

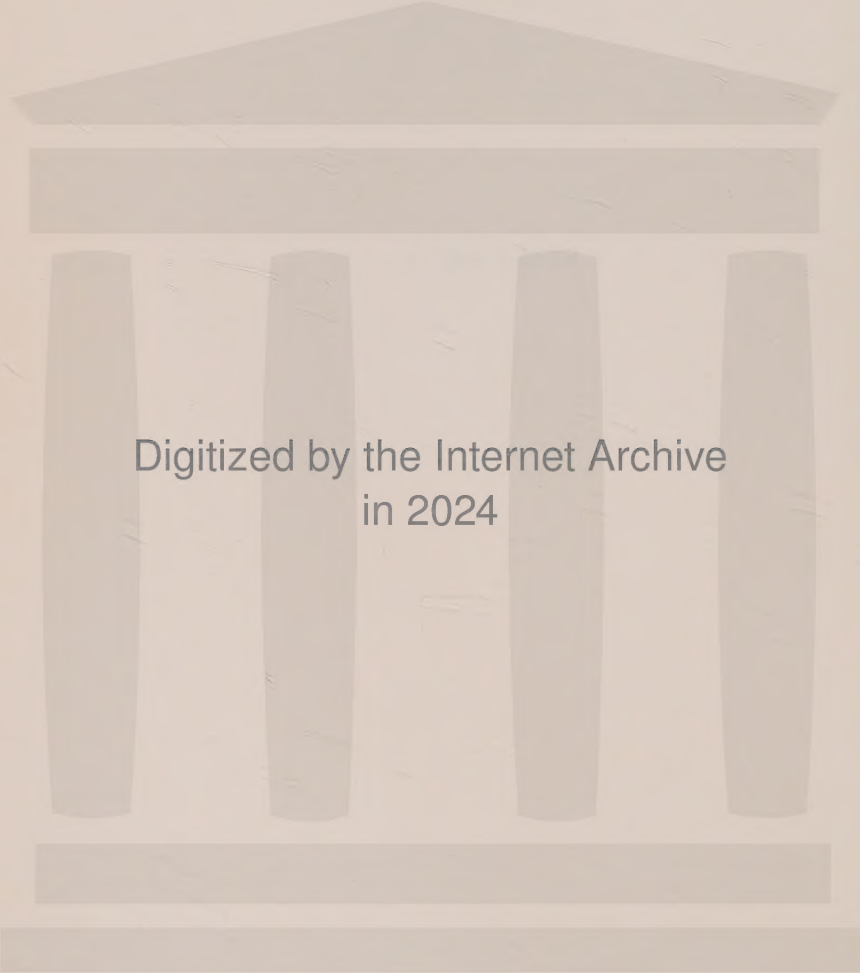
MOLECULAR PHYSICS

VOLUME 9

Printed and Published by

TAYLOR & FRANCIS LTD

RED LION COURT, FLEET STREET, LONDON, E.C.4



Digitized by the Internet Archive
in 2024

CONTENTS OF VOLUME 9

NUMBER 1

Far infra-red spectra of molecular crystals. IV. Ammonia, hydrogen sulphide and their fully deuterated analogues. A. ANDERSON and S. H. WALMSLEY	1
Formation of dimers in polar gases. A. K. BARUA, P. K. CHAKRABORTI and ANIL SARAN.. .. .	9
Quantum second virial coefficient of a two-dimensional Lennard-Jones gas. JOHN R. SAMS	17
The electronic structure of ionized molecules. III. Field ionization. J. C. LORQUET and G. G. HALL	29
On the tetragonal distortion of octahedral systems in an E_g electronic state. M. H. L. PRYCE, K. P. SINHA and Y. TANABE	33
The new equation of state of Longuet-Higgins and Widom. E. A. GUGGENHEIM	43
The high-resolution nuclear magnetic resonance spectrum of 2-carbomethoxy 5,6-dimethyl benzofuran. A. D. COHEN and K. A. McLAUCHLAN	49
Statistical mechanics of transport processes in adsorbed gases. J. POPIELAWSKI and B. BARANOWSKI	59
The influence of substitution on CH, CF and CF ₂ coupling constants. R. J. ABRAHAM and L. CAVALLI	67
Quantum second virial coefficient of a one-dimensional Lennard-Jones gas. JOHN R. SAMS	77
Normal coordinate analysis of Re(VII)O_4^- , $\text{Re(VII)O}_3\text{Cl}$ and $\text{Re(VII)O}_3\text{Br}$. WALTER A. YERANOS and FRED D. FOSS	87

RESEARCH NOTES

The relative signs of the proton coupling constants in the pyridine ring—the N.M.R. spectrum of 2,2'-dipyridine. V. M. S. GIL ..	97
--	----

NUMBER 2

The electronic structure of ionized molecules. II. Alkanes. J. C. LORQUET	101
Vacuum ultra-violet absorption spectra of various mono-substituted benzenes. K. KIMURA and S. NAGAKURA	117
The electron spin resonance spectrum and spin density distribution of the benzyl radical. A. CARRINGTON and I. C. P. SMITH	137

CONTENTS OF VOLUME 9

	Page
Rapid proton exchange of the free radical $\cdot\text{CH}_2\text{OH}$ as studied by E.S.R. HANNS FISCHER	149
Weak association between alkali metal ions and mononegative ions of aromatic hydrocarbons. H. NISHIGUCHI, Y. NAKAI, K. NAKAMURA, K. ISHIZU, Y. DEGUCHI and H. TAKAKI	153
Studies of sterically hindered and overcrowded molecules. Part I. Proton magnetic resonance studies of the relative steric and electronic effects of the methyl and <i>t</i> -butyl groups. W. A. GIBBONS and V. M. S. GIL	163
Studies of sterically hindered and overcrowded molecules. Part II. Comparative proton magnetic resonance studies of substituent effects in monoderivatives of benzene, mesitylene and 1,3,5-tri- <i>t</i> -butylbenzene. W. A. GIBBONS and V. M. GIL	167
Expansion theorems for solid spherical harmonics. J. P. DAHL and M. P. BARNETT	175
Solvent and temperature effects in the electron spin resonance spectrum of the hexamethylacetone-sodium ion-quartet. G. R. LUCKHURST	179
Isotope effects in electron spin resonance: the negative ion of cyclooctatetraene-1-d. A. CARRINGTON, H. C. LONGUET-HIGGINS, R. E. MOSS and P. F. TODD	187

RESEARCH NOTES

Spin densities in the alkyl groups of alkyl-substituted naphthalene negative ions, determined by N.M.R. E. DE BOER and C. MACLEAN	191
Two-dimensional second virial coefficients of krypton on graphitic carbon. JOHN R. SAMS	195
A test of Kihara's intermolecular potential. J. S. ROWLINSON	197
Variations on van der Waals' equation of state for high densities. E. A. GUGGENHEIM	199

NUMBER 3

The molecular orbital theory of some simple radicals. W. T. DIXON ..	201
The tricyano-sym-triazine anion: a permanent Jahn-Teller distortion? A. CARRINGTON, H. C. LONGUET-HIGGINS and P. F. TODD	211
Self-consistent approximations for molecular distribution functions. J. S. ROWLINSON	217
Molecular orbitals for H_3^+ using A.O.'s with angularly dependent Z_{eff} . K. C. BHALLA and P. G. KHUBCHANDANI	229
Microwave diamagnetic resonance associated with polysiloxanes. FLOYD HUGHES and FRANK W. PATTEN	233

CONTENTS OF VOLUME 9

	Page
The vibrational selection rules and torsional barrier of ferrocene. P. R. BUNKER	247
The vibrational selection rules and torsional barrier of methylsilyl-acetylene. P. R. BUNKER	257
A study of the valence electron approximation: application to LiH. J. D. STUART and R. P. HURST	265
Nouvelles recherches sur l'existence de cations complexes de structure définie dans les solutions d'électrolytes. ANTONIO DA SILVEIRA, MANUEL A. MARQUES et NOEMIO M. MARQUES	271
The electron distribution of the bonded hydrogen atom in carbon-hydrogen bonds. R. MASON, D. C. PHILLIPS and G. B. ROBERTSON	277
The Jahn-Teller effect in ReF_6 . M. S. CHILD and A. C. ROACH	281
The electron spin resonance spectra of paradinitrobenzene anions. J. M. GROSS and M. C. R. SYMONS	287

RESEARCH NOTES

Variation calculations for H_2^+ using A.O.'s with angularly dependent Z_{eff} . K. C. BHALLA and P. G. KHUBCHANDANI	291
Cobalt-59 spin-spin coupling and isotope shifts in $\text{K}_3\text{Co}(\text{CN})_6$. A. LOEWENSTEIN and M. SHPORER	293
Calculation of a triplet ground state for 1,2-diphenylphenanthro(1)-cyclobutene. J. W. HILPERN	295
Tetragonal splittings in cobalt complexes. A correction. J. H. DUNLOP and R. D. GILLARD	299

NUMBER 4

A molecular orbital theory of hydrocarbons, II. Ethane, ethylene and acetylene. J. A. POPLÉ and D. P. SANTRY	301
A molecular orbital theory of hydrocarbons, III. Nuclear spin coupling constants. J. A. POPLÉ and D. P. SANTRY	311
Double long-range spin-spin couplings between aldehydic and aromatic protons in the N.M.R. spectra of salicylaldehydes. DORA G. DE KOWALEWSKI and VALDEMAR J. KOWALEWSKI	319
Multiple long-range spin-spin couplings in di-substituted benzaldehydes and hindered rotation. DORA G. DE KOWALEWSKI and VALDEMAR J. KOWALEWSKI	331
Ligand field parameters of Mo(III) complexes. C. FURLANI and O. PIOVESANA	341

CONTENTS OF VOLUME 9

	Page
The long-range interaction of atoms and molecules. Y. M. CHAN and A. DALGARNO	349
The Renner effect in a nearly linear molecule, with application to NH_2 . R. N. DIXON	357
Fluorescence decay times of naphthalene and naphthalene excimers. NOBORU MATAGA, MASAO TOMURA and HITOSHI NISHIMURA ..	367
Electron resonance studies of fluorine hyperfine interactions. A. CARRINGTON, A. HUDSON and H. C. LONGUET-HIGGINS	377
Electric fields in fluorocyclohexanes and the magnitude of ^{19}F chemical shifts. J. W. EMSLEY	381

RESEARCH NOTES

E.P.R. studies of ionic association of pyrazine negative ion and alkali metal cations. J. DOS SANTOS-VEIGA and A. F. NEIVA-CORREIA ..	395
Note on the Paper "Proton spin-lattice relaxation in aqueous ionic solutions" by Jones and Powles. BURTON P. FABRICAND	399

NUMBER 5

The angular overlap model, an attempt to revive the ligand field approaches. CLAUS E. SCHÄFFER and CHR. KLIXBÜLL JØRGENSEN ..	401
Solvent effects on the visible spectra of nitrobenzene anion radicals. JAMES Q. CHAMBERS and RALPH N. ADAMS	413
Calculation on some excited states of helium and lithium. D. B. COOK and J. N. MURRELL	417
Détermination des signes relatifs des constantes de couplage ^{31}P - ^1H dans le tripropyl phosphate par R.M.N. dans le champ magnétique terrestre. E. DUVAL, J. RANFT et G. J. BÉNÉ	427
The distortions of the ethylene molecule in its low-lying excited states—a four-electron treatment. LOUIS BURNELLE and CLOTILDE LITT ..	433
H-H and ^{13}C -H coupling constants in pyridazine. V. M. S. GIL ..	443
Normal coordinate analysis of XeF_4 in the Urey-Bradley Field. WALTER A. YERANOS	449
Urey-Bradley potential constants of sulphur compounds: SF_5Cl . WALTER A. YERANOS	455
The dipole moment of dihexamethylbenzenecobalt. B. J. NICHOLSON and H. C. LONGUET-HIGGINS	461
The absorption spectra of solid CO and N_2 . M. BRITH and O. SCHNEPP	473

CONTENTS OF VOLUME 9

	Page
RESEARCH NOTES	
Long-range interaction of two 1s-hydrogen atoms expressed in terms of natural spin-orbitals. J. O. HIRSCHFELDER and P. O. LÖWDIN ..	491
Electron spin resonance spectrum of the NF_2 radical isolated in a neon matrix at 4°K. PAUL H. KASAI and EARL B. WHIPPLE	497
NUMBER 6	
Dielectric constants of homogeneous mixtures. H. LOOYENGA	501
A two-electron atomic integral. P. J. ROBERTS	513
Electron paramagnetic resonance study of the photo-excited triplet state of pyrene- <i>d</i> -10. S. W. CHARLES, P. H. H. FISCHER and C. A. McDOWELL	517
Long-range interactions between three hydrogen atoms. Y. M. CHAN and A. DALGARNO	525
An electron spin resonance and polarographic study of the sulphone group. R. GERDIL and E. A. C. LUCKEN	529
The intensity of the symmetry-forbidden electronic band of biphenylene. J. W. HILPERN	543
Multipolar theory of dielectric polarization in dense mixtures. S. KIELICH	549
Quadrupole relaxation in solutions of electrolytes. C. DEVERELL, D. J. FROST and R. E. RICHARDS	565
Nuclear magnetic energy levels and symmetry wave functions for six chemically equivalent spin $\frac{1}{2}$ nuclei with $C_{3v} \times C_i$ symmetry. A. NESZMÉLYI	579
The relationship between electron spin rotation coupling constants and <i>g</i> -tensor components. R. F. CURL, JR.	585
RESEARCH NOTE	
Electron spin resonance of the N_2O_2^+ radical. R. P. A. MUNIZ and J. DANON	599
Index of authors (with titles of papers)	601

Far infra-red spectra of molecular crystals

IV. Ammonia, hydrogen sulphide and their fully deuterated analogues

by A. ANDERSON

Basic Physics Division, National Physical Laboratory, Teddington, Middlesex†

and S. H. WALMSLEY

William Ramsay and Ralph Forster Laboratories, University College London

(Received 10 August 1964)

Absorption spectra of crystalline films of ammonia, 3-deutero ammonia, hydrogen sulphide and 2-deuterium sulphide have been measured at liquid nitrogen temperature using a Michelson interferometer. Changes in frequency on deuteration enable the modes to be classified as either translational or librational. In the case of ammonia, the spectrum is consistent with the stable cubic crystal form belonging to space group T^4 but the situation is complicated by the possible presence of metastable phases. The hydrogen sulphide spectrum indicates a site symmetry of C_s , and favours an orthorhombic over a tetragonal structure.

1. INTRODUCTION

In this paper the results of measurements on crystals of some simple hydrides and deuterides are presented. In contrast to crystals considered in earlier papers in this series [1–3], the molecules are not linear and additional lattice vibrations are expected due to torsion about the principal axis of the molecule.

Ammonia differs from the hydrogen halides and hydrogen sulphide in that the crystal structure is now well established [4–6]. The most recent determination by Olovsson and Templeton [6] gave some indication of hydrogen atom positions. The structure is the same as that of carbon dioxide, except that ammonia has no centre of symmetry. The space group is $T^4(P2_13)$ and the molecules have a threefold symmetry axis at the crystal site. In this work, the crystal sample is a film prepared by direct condensation from the vapour. According to Mauer and McMurdie [7] crystals in such a film contain two metastable non-cubic phases, the relative percentage of each depending on the rate of deposition of the film. No details have been published of either structure.

In hydrogen sulphide, three phases of the crystalline material have been distinguished with transition temperatures at 104°K and 126°K [8]. The low temperature phase is called phase III and the crystal passes successively to phase II and phase I. The early x-ray determinations [9–11] indicate that in all three phases the sulphur atoms form a face-centred cubic lattice. The lattice constant

† Present address: Frick Chemical Laboratory, Princeton University, Princeton, New Jersey, U.S.A.

is close to 5.74 \AA in each case. In more recent work [12] the changes in the electron diffraction pattern on passing through the transition point at 104°K have been investigated. The upper phase is consistent with a cubic lattice with spacing 5.74 \AA , but phase III has been indexed on the basis of a tetragonal cell with $a = 13.51 \text{ \AA}$ and $c = 4.14 \text{ \AA}$.

The near infra-red work of Reding and Hornig [13] supports the view that phases I and II are disordered with respect to the hydrogen atom positions, and that phase III is ordered. With the use of the polarizing microscope [14], phase III has been shown to be anisotropic, but the other two phases may be isotropic. In this paper only the low temperature phase has been studied.

2. EXPERIMENTAL

The gases in these investigations were supplied by I.C.I. Limited, (NH_3 —99.9 per cent pure), Mathieson Co. (H_2S —99.9 per cent) and Mecke, Sharpe and Dohme (Canada) Limited, (ND_3 and D_2S —99 per cent isotopic purity). The gases were dried before deposition on the reflecting surface. Special precautions were taken with the deuterated samples to avoid exchange with hydrogen.

The experimental procedures were identical with those described previously [15]. Suitable temperatures for the films, to avoid slow evaporation under vacuum, were 77°K for ammonia and 65°K for hydrogen sulphide. Normal spectral resolution was 4 cm^{-1} . Although no film thickness determinations were made, it was clear from the amount of gases deposited that the absorptions were in general more intense than those of previous investigations [1–3].

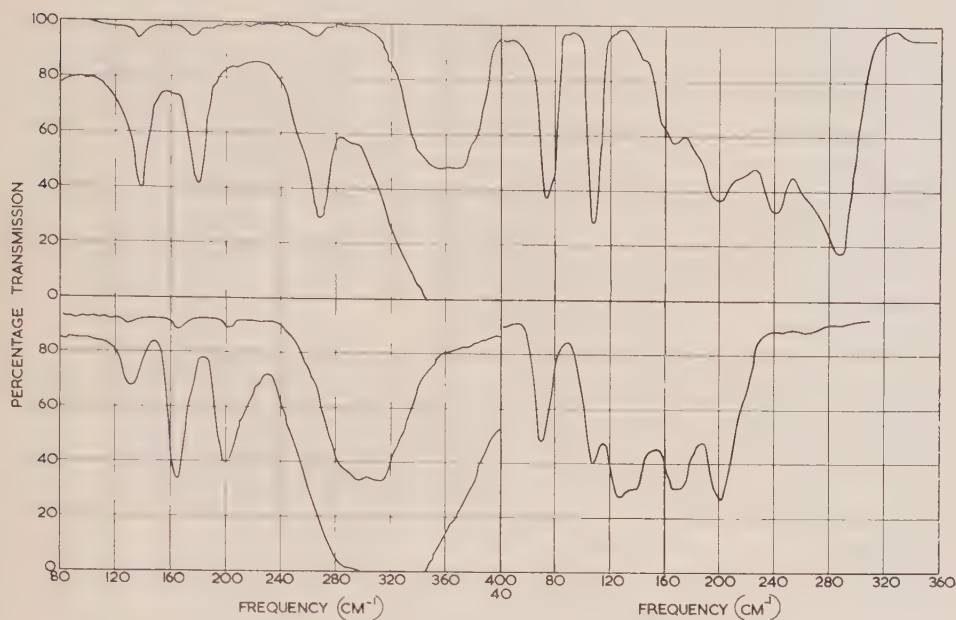
NH_3	138	180	268	362		
ND_3	132	167	200	297		
Ratio	1.04	1.08	1.34	1.22		
H_2S	74	108	167	199	240	287
D_2S	71	109	129	145	185	207
Ratio	1.04	0.99	1.30	1.37	1.30	1.40

Table 1. Frequencies in cm^{-1} of maximum absorption.

Absorption spectra, ratioed against the background, are shown in figures 1 to 4. The mean frequencies of maximum absorption are collected in table 1. In figures 1 and 2 the upper curves are for a film absorbing approximately 20 per cent of the total radiation over the frequency range, and the lower ones for thicker films absorbing about 50 per cent. In the latter, three weak bands at low frequency are clearly distinguishable in both NH_3 and ND_3 .

The strong absorption in hydrogen and deuterium sulphide is a broad band with a complicated structure. The frequencies and even the number of maxima observed in this band were found to be much less reproducible than for previous

samples. Although the spectra, reproduced in figures 3 and 4, for films absorbing about 50 per cent of the total signal are typical, it is not completely certain that there are four distinct bands present. The two low frequency bands are quite distinct and occur at nearly the same frequency in both compounds.

Figure 1. $\text{NH}_3(77^\circ\text{K})$.Figure 3. $\text{H}_2\text{S}(65^\circ\text{K})$.Figure 2. $\text{ND}_3(77^\circ\text{K})$.Figure 4. $\text{D}_2\text{S}(65^\circ\text{K})$.

The variability of the maxima in the intense band may be due to one or more of the following causes.

- Frequency dependence on thickness, which cannot be closely controlled in these experiments.
- Effect of reflected radiation reaching the detector, which may be considerable due to intense absorption.
- Possibility of orientational disorder, being 'frozen in' at the experimental temperature.

Further work with better annealing of the samples and then cooling to liquid helium or hydrogen temperatures to sharpen the bands will be necessary to resolve these difficulties.

3. DISCUSSION

The combined results of ammonia and deuterio-ammonia enable the observed bands to be classified as arising principally from translation or torsional vibrations. Table 1 includes the ratios of corresponding vibrations in NH_3 and ND_3 . For a pure translational vibration, the theoretical value is 1.1. For a torsion, the corresponding ratio is 1.4. This leads to the assignment of the two sharp, weak intensity lines at 138 and 180 cm^{-1} in ammonia as translational modes. The weak

band at 268 cm^{-1} and the broad very intense band at 362 cm^{-1} are both assigned as torsions. The intense torsional band has counterparts in both the hydrogen halides and hydrogen sulphide—the intensity presumably being due to alteration in the orientation of the molecular dipole moment during the vibration. In ammonia there is an additional degree of freedom corresponding to rotation about the dipolar axis. The very weak band at 268 cm^{-1} probably corresponds to torsion about this axis to a high degree of approximation.

Interpretation of the results is complicated by the possibility of a metastable phase [7] the structure of which is unknown. Staats and Morgan [16] observed changes in the near infra-red spectrum on heat treatment which they attributed to the two metastable phases and the cubic phase. In earlier work, Reding and Hornig looked at the near infra-red spectrum [17] in which the specimens were prepared by condensation from the vapour and also the Raman spectrum [18] in which the crystals are quite certainly cubic, being grown from a melt. They successfully interpreted *both* spectra on the basis of the stable cubic phase and a number of bands, which are expected to coincide in Raman and infra-red, were observed to do so within experimental error.

In this paper the spectrum is compared with the predictions for the cubic phase, with the proviso that the results may have to be re-examined when the position with respect to the metastable phases becomes clearer.

The stable crystal form of ammonia belongs to space group $T^4(P2_13)$. There are four molecules in the unit cell, each retaining a three-fold axis. The number of zero wave vector lattice vibrations predicted and their infra-red and Raman activity is summarized in table 2.

Type of free molecule motion	Symmetry		
	Molecular	Site	Crystal
	C_{3v}	C_3	T
Translation	A_1 E	A E }	$A + E + 2T^\dagger$
Rotation	A_2 E	A E	$A + T$ $E + 2T$

In the last column T is infra-red active. All vibrations are Raman active.

†In this entry the symmetry corresponding to pure translation of the lattice is not included.

Table 2. Symmetry and spectral activity of $K=0$ vibrations in crystalline ammonia.

Spectral information about the lattice vibrations of crystalline ammonia is available from three sources: the Raman spectrum [18] where direct observation is made, the near infra-red spectrum [17] in which certain bands are assigned as combinations involving lattice vibration and the far infra-red spectrum reported here. This is summarized in table 3.

NH ₃ (cm ⁻¹)			HD ₃ (cm ⁻¹)		
Near [16] infra-red	Far infra-red	Raman† [17]	Near [16] infra-red	Far infra-red	Raman† [17]
53†		99 s 129 m	41†		91.5 s 121 m
	138			132	142–161 vw
	180			167	
~ 250†	268		~ 200†	200	
		284 vs			213 vs
362	362	325–375 w ~ 386 vw	< 300	297	280–312 w
		430–462 vw			330–380 w
527			406		505–540 w

† Observed in combination bands.

‡ Hornig's qualitative estimates of intensities given after the frequency values.

Table 3. Summary of information from spectral sources on lattice vibrations of crystalline ammonia.

For the cubic structure, there are two infra-red and four Raman translation fundamentals predicted, two vibrations being common to both spectra. Experimentally, there are two bands found in each spectrum but no coincidences of frequency. In ND₃, additional weak scattering between 142 and 161 cm⁻¹ could correspond to translation vibration. It lies between the two bands in the infra-red spectrum and there is no corresponding feature in NH₃.

In the case of the torsional modes, three infra-red and five Raman active vibrations are predicted, the infra-red frequencies being coincident with three of the Raman frequencies. In the far infra-red only two maxima are observed, the weak 268 cm⁻¹ and the strong and broad band around 362 cm⁻¹. In both hydrogen chloride and hydrogen bromide [1] such an intense band was split into two on deuteration. Although the corresponding band in deuterio-ammonia does not exhibit this behaviour it is possible that this band in each case involves two fundamentals. The near infra-red spectrum suggests a torsional fundamental at 53 cm⁻¹ (41 cm⁻¹ in ND₃) from combination bands. The evidence suggests that this should have a T symmetry. No direct evidence for a vibration of this frequency is found in either Raman or far infra-red. Again, Reding and Hornig observe a sharp band at 527 cm⁻¹ (and 406 cm⁻¹ in the deuterated molecule). No corresponding Raman scattering was found. It could, nevertheless, represent a fundamental. The present work shows that it can also be assigned as the first overtone of the 268 cm⁻¹ vibration.

From the infra-red spectrum, Raman fundamentals are expected at 268 cm⁻¹ and 362 cm⁻¹ in ammonia. Corresponding to the latter there is a region of weak intensity scattering between 325 and 375 cm⁻¹. The same result is observed for ND₃, the corresponding figures being 297 in the infra-red, 280–312 cm⁻¹ in the Raman. In the region of 268 cm⁻¹ there is an intense scattering in the Raman,

having a maximum at a significantly higher frequency— 284 cm^{-1} . In fact this is the only intense Raman line in the torsional lattice region and can firmly be assigned as a fundamental of the cubic structure. Assuming the cubic structure for the infra-red work also, it is felt that 268 cm^{-1} represents a separate fundamental.

To summarize, the following fundamentals seem established:

NH_3	Translation :	99,	129,	<i>138,</i>	<i>180</i>
	Torsion :	<i>268,</i>	284,	<i>362 (2 ?)</i>	
ND_3	Translation :	92,	121,	<i>132,</i>	<i>167</i>
	Torsion.	<i>200,</i>	213,	<i>297 (2 ?)</i>	

Those in italics are derived from the far infra-red, the remainder from the Raman.

There remains the question of the nature of the crystal phase being examined in the films used in these experiments. Comparison with the Raman spectrum does not enable the problem to be resolved conclusively. The Raman spectrum is not as rich in bands as the simple theory suggests.

The far infra-red spectrum itself is consistent in general outline with a cubic structure. On the other hand, the broad intense torsional band could by comparison with the spectrum of the high temperature phase of hydrogen bromide [1] indicate a disordered structure. This could be a feature of a metastable phase.

The spectrum of hydrogen sulphide shows a marked similarity to the spectra of the other hydrides reported in this series. The two weak low frequency bands at 74 and 108 cm^{-1} in hydrogen sulphide correspond to bands observed in deuterium sulphide at 71 and 109 cm^{-1} . The small change in frequency indicates that the corresponding vibrations are translational in character. The broad intense band in hydrogen sulphide is displaced to longer wavelengths in deuterium sulphide. The ratios of the corresponding maxima all lie between 1.3 and 1.4 as seen in table 1 and can be ascribed to torsional vibrations.

These frequencies can be compared with lattice vibration frequencies deduced from other investigations. Thus Sirkar and Gupta [19], in their Raman work, observe a band at 80 cm^{-1} both in the Stokes and anti-Stokes spectrum of hydrogen sulphide. Although corresponding measurements for the deuterium compound have not been reported, it seems clear that this represents a further translation fundamental, by comparison with the results of the investigation reported here. In the near infra-red spectra measured by Reding and Hornig [13] lattice vibrations are not observed directly but certain bands are assigned as combinations involving them. In this way, a lattice vibration at 92 cm^{-1} in H_2S and 91 cm^{-1} in D_2S is deduced. This represents a translation from the change in frequency on deuteration and also is within the range of frequency in which such vibrations are found in the far infra-red. It is probably also a fundamental. Again, a lattice vibration at 170 cm^{-1} is suggested by the assignment of a further band in the near infra-red spectrum of H_2S . The corresponding value in deuterium sulphide is 125 cm^{-1} , indicating a torsional motion. These are close to the bands observed at 167 cm^{-1} (H_2S) and 129 cm^{-1} (D_2S) in the present investigation.

The interpretation of the crystal spectrum is hampered by lack of knowledge of the crystal structure. Reding and Hornig [13] have examined the crystal structure implications of their own near infra-red spectrum and the earlier Raman work [19, 20]. They considered both orthorhombic and tetragonal possibilities

and were able to show that the hydrogen sulphide retains a plane of symmetry at its site in the crystal which is perpendicular to the molecular plane. They further argued that the most likely structure involved a crystal of class D_{4h} , having eight molecules in the primitive unit cell. In this respect, however, the case cannot be said to have been proved conclusively since there is an error in the correlation table for D_{4h} , which influenced their choice.

It was found in the case of the hydrogen halides [1] that the predicted infra-red spectrum is diagnostic of the site symmetry for a given crystal system. There are only four possible site groups for hydrogen sulphide and the number of infra-red active fundamentals for each of these in a tetragonal or orthorhombic crystal is summarized in table 4. It is seen that the observed crystal spectrum agrees with an orthorhombic crystal having site symmetry C_s . The same site group in a tetragonal crystal differs only in the requirement of an additional translation fundamental.

Site Symmetry	Tetragonal		Orthorhombic	
	Translation	Torsion	Translation	Torsion
C_{2v}	1	2	0	2
C_s	3	4	2	4
C_2	3	5	2	5
C_1	7	9	6	9

Table 4. Number of infra-red fundamentals predicted for various site symmetries of hydrogen sulphide.

In the case of a crystal having n molecules in the unit cell, a total of $3n - 3$ translation fundamentals are predicted. The combined results of this and previous investigations give evidence for four translation fundamentals as follows: 74 (for infra-red), 80 (Raman), 92 (near infra-red) and 108 cm^{-1} (far infra-red). If this is correct the unit cell of hydrogen sulphide contains more than two molecules. This implies that an orthorhombic crystal would belong to crystal class D_{2h} . No further information is gained if the crystal is tetragonal. The site group C_s requires at least four molecules in the unit cell.

The authors would like to thank Professor D. F. Hornig for a helpful discussion.

This work forms part of the programme of Basic Physics Division of the National Physical Laboratory and is published by permission of the Director.

REFERENCES

- [1] ANDERSON, A., GEBBIE, H. A., and WALMSLEY, S. H., 1964, *Mol. Phys.*, **7**, 401.
- [2] WALMSLEY, S. H., and ANDERSON, A., 1964, *Mol. Phys.*, **7**, 411.
- [3] ANDERSON, A., and WALMSLEY, S. H., 1964, *Mol. Phys.*, **7**, 586.
- [4] MARK, H., and POHLAND, E., 1925, *Z. Kristallogr.*, **61**, 532.
- [5] DE SMEDT, J., 1925, *Bull. Cl. Sci., Acad. Belg.*, **11**, 655.
- [6] OLOVSSON, I., and TEMPLETON, D. H., 1959, *Acta Cryst.*, **12**, 832.

- [7] MAUER, F. A., and McMURDIE, H. F. (Reported at June 1958 meeting of American Crystallographic Association.)
- [8] CLUSIUS, K., 1933, *Z. Electrochem.*, **39**, 598.
- [9] NATTA, G., 1930, *R.C. Accad. Lincei*, **11**, 679, 749.
- [10] VEGARD, L., 1930, *Nature, Lond.*, **126**, 916; 1930, *Naturwissenschaften*, **18**, 1098; 1931, *Z. Kristallogr.*, **77**, 23.
- [11] JUSTI, E., and NIKTA, H., 1936, *Phys. Z.*, **37**, 435; 1937, *Ibid.*, **38**, 514.
- [12] KITAMURA, N., KASHWASE, Y., HARADA, J., and HONJO, G., 1961, *Acta Cryst.*, **14**, 687.
- [13] REDING, F. P., and HORNIG, D. F., 1957, *J. chem. Phys.*, **27**, 1024.
- [14] KREISS, A., and CLUSIUS, K., 1937, *Phys. Z.*, **38**, 510.
- [15] ANDERSON, A., and GEBBIE, H. A. (to be published).
- [16] STAATS, P. A., and MORGAN, H. W., 1959, *J. chem. Phys.*, **31**, 553.
- [17] REDING, F. P., and HORNIG, D. F., 1951, *J. chem. Phys.*, **19**, 594.
- [18] REDING, F. P., and HORNIG, D. F., 1954, *J. chem. Phys.*, **22**, 1926.
- [19] SIRKAR, S. C., and GUPTA, J., 1936, *Indian J. Phys.*, **10**, 227.
- [20] MURPHY, G. M., and VANCE, J. E., 1938, *J. chem. Phys.*, **6**, 426.

Formation of dimers in polar gases

by A. K. BARUA, P. K. CHAKRABORTI† and ANIL SARAN

Indian Association for the Cultivation of Science, Calcutta 32, India

(Received 4 May 1964; and revision received 6 July 1964)

In order to calculate the percentage of dimers in a polar gas at a particular pressure and temperature, the contribution of bound double molecules $B_b(T)$ to the second virial coefficient $B(T)$ has been calculated by assuming the dipoles to be in the head-to-tail position. $B_b(T)$ is related to the equilibrium constant for dimerization.

Sample calculation of the percentage of dimers as obtained from the values of $B_b(T)$ for several polar molecules have been made. The results obtained are quite reasonable.

1. INTRODUCTION

At high pressures an imperfect gas is an equilibrium mixture of single, double, triple, etc. molecules which are readily interconvertible [1]. The bound double molecules may be defined as systems whose relative kinetic energy is less than the negative value of the mutual potential energy [2]. These molecules exist only for the duration of a collision, but their number is determined by the usual type of chemical equilibrium constant. Consequently, for a proper representation of the equilibrium and non-equilibrium properties of gases at high pressures it is essential to know the percentage of various bound molecules. At not too high pressures it is sufficient to consider dimerization only.

According to Hill [2], the total second virial coefficient $B(T)$ may be written as

$$B(T) = B_f(T) + B_b(T) + B_m(T), \quad (1)$$

where $B_f(T)$, $B_b(T)$ and $B_m(T)$ are respectively the contributions of the free, bound and metastable double molecules. According to classical mechanics, metastable molecules can only be separated if perturbed by a third molecule. In this paper we have not considered the presence of metastable molecules and have calculated values of $B_b(T)$ only.

The formation of dimers in non-polar gases has been treated in detail by Stogryn and Hirschfelder [3] in terms of realistic intermolecular potentials. They have calculated $B_m(T)$ and $B_b(T)$ which can be related to the equilibrium constant for dimerization.

Due to the predominance of the dipole-dipole interaction term in the potential energy of interaction between two polar molecules at ordinary temperatures, dimerization plays a more significant part in determining properties of polar gases than in non-polar gases. In this paper we have calculated $B_b(T)$ for polar gases by assuming the dipoles of the two molecules to be in the head-to-tail position which corresponds to the Krieger potential [4]. This is a reasonably good approximation in the bound state as it corresponds to the maximum attractive

† Present Address: School of Chemistry, University of Leeds, England.

energy state and has been used with success by Barua and Das Gupta [5] in explaining the pressure dependence of the viscosity of super-heated steam.

It is relevant here to point out that if the two dipoles are taken in the head-to-tail position the total second virial coefficient become negative infinite. However, this difficulty with the Krieger potential is mathematical rather than physical as this particular orientation is also considered in the calculation of $B(T)$ for polar molecules on the Stockmayer potential [6]. Present calculations show that the values of $B_b(T)$ on the Krieger potential do not diverge. By elimination, then, the difficulty must be either with $B_f(T)$ or $B_m(T)$ or both. However, for the calculation of the percentage of dimers we are only concerned with $B_b(T)$ for which the difficulty encountered in the calculation of $B(T)$ on the Krieger potential is not present.

2. EVALUATION OF $B_b(T)$ FOR POLAR GASES

The interaction between two polar molecules separated by a distance r is given on the Stockmayer potential [6] as :

$$\phi(r) = 4\epsilon[(\sigma/r)^{12} - (\sigma/r)^6] - \frac{\mu^2}{r^3}(2 \cos \theta_1 \cos \theta_2 - \sin \theta_1 \sin \theta_2 \cos \phi), \quad (2)$$

where μ is the dipole moment of the interacting molecules, θ_1, θ_2 are the angles of inclination of the axes of the two dipoles to the line joining the centre of the molecules and ϕ is the azimuthal angle between them. For $\mu \rightarrow 0$, $\phi(r)$ is the usual Lennard-Jones (12:6) potential.

If the two dipoles of the interacting molecules are in the head-to-tail position, then equation (2) becomes effectively the Krieger potential [4] given by :

$$\phi(r) = 4\epsilon[(\sigma/r)^{12} - (\sigma/r)^6] - \frac{2\mu^2}{r^3}, \quad (3)$$

which is spherically symmetric.

For spherically symmetric molecules :

$$B_b(T) = -N\Lambda^6 Q_{2b}/V, \quad (4)$$

where Q_{2b} is the partition function for double molecules, N is Avogadro's number, V is the volume and $\Lambda^2 = h^2/2\pi mkT$. According to the expression for Q_{2b} as obtained by Hill [2] :

$$B_b(T) = -2\Pi N \int_{\sigma}^{\infty} r^2 \exp[-\phi(r)/kT] \left[\Gamma\left(\frac{3}{2}, -\frac{\phi(r)}{kT}\right) / \Gamma\left(\frac{3}{2}\right) \right] dr, \quad (5)$$

where $\Gamma\left(\frac{3}{2}, -\phi(r)/kT\right)$ is the incomplete gamma function. We define the following reduced quantities :

$$\phi^* = \phi/\epsilon, \quad r^* = r/\sigma, \quad T^* = kT/\epsilon, \quad B_b^* = \frac{B_b}{b_0}, \quad b_0 = \frac{2\pi}{3} N\sigma^3, \quad (6)$$

so that we get :

$$B_b^*(T^*) = -3 \int_1^{\infty} r^{*2} \exp[-\phi^*/T^*] \left[\Gamma\left(\frac{3}{2}, -\phi^*/T^*\right) / \Gamma\left(\frac{3}{2}\right) \right] dr^*. \quad (7)$$

The incomplete gamma function is a particular case of the confluent hypergeometric series [7]. By following the procedure of reference [3] and applying Kummer's transformation, we get:

$$B_b^*(T^*) = -\frac{2}{\Gamma(\frac{3}{2})} \sum_{n=0}^{\infty} \frac{\Gamma(1+n)\Gamma(\frac{5}{2})}{\Gamma(1)\Gamma(\frac{5}{2}+n)} \cdot \frac{1}{n!} \int_1^{\infty} r^{*2} (-\phi^*/T^*)^{n+3/2} dr^*. \quad (8)$$

In equation (3), we put:

$$\mu^* = \mu / \sqrt{(\epsilon \sigma^3)}, \quad (9)$$

so that

$$\phi^*(r^*) = 4 \left[r^{*-12} - r^{*-6} - \frac{\mu^{*2}}{2} r^{*-3} \right]. \quad (10)$$

Thus,

$$\begin{aligned} & \int_1^{\infty} r^{*2} (-\phi^*/T^*)^{n+3/2} dr^* \\ &= \left(\frac{4}{T^*} \right)^{n+3/2} \int_1^{\infty} r^{*2} [A r^{*-3} + r^{*-6} - r^{*-12}]^{n+3/2} dr^* \\ &= \left(\frac{4}{T^*} \right)^{n+3/2} \int_1^{\infty} (r^{*-3/2})^{2n} r^{*-5/2} [A + (r^{*-3/2})^2 - (r^{*-3/2})^6]^{n+3/2} dr^*, \end{aligned} \quad (11)$$

where

$$A = \mu^{*2}/2. \quad (12)$$

Putting $y = r^{*-3/2}$, we have:

$$\int_1^{\infty} r^{*2} (-\phi^*/T^*)^{n+3/2} dr^* = \left(\frac{4}{T^*} \right)^{n+3/2} \int_0^1 \left(\frac{2}{3} \right) y^{2n} [A + y^2 - y^6]^{n+3/2} dy. \quad (13)$$

It is not possible to integrate equation (13) analytically. It is to be noted that for $A = 0$, equation (13) corresponds to the expression approximate to the Lennard-Jones (12:6) potential. As an approximation we shall use an average of y within the bracket in equation (13) so that for $A = 0$, each term in equation (8) is equal to the corresponding term in the expression on the Lennard-Jones (12:6) model [3]. So we get:

$$[\bar{y}_n^2 - \bar{y}_n^6]^{n+3/2} = \frac{4^n \cdot n! (2n+2)! (2n+3)! (2n+1)!}{(4n+5)! (n+1)!}. \quad (14)$$

The values of \bar{y}_n thus obtained are shown in table 1. Consequently, equation (13) becomes:

$$\int_1^{\infty} r^{*2} (-\phi^*/T^*)^{n+3/2} dr^* = \frac{2}{3} \left[\frac{4(A + \bar{y}_n^2 - \bar{y}_n^6)}{T^*} \right]^{n+3/2} \cdot \frac{1}{2n+1}. \quad (15)$$

Substituting equation (15) into equation (8), we get:

$$B_b^*(T^*) = -\frac{2}{3}[2/\Gamma(\frac{3}{2})] \sum_{n=0}^{\infty} \frac{\Gamma(1+n)\Gamma(\frac{5}{2})}{\Gamma(1)\Gamma(\frac{5}{2}+n)} \cdot \frac{1}{n!} \left[\frac{4(A + \bar{y}_n^2 - \bar{y}_n^6)}{T^*} \right]^{n+3/2} \cdot \frac{1}{2n+1}$$

$$= -\frac{16}{(\pi)^{1/2}} \sum_{n=0}^{\infty} \frac{4^n \cdot (n+1)!}{(2n+3)!} \times \frac{1}{2n+1} \left[\frac{4(A + \bar{y}_n^2 - \bar{y}_n^6)}{T^*} \right]^{n+3/2}. \quad (16)$$

The values of $B_b^*(T^*)$ calculated from equation (16) at different values of A and T^* are shown in table 2.

n	0	1	2	3	4
\bar{y}_n	0.477	0.576	0.589	0.886	0.888
5	6	7	8	9	10
0.890	0.892	0.894	0.895	0.897	0.898

Table 1. Values of \bar{y}_n .

It may be seen from table 2 that, as expected, the values of $B_b^*(T^*)$ for polar molecules are much higher than those for non-polar molecules ($A=0$). It is interesting to see if the values of $B_b(T)$ as calculated on the Krieger potential are consistent with the values of $B(T)$ as calculated on the Stockmayer potential. For sample calculation we have chosen CHCl_3 for which the force constants on both the Krieger potential [8] and the Stockmayer potential are available. The values of $B_b(T)$ and $B(T)$ as calculated on the Krieger potential and the Stockmayer potential respectively are shown in table 3. It may be seen that the absolute values of $B_b(T)$ on the Krieger potential is less than the absolute values of $B(T)$ on the Stockmayer potential. This is due to the neglect of $B_r(T)$ and $B_m(T)$ which probably cannot be calculated on the Krieger potential. It may be seen that the values of $B_b(T)$ on the Krieger potential are quite consistent with the values of $B(T)$ on the Stockmayer potential. This shows that it is not unreasonable to use the Krieger potential in representing the interaction between two polar molecules in the bound state.

T ($^{\circ}\text{C}$)	$B_b(T)$ in cm^3/mole	$B(T)$ in cm^3/mole
300	-141.77	-260.24
500	-88.87	-150.52
700	-59.25	-100.35

Table 3. Sample calculation of $B_b(T)$ on the Krieger potential and $B(T)$ on the Stockmayer potential for CHCl_3 .

$\frac{I}{T^*}$	0	0.2	0.4	0.6	0.8	1.0	1.2	1.4	1.6	1.8	2.0
0.40	10.7306	52.9458									
0.50	6.3247	25.5834	83.5436								
0.60	4.2679	15.4682	42.7265	113.3121							
0.70	3.1223	10.6010	26.4208	60.9207	138.4733						
0.80	2.4100	7.8306	18.2711	38.5043	79.3479						
0.90	1.9325	6.0864	13.5722	26.8968	51.2738						
1.00	1.5940	4.9071	10.5897	20.0881	36.2078	97.4750	114.9761				
1.25	1.0738	3.1855	6.5299	11.5828	19.1785	64.3744	48.5044	76.8014	122.5877		
1.50	0.7857	2.2798	4.5390	7.7590	12.2714	18.6058	27.5382	40.4399	59.1538	86.7398	127.7081
1.75	0.6068	1.7352	3.3906	5.6641	8.7115	12.7789	18.2102	25.5228	35.4554	49.0859	67.9938
2.00	0.4868	1.3782	2.6588	4.3722	6.6026	9.4765	13.1674	17.9219	24.0843	32.1538	42.2796
2.50	0.3388	0.9469	1.7968	2.8966	4.2767	5.9800	8.0649	10.6102	13.7183	17.5287	22.2106
3.00	0.2531	0.6877	1.3174	2.1006	3.0595	4.2152	5.5902	7.2206	9.1438	11.4147	14.0977
4.00	0.1608	0.4413	0.8191	1.2887	1.8458	2.5087	3.2692	4.1410	5.1335	6.2610	7.5386
5.00	0.1135	0.3087	0.5714	0.8926	1.2712	1.7099	2.2082	2.7695	3.3975	4.0972	4.8736
10.00	0.0391	0.1056	0.1928	0.2968	0.4172	0.5528	0.7032	0.8677	1.0467	1.2399	1.4476

Table 2. Values of $-B_0^*(T^*)$ for polar molecules.

3. CALCULATION OF THE MOLEFRACTIONS OF DIMERS

When metastable double molecules are neglected, the equilibrium constant $K(T)$ for dimerization may be written as:

$$K(T) = -B_b(T) = n_2 V / n_1^2, \quad (17)$$

where n_1 , n_2 are the numbers of moles of monomers and dimers respectively and V is the volume. Recently, Itean *et al.* [8] have corrected the values of the collision integrals on the Krieger potential and have obtained the force constants for several polar gases on this model from viscosity data. We have made some sample calculations of the molefractions x_2 of dimers for HI, HBr and C_2H_5OH with the force constants of ref. [8] and the values of $B_b(T)$ from table 2. The results are shown in table 4. For the sake of comparison we have also given the corresponding values of x_2 for H_2O as obtained by Barua and Das Gupta [5], by the semi-empirical method given in ref. [1]. It may be seen that the values of x_2 as calculated from our values $B_b(T)$ are quite reasonable. The magnitude of the values of x_2 also show that dimerization must be considered for a proper representation of the properties of polar gases at high pressures.

Substance	Force constants on the Krieger potential [8]			μ (debyes)	P in atms.	x_2
	σ (Å)	ϵ/k (°K)	δ			
H I	4.264	252.5	0.033	0.42	0	0
					1	0.00155
					5	0.00769
					10	0.01515
					30	0.04292
					50	0.06786
HBr	3.858	161.2	0.251	0.80	0	0
					1	0.00159
					5	0.00789
					10	0.01555
					30	0.04401
					50	0.06948
C_2H_5OH	5.296	47.8	1.456	1.69	0	0
					1	0.00459
					5	0.02215
					10	0.04249
					30	0.11011
					50	0.16254
H_2O^\dagger				1.85	0	0
					1	0.006
					5	0.029
					10	0.054
					30	
					50	

† From ref. [5].

Table 4. Sample calculation of mole fractions of dimers of HI, HBr, and C_2H_5OH at 200°C.

The authors are grateful to Professor B. N. Srivastava, D.Sc., F.N.I., for his kind interest and encouragement. They wish to thank the referee of the paper for suggesting the approximation used in equation (13).

REFERENCES

- [1] HIRSCHFELDER, J. O., MCCLURE, F. T., and WEEKS, I. F., 1942, *J. chem. Phys.*, **10**, 201.
- [2] HILL, T. L., 1955, *J. chem. Phys.*, **23**, 617; 1956, *Statistical Mechanics* (New York: McGraw-Hill Book Co., Inc.), Chap. 5.
- [3] STOGRYN, D. E., and HIRSCHFELDER, J. O., 1959, *J. chem. Phys.*, **31**, 1531.
- [4] KRIEGER, F. J., 1951, *The Viscosity of Polar Gases*, Proj-RAND Report RM-646.
- [5] BARUA, A. K., and DAS GUPTA, A., 1963, *Trans. Faraday Soc.*, **59**, 2243.
- [6] STOCKMAYER, W. H., 1941, *J. chem. Phys.*, **9**, 398.
- [7] ERDELYI, A., 1953, *Higher Transcendental Functions*, Vol. I (New York: McGraw-Hill Book Co., Inc.).
- [8] ITEAN, E. C., GLUECK, A. R., and SVEHLA, R. A., 1961, NASA Technical Note, D-481.

Quantum second virial coefficient of a two-dimensional Lennard-Jones gas†

by JOHN R. SAMS

Department of Chemistry, University of British Columbia,
Vancouver 8, Canada

(Received 9 June 1964)

We consider the equation of state of a dilute two-dimensional quantum degenerate gas at moderately high temperatures, and calculate the second virial coefficient assuming a Lennard-Jones function for the pair potential. The physical systems of interest are the mobile adsorption of gases on solid surfaces at low surface densities. The net Slater sum corrections to the classical B are smaller than for the three-dimensional case, whereas the effect of different particle statistics is enhanced. This leads to markedly different results in the two-dimensional problem.

1. INTRODUCTION

The high temperature quantum corrections to the classical second virial coefficient for non-polar gases are well known [1–3], whereas little or no attention has been paid to the corresponding corrections for two- and one-dimensional gases. In recent years, however, other one- and two-dimensional systems have attracted considerable interest. For example, we might mention the Monte Carlo calculations of Metropolis *et al.* [4] and of Wood and Jacobson [5] on two-dimensional hard sphere fluids, the corresponding molecular dynamics calculations of Alder and Wainwright [6], the treatment of one- and two-dimensional hard sphere liquids by Helfand *et al.* [7], and the recent interest in one- and two-dimensional plasmas [8]. Moreover, the first six virial coefficients for a gas of hard discs have also been calculated [4, 9].

The apparent lack of interest in two-dimensional dilute quantum gases may well have been the result of a complete absence of experimental data to which such a theoretical development might be applied. Recent publications in the field of physical adsorption of non-polar gases on solids indicate, however, that such a treatment may indeed be of considerable value. Everett [10], Hill and Greenschlag [11], Steele and Ross [12], Sams *et al.* [13] and Barker and Everett [14] have all presented models in which the adsorbate is treated as an imperfect two-dimensional gas in an external potential field. Such models are essentially outgrowths of the Steele-Halsey [15] treatment of physical adsorption in which the adsorption isotherm is expanded in virial form, viz. [13]:

$$p = \frac{N_a k T}{B_{AS}} - \frac{N_a^2 k T C_{AAS}}{B_{AS}^3} - \frac{N_a^3 k T D_{AAAS}}{B_{AS}^4} - \dots \quad (1.1)$$

B_{AS} , C_{AAS} , etc. are the irreducible gas-surface cluster integrals, k the Boltzmann constant and N_a the number of molecules adsorbed at Kelvin temperature T and bulk gas pressure p . The expansion (1.1) can be related, through the Gibbs

† This research was supported by the National Research Council and the Research Fund of the University of British Columbia.

isotherm, to a two-dimensional gas virial expansion [13] to provide the relations

$$B^{(2)}/\mathcal{A} = -C_{\text{AAS}}/2B_{\text{AS}}^2, \quad (1.2)$$

$$C^{(2)}/\mathcal{A} = -[(2D_{\text{AAS}}/3B_{\text{AS}}^3) + (C_{\text{AAS}}^2/3B_{\text{AS}}^4)], \quad (1.3)$$

etc., where $B^{(2)}$ and $C^{(2)}$ are the second and third two-dimensional virial coefficients and \mathcal{A} is the surface area of the adsorbent. Since the gas-surface cluster integrals can be calculated directly from absorption isotherms, these two-dimensional virial coefficients are obtainable from precise experimental measurements at low surface densities.

The advantage of such a treatment is obvious from the form of the integrals involved in (1.2). C_{AAS} pertains to a 'three-body' cluster (two molecules and the surface), and hence its evaluation depends on either assuming pairwise additivity of the potentials or calculating an appropriate three-body interaction term, whereas $B^{(2)}$ pertains only to a two-body cluster and is readily evaluated. Thus the model allows n -body interactions to be treated as virtual $(n-1)$ -body interactions. Moreover, Freeman [16] has shown that the assumption of pairwise additivity for C_{AAS} leads to very appreciable errors. The two-dimensional model has been applied to the systems argon-graphite [13, 14] and xenon-graphite [17], using a Lennard-Jones (12-6) function for the pair potential, and the results have been in good agreement with independent theoretical predictions [18, 19] of the magnitude of the three-body dispersion energy.

Yaris and Sams [20] have recently presented a general quantum treatment of physical adsorption in the Henry's law region of the isotherm, i.e. where only the leading term in the expansion (1.1) need be retained. Since the systems of interest experimentally are necessarily at fairly high temperatures, the quantum deviations are small and may be accounted for simply by replacing the Boltzmann factor in B_{AS} by the Slater sum. In our paper [20] we derived an equation for B_{AS} correct to the fourth power in Planck's constant. The model provided an explanation for the unexpected behaviour observed in the H_2 - D_2 -graphite and CH_4 - CD_4 -graphite systems, and has also been applied to the system Ne-graphite [21]. It should be mentioned that in this last system, significant (~ 2 per cent) quantum deviations were observed at temperatures between 60-90°K, considerably higher than temperatures at which such deviations are observed in the gas phase. In fact, in all three systems the deviations persist to unusually high temperatures.

This enhancement of quantum defects in adsorption systems suggests that it may also be possible to measure quantum effects *between* molecules adsorbed on a surface, and that such effects might also persist to fairly high temperatures. If this were indeed the case, low-coverage adsorption studies using, say, hydrogen and deuterium on a homogeneous surface, might well lead to interesting and significant results on three-body dispersion effects in quantum systems. Classically, three-body terms in similar systems are reasonably large, amounting to ~ 15 -20 per cent of the gas phase interaction energy, and from Yaris' results [19] one predicts that the three-body dispersion energy in the hydrogen-graphite system would also be about 15 per cent. Hence the three-body effect should certainly be measurable, and one might hope that quantization would also be manifest in such systems. To this end, the present paper deals with the high temperature quantum corrections to the second virial coefficient of a two-dimensional Lennard-Jones gas.

2. THEORETICAL DEVELOPMENT

2.1. The equation of state

It is convenient to develop the two-dimensional gas equation of state through the grand potential q :

$$\Theta \mathcal{A} = kTq, \quad (2.1)$$

where \mathcal{A} is the area of the system and Θ the two-dimensional pressure. For a system of N particles with total energy ϵ , the grand potential can be written classically as:

$$\begin{aligned} e^q &= \sum_{N \geq 0} \frac{\exp(N\beta g)}{N!} \int \dots \int \exp(-\beta\epsilon) \prod_{i \geq 1} \frac{d\mathbf{p}_i d\mathbf{x}_i}{h^2} \\ &= \sum_{N \geq 0} \frac{\exp(N\beta g)}{\lambda^{2N} N!} \int \dots \int \exp\left[-\beta \sum_{k < l \leq N} \phi(r_{kl})\right] d\mathbf{x}_1 \dots d\mathbf{x}_{N'}, \end{aligned} \quad (2.2)$$

where $\beta = 1/kT$, g is the partial Gibbs function, ϕ the intermolecular pair potential and λ is given by the equation:

$$\lambda^2 = \beta h^2 / 2\pi\mu, \quad (2.3)$$

where μ is the molecular mass. Using the Mayer-Ursell cluster treatment, one may expand the right side of (2.2) in powers of $N\lambda^2/\mathcal{A}$:

$$\lambda^{-2N} \exp\left[-\beta \sum_{k < l \leq N} \phi(r_{kl})\right] = W_N(\mathbf{x}^N). \quad (2.4)$$

The two-dimensional second virial coefficient is then given in terms of the W_N by:

$$B_{\text{cl}}^{(2)} = -(N\lambda^4/2\mathcal{A}) \int [W_2(\mathbf{x}_1, \mathbf{x}_2) - W_1(\mathbf{x}_1)W_1(\mathbf{x}_2)] d\mathbf{x}_1 d\mathbf{x}_2 \quad (2.5)$$

$$= (N/2) \int_0^\infty (1 - \exp[-\beta\phi(r)]) 2\pi r dr. \quad (2.6)$$

In quantum statistics the situation is quite similar. One now has for the grand potential:

$$e^q = \text{Tr} \exp\left(\sum_i \mathbf{N}_i \beta g_i - \beta \mathcal{H}\right), \quad (2.7)$$

where the number operators \mathbf{N}_i are the Jordan-Klein matrices, \mathcal{H} is the Hamiltonian of the system, and the exponentials are defined by power series. One again introduces functions \mathcal{W}_N :

$$N! \text{Tr} \exp(-\beta \mathcal{H}_N) = \int \mathcal{W}_N d\mathbf{x}_1 \dots d\mathbf{x}_N. \quad (2.8)$$

\mathcal{W}_N is called the Salter sum [23], and is the exact quantum analogue of the Boltzmann factor W_N in classical statistics [3].

The second virial coefficient is still given by (2.5) if W_N is replaced by \mathcal{W}_N [3], but one now finds that potential interactions and quantum effects are mixed. Thus for an ideal gas, B is no longer zero, owing to symmetry effects. One can now write $B^{(2)}$ as [3]:

$$B^{(2)} = B_{\text{per}}^{(2)} + B_{\text{imp}}^{(2)}, \quad (2.9)$$

and evaluate the two parts separately.

For a perfect gas, the Hamiltonian is just the kinetic energy operator :

$$\mathcal{H}_N = \mathcal{T}_N = -(\hbar^2/2\mu) \sum_j \nabla_j^2, \quad (2.10)$$

and the Slater sum is simply :

$$\mathcal{W}_N^0(\mathbf{x}^N) = \lambda^{-2N} \sum_P (\pm 1)^P \exp \left[-(\pi/\lambda^2) \sum_l (\mathbf{x}_l - \mathbf{x}_{Pl})^2 \right]. \quad (\text{Upper sign B.E.}) \quad (2.11)$$

The identity permutation operator causes the argument of the exponent to vanish, so that if symmetry effects are absent, $\mathcal{W}_N^0 = \lambda^{-2N}$, which is the value of W_N when $\phi=0$ (see (2.4)).

For a real gas the complete Hamiltonian must be used and neglecting symmetry effects one finds [1, 3, 25] :

$$\mathcal{W}_N(\mathbf{x}^N) = W_N(\mathbf{x}^N) \left\{ 1 + \lambda^2 \sum_i w_2^{(i)} + \lambda^4 \sum_i w_4^{(i)} + \dots \right\} \quad (2.12)$$

where

$$w_2^{(i)} = -\frac{\beta}{24\pi} \left[\nabla_i^2 \phi - \frac{\beta}{2} (\nabla_i \phi)^2 \right], \quad (2.13)$$

$$w_4^{(i)} = +\frac{\beta}{960\pi^2} \left\{ \nabla_i^4 \phi - \frac{\beta}{6} \left[2\nabla_i^2 (\nabla_i \phi)^2 + 4\nabla_i \phi \cdot \nabla_i^3 \phi + 5(\nabla_i^2 \phi)^2 \right] \right. \\ \left. + \frac{\beta^2}{6} \left[5\nabla_i^2 \phi (\nabla_i \phi)^2 + 3\nabla_i \phi \cdot \nabla_i (\nabla_i \phi)^2 \right] - \frac{5\beta^3}{24} (\nabla_i \phi)^4 \right\}. \quad (2.14)$$

Kirkwood [25] and Uhlenbeck and Beth [1] give recursion formulae, so that higher terms can be written down as well. One should be rather careful about including higher terms, however, since there is no assurance that the series expansion in \hbar will converge, especially at fairly low temperatures [1, 24]. This will be discussed more fully in §3.

When the expansion (2.12) for two particles is substituted into (2.5), one has for the two-dimensional second virial coefficient :

$$B^{(2)} = B_{\text{cl}}^{(2)} + B_{\text{perf}}^{(2)} + B_{\text{I}}^{(2)} + B_{\text{II}}^{(2)} + \dots \quad (2.15)$$

B_{I} and B_{II} are contributions proportional to λ^2 and λ^4 , respectively, and are evaluated in the following section.

2.2. Second virial coefficient

We first derive B_{perf} . From (2.5) and (2.11) we have :

$$B_{\text{perf}}^{(2)} = \mp (N\lambda^4/2\mathcal{A}) \int [\exp(-\beta\mathcal{T}_2) \delta(\mathbf{x}_1 - \mathbf{x}'_2) \delta(\mathbf{x}_2 - \mathbf{x}'_1)]_{\mathbf{x}_1 = \mathbf{x}'_1} d\mathbf{x}_1 d\mathbf{x}_2 \\ = \mp (N/2\mathcal{A}) \int \exp[-(2/\lambda^2)(\mathbf{x}_1 - \mathbf{x}_2)^2] d\mathbf{x}_1 d\mathbf{x}_2, \\ B_{\text{perf}}^{(2)} = \mp N\lambda^2/4. \quad (\text{Upper sign B.E.}) \quad (2.16)$$

The distance over which the molecules influence each other due to symmetry of the wave functions is of the order of λ , which apart from a numerical factor is the thermal de Broglie wavelength of their relative motion.

We now consider the remaining terms in (2.15). From (2.5), (2.6), (2.12), (2.13) and (2.14) we have, where μ is now the reduced mass :

$$B_{\text{cl}}^{(2)} = -\pi N \int_0^\infty [\exp(-\beta\phi) - 1] r dr, \quad (2.17)$$

$$B_{\text{I}}^{(2)} = \pi N \frac{\hbar^2 \beta^2}{12\mu} \int_0^\infty \exp(-\beta\phi) [\nabla^2\phi - (\beta/2)(\nabla\phi)^2] r dr, \quad (2.18)$$

$$B_{\text{II}}^{(2)} = -\pi N \frac{\hbar^4 \beta^3}{240\mu^2} \int_0^\infty \exp(-\beta\phi) \left\{ \nabla^4\phi - \frac{\beta}{6} [2\nabla^2(\nabla\phi)^2 + 4\nabla\phi \cdot \nabla^3\phi + 5(\nabla^2\phi)^2] \right. \\ \left. + \frac{\beta^2}{6} [5\nabla^2\phi(\nabla\phi)^2 + 3\nabla\phi \cdot \nabla(\nabla\phi)^2] - \frac{5\beta^3}{24} (\nabla\phi)^4 \right\} r dr. \quad (2.19)$$

A series of partial integrations leads to:

$$B_{\text{cl}}^{(2)} = -\frac{1}{2}\pi N \beta \int_0^\infty \exp(-\beta\phi) \nabla\phi r^2 dr, \quad (2.20)$$

$$B_{\text{I}}^{(2)} = \pi N \frac{\hbar^2 \beta^2}{24\mu} \int_0^\infty \exp(-\beta\phi) \nabla^2\phi r dr, \quad (2.21)$$

$$B_{\text{II}}^{(2)} = -\pi N \frac{\hbar^4 \beta^3}{240\mu^2} \int_0^\infty \exp(-\beta\phi) \left[\frac{7}{8} \nabla^4\phi r + \frac{2}{3} \nabla^3\phi - \frac{7\beta}{24} (\nabla^2\phi)^2 r \right] dr. \quad (2.22)$$

For the pair potential we use a generalized Lennard-Jones function:

$$\phi = \gamma \epsilon (r^* - m - r^{*-n}), \quad m > n, \quad (2.23)$$

$$r^* = r/\sigma, \quad \gamma = \left(\frac{n}{m-n} \right) \left(\frac{n}{m} \right)^{m/(n-m)},$$

where σ is the collision diameter and ϵ the depth of the potential well. Integration of (2.20)–(2.22) then yields:

$$B_{\text{cl}}^{(2)} = -\pi N \sigma^2 \sum_{\tau \geq 0} \frac{1}{m\tau!} \left(\frac{T^*}{\gamma} \right)^{[\tau(n-m)-2]/m} \Gamma\left(\frac{\tau n - 2}{m} \right) = -\pi N \sigma^2 I_{\text{cl}}^{(2)}, \quad (2.24)$$

$$B_{\text{I}}^{(2)} = \frac{N\lambda^2}{48} \sum_{\tau \geq 0} \frac{n\tau(m-n)}{m\tau!} \left(\frac{T^*}{\gamma} \right)^{\tau(n-m)/m} \Gamma\left(\frac{\tau n}{m} \right) = \frac{N\lambda^2}{48} I_{\text{I}}^{(2)}, \quad (2.25)$$

$$B_{\text{II}}^{(2)} = -\frac{7N\lambda^4}{23040\pi\sigma^2} \sum_{\tau \geq 0} \frac{\tau^2 a + \tau b + c}{m\tau!} \left(\frac{T^*}{\gamma} \right)^{[\tau(n-m)+2]/m} \Gamma\left(\frac{\tau n + 2}{m} \right) \\ = -\frac{7N\lambda^4}{23040\pi\sigma^2} I_{\text{II}}^{(2)}, \quad (2.26)$$

in which

$$T^* = (\beta\epsilon)^{-1}, \quad (2.27)$$

$$a = -n^2(m-n)^2, \quad (2.28)$$

$$b = n\{3[(m+1)(m+2)(m+3) - (n+1)(n+2)(n+3)] \\ + (16/7)[(m+1)(m+2) - (n+1)(n+2)] \\ + [n(n+1)^2 + 4(m+1)(n+1) - (m+4)(m+1)^2]\}, \quad (2.29)$$

$$c = 2(m+1)(m+2)[3(m+3) - (m+1) + (16/7)]. \quad (2.30)$$

3. RESULTS AND DISCUSSION

The integrals $I_{\text{cl}}^{(2)}$, $I_{\text{I}}^{(2)}$ and $I_{\text{II}}^{(2)}$ have been calculated for a Lennard-Jones (12-6) potential at various values of reduced temperature in the region $0.2 < T^* < 40$, and numerical tables are given in the Appendix. Barker and Everett [14] have

published several values of $I_{cl}^{(2)}$ in the range $1.5 < T^* < 8.2$, and our results in this region are in essentially perfect agreement with theirs†.

For the purpose of estimating the actual magnitudes of the quantum correction terms, it is convenient to write (2.15) in reduced form as:

$$B^{(2)\star} = [B_{cl}^{(2)\star} + \Lambda^{*2} B_I^{(2)\star} + \Lambda^{*4} B_{II}^{(2)\star} + \dots] \mp \Lambda^{*2} B_{perf}^{(2)\star}, \quad (3.1)$$

where

$$B^{(2)} = \frac{1}{2} \pi N \sigma^2 B^{(2)\star}, \quad (3.2)$$

$$\Lambda^* = h/\sigma(\mu\epsilon)^{1/2}, \quad (3.3)$$

and where the upper sign refers to B.E. statistics. Then using the tabulations in the Appendix we can calculate the various contributions to $B^{(2)\star}$. Table 1

T^*	B_{cl}^*	B_I^*	B_{II}^*	B_{perf}^*
0.406	-6.237	3.989	-1.719	0.06229
0.510	-3.636	1.703	-0.7445	0.04962
0.827	-1.168	0.3761	-0.1511	0.03062
1.100	-0.4937	0.1745	-0.06511	0.02303
1.410	-0.1165	0.09540	-0.03277	0.01796
1.965	0.2097	0.04538	-0.01384	0.01289
2.786	0.4215	0.02199	-0.025888	0.029094
3.861	0.5445	0.01146	-0.02749	0.026561
6.289	0.6464	0.024723	-0.039269	0.024028
8.403	0.6769	0.02829	-0.034973	0.023014
11.24	0.6926	0.021714	-0.032700	0.022254
14.49	0.6972	0.021115	-0.031597	0.021748
20.41	0.6938	0.026317	-0.047965	0.021241
25.00	0.6877	0.024533	-0.045302	0.021013
31.25	0.6785	0.023157	-0.043404	0.028106
41.67	0.6636	0.021990	-0.041933	0.026079

Note: $0.031190 = 0.0001190$.

Table 1. Contributions to the second virial coefficient of a two-dimensional Lennard-Jones gas.

gives values of $B_{cl}^{(2)\star}$, $B_I^{(2)\star}$, $B_{II}^{(2)\star}$ and $B_{perf}^{(2)\star}$ for selected values of T^* . It is obvious from the table that at high temperatures $B_{cl}^{(2)\star}$ and $B^{(2)\star}$ do converge, as they should. It is also clear however, that at any given temperature the convergence of the Slater sum correction terms is relatively slow. A comparison of table 1 with the results given in Hirschfelder *et al.* [3] for three-dimensional gases reveals that the B_I^* are smaller for the two-dimensional gas, whereas the B_{II}^* are larger. Hence the expansion in powers of h is less rapidly convergent in the two-dimensional case and probably should not be used below $T^* \sim 5$. Below the Boyle temperature in fact, the expansion is apparently divergent.

Another point which we note in connection with table 1 is the enhanced effect of the symmetry of the wave functions, as reflected in the term $B_{perf}^{(2)\star}$. At high

† Our previously published [13] tabulation of $I_{cl}^{(2)}$ values was incorrect, owing to an error in the computer programme, and we are indebted to Professor D. H. Everett for bringing this to our attention. None of our conclusions are affected by this error, but a discussion of detailed changes *inter alia* is to be published.

temperatures ($T^* \gtrsim 10$) this term is larger even than $B_1^{(2)*}$, a situation which does not occur in the three-dimensional case. The perfect gas term seems the one which is most affected by the dimensionality of the problem and for all meaningful values of the temperature it is never really negligible relative to the other correction terms in the two-dimensional case.

To obtain values of $B^{(2)*}$, one must calculate the quantum mechanical parameter Λ^* , which requires a knowledge of the intermolecular potential parameters ϵ and σ . The usual procedure is to estimate ϵ and σ by fitting virial coefficients data to B_{cl} , and thence by a series of successive approximations to arrive at final best-fit values of Λ^* , ϵ and σ . Owing to the absence of suitable experimental data in the present case, however, we must estimate Λ^* in a different way. We could, of course, merely use three-dimensional potential parameters, but both experimentally [13, 14, 17] and theoretically [18, 19] it has been found (classically at least) that $\epsilon^{(2)} < \epsilon^{(3)}$ always, and a procedure which we feel to be somewhat more reasonable is the following.

From an equation due to Yaris [19] we can calculate the approximate magnitude of the three-body (admolecule-admolecule-surface) dispersion energy, and from this and $\epsilon^{(3)}$ obtain a value for $\epsilon^{(2)}$. Thus, according to Yaris [19], the three-body energy is

$$E_3 = \frac{1.5\epsilon_{gs}\alpha_g}{4r^3} \frac{2\chi_g/\alpha_g + \chi_s/\alpha_s}{\chi_g/\alpha_g + \chi_s/\alpha_s}, \quad (3.4)$$

where ϵ_{gs} is the gas-solid interaction energy as determined from Henry's law adsorption data using a virial treatment† [26], α the polarizability, χ the diamagnetic susceptibility and r the distance to the potential minimum ($r = 2^{1/6}\sigma^{(3)}$). Then $\epsilon^{(2)}$ is simply given by:

$$\epsilon^{(2)} = \epsilon^{(3)} - E_3. \quad (3.5)$$

Yaris and Sams [20] have published quantum-corrected Lennard-Jones (12-3) values of ϵ_{gs} for H_2 , D_2 , CH_4 and CD_4 on graphite, and we have used these to compute E_3 for these systems, and hence $\epsilon^{(2)}$. Polarizabilities and susceptibilities are those given by Yaris and Sams [20] and we have used the $\epsilon^{(3)}$ and $\sigma^{(3)}$ values of Hirschfelder *et al.* [3]. If it is assumed that three-body effects will influence the attractive part of the potential only, and leave the repulsive part unaltered, then for a (12-6) potential one can calculate $\sigma^{(2)}$ from the equation [14]:

$$\sigma^{(2)} = \sigma^{(3)} [\epsilon^{(3)}/\epsilon^{(2)}]^{1/12}. \quad (3.6)$$

The values of $\epsilon^{(2)}$ and $\sigma^{(2)}$ determined thusly are given in table 2, along with the

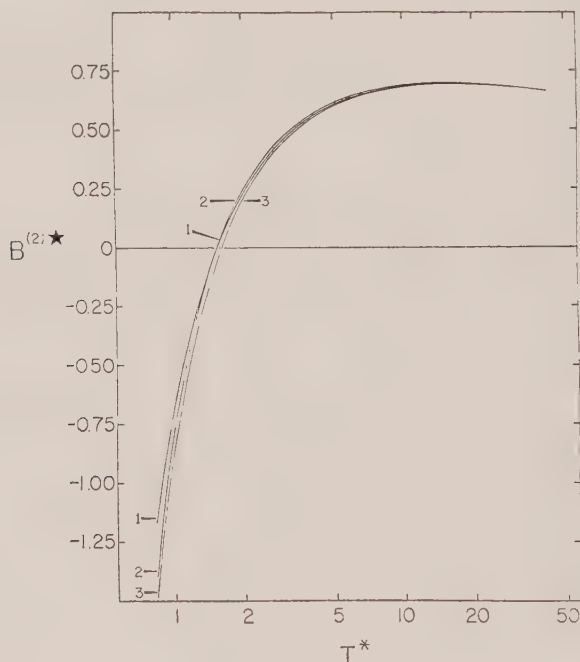
Molecule	$\epsilon^{(2)}/k(^{\circ}K)$	$\sigma^{(2)}(\text{\AA})$	Λ^*
H_2	31.47	2.968	1.851
D_2	31.63	2.967	1.306
CH_4	127.1	3.866	0.251
CD_4	127.9	3.864	0.224

Table 2. Estimated two-dimensional potential parameters and quantum parameters for several gases on graphite.

† This quantity may also be obtained from the isosteric heat of adsorption, q_{st} , at zero coverage, since $q_{st} = \epsilon_{gs} + \frac{1}{2}RT$, where T is taken as the middle of the temperature range of the experiments.

Λ^* values which can then be estimated for these gases on graphite. The new quantum mechanical parameters are not much different from those based on three-dimensional potential parameters [3], as the decrease in ϵ is largely offset by the concomitant increase in σ , but since Λ^* enters to the second and fourth powers in (3.1), these differences will be somewhat magnified. Note that $\epsilon^{(2)}$ and $\sigma^{(2)}$ are slightly different for isotopes of the same gas, owing to a difference in ϵ_{gs} . Actually the $\epsilon^{(3)}$ values should also exhibit small differences [27, 28].

Having now estimated the quantum parameter Λ^* , we may proceed to calculate the appropriate curves of $B^{(2)*}$ versus T^* . Such a graph for hydrogen is presented in the figure. So as to illustrate the various contributions, the figure contains three curves: (1) the classical curve $B_{cl}^{(2)*}$; (2) the quantum curve assuming Boltzmann statistics (only the first three terms in (3.1)); (3) the quantum curve assuming Bose-Einstein statistics (the full (3.1) with upper sign).



Reduced two-dimensional second virial coefficient $B^{(2)}$ of hydrogen on graphite, assuming a Lennard-Jones (12-6) pair potential. Curve 1 is the classical contribution. 2 is the quantum curve neglecting effects of symmetry on the wave functions (Boltzmann statistics), and only includes the terms of the Slater sum to order \hbar^4 . 3 is the full quantum corrected curve in Bose-Einstein statistics.

It is clear that the situation represented in the figure is not very like that for a three-dimensional gas. Above the Boyle point, the Boltzmann quantum curve lies above the classical curve and converges to the classical limit at high temperatures. This is the same as the situation with a three-dimensional gas, but here the similarity apparently ends. In the region of the Boyle point the two curves cross, indicating that the expansion in powers of \hbar is no longer convergent below this temperature, and the treatment presented here breaks down. Even in the

temperature region where the Slater sum appears to converge the discrepancies between the classical and quantum Boltzmann curves are smaller than in the corresponding T^* range for the three-dimensional case, amounting to no more than 4 per cent. We also note, in contrast to the three-dimensional case, that the Bose-Einstein curve always lies below the classical curve. This of course owes to the relatively large magnitude of the $B_{\text{perf}}^{(2)\star}$ term which enters with negative sign. It is clear that one cannot alter the relative positions of the classical and Bose-Einstein curves by altering the intermolecular potential parameters, as $B_1^{(2)\star}$ and $B_{\text{perf}}^{(2)\star}$ enter with the same coefficient. For all meaningful values of Λ^* , then, the situation exhibited in the figure will persist.

The results presented here raise several questions. Firstly, the temperature range of validity of the Slater sum expansion appears to be considerably smaller for a two-dimensional gas than for a three-dimensional one. Note that (2.12) is effectively a development in powers of the operator ∇ . Its validity consequently requires that the differential quotients of ϕ are small compared to ϕ and that the higher orders become successively smaller. This is the case over a much narrower temperature range in two dimensions than in three, and it may be that in one dimension there will be an even narrower region in which such an expansion is applicable. De Witt [29] has discussed the breakdown of this type of expansion in the three-dimensional case.

Secondly, the temperature at which the classical and quantum Boltzmann curves intersect is very close to the Boyle point. This point of intersection is, of course, the absolute lower limit of convergence of the expansion (2.12). Does this have some real significance, or is it merely fortuitous that the crossover occurs at this temperature? We feel that it probably *is* fortuitous, but this point would appear to warrant further study.

Thirdly, the perfect gas term is relatively much more important in two dimensions and in fact is the largest in absolute magnitude of all the correction terms at temperatures above $T^* \sim 10$. The contribution of this term should be even more greatly enhanced in the one-dimensional case, and it would probably dominate the Slater sum terms to considerably lower temperatures.

In connection with the above points it would appear that some further insight into these problems could be gained from a similar treatment of one-dimensional gases. This should provide more information on the limits of convergence of the Slater sum in such cases, and on the importance of the perfect gas correction. We are now at work on this problem.

Finally, we note that the predicted quantum defects are quite small at temperatures where the present treatment is valid, and there is some doubt that these defects could be detected experimentally. The principal experimental difficulty is that in order to obtain second two-dimensional virial coefficients, one must measure both second and third gas-surface virial coefficients. Clearly, the most sensitive region in which to fit data to the theoretical curves is $1 \leq T^* \leq 3$, but the treatment presented here appears to break down in just this region. A rather different treatment, perhaps along the lines used by Mohling [30] for helium at high temperatures, may well be required.

I am indebted to Mr. R. Wolfe for assistance with the numerical computations, and to Dr. A. Bear for helpful discussions.

APPENDIX

We present here numerical tabulations of the integrals $I_{\text{cl}}^{(2)}$, $I_{\text{I}}^{(2)}$ and $I_{\text{II}}^{(2)}$ of (2.24)–(2.26) for selected values of $\epsilon^{(2)}/kT$, assuming a Lennard-Jones (12–6) function for the intermolecular pair potential.

ϵ/kT	$I_{\text{cl}}^{(2)}$	$I_{\text{I}}^{(2)} \times 10^{-1}$	$I_{\text{II}}^{(2)} \times 10^{-4}$
0.024	0.331780	0.198019	1.09394
0.028	0.335969	0.217240	1.08771
0.032	0.339251	0.235656	1.08379
0.036	0.341833	0.253428	1.08154
0.040	0.343858	0.270675	1.08055
0.049	0.346877	0.307935	1.08168
0.059	0.348419	0.347629	1.08627
0.069	0.348619	0.385995	1.09339
0.079	0.347831	0.423415	1.10183
0.089	0.346285	0.460109	1.11158
0.099	0.344136	0.496357	1.12213
0.119	0.338445	0.567888	1.14504
0.139	0.331345	0.638765	1.16967
0.159	0.323186	0.709516	1.19550
0.209	0.299444	0.888164	1.26400
0.259	0.272267	1.05684	1.33606
0.309	0.242544	1.26296	1.41133
0.359	0.210736	1.46304	1.48959
0.409	0.177099	1.67344	1.57080
0.509	0.104863	2.12977	1.74235
0.609	0.026383	2.64057	1.92683
0.709	−0.058263	3.21431	2.12532
0.809	−0.149232	3.85981	2.33902
0.909	−0.246825	4.58666	2.56916
1.009	−0.351443	5.40535	2.81703
1.109	−0.463568	6.32746	3.08397
1.209	−0.583756	7.43117	3.37135
1.959	−1.81795	20.7636	6.32556
2.459	−3.11827	38.7513	9.26821

REFERENCES

- [1] UHLENBECK, G. E., and BETH, E., 1936, *Physica*, **3**, 729.
- [2] DE BOER, J., and MICHELS, A., 1938, *Physica*, **5**, 945.
- [3] HIRSCHFELDER, J. O., CURTISS, C. F., and BIRD, R. B., 1954, *Molecular Theory of Gases and Liquids* (John Wiley & Sons), Ch. 6.
- [4] METROPOLIS, N., ROSENBLUTH, A., ROSENBLUTH, M., TELLER, A., and TELLER, E., 1950, *J. chem. Phys.*, **21**, 1087.
- [5] WOOD, W. W., and JACOBSON, J. D., 1957, *J. chem. Phys.*, **27**, 1207.
- [6] ALDER, B. J., and WAINWRIGHT, T. E., 1957, *J. chem. Phys.*, **27**, 1208.
- [7] HELFAND, E., FRISCH, H. L., and LEBOWITZ, J. L., 1961, *J. chem. Phys.*, **34**, 1037.
- [8] PRAGER, S., 1962, *Advance chem. Phys.*, **4**, 201.
- [9] REE, F. H., and HOOVER, W. G., 1964, *J. chem. Phys.*, **40**, 939.
- [10] EVERETT, D. H., 1960, *Soc. chem. ind. Monographs*, **14**, 98.
- [11] HILL, T. L., and GREENSCHLAG, S., 1961, *J. chem. Phys.*, **34**, 1538.
- [12] STEELE, W. A., and ROSS, M., 1960, *J. chem. Phys.*, **33**, 464.
- [13] SAMS, J. R., CONSTABARIS, G., and HALSEY, G. D., 1962, *J. chem. Phys.*, **36**, 1334.

- [14] BARKER, J. A., and EVERETT, D. H., 1962, *Trans. Faraday Soc.*, **58**, 1608.
- [15] STEELE, W. A., and HALSEY, G. D., 1954, *J. chem. Phys.*, **22**, 979.
- [16] FREEMAN, M. P., 1958, *J. phys. Chem.*, **62**, 729.
- [17] SAMS, J. R., 1962, *J. chem. Phys.*, **37**, 1883.
- [18] SINANOGLU, O., and PITZER, K. S., 1960, *J. chem. Phys.*, **32**, 1279.
- [19] YARIS, R., 1962, Thesis, University of Washington.
- [20] YARIS, R., and SAMS, J. R., 1962, *J. chem. Phys.*, **37**, 571.
- [21] SAMS, J. R., and YARIS, R., 1963, *J. phys. Chem.*, **67**, 1931.
- [22] HILLS, T. L., 1956, *Statistical Mechanics* (McGraw-Hill), Ch. 5.
- [23] SLATER, J. C., 1931, *Phys. Rev.*, **38**, 237.
- [24] TER HAAR, D., 1954, *Elements of Statistical Mechanics* (Rinehart), p. 184.
- [25] KIRKWOOD, J. G., 1933, *Phys. Rev.*, **44**, 31.
- [26] SAMS, J. R., CONSTABARIS, G., and HALSEY, G. D., 1960, *J. phys. Chem.*, **64**, 1689.
- [27] KNAAP, H. F. P., and BEENAKKER, J. J. M., 1961, *Physica*, **27**, 523.
- [28] MICHELS, A., DE GRAAFF, W., and TEN SELDAM, C. A., 1960, *Physica*, **26**, 393.
- [29] DE WITT, H. E., 1962, *J. math. Phys.*, **3**, 1003.
- [30] MOHLING, F., 1963, *Phys. Fluids*, **6**, 1097.

The electronic structure of ionized molecules

III. Field ionization

by J. C. LORQUET†

Institut de Chimie de l'Université de Liège, quai F. Roosevelt, Liège, Belgique

and G. G. HALL

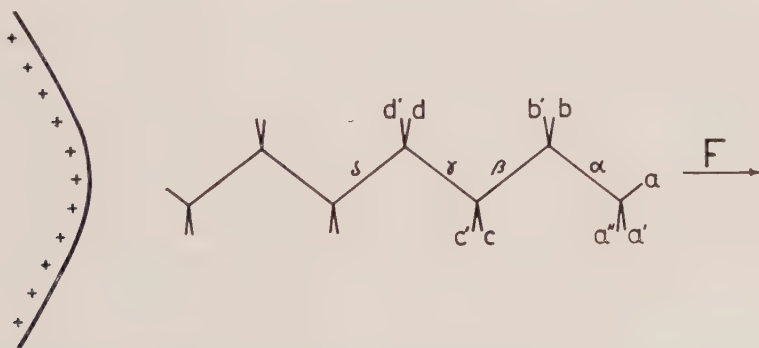
Department of Mathematics, University of Nottingham

(Received 4 August 1964)

The net positive charge distribution of n -alkane ions has been calculated in the presence of an electric field of the order of 1 v/\AA by the equivalent orbital method. The calculations explain satisfactorily the dissociation processes observed in the field ionization mass spectra.

Molecules adsorbed on a metallic surface may be ionized by the action of a high electric field, of the order of 10^7 – 10^8 v/cm . This process is called field ionization, and its mechanism has been adequately explained [1]. The molecular ions which are desorbed from the surface may be dissociated by the electric field at a distance of several angstroms from the tip of the positive electrode. This dissociation is a pure gas phase process and not the result of a surface reaction at the tip. If the ions so produced are analysed in a mass spectrometer, a relative abundance pattern is obtained which is called the field ionization mass spectrum of the molecule considered.

Beckey [2] has formulated a number of rules which rationalize the dissociation mechanisms characteristic of this phenomenon, and has justified them by approximate semi-classical considerations where the charge distribution of the ion in the



Schematic representation of a linear paraffin adsorbed on a field-ionization tip.

† Chercheur Qualifié du Fonds National Belge de la Recherche Scientifique.

presence of the electric field appears as the most important factor. It is the purpose of this paper to calculate this charge distribution for *n*-alkane ions using the methods of Part II [3].

Let us consider a *n*-paraffin molecule in the neighbourhood of the tip of the positive electrode. We shall assume that its long axis is oriented along the direction of the field, as shown in the figure. The validity of this assumption has been discussed in detail by Beckey [2]. A small orientation effect, due to the anisotropy of polarizability along the long and short molecular axis, already exists for the neutral molecule. This tendency will be much larger after ionization has taken place. Furthermore, only those ions which are oriented along the field will undergo dissociation and will be recorded in the mass spectrum as fragmentary ions.

The Hamiltonian of this system will contain an electrostatic potential term whose value will vary linearly with the distance from the effective centre of the tip. The matrix elements e_{mn}' of the equivalent orbitals associated with each CC and CH bond then take the form:

$$\begin{aligned} e_{mn}' &= \langle \chi_m | H^{\text{scf}} - eFz | \chi_n \rangle \\ &= \langle \chi_m | H^{\text{scf}} | \chi_n \rangle - eF \langle \chi_m | z | \chi_n \rangle \\ &\simeq e_{mn} - eF\bar{z} \langle \chi_m | \chi_n \rangle, \end{aligned}$$

where H^{scf} is the self-consistent Hamiltonian of the molecule in the absence of the electric field, χ_m and χ_n are the EO's associated to bonds *m* and *n*, e_{mn} are the matrix elements of H^{scf} considered in Part II, *F* is the field strength and *e* the electronic charge, \bar{z} is the distance between the effective centre of the tip and the centroid of a particular EO.

Since the EO's form an orthonormal basis, one thus sees that, to a first approximation, the off-diagonal elements e_{mn}' are equal to the e_{mn} , whereas the diagonal elements e_{mm}' differ from the e_{mm} by the term $-eF\bar{z}$. As the addition of a constant term to the diagonal elements of a matrix has no effect on its eigenvectors, the exact value of \bar{z} has not to be specified. One may use instead the differences $\Delta\bar{z}$ between the coordinates of the EO's centroids along the direction of the field.

Calculations were made for all *n*-paraffins from propane to *n*-octane, for two values of *F*: 0.3 and 1.0 v/Å. The results are given in the table. The designation of the bonds is shown in the figure. It may be seen that, for an electric field of 0.3 v/Å, the largest fraction of the positive charge lies on the CC β bond, in agreement with Beckey's predictions. Accordingly, a very large amount of C_2H_5^+ ions is found in the field ionization mass spectrum, for a field strength of this order of magnitude [4]. The dissociation of the β bond is probably favoured by another effect, also discussed by Beckey. During the extension of the β bond, the large amount of charge concentrated on the α and CH_n bonds is displaced in the direction of the field; as a result, the dissociation energy of the β bond is lowered. Beckey expresses this by the following statement: "Field dissociation of a specific bond in a molecular ion only occurs if the positive charge is on the tip-distant side of this bond".

At higher field strengths (1 v/Å), however, the α bond becomes much weaker than the β bond. The relative abundance of the CH_3^+ ions is thus expected to increase, and eventually to overcome that of the C_2H_5^+ ions, in agreement with the experimental observations.

	0 v/Å	0.3 v/Å	1.0 v/Å
<i>n</i> -propane			
CC α	0.33	0.45	0.43
CC β	0.33	0.18	0.06
CH $_a$	0.06	0.10	0.31
CH $_{a'}$	0.06	0.08	0.04
CH $_b$	0	0.02	0.05
CH $_c$	0.06	0.03	0.01
<i>n</i> -butane			
CC α	0.18	0.32	0.44
CC β	0.43	0.35	0.11
CC γ	0.18	0.08	0.01
CH $_a$	0.02	0.06	0.28
CH $_{a'}$	0.02	0.05	0.05
CH $_b$	0.02	0	0.03
CH $_c$	0.02	0.03	0.01
<i>n</i> -pentane			
CC α	0.10	0.26	0.44
CC β	0.32	0.36	0.11
CC γ	0.32	0.16	0.02
CC δ	0.10	0.03	0
CH $_a$	0.01	0.05	0.27
CH $_{a'}$	0.01	0.04	0.05
CH $_b$	0.02	0	0.03
CH $_c$	0	0.01	0.01
<i>n</i> -hexane			
CC α	0.06	0.24	0.44
CC β	0.23	0.35	0.11
CC γ	0.31	0.18	0.02
CC δ	0.23	0.06	0
CH $_a$	0.01	0.05	0.27
CH $_{a'}$	0.01	0.04	0.05
CH $_b$	0.01	0	0.03
CH $_c$	0	0.01	0.01
<i>n</i> -heptane			
CC α	0.04	0.23	0.44
CC β	0.16	0.34	0.11
CC γ	0.26	0.19	0.02
CC δ	0.26	0.07	0
CH $_a$	0	0.04	0.27
CH $_{a'}$	0	0.04	0.05
CH $_b$	0.01	0	0.03
CH $_c$	0	0.01	0.01
<i>n</i> -octane			
CC α	0.03	0.23	0.44
CC β	0.12	0.34	0.11
CC γ	0.21	0.19	0.02
CC δ	0.24	0.07	0
CH $_a$	0	0.04	0.27
CH $_{a'}$	0	0.04	0.05
CH $_b$	0.01	0	0.03
CH $_c$	0	0.01	0.01

Positive charge distribution of *n*-paraffin ions as a function of the field strength. Bond designation as indicated in the figure.

REFERENCES

- [1] GOMER, R., 1961, *Field Emission and Field Ionization* (Harvard University Press).
- [2] BECKEY, H. D., 1964, *Z. Naturf. A*, **19**, 71; 1964, *Bull. Soc. chim. Belg.*, **73**, 326; 1965, *Advances in Mass Spectrometry*, Vol. III (to be published).
- [3] LORQUET, J. C., 1965, *Mol. Phys.* (to be published in the next issue).
- [4] BECKEY, H. D., 1962, *Z. Naturf. A*, **17**, 1103.

On the tetragonal distortion of octahedral systems in an E_g electronic state

by M. H. L. PRYCE†, K. P. SINHA‡ and Y. TANABE§

H. H. Wills Physics Laboratory, University of Bristol

(Received 19 June 1964)

The tetragonal distortion of octahedral (ML_6) systems having two-fold orbital degeneracy is discussed on a model which takes into account covalency and the essential features of the Jahn–Teller effects. Theoretically both elongation and compression along the tetragonal axis are possible, depending on the sign of the coefficients involved in the first and the second-order terms. Covalency effects seem to influence this fact.

A qualitative discussion of these results is presented.

1. INTRODUCTION

The tetragonal distortion from cubic symmetry occurring in certain compounds has been treated on the basis of spatial ordering of distorted elementary octahedra [1, 2, 18]. The origin of distortion is to be related to the behaviour of some transition metal ions (e.g. Cu(II) or Mn(III)) located at the centre of each octahedron. While the explanation based on the ability of such cations to form the appropriate hybrid orbitals for covalent bonding with the overlapping anion orbitals [3] may not seem to be of general application, the approach which invokes crystal field effects and Jahn–Teller distortions of ligands presents scope for a wider generalization [4–6].

Recently, Liehr and Ballhausen [7] have attempted an extension of the treatment given by Van Vleck [8] and Öpik and Pryce [4] of the Jahn–Teller effect in inorganic complexes having E_g electronic states, by including additional quadratic terms. This amounts to introducing a new phenomenological constant, the sign of which is arbitrarily fixed to have agreement with the observed result. Furthermore, the calculations are carried out on the basis of an electrostatic model and no account is taken of the covalency between the central ion and the ligands. Since covalency of this kind does occur in such systems to a greater or lesser extent [9, 10] it is desirable to consider a model in which an account of this effect is included.

In what follows, we give a formal analysis of the energy states of octahedral systems in E_g electronic states following a molecular orbital approach which takes into account the essential features of the Jahn–Teller effects. The first and second order terms in this scheme include covalency effects which seem to have important bearing on the nature of tetragonal distortion, i.e. elongation or compression along the tetragonal axis.

† Present address: Department of Physics, University of Southern California.

‡ Present address: Chemical Physics Division, National Chemical Laboratory, Poona, India.

§ Present address: Department of Applied Physics, Faculty of Engineering, Tokyo University, Tokyo, Japan.

2. THEORETICAL MODEL

We consider an elementary octahedron with six ligands each situated at a corner and a transition metal ion having d^4 or d^9 electronic configuration at the centre. The positions and the displacements of ligands will be described in terms of normal coordinates which transform according to irreducible representations of the relevant symmetry group (O_h for the undistorted octahedron). The definitions and notations used here are the same as that of Öpik and Pryce [4] and Van Vleck [8]. We shall enumerate only those symmetry coordinates which are of physical interest for the problem. These are:

$$\left. \begin{aligned} Q_1(A_{1g}) &= [X_1 - X_4 + Y_2 - Y_5 + Z_3 - Z_6]/\sqrt{6}, \\ Q_2(E_g) &= [X_1 - X_4 - Y_2 + Y_5]/2, \\ Q_3(E_g) &= [2(Z_3 - Z_6) - (X_1 - X_4 + Y_2 - Y_5)]/2\sqrt{3}, \end{aligned} \right\} \quad (1)$$

where X_i , Y_i , Z_i represent the x , y , z components, respectively, of the displacement of the i th ligand. It will be useful to express the displacements of the ligands, whose regular octahedral positions are defined by $(\pm R_0, 0, 0)$, $(0, \pm R_0, 0)$ and $(0, 0, \pm R_0)$, in terms of normal coordinates given by (1). Thus:

$$\left. \begin{aligned} X_1 &= -X_4 = Q_1/\sqrt{6} + Q_2/2 - Q_3/2\sqrt{3}, \\ Y_2 &= -Y_5 = Q_1/\sqrt{6} - Q_2/2 - Q_3/2\sqrt{3}, \\ Z_3 &= -Z_6 = Q_1/\sqrt{6} + Q_3/\sqrt{3}. \end{aligned} \right\} \quad (2)$$

We assume all other normal coordinates to be zero.

In constructing the molecular orbitals for the system ML_6 by the MO, LCAO method we shall classify the orbitals into core and valence orbitals. Thus the orbitals on the metal ion important for mixing with those of the ligand ones are nd , $(n+1)s$, and $(n+1)p$. At this stage it may be useful to separate the behaviour of these sets of orbitals on the line suggested by Jørgensen [11]. For the present purpose, the effect of the 'central field' covalency arising out of the mixing of s and p orbitals of the central ion with the appropriate σ -bonding orbitals of the ligands will be considered to be relatively small. We shall therefore confine our attention to the study of symmetry restricted covalency which involves the mixing of partly filled d orbitals with the appropriate orbitals of the ligands. Among these, the admixture of $d\epsilon$ orbitals (i.e. d_{xy} , d_{yz} , d_{zx}) with the π -bonding orbitals of the ligands is expected to be much smaller and they may be regarded to be virtually in a non-bonding state.

Thus the most important contribution to covalency effects would seem to arise from the mixing of $d\gamma$ ($d_{3z^2-r^2}$, $d_{x^2-y^2}$) orbitals with the appropriate σ -orbitals of the ligands.

As typical examples of ligands we shall consider O^{2-} or F^- with $2p^6$ outer electronic configurations. Thus the appropriate linear combination of ligand orbitals will be constructed from the individual p_σ orbitals.

The explicit forms of the valence orbitals under consideration are taken as follows:

For the central metal ion;

$$\phi_a = R(r)Y_{20}(\theta\varphi), \quad (3a)$$

$$\phi_b = R(r)\{Y_{22}(\theta\varphi) + Y_{2-2}(\theta\varphi)\}/\sqrt{2}. \quad (3b)$$

The appropriate molecular orbitals constructed from the ligand orbitals are:

$$\chi_a(Q_{1s}) = (2[z] - [x] - [y])/2\sqrt{3}, \quad (4a)$$

$$\chi_b(Q_{1s}) = ([x] - [y])/2, \quad (4b)$$

where

$$[x] = (p_{\sigma_1}(X_1) - p_{\sigma_4}(X_4)), \text{ etc.}$$

It would be useful to note the transformation properties of the orbitals and the normal coordinates involved under symmetries of interest:

Q_3	a	X_a	$3z^2 - r^2$	$\left. \begin{array}{l} \\ \end{array} \right\}$	O_h	D_{4h}	D_{2h}
Q_2	b	X_b	$x^2 - y^2$		E_g	A_{1g}	A_{1g}
						B_{1g}	A_{1g}

With the simple model described above, we shall now proceed to develop a formalism suitable for the study of tetragonal distortions of the octahedral system (ML_6) having an electron in an E_g electronic state.

3. FORMULATION AND THE SOLUTION OF ENERGY MATRIX

We consider the Hamiltonian (in atomic units) as:

$$H = -\frac{1}{2} \sum \nabla_j^2 + V(\mathbf{r}, \hat{R}_n), \quad (5)$$

where the second term represents the total coulomb energy of electrons and nuclei. The potential V can be further decomposed into:

$$V_0(r) + \sum_{i=1}^6 V_i(|\mathbf{r} - \hat{R}_i|),$$

where V_0 has cubic symmetry and V_i has spherical symmetry about the i th nucleus. We have to start with a 4×4 secular matrix involving the orbitals ϕ_a , χ_a , ϕ_b and χ_b . Since we are interested in tetragonal distortion only we employ the following decomposition of this matrix by assuming $Q_2 = 0$, in the first instance. We construct the two 2×2 matrices given below to be diagonalized separately.

$$\begin{array}{c|cc} & \phi_a & \chi_a \\ \hline \phi_a & A_a - E & C_a - S_a E \\ \chi_a & & B_a - E \end{array} \quad (6a)$$

and

$$\begin{array}{c|cc} & \phi_b & \chi_b \\ \hline \phi_b & A_b - E & C_b - S_b E \\ \chi_b & & B_b - E \end{array} \quad (6b)$$

where $S_a = \langle \phi_a | \chi_a \rangle$ and $S_b = \langle \phi_b | \chi_b \rangle$.

The effect of Q_2 in the first and second-order terms in the development of the energy matrix will be included later.

Within this approximation we define the anti-bonding molecular orbitals ψ_a and ψ_b as follows:

$$\psi_a(Q_1 Q_2 Q_3) = \psi_a(Q_1 0 Q_3) + \dots, \quad (7a)$$

$$\psi_b(Q_1 Q_2 Q_3) = \psi_b(Q_1 0 Q_3) + \dots, \quad (7b)$$

Similarly, the Hamiltonian is taken as:

$$H(Q_1 Q_2 Q_3) = H(Q_1 0 Q_3) + \dots$$

Now, we have to consider the solutions of the 2×2 secular determinant:

$$\begin{vmatrix} \langle \psi_a | H | \psi_a \rangle - E & \langle \psi_a | H | \psi_b \rangle - E \langle \psi_a | \psi_b \rangle \\ \langle \psi_a | H | \psi_b \rangle - E \langle \psi_a | \psi_b \rangle & \langle \psi_b | H | \psi_b \rangle - E \end{vmatrix} = 0. \quad (8)$$

The two solutions within the approximation $Q_2 = 0$ can be defined as $E_a(Q_1 0 Q_3)$ and $E_b(Q_1 0 Q_3)$. These must be equal to:

$$E_a(Q_1 0 Q_3) = \langle \psi_a(Q_1 0 Q_3) | H(Q_1 0 Q_3) | \psi_a(Q_1 0 Q_3) \rangle \quad (9a)$$

and

$$E_b(Q_1 0 Q_3) = \langle \psi_b(Q_1 0 Q_3) | H(Q_1 0 Q_3) | \psi_b(Q_1 0 Q_3) \rangle. \quad (9b)$$

In order to find explicit forms of the solutions, we consider the following forms of anti-bonding and bonding orbitals which diagonalize the matrices (6a) and (6b):

$$\psi_a(Q_1 0 Q_3) = \{\cos \alpha_a \phi_a - \cos(\sigma_a + \alpha_a) \chi_a\} / \sin \sigma_a \quad (\text{anti-bonding}), \quad (10a)$$

$$\chi_a'(Q_1 0 Q_3) = \{\sin(\sigma_a + \alpha_a) \phi_a - \sin \alpha_a \phi_a\} / \sin \sigma_a \quad (\text{bonding}). \quad (10b)$$

Similarly:

$$\psi_b(Q_1 0 Q_3) = \{\cos \alpha_b \phi_b - \cos(\sigma_b + \alpha_b) \chi_b\} / \sin \sigma_b \quad (\text{anti-bonding}) \quad (11a)$$

and

$$\chi_b'(Q_1 0 Q_3) = \{\sin(\sigma_b + \alpha_b) \chi_b - \sin \alpha_b \phi_b\} / \sin \sigma_b \quad (\text{bonding}), \quad (11b)$$

where

$$\cos \sigma_a = S_a = \langle \phi_a | \chi_a \rangle \quad \text{and} \quad \cos \sigma_b = S_b = \langle \phi_b | \chi_b \rangle. \quad (12)$$

The coefficients involved in (10) and (11) can be determined from the relations given below; we write the relations in a general form without the suffixes a or b .

We have

$$\tan 2(\sigma + \alpha) = \frac{2(C - AS) \sin \sigma}{A - B + 2S(C - AS)} \quad (13)$$

and

$$\tan 2\alpha = \frac{2(C - BS) \sin \sigma}{A - B - 2S(C - BS)}. \quad (14)$$

Also:

$$\frac{(C - BS)}{\sin 2\alpha} + \frac{(C - AS)}{\sin 2(\alpha + \sigma)} = 0. \quad (15)$$

The diagonalization procedure for (6a) or (6b) finally gives:

$$\langle \chi | H | \psi \rangle = \{A + B - 2CS + \sqrt{[(A - B)^2 + 4(C - AS)(C - BS)]} / 2 \sin^2 \sigma. \quad (16)$$

It would be useful to write (16) in a form which separates the terms arising due to covalency from those which follow from an electrostatic model. Making use of relations (12) to (15) we get:

$$E(Q_1 0 Q_3) = \langle \psi | H | \psi \rangle = A - \{(C - AS) \cot(\alpha + \sigma) / \sin \sigma\}, \quad (17)$$

where the term in curly brackets represents the covalent part.

In order to derive suitable expressions for the derivatives

$$\partial E / \partial Q_i \quad \text{and} \quad \partial^2 E / \partial Q_i \partial Q_j, \text{ etc.}$$

involved in the expansion of the energy matrix with respect to normal coordinates, we introduce the following notations:

$$\psi = p\phi - q\chi, \quad (18)$$

where

$$\left. \begin{aligned} & \text{with relations} \\ & \text{and the normalization condition:} \end{aligned} \right\} \begin{aligned} & p = \cos \alpha / \sin \sigma; \quad q = \cos (\sigma + \alpha) / \sin \sigma \\ & p - qS = \sin (\sigma + \alpha) \quad pS - q = \sin \alpha \\ & p^2 + q^2 - 2pqS = 1. \end{aligned} \quad (19)$$

Thus (17) can be written as:

$$E = A - (C - AS)q / (p - qS). \quad (17')$$

It can also be written

$$E = A - 2(C - AS)pq + (B - A)q^2. \quad (17'')$$

We consider the case where all the algebraic entities E , A , C , S , q and p are functions of the normal coordinates. Let $[]_{Q_i}$ and $[]_{Q_i Q_j}$ stand for $\partial [] / \partial Q_i$ and $\partial^2 [] / \partial Q_i \partial Q_j$ respectively. Then after some complicated algebra involving relations given in (19), (17' and 17'') and their derivatives we get the following useful relations:

$$E_{Q_i} = A_{Q_i} - 2\{(C - AS)_{Q_i} + (A - E)S_{Q_i}\}pq - (A - B)_{Q_i}q^2 \quad (20)$$

and

$$\begin{aligned} E_{Q_i Q_j} = & A_{Q_i Q_j} - 2\{(C - AS)_{Q_i Q_j} + (A - E)S_{Q_i Q_j} + (A - E)_{Q_i}S_{Q_j} + (A - E)_{Q_j}S_{Q_i}\}pq \\ & - (A - B)_{Q_i Q_j}q^2 \\ & - \frac{2}{(A - E)}\{(A - E)_{Q_i}(p - qS) - [(C - AS)_{Q_i} + (A - E)S_{Q_i}]q\} \\ & \times \{(A - E)_{Q_j}(p - qS) - [(C - AS)_{Q_j} + (A - E)S_{Q_j}]q\}. \end{aligned} \quad (21)$$

With these relations in hand, we consider the 'Taylor Series' development of E_a and E_b (of equations (9) and (17)) with respect to Q_1 and Q_3 . We have:

$$\begin{aligned} E_a(Q_1 0 Q_3) = & E_a(000) + \left(\frac{\partial E_a}{\partial Q_1}\right)_0 Q_1 + \left(\frac{\partial E_a}{\partial Q_3}\right)_0 Q_3 \\ & + \frac{1}{2}\left(\frac{\partial^2 E_a}{\partial Q_1^2}\right)_0 Q_1^2 + \frac{1}{2}\left(\frac{\partial^2 E_a}{\partial Q_3^2}\right)_0 Q_3^2 + \left(\frac{\partial^2 E_a}{\partial Q_1 \partial Q_3}\right)_0 Q_1 Q_3 + \dots \end{aligned} \quad (22)$$

with a similar expression for $E_b(Q_1 0 Q_3)$.

Further, we have the following relations between the derivatives involved in the two expansions:

$$\left. \begin{aligned} & \frac{\partial E_a}{\partial Q_1} = \frac{\partial E_b}{\partial Q_1}; \quad \frac{\partial^2 E_a}{\partial Q_1^2} = \frac{\partial^2 E_b}{\partial Q_1^2}; \\ & \frac{\partial E_a}{\partial Q_3} = -\frac{\partial E_b}{\partial Q_3}; \quad \frac{\partial^2 E_a}{\partial Q_3^2} \neq \frac{\partial^2 E_b}{\partial Q_3^2}; \\ & \text{and} \\ & \frac{\partial^2 E_a}{\partial Q_1 \partial Q_3} = -\frac{\partial^2 E_b}{\partial Q_1 \partial Q_3}. \end{aligned} \right\} \quad (23)$$

Using these relations, we get a convenient development of the energy matrix

(cf. equation (8)) with respect to Q_i , S , up to the second order. We obtain:

$$\begin{pmatrix} W + \alpha Q_3 + \frac{1}{2}\beta(Q_3^2 - Q_2^2) & \alpha Q_2 - \beta Q_2 Q_3 \\ \alpha Q_2 - \beta Q_2 Q_3 & W - \alpha Q_3 - \frac{1}{2}\beta(Q_3^2 - Q_2^2) \end{pmatrix}, \quad (24)$$

where the various symbols stand for the following:

$$W = E_a(000) + \frac{\partial E_a}{\partial Q_1} Q_1 + \frac{1}{2} \frac{\partial^2 E_a}{\partial Q_1^2} Q_1^2 + \frac{1}{4} \left(\frac{\partial^2 E_a}{\partial Q_3^2} + \frac{\partial^2 E_b}{\partial Q_3^2} \right) (Q_3^2 + Q_2^2), \quad (25)$$

$$\alpha = \frac{\partial E_a}{\partial Q_3} + \frac{\partial^2 E_a}{\partial Q_1 \partial Q_3} Q_1 \quad (26)$$

and

$$\frac{1}{2}\beta = \frac{1}{4} \left(\frac{\partial^2 E_a}{\partial Q_3^2} - \frac{\partial^2 E_b}{\partial Q_3^2} \right). \quad (27)$$

The form of the dependence on Q_2 follows from the octahedral symmetry by observing that a cyclic permutation of the axes implies $Q_3 \rightarrow -(Q_3 + \sqrt{3}Q_2)/2$, $Q_2 \rightarrow (\sqrt{3}Q_3 - Q_2)/2$, $\psi_a \rightarrow -(\psi_a + \sqrt{3}\psi_b)/2$, $\psi_b \rightarrow (\sqrt{3}\psi_a - \psi_b)/2$; and that the energy matrix is invariant under this transformation.

Öpik and Pryce included a diagonal term of third order in the matrix, which arises from 'anharmonic terms' in the 'quasi-elastic' restoring forces. Such terms come in part from covalent effects already discussed, and in part from core overlaps not explicitly discussed here. They omitted the second-order terms represented by the coefficient β , however, Liehr and Ballhausen, on the other hand, pointed out the importance of β but neglected the third-order term. We shall supplement (24) by the third order matrix:

$$\begin{pmatrix} A_3(Q_3^3 - 3Q_3Q_2^2) + \delta Q_3(Q_2^2 + Q_3^2) & \delta Q_2(Q_2^2 + Q_3^2) \\ \delta Q_2(Q_2^2 + Q_3^2) & A_3(Q_3^3 - 3Q_3Q_2^2) - \delta Q_3(Q_2^2 + Q_3^2) \end{pmatrix}, \quad (24a)$$

whose form is given by the symmetry argument just outlined. But we shall not derive explicit expressions for A_3 and δ . A_3 is the same as in the notation of Öpik and Pryce, and its contribution to the energy can be comparable to that of β , which, being the difference of two quantities, may be smaller than would at first be expected of a second-order quantity. The contribution of δ is probably unimportant, as a detailed study of some model will reveal. Since A_3 arises in large measure from the overlap repulsion of several closed-shell electrons, and δ arises from only one d -electron, one may expect δ to be small compared with A_3 .

To solve (24) we define polar coordinates ρ and θ in the space of the coordinates Q_2 and Q_3 :

$$Q_3 = \rho \cos \theta; \quad Q_2 = \rho \sin \theta. \quad (28)$$

The eigenvalues of (24) + (24a) (cf. (8)) are:

$$E = W + A_3 \rho^3 \cos 3\theta \pm \sqrt{[(\alpha + \delta \rho^2)^2 + \frac{1}{4}\beta^2 \rho^2 + (\alpha + \delta \rho^2)\beta \rho \cos 3\theta]}. \quad (29)$$

When $Q_2 = 0$ the solutions are:

$$E_a = W \pm (\alpha Q_3 + \frac{1}{2}\beta Q_3^2 + \delta Q_3^3) + A_3 Q_3^3. \quad (30)$$

This can be written as:

$$\begin{aligned} E_a &= K + \alpha Q_3 + \gamma_a Q_3^2 + A_a Q_3^3, \\ E_b &= K - \alpha Q_3 + \gamma_b Q_3^2 + A_b Q_3^3, \end{aligned}$$

where

$$K = E_a(0, 0, 0) + \frac{\partial E_a}{\partial Q_1} Q_1 + \frac{1}{2} \frac{\partial^2 E_a}{\partial Q_1^2} Q_1^2 + \dots,$$

$$\gamma_a = \frac{1}{2} \frac{\partial^2 E_a}{\partial Q_3^2}, \quad \gamma_b = \frac{1}{2} \frac{\partial^2 E_b}{\partial Q_3^2}, \quad (31)$$

and

$$A_a = A_b \pm \delta.$$

Treating A_a , A_b as small quantities, the minima, with respect to variation of Q_3 , are:

$$E_a^{\min} = K - \alpha^2/4\gamma_a - A_a\alpha^3/8\gamma_a^3, \quad (32a)$$

$$E_b^{\min} = K - \alpha^2/4\gamma_b + A_b\alpha^3/8\gamma_b^3, \quad (32b)$$

and occur at

$$Q_3^a = -\alpha/2\gamma_a - 3A_a\alpha^2/8\gamma_a^3, \quad (33a)$$

$$Q_3^b = +\alpha/2\gamma_b - 3A_b\alpha^2/8\gamma_b^3. \quad (33b)$$

Finally

$$E_a^{\min} - E_b^{\min} = \alpha^2\beta/2\gamma_a\gamma_b - A_3\alpha^3(\gamma_a^3 + \gamma_b^3)/8\gamma_a^3\gamma_b^3 + \delta\alpha^3(\gamma_a^3 - \gamma_b^3)/8\gamma_a^3\gamma_b^3. \quad (34)$$

For a stable state γ_a and γ_b are positive. Also, as Öpik and Pryce have shown, on a reasonable model, A_3 is negative. We can summarize the configurations of lowest energy as follows (writing γ for an appropriate mean of γ_a and γ_b , and neglecting the term in δ):

$$\begin{array}{llll} \alpha > 0, & \beta > A_3\alpha/2\gamma, & E_b \text{ lowest,} & Q_3 > 0 \\ \alpha > 0, & \beta < \text{,,} & E_a \text{ ,,} & Q_3 < 0 \\ \alpha < 0, & \beta > \text{,,} & E_b \text{ ,,} & Q_3 < 0 \\ \alpha < 0, & \beta < \text{,,} & E_a \text{ ,,} & Q_3 > 0 \end{array} \quad (35)$$

The foregoing general conclusions include the various possibilities of distortion suggested by Öpik and Pryce [4] and the predictions of Liehr and Ballhausen [7] based on their electrostatic models. The inclusion of additional terms arising from covalency may influence the sign of the parameters involved in a different way than obtained before. This is examined in the next section.

4. DISCUSSION

The above analysis shows that the sign of the parameters α and β for any system would determine the nature of distortion, i.e. whether Q_3 would be positive or negative at the minimum. We shall now examine the explicit forms of α and β . We have:

$$\alpha = \frac{\partial E_a}{\partial Q_3} + \frac{\partial^2 E_a}{\partial Q_1 \partial Q_3} Q_1.$$

The explicit form as determined with the help of (20) and (21) turns out to be unwieldy, particularly the second term. A rough estimate on the basis of the electrostatic model (it should be noted that then our $\alpha = (\frac{1}{2}\alpha + \sqrt{2\beta q})$ of Liehr and Ballhausen [7]) shows that the second term is about one-hundredth of the

first. In the following, therefore, we shall neglect the effect of the second term even for the present model. Then it reduces to:

$$\alpha \simeq \frac{\partial E_a}{\partial Q_3} \\ \simeq [A_{Q_3}^a - 2\{(C^a - A^a S^a)_{Q_3} + (A^a - E^a)S_{Q_3}^a\}pq - (A - B)_{Q_3}^a q^2]$$

or alternatively

$$\alpha \simeq p^2 \frac{\partial A^a}{\partial Q_3} + q^2 \frac{\partial B^a}{\partial Q_3} - 2pq \frac{\partial C^a}{\partial Q_3} + 2pqE_0^a \frac{\partial S^a}{\partial Q_3} \quad (36)$$

Within this approximation for a moderate degree of covalency (i.e. p is not very much smaller than unity) it is likely that the first term of (36) dominates. Thus following Liehr and Ballhausen (and the accepted literature on cupric complexes before them) we assume that α is positive. This, however, may not be always true and the final answer would depend on the calculation of all the terms in (36) for the model chosen.

In view of the complicated form of (21) the reduction of the parameter

$$\beta = \frac{1}{2}(\gamma_a - \gamma_b) = \frac{1}{2} \left(\frac{\partial^2 E_a}{\partial Q_3^2} - \frac{\partial^2 E_b}{\partial Q_3^2} \right)$$

looks involved. However, if we make use of the symmetry relationship between E_a and E_b , in particular,

$$\frac{\partial E_a}{\partial Q_3} = - \frac{\partial E_b}{\partial Q_3}$$

some terms involved in the explicit form of β as written with the help of (21) cancel out. We get:

$$\beta = \frac{1}{2} \left[p^2 \left(\frac{\partial^2 A^a}{\partial Q_3^2} - \frac{\partial^2 A^b}{\partial Q_3^2} \right) + q^2 \left(\frac{\partial^2 B^a}{\partial Q_3^2} - \frac{\partial^2 B^b}{\partial Q_3^2} \right) - 2pq \left(\frac{\partial^2 C^a}{\partial Q_3^2} - \frac{\partial^2 C^b}{\partial Q_3^2} \right) + 2pqE_0^a \left(\frac{\partial^2 S^a}{\partial Q_3^2} - \frac{\partial^2 S^b}{\partial Q_3^2} \right) \right] \quad (37)$$

Once again it would be difficult to guess the sign of β from the form of (38) without carrying out the calculations based on the selected model for a particular system. Such calculations are obviously hard. However, it may be useful to develop some empirical relations based on some physical arguments as suggested from the nature of β .

According to the standard covalent point of view there is an appreciable transfer of σ -electrons from the ligands to the metal ion ($d\gamma$) in the bonding state and transfer of $d\gamma$ electrons from the metal ion to the ligands [10]. This is dependent on the electron affinity of the cation; in the present case the partially occupied $d\gamma$ orbitals which act as acceptors. That this tendency is enhanced for Cu (II) and Mn (III) can be related with the increased ionization potential for these ions [12]. These donor and acceptor properties of such cations are likewise influenced by the nature of the ligands. Thus the degree of covalency would depend on some specific property of both the central ion and the ligands.

Now, if we examine (37), ignoring the derivatives of the orbitals, we shall be left with the matrix elements of the second derivatives of the Hamiltonian, in fact, of the second derivatives of the potential of the nuclei with respect to the

electron in the anti-bonding orbitals. Such matrix elements would contain factors representing electric field gradient at the nuclei with respect to the appropriate symmetry axes. Such entities involved in nuclear quadrupole coupling are related linearly with the percentage ionic character of any bond which in turn is similarly related with the electronegativity difference between the atoms bonded [13].

It may not, therefore, seem unreasonable to suggest the following empirical relation for β :

$$\beta = |\text{const}| \left[1 - \frac{(|\kappa_M - \kappa_L|)}{|\mu|} \right] \quad (39)$$

where $|\mu|$ is a small number ≤ 3 , and $|\kappa_M - \kappa_L|$ is the number denoting electronegativity difference of the central metal ion and the ligand ion. The general predictions of (39) would be similar to that of (38). If the electronegativity difference is high, i.e. the covalency is small, the factor in the square bracket of (39) would either be negative or positive by a small margin; it would increase with decreasing electronegativity of ligands, i.e. increasing covalency. This is borne out by the series of compounds CuF_2 , CuCl_2 and CuBr_2 where the c/a ratios (for the elementary octahedron) are 1.17, 1.30 and 1.32 respectively [5, 14]. Assuming α to be positive, the elongation in this series of compounds is consistent with a positive β , whose value increases with the degree of covalency, i.e. decrease in the electronegativity difference; the electronegativity of F, Cl and Br are 4, 3 and 2.8 respectively. In crystals, where the covalency effect is very small, β is likely to be negative and a distortion where tetragonal axis is compressed could be expected. An example of this is furnished by the recently determined structure of K_2CuF_4 [15] where the four fluorine ions are at 2.08 Å and two at 1.95 Å, with $c/a = 0.94$. A purely electrostatic consideration would predict negative sign of β (see also Liehr and Ballhausen [7]). In compounds such as Fe_2CuO_4 a fair amount of covalency is expected and accordingly a positive β ; the observed distortion is elongation with $c/a = 1.08$. A similar situation exists in distorted spinels isomorphous with Fe_2CuO_4 [5].

A qualitative discussion of the distortions in MnF_3 and CrF_2 is possible only after the effect of Q_2 is also taken into account, i.e. the distortion is not purely tetragonal. In these compounds, the distortion of the octahedra is such that there are three different bond lengths [16, 17]. The origin of the distortion, however, is essentially the same and an extension of the present model taking into account the effect of both Q_3 and Q_2 (D_{2h} symmetry case) should lead to the desired result.

REFERENCES

- [1] FINCH, G. I., SINHA, A. P. B., and SINHA, K. P., 1957, *Proc. roy. Soc. A*, **242**, 28.
- [2] WOJTCOWICZ, P. J., 1959, *J. appl. Phys.*, Suppl., **30**, 305.
- [3] GOODENOUGH, J. B., and LOEB, A. L., 1955, *Phys. Rev.*, **98**, 391.
- [4] ÖPIK, U., and PRYCE, M. H. L., 1957, *Proc. roy. Soc. A*, **238**, 425.
- [5] DUNITZ, J. D., and ORGEL, L. E., 1957, *J. Phys. Chem. Solids*, **3**, 20.
- [6] SINHA, K. P., 1958, *Nature, Lond.*, **181**, 835.
- [7] LIEHR, A. D., and BALLHAUSEN, C. J., 1958, *Ann. Phys.*, **3**, 304.
- [8] VAN VLECK, J. H., 1939, *J. chem. Phys.*, **7**, 72.
- [9] OWEN, J., 1955, *Proc. roy. Soc. A*, **227**, 183.
- [10] OWEN, J., 1955, *Disc. Faraday Soc.*, **19**, 127.

- [11] JØRGENSEN, C. K., 1958, *Disc. Faraday Soc.*, **26**, 110.
- [12] WILLIAMS, R. J. P., 1958, *Disc. Faraday Soc.*, **26**, 123.
- [13] GORDY, W., 1955, *Disc. Faraday Soc.*, **19**, 14.
- [14] WILSON, A. J. C., 1947–1948, *Structure Reports*, **11**, 264.
- [15] KNOX, K., 1959, *J. chem. Phys.*, **30**, 991.
- [16] HEPWORTH, M. A., and JACK, K. H., 1957, *Acta Cryst.*, **10**, 345.
- [17] JACK, K. H., and MAITLAND, R., 1957, *Proc. chem. Soc.*, p. 232.
- [18] KANAMORI, J., 1960, *J. appl. Phys.*, Suppl., **31**, 148.

The new equation of state of Longuet-Higgins and Widom

by E. A. GUGGENHEIM

Chemistry Department, The University, Reading

(Received 26 November 1964)

The new equation of state for an ideal liquid proposed by Longuet-Higgins and Widom is reformulated in a slightly different form. Agreement with experiment becomes even more striking than in the original formulation.

In a recent paper Longuet-Higgins and Widom [1] have proposed a new equation of state for liquid and solid phases, but not the gas phase, obtained by taking the equation of state for non-interacting rigid spheres and adding a Van der Waals a type term to take account of the cohesive energy. This equation is simple, plausible and in striking agreement with available data on argon. Their treatment however calls for some comment. In one part of their paper they assume for non-interacting spheres numerical values obtained from a digital computer by Alder and Wainwright [2], but in another part they assume the equation of state derived by methods of statistical mechanics by Frisch [3, 4] and his collaborators. The two sets of data are similar but far from identical. It would be more consistent to assume throughout one or the other. The estimates of Alder and Wainwright are extremely interesting but only semi-quantitative, since, apart from other uncertainties, they involve an extrapolation from at most 500 molecules to effectively an infinite number. It therefore seems worth while to modify the analysis using only Frisch's equation of state for non-interacting spheres and experimental data on argon. We shall find that the self-consistency becomes even more remarkable than appears from the paper by Longuet-Higgins and Widom.

We use the following notation, which is a compromise between those of various authors.

L Avogadro's constant,

V molar volume,

σ molecular diameter,

$b = 2\pi L\sigma^3/3$ as in Van der Waals' equation,

$V_0 = L\sigma^3/\sqrt{2}$ molar volume in close packing,

$y = b/4V = 0.740 V_0/V$ as used by Helford and Frisch [4].

The subscripts l, s, t, b and c will be used to denote liquid, solid, triple-point, boiling point and critical point respectively. The subscripts e and f refer to evaporation and fusion respectively.

In this notation we have the following equations of state:

Van der Waals: $pV = RT(1 - 4y)^{-1} - aV^{-1},$

Frisch *et al.*: $pV = RT(1 - y^3)(1 - y)^{-4},$

Longuet-Higgins and Widom: $pV = RT(1 - y^3)(1 - y)^{-4} - aV^{-1}.$

For argon we use the experimental value $\Delta_e U/RT = a/V_1 RT_t = 8.56$. At the triple-point pV/RT is negligible so that the equation of state becomes:

$$(1 - y_1^3)(1 - y_1)^{-4} = a/V_1 RT_t = 8.56,$$

having the solution $y_1 = 0.427$ or $V_1/V_0 = 1.73_3$. We also have the experimental value $\Delta_f U/\Delta_e U = 0.22$, so that $V_1/V_s = 1.22$ as compared with the experimental value 1.14.

We now turn to the crucial test of the assumed equation of state namely the relation between temperature and vapour pressure. We begin by writing the equation of state in the abbreviated form:

$$pV = RT\phi(y) - aV^{-1}.$$

Then by straightforward thermodynamics we deduce:

$$\ln(pV_1/RT) = pV_1/RT - 1 + \int_0^y y^{-1}\{\phi(y) - 1\} dy - a/V_1 RT,$$

where p now denotes the saturated vapour pressure. The first term on the right is of course negligible. Setting $\phi(y) = (1 - y^3)(1 - y)^{-4}$ we obtain:

$$\int_0^y y^{-1}\{\phi(y) - 1\} dy = \frac{3}{2}(1 - y)^{-2} - \ln(1 - y) - \frac{3}{2}.$$

Inserting the values $a/V_1 RT_t = 8.56$ and $1 - y = 0.573$ we obtain:

$$\ln(pV_1/RT) = -8.56 T_t/T + 2.625.$$

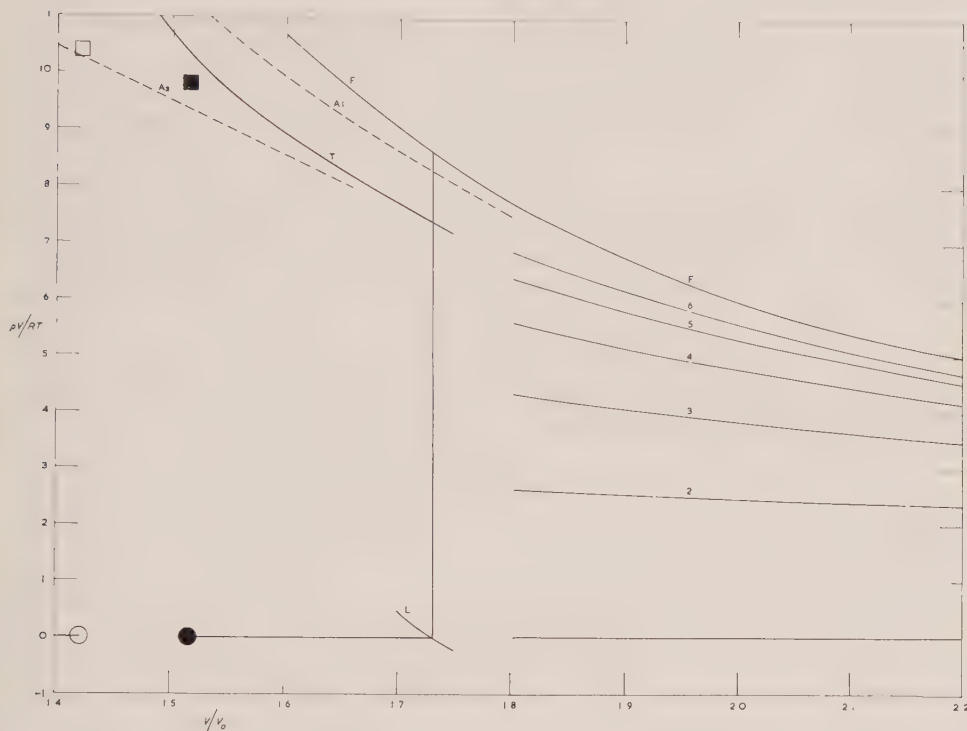
If we neglect the thermal expansion of the liquid this formula is valid at temperatures above the triple-point. At the triple-point we have:

$$\ln(p_t V_1/RT_t) = -5.93,$$

as compared with the experimental value -5.89 ; this striking agreement was already obtained by Longuet-Higgins and Widom. We may however also set $p = 1$ atm. and so calculate the normal boiling point. We find $T_b/T_t = 1.048$ as compared with the experimental value 1.042, a remarkable agreement.

It is to be noted that in this analysis no use has been made of the calculations of Alder and Wainwright [2]. It seems preferable to compare these calculations with the conclusions obtainable from the above analysis. The comparison is shown in the diagram where pV/RT is plotted against T/T_0 . The curves labelled 2-6 represent the virial expansion for rigid spheres including terms up to the 2nd-6th power in y or V/V_0 . The curve labelled F represents the analytical equation of state of Frisch *et al.* for non-interacting rigid spheres. The broken curve labelled A1 is that given by Alder and Wainwright for the fluid. The curve labelled L represents the equation of state of Longuet-Higgins and Widom. The horizontal line represents the liquid + solid phases at the triple-point. The points denoted by \circ and \bullet represent the solid phase at the triple-point when we use the calculated value $V_1/V_s = 1.22$ and the experimental value $V_1/V_s = 1.14$ respectively. The corresponding points on the curve for a solid composed of non-interacting rigid spheres are denoted by \square and \blacksquare respectively. The broken curve labelled As is that given by Alder and Wainwright for the solid.

We observe that curves F and A1 do not coincide; nor does the point ■ lie on the curve As. It is however interesting to observe that the distance of the point ■, measured horizontally, from the curve F is almost exactly equal to the horizontal distance between curves A1 and As at the same value of pV/RT . On the other hand the point □ lies practically on curve As.



A more stringent test of the equation of state is the evaluation of the coefficient of thermal expansion α . We have:

$$RT = (pV + aV^{-1})(1-y)^4(1-y^3)^{-1},$$

and differentiating logarithmically:

$$\begin{aligned} \alpha^{-1}T^{-1} &= \left(\frac{\partial \ln T}{\partial \ln V} \right)_p = \frac{pV - aV^{-1}}{pV + aV^{-1}} + \frac{4y}{(1-y)^4} - \frac{3y^3}{1-y^3} \\ &= -1 + 2.99 - 0.25 = 1.74, \end{aligned}$$

$$\alpha T = 0.57 \text{ as compared with the experimental value } \alpha T = 0.37.$$

We can also obtain a formula relating to the isothermal compressibility κ . We first rewrite the equation of state as:

$$pV = RT\phi(y) - aV^{-1},$$

and we deduce:

$$\frac{\alpha}{\kappa} = \left(\frac{\partial p}{\partial T} \right)_V = R\phi(y)V^{-1} = aV^{-2}T^{-1} = 8.6 RV^{-1},$$

as compared with the experimental value $\alpha/\kappa = 7.4 R/V$. It will be noticed that the last relation is independent of the form of $\phi(y)$. It is the same for the new equation of state as for Van der Waals' equation.

Although the equation of state is expected to be valid only for a condensed phase but not for the gas phase, it is nevertheless interesting to examine how well (or how badly!) it fits the dilute gas. The equation of state of Longuet-Higgins and Widom, like the equation of state of Van der Waals, reduces for low pressures to:

$$pV/RT = 1 + b/V - a/VRT.$$

Consequently the Boyle temperature T_B is determined by $a/bRT_B = 1$. At the triple point we have $a/bRT_t = a/4yV_1RT_t = 8.56/1.708 = 5.02$, so that $T_B/T_t = 5.02$ as compared with the experimental value $T_B/T_t = 411.5/83.8 = 4.91$, which is surprisingly good agreement. By contrast it is well known that the temperature-dependence of the second virial coefficient B is not at all well described by the relation $B = b - a/RT$.

Since the above text was written, Professor Rowlinson has drawn the author's attention to an alternative approximate equation of state for rigid spheres due to Thiele [5]. Whereas Frisch's formula, which alone we have used, may be described by

$$\phi(y) = (1 + y + y^2)(1 - y)^{-3};$$

the alternative approximation due to Thiele is shown on the diagram as the curve marked T and may be described by

$$\phi(y) = (1 + 2y + 3y^2)(1 - y)^{-2}.$$

It can be verified that, if we use Thiele's approximation in place of Frisch's, our conclusions are scarcely affected.

Whereas it was clearly explained by Longuet-Higgins and Widom [1] that their equation of state should be a good approximation for the liquid but a bad approximation for the dilute gas, they did not state at what density it would be expected to break down. It is clearly a good approximation when large clusters are more important than small clusters, but a bad approximation when small clusters are more important than large clusters. It therefore seemed likely that the approximation would be fairly good at the critical density. To study this we rewrite the equation of state as:

$$pb/4RT = y(1 - y^3)(1 - y)^{-4} - (4a/bRT)y^2.$$

The critical point is determined by

$$\partial p/\partial y = 0, \quad \partial^2 p/\partial y^2 = 0.$$

These conditions lead to the equation:

$$1 - 5y_c - 20y_c^2 - 12y_c^3 = 0,$$

with the solution $y_c = 0.129$ and to the equation:

$$a/RT_c V_c = 1.38$$

Combining this with $V_1/V_c = y_c/y_t = 0.129/0.427 = 0.302$ and with our earlier relation $a/RT_t V_1 = 8.56$ we obtain $T_t/T_c = 1.38/8.56 \times 0.302 = 0.535$ as compared with the experimental value for argon $T_t/T_c = 83.8/150.7 = 0.557$. Finally we have

$$(pV/RT)_c = (1 - y_c^3)(1 - y_c)^{-4}(4a/bRT_c)y_c^2 = 1.73_5 - 1.37_8 = 0.36$$

as compared with the experimental value 0.29.

The agreement between calculated and measured values, while far from perfect, is good enough to be interesting when we remember that the only experimental datum used here is the value of $\Delta_e U/RT_t$. Moreover because $\partial V/\partial P = \infty$ at the critical point it follows that a small inexactitude in the p - V curve may affect the calculated value of p_c only slightly but will have a pronounced effect on the apparent value of V_c . This is borne out by eliminating V_c from two previous relations. We have:

$$p_c V_t / RT_c = (pV/RT)_c y_c / y_t = 0.36 \times 0.302 = 0.109$$

as compared with the experimental value $0.29 \times 0.37 = 0.108$. No more need be said.

The author is grateful to Professor Longuet-Higgins and Professor Widom for letting him see their paper before its publication, and also to the former for encouraging comments.

REFERENCES

- [1] LONGUET-HIGGINS, H. C., and WIDOM, B., 1964, *Mol. Phys.*,
- [2] ALDER, B. J., and WAINWRIGHT, T. E., 1960, *J. chem. Phys.*, **33**, 1442.
- [3] REISS, H., FRISCH, H. L. and LEBOWITZ, J. L. 1959, *J. chem. Phys.*, **31**, 369, formula, (6.8).
- [4] HELFAND, E., and FRISCH, H. L., 1961, *J. chem. Phys.*, **34**, 1037, formula (2.20).
- [5] THIELE, E., 1963, *J. chem. Phys.*, **39**, 474.

The high-resolution nuclear magnetic resonance spectrum of 2-carbomethoxy 5,6-dimethyl benzofuran

by A. D. COHEN and K. A. McLAUCHLAN

Basic Physics Division, National Physical Laboratory, Teddington, Middlesex

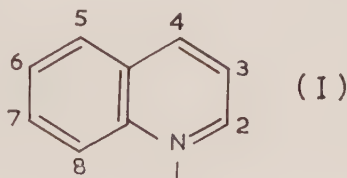
(Received 29 August 1964)

The high-resolution proton magnetic resonance spectrum of 2-carbomethoxy 5,6-dimethyl benzofuran has been obtained at 56.4 Mc/s. This N.M.R. (nuclear magnetic resonance) spectrum is complex since there are observable spin-spin coupled interactions between all the ring protons, between the protons of the 5 and 6 methyl groups and between the 4 and 7 protons and the protons of the 5 and 6 methyl groups. By taking advantage of solvent shifts and employing frequency-sweep spin decoupling techniques it was found that

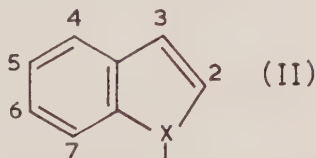
$$\begin{aligned} J_{H(3), H(4)} &= \mp 0.12 \pm 0.03 \text{ c/s}; \quad J_{H(3), H(7)} = \pm 0.60 \pm 0.03 \text{ c/s}; \\ J_{H(4), H(7)} &= \pm 0.99 \pm 0.03 \text{ c/s}, \quad J_{Me(5), Me(6)} = |0.37 \pm 0.04| \text{ c/s}, \\ J_{H(4), Me(5)} &= J_{Me(6), H(7)} = |0.74 \pm 0.1| \text{ c/s}, \\ \text{and } J_{H(4), Me(5)} &= J_{Me(6), H(7)} = |0.37 \pm 0.1| \text{ c/s}. \end{aligned}$$

1. INTRODUCTION

The first observed spin-spin coupling constant between protons on neighbouring rings of a fused ring compound was reported by Anet [1] in 1960. He demonstrated that in 5,7-dichloro- and 5,7-dimethyl-quinoline $J_{H(4), H(8)} = 0.8 \text{ c/s}$. In fact $J_{H(4), H(8)} = 1.0 \text{ c/s}$ is the only inter-ring coupling constant reported for quinoline (I) itself [2].

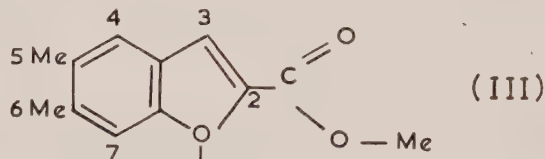


This implies that if the other inter-ring coupling constants are non-zero they are less than $|0.4| \text{ c/s}$. In compounds consisting of a fused benzene ring and a five membered ring of the type (II) the analogous



coupling constant is $J_{H(5), H(7)}$. In indene ($X = CH_2$), indole ($X = NH$), benzofuran ($X = O$), benzothiophene ($X = S$) and their derivatives, $J_{3,7}$ is the only inter-ring coupling constant that has been reported [3, 4]. Its size varies from 0.6 c/s to 1.0 c/s depending on X and on the nature of any substituents [3, 4].

The aim of this work was to find the sign of the inter-ring proton coupling constant in a compound of the type (I) or (II). This would be accomplished by finding its sign relative to a coupling constant whose sign was known relative to the positive [5] ortho proton coupling constant. The compound used was 2-carbomethoxy 5,6-dimethyl benzofuran (III):



subsequently referred to as (III). In (III), by analogy with other benzene derivatives (see the review article by Banwell and Sheppard [6]), the para coupling constant has the same sign as the ortho coupling constant so that $J_{H(4), H(7)}$ is necessarily positive. Thus it is necessary to find the sign of $J_{3,7}$ relative to $J_{4,7}$.

The proton-proton coupling constants involving the protons of Me(5) and Me(6) of (III) are also of interest because they give information about the π -electron system. McConnell [7, 8] calculated the π -electron contribution to the proton-proton coupling constants in benzene and naphthalene by considering configurational interaction. Hoffman [9] suggested that long-range proton couplings between the protons on a benzene ring and the protons on a substituent methyl group could be explained if hyperconjugation as well as configurational interaction was considered. Theoretical calculations of these coupling constants have been carried out [10, 11] by relating the π -electron contribution to the aromatic proton-proton coupling constants to the aromatic proton-methyl proton coupling constants via electron spin resonance data on hyperfine couplings.

2. EXPERIMENTAL

Compound (III) was prepared by Mr. G. O'Neill. All samples containing it were degassed and sealed into 5 mm sample tubes with T.M.S. (tetramethyl silane) added as an internal reference compound and also to give a convenient signal for actuating a field-frequency stabilization system.

Spectra were obtained at 56.4 Mc/s on a Varian V4300B spectrometer and both field-sweep and frequency-sweep double resonance techniques (see the review article by Baldeschwieler and Randall [12]) were employed. The field-sweep double resonance experiments were performed by the double modulation side-band method [13] using the Varian V-3521A integrator/decoupler. Field-frequency stabilization for the frequency sweep experiments was accomplished by the method of Freeman and Anderson [14].

In the frequency-sweep experiments the field homogeneity was continually monitored by observing the audio signal from T.M.S. after amplification but before phase-sensitive detection in the field-frequency stabilization unit. A tuned filter with a band pass of about 50 c/s was employed between the first and second stages of the audio amplifier. This caused no observable decrease in the response time of the system but prevented interference from other signals, providing that they were weak (as expected of signals arising when recording an

N.M.R. spectrum) and due to resonances more than 200 c/s from the T.M.S. resonance.

In order to facilitate analysis of the part of the N.M.R. spectrum of (III) due to the ring protons it was necessary to remove the coupling between the ring protons and the methyl-group protons on the benzene ring by double-resonance techniques [12]. The signals due to the methyl groups are chemically shifted from each other by less than 0.05 p.p.m. (as shown in the next section this depends on the solvent) and are about 2 c/s broad so that spin decoupling can be easily accomplished by irradiating strongly at their mean frequency.

Unfortunately these methyl groups are only about 2.3 p.p.m. down-field from T.M.S. and, despite the tuned filter in the lock-in phase sensitive detector, when sufficient audio-frequency power is supplied to the 'modulation' terminals of the V4311 radio frequency oscillator for efficient decoupling the stability of the field-frequency locking is disturbed. This was observed as loss of resolution as the apparent full line-width at half height increased from 0.24 ± 0.03 c/s to about 0.60 c/s. This difficulty was overcome by using centre-band to provide the irradiating field [15]. However, large radio-frequency fields (about 7.5 mc in the rotating component) obtained in the same way did not affect the field-frequency stabilization when the irradiating audio frequency was separated by more than 300 c/s from the audio-frequency used for field-frequency locking.

3. RESULTS

The N.M.R. spectrum of (III) can be conveniently separated into three parts:

(a) the signal due to the ring protons H(3), H(4) and H(7) occurring at about $\tau = 2.6$; (b) the single sharp line due to the protons on the methyl group of the 2-carbo-methoxy substituent, occurring at about $\tau = 5.9$. This signal contains no more information and will not be dealt with further; (c) the signals due to the protons on the 5 and 6 methyl groups occurring at about $\tau = 7.7$.

The spectrum of (III) was investigated by field-sweep techniques in a number of common solvents and substantial changes in the chemical shifts of H(3), H(4) and H(7) were observed. The τ values of (III) for solvents in which field-swept spin-decoupling was performed are given in the table. With dioxan as solvent, the spectrum of group (a) decoupled from group (c) was analysed as an ABC system to give:

$$J_{\text{H}(3), \text{H}(4)} < |0.3| \text{ c/s}; \quad J_{\text{H}(4), \text{H}(7)} = |0.98 \pm 0.1| \text{ c/s}$$

and $J_{\text{H}(4), \text{H}(7)(7)} = |0.55 \pm 0.1| \text{ c/s}.$

This indicated that the coupling constants were too small for their relative signs to be determined by nuclear magnetic triple resonance [16]. Before attempting any method based on the nuclear Overhauser effect [17], it was decided to attempt to make the spins of H(3), H(4) and H(7) sufficiently closely coupled at 56.4 Mc/s that the relative signs of $J_{\text{H}(3), \text{H}(7)}$ and $J_{\text{H}(4), \text{H}(7)}$ could be determined [18, 19]. The ABC spectrum of (a) field-sweep decoupled from (c) with carbon tetrachloride as solvent proved to be so strongly coupled that most of the lines were not resolvable and so it was decided to use frequency-sweep techniques. These can improve resolution [16] if full use is not being made

of the homogeneity of the magnetic field in space because the Bloch slow passage conditions are not being approached and/or the magnetic field is fluctuating in time.

Solvent	$\tau_{H(3)}^\dagger$	$\tau_{H(4)}$	$\tau_{H(7)}$	$\frac{1}{2}(\tau_{Me(5)} + \tau_{Me(6)})$	$ \tau_{Me(5)} - \tau_{Me(6)} $
Acetone [†]	2.561	2.574	2.658	7.673	0.047
Dioxan [†]	2.567	2.606	2.647	7.677	0.048
CCl ₄ and T.M.S. [§] 4 : 1	2.744	2.754	2.788	7.697	0.047
Deuterobenzene T.M.S. § 2.1 : 1	2.652	2.847	2.796	7.957	0.03

[†] $\tau_{H(3)}$ was measured without any spin-decoupling and then $\tau_{H(4)}$ and $\tau_{H(7)}$ were measured relative to $\tau_{H(3)}$. In this way Bloch-Siegert shifts due to the strong radio-frequency used spin decoupling could be neglected.

[‡] Measurements from field swept spectra with a mean deviation of ± 0.004 p.p.m.

[§] Measurements from frequency swept spectra with a mean deviation of ± 0.001 p.p.m.

Chemical shift data for compound (III).

The frequency-swept spectrum of group (a) with and without spin decoupling from group (c) is shown in figure 1 (i) and (ii). In the latter spectrum a combination line appears and is designated by an asterisk. A good fit to the observed spectrum can be obtained with both of two sets of parameters:

- (1) $J_{H(3), H(7)} = \pm 0.99$ c/s and $J_{H(4), H(7)} = \pm 0.60$ c/s with
 -0.2 c/s $< J_{H(3), H(4)} < 0.05$ c/s, and
- (2) $J_{H(3), H(7)} = \pm 0.99$ c/s and $J_{H(4), H(7)} = \pm 0.60$ c/s with
 0.10 c/s $< J_{H(3), H(4)} < 0.20$ c/s.

The limitation on the size of $J_{H(3), H(4)}$ is such that it should be less than 0.20 c/s so that it should be unobservable in the peaks due to H(3) and H(4). The intensity of the combination line could only be assessed approximately and so it did not allow accurate determination of $J_{H(3), H(4)}$. (However, it will be seen that the observation of the combination line gives the sign of $J_{H(3), H(4)}$ relative to the other couplings).

Unfortunately with $J_{H(3), H(7)}$ and $J_{H(4), H(7)}$ so small, the chemical shifts involved can allow $J_{H(3), H(4)}$ to modify the spectrum even though it is too small to be observed. However, if assignment (1) was correct and $J_{H(3), H(4)} \geq |0.06|$ c/s then solvent shift phenomena can be utilized to distinguish between the assignments. An ABX model is adequate to demonstrate this: suppose that

$$\delta_{AB} = 0, \delta_{AX} = \delta_{BX} \gg |J_{AX}| + |J_{BX}|; \quad J_{AB} = |0.12| \text{ c/s}, J_{AX} = |0.99| \text{ c/s and} \\ J_{BX} = |0.60| \text{ c/s,}$$

where the δ 's refer to chemical shifts. The effectiveness of the mixing of spin states A and B is dependent on the relative signs of J_{AX} and J_{BX} . If they are of the same sign, J_{AB} causes strong mixing so that the spectrum shown in figure 2 (i) would be observed. However, if they are of the opposite sign J_{AB} causes negligible mixing so that the spectrum shown in figure 2 (ii) would be observed. Further, if $J_{AB} = 0$, then no mixing can occur so that the relative

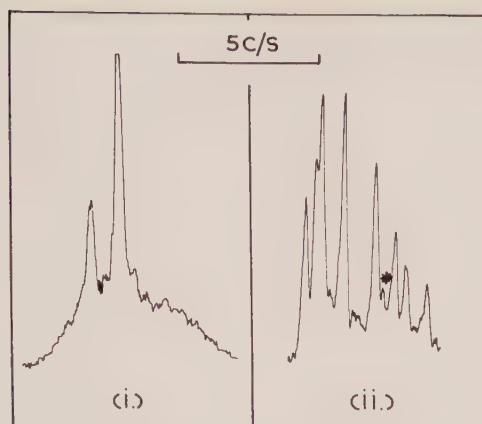


Figure 1. The frequency swept spectra† of H(3), H(4) and H(7) of compound (III) in a solution of carbon tetrachloride and T.M.S. in a ratio of 4 : 1.

- (i) The two sharp peaks are due to H(3). The broadness of the signals due to H(4) and H(7) originates from unresolved structure arising from spin interactions with Me(5) and Me(6).
- (ii) As (i) but with Me(5) and Me(6) spin decoupled from H(4) and H(7). Going up field: the first and third lines are due to H(4), the second and fourth lines are due to H(3), and the remaining lines are due to H(7). The line designated by an asterisk is a combination line.

†To avoid confusion these and the other frequency swept spectra have increasing magnetic field as their abscissa so as to conform with convention for field swept ones.

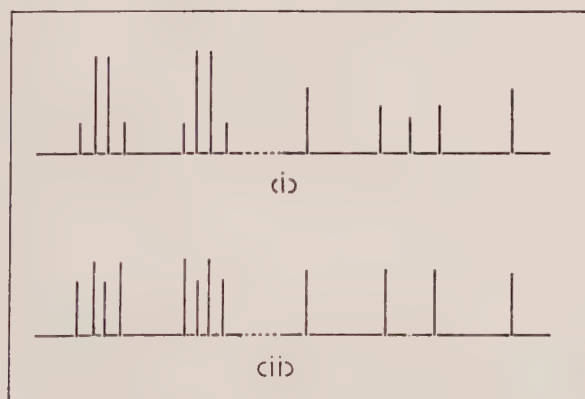


Figure 2. Calculated ABX spectra illustrating that an unobservable J_{AB} can allow the relative signs of J_{AX} and J_{BX} to be determined.

- (i) $\delta_{AX} = \delta_{BX} \gg |J_{AX}| + |J_{BX}|$; $\delta_{AB} = 0$;
 $J_{AB} = |0.12|$ c/s, $J_{AX} = \pm 0.99$ c/s and $J_{BX} = \pm 0.60$ c/s.
- (ii) $\delta_{AX} = \delta_{BX} \gg |J_{AX}| + |J_{BX}|$; $\delta_{AB} = 0$;
 $J_{AB} = |0.12|$ c/s, $J_{AX} = \pm 0.99$ c/s and $J_{BX} = \pm 0.60$ c/s.

signs of J_{AX} and J_{BX} could not be found by simply observing the spectrum since this spectrum must be AMX by definition.

Dioxan was carefully added to a saturated solution of (III) in carbon tetrachloride and T.M.S. until the lines due to H(4) were, as far as could be judged, enclosed by the lines due to H(3). This occurred when the ratios of dioxan to carbon tetrachloride to tetramethyl silane were about 1 : 3 : 1.5. This spectrum is shown in figure 3 (i) and it agrees only with spectra calculated on the basis of assignment (1). Before an exact calculation of the spectral parameters was attempted it was decided to obtain a better upper limit to the size of $J_{H(3), H(4)}$ in case virtual coupling was important [20]. Using deuterated benzene with T.M.S. (in the ratio 2.1 : 1) as a solvent for (III) a moderately coupled spectrum was obtained (see table). The frequency-swept spectrum of group (a) spin-decoupled from group (c) showed no splitting or line broadening of the doublets arising from H(3) (and H(4)). The lines observed had a full width at half-height of 0.24 c/s which gave, when the appropriate line shape factors were introduced, $J_{H(3), H(4)} < |0.15|\text{ c/s}$. A best fit for the spectrum in figure 3 (i) on the basis of assignment (1) is

$$J_{H(3), H(4)} = -0.12\text{ c/s}, J_{H(3), H(7)} = +0.99\text{ c/s}, J_{H(4), H(7)} = +0.60\text{ c/s}$$

with the assumption that the para ring coupling, $J_{H(4), H(7)}$, is positive.

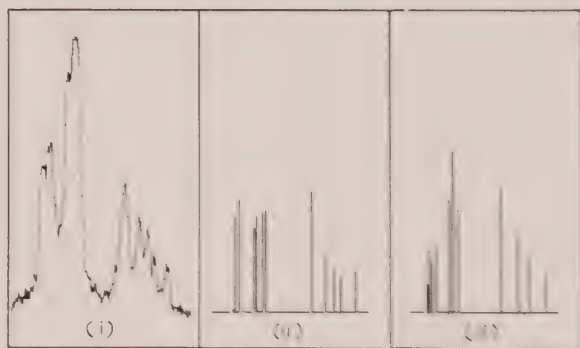


Figure 3. The observed frequency swept spectrum of H(3), H(4) and H(7) of compound (III) spin decoupled from Me(5) and Me(6) in dioxan, carbon tetrachloride and T.M.S. in the ratio of about 1.3 : 1 : 1.5 compared with the computed best fit spectra for cases (1) and (2) of text.

(i) The observed spectrum.

(ii) The ABC spectrum calculated for case (1) with the parameters:

$$\nu_A = 1.03\text{ c/s}, \nu_B = 0.86\text{ c/s}, \nu_C = -1.89\text{ c/s} \quad (\nu_A + \nu_B + \nu_C = 0)$$

$$J_{AB} = \mp 0.12\text{ c/s}, J_{AC} = \pm 0.60\text{ c/s}, J_{BC} = \pm 0.99\text{ c/s}.$$

(iii) The ABC spectrum calculated for case (2) with the parameters:

$$\nu_A = 0.93\text{ c/s}, \nu_B = 0.85\text{ c/s}, \nu_C = -1.78\text{ c/s} \quad (\nu_A + \nu_B + \nu_C = 0)$$

$$J_{AB} = \pm 0.15\text{ c/s}, J_{AC} = \pm 0.60\text{ c/s}, J_{BC} = \pm 0.99\text{ c/s}.$$

In figure 4 (iii) the frequency-sweep spectrum of group (c) is shown for a saturated solution of (III) in a solution of carbon tetrachloride and T.M.S. in the ratio 3 : 1. (From the N.M.R. spectrum of III alone it is not possible to assign the peaks to specific methyl groups.) Figure 4 (i) is a frequency-sweep spectrum of group (c) spin-decoupled from group (a). It is evident that this

is very nearly a first-order spectrum of the type A_3X_3 so that

$$J_{\text{Me}(5), \text{Me}(6)} = |0.37 \pm 0.04| \text{ c/s.}$$

On the basis of a first-order approximation the structure apparent in figure 4 (iii) can be explained, by assuming:

$$(1) J_{\text{H}(4), \text{Me}(5)} = J_{\text{Me}(6), \text{H}(7)} = |0.74 \pm 0.10| \text{ c/s,}$$

$$J_{\text{Me}(5), \text{H}(7)} = J_{\text{H}(4), \text{Me}(6)} = |0.37 \pm 0.10| \text{ c/s,}$$

$$(2) J_{\text{H}(3), \text{Me}(5)}, J_{\text{H}(4), \text{Me}(6)} < |0.1| \text{ c/s, } |0.1| \text{ c/s,}$$

where $J_{\text{H}(4), \text{Me}(5)}$, and $J_{\text{Me}(6), \text{H}(7)}$ have been chosen as $|0.74 \pm 0.10| \text{ c/s}$ rather than $J_{\text{Me}(5), \text{H}(7)}$, and $J_{\text{H}(4), \text{Me}(6)}$ due to the work of Acrivos [16] and Dewar and Fahey [17].

In view of the spectrum of group (a) in figure 1 (i) it may appear odd that the mixing of the spin-states of H(3), H(4) and H(7) is not sufficiently strong to cause their mixing to be apparent in group (c) but it must be remembered that

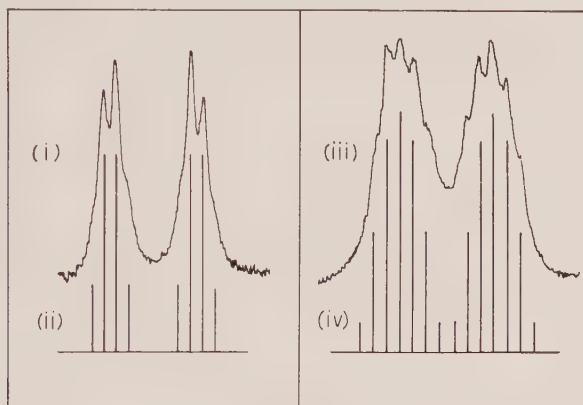


Figure 4. The frequency swept spectra of Me(5) and Me(6) of compound (III) in carbon tetrachloride and T.M.S. in the ratio 4 : 1 compared with calculated spectra.

- (i) Me(5) and Me(6) spin decoupled from H(4) and H(7). It is not possible to assign these peaks to specific methyl groups.
- (ii) The A_3X_3 spectrum with $J_{AX} = |0.37| \text{ c/s}$.
- (iii) Me(5) and Me(6) without spin decoupling.
- (iv) The first-order spectrum A_3N_3RX with $J_{AN} = |0.37| \text{ c/s}$, $J_{AR} = J_{RX} = |0.74| \text{ c/s}$ and $J_{AX} = J_{NR} = |0.37| \text{ c/s}$.

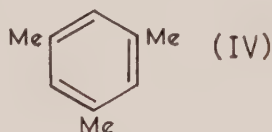
this is not equivalent to the statement that strong mixing of the spin-states of H(3), H(4) and H(7) does not occur. Thus it is only necessary for H(3), H(4) and H(7) not to be sufficiently strongly mixed for the majority of the 128 spin states possible for the Me(5) and Me(6) protons. This was demonstrated experimentally by noting that despite changes in the chemical shifts apparent between the ring protons, when acetone is used as a solvent for (III) (see table) the structure occurring in the (c) part of the spectrum remains invariant. (Actually the chemical shift between Me(5) and Me(6) does not vary noticeably on changing solvent from carbon tetrachloride to acetone so that the spectrum of (c) in the latter is as shown in figure 4 (i)).

4 DISCUSSION AND CONCLUSIONS

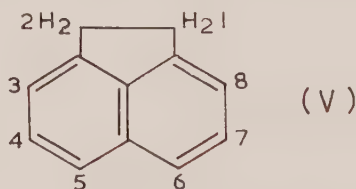
It has been shown that $J_{H(3) H(7)}$ in (III) is positive and by analogy it is to be expected that the similar inter-ring coupling constant in type (I) and (II) compounds is also positive. Qualitative discussions of the mechanism for long range inter-ring couplings in heterocyclic systems have been given by Gutowsky and Porte [21], Banwell and Sheppard [6], and Elvidge and Foster [4]. However, semi-quantitative or quantitative explanations will probably be lacking at least until the meta and para proton coupling constants in benzene can be quantitatively understood.

The negative sign of $J_{H(3), H(4)}$ is qualitatively expected if the reasonable assumption is made that the dominant contributions to it occurs through the three carbon pathway for then the σ -electron contribution to the coupling constant is negative from the Dirac vector model [22] and further the π -electron contribution is also expected to be negative from McConnell's [8] calculations for naphthalene.

The observation in (III) of the meta coupling constants $J_{H(4), Me(5)}$ and $J_{Me(5), H(7)}$ are of theoretical interest. Calculations for mesitylene [10] (IV)



gave good agreement for $J_{H(ortho), Me}$ and $J_{H(para), Me}$ while the calculation for $J_{Me, Me}$ gave 0.37 c/s, which apparently, was too small to cause anxiety when it was not observed. Also in acenaphthene [11] (V) the



ortho and para coupling to the methylene groups were observed but the meta coupling was not (this implies that the meta couplings were less than 0.3 c/s). However, calculations similar to those for (IV) predicted a readily observable meta coupling so that Dewar and Fahey [11] resorted to a less refined M.O. calculation which would always predict a zero meta coupling constant [7]. Thus the appearance in (III) of the meta coupling constants $J_{H(4), Me(6)}$ and $J_{Me(5), H(7)}$ shows that, as expected, the more sophisticated theories [8, 10] are superior to simple M.O. theory.

The observation in (III) of $J_{Me(5), Me(6)}$ is expected. From electron spin resonance data this observed coupling at Me(5) or Me(6) should change in sign but not substantially in size if Me(6) or Me(5), respectively, was replaced by a proton (see reference [23] for a discussion of this point). Since $J_{H(4), Me(5)}$ and $J_{Me(6), H(7)}$ are about twice the size of $J_{Me(5), Me(6)}$ then from simple M.O. theory [7] there is about $\sqrt{2}$ more π -bond order between C_4 and C_5 , and C_6 and C_7 than between C_5 and C_6 .

This work forms a part of the research programme of the National Physical Laboratory and is published by permission of the Director.

REFERENCES

- [1] ANET, F. A. L., 1960, *J. chem. Phys.*, **32**, 1274.
- [2] SCHAEFER, T., 1961, *Canad. J. Chem.*, **39**, 1864.
- [3] ELVIDGE, J. A., and FOSTER, R. G., 1963, *J. chem. Soc.*, p. 590.
- [4] ELVIDGE, J. A., and FOSTER, R. G., 1964, *J. chem. Soc.*, p. 981.
- [5] BUCKINGHAM, A. D., and McLAUCHLAN, K. A., 1963, *Proc. chem. Soc.*, p. 144.
- [6] BANWELL, C. N., and SHEPPARD, N., 1962, *Disc. Faraday Soc.*, **34**, 115.
- [7] McCONNELL, H. M., 1957, *J. mol. Spectrosc.*, **1**, 11.
- [8] McCONNELL, H. M., 1959, *J. chem. Phys.*, **30**, 26.
- [9] HOFFMAN, R. A., 1958, *Mol. Phys.*, **1**, 326.
- [10] ACRIVOS, J. V., 1962, *Mol. Phys.*, **5**, 1.
- [11] DEWAR, M. J. S., and FAHEY, R. C., 1963, *J. Amer. chem. Soc.*, **85**, 2704.
- [12] BALDESCHWIELER, J. D., and RANDALL, E. W., 1963, *Chem. Rev.*, **63**, 81.
- [13] FREEMAN, R., 1960, *Mol. Phys.*, **3**, 435.
- [14] FREEMAN, R., and ANDERSON, W. A., 1962, *J. chem. Phys.*, **37**, 2053.
- [15] FREEMAN, R., and WHIFFEN, D. H., 1962, *Proc. phys. Soc., Lond.*, **79**, 794.
- [16] COHEN, A. D., FREEMAN, R., McLAUCHLAN, K. A., and WHIFFEN, D. H., *Mol. Phys.*, **7**, 45.
- [17] HOFFMAN, R. A., and GESTBLOM, B., 1963, *J. chem. Phys.*, **39**, 486.
- [18] ANDERSON, W. A., 1956, *Phys. Rev.*, **102**, 151.
- [19] NARASIMHAN, P. T., and ROGERS, M. T., 1960, *J. chem. Phys.*, **33**, 727.
- [20] ABRAHAM, R. J., and BERNSTEIN, H. J., 1961, *Canad. J. Chem.*, **39**, 216.
- [21] GUTOWSKY, H. S., and PORTE, A. L., 1961, *J. chem. Phys.*, **35**, 839.
- [22] McCONNELL, H. M., 1955, *J. chem. Phys.*, **23**, 2454.
- [23] HOFFMAN, R. A., and GRONOWITZ, S., 1960, *Arkiv. Kemi.*, **16**, 471.

Statistical mechanics of transport processes in adsorbed gases

by J. POPIELAWSKI and B. BARANOWSKI

Institute of Physical Chemistry, Polish Academy of Sciences, Warsaw, Poland

(Received 6 May 1964; revision received 29 June 1964)

The integro-differential equation for the singlet distribution function describing the non-uniform state of a monolayer of adsorbed gas mixture has been derived by applying to the Liouville equation the Kirkwood time-smoothing procedure. In this equation Boltzman and Fokker-Planck dissipation terms appear. The general equation of change of molecular properties has been further derived which reduces to the laws of conservation of mass, momentum and energy. The correlation of surface diffusion and viscosity phenomena is demonstrated.

1. INTRODUCTION

Transport processes in adsorbed gases, although well established experimentally [1-4], have not been treated by statistical mechanics so far. The phenomenological description of such processes as surface diffusion, thermal diffusion, migration in an electrical field and viscous flow for multi-component monolayers on homogenous and isotropic surfaces has been given previously [5-8]. We now present the derivation of a basic integro-differential equation for the singlet distribution function for a monolayer of rarefied two-component gas mixture adsorbed on a uniform solid by van der Waals forces (physical adsorption). We assume that the adsorbed gas molecules are located at a constant distance r_m from the solid surface, which corresponds to the minimum of the potential of adsorption forces, and are capable of random two-dimensional motion. We assume further that the adsorbed molecules possess translatory degrees of freedom in two dimensions only and interact by binary encounters. In the picture of physical adsorption presented above the periodic structure of a solid has been neglected. If the molecules of the solid could not leave their equilibrium positions, the non-uniform state of the adsorbed gas could be described by a two-dimensional Boltzmann equation. In such a case the underlying solid could affect the interaction forces of molecules adsorbed, but could not modify the general form of the Boltzmann equation. This however, is not the case for temperatures above 0°K . The molecules of a solid undergo thermal oscillations about their equilibrium positions and can interact with the adsorbed molecules. The situation is well illustrated by the figure.

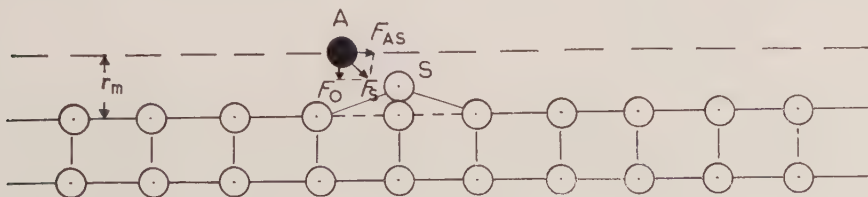


Figure 1.

The molecule of the solid S , which leaves its equilibrium position, acts on the adsorbed molecule A with the force \mathbf{F} . This force can be decomposed into two parts \mathbf{F}_{AS} and \mathbf{F}_0 . Force \mathbf{F}_0 , perpendicular to the surface, is compensated by the overall adsorption forces, thus only the force \mathbf{F}_{AS} , parallel to the solid surface, acts effectively on the adsorbed molecule. Summarizing the preliminary physical approximations of our treatment we can say that, for the adsorbed monolayer, two different interactions appear: a strong interaction with large momentum exchange between adsorbed molecules during binary encounters, and a weak interaction with a small momentum exchange between adsorbed molecules and the molecules of the underlying solid. We assume further that none of these interactions can lead to the desorption of the molecules adsorbed; thus the exchange of matter, momentum and energy with the neighbouring gas phase may be completely neglected. This assumption can be justified on the basis of comparison of the mean lifetime of adsorbed molecule on the solid surface with the mean time between surface collisions. The relaxation time for interaction of an adsorbed molecule with the solid substrate is assumed to be substantially shorter than the time between collisions for surface coverages for which the binary collision approximation can be applied. In the case of surface coverages of the order of a few per cent of the complete monolayer, for temperatures of order of $100\text{--}200^\circ\text{K}$, the simple kinetic theory of a two-dimensional gas leads to the mean time between collisions of order of $10^{-10}\text{--}10^{-11}$ sec. On the other hand the mean lifetime of a light adsorbed molecule has the order of magnitude of $10^{-5}\text{--}10^{-7}$ sec [9]. Thus the desorption of a molecule can be regarded as a relatively rare phenomenon, and the influence of the adsorption-desorption process on the transport processes within adsorbed layers may be neglected. Using the approximations presented above we are able to derive the integro-differential equation for the singlet distribution function by applying to the Liouville equation the Kirkwood time-smoothing procedure [10]. This equation can serve as the starting point for a detailed discussion of transport phenomena in the system considered, and makes possible the calculation of phenomenological coefficients on the basis of intermolecular forces.

2. DERIVATION OF BASIC EQUATION

We consider the non-uniform state of a physically adsorbed gas mixture in the conditions described above. The system considered contains K molecules of the solid, M_1 molecules of the first and M_2 molecules of the second gas adsorbed, thus we have:

$$K + M_1 + M_2 = N, \quad (1)$$

where N = number molecules of the system.

The non-uniform state of the system considered is most generally described by the Liouville equation:

$$\sum_{i=1}^N \left\{ \frac{\mathbf{p}_i}{m_i} \nabla_{\mathbf{r}_i} f^{(N)} + (\mathbf{X}_i + \mathbf{F}_i) \nabla_{\mathbf{p}_i} f^{(N)} \right\} + \frac{\partial f^{(N)}}{\partial t} = 0, \quad (2)$$

where $f^{(N)}$ = distribution function of N th order, \mathbf{p}_i = momentum of molecule i , m_i = mass of molecule i , \mathbf{X}_i = external force acting on molecule i , \mathbf{F}_i = internal force exerted on molecule i by other molecules of the system, \mathbf{r}_i = position vector of molecule i , t = time, $\nabla_{\mathbf{r}_i}$, $\nabla_{\mathbf{p}_i}$ = nabla operators acting on position and momentum coordinate of molecule i .

Now we adopt the time-smoothing method of Kirkwood [10], which makes it possible to obtain the equation for distribution functions of lower order from the Liouville equation. Defining the distribution function of n th order as:

$$f^{(n)}(\mathbf{p}, \mathbf{q}; t) = \int \dots \int f^{(N)}(\mathbf{p}, \mathbf{q}, \mathbf{P}, \mathbf{Q}; t) d\mathbf{P} d\mathbf{Q}, \quad (3)$$

where \mathbf{p}, \mathbf{q} denote momenta and position coordinates of n molecules in the system, while \mathbf{P}, \mathbf{Q} denote momenta and position coordinates of the remaining $N-n$ molecules, we introduce the time-smoothed functions:

$$\bar{f}^{(n)}(\mathbf{p}, \mathbf{q}; t) = \frac{1}{\tau} \int_0^\tau f^{(n)}(\mathbf{p}, \mathbf{q}; t+s) ds. \quad (4)$$

We then obtain in the usual way:

$$\frac{\partial \bar{f}_1^{(1)}}{\partial t} + \frac{\mathbf{p}_1}{m_1} \nabla_{\mathbf{r}_1} \bar{f}_1^{(1)} + \mathbf{X}_1 \nabla_{\mathbf{p}_1} \bar{f}_1^{(1)} = \nabla_{\mathbf{p}_1} \Omega_1^{(1)}, \quad (5)$$

where

$$\Omega_1^{(1)} = (M_1 - 1)\Omega_{11}^{(1)} + M_2\Omega_{12}^{(1)} + K\Omega_{1s}^{(1)}, \quad (6)$$

$$\begin{aligned} \Omega_{11}^{(1)} = & -\frac{1}{\tau} \int_0^\tau \int \dots \int \mathbf{F}_{11'}(\mathbf{R}_1, \mathbf{R}_{1'}) f^{(N)}(\mathbf{p}_1, \mathbf{R}_1, \mathbf{p}_{1'}, \mathbf{R}_{1'}, \mathbf{P}, \mathbf{Q}; t+s) \\ & \times d\mathbf{P} d\mathbf{Q} d\mathbf{p}_{1'} d\mathbf{R}_{1'} ds, \end{aligned} \quad (7)$$

$$\begin{aligned} \Omega_{12} = & -\frac{1}{\tau} \int_0^\tau \int \dots \int \mathbf{F}_{12}(\mathbf{R}_1, \mathbf{R}_2) f^{(N)}(\mathbf{p}_1, \mathbf{R}_1, \mathbf{p}_2, \mathbf{R}_2, \mathbf{P}, \mathbf{Q}; t+s) \\ & \times d\mathbf{P} d\mathbf{Q} d\mathbf{p}_2 d\mathbf{R}_2 ds, \end{aligned} \quad (8)$$

$$\begin{aligned} \Omega_{1s} = & -\frac{1}{\tau} \int_0^\tau \int \dots \int \mathbf{F}_{1s}(\mathbf{R}_1, \mathbf{R}_s) f^{(N)}(\mathbf{p}_1, \mathbf{R}_1, \mathbf{p}_s, \mathbf{R}_s, \mathbf{P}, \mathbf{Q}; t+s) \\ & \times d\mathbf{P} d\mathbf{Q} d\mathbf{p}_s d\mathbf{R}_s ds \end{aligned} \quad (9)$$

with: $\mathbf{F}_{11'}$ =force acting between two molecules of first adsorbed gas, \mathbf{F}_{12} =force acting between molecules of first and second adsorbed gas, \mathbf{F}_{1s} =force acting between the molecule of the first adsorbed gas and a molecule of underlying solid, $\mathbf{p}_1, \mathbf{R}_1$ =momentum and position coordinates of specified molecule 1 in the first adsorbed gas, $\mathbf{p}_2, \mathbf{R}_2$ =momentum and position coordinates of any molecule of the second adsorbed gas, and $\mathbf{p}_s, \mathbf{R}_s$ =momentum and position coordinates of a molecule in the underlying solid.

At this point a detailed specification of the averaging time is necessary. As stated above, we confine our treatment to the adsorption of rarefied gases in which only two-dimensional binary encounters can take place. The interaction of the adsorbed gas with the molecules of the underlying solid is assumed to be weak and not to affect the binary encounters between the molecules of adsorbed gas. Taking these remarks into account we choose the averaging time in such a manner that it includes the time of binary encounters between the adsorbed molecules τ_1 . The remaining part of the averaging time $\tau_s = \tau - \tau_1$ involves the interaction of an adsorbed molecule with the underlying solid. We assume that during the time

$\tau_1 \mathbf{F}_{1s} = 0$ and during the time τ_s , $\mathbf{F}_{11'} = \mathbf{F}_{12} = 0$. With this averaging time we are able to evaluate the integrals (7)–(9) in a way similar to that used by Rice and Alnatt [11] in the case of dense fluids. It can be shown that the integral $\nabla_{\mathbf{p}_1} \Omega_{11}^{(1)}$ takes the form of a two-dimensional Boltzmann collision integral:

$$\nabla_{\mathbf{p}_1} \Omega_{11}^{(1)} = \iint (f_1^{(1)*} f_{1'}^{(1)*} - f_1^{(1)} f_{1'}^{(1)}) q_{11'} db d\mathbf{p}_{1'}, \quad (10)$$

where

$$q_{11} = \left(\frac{\mathbf{p}_{1'}}{m_1} - \frac{\mathbf{p}_1}{m_1} \right) / \frac{1}{2} m_1$$

and b denotes the parameter of two-dimensional binary encounters, i.e. the distance between the axis moving with molecule 1, parallel to the relative momentum, and the asymptote of the relative momentum curve and $f_1^{(1)*}, f_{1'}^{(1)*}$ denote the distribution functions of molecules **1** and **1'** after encounter. In a quite similar way we obtain:

$$\nabla_{\mathbf{p}_1} \Omega_{12}^{(1)} = \iint (f_1^{(1)*} f_2^{(1)*} - f_1^{(1)} f_2^{(1)}) \mathbf{q}_{12} db d\mathbf{p}_2, \quad (11)$$

where

$$\mathbf{q}_{12} = \left(\frac{\mathbf{p}_2}{m_2} - \frac{\mathbf{p}_1}{m_1} \right) / \frac{m_1 m_2}{m_1 + m_2}.$$

The interaction of adsorbed molecule **1** with the underlying solid can be treated by the Brownian motion theory in which temperature T^s of the equilibrium environment of the molecule concerned can be safely identified with the temperature of the underlying solid. Thus we obtain after some calculations:

$$\Omega_{1s}^{(1)} = {}^1\langle \mathbf{F}_{1s} \rangle^0 f_1^{(1)}(\mathbf{p}_1, \mathbf{R}_1, t) + \zeta_{1s}^{(1)} \left\{ \frac{\mathbf{p}_1}{m_1} + kT^s \nabla_{\mathbf{p}_1} \right\} \bar{f}_1^{(1)}(\mathbf{p}_1, \mathbf{R}_1, t), \quad (12)$$

where

$${}^1\langle \mathbf{F}_{1s} \rangle^0 = \int \dots \int \mathbf{F}_{1s} {}^0 f^{(1/N)} d\mathbf{p}_s d\mathbf{R}_s d\mathbf{P} d\mathbf{Q}; \quad (13)$$

${}^0 f^{(1/N)}$ is the equilibrium relative distribution function

$$\begin{aligned} \zeta_{1s}^{(1)} &= \frac{1}{4kT^s} \int_{-\tau_s}^{+\tau_s} {}^1\langle F_s(t+s) F_{1s}^s \rangle^0 ds; \quad \mathbf{F}_{1s}^s = \sum_s \mathbf{F}_{1s}; \\ {}^1\langle F_{1s}(t+s) F_{1s}^s \rangle^0 &= \int \dots \int [F_{1s}(t+s) F_{1s}^s] {}^0 f^{(1/N)} d\mathbf{p}_s d\mathbf{R}_s d\mathbf{P} d\mathbf{Q}. \end{aligned} \quad (14)$$

The expression (12) has the form of the Fokker–Plank dissipation term. Introduction of expressions (10), (11) and (12) into equation (5) yields after the second averaging:

$$\begin{aligned} \frac{\partial \bar{f}_1^{(1)}}{\partial t} + \frac{\mathbf{p}_1}{m_1} \nabla_{\mathbf{R}_1} \bar{f}_1^{(1)} + \mathbf{X}_1 \nabla_{\mathbf{p}_1} \bar{f}_1^{(1)} - \nabla_{\mathbf{p}_1} \cdot \zeta_s^{(1)} \left\{ \frac{\mathbf{p}_1}{m_1} \bar{f}_1^{(1)} + kT^s \nabla_{\mathbf{p}_1} \bar{f}_1^{(1)} \right\} \\ = (M_1 - 1) \iint (\bar{f}_1^{(1)*} \bar{f}_{1'}^{(1)*} - \bar{f}_1^{(1)} \bar{f}_{1'}^{(1)}) \mathbf{q}_{11'} db d\mathbf{p}_{1'} \\ + M_2 \iint (\bar{f}_1^{(1)*} \bar{f}_2^{(1)*} - \bar{f}_1^{(1)} \bar{f}_2^{(1)}) \mathbf{q}_{12} db d\mathbf{p}_2, \end{aligned} \quad (15)$$

where

$$\zeta_s^{(1)} = k\zeta_{1s}^{(1)} = \frac{1}{4kT_s} \int_{-\tau_s}^{+\tau_s} {}^1\langle F_1^s(t+s)F_1^s \rangle^0 ds; \quad (16)$$

$\zeta_s^{(1)}$ is the friction coefficient.

In the derivation of equation (15) we have assumed that the mean force acting on molecule 1 obeys the equation

$${}^1\langle F_1^s \rangle^0 = k {}^1\langle F_{1s} \rangle^0 = 0 \quad (17)$$

and that

$$\overline{f^{(1)}f^{(1)}} = \bar{f}^{(1)}\bar{f}^{(1)}.$$

Introducing the generic distribution functions

$$f_1 = M_1 \bar{f}_1^{(1)}, \quad f_2 = M_2 \bar{f}_2^{(1)} \quad (18)$$

and the new variables

$$\mathbf{p}_1, \mathbf{R}_1 \rightarrow \mathbf{c}_1, \mathbf{r}, \quad \mathbf{p}_2, \mathbf{R}_2 \rightarrow \mathbf{c}_2, \mathbf{r}, \quad (19)$$

where \mathbf{c}_1 denotes the two dimensional velocity of the molecule of the first adsorbed gas, \mathbf{c}_2 denotes the two-dimensional velocity of the molecule of the second adsorbed gas, \mathbf{r} denotes the two-dimensional radius vector of any adsorbed molecule, we can write equation (15) in the more suitable form

$$\begin{aligned} & \frac{\partial f_1}{\partial t} + \mathbf{c}_1 \nabla_{\mathbf{r}} f_1 + \mathbf{Y}_1 \nabla_{\mathbf{c}_1} f_1 - \nabla_{\mathbf{c}_1} \beta_1 \left\{ \mathbf{c}_1 f_1 + \frac{kT_s}{m_1} \nabla_{\mathbf{c}_1} f_1 \right\} \\ &= \iint (f_1^* f_{1'}^* - f_1 f_{1'}) g_{11'} db d\mathbf{c}_{1'} + \iint (f_1^* f_2^* - f_1 f_2) g_{12} db d\mathbf{c}_2, \end{aligned} \quad (20)$$

where

$$\mathbf{Y}_1 = \frac{\mathbf{X}_1}{m_1}, \quad \beta_1 = \frac{\zeta_s^{(1)}}{m_1}; \quad (21)$$

g_{11} denotes the relative velocity of molecules 1 and 1' and g_{12} the relative velocities of molecules 1 and 2.

In a quite similar way we can obtain the equation for the distribution function f_2 of the second component. The functions f_1 and f_2 are normalized as follows:

$$\int f_1 d\mathbf{c}_1 = n_1; \quad \int f_2 d\mathbf{c}_2 = n_2, \quad (22)$$

where n_1 and n_2 denote the surface number densities of the first and second components of adsorbed gas respectively. Equation (20) can be solved by the Chapman-Enskog perturbation method (12). This solution renders possible the detailed discussion of such phenomena as surface viscous flow, diffusion, thermal diffusion and migration in external fields.

3. EQUATION OF CHANGE OF MOLECULAR PROPERTIES

We now present a discussion of some of the consequences of equation (20) which can be drawn without detailed solution. The notation used in the Chapman-Cowling monograph (12) will be followed throughout this section. Let Φ_1 denote any molecular property dependent on the molecular velocity \mathbf{c}_1 .

Φ_1 can be a scalar, vector or tensor quantity. Multiplying equation (20) by the quantity Φ_1 , performing integration over the whole velocity space and introducing the peculiar velocity of the first component \mathbf{C}_1 we obtain:

$$\begin{aligned} & \frac{Dn_1\Phi_1}{Dt} + n_1\Phi_1\nabla_{\mathbf{r}}\cdot\mathbf{c}_0 + \nabla_{\mathbf{r}}\cdot n_1\overline{\Phi_1\mathbf{C}_1} - n_1 \\ & \times \left\{ \frac{D\Phi_1}{Dt} + \overline{\mathbf{C}_1\cdot\nabla_{\mathbf{r}}\Phi_1} + \left(\mathbf{Y}_1 - \frac{D\mathbf{c}_0}{Dt} \right) \cdot \nabla_{\mathbf{c}_1}\Phi_1 \right. \\ & \left. + \nabla_{\mathbf{c}_1}\Phi_1\cdot\nabla_{\mathbf{r}}\mathbf{c}_0 + \overline{\beta_1(c_0 + C_1)}\cdot\nabla_{\mathbf{c}_1}\Phi_1 - \frac{\beta_1 k T^s}{m_1} \nabla_{\mathbf{c}_1}^2 \Phi_1 \right\} = n_1 \Delta \Phi_1, \end{aligned} \quad (23)$$

where

$$\begin{aligned} n_1 \Delta \Phi_1 &= \iiint \Phi_1 (f_1^* f_1'^* - f_1 f_1') g_{11} db d\mathbf{c}_1 d\mathbf{c}_1 \\ &+ \iint \Phi_1 (f_1^* f_2^* - f_1 f_2) g_{12} db d\mathbf{c}_2 d\mathbf{c}_1; \quad \Phi_1 = \frac{1}{n_1} \int \Phi_1 f_1 d\mathbf{c}_1, \end{aligned} \quad (24)$$

$$\frac{D}{Dt} = \frac{\partial}{\partial t} + u_0 \frac{\partial}{\partial x} + w_0 \frac{\partial}{\partial y};$$

u_0, w_0 are components of the mass velocity \mathbf{c}_0 , x_1, y are components of the radius vector \mathbf{r} .

Equation (23), similarly as in the case of three-dimensional gases, can be reduced to the hydrodynamic equations by taking into account the conservation of mass, momentum and energy during binary encounters. Introducing the quantity $\Phi_1 = m_1$ into equation (23) we can obtain the law of mass conservation in the same form as in the case of three-dimensional gases. Introducing the quantity $\Phi_1 = m_1 \mathbf{C}_1$ into equation (23) we obtain:

$$\begin{aligned} & \frac{D\rho\bar{\mathbf{C}}_1}{Dt} + \rho_1\bar{\mathbf{C}}_1\nabla_{\mathbf{r}}\cdot\mathbf{c}_0 + \nabla_{\mathbf{r}}\cdot(\rho_1\bar{\mathbf{C}}_1\mathbf{C}_1) - \rho_1\left(\mathbf{Y}_1 - \frac{D\mathbf{c}_0}{Dt}\right) \\ & + \rho_1\bar{\mathbf{C}}_1\cdot\nabla_{\mathbf{r}}\mathbf{c}_0 + \rho_1\beta_1\mathbf{c}_0 + \rho_1\beta_1\bar{\mathbf{C}}_1 = n_1\Delta m_1\bar{\mathbf{C}}_1. \end{aligned} \quad (25)$$

A similar equation can be derived for the second component. Adding these two equations and taking into account the momentum conservation during a binary collision we can express the law of momentum conservation for a two-component adsorbed gas in the following form:

$$\rho \frac{D\mathbf{c}_0}{Dt} = -\nabla_{\mathbf{r}}\cdot\boldsymbol{\pi} + \rho_1\mathbf{Y}_1 + \rho_2\mathbf{Y}_2 + \beta_1\mathbf{J}_1 + \beta_2\mathbf{J}_2 + (\rho_1\beta_1 + \rho_2\beta_2)\mathbf{c}_0, \quad (26)$$

where

$$\mathbf{J}_1 = \rho_2\mathbf{C}_1; \quad \mathbf{J}_2 = \rho_2\mathbf{C}_2; \quad \mathbf{J}_1, \mathbf{J}_2$$

are surface diffusion flows of the first and second components respectively and $\boldsymbol{\pi}$ is the surface pressure tensor, corresponding to the pressure tensor of a three-dimensional gas.

In equation (26) new terms appear in comparison to the corresponding expression for a three-dimensional gas [12]. These new terms describe the flow of momentum from the monolayer of adsorbed gas to the underlying solid $(\rho_1\beta_1 + \rho_2\beta_2)\mathbf{C}_2$ and a direct interaction between the diffusion and viscosity phenomena in the system considered $(\beta_1\mathbf{J}_1 + \beta_2\mathbf{J}_2)$. In the phenomenological

theory presented previously [7] the direct coupling of diffusion and viscosity phenomena had not been taken into account. In the case of a steady unidimensional flow of one-component adsorbed gas equation (26) takes the form

$$\frac{\partial \pi}{\partial x} + \rho \beta \mathbf{u}_0 = 0, \quad (27)$$

where π is the hydrostatic surface pressure.

Equation (27) has been already postulated, on the ground of physical arguments by Babbitt [13] for the description of the flow of adsorbed gases in microporous media. This author has shown that it fits experimental data reasonably well. Equation (27) has also been obtained in the phenomenological theory [7].

If the quantity $\Phi = \frac{1}{2} m_1 C_1 = E$ is introduced into equation (23) the following equation can be obtained:

$$\begin{aligned} \frac{Dn_1 \bar{E}_1}{Dt} + n_1 \bar{E}_1 (\nabla_{\mathbf{r}} \cdot \mathbf{c}_0) + \nabla_{\mathbf{r}} \cdot \mathbf{J}_u^1 - \rho_1 \mathbf{C}_1 \left(\mathbf{Y}_1 - \frac{D\mathbf{c}_0}{Dt} \right) \\ + \rho_1 \overline{\mathbf{C}_1 \mathbf{C}_1} : \nabla_{\mathbf{r}} \mathbf{c}_0 + \rho_1 \beta_1 (\mathbf{C}_1 \cdot \mathbf{c}_0) + \rho_1 \beta_1 \overline{\mathbf{C}_1 \cdot \mathbf{C}_1} - 2n_1 \beta_1 k T^s = n_1 \Delta \bar{E}_1, \end{aligned} \quad (28)$$

where $\mathbf{J}_u^1 = n_1 \mathbf{E}_1 \mathbf{C}_1$. A similar equation can be obtained for the second component. Adding these two equations and taking into account the conservation of energy during a binary encounter we can write the equation of energy conservation for a two-component adsorbed gas:

$$\begin{aligned} \frac{Dn\bar{E}}{Dt} = -n\bar{E} \nabla_{\mathbf{r}} \cdot \mathbf{c}_0 - \nabla_{\mathbf{r}} \cdot \mathbf{J}_u + \mathbf{J}_1 \cdot (\mathbf{Y}_1 - \beta_1 \mathbf{c}_0) + \mathbf{J}_2 \cdot \\ \times (\mathbf{Y}_2 - \beta_2 \mathbf{c}_0) - \boldsymbol{\pi} : \nabla_{\mathbf{r}} \mathbf{c}_0 + 2\beta_1 n_1 (\bar{E}_1 - k T^s) + 2\beta_2 n_2 (\bar{E}_2 - k T^s), \end{aligned} \quad (29)$$

where

$$\mathbf{J}_u = \mathbf{J}_u^1 + \mathbf{J}_u^2; \quad n\bar{E} = n_1 \bar{E}_1 + n_2 \bar{E}_2.$$

In equation (29) terms appear describing the flow of energy from the monolayer of adsorbed gas to the underlying solid. The interpretation of these terms is particularly clear in the case of a one-component adsorbed gas, where the equation of energy conservation takes the form:

$$\frac{DnkT}{Dt} = -nkT \nabla_{\mathbf{r}} \cdot \mathbf{c}_0 - \boldsymbol{\pi} : \nabla_{\mathbf{r}} \mathbf{c}_0 - \nabla_{\mathbf{r}} \cdot \mathbf{J}_u - 2nk\beta(T - T^s), \quad (30)$$

where the kinetic temperature of two-dimensional gas $\bar{E} = kT$ has been introduced. The term $-2nk\beta(T - T^s)$ describes the flow of energy per unit surface area from adsorbed gas to the underlying solid. It appears that this flow is directly proportional to the difference between the kinetic temperature of the monolayer and the temperature of the solid.

The considerations given above can be very easily generalized to monolayers of multi-component adsorbed gases.

4. DISCUSSION

In the above treatment we assume a strong interaction between the adsorbed molecules, that is, an intensive momentum exchange during surface binary encounters, and weak interactions, corresponding to a small momentum exchange, between adsorbed molecules and the underlying solid. The situation described

here is somewhat similar to that discussed by Rice and Allnatt [11] in the case of dense fluids. The application of the Kirkwood time-smoothing procedure to the Liouville equation for the system considered makes it possible to obtain an integro-differential equation for the singlet distribution function, in which both the Fokker-Planck and Boltzmann dissipation terms appear [20].

The general equation of change of molecular properties has been derived and it has been shown that this equation can be reduced to the conservation laws of mass, momentum and energy. It appears that the law of momentum conservation has an equivalent form to this discussed in the phenomenological theory [5, 7] only for a one-component adsorbed gas. The form of momentum conservation law for a two-component system clearly demonstrates the connection between the surface diffusion and viscosity phenomena. This connection will be fully discussed later on the basis of the solution of the integro-differential equation for the singlet distribution function (20) by the Chapman-Enskog perturbation method.

The interaction of adsorbed gas molecules with the underlying solid in the course of surface flow is described by friction coefficients β_1, β_2 . These can be calculated by approximate methods elaborated by Kirkwood [10] and Kirkwood *et al.* [14], and compared with the experimental data for the flow of adsorbed gases in microporous media. A detailed discussion of friction coefficients will be presented later.

REFERENCES

- [1] CARMAN, P. C., 1956, *The Flow of Gases Through Porous Media*, (London: Butterworths Scientific Publications)
- [2] TIMOFEEV, D. P., 1960, *Uspekhi Khimi*, **20**, 404.
- [3] HAUL, R. A. W., 1954, *Naturwissenschaften*, **41**, 255.
- [4] BARRER, R. M., and STRACHAN, E., 1955, *Proc. roy. Soc. A*, **231**, 52.
- [5] BARANOWSKI, B., and POPIELAWSKI, J., 1962, *Bull. Polon. Acad. Sci.*, ser. sci. chem., **10**, 445.
- [6] BARANOWSKI, B., and POPIELAWSKI, J., 1963, *Bull. Polon. Acad. Sci.*, ser. sci. chim., **11**, 33.
- [7] BARANOWSKI, B., and POPIELAWSKI, J., 1963, *Bull. Polon. Acad. Sci.*, ser. sci. chim., **11**, 39.
- [8] BARANOWSKI, B., and POPIELAWSKI, J., 1963, *Bull. Polon. Acad. Sci.*, ser. sci. chim., **11**, 253.
- [9] BOER DE, J. H., 1953, *The Dynamical Character of Adsorption* (Oxford: University Press).
- [10] KIRKWOOD, J. G., 1946, *J. chem. Phys.*, **14**, 180.
- [11] RICE, S. A., and ALLNATT, A. R., 1961, *J. chem. Phys.*, **34**, 2144.
- [12] CHAPMAN, S., and COWLING, T. G., 1960, *The Mathematical Theory of Non-uniform Gases* (Cambridge: University Press).
- [13] BABBITT, J. D., 1951, *Canad. J. Phys.*, **29**, 437.
- [14] KIRKWOOD, J. G., BUFF, F. P., and GREEN, M. S., 1949, *J. chem. Phys.*, **17**, 988.

The influence of substitution on CH.CF and CF.CF coupling constants

by R. J. ABRAHAM and L. CAVALLI†

The Robert Robinson Laboratories, University of Liverpool,
Oxford Street, Liverpool 7

(Received 14 August 1964)

The dependence of the coupling constants in CH.CF and CF.CF fragments on the electronegativities of the substituents are investigated. J_{AV}^{HF} obeys the equation $J_{AV}^{HF} = 53.03 - 3.38 \sum E$, where $\sum E$ is the sum of the electronegativities of the first atom of the remaining substituents, very closely. J_{AV}^{FF} follows the equation $J_{AV}^{FF} = 91.4 - 6.15 \sum E$ but only approximately. Consideration of these equations with that previously obtained for J_{AV}^{HH} shows that for highly electronegative substituents all three couplings decrease to zero. Thus although this limit cannot be reached for those couplings involving hydrogen, due to the low electronegativity of hydrogen, the 'peculiarly small' CF.CF couplings are shown to be the result of merely the high electronegativity of fluorine plus the relative ease of obtaining perfluorinated ethanes. Furthermore, the temperature dependence of the observed F-F couplings in some unsymmetrically substituted ethanes is shown to be not primarily due to the changing populations of the rotational isomers but due to the change in J^{FF} with temperature. This is not the case for the analogous H-H couplings, but may be so for the H-F couplings.

1. INTRODUCTION

The influence of the electronegativity of the substituents on the CH.CH coupling constant in substituted ethanes was originally discovered by Glick and Bothner-By [1]. Many authors extended their measurements and recently Banwell and Sheppard [2] from a consideration of the collected data in ethyl compounds, and Abraham and Pachler [3] using all types of CH.CH fragment, independently derived two virtually identical equations relating the average coupling constant to the electronegativity of the substituents: this can be written as:

$$J_{AV} = 18.0 - 0.80 \sum E, \quad (1)$$

where J_{AV} is the coupling constant which would be observed if all the rotational isomers of the ethane had equal free energies, and $\sum E$, is the sum of the Huggins electronegativities [4] of the first atom of all the substituent groups on the C.C fragment considered. This equation is obeyed to 0.3 c.p.s. over the entire range of J_{AV} (which however is not very large, *ca.* 4–8 c.p.s.), and thus provides a base from which all CH.CH couplings can be considered. Furthermore, such equations are of some theoretical significance in that any electronegativity effect must operate through bonds and therefore will only affect those couplings which are transmitted through bonds. This is known to be the case for CH.CH

† Society Edison Settore Chimico, Laboratorio Ricerche, Bollate, Milano, Italy.

couplings, but the mechanism of CH.CF and particularly CF.CF couplings is in doubt. Thus the validity or otherwise of a simple electronegativity relationship will be of some assistance in assessing the coupling mechanisms.

Recently Ng and Sederholm [5] have suggested that CF.CF couplings obey an electronegativity relationship, but much of their data is not unambiguous. CH.CF couplings have not been considered to date. Our attention was drawn to these problems during a study of CH.CF couplings in some substituted ethanes [6].

It is the purpose of this article to consider in the light of all acceptable data, the validity or otherwise of an equation of the form 1 for CH.CF and CF.CF coupling constants.

It is well known that CH.CH, CH.CF and CF.CF couplings in substituted ethanes are all dependent on the magnitude of the dihedral angle between the two C-X bonds, though the nature of this dependence is not known for the couplings involving fluorine. Thus to obtain a significant correlation of J versus the substituents this dependence must be eliminated, either by measuring J for a constant dihedral angle (a procedure which is mainly used in rigid cyclic systems), or by obtaining J_{AV} . Thus, considering now only CH.CF couplings, this is obviously the measured coupling in molecules of the type CH_3CFXY or CF_3CHXY . J_{AV} can also be derived by following the treatment given in reference [3] for $\text{XCH}_2\text{CH}_2\text{Y}$ compounds, for $\text{CF}_2\text{X}.\text{CH}_2\text{Y}$ systems, provided that all the vicinal coupling constants in these A_2B_2 type spectra can be deduced. J_{AV} may also be obtained from the relationship $J_{AV} = \frac{1}{3}(J_t + 2J_g)$ in those compounds for which $J_t(\text{trans})$ and $J_g(\text{gauche})$ have been found. As we shall see, these are only unambiguously obtained by direct measurements on the compound at such low temperatures that the rate of interconversion of the isomers is negligible. Finally, it may be possible to deduce by other measurements when the individual rotational isomers have equal energies. J_{AV} will then be the measured coupling. This was the case for the $\text{CH}_2\text{F}.\text{CH}_2\text{X}$ ($\text{X} = \text{Cl}, \text{Br}$) compounds shown in table 1 in which that value of J_{HF} is given for $L = (J_{HH} - J'_{HH}) = 0$.

These methods of obtaining J_{AV} have been stressed because J_{AV} is *not* in general the observed coupling in an unsymmetrically substituted ethane which should not be used for such correlations, e.g. Ng and Sederholm [5] take J_{AV}^{FF} in $\text{CF}_2\text{Br}.\text{CFHCl}$ to be the mean of the two CF.CF couplings (they are both 18 c.p.s.). However, the unequal free energies of the rotational isomers in this compound are clearly demonstrated by the existence of two very different CH.CF couplings of 3.5 and 6.3 c.p.s. respectively [7]. A large number of the compounds which Ng and Sederholm have used suffer from this defect, which is the reason for giving the CF.CF couplings here.

2. RESULTS AND DISCUSSION

The values of J_{AV} and the method by which they have been obtained are given in tables 1 and 2 and they are plotted against the sum of the electronegativities of the first atom of the four remaining substituent groups in the CH.CF and CF.CF fragments in figures 1 and 2. A comparison of figures 1 and 2 and equation (1) is most illuminating. Figure 1 demonstrates very clearly

Compound	J_{AV} (c.p.s.)	Obtained from	Reference
CH ₃ .CH ₂ F	25.2	Observed coupling	[8,9]
CH ₃ .CHF ₂	20.8	"	[8]
CH ₃ .CFCl.CH ₂ Cl	18.4	"	[10]
CH ₃ .CF ₂ .CH ₂ Cl	17.7	"	[10]
CH ₃ .CF ₂ Br	15.9	"	[8]
CH ₃ .CF ₂ Cl	15.0	"	[8]
(CF ₃ .CH ₂) ₂ Hg	15	"	[11]
CF ₃ .CH ₃	12.7	"	[8]
CF ₃ .CH ₂ .CH ₃	10.5	"	[8]
[CF ₃ .(CH ₂) ₃] ₂	10.4	"	[8]
CF ₃ .CH ₂ .CF ₃	9.17	"	[8]
CF ₃ .CH ₂ Br	8.92	"	[8]
CF ₃ .CH ₂ Cl	8.41	"	[8]
CF ₃ .CFH ₂	7.98	"	[8]
CF ₃ .CHCl.CF ₃	5.93	"	[8]
CF ₃ .CF ₂ H	2.60	"	[8]
CF ₂ Cl.CH ₂ Cl	9.5	$N\ 22.0; L-9$	[12]
CF ₂ Br.CH ₂ Br	10.6	$N\ 26.2; L-15$	[12]
CF ₃ .CF ₂ .CF ₂ .CH ₂ I	13.5	$N\ 34.6; L-23.0$	[12]
CH ₂ Cl.CH ₂ F	17.5	J_{HF} for $L=0$	[6]
CH ₂ Br.CH ₂ F	19.3	"	[6]
CF ₃ .(CF ₂) ₅ .CF ₂ H	3	Observed coupling	[29]
CF ₃ .CFH.CF ₃	5.5	"	[29]
(CF ₃) ₃ CH	7	"	[29]

Table 1. CH.CF coupling constants in various compounds.

Compound	J_{AV} (c.p.s.)	Obtained from	Reference
(CF ₃ CFH) ₂ Hg	17	Observed coupling	[11]
CF ₃ CFH ₂	15.3	"	[8]
(CF ₃) ₂ CFI	12.4	"	[13]
CF ₃ .CFI.CF ₂ Cl	11.8	"	[13]
(CF ₃) ₂ .CF.CF:(CF ₃) ₂	9.0	"	[13]
(CF ₃) ₂ .CFBr	8.7	"	[13]
CF ₃ CFCIBr	7.8	"	[7]
(CF ₃) ₂ CF.CH:CHF	7.6	"	[27]
(CF ₃) ₂ CFCI	6.4	"	[13]
CF ₃ .CFCI ₂	5.5	"	[7]
CF ₃ .CF ₂ I	4.6	"	[14]
(CF ₃) ₃ CF	4.0	"	[15]
CF ₃ .CF ₂ H	2.8	"	[8]
CF ₃ .CF ₂ Cl	1.6	"	[5]
CF ₃ .CF ₂ .CO ₂ H	1.48	"	[15, 16]
CF ₃ .CF ₂ .CF ₂ I	0.8	"	[13]
CF ₃ .CF ₂ .CF ₃	0.7	"	[14]
CF ₂ Br.CF ₂ Br	7.25	$N\ 13.1, L\ 4.2$	[17]
CF ₂ Cl.CF ₂ Cl	4.63	$N\ 7.4; L\ 5.5$	[17]
CF ₂ I.CF ₂ Cl	8.2	$N\ 14.6, L\sim 5$	[17]
CF ₃ .CFH.CF ₃	11	Observed coupling	[29]

Table 2. CF.CF coupling constants in various compounds.

that J_{AV}^{HF} in any CH.CF fragment is linearly dependent on the sum of the electronegativities of the substituents as is J_{AV}^{HH} . A least mean squares fit of all the points in figure 1 gives the equation:

$$J_{AV}^{HF} = 53.03 - 3.38 \sum E. \quad (2)$$

The mean deviation from equation (2) is 1.3 c.p.s. over a range of 22 c.p.s. This

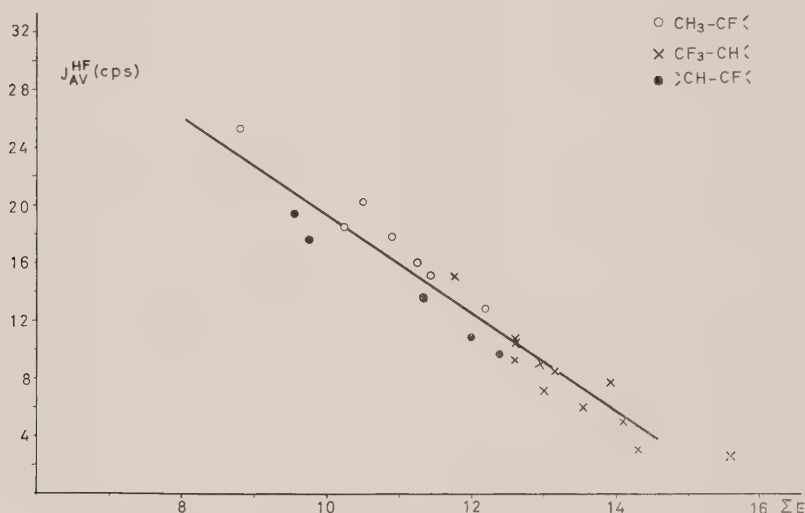


Figure 1. The CH.CF coupling constant J_{AV}^{HF} versus the sum of the electronegativities of the four remaining substituents.

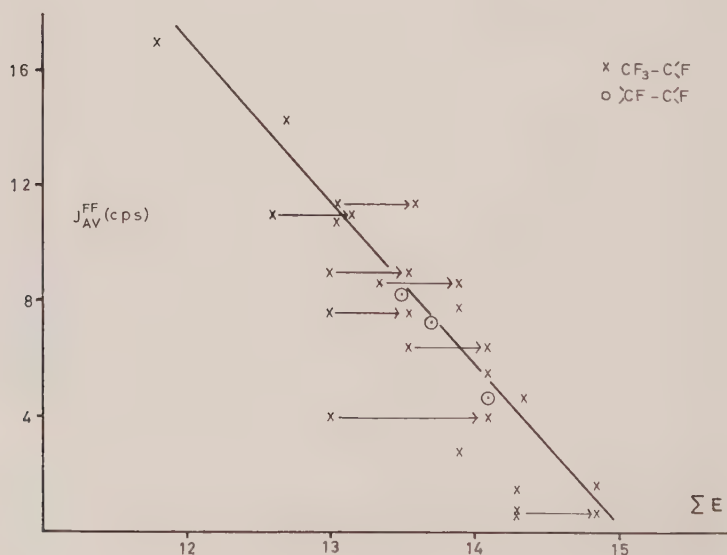


Figure 2. The CF.CF coupling constant J_{AV}^{FF} versus the sum of the electronegativities of the four remaining substituents.

large range of values of J_{AV}^{HF} is in marked contrast to the behaviour of J_{AV}^{HH} which changes only slightly with the electronegativity of the substituents. In order to compare equations (1) and (2) directly, it is convenient to re-write equation (1) in the same form as (2), in which it becomes:

$$J_{AV}^{HH} = 14.5 - 0.80 \sum E, \quad (3)$$

where now $\sum E$ is the sum of the electronegativities of the four remaining substituents in the CH.CH fragment.

It can be seen from equations (2) and (3) that the dependence of J_{AV}^{HF} on $\sum E$ is about four times that of J_{AV}^{HH} . However, this should not obscure the overall similarity of behaviour of the two cases, which demonstrates as expected theoretically the dominance of the through bond mechanism for these couplings.

It is also of interest to consider the results of variable temperature measurements of J^{HF} here. The detailed analysis of the J versus temperature curve enables the couplings of the individual isomers to be obtained and from these J_{AV} . This procedure necessarily makes a number of assumptions and the accuracy of the parameters obtained from such treatments are now seriously in doubt. The validity or otherwise of these underlying assumptions can be seen from the following argument.

Consider the case of a substituted ethane with only two distinct isomers, e.g. $\text{CHX}_2.\text{CFY}_2$. The J versus temperature curve will always have a finite slope except at $T=0$ or ∞ . As J_{AV} is by definition the coupling at infinite temperature any J versus temperature measurement will give one limit to J_{AV} (an upper or lower limit depending on whether the observed coupling is increasing or decreasing with temperature). This is not rigorously true for less symmetric molecules having three distinct isomers as the slope of the curve can change sign at finite temperatures, but is probably correct for those cases in which the energy differences between the isomers are relatively small (< 1 kcal/mole).

The values of J_{AV}^{HF} in $\text{CHCl}_2.\text{CFCl}_2$ and $\text{CHCl}_2.\text{CF}_2\text{Cl}$ are both 6.7 c.p.s. (from J_g and J_t values of 1.00 and 18.20 [18, 19] and 5 and 10 c.p.s. [20] respectively). These agree moderately well with equation (2) which predicts values of 9.0 and 7.2 c.p.s. respectively. However, the coupling in $\text{CHCl}_2.\text{CHFCl}$ is entirely anomalous. Even omitting the detailed analysis of this J versus temperature curve, which is a complex five-parameter analysis [19], the observed J^{HF} coupling decreases from 9.9 c.p.s. at 212°K to 8.4 c.p.s. at 470°K. Thus J_{AV}^{HF} may be expected to be less than 8.4 c.p.s. The predicted value from equation (2) is 13.6 c.p.s. The reason for this anomaly is not clear, though this may be a case in which the slope of the J versus temperature curve changes sign at higher temperatures. Alternatively this may be due to a change in the values of J_t and J_g with temperature (see below).

In the case of CF.CF couplings, figure 2 demonstrates quite clearly the much less significant correlation of J_{AV}^{FF} with the electronegativity of the substituents. This marked difference between F-F and F-H and H-H couplings strongly suggests that additional coupling mechanism are present in the former which do not obey the simple electronegativity rule. This does not necessarily mean that this additional mechanisms is "through space" as has been suggested [15].

The line shown in figure 2 (which is not the result of a least mean squares treatment) has the equation:

$$J_{AV}^{FF} = 91.4 - 6.15 \sum E \quad (4)$$

Again there is an increase in the magnitude of the dependence on the substituent electronegativity, which is now about twice that of J_{AV}^{HF} and almost ten times that of J_{AV}^{HH} . This large dependence on the electronegativity does seriously affect the discussion of such couplings, e.g. Petrakis and Sederholm report the 'anomalously high' value of J_{AV}^{FF} in $(CF_3)_3CF$ of 4.0 c.p.s. [15]. From figure 2 this is seen to be an anomalously low value. The reason for this discrepancy is that in reference [15] the coupling in $(CF_3)_3CF$ was compared with other perfluorinated hydrocarbons such as perfluoropropane ($J_{AV} = 0.7$) and perfluoroethane ($J_{AV} = 0$). However, in figure 2 this coupling is considered as that in a



fragment, in which J_{AV}^{FF} is much higher. It is of interest to note that CF_3 groups in fluorinated benzenes for example behave very similarly to a chlorine substituent, both as regards their effects on fluorine coupling constants and chemical shifts [13]. If the electronegativity of the CF_3 group is taken as that of chlorine (3.15) then this compound and indeed many of the anomalously low couplings now fall into line. This is shown in figure 2 by the horizontal arrows. The argument against this concept is that such group electronegativities (which are often defined and used in very similar measurements) were not necessary for H-H and H-F couplings.

It is of some interest to consider the electronegativity relationships of the three couplings in more detail. As an illustration, consider the various values of J_{AV} in CH_2F , CH_2F . (These will be equal to the observed couplings in CH_3CHF_2 for J_{AV}^{HH} and J_{AV}^{HF} .) Thus J_{AV}^{HH} equals 4.7 c.p.s. and for each replacement of a hydrogen by a fluorine atom it decreases by 1.4 c.p.s. (from equation (1)). Similarly J_{AV}^{HF} equals 20.8 c.p.s. and decreases by 5.8 c.p.s. for each replacement of H by F; and finally J_{AV}^{FF} would be expected to be *ca.* 37.3 c.p.s. and to decrease by *ca.* 10.5 c.p.s. for each replacement of H by F. Thus in the hypothetical case of a substituted ethane with substituents of such electronegativity that the total electronegativity of the substituents equals that in say, a perfluorinated hydrocarbon such as perfluoropropane, then J_{AV}^{HH} equals 0.0 c.p.s., J_{AV}^{HF} 1.5 c.p.s. and J_{AV}^{FF} 2.3 c.p.s. (These are obtained from the CH_2F , CH_2F values by replacing three hydrogens by fluorine and one by carbon, which has *ca.* one third the effect of a replacement of H by F.) The observed coupling in perfluoropropane is in fact 0.7 c.p.s., however, this does not affect the importance of this illustration, which is that *both* H-H and H-F couplings behave in precisely the same manner as the F-F couplings in that J_{AV} would approach zero for the same value of $\sum E$. (Of course this cannot be realized in practice as there must be at least two hydrogen substituents in a substituted ethane to measure the H-H coupling.) Thus the 'peculiarity' of the very small vicinal F-F couplings in substituted ethanes, which has been repeatedly commented upon, is in fact

nothing more than a consequence of the strongly electronegative character of the fluorine atom combined with the relative ease of obtaining perfluorinated hydrocarbons. Furthermore it is thus not necessary to invoke any additional coupling mechanism than those present in H-H and H-F couplings to explain this phenomenon alone [21].

This similarity in the behaviour of the three couplings with increasing $\sum E$ combined with the theoretical predictions that CH.CH couplings are always positive [22], also suggests that in all three cases, J_g and J_t decrease to small values when the electronegativity of the substituents is sufficiently large. This precludes the idea that J_g and J_t in CF.CF couplings are large but of opposite signs and thus cancel. Probably, as Harris and Sheppard have suggested [17], the true answer may well be a combination of both factors. This problem can only be resolved by the unambiguous determination of J_t and J_g .

Finally, it is of interest to consider the results of the variable temperature measurements of J^{FF} . Recently Brey and Ramey [23] have shown that J_{AV}^{FF} itself changes with temperature, e.g. in CF_3CFCl_2 , J_{AV}^{FF} decreases from 6.1 to 5.6 c.p.s. in going from -65 to $+90^\circ C$. Similarly in $CF_3.CF_2.CO_2H$ the coupling of 1.7 c.p.s. at -29° decreases to 1.3 c.p.s. at $85^\circ C$. These changes are small but are significant when compared with the observed change in J^{FF} with temperature in an unsymmetrical ethane. Thus they suggest that the values of J_g and J_t obtained from the detailed analysis of the J versus temperature curve (which analyses implicitly assume temperature independent J_g and J_t 's) are invalid. It is of interest to note here that in contrast J_{HH}^{AV} in substituted ethanes does not change with temperature in the few compounds for which it has been measured; e.g. the couplings in ethyl nitrate [24], 1,1-dichloroethane [25] and $CH_3.CHCl.CCl_3$ [25] show no detectable variation with temperature. No case of the temperature dependence of J_{AV}^{HF} has so far been reported and this would be of some significance in this context.

Brey and Ramey obtained considerable support for their argument in a study of $CF_2Br.CFBrCl$ [23]. The spectrum of this compound in $CFCl_3$ solution at $-120^\circ C$ consists of the spectra of the three rotational isomers, and this gives directly the coupling constants and relative populations (and therefore energy differences) of these isomers. These coupling constants were very different from those obtained by a five parameter analysis of the temperature dependence of the observed coupling constant at high temperatures [19]. However, Newmark and Sederholm [26] in a detailed study of the low and high temperature spectra in $CFCl_3$ solution concluded that the high temperature results were consistent with the low temperature measurements.

The low and high temperature spectra of this compound can be immediately checked by considering the observed couplings in the light of the discussion given previously for H-F couplings. There are two CF.CF couplings in $CF_2Br.CFBrCl$, but as only their sum can be obtained for all the isomers, we will consider here their average. This has the values of 13.3, 14.0 and 20.8 c.p.s. for the three isomers which we will label a , b and c . The assignment of the couplings to the isomers is not unambiguous but the energy differences are known uniquely and are $E_a 0$, $E_b 310$ and $E_c 750$ cal/mole [26]. The most stable isomer has the smallest coupling and therefore the observed coupling at high temperatures should increase uniformly from 13.3 c.p.s. to, at infinite temperatures,

J_{AV}^{FF} , which is 16.0 c.p.s. However, the observed coupling in $CFCl_3$ solution is 13.95 c.p.s. at 242°K which *decreases* to 13.70 c.p.s. at 371°K. It is clear that there is a considerable discrepancy between the two sets of results. This discrepancy is masked by the small temperature range over which the coupling can be measured in $CFCl_3$ solution. However, it is clearly seen in the more extensive measurements on the pure liquid [19]. Here the coupling decreases from 14.11 c.p.s. at 224°K to 13.36 c.p.s. at 466°K. This cannot be due to a change in the free energy differences between the rotaners on going from $CFCl_3$ solution to the pure liquid, as the observed couplings in the two solutions are practically identical. There is the possibility that the coupling constants of the individual isomers have different signs and thus the values of J_{AV}^{FF} and the calculated high temperature couplings would be changed. However, detailed inspection of all the possible sign combinations shows that the high temperature results in $CFCl_3$ and in the pure liquid cannot be obtained from the low temperature couplings without changing the energy differences by large and very improbable amounts. Thus we conclude that the temperature dependence of the coupling constants of $CF_2Br \cdot CFBrCl$ at high temperatures cannot be reconciled with the measured coupling constants of the individual isomers at -120°C. We note in the above case, the change in the observed coupling with temperature can only be from 13.3 c.p.s. to 16.0 c.p.s. and thus over any practical temperature range the change in J due to the changing population of the rotational isomers will be quite small. A more striking example is $CF_2Br \cdot CFBr_2$ in which the couplings of the individual isomers from low temperature measurements are (a) J_g 18.8 c.p.s., and (b) J_g 18.6 and J_t 16.2 c.p.s. [28]. Thus the variation in the high temperature coupling due to the change in the populations of the rotational isomers is only from 17.4 c.p.s. (isomer *b* is the more stable) to J_{AV}^{FF} which is 17.9 c.p.s. at infinite temperatures. Thus in this compound the change in the observed coupling due to the changing population of the rotational isomers over any normal temperature range will be less than the experimental error of measurement (± 0.1 c.p.s.). Indeed, consideration of these two unique factors in $CF \cdot CF$ couplings, i.e. the relatively small differences in the coupling constants of the individual isomers combine with the relatively large temperature dependence of J_{AV}^{FF} , suggests that the observed temperature dependence of the coupling constant at high temperatures is not primarily due to the changing populations of the rotational isomers, but presumably due to the change in the coupling constants of the individual isomers with temperature.

This situation is in contrast to H-H couplings, in which the differences between the couplings of the individual isomers are much larger and in which J_{AV}^{HH} does not change with temperature. The available evidence for H-F couplings is small but does suggest that they behave more like H-H than F-F couplings. However, until more experimental evidence is available the results of the temperature dependence of J^{HF} must also be considered with extreme caution.

ACKNOWLEDGMENTS

We are indebted to Drs. L. H. Sutcliffe and J. Feeney for the values before publication of J_{AV}^{FF} in a number of compounds and for much stimulating discussion.

REFERENCES

- [1] GLICK, R. E., and BOTHNER-BY, A. A., 1956, *J. chem. Phys.*, **25**, 362.
- [2] BANWELL, C. N., and SHEPPARD, N., 1962, *Disc. Faraday Soc.*, **34**, 115.
- [3] ABRAHAM, R. J., and PACHLER, K. G. R., 1963, *Mol. Phys.*, **7**, 165.
- [4] HUGGINS, M. L., 1953, *J. Amer. chem. Soc.*, **75**, 4123.
- [5] NG, S., and SEDERHOLM, C. H., 1964, *J. chem. Phys.*, **40**, 2090.
- [6] ABRAHAM, R. J., and CAVALLI, L., unpublished results.
- [7] LEE, J., and SUTCLIFFE, L. H., 1959, *Trans. Faraday Soc.*, **55**, 880.
- [8] ELLEMAN, D. D., BROWN, C., and WILLIAMS, D., 1961, *J. mol. Spectrosc.*, **7**, 037.
- [9] STAFFORD, S. L., 1962, *J. Amer. chem. Soc.*, **83**, 4473.
- [10] VARIAN ASSOCIATES, 1963, *N.M.R. Spectra Catalogue*, Vol. 2.
- [11] KRESPAN, C. G., 1960, *J. org. Chem.*, **25**, 105.
- [12] SHOOLERY, J. N., and CRAWFORD, B., 1957, *J. mol. Spectrosc.*, **1**, 270.
- [13] SUTCLIFFE, L. H. (private communication).
- [14] PITCHER, E., BUCKINGHAM, A. D., and STONE, F. G. A., 1962, *J. chem. Phys.*, **36**, 124.
- [15] PETRAKIS, L., and SEDERHOLM, C. H., 1961, *J. chem. Phys.*, **35**, 1243.
- [16] REILLY, C. A., 1956, *J. chem. Phys.*, **25**, 604.
- [17] HARRIS, R. K., and SHEPPARD, N., 1963, *Trans. Faraday Soc.*, **59**, 606.
- [18] ABRAHAM, R. J., and BERNSTEIN, H. J., 1961, *Canad. J. Chem.*, **39**, 39.
- [19] GUTOWSKY, H. S., BELFORD, G. G., and MCMAHON, P. E., 1962, *J. chem. Phys.*, **36**, 3353.
- [20] FESSENDEN, R. W., and WAUGH, J. S., 1961, *J. chem. Phys.*, **37**, 1466.
- [21] CRAPO, L., and SEDERHOLM, C. H., 1960, *J. chem. Phys.*, **33**, 1583.
- [22] KARPLUS, M., 1959, *J. chem. Phys.*, **30**, 11.
- [23] BREY, W. S., and RAMEY, K. C., 1963, *J. chem. Phys.*, **39**, 844.
- [24] SCHUG, J. C., MCMAHON, P. E., and GUTOWSKY, H. S., 1960, *J. chem. Phys.*, **33**, 843.
- [25] POWLES, J. G., and STRANGE, J. H., 1962, *Disc. Faraday Soc.*, **34**, 30.
- [26] NEWMARK, R. A., and SEDERHOLM, C. H., 1963, *J. chem. Phys.*, **39**, 3131.
- [27] BODEN, N., EMSLEY, J. W., FEENEY, J., and SUTCLIFFE, L. H., 1964, *Proc. roy. Soc. A*, **282**, 559.
- [28] MANATT, S. L., and ELLEMAN, D. D., 1962, *J. Amer. chem. Soc.*, **84**, 1305.
- [29] ANDREADES, S., 1964, *J. Amer. chem. Soc.*, **86**, 2003.

Quantum second virial coefficient of a one-dimensional Lennard-Jones gas†

by JOHN R. SAMS

Department of Chemistry, University of British Columbia,
Vancouver 8, Canada

(Received 31 August 1964)

We consider the equation of state of a dilute one-dimensional quantum degenerate gas at moderately high temperatures, and calculate the second virial coefficient assuming a Lennard-Jones function for the pair potential. Comparison with similar results for two- and three-dimensional gases reveals definite trends with changes in dimensionality. The Slater sum treatment of the quantum defects is found to be applicable over a narrower range of reduced temperatures as the dimensionality decreases.

1. INTRODUCTION

We have recently published high temperature quantum corrections to the second virial coefficient of a two-dimensional gas whose molecules interact through a Lennard-Jones (12-6) potential [1]. These results raised certain questions as to the applicability and convergence of the Slater sum (as embodied in the Wigner-Kirkwood expansion) in such a system, and it appeared that at least some of the answers might be found by examining the corresponding one-dimensional case.

The second virial coefficient can be written in reduced form as [2]:

$$B^{(n)}\star = [B_{\text{cl}}^{(n)}\star + \Lambda^{*2}B_{\text{I}}^{(n)}\star + \Lambda^{*4}B_{\text{II}}^{(n)}\star + \dots] \mp \Lambda^{*n}B_{\text{perf}}^{(n)}\star, \quad (1.1)$$

where

$$\Lambda^* = h/\sigma(\mu\epsilon)^{1/2}, \quad (1.2)$$

n is the dimensionality of the problem, h is Planck's constant, μ the molecular mass, ϵ the depth of the pair interaction well and σ the intermolecular separation at which the pair potential vanishes. B_{cl}^{\star} is the classical contribution, B_{I}^{\star} , B_{II}^{\star} , ..., the quantum corrections arising from the Wigner-Kirkwood expansion, and B_{perf}^{\star} the quantum perfect gas term reflecting the difference brought about by different particle statistics. The upper sign in (1.1) pertains to Bose-Einstein statistics, the lower sign to Fermi-Dirac statistics. In the two-dimensional case it was found [1] that the net Slater sum corrections were relatively smaller than the corresponding three-dimensional ones at high temperatures, while at temperatures below the Boyle point the expansion was divergent. This led

† This research was supported by the National Research Council and the Research Fund of the University of British Columbia.

to a crossing of the $B_{\text{Bo}}^{(2)}\star$ and $B_{\text{cl}}^{(2)}\star$ curves†: above the Boyle point, $B_{\text{Bo}}^{(2)}\star > B_{\text{cl}}^{(2)}\star$, whereas below the Boyle point, $B_{\text{Bo}}^{(2)}\star < B_{\text{cl}}^{(2)}\star$. This intersection of the curves should not, in itself, be taken too seriously, but merely as an indication that at these low temperatures the Wigner–Kirkwood expansion diverges and the treatment fails. However, it was not clear from these results whether there was any real significance in the fact that the Boyle temperature was the effective lower limit of convergence of the expansion. It was also found that when the perfect gas term for bosons was included the quantum curve lay below the classical one at all reduced temperatures, although as expected the two curves converged in the high temperature limit. This behaviour is very different from the three-dimensional case, for which the quantum curves lie above the classical one at all meaningful values of the reduced temperature. The explanation of this apparent inversion is simply that the perfect gas quantum contribution is larger than the net Slater sum contribution at all temperatures where the Wigner–Kirkwood explanation converges.

In the one-dimensional case the perfect gas term should be even larger relatively than in two dimensions, so we would anticipate that $B_{\text{cl}}^{(1)}\star$ will converge to $B_{\text{cl}}^{(1)}\star$ from below, as in the previous case. We also expect, however, that the convergence will be less rapid than in two dimensions. The main point of interest in the one-dimensional gas is, of course, the temperature limit of convergence of the Wigner–Kirkwood expansion. From a comparison of the two- and three-dimensional results, we would expect the expansion to diverge at an even higher relative reduced temperature unless the Boyle temperature *is* significant to the quantum corrections.

Unlike the two-dimensional gas treatment, which is applicable to high temperature physical adsorption systems, the one-dimensional gas does not correspond to a physically realizable system. However, there are two points of interest in the one-dimensional case, in addition to those mentioned above.

Firstly, as Halsey has pointed out [3], there is a strong coincidence between n -dimensional critical temperatures and $(n-1)$ -dimensional Boyle temperatures. Thus, the bulk critical temperature of a gas is effectively identical to the two-dimensional Boyle temperature; that is, the point at which attractions and repulsions just balance each other in the phase boundary. Hence the one-dimensional Boyle temperature is of interest in that it provides an estimate of the critical temperature in a mobile adsorbed film.

Secondly, the equations obtained in §3 are seen to be identical in form with those derived by Yaris and Sams [4] in their quantum treatment of physical adsorption in the Henry's law region. In the former paper [4], although the adsorbed molecules are free to translate over the surface, the adsorbate density is so small that one effectively has a perfect two-dimensional gas in an external field. One can therefore neglect interactions between the adsorbate molecules, and need treat only the interaction with the field, which is essentially a one-dimensional problem. In that case, the divergence of the Wigner–Kirkwood expansion was not apparent, although the reduced temperatures involved were considerably less than unity, and a comparison of the previous results with the present ones may therefore be of value.

† $B_{\text{Bo}}^{(2)}\star$ indicates the reduced quantum corrected second virial coefficient in Boltzmann statistics, i.e. only those terms within the square bracket of (1.1) are included.

2. THE EQUATION OF STATE

Our treatment of two-dimensional gases [1] can be taken over into one dimension with very slight modifications, and we give only a brief outline. For a one-dimensional gas the equation of state is

$$\vartheta L = kTq, \quad (2.1)$$

where ϑ is the one-dimensional pressure, L the length of the system, k the Boltzmann constant and T the Kelvin temperature. The grand potential q is given in quantum statistics by

$$q = \sum_{N=0}^{\infty} z^N \text{Tr} \exp(-\beta \mathcal{H}_N), \quad (2.2)$$

$$z \equiv \exp(\beta g), \quad \beta \equiv (kT)^{-1}, \quad (2.3)$$

where z is the activity, g the partial Gibbs function, and \mathcal{H}_N the Hamiltonian operator of the system of N molecules. One can introduce functions \mathcal{W}_N defined by

$$N! \text{Tr} \exp(-\beta \mathcal{H}_N) = \int \mathcal{W}_N d\mathbf{x}_1 \dots d\mathbf{x}_N, \quad (2.4)$$

from which it can be shown [1, 5],

$$\mathcal{W}_N(\mathbf{x}^N) = \left[\exp(-\beta \mathcal{H}_N) \sum_P (\pm 1)^P \prod_l \delta(\mathbf{x}'_l - \mathbf{x}_{Pl}) \right]_{\mathbf{x}'_l = \mathbf{x}_l} \quad (\text{upper sign B.E.}). \quad (2.5)$$

The summation is over all permutations P of the indices, and \mathbf{x}_{Pl} is the N -dimensional vector resulting from the application of this permutation to the vector \mathbf{x}_l .

For a perfect gas, the Hamiltonian is just the kinetic energy operator, where

$$\mathcal{H}_N = \mathcal{T}_N = -(\hbar^2/2\mu) \sum_j \nabla_j^2, \quad (2.6)$$

where ∇_j^2 is the Laplacian of the j th particle in one dimension. When (2.6) is substituted into (2.5) and the δ -function is written in terms of its Fourier integral, one finds:

$$\mathcal{W}_N^o(\mathbf{x}^N) = \lambda^{-N} \sum_P (\pm 1)^P \exp \left[-(\pi/\lambda) \sum_l (\mathbf{x}_l - \mathbf{x}_{Pl}) \right] \quad (\text{upper sign B.E.}), \quad (2.7)$$

$$\lambda \equiv (\beta \hbar^2 / 2\pi\mu)^{1/2}. \quad (2.8)$$

For a real gas, one must substitute the complete Hamiltonian in (2.5) to obtain [1, 2, 6, 7]:

$$\mathcal{W}_N(\mathbf{x}^N) = W_N(\mathbf{x}^N) \left\{ 1 + \lambda^2 \sum_i w_2^{(i)} + \lambda^4 \sum_i w_4^{(i)} + \dots \right\}, \quad (2.9)$$

where

$$W_N(\mathbf{x}^N) = \lambda^{-N} \exp \left[-\beta \sum_{k < l \leq N} \phi(x_{kl}) \right], \quad (2.10)$$

$$w_2^{(i)} = -\frac{\beta}{24\pi} \left[\nabla_i^2 \phi - \frac{\beta}{2} (\nabla_i \phi)^2 \right], \quad (2.11)$$

$$w_4^{(i)} = \frac{\beta}{960\pi^2} \left\{ \nabla_i^4 \phi - \frac{\beta}{6} [2\nabla_i^2 (\nabla_i \phi)^2 + 4\nabla_i \phi \cdot \nabla_i^3 \phi + 5(\nabla_i^2 \phi)^2] \right. \\ \left. + \frac{\beta^2}{6} [5\nabla_i^2 \phi (\nabla_i \phi)^2 + 3\nabla_i \phi \cdot \nabla_i (\nabla_i \phi)^2] - \frac{5\beta^3}{24} (\nabla_i \phi)^4 \right\}, \quad (2.12)$$

and where $\phi(x)$ is the intermolecular pair potential. The Slater sum, \mathcal{W}_N , is the exact quantum analogue of the Boltzmann factor, W_N , and approaches the classical limit as $\beta \rightarrow 0$.

3. SECOND VIRIAL COEFFICIENT

In terms of the Slater sum, the one-dimensional second virial coefficient can be written as:

$$B^{(1)} = -(N\lambda^2/2L) \int [\mathcal{W}_2(\mathbf{x}_1, \mathbf{x}_2) - \mathcal{W}_1(\mathbf{x}_1)\mathcal{W}_1(\mathbf{x}_2)] d\mathbf{x}_1 d\mathbf{x}_2, \quad (3.1)$$

which leads to a development of the form:

$$B^{(1)} = B_{\text{cl}}^{(1)} + B_{\text{perf}}^{(1)} + B_{\text{I}}^{(1)} + B_{\text{II}}^{(1)} + \dots \quad (3.2)$$

$B_{\text{perf}}^{(1)}$ is the quantum mechanical second virial for a perfect gas, arising from $\mathcal{W}^{(1)}$, $B_{\text{cl}}^{(1)}$ is the classical second virial and $B_{\text{I}}^{(1)}$ and $B_{\text{II}}^{(1)}$ are quantum terms proportional to λ^2 and λ^4 , respectively.

From (2.7) and (3.1) we may evaluate $B_{\text{perf}}^{(1)}$ as:

$$\begin{aligned} B_{\text{perf}}^{(1)} &= \mp (N/2L) \int \exp[-(2\pi/\lambda)(\mathbf{x}_1 - \mathbf{x}_2)^2] d\mathbf{x}_1 d\mathbf{x}_2 \\ &= \mp N\lambda/2^{3/2} \quad (\text{upper sign B.E.}). \end{aligned} \quad (3.3)$$

The remaining terms in (3.2) are found by substituting the appropriate terms of the expansion (2.9), written for two particles, into (3.1). The resulting equations may be simplified by a series of partial integrations to yield:

$$B_{\text{cl}}^{(1)} = -\frac{N\beta}{2} \int_0^\infty \exp(-\beta\phi) \nabla\phi x dx, \quad (3.4)$$

$$B_{\text{I}}^{(1)} = -\frac{N\hbar^2\beta^2}{2 \cdot 24\mu} \int_0^\infty \exp(-\beta\phi) \nabla^2\phi dx, \quad (3.5)$$

$$B_{\text{II}}^{(1)} = -\frac{N\hbar^2\beta^3}{2 \cdot 240\mu^2} \int_0^\infty \exp(-\beta\phi) \left[\frac{7}{8} \nabla^4\phi - \frac{7\beta}{24} (\nabla^2\phi)^2 \right] dx, \quad (3.6)$$

where μ is now the reduced mass. For the intermolecular pair potential we use a generalized Lennard-Jones function:

$$\begin{aligned} \phi &= \gamma \epsilon (r^{*-m} - r^{*-n}), \quad m > n, \\ r^* &= x/\sigma, \quad \gamma = \left(\frac{n}{m-n} \right) \left(\frac{n}{m} \right)^{m/(n-m)} \end{aligned} \quad (3.7)$$

When (3.7) is employed in (3.4)–(3.6), the integrations may be carried out in terms of series of gamma functions, and we find:

$$B_{\text{cl}}^{(1)} = -\frac{N\sigma}{2} \sum_{\tau \geq 0} \frac{1}{m\tau!} \left(\frac{T^*}{\gamma} \right)^{[\tau(n-m)-1]/m} \Gamma\left(\frac{\tau n - 1}{m}\right) = -\frac{N\sigma}{2} I_{\text{cl}}^{(1)}, \quad (3.8)$$

$$\begin{aligned} B_{\text{I}}^{(1)} &= \frac{N\lambda^2}{96\pi\sigma} \sum_{\tau \geq 0} \frac{\tau n(m-n) + m + 1}{m\tau!} \left(\frac{T^*}{\gamma} \right)^{[\tau(n-m)+1]/m} \Gamma\left(\frac{\tau n + 1}{m}\right) \\ &= \frac{N\lambda^2}{96\pi\sigma} I_{\text{I}}^{(1)}, \end{aligned} \quad (3.9)$$

$$B_{II}^{(1)} = -\frac{7N\lambda^4}{46080\pi^2\sigma^3} \sum_{\tau \geq 0} \frac{\tau^2 a + \tau b + c}{m\tau!} \left(\frac{T^*}{\gamma}\right)^{[\tau(n-m)+3]/m} \Gamma\left(\frac{\tau n + 3}{m}\right) \quad (3.10)$$

$$= -\frac{7N\lambda^4}{46080\pi^2\sigma^3} I_{II}^{(1)},$$

where

$$T^* = (\beta\epsilon)^{-1}, \quad (3.11)$$

$$a = -n^2(m-n)^2, \quad (3.12)$$

$$b = n\{3[(m+1)(m+2)(m+3) - (n+1)(n+2)(n+3)] + n(n+1)^2 + 6(m+1)(n+1) - (m+6)(m+1)^2\}, \quad (3.13)$$

$$c = 3(m+1)(m+3)[3(m+2) - (m+1)]. \quad (3.14)$$

4. RESULTS AND DISCUSSIONS

The equations of the preceding section allow one to calculate the various contributions to the one-dimensional second virial coefficient for any pair potential having a Lennard-Jones ($m-n$) form, although we restrict ourselves here to the commonly used (12-6) function. The Appendix contains selected values of the integrals $I_{cl}^{(1)}$, $I_I^{(1)}$ and $I_{II}^{(1)}$ calculated for this potential at various reduced temperatures in the range $0.4 < T^* < 40$. Similar tables for three other Lennard-Jones type potentials [(9-3), (12-3) and (10-4)] have previously been published [4].

Using the tables in the Appendix we can estimate the magnitudes of the contributions to $B^{(1)*}$ through (1.1). Values of $B_{cl}^{(1)*}$, $B_I^{(1)*}$, $B_{II}^{(1)*}$ and $B_{perf}^{(1)*}$ are given in the table for selected values of T^* . It is instructive to compare these

T^*	B_{cl}^*	B_I^*	B_{II}^*	B_{perf}^*
0.381	-2.310	2.513	-2.639	0.4567
0.471	-1.107	1.137	-1.116	0.4110
0.617	-0.2977	0.4797	-0.4121	0.3594
0.891	0.2533	0.1787	-0.1220	0.2987
1.147	0.4598	0.1015	-0.05707	0.2634
1.385	0.5659	0.06940	-0.03357	0.2399
1.748	0.6597	0.04524	-0.01803	0.2134
2.370	0.7413	0.02735	-0.008383	0.1833
3.106	0.7883	0.01821	-0.004393	0.1601
4.505	0.8274	0.01092	-0.0021886	0.1329
6.579	0.8473	0.006760	-0.0018276	0.1100
8.197	0.8525	0.005195	-0.0015216	0.09854
9.804	0.8542	0.004220	-0.0013607	0.09010
12.20	0.8537	0.003297	-0.0012316	0.08079
14.93	0.8513	0.002638	-0.0011546	0.07301
19.23	0.8460	0.002008	-0.0009418	0.06432
25.00	0.8384	0.001523	-0.00085634	0.05642
31.25	0.8307	0.001209	-0.00083671	0.05047
35.71	0.8256	0.001055	-0.00082847	0.04719
41.67	0.8193	0.0009019	-0.00082133	0.04370

Note: $0.0034267 = 0.0004267$.

Contributions to the second virial coefficient of a one-dimensional Lennard-Jones gas.

results with those for two-dimensional [1] and three-dimensional [2] Lennard-Jones gases. Owing to the differences in Boyle temperatures, such a comparison should be made not at the same values of reduced temperature, but at reduced temperatures which are the same relative to the Boyle point. One then finds the magnitudes of all the quantum corrections increase as the dimensionality of the gas decreases. These increases are not all proportional, however, B_{11}^* increasing relatively more than B_1^* , while B_{perf}^* shows an enormous increase. These trends have the effect of raising the relative temperature limit of convergence of the Wigner-Kirkwood expansion while lowering the rate of convergence to the classical result, as the dimensionality decreases. This means that the temperature range in which a Slater sum treatment of quantum defects can safely be employed is narrower for a one-dimensional gas than for a two-dimensional one, which is in turn narrower than the range of validity of the treatment in three dimensions. At the same time the perfect gas contribution is of much greater importance in the lower dimensional cases.

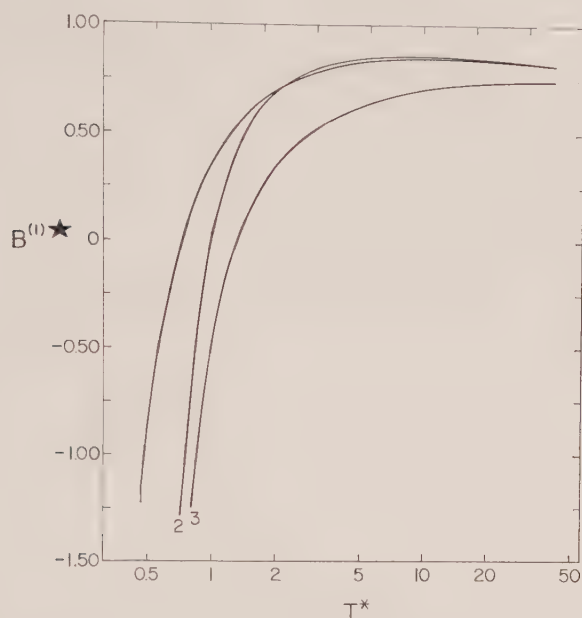
To construct curves of $B^{(1)*}$ versus T^* it is necessary to evaluate the quantum parameter Λ^* . This cannot be done in the present case, as there is no way to obtain the one-dimensional intermolecular potential parameters $\epsilon^{(1)}$ and $\sigma^{(1)}$. By the same token, however, since our system is purely a hypothetical one, we can allow some reasonable latitude in our choice of Λ^* . That is to say, we are primarily interested in the trends shown by the various curves which together make up the total $B^{(1)*}$, rather than in the exact magnitudes of the contributions, and these trends will not be particularly sensitive to the exact choice of Λ^* . Moreover, the theoretically estimated two-dimensional quantum parameters [1] are not much different from the three-dimensional ones [2], so that by using, say, the two-dimensional values we should certainly obtain a fairly accurate notion of the trends shown by the curves.

The figure shows plots of $B^{(1)*}$ versus T^* for hydrogen, which have been calculated from (1.1) using the values of the table along with the estimated two-dimensional Λ^* value previously published [1]. Curve 1 is the classical curve; 2 is the quantum corrected curve in Boltzmann statistics (only the terms in square brackets in (1.1) are included); 3 is the quantum corrected curve in Bose-Einstein statistics (the complete equation (1.1) with upper sign).

As in two dimensions, the divergence of the Wigner-Kirkwood expansion is evident at the low end of the temperature spectrum, and in fact, it is even more pronounced in the one-dimensional case. The Boltzmann quantum curve and the classical curve exhibit a cross-over point, which is the effective lower limit of convergence of the Slater sum. The importance of the perfect gas correction term is readily apparent from a comparison of the Boltzmann and Bose quantum curves. At low temperatures the perfect gas term is small compared to the terms in the Slater sum, but as the temperature increases the relative importance is greatly enhanced and at the high temperature end of the plot it constitutes by far the major contribution to the quantum corrections. The influence of the $B_{\text{perf}}^{(1)*}$ term is somewhat diminished by the fact (see (1.1)) that it enters with a smaller coefficient of Λ^* than does $B_1^{(1)*}$, but this effect is not nearly large enough to prevent it from dominating the Slater sum terms. For example, at $T^* = 41.67$, $B_{\text{perf}}^{(1)*} \sim 50 B_1^{(1)*}$, while $\Lambda^* B_{\text{perf}}^{(1)*} \sim 30 \Lambda^{*2} B_1^{(1)*}$.

It is clear from the figure that the temperature limit of convergence of the Wigner-Kirkwood expansion is well above the one-dimensional Boyle point.

In the two-dimensional case [1] it was not entirely clear whether or not there was any significance in the fact that the classical and Boltzmann quantum curves crossed just at the Boyle temperature, but the present results indicate that this was nothing more than coincidental.



Reduced one-dimensional second virial coefficient $B^{(1)*}$ for hydrogen, assuming a Lennard-Jones (12-6) pair potential. Λ^* based on two-dimensional parameters. Curve 1 is the classical contribution. 2 is the quantum curve neglecting effects of symmetry of the wave functions (Boltzmann statistics), and includes terms in the Slater sum to order \hbar^4 . 3 is the full quantum corrected curve in Bose-Einstein statistics.

As we mentioned above, the one-dimensional Boyle temperature can be used to obtain an estimate of the critical temperature of a two-dimensional mobile adsorbed film [3]. Owing to the fact that the present treatment of the quantum defects is not applicable down to the Boyle point we cannot make such an estimate for quantum degenerate gases. One can, however, use the classical results to estimate, for example, the critical temperature of an argon film adsorbed on graphite. From the figure, the one-dimensional Boyle point is seen to occur at $T_{1B}^* = 0.727$, which gives $T_{1B}^*/T_{2B}^* = 0.466$ [1]. From this and the critical temperature of bulk argon [8], the predicted two-dimensional critical temperature for argon on graphite is $T_{2c} = 70^\circ\text{K}$, which compares very favourably with the experimental value of 68°K estimated by Prezlow and Halsey [9].

In light of the present findings, we should comment briefly on the results of Yaris and Sams [4] for the adsorption of isotopic species in the Henry's law region of the adsorption isotherm. The two treatments are essentially the same, except that whereas here we have dealt with a strictly one-dimensional gas whose molecules interact only with each other, Yaris and Sams consider the case of isolated molecules interacting in one dimension with an external field, and for

this reason they employed somewhat different models for the interaction potential. It seems clear, however, that the reason the divergence of the Slater sum did not appear in the previous results was not owing to slight differences in the potential models, but rather to very large differences in the quantum parameters Λ^* . The Λ^* value for hydrogen used here is based on the interaction energy $\epsilon^{(2)}/k = 31.5^\circ\text{K}$ [1], whereas in the adsorption case the gas-solid interaction energy is $\epsilon_{\text{gs}}/k = 617^\circ\text{K}$ for the hydrogen-graphite system [4]. This increase in ϵ would reduce Λ^* by a factor of about 4. In other words, Λ^* for the gas-surface case is about 0.5 rather than the value of about 2 employed here. Hence, $B_{\text{I}}^{(1)*}$ enters with a coefficient of ~ 0.25 , and $B_{\text{II}}^{(1)*}$ with a coefficient of ~ 0.06 . This means that $B_{\text{II}}^{(1)*}$ would have to be about four times as large as $B_{\text{I}}^{(1)*}$ at this value of Λ^* for the divergence of the series to appear, and this is not the case even at the very low reduced temperatures ($0.15 \lesssim T^* \lesssim 0.25$) which were used.

This indicates that really sizeable changes in the quantum parameter Λ^* can markedly alter the convergence properties of a Slater sum type treatment, and that one should examine the experimental conditions carefully before trying to apply such a treatment.

The assistance of Mr. Robert Wolfe with some of the numerical computations is gratefully acknowledged.

APPENDIX

We present here numerical tabulations of the integrals $I_{\text{cl}}^{(1)}$, $I_{\text{I}}^{(1)}$ and $I_{\text{II}}^{(1)}$ of (3.8)–(3.10) for selected values of $\epsilon^{(1)}/kT$, assuming a Lennard-Jones (12-6) function for the pair potential.

ϵ/kT	$I_{\text{cl}}^{(1)}$	$I_{\text{I}}^{(1)} \times 10^{-2}$	$I_{\text{II}}^{(1)} \times 10^{-4}$
0.024	0.819311	0.179531	1.20382
0.028	0.825560	0.179916	1.18407
0.032	0.830655	0.180460	1.16898
0.040	0.838388	0.181861	1.14809
0.052	0.845952	0.184462	1.13572
0.067	0.851270	0.188112	1.12287
0.082	0.853743	0.192073	1.12305
0.102	0.854224	0.197627	1.13023
0.122	0.853604	0.203412	1.14276
0.152	0.847307	0.212480	1.16795
0.222	0.827403	0.234920	1.24790
0.322	0.788310	0.270139	1.38162
0.422	0.741338	0.309563	1.53481
0.572	0.659675	0.377876	1.79709
0.722	0.565859	0.459226	2.09976
0.872	0.459797	0.556209	2.44700
1.022	0.340645	0.671838	2.85024
1.122	0.253315	0.761005	3.16072
1.372	0.003827	1.04383	4.02937
1.622	-0.297735	1.41295	5.10724
1.872	-0.663092	1.90496	6.43932
2.122	-1.10708	2.55937	8.07752
2.372	-1.64837	3.42807	10.0814
2.622	-2.31036	4.57809	12.5174

REFERENCES

- [1] SAMS, J. R., 1965, *Mol. Phys.*, **9**, 17.
- [2] HIRSCHFELDER, J. O., CURTISS, C. F., and BIRD, R. B., 1954, *Molecular Theory of Gases and Liquids* (John Wiley & Sons), Chap. 6.
- [3] HALSEY, G. D., 1962, *J. chem. Phys.*, **36**, 1688.
- [4] YARIS, R., and SAMS, J. R., 1962, *J. chem. Phys.*, **37**, 571.
- [5] TER HAAR, D., 1954, *Elements of Statistical Mechanics* (Rinehart), p. 184.
- [6] KIRKWOOD, J. G., 1933, *Phys. Rev.*, **44**, 31.
- [7] UHLENBECK, G. E., and BETH, E., 1936, *Physica*, **3**, 729.
- [8] LEVELT, J. M. H., 1960, *Physica*, **26**, 361.
- [9] PRENZLOW, C. F., and HALSEY, G. D., 1957, *J. phys. Chem.*, **6**, 1158.

Normal coordinate analysis of Re(VII)O_4^- , $\text{Re(VII)O}_3\text{Cl}$ and $\text{Re(VII)O}_3\text{Br}^\dagger$

by WALTER A. YERANOS[‡] and FRED D. FOSS

Department of Chemistry,
Northern Illinois University, DeKalb, Illinois 60115

(Received 7 July 1964)

Using published infra-red and Raman data, the potential constants of ReO_4^- , ReO_3Cl and ReO_3Br have been determined in a modified Urey-Bradley field. A normal coordinate analysis have been carried within the formalism of Wilson's F - G matrix method, and the force constants have been evaluated by a computer routine which refined the differences of experimental and calculated frequencies in the least-square sense. Transferability of Urey-Bradley force constants has been assumed.

1. INTRODUCTION

The infra-red and Raman spectra of ReO_4^- have been reported by Claassen and Zielen [1], while on the other hand, the spectra of ReO_3Cl and ReO_3Br have been reported by Miller and Carlson [2]. The reported band assignments, as well as calculated frequencies, are given in table 1.

The ReO_4^- ion belongs to the T_d point group, and since it has nine degrees of freedom, one expects, from group theoretical considerations [3], these nine fundamental vibrations to belong to the irreducible representations given in table 1. On the other hand, in the ReO_3X molecule, ($\text{X} = \text{Cl}, \text{Br}$), which also has nine degrees of freedom, because of the descent in symmetry from T_d to C_{3v} , the irreducible representations spanned by these vibrations are different from those of T_d . These fundamental vibrational modes and the irreducible representations to which they belong in C_{3v} are also given in table 1.

A diagram depicting the 'general' geometry of the molecules considered in this investigation is given in figure 1. The internal coordinates chosen for the vibrational analysis were δr_1 , δr_2 , δr_3 , δR , $\rho\delta\alpha_1$, $\rho\delta\alpha_2$, $\rho\delta\alpha_3$, $\rho\delta\beta_1$, $\rho\delta\beta_2$ and $\rho\delta\beta_3$, where the internal coordinates involving changes of angles have been multiplied by ρ , the internuclear equilibrium bond distance, so that *all* the force constants be given in units of mdyn/Å.

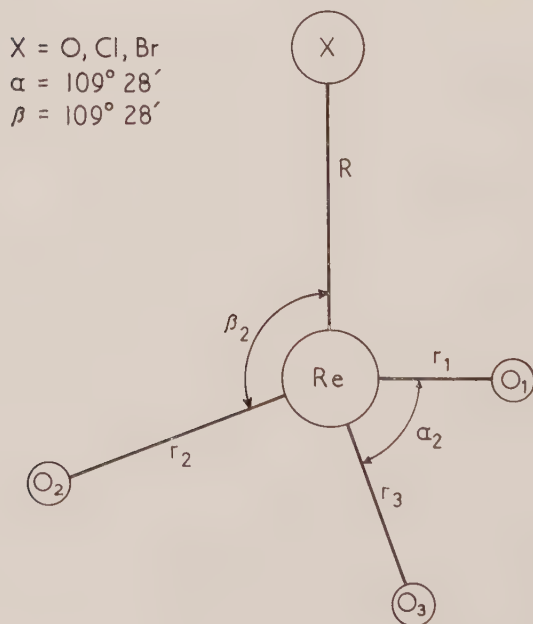
[†] Supported by the Dean's Fund for Research at N.I.U.

[‡] All correspondence should be addressed to this author.

	Mode	Activ.	Exp.	Calc. 1 $\Delta\nu$ per cent	Calc. 2 $\Delta\nu$ per cent	Calc. 3 $\Delta\nu$ per cent
ReO_4^-	$\nu_1(a_1)$	R	971	972 0	981 +1	986 +2
	$\nu_2(e)$	R	331	399 +20	334 +1	335 +1
	$\nu_3(t_2)$	IR, R	918	847 - 8	941 +3	940 +2
	$\nu_4(t_2)$	IR, R	331	396 +17	325 -2	326 -1
ReO_3Cl	$\nu_1(a_1)$	IR, R	1001	925 - 8	986 -2	986 -2
	$\nu_2(a_1)$	IR, R	435	377 -13	440 +1	436 0
	$\nu_3(a_1)$	IR, R	293	315 + 7	290 -1	293 0
	$\nu_4(e)$	IR, R	960	825 -14	953 -1	949 -1
	$\nu_5(e)$	IR, R	344	384 +12	348 +1	345 0
	$\nu_6(e)$	IR, R	196	244 +24	197 0	196 0
ReO_3Br	$\nu_1(a_1)$	IR, R	997	925 - 7	988 -1	989 -1
	$\nu_2(a_1)$	IR, R	350	335 - 4	354 +1	351 0
	$\nu_3(a_1)$	IR, R	195	237 +22	194 -1	195 0
	$\nu_4(e)$	IR, R	963	825 -14	958 -1	954 -1
	$\nu_5(e)$	IR, R	332	384 +16	330 0	331 0
	$\nu_6(e)$	IR, R	168	216 +29	168 0	168 0

Table 1. Experimental and calculated frequencies† (in cm^{-1}).

† Percentage errors calculated to the nearest wave number.



Geometry of the molecules considered in the present investigation. In the case of $X \equiv \text{O}_4$, $R \equiv r_4$ and the angles are labelled α_{12} instead of α_3 , etc.

The molecular dimensions of ReO_3Cl were taken from the microwave spectrum to be Re-O 1.702 Å, Re-Cl 2.230 Å and $\angle \text{Cl-Re-O}$ $109^\circ 28'$ [4]. Since no such information was available for ReO_3Br , we have assumed all the angles in this molecule to be tetrahedral just as in the case of ReO_3Cl . We have furthermore, estimated Re-Br to be a scaled† sum of the covalent radii of Re and Br . This gave us Re-Br 2.377 Å.

2. SYMMETRY COORDINATES

The symmetry coordinates belonging to the different irreducible representations in T_d and C_{3v} were generated by the projection operator

$$P_{\lambda k}^{(j)} = \frac{l_j}{h} \sum \Gamma^{(j)}(R)_{\lambda k}^* R[3],$$

as shown by Nielson and Berryman [5]. Note that, because of our choice of ten internal coordinates to describe nine degrees of internal freedom, a redundant symmetry coordinate was also generated. After the elimination of the redundant coordinates we were left with the following symmetry coordinates for both of the point groups, T_d and C_{3v} , under consideration.

For ReO_4^- in T_d :

$$S_1(a_1) = \frac{1}{2}(\delta r_1 + \delta r_2 + \delta r_3 + \delta r_4),$$

$$S_{2_a}(e) = \frac{\rho}{\sqrt{12}}(2\delta\alpha_{12} + 2\delta\alpha_{34} - \delta\alpha_{13} - \delta\alpha_{23} - \delta\alpha_{24} - \delta\alpha_{14}),$$

$$S_{2_b}(e) = \frac{\rho}{2}(\delta\alpha_{13} - \delta\alpha_{23} + \delta\alpha_{24} - \delta\alpha_{14}),$$

$$S_{3_a}(t_2) = \frac{1}{2}(\delta r_1 - \delta r_2 - \delta r_3 + \delta r_4),$$

$$S_{3_b}(t_2) = \frac{1}{2}(\delta r_1 - \delta r_2 + \delta r_3 - \delta r_4),$$

$$S_{3_c}(t_2) = \frac{1}{2}(\delta r_1 + \delta r_2 - \delta r_3 - \delta r_4),$$

$$S_{4_a}(t_2) = \frac{\rho}{\sqrt{2}}(\delta\alpha_{23} - \delta\alpha_{14}),$$

$$S_{4_b}(t_2) = \frac{\rho}{\sqrt{2}}(\delta\alpha_{24} - \delta\alpha_{13}),$$

$$S_{4_c}(t_2) = \frac{\rho}{\sqrt{2}}(\delta\alpha_{34} - \delta\alpha_{12}).$$

† By this we mean

$$\frac{\text{Re-Cl (sum of covalent radii)}}{\text{Re-Br (sum of covalent radii)}} = \frac{\text{Re-Cl (actual)}}{\text{Re-Br (scaled sum of covalent radii)}}$$

And for ReO_3X in C_{3v} :

$$S_1(a_1) = \frac{1}{\sqrt{3}} (\delta r_1 + \delta r_2 + \delta r_3),$$

$$S_2(a_1) = \frac{\rho}{\sqrt{6}} (\delta \alpha_1 + \delta \alpha_2 + \delta \alpha_3 - \delta \beta_1 - \delta \beta_2 - \delta \beta_3),$$

$$S_3(a_1) = \delta R,$$

$$S_{4a}(e) = \frac{1}{\sqrt{6}} (2\delta r_1 - \delta r_2 - \delta r_3),$$

$$S_{4b}(e) = \frac{1}{\sqrt{2}} (\delta r_2 - \delta r_3),$$

$$S_{5a}(e) = \frac{\rho}{\sqrt{6}} (2\delta \alpha_1 - \delta \alpha_2 - \delta \alpha_3),$$

$$S_{5a}(e) = \frac{\rho}{\sqrt{2}} (\delta \alpha_2 - \delta \alpha_3),$$

$$S_{6a}(e) = \frac{\rho}{\sqrt{6}} (2\delta \beta_1 - \delta \beta_2 - \delta \beta_3),$$

$$S_{6b}(e) = \frac{\rho}{\sqrt{2}} (\delta \beta_2 - \delta \beta_3).$$

3. F AND G MATRIX ELEMENTS

For a system of vibrating nuclei, the potential energy V and the kinetic energy T are given by:

$$2V = S'FS$$

and

$$2T = \dot{S}'G^{-1}\dot{S},$$

where F is the force constant matrix, G is the inverse kinetic energy matrix and S is the column vector of the symmetry coordinates. In these coordinates, the vibrational secular equation takes the familiar form [6]:

$$L^{-1}GFL = \Lambda,$$

where Λ is the diagonal matrix of the frequency parameters $\lambda_i (\equiv 4\pi^2 c^2 \nu_i^2)$ and L is the transformation matrix from the normal coordinates, Q , to the symmetry coordinates:

$$S = LQ$$

or its inverse:

$$Q = L^{-1}S.$$

In the present investigation we have assumed a Urey-Bradley field force [7], with the standard force constants of stretches denoted by K , of bends denoted by H and of repulsions denoted by F . These have, furthermore, been supplemented by the 'intramolecular tension force constant' k defined by Shimanouti [8]. Assuming all angles in the molecules to be tetrahedral, the G and F matrices of ReO_4^- in T_d and ReO_3X , ($\text{X} = \text{Cl}, \text{Br}$), in C_{3v} are given in tables 2 and 3 respectively. Where μ_0 , μ_{Re} and μ_x are the reciprocals of the atomic masses (in a.m.u.) of oxygen, rhenium and the halide respectively and $r_{\text{Re-O}}$ and $r_{\text{Re-X}}$ are the equilibrium distances (in angstroms) of the bonds Re-O and Re-X respectively.

ReO ₄ ⁻ (<i>T_d</i>)	$G_{1,1}(a_1)$ $G_{2,2}(e)$ $G_{3,3}(t_2)$ $G_{3,4}(t_2) = G_{4,3}(t_2)$ $G_{4,4}(t_2)$	μ_0 $3\mu_0$ $\mu_0 + \frac{4}{3}\mu_{\text{Re}}$ $-\frac{8}{3}\mu_{\text{Re}}$ $\frac{16}{3}\mu_{\text{Re}} + 2\mu_0$
ReO ₃ X(<i>C_{3v}</i>)	$G_{1,1}(a_1)$ $G_{1,2}(a_1) = G_{2,1}(a_1)$ $G_{1,3}(a_1) = G_{3,1}(a_1)$ $G_{2,2}(a_1)$ $G_{2,3}(a_1) = G_{3,2}(a_1)$ $G_{3,3}(a_1)$ $G_{4,4}(e)$ $G_{4,5}(e) = G_{5,4}(e)$ $G_{4,5}(e) = G_{6,4}(e)$ $G_{5,5}(e)$ $G_{5,6}(e) = G_{6,5}(e)$ $G_{6,6}(e)$	$\mu_0 + 0.333\mu_{\text{Re}}$ $-1.333\mu_{\text{Re}}$ $-0.577\mu_{\text{Re}}$ $2\mu_0 + 5.333\mu_{\text{Re}}$ $2.309\mu_{\text{Re}}$ $\mu_{\text{Re}} + \mu_{\text{X}}$ $\mu_0 + 1.333\mu_{\text{Re}}$ $1.885\mu_{\text{Re}}$ $\left(-0.471 - 1.414\left(\frac{r_{\text{Re}-0}}{r_{\text{Re}-\text{X}}}\right)\right)\mu_{\text{Re}}$ $2.5\mu_0 + 2.666\mu_{\text{Re}}$ $+0.5\mu_0 - \left(0.666 + 2\left(\frac{r_{\text{Re}-0}}{r_{\text{Re}-\text{X}}}\right)\right)\mu_{\text{Re}}$ $\mu_0 + 1.5\left(-0.333 - \left(\frac{r_{\text{Re}-0}}{r_{\text{Re}-\text{X}}}\right)\right)^2\mu_{\text{Re}}$ $+1.5\left(\frac{r_{\text{Re}-0}}{r_{\text{Re}-\text{X}}}\right)^2\mu_{\text{X}}$

Table 2. *G* matrix elements.

4. CALCULATION OF U.B. FORCE CONSTANTS

Since we have assumed the transferability of force constants among similar molecules in the Urey-Bradley field, we have the 11 independent force constants given in table 4 to be calculated from the 16 observed frequencies of table 1. This abundance of observed frequencies over the force constants has the net mathematical effect of making the vibrational secular determinant overdetermined and thus the problem essentially reduces to the refinement of initially estimated force constant to give a least squares fit of the calculated frequencies to the observed frequencies. A FORTRAN programme† was written for the I.B.M. 1620 Mark II computer for this purpose. The general outline of procedure used is as follows.

† A manuscript is in preparation entitled "A computer Program for Vibrational Analyses," with C. Givens of the Computer Center of Northern Illinois University as co-author. In this paper we give the programme, sub-programmes and a detailed mathematical analysis of our results, as applied to the 60K, I.B.M. 1620 Mark II computer.

$\text{ReO}_4^-(T_d)$	$F_{1,1}(a_1)$ $F_{2,2}(e)$ $F_{3,3}(t_2)$ $F_{3,4}(t_2) = F_{4,3}(t_2)$ $F_{4,4}(t_2)$	$1 \text{ K(Re-O)} + 4\text{F(O} \dots \text{O)}$ $1\text{H(O-Re-O)} + 0.37\text{F(O} \dots \text{O)}$ $1\text{K(Re-O)} + 1.2\text{F(O} \dots \text{O)}$ $0.6\text{F(O} \dots \text{O)}$ $1\text{H(O-Re-O)} + 0.5\text{F(O} \dots \text{O)}$
$\text{ReO}_3\text{X}(\text{C}_{3v})$	$F_{1,1}(a_1)$ $F_{1,2}(a_1) = F_{2,1}(a_1)$ $F_{1,3}(a_1) = F_{3,1}(a_1)$ $F_{2,2}(a_1)$ $F_{2,3}(a_1) = F_{3,2}(a_1)$ $F_{3,3}(a_1) = F_{3,3}(a_1)$ $F_{4,4}(e)$ $F_{4,5}(e) = F_{5,4}(e)$ $F_{4,6}(e) = F_{6,4}(e)$ $F_{5,5}(e)$ $F_{5,6}(e) = F_{6,5}(e)$ $F_{6,6}(e)$	$1\text{K(Re-O)} + 2.695\text{F(O} \dots \text{O)}$ $+ 0.536\text{F(O} \dots \text{x)}$ $0.586\text{F(O} \dots \text{O}) - 0.304\text{F(O} \dots \text{x)}$ $1.188\text{F(O} \dots \text{x)}$ 0.483H(O-Re-O) $+ 0.517\text{H(O-Re-x)}$ $+ 0.191\text{F(O} \dots \text{O)}$ $+ 0.261\text{F(O} \dots \text{x}) + 0.646k_x$ $- 0.645\text{F(O} \dots \text{x)}$ $1\text{K(Re-x)} + 2.131\text{F(O} \dots \text{x)}$ $1\text{K(Re-O)} + 0.576\text{F(O} \dots \text{O)}$ $+ 0.536\text{F(O} \dots \text{x)}$ $- 0.422\text{F(O} \dots \text{O)}$ $0.423\text{F(O} \dots \text{x)}$ $1\text{H(O-Re-O)} + 0.393\text{F(O} \dots \text{O)}$ $+ 0.185k_x$ $- 0.382k_x$ $1\text{H(O-Re-x)} + 0.505\text{F(O} \dots \text{x)}$ $+ 0.185k_x$

Table 3. F matrix elements.

(1) A set of estimates of the force constants is used to calculate a set of theoretical frequencies, the error vector ϵ_λ (observed-calculated), and the Jacobian matrix (JZ), with matrix elements:

$$(JZ)_{ij} = \sum_{Kl} (L)_{Kl} (L)_i Z_{Kl}^{(j)},$$

where L is obtained from

$$L^{-1}GFL = \Lambda$$

and the $Z_{Kl}^{(j)}$ is the coefficient of j th Urey-Bradley force constant in the F_{Kl} matrix element of the symmetrized F matrix, such that

$$F_{Kl} = \sum_j Z_{Kl}^{(j)} \Phi_j.$$

(2) The Jacobian (JZ) is used to construct a set of linear equations relating the variations in the force constants $\delta\Phi$ with respect to small variations in the calculated frequencies $\delta\lambda$, such that

$$(JZ)\delta\Phi = \epsilon_\lambda$$

and defining the residual vector as:

$$r = (JZ) \cdot \delta\Phi - \epsilon_\lambda,$$

	$K(\text{Re}=\text{O})$	$K(\text{Re}-\text{Cl})$	$K(\text{Re}-\text{Br})$	$H(\text{O}-\text{Re}-\text{O})$	$H(\text{O}-\text{Re}-\text{Cl})$	$H(\text{O}-\text{Re}-\text{Br})$	$F(\text{O}\dots\text{O})$	$F(\text{O}\dots\text{Cl})$	$F(\text{O}\dots\text{Br})$	k_1/ρ^2 [†]	k_2/ρ^2	k_3/ρ^2
Calc. 1	5.02	1.34	1.11	0.14	0.12	0.10	0.97	0.50	0.50	0.09	0.07	0.07
Calc. 2	6.95	0.89	0.81	0.16	-0.28	-0.38	0.53	1.02	1.18	0.05	0.38	0.15
Calc. 3	6.90	1.07	0.72	0.14	-0.26	-0.36	0.56	0.96	1.13	0.05	0.34	0.17

[†] Calculated from $k_1/\rho^2 = 0.1F(\text{O}\dots\text{O}) \sin 109^\circ 28'$.

Table 4. Calculated Urey-Bradley force constants (in mdyn/Å).

we obtain by the usual least squares procedure [9]: a set of normal equations which upon rearrangement gives us:

$$\delta\Phi = [(JZ)'W(JZ)]^{-1}(JZ)'W\epsilon_\lambda,$$

where W is a diagonal matrix taken by some investigators to have $W_{ii} = 1/\lambda_i$ matrix elements [10], and by others as $W_{ii} = 1/\lambda_i^2$ [9 d].

(3) These variations in Φ are used to set up a new set of force constants:

$$\Phi_{\text{new}} = \Phi_{\text{old}} + c\delta\Phi,$$

where c is an arbitrary scaling factor, necessary for damping purposes and the force constants thus obtained are used over again till the desired number of reiterations is completed.

The bases of our initial estimates were as follows: $K(\text{Re-O})$, $H(\text{O-Re-O})$, and $F(\text{O}\dots\text{O})$ were roughly calculated, only considering three vibrations of ReO_4^- . The values of $K(\text{Re-Cl})$ and $K(\text{Re-Br})$ were transferred from ReX_6^- molecules [11]. The repulsive force constants were approximated to:

$$F(\text{O}\dots\text{X}) = \frac{1}{2}[F(\text{O}\dots\text{O}) + F(\text{X}\dots\text{X})]$$

where the $F(\text{X}\dots\text{X})$'s were read from graphs of $(\partial^2 U / \partial r^2) \text{ v/s } r_e$ of the Lennard-Jones (6-12) potential for Ar and Kr [12]. r_e the bending force constants were estimated to be $H(\text{O-Re-O}) > H(\text{O-Re-Cl}) > H(\text{O-Re-Br})$. Finally, the 'intramolecular force constants' k were estimated by

$$k/\rho^2 = 0.1F \sin 109^\circ 28'.$$

In the present investigation we have used two series of iterations. One with $c=0.5$, which took 11 iterations for convergence, and the other with $c=1.0$ which took four iterations for convergence†. The final force constants and calculated frequencies ended up to be identical in both series. We, furthermore, performed these iterations with both types of statistical weighing factors of $1/\lambda_i$ and $1/\lambda_i^2$. The force constants and the calculated frequencies from them are given in tables 4 and 1 respectively. It is perhaps necessary to comment that even though the use of $1/\lambda_i$ is claimed by some investigators [11] to ensure the frequency fit to be on the percentage rather than absolute basis, we found that the use of $1/\lambda_i^2$ is better than $1/\lambda_i$ in *both*, the absolute and the percentage basis. Since we also believe that the uncertainties in the ν 's arise from anharmonicity effects we consider that $1/\lambda_i^2$ is a better statistical weighing factor than $1/\lambda_i$ and consequently believe that Set 3 in both the calculated frequencies as well as force constants is a more realistic fit.

	S_1	S_2	S_3	S_4
Q_1	4.000			
Q_2		2.309		
Q_3			3.813	0.145
Q_4			0.316	2.572

Table 5. Normal coordinates of ReO_4^- .

† Convergence here implies that $\delta\Phi$ has become so small that the changes in ϵ_λ are negligible. In the case of $W_{ii} = 1/\lambda_i$, $C=1.0$ even after 14 iterations it was not possible to obtain any convergence.

Using the force constants of Set 3, we have also calculated the normalized L^{-1} which connects the symmetry coordinates S to the normal coordinates Q . Tables 5, 6 and 7 give the normal coordinates of ReO_4^- , ReO_3Cl and ReO_3Br in terms of the symmetry coordinates previously described.

Finally, one may argue that some of our force constants† are not perhaps the best. The only answer we have is that a statistical method has been used when only five statistical degrees of freedoms were available. One should remember that statistical analysis attains significance when a relatively large number of observed data are being fitted to a relatively small number of force

	S_1	S_2	S_3	S_4	S_5	S_6
Q_1	3.949	-0.010	0.560			
Q_2	0.273	1.680	-4.753			
Q_3	0.108	1.980	2.809			
Q_4				3.817	-0.093	0.186
Q_5				-0.293	2.455	-0.783
Q_6				0.168	0.198	3.173

Table 6. Normal coordinates of ReO_3Cl .

constants. We are certain that discrepancies in some of the force constants would be minimized and even perhaps disappear if the number of statistical degrees of freedom would have been increased by the inclusion of coriolis zeta interaction constants, centrifugal stretching constants, vibrational-rotational interaction constants, etc. But, alas, in the absence of these, one has to be satisfied with the force constants of table 4.

	S_1	S_2	S_3	S_4	S_5	S_6
Q_1	3.959	-0.020	0.611			
Q_2	0.171	2.188	-5.636			
Q_3	0.171	1.459	5.239			
Q_4				3.820	-0.095	0.225
Q_5				-0.263	2.453	-0.219
Q_6				0.222	-0.295	3.580

Table 7. Normal coordinates of ReO_3Br .

ACKNOWLEDGMENTS

We would like to express our gratitude to Professor M. J. Joncich for his encouragement and Mr. C. Givens of the Computer Center of Northern Illinois University for his expert assistance in several phases of our computer work. We would also like to thank Dean John Skok of Northern Illinois University for his support of this work.

† Those for instance concerned with the angle bends.

REFERENCES

- [1] CLAASSEN, H. H., and ZIELEN, A. J., 1954, *J. chem. Phys.*, **22**, 707.
- [2] MILLER, F. A., and CARLSON, G. I., 1960, *Spectrochim. Acta*, **16**, 1148.
- [3] TINKHAM, M., 1964, *Group Theory and Quantum Mechanics* (New York: McGraw-Hill Book Co., Inc.).
- [4] AMBLE, E., MILLER, S. L., SCHAWLOW, A. L., and TOWNES, C. H., 1952, *J. chem. Phys.*, **20**, 192.
- [5] NIELSEN, J. R., and BERRYMAN, L. H., 1949, *J. chem. Phys.*, **17**, 659.
- [6] BRIGHT WILSON, E., JR., DECIUS, J. C., and CROSS, P. C., 1955, *Molecular Vibrations* (New York: McGraw-Hill Book Co., Inc.). p. 309.
- [8] SHIMANOUTI, T., 1949, *J. chem. Phys.*, **17**, 245.
- [9] (a) ARLEY, N., and BUCH, K. R., 1950, *Probability and Statistics* (New York: John Wiley).
(b) Overend, J., and SCHERER, J. R., 1960, *J. chem. Phys.*, **32**, 1289, 1296, 1720; **34**, 446.
(c) MILLS, I. M., 1960, *Spectrochim. Acta*, **16**, 35. (d) ALDOUS, J., and MILLS, I. M., 1962, *Spectrochim. Acta*, **18**, 1073; 1963, *Ibid.*, **19**, 1567. (e) DUNCAN, J. L., and MILLS, I. M., 1964, *Spectrochim. Acta*, **20**, 523.
- [10] MANN, D. E., SHIMANOUTI, T., MEAL, J. H., and FANO, L., 1957, *J. chem. Phys.*, **27**, 43.
- [11] YERANOS, WALTER, A., 1965, *Bull. soc. chem. Belge* (to be published).
- [12] DAVIDSON, NORMAN, 1962, *Statistical Mechanics* (New York; McGraw-Hill Book Co., Inc.).

RESEARCH NOTE

The relative signs of the proton coupling constants in the pyridine ring—the N.M.R. spectrum of 2,2'-dipyridine

by V. M. S. GIL†

Chemistry Department, University of Sheffield

(Received 19 October 1964)

Two papers have been published in which the double resonance technique has been used to determine the relative signs of the nuclear spin coupling constants in the pyridine ring. However, the compounds studied, 2-amino-3-picoline [1] and quinoline [2], only allowed the signs of three out of the possible six coupling constants to be determined. In this note we report a double resonance experiment on 2,2'-dipyridine which yields the relative signs of all the pyridine ring coupling constants except J_{26} (absolute value ~ 0.4 c.p.s.).

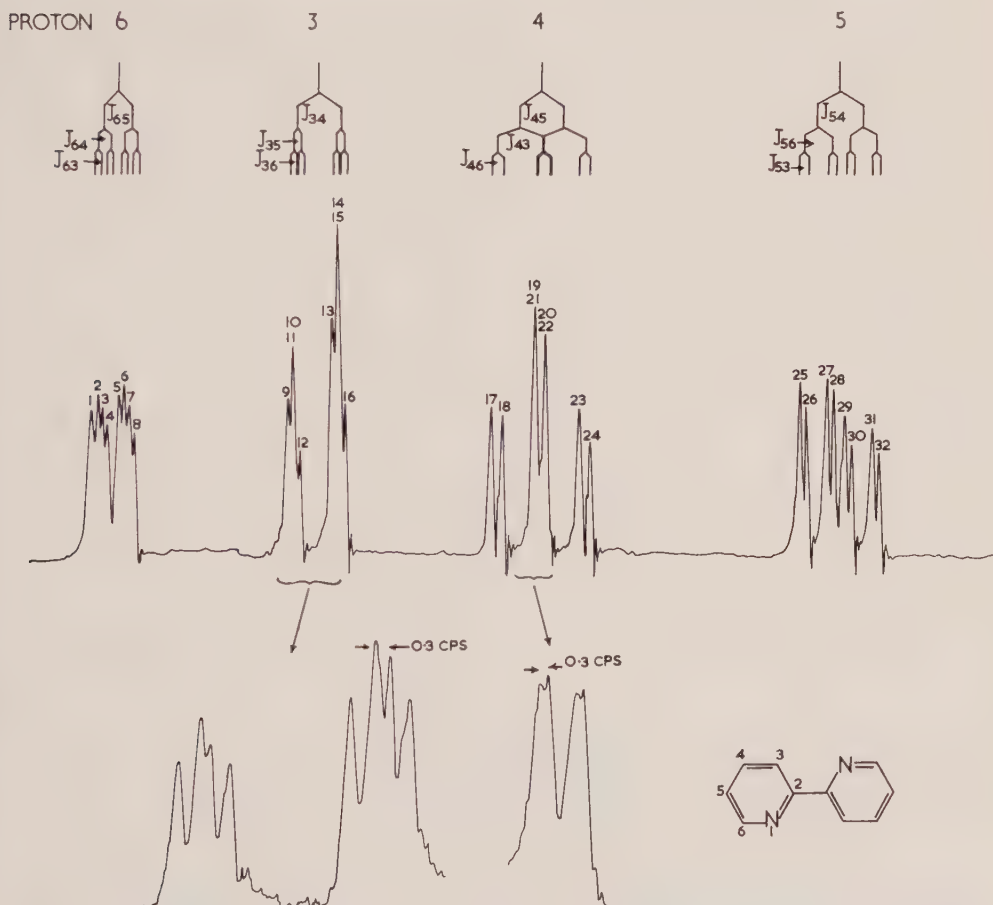


Figure 1. The 100 Mc/s proton resonance spectrum of 2,2'-dipyridine in CH_3OH (3 per cent mole solution).

† On leave of absence from the University of Coimbra, Portugal.

Figure 1 shows the nearly first-order 100 Mc/s spectrum of 2,2'-dipyridine in methanol (3 per cent mole solution). Since there is no detectable coupling between protons in different rings, the observed spectrum is one of a four-spin ($\frac{1}{2}$) system. In such a spectrum the relative intensities of the lines can give no reliable information about the relative signs of the coupling constants.

Collapsed lines	Expected $\nu_2 - \nu_1$ values (c.p.s.). (In brackets, lines to be irradiated)	
(a)	$J_{63} \cdot J_{43} > 0$	$J_{63} \cdot J_{43} < 0$
17, 18 ... $J_{56} \cdot J_{45} > 0$ $J_{56} \cdot J_{45} < 0$	67.2 (1,3) 62.1 (5,7)	66.3 (2,4) 61.2 (6,8)
(b)	$J_{56} \cdot J_{36} > 0$	$J_{56} \cdot J_{36} < 0$
25, 26 ... $J_{34} \cdot J_{45} > 0$ [29, 30] $J_{34} \cdot J_{45} < 0$	88.5 (9,11) [88.8 (13,15)] 81.2 (13,15) [96.1 (9,11)]	87.6 (10,12) [88.2 (14,16)] 80.5 (14,16) [95.3 (10,12)]
(c)	$J_{53} \cdot J_{63} > 0$	$J_{53} \cdot J_{63} < 0$
1, 5 ... $J_{45} \cdot J_{46} > 0$ [2,6] $J_{45} \cdot J_{46} < 0$	-121.7 (25,27) [-122.0 (26,28)] -129.1 (29,31) [-129.4 (30,32)]	-122.9 (26,28) [-120.8 (25,27)] -130.3 (30,32) [-128.2 (29,31)]
(d)	$J_{34} \cdot J_{64} > 0$	$J_{34} \cdot J_{64} < 0$
9, 10 ... $J_{35} \cdot J_{56} > 0$ $J_{35} \cdot J_{56} < 0$	33.3 (1,2) 28.3 (5,6)	31.5 (3,4) 26.4 (7,8)
(e)	$J_{34} \cdot J_{54} > 0$	$J_{34} \cdot J_{54} < 0$
9, 11 ... $J_{36} \cdot J_{56} > 0$ $J_{36} \cdot J_{56} < 0$	-88.5 (25,26) -93.6 (27,28)	-96.2 (29,30) -100.9 (31,32)
(f)	$J_{34} \cdot J_{64} > 0$	$J_{34} \cdot J_{64} < 0$
5, 6 ... $J_{35} \cdot J_{56} > 0$ $J_{35} \cdot J_{56} < 0$	-29.2 (11,12) -28.3 (9,10)	-36.3 (15,16) -35.6 (13,14)

A comparison with the chemical shifts in pyridine itself [3] and the structure of the signals enabled a straightforward assignment of the spectrum.† A first-order analysis gave the following τ -values and coupling constants‡ (the values in

† The 3 proton chemical shift is very sensitive to the nature of the solvent. It decreases by about 0.30 p.p.m. on going from a CH₃OH to a CCl₄ solution. Work on this and related phenomena is in progress.

‡ In each spectrum an average of the observed splittings corresponding to the same J has been performed. The chemical shifts and the J 's reported are expected to differ from those of an exact ABCD analysis by 0.2 c.p.s. at the most [5].

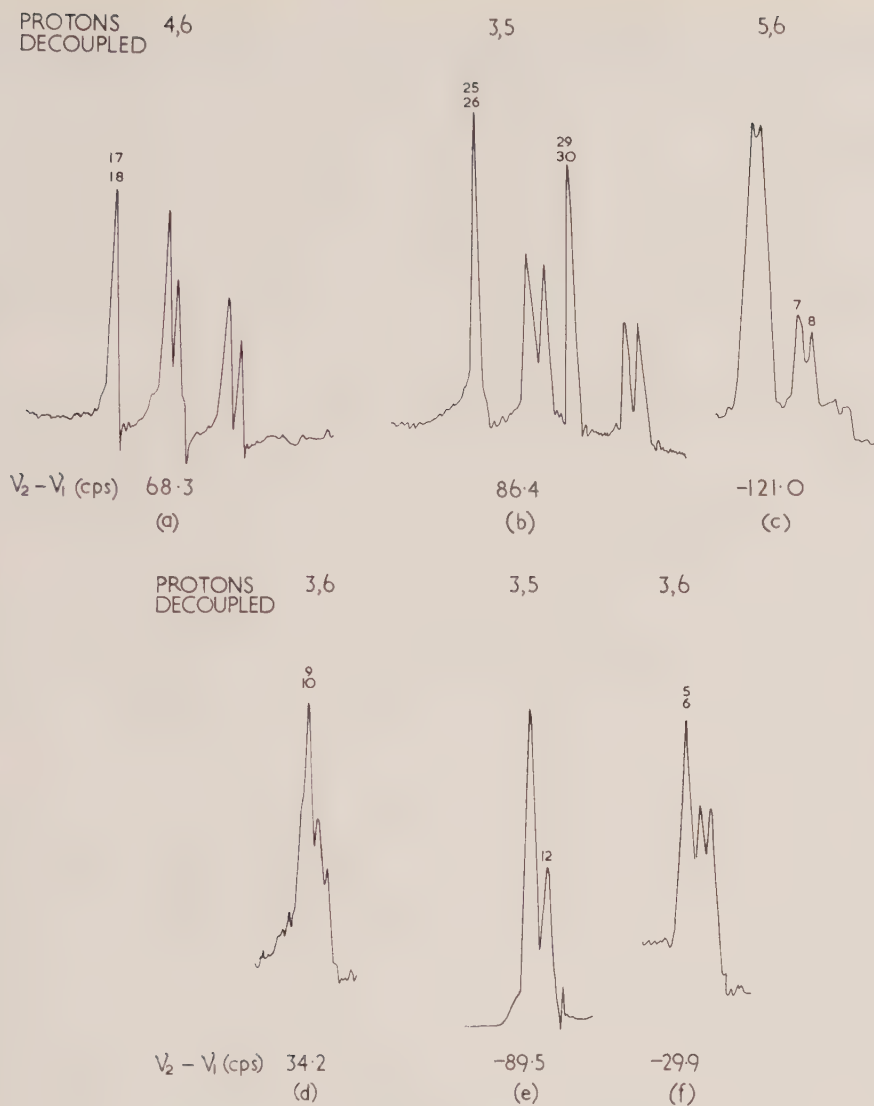


Figure 2. Spin-decoupled spectra and the observed $\nu_2 - \nu_1$ values.

brackets are for pyridine in an infinitely dilute solution in CCl_4 [3]):

$$\begin{aligned}\tau_5 - \tau_4 &= 0.52 \quad (0.38) \\ \tau_4 - \tau_3 &= 0.39 \quad (-0.38) \\ \tau_3 - \tau_6 &= 0.34 \quad (1.31) \\ \tau_6 &= 1.37 \quad (1.38)\end{aligned}$$

$$\begin{aligned}|J_{34}| &= 7.6 \text{ c.p.s.} \quad (7.5); & |J_{45}| &= 7.8 \text{ c.p.s.} \quad (7.5); \\ |J_{35}| &= 1.2 \text{ ,,} \quad (1.6); & |J_{46}| &= 1.9 \text{ ,,} \quad (1.9); \\ |J_{36}| &= 0.9 \text{ ,,} \quad (0.9); & |J_{56}| &= 5.0 \text{ ,,} \quad (5.5).\end{aligned}$$

A probable error of about ± 0.1 c.p.s. is estimated for the average spacing between the lines among several spectra.

A single spin-decoupling experiment in a first-order four-spin system can, in principle, give the relative signs of coupling constants within two distinct pairs. For example, collapsing of lines 9 and 11 is obtained by irradiating: (a) lines 25, 26 if $J_{36} \cdot J_{56} > 0$ and $J_{34} \cdot J_{45} > 0$, (b) lines 27, 28 if $J_{36} \cdot J_{56} < 0$ and $J_{34} \cdot J_{45} > 0$, (c) lines 29, 30 if $J_{36} \cdot J_{56} > 0$ and $J_{34} \cdot J_{45} < 0$, and (d) lines 31, 32 if $J_{36} \cdot J_{56} < 0$ and $J_{34} \cdot J_{45} < 0$. In this manner it is possible to determine the signs of all the six coupling constants relative to one another from only three independent irradiations. Nevertheless six spin-decoupling experiments have been performed in order to eliminate ambiguities. The spin-decoupled spectra are shown in figure 2 together with the actual differences between the frequencies of the irradiating r.f. field, ν_2 , and the observing r.f. field, ν_1 . In some cases the collapse to a single line remained for a variation of ν_2 as large as 1 c.p.s.

In the table we show, for each pair of collapsed lines, the expected $\nu_2 - \nu_1$ values (in brackets, the lines to be irradiated) for the various sign combinations of the coupling constants. From the table and the actual $\nu_2 - \nu_1$ values in figure 2 we conclude that the coupling constants have all the same sign. Since J_{56} probably has the sign of the coupling between aromatic protons *ortho* to each other in *p*-nitrotoluene [4], then they are all positive.

The compound studied therefore constitutes one more example of positive coupling between ring protons *meta* to one another. The Dirac vector model predicts a negative value for this coupling. However, a calculation of coupling constants in the benzene molecule, based on a recent theory by Pople and Santry [6] and in which long-range resonance integrals are included, gives a positive value of about 2 c.p.s. for the *meta* coupling. Details will appear elsewhere.

The author would like to thank Dr. J. N. Murrell for his comments and interest in this work, and Drs. K. A. McLauchlan and A. D. Cohen for their invaluable help. Acknowledgment is made to the Comissão Coordenadora da Investigação para a NATO, Portugal, for the award of a post-graduate scholarship, and the National Physical Laboratory, Teddington, for guest worker facilities.

REFERENCES

- [1] RAO, B. D. N., and BALDESCHWIELER, J. D., 1962, *J. chem. Phys.*, **37**, 2473.
- [2] PATERSON, W. G., and BIGAM, G., 1963, *Canad. J. Chem.*, **41**, 1841.
- [3] SCHNEIDER, W. G., BERNSTEIN, H. J., and POPLER, J. A., 1957, *Canad. J. Chem.*, **35**, 1487.
- [4] BUCKINGHAM, A. D., and MACLAUCHLAN, K. A., 1963, *Proc. chem. Soc.*, p. 144.
- [5] KOWALEWSKI, V. J., and KOWALEWSKI, D. G., 1962, *J. chem. Phys.*, **36**, 266.
- [6] POPLER, J. A., and SANTRY, D. P., 1964, *Mol. Phys.*, **8**, 1.

The electronic structure of ionized molecules

II. Alkanes

by J. C. LORQUET†

Institut de Chimie de l'Université de Liège, quai F. Roosevelt, Liège, Belgique
and

Centre de Mécanique Ondulatoire Appliquée, 23, rue du Maroc, Paris 19°, France

(Received 4 August 1964)

The ionization of linear and branched alkanes and cyclanes has been studied by the semi-empirical EO method developed by Hall and Lennard-Jones. Three improvements have been introduced:

- (A) All CH bonds have been taken into account.
- (B) The inductive effect has been introduced into the calculations.
- (C) The error made by using the same MO's for both the molecule and its positive ion has been estimated and found to be negligible in the present method.

The calculated ionization energies are in good agreement with the available experimental values. Finally, the relation between the net positive charge on the different bonds of the ion and its dissociation pattern has been clarified.

1. INTRODUCTION

Some time ago, a very elegant method of calculating the ionization energies and the positive charge distribution in an ionized molecule was developed by Hall and Lennard-Jones [1,2]. The basic entities of this method are the equivalent orbitals (EO's) associated with the different bonds and lone pairs of the molecule. These EO's derive from the molecular orbitals by a linear transformation which concentrates them around one or two atoms. This localization property makes them the closest analogue in quantum chemistry of chemical bonds, inner shells and lone pairs. They form an orthonormal basis which spans the same space as the molecular orbitals. In a highly symmetrical molecule, or in a molecule containing only a limited number of chemically equivalent bonds (such as the alkanes), the number of their matrix elements will be small. If these are known, the eigenvalues and eigenvectors of this matrix will give directly the one-electron energies (which represent an approximation to molecular ionization potentials), as well as the coefficients of the expansion of the MO's on the orthonormal basis of the EO's. In Hall's method, the matrix elements between equivalent orbitals are determined from experimentally known ionization potentials of the first terms of a series of molecules, and then used to predict those of the others.

Conceptually, the basis of the method is extremely sound [1], since its equations are those of the accurate self-consistent field treatment (and not of its LCAO approximation). However, in all applications which have been made so far (mainly to linear paraffins), at least three approximations have been introduced.

† Chercheur Qualifié du Fonds National Belge de la Recherche Scientifique.

(A) A n -paraffin C_nH_{2n+2} is treated as a linear chain of n CH_2 groups. (The end CH bonds are disregarded in order to simplify the resolution of the secular equations.)

(B) The parameters of the method (i.e. the matrix elements of the EO's) are supposed to keep a constant value on a set of homologous molecules, and are not allowed to vary with their neighbourhood. (Neglect of the inductive effect.)

(C) The wave function of the ion is formed from the Slater determinant representing the neutral molecule by crossing out the row and column corresponding to the electron which is removed by ionization; but the same MO's are used for both the neutral molecule and its positive ion.

It is the purpose of this work to undertake a systematic study of the possibilities of this method, and to investigate the influence of the approximations which must be introduced. In the present paper we shall be concerned only with alkanes, linear, branched and cyclic. We shall first describe a conventional treatment where only approximation (A) has been removed, and then examine the influence of approximations (B) and (C).

2. THE FIRST APPROXIMATION

Five parameters are needed in the case of the alkanes. They are defined as follows:

- (a) diagonal matrix element of the self-consistent Hamiltonian with respect to the EO associated to a CH bond.
- (b) matrix element between the EO's associated to two adjacent CH bonds.
- (c) diagonal matrix element of the EO associated to a CC bond.
- (d) matrix element between a CC bond and an adjacent CH bond.
- (e) matrix element between two adjacent CC bonds.

The interaction between non-adjacent bonds is supposed to lead to negligible matrix elements.

In order to be consistent we shall use throughout the ionization potentials determined by Honig [3] for the linear paraffins. The first ionization energy of CH_4 is 13.04 eV. Using a RPD technique, Frost and McDowell [4] have measured the second ionization potential, corresponding to the removal of an electron from the a_1 orbital. They find an energy difference of 6.26 eV between the two ionization energies. Collin [5] has found 6.17 eV by the same method. From these data, the value of a and b can be easily obtained [1]:

$$\left. \begin{aligned} a &= -14.605 \text{ eV,} \\ b &= -1.565 \text{ eV.} \end{aligned} \right\} \quad (1)$$

The value of the other three parameters c , d and e must be obtained from experimental values of ionization potentials of other alkanes.

An unsolved problem then arises concerning the species of the uppermost orbital of a given n -paraffin. This orbital may either be built from CC EO's and in-phase combinations of CH EO's (thus leading to a a_1 or b_2 orbital in the classification of group C_{2v}), or it may be built from out-of-phase combinations of CH bonds only (b_1 or a_2 orbital). Hall has successively examined these

two assumptions [1, 6], and has found that both could give agreement with the existing experimental data. The first assumption seems however to be more reasonable, since it leads to a secular equation of a higher degree with relatively large off-diagonal elements, while in the second, one has to introduce small interaction parameters between distant orbitals in order to explain the variation of the first ionization potential in a series of molecules. Moreover, the dissociation processes observed in the mass spectra of alkanes are more easily understood if one assumes that the ionization affects CC bonds (*vide infra*). The first assumption was thus preferred.

With this assignment, the order of stability of the orbitals of ethane is the following: $(a_{1g})^2(a_{2u})^2(e_g)^4(e_u)^4(a_{1g})^2$, in agreement with Mulliken's [7] and Hall's [1] suggestions, but in partial disagreement with recent calculations by Hoffmann [8] and by Pitzer [9] where the e_u is above the a_{1g} orbital. The difference of stability between the latter orbitals is quite small; in Hoffmann's semi-empirical theory it depends very sensitively on the choice of the parameters, and it may easily be reversed (cf. figure 10 of ref. [8]). In all calculations, however, the energy of the a_{1g} is above the average energy of the e_g and e_u orbitals. The splitting between the latter is determined in the present treatment by the intensity of the interactions between distant CH orbitals which have been neglected in this approximation, and which will raise the energy of the e_u orbital and lower that of the e_g [1]. It is probable that the e_u and a_{1g} orbitals are of comparable stability and thus, that even if the e_u was the less stable, the error made by attributing a value of 11.76 eV (first ionization energy of ethane), to the energy of the a_{1g} orbital would be numerically small.

The secular equations for all n -alkanes up to decane were solved numerically on a computer (IBM 7040). The values of parameters a and b were those derived from the ionization energies of methane (1), and the other three were adjusted to fit the experimental values of the lowest ionization potential of the other n -paraffins. The following set of parameters:

$$\left. \begin{aligned} c &= -20.205 \text{ eV,} \\ d &= -2.9 \text{ eV,} \\ e &= -5.129 \text{ eV,} \end{aligned} \right\} \quad (2)$$

gives a very good agreement between experimental and calculated values for the first ionization potential of n -alkanes. If, however, the same set is used for the branched paraffins, one obtains ionization potentials which are systematically too high by a few tenths of an electron volt. This discrepancy was attributed to the neglect of the inductive effect. A method of correcting approximation (B) is therefore developed in the next section.

3. THE INDUCTIVE EFFECT

The evaluation of the influence of the inductive effect follows closely the calculation of the matrix elements in the Pariser-Parr method [10]. Let χ_m be the equivalent orbital associated to bond m . By definition, one has:

$$e_{mn} \equiv \int \chi_m^* \left\{ H^c + \sum_p (2J_p - K_p) \right\} \chi_n d\tau, \quad (3)$$

where H^c is the sum of the kinetic energy operators and of the potential energy operators between electrons and cores. J_p and K_p are the Coulomb and exchange

operators expressed in terms of the EO's. Since the EO's are both localized and orthogonal, the zero differential approximation should be quite justified. It was already shown by Lennard-Jones and Pople [11] that the sum of the exchange integrals is smallest when equivalent orbitals are used. The exchange and hybrid integrals occurring in (3) may thus be neglected before the Coulombic terms.

Let us now evaluate the matrix element a in two molecules: methane and ethane. In CH_4 ,

$$a = (h_1|h_1) + (h_1h_1|h_1h_1) + 6(h_1h_1|h_2h_2). \quad (4)$$

In C_2H_6 ,

$$a = (h_1|h_1) + (h_1h_1|h_1h_1) + 4(h_1h_1|h_2h_2) + 2(h_1h_1|cc) + 2(h_1h_1|h_4h_4) + 4(h_1h_1|h_5h_5). \quad (5)$$

h_i is the EO associated to the i th CH bond. In C_2H_6 they are numbered according to figure 1. $(h_1|h_1)$ is the matrix element of the core Hamiltonian H^c ; it has

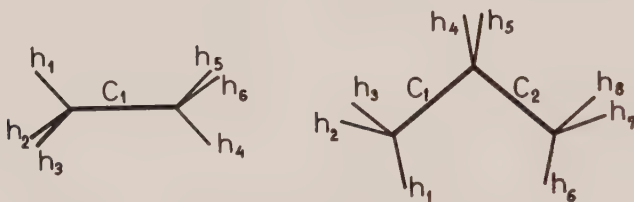


Figure 1. Bond designation in ethane and propane.

a different value in CH_4 and in C_2H_6 . These terms will now be evaluated using the Goeppert-Mayer-Sklar approximation [10][12]. Let us put:

$$(q:pp) \equiv - \int U_q^*(i) \chi_p^*(i) \chi_p(i) d\tau_i. \quad (6)$$

where U_q^* designates the potential due to a neutral bond q . $(q:pp)$ is called a penetration integral:

$$W_{\text{CH}} \equiv \int h_1^*(i) [T(i) + U_{\text{CH}}(i)] h_1(i) d\tau_i. \quad (7)$$

$T(i)$ is the kinetic energy operator associated to electron i , and U_{CH} is the potential due to a CH bond without its two valence electrons. One then finds for CH_4 :

$$(h_1|h_1) = W_{\text{CH}} - 6(h_1h_1|h_2h_2) - 3(h_2:h_1h_1). \quad (8)$$

For C_2H_6 :

$$\begin{aligned} (h_1|h_1) = & W_{\text{CH}} - 4(h_1h_1|h_2h_2) - 2(h_1h_1|h_4h_4) - 4(h_1h_1|h_5h_5) \\ & - 2(h_1h_1|cc) - 2(h_2:h_1h_1) - (h_4:h_1h_1) \\ & - 2(h_5:h_1h_1) - (c:h_1h_1). \end{aligned} \quad (9)$$

The penetration integrals involving non-adjacent bonds are negligible. Substituting in (4) and (5), one gets for CH_4 :

$$a_0 = W_{\text{CH}} + (h_1h_1|h_1h_1) - 3(h_2:h_1h_1). \quad (10)$$

For C_2H_6 :

$$a_1 = W_{\text{CH}} + (h_1h_1|h_1h_1) - 2(h_2:h_1h_1) - (c:h_1h_1). \quad (11)$$

We denote by a_n the diagonal matrix element associated to a CH bond linked to n CC bonds (a_1 for the CH bonds of a methyl group, a_2 for those of a methylene group, a_3 for a tertiary CH bond). Let us put:

$$\delta \equiv (h_2 : h_1 h_1) - (c : h_1 h_1). \quad (12)$$

One has:

$$a_n = a_0 + n\delta. \quad (13)$$

In a similar way, one gets the equations:

$$c_0 = W_{CC} + (cc|cc) - 6(h_1 : cc), \quad (14)$$

$$c_n = c_0 + n\epsilon, \quad (15)$$

$$\epsilon \equiv (h_1 : c_1 c_1) - (c_2 : c_1 c_1). \quad (16)$$

c_0 is the diagonal matrix element of the CCEO of ethane and c_n that of a CCEO substituted by n CC bonds. In this approximation, the mode of substitution has no importance. For instance, the diagonal matrix element of the central CC bond of n -butane is equal to that of a CC bond of isobutane (two CC neighbours each). δ and ϵ are treated as two additional parameters, and will be determined by comparison with experiment. As a simplifying assumption, we take $\delta \simeq \epsilon$, this being based on an approximate relation between penetration integrals involving atomic orbitals [13, 14] $((a : bb) \simeq (a : cc)$, where a , b and c are atomic orbitals). The value of the off-diagonal elements b , d and e does not, to a good approximation, depend upon neighbouring bonds or atoms. Our final set of parameters is then:

$$\left. \begin{aligned} a_0 &= -14.605 \text{ ev}, \\ b &= -1.565 \text{ ev}, \\ c_0 &= -18.443 \text{ ev}, \\ d &= -2.492 \text{ ev}, \\ e &= -3.792 \text{ ev}, \\ \delta = \epsilon &= +0.4 \text{ ev}. \end{aligned} \right\} \quad (17)$$

The value of δ and ϵ is very inaccurate, and indicates an order of magnitude only.

The present set of parameters eliminates an inconsistency concerning the value of a and b . In Hall and Lennard-Jones's work, $(a+b)$ was equal to

Sym. sp.	Orb. en. (ev)	
a_{1g}	-11.76	$0.6744 c - 0.3014 (h_1 + h_2 + h_3 + h_4 + h_5 + h_6)$
e_g	-12.64	$\begin{cases} (12)^{-1/2} (2h_1 - h_2 - h_3 + 2h_4 - h_5 - h_6) \\ 0.5 (h_2 - h_3 + h_5 - h_6) \end{cases}$
e_u	-12.64	$\begin{cases} (12)^{-1/2} (2h_1 - h_2 - h_3 - 2h_4 + h_5 + h_6) \\ 0.5 (h_2 - h_3 - h_5 + h_6) \end{cases}$
a_{2u}	-17.33	$(6)^{-1/2} (h_1 + h_2 + h_3 - h_4 - h_5 - h_6)$
a_{1g}	-24.02	$0.7384 c + 0.2753 (h_1 + h_2 + h_3 + h_4 + h_5 + h_6)$

Table 1. Molecular orbitals of ethane

–16.2 eV in the case of CH_4 , and to –12 eV for the other alkanes. Although in the right direction, this difference is much too large to be explained by an inductive effect.

The orbital energies and the molecular orbitals of a particular molecule are given by the eigenvalues and eigenvectors of the associated matrix. For sake of brevity, these will be given for ethane and propane only (tables 1 and 2). The next two sections are devoted to a discussion of the ionization potentials and of the charge distributions.

Sym. sp.	Orb. en. (eV)	
b_2	–11.21	$0.5780 (c_1 - c_2) - 0.2352 (h_1 + h_2 + h_3 - h_6 - h_7 - h_8)$
a_1	–11.72	$0.3806 (c_1 + c_2) - 0.1688 (h_1 + h_2 + h_3 + h_6 + h_7 + h_8) - 0.5193 (h_4 + h_5)$
b_1	–12.24	$(2)^{-1/2} (h_4 - h_5)$
a_1	–12.64	$(12)^{-1/2} (2h_1 - h_2 - h_3 + 2h_6 - h_7 - h_8)$
a_2	–12.64	$0.5 (h_2 - h_3 - h_7 + h_8)$
b_1	–12.64	$0.5 (h_2 - h_3 + h_7 - h_8)$
b_2	–12.64	$(12)^{-1/2} (2h_1 - h_2 - h_3 - 2h_6 + h_7 + h_8)$
a_1	–16.60	$0.0980 (c_1 + c_2) - 0.3331 (h_1 + h_2 + h_3 + h_6 + h_7 + h_8) + 0.3968 (h_4 + h_5)$
b_2	–20.38	$0.4073 (c_1 - c_2) + 0.3337 (h_1 + h_2 + h_3 - h_6 - h_7 - h_8)$
a_1	–26.22	$0.5878 (c_1 + c_2) + 0.1649 (h_1 + h_2 + h_3 + h_6 + h_7 + h_8) + 0.2700 (h_4 + h_5)$

Table 2. Molecular orbitals of propane.

4. IONIZATION POTENTIALS

The calculated and experimental values of the lowest ionization potentials are compared in table 3. The quoted experimental error is of the order of 0.02 eV. However, as discussed by Chupka and Kaminsky [15], a more realistic estimate of the absolute error involved would be 0.1–0.2 eV, perhaps more for the branched paraffins. The overall agreement is thus very good. Since our calculations pertain to vertical processes, photoionization values are expected to be consistently low by a few tenths of an electron volt. They are indicated in parenthesis.

The present calculations predict an alternation in the value of the ionization potentials of the unstrained cyclanes. This unusual behaviour has been experimentally observed by Natalis, Steiner and Inghram [16].

The secular equations also give an estimate of the lower orbital energies. These are given in table 4 for the n -alkanes where they have been classified according to the representations of group C_{2v} (except for ethane).

The electron which is removed by ionization belongs to a totally symmetric orbital if the number of carbon atoms is even; if it is odd, the uppermost occupied orbital is antisymmetric with respect to the plane perpendicular to the CC bonds. One notices a set of accidentally degenerate levels at $a_1 - b$ (–12.64 eV) and at $a_2 - b$ (–12.24 eV). As in the case of ethane, these degeneracies will be split by higher-order interactions, but the extent of this splitting is difficult to estimate.

Moreover, this treatment only gives the ionization potentials which may be described in the self-consistent field theory by the simple removal of a valence electron. In addition, one also has to consider another set where this removal is accompanied by the excitation of one or more remaining electrons to unoccupied orbitals. The density of these states will be greater than that of the states produced by the first process and will increase rapidly with the energy. Quartet states will be found among them.

	Calc.	Experimental			
Ethane	11.76	11.76			(11.65)
Propane	11.21	11.21			(11.07)
<i>n</i> -butane	10.81	10.80			(10.63)
<i>n</i> -pentane	10.58	10.55			(10.35)
<i>n</i> -hexane	10.43	10.43			(10.18)
<i>n</i> -heptane	10.34	10.35			(10.08)
<i>n</i> -octane	10.28	10.24			
<i>n</i> -nonane	10.23	10.21			
<i>n</i> -decane	10.20	10.19			
<i>isobutane</i>	10.94	10.79	11.06	10.7	(10.57)
<i>isopentane</i>	10.49	10.60			(10.32)
<i>neopentane</i>	10.66		10.29		(10.35)
2-methylpentane	10.32	10.34			(10.12)
3-methylpentane	10.31	10.30			(10.08)
2,2-dimethylbutane	10.18				(10.06)
2,3-dimethylbutane	10.13	10.24	10.19	10.5	(10.02)
Cyclopentane	10.53	10.92			(10.53)
Methylcyclopentane	10.28	10.45			
Cyclohexane	10.06	10.50			(9.88)
Methylcyclohexane	9.91	10.19			(9.85)
Cycloheptane	10.32				
Cyclooctane	10.06				

Table 3. Calculated and observed [31] values of the first ionization potential of alkanes and cyclanes (in electron volts). Photoionization data are included in parenthesis.

For these reasons, the data of table 4 are not expected to give an accurate estimate of the position of the electronic levels of the ion. A configuration interaction treatment involving unoccupied orbitals would probably give results more directly comparable to experimental observations. Unfortunately, the latter are at present so scarce and unreliable that sufficient data are not available to allow any such refinement†.

† The ionization efficiency curves of a few alkanes have been very recently studied by the RPD method (C. E. Melton and W. H. Hamill, *J. chem. Phys.*, **41**, 546 (1964)). One observes breaks at 11.6, 12.1, and 12.7 eV for C₂H₆ and at 11.1, 11.4, 11.8 and 12.2 eV for C₃H₈ which closely match the calculated values. The additional breaks observed at 12.1 and 11.4 eV are probably due to auto-ionization and metastable decomposition reactions. The author is indebted to Drs. C. E. Melton and W. H. Hamill for communicating their results before publication.

5. CHARGE DISTRIBUTION

The net positive charge distribution in the ground state of the ion is shown in figures 2, 3 and 4. It may be seen that the present results are not very different from those given by Lennard-Jones and Hall [2] and by Fueki and Hirota [17] for the other linear alkanes.

Methane 13.04 (t_1); 19.30 (a_1).
Ethane 11.76 (a_{1g}); 12.64 ($e_g + e_u$); 17.33 (a_{2u}); 24.02 (a_{1g}).
Propane 11.21 (b_2); 11.72 (a_1); 12.24 (b_1); 12.64 ($a_1 + a_2 + b_1 + b_2$); 16.60 (a_1); 20.38 (b_2); 26.22 (a_1).
<i>n</i> -butane 10.81 (a_1); 11.56 (b_2); 11.71 (a_1); 12.24 ($a_2 + b_1$); 12.64 ($a_1 + a_2 + b_1 + b_2$); 16.21 (b_2); 18.64 (a_1); 22.98 (b_2); 27.23 (a_1).
<i>n</i> -pentane 10.58 (b_2); 11.31 (a_1); 11.64 (b_2); 11.71 (a_1); 12.24 ($a_2 + 2b_1$); 12.64 ($a_1 + a_2 + b_1 + b_2$); 15.97 (a_1); 17.70 (b_2); 20.79 (a_1); 24.68 (b_2); 27.76 (a_1).
<i>n</i> -hexane 10.43 (a_1); 11.09 (b_2); 11.50 (a_1); 11.67 (b_2); 11.70 (a_1); 12.24 ($2a_2 + 2b_1$); 12.64 ($a_1 + a_2 + b_1 + b_2$); 15.83 (b_2); 17.13 (a_1); 19.40 (b_2); 22.57 (a_1); 25.77 (b_2); 28.07 (a_1).
<i>n</i> -heptane 10.34 (b_2); 10.90 (a_1); 11.34 (b_2); 11.57 (a_1); 11.68 (b_2); 11.70 (a_1); 12.24 ($2a_2 + 3b_1$); 12.64 ($a_1 + a_2 + b_1 + b_2$); 15.72 (a_1); 16.74 (b_2); 18.49 (a_1); 21.00 (b_2); 23.89 (a_1); 26.50 (b_2); 28.27 (a_1).
<i>n</i> -octane 10.28 (a_1); 10.76 (b_2); 11.20 (a_1); 11.47 (b_2); 11.62 (a_1); 11.69 (b_2); 11.70 (a_1); 12.24 ($3a_2 + 3b_1$); 12.64 ($a_1 + a_2 + b_1 + b_2$); 15.65 (b_2); 16.47 (a_1); 17.86 (b_2); 19.87 (a_1); 22.35 (b_2); 24.87 (a_1); 27.00 (b_2); 28.41 (a_1).

Table 4. Higher ionization potentials of *n*-alkanes.

For all paraffinic ions in their ground state, most of the positive charge is distributed on the CC bonds, and a very small fraction of it remains on the CH bonds.

It has often been assumed that there is a relation between the weakening of a particular bond after ionization, and its ability to dissociate. The striking parallelism between the fragmentation pattern of *n*-octane at 50 v and the charge densities on the different CC bonds was noticed by Thompson [18, 19]. It was shown by Coggeshall [20], however, that the positive charge has its maximum value on the central CC bond of a linear paraffin, whereas the most probable dissociation at 50 v always involves the production of a C_3 or C_4 fragment. The correlation just mentioned holds thus only up to octane and does not maintain for larger linear alkanes.

As far as large *n*-paraffins are concerned, we think that the charge distribution is too evenly distributed to have a decisive influence on the fragmentation of the ion. For *n*-dectane, for instance, the net positive charges on the different CC bonds, starting from the central one, are respectively: 0.20, 0.18, 0.13, 0.06 and 0.02. Clearly, in this case, the dissociation must be determined by other factors than the bond strengths, especially at 50 v.

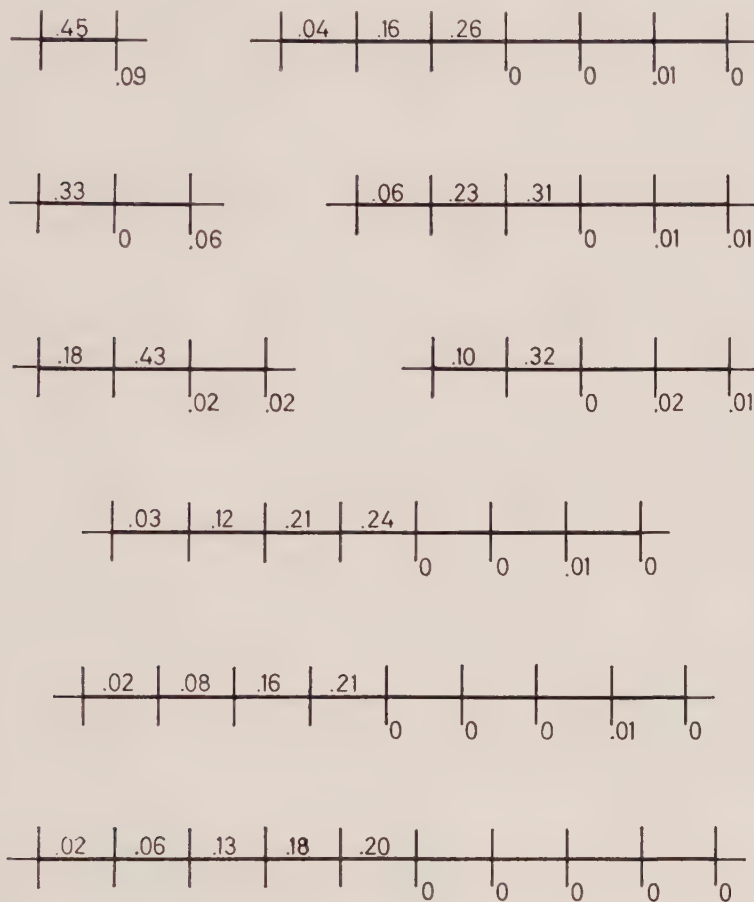


Figure 2. Net positive charge distribution in the ground state of the ions of linear alkanes.

The situation, however, is quite different for the branched alkanes (figure 3). For these ions, the positive charge is substantially greater on a particular bond (viz. the CC bond which is substituted by the largest number of CC bonds), which may then correspond to a point of greater fragility. According to the results reported on figure 3, isopentane, 2-methylpentane and 2,3-dimethylbutane are expected to give large amounts of C_3 ions, while 3-methylpentane and 2,2-dimethylbutane will yield C_4 ions preferentially. This is indeed found to be the case at 50 v [21]. In figures 5–9, the sums of the relative abundances of ions corresponding to the same number of carbon atoms have been plotted as a function of the energy of the impinging electrons (spectra taken on an AEI MS9 mass spectrometer). It may be seen that the correlation holds for

all values of V . This fact is probably connected with the existence of radiationless transitions which convert an appreciable fraction of ions, first created in excited states by the interaction with a 50 v electron, to the ground state with a large excess of vibrational energy.

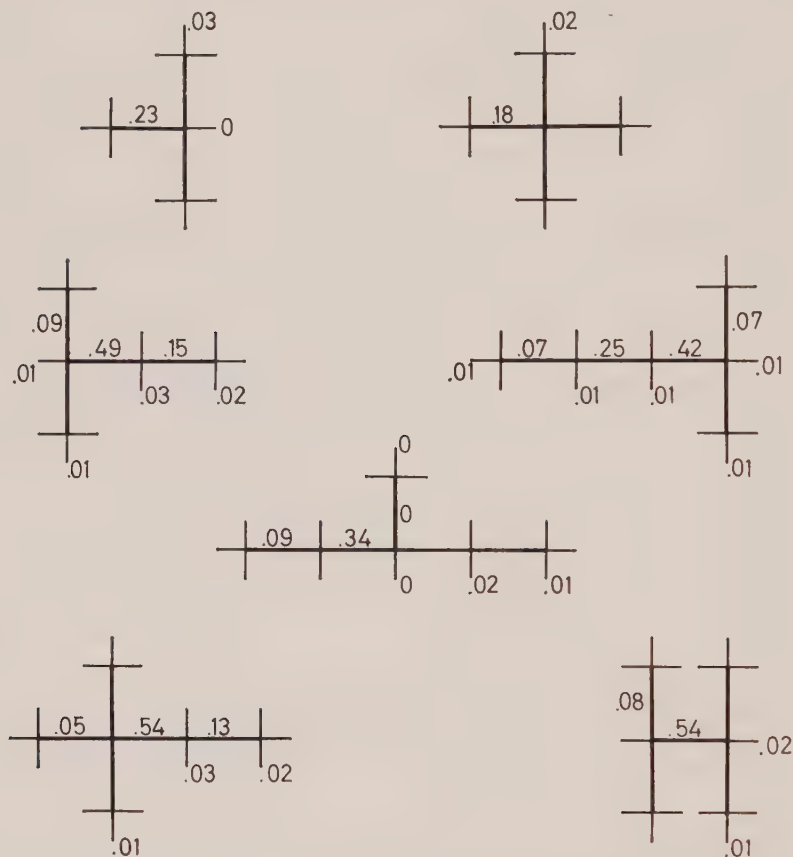


Figure 3. Net positive charge distribution in the ground state of the ions of branched alkanes.

6. INFLUENCE OF ORBITAL REARRANGEMENT

In the calculations described so far, the same MO's were used for the ground state of the neutral molecule and of its ion. Partial justification of this approximation has been given [22-24]. However, several numerical calculations using the SCFLCAO method, on NH_3^+ [25] (Part I of this series), on CH^+ [16] and on the ions of aromatic hydrocarbons [27] have shown it to be unreliable. It was therefore attempted to get an estimate of the accuracy of this approximation by calculating the true self-consistent orbitals of the positive ion, using those of the neutral molecule as a starting point for the iterative process.

The method of the self-consistency conditions proposed by Longuet-Higgins and Pople [28] and especially developed by Lefebvre [29] was found quite

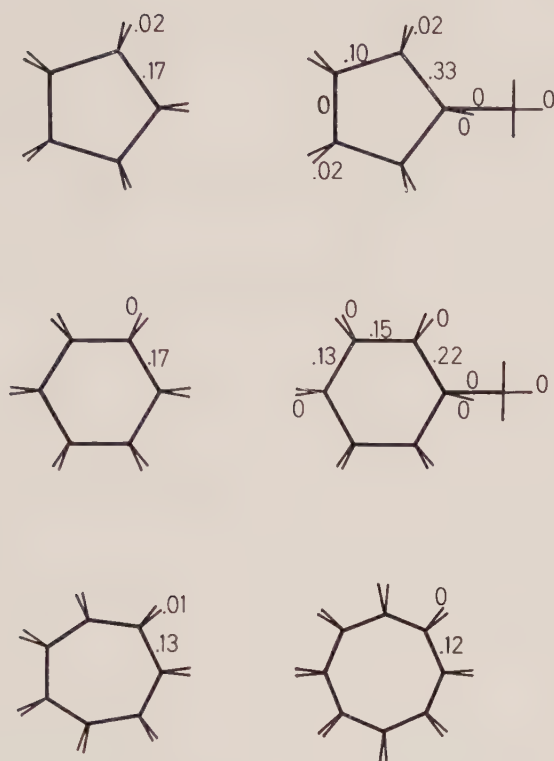


Figure 4. Net positive charge distribution in the ground state of the ions of cyclanes.

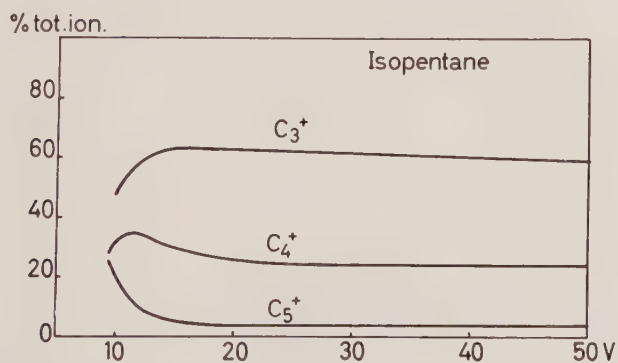


Figure 5. Relative abundances as a function of the energy of the electrons (isopentane).

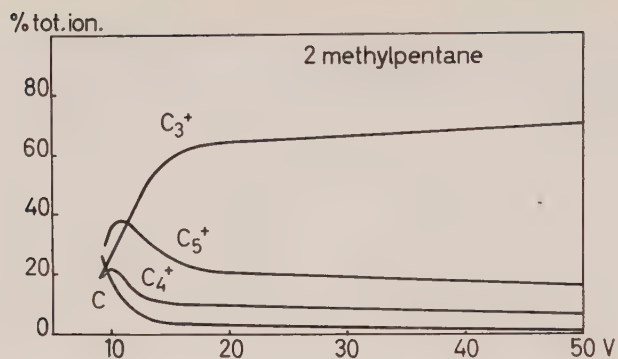


Figure 6. Relative abundances as a function of the energy of the electrons (2-methylpentane).

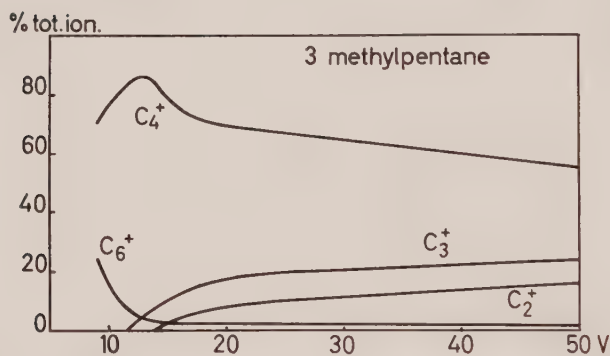


Figure 7. Relative abundances as a function of the energy of the electrons (3-methylpentane).

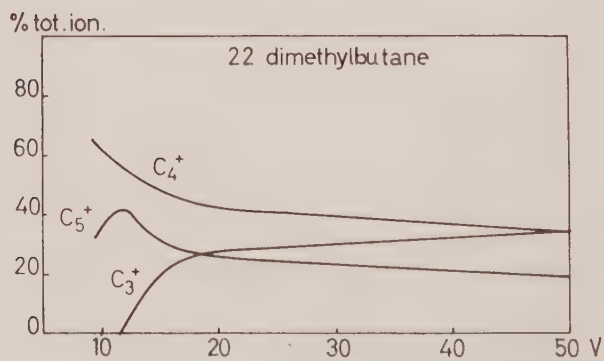


Figure 8. Relative abundances as a function of the energy of the electrons (2,2-dimethylbutane).

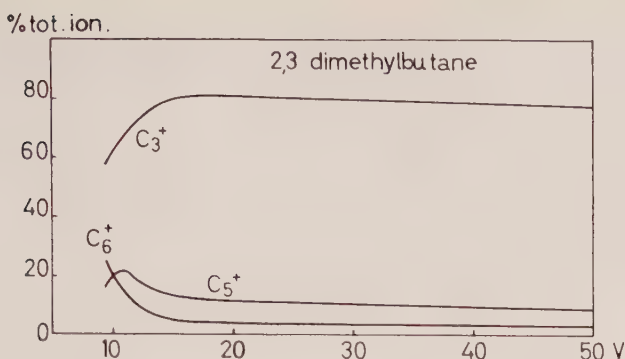


Figure 9. Relative abundances as a function of the energy of the electrons (2,3-dimethylbutane).

suitable to handle this open shell problem. In order to be self-consistent, the MO's of the ion must obey the following equations:

$$\epsilon_{i0} + \frac{1}{2}(\phi_0\phi_0|\phi_0\phi_i) = 0, \quad (18)$$

$$\epsilon_{ik} = 0, \quad (19)$$

$$\epsilon_{0k} - \frac{1}{2}(\phi_0\phi_0|\phi_0\phi_k) = 0. \quad (20)$$

In these expressions, ϕ_0 represents the orbital which is singly occupied as a result of the ionization process, ϕ_i is a doubly occupied orbital and ϕ_k an unoccupied MO. The ϵ 's are the matrix elements of the self-consistent Hamiltonian of the ion:

$$H_{\text{ion}} = H^c + \sum_j (2J_j - K_j) + \frac{1}{2}(2J_0 - K_0). \quad (21)$$

If one now uses the MO's of the molecule as the starting point of the iterative process, it is easily seen that conditions (18) are automatically fulfilled since they are equivalent to the self-consistency conditions of the molecule (i.e. the conditions that the off-diagonal matrix elements of the molecular Hamiltonian should be equal to zero). This result was already demonstrated by Koopmans [22].

To insure additional flexibility, one then introduces a set of unoccupied orbitals ϕ_k , orthogonal to the ϕ_i 's and ϕ_0 . The ϕ_k 's may, for example, be expanded on the antibonding EO's associated to each bond of the molecule. Since, by definition, the ϕ_i 's and ϕ_0 are the result of an accurate self-consistent field calculation, the subspace they determine is orthogonal to the subspace spanned by the ϕ_k 's. This means that no EO will enter into the expansion of a ϕ_k orbital of the molecule, and conversely, that no member of the new set will enter into the expansion of the MO's of the neutral molecule. In the ion, however, both sets will be mixed to an extent determined by equations (18), (19) and (20). Therefore, if one expands integrals such as $(\phi_0\phi_0|\phi_0\phi_k)$, $(\phi_0\phi_0|\phi_i\phi_k)$ and $(\phi_0\phi_i|\phi_0\phi_k)$ over the extended set of EO's, one gets a sum of exchange and hybrid integrals only. Now, as already discussed, the EO's should verify the zero differential approximation, and these non-coulombic integrals are negligible. As to the ϵ 's, they may be expressed as a sum of the matrix elements of the self-consistent molecular Hamiltonian, which are equal to zero by hypothesis, and of bielectronic integrals of the type just discussed. They are thus negligible.

Thus, if the molecular orbitals of the ion are allowed to expand on an increased basis, equations (19) and (20) are verified to a good approximation, and the resulting correction is found to be negligible. The MO's of the molecule are thus also self-consistent for the ion to a good approximation. This result is peculiar to the EO method only. It is not valid for LCAO calculations.

This may be interpreted as follows. The square moduli of the coefficients $|c_{ij}|^2$ are related to the electronic charge density obtained by an integration process, around an atom in the LCAO scheme, or in the region between two linked nuclei in the EO method. If one visualizes the charge displacements which accompany the ionization as shifts of electron pairs between bonded atoms, one sees that the charge distribution (and the c_{ij} 's) will be very sensitive to such displacements in the LCAO approximation, and much less so in the EO method. This is due to the particular dissection of space used in the population analysis of each method. This is similar to a result obtained by Daudel [30], showing that the EO method is unable to describe the charge transfers induced by the substitution of a hydrogen atom in a paraffin by a heteroatom.

The author is grateful to Professors R. Daudel, L. D'Or and G. G. Hall and to Drs. S. Bratoz and R. Lefebvre for many helpful discussions. He also wishes to thank the staff of the Computing Centre of the University of Liege (CECTI) for assistance with the numerical computations.

La méthode semi-empirique des orbitales équivalentes introduite par Hall et Lennard-Jones a été appliquée à l'étude de l'ionisation des alcanes linéaires et ramifiés et des cyclanes. Cette méthode a été améliorée en trois points:

- (A) Toutes les liaisons CH ont été prises en considération.
- (B) L'effect inductif a été introduit dans les calculs.
- (C) On a estimé l'importance du remaniement de l'atmosphère électronique consécutif à l'ionisation. Dans la méthode décrite, l'erreur commise en utilisant les mêmes orbitales moléculaires pour représenter la molécule et son ion positif peut être considérée comme négligeable.

Les énergies d'ionisation calculées sont en bon accord avec les valeurs expérimentales existantes. Enfin, on précise la relation existant entre la distribution de la charge positive dans l'ion et les processus de dissociation observés.

REFERENCES

- [1] HALL, G. G., 1951, *Proc. roy. soc.*, A **205**, 541.
- [2] LENNARD-JONES, J. E., and HALL, G. G., 1952, *Trans. Faraday Soc.*, **48**, 581.
- [3] HONIG, R. E., 1948, *J. chem. Phys.*, **16**, 105.
- [4] FROST, D. C., and McDOWELL, C. A., 1957, *Proc. roy. Soc.*, A, **241**, 194.
- [5] COLLIN, J. E., 1961, *IX Colloquium Spectroscopicum Internationale*, Lyon, p. 596.
- [6] HALL, G. G., 1954, *Trans. Faraday Soc.*, **50**, 319.
- [7] MULLIKEN, R. S., 1935, *J. chem. Phys.*, **3**, 517.
- [8] HOFFMANN, R., 1963, *J. chem. Phys.*, **39**, 1397.
- [9] PITZER, R. M., and LIPSCOMB, W. N., 1963, *J. chem. Phys.*, **39**, 1995.
- [10] PARISER, R., and PARR, R. G., 1953, *J. chem. Phys.*, **21**, 466.
- [11] LENNARD-JONES, J. E., and POPL, J. A., 1950, *Proc. roy. Soc.*, A **202**, 166.
- [12] GOEPPERT-MAYER, M., and SKLAR, A. L., 1938, *J. chem. Phys.*, **6**, 645.
- [13] LEROY, G., VAN MEERSSCHE, M., and GERMAIN, G., 1963, *J. Chim. Phys.*, **60**, 1283.
- [14] DAHL, J. P., and HANSEN, A. E., 1963, *Theor. chim. Acta*, **1**, 199.
- [15] CHUPKA, W. A., and KAMINSKI, M., 1961, *J. chem. Phys.*, **35**, 1991.
- [16] NATALIS, P. (private communication).

- [17] FUEKI, K., and HIROTA, K., 1960, *Nippon Kagaku Zasshi*, **81**, 212.
- [18] THOMPSON, R., 1953, *Conference on Applied Mass Spectroscopy* (London: Institute of Petroleum), p. 185.
- [19] FIELD, F. H., and FRANKLIN, J. L., 1957, *Electron Impact Phenomena* (New York. Academic Press), p. 171.
- [20] COGGESHALL, N. D., 1959, *J. chem. Phys.*, **30**, 595.
- [21] AMERICAN PETROLEUM INSTITUTE, 1953, *Catalog of Mass Spectral Data*, Pittsburgh.
- [22] KOOPMANS, T., 1933, *Physica*, **1**, 104.
- [23] MULLIKEN, R. S., 1949, *J. Chim. phys.*, **46**, 497.
- [24] HALL, G. G., and LENNARD-JONES, J. E., 1950, *Proc. roy. Soc. A*, **202**, 155.
- [25] LORQUET, J. C., and LEFEBVRE-BRION, H., 1960, *J. Chim. Phys.*, **57**, 85.
- [26] CORNILLE, M., 1960, *Cah. Phys.*, **124**, 497.
- [27] HOYLAND, J. R., and GOODMAN, L., 1962, *J. chem. Phys.*, **36**, 12.
- [28] LONGUET-HIGGINS, H. C., and POPE, J. A., 1955, *Proc. phys. Soc., Lond. A*, **68**, 591.
- [29] LEFEBVRE, R., 1957, *J. Chim. phys.*, **54**, 168.
- [30] DAUDEL, R., 1962, *Structure Electronique des Molécules* (Paris: Gauthier-Villars), p. 129.
- [31] KISER, R. W., 1960, and 1962 *Tables of Ionization Potentials*, USAEC Office of Technical Information, TID-6142.

Vacuum ultra-violet absorption spectra of various mono-substituted benzenes

by K. KIMURA† and S. NAGAKURA

The Institute for Solid State Physics, The University of Tokyo,
Minato-ku, Tokyo, Japan

(Received 5 August 1964)

The vacuum ultra-violet spectra of various mono-substituted benzenes were measured in the wavelength region of 1550 Å to 2200 Å in the vapour phase by a recording vacuum ultra-violet spectrophotometer. The compounds studied here are phenols (phenol, anisole, phenetole and thiophenol), halogenobenzenes (fluorobenzene, chlorobenzene, bromobenzene and iodobenzene), and toluene. It was found that four $\pi \rightarrow \pi^*$ transition bands appear in the wavelength region of 1550 Å to 3000 Å for phenol, anisole, phenetole, fluorobenzene, chlorobenzene and bromobenzene. On the other hand, six $\pi \rightarrow \pi^*$ transition bands were found in the same wavelength region for thiophenol and iodobenzene. The absorption spectra of the former group are similar to that of benzene itself. On the other hand, the absorption spectra of the latter group are very different from that of benzene and rather similar to those of the anilines studied in a previous paper. From this point of view, the former group may be regarded as the molecules with weak substituents, and the latter as the molecules with strong substituents.

Theoretical studies of π -electron structures have been carried out with the phenols and halogenobenzenes by considering configurational interactions among the ground, locally excited, and intramolecular charge-transfer configurations. Good agreement was obtained between the experimental and theoretical values for both transition energies and oscillator strengths. It was concluded that the energies of charge-transfer configurations have a great effect upon the absorption spectra of the mono-substituted benzene molecules. That is to say, the charge-transfer configurations lie intermediate between the locally excited configurations for the molecules with strong substituents, while for the molecules with weak substituents they have higher energies than the locally excited configurations. Intramolecular charge-transfer bands were observed for the molecules with strong substituents.

The electron affinity of benzene was determined to be -1.1 ± 0.3 eV from the energy of the charge-transfer configuration estimated in such a way as to explain as well as possible the observed absorption spectra of the mono-substituted benzenes under consideration.

1. INTRODUCTION

Since a study on the electronic spectra of nitrobenzene, benzaldehyde, acetophenone and benzoic acid by Nagakura and Tanaka [1], electronic spectra of some substituted benzenes have been studied in terms of intramolecular charge-transfer between substituents and the benzene ring [2-10]. It was surmised from the theoretical studies that there appear additional bands characteristic of the charge-transfer interaction between substituents and the

† Present address: Department of Chemistry, Faculty of Engineering Science, Osaka University, Toyonaka, Osaka.

benzene ring. One of the methods of demonstrating experimentally the appearance of the additional bands of this kind, which may be called the intramolecular charge-transfer band by an analogy with Mulliken's terminology for the intermolecular case [11], is to find new $\pi \rightarrow \pi^*$ transition bands in addition to the four $\pi \rightarrow \pi^*$ transition bands pertinent to benzene. In this sense, it seems to be important to measure the absorption spectra of mono-substituted benzenes in both near and vacuum ultra-violet regions. So far, however, no detailed and extensive measurements of vacuum ultra-violet absorption have been made with mono-substituted benzenes, although some studies were made by Klevens and Platt [12], and by Walsh *et al.* [13].

Very recently we have measured in detail the vacuum ultra-violet absorption spectra of nitrobenzene and aniline (and its derivatives) with a spectrophotometer constructed in our laboratory [14]. The result for nitrobenzene showed that five $\pi \rightarrow \pi^*$ transition bands can be observed in the wavelength region of 3000 Å to 1550 Å. By comparing the observed band positions and intensities with the theoretical results, we were led to the conclusion that the 240 mμ band of nitrobenzene may be assigned to an intramolecular charge-transfer band, the transition of which is accompanied by electron transfer from the benzene ring to the nitro group [9]. This assignment may be said to be supported by the direction of the transition moment determined by Labhart from the absorption measurement under strong electric field [15].

A similar experimental and theoretical study was made with aniline and some of its N-derivatives [10] with the result that each of these compounds exhibits six $\pi \rightarrow \pi^*$ transition bands in the wavelength region of 3000 Å to 1550 Å. This means that the intramolecular charge-transfer bands accompanied by electron transfer from the substituent groups to the benzene ring appear for these compounds.

These studies have prompted the present investigation including the phenols, thiophenol, the halogenobenzenes and toluene. The results have shown that these compounds can be divided into two classes from the observed absorption spectra. Phenol, fluorobenzene, chlorobenzene and bromobenzene belong to one group. These molecules show three or four $\pi \rightarrow \pi^*$ transition bands which can satisfactorily be interpreted in terms of the $A_{1g} \rightarrow B_{2u}$, $A_{1g} \rightarrow B_{1u}$ and $A_{1g} \rightarrow E_{1u}$ bands of benzene. On the other hand, six bands have been observed with thiophenol and iodobenzene. Furthermore, in order to interpret the difference in absorption spectra between the two groups, theoretical studies have been carried out by considering the interaction between the benzene ring and substituent groups by configurational interaction among ground, locally excited and charge-transfer configurations.

2. MEASUREMENTS OF VACUUM ULTRA-VIOLET ABSORPTION SPECTRA

The absorption in the wavelength region of 1550 Å to 2200 Å were measured at room temperature† by a recording vacuum ultra-violet spectrophotometer constructed in our laboratory, the apparatus using a Bausch and Lomb concave grating with a radius of 995.4 mm. The details of this apparatus have recently

† The absorption spectrum of phenol was measured at the room temperature of 30.0°C, and the spectra of the other compounds were at about 25°C.

been published elsewhere [14]. A hydrogen discharge lamp of hot-cathode type from Hitachi Co. was used as a light source. Gas cells with light paths 7, 10 and 30 mm long and with lithium fluoride windows were used.

The mono-substituted benzenes studied here are phenol, anisole, phenetole, thiophenol, fluorobenzene, bromobenzene, iodobenzene and toluene. The commercial materials of the compounds were fractionally distilled in a vacuum system and the vapours of the purified samples were transferred through it into an absorption cell placed in the cell compartment of the spectrophotometer. The vapour pressure was measured with an accuracy of ± 0.02 mm Hg, a mercury manometer with a travelling microscope attached being used. The vacuum ultra-violet spectra for the respective compounds were carefully measured several times with different vapour pressures and under identical optical conditions. The value of $\log(I_0/I)$ at each wavelength was calculated from the observed light intensity for the reference and for a sample†. The extinction coefficients at about 2000 Å measured with our vacuum ultra-violet spectrophotometer were in good agreement with those measured with a Cary recording spectrophotometer model 14 M.

3. EXPERIMENTAL RESULTS

The absorption spectrum of gaseous benzene was measured in order to obtain a reference data for interpreting the electronic spectra of the mono-substituted benzenes. The result is shown in figure 1. The transition energies corresponding to the observed absorption peak wavelengths of the spectrum of benzene are given in table 1, together with the wave function of the excited state corresponding to each transition.

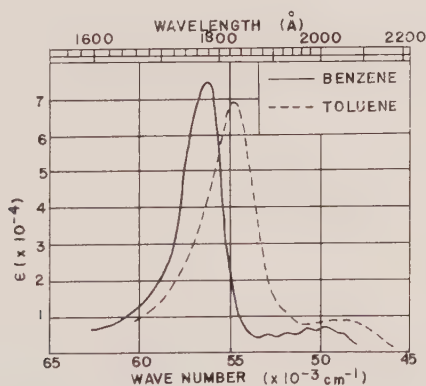


Figure 1. Ultra-violet absorption spectra of benzene and toluene from 1550 Å to 2200 Å.

The spectra of the phenols are shown in figure 2 and those of the halogenobenzenes are in figure 3. The spectra of aniline and N,N-dimethylaniline measured in our previous work [10] are shown in figure 4, for the purpose of comparison. As is seen in figures 2–4, the observed spectra for the respective compounds can be decomposed into several single bands, which are shown by dotted curves designated by A, B, C, ... from the longest-wavelength band

† The procedures for removing the effect of a stray light were described in reference [14].

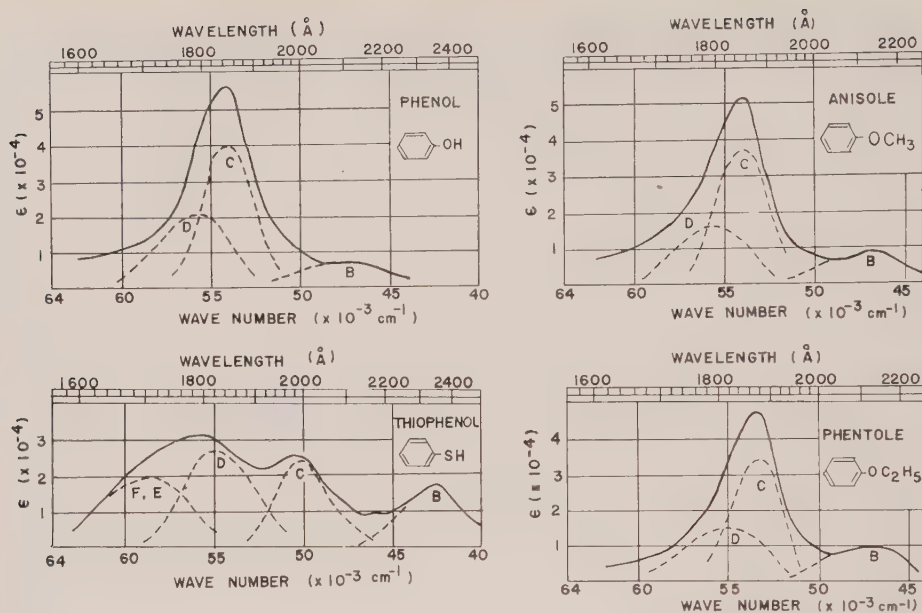


Figure 2. Ultra-violet absorption spectra of phenol, anisole, phenetole and thiophenol from 1550 Å to 2500 Å.

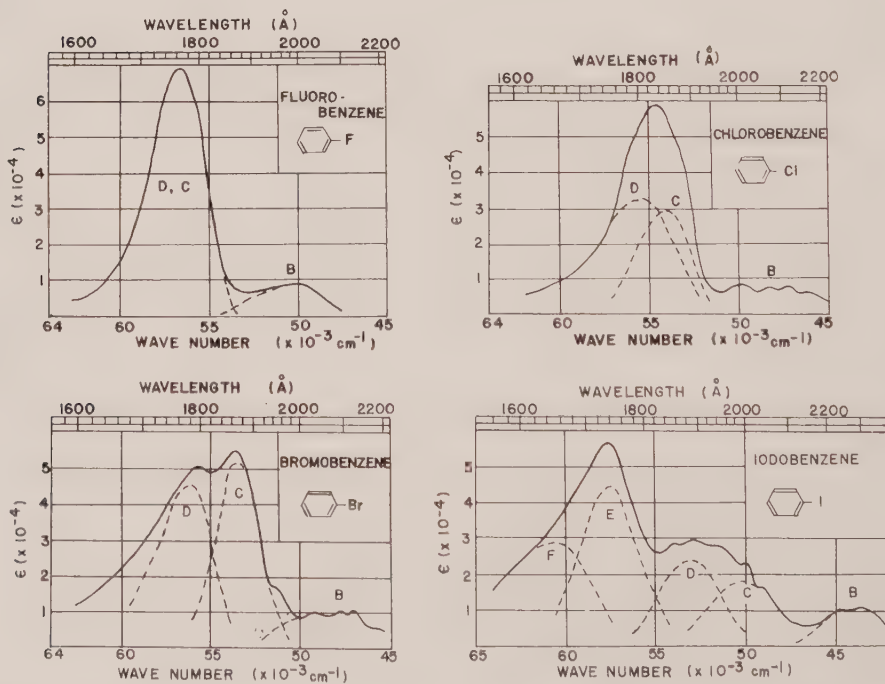


Figure 3. Ultra-violet absorption spectra of fluorobenzene, chlorobenzene, bromobenzene and iodobenzene from 1550 Å to 2200 Å.

toward shorter wavelength band. Band A is not shown in the figures, since it is too weak to be shown in a same extinction coefficient scale as the other bands. The resolutions of the overlapping bands into individual bands were carried out by assuming the Gaussian curve for each band. The transition energy, $(E-E_0)$, and the oscillator strength, f , of each band are summarized in tables 2-4. The experimental f values were evaluated from the integral areas under the absorption curves by the use of the following equation:

$$f = 4.32 \times 10^{-9} \int \epsilon d\nu, \quad (1)$$

where ϵ is the molar extinction coefficient and ν is the frequency in cm^{-1} .

The spectrum of toluene is also shown in figure 1; it has a strong band at 1828 Å (6.78 eV) with $f=1.075$ and a weaker band at 2150 Å (5.76 eV) with $f=0.168$. These bands appear at longer wavelengths than the corresponding bands of benzene.

The spectrum of fluorobenzene exhibits a strong band at 1765 Å (7.02 eV); it is accompanied by a shoulder at the longer wavelength side (around 1800 Å). In this case, the C and D bands overlap very closely with each other.

Wave function	Observed wavelength (Å)	Energy (ev)
$\psi_{B2u} = 2^{-1/2}\{(\phi_3^{-1}\phi_5) - (\phi_2^{-1}\phi_4)\}$	2534	4.89
$\psi_{B1u} = 2^{-1/2}\{(\phi_3^{-1}\phi_4) + (\phi_2^{-1}\phi_5)\}$	2008	6.17
$\psi_{E'1u} = 2^{-1/2}\{(\phi_3^{-1}\phi_5) + (\phi_2^{-1}\phi_4)\}$	1776	6.98
$\psi_{E1u} = 2^{-1/2}\{(\phi_3^{-1}\phi_4) - (\phi_2^{-1}\phi_5)\}$	1776	6.98
$\phi_2 = 12^{-1/2}(2x_1 + x_2 - x_3 - 2x_4 - x_5 + x_6)$ $\phi_3 = 2^{-1}(x_2 + x_3 - x_5 - x_6)$ $\phi_4 = 2^{-1}(x_2 - x_3 + x_5 - x_6)$ $\phi_5 = 12^{-1/2}(-2x_1 + x_2 + x_3 - 2x_4 + x_5 + x_6)$		

Table 1. Wave functions and energies for the excited levels of benzene†.

† $x_i (i=1, 2, \dots, 6)$ is the 2p-orbital of the i th carbon atom.

4. THEORETICAL

The present method of theoretical consideration is essentially based on that originally presented by Longuet-Higgins and Murrell [2], and employed in our previous studies of nitrobenzene [9], and of aniline and its N-derivatives [10]. The π -electron system for each of the mono-substituted benzenes under consideration was divided into two components, one is the benzene ring, and the other is a substituent group with non-bonding π -electrons. The non-bonding orbitals which are designated as θ , in the present paper; an oxygen 2p π -orbital for the phenols, a fluorine 2p π -orbital for fluorobenzene, a sulphur 3p π -orbital for thiophenol, a chlorine 3p π -orbital for chlorobenzene, a bromine 4p π -orbital for bromobenzene, and an iodine 5p π -orbital for iodobenzene.

The interaction between the substituent group and the benzene ring was considered by the configurational interaction among several electron configurations

Phenol						
Band	Experimental		Theoretical			Transition
	$(E-E_0)$	f	$(E-E_0)$	f	$(f')^\dagger$	
A	4.59	0.020	4.88	0.006		$W_0 \rightarrow W_1$
B	5.82	0.132	5.87	0.127(0.225)		$W_0 \rightarrow W_2$
C	6.70	0.636	6.72	0.787		$W_0 \rightarrow W_3$
D	6.93	0.467	6.84	0.741(0.881)		$W_0 \rightarrow W_4$
E			8.14	0.260(0.130)		$W_0 \rightarrow W_5$
F			8.30	0.399		$W_0 \rightarrow W_6$
Anisole						
Band	Experimental		Theoretical			Transition
	$(E-E_0)$	f	$(E-E_0)$	f	$(f')^\dagger$	
A	4.59	0.023	4.86	0.007		$W_0 \rightarrow W_1$
B	5.78	0.175	5.78	0.141(0.259)		$W_0 \rightarrow W_2$
C	6.68	0.585	6.67	0.684		$W_0 \rightarrow W_3$
D	6.90	0.371	6.82	0.690(0.784)		$W_0 \rightarrow W_4$
E			8.00	0.316(0.210)		$W_0 \rightarrow W_5$
F			8.12	0.500		$W_0 \rightarrow W_6$
Phenetole						
Band	Experimental		Theoretical			Transition
	$(E-E_0)$	f	$(E-E_0)$	f	$(f')^\dagger$	
A	4.59	0.028	4.86	0.008		$W_0 \rightarrow W_1$
B	5.75	0.188	5.75	0.152(0.271)		$W_0 \rightarrow W_2$
C	6.60	0.529	6.65	0.648		$W_0 \rightarrow W_3$
D	6.81	0.362	6.81	0.672(0.750)		$W_0 \rightarrow W_4$
E			7.96	0.372(0.223)		$W_0 \rightarrow W_5$
F			8.07	0.537		$W_0 \rightarrow W_6$
Thiophenol						
Band	Experimental		Theoretical			Transition
	$(E-E_0)$	f	$(E-E_0)$	f	$(f')^\dagger$	
A	4.58	0.013	4.70	0.015		$W_0 \rightarrow W_1$
B	5.30	0.347	5.40	0.170(0.340)		$W_0 \rightarrow W_2$
C	6.22	0.398	6.29	0.358		$W_0 \rightarrow W_3$
D	6.79	0.587	6.73	0.524(0.649)		$W_0 \rightarrow W_4$
E			7.75	0.355		$W_0 \rightarrow W_5$
F	(7.30)	(0.438)	7.76	0.510(0.358)		$W_0 \rightarrow W_6$

† Oscillator strength values calculated including the following integrals:

$$\left. \begin{aligned} \int \psi_{E_{1u}} r \psi_{CT_a} dv &\approx (-Sk/\sqrt{6})\mathbf{j}, \\ \int \psi_{B_{1u}} r \psi_{CT_b} dv &\approx (Sk/\sqrt{6})\mathbf{j}, \\ \int \psi_{C_1} r \psi_{CT_b} dv &\approx (-2Sk/\sqrt{6})\mathbf{j}, \end{aligned} \right\}$$

which have been usually neglected in such calculations. Here, \mathbf{j} is a unit vector along the molecular axis, k is the distance between the centres of the benzene ring and the C-X bond. S is overlap integral.

Table 2. The experimental and the theoretical results of transition energy, $(E-E_0)$ given in ev units, and oscillator strength, f , for phenol, anisole, phenetole and thiophenol.

Fluorobenzene						
Band	Experimental		Theoretical		Transition	Symmetry
	$(E-E_0)$	f	$(E-E_0)$	f $(f')^\dagger$		
A	4.84	0.003	4.91	0.001	$W_0 \rightarrow W_1$	B_2
B	6.19	0.150	6.05	0.053(0.094)	$W_0 \rightarrow W_2$	A_1
C, D	7.00	1.433	6.87	0.961(1.032)	$W_0 \rightarrow W_3$	A_1
			6.90	1.042	$W_0 \rightarrow W_4$	B_2
E			8.26	0.191(0.097)	$W_0 \rightarrow W_5$	A_1
F			8.88	0.163	$W_0 \rightarrow W_6$	B_2
Chlorobenzene						
Band	Experimental		Theoretical		Transition	Symmetry
	$(E-E_0)$	f	$(E-E_0)$	f $(f')^\dagger$		
A	4.71	0.005	4.85	0.005	$W_0 \rightarrow W_1$	B_2
B	5.95	0.195	5.92	0.098(0.174)	$W_0 \rightarrow W_2$	A_1
C	6.72	0.471	6.78	0.895	$W_0 \rightarrow W_3$	B_2
D	6.88	0.732	6.85	0.909(1.010)	$W_0 \rightarrow W_4$	A_1
E			8.38	0.199(0.072)	$W_0 \rightarrow W_5$	A_1
F			8.54	0.250	$W_0 \rightarrow W_6$	B_2
Bromobenzene						
Band	Experimental		Theoretical		Transition	Symmetry
	$(E-E_0)$	f	$(E-E_0)$	f $(f')^\dagger$		
A	4.76	0.007	4.72	0.014	$W_0 \rightarrow W_1$	B_2
B	5.84	0.254	5.64	0.165(0.300)	$W_0 \rightarrow W_2$	A_1
C	6.65	0.625	6.60	0.725	$W_0 \rightarrow W_3$	B_2
D	6.98	0.745	6.82	0.785(0.853)	$W_0 \rightarrow W_4$	A_1
E			8.46	0.234(0.091)	$W_0 \rightarrow W_5$	A_1
F			8.48	0.458	$W_0 \rightarrow W_6$	B_2
Iodobenzene						
Band	Experimental		Theoretical		Transition	Symmetry
	$(E-E_0)$	f	$(E-E_0)$	f $(f')^\dagger$		
A	4.83	0.011	4.70	0.008	$W_0 \rightarrow W_1$	B_2
B	5.45	0.211	5.43	0.063(0.201)	$W_0 \rightarrow W_2$	A_1
C	6.20	0.360	6.21	0.321	$W_0 \rightarrow W_3$	B_2
D	6.56	0.394	6.55	0.273(0.395)	$W_0 \rightarrow W_5$	A_1
E	7.12	0.720	7.42	0.800(0.606)	$W_0 \rightarrow W_6$	A_1
F	7.55	0.755	7.44	0.865	$W_0 \rightarrow W_4$	B_2

† See footnote in table 2.

Table 3. The experimental and the theoretical results of transition energy, $(E-E_0)$ given in ev units, and oscillator strength, f , for fluorobenzene, chlorobenzene, bromobenzene, and iodobenzene.

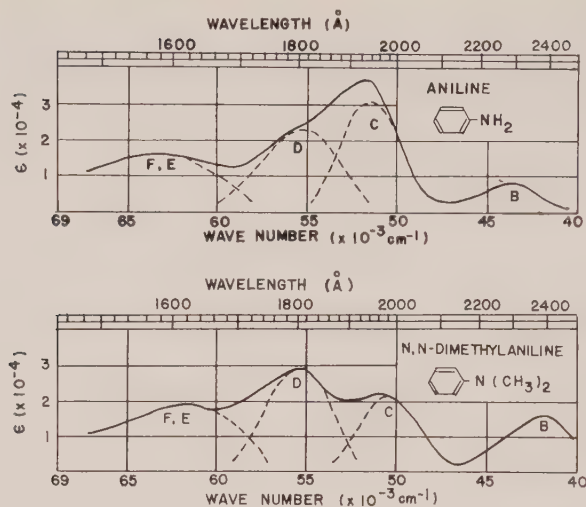


Figure 4. Ultra-violet absorption spectra of aniline and N,N-dimethylaniline from 1500 Å to 2500 Å. The absorption spectrum of gaseous aniline exhibits vibrational structures in the wavelength region longer than 2000 Å. These vibrational structures are neglected in this figure.

Aniline						
Band	Experimental		Theoretical			Transition
	$(E-E_0)$	f	$(E-E_0)$	f	$(f')^\dagger$	
A	4.40	0.028	4.72	0.021		$W_0 \rightarrow W_1$
B	5.39	0.144	5.45	0.174(0.375)		$W_0 \rightarrow W_2$
C	6.40	0.510	6.42	0.416		$W_0 \rightarrow W_3$
D	6.88	0.570	6.86	0.505(0.624)		$W_0 \rightarrow W_4$
E			8.04	0.745		$W_0 \rightarrow W_5$
F	(7.87)	(0.68)	8.05	0.416(0.254)		$W_0 \rightarrow W_6$
N,N-Dimethylaniline						
Band	Experimental		Theoretical			Transition
	$(E-E_0)$	f	$(E-E_0)$	f	$(f')^\dagger$	
A	4.30	0.044	4.61	0.026		$W_0 \rightarrow W_1$
B	5.15	0.256	5.17	0.182(0.394)		$W_0 \rightarrow W_2$
C	6.25	0.350	6.25	0.279		$W_0 \rightarrow W_3$
D	6.88	0.575	6.85	0.409(0.503)		$W_0 \rightarrow W_4$
E			7.90	0.875		$W_0 \rightarrow W_5$
F	(7.68)	(0.81)	7.93	0.497(0.354)		$W_0 \rightarrow W_6$

† See footnote in table 2.

Table 4. The experimental and the theoretical results of transition energy, $(E-E_0)$ given in ev units, and oscillator strength, f , for aniline and N,N-dimethylaniline.

including ground, locally excited, and charge-transfer configurations. For the locally excited configurations of the benzene ring, we used the wave functions and transition energies shown in table 1.

Two charge-transfer configurations were taken into account for each molecule; they are caused by an electron transfer from the non-bonding electron orbital of the substituent toward the lowest vacant orbitals of the benzene ring. One of the charge-transfer configurations is symmetric and the other is antisymmetric with regard to the symmetry plane vertical to the molecular plane; they are represented by:

$$\psi_{CTa} = (\theta^{-1}\phi_5) \text{ and } \psi_{CTb} = (\theta^{-1}\phi_4) \quad (2)$$

their energies are as follows:

$$\left. \begin{aligned} E_{CTa} &= I - A - Q_1, \\ E_{CTb} &= I - A - Q_2, \end{aligned} \right\} \quad (3)$$

where I is the ionization potential of the substituent, A is the electron affinity of benzene, and Q_1 and Q_2 are the electrostatic energies given by

$$\left. \begin{aligned} Q_1 &= \frac{1}{3}\{(C_1C_1/XX) + \frac{1}{2}(C_2C_2/XX) + \frac{1}{2}(C_3C_3/XX) + (C_4C_4/XX)\}, \\ Q_2 &= \frac{1}{3}\{(C_2C_2/XX) + (C_3C_3/XX)\}. \end{aligned} \right\} \quad (4)$$

Here X represents the O, S, F, Cl, Br and I atoms for phenol, thiophenol, fluorobenzene, chlorobenzene, bromobenzene and iodobenzene, respectively. Two-centre repulsion integrals, (CC/XX) , were calculated by the use of the following quadratic equations of atomic distances, r_{C-X} . These equations were obtained in the way suggested by Pariser and Parr [16]†.

$$\left. \begin{aligned} (CC/00) &= 0.2865r_{C-O}^2 - 3.100r_{C-O} + 11.35, \\ (CC/SS) &= 0.1667r_{C-S}^2 - 2.350r_{C-S} + 10.20, \\ (CC/FF) &= 0.5300r_{C-F}^2 - 4.700r_{C-F} + 13.96, \\ (CC/ClCl) &= 0.2332r_{C-Cl}^2 - 2.785r_{C-Cl} + 10.93, \\ (CC/BrBr) &= 0.1742r_{C-Br}^2 - 2.385r_{C-Br} + 10.29, \\ (CC/II) &= 0.1255r_{C-I}^2 - 2.100r_{C-I} + 9.83. \end{aligned} \right\} \quad (5)$$

The values of Q_1 and Q_2 calculated for the various mono-substituted benzenes by the use of equation (4) are shown in table 5. The $I-A$ value was taken as

	C ₆ H ₅ OH	C ₆ H ₅ SH	C ₆ H ₅ F	C ₆ H ₅ Cl	C ₆ H ₅ Br	C ₆ H ₅ I	C ₆ H ₅ NH ₂
Q_1	5.26	4.59	5.72	4.77	4.54	4.23	5.44
Q_2	4.71	4.24	4.83	4.32	4.18	3.93	5.00

Table 5. Coulombic energies (in ev units) calculated for the various mono-substituted benzenes.

a parameter for each of the mono-substituted benzene molecules studied here, and the details of their determination will be described later. The energies of the locally excited and charge-transfer configurations are shown diagrammatically in figure 7, the energy of the ground configuration being taken as the standard.

† In the derivation of equation (5), data for the valence-state ionization potentials and electron affinities of carbon, nitrogen, and oxygen were taken from the table of reference [17], and those for the other atoms were taken from the table of reference [18].

Off-diagonal matrix elements of the total electron Hamiltonian were reduced to the following simple formulae:

$$\left. \begin{aligned} H_{G, CT_a} &= -\frac{2}{\sqrt{6}}(\beta - \beta'), & H_{CT_b, B_{2u}} &= \frac{1}{\sqrt{6}}(\beta + \beta'), \\ H_{CT_a, B_{1u}} &= -\frac{1}{\sqrt{6}}(\beta + \beta'), & H_{CT_b, E_{1u}'} &= -\frac{1}{\sqrt{6}}(\beta + \beta'), \\ H_{CT_a, E_{1u}} &= \frac{1}{\sqrt{6}}(\beta + \beta'), \end{aligned} \right\} \quad (6)$$

where β is the resonance integral between two atomic orbitals belonging to the atom, X, and the adjacent carbon atom, C_1 , and β' is the resonance integral between the atom, X, and the ortho-position carbon atom, C_2 or C_6 (see figure 5). The values for β' were calculated on the assumption that the resonance integrals are proportional to the corresponding overlap integrals, S ; that is to say:

$$\beta' = \beta(S'/S), \quad (7)$$

In table 6 are shown the values of S and S' taken from the table of Mulliken *et al.* [19], and their ratios for the various mono-substituted benzenes. The inclusion of β' is one of the characteristics of the present calculation.

In the present calculation, the secular determinants have the same form for all the molecules under consideration. The energies of the charge-transfer

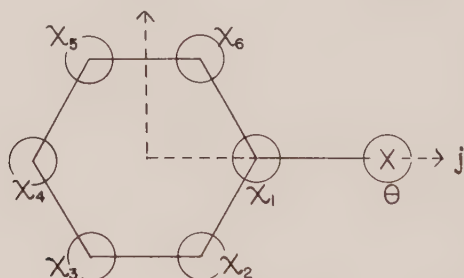


Figure 5. Atomic orbitals in the mono-substituted benzene.

Compound (C_6H_5-X)	Distance† (C_1-X), Å	$S(C_1-X)$	Distance ($C_2 \dots X$),	$\text{\AA} S'(C_2 \dots X)$	S'/S
C_6H_5OH	1.36	0.158	2.38	0.015	0.095
C_6H_5SH	(1.75)‡	0.169	2.73	0.024	0.142
C_6H_5F	1.31	0.139	2.35	0.013	0.094
C_6H_5Cl	1.70	0.151	2.69	0.021	0.139
C_6H_5Br	1.86	—	2.84	—	(0.190)‡
C_6H_5I	2.00	0.184	2.96	0.046	0.250
$C_6H_5NH_2$	1.407	0.181	2.425	0.021	0.116

† These values, except for the cases of aniline and thiophenol are taken from "Tables of Interatomic Distances and Configuration in Molecules and Ions". The values for aniline is taken from the values for 2,5-dichloroaniline (T. Sakurai, M. Sundaralingam and G. A. Jefferey, 1963, *Acta Cryst.*, **16**, 354).

‡ Estimated values.

Table 6. Overlap integrals calculated for various atom pairs.

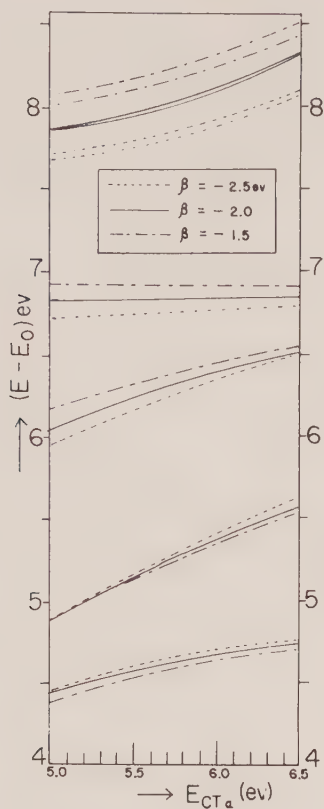


Figure 6. Plot of calculated transition energies for thiophenol against the energy of the charge-transfer configuration.

	$E_{1u}(E_{1u}')$	B_{1u}	B_{2u}	
PHENOL				
ANISOLE				
PHENETOLE				
THIOPHENOL				
FLUOROBENZENE				
CHLOROBENZENE				
BROMOBENZENE				
IODOBENZENE				
ANILINE				
N,N-DIMETHYLANILINE				
	8	7	6	5ev

Figure 7. Energies of charge-transfer configurations for the various mono-substituted benzenes (shown with the dotted lines) and the excitation energies of benzene (shown with the solid lines).

configurations and the resonance integrals only change on going from one mono-substituted benzene molecule to another. Therefore, $(I-A)$ and β were taken as parameters to be determined from a comparison between the experimental and theoretical transition energies. In order to select a best set of the parameters for each molecule, a hundred of secular equations with the different parameter values were solved by a Facom 202 electronic computer, in considerably wide ranges of the parameter values with intervals of 0.1 ev for $(I-A)$ and of 0.2 ev for β .

Compound	$I-A$	$I(\text{CH}_3\text{X})$	A
$\text{C}_6\text{H}_5\text{OH}$	12.16	10.83(CH_3OH) [20]	-1.36
$\text{C}_6\text{H}_5\text{OCH}_3$	11.86	10.50(CH_3OCH_3) [21]	-1.36
$\text{C}_6\text{H}_5\text{OC}_2\text{H}_5$	11.76		
$\text{C}_6\text{H}_5\text{SH}$	10.49	9.44(CH_3SH) [22]	-1.05
$\text{C}_6\text{H}_5\text{F}$	13.32	12.61(CH_3F) [23]	-0.71
$\text{C}_6\text{H}_5\text{Cl}$	12.17	11.34(CH_3Cl) [24]	-0.83
$\text{C}_6\text{H}_5\text{Br}$	11.54	10.50(CH_3Br) [23]	-1.04
$\text{C}_6\text{H}_5\text{I}$	10.23	9.55(CH_3I) [23]	-0.68

Table 7. Experimental $(I-A)$ values and estimation of the electron affinity of benzene, A , for the various mono-substituted benzenes. (Values are given in ev units.)

	$\text{C}_6\text{H}_5\text{OH}$	$\text{C}_6\text{H}_5\text{SH}$	$\text{C}_6\text{H}_5\text{F}$	$\text{C}_6\text{H}_5\text{Cl}$	$\text{C}_6\text{H}_5\text{Br}$	$\text{C}_6\text{H}_5\text{I}$	$\text{C}_6\text{H}_5\text{NH}_2$
β	-1.64	-1.66	-1.28	-1.58	-1.93	-1.20	-1.94
β'	-0.16	-0.24	-0.12	-0.22	-0.37	-0.30	-0.23

Table 8. Resonance-integral values, β and β' given in ev units, obtained from the present analysis of the electronic spectra of the various mono-substituted benzenes.

For a given β value, a set of transition energy curves was obtained by plotting calculated transition energies against the $(I-A)$ values, as is shown in figure 6. In this figure the transition energy curves for thiophenol are shown as an example. From a systematic graphical comparison of the calculated energy curves with the experimental transition energies, the best set of the calculated transition energies was obtained for each mono-substituted benzene, as is given in tables 2, 3 and 4. The best values of $(I-A)$ and of β thus obtained for the mono-substituted benzenes under consideration are shown in tables 7 and 8, respectively. The final results on the energy levels and wave functions for phenol, anisole, phenetole, and thiophenol are summarized in table 9. Furthermore, those for the halobenzenes are in table 10.

The theoretical oscillator strengths shown in tables 2, 3 and 4, were obtained by the use of the following equation:

$$f_{ij} = 1.085 \times 10^{11} \nu_{ij} D_{ij}^2, \quad (8)$$

where ν_{ij} and D_{ij} are respectively the frequency (in cm^{-1}) and moment (in cm) of the ij transition.

Phenol	
Energy (ev)	Wave function
$W_6 = 8.10$	$\psi_6 = -0.188\psi_{B_{2u}} + 0.539\psi_{E_{1u'}} + 0.821\psi_{CT_b}$
$W_5 = 7.94$	$\psi_5 = 0.311\psi_{B_{1u}} - 0.572\psi_{E_{1u}} + 0.112\psi_G + 0.750\psi_{CT_a}$
$W_4 = 6.64$	$\psi_4 = 0.541\psi_{B_{1u}} + 0.763\psi_{E_{1u}} + 0.062\psi_G + 0.349\psi_{CT_a}$
$W_3 = 6.52$	$\psi_3 = 0.222\psi_{B_{2u}} + 0.838\psi_{E_{1u'}} - 0.499\psi_{CT_b}$
$W_2 = 5.67$	$\psi_2 = 0.781\psi_{B_{1u}} - 0.300\psi_{E_{1u}} - 0.112\psi_G - 0.536\psi_{CT_a}$
$W_1 = 4.68$	$\psi_1 = 0.957\psi_{B_{2u}} - 0.088\psi_{E_{1u'}} + 0.277\psi_{CT_b}$
$W_0 = -0.20$	$\psi_0 = 0.019\psi_{B_{1u}} - 0.017\psi_{E_{1u}} + 0.985\psi_G - 0.169\psi_{CT_a}$
Anisole	
Energy (ev)	Wave function
$W_6 = 7.91$	$\psi_6 = -0.188\psi_{B_{2u}} + 0.609\psi_{E_{1u'}} + 0.771\psi_{CT_b}$
$W_5 = 7.79$	$\psi_5 = 0.317\psi_{B_{1u}} - 0.635\psi_{E_{1u}} + 0.106\psi_G + 0.697\psi_{CT_a}$
$W_4 = 6.61$	$\psi_4 = 0.605\psi_{B_{1u}} + 0.707\psi_{E_{1u}} + 0.065\psi_G + 0.359\psi_{CT_a}$
$W_3 = 6.46$	$\psi_3 = 0.262\psi_{B_{2u}} + 0.787\psi_{E_{1u'}} - 0.558\psi_{CT_b}$
$W_2 = 5.57$	$\psi_2 = 0.730\psi_{B_{1u}} - 0.311\psi_{E_{1u}} - 0.127\psi_G - 0.596\psi_{CT_a}$
$W_1 = 4.65$	$\psi_1 = 0.947\psi_{B_{2u}} - 0.097\psi_{E_{1u'}} + 0.307\psi_{CT_b}$
$W_0 = -0.21$	$\psi_0 = 0.020\psi_{B_{1u}} - 0.018\psi_{E_{1u}} + 0.984\psi_G - 0.176\psi_{CT_a}$
Phenetole	
Energy (ev)	Wave function
$W_6 = 7.85$	$\psi_6 = -0.186\psi_{B_{2u}} + 0.633\psi_{E_{1u'}} + 0.751\psi_{CT_b}$
$W_5 = 7.74$	$\psi_5 = 0.317\psi_{B_{1u}} - 0.656\psi_{E_{1u}} + 0.104\psi_G + 0.677\psi_{CT_a}$
$W_4 = 6.59$	$\psi_4 = 0.627\psi_{B_{1u}} + 0.687\psi_{E_{1u}} + 0.065\psi_G + 0.361\psi_{CT_a}$
$W_3 = 6.43$	$\psi_3 = 0.277\psi_{B_{2u}} + 0.767\psi_{E_{1u'}} - 0.578\psi_{CT_b}$
$W_2 = 5.53$	$\psi_2 = 0.711\psi_{B_{1u}} - 0.313\psi_{E_{1u}} - 0.132\psi_G - 0.616\psi_{CT_a}$
$W_1 = 4.64$	$\psi_1 = 0.943\psi_{B_{2u}} - 0.100\psi_{E_{1u'}} + 0.318\psi_{CT_b}$
$W_0 = -0.22$	$\psi_0 = 0.021\psi_{B_{1u}} - 0.018\psi_{E_{1u}} + 0.984\psi_G - 0.179\psi_{CT_a}$
Thiophenol	
Energy (ev)	Wave function
$W_6 = 7.55$	$\psi_6 = -0.315\psi_{B_{1u}} + 0.761\psi_{E_{1u}} - 0.083\psi_G - 0.561\psi_{CT_a}$
$W_5 = 7.54$	$\psi_5 = -0.170\psi_{B_{2u}} + 0.797\psi_{E_{1u'}} + 0.580\psi_{CT_b}$
$W_4 = 6.52$	$\psi_4 = 0.751\psi_{B_{1u}} + 0.566\psi_{E_{1u}} + 0.058\psi_G + 0.336\psi_{CT_a}$
$W_3 = 6.08$	$\psi_3 = -0.442\psi_{B_{2u}} - 0.587\psi_{E_{1u'}} + 0.678\psi_{CT_b}$
$W_2 = 5.19$	$\psi_2 = -0.580\psi_{B_{1u}} + 0.318\psi_{E_{1u}} + 0.158\psi_G + 0.733\psi_{CT_a}$
$W_1 = 4.49$	$\psi_1 = 0.881\psi_{B_{2u}} - 0.141\psi_{E_{1u'}} + 0.452\psi_{CT_b}$
$W_0 = -0.21$	$\psi_0 = 0.225\psi_{B_{1u}} - 0.200\psi_{E_{1u}} + 0.982\psi_G - 0.185\psi_{CT_a}$

Table 9. Calculated energy levels and wave functions of phenol, anisole, phenetole and thiophenol.

Fluorobenzene	
Energy (ev)	Wave function
$W_6 = 8.77$	$\psi_6 = -0.139\psi_{B_{2u}} + 0.310\psi_{E_{1u'}} + 0.940\psi_{CT_b}$
$W_5 = 8.15$	$\psi_5 = 0.248\psi_{B_{1u}} - 0.422\psi_{E_{1u}} + 0.098\psi_G + 0.866\psi_{CT_a}$
$W_4 = 6.80$	$\psi_4 = 0.082\psi_{B_{2u}} + 0.950\psi_{E_{1u'}} - 0.300\psi_{CT_b}$
$W_3 = 6.76$	$\psi_3 = 0.330\psi_{B_{1u}} + 0.886\psi_{E_{1u}} + 0.045\psi_G + 0.320\psi_{CT_a}$
$W_2 = 5.94$	$\psi_2 = 0.911\psi_{B_{1u}} - 0.196\psi_{E_{1u}} - 0.055\psi_G - 0.365\psi_{CT_a}$
$W_1 = 4.80$	$\psi_1 = 0.988\psi_{B_{2u}} - 0.044\psi_{E_{1u'}} + 0.160\psi_{CT_b}$
$W_0 = -0.11$	$\psi_0 = -0.011\psi_{B_{1u}} - 0.010\psi_{E_{1u}} + 0.993\psi_G - 0.120\psi_{CT_a}$
Chlorobenzene	
Energy (ev)	Wave function
$W_6 = 8.39$	$\psi_6 = -0.183\psi_{B_{2u}} + 0.455\psi_{E_{1u'}} + 0.871\psi_{CT_b}$
$W_5 = 8.23$	$\psi_5 = 0.293\psi_{B_{1u}} - 0.482\psi_{E_{1u}} + 0.105\psi_G + 0.819\psi_{CT_a}$
$W_4 = 6.70$	$\psi_4 = 0.451\psi_{B_{1u}} + 0.831\psi_{E_{1u}} + 0.051\psi_G + 0.322\psi_{CT_a}$
$W_3 = 6.63$	$\psi_3 = 0.180\psi_{B_{2u}} + 0.887\psi_{E_{1u'}} - 0.425\psi_{CT_b}$
$W_2 = 5.77$	$\psi_2 = 0.843\psi_{B_{1u}} - 0.277\psi_{E_{1u}} - 0.083\psi_G - 0.453\psi_{CT_a}$
$W_1 = 4.70$	$\psi_1 = 0.966\psi_{B_{2u}} - 0.079\psi_{E_{1u'}} + 0.245\psi_{CT_b}$
$W_0 = -0.15$	$\psi_0 = 0.016\psi_{B_{1u}} - 0.015\psi_{E_{1u}} + 0.990\psi_G - 0.141\psi_{CT_a}$
Bromobenzene	
Energy (ev)	Wave function
$W_6 = 8.29$	$\psi_6 = -0.219\psi_{B_{2u}} + 0.568\psi_{E_{1u'}} + 0.793\psi_{CT_b}$
$W_5 = 8.27$	$\psi_5 = 0.338\psi_{B_{1u}} - 0.551\psi_{E_{1u}} + 0.106\psi_G + 0.756\psi_{CT_a}$
$W_4 = 6.63$	$\psi_4 = 0.584\psi_{B_{1u}} + 0.759\psi_{E_{1u}} + 0.050\psi_G + 0.284\psi_{CT_a}$
$W_3 = 6.41$	$\psi_3 = 0.308\psi_{B_{2u}} + 0.812\psi_{E_{1u'}} - 0.496\psi_{CT_b}$
$W_2 = 5.45$	$\psi_2 = 0.737\psi_{B_{1u}} - 0.348\psi_{E_{1u}} - 0.121\psi_G - 0.567\psi_{CT_a}$
$W_1 = 4.53$	$\psi_1 = 0.926\psi_{B_{2u}} - 0.135\psi_{E_{1u'}} + 0.353\psi_{CT_b}$
$W_0 = -0.19$	$\psi_0 = 0.024\psi_{B_{1u}} - 0.022\psi_{E_{1u}} + 0.986\psi_G - 0.165\psi_{CT_a}$
Iodobenzene	
Energy (ev)	Wave function
$W_6 = 7.38$	$\psi_6 = -0.134\psi_{B_{2u}} + 0.828\psi_{E_{1u'}} + 0.545\psi_{CT_b}$
$W_5 = 7.36$	$\psi_5 = -0.262\psi_{B_{1u}} + 0.820\psi_{E_{1u}} - 0.042\psi_G - 0.507\psi_{CT_a}$
$W_4 = 6.49$	$\psi_4 = 0.772\psi_{B_{1u}} + 0.495\psi_{E_{1u}} + 0.038\psi_G + 0.398\psi_{CT_a}$
$W_3 = 6.15$	$\psi_3 = -0.366\psi_{B_{2u}} - 0.552\psi_{E_{1u'}} + 0.749\psi_{CT_b}$
$W_2 = 5.37$	$\psi_2 = -0.579\psi_{B_{1u}} + 0.288\psi_{E_{1u}} + 0.087\psi_G + 0.758\psi_{CT_a}$
$W_1 = 4.64$	$\psi_1 = 0.921\psi_{B_{2u}} - 0.099\psi_{E_{1u'}} + 0.377\psi_{CT_b}$
$W_0 = -0.06$	$\psi_0 = 0.010\psi_{B_{1u}} - 0.009\psi_{E_{1u}} + 0.995\psi_G - 0.103\psi_{CT_a}$

Table 10. Calculated energy levels and wave functions of fluorobenzene, chlorobenzene, bromobenzene and iodobenzene.

5. DISCUSSION

As is clearly seen from the experimental and theoretical results summarized in tables 2 and 3, it may be said in general that a very good agreement was obtained between the experimental and theoretical results for both the transition energies and the oscillator strengths. It is interesting that the spectra of various mono-substituted benzenes are well interpreted systematically in terms of a considerably simple model in which the seven electron configurations including the ground, four locally excited and two charge-transfer configurations were taken into account.

Compound	Band A	Band B		Band C		Band D		
	B_{2u}	B_{1u}	CT_a	$E_{1u'}$	CT_a	B_{1u}	E_{1u}	CT_a
C_6H_5OH	92	61	29	70	25	29	58	12
$C_6H_5OCH_3$	90	53	36	62	31	37	50	13
$C_6H_5OC_2H_5$	89	51	38	59	33	39	47	13
C_6H_5SH	78	34	54	34	46	56	32	11
C_6H_5F	98	83	13	90	9	11	79	10
C_6H_5Cl	93	71	31	79	18	20	69	10
C_6H_5Br	86	54	32	66	25	34	57	8
C_6H_5I	85	34	57	30	56	60	24	16
$C_6H_5NH_2$	75	35	50	40	39	53	37	9
$C_6H_5N(CH_3)_2$	65	26	59	28	40	63	29	8

Table 11. Charge-transfer contributions to band A, B, C and D for the various mono-substituted benzenes. (Values are given in percentages.)

In the spectra of phenol, anisole, and phenetole (figure 2) and those of fluorobenzene and chlorobenzene (figure 3), bands C and D overlap with each other so closely that they might be regarded as a single band. However, a detailed comparison of these superposed bands with the E_{1u} band of benzene indicates that there exists a considerable difference in shape between them; i.e. the bands of the phenols are asymmetric; that is to say, their intensities decrease more gently at the shorter wavelength side than at the longer wavelength side, and the band of chlorobenzene is much broader than the E_{1u} band of benzene. These spectral features suggest that these bands consist of two bands due to different transitions. The present analysis indicates that the splittings between bands C and D are within about 0.2 eV for these compounds, although the resolution of the bands were made somewhat arbitrarily.

For bromobenzene and thiophenol, however, C and D bands split so appreciably that they can easily be separated into two bands, the resulting separations being 0.33 and 0.55 eV, respectively. These values are in good agreement with the calculated ones (see tables 2 and 3). In the case of N,N-dimethylaniline, the splitting was about 0.6 eV; this is also in good agreement with the theoretical value [10].

The spectrum of iodobenzene is very complicated. The 173 m μ band is broad and has a shoulder in the shorter wavelength side, and the 195 m μ band shows a vibrational structure. From the comparison of the observed spectrum

with the theoretical result four bands C, D, E and F are safely separated in the region $155\text{ m}\mu \sim 200\text{ m}\mu$ and they are assigned as is shown in table 3.

From the wave functions of the mono-substituted benzenes under consideration for the ground and excited states (tables 9 and 10), we can evaluate the magnitudes of the contributions of the original electron configurations to each electronic state. The results are shown in table 11, together with those about aniline and *N,N*-dimethylaniline. The longest wavelength absorption bands (bands A) are predominantly of the $A_{1g} \rightarrow B_{2u}$ character for all the molecules studied here. Concerning B, C and D bands, it is difficult to discuss their characteristics commonly for all the molecules under consideration, since the magnitudes of the contributions of the respective electron configurations to

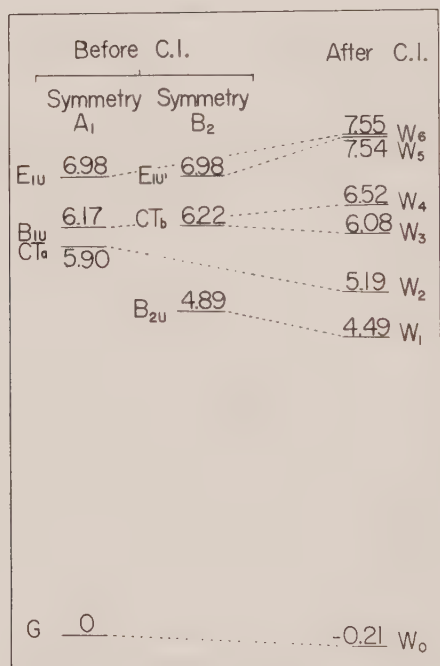


Figure 8. The energy level diagram of thiophenol.

the excited state largely change from one molecule to another. For example, the contribution of the B_{1u} configuration to the excited state of B band changes from 26 per cent for *N,N*-dimethylaniline to 83 per cent for fluorobenzene: for the former B band may safely be regarded as the shifted band of the $A_{1g} \rightarrow B_{1u}$ transition and of benzene but for the latter case, B band may rather be interpreted as an intramolecular charge-transfer band [10]. From this point of view, the mono-substituted benzene molecules given in table 11 can be classified into two groups.

One of them includes thiophenol, iodobenzene, aniline and *N,N*-dimethylaniline in which the contribution of the CT_a configuration in the excited state of B band is equal to or exceeds 50 per cent. The other group consists of the molecules in which the B_{1u} configuration is the most important contributor in

Symmetry	Present work			Klevens and Platt [12]		Baba [4]		Bloor and Paradejordi [5]	
	Experimental (gas)		Theoretical		Experimental (heptane solu.)	Theoretical		Theoretical	
	$(E - E_0)$	f	$(E - E_0)$	f		$(E - E_0)$	f	$(E - E_0)$	f
B_2	4.59	0.020	4.88	0.006	4.55	4.61	0.059	4.80	0.01
A_1	5.82	0.132	5.87	0.127(0.225)	5.83	5.80	0.125	5.96	0.06
B_2	6.70	0.636	6.74	0.787	6.53	6.62	0.956	6.82	1.20
A_1	6.93	0.467	6.84	0.741(0.881)		6.64	1.142	6.83	1.09
A_1			8.14	0.260(0.130)					
B_2			8.30	0.399					

†See footnote in table 2.

Table 12. Comparison of the present results of phenol with those by other authors. (Transition energies, $E - E_0$, are given in ev units.)

the same excited state: this group includes the phenols, fluorobenzene, chlorobenzene and bromobenzene. The observed absorption spectra of the latter group, which consists of four bands, can generally be interpreted as the shifted or splitted bands of the corresponding benzene bands; for instance A and B bands of the phenols may be regarded as the shifted bands of the $A_{1g} \rightarrow B_{2u}$ transition band and the $A_{1g} \rightarrow B_{1u}$ transition band of benzene, respectively, and C and D bands as the splitted ones of the $A_{1g} \rightarrow E_{1u}$ bands of benzene.

On the other hand, the absorption spectra of the former group are more complicated than those of the latter group and cannot satisfactorily be interpreted only from the view-point of the shifted or splitted bands of the corresponding benzene bands. The molecules like the anilines, thiophenol and iodobenzene commonly have the seven strong $\pi-\pi^*$ transition bands in the wavelength region of 3000–1500 Å. This fact means that some additional bands, namely the intra-molecular charge-transfer bands appear for these molecules. It may be said that the molecules belonging to the former and latter groups have the strong and weak substituents, respectively, in view of their effects upon the absorption spectrum of benzene.

The striking contrast of the absorption spectra of the molecules with the strong substituent groups to those of the molecules with the weak substituent groups may be brought about by the difference in the energy of the charge-transfer configuration. The energies of the charge-transfer configurations of the former group molecules are lower than those of the E_{1u} or B_{1u} locally excited configurations while the molecules of the latter group has the charge-transfer configurations at the higher position than the B_{1u} locally excited configuration.

In the first column of table 7 are listed the $(I-A)$ values determined in such a way as the calculated transition energies and intensities fit to the observed spectral data as well as possible. Assuming that I is equal to the ionization potential of CH_3X , the parent molecule of the substituent, X, we may estimate the electron affinity of benzene (A) from the $(I-A)$ values given in table 7. Using the reported ionization potential values [20–24], the electron affinity of benzene was estimated to be about -1.1 eV with some fluctuation of (± 0.3) eV (see table 7). It is interesting to see that this average value for A comes between the two theoretical values; one of which is -1.63 eV given by Hedges and Matsen [25], and the other is -0.54 eV by Pople and Hush [26]†. This fact seems to suggest that the present analysis obtaining the $(I-A)$ values from the electronic spectra may be valid.

It was found from tables 9 and 10 that the charge-transfer configuration contributes by a few per cent to the ground state and the resulting stabilization energies are: 4.6 kcal/mol for phenol, 4.8 kcal/mol for anisole, 5.1 kcal/mol for phenetole, 4.8 kcal/mol for thiophenol, 2.5 kcal/mol for fluorobenzene, 3.5 kcal/mol for chlorobenzene, 4.3 kcal/mol for bromobenzene and 1.4 kcal/mol for iodobenzene. In the previous work [10] the stabilization energies for aniline and N,N-dimethylaniline were found to be 7.4 kcal/mol and 8.1 kcal/mol,

† Scott and Becker obtained -1.50 eV for the electron affinity of benzene by the aid of the semi-empirical ω technique (1962, *J. Amer. chem. Soc.*, **66**, 2713). According to a private communication from Dr. Scott, however, this value seems to be too high and the best estimate may be -1.1 eV in excellent agreement with our estimated value. The authors should like to express their sincere thanks to Dr. Scott for his kindness in giving them this information.

respectively. It is interesting to compare these values with the empirical resonance energy values given by Pauling [27], which are 7 kcal/mol for phenol and 6 kcal/mol for aniline.

Finally it should be mentioned about the toluene spectrum, although no theoretical treatment was given here for this molecule. It is no doubt that the 1828 Å band of toluene is a shifted band of the E_{1u} band of benzene, the shift being 0.28 eV, which is considerably large and comparable with that of chlorobenzene. This suggests that the methyl group has a considerable charge-transfer effect to the phenyl group. This is also confirmed by the fact that the second band of toluene (2150 Å) shifts in a considerable amount (0.41 eV) from the B_{1u} band of benzene.

REFERENCES

- [1] NAGAKURA, S., and TANAKA, J., 1954, *J. chem. Phys.*, **22**, 236. NAGAKURA, S., 1955, *J. chem. Phys.*, **23**, 1441.
- [2] LONGUET-HIGGINS, H. C., and MURRELL, J. N., 1955, *Proc. phys. Soc., Lond.*, A **68**, 601. MURRELL, J. N., 1955, *Proc. phys. Soc., Lond.* A, **68**, 969.
- [3] PEACOCK, T. E., 1960, *Mol. Phys.*, **3**, 453.
- [4] BABA, H., 1961, *Bull. chem. Soc., Japan*, **34**, 76.
- [5] BLOOR, J. E., 1961, *Canad. J. Chem.*, **39**, 2256. BLOOR, J. E., and PERADEJORDI, F., 1962, *Theoret. chim. Acta, (Berl.)*, **1**, 83.
- [6] FISCHER-HJALMARS, I., 1962, *Ark. Fys.*, **21**, 123.
- [7] MURRELL, J. N., 1963, *Tetrahedron*, Suppl. 2, **19**, 277.
- [8] TANAKA, J., 1963, *Bull. chem. Soc., Japan*, **36**, 833.
- [9] NAGAKURA, S., 1963, *Pure appl. Chem.*, **7**, 79. NAGAKURA, S., KOJIMA, M., and MARUYAMA, Y., 1964, *Mol. Spectrosc.*, **13**, 174.
- [10] KIMURA, K., TSUBOMURA, H., and NAGAKURA, S., 1964, *Bull. chem. Soc., Japan*, **37**, 1336.
- [11] MULLIKEN, R. S., 1952, *J. Amer. chem. Soc.*, **74**, 811; 1952, *J. phys. Chem.*, **56**, 801.
- [12] KLEVEN, H. B., and PLATT, J. R., 1949, *J. Amer. chem. Soc.*, **71**, 1714. KLEVEN, H. B., and PLATT, J. R., 1954-55, Technical Report of the Laboratory of Molecular Structure and Spectra, Department of Physics, University of Chicago.
- [13] HAMMOND, V. J., PRICE, W. C., TEEGAN, J. P., and WALSH, A. D., 1950, *Disc. Faraday Soc.*, **9**, 53. PRICE, W. C., and WALSH, A. D., 1946, *Proc. roy. Soc., Lond.* A, **185**, 182.
- [14] TSUBOMURA, H., KIMURA, K., KAYA, K., TANAKA, J., and NAGAKURA, S., 1964, *Bull. chem. Soc., Japan*, **37**, 417.
- [15] LABHART, H., and WAGNIÈRE, G., 1963, *Helv. chim. Acta*, **46**, 1314.
- [16] PARISER, R., and PARR, R. G., 1953, *J. chem. Phys.*, **21**, 767.
- [17] PILCHER, G., and SKINNER, H. A., 1962, *J. inorg. nucl. Chem.*, **24**, 937.
- [18] PRICHARD, H. O., and SKINNER, H. A., 1955, *Chem. Rev.*, **55**, 745.
- [19] MULLIKEN, R. S., PIEKE, C. A., ORLOFF, D., and ORLOFF, H., 1949, *J. chem. Phys.*, **17**, 1248.
- [20] MORRISON, J. D., and NICHOLSON, A. J. C., 1952, *J. chem. Phys.*, **20**, 1021.
- [21] FIELD, F. H., and FRANKLIN, J. L., *Electron Impact Phenomena and the Properties of Gaseous Ions* (New York: Academic Press Inc.).
- [22] PRICE, W. C., TEEGAN, J. P., WALSH, A. D., 1950, *Proc. roy. Soc., Lond.* A, **201**, 600.
- [23] DIBELER, V. H., and REESE, R. M., 1955, *J. Res. nat. Bur. Stand.*, **54**, 127.
- [24] DIBELER, V. H., and REESE, R. M., 1958, *Analyt. Chem.*, **30**, 604.
- [25] HEDGES, R. M., and MATSEN, F. A., 1958, *J. chem. Phys.*, **28**, 950.
- [26] POPLE, J. A., and HUSH, N. S., 1955, *Trans. Faraday Soc.*, **51**, 600.
- [27] PAULING, L., *The Nature of the Chemical Bond* (Cornell University Press) p. 208.

The electron spin resonance spectrum and spin density distribution of the benzyl radical

by A. CARRINGTON and I. C. P. SMITH

Department of Theoretical Chemistry, University of Cambridge

(Received 19 May 1964 ; revision received 14 October 1964)

The benzyl radical has been generated in aqueous solution by means of a continuous flow system. The electron spin resonance spectrum is almost completely resolved, and accurate values for the four proton hyperfine splittings are obtained. The spin density distribution in the benzyl radical is calculated by various methods and the relationship between theoretical spin densities and proton hyperfine constants is studied.

1. INTRODUCTION

The benzyl radical has always been a favourite with theoretical chemists. It is one of the simplest odd-alternant hydrocarbons and has served as an excellent model for electronic structure calculations. Theoretical studies far exceed experimental information, however, for rather few measurements of the physical properties of this radical have been possible. Its electronic spectrum has been measured in the gas phase by flash photolysis of toluene and an adequate theoretical interpretation provided [1, 2]. The ionization potential of the benzyl radical has been measured by Franklin and Lumpkin [3]. Szwarc [4] determined its heat of formation from toluene by pyrolysis experiments and thus made an estimate of the resonance energy for comparison with theoretical predictions. No other physical properties were known until quite recently.

There has been considerable interest in the electron resonance spectrum of benzyl since the isotropic proton hyperfine splittings should provide an accurate experimental estimate of the unpaired electron distribution. It is not difficult to prepare and stabilize benzyl in rigid matrices at low temperatures and several authors have described such investigations. Tolkachev, Chkeidze and Buben found that ultra-violet irradiation of benzyl iodide on silica gel at 77°K yielded a poorly resolved spectrum which they attributed to benzyl [5]. Proton splittings of 16.5 gauss (triplet) and 5.5 gauss (quartet) were obtained, the quartet splitting being interpreted in terms of near-equivalence of the ortho and para protons. The large triplet splitting was assigned to the methylene group.

Rather similar results were obtained by Bennett and Thomas [6] using a rotating cryostat at 77°K. Sodium atoms were fired at solid benzyl chloride and the resulting free-radical-containing solid was examined in an electron resonance spectrometer. A poorly resolved spectrum gave a triplet splitting at 16.9 gauss.

Using a somewhat different approach, Vincow and Johnson [7] irradiated toluene in a sulphuric acid glass at 77°K and measured the second moment of

the electron resonance absorption. They compared this with the second moment calculated by using a theoretical spin distribution obtained from the method of alternant molecular orbitals. A particular merit of this study is that it takes account of the anisotropic hyperfine interaction, which is the reason for the poor resolution usually obtained with randomly oriented solids.

The most significant experimental contribution is that of Dixon and Norman [8] who succeeded in generating a high enough stationary concentration of benzyl in aqueous solution to yield a resolvable electron resonance spectrum. They developed a flow system in which an aqueous sulphuric acid solution containing titanous ion was mixed with a similar solution containing hydrogen peroxide. Hydroxyl radicals are generated in high concentration and are easily detected by electron spin resonance [9]; more importantly, if the solutions also contain an organic substrate, secondary radicals formed by hydroxyl addition or hydrogen atom abstraction can be detected. Dixon and Norman discovered that if the solutions were saturated with toluene, the electron resonance spectrum of the benzyl radical was obtained. The spectrum was weak but well enough resolved to yield reasonably reliable values for all the proton splitting constants. The values given were 15.9, 4.9, 1.5 and 6.1 gauss for the methylene, ortho, meta and para protons respectively.

The resolution of the spectrum obtained by Dixon and Norman was limited by the low signal-to-noise ratio, which in turn was probably due to the rather low solubility of toluene in dilute aqueous sulphuric acid. In this paper we describe a modification of the flow experiment in which phenylacetic acid is used instead of toluene. We chose this compound because of an earlier observation [8] that attack of acetic acid by hydroxyl leads to a detectable concentration of methyl radicals. Phenylacetic acid is quite soluble in dilute aqueous acid and as a result of attack by hydroxyl radicals yields a spectrum which can be almost completely resolved and unambiguously interpreted in terms of the benzyl radical.

2. EXPERIMENTAL

The mixing chamber used in the flow system employs the Varian aqueous solution sample cell, and is similar to the one described by Dixon and Norman [9]. Two solutions were mixed approximately 1 in. from the centre of the microwave cavity and a flow rate of 5 ml/sec. was employed. Both solutions were 1 N with respect to sulphuric acid and both were saturated with phenylacetic acid. One solution contained titanous ion (10^{-3} M) and the other hydrogen peroxide (10^{-3} M).

Twelve litres of solution were passed through the cavity during each experiment, and instrumental controls, principally high frequency modulation amplitude and microwave power level were optimized during successive runs. Finally, the spectrum shown in the figure was recorded, the scanning rate being 3.5 gauss per minute. Out of a possible total of 54 lines, 48 are resolved. The reconstruction shown beneath the spectrum is based on the hyperfine coupling constants listed in table 2; these are believed to be accurate to within ± 0.05 gauss.

The spectrum was recorded using a Varian 100 kc spectrometer in conjunction with a Varian 6 in. magnet.



3. SPIN DENSITY CALCULATIONS

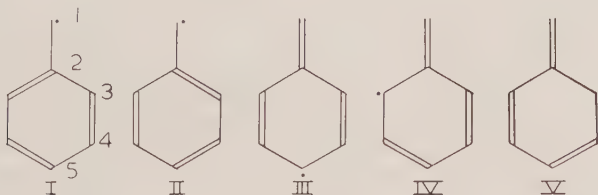
To a good approximation an aromatic proton hyperfine coupling constant a_H is related to the spin density ρ on the adjacent carbon atom through the well-known relationship [10] $a_H = Q\rho$, where Q is a constant whose value is usually chosen in the range 22.5–30 gauss. In order to facilitate comparison between theoretical spin densities ρ_i and experimental hyperfine constants a_i in benzyl we have obtained theoretical hyperfine constants a_i' as follows:

Defining

$$\bar{Q} = \frac{2a_1 + 2a_3 - 2a_4 + a_5}{2\rho_1 + 2\rho_3 + 2\rho_4 + \rho_5},$$

where the atoms are numbered as in (I) below, we set $a_i' = \bar{Q}\rho_i$, so that the sum of the a_i' is automatically equal to the sum of the a_i . We present the ρ_i values in table 1 and the predicted hyperfine constants a_i' in table 2. We now describe various methods which we have used for calculating the ρ_i .

Simple valence bond theory has been used successfully to interpret the spectra of other odd-alternant hydrocarbon radicals, notably triphenylmethyl [14] and perinaphthenyl [15]. The first valence bond calculations for the benzyl radical were made by Wheland and Pauling [16] who considered five resonance structures (I to V):



but simplified their calculation by assuming that III, IV and V contribute equally to the ground state resonance hybrid. They calculated the resonance energy correctly but, as has been pointed out independently by Pullman [17] and Bingel [1], their wave function is in error. This incorrect wave function has been used

	Method	Reference	Spin density†				
			1	2	3	4	5
1 (a)	Valence bond method (five structures)	†	0.685	-0.321	0.330	-0.177	0.330
1 (b)	Valence bond method (fourteen structures)	†	0.651	-0.323	0.407	-0.256	0.370
2 (a)	Hückel molecular orbital method (H.M.O.)	†	0.571	0.000	0.143	0.000	0.143
2 (b)	H.M.O. with C.I. (perturbation method for all singly excited states)	†	0.797	-0.082	0.150	-0.052	0.089
2 (c)	H.M.O. with C.I. (perturbation method for all singly and doubly excited states)	†	0.785	-0.076	0.149	-0.048	0.089
2 (d)	H.M.O. with C.I. (variation method for all singly excited states)	†	0.706	-0.084	0.170	-0.058	0.154
3 (a)	S.C.F.M.O. (without C.I., method of Lefebvre [28])	7	0.772	0.000	0.088	0.000	0.052
3 (b)	S.C.F.M.O. with C.I. (perturbation method for all singly excited states)	†	0.776	-0.072	0.134	-0.035	0.098
3 (c)	S.C.F.M.O. with C.I. (perturbation method for all singly and doubly excited states)	†	0.774	-0.067	0.131	-0.032	0.095
3 (d)	S.C.F.M.O. with C.I. (variation method for all singly excited states)	†	0.774	-0.077	0.143	-0.045	0.107
4 (a)	S.C.F.M.O. with C.I. (approximate method of McLachlan)	26	0.770	-0.102	0.161	-0.063	0.137
4 (b)	S.C.F.M.O. with C.I. (unrestricted Hartree-Fock method, after projection, Baudet and Berthier)	25	0.673	-0.103	0.200	-0.089	0.208
4 (c)	S.C.F.M.O. with C.I. (unrestricted Hartree-Fock method, after projection, Amos and Snyder)	32	0.718	—	0.157	-0.050	0.127
5	Alternant molecular orbital method (Vincow and Johnson, using method of Löwdin [29])	7	0.600	-0.067	0.200	-0.067	0.200

† Refers to present work.

‡ Numbering scheme as previously given.

Table 1. Computed spin densities (ρ_i).

	Method	Reference	\bar{Q}	Predicted hyperfine splitting (gauss) †				
				a_1'	a_3'	a_4'	a_5'	
1 (a)	Valence bond method (five structures)	†	22.74	15.58	7.50	4.03	7.50	
1 (b)	Valence bond method (fourteen structures)	†	23.11	15.04	9.41	5.92	8.55	
2 (a)	Hückel molecular orbital method (H.M.O.)	†		16.58	4.15	0.00	4.15	
2 (b)	H.M.O. with C.I. (perturbation method for all singly excited states)	†	29.04 24.28	19.35	3.64	1.26	2.16	
2 (c)	H.M.O. with C.I. (perturbation method for all singly and doubly excited states)	†	24.51	19.24	3.65	1.18	2.18	
2 (d)	H.M.O. with C.I. (variation method for all singly excited states)	†	25.49	18.00	4.33	1.48	3.93	
3 (a)	S.C.F.M.O. (without C.I., method of Lefebvre [27, 28])	7	25.76	19.86	2.28	0.00	1.34	
3 (b)	S.C.F.M.O. with C.I. (perturbation method for all singly excited states)	†	24.69	19.16	3.31	0.86	2.42	
3 (c)	S.C.F.M.O. with C.I. (perturbation method for all singly and doubly excited states)	†	24.78	19.18	3.25	0.79	2.35	
3 (d)	S.C.F.M.O. with C.I. (variation method for all singly excited states)	†	24.65	19.08	3.53	1.11	2.64	
4 (a)	S.C.F.M.O. with C.I. (approximate method of McLachlan)	26	24.36	18.76	3.92	1.54	3.34	
4 (b)	S.C.F.M.O. with C.I. (unrestricted Hartree-Fock method, after spin projection, Baudet and Berthier)	25	25.69	17.29	5.14	2.29	5.34	
4 (c)	S.C.F.M.O. with C.I. (unrestricted Hartree-Fock method, after spin projection, Amos and Snyder)	32	25.67	18.43	4.03	1.28	3.26	
5	Alternant molecular orbital method (Vincow and Johnson, using method of Löwdin [29])	7	27.38	16.43	5.48	1.83	5.48	
Experimental hyperfine splitting constants		†		a_1 16.35	a_3 5.14	a_4 1.75	a_5 6.14	

† Refers to present work.
‡ Numbering scheme as previously given.

Table 2. Experimental and predicted hyperfine splitting constants.

by Dearman and McConnell [18] to calculate the spin density distribution. The correct wave function using this approximation is

$$\Psi = 0.3816 (\psi_I + \psi_{II}) + 0.2311 \psi_{III} + 0.2440 (\psi_{IV} + \psi_V),$$

and its energy is $E = \alpha + 2.4093\beta$, where α and β are the usual valence bond coulomb and exchange integrals. The spin density distribution corresponding to this wave function is shown in table 1, row 1 (a) and the predicted splitting constants in table 2, row 1 (a).

We have also performed a valence bond calculation using a full set of canonical structures. For a system which has n bonds between $2n$ atoms the number of linearly independent canonical structures that can be drawn is $(2n)!/n!(n+1)!$ [19]. For free radicals a phantom atom with an unpaired electron must be introduced. Thus, for the benzyl radical $n=4$ and there are 14 such structures. Difficulties arise in this case when using a complete set of structures to calculate the spin density distribution. Because some of the unsymmetrical 'excited' structures do not necessarily occur in pairs in the complete set one may not assign equal coefficients to those which do occur in pairs, e.g. structures I and II, and IV and V. Failure to recognize this point leads to a spin distribution incompatible with the molecular symmetry. This lack of simplification by symmetry necessitates the diagonalization of a 14×14 matrix. The energy of the benzyl radical obtained by this method is $E = \alpha + 2.5897\beta$. The resulting spin densities and predicted hyperfine constants are given in tables 1 and 2, row 1 (b).

Another simple theoretical interpretation is provided by Hückel molecular orbital theory which predicts that the unpaired electron in an odd-alternant hydrocarbon occupies a non-bonding orbital [31]. Its distribution is thus easily calculated (tables 1 and 2, row 2 (a)). A similar prediction is made if one employs self-consistent field orbitals without configuration interaction (row 3 (a)).

In other radicals where negative spin densities are important, molecular orbital theory with configuration interaction has been shown to give results in good agreement with experiment [20] and we have therefore applied it to the benzyl radical. The doublet ground state of the benzyl radical may be represented by the Slater determinant:

$$\Psi_0 = ||\phi_1\bar{\phi}_1\phi_2\bar{\phi}_2\phi_3\bar{\phi}_3\phi_0||,$$

where the ϕ 's are molecular orbitals. We describe the excited states by means of the basis set of molecular orbitals used to construct the ground state configuration. There are nine singly excited states and forty doubly excited states of the correct symmetry for combining with the ground state. The singly excited states may be represented by Slater determinants of the form,

$$\begin{aligned} \text{or } \Psi_a &= ||\dots\phi_i\phi_k\phi_0|| (2\alpha\alpha\beta - \alpha\beta\alpha - \beta\alpha\alpha)/\sqrt{6}, \\ \Psi_b &= ||\dots\phi_i\phi_k\phi_0|| (\alpha\beta\alpha - \beta\alpha\alpha)/\sqrt{2}, \end{aligned} \quad \left. \vphantom{\begin{aligned} \Psi_a \\ \Psi_b \end{aligned}} \right\} \text{excitation } i \rightarrow k$$

$$\text{or } \Psi_c = ||\dots\phi_i\bar{\phi}_0\phi_0||, \quad \text{excitation } i \rightarrow 0$$

$$\text{or } \Psi_d = ||\dots\phi_i\bar{\phi}_i\phi_1||, \quad \text{excitation } 0 \rightarrow i.$$

States Ψ_c and Ψ_d are the result of excitations to and from the non-bonding orbital ϕ_0 . If the Hamiltonian operator contains electron repulsion terms it

may have non-zero off-diagonal elements between Ψ_0 and excited states of all four types. The spin density operator has zero matrix elements between Ψ_0 and states of the form Ψ_b . However, the Ψ_b states may have non-vanishing spin density matrix elements with the other excited states, so it is useful to include them in a spin density calculation.

We have used the configuration interaction method at various levels of approximation. The wave function for the benzyl radical is represented by

$$\Psi = \sum_i c_i \Psi_i,$$

where the c_i are to be determined by calculation. It is therefore necessary to evaluate matrix elements of the form $\langle \Psi_i | \mathcal{H} | \Psi_j \rangle$, where \mathcal{H} is the Hamiltonian operator containing two-electron interaction terms of the type e^2/r_{12} . Because the molecular orbitals are linear combinations of atomic orbitals, these matrix elements can be expressed as sums of products of atomic integrals and LCAO coefficients. These atomic integrals have been evaluated from the information given by Pariser and Parr [23, 24]. All bond lengths have been assumed equal to 1.39 Å, and we have used -2.39 eV for the carbon-carbon resonance integral β . In the calculation of the carbon coulomb integrals we have neglected penetration integrals and used -11.22 eV for the valence state ionization potential. We have carried out calculations using as basis functions both the simple Hückel orbitals and the self-consistent field orbitals determined by the method of Lefebvre [28].

We have obtained configuration interaction wave functions by several methods. In the first method we used first order perturbation theory to make an approximation to the full variational solution; the approach was similar to that used by Hoijtink [30]. We took the wave function for the doublet ground state of the benzyl radical to be:

$$\Psi = N \left(\Psi_0 - \sum_i \lambda_i \Psi_i \right),$$

where N is a normalization factor and

$$\lambda_i = \frac{\langle \Psi_i | \mathcal{H} | \Psi_0 \rangle}{E_i - E_0}.$$

For excited configurations which are degenerate because of the pairing theorem, one must take the appropriate linear combinations and include the matrix element of the Hamiltonian between them in the denominator of λ . In the case of Hückel orbitals we have used the Hückel energies for the E_i , but for the self-consistent orbitals we have used the diagonal matrix elements of the Hamiltonian operator. The states with spin function $(\alpha\beta\alpha - \beta\alpha\alpha)/\sqrt{2}$ were not included in this perturbation calculation. For the Hückel orbitals these states have small \mathcal{H}_{0j} relative to those for the other excited states. With the self-consistent field orbitals these \mathcal{H}_{0j} are identically zero, this being a necessary condition for self-consistency [22]. After normalization the spin density matrix was determined and the atomic contributions summed. The results are shown in tables 1 and 2, rows 2 (b) and 3 (b).

We have also used perturbation theory to investigate the importance of doubly excited states in the spin density calculation. As well as states with one or three unpaired electrons in one or three molecular orbitals there are doubly excited states with five electrons in five orbitals. One can derive ten spin functions

for these, only five of which are linearly independent. Of these five, only two give non-zero matrix elements of the Hamiltonian with the ground state. They are:

$$(-\beta\alpha\alpha\beta\alpha - \alpha\beta\alpha\beta\alpha + 2\alpha\alpha\beta\beta\alpha + 2\beta\beta\alpha\alpha\alpha - \beta\alpha\beta\alpha\alpha - \alpha\beta\beta\alpha\alpha)/2\sqrt{3}$$

and

$$(-\beta\alpha\alpha\beta\alpha + \alpha\beta\alpha\beta\alpha + \beta\alpha\beta\alpha\alpha - \alpha\beta\beta\alpha\alpha)/\sqrt{2}.$$

The 40 doubly excited states of the benzyl radical, and the nine singly excited states, all described by appropriate spin functions, were mixed with the ground state in the first order. The approximation of using only Hückel energies in the denominators of the mixing coefficients of the doubly excited states was employed for both the Hückel and the self-consistent field orbitals. Thus, the results of this calculation give only a qualitative estimate of the effect of inclusion of doubly excited states. The results are given in tables 1 and 2, rows 2(c) and 3(c).

Finally we have used the variational method to find the best wave function of the form

$$\Psi = \lambda_0 \Psi_0 + \sum_i \lambda_i \Psi_i \quad \left(\lambda_0^2 + \sum_i \lambda_i^2 = 1 \right),$$

where the sum \sum_i is over all singly excited configurations, but omits all doubly excited configurations. Two such calculations were performed; the first (table 1, row 2(d)) was based on Hückel orbitals, and the second (row 3(d)) upon self-consistent molecular orbitals.

4. DISCUSSION

The simple valence bond method exaggerates the amount of electron correlation, but does give fairly good results for the magnitudes and signs of the spin densities, as seen from tables 1 and 2, row 1(a). The use of a complete set of non-ionic structures tends to exaggerate electron correlation even more, and the agreement with experiment is consequently worse (row 1(b)).

Neither the simple Hückel method, row 2(a), nor the self-consistent field method, row 3(a), predicts negative spin densities for odd-alternant radicals without the inclusion of configuration interaction. The results of these methods are therefore only in very rough agreement with experiment.

Better agreement with experiment can be expected from the configuration interaction method where a certain amount of electron correlation is explicitly introduced. Thus, starting from both Hückel and self-consistent field orbitals, we find better agreement with experiment than with the less accurate methods; in particular, significant negative spin densities appear at the unstarred positions. The variational treatment of the configuration interaction with singly excited states gives somewhat better agreement than the perturbation treatment, as one would expect. The effect of the inclusion of doubly excited states in the spin density calculations can be seen to be negligibly small even when starting from Hückel orbitals. All of the above calculations give only approximate agreement with experiment, and all fail to predict correctly the relative magnitudes of the ortho and para proton hyperfine splittings.

A previous configuration interaction calculation on the benzyl radical yielded excellent agreement with experiment [21]. Atherton, Land and Porter used the

method of Hoiijtink and started from Hückel orbitals. Apart from states of the form Ψ_a above, they neglected excited states involving excitations to and from the non-bonding orbital, a valid procedure if the orbitals resemble closely the self-consistent orbitals [22]. However, excited states of the form Ψ_c and Ψ_d make appreciable contributions to the ground-state wave function when Hückel orbitals are used, so the good agreement must be regarded as fortuitous.

5. OTHER METHODS

In the tables we have listed the results of three other configuration interaction calculations involving self-consistent field orbitals. One would expect such intensive calculations, which take a major portion of electron correlation into account, to give the best estimates of spin density for comparison with experiment.

The method of McLachlan [26] is a semi-empirical treatment which has been of great value in accounting for the spectra of other radicals and radical-ions. From table 2, row 4 (a) we see that it gives results which are only in rough agreement with experiment, but which agree as well as the results of the detailed configuration interaction calculation starting from self-consistent field orbitals (row 3 (d)). The calculations of Baudet and Berthier [25], row 4 (b), and Amos and Snyder [32], row 4 (c), are applications of the unrestricted Hartree-Fock method which involves the computation of separate sets of orbitals for electrons of different spin. The results of Baudet and Berthier are in good agreement with experiment. Those of Amos and Snyder are less satisfactory, predicting the magnitudes of the ortho and para proton hyperfine splittings in the wrong order. This discrepancy between two independent applications of the same method must presumably be due to different choices of the integrals and parameters involved.

We have also included in the tables, row 5, the results of an alternant molecular orbital calculation by Vincow and Johnson [7] applying the method described by Lefebvre, Dearman, and McConnell [33], and originally proposed by Löwdin [29]. This method introduces configuration interaction by mixing each bonding orbital of the basis set with the corresponding antibonding orbital. Vincow and Johnson used a basis set of Hückel orbitals and employed the same parameter to specify the amount of mixing of every bonding orbital with the corresponding antibonding orbital. (The single mixing parameter was fixed by considering the values used by Lefebvre *et al.* [33] to fit one value of the 'experimental' spin density in the perinaphthényl and triphenylmethyl radicals.) Their method is therefore less flexible than a variational treatment in which each singly excited state is introduced with an independent coefficient. The good agreement of the results of this method with experiment is thus attributable to the element of semi-empiricism.

Thus far in comparing the various theoretical results with experiment we have said nothing about the values of \bar{Q} , which is an average value for the different sorts of proton. There is a possibility that \bar{Q} might have different values for the CH_2 and ring protons [36]. It is obvious from table 2 that a smaller value of \bar{Q} for the CH_2 protons and a larger value for the ring protons would give improved agreement with experiment for most of the methods of calculation. We have not examined this matter in detail. Various modifications to the simple McConnell relationship have indeed been proposed; in particular, proton splittings seem to

be sensitive to charge densities as well as to spin densities [11, 12, 34]. This particular complication, which may be serious in the case of radical-ions, does not concern us here, since within the Pariser–Parr–Pople approximation the net electron density distribution in a neutral alternant hydrocarbon is uniform [13]. But, there is considerable evidence from the electron spin resonance studies of free radicals in crystals that the proton hyperfine splitting constant may depend upon the spin densities on the next-nearest carbon atoms as well as upon that on the adjacent carbon atom [35]. This effect may be particularly important in radicals where large or negative spin densities occur, and may be responsible for the failure of the more thoroughgoing methods of spin density calculation (e.g. S.C.F.M.O. with C.I., row 3 (*d*)) to explain the relative magnitude of the ortho and para hyperfine splittings in the benzyl radical. The only calculation predicting them in the observed order is the unrestricted Hartree–Fock calculation of Baudet and Berthier [25] upon which we have already commented.

With regard to the calculations which we have performed, it would certainly be possible to improve the agreement with experiment by semi-empirical adjustment of such parameters as the resonance integral between carbon atoms 1 and 2 and the atomic electron repulsion integrals. We have preferred to employ the values most commonly used in the literature for calculations of this type. There seems little point in introducing such further complications until the precise relationship between spin densities and hyperfine splittings is more fully established.

6. CONCLUSION

In comparing the results of the various calculations with experiment it must be borne in mind that experiment provides values of a_{H} , whereas the calculations give ρ_{c} in the first instance, and the relation $a_{\text{H}} = Q\rho_{\text{c}}$ is liable to various uncertainties, as we have already explained. Subject to this qualification, the results in table 2 show that methods 3, 4 and 5 and their variants give little improvement over methods 2 (*b*), 2 (*c*) and 2 (*d*), but that the latter methods are superior to 2 (*a*) and to the valence bond method in their estimates of the meta spin density, which is almost certainly negative. The essence of methods 2 (*b*) and 2 (*d*) is that they allow for configurational interaction with the singly excited states, in particular those discussed by Hoijtink, and perturbation theory seems to be adequate for taking them into account. The inclusion of configuration interaction with doubly excited states has a negligible effect on the predicted spin densities. The method of McLachlan is also to be recommended because of its favourable combination of accuracy and labour. But it would be unwise to attach too much significance to precise numerical comparisons in view of the sensitivity of the theoretical results to the values assigned to the one- and two-electron integrals.

We would like to thank Professor H. C. Longuet-Higgins, F.R.S., and Dr. A. D. McLachlan for their helpful advice, and Dr. P. Rajagopal and Mr. J. Ternan for assistance in writing computer programmes for the numerical calculations. We are grateful to the referee for his useful criticism and to Dr. R. Lefebvre and Dr. N. Atherton for correspondence regarding their respective calculations for the benzyl radical. I.C.P.S. thanks the Shell Oil Company of Canada for a Postgraduate Research Scholarship and we are both indebted to the D.S.I.R. for financial assistance towards the purchase of apparatus.

REFERENCES

- [1] BINGEL, W., 1955, *Z. Naturf. A*, **10**, 462.
- [2] PORTER, G., and WRIGHT, F. J., 1955, *Trans. Faraday Soc.*, **51**, 1469; PORTER, G., and WINDSOR, M. W., 1957, *Nature, Lond.*, **180**, 187; PORTER, G., and STRACHAN, E., 1958, *Spectrochim. Acta*, **12**, 299.
- [3] FRANKLIN, J. L., and LUMPKIN, H. E., 1951, *J. chem. Phys.*, **19**, 1073.
- [4] SZWARC, M., 1947, *J. chem. Phys.*, **16**, 128.
- [5] TOLKACHEV, V. A., CHKEIDZE, I. I., and BUBEN, N. YA., 1962, *Dokl. Akad. Nauk., SSSR*, **147**, 643.
- [6] BENNETT, J. E., and THOMAS, A., 1962, *Nature, Lond.*, **195**, 995.
- [7] VINCOW, G., and JOHNSON, P. M., 1963, *J. chem. Phys.*, **39**, 1143.
- [8] DIXON, W. T., and NORMAN, R. O. C., 1963, *Proceedings of the Sixth International Symposium on Free Radicals*, Cambridge.
- [9] DIXON, W. T., and NORMAN, R. O. C., 1963, *J. chem. Soc.*, p. 3119.
- [10] MCCONNELL, H. M., and CHESNUT, D. B., 1958, *J. chem. Phys.*, **28**, 107.
- [11] WEISSMAN, S. I., DE BOER, E., and CONRADI, J. J., 1957, *J. chem. Phys.*, **26**, 963; CARRINGTON, A., DRAVNIKS, F., and SYMONS, M.C.R., 1959, *J. chem. Soc.*, p. 947.
- [12] COLPA, J. P., and BOLTON, J. R., 1963, *Mol. Phys.*, **6**, 273.
- [13] COULSON, C. A., and RUSHBROOKE, G. S., 1940, *Proc. Camb. phil. Soc.*, **36**, 193. POPLE, J. A., 1953, *Trans. Faraday Soc.*, **49**, 1375.
- [14] BROVETTO, P., and FERRONI, S., 1957, *Nuovo Cim.*, **5**, 142.
- [15] MCCONNELL, H. M., and CHESNUT, D. B., 1957, *J. chem. Phys.*, **27**, 984.
- [16] PAULING, L., and WHELAND, G. W., 1933, *J. chem. Phys.*, **1**, 362.
- [17] PULLMAN, A., 1947, *Disc. Faraday Soc.*, **2**, 26.
- [18] DEARMAN, H. H., and MCCONNELL, H. M., 1960, *J. chem. Phys.*, **33**, 1877.
- [19] PAULING, L., 1933, *J. chem. Phys.*, **1**, 280.
- [20] HOIJTINK, G. J., TOWNSEND, J., and WEISSMAN, S. I., 1960, *J. chem. Phys.*, **34**, 507.
- [21] ATHERTON, N. M., LAND, E. J., and PORTER, G., 1963, *Trans. Faraday Soc.*, **59**, 818.
- [22] LONGUET-HIGGINS, H. C., and POPLE, J. A., 1955, *Proc. Phys. Soc., Lond.*, **68**, 591.
- [23] PARISER, R., and PARR, R. G., 1953, *J. chem. Phys.*, **21**, 466, 767.
- [24] PARISER, R., and PARR, R. G., 1956, *J. chem. Phys.*, **24**, 250.
- [25] BAUDET, J., and BERTHIER, G., 1963, *J. Chim. phys.*, **60**, 1161.
- [26] McLACHLAN, A., 1960, *Mol. Phys.*, **3**, 233.
- [27] BEN JEMIA, H., and LEFEBVRE, R., 1962, *J. Chim. phys.*, **59**, 754.
- [28] BRION, H., LEFEBVRE, R., and MOSER, C., 1957, *J. Chim. phys.*, **54**, 363.
- [29] LÖWDIN, P.-O., 1955, *Phys. Rev.*, **97**, 1509.
- [30] HOIJTINK, G. J., 1958, *Mol. Phys.*, **1**, 157.
- [31] LONGUET-HIGGINS, H. C., 1950, *J. chem. Phys.*, **18**, 265, 275, 283.
- [32] AMOS, T., and SNYDER, L., (personal communication).
- [33] LEFEBVRE, R., DEARMAN, H. H., and MCCONNELL, H. M., 1960, *J. chem. Phys.*, **32**, 176.
- [34] GIACOMETTI, G., NORDIO, P. L., and PAVAN, M. P., 1963, *Theor. Chem. Acta*, **1**, 404.
- [35] HORSFIELD, A., MORTON, J. R., and WHIFFEN, D. H., 1961, *Trans. Faraday Soc.*, **57**, 1657.
- [36] MCCONNELL, H. M., 1958, *J. chem. Phys.*, **28**, 1188.

Rapid proton exchange of the free radical $\cdot\text{CH}_2\text{OH}$ as studied by E.S.R.

by HANNS FISCHER

Deutsches Kunststoff-Institut, Darmstadt

(Received 12 October 1964)

From the pH-dependence of the hydroxy proton splitting in the electron spin resonance spectra of the free radical $\cdot\text{CH}_2\text{OH}$ in acidified aqueous solutions a rapid exchange of the hydroxy protons is detected. This exchange is explained by the reaction $\cdot\text{CH}_2\text{OH} + \text{H}_3\text{O}^+ \rightleftharpoons \cdot\text{CH}_2\text{OH}_2^+ + \text{H}_2\text{O}$ with a rate constant $k = 1.76 \times 10^8 \text{ l. mol}^{-1} \text{ sec}^{-1}$ at 17°C .

By means of nuclear magnetic resonance the rapid exchange of hydroxy protons of organic compounds has been studied by many authors [1]. Electron spin resonance (E.S.R.) investigations published recently now indicate that protolysis also occurs in unstable carbon radicals containing hydroxy- and carboxy-groups, and they suggest that E.S.R.-spectroscopy may be applied in the study of such exchange phenomena [2, 3].

In this paper we describe and discuss a pH-dependent exchange of the hydroxy protons of the free radicals $\cdot\text{CH}_2\text{OH}$ in aqueous solution, as observed by E.S.R.-methods.

The generation of the free radicals was carried out in a flow system, similar to that of Dixon and Norman [2], in which two aqueous methanol solutions containing TiCl_3 and H_2O_2 respectively, mix directly before entering the cavity of the E.S.R.-spectrometer. In the continuous flow the hydroxyl radicals from the reaction of TiCl_3 with H_2O_2 react with methanol to give the free radicals $\cdot\text{CH}_2\text{OH}$ [2]. The flow rate used was $2.5 \text{ cm}^3/\text{sec}$, the methanol concentration was varied from 0.07 to 3.1 mol/l . pH-values were changed by addition of H_2SO_4 or NaOH to the solutions and were measured with a pH-meter type 390 of WTW, Weilheim, combined with the electrode UX of Metrohm AG, Herisau. The E.S.R.-spectra of the free radicals were recorded on a Varian-E.S.R.-spectrometer, the magnetic field of which was calibrated with proton resonance.

In figure 1 two typical spectra, recorded at different pH-values, are given. They show a pH-independent triplet splitting by the CH_2 -protons [2] ($a_{\text{H}}^{\text{CH}_2} = (17.62 \pm 0.06) \text{ oe}$) and a doublet splitting which is ascribed to the hydroxyl protons and which depends considerably on the pH-value. As shown in figure 2 the doublet splitting is observed above $\text{pH} = 1.11$, increases with increasing pH, and reaches a maximum value of $a_{\text{H}}^{\text{OH}} = (0.96 \pm 0.01) \text{ oe}$. Moreover, no dependence of this splitting on methanol and free radical concentrations could be detected.

The explanation of these findings follows easily from the assumption that the hydroxy protons of $\cdot\text{CH}_2\text{OH}$ exchange with protons of the solvent as the hydroxy protons of alcohols do. Now, introduction of a rate of exchange ν , defined as



Figure 1. E.S.R.-spectra of $\cdot\text{CH}_2\text{OH}$. (a) $\text{pH} = 1.40$. (b) $\text{pH} = 1.03$.

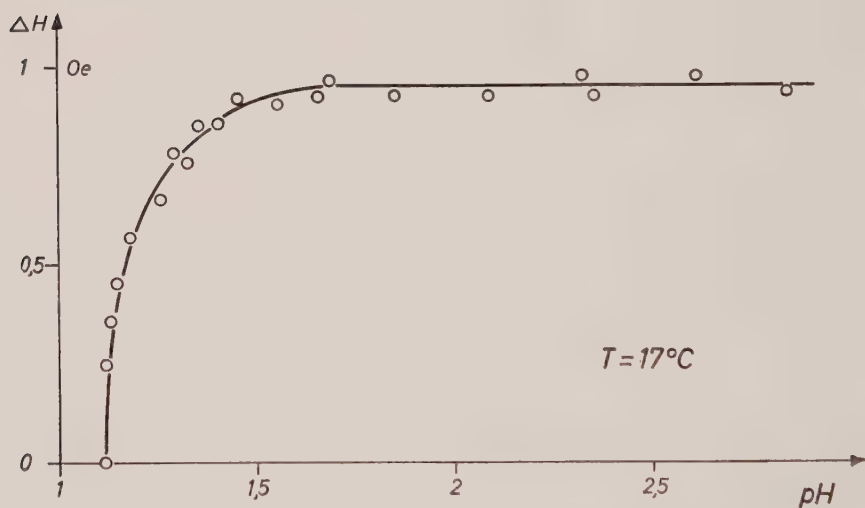


Figure 2. pH-dependence of the doublet splitting.

the reciprocal of the mean life time of the radicals between succeeding exchanges (as in nuclear magnetic resonance [4]), gives for the doublet splitting:

$$\Delta H = a_{\text{H}}^{\text{OH}} \left[1 - 2 \left(\frac{\nu}{\gamma \cdot a_{\text{H}}^{\text{OH}}} \right)^2 \right]^{1/2}, \quad (1)$$

if the linewidth without exchange is small compared with the maximum splitting. γ is the gyromagnetic ratio of the free radicals. Though the linewidth for slow exchange (0.35 oe) is not very small compared with a_{H}^{OH} in our spectra we

apply formula (1) for calculating ν , keeping aware of the line broadening by oxygen [3] which develops during the redox reaction. The dependence of ν on the H_3O^+ -concentration thus derived is plotted in figure 3 and shows a straight line.

Meiboom and co-workers [5] explain a similar pH-dependent proton exchange in acidified methanol- and ethanol-water mixtures observed by nuclear magnetic resonance in the frame of the following reaction scheme:



where $\text{R} = \text{CH}_3$ or $\text{R} = \text{CH}_2\text{CH}_3$. Applying these reactions to our observations we may exclude reaction (II), since the rate ν does not depend on the methanol or radical concentrations. On the other hand, since:

$$\nu = \frac{1}{\tau} = \frac{1}{\text{ROH}} \cdot \frac{d\text{ROH}}{dt} = k_1 \cdot \text{H}_3\text{O}^+,$$

reaction (I) explains the straight line of figure 3, from the slope of which we obtain $k_1 = 1.76 \times 10^8 \text{ l. mol}^{-1} \text{ sec}^{-1}$. This value agrees fairly well with the rate constants $k_1 = 2.8 \times 10^6 \text{ l. mol}^{-1} \text{ sec}^{-1}$ for ethanol and $k_1 \approx 10^7$ to $10^8 \text{ l. mol}^{-1} \text{ sec}^{-1}$ for methanol found by Meiboom *et al.* [5]. Thus, the protolysis of simple free carbon radicals with hydroxy substituents does not differ remarkably from the exchange of the corresponding alcohols.

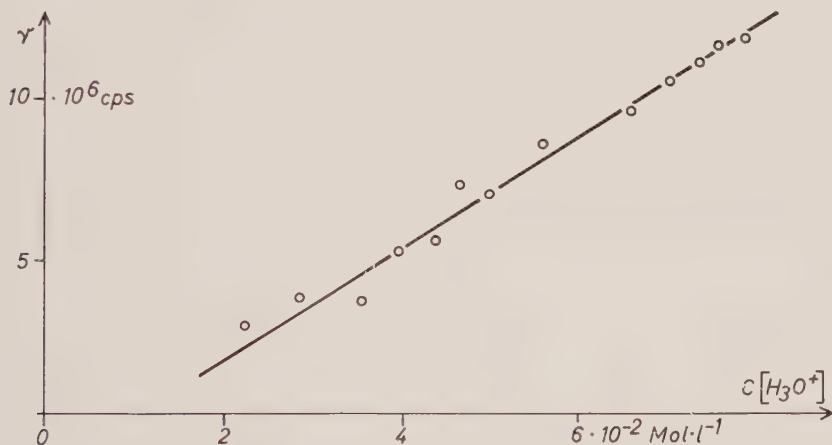


Figure 3. Rate of exchange versus H_3O^+ -concentration.

Furthermore, together with some recent observations on pH-dependent line narrowing in the E.S.R.-spectra of a large number of unstable carbon radicals listed previously [3], this paper verifies the assumption [2, 3] that the lack of hydroxy and carboxy proton splittings in acidified aqueous solutions is caused by rapid exchange. Finally, it explains, by the small value of a_{H}^{OH} , why a doublet splitting has never been observed in the anisotropy broadened spectra of the free radical $\cdot\text{CH}_2\text{OH}$ in irradiated solid methanol [6, 7].

REFERENCES

- [1] STREHLOW, H., 1963, In A. Weissberger: *Investigation of Rates and Mechanism of Reactions* (New York: Interscience Publ.), p. 865.
- [2] DIXON, W. T., and NORMAN, R. O. C., 1963, *J. chem. Soc.*, p. 3119.
- [3] FISCHER, H., 1964, *Z. Naturf. A*, **19**, 267; 1964, *Ibid.*, **19**, 866.
- [4] POPLE, J. A., SCHNEIDER, W. G., and BERNSTEIN, H. J., 1959, *High Resolution Nuclear Magnetic Resonance* (New York: McGraw-Hill), p. 224.
- [5] LUZ, Z., GILL, D., and MEIBOOM, S., 1959, *J. chem. Phys.*, **30**, 1540.
- [6] SYMONS, M. C. R., 1959, *J. chem. Soc.*, p. 269, 277.
- [7] FUJIMOTO, M., and INGRAM, D. J. E., 1958, *Trans. Faraday Soc.*, **54**, 1304.

Weak association between alkali metal ions and mononegative ions of aromatic hydrocarbons

by H. NISHIGUCHI, Y. NAKAI, K. NAKAMURA, K. ISHIZU,
Y. DEGUCHI and H. TAKAKI

Department of Chemistry, Faculty of Science, Kyoto University,
Kyoto, Japan

(Received 31 August 1964)

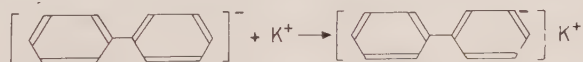
Extra hyperfine splittings due to alkali metal cations have been observed in the electron spin resonance (E.S.R.) spectra of biphenyl, naphthalene, anthracene and pyrene mononegative ions. It is interpreted as being due to ion-pair association between the aromatic anions and the metal cations. The unpaired spin densities at the metal nuclei are estimated using the data from the atomic beam experiments. In the case of biphenyl-alkali metal systems the appropriateness of the model described in a previous paper has been checked by studying the temperature dependence of the cation hyperfine splittings and the E.S.R. spectra of some methyl substituted biphenyl anions. The structure of the ion-pairs are discussed using Mulliken's theory of charge-transfer complexes.

1. INTRODUCTION

The electron spin resonance (E.S.R.) spectra of the mononegative ions of alternant hydrocarbons have been extensively studied by a number of investigators from both experimental and theoretical points of view [1]. Consequently, it was found that the experimental results can be explained under the assumption that the radicals exist as free ions. Recently, however, the fully resolved spectra of several ion radicals have shown extra hyperfine lines speculated to be due to the positive ions of alkali metals [2-4]. This is consistent with the assumption of ion pair formation between the aromatic anions and the metal cations [2]. Furthermore, the existence of an ion-ion pair equilibrium was demonstrated by the aid of the E.S.R. spectroscopy [2, 5].

On the other hand, in the electronic absorption spectra of the naphthalene and anthracene anions in tetrahydrofuran solution, the peak wavelengths showed slight shifts by changing alkali metals used as reductants [6]. This was interpreted as an ion-association effect that the anion and the counter ion are practically undissociated at concentrations 10^{-3} to 10^{-4} mol/l. at room temperature.

Previously we reported on the E.S.R. spectrum of the biphenyl mononegative ion produced by reduction with potassium [7]. We were led to the conclusion that a weak ion association between the biphenyl anion and the potassium cation takes place:



and that the spin density of the unpaired electron at the potassium nucleus amounts to 0.0010 at room temperature. In order to obtain further knowledge on the structure of the 'ion-pair', we have measured the E.S.R.

spectra of the biphenyl anion in the presence of other alkali metals such as lithium, sodium, rubidium, and caesium. Since the isotropic hyperfine splittings of 2s term of Rb and Cs are larger than those of other alkali metals, the hyperfine splitting constants in the case of Rb and Cs derivatives may be expected to be about 1–2 gauss provided that the contributions of np or nd states to the hyperfine structure are negligibly small. In fact we have found a remarkable effect of alkali metals in the case of rubidium- and caesium-biphenyl, using tetrahydropyran (THP) as solvent (§ 3).

In order to interpret the temperature dependence of the potassium coupling constants, in the previous paper [7] we took a simple model that the counter ion rests on either the 1–1' or 2–3 bond of the biphenyl benzene ring. The appropriateness of this model has been checked by the E.S.R. spectrum measurements of some methylated biphenyl anions (§ 3.2). Furthermore, we have re-measured the spectra of the anions of naphthalene, anthracene and pyrene prepared by reduction with the alkali metals in THP, and have found the extra lines due to the counter ions as will be described in § 3.3. In § 4 we shall discuss the structure of the ion pair, using Mulliken's theory on charge-transfer complexes which involves resonance between the no-bond structure ($A \cdots B$) and the dative structure ($A^- - B^+$).

2. EXPERIMENTAL

The anions were prepared by reduction of the hydrocarbons with various alkali metals in THP. The spectra were measured at the range of room temperature to -60°C , a JES-3B type E.S.R. spectrometer equipped with 100 kc/s field modulation and a JES 12 in. magnet being used. Details of the experiments were described elsewhere [8]. On measuring the spectra of ion pairs, complete reduction was essential, which was usually indicated by slight change in colour.

3. RESULTS

3.1. Biphenyl anion

3.1.1. Lithium and sodium derivatives

The spectra shown in figure 1 are very simple and easily analysed. These consist of normal 45 lines due to 10 ring protons [7] and further 1 : 1 : 1 : 1 quartet splittings due to the lithium or sodium nucleus with spacings of 0.136 and 0.079

	Li		Na	K		Rb		Cs
Mass number	6	7	23	39	41	85	87	133
Spin†	1	3/2	3/2	3/2	3/2	5/2	3/2	7/2
Natural abundance (per cent)	7.43	92.57	100	93.08	1.092	72.8	27.2	100
Q_M (gauss)‡	44.299	143.3	316.2	82.38	—	316.08	1219.4	820.08

† See, for example, J. A. Pople, W. G. Schneider and H. J. Bernstein, 1959, *High-Resolution Nuclear Magnetic Resonance* (McGraw-Hill Book Co.).

‡ See P. Kusch and H. Taub, 1949, *Phys. Rev.*, **75**, 1477.

Table 1. Nuclear properties of the alkali metals.

(± 0.005) gauss for the lithium and sodium derivatives respectively. The spin densities (ρ_M) on the metal nuclei were estimated to be 9.49×10^{-4} and 2.5×10^{-4} for lithium and sodium, respectively, from the comparison of the above-mentioned hyperfine splittings, a_M , with those of the free atoms, Q_M , determined from the

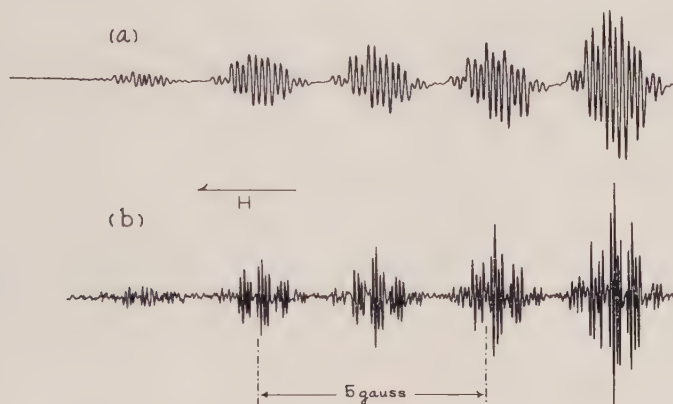


Figure 1. First derivatives of the E.S.R. absorption versus magnetic field for the biphenyl mononegative ion produced with: (a) lithium and (b) sodium in tetrahydropyran at room temperature. The magnetic field increases to the left.

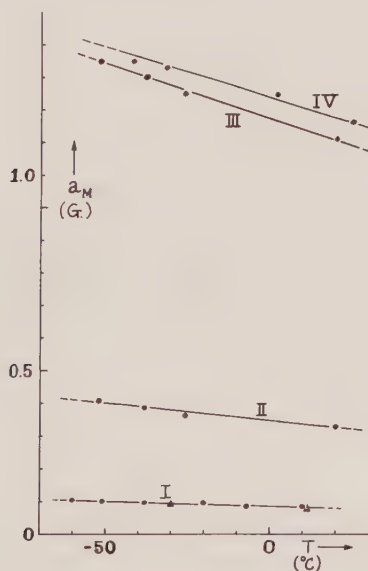


Figure 2. Temperature dependence of the alkali metal hyperfine splittings (a_M) for the alkali metal-biphenyl systems in THP; I: K and Na, II: ^{85}Rb , III: ^{87}Rb and IV: Cs.

atomic beam experiments; the latter quantities are given in table 1. The coupling constants of the ring protons and the spin density at the lithium nucleus are almost equal to the corresponding quantities of the potassium-biphenyl system in THP, while the spin density on the sodium nucleus is very small.

The temperature dependence of the a_M values were measured with the results shown in figure 2. The sodium hyperfine splitting increases with decreasing temperature as in the case of the potassium derivative described in the previous paper [7].

3.1.2. Rubidium derivative

As is shown in figure 3, the spectrum of rubidium derivative at room temperature is complicated because of the appearance of the hyperfine structures due to the nuclear spins of the two isotopes ($5/2$ and $3/2$). It can be analysed, however,

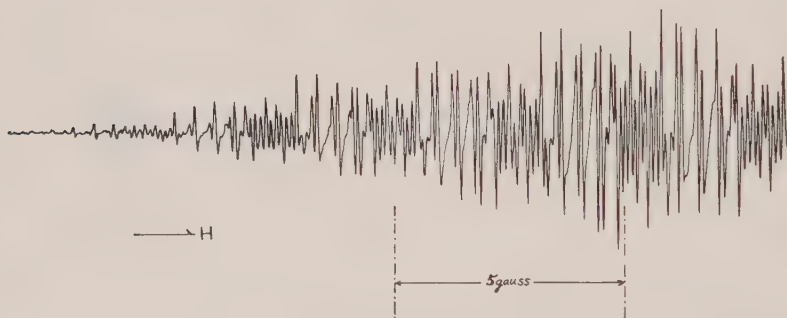


Figure 3. Lower half of first derivative of the E.S.R. absorption versus magnetic field for the biphenyl mononegative ion produced with rubidium in tetrahydropyran at room temperature.

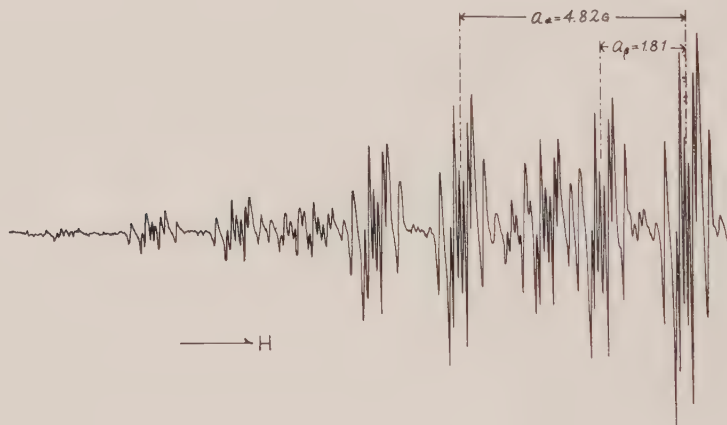


Figure 4. Lower half of first derivative of the E.S.R. absorption versus magnetic field for the naphthalene mononegative ion produced with rubidium in tetrahydropyran at room temperature.

in comparison with that of the naphthalene anion in the presence of the Rb cation (figure 4). The patterns obtained show that each line of the spectrum due to protons splits further into eight lines which are probably a superposition of an equivalent sextet due to ^{85}Rb and an equivalent quartet due to ^{87}Rb , the ratio of the spacings being 1:3. The metal hyperfine splitting constants obtained from the spectrum and the spin densities thus calculated are given in table 2. The spin

density at the ^{87}Rb nucleus in the solution of Rb in methylamine was reported to be 3.5 per cent of the value for the free atom [9]. It is interesting to note that the spin density on the metal ion in the present system is about 1/40 of that in the Rb-methylamine system. The temperature dependence of the ^{85}Rb and ^{87}Rb splittings are shown in figure 2.

Alkali metals	Li	Na	K	Rb	Rb	Cs
Mass number	7	23	39	85	87	133
Biphenyl	$a_{\text{M}}(\text{G})$	0.136	0.079	0.083	0.331	1.11 ₃
	$\rho_{\text{M}} \times 10^{-4}$	9.49	2.5	10.1	9.17	14.21
	$\lambda \times 10^{-2}$	3.08	1.6 ₆	3.18	3.10	3.76
Naphthalene	$a_{\text{M}}(\text{G})$	0.371	1.26†	†	0.093	0.327
	$\rho_{\text{M}} \times 10^{-4}$	25.9	39.9	†	2.58	2.68
	$\lambda \times 10^{-2}$	5.09	6.32	†	1.60	1.64
Pyrene	$a_{\text{M}}(\text{G})$	†	†	†	0.246	0.763
	$\rho_{\text{M}} \times 10^{-4}$	†	†	†	6.81	6.25
	$\lambda \times 10^{-2}$	†	†	†	2.61	2.50
Anthracene	$a_{\text{M}}(\text{G})$	†	0.080	†	†	0.54 ₃
	$\rho_{\text{M}} \times 10^{-4}$	†	2.5	†	†	6.6 ₂
	$\lambda \times 10^{-2}$	†	1.6 ₆	†	†	2.5 ₈

† Not observed.

‡ See reference [2].

Table 2. Alkali metal splitting constants (a_{M}), spin densities at the metal nuclei (ρ_{M}) and mixing parameters (λ) in some alkali metal-aromatic hydrocarbon systems.

3.1.3. Caesium derivative

Since the nuclear spin angular momentum of caesium is $7/2$ in unit of $\hbar/2\pi$, it may be expected that each line of the normal spectrum in the absence of metal splittings splits further into equivalent eight lines of equal spacing. The experimental result completely satisfies this expectation. The spectrum actually obtained (figure 5 (a)) consists of 45 lines due to 10 ring protons, each of which is led to equivalent octet splittings due to the caesium nucleus (spacing 1.166 gauss at room temperature). The Cs splitting increases with decreasing temperature as is shown in figure 2. That is to say, at -32°C it amounts to 1.35 gauss. As is seen from figure 5 (b), the value is almost three times as large as the coupling constant of the meta ring protons. The ratio among the hyperfine coupling constants due to the metal and the ring protons on the ortho, meta and para positions can be represented by the following equation:

$$a_{\text{p}}^{\text{H}} : a_{\text{m}}^{\text{H}} : a_{\text{o}}^{\text{H}} : a_{\text{Cs}} = 12 : 1 : 6 : 3 \quad (\text{at } -32^\circ\text{C}),$$

where $a_{\text{p}, \text{m}, \text{o}}^{\text{H}}$ are the hyperfine coupling constants of the ring protons attached to the para-, meta-, and ortho- positions of the biphenyl anion. The spin density at the Cs nucleus was estimated by the same method as described for the lithium and sodium derivatives.

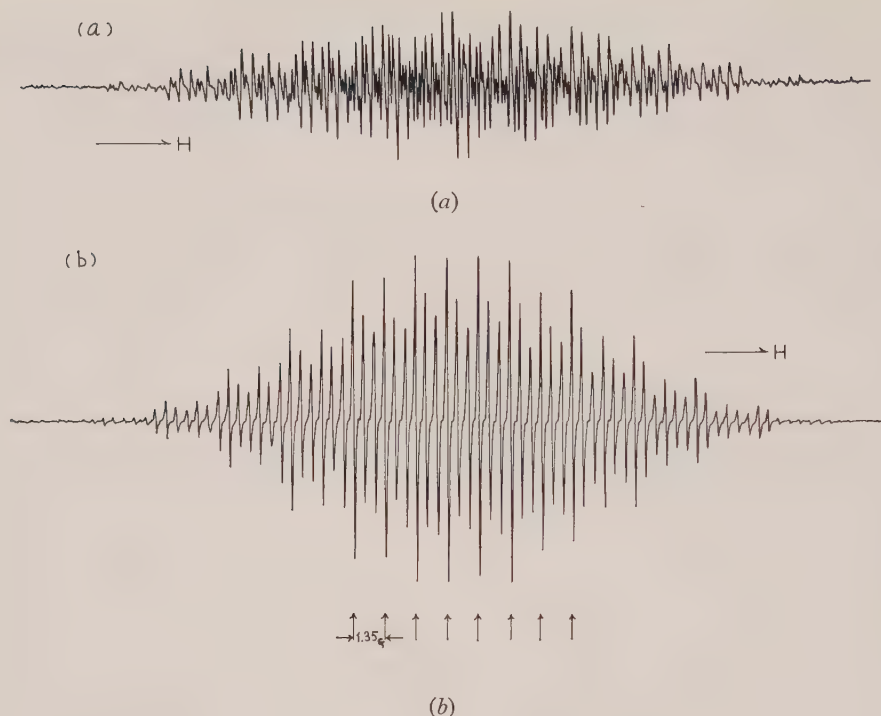


Figure 5. First derivatives of the E.S.R. absorption versus magnetic field for the biphenyl mononegative ion produced with caesium in tetrahydropyran at: (a) 25°C and (b) -32°C. Lower eight arrows indicate the total proton spin state $M_0(H) = M_m(H) = M_p(H) = 0$ and the caesium nuclear spin states $M(\text{Cs}) = -7/2$ to $+7/2$.

3.2. Anions of methyl derivatives of biphenyl

In order to check the hypothesis on the position of the metal ion described in the previous paper [7] somewhat more fully, the potassium splitting in the E.S.R. spectra was measured with the p-methylbiphenyl, p, p'-, m, m'- and o, o'-bitolyl anions in THP whose proton coupling constants in THF or DME had been determined by K. Ishizu [8a, 10]. According to his result, the spectra of p-methylbiphenyl and m, m'-bitolyl anions at room temperature, and p, p'-bitolyl at -60°C exhibited extra hyperfine lines with splittings of 0.062, 0.094 and 0.055 ± 0.005 gauss, respectively, which are conceivably due to the counter ion. On the other hand, concerning the spectrum of the o, o'-bitolyl anion, the hyperfine splittings due to alkali metal have never been observed, although those due to the ring and methyl protons were found. The disappearance of alkali metal hyperfine splitting only in the case of the o, o'-bitolyl anion radical shows implicitly that the counter ion localizes on the position where it is not affected by the para or meta substitution but is affected by the ortho substitution above. Therefore, the most probable position of the metal ion is considered to be above or below the 1-1' bond.

Fukui *et al.* [11] calculated the delocalization energies of the aromatic hydrocarbon-silver ion complex and concluded that, in the biphenyl complex, the silver ion is probably located on either 1-1' or 2-3 bond. This conclusion seems to be consistent with our hypothesis about the position of the alkali metal cations.

In table 2 we have summarized the alkali metal hyperfine splittings and spin densities under consideration, together with the mixing parameters obtained by the method which will be given in the next section. It will be seen from table 2 that the spin densities at the alkali metal nuclei are of the order of magnitude of 10^{-3} except for the sodium case. These values are comparable order of magnitude with these for other ion pair systems [2, 3].

3.3. Anions of another aromatic hydrocarbon

The E.S.R. spectra of the anion of naphthalene, anthracene, and pyrene (figure 6) prepared by the reduction with alkali metals in THP exhibited the counter ion hyperfine lines. This directly demonstrates the ion pair formation between these aromatic anions and the metal cation. The metal hyperfine constants in these systems are tabulated in table 2. Here we have omitted the proton hyperfine coupling constants which are almost equal to the values summarized in the reference [1*b*].



Figure 6. Lower half of first derivative of the E.S.R. absorption versus magnetic field for the pyrene mononegative ion produced with caesium in tetrahydropyran at -30°C , the metal coupling constant being 0.773 gauss. Lower figure indicates the total proton spin state $M_1(H)=M_2(H)=M_4(H)=0$ and the caesium nuclear spin states $M(\text{Cs}) = -7/2$ to $+7/2$.

4. DISCUSSION

The appearance of the metal hyperfine splittings in the E.S.R. spectra of the aromatic hydrocarbon anions is direct evidence for ion pair formation between a metal cation and an aromatic radical anion with the ratio of 1:1. The mechanism of the ion pair formation may be understood by applying [12] Mulliken's charge-transfer complex model [13] to the systems under consideration:

$$\Psi_{\text{ion-pair}} = \Psi_0(\text{Ar}^-, \text{M}^+) + \lambda \Psi_1(\text{Ar}, \text{M}), \quad (1)$$

where $\Psi_{\text{ion-pair}}$ is the ground state wave function of the system, $\Psi_0(\text{Ar}^-, \text{M}^+)$ represents the no-bond structure in which an unpaired electron occupies the lowest vacant molecular orbital and the alkali metal is positively charged, $\Psi_1(\text{Ar}, \text{M})$ the charge-transfer structure, and λ a mixing parameter. According to

the perturbation theory, the alkali metal isotropic hyperfine coupling constant, a_M , in this system will be given by the following equation:

$$a_M = [8\pi/3 \cdot g |\beta| (\mu/I) |S(0)^2| \lambda^2, \quad (2)$$

under the assumption that the unpaired electron in the Ψ_1 structure occupies the ns orbitals of the metal atom. Since the quantity inside the bracket of equation (2) is equivalent to Q_M , the mixing parameter can be estimated from the equation:

$$\lambda^2 = a_M/Q_M = \rho_M. \quad (3)$$

On the other hand, the second-order perturbation theory gives the following approximate relation [12]:

$$\lambda \simeq -H_{10} / \left(I - A + \frac{e^2}{\bar{r}} \right), \quad (4)$$

where I and A denote the ionization potential of the metal and the electron affinity of the aromatic hydrocarbon, respectively, and e^2/\bar{r} electrostatic interaction energy between the radical anion and the metal cation. H_{10} is the matrix element like $\langle \Psi_1 | H | \Psi_0 \rangle$. Since λ depends drastically on H_{10} , one may regard it as the measure of the ion pairing. The parameters determined from the experiments are tabulated in table 2. It will be noticed that the values are almost equal through all metals except for sodium, and about 1/5 or 1/10 of that for the benzene iodine complex [12] in which λ is of the order of 1.7×10^{-1} .

Since the temperature dependence of the hyperfine splittings due to Li, Na, Rb and Cs metals shown in figure 2 exhibits the same tendency as that in the potassium-biphenyl system, the speculation mentioned in the previous paper [7] that, with decreasing temperature, the metal ion may approach a more stable position such as the 1-1' or 2-3 bond may be applied to all alkali metal-biphenyl systems. One can recognize that this is consistent with the results of the substitution effect mentioned in § 3.2. However, real behaviour of the ion pairs, one can imagine, is that the counter ion is not fixed on the position above the molecular plane but vibrates around the position with a frequency ν . Equal intensity and line width of the multiplet hyperfine lines in all cases of various alkali metal-biphenyl systems exhibit vividly a frequency condition $\nu \gg (\Delta\omega/2\pi)$, where $\Delta\omega$ is the relative change in a resonance angular frequency. On the other hand, a line alternation which has been observed in the spectrum of lithium-naphthalene system in THP at room temperature may be explained by a condition $\nu \sim (\Delta\omega/2\pi)$. We are planning to publish a more complete account of this line-width variation.

REFERENCES

- [1] See, for example, (a) INGRAM, D. J. E., 1958, *Free Radicals as Studied by Electron Spin Resonance* (London: Butterworth Scientific Publication); and (b) STREITWIESER, A., Jr., 1961, *Molecular Orbital Theory for Organic Chemists* (New York, London: John Wiley and Sons, Inc.), p. 160. Other references cited therein.
- [2] (a) ADAM, H. C., and WEISSMAN, S. I., 1958, *J. Amer. chem. Soc.*, **80**, 1518, (b) ATHERTON, N. M., and WEISSMAN, S. I., 1961, *J. Amer. chem. Soc.*, **83**, 1330.
- [3] DE BOER, E., and MACKOR, E. L., 1963, *Proc. chem. Soc.*, p. 23.
- [4] BOLTON, J. R., and CARRINGTON, A., 1961, *Mol. Phys.*, **4**, 497.
- [5] ZANDSTRA, D. J., and WEISSMAN, S. I., 1962, *J. Amer. chem. Soc.*, **84**, 4408.
- [6] HUSH, N. S., and ROWLANDS, J. R., 1963, *Mol. Phys.*, **6**, 201.

- [7] NISHIGUCHI, H., NAKAI, Y., NAKAMURA, K., ISHIZU, K., DEGUCHI, Y., and TAKAKI, H., 1964, *J. chem. Phys.*, **40**, 241.
- [8] (a) ISHIZU, K., 1963, *Bull. chem. Soc., Japan*, **36**, 938; (b) DEGUCHI, Y., 1960, *J. chem. Phys.*, **32**, 1584.
- [9] VOS, K. D., and DYE, J. L., 1963, *J. chem. Phys.*, **38**, 2033.
- [10] ISHIZU, K., 1964, *Bull. chem. Soc., Japan*, **37**, 1093.
- [11] FUKUI, K., IMAMURA, A., YONEZAWA, T., and NAGATA, C., 1961, *Bull. chem. Soc., Japan*, **34**, 1076.
- [12] MULLIKEN, R. S., 1952, *J. Amer. chem Soc.*, **74**, 811.
- [13] AONO, S., and OOHASHI, K., 1963, *Prog. theor. Phys.*, **30**, 162. Another mechanism interpreting the ion pairing effect is presented in a recent review article by McClelland, B. J., 1964, *Chem. Rev.*, **64**, 301.

Studies of sterically hindered and overcrowded molecules

Part I. Proton magnetic resonance studies of the relative steric and electronic effects of the methyl and *t*-butyl groups

by W. A. GIBBONS† and V. M. S. GIL‡

Department of Chemistry, Sheffield University

(Received 4 August 1964 ; revision received 19 October 1964)

A comparative study of the proton magnetic resonance spectra of the mono-, di-, tri- and tetra-*t*-butyl and methyl substituted benzenes shows that a *t*-butyl group interacts with the ring as strongly as a methyl group.

Low-field chemical shifts of ring protons (amounting to -0.50 p.p.m.) and *t*-butyl protons (amounting to -0.23 p.p.m.) *ortho* to a *t*-butyl group are attributed to intramolecular van der Waals forces.

The possibility of severe ring puckering in the *t*-butylbenzenes is rejected since it is felt that this phenomenon should produce high-field shifts of the ring proton signals.

1. INTRODUCTION

One of the predominant factors governing the chemical shifts of aromatic ring protons is the π -electron density on the bonded carbon atom [1]. Proton magnetic resonance spectroscopy has thus proved a very important technique for studying electronic interaction of substituents with the benzene ring [2]. However a full explanation of the results cannot ignore contributions to the chemical shifts arising from the magnetic anisotropy [3] and the electric dipole [4] of neighbouring groups. Recently [5, 6] it was shown that intramolecular van der Waals forces may also be an important factor (low-field shifts) particularly when bulky groups are involved.

Alkyl groups may be expected to have neither a high magnetic anisotropy nor appreciable electric dipole. Comparison of chemical shifts of ring protons not affected by van der Waals forces in a series of methyl and *t*-butyl benzenes should therefore give the N.M.R. answer to the controversial question of the relative interaction of methyl and *t*-butyl groups with the benzene ring. Also the *t*-butylbenzenes should be an interesting class of compounds where the importance of intramolecular van der Waals forces in N.M.R. could be tested. Finally from the N.M.R. results we can get information on how an overcrowded molecule will relieve steric strain.

† Present address: Bell Telephone Laboratory, Murray Hill, New Jersey.

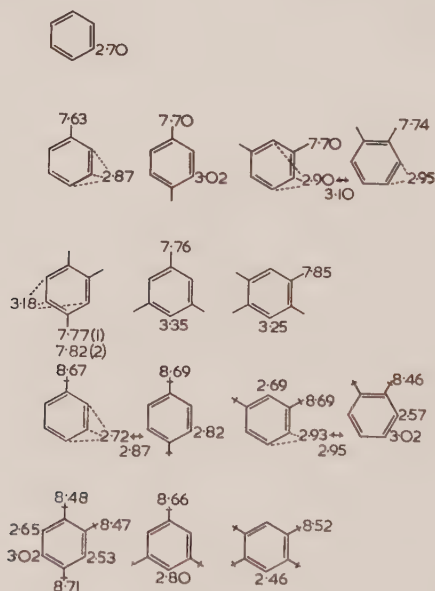
‡ On leave of absence from the University of Coimbra, Portugal.

2. EXPERIMENTAL

The spectra of the methylbenzenes and the *t*-butylbenzenes were recorded, respectively, on a AEI-RS-2 spectrometer operating at 60 Mc/s and on a 100 Mc/s Varian N.M.R. spectrometer. 1 mole per cent solutions in carbon tetrachloride were used. Ortho-di-*t*-butyl-, 1,2,4,5-tetra-*t*-butyl- and 1,2,4-tri-*t*-butylbenzene were donated by Dr. Hoogzand of European Research Associates, Brussels. Dr. Carl E. Johnson of the Amoco Chemical Company, Whiting, Indiana, supplied 1,3- and 1,4-di-*t*-butylbenzene. 1,3,5-tri-*t*-butylbenzene was synthesized by the method of Barclay and Betts [7]. Its melting point and analysis agreed with the published data. *t*-butylbenzene was prepared by simple Friedel-Crafts alkylation of benzene and purified by two fractional distillations [8].

3. RESULTS AND DISCUSSION

The figure gives the τ -values for the various methyl and *t*-butylbenzenes used in this study. The aromatic regions of the spectra of 1,2-di-*t*-butyl- and 1,2,4-tri-*t*-butylbenzene have been treated as A_2X_2 and AMX systems, respectively.



τ -values for benzene, and methyl and *t*-butylbenzenes (1 mole per cent solutions in CCl_4).

Consistent with the accepted electron-donating character of the methyl group, a high field shift of the ring proton signals relative to benzene is invariably found in the methylbenzenes.

In order to get information on the electronic interaction of a *t*-butyl group with the benzene ring relative to a methyl group, we must compare those ring

proton chemical shifts whose changes relative to benzene are thought to depend mainly on the π -electron density on the bonded carbon atom. Protons 3, 4 and 5 in the mono-derivatives, proton 5 in the 1,3-di-alkylbenzenes, and protons 4 and 5 in the 1,2-di-alkylbenzenes† are in these circumstances. Only in the latter, can the chemical shifts be obtained directly from the spectrum: τ -values 3.02 and 2.95 for 1,2-di-*t*-butylbenzene and *o*-xylene, respectively. The τ -value for the 5-proton in 1,3-di-*t*-butylbenzene is about 2.95 and that for *m*-xylene is probably close to this value since it is expected that proton 5 (*meta* to both methyl groups) is the less affected on going from benzene to *m*-xylene. Similarly proton 4 in *t*-butylbenzene is likely to have a τ -value close to 2.87, a value near to 2.72 being expected for the *ortho* protons (see discussion below on the effect of van der Waals forces). These results suggest that *t*-butyl and methyl groups interact with the ring about equally, in agreement with Ingold's work on rates of nitration of toluene and *t*-butylbenzene [9], and with the results of Heilbronner from ultra-violet spectroscopy [10].

In contrast to methylbenzenes where the ring proton chemical shifts are approximately the same, protons *ortho* to a *t*-butyl group always show an appreciable low-field shift. In some cases this shift is even to the low-field side of the benzene signal. Since, due to its large size, a *t*-butyl group interferes strongly with an *ortho* ring proton, it is felt that these low-field shifts are almost certainly due to van der Waals forces. Having shown that the electronic interaction of a *t*-butyl and a methyl group with the ring is about the same, a rough idea of the contribution of these forces to the *ortho* ring proton chemical shift can be obtained by subtracting the τ -values of *ortho*-protons in the corresponding compounds of both series. It is then found that the dispersion effect per *t*-butyl group lies in the range -0.15 to -0.28 p.p.m., except when two groups are *ortho* to each other in which case the effect is still larger: -0.38 to -0.53 p.p.m. This is not surprising since groups in *ortho* positions tend to repel each other, being therefore driven to interfere more strongly with the neighbouring ring hydrogen atoms. No major change in the distance, R , between interacting atoms needs to be assumed as the reduction in screening is probably roughly proportional to R^{-6} [11].

The abnormal low-field shift of *t*-butyl groups in *ortho* positions as compared to *t*-butylbenzene can also be understood in terms of a dispersion effect involving the two bulky groups. This effect amounts to -0.23 p.p.m.

Examination of models of 1,2-di-*t*-butyl-, 1,2,4-tri-*t*-butyl- and 1,2,4,5-tetra-*t*-butylbenzene shows that the *t*-butyl groups approach closer than the van der Waals radii of the hydrogen atom. The presence of considerable steric strain due to this molecular overcrowding has been clearly demonstrated by thermochemical studies [12–14]. According to Coulson [15] molecular overcrowding can be relieved by (a) ring puckering or (b) distortion of the angle between the ring and the substituent. Severe ring puckering must be absent in the above molecules since this should manifest itself by appreciable high field shifts of the protons attached to the ring which is opposite to what is observed. Molecular overcrowding in the above molecules is therefore relieved predominantly by changes in the angle between the ring and the substituent.

† It is shown below that severe ring puckering is absent in these molecules. Therefore any change on the ring current can affect the ring proton chemical shifts only slightly.

W. A. G. thanks Professor G. Porter and the British Petroleum Company for the award of a Fellowship. V. M. S. G. thanks the Comissão Coordenadora da Investigação para a NATO (Portugal) for the award of a postgraduate scholarship. We are grateful to Dr. J. N. Murrell and Dr. A. D. Cohen for helpful discussions and the National Physical Laboratory, Teddington, for use of their 100 Mc/s N.M.R. Spectrometer and for their hospitality while one of us (V. M. S. G.) was a guest worker.

REFERENCES

- [1] SCHAEFER, T., and SCHNEIDER, W. G., 1963, *Canad. J. Chem.*, **41**, 966.
- [2] MARTIN, J. S., and DAILEY, B. P., 1963, *J. chem. Phys.*, **39**, 1722.
- [3] McCONNELL, H., 1956, *J. chem. Phys.*, **24**, 1111.
- [4] BUCKINGHAM, A. D., 1960, *Canad. J. Chem.*, **38**, 300.
- [5] SCHAEFER, T., REYNOLDS, W. F., and YAMEMOTO, T., 1963, *Canad. J. Chem.*, **41**, 2969.
- [6] GIL, V. M. S., and GIBBONS, W. A., 1964, *Mol. Phys.*, **8**, 199.
- [7] BARCLAY, L. R. C., and BETTS, E. E., 1955, *Canad. J. Chem.*, **33**, 672.
- [8] ARNETT, E. M., and STREM, M. E., 1961, *Chem. & Ind.*, **49**, 2008.
- [9] INGOLD, C. K., 1953, *Structure and Mechanism in Organic Chemistry* (London: G. Bell & Sons).
- [10] HEILBRONNER, E., 1963, *Tetrahedron*, Suppl., **2**, 289.
- [11] MARSHALL, T. W., and POPLE, J. A., 1960, *Mol. Phys.*, **3**, 339.
- [12] DALE, J., 1963, *Chem. Ber.*, **94**, 2821.
- [13] HOOZAND, C., and HÜBEL, W., 1961, *Tetrahedron Letters*, **18**, 637.
- [14] HOOZAND, C., and HÜBEL, W., 1961, *Angew. Chem.*, **73**, 680.
- [15] COULSON, C. A., 1958, *Steric Effects in Conjugated Systems*, Ed. G. W. Gray (London: Butterworths).

Studies of sterically hindered and overcrowded molecules Part II. Comparative proton magnetic resonance studies of substituent effects in monoderivatives of benzene, mesitylene and 1,3,5-tri-*t*-butylbenzene

by W. A. GIBBONS† and V. M. S. GIL‡
Department of Chemistry, Sheffield University

(Received 4 August 1964 ; revision received 19 October 1964)

The proton magnetic resonance spectra of ten mono-derivatives of benzene, mesitylene and 1,3,5-tri-*t*-butylbenzene have been compared to investigate (a) the effect of substituent-ring angle on the chemical shifts of ring protons, substituent protons and protons of groups attached to the ring, and (b) the properties of molecules in which the atoms approach closer than their van der Waals radii.

1. INTRODUCTION

It is possible to prevent coplanarity of a substituent and the benzene ring by substituting alkyl groups in the *ortho* positions. Ultra-violet spectroscopy has been the principal means of studying this phenomenon, and the results have recently been summarized [1,2]. By changing the *ortho*-alkyl group through methyl, ethyl, isopropyl to *t*-butyl, it is possible to vary the angle between the substituent and the ring by increasing amounts. This variation is reflected in changes in the 250 m μ band of the molecule, and from the ratio of the extinction coefficient of this band relative to that in the planar molecule (e.g. nitrobenzene, benzaldehyde, aniline) the angle between the ring and the substituent can be calculated.

Changing the angle between the substituent and the plane of the ring affects the electron density within a molecule and hence it must also affect the chemical shifts of protons attached to the ring or the substituent. Investigations of this phenomenon by nuclear magnetic resonance [3-6,9] have been restricted to cases where the *ortho*-alkyl groups are methyl. In this paper we report the results for derivatives of mesitylene and 1,3,5-tri-*t*-butylbenzene and compare these with the corresponding benzenes.

In addition to being able to exert the largest obstacle to coplanarity, the substituted tri-*t*-butylbenzenes are interesting from another point of view. Examination of a scale model shows that the protons of the *ortho*-*t*-butyl groups and the substituent approach closer than their van der Waals radii. Although little is known about the effect of molecular overcrowding and intramolecular van der Waals forces on chemical shifts [10], in a recent communication it was shown that these phenomena manifest themselves by low field shifts of the *o*-*t*-butyl protons and those of the substituents [7]. Schaeffer *et al.* [8] came to this same conclusion in an examination of the chemical shifts of monohalogeno derivatives of methane and mesitylene.

† Present address: Bell Telephone Laboratories, Murray Hill, New Jersey.

‡ On leave of absence from the University of Coimbra, Portugal.

2. EXPERIMENTAL

Solute concentrations of 1 mole per cent in cyclohexane or carbon tetrachloride were used throughout to minimize possible intermolecular contributions to chemical shifts. Tetra-methylsilane was the internal standard. The spectra were recorded on an A.E.I. RS2 nuclear magnetic resonance spectrometer operating at 60 Mc/sec.

All substituted tri-*t*-butylbenzenes were synthesized in this laboratory from *para*-di-butylbenzene supplied by Dr. Carl S. Johnson of the Amoco Chemical Company, Indiana. Satisfactory analysis, melting point, infra-red and other relevant data were obtained for all compounds used. Preliminary attempts at preparing the CN, COCH₃, F and I derivatives of 1,3,5-tri-*t*-butylbenzene have been unsuccessful, but the problem is still being pursued.

The mesitylenes used in this study were synthesized by common literature methods. Correct boiling points and analysis were obtained.

3. RESULTS AND DISCUSSION

The discussion will be divided into three sections:

3.1. The effect of the substituent on the *meta* ring proton magnetic shielding in the three series.

3.2. The effect of substitution on the chemical shift of the *ortho* and *para*-alkyl groups in the mesitylene and 1,3,5-tri-*t*-butylbenzene derivatives.

3.3. Changes of the chemical shift of the protons of the substituent group in going from the benzene derivatives to the corresponding mesitylene and 1,3,5-tri-*t*-butylbenzene (TTBB) series.

3.1. *Meta* ring proton shifts

The differing electronic interaction of a group, X, with the ring in the tri-alkylbenzene derivatives, as compared to the benzene derivatives, should be observable in the shifts of *meta*-proton signals relative to the parent hydrocarbon—although the *meta* position is not usually associated with the largest changes in π -electron density. Table 1 shows these *meta* proton shifts in the benzene, mesitylene and TTBB derivatives relative to the parent hydrocarbon. A positive sign indicates a high-field shift, and 1 mole per cent solutions in cyclohexane were used.

The extent to which X interacts with the ring in the tri-alkylbenzene derivatives, as compared to the benzene derivatives, depends not only on the angle of twisting with the ring plane but also on the presence of the alkyl groups which themselves behave as electron-donating groups. It is therefore, in general, difficult to correlate changes in ring proton chemical shift with the ring-substituent angle alone. Also we are dealing with overcrowded molecules where intramolecular forces are expected to contribute noticeably to the magnetic screening. Nevertheless some qualitative conclusions can be inferred, particularly on comparing the mesitylenes with the tri-*t*-butylbenzene derivatives. Our conclusions on the planarity of the aromatic ring in the poly-*t*-butylbenzenes [15] and the presence of 'abnormal, low field shifts' lead us to believe that the present molecules do not relieve strain by ring puckering. Any changes on ring current due to other factors are supposed to be negligible.

The CH_3 , NH_2 , OH and OCH_3 substituents do not possess appreciable magnetic anisotropy, nor should the electric dipole influence the *meta* position to any great extent. Any explanation of observable shifts for these groups should therefore involve only changes in electronic interaction and van der Waals forces.

The presence of other electron-releasing groups on the tri-alkylbenzenes, and twisting out of the plane (except for CH_3) are expected to decrease the interaction of X with the ring but are not likely to change its sign. Therefore a high-field contribution to the *meta*-proton chemical shift should still be present although smaller than in the benzene derivatives.

By analogy with proton shifts in *t*-butylbenzenes possessing *t*-butyl groups in *ortho* positions [15], we postulate that the X substituent forces the *ortho*-alkyl groups towards the ring proton. This would be reflected in a de-shielding of the ring proton (van der Waals contribution) and seems to be the predominant factor in tri-*t*-butyltoluene (shift to low field, -0.10 p.p.m.).

X	$\text{C}_6\text{H}_5\text{X}\S$	$1\text{-X-2,4,6-(CH}_3)_3\text{C}_6\text{H}_2^\dagger$	$1\text{-X-2,4,6-(t-Bu)}_3\text{-C}_6\text{H}_2^\dagger$
F	+0.02	-0.03†	—
Cl	+0.06	-0.10†	-0.12
Br	+0.13	-0.12	-0.21
I	+0.26	-0.09	—
CH_3	+0.11	-0.01	-0.10
NH_2	+0.24	+0.08	+0.03
OH	+0.14	+0.06	+0.04
OCH_3	+0.09	+0.01	+0.05
CHO	-0.21	-0.10	-0.08
NO_2	-0.17	-0.21	-0.23

† This work.

‡ DIEHL, P., and SVEGLIADO, G., 1963, *Helv. chim. Acta.*, **46**, 461. (5 mole per cent solution in hexane.)

§ LANGENBUCHER, F., SCHMIDT, E. D., and MECKE, R., 1963, *J. chem. Phys.*, **39**, 1901.

|| SPIESECKE, H., and SCHNEIDER, W. G., 1961, *J. chem. Phys.*, **35**, 731. (5 mole per cent solutions in C_6H_{12} .)

Table 1. Meta ring proton chemical shifts (p.p.m.).

Halogen substituents have a high magnetic anisotropy, appreciable electric dipole effect and interact with the ring. It is difficult to see how any of these factors will change their relative contributions to the *meta*-proton shifts in going from the halobenzenes to the halo-tri-alkylbenzenes. However, the negative shifts of the *meta*-protons in the latter molecules, compared to the positive shifts in the halobenzenes, must be due largely to the van der Waals interactions already invoked for tri-*t*-butyltoluene. In fact, the difference between the effect in the halomesitylenes and the halobenzene derivatives is -0.05 p.p.m., -0.16 p.p.m., -0.25 p.p.m. and -0.35 p.p.m. respectively for F, Cl, Br and I, in qualitative agreement with the increasing size of the substituent. The larger shifts for the Cl and Br derivatives of TTBB support this conclusion.

The CHO and NO_2 groups are similar to the halogens in that they are expected to have a high magnetic anisotropy and electric dipole effect. The ultra-violet

spectrum of nitrobenzene and benzaldehyde shows that they interact very strongly with the ring. Unlike the halogens, however, the angle between these substituents and the ring increases with increasing size of the *ortho*-alkyl substituent. Unfortunately, neither theory nor experiment have yet revealed to what extent the substituent-ring angle affects the relative contributions of the above factors to the ring proton chemical shifts. The CHO derivatives follow the general pattern observed for the NH₂ and OH derivatives. Thus the *increased* electron density at the *meta* carbon atom (relative to benzaldehyde) due to the *increased* twisting (and thus *decreased* interaction) is reflected by the values -0.21 p.p.m., -0.10 p.p.m. and -0.08 p.p.m. for benzaldehyde, mesitaldehyde and TTBbenzaldehyde. Surprisingly, the corresponding NO₂ derivatives show the opposite effect, which is contrary to the expectation in terms of electron density changes alone; the shifts for nitrobenzene, etc. being -0.17 p.p.m., -0.21 p.p.m. and -0.23 p.p.m. These figures certainly show that for the NO₂ derivatives at least, there are effects, operative at the *meta* position, which compensate for the electron density increase due to twisting. Presumably some of the low-field shift in nitromesitylene and TTBnitrobenzene is due to van der Waals forces, but the electric dipole effect and magnetic anisotropy may also play their part.

Obviously a fuller interpretation of the results for the *meta* shifts must await more experimentation and further advances in the theory of proton chemical shifts. It can be said for certain that care must be taken in using N.M.R. data to determine the relative electronic interaction of substituents with the ring. Even at the *meta* position factors other than electron density are important. A similar study of the 1-X-2,6-di-alkylbenzenes will be interesting since in these we have both *para* and *meta* ring protons. The shifts of the *para* protons should better reflect changing electronic interaction due to twisting about the substituent ring bond.

3.2. The alkyl proton chemical shifts

The shifts of the *ortho* and *para*-alkyl protons of the 1-X-2,4,6-tri-alkylbenzenes relative to the parent hydrocarbon are shown in table 2. Again a positive sign refers to a high-field shift, and 1 mole per cent solutions in carbon tetrachloride were used. Δ_{op} is the difference, in p.p.m., between the *ortho* and *para*-alkyl groups shifts within the same molecule.

Whereas the *para*-alkyl group shift relative to the parent hydrocarbon always reflects a residual interaction of X with the ring of the right sign (except perhaps for the tri-*t*-butylbenzaldehyde where a positive shift of 0.01 p.p.m. is observed), the *ortho*-alkyl shifts are very often in the opposite direction. These cannot be interpreted in terms of the π -electron density.

If we assume that the electronic interaction of X with the ring affects the *ortho* and *para* positions to the same extent, the shift of the *ortho*-alkyl group protons relative to the *para* group protons (Δ_{op} in table 2) should be a measure of those factors, additional to π -electron density, which affect the *ortho* and not the *para* position. These factors are the magnetic anisotropy and electric dipole of the substituent and van der Waals interactions between the substituent and the *ortho*-alkyl groups.

For TTBtoluene, only van der Waals forces can be significant, and these produce a Δ_{op} of -0.16 p.p.m. The absence of a Δ_{op} in 1-CH₃-mesitylene

supports this conclusion. The same consideration holds for the NH_2 , OH and OCH_3 derivatives of TTBB where Δ_{op} is -0.18 p.p.m., -0.14 p.p.m. and -0.13 p.p.m. respectively. The values (p.p.m.) for the corresponding mesitylenes are $+0.08$, $+0.02$ and -0.02 , showing that van der Waals forces do not contribute significantly to the chemical shift of the *ortho*-methyl groups.

The large low-field shifts of the *ortho*-*t*-butyl protons in the halogenated TTBB are also due to van der Waals forces since the magnetic anisotropy effect averaged over rotation in the alkyl group is probably very small. The negative values for Δ_{op} in the halomesitylenes (except the F-derivative) have also been attributed to similar interactions by Schaeffer *et al.* [8].

X	X-mesitylene		Δ_{op}	X-TTBBbenzene		Δ_{op}
	<i>ortho</i>	<i>para</i>		<i>ortho</i>	<i>para</i>	
F	$+0.04\dagger$	$+0.02\dagger$	$+0.02$	—	—	—
Cl	$-0.07\dagger$	$+0.05\dagger$	-0.12	-0.19	$+0.02$	-0.21
Br	-0.06	$+0.07$	-0.13	-0.26	$+0.00$	-0.26
I	$-0.19\dagger$	$+0.02\dagger$	-0.21	—	—	—
CH_3	$+0.02$	$+0.02$	0.00	-0.15	$+0.01$	-0.16
NH_2	$+0.22$	$+0.14$	$+0.08$	-0.13	$+0.05$	-0.18
OH	$+0.14$	$+0.12$	$+0.02$	-0.10	$+0.04$	-0.14
OCH_3	$+0.08$	$+0.10$	-0.02	-0.07	$+0.06$	-0.13
CHO	-0.30	-0.05	-0.25	-0.01	$+0.01$	-0.02
NO_2	-0.02	-0.15	$+0.13$	-0.05	-0.01	-0.04

\dagger DIEHL, P., and SVEGLIADO, G., 1963, *Helv. chim. Acta.*, **46**, 461.

Table 2. Alkyl proton chemical shifts (p.p.m.).

Finally the apparently anomalous results for the CHO and NO_2 derivatives. Yamaguchi [9] explained the high-field shift of the *ortho*-methyl protons relative to the *para* in nitromesitylene (angle of twisting 65° [13]) in terms of a change in the magnetic susceptibility tensor of the nitro group relative to the planar nitrobenzene. It is, however, felt that a similar reason cannot be invoked to explain, through a partial cancellation of a low-field van der Waals shift, the small value of Δ_{op} for TTBNitrobenzene (angle of twisting 72° [13]) as the magnetic anisotropy effect averaged over rotation in the *t*-butyl group and possible oscillations of the NO_2 groups itself should be very small. The same applies to TTBBenzaldehyde (angle of twisting 68° [11]). It should, however, be noted that the biggest low-field shift is shown by the *ortho*-methyl groups in mesitaldehyde where the angle of twisting is thought to be only 22° [12]. For this almost planar configuration, the *ortho*-methyl protons probably see a magnetic anisotropy effect of the same sign as that of the aldehydic proton—a de-shielding effect [14]. Also a stronger interaction of the carbonyl lone pairs with the methyl protons for that configuration must contribute to the total low-field shift. As far as the Δ_{op} values for the other CHO and NO_2 compounds are concerned it could be said that for substituent-ring angles of 65° – 72° any interaction particularly with the *t*-butyl groups should be weaker, but we do not feel very sure about it; after all, such a large angle of twist can only arise from strong interaction with the *ortho* groups.

3.3. Substituent chemical shifts

Table 3 shows the τ -values for protons of the substituent, X, in the benzene derivatives and the changes, Δ_X , on these chemical shifts observed for the corresponding mesitylene and TTBB derivatives. A positive sign indicates high-field shift. All solutions are one mole per cent in carbon tetrachloride.

The electron-releasing properties of the NH_2 , OH and OCH_3 groups will be decreased in the tri-alkylbenzene derivatives relative to the benzene derivative, (1) by an increase in the ring-substituent angle and (2) due to the presence of three electron releasing groups on the ring. These two effects, through an increase in electron density on X relative to the benzene derivative, should lead to a high-field shift of the X proton chemical shift. In addition, this high-field shift should be enhanced since, in the twisted position, the X protons will experience a ring current effect which is more shielding than in a non-twisted group. For the CH_3 group, only effect (2) can be present.

X	$\text{C}_6\text{H}_5\text{-X}$ τ	Mesitylene-X Δ_X (p.p.m.)	TTBB-X Δ_X (p.p.m.)
CH_3	7.63	+0.18	-0.27
NH_2	6.62	+0.17	-0.49
OH	5.43	+0.44	-0.32
OCH_3	6.23	+0.16	+0.10
CHO	0.03	-0.56	-1.09

Table 3. Substituent chemical shifts.

A high-field shift is observed for the X-mesitylenes ($\text{X} = \text{CH}_3$, NH_2 , OH and OCH_3), but for the X-TTBB derivatives ($\text{X} = \text{CH}_3$, NH_2 and OH) the opposite effect is observed. This has been attributed [7] to intramolecular van der Waals forces involving the substituent and the *ortho-t*-butyl protons. The tri-*t*-butylanisole is anomalous, the shift being +0.10 p.p.m. This can in part be due to the fact that the OCH_3 group protons in the highly twisted position see a more shielding ring current effect than that experienced by the protons of the other groups.

The observed shifts for the CHO protons in mesitaldehyde and TTBB-benzaldehyde can only be explained by assuming that, as the angle of twist increases, the electron density on the carbonyl carbon atom decreases thus de-shielding the carbonyl proton. Van der Waals forces must also contribute to the low-field shift, but there must be some compensation due to changed ring current and, probably, magnetic anisotropy effects.

W. A. G. thanks Professor G. Porter and the British Petroleum Company for the award of a Fellowship. V. M. S. G. thanks the Comissão Coordenadora da Investigação para a NATO (Portugal) for the award of a postgraduate scholarship. We are grateful to Dr. J. N. Murrell and Mr. Dennis Williams for helpful discussions. Dr. Herbert Fischer is thanked for help with the synthesis of the tri-*t*-butylbenzene derivatives.

REFERENCES

- [1] MURRELL, J. N., 1963, *Theory of the Electronic Spectra of Organic Molecules* (London: Methuen).
- [2] JAFFE, H. H., and ORCHIN, M., 1962, *Theory and Application of Ultraviolet Spectroscopy* (New York: Wiley and Sons).
- [3] BULLOCK, F., 1963, *Canad. J. Chem.*, **41**, 711.
- [4] FRASER, R. R., 1960, *Canad. J. Chem.*, **38**, 2226.
- [5] DIEHL, P., and SVEGLIADO, G., 1963, *Helv. chim. Acta*, **46**, 461.
- [6] LAUTERBUR, P. C., 1963, *J. chem. Phys.*, **38**, 1406.
- [7] GIL, V. M. S., and GIBBONS, W. A., 1964, *Mol. Phys.*, **8**, 199.
- [8] SCHAEFER, T., REYNOLDS, W. F., and YAMEMOTO, T., 1963, *Canad. J. Chem.*, **41**, 2969.
- [9] YAMAGUCHI, I., 1963, *Mol. Phys.*, **6**, 105.
- [10] FERGUSON, G., and ROBERTSON, J., 1963, *Advances in Physical Organic Chemistry*, Vol. I (Academic Press), p. 203.
- [11] GIBBONS, W. A., unpublished results.
- [12] BRAUDE, E. A., and SONDHEIMER, F., 1955, *J. chem. Soc.*, 3754.
- [13] BURGERS, J., HOEFNAGEL, M. A., VERKADE, P. E., VISSER, H., and WEPSTER, B. M., 1958, *Rec. Trav. chim. Pays-Bas*, **77**, 491.
- [14] POPL, J. A., 1962, *Disc. Faraday Soc.*, **34**, 7.
- [15] GIBBONS, W. A., and GIL, V. M. S., 1965, *Mol. Phys.*, **9**, 163.

Expansion theorems for solid spherical harmonics

by J. P. DAHL

H. C. Ørstedinstituttet, Laboratory for Physical Chemistry,
University of Copenhagen, Copenhagen, Denmark

and M. P. BARNETT

Institute of Computer Science, 44 Gordon Square,
London, W.C.1

(Received 10 October 1964)

An inductive method has been used to derive formulae for the expansion of a solid spherical harmonic $(r_n$ or $r^{-n-1})P_n^m(\cos \theta) \exp(im\phi)$ on one centre in terms of solid spherical harmonics on another centre.

Solid spherical harmonics are solutions of Laplace's equation $\nabla^2\psi=0$ of the form:

$$r^N P_N^M(\cos \theta) \exp(iM\phi) \quad (\text{regular harmonics})$$

or

$$r^{-N-1} P_N^M(\cos \theta) \exp(iM\phi) \quad (\text{irregular harmonics}).$$

Since Laplace's equation is invariant under translations and rotations it is possible to express a solid spherical harmonic on one centre as a linear combination of solid spherical harmonics on another centre. Formulae affecting the expansion are of importance in the calculation of molecular integrals [1] and have attracted considerable attention in the literature. Hobson [2] treated the case where the coordinate systems on the two centres have their z -axes pointing towards each other. In the more general case, where the coordinate systems on the two centres have parallel axes, the expansion theorem for the regular harmonics was first derived by Rose [3], who applied the algebra of irreducible tensors. The corresponding expansion for the irregular harmonics was derived simultaneously by Chiu [4], Sack [5] and the present authors. Chiu applied the theory of irreducible tensors, while Sack used a differential equation method. Our own method, which is inductive in nature, has only been described in technical reports [6, 7], but since it is quite simple to apply we have found reason to present it here.

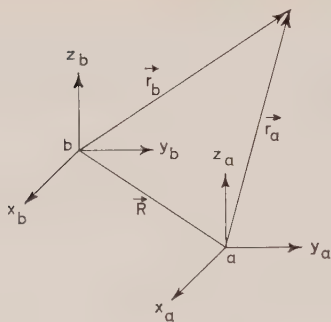
Consider the two coordinate systems a and b (figure) with parallel axes. The location of b relative to a is specified by giving the vector $\mathbf{R} = (X, Y, Z) = (R, \Theta, \Phi)$, where the rectangular and spherical coordinates of \mathbf{R} expressed in a have been denoted (X, Y, Z) and (R, Θ, Φ) respectively. With a similar notation a field point P may be specified by giving its coordinates in b , i.e.

$$\mathbf{r}_b = (x_b, y_b, z_b) = (r_b, \theta_b, \phi_b)$$

or in a , $\mathbf{r}_a = (x_a, y_a, z_a) = (r_a, \theta_a, \phi_a)$. The relation

$$(x_b, y_b, z_b) = (x_a - X, y_a - Y, z_a - Z) \quad (1)$$

obviously holds.



The following expansions are then valid:

$$r_b^N P_N^M(\cos \theta_b) \exp(iM\phi_b) = \sum_{n=0}^N \sum_m (-1)^{N-n} \binom{N+M}{n+m} r_a^n R^{N-n} \\ \times P_n^m(\cos \theta_a) P_{N-n}^{M-m}(\cos \Theta) \exp(im\phi_a) \exp[i(M-m)\Phi] \quad (2)$$

and

$$\frac{P_N^M(\cos \theta_b)}{r_b^{N+1}} \exp(iM\phi_b) = \delta^N \sum_{n=0}^{\infty} \frac{r_{<}^n}{r_{>}^{N+n+1}} \sum_m (-1)^{M-m} \binom{N+n-m}{N-M} \\ \times P_{N+n}^m(\cos \theta_{>}) P_n^{M-m}(\cos \theta_{<}) \exp(im\phi_{>}) \exp[i(M-m)\phi_{<}]. \quad (3)$$

In (3) $r_{<}$ denotes the smaller, $r_{>}$ the larger of r_a and R . $\theta_{>}$, $\phi_{>}$ and $\theta_{<}$, $\phi_{<}$ are the angles associated with $r_{>}$ and $r_{<}$, respectively. δ is -1 for $r_a < R$ and $+1$ for $r_a > R$. The associated Legendre functions are those defined by Hobson [2]:

$$P_n^m(\cos \theta) = (-1)^m \sin^m \theta \frac{d^m}{d(\cos \theta)^m} P_n(\cos \theta), \quad m \geq 0, \quad (4)$$

$$P_n^{-m}(\cos \theta) = (-1)^m \frac{(n-m)!}{(n+m)!} P_n^m(\cos \theta). \quad (5)$$

The relation (5) holds for all m values. Further it is contained in (4) that $P_n^m(\cos \theta) = 0$ for $m > n$, so that the sums over m in (2) and (3) usually contain less than $2n+1$ terms. The notation $\binom{p}{q}$ has been used for the binomial coefficient:

$$\binom{p}{q} = \frac{p!}{q!(p-q)!}.$$

To derive (2) we note that the defining equation (4) involves that

$$P_N^N(\cos \theta_b) = (-1)^N \frac{(2N)!}{2^N N!} \sin^N \theta_b$$

or

$$r_b^N P_N^N(\cos \theta_b) \exp(iN\phi_b) = (-1)^N \frac{(2N)!}{2^N N!} (x_b + iy_b)^N. \quad (6)$$

If (1) is substituted into the right-hand side of (6), application of the binomial expansion immediately gives:

$$r_b^N P_N^N(\cos \theta_b) \exp(iN\phi_b) = \sum_{n=0}^N (-1)^{N-n} \binom{2N}{2n} r_a^n R^{N-n} P_n^n(\cos \theta_a) \\ \times P_{N-n}^{N-n}(\cos \Theta) \exp(in\phi_a) \exp[i(N-n)\Phi], \quad (7)$$

which is recognized as equation (2) for $M=N$.

To derive (2) for $M \neq N$ we consider simultaneous, infinitesimal rotations of the coordinate systems a and b through the same angle about parallel axes. The changes in the functions involved may then be found by applying the operators of angular momentum, since these operators are proportional to the operators for small rotations. The fact that \mathbf{r}_a , \mathbf{r}_b and \mathbf{R} are all rotated through the same angle then implies that operating with an angular momentum operator \hat{l}_b on the left side of, for instance, equation (7) is equivalent to operating with the operator $\hat{l} + \hat{l}_a$ on the right side. Here \hat{l} and \hat{l}_a are the same functions of (Θ, Φ) and (θ_a, ϕ_a) as \hat{l}_b is of (θ_b, ϕ_b) .

From the well-known properties of the operator $\hat{l}_x - i\hat{l}_y$ it follows that

$$(\hat{l}_x - i\hat{l}_y) P_n^m(\cos \theta) \exp(im\phi) = (n+m)(n-m+1) P_n^{m-1}(\cos \theta) \exp[i(m-1)\phi]. \quad (8)$$

Operating on the left-hand side of (7) with the operator $\hat{l}_{x_b} - i\hat{l}_{y_b}$ and on the right-hand side with the operator $(\hat{l}_x - i\hat{l}_y) + (\hat{l}_{x_a} - i\hat{l}_{y_a})$ the expansion formula for the case $M=N-1$ is readily derived. From this formula the general formula (2) is inferred, and the validity of (2) is finally proved by induction, i.e. validity for the value M is shown to imply validity for the value $M-1$. This step is again carried out by applying the operators $\hat{l}_x - i\hat{l}_y$.

To derive equation (3) the starting point is taken in the well-known expansion for the $N=0$, $M=0$ case:

$$\frac{1}{r_b} = \sum_{n=0}^{\infty} \frac{r_{<}^n}{r_{>}^{n+1}} \sum_{m=-n}^n (-1)^m P_n^m(\cos \theta_{>}) P_n^{-m}(\cos \theta_{<}) \quad (9)$$

and the expressions:

$$\frac{P_n^m(\cos \theta) \exp(im\phi)}{r^{n+1}} = (-1)^{n-m} \frac{1}{(n-m)!} \frac{\partial^{n-m}}{\partial z^{n-m}} \frac{\partial^m}{\partial \eta^m} \left(\frac{1}{r} \right), \quad (10)$$

$$\frac{P_n^m(\cos \theta) \exp(-im\phi)}{r^{n+1}} = (-1)^{n-m} \frac{1}{(n-m)!} \frac{\partial^{n-m}}{\partial z^{n-m}} \frac{\partial^m}{\partial \xi^m} \left(\frac{1}{r} \right), \quad (11)$$

where

$$m \geq 0 \quad \text{and} \quad \eta = \frac{1}{2}(x - iy), \quad \xi = \frac{1}{2}(x + iy).$$

From (9), (10) and (11) the expansion formula for $M=0$, arbitrary N is obtained by differentiating the left side of (9) with respect to \mathbf{r}_b 's coordinates. For each differentiation on the left a differentiation is performed on the right with respect to \mathbf{r}_a or $-\mathbf{R}$, whichever is the larger (cf. equation (1)). (10) and (11) are then used to identify the terms on the right-hand side.

Having derived (3) for $M=0$, arbitrary N , the expansion formula for $M=1$ may be derived applying the operators for infinitesimal rotations. From the $M=1$ case the general formula (3) is inferred, and the method of induction is finally used to prove the general validity of this formula.

The present work was done at the Solid State and Molecular Theory Group, M.I.T., and it is a pleasure to thank Professor J. C. Slater for his interest. We express appreciation to the National Science Foundation for financial support and J. P. D. is grateful to the U.S. Government for a travel grant under the Fulbright-Hays Act.

REFERENCES

- [1] PITZER, R. M., KERN, C. W., and LIPSCOMB, W. N., 1962, *J. chem. Phys.*, **37**, 267.
- [2] HOBSON, E. W., 1955, *The Theory of Spherical and Ellipsoidal Harmonics* (New York: Chelsea Publishing Company).
- [3] ROSE, M. E., 1958, *J. math. Phys.*, **37**, 215.
- [4] CHIU, Y., 1964, *J. math. Phys.*, **5**, 283.
- [5] SACK, R. A., 1964, *J. math. Phys.*, **5**, 252.
- [6] DAHL, J. P., and BARNETT, M. P., 1963, Quarterly Progress Report No. 48, Solid State and Molecular Theory Group, M.I.T., April 15, p. 53.
- [7] DAHL, J. P., 1964, Quarterly Progress Report No. 52, Solid State and Molecular Theory Group, M.I.T., April 15, p. 47.

Solvent and temperature effects in the electron spin resonance spectrum of the hexamethylacetone-sodium ion-quartet

by G. R. LUCKHURST

Department of Theoretical Chemistry, University Chemical Laboratory,
Lensfield Road, Cambridge

(Received 17 September 1964)

The sodium coupling constant of the radical obtained by reduction of hexamethylacetone in tetrahydrofuran, methyltetrahydrofuran and their binary mixtures has been studied as a function of solvent composition and temperature. The solvent dependence of the sodium coupling constant may be explained by a simple model involving equilibria between radicals differing only in the composition of the solvent sheath. The increase of the sodium coupling constant on cooling the solution may be caused by structural changes in the solvent sheath and a depopulation of vibrational levels.

1. INTRODUCTION

Adam and Weissman [1] were the first to demonstrate the formation of ion-pairs from alkali-metal cations and radical anions in solvents of low dielectric constant. They found that the electron spin resonance spectrum of a solution of benzophenone ketyl formed by sodium reduction was more complex than that of the free anion. This difference could be accounted for by supposing that each line of the anion spectrum was split into four components of equal intensity through interaction with the nuclear moment of a sodium cation ($I = \frac{3}{2}$). Since then electron spin resonance has been used to study ion-pair formation and ion-pair equilibria in a variety of systems [2, 3, 4].

In principle such studies should help to determine the structure of ion-pairs and the nature of the solvent sheaths surrounding them, but in practice the partial dissociation of the ion-pairs usually complicates the interpretation of the spectra. To avoid this complication we have worked with the ion-quartet, formed by sodium reduction of hexamethylacetone, which does not dissociate appreciably in tetrahydrofuran or similar solvents [5, 6].

2. ANALYSIS OF THE ELECTRON SPIN RESONANCE SPECTRA

Hexamethylacetone was prepared by methylation of di-isopropyl ketone [7] and purified by distillation *in vacuo*. Solutions of the ketyl were obtained by reduction with sodium [8]. The spectra were recorded at a number of temperatures on a Varian 100 kc E.P.R. spectrometer using the Varian variable temperature accessory.

At room temperature the hyperfine structure of the spectrum (figure 1 (a)) of solutions of the radical in tetrahydrofuran is due to the interaction of the odd

electron with 18 equivalent protons and two equivalent sodium nuclei [5]. Our values of the sodium, proton and carbon-13 coupling constants are in good agreement with those obtained by Hirota and Weissman [5]. Surprisingly the spectrum 1(*d*) obtained from the solution in methyltetrahydrofuran differs drastically from that in tetrahydrofuran. However, the difference between spectra 1(*a*) and 1(*d*) depends only on a change in the sodium coupling constant which is 1.58 gauss in tetrahydrofuran and 0.65 gauss in methyltetrahydrofuran. Because of the large difference between these sodium coupling constants we thought it interesting to measure the spectrum of the radical in mixtures of the two solvents; two typical spectra are shown in figure 1.

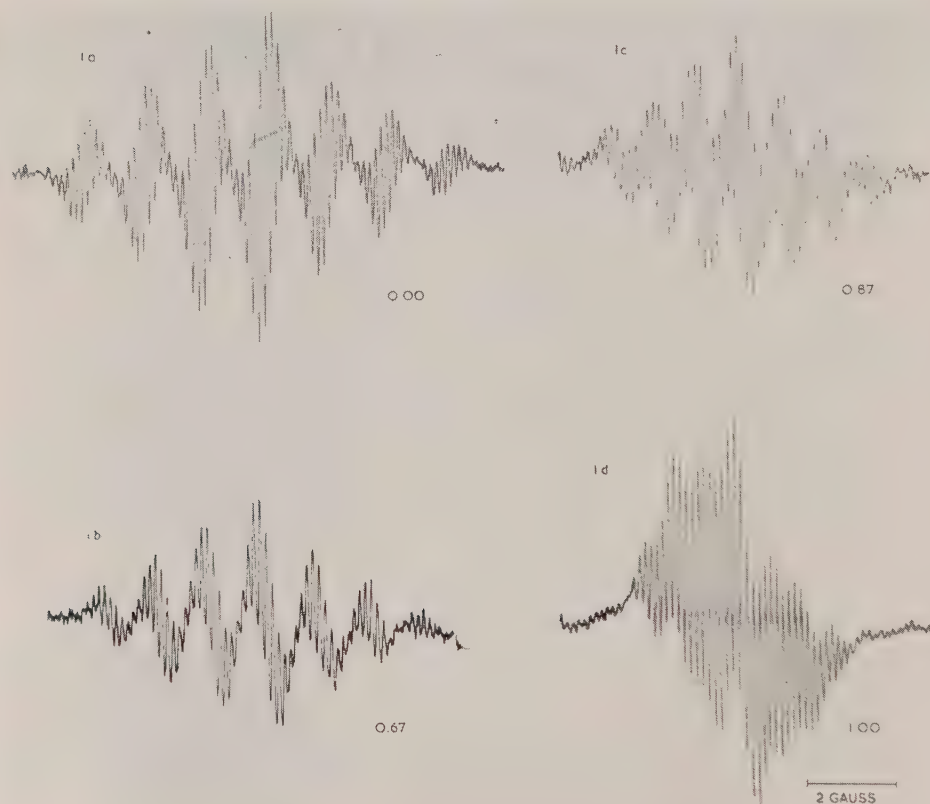


Figure 1. The electron spin resonance spectra of the radical obtained by sodium reduction of hexamethylacetone. The numbers give the mole fraction of methyltetrahydrofuran.

Whereas the proton coupling constant in all solvents and the sodium coupling constant in tetrahydrofuran are insensitive to the temperature, in methyltetrahydrofuran the sodium coupling constant depends critically on temperature increasing from 0.65 gauss at 20°C to a limiting value of 1.90 gauss at -100°C. This temperature dependence is shown in figure 2 for the pure solvents and

their binary mixtures. The sodium coupling constant in all solvent mixtures tends to the same limiting value, 1.70 gauss at low temperatures.

The sodium coupling constant at various temperatures was obtained as a function of solvent composition by taking values from the smoothed curves in figure 2, these are plotted in figure 3.

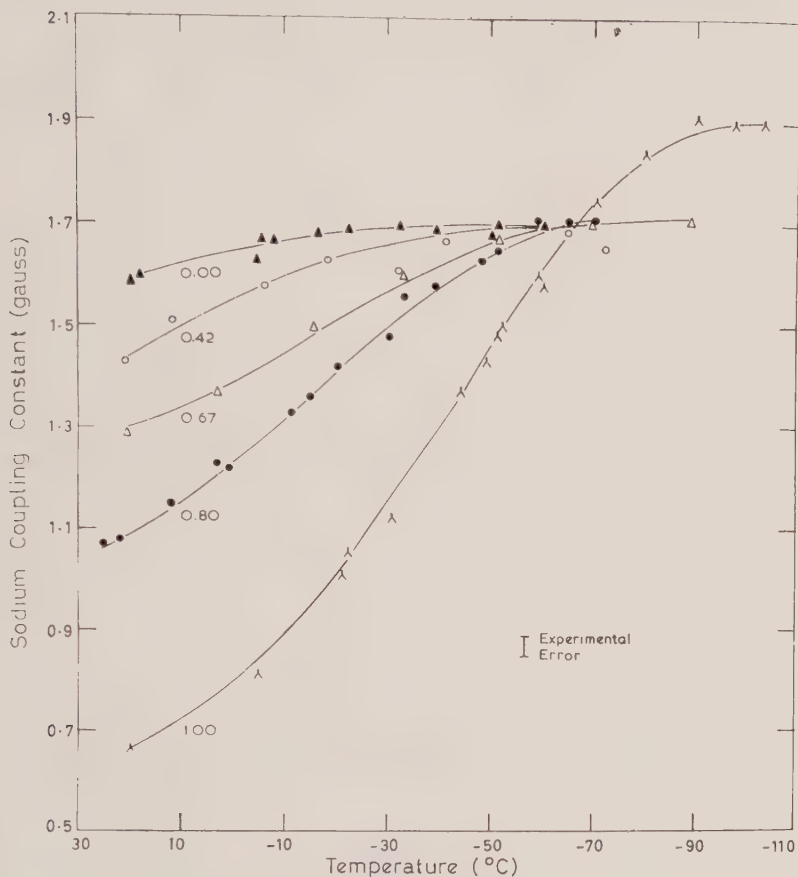


Figure 2. The temperature dependence of the sodium coupling constant for the pure solvents and their mixtures.

3. A SIMPLE MODEL FOR THE SOLVENT EFFECT

The solvent dependence of proton coupling constants of polar radicals in binary mixtures of an ether and an alcohol is well understood [9,10]. This variation is caused by a single equilibrium between a 1 : 1 alcohol-radical complex and the free radical-anion. In ether-type solvents such complex formation by hydrogen-bonding cannot occur so that variation of the sodium coupling constant must be caused by a different modification of the solvent sheath.

Suppose that the radical X has an average coordination number n and that these n sites are spatially equivalent. Then in a solvent mixture of A and B there will be n equilibria of the form:



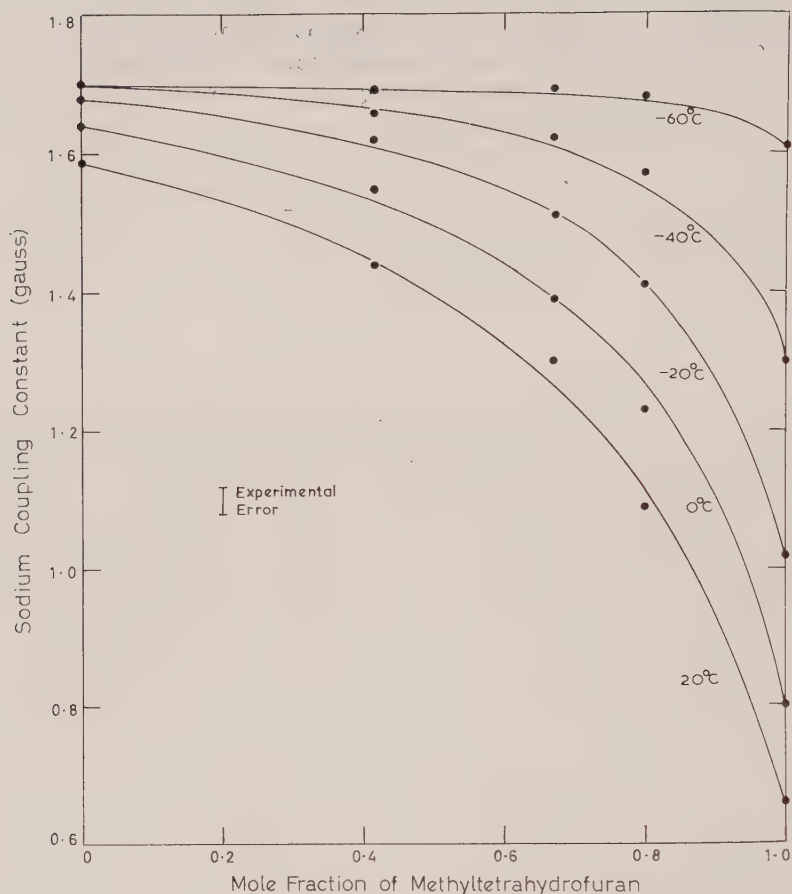


Figure 3. The sodium coupling constant as a function of the mole fraction of methyltetrahydrofuran at various temperatures.

Now the high resolution of the spectra in all solvent mixtures shows that the molecules in the solvent sheath are exchanging rapidly with those in the bulk solvent, so that the observed sodium coupling constant \bar{a} will be the statistical average of the coupling constants in the $(n+1)$ distinct solvated radicals. Thus:

$$\bar{a} = \frac{\sum_{m=0}^n p_m a_m}{\sum_{m=0}^n p_m}, \quad (3.1)$$

in which p_m is proportional to the number of moles of solvated radical $XA_{n-m}B_m$ with a sodium coupling constant a_m .

The calculation of both a_m and p_m is difficult and we are forced to make some drastic assumptions. Since the sodium coupling constant, a_m , cannot be measured we shall assume that it is independent of the order of A and B on the sites and is linearly related to the values a^A and a^B in the pure solvents, i.e.:

$$a_m = \frac{(n-m)a^A + ma^B}{n}. \quad (3.2)$$

We shall also assume that the Gibbs free energy, $\Delta G^X(m)$, of the solvated radical $XA_{n-m}B_m$ relative to a solution of its components is:

$$\Delta G^X(m) = \frac{n-m}{n} \Delta G^{XA} + \frac{m}{n} \Delta G^{XB} + (n-m)\Delta G^A + m\Delta G^B, \quad (3.3)$$

where ΔG^{XA} is the difference in free energy of unsolvated X and X solvated by n molecules of A; ΔG^{XB} is defined similarly. ΔG^A (or ΔG^B) is the difference in free energy between a molecule of A (or B) in the solvent sheath and in the solvent. Equation (3.3) may be written as:

$$\Delta G^X(m) = (n-m)\Delta G^A + m\Delta G^{B'}, \quad (3.4)$$

where

$$\Delta G^{A'} = \frac{\Delta G^{XA}}{n} + \Delta G^A,$$

$$\Delta G^{B'} = \frac{\Delta G^{XB}}{n} + \Delta G^B,$$

and we assume that $\Delta G^{A'}$ and $\Delta G^{B'}$ are independent of m and the composition of the solvent mixture. This assumption will be valid if the solvents A and B are very similar for then the A-B interaction will be close to the mean of the A-A and B-B interactions so that $\Delta G^{A'}$ and $\Delta G^{B'}$ will depend only on the interaction of A and B with the radical X .

The ideal nature of the solvents and the low concentration of radicals permits us to replace activities by concentrations. Thus in a solution of N_1 moles of A and N_2 moles of B the value of p_m is:

$$p_m = \frac{n!}{(n-m)!m!} N_1^{n-m} N_2^m \exp \left\{ \frac{-(n-m)\Delta G^{A'} - m\Delta G^{B'}}{kT} \right\}. \quad (3.5)$$

The factor $[n!/(n-m)!m!]$ allows for the number of different ways of arranging the $(n-m)$ molecules of A and the m molecules of B on the solvent sites in the radical $XA_{n-m}B_m$. The term $N_1^{n-m}N_2^m$ is proportional to the probability of forming $XA_{n-m}B_m$ if there was no difference in free energy between the solvated radical and its components. However there is a difference, namely $\Delta G^X(m)$, and this accounts for the exponential term in equation (3.5). Substitution of equations (3.2) and (3.5) into equation (3.1) leads to the result that:

$$\bar{a} = \frac{a^A N_1 \exp(-\Delta G^{A'}/kT) + a^B N_2 \exp(-\Delta G^{B'}/kT)}{N_1 \exp(-\Delta G^{A'}/kT) + N_2 \exp(-\Delta G^{B'}/kT)}. \quad (3.6)$$

This is conveniently written in terms of the mole fraction, x , of B and an equilibrium constant, K , defined by:

$$\Delta G^{A'} - \Delta G^{B'} = -kT \log_e K, \quad (3.7)$$

so that the observed sodium coupling constant is:

$$\bar{a} = \frac{a^A(1-x) + a^B Kx}{1+x(K-1)}. \quad (3.8)$$

The equilibrium constant is for any equilibrium in which solvent A tends to be replaced by solvent B on one site in the solvent sheath. This result is independent of the number of sites so that it is identical to that obtained by Gendell *et al.* [9] who restricted themselves to the one site problem.

We have fitted our results to equation (3.8). The table gives the equilibrium constants estimated in this way. The curves in figure 3 have been calculated using these constants. In view of the naive assumptions in our model the agreement with experiment is surprisingly good.

Temperature (°K)	Equilibrium constant K
293	0.257 ± 0.017
273	0.200 ± 0.017
253	0.158 ± 0.020
233	0.143 ± 0.033
213	0.100

Equilibrium constants for the replacement of solvent molecules.

We can now calculate the molar enthalpy, ΔH , and entropy ΔS for the replacement of tetrahydrofuran (A) by that of methyltetrahydrofuran (B) on one site of the solvent sheath. A plot of $\log_e K$ against $1/T$, shown in figure 4, is reasonably linear. From the slope of this line we find that ΔH is 1.5 ± 0.3 kcal mole⁻¹ and ΔS is 2.1 ± 0.2 cal deg⁻¹ mole⁻¹.

Although the factors determining ΔH and ΔS are complex and indeed their experimental values uncertain it seems probable that the steric effect of the methyl group is amongst the most important. Thus the replacement of a molecule of tetrahydrofuran by one of methyltetrahydrofuran could disturb the ordered arrangement slightly and so account for the small positive change in entropy. Similarly the positive enthalpy change shows that the radical interacts more strongly with tetrahydrofuran than methyltetrahydrofuran. Possibly the second solvent cannot approach as close to the radical as tetrahydrofuran. It is interesting that the radical is unstable in methyltetrahydrofuran but not in tetrahydrofuran perhaps the decrease in solvation energy is a dominating factor here.

4. THE TEMPERATURE VARIATION OF THE SODIUM COUPLING CONSTANT

The sodium coupling constant in solutions of tetrahydrofuran and its mixtures with methyltetrahydrofuran tends to the limiting value of 1.70 gauss on lowering the temperature. This is caused by the decrease in equilibrium constant K with decreasing temperature so that the amount of tetrahydrofuran in the solvent sheath increases.

Let us now consider why the sodium coupling constant changes with temperature in the pure solvents. Although the majority of aromatic radical-anions give proton coupling constants which are insensitive to temperature changes there are cases when they are critically temperature dependent [11]. The behaviour of these systems may be understood in terms of a thermal population of two near-degenerate electronic levels with energies E_1 and E_2 and corresponding hyperfine coupling constants a_1 and a_2 . Thus the observed coupling constant is given by:

$$\bar{a} = \frac{a_1 \exp(-E_1/kT) + a_2 \exp(-E_2/kT)}{\exp(-E_1/kT) + \exp(-E_2/kT)} \quad (4.1)$$

Atherton and Weissman [2] have extended this idea to explain the temperature variation of the sodium coupling constant in sodium naphthalenide. They suggest that the sodium cation may occupy a large number of thermally accessible vibrational levels so that (4.1) becomes:

$$\bar{a} = \frac{\sum_{n=0}^{\infty} a_n \exp(-E_n/kT)}{Z}, \quad (4.2)$$

where Z is the partition function, a_n is the coupling constant in the n th level with energy E_n . The problem of calculating \bar{a} for most cases is impossible and the

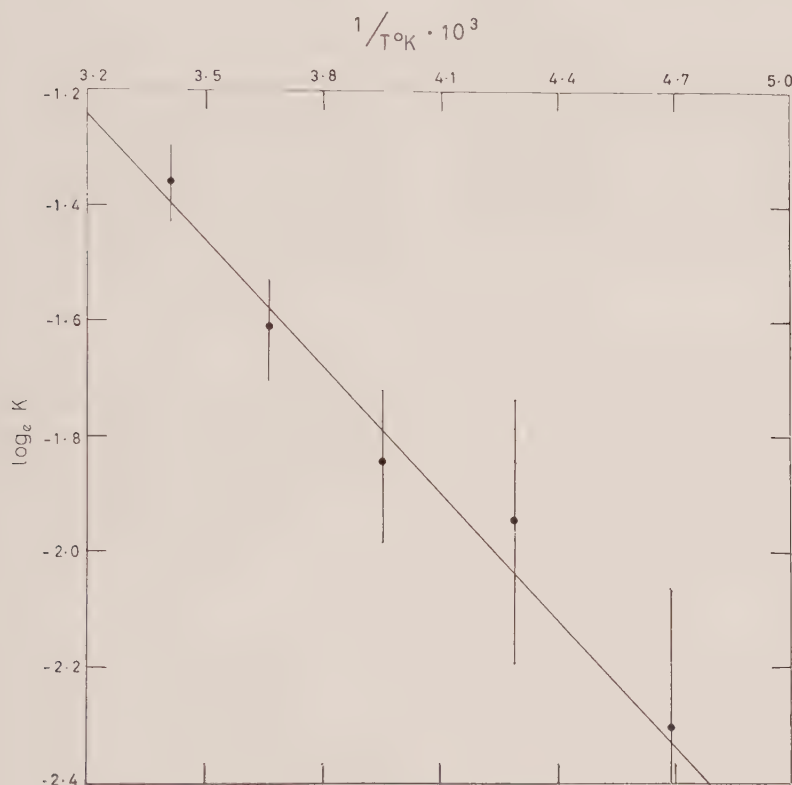
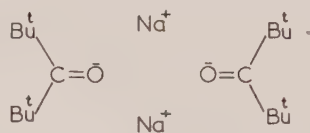


Figure 4. Plot of $\log_e K$ against I/T . The vertical lines give an estimate of the experimental error.

best we can do is to make rather general observations. Thus our results for the temperature dependence of the sodium coupling constant in pure solvents are completely consistent with this model if $a_n > a_{n+1}$ and if a_n depends on n in such a way as to make \bar{a} tend to a limiting value. However a somewhat simpler explanation is available.

The way in which the sodium splitting arises in ion-pairs has been discussed by Atherton and Weissman [2] and it seems likely that unpaired spin in the 3s orbital is responsible. In turn this may depend on the overlap of the 3s orbital with the unpaired spin in the antibonding π orbital of the carbonyl group and unpaired spin in the sp^2 hybrid orbitals containing the lone pairs of the oxygen

atom, caused by spin polarization [12]. The intimate details of this interaction are not too important, the main point being that the sodium coupling constant will be sensitive to the nuclear positions. Hirota and Weissman [6] have suggested that the structure of this ion-quartet is:



but the actual arrangement of the ions will depend on electrostatic forces and the structure of the solvent sheath. It is reasonable to assume that the solvent sheath will become more compact as the temperature is lowered and that the change for methyltetrahydrofuran will be greater than that for tetrahydrofuran for steric reasons. Thus the sodium coupling constants will be more sensitive to temperature for the ion-quartet in methyltetrahydrofuran. The fact that the sodium coupling constant increases on cooling implies that the overlap between the 3s and π orbitals or sp^2 orbitals is increased as the solvent sheath contracts. It seems that both effects may be important in determining the sodium coupling constant.

5. CONCLUSION

A simple model of equilibria in a binary solvent mixture is able to explain the solvent dependence of the sodium coupling constant in this ion-quartet. Detailed analysis of the results in terms of this model allow us to estimate the differential enthalpy and entropy of solvation. The change of the sodium coupling constant with temperature in the pure solvents is probably caused by a combination of two changes (*a*) in the structure of the solvent sheath and (*b*) in the thermal population of vibrational levels.

It is a pleasure to acknowledge the interest and encouragement of Dr. L. E. Orgel, F.R.S. during the course of this work. I also wish to thank the D.S.I.R. for the award of a studentship.

REFERENCES

- [1] ADAM, F. C., and WEISSMAN, S. I., 1958, *J. Amer. chem. Soc.*, **80**, 1518.
- [2] ATHERTON, N. M., and WEISSMAN, S. I., 1961, *J. Amer. chem. Soc.*, **83**, 1330.
- [3] STRAUSS, H., KATZ, T., and FRAENKEL, G. K., 1963, *J. Amer. chem. Soc.*, **85**, 2360.
- [4] DE BOER, E., and MACKOR, E. L., 1964, *J. Amer. chem. Soc.*, **86**, 1513.
- [5] HIROTA, N., and WEISSMAN, S. I., 1960, *J. Amer. chem. Soc.*, **82**, 4424.
- [6] HIROTA, N., and WEISSMAN, S. I., 1964, *J. Amer. chem. Soc.*, **86**, 2538.
- [7] WHITMORE, F. C., and STAHLY, E. E., 1933, *J. Amer. chem. Soc.*, **55**, 4153.
- [8] PAUL, D. E., LIPKIN, D., and WEISSMAN, S. I., 1956, *J. Amer. chem. Soc.*, **78**, 116.
- [9] GENDELL, J., FREED, J. H., and FRAENKEL, G. K., 1962, *J. chem. Phys.*, **37**, 2832.
- [10] LUCKHURST, G. R., and ORGEL, L. E., 1964, *Mol. Phys.*, **8**, 117.
- [11] CARRINGTON, A., MOSS, R. E., and TODD, P. F. (to be published).
- [12] MCCONNELL, H. M., 1956, *J. chem. Phys.*, **24**, 764.

Isotope effects in electron spin resonance: the negative ion of cyclo-octatetraene-1-d

by A. CARRINGTON, H.C. LONGUET-HIGGINS,

R. E. MOSS and P. F. TODD

Department of Theoretical Chemistry, University of Cambridge

(Received 23 September 1964)

Replacement of one hydrogen atom by deuterium in the negative ion of cyclo-octatetraene, makes no significant difference to the electron spin densities at the hydrogen nuclei. This result contrasts with a recent observation that mono-deuteration produces a measurable change in the spin distribution in the benzene negative ion. The difference between the two systems is interpreted in terms of the Jahn-Teller effect.

1

Lawler *et al.* [1] recently measured the electron spin resonance spectrum of the benzene-1-d negative ion and discovered that the spin distribution differs significantly from that in the negative ion of benzene itself. We here report corresponding measurements on the negative ion of cyclo-octatetraene-1-d where no such isotope effect appears. We first present our results and then offer a qualitative explanation for the difference between the two ring systems.

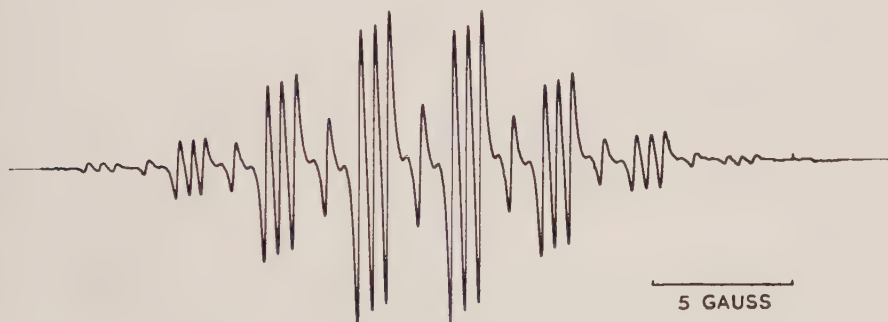


Figure 1. The electron spin resonance spectrum of the negative ion of cyclo-octatetraene-1-d.

2

Cyclo-octatetraene-1-d was prepared by the action of deuterium oxide on a solution of cyclo-octatetraenyl lithium in dry ether. It was dissolved in tetrahydrofuran, and reduced with metallic lithium to the ion radical. The electron resonance spectrum of the solution was recorded at -70°C using a Varian 100 kc spectrometer, and is shown in figure 1. The eight triplets are presumed

to arise from $\text{C}_8\text{H}_7\text{D}^-$. In between the triplets are seven weaker lines, which we attribute to the undeuterated ion C_8H_8^- ; there should be two more lines, but they are not visible. The main spacing (a_{H}) in each spectrum is 3.2 ± 0.05 gauss, and the triplet splitting (a_{D}) is 0.50 ± 0.02 gauss. Both spectra are accurately symmetrical about the centre line in the C_8H_8^- spectrum, and the widths of all the lines are equal within experimental error, and not unusually great. The relative intensities of the two sets of lines indicate that the deuterated material was better than 85 per cent isotopically pure.

3

If there were a significant electronic isotope effect, leading to inequivalence of the various hydrogen nuclei in the deuterated radical ion, one would observe a splitting of at least some of the lines in the spectrum of $\text{C}_8\text{H}_7\text{D}^-$, and/or a discrepancy between $a_{\text{H}}/a_{\text{D}}$ and the ratio of the nuclear g factors. Actually $a_{\text{H}}/a_{\text{D}} = 6.4 \pm 0.2$, in agreement with $g_{\text{H}}/g_{\text{D}} = 6.514$, and there is no sign of any further splittings. In fact, the isotope effect is too small for us to detect. Why, then, is it so much smaller than in $\text{C}_6\text{H}_5\text{D}^-$?

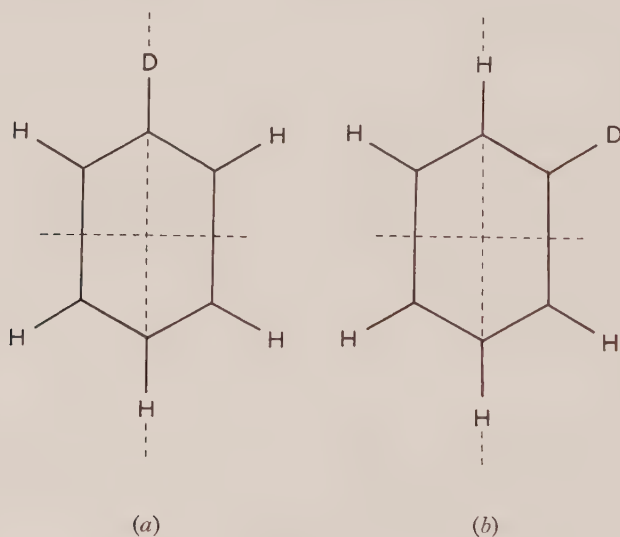


Figure 2.

The answer, we suggest, is to be found in the Jahn–Teller effect, and in an interesting difference between the ways in which it operates in the two ions. Let us consider C_6H_6^- first. Here, as shown by McConnell and McLachlan [2], the odd electron occupies an e_{2u} orbital, so that the D_{6h} nuclear configuration is unstable against distortions of species e_{2g} . As a result the ion possesses not one but several configurations of minimum electronic energy. In the lowest approximation, used by these authors, there are infinitely many equilibrium configurations, forming a circle in configuration space; if anharmonicity is taken into account their number is reduced to three, corresponding to an elongation or, alternatively, a shortening of the ring along one of the three principal diagonals. Figures 2 and 3 illustrate these alternative possibilities for $\text{C}_6\text{H}_5\text{D}^-$, which has

the same electronic energy surface as $C_6H_6^-$; the dotted lines in each diagram indicate the nodes of the more stable orbital for the odd electron, on the principle that a bond crossed by a node tends to be longer than one which is not.

If the nuclei had no kinetic energy, there would be nothing to favour a distortion along any particular diagonal, and every hydrogen nucleus, whether H or D, would experience the same mean spin density. But as soon as one takes the nuclear kinetic energy into account it becomes clear that configurations of type (a) need not occur with the same probability as those of type (b). This is because there are many degrees of freedom, other than those associated with the Jahn-Teller distortion, for which the zero-point energy will differ as between configurations (a) and (b). In particular, the C-H stretching vibrations, which are largely independent of the ring modes, may well have a different zero-point energy in the two types of structure. This will be the case if the force constant of a C-H bond is sensitive to the electronic charge on the C atom; in figure 2 (a) the D atom is at a position of zero charge, whereas in 2 (b) the net charge on the neighbouring C atom is $\frac{1}{4}$.

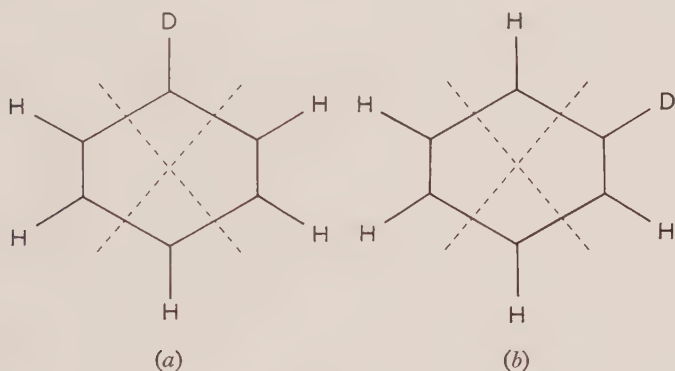


Figure 3.

It is, of course, over-simple to regard (a) and (b) as distinct isomers; there will be tunnelling between them, and not all the molecules will be in their vibronic ground states. But it remains true that the effective potential energy need not be the same for configurations of type (a) and (b), and that whichever has the lower effective potential energy will be statistically favoured in equilibrium.

We now turn to the negative ion of cyclo-octatetraene. Here there are three electrons in the e_{2u} orbitals and, as shown by McLachlan and Snyder [3], the D_{8h} configuration is unstable against distortions of species b_{1g} or b_{2g} . A b_{1g} distortion of the ring leads to an alternation of the C-C-C bond angles, and a b_{2g} distortion to an alternation of bond lengths (see figure 4). Since the orbital energy is undoubtedly more sensitive to changes in bond length than to changes in bond angle, the b_{2g} distortion will almost certainly be the favoured one, and there will be two equivalent equilibrium configurations, in each of which the C-C bonds alternate in length round the ring. But now an essential difference arises: whereas in $C_6H_6^-$ the favoured distortion made the H nuclei inequivalent, in $C_8H_8^-$ the H nuclei are *still* equivalent even in the *distorted* equilibrium configuration. This would not be true, of course, if the ion distorted in the b_{1g} mode, but this possibility may safely be dismissed for the reason already given.

If this is granted, the two equilibrium configurations are isotopically indistinguishable, and there is nothing to choose between the different positions as far as mean spin density is concerned. The absence of a detectable isotope effect is thus accounted for.

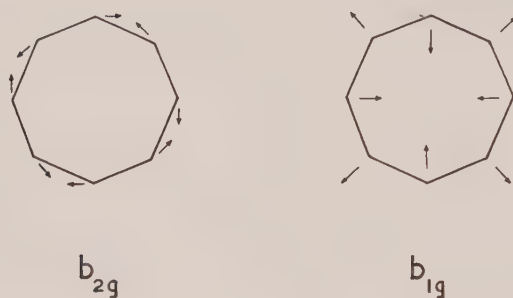


Figure 4.

4

On the basis of these ideas it is possible to predict which of the polydeuterated benzene anions ought to show an electronic isotope effect. The prediction is simple, because there are only two deuterated benzenes for which the distorted anions are isotopically indistinguishable, namely benzene-1,3,5- d_3 and benzene- d_6 . All the others, we predict, should exhibit measurable isotope effects. As for the deuterated cyclo-octatetraenes, the situation is a little more complicated because the distorted forms of, say, cyclo-octatetraene-1,2- d_2 are isotopically distinguishable. But the spin densities are the same at all positions in both distorted forms, so that there cannot even be a difference of C-H zero-point energy to give rise to an isotope effect in the deuterated cyclo-octatetraene anions.

We should like to record that the interpretation of the benzene-1- d negative ion spectrum in terms of the Jahn-Teller effect was appreciated independently by Dr. L. E. Orgel, F.R.S. We thank the D.S.I.R. for the purchase of a Varian spectrometer and for a maintenance grant to R.E.M. P.F.T. thanks I.C.I. Ltd., Petrochemical and Polymer Laboratory, for leave of absence.

REFERENCES

- [1] LAWLER, R. G., BOLTON, J. R., FRAENKEL, G. K., and BROWN, T. H., 1964, *J. Amer. chem. Soc.*, **86**, 520.
- [2] McCONNELL, H. M., and McLACHLAN, A. D., 1961, *J. chem. Phys.*, **34**, 1.
- [3] McLACHLAN, A. D., and SNYDER, L. C., 1962, *J. chem. Phys.*, **36**, 1159.

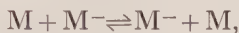
RESEARCH NOTES

Spin densities in the alkyl groups of alkyl-substituted naphthalene negative ions, determined by N.M.R.

by E. DE BOER and C. MACLEAN
Koninklijke/Shell-Laboratorium, Amsterdam
(Shell Research N.V.)

(Received 11 January 1965)

In solutions containing both neutral molecules and the corresponding negative ions, electron transfer reactions may occur between these two species [1]. Such a reaction may be symbolized by:



where M represents the neutral molecule.

This electron transfer process modifies the proton magnetic resonance spectrum of the neutral molecule in two ways. Firstly, it causes a broadening of the proton lines [2] and secondly the proton resonance lines are shifted [3]. The figure illustrates this for 1-n-propylnaphthalene. The concentration of negative ions $[M^-]$ increases from zero (*a*) to 3.8×10^{-1} mole/l. (*d*). The broadening of the lines is caused by the time-dependent contact hyperfine interaction; this interaction is also responsible for the observed shifts of the resonance lines.

With the aid of the modified Bloch equations [4] or with the spin-density matrix method [5, 2] one can account for the broadening effect as well as for the contact shift. If we consider only the diagonal part of the scalar interaction $a(t)S \cdot I$, we find with both methods that the absorption signal is a Lorentz curve centred at:

$$\omega = \omega_I - a \frac{g\beta H}{4kT} f_{M^-} \left\{ \frac{1}{1 + (f_{M^-} \tau_p^2 a^2 / 4) / (1 + 2\tau_p T_1^{-1})} \right\}$$

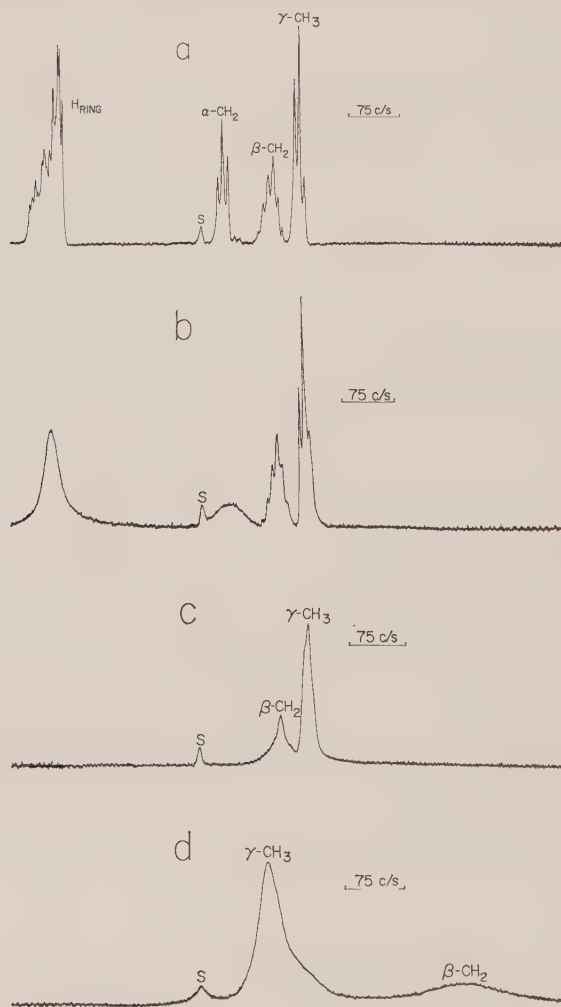
and that the exchange contribution to the transverse relaxation time is given by:

$$(1/T_2)_{\text{ex}} = \frac{f_{M^-} \tau_p a^2 / 4}{1 + f_{M^-} \tau_p^2 a^2 / 4 + 2\tau_p T_1^{-1}}.$$

In these expressions τ_p is the lifetime of M^- , T_1 the longitudinal relaxation time of the electron, a the hyperfine interaction constant in radians/sec, f_{M^-} the fraction of negative ions, f_M the fraction of neutral molecules, ω_I the Larmor frequency of the proton and ω the radiofrequency. All other symbols have their usual meaning.

The direction of the shift is governed by the sign of the splitting constant a ; if $\tau_p^2 a^2/4 \ll 1$ the magnitude of the shift is determined by the absolute value of a and the fraction of paramagnetic molecule f_{M^-} , irrespective of the value of T_1 [6].

We measured the N.M.R. spectra of 1- and 2-(n)-alkyl-substituted naphthalenes in the presence of their negative ions, in order to get information



Proton magnetic resonance spectra of 1-n-propylnaphthalene (M) in tetrahydrofuran-d₈ (isotopic purity ≥ 98 per cent) at 56.4 Mc/s and 20°C. Our experimental set-up prevented spinning of the sample tube.

(a) $[M^-] = 1.15$ mole/l. $[M] = 0$; the peak indicated by S is due to the isotopic impurity.

(b) $[M^-] = \leq 10^{-7}$ mole/l.

(c) $[M] = 9 \times 10^{-3}$ mole/l.

(d) $[M^-] = 3.8 \times 10^{-1}$ mole/l; this spectrum has been recorded with a higher r.f. power level for clarity. The scale (75 c/s) is indicated in the spectra. The magnetic field increases from left to right.

about the sign and the magnitude of the spin densities at the hydrogen nuclei of the alkyl group. For the rate of electron transfer between naphthalene and its sodium derivative in 1,2-dimethoxyethane Ward and Weissman [1] found a value of $10^9 \text{ l. mole}^{-1} \text{ sec}^{-1}$. This implies for our measurements, which were carried out under identical conditions (see table), that $\tau_p \approx 10^{-9} \text{ sec}$, so that $\tau_p^2 a^2 / 4 \ll 1$. Hence the splitting constants, which are related to the spin densities, can be deduced direct from the observed shifts and f_M . The latter quantity has been determined from the solvent shift due to the susceptibility change of

Substituent	Splitting constant (in milligauss) of protons in (positions)			
	α	β	γ	δ
1-CH ₃	+3860			
1-C ₂ H ₅	+3240	-74		
1-C ₃ H ₇	+2670	-212	+64	
1-C ₄ H ₉	+2800	-155	+45	+35
2-CH ₃	+1810			
2-C ₂ H ₅	+1130	+32		
2-C ₃ H ₇	+1080	≤ 2	+27	
2-C ₄ H ₇	+1050	†	†	+20

† Not measured.

Hyperfine splitting constants for the sets of alkyl protons in alkyl-substituted naphthalene negative ions, prepared in 1,2-dimethoxyethane with sodium.

the solution caused by the reduction of M. As Bennett and Torrey [7] and Friedrich [8] have shown, this procedure is justified in our case. The results are given in the table. The various protons in the alkyl group are denoted by α , β , γ and δ . The large splitting constants of the α -protons, not easily determined by N.M.R., have been obtained from E.S.R. At the same time the E.S.R. spectra enabled us to check in some cases the N.M.R. results for the β , γ and δ protons. No discrepancy was found.

A more extensive survey and discussion of the results will be given later.

The authors are thankful to Mr. M. J. van den Brink for preparing the compounds. The experimental assistance of Mr. C. W. Hilbers and Mr. A. P. Praat is gratefully acknowledged.

REFERENCES

- [1] WARD, R. L., and WEISSMAN, S. I., 1956, *J. Amer. chem. Soc.*, **79**, 2086.
- [2] (a) BRUCE, C. R., NORBERG, R. E., and WEISSMAN, S. I., 1956, *J. chem. Phys.*, **24**, 473.
(b) MCCONNELL, H. M., and BERGER, S. B., 1957, *J. chem. Phys.*, **27**, 230.
(c) JOHNSON, C. S., 1963, *J. chem. Phys.*, **39**, 2111. (d) JOHNSON, C. S., and TULLY, J. C., 1964, *J. chem. Phys.*, **40**, 1744.
- [3] (a) BLOEMBERGEN, N., 1957, *J. chem. Phys.*, **27**, 595. (b) MCCONNELL, H. M., and CHESTNUT, D. B., 1958, *J. chem. Phys.*, **28**, 107.
- [4] MCCONNELL, H. M., 1956, *J. chem. Phys.*, **25**, 709.
- [5] ALEXANDER, S., 1962, *J. chem. Phys.*, **37**, 974.
- [6] BINGÖL, G., and MÜLLER-WARMUTH, W., 1964, *Phys. Letters*, **11**, 292.
- [7] BENNETT, L. H., and TORREY, H. C., 1957, *Phys. Rev.*, **108**, 499.
- [8] FRIEDRICH, H. J., 1964, *Z. Naturf.*, **196**, 663.

Two-dimensional second virial coefficients of krypton on graphitic carbon

by JOHN R. SAMS

Department of Chemistry, University of British Columbia, Vancouver 8, Canada

(Received 8 December 1964)

In studies of physical adsorption at high temperatures ($T \gtrsim T_c$, the critical temperature of the adsorbate), it is convenient to expand the isotherm in virial form [1], viz.

$$N_a = B_{AS}(p/kT) + C_{AAS}(p/kT)^2 + \dots, \quad (1)$$

where N_a is the number of molecules adsorbed at pressure p and temperature T , and the coefficients are the gas-surface cluster integrals. B_{AS} is the effective Henry's law constant, describing the interactions of single gas molecules with the surface, while C_{AAS} accounts for initial deviations from Henry's law caused by interactions between admolecules. As C_{AAS} relates to a three-body cluster, it is usually more convenient to treat the deviations from Henry's Law as imperfections in a two-dimensional gas.

Formally, the two-dimensional equation of state can be written as [1, 2, 3]

$$\Theta \mathcal{A} / N_a kT = 1 + B^{(2)}(N_a / \mathcal{A}) + \dots, \quad (2)$$

where Θ is the two-dimensional pressure and \mathcal{A} the area of the system. Inversion of (1) gives p/kT as a power series in N_a which can be used to integrate the Gibbs isotherm, yielding [1]:

$$\Theta \mathcal{A} / N_a kT = 1 - (C_{AAS} / 2B_{AS}^2) N_a - \dots \quad (3)$$

Comparison of (2) and (3) provides the identification:

$$B^{(2)} / \mathcal{A} = -C_{AAS} / 2B_{AS}^2, \quad (4)$$

Theoretical equations for $B^{(2)}$ for a generalized (m, n) pair potential have been derived [1, 4]. One finds:

$$B^{(2)} / \frac{1}{2} \pi \bar{N} \sigma_2^2 \equiv B^{(2)*} = f(\epsilon_2 / kT), \quad (5)$$

where σ_2 and ϵ_2 are the two-dimensional collision diameter and depth of the pair well, respectively. Tabulations of $f(\epsilon_2 / kT)$ at various values of $T^* \equiv kT / \epsilon_2$ for a (12, 6) potential have been published [4]. It is clear that if one fits experimental values of $B^{(2)} / \mathcal{A}$ determined over a range of temperatures to $f(\epsilon_2 / kT)$ versus T^* , the parameters ϵ_2 and \mathcal{A} / σ_2^2 can be evaluated. The procedure is entirely analogous to that used to derive potential parameters from gas-phase virials. σ_2 is obtainable from the corresponding three-dimensional quantity [2, 4] so that the area of the adsorbent can be found.

Constabaris *et al.* [5] have published precise isotherms for the heavy rare gases interacting with graphitic carbon, from which B_{AS} and C_{AAS} values can be calculated. Their data for Ar and Xe have previously been analysed [1, 6, 7], and we treat the Kr data here. Values of B_{AS} and C_{AAS} for Kr are given in table 1 from which $B^{(2)} / \mathcal{A}$ values follow from (4). These data have been fitted

to (5) to yield the (12, 6) parameters of best fit given in table 2. For comparison, the three-dimensional (12, 6) potential parameters [8] are also quoted.

The present results follow the general behaviour found for Ar and Xe [1, 6, 7]. ϵ_2 is 15 per cent smaller than ϵ_3 , indicating an additional repulsion between the admolecules over what prevails in the gas. This is in good agreement with the predicted [9] magnitude of the three-body effect (14 per cent) in this system.

T ($^{\circ}\text{K}$)	B_{AS} ($\text{cm}^3 \text{g}^{-1}$)	C_{AAS} ($\text{cm}^6 \text{g}^{-1} \text{mole}^{-1}$)
245.173	0.2645	-202.1
255.401	0.2147	-184.5
279.472	0.1382	-105.2
285.119	0.1264	-108.2
291.173	0.1161	-93.6
297.159	0.1066	-84.5
307.171	0.0924	-68.4

Table 1. Second and third gas-surface virial coefficients for krypton with graphitic carbon.

Two-dimensional			Three-dimensional [8]	
ϵ/k ($^{\circ}\text{K}$)	σ (\AA)	\mathcal{A} ($\text{m}^2 \text{g}^{-1}$)	ϵ/k ($^{\circ}\text{K}$)	σ (\AA)
142	3.73	9.3	167	3.68

Table 2. (12, 6) potential parameters for krypton.

Barker and Everett [2] have introduced a correction term to (5) to account for the departure of the adsorbed phase from planarity. When this correction is applied to the present data, the parameters of best fit are: $\epsilon_2/k=140^{\circ}\text{K}$, $\sigma_2=3.74\text{\AA}$ and $\mathcal{A}=8.2\text{m}^2\text{g}^{-1}$. The energy is lowered only slightly, but the effect on \mathcal{A} is considerable. A detailed discussion of surface areas determined by this method is to be published [7].

I am indebted to Mr. Robert Wolfe for calculating the non-planarity corrections.

REFERENCES

- [1] SAMS, J. R., CONSTABARIS, G., and HALSEY, G. D., 1962, *J. chem. Phys.*, **36**, 1334.
- [2] BARKER, J. A., and EVERETT, D. H., 1962, *Trans. Faraday Soc.*, **58**, 1608.
- [3] ROWLINSON, J. S., 1964, *Mol. Phys.*, **7**, 593.
- [4] SAMS, J. R., 1965, *Mol. Phys.*, **9**, 17.
- [5] CONSTABARIS, G., SAMS, J. R., and HALSEY, G. D., 1962, *J. chem. Phys.*, **37**, 915.
- [6] SAMS, J. R., 1962, *J. chem. Phys.*, **37**, 1883.
- [7] WOLFE, R., and SAMS, J. R., 1965, *J. phys. Chem.* (in the press).
- [8] WHALLEY, E., and SCHNEIDER, W. G., 1955, *J. chem. Phys.*, **23**, 1644.
- [9] YARIS, R., 1962, Thesis, University of Washington.

A test of Kihara's intermolecular potential

by J. S. ROWLINSON

Department of Chemical Engineering and Chemical Technology,
Imperial College of Science and Technology, London, S.W.7

(Received 15 January 1965)

It is now generally agreed that the inverse-power potential of Lennard-Jones is an inadequate representation of the intermolecular energy even of the inert gases. The simplest function that might serve is the three-parameter potential of Kihara [1]:

$$u(r) = A \left(\frac{m}{n} \right) \epsilon \left[\left(\frac{1-\gamma}{r-\gamma} \right)^n - \left(\frac{1-\gamma}{r-\gamma} \right)^m \right], \quad (1)$$

where R is the separation, $r = R/\sigma$, σ is the collision diameter (that is, $u(\sigma) = 0$), $-\epsilon$ is the minimum value of u , $(\gamma\sigma)$ is a small hard-core within which u is supposed to be infinite, and $A(m/n)$ is a pure number

$$A(x) = x^{-x/(1-x)}(1-x)^{-1}, \text{ or } A(\tfrac{1}{2}) = 4. \quad (2)$$

This potential has been used recently by Sherwood and Prausnitz [2] to fit the second and third virial coefficients of argon (after correction of the latter for the effects of three-body forces) and by Barker *et al.* [3] to fit the second virial coefficient and the transport coefficients. Their potentials are similar:

$$\text{S. and P.} \quad n = 12, \quad m = 6, \quad \gamma = 1/9, \quad \sigma = 3.314 \text{ \AA}, \quad \epsilon/k = 147.2^\circ \text{K},$$

$$\text{B., F. and S.} \quad n = 12, \quad m = 6, \quad \gamma = 1/10, \quad \sigma = 3.363 \text{ \AA}, \quad \epsilon/k = 142.9^\circ \text{K}.$$

This potential has three merits. First, it fits well the properties of the dilute gas. Secondly, it yields a coefficient of $(-R^{-6})$ of about $60 \times 10^{-60} \text{ erg cm}^6$, which is about half that of the best Lennard-Jones potential, but which agrees well with quantal calculations and with a value derived from the absorption spectrum [4]. Thirdly, it resembles the potential that Guggenheim and McGlashan [5] derived from a study of the crystal, although it predicts too large a lattice energy. This discrepancy has been ascribed to the multi-body forces [3].

The purpose of this note is to provide a test of this potential by using the properties of argon in a state intermediate between that of the dilute gas and that of the crystal at low temperatures. The property used is the mean value in the liquid of the second derivative of $u(r)$. This property can be derived from measurements of the isotopic separation factor between liquid and vapour [6].

Define the virial function $v(r)$, its derivative $w(r)$ and the macroscopic equivalents \mathcal{V} and \mathcal{W} by

$$v(r) = ru'(r), \quad w(r) = rv'(r), \quad (3)$$

$$\mathcal{U} = \sum_{i < j} \sum u_{ij}, \quad \mathcal{V} = -\frac{1}{3} \sum_{i < j} \sum v_{ij}, \quad \mathcal{W} = \frac{1}{9} \sum_{i < j} \sum w_{ij}. \quad (4)$$

The mean values of \mathcal{U} and \mathcal{V} in a classical fluid are

$$\overline{\mathcal{U}} = U, \quad \overline{\mathcal{V}} = pV - NkT, \quad (5)$$

where U is the configurational energy. The mean of \mathcal{W} in liquid argon at its triple point is [6] :

$$\overline{\mathcal{W}} = 4.55 \times 10^4 \text{ J mole}^{-1}. \quad (6)$$

The only assumptions made in obtaining $\overline{\mathcal{W}}$ from the experimental results are that $\sigma \sim 3.4 \text{ \AA}$ and that \mathcal{W} is a sum of pair functions.

A test of (1) can now be made since there is, for this potential, an identity relating $w(r)$ to $u(r)$ and $v(r)$. By differentiation of (1)

$$\left(1 - \frac{\gamma}{r}\right)^2 w(r) + \left(1 - \frac{\gamma}{r}\right) \left(n + m + \frac{\gamma}{r}\right) v(r) + nm u(r) = 0. \quad (7)$$

If $\gamma = 0$ this reduces to an equation used previously [7] to provide a discriminant for the Lennard-Jones potential. The average of \mathcal{W} is found by multiplying (7) by the distribution function and integrating over all separations. In performing this operation it is sufficient to put $r = 1$ in the terms containing γ , for reasons discussed previously in a different context [6]. Hence

$$(1 - \gamma)^2 \overline{\mathcal{W}} - \frac{1}{3}(1 - \gamma)(n + m + \gamma)(pv - NkT) + \frac{nm}{9} U = 0 \quad (8)$$

and so,

$$\text{for } \gamma = 0 \quad \overline{\mathcal{W}} = 4.33 \times 10^4 \text{ J mole}^{-1},$$

$$\text{for } \gamma = 0.1 \quad \overline{\mathcal{W}} = 5.40 \times 10^4 \text{ J mole}^{-1},$$

The first value agrees moderately well with (6) but, as shown previously [7], is just too low to satisfy Schwarz's inequality for the mean fluctuations of \mathcal{U} and \mathcal{V} . The lowest value permitted is $4.49 \times 10^4 \text{ J mole}^{-1}$. The second value satisfies Schwarz's inequality but is in direct conflict with the experimental value (6). That is either (1) has too great a curvature at separations near σ , or else \mathcal{W} is not given adequately by a sum of pair terms.

The evidence of the properties of the dilute gas is that (1) is a fair representation of the true two-body potential at all separations equal to and greater than σ . The tests of Sherwood and Prausnitz [2] and of Barker *et al.* [3] are searching and convincing, and it is unlikely that the curvature of the two-body potential is as low as is implied by (6). The evidence from the third virial coefficient of the gas [2], from the lattice energy of the crystal [3], and now from the isotopic separation factor of the liquid is that a sum of true pair potentials is an incomplete representation of \mathcal{U} at high densities.

REFERENCES

- [1] KIHARA, T., 1953, *Rev. mod. Phys.*, **25**, 831.
- [2] SHERWOOD, A. E., and PRAUSNITZ, J. M., 1964, *J. chem. Phys.*, **41**, 429.
- [3] BARKER, J. A., FOCK, W., and SMITH, F., 1964, *Phys. Fluids*, **7**, 897.
- [4] BARKER, J. A., and LEONARD, P. S., 1964, *Phys. Letters*, **13**, 127.
- [5] GUGGENHEIM, E. A., and MCGLASHAN, M. L., 1960, *Proc. roy. Soc. A*, **225**, 456.
- [6] ROWLINSON, J. S., 1964, *Mol. Phys.*, **7**, 477.
- [7] BROWN, W. B., and ROWLINSON, J. S., 1960, *Mol. Phys.*, **3**, 35.

Variations on van der Waals' equation of state for high densities

by E. A. GUGGENHEIM

Chemistry Department, The University, Reading

(Received 27 January 1965)

Van der Waals' equation of state contains two parameters a and b . While $-a$ is a measure of the excess energy compared with that at zero density, b determines the excess entropy. It has long been well known that the contribution of b to the entropy is inaccurate except at densities so low that interactions between three or more molecules are negligible; in other words only the second virial coefficient, but no higher virial coefficient, depends on b in the manner implied by the equation. It is much less well known that the contribution of a to the energy, while inaccurate at low densities, is a useful approximation at high densities. This has been clearly stated and explained [1] by Longuet-Higgins and Widom. For high densities they accordingly recommend taking the equation of state for non-interacting rigid spheres expressed in terms of a volume b and adding a van der Waals' a type term to take account of the energy. They did not however express an unambiguous preference for a particular equation for non-interacting rigid spheres. One possible choice has been examined in a previous paper [2]. The object of the present note is to discuss and compare alternative choices.

We use the following symbols: V for molar volume, y for the volume of a spherical molecule multiplied by the number of molecules per unit volume, a as in van der Waals' equation, P pressure. We use the subscripts l for liquid, g for gas, c for critical, t for triple point, B for Boyle point, s for saturation.

There are available two recent approximate formulae for non-interacting rigid spheres. The one due to Frisch *et al.* [3] will be denoted by F. The other due to Thiele [4] will be denoted by T. These two approximations agree in the virial coefficients up to the third but differ slightly in the values predicted for the fourth. When each of these approximations is used in the manner proposed by Longuet-Higgins and Widom, the values predicted for experimental properties are almost identical. It therefore seems likely that yet other approximations will also lead to almost identical predictions and it is possible that an algebraically simpler approximation may be satisfactory. We accordingly study a third approximation which will be denoted by G. All these will be compared with one another and with van der Waals' equation, denoted by v.d.W., and with experiment.

These four equations of state are:

$$\begin{aligned} PV/RT &= -a/RTV + (1-4y)^{-1}, & \text{v.d.W.} \\ PV/RT &= -a/RTV + (1+y+y^2)(1-y)^{-3}, & \text{F} \\ PV/RT &= -a/RTV + (1+2y+3y^2)(1-y)^{-3}, & \text{T} \\ PV/RT &= -a/RTV + (1-y)^{-4}, & \text{G} \end{aligned}$$

We first compare virial expansions when $a=0$:

$$PV/RT = 1 + 4y + 16y^2 + 64y^3 + 256y^4 + 1024y^5 +, \quad \text{v.d.W.}$$

$$PV/RT = 1 + 4y + 10y^2 + 19y^3 + 31y^4 + 46y^5 +, \quad \text{F}$$

$$PV/RT = 1 + 4y + 10y^2 + 16y^3 + 22y^4 + 28y^5 +, \quad \text{T}$$

$$PV/RT = 1 + 4y + 10y^2 + 20y^3 + 35y^4 + 56y^5 +, \quad \text{G}$$

whereas the accurate virial expansion is known to be:

$$PV/RT = 1 + 4y + 10y^2 + 18.36y^3 + 28.2y^4 + 40y^5 +.$$

We see that the order of accuracy is $F > G > T > \text{v.d.W.}$

Some comparisons with experiment can be made without any further assumption. Others require a single assumption equivalent to fixing the ratio a/b in van der Waals' equation. For this we equate $a/RT_t V_1$ to the experimental value of $\Delta_e U/RT_t$ where $\Delta_e U$ is the molar energy of evaporation of the liquid. Using the value for argon, or indeed any substance [5] obeying the principle of corresponding states relative to argon, we have $a/RT_t V_1 = 8.56$. Without using any other experimental data we obtain by straightforward thermodynamics the results shown in the table.

	v.d.W.	F	T	G	Experiment
$(PV/RT)_c$	0.375	0.36	0.40	0.36	0.29
T_B/T_c	3.375	2.68	2.54	2.72	2.73
V_1/V_c	0.377	0.302	0.298	0.303	0.374
T_t/T_c	0.350	0.535	0.529	0.528	0.557
$\ln(P_s V_1/RT_t)$	-7.40	-5.93	-5.90	-6.01	-5.89
$P_c V_1/RT_c$	0.141	0.109	0.12	0.109	0.108

We draw the following conclusions. There is nothing to choose between the approximations F, T and G as far as agreement with experiment is concerned. Each of them is much better than van der Waals' equation. The only conspicuous failure is in quantities containing V_c , in particular $(PV/RT)_c$. This is not surprising. Because $\partial V/\partial P = \infty$ at the critical point a small inexactitude in the $P-V$ curve may affect P_c only slightly but will have a pronounced effect on the predicted value of V_c . This is borne out by multiplying $(PV/RT)_c$ by V_1/V_c and obtaining the values of $P_c V_1/RT_c$ in the last line of the table.

SUMMARY

The equation of state $PV = -a/V + RT(1-y)^{-4}$ is shown to be considerably better at high densities than van der Waals' equation $PV = -a/V + RT(1-4y)^{-1}$ and to be equal in accuracy to two other slightly more complicated equations for PV .

REFERENCES

- [1] LONGUET-HIGGINS, H. C., and WIDOM, B., 1965, *Mol. Phys.*, **8**, 549.
- [2] GUGGENHEIM, E. A., 1965, *Mol. Phys.*, **9**, 43.
- [3] REISS, N. R., FRISCH, H. L. F., and LEBOWITZ, J. L. L., 1959, *J. chem. Phys.*, **31**, 369.
HELFAHD, E. H., and FRISCH, H. L. F., 1961, *J. chem. Phys.*, **34**, 1037.
- [4] THIELE, E. T., 1963, *J. chem. Phys.*, **39**, 474.
- [5] GUGGENHEIM, E. A., 1959, *Thermodynamics*, 4th Edition (North Holland), p. 165.

The molecular orbital theory of some simple radicals

by W. T. DIXON†

Department of Theoretical Chemistry, Cambridge

(Received 6 November 1964)

In this paper the molecular orbital theory of hyperconjugation is extended in order to account for the hyperfine coupling constants observed in some simple but interesting free radicals, e.g. cyclopentyl, vinyl. Predictions are made for the phenyl radical.

1. INTRODUCTION

Much evidence for the theory of hyperconjugation has accumulated from electron spin studies and it is difficult to visualize how the relatively large coupling constants of methyl protons could arise except by actual delocalization of the odd electron. Indeed, recent calculations [1] have shown that the splitting observed from such protons is an order of magnitude larger than that predicted by a spin polarization mechanism similar to that which accounts for the coupling constants of protons situated in the nodal plane of the odd electron [2]. The assumption of hyperconjugation, on the other hand, does lead to estimates for the splitting due to methyl protons which are the right order of magnitude, for example in semiquinones [3] and alkyl radicals [4].

Coupling is observed not only from protons attached to a carbon atom of the conjugated system in which the odd electron is most likely to be found and those bonded to adjacent carbon atoms, but also from protons separated from the unsaturated system by two carbon atoms. To label these three types of proton, we shall call them α , β and γ protons respectively. β and γ protons are not in general held fixed in the nodal plane of the odd electron and our object in this paper will be to develop a molecular orbital theory which enables us to predict, within reasonable limits, the hyperfine coupling constants of such protons. Initially we shall consider symmetrical molecules to which we can apply the concepts of hyperconjugation theory [5, 6]. Having found it necessary to incorporate certain modifications into the model developed by Coulson and Crawford [6], in order to account for the experimental results, we shall derive a rather more general theory which can be applied, in principle, to any hydrocarbon. We shall then be able to account for the splittings of the protons in vinyl and to predict the proton coupling constants in the phenyl radical. Since we neglect configurational interaction throughout, we shall only be concerned with regions of positive spin density and make no attempt to calculate the coupling constants of protons held in the nodal plane of the odd electron.

2. THE HYPERCONJUGATION MODEL

One usually thinks of the methyl group being held together by two-centre bonds between tetrahedral hybrids of the carbon atom and the three hydrogen

† Now at Bedford College, Regent's Park, London, N.W.1.

1s orbitals. An equivalent way of looking at it would be to consider multi-centre bonds formed between linear combinations of the hydrogen orbitals and appropriate orbitals of the carbon atom. These linear combinations can be chosen in such a way that only one of them has a non-zero overlap integral with the $2p_\pi$ orbital of the methyl carbon atom and it is this combination which leads to an extension of the π -electron system. When the methyl group is described in these terms the coulomb and more important resonance integrals associated with the hydrogen group orbitals are independent of the molecular conformation. Such a choice of basic wave-functions greatly simplifies calculations, for the π -electron system in the ethyl radical becomes similar to that in allyl and the molecular orbital of the odd electron can be written in the following manner:

$$\psi_{\text{M.O.}} = c_1\psi_1 + c_2\psi_2 + c_3\psi_3,$$

where ψ_1 , ψ_2 are $2p_z$ orbitals of the α and β carbon atoms respectively and ψ_3 is the appropriate linear combination of the β hydrogen atomic orbitals. The coefficients c_1 , c_2 and c_3 can, of course, be found by solving the secular equations.

In order to simplify the algebra, the matrix elements are defined in terms of α , β and S , which are the coulomb, resonance and overlap integrals occurring in the secular equations of benzene. If we assume that overlap integrals are proportional to the corresponding resonance integrals, we can define the following relationships for the normalized wave functions ψ_r [6]:

$$\begin{aligned} \int_{\tau} \psi_r \psi_s d\tau &= \rho_{rs} S_1, \quad r \neq s, \\ \int_{\tau} \psi_r \mathcal{H} \psi_s d\tau &= \rho_{rs} (\beta + \alpha S), \quad r \neq s, \\ \int_{\tau} \psi_r \mathcal{H} \psi_r d\tau &= \alpha_r = \alpha + \delta_r \beta. \end{aligned}$$

When we have either calculated or simply chosen values for the ρ_{rs} and δ_r it will be possible to solve the secular equations and find the molecular orbital of the odd electron. The splitting due to a proton will be proportional to the value of the probability functions of the odd electrons [7] at that proton, so we can write the following expression for the hyperfine coupling constant a , taking the ethyl radical as an example:

$$a = k |\psi_{\text{M.O.}}(p)|^2 = k |c_1\psi_1(p) + c_2\psi_2(p) + c_3\psi_3(p)|^2. \quad (1)$$

p defines the position in space of the proton in question and the constant k can be calculated directly in the case of the hydrogen atom. If ψ_0 is the value of the electronic ground-state wave function of the free hydrogen atom at its nucleus, then we can re-write equation (1) as follows:

$$a = 508 \left| c_1 \frac{\psi_1(p)}{\psi_0} + c_2 \frac{\psi_2(p)}{\psi_0} + c_3 \frac{\psi_3(p)}{\psi_0} \right|^2. \quad (1a)$$

Now in every radical considered here, the odd electron goes into an orbital which is approximately non-bonding and this implies that by far the largest contribution to the coupling constant of a proton arises from spin density in the atomic orbital associated with it and that the small effects from more distant

orbitals tend to cancel each other. We are therefore justified in simplifying equation (1a) to the following form:

$$a \approx 508 \left(\frac{\chi_0}{\psi_0} \right)^2 c_h^2 = k c_h^2, \quad (2)$$

where c_h is the coefficient of the hydrogen atomic orbital, χ_0 is the value of this orbital at the proton, and k is the proportionality factor connecting spin density and the corresponding hyperfine coupling constant. If the atomic orbital, χ , to associate with hydrogen in a molecular orbital treatment of hydrocarbons is a hydrogen like 1s orbital with effective atomic number Z_h , then we can write from equation (2):

$$a = 508 Z_h^3 c_h^2. \quad (2a)$$

In the first set of calculations the spin density in a methyl hydrogen orbital calculated for ethyl, using a given set of parameters, and by dividing into the observed coupling constant, 26.87 g. [11], a value for k is derived which can be used in similar calculations for other molecules. In effect this procedure eliminates the need to determine the best hydrogen wave-function to use in such a molecular orbital treatment, partly off-setting the weakness of introducing yet another empirical quantity into the theory.

The numbers ρ_{rs} and δ_r have in practice been used as parameters and we take the following values for them: $\rho_{12} = 0.76$ or 1.0 , $\rho_{13} = 0$, $\rho_{23} = 2.5$, $\delta_1 = 0$, $\delta_2 = -0.1$, $\delta_3 = -0.5$. These two sets of parameters are close to those which have been used previously in calculations of dipole moments [6] and hyperfine coupling constants [3, 4]. In the radicals considered here, we assume that the carbon skeleton is planar and as symmetrical as possible, with carbon-carbon bond lengths 1.54 Å, carbon-hydrogen bond lengths 1.09 Å and angles between carbon-hydrogen bonds of $109\frac{1}{2}^\circ$. In the case of cyclohexadienyl, the bond lengths in the conjugated system are taken to be 1.40 Å. The secular equations in the case of ethyl are as follows:

$$\begin{aligned} (\alpha - E)c_1 + \rho_{12}[\beta + S(\alpha - E)]b_2 &= 0, \\ \rho_{12}[\beta + S(\alpha - E)] + (\alpha - E - 0.1\beta)c_2 + 2.5[\beta + S(\alpha - E)]c_3 &= 0, \\ 2.5[\beta + S(\alpha - E)]c_2 + (\alpha - E - 0.5\beta)c_3 &= 0. \end{aligned}$$

If we assume that the methyl group is rotating rapidly enough, then we can identify c_h^2 with $\frac{1}{3}c_3^2$ and thence calculate values for a_β . The results are shown in table 1.

	k	$(\text{CH}_3)_2\dot{\text{C}}\text{H}$	$(\text{CH}_3)_3\dot{\text{C}}$	Cyclo- C_3H_5	Cyclo- C_5H_9		Cyclo- C_6H_7
		a_β	a_β	a_β	a_β	a_γ	a_{CH_3}
$\rho_{12} = 0.76$	948	24.6	22.7	38.8	36.2	0.08	52 gauss
$\rho_{12} = 1.0$	585	23.4	20.8	35.8	35.4	0.10	51 "
Experimental [11]	—	24.68	22.72	23.42	35.12	0.53	47.72 "

Table 1. Methyl or methylene proton coupling constants.

The agreement between theory and experiment is generally quite good, except for the β -coupling in cyclopropyl and the γ -coupling constants in cyclopentyl. These points of disagreement together with the empirical method for determining constitute rather unsatisfactory features of the theory, and so we shall now examine the basis of hyperconjugation theory to see whether any simple modification will lead to improved agreement with observation.

3. MODIFIED HYPERCONJUGATION MODEL

In order to keep expressions relatively simple we shall consider a methylene group in a planar network of carbon atoms and omit overlap terms where they occur in the secular equations. In the actual computations we shall include overlap.

The hydrogen group orbital of π -symmetry is $(1/\sqrt{2})(\chi' - \chi'')$, where χ', χ'' are the two hydrogen wave functions.

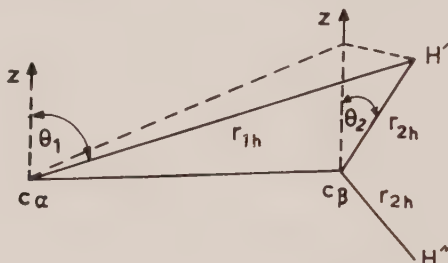


Figure 1. Diagram of C-CH₂ fragment.

If ψ_1, ψ_2 are the $2p_\pi$ orbitals of the α, β carbon atoms, respectively, then the overlap integrals of the system are as follows:

$$S_{12} = \int_{\tau} \psi_1 \psi_2 d\tau,$$

$$S_{13} = \int_{\tau} \psi_1 (1/\sqrt{2})(\chi' - \chi'') d\tau = \sqrt{2} \int_{\tau} \psi_1 \chi' d\tau = \sqrt{2} S_{1h} \cos \theta_1$$

$$S_{23} = \sqrt{2} S_{2h} \cos \theta_2;$$

S_{1h} and S_{2h} are the overlap integrals between carbon $2p_\sigma$ orbitals and hydrogen $1s$ orbitals at distances r_{1h}, r_{2h} respectively. θ_1 and θ_2 are the corresponding angles. These overlap integrals can be calculated exactly if we take the carbon and hydrogen atomic orbitals to be hydrogen-like. From the molecular orbital treatment of H_2 and H_2^+ , we would expect the effective atomic number of hydrogen in a molecule to be about 1.2 [8, 9] and using Slater's rules [10] this parameter for carbon $2p$ orbitals is 3.25. Using these assumptions, the overlap integrals are as follows:

$$S_{12} = 0.189, S_{13} = 0.083, S_{23} = 0.563, S_{h'h''} = 0.192.$$

Assuming the overlap and resonance integrals are proportional to each other and that each carbon $2p$ orbital has a coulomb integral α , we can solve the secular equations, once we have decided on the relative value of the coulomb integral of the hydrogen group orbital. In order to be able to reproduce approximately

the results of Coulson and Crawford [6], we give δ_3 the value -0.5 . From equation (2), k has a value of 878. The results of calculations using this modified hyperconjugation model, are shown in table 2.

	C_2H_5	$(CH_3)_2CH$	$(CH_3)_3C$	Cyclo- C_3H_5	Cyclo- C_4H_7		
	a_β	a_β	a_β	a_β	a_β	a_γ	
Calculated	27.1	22.8	20.3	24.1	38.2	2.9	gauss
Observed [11]	26.87	24.68	22.72	23.4	36.66	1.12	,,
	Cyclo- C_3H_9			Cyclo- C_6H_7			
	a_β	a_γ		a_{CH_2}			
Calculated	37.2	0.57		54			gauss
Observed [11]	35.12	0.53		47.72			,,

Table 2. Coupling constants using modified hyperconjugation model.

The agreement between theory and experiment is very good considering the rather crude assumptions concerning the geometry of the molecules, and we see that there is great improvement in the estimates of the coupling constants in cyclopentyl and cyclopropyl. The comparatively poor results for cyclobutyl can be attributed, at least partly, to the poor geometrical model and the calculations for isopropyl and tertiary butyl were not exact since the interactions between the methyl groups are dependent on the molecular conformations. In the latter case, an average was taken between extreme conformations. Long-range interactions were important especially in determining the order of magnitude of the γ -coupling constants and therefore it was necessary to include all possible resonance integrals when setting up the secular equations.

Similar calculations were carried out using 1.0 and $\sqrt[3]{2}$ for the effective number of hydrogen. The corresponding values for k should be 508 and 1016 if we were to be consistent, but it was necessary to adjust k using the ethyl radical standard in order to get realistic values for the coupling constants. The results shown in table 3 imply that 1.2 was indeed the best choice to make for the effective number of hydrogen.

	k	Cyclo- C_3H_5	Cyclo- C_5H_9		
		a_β	a_β	a_γ	
$Z_h = 1.0$	838	22.8	36.9	0.91	gauss
$Z_h = \sqrt[3]{2}$	862	26.1	36.9	0.19	,,

Table 3. Variation of effective atomic number of hydrogen.

Now we shall generalize the theory developed in this section so that we can treat less symmetrical molecules to which hyperconjugation theory cannot be applied.

4. MORE GENERAL THEORY APPLIED TO VINYL AND PHENYL

All we need, to generalize the modified hyperconjugation model, is the relationship between the coulomb integrals for carbon 2s and carbon 6p orbitals, and this can be roughly estimated as follows:

By taking the coulomb integral α_3 in the previous section to be $\alpha = 0.5\beta$, we fixed the coulomb integral of hydrogen α_h , for we have:

$$\begin{aligned}\alpha_3 &= \int_{\tau} (1/\sqrt{2})(\chi' = \chi'') \mathcal{H} (1/\sqrt{2})(\chi' = \chi'') d\tau \\ &= \alpha_h - \beta_{h'h''} \\ &= \alpha_h - \frac{S_{h'h''}}{S} \beta \\ &= \alpha_h - 0.78\beta,\end{aligned}$$

i.e.

$$\alpha_h = \alpha + 0.28\beta.$$

Now we assume, with Coulson and Crawford, that there is little or no contribution towards the dipole moment of the hydrocarbon in question from the σ -electron system [6]. If there is no net dipole moment between the hydrogen group orbital of σ -symmetry and the corresponding sp hybrid orbital of the methyl carbon atom, then their coulomb integrals must be identical. If α_s is the coulomb integral of a carbon 2s orbital, we can then deduce the required relationship:

$$\alpha + \frac{1}{2}(\alpha_s - \alpha) \doteq \alpha_h + 0.78\beta,$$

i.e.

$$\alpha_s \doteq \alpha + 2.12\beta.$$

We are now in a position to calculate, for any hydrocarbon, properties which are not too sensitive to the choice of the coulomb integrals α_h and α_s .

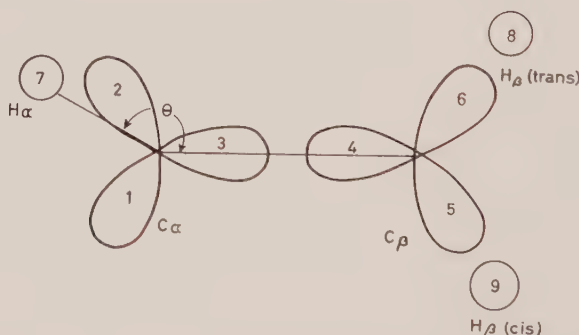


Figure 2. Atomic orbitals of the σ -electron system in vinyl.

The radical was assumed to be planar with carbon-carbon bond length 1.34 Å and carbon-hydrogen bond lengths 1.09 Å. The bond angles at the β carbon atom were taken to be 120°. As with ethylene and benzene, the secular determinant can be factorized to give σ and π molecular orbitals which, in the

simple L.C.A.O. approximation, are independent of each other. The odd electron goes into the first antibonding orbital and is therefore associated with the σ -electron system which is symmetrical with respect to reflection through the plane of the page (figure 2). Solutions of the secular equations were obtained by means of a standard programme on the EDSAC computer and the results are shown in table 4:

	$\theta = 120$	$\theta = 150$	$\theta = 180$	Expt. [12]	
c_1	0.91	0.86	0.94†	—	
a_α	+35.8	+14.5	—	15.6	gauss
a_β (cis)	+32.7	+52.3	+72.2	34	„
a_β (trans)	+79.3	+82.0	+72.2	68	„

† In this case orbital 1 and $2p_\pi$ orbital of the α carbon atom.

Table 4. Coupling constants for the vinyl radical.

It is clear from these results, that we have accounted for most of the features of the observed spectrum and that θ probably lies between 120° and 150° . The large odd electron density in orbital 1, leads us to expect strong spin polarization of the orbitals around the α carbon atom, so the exact magnitude and sign of a_α is uncertain.

Further calculations show that the large trans-proton splitting arises almost entirely from the negative resonance integral of π -type between orbitals 1 and 2. Such a trans effect has been observed already in the M.O. theory of σ -electron systems [13]. Another interesting point is that the positive spin density associated

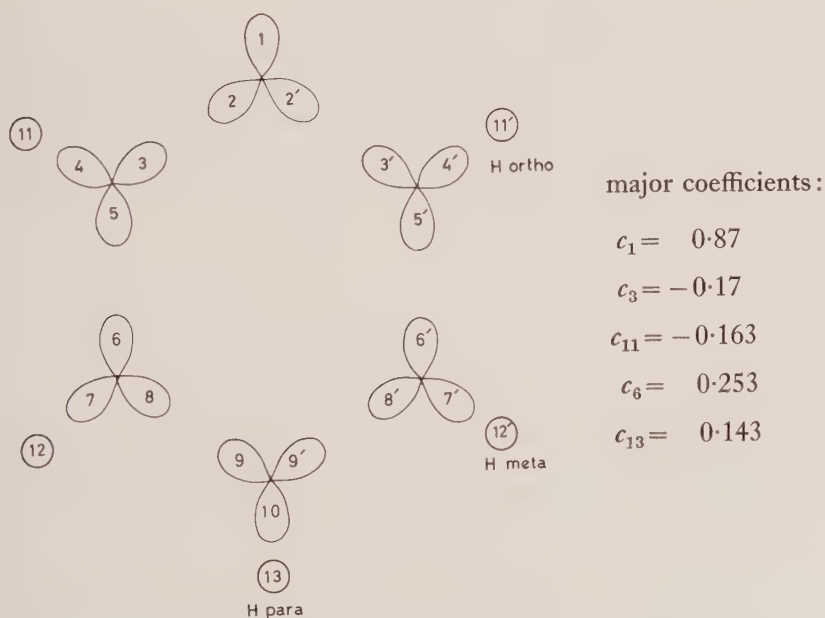


Figure 3. Atomic orbitals used in the phenyl calculation.

with the α hydrogen orbital is due almost completely to the inclusion of resonance integrals between sp_2 hybrid orbitals on the same carbon atoms.

When the coulomb integrals were estimated by the method of Pople and Santry [13], the results were almost exactly the same as those given in table 4. The geometry of the phenyl radical was assumed to be the same as that of benzene apart from the absence of one hydrogen atom. The odd electron goes into the first antibonding orbital which is the seventh of the thirteen molecular orbitals, symmetrical with respect to reflection through the two planes of symmetry. The coefficients of the orbitals are shown in figure 3, and the predicted coupling constants are $a_{\text{ortho}} = +23.3$ g, $a_{\text{meta}} = +4.2$ g and $a_{\text{para}} = +17.9$ g. a_{ortho} is about the magnitude expected by comparison with a_β (cis) for vinyl and one would expect a_{meta} to be small, since the meta hydrogen atom is a long way from orbital 1. The large value of a_{para} is rather unexpected, but can be explained in the following manner: the comparatively large coefficient of orbitals 6 might be expected to arise from a similar trans effect to that which leads to the large a_β (trans) in vinyl. The para hydrogen is, however, in a trans position with respect to orbitals 6, so it would appear that the large a_{para} arises from a combination of two trans effects. Actually, we could estimate, roughly, all the coupling constants in phenyl from the known experimental coupling constants in vinyl and would get similar orders of magnitude to those calculated above. It would appear then, that the large a_{para} is a general consequence of molecular orbital theory and does not depend very much on the numerical approximations employed. Actually if negative overlap integrals are neglected the predicted coupling constants are: $a_{\text{ortho}} = 19.2$ g, $a_{\text{meta}} = 3.1$ g, $a_{\text{para}} = 0.1$ g.

5. CONCLUSIONS

We may seem to have travelled a long way from the hyperconjugation theory of Coulson and Crawford, but our assumptions are identical with theirs, apart from a few numerical factors. It is probably worthwhile listing these assumptions: (a) Atomic wave functions are given by Slater's rules [10] except in the case of hydrogen, when the effective atomic number parameter is 1.2. (b) Resonance integrals are proportional to the corresponding overlap integrals. (c) The coulomb integrals are approximately as follows:

$$\text{carbon (2p)} - \alpha$$

$$\text{carbon (2s)} - \alpha + 2.1\beta$$

$$\text{hydrogen (1s)} - \alpha + 0.28\beta.$$

With this theory we have been able to predict, within reasonable limits, coupling constants in a variety of radicals and have confirmed the existence of a trans effect by means of which spin density may be transmitted through σ -electron systems.

The author would like to thank Professor H. C. Longuet-Higgins, F.R.S., for his help and encouragement and the Salters' Company for a maintenance grant.

REFERENCES

- [1] COLPA, J. P., and DE BOER, E., 1964, *Mol. Phys.*, **7**, 333.
- [2] MCCONNELL, H. M., 1956, *J. chem. Phys.*, **24**, 764.
- [3] BERSOHN, R., 1956, *J. chem. Phys.*, **24**, 1066.
- [4] CHESNUT, D. B., 1958, *J. chem. Phys.*, **29**, 43.
- [5] MULLIKEN, R. S., RIEKE, C. A., and BROWN, W. G., 1941, *J. Amer. chem. Soc.*, **63**, 41.
- [6] COULSON, C. A., and CRAWFORD, V. A., 1953, *J. chem. Soc.*, p. 2052.
- [7] FERMI, E., 1930, *Z. Phys.*, **60**, 320.
- [8] WANG, S., 1928, *Phys. Rev.*, **31**, 579.
- [9] WEINBAUM, S. J., 1933, *J. chem. Phys.*, **1**, 317.
- [10] SLATER, J. C., 1930, *Phys. Rev.*, **36**, 57.
- [11] FESSENDEN, R. W., and SCHULER, R. H., 1963, *J. chem. Phys.*, **39**, 2147.
- [12] COCHRAN, E. L., ADRIAN, F. J., and BOWERS, V. A., 1964, *J. chem. Phys.*, **40**, 213.
- [13] POPL, J. A., and SANTRY, D. B., 1964, *Mol. Phys.*, **7**, 269.

The tricyano-sym-triazine anion : a permanent Jahn-Teller distortion ?

by A. CARRINGTON, H. C. LONGUET-HIGGINS and P. F. TODD

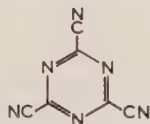
Department of Theoretical Chemistry, University of Cambridge

(Received 28 October 1964)

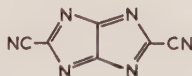
The electron resonance spectrum of the mono-anion of tricyano-sym-triazine, at 25°C and below, reveals the presence, not of two sets of three equivalent nitrogen atoms, but a set of two and another set of four. It is suggested that the radical-ion undergoes a permanent Jahn-Teller distortion to one of three equivalent distorted forms.

1. INTRODUCTION

We have prepared the negative ion of 2:4:6-tricyano-sym-triazine (I) and measured its electron resonance spectrum in tetrahydrofuran solution. This experiment was undertaken as part of a study of the Jahn-Teller effect in molecules with degenerate ground states, and the result was startling. At room temperature the spectrum reveals that the radical-ion possesses, not two sets of three equivalent nitrogen atoms, but a set of two and another set of four.



I



II

The spectrum is shown in figure 1, and the reconstruction is based on $a_N^{(2)} = 3.78$ gauss and $a_N^{(4)} = 0.84$ gauss, where the superscripts indicate the number of equivalent atoms in the set. The agreement is too good for the interpretation to be in serious doubt.

It is conceivable that the addition of an electron to tricyano-sym-triazine causes a revolutionary change in the molecular structure, yielding an isomer such as (II), but this seems extremely unlikely in view of the immediacy with which the radical-ion is formed in contact with metallic lithium, sodium and potassium, even in the cold (the experimental details are set out below). We propose an alternative explanation of the electron resonance data, based on the Jahn-Teller rule.

The π orbitals of $C_3N_3(CN)_3$ are of two symmetry types in the group D_{3h} , namely A_2'' (non-degenerate) and E'' (doubly degenerate). To obtain the electron configuration of the ground state of the negative ion we have performed a simple molecular orbital calculation of the Hückel type, with all resonance integrals

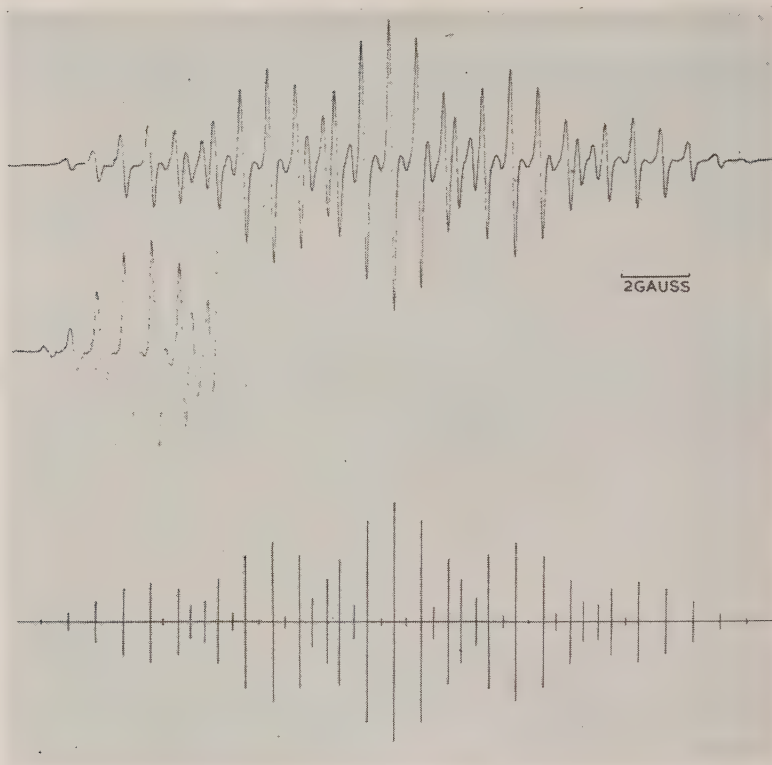


Figure 1. Tricyano sym-triazine anion.

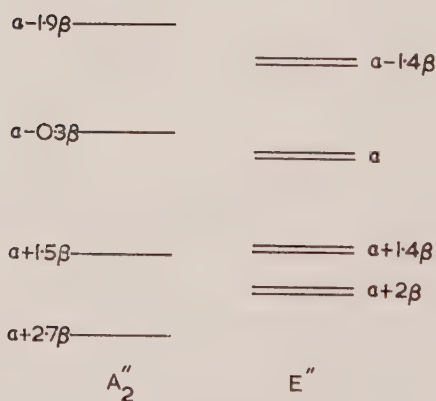


Figure 2.

equal to β , all carbon coulomb integrals equal to α and all nitrogen coulomb integrals equal to $\alpha + \beta$. Figure 2 shows the resulting pattern of orbital energies. The lowest six orbitals are well separated from the others, and are all strongly bonding, giving a stable closed shell structure for the neutral molecule. The next orbital is doubly degenerate, of species E'' , so that the mono-negative ion

should have an orbitally degenerate ground state. (This conclusion is, furthermore, unaffected by small changes in the coulomb and resonance integrals.) In real form the degenerate orbitals for the odd electron have the atomic orbital coefficients shown in figure 3.

Now by the Jahn-Teller rule a molecule in an orbitally degenerate state will tend to distort in such a way as to remove the degeneracy. If the distortion is severe enough, the molecule may become locked in one of the equivalent distorted forms, and all trace of the original symmetry be lost. Assume for a moment that this happens to the tricyano-sym-triazine mono-anion. Then according to which of the two orbitals becomes the more stable, the spin densities on the nitrogen atoms would be *either* $\rho_N^{(2)} = \frac{1}{6}$, $\rho_N^{(4)} = \frac{1}{24}$ *or* $\rho_N^{(2)} = 0$, $\rho_N^{(4)} = \frac{1}{8}$. Using the relationship $a_N = Q\rho_N$ with $Q = 24$ gauss [1] we obtain the alternative possibilities *either* $a_N^{(2)} = 4$ gauss, $a_N^{(4)} = 1$ gauss, *or* $a_N^{(2)} = 0$, $a_N^{(4)} = 3$ gauss. The former pair of splitting constants fit the observed values remarkably well.

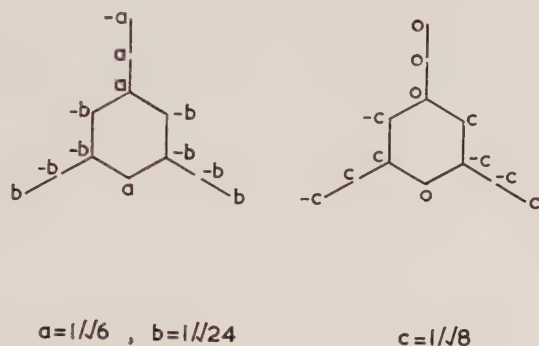


Figure 3.

The theoretical values of a_N just given are based on a very primitive calculation, and it might be supposed that a more careful choice of coulomb or resonance integrals, allowing for the different valence states of the different nitrogen or carbon atoms, and the undoubtedly different bond lengths, would spoil the agreement with experiment. To these objections two comments are relevant. First, the *equivalence* of the nitrogen atoms in each of the two sets, though in a sense accidental, does not depend on the value of $(\alpha_N - \alpha_C)/\beta$, or on the value of β_{CN}/β_{CC} . It is enough that the antisymmetric orbital in figure 3 should have equal squared coefficients at the two pairs of nitrogen atoms at which it does not vanish. This ensures that in the symmetric orbital (which is a simple transform of the antisymmetric one) four of the values of c_N^2 are equal, and the other two are also equal. Secondly, if this single coincidence is satisfied for the antisymmetric orbital, it follows from symmetry alone that not only are the squared coefficients in the symmetric orbital equal in sets of two and four, but that the value of $\rho_N^{(2)}$ is exactly four times the value of $\rho_N^{(4)}$. Within experimental error this relation is exactly satisfied by the experimental splitting constants, and this increases our confidence in assigning the unpaired electron to the symmetric orbital.

The fact that at 25°C we observe a spectrum characteristic of a distorted radical implies that at this temperature the radical does not change rapidly from one

distorted form to another; if it did we should see six nitrogen atoms with equal splitting constants (or under higher resolution, perhaps two sets of three equivalent atoms). It is disappointing to find that at higher temperatures (above 50°C) the spectrum changes, but not simply or reversibly; the radical seems to decompose before the onset of internal equilibration. But in spite of this negative result we believe that at 25°C the addition of an electron to tricyano-sym-triazine produces a Jahn-Teller distortion which stabilizes the symmetric orbital as against the antisymmetric one, and that the distortion is strong enough to prevent the radical-ion from tunnelling between the three equivalent potential minima.

Two further questions arise: first, why should the radical distort in such a way as to stabilize the symmetric orbital rather than the antisymmetric one; and secondly, why should it take so long for the radical to pass from one potential minimum to the others?

Neither of these questions is easy to answer. First, in the harmonic approximation, which neglects second-order coupling terms in the potential energy, there is nothing to choose between one kind of distortion and the other; the difference in depth of the minima only appears in the second order. A definitive quantum-mechanical calculation would therefore be very difficult, but perhaps the following remarks are relevant. The inverse relation between bond order and bond length implies that if c_r is the coefficient of the r th atomic orbital in the molecular orbital of the odd electron, then the bond $r-s$ will tend to shorten

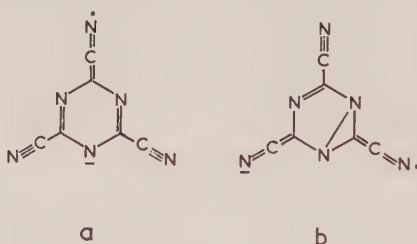


Figure 4.

if $c_r c_s$ is positive and to lengthen if it is negative. Figure 4(a) presents a 'structure' which largely accords with this rule if the odd electron is in the symmetric orbital, but there is no structure more satisfactory than 4(b) to represent occupation of the antisymmetric orbital. The drawing of structures is not, of course, any substitute for quantum-mechanical reasoning; but perhaps figure 4 may appeal to the intuition of the organic chemist.

As to the permanence of the distortion, it is possible that the radical-ion is clamped in one conformation by an associated positive ion. There is, however, no trace of metal hyperfine structure in the spectrum, which is altogether indifferent to the chemical nature of the gegenion. An alternative suggestion, which we prefer, is that the tunnelling frequency is low because of a very small Franck-Condon factor; passage from one minimum to another requires a change in a large number of bond lengths, and this may be the essential reason for the difference between the negative ions of tricyano-sym-triazine and, say, benzene.

To sum up, the evidence points to a permanent Jahn-Teller distortion in the mono-anion of tricyano-sym-triazine. Such a distortion would be the first of its kind to be observed in an organic radical-ion.

2. EXPERIMENTAL

2 : 4 : 6-tricyano-sym-triazine was prepared from ethyl cyanoformate by the sequence of steps described by Weddidge [2] and Ott [3]. The product melted at 118–120°C; the quoted melting point is 119°C. Analysis: C, 46.0 per cent; N, 53.9 per cent (C_6N_6 requires C, 46.2 per cent; N, 53.8 per cent). Molecular weight determined from vapour pressure of solution in CH_2Cl_2 : 161 (C_6N_6 requires 156).

The mono-anion was formed by the action of metallic Li, Na or K on the solution in tetrahydrofuran or 1 : 2-dimethoxy-ethane. The same, strongly paramagnetic, blue-violet solution was obtained immediately in all cases and the electron resonance spectra, recorded on a Varian 100 kc spectrometer, were identical: at room temperature there was no detectable difference in line width between the spectra obtained with different alkali metals. The same spectrum was, furthermore, obtained when the neutral compound was dissolved in tetrahydrofuran in the presence of hexamethyl melamine (tri-dimethylamino-sym-triazine) and then irradiated with ultra-violet light.

At temperatures above 50°C the spectrum degenerated irreversibly into a quite different and much less well-resolved spectrum of lower intensity; this spectrum persisted when the solution was re-cooled to 25°C.

We thank the D.S.I.R. for the purchase of a Varian spectrometer and I.C.I. Ltd., Petrochemical and Polymer Laboratory, for leave of absence to P.F.T.

REFERENCES

- [1] CARRINGTON, A., and DOS SANTOS-VEIGA, J., 1962, *Mol. Phys.*, **5**, 21.
- [2] WEDDIDGE, A., 1874, *J. prakt. Chem.*, **10**, 208.
- [3] OTT, E., 1919, *Ber. dtsh. chem. Ges.*, **52**, 656.

Self-consistent approximations for molecular distribution functions

by J. S. ROWLINSON

Department of Chemical Engineering and Chemical Technology,
Imperial College of Science and Technology, London, S.W.7

(Received 15 January 1965)

The molecular distribution functions of a classical fluid are related to the pressure both by the virial equation of the canonical ensemble and by the equation for the compressibility of the grand canonical ensemble. In general, the two values of the pressure do not agree if approximations to the functions are used. It is shown that a direct correlation function can be devised which removes this discrepancy, and that its removal leads to a significant improvement in the equation of state for hard spheres over those of the Percus-Yevick and hyper-netted chain approximations. Two other inconsistencies are discussed more briefly but are not used constructively.

1. INTRODUCTION

Several thermodynamic properties, such as pressure, compressibility and energy, can be expressed directly in terms of the molecular distribution functions by means of the equations of classical statistical mechanics. The derived properties are self-consistent if exact functions are used; that is, all known thermodynamic relations between them are satisfied. However, the properties are usually inconsistent if approximate distribution functions are used.

The most notorious of these discrepancies is that between the pressure calculated from the canonical ensemble by the virial theorem, and the compressibility calculated from the fluctuations of density in the grand canonical ensemble. It is shown here that distribution functions can be devised which remove this discrepancy and that these functions are superior to those used hitherto. Thus the existence of two independent routes to the pressure can be used to improve the distribution functions and so to obtain a better equation of state.

Two other discrepancies are also discussed, but not used constructively, in §§ 5 and 6 below. It is shown that the improved distribution functions reduce but do not remove one of these discrepancies.

2. MOLECULAR DISTRIBUTION FUNCTIONS

Let $g(r)$ be the radial distribution function of a fluid, normalized to unity at large r , and define a total correlation function $h(r)$ by:

$$h(r) = g(r) - 1. \quad (2.1)$$

Let the limit of $h(r)$ in a gas of low density be $f(r)$:

$$f(r) = \exp [-u(r)/kT] - 1, \quad (2.2)$$

where $u(r)$ is the intermolecular potential. Define a direct correlation function $c(r)$ by the integral equation:

$$h(r_{12}) = c(r_{12}) + n \int c(r_{13}) h(r_{23}) d\mathbf{r}_3 \quad (2.3)$$

where n is the number density. It follows that $f(r)$, $g(r)$, $h(r)$ and $c(r)$ have discontinuities at any separation at which $u(r)$ is discontinuous. However, the function

$$y(r) = g(r) \exp [u(r)/kT] \quad (2.4)$$

is always continuous.

The pressure and compressibility are related to the distribution and correlation functions by:

$$\frac{p}{nkT} = 1 + \frac{n}{2s} \int r f'(r) y(r) d\mathbf{r}, \quad (2.5)$$

$$(kT)^{-1} \left(\frac{\partial p}{\partial n} \right)_T = 1 - n \int c(r) d\mathbf{r} = \left[1 + n \int h(r) d\mathbf{r} \right]^{-1}, \quad (2.6)$$

where s is the number of dimensions of the system.

If an approximation is used for $y(r)$, and hence for $h(r)$ and $c(r)$, then (2.5) and (2.6) yield different pressures. The two parts of (2.6) are always self-consistent since one can be obtained from the other by integrating (2.3) over \mathbf{r}_2 .

Any guess at $c(r)$ leads, by (2.3), to an approximation for $h(r)$ and so to the pressure by two independent routes. It is known from the expansion of $c(r)$ and $y(r)$ in powers of the density [1] that the former is predominantly of short range, that is of the range of $f(r)$, whereas the latter is of long range and all the cluster integrals of its expansion are free from factors of $f(r)$. Therefore, let $c(r)$ be written:

$$c(r) = f(r)e(r) + d(r), \quad (2.7)$$

where $d(r)$ and $e(r)$ are functions of r , n and T that are yet to be determined, but where $d(r)$ is expected to be smaller everywhere than $e(r)$. Substitute (2.4) and (2.7) into (2.3):

$$y_{12} = 1 + f_{12}(e_{12} - y_{12}) + d_{12} + n \int [f_{13}e_{13} + d_{13}][y_{23}(1 + f_{23}) - 1] d\mathbf{r}_3. \quad (2.8)$$

Hence $e(r) \equiv y(r)$ since $y(r)$ must have no terms in $f(r)$. This prohibition applies not only to the exact $y(r)$ but also to any acceptable approximation; if it did not then (2.5) would be indeterminate for discontinuous potentials. The approximation of Percus and Yevick [2] is obtained from (2.7) by putting $e(r) = y(r)$ and $d(r) = 0$. An exact integral equation for $y(r)$ in terms of $d(r)$, the unknown 'tail' of the direct correlation function is:

$$y_{12} = 1 + d_{12} + n \int [f_{13}y_{13} + d_{13}][y_{23}(1 + f_{23}) - 1] d\mathbf{r}_3. \quad (2.9)$$

The form of $d(r)$ is not so easily found, but the hyper-netted chain (HNC) approximation [3] for the clusters in the density expansion of $y(r)$ sets it equal to $[y(r) - 1 - \ln y(r)]$. Although $d(r)$ is, for convenience, called the tail of $c(r)$ it also contributes to this function at small separations where $f(r)$ is not zero.

Its exact density expansion starts, in the usual notation [4]:

$$d(r) = n^2 \frac{1}{2} \left[\text{diag}_1 + \text{diag}_2 \right] + \dots \quad (2.10)$$

The form of $c(r)$ used here is:

$$\begin{aligned} c(r) &= f(r) y(r) + d(r), \\ d(r) &= \Phi(n, T) [y(r) - 1 - \ln y(r)], \end{aligned} \quad (2.11)$$

where $c(r)$ and $y(r)$ are also functions of n and T but where the parameter Φ is independent of r , and is a function of only n if $u(r)$ is everywhere zero or $+\infty$. It is to be determined by equating the pressures from (2.5) and (2.6). The approximation can be written formally:

$$c(r) = (1 - \Phi) c^0(r) + \Phi c^1(r), \quad (2.12)$$

where $c^0(r)$ and $c^1(r)$ are, respectively, the correlation functions of the Percus-Yevick and hyper-netted chain approximations.

3. ITERATIVE SOLUTION IN POWERS OF THE DENSITY

An analytical solution of the integral equation obtained by substituting (2.11) into (2.3) has been obtained for a fluid of hard spheres only if $\Phi = 0$, the Percus-Yevick (PY) approximation. However, (2.9) can be solved for any potential by iteration in powers of the density by putting:

$$\Phi(n, T) = \sum_{l=4} \phi_l(T) n^{l-4}. \quad (3.1)$$

The subscripts are started at 4 since the first term affects only the fourth and higher coefficients of the virial expansion of p .

The coefficients of n^{l-2} in the expansion of $y(r)$ is a linear function of ϕ_l and has terms with products of lower coefficients down to ϕ_4^{l-3} . Thus,

$$\begin{aligned} y(r) &= 1 + n \left[\text{diag}_1 \right] + n^2 \left[\text{diag}_2 + 2 \text{diag}_3 + \frac{1}{2} \phi_4 \text{diag}_4 \right] \\ &+ n^3 \left[\text{diag}_5 + 2 \text{diag}_6 + 2 \text{diag}_7 + \text{diag}_8 \right] \\ &+ 2 \left[\text{diag}_9 + 2 \text{diag}_{10} + \text{diag}_{11} \right] \\ &+ \phi_4 \left[\text{diag}_{12} + 2 \text{diag}_{13} + \text{diag}_{14} + \text{diag}_{15} \right] \\ &+ \phi_4 \left(\frac{1}{2} \phi_4 - \frac{1}{3} \right) \text{diag}_{16} + \frac{1}{2} \phi_5 \text{diag}_{17} \left] + \dots \end{aligned} \quad (3.2)$$

The next term has also been obtained but is too long to quote. The derived virial coefficients contain terms with coefficients of $\phi_4(\phi_4 - 1)$ which therefore appear in neither the PY ($\phi_4 = 0$) nor the HNC ($\phi_4 = 1$) approximation.

The l th virial coefficient L_l is found from (3.2) by choosing ϕ_l to give a single solution to (2.5) and (2.6) after all lower coefficients ϕ_{l-1} , etc. have been fixed from the lower virial coefficients. It is readily seen that for hard spheres a

small departure from this consistent value leads to 'pressure' and 'compressibility' coefficients, $(L_l)_p$ and $(L_l)_c$ which bracket the consistent value. This follows from the fact that the lowest power of n in $y(r)$ that contains ϕ_l arises from the direct term d_{12} in (2.9). It is of the form:

$$\phi_l n^{l-2\frac{1}{2}} \begin{array}{c} \diagup \diagdown \\ \diagdown \diagup \end{array}, \quad (3.3)$$

where the cluster integral is the first term in the expansion of $[y-1-\ln y]$. Hence, from the two parts of (2.11), the contribution of lowest term in ϕ_l to $c(r)$ is:

$$\phi_l n^{l-2\frac{1}{2}} \left(\begin{array}{c} \diagup \diagdown \\ \diagdown \diagup \end{array} + \begin{array}{c} \diagdown \diagup \\ \diagup \diagdown \end{array} \right). \quad (3.4)$$

The corresponding contributions to the virial coefficients are:

$$(L_l)_p \text{ from (2.5)} \quad + \frac{b}{2} \phi_l \left(\begin{array}{c} \diagup \diagdown \\ \diagdown \diagup \end{array} \right)_{r=\sigma}, \quad (3.5)$$

$$(L_l)_c \text{ from (2.6)} \quad - \frac{1}{2l} \phi_l \left(\begin{array}{c} \square \\ \square \end{array} + \begin{array}{c} \diagup \diagdown \\ \diagdown \diagup \end{array} \right), \quad (3.6)$$

where (in three dimensions) $b = \frac{2}{3}\pi N\sigma^3$ and σ is the diameter of a sphere. These terms are respectively positive and negative if ϕ_l is positive.

The coefficients $\phi_4 - \phi_6$ can be found for those potentials for which the open cluster integrals of (3.2) are either known or are reducible to known combinations of irreducible clusters [1]. The following sources of open and irreducible clusters have been used here:

<i>two dimensions—hard spheres</i>	Rowlinson [5]
<i>three dimensions—hard spheres</i>	Hutchinson [6]
<i>three dimensions—square-well potential</i>	Katsura [7]
	McQuarrie [8]

The following values of ϕ_l are obtained.

Hard spheres of diameter σ

One dimension

$$\Phi = 0. \quad (3.7)$$

This is not exact since $d(r) \neq 0$ for $r < \sigma$, cf. (2.10), although $c(r)$ is here confined entirely to σ (see below).

Two dimensions

$$\begin{aligned} \phi_4 &= - \left(1 - \frac{6\sqrt{3}}{\pi} + \frac{39}{2\pi^2} \right) \left(8 - \frac{3\sqrt{3}}{\pi} - \frac{29}{\pi^2} \right)^{-1} \\ &= 0.0920. \end{aligned} \quad (3.8)$$

Three dimensions

$$\left. \begin{aligned} \phi_4 &= \frac{1260}{7607} = 0.1656, \\ \phi_5/b &= \frac{267}{2064} \frac{766}{559} \frac{349}{167} \frac{445}{422} = 0.1297, \\ \phi_6/b^2 &= 0.02832. \end{aligned} \right\} \quad (3.9)$$

All coefficients are rational fractions of the appropriate powers of b , but ϕ_6 was calculated only in decimal form.

Square-well potential—three dimensions

for which $u(r) = -\epsilon \quad (\sigma < r < 2\sigma)$, (3.10)

$$\phi_4 = \frac{1260 - 51 \cdot 412f + 360 \cdot 640f^2 - 974 \cdot 288f^3 + 482 \cdot 240f^4 - 1 \cdot 224 \cdot 720f^5}{7607 - 78 \cdot 781f + 544 \cdot 796f^2 - 1 \cdot 568 \cdot 560f^3 + 2 \cdot 001 \cdot 220f^4 + 306 \cdot 180f^5} \quad (3.11)$$

where $f = \exp(\epsilon/kT) - 1$. (3.12)

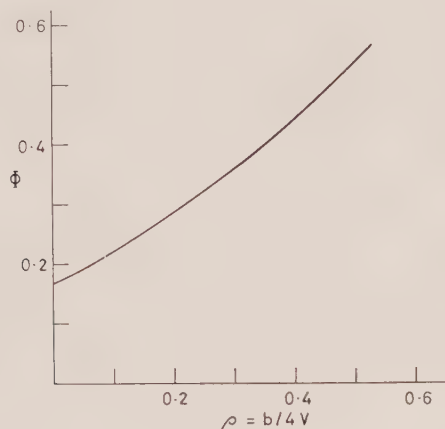


Figure 1. Φ as a function of reduced density from the first three terms of (3.1) for hard spheres in three dimensions.

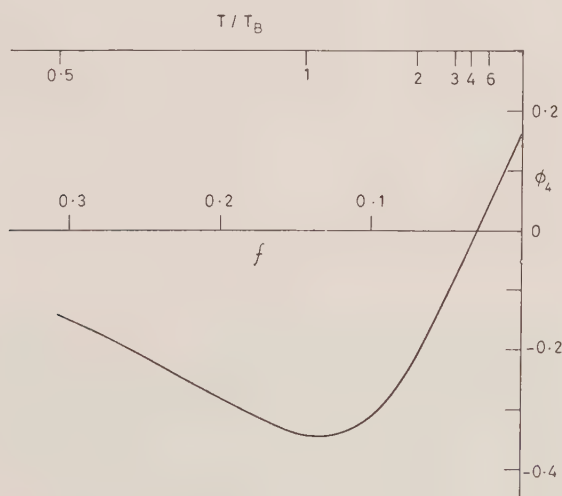


Figure 2. ϕ_4 as a function of f (3.12). The upper scale is a reduced temperature T/T_B , where T_B is the Boyle temperature at which $B=0$ and $7f=1$.

Figure 1 shows Φ as a function of density, from the coefficients of (3.9). It is probably less than unity at all densities at which the fluid phase is stable [9], that is for $\rho < 0.47$, where the reduced density ρ is given by:

$$\rho = b/4V = bn/4N. \quad (3.13)$$

Since Φ is less than unity it seems that the HNC approximation ($\Phi=1$) overestimates the tail of $c(r)$ for hard spheres, but that this tail becomes more important at higher densities.

Figure 2 shows ϕ_4 of (3.11) as a function of f , and hence of temperature, for the square-well potential. The coefficient is again small but is now negative at moderately low temperatures.

4. THE VIRIAL COEFFICIENTS

The following virial coefficients have been calculated from the values of Φ above. They are compared in table 1 with those of the PY approximation ($\Phi=0$), of the HNC approximation ($\Phi=1$) and with the directly computed values, see [4].

Two dimensions $(b = \frac{1}{2}\pi N\sigma^2)$				
	PY ($\Phi = 0$)	HNC ($\Phi = 1$)	Consistent approx.	Exact Value
D_p/b^3	0.5008	0.8066	} 0.5290	0.5322
D_c/b^3	0.5377	0.4423		
Three dimensions $(b = \frac{2}{3}\pi N\sigma^3)$				
D_p/b^3	0.25	0.4453	} 0.2824	0.2869
D_c/b^3	0.2969	0.2092		
E_p/b^4	0.0859	0.1447	} 0.1041	0.1102 ± 0.0003
E_c/b^4	0.1211	0.0493		
F_p/b^5	0.0273	0.0382	} 0.0341	0.0386 ± 0.0004
F_c/b^5	0.0449	0.0281		

Table 1. Virial coefficients for hard spheres.

The value obtained for the fourth coefficient namely

$$D/b^3 = \frac{68}{243} \frac{731}{424} = 0.2824 \quad (4.1)$$

was obtained earlier by Hutchinson and Rushbrooke [10] by means of an approximation that was consistent to the fourth coefficient but not beyond. Hurst [11] has recently modified the treatment of Hutchinson and Rushbrooke in a way that produces accurate values of E_c , but which does not produce consistency beyond D . The improvement effected here is two-fold, first the theory is self-consistent at all densities and secondly the virial coefficients are uncommonly accurate. The approximation is, moreover, quite as tractable as the HNC approximation.

Since the term in n^2 in $y(r)$, (3.2), is linear in ϕ_4 it follows that D is also a linear function of ϕ_4 and the self-consistent value can be written:

$$D^\phi = \frac{D_p^0 D_c^1 - D_p^1 D_c^0}{(D_p^0 - D_c^0) - (D_p^1 - D_c^1)}, \quad (4.2)$$

where the superscripts denote the value of ϕ_4 . Hence D^b for the square-well potential is readily found from those for the PY and HNC approximations listed by McQuarrie [8]. It is compared with them and with the directly computed values of Barker and Monaghan [12] in figure 3. It is seen that this approximation is at least as accurate as any previously obtained and, as is shown below, yields a good value for the internal energy of the fluid.

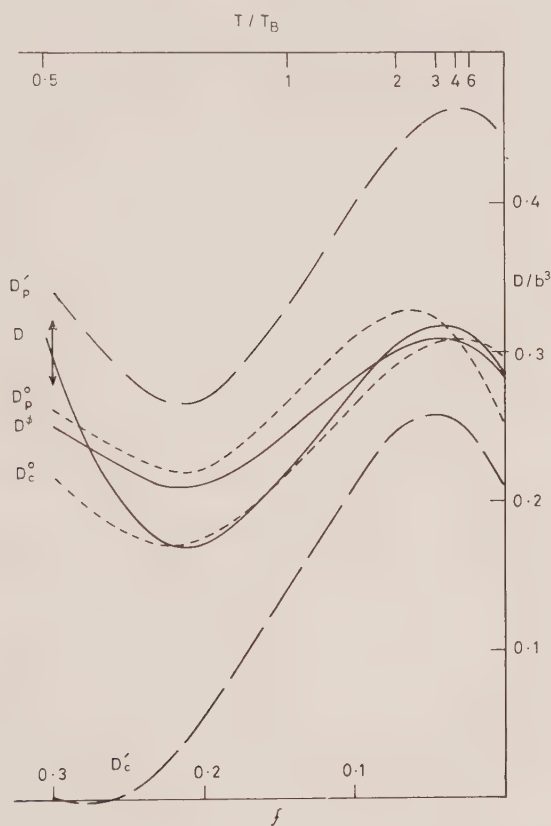


Figure 3. D as a function of f . The short-dashed curves are the PY approximations, the long-dashed curves the HNC approximations, and the full curves the self-consistent approximation and the exact value. The arrow on the last curve is an estimate of the uncertainty of the calculations at low temperature.

5. THE TEST OF HOOVER AND POIRIER

Hoover and Poirier [13] point out that, for hard spheres, the potential of average force at zero separation is equal to the configurational part of the chemical potential. The latter can also be expanded in powers of the density, and so

for this potential there is a third route to the virial coefficients. Their results can be written:

$$-\ln y(0) = \mu^*/NkT = \sum_{l=2}^{\infty} \frac{l}{l-1} L_l n^{l-1}, \quad (5.1)$$

where μ^* is the configurational part of the chemical potential.

By expanding $y(0)$ it is seen that the l th virial coefficient is now given by degenerate forms ($r=0$) of the cluster integrals usually associated with the $(l+1)$ th virial coefficient. Hence approximate theories of fluids are now inconsistent at the third and not the fourth coefficient. The test of consistency is a severe one.

The third coefficient, C^ϕ , is now given by

$$C^\phi = 2C + \frac{4}{3}(\phi_4 - 1)B^2, \quad (5.2)$$

where B and C are the exact coefficients. It is seen in table 2 that none of the theories discussed, the PY approximation ($\phi_4=0$), the HNC approximation ($\phi_4=1$), or the 'self-consistent' approximation yields good values of C . However, the last is the least in error, and, in particular, is still superior to the PY approximation, whose compressibility coefficients were the second-best in table 1.

	One dimension	Two dimensions	Three dimensions
C/b^2	1.0000	0.7820	0.6250
C^0/b^2	0.6667	0.2307	-0.0833
C^ϕ/b^2	0.6667	0.3534	0.1375
C^1/b^2	2.0000	1.5640	1.2500

Table 2. Third virial coefficient from (5.2).

This superiority may not persist at high densities. All values of the fourth coefficient are bad, but the 'self-consistent' value is worse than the PY value. In three dimensions:

$$D^0/b^3 = 0.0781, \quad D^\phi/b^3 = -0.0076, \quad D^1/b^3 = 0.8906. \quad (5.3)$$

Hoover and Poirier observe that Kirkwood's integral equation with the superposition approximation is exact to C and good to D by this test. However, the approximation is inadequate when tested by the usual calculations of §4.

It is seen that the PY approximation is not correct even in one dimension although it gives a consistent and exact equation of state from (2.5) and (2.6). The differences between the exact and the PY versions of $y(r)$ and $c(r)$ are, to the term in n^2 :

$$y(r) - y^0(r) = n^{2\frac{1}{2}} \left[\text{diagram 1} + \text{diagram 2} \right], \quad (5.4)$$

$$c(r) - c^0(r) = n^{2\frac{1}{2}} \left[\text{diagram 1} + \text{diagram 2} + \text{diagram 3} + \text{diagram 4} \right]. \quad (5.5)$$

Now in one dimension:

$$\text{diagram 1} + \text{diagram 2} = 0 \quad (r \geq \sigma) \quad (5.6)$$

and in all dimensions :

$$\begin{array}{c} \diagup \diagdown \\ \circ \quad \circ \end{array} + \begin{array}{c} \diagdown \diagup \\ \circ \quad \circ \end{array} = 0; \quad \begin{array}{c} \diagup \diagdown \\ \diagdown \diagup \\ \circ \quad \circ \quad \circ \quad \circ \end{array} + \begin{array}{c} \diagdown \diagup \\ \diagup \diagdown \\ \circ \quad \circ \quad \circ \quad \circ \end{array} = 0 \quad (r \leq \sigma). \quad (5.7)$$

These equations (and equivalent ones for higher clusters) are sufficient to ensure that (2.5) and (2.6) are self-consistent and exact. They are, however, not sufficient to satisfy the test of Hoover and Poirier, which appears to be too searching for current theories. It might be valuable if it could be used constructively to produce more accurate functions for $y(r)$.

6. THE TEST OF HIROIKE

The test used in the last section was applicable only to hard spheres. The test proposed by Hiroike [14] and used recently by McQuarrie [15] is, in a sense, complementary to it, since it is useful only for potentials for which $u(r)$ is finite and not zero over a finite non-zero range of r . For such potentials the mean configurational energy of the fluid is not zero and is given by :

$$\frac{U}{N} = \frac{n}{2} \int u(r) g(r) dr. \quad (6.1)$$

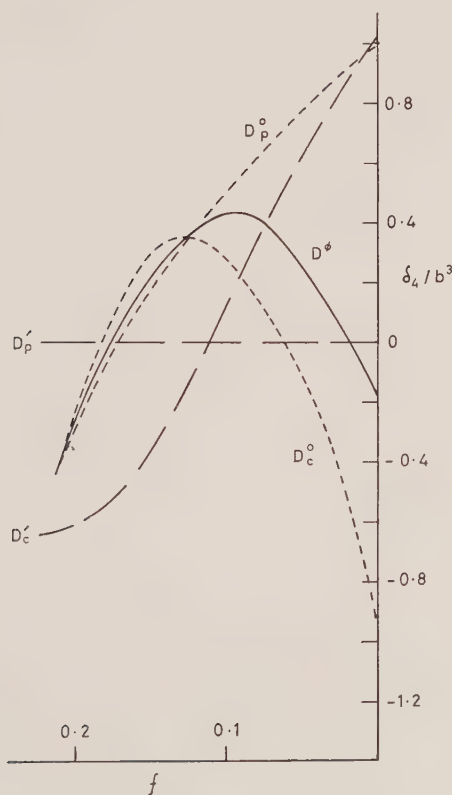


Figure 4. The difference δ_4 (6.3). Conventions as in figure 3.

The test of Hiroike is an examination of difference between the two sides of the following equation:

$$\left(\frac{\partial U}{\partial V}\right)_T = -p + T\left(\frac{\partial p}{\partial T}\right)_V, \quad (6.2)$$

when U is given by (6.1) and p by (2.5) or (2.6). A difference usually appears at the fourth virial coefficient and, for the square-well potential of (3.10), is conveniently measured by δ_4 where

$$\delta_4 = \frac{dD}{df} + \frac{3}{2} \int_{\sigma}^{2\sigma} \eta_4(r) 4\pi r^2 dr, \quad (6.3)$$

where f is given by (3.12) and $\eta_4(r)$ is the term in n^2 in the expansion of $y(r)$. Figure 4 shows the value of δ_4 found for the PY and HNC approximations (using cluster integrals from the sources quoted above) and for the 'self-consistent' approximation of §4 by using the values of ϕ_4 from (3.11). It is seen that δ_4 is, on the whole, smaller for this last approximation than for either version of the PY approximation.

One striking result of figure 3 is that $\delta_4 = 0$ at all temperatures for the 'pressure' version of the HNC approximation. This result was not found by McQuarrie for two reasons; first, because of an error in the coefficient of f^2 in the second term of (6.3), and secondly, because he chose to compare this second term with the exact value of dD/df and not with the value given by the same approximation. The $(\text{HNC})_p$ approximation can be shown to be consistent to the fourth coefficient by the following argument.

It omits from the exact integral of (2.5) the cluster integral

$$\int r f'(r)^{\frac{1}{2}} \text{[diagram]} d\mathbf{r} = -\frac{3}{4} \text{[diagram]}. \quad (6.4)$$

(The equation is due to Rushbrooke and Scoins [1].)

Now

$$\frac{d}{df} \text{[diagram]} = 6 \int_{\sigma}^{2\sigma} \text{[diagram]} 4\pi r^2 dr \quad (6.5)$$

or

$$\frac{d}{df} \frac{1}{6} \int r f'(r)^{\frac{1}{2}} \text{[diagram]} d\mathbf{r} + \frac{3}{2} \int_{\sigma}^{2\sigma} \frac{1}{2} \text{[diagram]} 4\pi r^2 dr = 0. \quad (6.6)$$

But the two parts of this equation are just the amounts by which the two terms in (6.3) differ from their exact values. Hence $\delta_4 = 0$, but this consistency does not have any great significance.

7. CONCLUSIONS

Three types of inconsistency are discussed above. One is common to all potentials whilst the other two are applicable only to mutually exclusive types of potential. It is shown that the first can be removed (with no reduction in the second but some in the third) and that its removal leads to a significant improvement in the first six virial coefficients of a fluid of hard spheres. Numerical solutions of integral equations are needed to assess this improvement for densities beyond the range of the virial expansion and for less simple potentials. Such solutions appear to be no more difficult than those for the HNC equations.

This method of approximation cannot yet be compared with the second approximation of Percus [16], which is denoted PY2 by Verlet [17]. The latter shows that PY2 is exact to the fourth virial coefficient of (2.5) and (2.6), and hence to the third of (5.1), and is good, but inconsistent, to the fifth coefficient of (2.5) and (2.6). Only the compressibility value is known for hard spheres [18]:

$$E_c/b^4 = 0.107. \quad (7.1)$$

Its performance at higher densities is yet to be tested since it is less tractable than the approximation of this paper.

REFERENCES

- [1] RUSHBROOKE, G. S., and SCOINS, H. E., 1953, *Proc. roy. Soc. A*, **216**, 203.
- [2] PERCUS, J. K., and YEVICK, G. J., 1958, *Phys. Rev.*, **110**, 1.
- [3] VAN LEEUWEN, J. M. J., GROENEVELD, J., and DE BOER, J., 1959, *Physica*, **25**, 792.
- [4] ROWLINSON, J. S., 1965, *Rep. Prog. Phys.*, **28** (in the press).
- [5] ROWLINSON, J. S., 1964, *Mol. Phys.*, **7**, 593.
- [6] HUTCHINSON, P., 1964, AERE Report R-4494.
- [7] KATSURA, S., 1959, *Phys. Rev.*, **115**, 1417; 1960, *Ibid.*, **118**, 1667.
- [8] MCQUARRIE, D. A., 1964, *J. chem. Phys.*, **40**, 3455.
- [9] ALDER, B. J., and WAINWRIGHT, T. E., 1960, *J. chem. Phys.*, **33**, 1439.
- [10] HUTCHINSON, P., and RUSHBROOKE, G. S., 1963, *Physica*, **29**, 675.
- [11] HURST, C., 1965, *Phys. Letters*, **14**, 192.
- [12] BARKER, J. A., and MONAGHAN, J. J., 1962, *J. chem. Phys.*, **36**, 2558.
- [13] HOOVER, W. G., and POIRIER, J. C., 1962, *J. chem. Phys.*, **37**, 1041.
- [14] HIROIKE, K., 1957, *J. phys. Soc., Japan*, **12**, 326.
- [15] MCQUARRIE, D. A., 1964, *J. chem. Phys.*, **41**, 1197.
- [16] PERCUS, J. K., 1962, *Phys. Rev. Letters*, **8**, 462.
- [17] VERLET, L., 1964, *Physica*, **30**, 95.
- [18] RUSHBROOKE, G. S., 1965, *Statistical Mechanics of Equilibrium and Non-Equilibrium*, Ed. J. Meixner (North-Holland), p. 222.

Molecular orbitals for H_2^+ using A.O.'s with angularly dependent Z_{eff}

by K. C. BHALLA and P. G. KHUBCHANDANI
Atomic Energy Establishment, Trombay, Bombay, India

(Received 15 September 1964)

The H_2^+ molecule is studied using the variational approach. The wave function is written following Dalgarno and Poots and using the angular dependent z type atomic orbitals as used by Scrocco and Tomasi. A better result has been obtained than the later authors.

Recently Scrocco and Tomasi [1] have used the variation method for the ground state of the H_2^+ molecule, using a wave function of the type:

$$\psi = \frac{\chi_a + \chi_b}{\sqrt{N}},$$

where N is the normalizing factor and

$$\chi_a = \exp[-z(1 + \gamma \cos \theta_a)\gamma_a],$$

with z, γ as variational parameters. In effect this amounts to using the orbitals in a hybrid form [1]. Using elliptic coordinates the above authors have calculated the various integrals required, in closed forms. This is convenient for the variation method. Further their integrals are true for all values of inter-nuclear separation R . Using z and γ as variation parameters and $R=2$ A.U., they have been able to calculate the bond energy with 2.08 per cent error as compared to the exact value obtained by Bates *et al.* [2].

Following Dalgarno and Poots [3], we have written our molecular wave-function in the form

$$\psi = \frac{(\chi_a + \chi_b) + p\chi_a\chi_b}{\sqrt{N}},$$
$$\chi_b = \exp[-z(1 + \gamma \cos \theta_b)\gamma_b],$$

with a suitable normalization factor. (This wave-function differs from that used by Dalgarno and Poots, since we have taken $\alpha = \beta = z$ in their choice of the function and introduced angle dependence through γ .) This wave-function behaves correctly at the two limits $R \rightarrow 0$ and $R \rightarrow \infty$, and is an obvious improvement on the function used by Scrocco and Tomasi. We have been able to calculate the required integrals in a closed form and they are true for all inter-nuclear separations. We report them below:

$$\int \chi_a \chi_b (-\nabla^2) \chi_a \chi_b d\tau = \frac{\pi(1+2zR)}{2z} \exp[-2zR(1+\gamma)], \quad (1)$$

$$\int \chi_a (-\nabla^2) \chi_a \chi_b d\tau = \frac{4\pi}{z\gamma^2} \left\{ \left(\frac{2\gamma(2-\gamma)}{(3-\gamma)^2} + \frac{(1-\gamma)zR}{(3-\gamma)} \right) \exp[-zR(1+\gamma)] \right. \\ \left. - \left(\frac{2\gamma(2+\gamma)}{(3+\gamma)^2} + \frac{(1-\gamma)zR}{(3+\gamma)} \right) \exp[-2zR(1+\gamma)] - \frac{zR}{2} \left(2 + (1-\gamma^2) \frac{zR}{\gamma} \right) \epsilon_2 \right\}, \quad (2)$$

$$\int \chi_a (-\nabla^2) \chi_a d\tau = \frac{\pi}{z(1-\gamma^2)}, \quad (3)$$

$$\int \chi_a (-\nabla^2) \chi_b d\tau = \frac{\pi}{z} \left\{ (1-\gamma^2) + (1-\frac{2}{3}\gamma-\gamma^2)zR - (1+\gamma)^2 \frac{z^2 R^2}{3} \right\} \\ \times \exp[-zR(1+\gamma)] \quad (4)$$

$$\int \chi_a^2 \chi_b^2 \left(-\frac{2}{r_a} \right) d\tau = \frac{-\pi}{2z^2} (1+2zR) \exp[-2zR(1+\gamma)], \quad (5)$$

$$\int \chi_a^2 \chi_b \left(-\frac{2}{r_a} \right) d\tau = \frac{-4\pi}{\gamma z^2} \left\{ \frac{-2(1-\gamma) \exp[-zR(1+\gamma)]}{(1+\gamma)(3-\gamma)} \right. \\ \left. + \frac{2 \exp[-2zR(1+\gamma)]}{(1+\gamma)(3+\gamma)} + \frac{zR}{\gamma} \epsilon_2 \right\}, \quad (6)$$

$$\int \chi_a^2 \chi_b \left(-\frac{2}{r_b} \right) d\tau = \frac{-8\pi}{\gamma z^2} \left\{ \frac{2 \exp[-zR(1+\gamma)]}{(1+\gamma)(3-\gamma)} - \frac{(2+\gamma) \exp[-2zR(1+\gamma)]}{(1+\gamma)(3+\gamma)} \right. \\ \left. - \frac{zR}{\gamma} \epsilon_2 \right\}, \quad (7)$$

$$\int \chi_a^2 \left(-\frac{2}{r_a} \right) d\tau = \frac{-2\pi}{z^2(1-\gamma^2)}, \quad (8)$$

$$\int \chi_a^2 \left(-\frac{2}{r_b} \right) d\tau = \frac{-2\pi}{z^2} \left\{ \frac{1}{\gamma(1-\gamma^2)} - \frac{\exp[-2zR(1+\gamma)]}{\gamma(1+\gamma)} - \frac{zR}{\gamma^2} \epsilon_1 \right\}, \quad (9)$$

$$\int \chi_a \chi_b \left(-\frac{2}{r_a} \right) d\tau = \frac{-2\pi}{z^2} (1+zR) \exp[-zR(1+\gamma)], \quad (10)$$

$$\int \chi_a^2 \chi_b^2 d\tau = \frac{\pi}{24z^3} (3+6zR+4z^2R^2) \exp[-2zR(1+\gamma)], \quad (11)$$

$$\int \chi_a^2 \chi_b d\tau = \frac{8\pi}{\gamma z^3} \left\{ \left(\frac{zR}{\gamma} - \frac{2(1-\gamma)}{(1+\gamma)(3-\gamma)} \right) \frac{\exp[-zR(1+\gamma)]}{(1+\gamma)(3-\gamma)} \right. \\ \left. - \left(\frac{zR}{\gamma} - \frac{(2+\gamma)}{(1+\gamma)(3+\gamma)} \right) \frac{\exp[-2zR(1+\gamma)]}{(1+\gamma)(3+\gamma)} - \frac{z^2 R^2}{2\gamma^2} \epsilon_2 \right\}, \quad (12)$$

$$\int \chi_a^2 d\tau = \frac{\pi}{z^3(1-\gamma^2)^2}, \quad (13)$$

$$\int \chi_a \chi_b d\tau = \frac{\pi}{z^3} \left(1+zR + \frac{z^2 R^2}{3} \right) \exp[-zR(1+\gamma)], \quad (14)$$

where

$$\epsilon_1 = (E_i(-x_2) - E_i(-x_1)) \exp \left[\frac{zR}{\gamma} (1 - \gamma^2) \right] \quad \text{with} \quad \begin{cases} x_2 = \frac{zR}{\gamma} (1 + \gamma)^2, \\ x_1 = \frac{zR}{\gamma} (1 - \gamma^2), \end{cases}$$

$$\epsilon_2 = (E_i(-x_4) - E_i(-x_3)) \exp \left[\frac{3}{2} \frac{zR}{\gamma} (1 - \gamma^2) \right] \quad \text{with} \quad \begin{cases} x_4 = \frac{zR}{2} \frac{(1 + \gamma)}{\gamma} (3 + \gamma), \\ x_3 = \frac{zR}{2} \frac{(1 + \gamma)}{\gamma} (3 - \gamma), \end{cases}$$

and $E_i(-y)$ is the Exponential Integral [4], defined by

$$E_i(-y) = - \int_y^\infty \frac{\exp(-t)}{t} dt.$$

It will be seen that equations (3), (4), (8), (9), (10), (13) and (14) are the same as obtained by Scrocco and Tomasi.

The calculations of energy were performed on CDC 3600 at the Tata Institute of Fundamental Research. For $R = 2$ A.U. the z and γ parameters were varied and their choice fixed the value of p through energy minimization. The results obtained are shown below.

Molecular orbitals used	Optimum values of parameters (Å)	Bond energy (ev)	Relative error (per cent)
(a) $\frac{X_a + X_b}{\sqrt{N}}$	$R = 1.06$ $z = 1.275$ $\gamma = -0.19$	2.734	2.08
(b) $\frac{(X_a + X_b) + pX_aX_b}{\sqrt{N}}$	$R = 1.06$ $z = 1.2390$ $\gamma = -0.1490$ $p = 0.7045$	2.744	1.73
(c) Exact solution	—	2.792	—

(a) Scrocco and Tomasi; (b) This paper.

Thus the present wave function is an improvement over the one used by Scrocco and Tomasi. The energy value obtained is -2.20171 ry, exact value being -2.20525 ry.

We are thankful to Shri P. Chandrasekhar for his help in programming the calculations.

REFERENCES

- [1] SCROCCO, E., and TOMASI, J., 1961, *Mol. Phys.*, **4**, 193.
- [2] BATES, D. R., LEDSHAM, K., and STEWART, A. L., 1953, *Phil. Trans.*, A, **246**, 215.
- [3] DALGARNO, A., and POOTS, G., 1954, *Proc. phys. Soc., Lond.*, A, **67**, 343.
- [4] WHITTAKER, E. T., and WATSON, G. N., 1961, *Modern Analysis* (Cambridge University Press).

Microwave diamagnetic resonance associated with polysiloxanes†

by FLOYD HUGHES and FRANK W. PATTEN

U.S. Naval Research Laboratory, Washington, D.C.

(Received 12 September 1964)

Diamagnetic resonance has been observed at 9.3 Gc/s and 23 Gc/s with thin films of several methyl-phenyl substituted siloxanes. The films (thickness $< 200 \text{ \AA}$) were deposited upon insulator substrates mounted in evacuated cavity resonators. The resonance, which appears as a carrier avalanche ionization, occurs above microwave electric fields of approximately 1–10 V/cm. Fields and frequencies satisfy the cyclotron resonance equation $\nu = eB/2\pi m^*c$ (where $m^* = 1.000 \pm 0.001 m_e$). The mean collision lifetime at low power is $\tau \sim 10^{-9}$ sec. The lifetime is relatively insensitive to ambient gas pressures in the range from less than 5×10^{-6} torr to 0.2 torr and to cavity temperatures in the range from 300°K to 20°K. Results of application to the films of d.c. electric fields are described. A tentative interpretation of the phenomena is given.

1. BACKGROUND

In recent years diamagnetic resonance has been observed in semiconductors and metals [1] and in low pressure gases [2]. To obtain a well defined resonance, it is necessary that the mean time, between collisions of the charge carriers with a lattice or with gas molecules, be sufficiently long so that the carrier may complete a cyclotron orbit, i.e. $\omega\tau \geq 1$. At X-band frequencies ($\nu \sim 9.2 \text{ Gc/s}$) this requires a carrier mobility $\mu > 10^4 \text{ cm}^2/\text{V/sec}$. (There are other, more stringent requirements for observation of the resonance in metals which will not be discussed here.)

For insulators and semiconductors it is necessary that provision be made to ionize carriers into a conduction band. In the early work on germanium, at microwave frequencies, low temperatures were required in order to satisfy the condition $\omega\tau > 1$ [3]. At these temperatures the carriers were 'frozen out'. Fortunately the carriers were located in such shallow traps that they could easily be ionized by the microwave electric field. In recent semiconductor work at microwave frequencies, carriers have been ionized by irradiation of the sample with an auxiliary infra-red source [4].

In the organic insulators which are of particular interest here, it is possible to obtain an adequate carrier population with the use of ultra-violet or ionizing radiation. Unfortunately in most cases the carrier mobilities appear to be too low for resonance at microwave frequencies [5]. To our knowledge, no attempts have been made to observe diamagnetic resonance in these materials in the infra-red region.

† A preliminary discussion of this work was given in *Bull. Amer. phys. Soc.*, **9**, 573 (1964).

In recent pulse conductivity measurements [6] of a number of aliphatics the carriers were provided by low intensity ionizing radiation. Evidence was found for a higher 'local' carrier mobility than was expected from the 'unirradiated' conductivity. In the present work on polysiloxane films, the 'local' mobility, as determined by microwave diamagnetic resonance, is orders of magnitude greater than the long range mobility obtained by d.c. conductivity measurements which were made during the resonance.

It is tempting to assign the 'local' mobility to intra-molecular carriers and to relate the low, long range mobility to inter-molecular carrier movement. Unfortunately, the present data (in particular, the computed diameter of the cyclotron orbits) do not support this hypothesis. Whatever may be the precise mechanism for the high 'local' mobility, its existence in such diverse compounds as the aliphatics and the siloxanes suggests that a search should be made for it in other materials.

1.1. Introduction

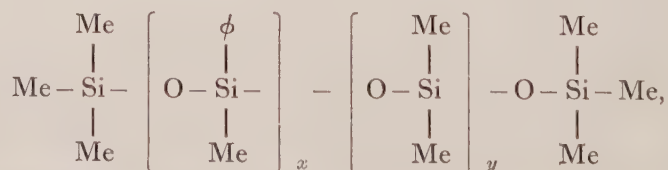
Electron diamagnetic resonances have been observed at X-band and K-band ($\nu \sim 24$ Gc/s) which are associated with thin films of methyl-phenyl substituted polysiloxanes. The films were evaporated on various solid substrates which were affixed to the walls of evacuated, microwave, cavity resonators. Evidence will be presented which suggests that interaction between substrate dipolar field and the molecular electric dipole introduces a preferred arrangement of the molecules upon the substrate.

A small initial carrier population appears to be provided by heating via a strong dielectric loss mechanism. Cyclotron resonance absorption of these initial carriers leads to multiple ionization of new carriers. At higher microwave power levels the multiplication causes a carrier avalanche. The appearance of the resonance is superficially the same as that observed in the early work in germanium [3] although the initial excitation processes do not appear to be the same. The carriers appear to be localized upon the film surface, perhaps in something resembling the so-called Tamm states [7]. This interpretation is supported by observation of the effects upon the resonance of d.c. electric fields and changes in residual gas pressures.

Since these results do not seem to have been discussed elsewhere†, the description will be somewhat more detailed than is customary for such straightforward experiments.

2. EXPERIMENTAL

These polysiloxanes have a composition which may be represented by the schematic:



† Diamagnetic resonances similar to those reported in the present work have been noted without interpretation by Thomas [8].

where Me=methyl and ϕ =phenyl. Although they are prepared as fairly 'sharp-cut' boiling fractions (for example, in the methyl substituted polysiloxanes a change of one silicon unit gives a change of 10°C to 20°C in the boiling point) [9], they may at best be viewed as mixtures of isomers, with X and Y approximately constant, and with various Me-Me and ϕ -Me arrangements along the molecular chain. Undoubtedly there are 'impurities' of molecules whose molecular weights are very large or very small compared to the average molecular weight as determined by viscosity measurements. In addition, arc-spectrographic analysis shows impurities of a few parts per million of alkaline earth metals.

The O-Si-O bond angle is approximately 140° and the O-Si bond length is approximately 1.6 Å [10].

Although the precise connection with the present work is not clear to us, it may be noted that all polysiloxanes have a resonant dielectric absorption in the region of 25 Gc/s [11].

The quantitative differences among the various materials were no greater than the variations among different samples prepared from the same material. The table below gives their average molecular weight, X/Y ratios and commercial origin; they will not be further distinguished during the course of the discussion.

Composition	Average mol. weight	X/Y	Origin
1	530	0.7	D.C. 702†
2	484	1.0	D.C. 704
3	?	1.0	D.C. 258
Dodeca methyl pentasiloxane	384	($X=0$)	G.E. Co.

† Dow Corning.

Although most of the data in this table appears in Gunderson [12], some of the ϕ -Me ratios were determined in this laboratory from the ratio of the 3.29 μ and 3.37 μ infra-red absorption lines. These ratios were measured with several different Beckman I.R. spectrophotometers.

2.1. Sample preparation and apparatus

The samples were vacuum evaporated on insulator substrates which were affixed to the walls of evacuated microwave cavity resonators. There were no significant differences observed in the results obtained from such diverse substrate materials as cleaved KCl crystals, fused silica, naphthalene and Pyrex. Of the various cements and greases which, for cryogenic purposes, were used to hold the substrate to the cavity wall, only those containing silicones produced any effect of their own. The silicone greases were not used for most of this work.

The cavities were mounted on 'cold finger' type Dewars and could be cooled by conduction to liquid nitrogen or helium temperatures. They were exposed to the same vacuum conditions as the Dewar vacuum insulation walls. The Dewars were coupled to conventional hybrid-T bridge, microwave spectrometers operating at 9.2 and 23.0 Gc/s.

No resonance was observed in cavities which had only the siloxane film on the walls. This is consistent with the fact that E_{rf} is analytically zero at the walls. The observation is inconsistent with the assumption that the phenomenon is due to a low pressure gas breakdown. No resonance was observed in a 2 mm thick sample of siloxane, indicating that the results are not characteristic of the bulk compounds. No E.P.R. absorption was found which could be attributed to the siloxane.

Due to the fact that the diffusion pump utilized one of the siloxane compositions (No. 1, see table) as a pump fluid, blank runs and changes of sample composition were not completely satisfactory. It was found that with a siloxane-free sample and cavity it required a long pumping time with 12–15 hours of exposure to the diffusion pump fluid to deposit a siloxane film thick enough for the resonance. The negative result which occurred after 1–2 hours of pumping thus served as a blank run on the substrate and cryogenic cement. If a drop of siloxane was placed in the cavity, however, 1–2 hours pumping produced a film of adequate thickness. Obviously all samples were somewhat contaminated by the pump fluid composition. At present a siloxane-free Dewar and pump station are being constructed. It is not believed that the results to be expected from their use will modify the conclusions of the present work.

An upper limit to the film thickness was made with a Cary model 14 spectrophotometer with a 'fine slide wire' attachment. The phenyl groups present in most of the compositions produce strong optical absorption bands in the region of 2500–2700 Å. Dilute solutions of the siloxanes in spectroscopically pure *n*-heptane were used to establish the absorption strength, which is $\sim 10^4 \text{ cm}^{-1}$. From this number and the known minimum sensitivity of the spectrophotometer it was found that the film thickness must be less than 200 Å. This was true of films on substrates which had been exposed to the diffusion pump vapour for at least five times as long as was required to obtain the microwave resonance.

In the TE_{102} mode cavities which were used for most of this work, the substrate could be placed either on the cavity bottom or along a narrow side wall. The plane of the cyclotron orbit is parallel to the macroscopic substrate surface in the side wall position and perpendicular to the surface in the bottom position. The lack of differences in the resonance results for substrates in the two different positions is somewhat disturbing. However, it must be realized that all substrates had 'stair-steps' and other irregularities many times the cyclotron orbit diameter and thus always presented some surface which was parallel to the orbit plane.

2.2. The resonance

Figure 1 shows the first derivative of absorption with respect to magnetic field. The curve was taken with 400 cycle field modulation with amplitude much less than the line width. (Such derivative curves could also be observed with electric field modulation at audio frequencies and amplitudes of 1–10 v/cm.) The sharp rise and descent of the curve are the result of sudden changes in the number of carriers during the ionization.

The microwave electric field E_{rf} was less than 2 v/cm at the sample surface. This value corresponded to approximately 0.2 mw of power incident upon the cavity. The accuracy in power measurement was probably no better than a factor of two.

From a simple semi-classical treatment of cyclotron resonance [3] which assumes an isotropic, velocity independent, relaxation process, the mean collision time may be related to the half-width of the absorption curve. For figure 1, $\tau_R \sim 10^{-10}$ sec. The field position and frequency of the line centre are related by the cyclotron resonance condition $\nu = eB/2\pi m^*c$. The effective mass $m^* = (1.000 \pm 0.001)m$, where m is the free electron mass. Within experimental error m^* is the same at K-band frequencies.

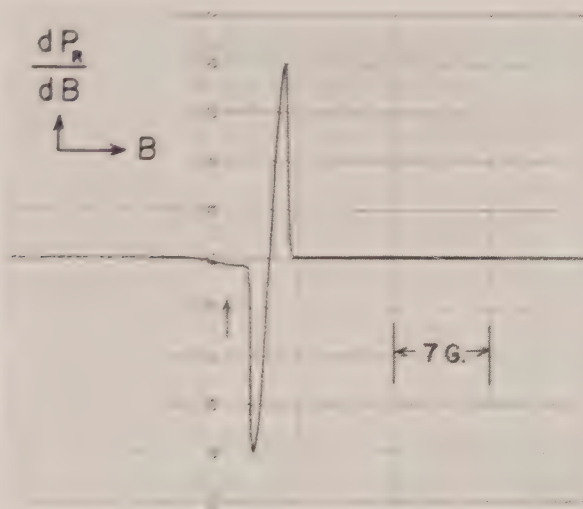


Figure 1. Diamagnetic resonance absorption derivative versus magnetic field at He temperature. The marked (arrow) peak is an E.P.R. line due to an impurity in the silica substrate.

The total number of carriers present, n , may be approximately determined by comparing the strength of the cyclotron resonance absorption with that of the E.P.R. absorption of a known quantity of the free radical DPPH. The computation depends upon the assumptions that (a) the ratio of an electric dipole transition probability to that of a magnetic dipole is 10^3 and (b) the effective absorption strength of magnetic dipoles is reduced by 10^3 due to the Boltzmann factor. For figure 1, n is at least 10^{10} electrons.

From the above data one may compute an electron mobility $\mu_R = e\tau_R/m^* \sim 10^6$ $\text{cm}^2/\text{V sec}$. It is to be emphasized that this number represents a purely 'local' mobility which is not to be associated with the long range transport properties of the bulk siloxanes.

If the carriers are assumed to be in quasi-thermal equilibrium with the substrate then the cyclotron orbit diameter may be computed. For the conditions of figure 1 it is of the order of 10^3 \AA .

2.3. Carrier avalanche

The data of figure 1 were observed at the lowest microwave power which produced carrier ionization. (The existence of this power threshold provides the sharpest distinction between diamagnetic resonance absorption and paramagnetic

resonance absorption.) At higher microwave power, n increases enormously and the impedance relationship between cavity and microwave line changes drastically. This impedance mis-match prevents an accurate observation of line shape and position at these power levels. Information may still be obtained however by measurements of the kind which are used for microwave breakdown in gases [2]. This procedure is shown in figure 2. One sets the microwave power at a known value and then sweeps the magnetic field toward the line from a low field, off-resonant value. At a certain value of magnetic field the carrier ionization avalanche occurs. This is indicated by a sudden increase in microwave power reflected from the cavity. This field position is noted and the field is lowered to an off-resonant position. The power is then changed and the process is repeated. After observing the low field side of the breakdown curve of figure 2 the data are completed by approaching the ionization onset from the off-resonant high field side.

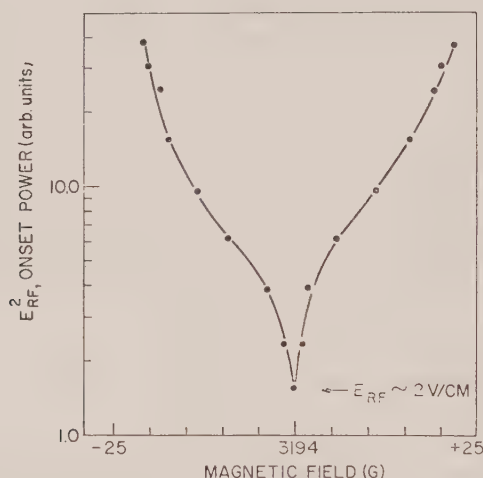


Figure 2. Ionization onset versus magnetic field; silica substrate at 80°K.

The shape of the curves and the power threshold are dependent upon ambient gas pressure and substrate temperature. These effects will be discussed later. It may be noted here that the width of the curves at the very lowest power correlates with the width of derivative curves similar to figure 1. It is reasonable then to assign the change in character of the curves at higher powers to a decrease in mean collision time and to assume that the width at any power level is inversely proportional to an effective collision time, τ_{eff} .

In making such measurements certain complications appear. If a sample has been held in an off-resonant field position for a time $(\Delta t)_1 \sim 30$ min, the sample does not become ionized and, even at the highest power, the resonance is not observed as the magnetic field is varied across the line. By adjusting the field to the line centre and waiting for a time $(\Delta t)_2$, the ionization takes place. After the sample is thus 'prepared' the data similar to figure 2 may be taken.

Figure 3 shows additional effects. If, after 'preparation', the field is increased from an off-resonant position to the point at which ionization takes place (path A) and then slowly lowered, the resonance remains 'on' to some lower field position

and then disappears. If the field is then immediately increased, path B is traced. The effect indicates that all carriers have not recombined after the ionization of path A was 'turned off' and that it is thus easier to start the second ionization (i.e. path B) at a lower field. We define the time $(\Delta t)_3$ as the wait time required between observations so that path A and path B coincide. This time is of the order of seconds at room temperature and of the order of minutes at liquid He temperatures. The times $(\Delta t)_1$ and $(\Delta t)_3$ are primarily the result of complicated carrier recombination processes. Figure 2 was plotted after the sample had been 'prepared' and after a time $(\Delta t)_3$ since the last ionization.

The wait time $(\Delta t)_2$ for a freshly evaporated sample varies in such a way as to suggest that it is influenced by molecular arrangement upon the substrate.

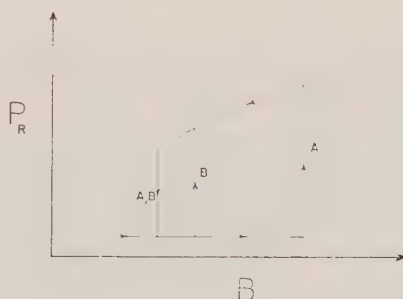


Figure 3. Constant power section of figure 2 (see text).

2.4. Molecular arrangement

Figure 4 shows an oscilloscope presentation of the reflected microwave power versus magnetic field at high microwave power. As was mentioned above, the shape of the curve is not relevant since it is distorted by cavity-microwave line mis-match. The significant observation here is the breakdown noise which is superposed upon the absorption curve. This noise, with components from low audio frequencies up to at least 200 kc/s, was used as a qualitative signature in the following experiments.

Samples were evaporated in the usual way, placed in a 9000 G magnetic field for 30 min, cooled to 80°K and then held for 30 min more. The field was then lowered to the X-band resonance value. For samples frozen with the polarizing field (9000 G) direction at right angles to the resonant field (3000 G), the wait time $(\Delta t)_2$ was of the order of seconds. The relative noise amplitude was similar to that of figure 4 which was taken after freezing the sample outside the magnetic field. When the polarizing field direction was parallel to the resonance field the time, $(\Delta t)_2$, was an order of magnitude greater and the ionization noise practically disappeared. The effect was quite reproducible. A sample could be repeatedly cycled by cooling in one polarizing field orientation, observing the resonance, warming to room temperature, recooling in the other orientation, etc. Experiments were performed by freezing the sample in the field near the edge of the magnet pole caps. They indicated that the effect is due to B and not $\text{grad } B$. Other experiments showed that the substrate position within the cavity during polarization was not relevant (see § 2.1). No polarizing effects were observed with electric fields up to 10^3 v/cm.

By assuming that the polarizing field orientation to produce the least noise and the longest $(\Delta t)_2$ is the one which gives the most ordered sample condition, one may draw some conclusions as to the precise molecular arrangement. The data at present do not warrant such discussion. However, the above results do suggest that the dipolar field of the substrate causes preferential ordering of the molecules and that, under certain circumstances, magnetic fields enhance the ordering. This view is not unreasonable in the light of the results obtained with certain liquid crystals which also have molecular dipole moments [13].

After the above observations were made, polysiloxane films upon KCl substrates were examined by high energy electron diffraction techniques [14]. The work was carried out with the electron beam at grazing incidence which means that the electrons penetrated only a few angstroms into the surface. Due to charging of the insulating substrate, the molecular orientation could not be obtained but the results supported the postulate of preferential order in the siloxane superstructure above the substrate.

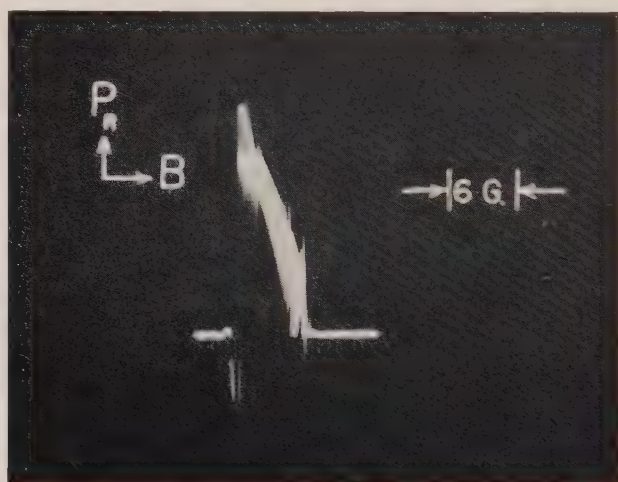


Figure 4. Reflected power versus magnetic field with KCl substrate at 80°K.
 $P \sim 10^{-4}$ torr.

2.5. Effect of residual gas and substrate temperature

Only very qualitative statements may be made here since the two parameters are interdependent due to cryogenic pumping in the experimental Dewar vessels. (a) With the Dewar at liquid He temperature the pressure at the room temperature vacuum wall was 5×10^{-6} torr. The sample, which in most cases faced only liquid He cooled surfaces, experienced a pressure only of gaseous He. From the natural fraction of He in the atmosphere, the sample pressure is estimated to be 5×10^{-10} torr. No attempts were made to vary the pressure at this temperature. (b) At 80°K the pressure at the outer vacuum wall was 5×10^{-4} torr. The sample pressure was estimated to be somewhat less than this value due to cryogenic pumping of H_2O . By adding either He or dry air, the pressures were varied from 5×10^{-4} to 0.5 torr. (c) At room temperature the pressure could be varied from 10^{-3} to 0.5 torr.

At 80°K and 5×10^{-4} torr the resonance plots and breakdown curves of the type of figures 1 and 2 are similar to the liquid He runs. At the higher temperature the minimum required threshold power is about a factor of two greater than at liquid He temperature and the 'long', $(\Delta t)_1$, carrier recombination time is about one tenth as long.

At 80°K it is possible to hold the sample temperature and vary the pressure independently. No significant differences are noted between the effects of ambients of He or dry air. As the pressure increases from 5×10^{-4} torr the minimum power threshold becomes greater. At 5×10^{-3} torr the noise which is superposed upon the resonance diminishes. Figure 5 shows this effect. In this pressure region $(\Delta t)_3$ remains approximately the same. The magnetic field separation between the onset of paths A and B of figure 3 increases

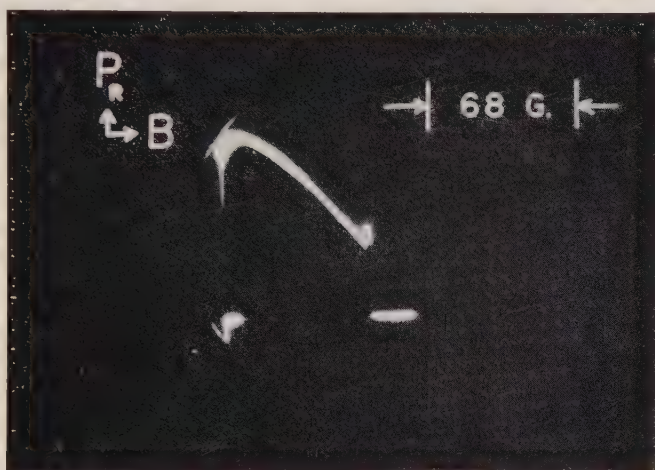


Figure 5. Same sample as figure 4, $P \sim 5 \times 10^{-3}$ torr; E_{rf} ten times greater.

with pressure. (That is, the resonance remains on for lower and higher field values which were non-resonant at the reduced pressure.) These two results indicate that at higher pressure either the carrier multiplication by orbiting electrons is more efficient in production of new carriers or the recombination time is longer. The width of curves such as figure 2 however does not seem to change much with pressure and, at lower power levels, τ_{eff} (see §2.3) is longer at higher pressure.

As the pressure is raised to 0.2 torr the resonance disappears. Although at room temperature the power threshold is about ten times greater than at 80°K , the pressure effects are qualitatively the same and the resonance disappears at about the same pressure.

The pressure effects are reversible. If the temperature is held constant at 80°K the low pressure results may be obtained by merely pumping down to the original pressure.

Although the above results are qualitative, some fairly definite conclusions concerning the *locale* of the carriers may be drawn from them. If the carriers are free electrons existing in the vacuum space of the cavity, then the mean

collision frequency for electron-gas molecule collisions, in He at least, is fairly independent of electron velocity [15], and one might expect that $\tau_{\text{eff}} \propto 1/P$. This is supported by Lax's work [2] where the width of the breakdown curves of the type of figure 2 above is very nearly proportional to pressure. This is contrary to the present results.

At the lowest pressures and powers, $\tau_R \sim 10^{-9}$ sec. At these pressures the reciprocal of the mean collision frequency in He gas is 1 sec. Thus the energy loss mechanism represented by τ_R is not related to electron-molecule collisions. At 0.2 torr, the reciprocal of mean collision frequency is still somewhat longer than τ_R and interparticle collisions could be expected to produce only slight effects rather than to completely prevent the resonance.

The residual gas effects are incompatible with the assumption that the carriers are in the vacuum space. However, all results are consonant with the hypothesis that they are on or near the siloxane surface. In this, one assumes that, at even the lowest pressures, the surface is 'dirty' (compared to the 'clean' surfaces which are obtainable by contemporary vacuum technique) because of residual gas adsorption. By this one means that the surface has adsorbed a large portion of the total residual gas which may be held at any given temperature [16]. All effects of residual gas may be ascribed to collisions of the carriers with adsorbed residual gas molecules. The small changes in the phenomena with pressure are then attributed to a condition where the curve of the number of adsorbed molecules *versus* pressure is almost saturated.

2.6. K-band results

At K-band the microwave frequency and photon energy are approximately three times those at X-band. All other things being equal (temperature, substrate, sample composition and cavity vibrational mode) no resonance was observed at a microwave power level which was approximately 30 times the minimum threshold power at X-band.

A cylindrical bi-modal cavity was constructed which resonated in the TE_{111} mode at X-band and in the TM_{113} mode at K-band. For a sample mounted at the base of the cavity E_{rf} had the same direction for both modes. In both modes the Q of the cavity was approximately ten times that in the rectangular TE_{102} cavities which were used in the earlier part of the work. The increase in E_{rf} at K-band due to the different mode and higher Q permitted the observation of the diamagnetic resonance at K-band.

Within experimental error m^* is the same at the two frequencies. Regarding the microwave photon number as proportional to (power/ν^2) , the number of photons for minimum ionization threshold at K-band, and at 80°K, is somewhat larger but of the same order of magnitude as that for X-band.

It was possible to 'prepare' the sample (see §2.3) at one frequency and then quickly change the magnetic field to observe it at the other frequency. There were no observable changes in the resonance at one frequency when the other frequency was suddenly 'turned on'. No effects were observed with exposure during resonance, of the sample to light from a strong photographic lamp. A small α -particle emitter which was placed in the sample cavity also produced no obvious differences. This is consistent with the earlier results and indicates merely that the initial number of carriers produced by any mechanism is very small compared to those resulting from cyclotron resonance multiplication.

It should also be mentioned that with this cavity, the maximum value of field is $E_{rf} \sim 400$ v/cm; at these fields and at a relatively high pressure of ~ 1.0 torr, a resonance was observed which could be attributed to residual gas breakdown [2].

2.7. Electric field effects

By applying thin silver paste electrodes to the edges of fused silica plates and using the plates as substrates it was possible to apply electric fields tangential to the siloxane films. Conductivity measurements at d.c. fields of ~ 100 v/cm were made with a G.R. mod. 544 B impedance bridge. With the sample at low temperatures and the magnetic field in an off-resonant position the resistance of the film was greater than 10^{12} ohms. When the magnetic field was turned to the resonance centre, the resistance dropped to the order of 10^8 ohms. If the electrodes are spaced d cm apart and the total number of carriers n is measured by the resonance intensity, then the mobility tangential to the film, *during resonance*, is $\mu_{d.c.} = (d^2/eRn)$ (where e is the electronic charge and R is the resistance). It was found that $\mu_{d.c.} \sim 1$ cm²/v/sec which is of the same order of magnitude as the bulk mobilities found in organic single crystals by photoconductivity methods [5]. It is to be noted that this is several orders of magnitude smaller than the 'local' mobility, μ_R , obtained from the resonance parameters.

Depending upon the microwave power level it was possible to suppress the resonance by applying the d.c. electric field. At the highest microwave power this suppression required fields of the order of 1000 v/cm. As mentioned earlier, absorption derivative curves could be obtained by applying an audio frequency field to the electrodes.

In another experiment an insulated, polished copper post was inserted through the bottom of the cavity and a siloxane film was evaporated upon it. Potentials of the order of 10^2 – 10^3 v which were applied between the post and the cavity produced fields radial to the film and, during resonance, currents could be drawn from the post to the cavity through the vacuum space. The results were poorly reproducible due to destruction of the film during the measurements. Although films on insulator substrates withstood hours of observation under the highest microwave power, the resonance intensity of the copper substrate films dropped noticeably after only a few minutes with applied d.c. electric fields. Regarding all charge as originating at the post (the zero E_{rf} fields at the cavity walls should permit no charge to arise there), at 80°K the sign of the net charge was negative, at helium temperatures the sign was positive. At present one may only speculate that either electrons or ions may be drawn from the post depending on the temperature and field polarity.

To check the rather unlikely possibility that the initial carriers are liberated by direct microwave field ionization, bulk d.c. conductivity measurements were made in the presence and absence of microwave irradiation (both measurements were in the absence of the magnetic field). The sample was outgassed by vacuum boiling and transferred to a cavity which could be evacuated. The sample partially filled a TE₀₁₁ cavity whose bottom plate was electrically insulated from the cylindrical walls. Room temperature conductivity was measured by observing the time rate of charge of a standard capacitor. The potential detector was a Cary model 31 vibrating reed electrometer. Within experimental error no effects were observed which could be attributed to direct microwave field ionization. If one assumes a bulk mobility of the order of that for the tangential film mobility, the experiment sets an upper limit of 10^4 electrons/cm³.

From long term changes in the conductivity with fluctuations in room temperature, an estimate of 0.3–0.5 eV was obtained for the activation energy for conduction.

3. DISCUSSION

From the extremely long carrier recombination times and the film orientation effects it is evident that the phenomena reported above originate, at least at low temperatures, in the solid state. The ambient gas effects indicate that the carriers are not free electrons in the cavity vacuum space. The low value of $\mu_{\text{d.c.}}$, the absence of resonance in the bulk siloxanes and the thickness of the films relative to the computed orbit diameter all suggest that the carriers are localized on the film surface. Two possible interpretations of the phenomena may be given.

(A) At pressures below 10^{-5} torr, a pressure-independent, electron avalanche has been observed in electrodeless discharge tubes [17]. The avalanche occurred only at certain critical relationships between the frequency and amplitude of the applied field and the physical dimensions of the discharge tube. The explanation is that a stray electron in the tube near one wall may be accelerated to the opposite wall during one portion of the r.f. cycle. If the frequency, and tube dimensions have the proper relations to one another the electron may pass across the tube in one half-cycle. If the field amplitude is large enough, the incident electron may have great enough energy to liberate secondary electrons which are in positions to reverse the first traverse of the tube in phase with the r.f. Evidence was also found for avalanches which originated with electrons requiring two and three, half-cycles to cross the tube.

To interpret the present data in terms of this effect one would expect the analogue of the discharge tube walls to be the random surface irregularities of the substrates. The secondary electron emission ratio would necessarily approach unity at energies corresponding to the lowest microwave threshold value of E_{rf} . Although it has not been possible to perform an experiment which definitely eliminates this interpretation, the above considerations lead us to favour another one.

(B) It is assumed that the evidence for a preferred orientation of molecules in the films is support for a discussion in terms of simple band theory. In the problem of the interaction of an electron with a periodic potential, Tamm [7] first pointed out that if one uses a finite boundary condition rather than the usual infinite or cyclic conditions, additional allowed levels arise. From this and later work [18, 19] it seems that in the case of 'non-crossing' bands, the new 'surface' levels should appear just above the valence band and just above the conduction band.

There have been no previous experimental results concerning insulator surface states and the existing theory is inadequate for a detailed picture of their properties. The behaviour of the carriers on siloxane surfaces is more characteristic of loosely bound trapping states than of carriers moving in allowed bands. The long range transport resembles a 'hopping' movement (between high mobility points) with a mobility which is of the order of magnitude expected for the bulk samples.

In so far as a band theory model [5] can be applied to a two dimensional array of siloxane molecules, we expect the following: very narrow, low mobility bands with a forbidden gap of at least 6 eV (the optical 'edge' starts at $\sim 2300 \text{ \AA}$); excitation levels due to the phenyl groups near 4.5 eV; and a set of surface levels

just above each allowed band. Assuming the carriers are intrinsic electrons, the surface levels must be a few tenths of an electron volt above the filled band in order to account for the weak temperature dependence of the resonance. No attempt has been made to incorporate the residual gas effects into this model.

Although the multiplication of the initial carriers appears to be a straightforward, impact ionization process, the mechanism by which the few initial carriers are produced is uncertain. Either room temperature radiation from the top of the Dewars or microwave dielectric heating could produce a small population in the final state. The behaviour of the wait time $(\Delta t)_2$ (§ 2.3) with power gives support to the latter mechanism.

In recent work with anthracene single crystals [20], it has been found that carriers are produced when excitons migrate to a crystal surface. At present there is no information which excludes the possibility that in the siloxanes an exciton is the intermediary between the initial, low mobility state and the final, high mobility state.

Although this simple model is in accord with current experimental and theoretical information, it must be emphasized that at best, it is a very tentative one. Much more sophisticated experiments must be devised before it can be verified. At present the most promising approach for future work appears to be experiments using very clean metal substrates.

The authors wish to thank A. U. McRae for permission to quote the results of the electron diffraction work. They are further indebted to D. L. Mitchell, J. H. Woodson, and S. Teitler for a number of stimulating and informative discussions and to V. Ritz for the use of the d.c. conductivity apparatus. J. M. Nielson of G. E. Co. very kindly contributed the completely methylated siloxane sample.

REFERENCES

- [1] KIP, A. F., LANGENBERG, D. N., ROSENBLUM, B., and WAGONER, G., 1957, *Phys. Rev.*, **108**, 494.
- [2] LAX, B., ALLIS, W. P., and BROWN, S. C., 1950, *J. appl. Phys.*, **21**, 1297.
- [3] DRESSELHAUS, G., KIP, A. F., and KITTEL, C., 1955, *Phys. Rev.*, **98**, 368.
- [4] DEXTER, R. N., ZEIGER, H. J., and LAX, B., 1954, *Phys. Rev.*, **95**, 557.
- [5] FRIEDMAN, L., 1964, *Phys. Rev.*, **A**, **133**, 1668.
- [6] SAMUEL, A. H., HALLIDAY, F. O., KEAST, A. K., and TAIMUTY, S. I., 1964, *Proc. nat. Acad. Sci., Wash.*, **51**, 839.
- [7] TAMM, I., 1932, *Phys. Z. Sowjet.*, **1**, 733.
- [8] THOMAS, D. D., KELLER, H., and MCCONNELL, H. M., 1963, *J. chem. Phys.*, **39**, 2321.
- [9] WILCOCK, D. F., 1946, *J. Amer. chem. Soc.*, **68**, 691.
- [10] BAUER, S. H., 1950, *Non-Crystalline Solids*, Ed. by V. D. Frechette (New York: John Wiley), p. 74.
- [11] DIELECTRIC MATERIALS AND APPLICATIONS, 1954, Ed. by A. von Hippel (New York: John Wiley), p. 366.
- [12] SYNTHETIC LUBRICANTS, 1962, Ed. by R. L. Gunderson and A. W. Hart (New York: Reinhold), p. 275.
- [13] CARR, E. F., 1963, *J. chem. Phys.*, **39**, 1979.
- [14] McRAE, A. U. (personal communication).
- [15] HANDBOOK OF PHYSICS, 1958, Ed. by E. U. Condon, and H. Odishaw (New York: McGraw-Hill), p. 4.
- [16] DUSHMAN, S., 1949, *Vacuum Technique* (New York: John Wiley), p. 387.
- [17] GILL, E. W. B., and VAN ENGEL, A., 1949, *Proc. roy. Soc. A*, **197**, 107.
- [18] GOODWIN, E. T., 1939, *Proc. Camb. phil. Soc.*, **35**, 205, 221, 232.
- [19] PUGH, D., 1964, *Phys. Rev. Letters*, **12**, 390.
- [20] KEPLER, R. G., 1960, *Phys. Rev.*, **119**, 1226.

The vibrational selection rules and torsional barrier of ferrocene

by P. R. BUNKER

Department of Theoretical Chemistry,
University Chemical Laboratory, Cambridge

(Received 15 December 1964)

The double group of the molecular symmetry group of ferrocene is used to classify the rotational and torsional wavefunctions and the 'approximate normal coordinates' of the molecule. The approximate normal coordinates do not depend on either the torsional angle or the torsional quantum number, and from their symmetry species the infra-red and Raman selection rules are determined. It is also shown how an ultra-high resolution analysis of some of the infra-red bands might yield the height of the torsional barrier.

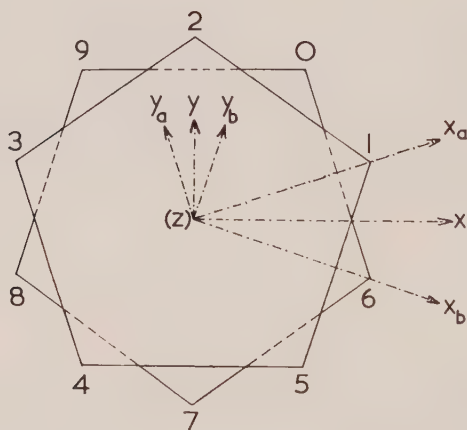
1. INTRODUCTION

In a previous paper [1] it was shown how to determine the vibrational selection rules of dimethylacetylene by using approximate normal coordinates that do not depend on the torsional quantum number. It has also been shown [2] how to determine the torsional barrier of dimethylacetylene from the fine structure of some of the infra-red bands. In this paper these ideas are applied to the interpretation of the infra-red and Raman spectra of ferrocene. It is shown how to determine the symmetry species of the approximate normal coordinates from the transformation properties of the internal coordinates.

2. THE SYMMETRY GROUP

Longuet-Higgins [3] has defined the molecular symmetry group of a non-rigid molecule and he has shown how to use the group to classify the rotational-torsional wavefunctions of such molecules. In order to classify separately the rotational, torsional and vibrational wavefunctions of molecules such as dimethylacetylene and ferrocene that have co-axial internal rotors it is necessary to use the double group of the molecular symmetry group of the molecule. Hougen [4] first realized this and used the group to classify the states of dimethylacetylene. The molecular symmetry group of ferrocene (G_{100}) has been obtained previously [5] and we will now determine its double group.

The atom numbering convention is shown in the figure together with the molecule-fixed xyz -axes and the rotor-fixed $x_a y_a$ - and $x_b y_b$ -axes. These axis systems are defined when the molecule is in a potential energy minimum configuration and their common origin is the centre of gravity of the molecule. We will label the centre of gravity of ring '12345' as O_a and that of ring '67890' as O_b . The z -axis points in the direction $O_b \rightarrow O_a$ and its orientation in space is measured by the Eulerian angles θ and ϕ . The angle of twist of the x_a -axis (which rotates in the C_1-O_a-Fe plane) is χ_a , and that of the x_b -axis (which rotates in the C_6-O_b-Fe plane) is χ_b . We define the angles $\gamma = (\chi_a - \chi_b)/2$ and $\chi = (\chi_a + \chi_b)/2$; the angle of twist of the x -axis is defined to be χ . The angles χ and γ are not single-valued functions of the molecular configuration and because of this we must use the double group to classify separately the rotational, torsional and vibrational wavefunctions.



The atom numbering convention used and the definitions of the axis systems.

The molecular symmetry group of this molecule is generated by the four operators A^2 , B^2 , C and D where

$$A^2 \equiv (12345)^2 = (13524),$$

$$B^2 \equiv (67890)^2 = (68079),$$

$$C \equiv (16)(20)(39)(48)(57)^*,$$

$$D \equiv (25)(34)(70)(89)^*,$$

and A^2 and B^2 are of order 5. The group has 100 elements which divide into 16 classes. The double group G_{100}^\dagger is the direct product of this group and the group that consists of the two elements E and A^5 . The character table of G_{100}^\dagger is shown in the Appendix. The transformation properties of the Eulerian angles under the effect of the operators A , B , C and D are shown in table 1.

E	A	B	C	D
θ	θ	θ	θ	$\pi - \theta$
ϕ	ϕ	ϕ	ϕ	$\phi + \pi$
χ_a	$\chi_a - \frac{2\pi}{5}$	χ_a	$\chi_b + \pi$	$-\chi_a - \pi$
χ_b	χ_b	$\chi_b + \frac{2\pi}{5}$	$\chi_a + \pi$	$-\chi_b - \pi$
χ	$\chi - \frac{2\pi}{10}$	$\chi + \frac{2\pi}{10}$	$\chi + \pi$	$-\chi - \pi$
γ	$\gamma - \frac{2\pi}{10}$	$\gamma - \frac{2\pi}{10}$	$-\gamma$	$-\gamma$

Table 1. The transformation properties of the Eulerian angles.

3. THE SYMMETRY CLASSIFICATION OF THE ROTATIONAL AND TORSIONAL WAVEFUNCTIONS

The rotational-torsional wavefunctions of the molecule, assuming it to have a zero torsional barrier, are of the form:

$$\Psi_{\text{RT}} = S_{JKM}(\theta, \phi) \exp(ik_a \chi_a) \exp(ik_b \chi_b),$$

where $K = |k_a + k_b|$. We can rewrite this as:

$$\Psi_{\text{RT}} = S_{JKM}(\theta, \phi) \exp(ik\chi) \exp(iL_s \gamma),$$

where $k = k_a + k_b$, $L_s = k_a - k_b$, and $L = |L_s|$. We define the rotational wavefunction to be:

$$\Psi_{\text{R}} = S_{JKM}(\theta, \phi) \exp(ik\chi)$$

and the torsional wavefunction to be:

$$\Psi_{\text{T}} = \exp(iL_s \gamma).$$

Value of K	0	$5n \pm 1$	$5n \pm 2$	$5n$
Rotational	A_{1s} (J even)	E_{5s} (K even)	E_{7s} (K even)	$A_{1s} + A_{2s}$ (K even)
Species	A_{2s} (J odd)	E_{6d} (K odd)	E_{8d} (K odd)	$A_{3d} + A_{4d}$ (K odd)
Values of L	0	$5n \pm 1$	$5n \pm 2$	$5n$
Torsional	A_{1s}	E_{1s} (L even)	E_{3s} (L even)	$A_{1s} + A_{3s}$ (L even)
Species		E_{1d} (L odd)	E_{3d} (L odd)	$A_{1d} + A_{3d}$ (L odd)

Table 2. The species of the rotational and torsional wavefunctions of ferrocene in G_{100}^\dagger .

The wavefunctions Ψ_R and Ψ_T are not single-valued and they cannot be classified in G_{100} although we can heuristically derive species which will multiply to give the correct overall species of Ψ_{RT} [5]. However, they can be classified separately in G_{100}^\dagger using the results of table 1. The species of the rotational and torsional wavefunctions are given in table 2. In Ψ_{RT} the quantum numbers K and L must have the same parity so that the wavefunction is single-valued.

4. THE SYMMETRY CLASSIFICATION OF THE APPROXIMATE NORMAL COORDINATES

The exact normal coordinates of this molecule, like those of dimethylacetylene [1], will depend on both the torsional angle γ and the torsional quantum number L . Using these exact normal coordinates it is impossible to obtain separate vibrational selection rules. However, by approximating the potential function we can obtain approximate normal coordinates that are independent of γ and L . The approximation involved is that of ignoring the coupling of the degenerate vibrations of the cyclopentadienyl rings across the Fe atom, and it means that these vibrations will be four-fold degenerate. From the species of these approximate normal coordinates in G_{100}^\dagger we can determine the vibrational selection rules. In this section we show how the species of the approximate normal coordinates can be obtained.

Assuming the torsional barrier to be zero there will be 56 vibrational normal coordinates and they will be functions of changes in the internal coordinates. The species of the 56 *approximate* normal coordinates (not involving γ) will be the same as that of 56 independent internal coordinate changes (not including changes in γ). The internal coordinates are defined below:

r_i is the length of the C_i-H_i bond,

r_{ij} is the length of the C_i-C_j bond,

ρ_i is the angle between the C_i-H_i bond and the $C_{i-1}-C_i-C_{i+1}$ plane,

$$\epsilon_1 = \alpha_1 - \alpha_2, \quad \epsilon_2 = \alpha_3 - \alpha_4, \quad \text{etc. up to } \epsilon_{10},$$

and

$$\sigma_1 = \alpha_1 + \alpha_2, \quad \sigma_2 = \alpha_3 + \alpha_4, \quad \text{etc. up to } \sigma_{10},$$

where α_1 is the angle $H_1-C_1-C_5$, α_2 is the angle $C_2-C_1-H_1$, α_3 is the angle $H_2-C_2-C_1$, α_4 is the angle $C_3-C_2-H_2$, and so on up to α_{20} .

β_i is the angle $Fe-O_a-C_i$ or $Fe-O_b-C_i$,

r is the length of $Fe-O_a$,

r' is the length of $Fe-O_b$,

ϕ_x is the angle O_a-Fe-O_b measured in the xz -plane, and

ϕ_y is the angle O_a-Fe-O_b measured in the yz -plane.

The species in G_{100}^\dagger of sets of equivalent internal coordinate changes are:

$$\Gamma(\Delta r_i) = A_{1s} + A_{4s} + G_{1s} + G_{4s},$$

$$\Gamma(\Delta r_{ij}) = A_{1s} + A_{4s} + G_{1s} + G_{4s},$$

$$\Gamma(\Delta \rho_i) = A_{1s} + A_{4s} + G_{1s} + G_{4s},$$

$$\Gamma(\Delta \epsilon_i) = A_{2s} + A_{3s} + G_{1s} + G_{4s},$$

$$\Gamma(\Delta \sigma_i) = A_{1s} + A_{4s} + G_{1s} + G_{4s} \text{ (the } A_{1s}, A_{4s} \text{ and } G_{1s} \text{ combinations are redundant),}$$

$$\Gamma(\Delta \beta_i) = A_{1s} + A_{4s} + G_{1s} + G_{4s} \text{ (the } A_{1s} \text{ and } A_{4s} \text{ combinations are redundant),}$$

$$\Gamma(\Delta r, \Delta r') = A_{1s} + A_{4s}, \text{ and}$$

$$\Gamma(\Delta \phi_x, \Delta \phi_y) = E_{6d}.$$

Thus the species in G_{100}^\dagger of the approximate normal coordinates are[†],

$$\Gamma_v = 4A_{1s} + A_{2s} + A_{3s} + 4A_{4s} + 5G_{1s} + 6G_{4s} + E_{6d}.$$

Frequency number	Description	Species
1	Sym. C-H stretching	A_{1s}
2	Sym. C-H bending (\perp)	A_{1s}
3	Sym. ring breathing	A_{1s}
4	Sym. ring-metal stretching	A_{1s}
5	C-H bending (\parallel)	A_{2s}
6	C-H bending (\parallel)	A_{3s}
7	C-H stretching	A_{4s}
8	C-H bending (\perp)	A_{4s}
9	Anti-sym. ring breathing	A_{4s}
10	Anti-sym. ring-metal stretching	A_{4s}
11	C-H stretching	G_{1s}
12	C-H bending (\parallel)	G_{1s}
13	C-H bending (\perp)	G_{1s}
14	Sym. C-C stretching	G_{1s}
15	Sym. ring tilt	G_{1s}
16	C-H stretching	G_{4s}
17	C-H bending (\parallel)	G_{4s}
18	C-H bending (\perp)	G_{4s}
19	C-C stretching	G_{4s}
20	Ring distortion (\parallel)	G_{4s}
21	Ring distortion (\perp)	G_{4s}
22	Ring-metal-ring bending	E_{6d}

Table 3. A description of the symmetry coordinates of ferrocene.

[†] The reader should be warned against attempting to determine the species of the normal coordinates from the transformation properties of the Cartesian displacement coordinates. Using the molecular symmetry group the transformed Cartesian displacement coordinates are not generally infinitesimal and do not bear a simple relation to the untransformed (infinitesimal) displacement coordinates.

Approximate descriptions of these coordinates and their species in G_{100}^\dagger are given in table 3. In this the \parallel and \perp signs describe vibrations that are in the planes of or perpendicular to the planes of the cyclopentadienyl rings.

With dimethylacetylene the introduction of the coupling of the degenerate methyl group vibrations across the acetylene bond changes the G_s coordinates into coordinates that involve γ , and these coordinates are of species $E_{1d} + E_{2d}$ in G_{36}^\dagger . For ferrocene the coupling of the degenerate vibrations changes the G_{1s} coordinates into coordinates of species $E_{5d} + E_{6d}$ and the G_{4s} coordinates into coordinates of species $E_{7d} + E_{8d}$.

Table 3 should be compared with table 5 in the paper of Lippincott and Nelson [6] in which the coordinates are classified in the symmetry group D_{5d} . Note the correlation of the species of D_{5d} with those of G_{100}^\dagger ,

	A_{1g} with A_{1s} ,
	A_{1u} with A_{3s} ,
	A_{2g} with A_{2s} ,
	A_{2u} with A_{4s} ,
	E_{1g} and E_{1u} with $G_{1s} = E_{5d} + E_{6d}$ after coupling,
	E_{1u} (skeletal bend) with E_{6d} ,
and	E_{2g} and E_{2u} with $G_{4s} = E_{7d} + E_{8d}$ after coupling.

5. THE VIBRATIONAL SELECTION RULES

In table 3 we have given the symmetry species of the approximate normal coordinates when expressed in terms of internal coordinate changes. In table 4 we give the species of the components of the dipole moment operator and polarizability tensor along the molecule-fixed and rotor-fixed axes shown in the figure. We can easily deduce from these results that in the infra-red spectrum

$$\begin{aligned}
 \Gamma(\mu_z) &= A_{4s}, \\
 \Gamma(\mu_{x_a}, \mu_{y_a}, \mu_{x_b}, \mu_{y_b}) &= G_{1s}, \quad \Gamma(\mu_x, \mu_y) = E_{6d} \\
 \Gamma(\alpha_{z^2}) &= \Gamma(\alpha_{x^2+y^2}) = \Gamma(\alpha_{x_a^2+y_a^2+x_b^2+y_b^2}) = A_{1s} \\
 \Gamma(\alpha_{xz}, \alpha_{yz}) &= E_{5d}, \quad \Gamma(\alpha_{xy}, \alpha_{x^2-y^2}) = E_{7s} \\
 \Gamma(\alpha_{x_a z}, \alpha_{y_a z}, \alpha_{x_b z}, \alpha_{y_b z}) &= G_{1s} \\
 \Gamma(\alpha_{x_a^2-y_a^2}, \alpha_{x_a y_a}, \alpha_{x_b^2-y_b^2}, \alpha_{x_b y_b}) &= G_{4s}
 \end{aligned}$$

Table 4. The species in G_{100}^\dagger of the components of the polarizability tensor and dipole moment operator.

there will be four parallel fundamental bands (ν_7 - ν_{10}). In the infra-red spectrum there will also be six perpendicular fundamental bands; one will be the skeletal bending band ν_{22} and the others will be the five G_{1s} type bands ν_{11} - ν_{15} . In the Raman spectrum there will be four polarized bands (ν_1 - ν_4) and eleven depolarized bands (ν_{11} - ν_{21}). Of the depolarized Raman bands the five of species G_{1s} (ν_{11} - ν_{15}) will have $\Delta K = \pm 1$ selection rules and the six of species G_{4s} (ν_{16} - ν_{21}) will have $\Delta K = \pm 2$ selection rules.

The first excited states of each of the five G_{18} vibrations are infra-red and Raman active and there could be five coincidences of fundamental bands. Coupling of these vibrations across the metal atom will remove these coincidences [1]. For a particular one of these five vibrations the extent of the coupling is measured by the degree to which the Raman and infra-red frequencies are split (i.e. the differences $\nu_{12}-\nu_{17}$, $\nu_{13}-\nu_{18}$, $\nu_{14}-\nu_{19}$, $\nu_{15}-\nu_{20}$ and $\nu_{16}-\nu_{21}$ using Lippincott and Nelson's numbering convention). From the work of Lippincott and Nelson we see that the coupling is only significant for the ring tilting vibration ($\nu_{16}-\nu_{21} = -114 \text{ cm}^{-1}$).

6. THE INFRA-RED PERPENDICULAR FUNDAMENTAL BANDS AND THE TORSIONAL BARRIER

The Q -branches in each of the G_{18} infra-red perpendicular fundamental bands will occur in bunches. If the torsional barrier and vibrational coupling potential for the vibration are both zero then the separation of the bunches will be $4A(1-\zeta_i)-2B$ and the spacing within each bunch will be $2B$ ($\approx 0.05 \text{ cm}^{-1}$), where A and B are the inertial constants for the whole molecule and ζ_i is the Coriolis coupling constant for the vibration concerned. It was shown in [5] that a torsional barrier of the form

$$V_5/2 \cos 5(\chi_b - \chi_a)$$

splits the ground vibrational state levels for which $L = |k_a - k_b| = 5$. Thus the most easily observed effect of a torsional barrier on the perpendicular band is the splitting of the Q -branches that result from transitions from the ground state levels for which $L = 5$. If we could resolve this splitting then we could determine the height of the torsional barrier.

ACKNOWLEDGEMENTS

I would like to thank Professor H. C. Longuet-Higgins, F.R.S., and Dr. A. J. Stone, for discussions. I acknowledge a D.S.I.R. research studentship.

REFERENCES

- [1] BUNKER, P. R., 1965, *J. chem. Phys.*, **42**, 2991.
- [2] BUNKER, P. R., and LONGUET-HIGGINS, H. C., 1964, *Proc. roy. Soc. A*, **280**, 340.
- [3] LONGUET-HIGGINS, H. C., 1963, *Mol. Phys.*, **6**, 445.
- [4] HOUGEN, J. T., 1964, *Canad. J. Phys.*, **40**, 1920.
- [5] BUNKER, P. R., 1964, *Mol. Phys.*, **8**, 81.
- [6] LIPPINCOTT, E. R., and NELSON, R. D., 1958, *Spectrochim. Acta*, **10**, 307.

APPENDIX

The character table of G_{100}^\dagger

E	A^6B^6	A^2B^2	C	A^6B^4	A^2	A^6B^8	A^2C	A^3B^8	A^4	A^6C	CD	A^2CD	A^6CD	D
1	1	2	5	2	4	4	10	2	4	10	5	10	10	25
A_{1s}	1	1	1	1	1	1	1	1	1	1	1	1	1	1
A_{2s}	1	1	1	1	1	1	1	1	1	1	-1	-1	-1	-1
A_{3s}	1	1	-1	1	1	1	-1	1	1	-1	1	1	1	-1
A_{4s}	1	1	-1	1	1	1	-1	1	1	-1	-1	-1	-1	1
E_{1s}	2	2a	0	2	2a	2b	0	2	2b	0	2	2a	2b	0
E_{2s}	2	2a	0	2	2a	2b	0	2	2a	0	-2	-2a	-2b	0
E_{3s}	2	2b	0	2	2b	2a	0	2	2a	0	2	2b	2a	0
E_{4s}	2	2a	0	2	2a	2a	0	2	2a	0	-2	-2b	-2a	0
E_{5s}	2	2	2	2a	2a	2a	2a	2b	2b	2b	0	0	0	0
E_{6s}	2	2	-2	2a	2a	2b	-2a	2b	2b	-2b	0	0	0	0
E_{7s}	2	2	2	2b	2b	2b	2b	2a	2a	2a	0	0	0	0
E_{8s}	2	2	-2	2b	2b	2b	-2b	2a	2a	-2a	0	0	0	0
G_{1s}	4	4a	0	4a	4a ²	4ab	0	4b	4b ²	0	0	0	0	0
G_{2s}	4	4b	0	4a	4ab	4a ²	0	4b	4ab	0	0	0	0	0
G_{3s}	4	4a	0	4b	4ab	4b ²	0	4a	4a ²	0	0	0	0	0
G_{3s}	4	4b	0	4b	4b ²	4ab	0	4a	4ab	0	0	0	0	0
A_{1d}	1	1	1	1	1	1	1	1	1	1	1	1	1	1
A_{2d}	1	1	1	1	1	1	1	1	1	1	-1	-1	-1	-1
A_{3d}	1	1	-1	1	1	1	-1	1	1	-1	-1	-1	-1	1
A_{4d}	1	1	-1	1	1	1	-1	1	1	-1	-1	-1	-1	1
E_{1d}	2	2a	0	2	2a	2b	0	2	2b	0	2	2a	2b	0
E_{2d}	2	2a	0	2	2a	2b	0	2	2b	0	-2	-2a	-2b	0
E_{3d}	2	2b	0	2	2b	2a	0	2	2a	0	2	2b	2a	0
E_{4d}	2	2b	0	2	2b	2a	0	2	2a	0	-2	-2b	-2a	0
E_{5d}	2	2	2	2a	2a	2a	2a	2b	2b	2b	0	0	0	0
E_{6d}	2	2	-2	2a	2a	2b	-2a	2b	2b	-2b	0	0	0	0
E_{7d}	2	2	2	2b	2b	2b	2b	2a	2a	2a	0	0	0	0
E_{8d}	2	2	-2	2b	2b	2b	-2b	2a	2a	-2a	0	0	0	0
G_{1d}	4	4a	0	4a	4a ²	4ab	0	4b	4ab	0	0	0	0	0
G_{2d}	4	4b	0	4b	4ab	4a ²	0	4b	4b ²	0	0	0	0	0
G_{3d}	4	4a	0	4b	4ab	4b ²	0	4a	4a ²	0	0	0	0	0

	A^5	AB^6	A^7B^2	A^5C	AB^4	A^7	AB^8	A^7C	A^7B^8	AB^2	A^9	AC	A^5CD	A^7CD	ACD	A^{5D}
A_{1s}	1	1	1	1	1	1	1	1	1	1	1	10	5	10	10	25
A_{2s}	1	1	1	1	1	1	1	1	1	1	1	1	-1	-1	-1	1
A_{3s}	1	1	1	-1	1	1	1	-1	1	1	1	-1	1	1	1	-1
A_{4s}	1	1	1	-1	1	1	1	-1	1	1	1	-1	-1	-1	-1	1
E_{1s}	2	2a	2b	0	2	2a	2b	0	2	2a	2b	0	2	2a	2b	0
E_{2s}	2	2a	2b	0	2	2a	2b	0	2	2a	2b	0	-2	-2a	-2b	0
E_{3s}	2	2b	2a	0	2	2b	2a	0	2	2b	2a	0	2	2b	2a	0
E_{4s}	2	2b	2a	0	2	2b	2a	0	2	2b	2a	0	-2	-2b	-2a	0
E_{5s}	2	2	2	2	2a	2a	2a	2a	2b	2b	2b	2b	0	0	0	0
E_{6s}	2	2	2	-2	2a	2a	2a	-2a	2b	2b	2b	-2b	0	0	0	0
E_{7s}	2	2	2	2	2b	2b	2b	2b	2a	2a	2a	2a	0	0	0	0
E_{8s}	2	2	2	-2	2b	2b	2b	-2b	2a	2a	2a	-2a	0	0	0	0
G_{1s}	4	4a	4b	0	4a	4a ²	4ab	0	4b	4ab	4b ²	0	0	0	0	0
G_{2s}	4	4b	4a	0	4a	4a ²	4a ²	0	4b	4b ²	4ab	0	0	0	0	0
G_{3s}	4	4a	4b	0	4b	4ab	4b ²	0	4a	4a ²	4ab	0	0	0	0	0
G_{4s}	4	4b	4a	0	4b	4b ²	4ab	0	4a	4ab	4a ²	0	0	0	0	0
A_{1d}	-1	-1	-1	-1	-1	-1	-1	-1	-1	-1	-1	-1	-1	-1	-1	-1
A_{2d}	-1	-1	-1	-1	-1	-1	-1	-1	-1	-1	-1	-1	1	1	1	1
A_{3d}	-1	-1	-1	1	-1	-1	-1	1	-1	-1	-1	-1	1	1	1	1
A_{4d}	-1	-1	-1	1	-1	-1	-1	1	-1	-1	-1	1	1	1	1	-1
E_{1d}	-2	-2a	-2b	0	-2	-2a	-2b	0	-2	-2a	-2b	0	-2	-2a	-2b	0
E_{2d}	-2	-2a	-2b	0	-2	-2a	-2b	0	-2	-2a	-2b	0	2	2a	2b	0
E_{3d}	-2	-2b	-2a	0	-2	-2b	-2a	0	-2	-2b	-2a	0	-2	-2b	-2a	0
E_{4d}	-2	-2b	-2a	0	-2	-2b	-2a	0	-2	-2b	-2a	0	2	2b	2a	0
E_{5d}	-2	-2	-2	-2	-2	-2a	-2a	-2a	-2b	-2b	-2b	-2b	0	0	0	0
E_{6d}	-2	-2	-2	-2	-2a	-2a	-2a	-2a	-2b	-2b	-2b	-2b	0	0	0	0
E_{7d}	-2	-2	-2	-2	-2b	-2b	-2b	-2b	-2a	-2a	-2a	-2a	0	0	0	0
E_{8d}	-2	-2	-2	-2	-2b	-2b	-2b	-2b	-2a	-2a	-2a	-2a	0	0	0	0
G_{1d}	-4	-4a	-4b	0	-4a	-4a ²	-4ab	0	-4b	-4ab	-4b ²	0	0	0	0	0
G_{2d}	-4	-4b	-4a	0	-4a	-4a ²	-4a ²	0	-4b	-4b ²	-4ab	0	0	0	0	0
G_{3d}	-4	-4a	-4b	0	-4b	-4ab	-4b ²	0	-4a	-4a ²	-4ab	0	0	0	0	0
G_{4d}	-4	-4b	-4a	0	-4b	-4b ²	-4ab	0	-4a	-4a ²	-4ab	0	0	0	0	0

Where $a = \cos 2\pi/5 = \frac{\sqrt{5}-1}{4}$ and $b = \cos 4\pi/5 = -\frac{\sqrt{5}+1}{4}$.

The vibrational selection rules and torsional barrier of methylsilylacetylene

by P. R. BUNKER

Department of Theoretical Chemistry,
University Chemical Laboratory, Cambridge

(Received 15 December 1964)

The molecular symmetry group of methylsilylacetylene is determined and used to classify the rotational-torsional wavefunctions and normal vibrations of the molecule. The vibrational selection rules are also derived and it is shown how a high resolution analysis of some of the perpendicular fundamental bands in the infra-red spectrum might yield the height of the torsional barrier. The experimental results are shown to be consistent with there being a near zero torsional barrier.

1. INTRODUCTION

The infra-red spectrum of methylsilylacetylene and of methylsilyl- d_3 -acetylene has been measured by Robinson and Reeves [1, 2]. From the microwave spectrum Lide [3] concludes that the height of the torsional barrier is less than 2 cm^{-1} but not identically zero. The theory necessary for determining the height of the torsional barrier in dimethylacetylene from a highly resolved infra-red spectrum has been presented [4], and we now show how a similar high resolution analysis of the infra-red spectrum of methylsilylacetylene might also yield the height of the torsional barrier in this molecule. We conclude that the results of Robinson and Reeves are consistent with there being a near zero torsional barrier but that the exact height cannot be determined until we know the accurate values of the rotational constants for the molecule and have an infra-red spectrum of higher resolution than so far obtained.

Longuet-Higgins [5] has defined the elements of the molecular symmetry group of a non-rigid molecule and we use his ideas to determine the molecular symmetry group of methylsilylacetylene. We use this group to classify the rotational-torsional wavefunctions of the molecule. To determine the vibrational selection rules we use the method adopted for dimethylacetylene [6] and ferrocene [7]. This involves assuming that there is no coupling of the perpendicular vibrations of the methyl and silyl groups across the acetylenic bond; since these vibrations will be nowhere near degenerate this approximation will be a very good one. Robinson and Reeves also considered the coupling to be very small. These 'non-coupled' vibrational coordinates can be classified in the molecular symmetry group of the molecule and the selection rules derived. The selection rules are in satisfactory agreement with experiment.

2. THE MOLECULAR SYMMETRY GROUP

The atom labelling convention used is shown in figure 1. The number of feasible permutations and permutations with inversion is found to be eighteen

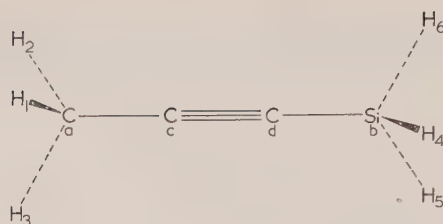


Figure 1. The atom-labelling convention.

(including the identity). There are thus 18 elements in the molecular symmetry group, which we shall call G_{18} . The elements of G_{18} and the character table of the group is shown in table 1.

	E	(123) (132)	(456) (465)	(123) (456) (132) (465)	(123) (465) (132) (456)	(12) (45)* (12) (56)* (12) (64)* (23) (45)* (23) (56)* (23) (64)* (31) (45)* (31) (56)* (31) (64)
A_1	1	1	1	1	1	1
A_2	1	1	1	1	1	-1
E_1	2	2	-1	-1	-1	0
E_2	2	-1	2	-1	-1	0
E_3	2	-1	-1	2	-1	0
E_4	2	-1	-1	-1	2	0

Table 1. The molecular symmetry group of methylsilylacetylene, G_{18} .

3. THE ROTATIONAL-TORSIONAL WAVEFUNCTIONS

Assuming the molecule to have no torsional barrier the rotational-torsional wavefunctions of the molecule will be of the form:

$$S_{JKM}(\theta, \phi) \exp(\pm iK_{\text{Si}}\chi_{\text{Si}}) \exp(\pm iK_{\text{C}}\chi_{\text{C}})$$

where $(\theta, \phi, \chi_{\text{Si}})$ and $(\theta, \phi, \chi_{\text{C}})$ are the Eulerian angles of the silyl group and methyl group respectively and $K = (K_{\text{Si}} + K_{\text{C}})$. The transformation properties of the Eulerian angles are shown in table 2.

From these transformation properties we can determine the species of the rotational-torsional wavefunctions and these species are given in table 3. If we

want to determine the separate species of the rotational wavefunctions (involving $(\chi_C + \chi_{Si})/2$) and torsional wavefunctions (involving $(\chi_C - \chi_{Si})/2$) we would need to use the double group of G_{18} [6, 7, 8] but there seems little point (we can classify all the approximate vibrational coordinates in G_{18}).

The rotational-torsional energy levels are (in cm^{-1}):

$$BJ(J+1) - BK^2 + A_{Si}K_{Si}^2 + A_C K_C^2,$$

where A_{Si} is the inertial constant for the silyl group about its 3-fold axis, A_C is that of the methyl group, and B is the inertial constant of the whole molecule about an axis perpendicular to the figure axis. The effect of the torsional barrier on these energy levels is discussed in the final sections of the paper.

E	(123)	(456)	(123) (456)	(123) (456)	(23) (56)*
θ	θ	θ	θ	θ	$\pi - \theta$
ϕ	ϕ	θ	ϕ	ϕ	$\phi + \pi$
χ_{Si}	χ_{Si}	$\chi_{Si} + 2\pi/3$	$\chi_{Si} + 2\pi/3$	$\chi_{Si} - 2\pi/3$	$-\chi_{Si} + \pi$
χ_C	$\chi_C - 2\pi/3$	χ_C	$\chi_C - 2\pi/3$	$\chi_C - 2\pi/3$	$-\chi_C + \pi$

Table 2. The transformation properties of the Eulerian angles.

K_{Si}	K_C	Species
0	0	A_1 J even A_2 J odd
	$3n \pm 1$	E_2
	$3n$	$A_1 + A_2$
$3n \pm 1$	0	E_1
	$3n \pm 1$	$E_3 + E_4$
	$3n$	$2E_1$
$3n$	0	$A_1 + A_2$
	$3n \pm 1$	$2E_2$
	$3n$	$2A_1 + 2A_2$

Table 3. The species of the rotational-torsional wavefunctions.

4. THE SYMMETRY CLASSIFICATION OF THE APPROXIMATE NORMAL COORDINATES

The frequencies of the perpendicular vibrations of the methyl group and silyl group are very different and their coupling together will be very small. From the results of Robinson and Reeves we see that the $\text{C}-\text{C}\equiv\text{C}$ and $\text{Si}-\text{C}\equiv\text{C}$ skeletal bending frequencies are also very different. There will, therefore, be little coupling of these vibrations. Ignoring the end-to-end coupling the normal coordinates will all be single valued functions of molecular configuration and none will involve the torsional angle. The species of these approximate normal coordinates is the same as that of 23 (i.e. $3N-7$, where N is the number of atoms in the molecule) independent internal coordinate changes, not involving changes in the torsional angle. We will now determine the species of the coordinates.

The rotor-fixed $(x_a y_a)$ and $(x_b y_b)$ -axes and the molecule-fixed z -axis are defined, as shown in figure 2, for the molecule when it is in a potential energy minimum configuration. The z -axis points in the $\text{Si}\rightarrow\text{C}$ direction and its orientation in space is measured by the Eulerian angles θ and ϕ . The common

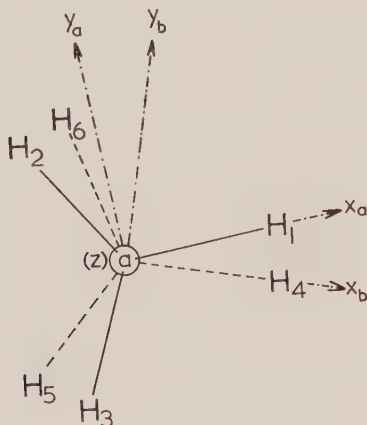


Figure 2. The molecule-fixed axis systems.

origin of the two coordinate axis systems is the centre of gravity of the molecule, O. The $(x_a y_a)$ -axes rotate with the methyl group so that the x_a -axis is in the $\text{Si}-\text{C}-\text{H}_1$ plane and the angle of twist of x_a is χ_C . The $(x_b y_b)$ -axes rotate with the silyl group so that the x_b -axis is in the $\text{C}-\text{Si}-\text{H}_4$ plane and the angle of twist of x_b is χ_{Si} .

The internal coordinates of the molecule are defined in figure 3. The angles ϕ_{cx} , ϕ_{cy} , ϕ_{dx} and ϕ_{dy} are measured in the $x_a\text{Oz}$, $y_a\text{Oz}$, $x_b\text{Oz}$ and $y_b\text{Oz}$ planes respectively.

The species of the 23 independent internal coordinate changes is easily determined to be:

$$7A_1 + 4E_1 + 4E_2,$$

which is, therefore, the species of the approximate normal coordinates. Symmetry coordinates for methylsilylacetylene are given in table 4 together with their symmetry species. Vibrational coupling will mix the E_1 and E_2 vibrations but this will be a small effect.

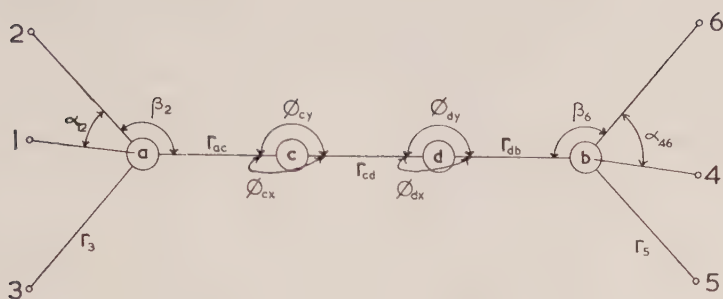


Figure 3. The internal coordinates.

$7A_1$	$S_1 = \Sigma_a \Delta r_i / \sqrt{3},$	
	$S_2 = \Sigma_b \Delta r_i / \sqrt{3},$	
	$S_3 = \Delta r_{cd},$	
	$S_4 = \Sigma_a (\Delta \alpha - \Delta \beta) / \sqrt{6},$	
	$S_5 = \Delta r_{ac},$	
	$S_6 = \Sigma_b (\Delta \alpha - \Delta \beta) / \sqrt{6},$	
	$S_7 = \Delta r_{db}.$	
$4E_1$	$S_{8a} = (\Delta r_4 + \omega \Delta r_5 + \omega^2 \Delta \theta r_6) / \sqrt{3},$	$S_{8b} = (\Delta r_4 + \omega^2 \Delta r_5 + \omega \Delta r_6) / \sqrt{3},$
	$S_{9a} = (\Delta \alpha_{56} + \omega \Delta \alpha_{64} + \omega^2 \Delta \alpha_{45}) / \sqrt{3},$	$S_{9b} = (\Delta \alpha_{56} + \omega^2 \Delta \alpha_{64} + \omega \Delta \alpha_{45}) / \sqrt{3},$
	$S_{10a} = (\Delta \beta_4 + \omega \Delta \beta_5 + \omega^2 \Delta \beta_6) / \sqrt{3},$	$S_{10b} = (\Delta \beta_4 + \omega^2 \Delta \beta_5 + \omega \Delta \beta_6) / \sqrt{3},$
	$S_{11a} = \Delta \phi_{dx},$	$S_{11b} = \Delta \phi_{dy}.$
$4E_2$	$S_{12a} = (\Delta r_1 + \omega r_2 + \omega^2 \Delta r_3) / \sqrt{3},$	$S_{12b} = (\Delta r_1 + \omega^2 \Delta r_2 + \omega \Delta r_3) / \sqrt{3},$
	$S_{13a} = (\Delta \alpha_{23} + \omega \Delta \alpha_{31} + \omega^2 \Delta \alpha_{12}) / \sqrt{3},$	$S_{13b} = (\Delta \alpha_{23} + \omega^2 \Delta \alpha_{31} + \omega \Delta \alpha_{12}) / \sqrt{3},$
	$S_{14a} = (\Delta \beta_1 + \omega \Delta \beta_2 + \omega^2 \Delta \beta_3) / \sqrt{3},$	$S_{14b} = (\Delta \beta_1 + \omega^2 \Delta \beta_2 + \omega \Delta \beta_3) / \sqrt{3},$
	$S_{15a} = \Delta \theta_{cx},$	$S_{15b} = \Delta \phi_{cy}.$

Table 4. Symmetry coordinates of methylsilylacetylene. Each summation Σ_a is over H_1 , H_2 and H_3 and Σ_b is over H_4 , H_5 and H_6 . The internal coordinates are as defined in figure 3.

5. THE VIBRATIONAL SELECTION RULES

The rotor-fixed ($x_a y_a$) and ($x_b y_b$)-axes and the molecule-fixed z -axis were defined in figure 2. The species of the components of the dipole moment operator and polarizability tensor along these axes are:

$$\Gamma(\mu_z) = A_1, \quad \Gamma(\mu_{x_a}, \mu_{y_a}) = E_2, \quad \Gamma(\mu_{x_b}, \mu_{y_b}) = E_1;$$

and

$$\Gamma(\alpha_z^2) = \Gamma(\alpha_{x_a^2+y_a^2}) = \Gamma(\alpha_{x_b^2+y_b^2}) = A_1,$$

$$\Gamma(\alpha_{zx_a}, \alpha_{zy_a}) = \Gamma(\alpha_{x_a y_a}, \alpha_{x_a^2-y_a^2}) = E_2,$$

$$\Gamma(\alpha_{zx_b}, \alpha_{zy_b}) = \Gamma(\alpha_{x_b y_b}, \alpha_{x_b^2-y_b^2}) = E_1.$$

We see that vibrations ν_1 through ν_7 , of species A_1 , will give rise to infra-red parallel fundamental bands and Raman polarized bands; the vibrations ν_8 through ν_{15} , of species E_1 or E_2 , will give rise to infra-red perpendicular fundamental bands and Raman depolarized bands. In the next section we will determine the detailed shapes of the perpendicular fundamental bands, assuming there to be a zero torsional barrier. The effect of a torsional barrier will be discussed.

6. THE PERPENDICULAR BANDS AND THE TORSIONAL BARRIER

As with dimethylacetylene it might be possible to determine the torsional barrier from a high resolution analysis of the infra-red perpendicular fundamental bands. We now present the necessary theory and show that the bands obtained by Robinson and Reeves are consistent with there being a near zero torsional barrier. The effect of the coupling of the perpendicular methyl group vibrations with the perpendicular silyl group vibrations will be neglected.

Assuming a zero torsional barrier the energy levels of the molecule when it is in the first excited state of one of the perpendicular silyl vibrations (E_1 type) are (in cm^{-1}):

$$\nu_0 + BJ(J+1) - B(K_C + K_{\text{Si}})^2 + A_C K_C^2 + A_{\text{Si}}(K_{\text{Si}} - \zeta 1_{\text{Si}})^2,$$

where ν_0 is the fundamental frequency and ζ the Coriolis coupling constant for the vibration and $1_{\text{Si}} = \pm 1$. The infra-red selection rules on transitions from the ground vibrational state to the first excited state of such a perpendicular vibration are deduced to be:

$$\Delta K_C = 0, \Delta K = \Delta K_{\text{Si}} = +1 \text{ for transitions to the } 1_{\text{Si}} = +1 \text{ levels and}$$

$$\Delta K_C = 0, \Delta K = \Delta K_{\text{Si}} = -1 \text{ for transitions to the } 1_{\text{Si}} = -1 \text{ levels,}$$

both with $\Delta J = 0, \pm 1$. The most conspicuous features of the infra-red band will be the Q -branches, for which $\Delta J = 0$. Including the effect of second-order vibration-rotation interaction the positions of the Q -branches in an E_1 -type perpendicular fundamental band are:

$$\nu_0 + A_{\text{Si}}'(1-\zeta)^2 - B' \pm 2K_{\text{Si}}[A_{\text{Si}}'(1-\zeta) - B'] \mp 2B'K_C + [(A_C' - B') - (A_C'' - B'')]K_C^2 + [(A_{\text{Si}}' - B') - (A_{\text{Si}}'' - B'')]K_{\text{Si}}^2, \quad (1)$$

where K_{Si} and K_C are ground vibrational state quantum numbers. A similar analysis of the E_2 -type perpendicular methyl bands shows that the Q -branches in these bands have the positions:

$$\nu_0 + A_C'(1-\zeta)^2 - B' \pm 2K_C[A_C'(1-\zeta) - B'] \mp 2B'K_{\text{Si}} + [(A_C' - B') - (A_C'' - B'')]K_C^2 + [(A_{\text{Si}}' - B') - (A_{\text{Si}}'' - B'')]K_{\text{Si}}^2. \quad (2)$$

The relative intensities of the Q -branches can be determined; this involves the determination of the statistical weights and Boltzmann factors for the ground vibrational state levels. The theoretically predicted perpendicular bands can then be constructed, and the perpendicular methyl-group vibrational bands (ν_{12} , ν_{13} and ν_{14}) will be as shown in figure 4 (for simplicity second-order vibration-rotation interaction is ignored). The Q -branches occur in bunches and the separation of the bunches is $2[A_C(1-\zeta)-B]$. The separation of the Q -branches within each bunch is $2B$. Each bunch can be assigned a K_C value and each line within a bunch can be assigned a K_{Si} value, as done in figure 4, where these quantum numbers refer to the ground vibrational state levels from which the transitions originate. Transitions between states for which $K_{Si}=0$ give rise

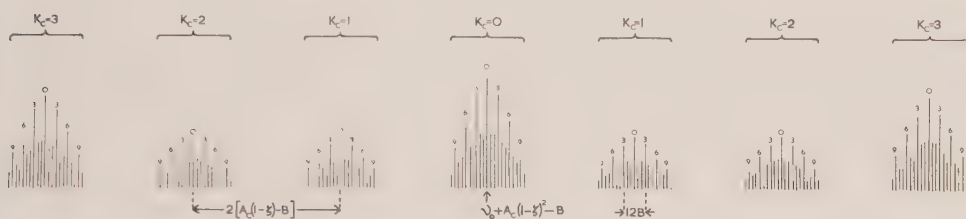


Figure 4. An E_2 -type infra-red perpendicular band. The numbers at the top of each Q -branch are the K_{Si} values of the ground state from which the transition occurs.

to the $K_{Si}=0$ series of Q -branches which mark the centres of the bunches. The $K_{Si}=0$ Q -branches have the same positions (even including the effect of second-order vibration-rotation interaction) and relative intensities as the Q -branches in the perpendicular bands of an Me-X type molecule such as methylchloride. The position of the $K_{Si}=0$ Q -branches, i.e. the positions of the centres of the bunches, are given by:

$$\nu_0 + A_C'(1-\zeta)^2 - B' \pm 2K_C[A_C'(1-\zeta) - B'] + [(A_C' - B') - (A_C'' - B'')]K_C^2.$$

Transitions between states for which $K_{Si} \neq 0$ give rise to fine structure lines on either side of the $K_{Si}=0$ lines. The band ν_{12} of methylsilyl- d_3 -acetylene has been studied [2] and the centres of the bunches found to fit the expression:

$$\nu = 2987.75 \pm 10.09K_C - 0.03K_C^2,$$

where we have replaced the K of reference 2 by K_C , as a result of the theory developed here. The intensity alternation is approximately 2.1.1.2.1.1.2 for successive bunches and for successive Q -branches within each bunch.

The Q -branches in the particular silyl bands also occur in bunches. The separation of the bunches is $2[A_{Si}(1-\zeta)-B]$ and the separation within the bunches is $2B$. Each bunch can be assigned a K_{Si} value and each line within a bunch a K_C value. The positions of the centres of the bunches (i.e. $K_C=0$ branches) is given by:

$$\nu_0 + A_{Si}'(1-\zeta)^2 - B' \pm 2K_{Si}[A_{Si}'(1-\zeta) - B'] + [(A_{Si}' - B') - (A_{Si}'' - B'')]K_{Si}^2,$$

and such an expression holds for all the perpendicular silyl bands [1].

The effect of a torsional barrier on the positions of the Q -branches can only be determined when A_{Si} and A_{C} are accurately known. However we can outline the qualitative effect. We assume that the torsional barrier is of the form

$$V_3' = \frac{V_3}{2} \cos 3(\chi_{\text{Si}} - \chi_{\text{C}}),$$

where V_3 is the barrier height. This can be seen to couple the rotor-vibrational state $(K_{\text{Si}}', K_{\text{C}}')$ with the rotor-vibrational state $(K_{\text{Si}}'', K_{\text{C}}'')$ when both are in the same vibrational state and have the same J value and when either

$$K_{\text{Si}}' = K_{\text{Si}}'' + 3 \text{ and } K_{\text{C}}' = K_{\text{C}}'' - 3$$

or

$$K_{\text{Si}}' = K_{\text{Si}}'' - 3 \text{ and } K_{\text{C}}' = K_{\text{C}}'' + 3.$$

Since $A_{\text{C}} \neq A_{\text{Si}}$ there will not be any exact degeneracies between states that are coupled by V_3' . However, there ought to be several near degeneracies, and these levels will suffer a relatively large shift as a result of a torsional barrier. Q -branches which result from transitions to or from such highly perturbed levels should suffer a measurable energy shift. From the values of such shifts it ought to be possible to determine the height of the torsional barrier.

I should like to thank Professor H. C. Longuet-Higgins, F.R.S., for reading the manuscript and for helpful suggestions. I acknowledge a D.S.I.R. research studentship.

REFERENCES

- [1] ROBINSON, D. W., and REEVES, R. B., 1962, *J. chem. Phys.*, **37**, 2625.
- [2] REEVES, R. B., and ROBINSON, D. W., 1964, *J. chem. Phys.*, **41**, 1699.
- [3] LIDE, D. R. (private communication).
- [4] BUNKER, P. R., and LONGUET-HIGGINS, H. C., 1964, *Proc. roy. Soc. A*, **280**, 340.
- [5] LONGUET-HIGGINS, H. C., 1963, *Mol. Phys.*, **6**, 445.
- [6] BUNKER, P. R., 1965, *J. chem. Phys.*, **42**, 2991.
- [7] BUNKER, P. R., 1965, *Mol. Phys.*, **9**, 247.
- [8] HOUGEN, J. T., 1964, *Canad. J. Phys.*, **40**, 1920.

A study of the valence electron approximation: application to LiH

by J. D. STUART†

The John Hopkins University, Applied Physics Laboratory,
Silver Spring, Maryland

and R. P. HURST‡

The State University of New York at Buffalo,
Department of Physics, Buffalo, New York

(Received 11 March 1965)

Using the valence bond approach and a six-term wave function valence electron calculations are made of the energy and dipole moment of lithium hydride. Comparisons are then made with previous two- and with four-electron results. It is found that reasonable agreement with four-electron calculations of the dipole moment is obtained when the valence orbitals are made orthogonal to the orbitals of the neglected lithium inner shell 1s electrons and that an approximate variational theorem for the energy is then valid. On the other hand, when one fails to require the valence orbitals to be orthogonal to the inner shell an energy lower than the 'experimental' energy can be obtained and the computed dipole moment is in poor agreement with the computed four-electron moment and with the experimentally determined moment. Finally, as with four-electron calculations, hybridization with the 2p covalent structure is necessary to give a reasonable dipole moment.

1. INTRODUCTION

The valence electron approximation has received considerable attention for a number of polyatomic molecular problems for which the numerical difficulties resulting from more exact treatments have been almost insurmountable. Thus, for aromatic organic systems or for problems involving the solid state rather drastic approximations are nearly always necessary and the approximation of considering only the valence electrons is frequently made. In valence electron calculations the electrons of the inner shells are often treated as point charges coinciding with the nuclei.

Lithium hydride is a sufficiently simple system such that very accurate calculations have been made in which all four electrons are considered. These results have been carefully reviewed in the literature. Hence, those will not be extensively considered here [1-3]. Lithium hydride molecule contains two tightly bound inner-shell electrons on the lithium atoms and is therefore a system for which the simplified treatment is possible. Thus, this system should be an ideal one to make a critical evaluation of the valence electron approximation.

† This work was supported by the United States Department of the Navy, Bureau of Naval Weapons, under contract N0w 62-0604-c.

‡ Supported in part by the Air Force Office of Scientific Research grant AF-AFOSR-191-63.

In the present paper we are reporting singlet ground-state valence bond two-electron calculations of the energy and dipole moment for LiH. Comparisons are then made with other two- and with four-electron results.

2. METHODS AND CALCULATIONS

When one considers the two 1s electrons on lithium as point charges coinciding with that nucleus a simplified Hamiltonian, H , results for the molecule. Thus, with this approximation, if A and B refer to the lithium and hydrogen centres respectively, and ρ is the internuclear distance H is then given in atomic units by:

$$H = -\frac{1}{2}\nabla_1^2 - \frac{1}{2}\nabla_2^2 - \frac{1}{r_{1A}} - \frac{1}{r_{1B}} - \frac{1}{r_{2A}} - \frac{1}{r_{2B}} + \frac{1}{r_{12}} + \frac{1}{\rho}. \quad (1)$$

The energy corresponding to this approximate Hamiltonian is considered to be the sum of the first ionization potential of the lithium and hydrogen atoms, the binding energy of LiH molecule and the zero point vibrational energy. In addition, it is intended that the wave function approximate that of the outermost two electrons such as to give a reasonable prediction of the molecular dipole moment.

Wave function configurations (see equation (2) of text)	
$\phi_1 = [b(1)d(2) + b(2)d(1)]/N_{11}$	Li-H
$\phi_2 = [c(1)d(2) + c(2)d(1)]/N_{22}$	Li-H
$\phi_3 = [d(1)d(2)]/N_{33}$	Li ⁺ H ⁻
$\phi_4 = [b(1)b(2)]/N_{44}$	Li ⁻ H ⁺
$\phi_5 = [c(1)b(2) + c(2)b(1)]/N_{55}$	Li ⁻ H ⁺
$\phi_6 = [c(1)c(2)]/N_{66}$	Li ⁻ H ⁺
Non-orthogonal to inner shell	Orthogonal to inner shell
$b = \psi_{2sLi} = \left(\frac{0.65^5}{3\pi}\right)^{1/2} r_{Li} \exp(-0.65r_{Li})$	$b = \psi_{2sLi} - \lambda\psi_{1sLi}$
$c = \psi_{2pLi} = \left(\frac{0.65^5}{\pi}\right)^{1/2} r_{Li} \exp(-0.65r_{Li}) \cos \theta_{Li}$	$c = \psi_{2pLi}$
$d = \psi_{1sH} = \left(\frac{1}{\pi}\right)^{1/2} \exp(-r_H)$	$d = \psi_{1sH} - \eta\psi_{1sLi}$
$\lambda = \int \psi_{1sLi} \psi_{2sLi} d\tau$	
$\eta = \int \psi_{1sLi} \psi_{1sH} d\tau$	
$\psi_{1sLi} = \left(\frac{2.7^3}{\pi}\right)^{1/2} \exp(-2.7r_{Li})$	

Table 1.

On inspection of our approximate Hamiltonian it is apparent that this operator has the same form generally assumed for the hydrogen molecule. Thus, despite the form of equation (1) the trial variational function is constructed to have not $^1\Sigma_g^+$ symmetry of hydrogen molecule but the lesser symmetry $^1\Sigma^+$ of lithium hydride. It is, of course, evident that if the trial variational function were to be given $^1\Sigma_g^+$ symmetry our results would represent a poor calculation for the H_2 molecule and would give a zero dipole moment. Both the computed energy and dipole moment would have no relation to LiH molecule.

The wave function ψ is of the usual superposition of configuration type:

$$\psi = \sum_{i=1}^n C_i \phi_i, \quad (2)$$

where the ϕ_i are listed in table 1. The electronic energies E and the coefficients C_i are determined from:

$$\sum_{i=1}^n C_j (H_{ij} - S_{ij} E) = 0. \quad (3)$$

Finally, the dipole moment μ is computed from:

$$\mu = e(\rho - \bar{Z}), \quad (4)$$

where

$$\bar{Z} = \int \psi (z_1 + z_2) \psi d\tau. \quad (5)$$

Two cases are considered, first with the 2s and 1h (1s on hydrogen) orbitals non-orthogonal to the inner shell 1s orbitals and second, with these orbitals transformed by the Schmidt process so that they are orthogonal to the lithium 1s orbital but not orthogonal to each other. In table 2 are given C_i , μ and E that resulted from including various combinations of the six wave function configurations with non-orthogonal orbitals. Table 3 contains the corresponding results with the valence orbitals orthogonal to the inner shell 1s orbitals. In addition, the dipole moment results [4, 5] for directly comparable four-electron calculations (i.e. four-electron calculations involving the same orbitals, orbital exponents, and internuclear distance) are given in tables 2 and 3 along with the molecular beam measurement of the dipole moment of Wharton *et al.* [6].

3. DISCUSSION

Several conclusions can be drawn from the present and previous results. First the necessity for making the valence orbitals orthogonal to the neglected inner shell is readily apparent. The computed electronic energy results obtained by considering the non-orthogonal Slater orbitals (table 2) lie below the 'experimental' energy. Furthermore, the dipole moment corresponding to the most complete calculation in table 2 is about two-thirds as large as was obtained from numerous four-electron calculations [1-3]. By contrast, the energies obtained by considering the transformed orbitals (table 3) always lie above the 'experimental' energy and dipole moment $-6.59 D$ (hydrogen negative) is in approximate agreement with the computed four-electron moments which lie in the range -5.4 to $-6.4 D$. The most directly comparable [4, 5] computed four-electron calculation of the moment is $-6.040 D$ while the experimental value [6] is $-5.882 D$.

Coefficients ^a				
Calculation No.	1	2	3	4
ϕ_1	1.0000	0.78214	0.81272	0.82046
ϕ_2	0.0	0.17561	0.0	0.22096
ϕ_3	0.0	0.21369	0.27950	0.19199
ϕ_4	0.0	0.0	-0.013275	-0.027037
ϕ_5	0.0	0.0	0.0	-0.039604
ϕ_6	0.0	0.0	0.0	-0.029163
E (ev)	-21.911	-22.428	-22.312	-22.444
μ (D)	-0.793	-4.086	-2.786	-4.141
μ (D) ^b	-0.871	-5.979		-6.040

$\rho = 1.5953 \text{ \AA}^c$.

Experimental energy^d = -21.671 ev.

Experimental dipole moment^e = -5.882 D.

^aNormalized to $\int \psi \psi d\tau = 1$.

^bCalculated in comparable four-electron calculations (see reference [4]).

^cExperimental internuclear distance, G. Herzberg, *Spectra of Diatomic Molecules* (D. van Nostrand, Company, Inc., Princeton, 1950), p. 546.

^dSum of experimental energies: first ionization potential of lithium, the ionization energy of hydrogen, the binding of LiH, and the zero point energy.

^eSee reference [6].

Table 2. Dipole moment and energy results using valence orbitals not orthogonalized to inner shell.

It is well to note in this connection that *all* of the integrals required for the equivalent case of the four-electron calculations are required for the present valence electron calculation with the orthogonalized orbitals. Thus, accepting the conclusion that the valence orbitals must be orthogonal to the inner shell the only labour saving to be gained by neglecting the inner shell electrons results when combining the integrals to obtain the Hamiltonian and overlap matrix elements.

It is of interest to note the importance of allowing for hybridization by the 2p covalent structure (ϕ_2 of table 1). This fact is clearly demonstrated on comparing calculation 3 of table 3 with the corresponding calculations 2 and 4. Here it is seen that including the 2p structure produces a greater improvement in energy than the ionic structures ϕ_4 , ϕ_5 and ϕ_6 and increases the magnitude of the dipole moment by about 1.7 D.

Finally, there have been previous valence electron calculations made by Adamov [7], Fischer [8], Hutchisson and Muskat [9] and by Mueller and Eyring [10]. Of these only Adamov made calculations in which all valence orbitals are orthogonal to the neglected inner shell. This also is the only valence electron calculation of the dipole moment. Since the present results clearly show that it is possible, when one has neglected to require orthogonality to the inner shell, for the computed valence electron energies to lie well below the 'experimental energy' a comparison of energy results from calculations based on orbitals which are not orthogonal to the inner shell is nearly meaningless. For these reasons we will consider only Adamov's results further.

Coefficients ^a				
Calculation No.	1	2	3	4
ϕ_1	1.0000	0.33680	0.64883	0.45060
ϕ_2	0.0	0.55826	0.0	0.63318
ϕ_3	0.0	0.33079	0.51459	0.27550
ϕ_4	0.0	0.0	-0.095059	-0.081107
ϕ_5	0.0	0.0	0.0	-0.093508
ϕ_6	0.0	0.0	0.0	-0.038238
E (ev)	-17.334	-19.252	-18.361	-19.337
$\mu(D)$	-0.871	-6.529	-4.842	-6.586
$\mu(D)^b$	-0.871	-5.979		-6.040

$\rho = 1.5953 \text{ \AA}^c$.

Experimental energy^d = -21.671 ev.

Experimental dipole moment^e = -5.882 D .

^aNormalized to $\int \psi \psi \, d\tau = 1$.

^bCalculated in comparable four-electron calculations (see reference [4]).

^cExperimental internuclear distance, G. Herzberg, *Spectra of Diatomic Molecules* (D. van Nostrand, Company, Inc., Princeton, 1950), p. 546.

^dSum of experimental energies: first ionization potential of lithium, the ionization energy of hydrogen, the binding energy of LiH, and the zero point energy.

^eSee reference [6].

Table 3. Dipole moment and energy results using valence orbitals orthogonalized to inner shell.

In Adamov's calculation hybridization by the 2p covalent structure is omitted so that his most complete calculation is very nearly equivalent to that presented as calculation 3 of table 3. His computed dipole moment is -3.4 D where ours is -4.8 D . This discrepancy in the computed moments is at least partially explainable by the differences in the 2s orbital exponent and the slight differences in the internuclear distances. In the present calculation the Slater exponent 0.65 is used while Adamov's 2s exponent is 0.8. In addition, Adamov's calculations are made for $\rho = 1.587 \text{ \AA}$ where in the present work $\rho = 1.5953 \text{ \AA}$. It would seem probable that some of this discrepancy is due to the numerical precision to which his calculations are made. In the present work eight figures are maintained throughout the entire calculation and only later are they rounded off; Adamov lists some of his moment integrals to only two figures. Adamov obtained the result 1.29 ev for the binding energy. However, he did not state the atomic reference energies to which his result corresponds. The present calculation gives a binding energy of 0.45 ev when compared with the *experimental* first ionization potential of lithium and hydrogen. The experimental binding energy of LiH is 2.56 ev [11].

REFERENCES

- [1] MATSEN, F. A., and BROWNE, J. C., 1962, *J. phys. Chem.*, **66**, 2332.
- [2] EBBING, D. D., 1962, *J. chem. Phys.*, **36**, 1361.
- [3] KAHALAS, S. L., and NESBET, R. K., 1963, *J. chem. Phys.*, **39**, 529.
- [4] HURST, R. P., MILLER, J., and MATSEN, F. A., 1957, *J. chem. Phys.*, **26**, 1092.

- [5] MILLER, J., FRIEDMAN, R. H., HURST, R. P., and MATSEN, F. A., 1957, *J. chem. Phys.*, **27**, 1385.
- [6] WHARTON, L., GOLD, L. P., and KLEMPERER, W., 1960, *J. chem. Phys.*, **33**, 1255.
- [7] ADAMOV, M. H., 1949, *J. phys. Chem., Moscou*, **23**, 1172.
- [8] FISHER, I., 1952, *Ark. Fys.*, **5**, 349.
- [9] HUTCHISSON, E., and MUSKAT, M., 1932, *Phys. Rev.*, **40**, 340.
- [10] MUELLER, C. R., and EYRING, H., 1951, *J. chem. Phys.*, **19**, 934.
- [11] NAKAMURA, G., 1930, *Z. Phys.*, **59**, 218.

Nouvelles recherches sur l'existence de cations complexes de structure définie dans les solutions d'électrolytes

par ANTONIO DA SILVEIRA, MANUEL A. MARQUES et NOEMIO M. MARQUES

Laboratoire de Physique de la Faculté des Sciences de Lisbonne

(Received 25 November 1964)

On donne les fréquences et les facteurs de dépolarisation de certaines bandes observées dans les spectres Raman des solutions de sels de magnésium, zinc, aluminium et beryllium, dans l'eau légère et dans l'eau lourde, que l'on attribue à des cations complexes de la forme $\text{Me}(\text{OH}_2)_n$ et $\text{Me}(\text{OD}_2)_n$, complexes dont la structure serait analogue à celle que l'on observe dans les cristaux hydratés. Avec certaines hypothèses on peut calculer les fréquences propres totalement symétriques de ces complexes et celles-ci sont voisines des fréquences expérimentales.

1. INTRODUCTION

De recherches faites naguère par l'effet Raman [1] sur l'existence de cations complexes de structure définie, dans les solutions concentrées d'électrolytes, il ressortait avec une certaine évidence que de tels complexes sont effectivement présents notamment dans les solutions des sels de magnésium, aluminium, cuivre et zinc. Un calcul un peu simpliste avait montré d'ailleurs que la vibration totalement symétrique de ces complexes devait avoir une fréquence propre voisine de la fréquence expérimentale qu'on pouvait leur attribuer.

Ces résultats expérimentaux ont été confirmés d'abord par J.-P. Mathieu [2] qui a étudié, par l'effet Raman, des cristaux et solutions aqueuses de certains sels; et plus récemment par Lafont [3], Hester et Plane [4], et par Irish [5].

Nous avons repris il y a quelque temps les recherches [6], nous les avons complétées par une mesure assez précise du facteur de dépolarisation des bandes Raman, et nous avons fait une étude parallèle de quelques solutions dans l'eau lourde. Cet article contient l'ensemble des résultats expérimentaux obtenus avec les solutions de certains sels de magnésium, de zinc, d'aluminium et de beryllium, et un calcul de la fréquence totalement symétrique des complexes.

Le montage spectrographique et la technique que nous avons employés pour l'ultrafiltration des solutions ont été déjà indiqués [1]. Pour les facteurs de dépolarisation nous avons employé une méthode dont l'optique ne diffère pas beaucoup de celle de Cabannes et Rousset [7]. Les mesures d'intensité ont été facilitées, et rendues plus précises, par l'emploi d'un condenseur à diaphragme échellonné de Zeiss.

2. RÉSULTATS EXPÉRIMENTAUX

Dans nos spectres des solutions des sels de Mg, de Zn et de Al nous avons identifié d'abord les bandes attribuées aux ions NO_3^- et SO_4^{--} , et aux molécules OH_2 et OD_2 . Dans les solutions de Cl_2Zn nous avons encore repéré deux

autres bandes, de fréquences 108 cm^{-1} (dépolarisée) et 288 cm^{-1} (polarisée), déjà signalées d'ailleurs dans les solutions dans l'eau légère [1, 5 et 8]. En plus nous avons trouvé les bandes de fréquences ν , avec des facteurs de dépolarisation ρ et des intensités I , données dans le tableau 1. Dans ce tableau les intensités relatives ne sont généralement significatives que pour les solutions d'un même sel. Les points d'interrogation signifient ou que les bandes prévues n'ont pas été observables ou que nous ne pouvons pas garantir leur intensité avec la même précision; ces dernières bandes sont d'ailleurs très faibles. Dans le cas des solutions très diluées ou très absorbantes nous n'avons pas mesuré les intensités, ce qui est indiqué par un trait.

Substance	Conc.	ν_1 (cm^{-1})	ρ	I	ν_2 (cm^{-1})	ρ	I	ν_3 (cm^{-1})	ρ	I
(NO ₃) ₂ Mg	7,6 N	365	<0,2	7	315	dp	<1	240	dp	7 ?
sol.en OH ₂	1,9 N	365	p	—	?					
SO ₄ Mg	5,2 N	365	<0,2	7	?			240	dp	7 ?
sol.en OH ₂	1,5 N	365	p	—	?			?		
Cl ₂ Mg	7,2 N	361	<0,2	7	315	dp	<1	240	dp	7 ?
sol.en OH ₂	3,7 N	363	<0,2	4	?			240	dp	
	1,4 N	360	p	1	?					
Cl ₂ Mg	4,2 N	344	<0,2	4	302	?	?	240	dp	?
sol.en OD ₂										
(NO ₃) ₂ Zn	11,0 N	390	<0,2	7	335	dp	1	230	dp	6
sol.en OH ₂										
SO ₄ Zn	6,3 N	400	<0,2	7	335	dp	1	240	dp	?
sol.en OH ₂										
Cl ₂ Zn	17,5 N	385	<0,2	3	335	dp	?	230	dp	?
sol.en OH ₂	10,8 N	382	p	2	335	dp	?	230	dp	2
	2,3 N	387	p	2	335	dp	<1	230	dp	?
Cl ₂ Zn	7,3 N	369	p	2	?			210	dp	2
sol.en OD ₂										
(NO ₃) ₃ Al	7,1 N	524	<0,2	6	447	dp	1	342	0,8	8
sol.en OH ₂	5,1 N	524	<0,2	4,5	446	dp	1	343	0,8	4,5
	2,4 N	524	p	2	452		<1	343	dp	2
(SO ₄) ₃ Al ₂	6,2 N	520	<0,2	6				339	0,8	8
sol.en OH ₂	1,5 N	523 ?	p	—				338	dp	—
Cl ₃ Al	6,9 N	526	<0,2	6	447	dp	1	340	0,8	8
sol.en OH ₂	5,6 N	525	<0,2	—	447	dp	—	340	0,8	—
	1,0 N	525	p	—	?			340	dp	—
Cl ₃ Al	4,6 N	503	<0,2	6	433	dp	1	313	0,8	8
sol.en OD ₂										

Tableau 1.

Dans ce qui suit nous employons les notations de [9] pour les modes d'oscillation. Pour préciser, nous nous référons d'abord aux solutions dans l'eau légère. Les bandes de fréquence plus élevée des solutions des sels de Mg (363 cm^{-1}), de Zn (389 cm^{-1}) et de Al (524 cm^{-1}), avec un facteur de dépolarisation $\rho < 0,2$, sont attribuées—d'accord avec les considérations qui suivent et les calculs faits plus loin, à la vibration totalement symétrique, ν_1 , de complexes octaédriques du cation respectif.

Les deux autres bandes observées avec les mêmes sels de Mg, de Zn et de Al, données dans le tableau 1 avec leurs facteurs de dépolarisation, sont attribuées aux deux autres fréquences actives dans l'effet Raman : ν_2 doublement dégénérée et ν_3 triplement dégénérée.

Nous avons cherché une vérification de ces attributions en étudiant des solutions de chlorures dans l'eau lourde. Remarquons que d'après le même tableau, le rapport $\nu_1(\text{OH}_2)/\nu_1(\text{OD}_2)$ des valeurs mesurées donne, dans le cas des complexes de Mg^{2+} : 1,05 et dans le cas des complexes de Zn^{2+} et Al^{3+} : 1,04; dans l'hypothèse où—toute chose égale d'ailleurs—seule la masse de H est remplacée par la masse de D, le rapport calculé des mêmes fréquences donne 1,054.

Pour les autres bandes, dans le cas du cation Al^{3+} , on obtient

$$\begin{aligned} \text{mesuré : } \frac{\nu_2(\text{OH}_2)}{\nu_2(\text{OD}_2)} &= 1,04 \quad \frac{\nu_3(\text{OH}_2)}{\nu_3(\text{OD}_2)} = 1,08, \\ \text{calculé : } \frac{\nu_2(\text{OH}_2)}{\nu_2(\text{OD}_2)} &= 1,054 \quad \frac{\nu_3(\text{OH}_2)}{\nu_3(\text{OD}_2)} = 1,087. \end{aligned}$$

Dans le cas du cation Mg^{2+} on obtient, pour ν_2 , un rapport des valeurs mesurées égale à 1,04, le rapport théorique étant 1,054; le changement de la fréquence ν_3 ne peut pas être mesuré à cause de l'aspect très flou de cette bande.

Dans le cas du cation Zn^{2+} , on obtient pour ν_3 un rapport des valeurs mesurées égale à 1,09, le rapport théorique étant 1,084; la bande ν_2 , dans l'eau lourde, se trouverait noyée dans l'aile de la bande large et très intense de 288 cm^{-1} . Cette bande a été attribuée [8] à des complexes de la forme $(\text{Cl}_4\text{Zn})^{2-}$; en consonnance avec ceci nous observons qu'elle ne change pas de fréquence dans le passage de OH_2 à OD_2 .

En ce qui concerne les solutions des sels de Be—les bandes de l'eau et des anions NO_3^- et SO_4^{--} mises à part—nous observons un grand nombre de bandes non encore signalées mais, ici, nous ne retiendrons que deux de ces bandes, celles qui présentent à peu près la même fréquence et le même facteur de dépolarisation dans les différentes solutions (tableau 2). Nous pensons qu'on

Substance	Conc.	ν (cm^{-1}) ρ I			ν (cm^{-1}) ρ I		
$(\text{NO}_3)_2\text{Be}$	11,0 N	345	0,8	6	533	0,2	7
sol.en OH_2	6,3 N	350	0,8	3	538	<0,2	4
SO_4Be	6,7 N	347	0,8	5	533	0,2	7
sol.en OH_2	3,4 N	356	0,8	2	538	0,2	3
F_2Be	15,6 N	360	0,8	5	543	<0,2	7
sol.en OH_2	7,8 N	354	dp	1	530	p	2
Cl_2Be	3,2 N	350	0,8	3	535	<0,2	3
sol.en OH_2							
Cl_2Be	3,2 N	335	0,8	3	510	<0,2	3
sol.en OD_2							

Tableau 2.

peut considérer celles-ci comme dues à la présence de complexes de coordination de molécules d'eau autour du cation Be^{2+} , probablement tetracoordonnées et quasi-tetraédriques, comme dans les cristaux [10].

La bande de fréquence (536 cm^{-1}), polarisée, relativement intense et étroite est attribuée à la vibration totalement symétrique ν_1 , du complexe $\text{Be}^{2+}(\text{OH}_2)_4$; la bande de fréquence (352 cm^{-1}), dépolarisée, relativement intense et plus large, est attribuée à une des vibrations non totalement symétriques (dégénérée ou antisymétrique) du même complexe.

Le changement de fréquence pour ν_1 , du à la substitution isotopique $\text{H} \rightarrow \text{D}$, s'accorde avec l'attribution faite :

$$\text{observé : } \frac{\nu_1(\text{OH}_2)}{\nu_1(\text{OD}_2)} = 1,05; \quad \text{calculé : } \frac{\nu_1(\text{OH}_2)}{\nu_1(\text{OD}_2)} = 1,054.$$

Pour l'autre bande, la valeur théorique de ce rapport ne peut pas être précisée sans préciser d'abord le mode de vibration—et nous n'avons pas d'éléments pour le faire à ce stade—mais les valeurs mesurées des fréquences donnent un rapport $\nu(\text{OH}_2)/\nu(\text{OD}_2) = 1,05$ lequel est voisin des rapports théoriques que l'on peut prévoir pour les modes de vibration du complexe tetraédrique.

Dans un travail récent, Bobovich [11] donne une bande de fréquence 530 cm^{-1} , polarisée, trouvée dans le spectre Raman d'une solution de Cl_2Be (14 N) dans l'eau légère, ce qui est en accord avec nos observations pour des concentrations beaucoup plus petites (3 N). L'interprétation de cet auteur est, néanmoins, totalement différente de la nôtre.

3. CALCUL DE LA FRÉQUENCE TOTALEMENT SYMÉTRIQUE

Pour calculer la fréquence de la vibration totalement symétrique il faut introduire certaines hypothèses et faire quelques simplifications que nous allons expliciter.

Nous admettons que les molécules d'eau vibrent en entier, par rapport à l'ion central, dans un complexe ayant la symétrie d'un octaèdre régulier dans le cas de Mg^{2+} , Zn^{2+} et Al^{3+} , et d'un tétraèdre régulier dans le cas du Be^{2+} . La molécule OH_2 a été réduite à un dipole centré sur le noyau d'oxygène en négligeant le quadripole quasi-sphériquement symétrique [12]. Nous admettons que l'énergie potentielle des complexes est donnée par :

$$U(r) = N \left[-\frac{(\mu + \mu')Ze}{r^2} + \frac{D(\mu + \mu')^2}{r^3} + \frac{\mu'^2}{2\alpha} \right] + \frac{a}{r^n} + \frac{b}{r^m} + U_1^d(r) + U_2^d(r).$$

Dans cette formule N est le nombre de molécules d'eau coordonnées, Ze la charge de l'ion central, r la distance du cation à l'oxygène des molécules d'eau, α la polarisabilité électrique moyenne de ces dernières. $-(\mu + \mu')Ze/r^2$ donne l'énergie d'attraction électrostatique entre le cation et la molécule OH_2 polarisée; μ est le moment dipolaire permanent de OH_2 et μ' , qui dépend de r , son moment induit. Nous avons pris $\mu = 1,87$ Debye. Pour les rayons d'équilibre des complexes (donnés plus loin) nous avons trouvé $\mu' = 1,85$ Debye dans le cas de Mg^{2+} , $\mu' = 1,83$ Debye dans le cas de Zn^{2+} et $\mu' = 3,27$ Debye dans le cas de Al^{3+} et Be^{2+} . $+D(\mu + \mu')^2/r^3$ représente l'énergie de répulsion mutuelle dipolaire des molécules d'eau; D est un facteur dépendant de la configuration

géométrique du complexe, que l'on calcule facilement : $D=1,19$ pour un octaèdre et $D=0,573$ pour un tétraèdre.

$+\mu'^2/2\alpha$ est l'énergie des dipôles induits sur les molécules d'eau ($\alpha=1,48 \times 10^{-24}$ cgs).

a/r^n est l'expression simplifiée de Born pour l'énergie de répulsion des actions de courte portée (overlap energy) entre le cation et les molécules d'eau ; b/r^m est l'énergie du même type entre les molécules d'eau adjacentes du complexe ; a et b sont les constantes de répulsion de Born multipliées par des facteurs géométriques qui dépendent du type de complexe. Pour les exposants n et m nous avons adopté des valeurs, déduites des résultats des mesures de compressibilité sur les oxides cristallisés, données par Pauling [13]. Nous admettons que le comportement des molécules d'eau dans les complexes est semblable, du point de vue de ces actions de courte portée, à celui des ions O^{2-} dans les oxides cristallisés des mêmes cations. Dans le cas des complexes de Mg^{2+} et de Al^{3+} on a $n=m=7$, ce qui nous permet de fondre dans un seul terme, A/r^7 , les deux répulsions de courte portée. Pour les complexes de Zn^{2+} et de Be^{2+} on a $n \neq m$ (Zn^{2+} : $n=8$ et $m=7$; Be^{2+} : $n=6$ et $m=7$). Dans ce dernier cas, ne pouvant pas calculer séparément les deux termes de répulsion, nous avons dû les représenter encore par un terme unique. Nous avons adopté, un peu arbitrairement, la même loi d'interaction entre le cation et la molécule d'eau et entre les molécules d'eau elles-mêmes, c'est à dire : A/r^8 dans le cas des complexes de Zn^{2+} et A/r^6 dans le cas des complexes de Be^{2+} .

La constante A a été déterminée par la condition d'équilibre $dU/dr=0$ pour $r=r_0$, r_0 étant une valeur moyenne des rayons d'équilibre des complexes dans les cristaux [10, 14 et 15]. Nous avons pris $r_0=2,08$ Å pour les complexes $Mg^{2+}(OH_2)_6$, $2,10$ Å pour $Zn^{2+}(OH_2)_6$, $r_0=1,90$ Å pour $Al^{3+}(OH_2)_6$ et $r_0=1,65$ Å pour $Be^{2+}(OH_2)_4$. Remarquons ici qu'un accroissement de 1 pour cent sur r_0 entraîne une réduction de 2 pour cent sur la fréquence ν_1 calculée.

$U_1^d(r)$ est l'énergie de dispersion entre le cation et les molécules d'eau. $U_2^d(r)$ est l'énergie de dispersion entre les molécules d'eau coordonnées autour du cation.

Il semble que, des expressions proposées pour les forces de dispersion, aucune n'est ici rigoureusement applicable. Néanmoins on peut admettre que ces forces de dispersion varient, à part le signal, comme $1/r^7$, loi très proche de celle que, dans le cas présent, assument les forces répulsives de courte portée ; comme, d'autre part, la constante A a été fixée par la condition que les forces répulsives équilibrent les forces attractives, il en résulte qu'un petit changement dans la constante des forces de dispersion n'affecte pas sensiblement les résultats.

Nous avons pris pour $U_1^d(r)$ et $U_2^d(r)$ des expressions du type proposé par Slater et Kirkwood [16] avec les valeurs de la polarisabilité des cations données par Pauling [17]. D'ailleurs, l'inclusion dans l'énergie $U(r)$ de ces termes de dispersion entraîne un accroissement soit de $-U(r_0)$ soit de ν_1 qui atteint tout au plus 3 pour cent.

La fréquence ν_1 de la vibration totalement symétrique est donnée, en nombre d'ondes, par $4\pi^2 N m c^2 \nu_1^2 = (d^2 U / dr^2)_{r=r_0}$, m étant la masse de la molécule OH_2 , c la vitesse de la lumière.

Nous pensons qu'on peut identifier l'énergie d'hydratation du cation avec l'énergie $-U(r_0)$ de la fixation autour de celui-ci de la première couche de 6 ou de 4 molécules d'eau, selon les cas.

	$-U(r_0)$ (kcal/iongr)		ν_1 (cm ⁻¹)	
	Auteurs	Bernal et Fowler	Mesurée (moyenne)	Calculée
Mg ²⁺ (OH ²) ₆	325	335	363	365
Zn ²⁺ (OH ²) ₆	335	360	389	395
Al ³⁺ (OH ²) ₆	730	870	524	605
Be ²⁺ (OH ²) ₄	390	455	536	600

Tableau 3.

Le tableau 3 donne l'ensemble des nouveaux résultats et pour l'énergie $-U(r_0)$ d'hydratation des cations et pour la fréquence ν_1 de la vibration totalement symétrique. Nous y comparons nos valeurs de $-U(r_0)$ avec les valeurs prises dans les graphiques de Bernal et Fowler [18] correspondant à la première couche d'hydratation.

L'accord entre les fréquences mesurées et calculées, bien qu'il ne soit pas parfait, est satisfaisant, étant donné les approximations.

Les auteurs M. A. Marques et N. M. Marques remercient le Instituto de Alta Cultura pour les Bourses accordées.

REFERENCES

- [1] DA SILVEIRA, A., et BAUER, E., 1932, *C.R. Acad. Sci., Paris*, **195**, 416. DA SILVEIRA, A., 1933, *C.R. Acad. Sci., Paris*, **197**, 1033; 1939, *J. chem. Phys.*, **7**, 380.
- [2] MATHIEU, J. P., 1950, *C.R. Acad. Sci., Paris*, **231**, 896.
- [3] LAFONT, R., 1957, *C.R. Acad. Sci., Paris*, **244**, 1481.
- [4] HESTER, R., 1962 Thèse, Cornell University, Juin. HESTER, R., et PLANE, R. A., 1964, *J. inorg. Chem.*, **3**, 768.
- [5] IRISH, D. E., MCCARROLL, B., et YOUNG, T. F., 1963, *J. chem. Phys.*, **39**, 3436.
- [6] DA SILVEIRA, A., MARQUES, M. A., et MARQUES, N. M., 1961, *C.R. Acad. Sci., Paris*, **252**, 3983.
- [7] CABANNES, J., et ROUSSET, A., 1933, *Ann. Phys., Paris*, **19**, 271.
- [8] DELWAULLE, M. L., 1955, *C.R. Acad. Sci., Paris*, **240**, 2132.
- [9] WU, T.-Y., 1946, *Vibrational Spectra and Structure of Polyatomic Molecules*, Ed. J. W. Edwards,
- [10] BEEVERS, C. A., et LIPSON, H., 1932, *Z. Kristallogr.*, **82**, 297.
- [11] BOBOVICH, Y. S., 1963, *Optics and Spectroscopy*, **13**, 382.
- [12] DUNCAN, A., et POPLE, J., 1953, *Trans. Faraday Soc.*, **49**, 217.
- [13] PAULING, L., 1948, *The Nature of the Chemical Bond* (Oxford University Press).
- [14] HÜCKEL, W., 1951, *Structural Chemistry of Inorganic Compounds* (Amsterdam : Elsevier Publishing Company).
- [15] WELLS, A. F., 1950, *Structural Inorganic Chemistry*, 2nd edition (Oxford University Press).
- [16] SLATER, J. C., et KIRKWOOD, J. G., 1931, *Phys. Rev.*, **37**, 682.
- [17] PAULING, L., 1927, *Proc. roy. Soc.*, **114**, 191.
- [18] BERNAL, J., et FOWLER, R., 1933, *J. chem. Phys.*, **1**, 515.

The electron distribution of the bonded hydrogen atom in carbon-hydrogen bonds

by R. MASON, D. C. PHILLIPS† and G. B. ROBERTSON

Department of Chemistry, The University, Sheffield, and
The Royal Institution, London, W.1

(Received 22 February 1965)

Evidence, from x-ray diffraction data, that the effective nuclear charge of the bonded hydrogen atom in a \geq C-H bond differs from that in the free atom is summarized.

1. INTRODUCTION

X-ray analyses of the structures of simple aromatic molecules have recently progressed to the point where the atomic positions of the hydrogen atoms can be determined with reasonable precision ($\sigma \sim 0.02$ to 0.05 Å). Moreover, detailed comparisons of the electron distribution in the bonded atoms with the free atom 1s distribution function can be made and discrepancies have been noted by Cochran [1, 2] and Mason [3]. A possible explanation [3] of these discrepancies may be that the effective nuclear charges of the bonded and non-bonded atoms are different in the same sense as is found for the hydrogen molecule [4, 5]; accurate refinement analyses of acridine III [6, 7], diphenyl [8], dipyridyl [9, 10] and perylene [11, 12] confirm this view.

2. RESULTS

The x-ray analysis of acridine III has now been completed so that the discrepancy index, R , for the three-dimensional data is 0.065. Refinement of the hydrogen positional and thermal parameters for the nine crystallographically non-equivalent hydrogens was begun when the refinement of the carbon and nitrogen parameters was essentially complete ($R=0.075$). The hydrogen parameter refinement was based initially on the McWeeny scattering factor [13] and provided acceptable results for the coefficients b_{ij} of the thermal parameters

$$T = \exp \{ -b_{11}h^2 + b_{22}k^2 + b_{33}l^2 + b_{12}hk + b_{13}hl + b_{23}kl \}$$

in so far as the refined vibration ellipsoid axes were all real—the b_{ii} terms were not too small while the cross-terms, b_{12} , etc, were not prohibitively large. The orientation of the hydrogen vibration ellipsoids were also related to those of the carbon atoms to which the hydrogens are directly bonded, but the calculated mean square amplitudes of vibration, $\overline{u^2}_{\text{hydrogen}}$, were such that they were all systematically lower than the values of these adjacent carbons. This latter result is not acceptable since the major proportion of the atomic displacements in a molecular crystal at room temperature originates from rigid body molecular

† Medical Research Council External Staff.

'Sharpening' of a 1s curve in this way has only limited validity but the agreement between this semi-empirical f_H and the orbitally contracted 1s function is good (figure); the deviations at high $\sin \theta/\lambda$ values result principally from the fact that the convolution of a positive exponential with the 1s atomic scattering factor is not properly convergent.

The results have been confirmed, at least qualitatively, in our refinement analyses of dipyrindyl and perylene.

3. DISCUSSION

The proposed contraction of *ca.* 20 per cent in the 1s radial function is in qualitative agreement with the results of electron scattering cross section measurements for hydrogen which have been reported recently [15] and with the theoretical estimate of Z_{eff} in the hydrogen molecule [4, 5]. The precise amount of orbital contraction in a \geq C-H bond is, perhaps, quantitatively different from that in the hydrogen molecule but our present results are not sufficiently accurate to allow us to comment on this point.

We are grateful to the Department of Scientific and Industrial Research for support of these studies.

REFERENCES

- [1] COCHRAN, W., 1953, *Acta Cryst.*, **6**, 260.
- [2] COCHRAN, W., 1956, *Acta Cryst.*, **9**, 924.
- [3] MASON, R., 1960, *Proc. roy. Soc. A*, **258**, 302.
- [4] DICKINSON, B., 1933, *J. chem., Phys.* **1**, 317.
- [5] HELLMAN, H., 1937, *Einführung in die Quantenchemie* (Leipzig: Deuticke).
- [6] PHILLIPS, D. C., 1956, *Acta Cryst.*, **9**, 237.
- [7] MASON, R., and PHILLIPS, D. C. (in preparation).
- [8] ROBERTSON, G. B., 1961, *Nature, Lond.*, 1961, **191**, 593, and in preparation.
- [9] MERRITT, L. T., and SCHROEDER, E. D., 1956, *Acta Cryst.*, **9**, 801.
- [10] MASON, R., and ROBERTSON, G. B. (in preparation).
- [11] CAMERMAN, A., and TROTTER, J., 1964, *Proc. roy. Soc. A*, **279**, 129.
- [12] MASON, R., and ROBERTSON, G. B. (in preparation).
- [13] McWEENY, R., 1951, *Acta Cryst.*, **4**, 513.
- [14] BACON, G. E., CURRY, N. A., and WILSON, S. A., 1964, *Proc. roy. Soc. A*, **279**, 98.
- [15] IJUIMA, T., and BONHAM, R. A., 1963, *Acta. Cryst.*, **16**, 1061.

The Jahn-Teller effect in ReF_6

by M. S. CHILD and A. C. ROACH

Chemistry Department, The University of Glasgow

(Received 4 March 1965)

Calculations on the strength of the Jahn-Teller effect in ReF_6 (d^1) on the basis of a purely electrostatic interaction between the fluorine atoms and the non-bonding t_{2g} electron predict a large ν_2 splitting in the Raman spectrum $(130\text{--}200\text{ cm})^{-1}$ and a small tetragonal distortion of the molecule ($\sim 0.005\text{ \AA}$).

A recent analysis of the vibrational spectra of ReF_6 ($5d^1$) has shown evidence for the probable existence of a fairly strong Jahn-Teller effect [1]. In this paper we have tried to estimate the strength of this effect on the assumption that it arises from the electrostatic forces between the non-bonded rhenium t_{2g} electron and the fluorine atoms. Our results, which are rather insensitive to the precise details of the model, agree in order of magnitude with the spectroscopic data. They also predict a small ($\sim 0.005\text{ \AA}$) tetragonal distortion of the molecule.

The Jahn-Teller effect is actually due to a vibrationally-induced coupling between electronic states which would otherwise be degenerated [2]. In the present case, in the absence of such coupling, the electronic state is four-fold degenerate (Γ_8) as a result of a strong spin-orbit coupling among the t_{2g} orbitals which are well separated from the e_g level [3]. The resulting states, which can be regarded as the components of a manifold with pseudo angular momentum quantum number $j' = \frac{3}{2}$, can be written in an obvious notation:

$$\left. \begin{aligned} \left| \frac{3}{2} \right\rangle &= \sqrt{\frac{1}{2}}(|zx, \alpha\rangle - i|yz, \alpha\rangle), \\ \left| \frac{1}{2} \right\rangle &= \sqrt{\frac{1}{6}}(2i|xy, \alpha\rangle + |zx, \beta\rangle - i|yz, \beta\rangle), \\ \left| -\frac{1}{2} \right\rangle &= \sqrt{\frac{1}{6}}(2i|xy, \beta\rangle + |zx, \alpha\rangle + i|yz, \alpha\rangle), \\ \left| -\frac{3}{2} \right\rangle &= -\sqrt{\frac{1}{2}}(|zx, \beta\rangle + i|yz, \beta\rangle), \end{aligned} \right\} \quad (1)$$

and

where α and β are spin functions.

We have supposed that vibronic coupling between these states arises only from electrostatic interaction with the ligand groups. The electrostatic potential at a point distance r from a fluorine ligand at an angle α from the ReF bond was taken to be:

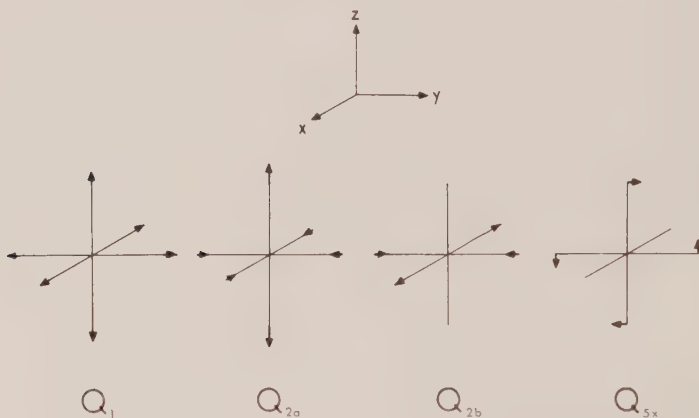
$$\begin{aligned} U(r) = & \left\{ \frac{1}{r} - \frac{10}{r} \exp(-2.674r) - 147r^2 \exp(-5.365r) \right\} \\ & - (1-g) \left\{ \frac{1}{r} - \exp(-2cr) \left[\frac{1}{r} + c\frac{3}{2} + c^2r + \frac{c^3r^2}{3} \right] \right. \\ & - h(1-3\cos^2\alpha) \left[\frac{3}{2c^2r^3} - \exp(-2cr) \left(\frac{3}{2c^2r^3} \right. \right. \\ & \left. \left. + \frac{3}{cr^2} + \frac{3}{r} + 2c + c^2r + \frac{c^3r^2}{3} \right) \right] \left. \right\}, \end{aligned} \quad (2)$$

where the terms in the first parentheses $\{ \}$ are due to the Hartree-Fock electron distribution in the F^- ion [4], and those in the second are the potential due to one electron in a hybrid $2s2p$ Slater-type orbital with exponent c ; h is a hybridization constant ($h=0$ corresponds to a pure s orbital and $h=1$ to a pure p -function) and g is a measure of the bond polarity (completely covalent and completely ionic bonds correspond to $g=0$ and $g=1$ respectively).

Conventionally, the term 'Jahn-Teller effect' is confined to interactions that are linear in the normal coordinates of the molecule, and our attention will be restricted to these. Group theoretical considerations show that the only Jahn-Teller active coordinates are $Q_1(A_{1g})$, $Q_2(E_g)$ and $Q_5(T_{2g})$ [5]. Q_1 and Q_2 are bond stretching vibrations and Q_5 involves changes in bond angles (figure 1). When referred to the above electronic states (1), the vibronic interaction matrix takes the form:

$$\begin{bmatrix} k_1 Q_1 + k_2 Q_{2a} & k_5(Q_{5y} - iQ_{5x}) & k_2 Q_{2b} - ik_5 Q_{5z} & 0 \\ k_5(Q_{5y} + iQ_{5x}) & k_1 Q_1 - k_2 Q_{2a} & 0 & -k_2 Q_{2b} + ik_5 Q_{5z} \\ k_2 Q_{2b} + ik_5 Q_{5z} & 0 & k_1 Q_1 - k_2 Q_{2a} & k_5(Q_{5y} - iQ_{5x}) \\ 0 & -k_2 Q_{2b} - ik_5 Q_{5z} & k_5(Q_{5y} + iQ_{5x}) & k_1 Q_1 + k_2 Q_{2a} \end{bmatrix} \quad (3)$$

The constants k_1 , k_2 and k_5 therefore determine the strength of vibronic coupling.



The vibronically active modes of vibration.

It is clear from equations (1) that the above matrix elements, and hence k_1 , k_2 and k_5 , can be expressed in terms of integrals involving the original t_{2g} orbitals, and it is most convenient to work with these. Further, by expressing the interactions as combinations of single-ligand contributions, we find that only four basic two-centre integrals are required. If the bond is supposed to be along the z axis, the constants k_1 and k_2 depend on the integrals:

$$\left. \begin{aligned} u'_{xy} &= \left[\frac{\partial}{\partial z} \langle xy | U | xy \rangle \right]_{z=R_0} \\ u'_{zx} &= \left[\frac{\partial}{\partial z} \langle zx | U | zx \rangle \right]_{z=R_0} \end{aligned} \right\} \quad (4)$$

and k_5 can be expressed in terms of

$$\left. \begin{aligned} u_{xy} &= [\langle xy | U | xy \rangle]_{z=R_0} \\ u_{zx} &= [\langle zx | U | zx \rangle]_{z=R_0} \end{aligned} \right\} \quad (5)$$

R_0 in these equations is the bond length in the initial undistorted configuration. The exact expressions for k_1 , k_2 and k_5 take the forms:

$$\left. \begin{aligned} k_1 &= \sqrt{\frac{2}{3}} (u'_{xy} + 2u'_{zx}), \\ k_2 &= -\frac{1}{\sqrt{3}} (u'_{xy} - u'_{zx}), \\ k_5 &= \frac{2}{\sqrt{3}} \left(\frac{u_{xy} - u_{zx}}{R_0} \right). \end{aligned} \right\} \quad (6)$$

The dimensionless quantities

$$D_i = \frac{1}{2} \frac{k_i^2}{\lambda_i \nu_i} \quad (i=1, 2, 5), \quad (7)$$

where λ_i and ν_i are the vibrational force constants and vibrational frequencies respectively, then provide a convenient measure of the Jahn-Teller effect [6].

The values $\nu_1 = 755 \text{ cm}^{-1}$, $\nu_2 = 670 \text{ cm}^{-1}$ and $\nu_5 = 295 \text{ cm}^{-1}$ have been adopted. ν_1 is taken directly from the Raman spectrum [1], but ν_2 and ν_5 are interpolated from the sequence WF_6 , IrF_6 and PtF_6 [7-9] because the observed ReF_6 frequencies must partly depend on the Jahn-Teller effect. The bond length R_0 was given the WF_6 value of 1.830 \AA [9]. The remaining unknown quantities are the t_{2g} orbitals themselves, for which we have assumed a 5d Slater-type form with various values of the screening constant p , to eliminate any fortuitous cancellations. The integrals were evaluated by Gaussian quadrature on an English Electric KDF9 computer.

The results are set out in the table. The fluorine orbital exponent c in equation (2) was given the value of 2.425 throughout, in accordance with Slater's rules. (The value $c=2.6$ was found, in one case, to increase the calculated coupling constants by about 2 per cent so the results do not seem very sensitive to this choice.) The t_{2g} orbital exponent p was varied widely around the Slater value of 1.4, and comparison of the resulting radial distributions with the dimensions of the molecule suggests that the extreme values of 1.0 and 2.5, with corresponding orbital maxima at 2.12 \AA and 0.85 \AA respectively, may be rather unrealistic. In the first two sections of the table the ReF bonds are assumed to be purely covalent ($g=0$) using 2p fluorine orbitals in the first section ($h=1$) and 2s orbitals in the second ($h=0$). It is clear that the results are not very sensitive to the values of h but that variation in the size of the Re orbital by means of the exponent p does cause significant changes in the constants D_2 and D_5 . Their order of magnitude, however, particularly in the most probable region $1.4 \leq p \leq 2.0$ remains much the same. The final section shows the effect of increasing the bond polarity. g is the fractional electronic charge transferred to each F atom and the values of orbital exponent p were derived by applying Slater's rules to the Re configuration $5d(t_{2g})^1[5d(e_g)^4 6s^2]^{1-g}$. The values of

p	g	h	$r_{\max}(\text{\AA})$	D_1	D_2	D_3	$\Delta\nu_2$ (cm^{-1})	k_2/λ_2 (cm^{-1})	k_5/λ_5 (cm^{-1})	$\Delta Q_1(\text{\AA})$	$\Delta Q_2(\text{\AA})$	$\Delta Q_5(\text{\AA})$
1.0	0	1	2.12	0.038	0.0069	0.068	13	9.27	40.2	-0.0055		± 0.014
1.4	0	1	1.51	0.413	0.062	0.188	130	82.3	111	-0.018		± 0.025
1.7	0	1	1.25	0.760	0.101	0.188	190	136	111	-0.024	± 0.0067	
2.0	0	1	1.06	0.866	0.101	0.140	190	135	82.4	-0.026	± 0.0067	
2.5	0	1	0.85	0.714	0.061	0.068	130	81.0	39.9	-0.024	± 0.0052	
1.0	0	0	2.12	0.065	0.0093	0.092	20	12.4	54.1	-0.0072		± 0.017
1.4	0	0	1.51	0.543	0.079	0.200	160	106	118	-0.021		± 0.025
1.7	0	0	1.25	0.813	0.117	0.164	210	157	96.7	-0.025	± 0.0072	
2.0	0	0	1.06	0.738	0.104	0.096	200	139	56.7	-0.024	± 0.0068	
2.5	0	0	0.85	0.371	0.048	0.029	110	64.4	16.9	-0.017	± 0.0046	
1.4	0.0	1	1.51	0.413	0.062	0.188	130	82.3	111	-0.018		± 0.025
1.435	0.1	1	1.47	0.222	0.063	0.110	140	83.9	65.0	-0.013	± 0.0053	
1.505	0.3	1	1.41	0.0034	0.059	0.015	130	78.6	8.62	-0.0016	± 0.0051	
1.61	0.6	1	1.31	0.482	0.043	0.041	100	57.9	24.2	+0.019	± 0.0044	
1.75	1.0	1	1.21	3.693	0.016	0.394	40	21.4	232	+0.054		± 0.034

r_{\max} = radial distribution maximum of t_{2g} orbital.

ΔQ_1 = increase in average bond length.

ΔQ_2 = increase in equatorial bond length = $\frac{1}{2}$ (decrease in axial bond length).

ΔQ_5 = atomic displacement in a Q_5 mode.

D_2 appear (perhaps fortuitously) remarkably insensitive to g but k_5 , from which D_5 is calculated by equation (7), falls off rapidly with increasing ionicity and indeed changes sign between $g=0.3$ and 0.6 . We would think it unlikely, however, that g would much exceed the value 0.3 with a corresponding charge $+1.8e$ on the central atom. Broadly speaking therefore the magnitudes of D_2 and D_5 do not vary much over the range of physically reasonable parameters in our model.

The values of D_2 and D_5 determine the expected splitting in the Raman spectrum. Assuming that Q_2 and Q_5 act independently, the present case for Q_2 is identical with that analysed by Longuet-Higgins and others [10] and the $\Delta\nu_2$ values in column 7 are derived from their tables of vibronic energy levels. In the region $1.4 \leq p \leq 2.0$ these values are in good agreement with the reported value of $\sim 150 \text{ cm}^{-1}$ [1]. There are no comparable tables from which we could predict the structure of the ν_5 band.

Finally we consider the effect of vibronic interactions on the equilibrium configuration of the molecule. Moffitt and Thorson have shown [5] that Jahn-Teller forces would cause a distortion either of $\pm k_2/\lambda_2$ in Q_2 alone (if $k_2^2/\lambda_2 > k_5^2/\lambda_5$) or of $\pm k_5/\lambda_5$ in Q_5 alone (if $k_2^2/\lambda_2 < k_5^2/\lambda_5$) but never in both at once. Furthermore any second-order effects ensure that Q_2 distortion will be in the Q_{2a} component [11] (figure 1). Superimposed on this there will also be a distortion of $(-k_1/\lambda_1)$ in the symmetrical stretching coordinate Q_1 . The calculated atomic displacements are given in the final three columns. It is clear that neither Q_2 nor Q_5 distortions predominate over the entire range of p and that no firm prediction is possible. A small amount of ionicity tends to favour Q_2 , however, and a distortion in this mode appears the more likely. We would predict therefore a probable small decrease in average bond length ($\sim 0.01 \text{ \AA}$) from the WF_6 value of 1.83 \AA superimposed on a tetragonal distortion (change in equatorial bond length $\sim 0.005 \text{ \AA}$).

It is interesting to find that the actual Jahn-Teller distortion in the isolated molecule will probably be rather small, although the effect on the vibrational spectrum appears quite striking. There may however be cooperative Jahn-Teller effects between different molecules in a crystal and this aspect of the problem has not yet been discussed.

One of us (A.C.R.) is grateful for a grant from the Carnegie Trust for the Universities of Scotland.

REFERENCES

- [1] WEINSTOCK, B., and GOODMAN, G. L., *Adv. chem. phys.* (in course of publication).
- [2] LONGUET-HIGGINS, H. C., 1960, *Advanc. Spectrosc.*, **2**, 249.
- [3] MOFFITT, W., GOODMAN, G. L., FRED, M., and WEINSTOCK, B., 1959, *Mol. Phys.*, **2**, 109.
- [4] CRAIG, D. P., and ZAULI, C., 1962, *J. chem. Phys.*, **37**, 601.
- [5] MOFFITT, W., and THORSON, W. R., 1957, *Phys. Rev.*, **108**, 1256.
- [6] MOFFITT, W., and THORSON, W. R., 1958, *Rec. Mém. Centre Nat. Rech. Sci.*, November.
- [7] BURKE, T. G., SMITH, D. F., and NIELSON, A. H., 1952, *J. chem. Phys.*, **20**, 447.
- [8] CLAASSEN, H. H., MALM, J. G., and SELIG, H., 1962, *J. chem. Phys.*, **36**, 2890.
- [9] WEINSTOCK, B., CLAASSEN, H. H., and MALM, J. G., 1960, *J. chem. Phys.*, **32**, 181.
- [10] LONGUET-HIGGINS, H. C., ÖPIK, U., PRICE, M. H. L., and SACK, R. A., 1958, *Proc. roy. Soc. A*, **244**, 1.
- [11] BALHAUSEN, C. J., and LIEHR, A. D., 1958, *Annals of Physics*, **3**, 304.

The electron spin resonance spectra of paradinitrobenzene anions

by J. M. GROSS and M. C. R. SYMONS

Department of Chemistry, The University, Leicester

(Received 19 October 1964)

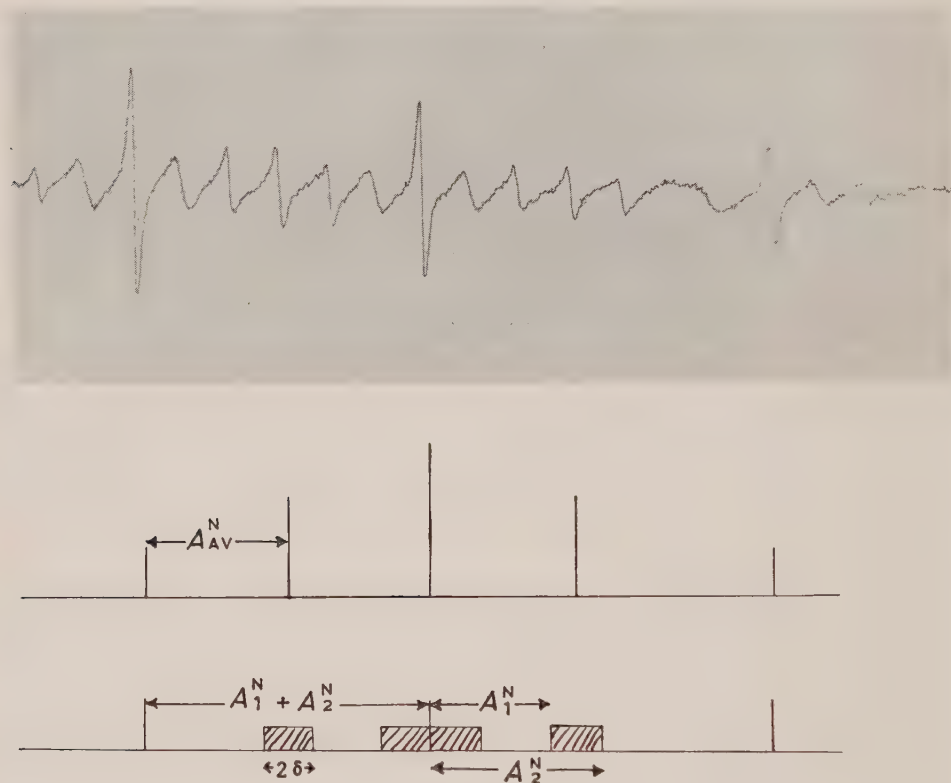
Electron spin resonance spectra of paradinitrobenzene anions in methanol-dioxane mixtures exhibit a very marked line-width alternation. It is shown that such alternation, stemming from a relatively small difference between the isotropic hyperfine coupling constants of the two nitrogen atoms can account for the apparently anomalous spectra in solvents of low dielectric constant.

Considerable attention has been given to the observation that both *meta* [1] and *paradinitrobenzene* [2] anions, when prepared by alkali metal reduction in ethers, exhibit spectra apparently showing a large hyperfine interaction with only one nitrogen, whereas electrolytic preparation of the anions in acetonitrile [3] or dimethyl formamide [4] gives spectra which show clearly the presence of two equivalent nitrogens.

Since, at least for the *meta*-isomer, the 'normal' spectrum can be regenerated from the 'abnormal' simply by dilution of ether solutions with acetonitrile [5], it seems that chemical reaction does not take place and that the dissymmetry is caused by ion-pairing. This raises a major problem, however, since it is then necessary to invoke a molecular orbital scheme which allows the relatively minor perturbation of replacing solvent molecules close to one of the nitro groups by a cation to alter the structure so drastically that one nitrogen and, for the *para*-isomer two protons, virtually cease to interact with the electron spin. As has been stressed by Weissman [6] and verified for other systems by Bolton *et al.* [7], this situation is only likely to arise when there is a near-degeneracy in the molecular orbital of the unpaired electron so that the perturbation effectively confines the electron to one level only. The difficulty is to find suitable levels for both the *meta* and *para*-isomers.

The purpose of this note is to report results for the *para*-isomer in methanol-dioxan mixtures which show that there is such a marked line-width alternation that some lines become almost undetectable when the concentration of methanol is small. Extrapolation of these results together with the values of A^N and A^H to pure dioxan suggests strongly that the spectrum obtained by Ward was subject to a similar line-width alternation. This means that, rather than postulating a very large difference between the two nitrogens (N_1 and N_2) with a slow fluctuation (probably caused by migration of the cation [8]), it is only necessary to postulate a minor difference between A_1^N and A_2^N together with a fluctuation of frequency comparable with that of the inverse of the hyperfine interaction energy.

The ways in which such a fluctuation can cause line-broadening have been discussed in depth by Freed and Fraenkel [9] and a simple pictorial representation for the case of two nitrogen nuclei is given in the figure together with a typical spectrum. The nitrogen contribution changes from a quintet with relative intensities 1:2:3:2:1 (in the absence of trends caused by g and A -tensor anisotropies) with hyperfine splitting A_{AV}^N to a 1:1:1 triplet with splitting $2A_{AV}^N$ in the limit of very broad intermediate lines. Following behind this



Spectrum of *para*dinitrobenzene anions in a methanol-dioxan mixture containing 54.3 percent mole fraction dioxan. Theoretical reconstruction showing the effect of fluctuation in the nitrogen hyperfine coupling constants A_1^N and A_2^N about the mean value A_{AV}^N .

$$\begin{aligned} A_1^N + A_2^N &= 2A_{AV}^N, \\ A_2^N - A_1^N &= \delta. \end{aligned}$$

trend (because of the smaller hyperfine interaction energy) the proton contribution passes from a 1:4:6:4:1 quintet with splitting A_{AV}^H to a 1:4:1 triplet with splitting $2A_{AV}^H$. This is closely the situation found by Ward. It should be noted that A_{AV}^N estimated in this way is smaller than that found in good solvents such as methanol [10], but is close to that found in acetonitrile, dimethylformamide and other poor hydrogen-bonding media.

Thanks are due to the Department of Scientific and Industrial Research for a maintenance grant to J. M. G.

REFERENCES

- [1] WARD, R. L., 1960, *J. chem. Phys.*, **32**, 410.
- [2] WARD, R. L., 1961, *J. Amer. chem. Soc.*, **83**, 1296.
- [3] GESKE, D. H., and MAKI, A. H., 1960, *J. chem. Phys.*, **33**, 825.
- [4] RIEGER, P. H., and FRAENKEL, G. K., 1963, *J. chem. Phys.*, **39**, 609.
- [5] BLANDAMER, M. J., GROSS, J. M., and SYMONS, M. C. R., 1963, *J. chem. Soc.*, p. 559.
- [6] WEISSMAN, S. I., 1961, *Ann. Rev.*, **12**, 162.
- [7] BOLTON, J. R., CARRINGTON, A., FORMAN, A., and ORGEL, L. E., 1962, *Mol. Phys.* **5**, 43.
- [8] DE BOER, E., and MACKOR, E. L., 1964, *J. Amer. chem. Soc.*, **86**, 1513.
- [9] FREED, J. H., and FRAENKEL, G. K., 1963, *J. chem. Phys.*, **89**, 326.
- [10] AYSCOUGH, P. B., SARGENT, F. P., and WILSON, R., 1963, *J. chem. Soc.*, p. 5418.

RESEARCH NOTES

Variation calculations for H_2^+ using A.O.'s with angularly dependent Z_{eff}

by K. C. BHALLA and P. G. KHUBCHANDANI

Atomic Energy Establishment Trombay, Chemistry Division, Bombay 28,
India

(Received 9 March 1965)

The H_2^+ molecule has been studied by the variational method by Scrocco and Tomasi [1] using angularly dependent Z_{eff} . They have used the wave function $\psi = \chi_a + \chi_b$ with $\chi_a = \exp[-Z\lambda_{ra}(1 + \gamma \cos \theta_a)]$ and a similar expression for χ_b . When χ is expanded, one gets in terms of atomic orbitals

$$\chi = (1 - \gamma^2) \left\{ (1s) - \gamma(2p_\sigma) + \frac{\sqrt{5}}{8} \gamma^2(3s) - \dots \right\},$$

where $1s$, $2p_\sigma$, $3s$ are normalized slater orbitals. In this expansion we see that the orbitals $2s$, $4s$, $3p_\sigma$, $5p_\sigma$. . . are missing. We have in the present work written the wave function in a form so as to include these missing orbitals which are of the right symmetry. As expected we have been able to lower the energy calculated by them.

We write $\psi = \phi_a + \phi_b$,

where $\phi_a = \exp[-Z(1 + \gamma \cos \theta_a)r_a](1 + p r_a)$.

On expansion we get:

$$\begin{aligned} \phi = (1 - \gamma^2) \left[\left\{ (1s) - \gamma(2p_\sigma) + \frac{\sqrt{5}}{8} \gamma^2(3s) - \dots \right\} \right. \\ \left. + p \left\{ \frac{\sqrt{3}}{Z} (2s) - \frac{\gamma}{Z} \left(\frac{15}{2} \right)^{1/2} (3p_\sigma) + \dots \right\} \right] \end{aligned}$$

This includes the terms missing in χ . Also the parameter p gives laxity to the problem.

The various integrals could be obtained in closed form and the calculations were performed on CDC 3600. The bond energy obtained was 2.759 ev against 2.734 ev obtained by Scrocco and Tomasi. The exact value [2] is 2.792 ev. Thus we have nearly halved the error by including an extra term.

REFERENCES

- [1] SCROCCO, E., and TOMASI, J., 1961, *Mol. Phys.*, **4**, 193.
- [2] BATES, D. R., LEDSHAM, K., and STEWART, A. L., 1953, *Phil. Trans. A*, **246**, 215.

Cobalt-59 spin-spin coupling and isotope shifts in $K_3Co(CN)_6$

by A. LOEWENSTEIN and M. SHPORER

Department of Chemistry, Technion—Israel Institute of Technology,
Haifa, Israel

(Received 9 February 1965)

Carbon-13 spin-spin coupling constants with 1H , ^{19}F have been studied extensively [1]. The shifts due to substitution of ^{12}C by ^{13}C on the 1H or ^{19}F nuclear magnetic resonances were observed before [2]. Their magnitudes are extremely small and difficult to measure with sufficient accuracy for quantitative calculations.

We have measured the nuclear magnetic resonance spectrum of ^{59}Co in an aqueous solution of $K_3Co(CN)_6$ (about 1 M) prepared from KCN enriched to 15 atom per cent with ^{13}C . The fractions of zero-, mono-, di- and tri-substituted complexes are 0.377; 0.400; 0.176; and 0.041 respectively. The measurements were performed at two constant frequencies: 4.3 and 14.1 Mc (^{59}Co frequency is 10.1 Mc at 10 kG).

The results are shown in the figure and the measured data summarized in the table.

Frequency (Mc)	$J^{59}Co-^{13}C$ (c.p.s.)	$\delta\sigma(^{13}C-^{12}C)†$ (c.p.s.)		
		One ^{13}C	Two ^{13}C	Three ^{13}C
14.1	128 ± 0.5	12.0 ± 0.7	24.1 ± 1.0	36.1 ± 1.5
4.3	127 ± 1	3.5 ± 1.0	6.2 ± 1.5	—

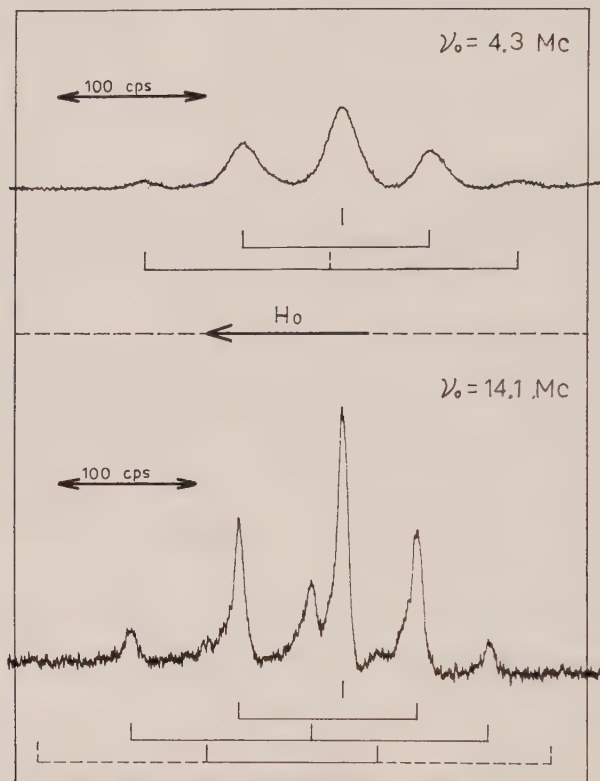
† Measured relative to zero substituted $K_3Co(CN)_6$; all isotopic shifts are to higher magnetic fields.

^{59}Co spin-spin coupling and isotope shifts in $K_3Co(CN)_6$

Benedek *et al.* [3] have measured the pressure dependence of ^{59}Co and from their results estimated the quantity n defined as $n = -\partial \ln \Delta / \partial \ln R$ where Δ is the crystal field splitting and R the cobalt ligand distance. Following the arguments given by Benedek *et al.* [3] and assuming that the changes in σ , ($\delta\sigma$) caused by the substitution of ^{13}C are wholly due to changes, δR , in R , one readily obtains $\delta\sigma/\sigma_p = -n\delta R/R$ where σ_p is the paramagnetic contribution to the ^{59}Co shift. Substituting $n=5$, $\sigma_p=0.0141$ [3], $\delta\sigma=12/14.1 \times 10^6$ one obtains $\delta R/R = -1.2 \times 10^{-5}$, i.e. substitution of one ^{12}C by ^{13}C decreases the mean Co ligand distance ($R \approx 1.8 \text{ \AA}$) by 1.2×10^{-3} per cent. Since ^{13}C shifts seem to be additive (see table) total substitution of ^{12}C by ^{13}C in $K_3Co(CN)_6$ would decrease the Co ligand mean distance by about 7×10^{-3} per cent. This estimate is obviously an upper limit since it is assumed that the change in Δ can be completely attributed to the change in distance. The change in R is in the same direction as is observed

when pressure is applied to the system [3] and indicates shortening of the Co ligand distance. Shortening of the bonds by isotopic substitution is also expected if the vibrational potential curve remains unaltered [4].

The compound was prepared from ^{13}C enriched KCN \dagger by a procedure given by Bigelow [5]. Measurements were performed on a Varian DP spectrometer using a V4311 fixed frequency unit operating at 4.3 Mc and a V4210A variable



^{59}Co n.m.r. spectra of $\text{K}_3\text{Co}(\text{CN})_6$ in aqueous solution at 14.1 and 4.3 Mc.

frequency unit operating at 14.1 Mc. Detection with the latter unit was done through a V3521 integrator applying a 2 kc low index modulation and recording the centre-band of the output.

Note:—While this note was in press P. C. Lauterbur has reported similar measurements in *J. chem. Phys.*, **42**, 799 (1965).

REFERENCES

- [1] See for example : LAUTERBUR, P. C., 1962, *Determination of Organic Structures by Physical Methods*, Ed. F. C. Nachod and W. D. Philips (New York: Academic Press), p. 465.
- [2] FRANKISS, S. G., 1963, *J. phys. Chem.*, **67**, 752. SHOOLERY, J. N., JOHNSON, L. F. and W. A., ANDERSON, 1960, *J. mol. Spectrosc.*, **5**, 100.
- [3] BENEDEK, G. B., ENGELMAN, R., and ARMSTRONG, J. A., 1963, *J. chem. Phys.*, **39**, 3349.
- [4] HALEVI, E. A., 1963, *Progress in Physical Organic Chemistry*, Vol. I, Ed. S. G. Cohen, A. Steitwieser, Jr., and R. W. Taft (New York: Interscience Publishers), p. 109.
- [5] BIGELOW, J. H., 1946, *Inorg. Syn.*, **2**, 225.

\dagger The authors thank Professor G. Stein and Mr. G. Navon of the Department of Physical Chemistry, The Hebrew University, Jerusalem, for their kind assistance.

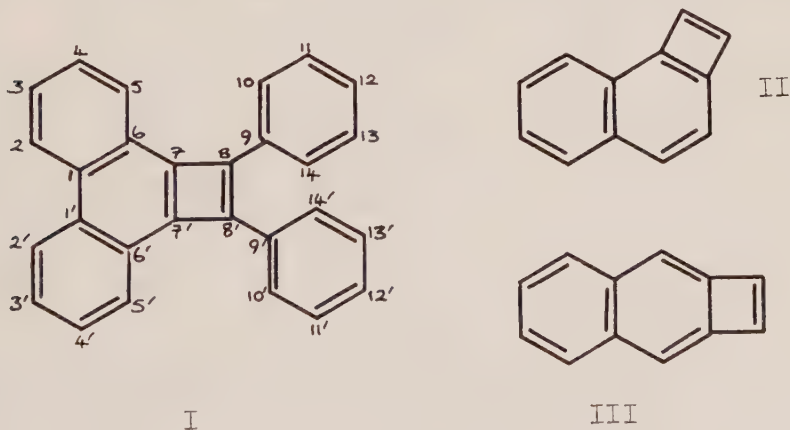
Calculation of a triplet ground state for 1,2-diphenylphenanthro[1]-cyclobutene

by J. W. HILPERN

Department of Chemistry, The University, Sheffield 10

(Received 6 January 1965)

Cava *et al.* [1] have recently reported that 1,2-diphenylphenanthro [1] cyclobutene, I, is formed as an unstable intermediate on the debromination of 1,2-dibromo-1,2-diphenylphenanthro [1]-cyclobutene. The behaviour of (I) lead them to postulate that this molecule might exist as a triplet in the ground state. Coulson and Poole [2] have carried out a molecular orbital study on 1 : 2 (II) and 2 : 3 naphthocyclobutadiene (III) and related compounds. Cava *et al.* [3] has reported the synthesis of diphenyl 2 : 3 naphthocyclobutadiene which they have isolated but which readily undergoes dimerization. Coulson's calculations on (II) have shown that there is a large degree of double bond fixation in the four membered ring and that the molecule should be very reactive, although more stable and less reactive than the 1 : 2 compound. (I) does not appear to show a comparable dienophilic reactivity of the double bond and we have carried out a Pariser-Parr-Pople calculation on (I) as described by Murrell [4].



This is a semi-empirical method based on the zero-differential-overlap approximation but including electron repulsion terms. The Huckel coefficients were first calculated and the same procedure then followed as in calculations on biphenylene by Hilpern [5].

The molecule has C_{2v} symmetry and all the π orbitals, with which we are dealing, have symmetry A_2 or B_2 . Table 1 shows the Huckel bonding orbitals and orbital energies.

	C_1	C_2	C_3	C_4	C_5	C_6	C_7	C_8	C_9	C_{10}	C_{11}	C_{12}	C_{13}	C_{14}	m
$\psi_1(B_2)$	0.1667	0.0892	0.1724	0.0781	0.1774	0.0667	0.3484	0.3927	0.0190	0.1969	0.0064	0.1974	0.0064	0.1969	-0.0644
$\psi_2(A_2)$	0.2990	0.3720	0.0103	0.3800	0.2846	0.1592	0.1091	0.0346	0.0477	0.0385	0.0199	0.0512	0.0199	0.0358	-0.7761
$\psi_3(B_2)$	0.0878	0.2196	0.2612	0.0134	0.2718	0.2012	0.2008	0.1589	0.2343	0.1719	0.0986	0.2497	0.0986	0.1719	-0.7894
$\psi_4(B_2)$	0	0	0	0	0	0	0	0	0	0.3536	0.3536	0	0.3536	0.3536	-1.0000
$\psi_5(A_2)$	0	0	0	0	0	0	0	0	0	0.3536	0.3536	0	0.3536	0.3536	-1.0000
$\psi_6(A_2)$	0.0309	0.2281	0.2821	0.0824	0.1913	0.2930	0.1005	0.0820	0.2727	0.1091	0.1525	0.2770	0.1525	0.1091	-1.1010
$\psi_7(B_2)$	0.1819	0.2611	0.1400	0.0884	0.2490	0.2186	0.2024	0.1715	0.2424	0.0637	0.1638	0.2657	0.1638	0.0637	-1.2331
$\psi_8(A_2)$	0.0264	0.1872	0.2616	0.1414	0.0839	0.2468	0.1997	0.2037	0.2599	0.0614	0.1828	0.2910	0.1828	0.0614	-1.2562
$\psi_9(B_2)$	0.3272	0.0054	0.3200	0.4291	0.2481	0.1006	0.0542	0.0831	0.0810	0.0122	0.0650	0.0981	0.0650	0.0122	-1.3240
$\psi_{10}(B_2)$	0.1736	0.1767	0.1525	0.1045	0.0404	0.0301	0.2694	0.1976	0.1025	0.1933	0.2541	0.2755	0.2541	0.1933	-1.8448
$\psi_{11}(A_2)$	0.1870	0.2371	0.2765	0.3033	0.3165	0.3153	0.1129	0.0184	0.0585	0.0664	0.0713	0.0730	0.0713	0.0664	-1.9548
$\psi_{12}(A_2)$	0.0433	0.0443	0.0489	0.0573	0.0704	0.0892	0.0717	0.1317	0.3339	0.2815	0.2516	0.2419	0.2516	0.2815	-2.0802
$\psi_{13}(B_2)$	0.3310	0.2172	0.1570	0.1354	0.1472	0.1954	0.0394	0.2444	0.2653	0.1758	0.1296	0.1154	0.1296	0.1758	-2.2465
$\psi_{14}(B_2)$	0.2384	0.1168	0.0730	0.0778	0.1343	0.2804	0.3748	0.3441	0.1986	0.0926	0.0484	0.0363	0.0484	0.0926	-2.6661

Table 1. Huckel bonding orbitals and orbital energies of I.

Coefficients of C_1' , etc. = C_1 , etc., for orbitals of B_2 symmetry, = $-C_1$, etc. for orbitals of A_2 symmetry.

For reasons of space -0.2990 is written as 0.2990 etc.).

As in reference [5], the triplet energy of the first excited state is given by

$$\langle {}^3\psi_1^{-1} | \mathcal{H} | {}^3\psi_1^{-1} \rangle - E_0 = F_{-1-1} - F_{11} - \langle 1_1 - 1 | G | 1_1 - 1 \rangle. \quad (1)$$

Calculation of $(F_{-1-1} - F_{11})$ gives a value of 3.88 eV, and the electron repulsion integral a value of 4.64 eV. Thus the energy of triplet state is seen to be -0.76 eV, 0.76 eV, below the closed-shell configuration state of the molecule, in other words is the ground state. Coulson [2] has given formulae connecting bond length with overlap. The overlap integral for a single C-C bond corresponds to two-thirds that for an aromatic C-C bond. Substituting this value for the 7,8 bond in the cyclobutadiene ring gives a triplet energy equal to that of the ground state energy. Since even in the limiting case of single bond overlap in the cyclobutadiene ring the closed-shell ground state is no more stable than the triplet level, it seems probable that this molecule does indeed have a triplet ground state as suggested by Cava. This is important as it means that this is the first even alternant aromatic hydrocarbon to have been observed with a triplet ground state. The existence of a triplet ground state is associated with the small difference in energy between highest bonding and lowest antibonding Huckel orbitals. Coulson and Poole [2] found an energy separation of $0.295\beta_0$ for 1:2 naphthocyclobutadiene (II) where the naphthalene double bond is mainly localized in the cyclobutadiene ring, but a larger energy separation of $0.67\beta_0$ for 2:3 naphthocyclobutadiene (III) where the naphthalene double bonds are mainly exocyclic to the cyclobutadiene ring. In (I), the phenanthrene 9,10 bond has considerably more double bond character and the energy separation is only $0.13\beta_0$.

Band Clar's/Platt's classification	Wavefunction	Symmetry	Calculated energy (eV)
		$\beta_{78} = \frac{2}{3}\beta_{12}$ in brackets	
p 1L_a	${}^1\psi_1^{-1}$	B_1	0.36 (1.98)
α 1L_b	${}^1\psi_1^{-2} - {}^1\psi_2^{-1}$ (forbidden)	A_1	2.72 (3.34)
β 1B_b	${}^1\psi_1^{-2} + {}^1\psi_2^{-1}$ (forbidden)	A_1	2.76 (3.88)
β' 1B_a	${}^1\psi_2^{-2}$	B_1	4.64 (5.26)
${}^3\beta$ 3B_b	${}^3\psi_1^{-2} + {}^3\psi_2^{-1}$ (forbidden)	A_1	1.91 (3.03)
${}^3\alpha$ 3L_b	${}^3\psi_1^{-2} - {}^3\psi_2^{-1}$ (forbidden)	A_1	2.32 (3.34)
${}^3\beta'$ 3B_a	${}^3\psi_2^{-2}$	B_1	3.51 (4.13)

Table 2. Calculated electronic spectrum of I.

Table 2 gives the calculated electronic spectrum, the energy differences being calculated with reference to the triplet ground state. The first excited singlet state, the p band, is in the infra-red, the α and β bands are symmetry forbidden, the β band at 2.76 eV probably appearing as a weak band, but the maximum absorption band expected would be the allowed β' band at 4.64 eV. The first excited triplet level lies above the first excited singlet but still in the infra-red region.

It should be pointed out that the two phenyl rings have been taken to be planar in this calculation. Steric hindrance would probably lead to distortion of the 13-14-9 and 13'-14'-9' bonds but would not appreciably effect the conjugation

within the phenyl ring itself. Calculations on the molecule reducing β for the 8-9 and 8'-9' bonds to the single bond value were, however, carried out; ($F_{-1-1} - F_{11}$) in this case was 3.92 eV, 0.04 eV different from the previous calculation. It is thus seen that a reduction in the 8-9, 8'-9' bond orders does not affect the main conclusion, that the molecule probably exists as a triplet in the ground state.

The author would like to thank the Air Force Cambridge Research Laboratories, O.A.R. of the office of Aerospace Research, United States Air Force, through its European Office for support of this work under contract AF 61(052)-848.

REFERENCES

- [1] CAVA, M. P., and MARIGOLD, D., 1964, *Tetrahedron Letters*, **26**, 1751.
- [2] COULSON, C. A., and POOLE, M. P., 1964, *Tetrahedron*, **20**, 1859.
- [3] CAVA, M. P., HWANG, B., and VAN METER, J., 1963, *J. Amer. chem. Soc.*, **85**, 4032.
- [4] MURRELL, J. N., 1963, *The Theory of the Electronic Spectra of Organic Molecules* (London: Methuen), pp. 109 and 318.
- [5] HILPERN, J. W., 1965, *Trans. Faraday Soc.*, **61**, 605.

Tetragonal splittings in cobalt complexes. A correction

by J. H. DUNLOP and R. D. GILLARD

Department of Chemistry, The University, Sheffield, 10

(Received 6 March 1965)

It has been brought to our attention that the circular dichroism spectrum of *trans*-dichlorobis (—) propylenediaminecobalt (III) chloride which we reported [1] recently is incorrect, owing to a base-line error. The corrected circular dichroism agrees with that reported by Mathieu [2] and, more recently, by Wentworth and Piper [3].

REFERENCES

- [1] DUNLOP, J. H., and GILLARD, R. D., 1964, *Mol. Phys.*, **7**, 493.
- [2] MATHIEU, J. P., 1944, *Ann. Phys., Paris*, **19**, 335.
- [3] WENTWORTH, R. A. D., and PIPER, T. S., 1965, *Inorganic Chem.*, **4**, 202.

A molecular orbital theory of hydrocarbons

II. Ethane, ethylene and acetylene

by J. A. POPLE

Carnegie Institute of Technology and Mellon Institute, Pittsburgh, Pa., U.S.A.

and D. P. SANTRY

Carnegie Institute of Technology, Pittsburgh, Pa., U.S.A.

(Received 15 September 1964)

The molecular orbital theory of hydrocarbons developed in a previous paper [1] has been extended and applied to the molecules ethane, ethylene and acetylene, enabling the long-range bond orders, and hence the extent of the delocalization of electrons between σ bonds, to be compared for the three hybridizations sp^3 , sp^2 and sp . It is found that the geminal bond orders are sensitive to changes in hybridization as they depend directly on the s-character of the bonds. Vicinal bond orders are quite large and found to be closely related to the extent of second-order hyperconjugation.

1. INTRODUCTION

In part I of this series [1], an independent electron molecular orbital theory was described and applied in some detail to paraffin molecules. The theory used the 2s and 2p atomic orbitals of carbon and the 1s orbitals of hydrogen as a basis for a linear combination of atomic orbital (LCAO) expansion of the molecular orbitals. Sufficient conditions for a transformation to completely localized bond orbitals were derived and a perturbation approach was then used to study the extent and causes of partial delocalization of the bonding electrons. Zero-order wave functions were built up from hybrid orbitals localized in each bond, and the effect of interaction between bonds allowed for by the method of polarizabilities introduced by Coulson and Longuet-Higgins [2] for π -electrons. It was found that long-range bond orders, which are a measure of electron delocalization, could be quite large and extend over several bonds. The delocalization also introduced significant extra terms in the expression for the total energy of the molecule, but it was found possible to retain a good additivity law by appropriate redefinitions of C-C and C-H bond energies.

In this paper, we aim to extend these methods to hydrocarbons with double and triple carbon-carbon bonds. This will be done by applying similar techniques to a comparative study of the three basic molecules ethane, ethylene and acetylene. Emphasis will again be on the calculation of charge densities, bond orders (including the long-range ones which indicate bond delocalization) and corresponding contributions to the total energy. All electrons in the valence shell (that is all except those in carbon inner shells) are considered explicitly.

Mention should be made of important work by Hoffmann [3], who has made extensive numerical calculations on a wide range of hydrocarbons using a

similar basic theory. Our study differs from his in attempting to avoid commitment to particular numerical parameters as far as possible and in developing perturbation methods so that the theory can be applied in a comparative manner to related molecules. It is encouraging that some of his detailed results parallel our predictions.

2. GENERAL LCAO THEORY

The details of the general theory were given in part I and only a summary of the more important points need be presented here. Molecular orbitals are written in LCAO form:

$$\psi_i = \sum_{\mu} c_{i\mu} \phi_{\mu}, \quad (2.1)$$

where the basic functions ϕ_{μ} are all hydrogen 1s (written h), carbon 2s (written s) and carbon 2p (written p) atomic orbitals. The coefficients satisfy the linear equations:

$$\sum_{\nu} (H_{\mu\nu} - \epsilon_i \delta_{\mu\nu}) c_{i\nu} = 0, \quad (2.2)$$

overlap integrals having been neglected. The charge density and bond order matrix is then defined as:

$$P_{\mu\nu} = 2 \sum_i^{\text{occ}} c_{i\mu} c_{i\nu}, \quad (2.3)$$

the sum being over (doubly) occupied molecular orbitals.

The Hamiltonian matrix elements $H_{\mu\nu}$ are classified as follows:

- (i) Diagonal elements $H_{\mu\mu}$, denoted by α_h , α_s and α_p for hydrogen 1s, carbon 2s and carbon 2p orbitals respectively
- (ii) Elements $H_{\mu\nu}$ between different s, p atomic orbitals on the same atom. These are neglected.
- (iii) Elements $H_{\mu\nu}$ between atomic orbitals on neighbouring atoms. For C-H bonds these are written β_{sh} and $\beta_{\sigma h}$, σ denoting a p-function along the bond. For C-C bonds there are four types of element β_{ss} , β_{os} , $\beta_{\sigma\sigma}$ and $\beta_{\pi\pi}$ (see figure 1 of part I).
- (iv) Elements $H_{\mu\nu}$ between more distant atoms. Initially these are neglected but they are reintroduced in certain cases later in the paper.

In numerical calculations, the diagonal elements (i) are given values:

$$\alpha_h = -13.6 \text{ eV}, \quad \alpha_p = 11.5 \text{ eV}, \quad \alpha_s = -21.34 \text{ eV}, \quad (2.4)$$

which are the sp^3 valence state ionization potentials given by Skinner and Pritchard [4]. Off-diagonal elements (iii) between orbitals or neighbouring atoms are assumed to be proportional to the corresponding overlap integral:

$$H_{\mu\nu} = \beta_0 S_{\mu\nu}, \quad (2.5)$$

β_0 being a constant taken as -10 eV to obtain values comparable with those used in empirical π -electron theories. Overlap integrals were taken from the tables of Mulliken, Rieke, Orloff and Orloff using Slater exponents of 1.0 for the hydrogen 1s orbital and 2s and 2p for carbon 2s and 2p orbitals. Values are listed in table 1.

	S_{hh}^\dagger	S_{sh}	S_{oh}	S_{ss}	S_{os}	S_{oo}	$S_{\pi\pi}$
Ethane ($r_{CC}=1.54 \text{ \AA}$, $r_{CH}=1.114 \text{ \AA}$)	0.269	0.557	0.457	0.030	0.365	-0.328	0.192
Ethylene ($r_{CC}=1.35 \text{ \AA}$, $r_{CH}=1.06 \text{ \AA}$)	0.264	0.585	0.468	0.431	0.430	-0.326	0.265
Acetylene ($r_{CC}=1.20 \text{ \AA}$, $r_{CH}=1.06 \text{ \AA}$)	—	0.585	0.468	0.511	0.472	-0.290	0.337

† Between geminal hydrogens.

Table 1. Atomic overlap integrals.

3. HYBRID ORBITAL TREATMENT OF ETHANE, ETHYLENE AND ACETYLENE

The general LCAO method based on s and p atomic orbitals outlined in the previous section is applicable in principle to all hydrocarbons in any configuration. To study bond delocalization, however, it is more convenient to use an alternative, but equivalent, set of *hybrid orbitals*. For ethane and other paraffinic hydrocarbons discussed in part I, carbon s and p functions are replaced by four tetrahedral sp^3 hybrids having the form:

$$(te) = (s + 3^{1/2}p)/2 \quad (3.1)$$

directed along four bond directions. For ethylene, a more appropriate set of hybrids consists of three sp^2 or trigonal orbitals:

$$(tr) = (s + 2^{1/2}p)/3^{1/2}, \quad (3.2)$$

directed from each carbon atom along the C-C and C-H bonds in the molecular plane (assuming 120° bond angles as a simplified model). The set is completed by carbon 2p orbitals (usually denoted by $2p\pi$) with nodes in the molecular plane. For acetylene, appropriate hybrids are digonal orbitals:

$$(di) = (s + p)/2^{1/2}, \quad (3.3)$$

directed along the C-C and C-H bonds, together with two carbon $2p\pi$ orbitals for each carbon atom with perpendicular nodes in the molecular plane.

It should be emphasized that these choices of basis functions imply no particular assumptions about the chemical bonding. The hybrid basis sets are simply orthogonal transformations of the original s-p sets and the molecular orbitals derived by solution of the LCAO equations (2.2) will be identical, whichever set is used.

Hamiltonian matrix elements referred to the hybrid set are easily expressed in terms of previously defined quantities. The diagonal elements will be denoted by α_{te} , α_{tr} and α_{di} and off-diagonal elements as shown in figure 1.

Off-diagonal elements may be classified into those between orbitals directly bonded in the primary valence structure (β_{CH} and β_{CC}) and the remainder which connect orbitals in different bonds. The importance of this distinction is that the directly bonded interactions localize electrons in the bonds while the others delocalize them between bonds and are responsible for long range bond orders. In the theory developed here, the delocalizing elements are treated as perturbations.

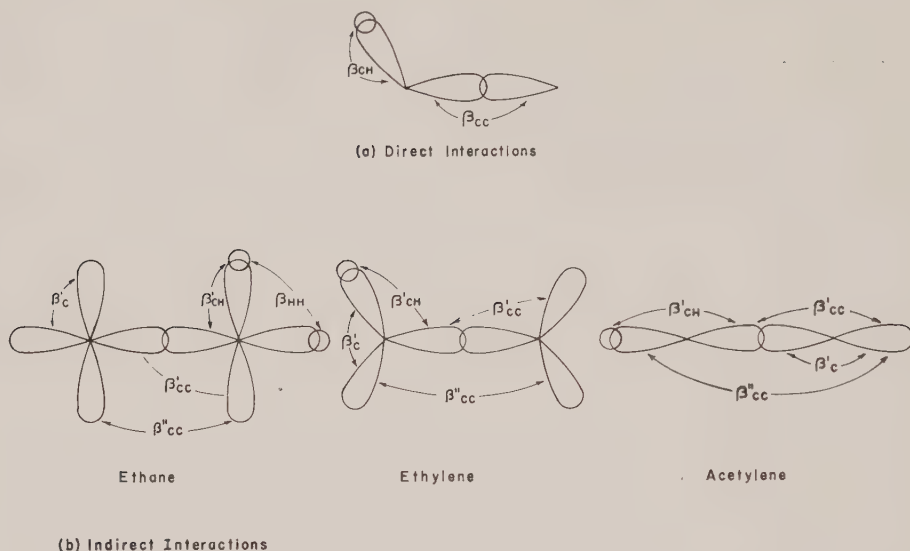


Figure 1. Off-diagonal Hamiltonian matrix elements referred to hybrid basis set.

It should be noted that the values of hybrid matrix elements depend on the molecule under consideration. Explicit expressions for them in terms of the matrix elements involving s and p functions are:

Ethane

$$\text{One-centre:} \quad \alpha_{te} = \frac{1}{4}(\alpha_s + 3\alpha_p), \quad (3.4)$$

$$\beta'_C = \frac{1}{4}(\alpha_s - \alpha_p). \quad (3.5)$$

$$\text{C-H bonds:} \quad \beta_{CH} = \frac{1}{2}\beta_{sh} + \frac{1}{2}3^{1/2}\beta_{\sigma h}, \quad (3.6)$$

$$\beta'_{CH} = \frac{1}{2}\beta_{sh} - \frac{1}{2}3^{-1/2}\beta_{\sigma h}. \quad (3.7)$$

$$\text{C-C bond:} \quad \beta_{CC} = \frac{1}{4}\beta_{ss} + \frac{1}{2}3^{1/2}\beta_{\sigma s} - \frac{3}{4}\beta_{\sigma\sigma}, \quad (3.8)$$

$$\beta'_{CC} = \frac{1}{4}\beta_{ss} + \frac{1}{2}3^{-1/2}\beta_{\sigma s} + \frac{1}{4}\beta_{\sigma\sigma}, \quad (3.9)$$

$$\beta''_{CC} = \frac{1}{4}\beta_{ss} - \frac{1}{2}3^{-1/2}\beta_{\sigma s} - \frac{1}{12}\beta_{\sigma\sigma} + \frac{2}{3}\beta_{\pi\pi} \cos \phi. \quad (3.10)$$

Here ϕ is the azimuthal angle between the hybrids on neighbouring atoms. In this paper, only the staggered configuration (D_{3d}) is discussed, for which ϕ may have the values 60° (gauche) or 180° (trans):

Ethylene

$$\text{One-centre:} \quad \alpha_{tr} = \frac{1}{3}(\alpha_s + 2\alpha_p), \quad (3.11)$$

$$\beta'_C = \frac{1}{4}(\alpha_s - \alpha_p). \quad (3.12)$$

$$\text{C-H bonds:} \quad \beta_{CH} = 3^{-1/2}\beta_{sh} + \left(\frac{2}{3}\right)^{1/2}\beta_{\sigma h}, \quad (3.13)$$

$$\beta'_{CH} = 3^{-1/2}\beta_{sh} - 6^{-1/2}\beta_{\sigma h}. \quad (3.14)$$

$$\text{C-C bonds:} \quad \beta_{CC} = \frac{1}{3}\beta_{ss} + \frac{2}{3}2^{1/2}\beta_{\sigma s} - \frac{2}{3}\beta_{\sigma\sigma}, \quad (3.15)$$

$$\beta'_{CC} = \frac{1}{3}\beta_{ss} + \frac{1}{3}2^{-1/2}\beta_{\sigma s} + \frac{1}{3}\beta_{\sigma\sigma}, \quad (3.16)$$

$$\beta''_{CC} = \frac{1}{3}\beta_{ss} - \frac{1}{3}2^{1/2}\beta_{\sigma s} - \frac{1}{6}\beta_{\sigma\sigma} + \frac{1}{2}\beta_{\pi\pi} \cos \phi. \quad (3.17)$$

In this case ϕ is 0° for cis hybrids and 180° for trans:

Acetylene

$$\text{One-centre:} \quad \alpha_{\text{di}} = \frac{1}{2}(\alpha_s + \alpha_p), \quad (3.18)$$

$$\beta'_{\text{C}} = \frac{1}{2}(\alpha_s - \alpha_p). \quad (3.19)$$

$$\text{C-H bonds:} \quad \beta_{\text{CH}} = 2^{-1/2}(\beta_{\text{sh}} + \beta_{\text{oh}}), \quad (3.20)$$

$$\beta'_{\text{CH}} = 2^{-1/2}(\beta_{\text{sh}} - \beta_{\text{oh}}). \quad (3.21)$$

$$\text{C-C bonds:} \quad \beta_{\text{CC}} = \frac{1}{2}(\beta_{\text{ss}} + 2\beta_{\text{os}} - \beta_{\text{os}}), \quad (3.22)$$

$$\beta'_{\text{CC}} = \frac{1}{2}(\beta_{\text{ss}} + \beta_{\text{os}}), \quad (3.23)$$

$$\beta''_{\text{CC}} = \frac{1}{2}(\beta_{\text{ss}} - 2\beta_{\text{os}} - \beta_{\text{os}}). \quad (3.24)$$

Values for these elements are listed in table 2.

4. BOND POLARITIES

If the indirect interactions (figure 2 (*b*)) are neglected, all molecular orbitals will be localized in individual bonds and each pair of electrons may be treated independently. All C-C bonds are then non-polar as they connect equivalent atomic orbitals. The polarity of C-H bonds, on the other hand, will vary from one molecule to another and will depend on the relative magnitudes of the diagonal matrix elements.

The charge densities $P_{\mu\mu}$ in the component atomic orbitals of a C-H bond in ethane will be unity if

$$\alpha_{\text{te}} = \frac{1}{4}(\alpha_s + 3\alpha_p) = \alpha_h, \quad (4.1)$$

as already noted in part I. This equation is approximately satisfied using values quoted in §2, so that for paraffins C-H bonds are non-polar. For the other molecules, the α -elements are lower because of the greater s-character and are given by:

$$\left. \begin{array}{ll} \text{Ethylene:} & \alpha_{\text{tr}} = \alpha_{\text{te}} + \frac{1}{12}(\alpha_s - \alpha_p), \\ \text{Acetylene:} & \alpha_{\text{di}} = \alpha_{\text{te}} + \frac{1}{4}(\alpha_s - \alpha_p), \end{array} \right\} \quad (4.2)$$

indicating that the polarity is C-H⁺ and greatest for acetylene.

Molecule	β'_{HH}	β_{CC}	β'_{CC}	β''_{CC}	β'_{CH}	β_{CH}	$\beta_{\text{C}'}$
Ethane	0.269	0.6471	0.1084	$\left\{ \begin{array}{l} \text{gauche } 0.071 \\ \text{trans } -0.121 \end{array} \right.$	0.1466	0.6743	0.245
Ethylene	0.264	0.7663	0.1363	$\left\{ \begin{array}{l} \text{cis } 0.1189 \\ \text{trans } -0.1471 \end{array} \right.$	0.1466	0.7199	0.3266
Acetylene	—	0.8725	0.1105	-0.0715	0.0827	0.7446	0.4900

Table 2. Matrix elements in units of -10 ev.

The magnitudes of the charge densities for C-H bonds in ethylene and acetylene may be estimated by treating $(\alpha_{tr} - \alpha_{te})$ and $(\alpha_{di} - \alpha_{te})$ as perturbations on a non-polar bond. Using the formula

$$P_{\mu\mu} = \sum_{\nu} \pi_{\mu\nu} \delta\alpha_{\nu}, \quad (4.3)$$

where $\pi_{\mu\nu}$ is a Coulson and Longuet-Higgins type polarizability coefficient (see part I), we obtain the charge densities given in table 3. Numerical values follow from the procedure outlined in §2.

	Hydrogen 1s	Carbon hybrid
Ethane	1	1
Ethylene	$1 - \frac{\alpha_s - \alpha_p}{24\beta_{CH}} = 0.943$	$1 + \frac{\alpha_s - \alpha_p}{24\beta_{CH}} = 1.057$
Acetylene	$1 - \frac{\alpha_s - \alpha_p}{8\beta_{CH}} = 0.836$	$1 + \frac{\alpha_s - \alpha_p}{8\beta_{CH}} = 1.165$

Table 3. Calculated charge densities in C-H bonds.

5. LONG-RANGE BOND ORDERS AND ELECTRON DELOCALIZATION

Long-range bond orders between hydrogen functions or hybrid orbitals involved in different bonds can also be calculated by perturbation methods along lines already indicated in part I. For all three molecules, the unperturbed system is chosen as one in which indirect elements are neglected and the diagonal elements for carbon hybrids are all equal to α_{te} which is in turn equal to α_h . The electronegativity perturbation $(\alpha_{tr} - \alpha_{te})$ and $(\alpha_{di} - \alpha_{te})$ which were dealt with in the previous section, need not be considered in the calculation of bond orders, for they are independent of the indirect interaction elements β'_C , β'_{CH} , β'_{CC} and β''_{CC} . This is because of the following results which apply to the leading terms in a perturbation expansion:

- (1) All bond orders are independent of the electronegativity perturbation.
- (2) The inclusion of the indirect interaction elements produces no changes in charge density.
- (3) There are no cross terms between the two kinds of Hamiltonian perturbation matrix elements in the expansion of the total energy.

These are proved by the same method as the corresponding results for paraffins (part I).

The hybrid orbitals and hydrogen functions will be numbered as shown in figure 2. Using the Coulson and Longuet-Higgins polarizability coefficients given in part I (which apply also for other hybridizations), the long-range bond orders are:

Interactions between geminal bonds (bonds on some carbon)

$$P_{56} = -P_{23} = (\beta'_{HH} - \beta'_C)/2\beta_{CH}, \quad (5.1)$$

$$P_{26} = P_{35} = 0, \quad (5.2)$$

$$P_{15} = -P_{1'2} = (\beta'_{CH} - \beta'_{CC})/(\beta_{CC} + \beta_{CH}), \quad (5.3)$$

$$P_{1'5} = -P_{12} = -\beta'_C/2\beta_{CH}. \quad (5.4)$$

Molecule	P_{56}	P_{23}	P_{12}	P'_{51}	P'_{21}	P_{51}	P'_{55}	P'_{22}
Ethane	0.0178	-0.0178	0.1854	-0.1854	-0.0289	0.0289	{ gauche trans	0.053 -0.090
Ethylene	-0.0435	0.0435	0.2198	0.2198	-0.0069	0.0069	{ cis trans	0.079 -0.102
Acetylene	—	—	0.3030	-0.3030	0.0172	-0.0172	0.048	-0.048

$P_{53} = 0$ all molecules.

Table 4. Long-range bond orders.

Interactions between vicinal bonds (bonds on neighbouring carbons)

$$P_{55'} = -P_{22'} = -\beta''_{CC}/2\beta_{CH}, \quad (5.5)$$

$$P_{25'} = P_{2'5} = 0. \quad (5.6)$$

For vicinal long-range bond orders, the same formulae apply to other $P_{\mu\nu}$ such as $P_{66'}$, $P_{77'}$, the dependence on azimuthal angle ϕ being that of β''_{CC} (as given by (3.10) and (3.17)). Numerical values, using the parameters listed in §2 are given in table 4.

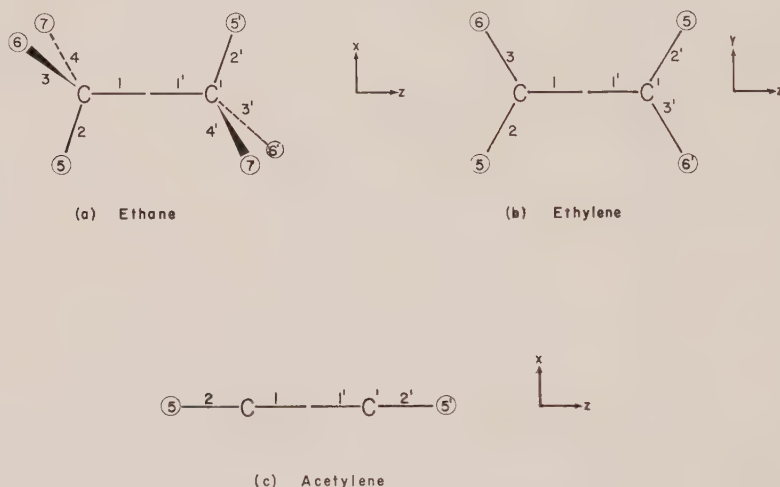


Figure 2. Labelling of hybrids (1-4, 1'-4') and hydrogen orbitals (5-7, 5'-7') for ethane, ethylene and acetylene.

6. TRANSFORMATION OF CHARGE DENSITIES AND BOND ORDERS FROM HYBRID TO s-p BASIS

From some points of view, it is preferable to discuss charge densities and bond orders (including long-range ones) referred to the s and p atomic orbitals on the carbon atoms. In a later paper, we shall see that this is required in the theory of nuclear spin coupling. The charge density and bond order matrix using the s-p basis is related to that based on hybrid orbitals by a simple transformation.

Let ϕ_μ and ϕ'_m denote the atomic orbital and hybrid set respectively. The two sets of functions are connected by an orthogonal transformation

$$\phi'_m = \sum O_{m\mu} \phi_\mu, \quad (6.1)$$

where the elements $O_{m\mu}$ are determined by the geometry of the molecule. For example, the transformation for the carbon orbitals of the left-hand carbon in ethane, using the axes of figure 2 (a) is:

$$\begin{bmatrix} \phi'_1 \\ \phi'_2 \\ \phi'_3 \\ \phi'_4 \end{bmatrix} = \begin{bmatrix} \frac{1}{2} & 0 & 0 & (3/4)^{1/2} \\ \frac{1}{2} & -(2/3)^{1/2} & 0 & -(1/12)^{1/2} \\ \frac{1}{2} & (1/6)^{1/2} & (1/2)^{1/2} & -(1/12)^{1/2} \\ \frac{1}{2} & (1/6)^{1/2} & -(1/2)^{1/2} & -(1/12)^{1/2} \end{bmatrix} \begin{bmatrix} s \\ p_x \\ p_y \\ p_z \end{bmatrix}. \quad (6.2)$$

Corresponding transformations for the left hand carbons in ethylene and acetylene (figures 2 (b) and 2 (c)) are

$$\begin{bmatrix} \phi'_1 \\ \phi'_2 \\ \phi'_3 \end{bmatrix} = \begin{bmatrix} (1/3)^{1/2} & 0 & (2/3)^{1/2} \\ (1/3)^{1/2} & -(1/2)^{1/2} & -(1/6)^{1/2} \\ (1/3)^{1/2} & (1/2)^{1/2} & (1/6)^{1/2} \end{bmatrix} \begin{bmatrix} s \\ p_y \\ p_z \end{bmatrix} \quad (6.3)$$

and

$$\begin{bmatrix} \phi'_1 \\ \phi'_2 \end{bmatrix} = \begin{bmatrix} (1/2)^{1/2} & (1/2)^{1/2} \\ (1/2)^{1/2} & -(1/2)^{1/2} \end{bmatrix} \begin{bmatrix} s \\ p_z \end{bmatrix}. \quad (6.4)$$

Somewhat similar matrices are easily written down for the right-hand carbon atoms.

The corresponding transformation between the hybrid system matrix P_{mn} and that for atomic orbitals $P_{\mu\nu}$ is:

$$P_{\mu\nu} = \sum_{mn} P_{mn} O_{m\nu} O_{n\mu}. \quad (6.5)$$

Thus, using the notation of figure 2, the bond orders between the carbon 2s orbitals and the directly bonded hydrogen atoms are

$$\text{Ethane:} \quad P_{s5} = \frac{1}{2}(P_{15} + P_{25} + P_{35} + P_{45}), \quad (6.6)$$

$$\text{Ethylene:} \quad P_{s5} = (1/3)^{1/2}(P_{15} + P_{25} + P_{35}), \quad (6.7)$$

$$\text{Acetylene:} \quad P_{s5} = (1/2)^{1/2}(P_{15} + P_{25}). \quad (6.8)$$

The bond orders between carbon 2s orbitals are

$$\text{Ethane:} \quad P_{ss'} = \frac{1}{4} \sum_{m=1}^4 \sum_{n=1'}^{4'} P_{mn}, \quad (6.9)$$

$$\text{Ethylene:} \quad P_{ss'} = \frac{1}{3} \sum_{m=1}^3 \sum_{n=1'}^{3'} P_{mn}, \quad (6.10)$$

$$\text{Acetylene:} \quad P_{ss'} = \frac{1}{2} \sum_{m=1}^2 \sum_{n=1'}^{2'} P_{mn}. \quad (6.11)$$

Finally, the carbon-carbon π -bond orders (between 2p orbitals perpendicular to the bond) are given by

$$\text{Ethane:} \quad P_{xx'} = P_{yy'} = -P_{22'} + P_{23'}, \quad (6.12)$$

$$\text{Ethylene:} \quad P_{xx'} = 1; \quad P_{yy'} = -P_{22'} + P_{23'}, \quad (6.13)$$

$$\text{Acetylene:} \quad P_{xx'} = P_{yy'} = 1. \quad (6.14)$$

Values of these bond orders given in table 5, together with values corresponding to completely localized bonding orbitals:

	P_{hs}	$P_{ss'}$	$P_{xx'}$	$P_{yy'}$
Ethane	0.515 (0.5)	0.218 (0.25)	0.142 (0)	0.142 (0)
Ethylene	0.581 (0.577)	0.311 (0.33)	1.00 (1.00)	0.185 (0)
Acetylene	0.695 (0.707)	0.493 (0.50)	1.00 (1.00)	1.00 (1.00)

Table 5. Some atomic orbital bond orders (values in brackets are those for localized bonding orbitals).

7. CONCLUSIONS

The main aim of this paper has been to calculate charge densities and bond orders (including long-range ones) for the molecules ethane, ethylene and acetylene, thereby providing a comparison of the delocalization of electrons in sp^3 , sp^2 and sp hybridization. As stressed in part I, the crudity of the independent electron model limits the numerical significance of the results, but the following qualitative conclusions emerge.

(i) The energy difference between carbon 2s and 2p orbitals is an important factor in the determination of charge distributions. The increasing polarity $C-H^+$ along the series is a consequence of this [6] and is included quantitatively in the treatment.

(ii) Long-range bond orders between geminal hydrogen 1s orbitals (P_{56}) involve the cancellation of large terms and are sensitive to the type of hybridization. According to the numerical values used, there is a change from a positive value in ethane to a negative value in ethylene (table 4) primarily because of the increased s-character of the bonds in the latter molecule.

(iii) Long-range bond orders between vicinal hydrogen 1s orbitals are positive for the *trans* configuration, but negative for the *cis* (ethylene) and *gauche* (ethane) configurations. The fact that these have opposite signs means that the interactions between such hydrogen atoms occur via a π -bonding mechanism. This shows up in the calculated π -bond orders shown in table 5. The values for $P_{xx'}$ (ethane) and $P_{yy'}$ (ethane and ethylene) correspond to what was termed 'second order hyperconjugation' by Mulliken *et al.* [7]. Indeed the figures given in table 2 are similar to those obtained by these authors.

(iv) Other bond orders for directly bonded atoms are also modified by electron delocalization. For example, it is noteworthy that bond orders between hydrogen 1s orbitals and neighbouring carbon 2s orbitals deviate from the values pertinent to localized bonding.

The results on bond orders are very relevant to the molecular orbital theory of nuclear spin coupling constants in these molecules. This topic will be taken up in detail in a following paper.

REFERENCES

- [1] POPLER, J. A., and SANTRY, D. P., 1964, *Mol. Phys.*, **7**, 269.
- [2] COULSON, C. A., and LONGUET-HIGGINS, H. C., 1949, *Proc. roy. Soc., A*, **92**, 16.
- [3] HOFFMAN, R., 1963, *J. chem. Phys.*, **39**, 1397.
- [4] SKINNER, H. A., and PRITCHARD, H. O., 1953, *Trans. Faraday Soc.*, **49**, 1254.
- [5] MULLIKEN, R. S., RIEKE, C. A., ORLOFF, D., and ORLOFF, H., 1949, *J. chem. Phys.*, **17**, 1248.
- [6] WALSH, A. D., 1947, *Disc. Faraday Soc.*, **2**, 18.
- [7] MULLIKEN, R. S., RIEKE, C. A., and BROWN, W. G., 1941, *J. Amer. chem. Soc.*, **63**, 41.

A molecular orbital theory of hydrocarbons

III. Nuclear spin coupling constants

by J. A. POPLE

Carnegie Institute of Technology and Mellon Institute, Pittsburgh,
Pennsylvania 15213, U.S.A.

and D. P. SANTRY

Carnegie Institute of Technology
Pittsburgh, Pennsylvania 15213, U.S.A.

(Received 15 September 1964)

The molecular orbital theory of hydrocarbons developed in the previous two papers [1, 2] has been adapted to the calculation of nuclear spin coupling constants. Using perturbation theory, long range coupling constants are related to those interactions within the molecule which are responsible for electron delocalization between bonds. The theory is applied to the calculation of all nuclear spin coupling constants in ethane, ethylene and acetylene. For nuclei separated by two bonds, the calculations lead to positive constants in all cases, whereas some negative values are found experimentally. However, the observed trend of increasingly positive values with increasing bond angle is well reproduced. For protons separated by three bonds, the theory gives results comparable with those already achieved by valence bond calculations.

1. INTRODUCTION

In previous papers [1, 2], the electron localization between σ -bonds in simple hydrocarbons has been discussed. It has frequently been pointed out that the existence of long range nuclear spin coupling constants provides experimental evidence for delocalization, so it should be possible to interpret observed trends of coupling constants in terms of the structural features leading to delocalization. In this paper, the molecular orbital theory developed in parts I and II is adapted to the calculation of these constants in simple hydrocarbons and compared with experiment, particularly the very complete data of Lynden-Bell and Sheppard [3] on ethane, ethylene and acetylene.

Most previous theoretical work on long-range spin coupling constants has been in terms of valence bond theory, where the magnitude is related to deviations from perfect pairing [4-6]. The calculations were relatively successful for protons in vicinal positions [5], but led to some misleading predictions for geminal interactions. These difficulties were attributed by Karplus [7] to sensitivity to cancellation of large terms of opposite sign. We shall find similar effects in this molecular orbital theory.

2. GENERAL THEORY

The background of the molecular orbital theory of indirect isotropic nuclear spin coupling has been discussed in detail elsewhere [8–10] and we shall content ourselves with a statement of the results to be used. For the molecules considered in this paper, it is found that the Fermi contact mechanism is the most important in all coupling constants discussed and the other contributions will not be examined in detail. For the contact part, McConnell [9] developed a theory using a mean energy approximation, in which all the excitation energies to triplet states are replaced by a single value ΔE . This leads to the expression†:

$$K_{AB} = (8\pi\beta^\dagger/3)^2(\Delta E)^{-1}s_A^2(0)s_B^2(0)P_{s_A s_B}^2, \quad (2.1)$$

where $s_A(0), s_B(0)$ are the values of the valence s-orbitals of atoms A and B at the nuclei and $P_{s_A s_B}$ is the molecular orbital bond order between them. (It should be noted that we use reduced coupling constants K_{AB} [10] in units of cm^{-3} .) The principal drawback of (2.1) is that it predicts K to be always positive, whereas many negative values are known experimentally.

If the mean excitation energy is avoided, the following more general expression can be obtained [10]:

$$K_{AB} = (8\pi\beta^\dagger/3)^2 s_A^2(0)s_B^2(0)\pi_{s_A s_B} \quad (2.2)$$

where

$$\pi_{\mu, \nu} = 4 \sum_i^{\text{occ}} \sum_j^{\text{unocc}} (\epsilon_i - \epsilon_j)^{-1} c_{i\mu} c_{i\nu} c_{j\mu} c_{j\nu}. \quad (2.3)$$

$c_{i\mu}$ is the LCAO coefficient of the atomic orbital ϕ_μ in the molecular orbital ψ_i , the energy of which is ϵ_i . $\pi_{\mu, \nu}$ is the mutual polarizability introduced into π -electron theory by Coulson and Longuet-Higgins [15].

The analysis of reference [10] suggested that the simpler formula (2.1) is probably adequate for directly bonded CH atoms and it will be so used in this paper. However, we shall attempt to calculate long range coupling constants using (2.2). For this purpose, the simplified MO theory of hydrocarbons has to be developed to calculate $P_{s_A s_B}$ and π_{s_A, s_B} . This will be done by perturbation techniques.

In its primary form, the LCAO theory [1, 2] uses as a set of basis hydrogen functions, 1s orbitals and a hybrid set on each carbon (tetrahedral, trigonal and digonal in ethane, ethylene and acetylene respectively). This leads to bond orders and mutual polarizabilities referred to this same basis set, which are all that is needed for hydrogen-hydrogen coupling constants but are not appropriate for carbon atoms. To calculate coupling constants to carbon, therefore, it is necessary to transform to the atomic orbital (s, p) set. If the hybrid set is denoted by ϕ_m' , the atomic orbital (s, p) set by ϕ_μ and the transformation between them by:

$$\phi_m' = \sum_\mu O_{m\mu} \phi_\mu, \quad (2.4)$$

then the new set of $P_{\mu\nu}$ and $\pi_{\mu, \nu}$ are given by:

$$P_{\mu\nu} = \sum_{mn} P_{mn} O_{m\mu} O_{n\nu} \quad (2.5)$$

† The symbol β^\dagger is used for the Bohr magneton to avoid confusion with the Hamiltonian matrix element β used later in the paper.

and

$$\pi_{\mu\nu} = \sum_{m,n} \pi_{m,n} O_{m\mu}^2 O_{n\nu}^2 + 2 \sum_m \sum_{n < q} \pi_{nq,m} O_{m\mu}^2 O_{n\nu} O_{q\nu} + 2 \sum_{m < p} \sum_n \pi_{mp,n} O_{n\nu}^2 O_{m\mu} O_{p\mu} + 2 \sum_{m < p} \sum_{n < q} \pi_{mp,nq} O_{m\mu} O_{n\nu} O_{p\mu} O_{q\nu}, \quad (2.6)$$

where $\pi_{m,n}$, $\pi_{mp,n}$ and $\pi_{mp,nq}$ are defined by:

$$\pi_{m,n} = 4 \sum_i^{\text{occ}} \sum_j^{\text{unocc}} (\epsilon_i - \epsilon_j)^{-1} c_{im} c_{in} c_{jm} c_{jn}, \quad (2.7)$$

$$\pi_{mp,n} = 2 \sum_i^{\text{occ}} \sum_j^{\text{unocc}} (\epsilon_i - \epsilon_j)^{-1} (c_{im} c_{jp} + c_{ip} c_{jm}) c_{in} c_{jn}, \quad (2.8)$$

$$\pi_{mp,nq} = 2 \sum_i^{\text{occ}} \sum_j^{\text{unocc}} (\epsilon_i - \epsilon_j)^{-1} (c_{im} c_{jp} + c_{ip} c_{jm}) (c_{in} c_{jq} + c_{iq} c_{jn}), \quad (2.9)$$

c_{im} denoting LCAO coefficients using the hybrid basis set ϕ_m' .

The details of the transformation matrices $O_{m\mu}$ have been given in part II [2], together with calculations of those bond orders needed in the discussion of directly bonded coupling constants using the McConnell formula (2.1). For coupling constants between non-bonded hydrogens, the mutual polarizability required in (2.2) can be obtained directly from the theory using the hybrid basis set. Only for non-bonded hydrogen-carbon coupling (HCC) is it necessary to use the transformation (2.6). Using the notation of figure 3 of part II, the mutual polarizabilities between the 2s orbitals of one carbon atom (s) and the 1s orbital of a hydrogen attached to the other carbon (5') are:

$$\text{Ethane} \quad \pi_{s,5'} = \frac{1}{4}(\pi_{1,5'} + \pi_{2,5'} + 2\pi_{3,5'}) + \frac{1}{2}(\pi_{12,5'} + 2\pi_{13,5'} + 2\pi_{23,5'} + \pi_{34,5'}); \quad (2.10)$$

$$\text{Ethylene} \quad \pi_{s,5'} = \frac{1}{3}(\pi_{1,5'} + \pi_{2,5'} + \pi_{3,5'}) + \frac{2}{3}(\pi_{12,5'} + \pi_{13,5'} + \pi_{23,5'}); \quad (2.11)$$

$$\text{Acetylene} \quad \pi_{s,5'} = \frac{1}{2}(\pi_{1,5'} + \pi_{2,5'}) + \pi_{12,5'}. \quad (2.12)$$

3. PERTURBATION CALCULATION OF POLARIZABILITY COEFFICIENTS

In this section we shall develop explicit expressions for the polarizability coefficients $\pi_{m,n}$ and $\pi_{mp,n}$ by perturbation methods analogous to those used for the calculation of bond orders in parts I and II. m, n and p refer to hydrogen or hybrid orbitals ϕ' which are not directly bonded in the usual valence structure.

In the unperturbed system, Hamiltonian matrix elements β_{CC} and β_{CH} are only introduced between directly bonded orbitals so that the bonding orbitals are completely localized. The polarizability coefficients $\pi_{m,n}$ and $\pi_{mp,n}$ under consideration are then strictly zero. To simplify the calculation, we shall assume

- (1) that diagonal Hamiltonian matrix elements for all hybrids and hydrogen functions ϕ' are equal (and chosen to be zero for convenience), so that the unperturbed localized molecular orbitals are non-polar and have the form (for bond r):

$$\left. \begin{aligned} \chi_r^{(b)} &= 2^{-1/2}(\phi_{1r}' + \phi_{2r}'), & (\text{bonding}), \\ \chi_r^{(a)} &= 2^{-1/2}(\phi_{1r}' - \phi_{2r}'), & (\text{antibonding}), \end{aligned} \right\} \quad (3.1)$$

where ϕ_{1r}' and ϕ_{2r}' are the component atomic functions for bond r ; and

- (2) that the carbon-carbon and carbon-hydrogen bonding elements β_{CC} and β_{CH} are equal (to a common value β), so that all the occupied bonding localized molecular orbitals $\chi_r^{(b)}$ have energy β and the unoccupied antibonding ones $\chi_r^{(a)}$ have energy $-\beta$.

Having specified the unperturbed system, we now introduce matrix elements $\beta_C', \beta_{CH}', \beta_{CC}', \beta_{CC}'', \beta_{HH}$ between functions in different bonds (see figure 2 of part II for notation). As the unperturbed orbitals are degenerate, there will be changes in individual molecular orbital energies, which become:

$$\left. \begin{aligned} \epsilon_i &= \beta + \eta_i, & (\text{occupied}), \\ \epsilon_j &= -\beta + \eta_j, & (\text{unoccupied}), \end{aligned} \right\} \quad (3.2)$$

η_i, η_j being first order in the perturbing elements.

Expanding the energy denominators in (2.7) and (2.8), we may write, correct to the second order:

$$\begin{aligned} & \sum_i^{\text{occ}} \sum_j^{\text{unocc}} (\epsilon_i - \epsilon_j)^{-1} c_{im} c_{jp} c_{in} c_{jn} \\ &= (2\beta)^{-1} \sum_i^{\text{occ}} \sum_j^{\text{unocc}} c_{im} c_{jp} c_{in} c_{jn} \{1 - (2\beta)^{-1}(\eta_i - \eta_j) + (2\beta)^{-2}(\eta_i - \eta_j)^2\}. \end{aligned} \quad (3.3)$$

Next, noting that:

$$\sum_i^{\text{occ}} c_{im} c_{in} = \frac{1}{2} P_{mn}, \quad \sum_j^{\text{unocc}} c_{jp} c_{jn} = -\frac{1}{2} P_{pn} \quad (3.4)$$

and that P_{mn}, P_{pn} will already be first order in the perturbation, (3.3) is replaced by:

$$\begin{aligned} & \sum_i^{\text{occ}} \sum_j^{\text{unocc}} (\epsilon_i - \epsilon_j)^{-1} c_{im} c_{jp} c_{in} c_{jn} \\ &= (8\beta)^{-1} \left\{ -P_{mn} P_{pn} + \beta^{-1} P_{pn} \sum_i^{\text{occ}} c_{im} c_{in} \eta_i + \beta^{-1} P_{mn} \sum_j^{\text{unocc}} c_{jp} c_{jn} \eta_j \right. \\ & \quad \left. - 2\beta^{-2} \left(\sum_i^{\text{occ}} c_{im} c_{in} \eta_i \right) \left(\sum_j^{\text{unocc}} c_{jp} c_{jn} \eta_j \right) \right\}. \end{aligned} \quad (3.5)$$

All terms omitted in the passage from (3.4) to (3.5) are third order or smaller.

We now have to evaluate the two summations remaining in (3.5), but this need only be done to first order since the full expression is only required to second. This requires the solution of the separate first order perturbation problems for the degenerate sets of bonding and antibonding orbitals. For the bonding orbitals, zero-order combinations:

$$\psi_i = \sum_r d_{ir} \chi_r^{(b)}, \quad (3.6)$$

have to be found, where the coefficient d_{ir} satisfy:

$$\sum_s H_{rs}^{(b)} d_{is} = \eta_i d_{ir} \quad (3.7)$$

and

$$H_{rs}^{(b)} = \int \chi_r^{(b)} H \chi_s^{(b)} d\tau. \quad (3.8)$$

From (3.7), it follows that:

$$\sum_i^{\text{occ}} d_{ir} d_{it} \eta_i = \sum_s^{\text{occ}} \sum_i^{\text{occ}} d_{is} d_{it} H_{rs}^{(b)} = H_{rt}^{(b)}. \quad (3.9)$$

Since η_i is already of first order, only zero-order values of c_{im}, c_{in} are required in the evaluation of

$$\sum_i^{\text{occ}} c_{im} c_{in} \eta_i.$$

Using (3.1) we may then write:

$$\sum_i^{\text{occ}} c_{im} c_{in} \eta_i = \frac{1}{2} H_{mn}^{(b)}, \quad (3.10)$$

where the suffixes m and n in $H_{mn}^{(b)}$ serve to label the bond orbitals $\chi_m^{(b)}, \chi_n^{(b)}$ which contain the hybrid (or hydrogen) orbitals ϕ_m', ϕ_n' .

Proceeding similarly for antibonding orbitals, we obtain:

$$\sum_j^{\text{unocc}} c_{jp} c_{jn} \eta_j = \frac{1}{2} H_{pn}^{(a)}, \quad (3.11)$$

where $H_{pn}^{(a)}$ is defined by an expression similar to (3.8) and we have arranged for the orbitals ϕ_p', ϕ_n' to occur with *positive* signs in the antibonding orbitals $\chi_p^{(a)}, \chi_n^{(a)}$ to which they contribute.

Using (3.5), (3.10) and (3.11), we obtain the following formulae for the polarizability coefficients:

$$\pi_{m,n} = \frac{1}{2} \beta^{-1} P_{mn}^2 + \frac{1}{4} \beta^{-2} P_{mn} (H_{mn}^{(b)} + H_{mn}^{(a)}) - \frac{1}{4} \beta^{-3} H_{mn}^{(b)} H_{mn}^{(a)}, \quad (3.12)$$

$$\pi_{mp,n} = -\frac{1}{2} \beta^{-1} P_{mn} P_{pn} + \frac{1}{8} \beta^{-2} [P_{mn} (H_{pn}^{(b)} + H_{pn}^{(a)}) + P_{pn} (H_{mn}^{(b)} + H_{mn}^{(a)})] \\ - \frac{1}{8} \beta^{-3} (H_{mn}^{(b)} H_{pn}^{(a)} + H_{pn}^{(b)} H_{mn}^{(a)}). \quad (3.13)$$

Using the definitions of $H_{mn}^{(b)}, H_{mn}^{(a)}$ and the perturbed bond orders derived in part II, (3.12) and (3.13) lead to explicit expressions for the polarizability coefficients and hence for the long range coupling constants.

4. COUPLING CONSTANTS FOR DIRECTLY BONDED ATOMS

In this section we consider the coupling constants between directly bonded atoms in ethane, ethylene and acetylene, using the McConnell formula (2.1). It is convenient to denote these by symbols ${}^1K_{\text{CH}}$ and ${}^1K_{\text{CC}}$, the upper left-hand index showing that the atoms are separated by one bond. In later sections we shall use 2K and 3K for coupling constants between atoms separated by two and three bonds.

The bond orders between valence s orbitals on neighbouring atoms in C_2H_6 , C_2H_4 and C_2H_2 have already been calculated in part II. The values chosen for $1s_{\text{H}}^2(0)$ and $2s_{\text{C}}^2(0)$ are 0.5500 and 2.767 atomic units respectively [10]. The

Coupling constant	ΔE (ev)	$10^{-20} K_{\text{calc}}$	$10^{-20} K_{\text{calc}}$ (localized)	$10^{-20} K_{\text{obs}}$ (ref. [3])	J (c/s) _{obs}
${}^1K_{\text{CH}}(\text{C}_2\text{H}_6)$	13.2	52.3	49.4	41.7	124.9
${}^1K_{\text{CH}}(\text{C}_2\text{H}_4)$	14.8	59.4	58.5	52.3	156.4
${}^1K_{\text{CH}}(\text{C}_2\text{H}_2)$	16.2	78.0	80.7	83.1	248.7
${}^1K_{\text{CC}}(\text{C}_2\text{H}_6)$	13.2	47.2	62.1	45.6	34.6
${}^1K_{\text{CC}}(\text{C}_2\text{H}_4)$	14.8	85.4	98.1	89.0	67.6
${}^1K_{\text{CC}}(\text{C}_2\text{H}_2)$	16.2	197.4	203	225.9	171.5

Table 1. Calculated and observed coupling constants for directly bonded atoms.

mean triplet excitation energy is chosen to be -2β where β is the mean of the direct bonding interaction elements β_{CC} and β_{CH} . Calculated and observed coupling constants are given in table 1.

The performance of the theory is fairly satisfactory and provides some support for the assignment of a positive sign to all these constants. The main cause of increases along the series C_2H_6 , C_2H_4 , C_2H_2 is the bond orders $P_{s_A s_B}$ which are in turn related to the hybridization factors. However, there is no significant improvement over the theory in which bond orders obtained from localized bonding orbitals are used (corresponding to the formulae proposed by Muller and Pritchard [11] and by Frei and Bernstein [12]).

5. COUPLING CONSTANTS FOR ATOMS SEPARATED BY TWO BONDS

To calculate the constants ${}^2K_{HH}$ and ${}^2K_{CH}$, we use the formula (2.2). For the coupling between geminal hydrogens, the mutual polarizability $\pi_{s_A s_B}$ is given directly by the theory using a hybrid basis set. The bond order between the hydrogen 1s orbitals was determined in part II and the quantities $H_{mn}^{(b)}$ and $H_{mn}^{(a)}$ appearing in (3.12) are easily determined.

Thus:

$$P_{mn} = (\beta_{HH}' - \beta_C')/2\beta; \quad H_{mn}^{(b)} = \frac{1}{2}(\beta_{HH}' + 2\beta_{CH}' + \beta_C'); \\ H_{mn}^{(a)} = \frac{1}{2}(\beta_{HH}' - 2\beta_{CH}' + \beta_C'). \quad (5.1)$$

Substitution into (3.12) and (2.2) gives:

$${}^2K_{HH} = (8\pi\beta^\dagger/3)^2 s_H^4(0) \{4\beta_{CH}'^2 - 4\beta_C'^2 - (\beta_{HH}' - \beta_C')^2\}/16\beta^3. \quad (5.2)$$

This result applies to geminal couplings in both ethane and ethylene (with different values of the β -parameters).

For the calculation of ${}^2K_{CH}$, it is necessary to determine all the polarizabilities in equations (2.10), (2.11) and (2.12) using (3.12) and (3.13). The final results are:

Ethane

$${}^2K_{CH} = (8\pi\beta^\dagger/3)^2 s_C^2(0) s_H^2(0) \\ \times \{-5\beta_C'^2 + [\beta_{CH}' + \beta_{CC}' + \beta_{CC}''(\text{trans}) + 2\beta_{CC}''(\text{gauche})]^2\}/64\beta^3. \quad (5.3)$$

Ethylene

$${}^2K_{CH} = (8\pi\beta^\dagger/3)^2 s_C^2(0) s_H^2(0) \\ \times \{-5\beta_C'^2 + [\beta_{CH}' + \beta_{CC}' + \beta_{CC}''(\text{trans}) + \beta_{CC}''(\text{cis})]^2\}/48\beta^3. \quad (5.4)$$

Acetylene

$${}^2K_{CH} = (8\pi\beta^\dagger/3)^2 s_C^2(0) s_H^2(0) \{-5\beta_C'^2 + [\beta_{CH}' + \beta_{CC}' + \beta_{CC}'']^2\}/32\beta^3. \quad (5.5)$$

Equations (5.2) to (5.5) are all rather similar and lead one to expect variations in ${}^2K_{HH}$ and ${}^2K_{CH}$ to be closely related. Two main features determine the calculated coupling constants:

- (1) The element β_C' connects different hybrids on the same carbon atom and is proportional to the energy difference between 2s and 2p orbitals. It leads to a *positive* contribution (noting that β is negative).
- (2) The remaining elements β_{CH}' , β_{CC}' , β_{CC}'' connect orbitals on neighbouring atoms which are not directly bonded in the primary valence structure. These give *negative* contributions.

These two trends can be interpreted qualitatively in terms of electron spin coupling (figure 1). For a CH_2 group, if there is an electron of α spin in one of the hydrogen orbitals h , there will be an excess of β electrons in the hybrid t to which it is bonded. As the matrix element β_C' leads to some 'bonding' between hybrids t and t' , there will an excess α population in t' leading finally to an excess β population in h' . This corresponds to positive nuclear spin coupling constants ${}^2K_{\text{HH}}$. On the other hand the 'other bond' interaction β_{CH} leads to a tendency for opposed electron spins in h and t' and hence to parallel alignment in h and h' and a negative contribution to ${}^2K_{\text{HH}}$.

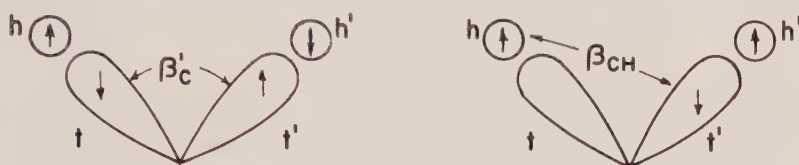


Figure 1. Electron spin coupling tendencies in CH_2 groups.

As the coupling constants are calculated as a difference of two opposing effects, accurate results are not to be expected. Numerical results using the parameters introduced in part II are given in table 2. These predict all the constants to be positive, whereas negative values are found experimentally in certain cases. It would appear, therefore, that although molecular orbital theory may lead to negative coupling constants, the neglect of correlation between electrons of different spin tends to over emphasize the positive contributions.

Molecule	10^{-20} $({}^2K_{\text{HH}})_{\text{calc}}$	10^{-20} $({}^2K_{\text{HH}})_{\text{obs}}$	10^{-20} $({}^2K_{\text{CH}})_{\text{calc}}$	10^{-20} $({}^2K_{\text{CH}})_{\text{obs}}$
Ethane	+1.74	-1.00	+3.17	-1.5
Ethylene	+2.72	+0.21	+6.21	-0.8
Acetylene	—	—	+18.28	+16.4

Table 2. Calculated and observed coupling constants for atoms separated by two bonds (observed values from reference [3]; ${}^2K_{\text{HH}}$ (ethane) is the value for methane).

On the other hand, the trends along the series ethane, ethylene and acetylene are well reproduced, the increasing (becoming more positive) values being ascribed to the increase of β_C' .

6. COUPLING CONSTANTS FOR ATOMS SEPARATED BY THREE BONDS

Only proton-proton coupling constants ${}^3K_{\text{HH}}$ occur in the molecules considered. Again using (2.2), (3.12) and the results of part II, we find:

$$P_{mn} = -\beta_{\text{CC}}''/2\beta; \quad H_{mn}^{(b)} = H_{mn}^{(a)} = \frac{1}{2}\beta_{\text{CC}}'', \quad (6.1)$$

whence

$${}^3K_{\text{HH}} = -(8\pi\beta^3/3)^2 s_{\text{H}}^4(0)[5\beta_{\text{CC}}''^2/16\beta^3], \quad (6.2)$$

in all cases. The following general points about this result may be noted.

- (1) All vicinal hydrogen-hydrogen coupling constants are predicted to be positive for these three molecules.
- (2) The values by (6.2) are exactly (5/2) times as great as those given by (2.1) with $\Delta E = 2\beta$. The McConnell formula underestimates coupling constants in these cases and may not be used in reverse to obtain reliable long range bond orders.
- (3) It has been noted in parts I and II that the vicinal interaction parameter $\beta_{CC''}$ is closely approximated by $\frac{2}{3}\beta_{\pi\pi}\cos\phi$ where ϕ is the dihedral angle between the bonds. The theory therefore gives a derivation of the approximate rule for vicinal protons separated by C-C single bonds:

$$^3K_{HH} \propto \cos^2 \phi, \quad (6.3)$$

suggested by Karplus [5] and Conroy [13].

Molecule		$10^{-20}(^3K_{HH})_{\text{calc}}$	$10^{-20}(^3K_{HH})_{\text{obs}}$
Ethane	trans	+0.823	—
	gauche	+0.283	—
	average	+0.463	+0.67
Ethylene	trans	+0.855	+1.59
Acetylene	cis	+0.558	+0.98
		+0.157	+0.79

Table 3. Calculated and observed coupling constants for atoms separated by three bonds (observed values from reference [3]).

Numerical values calculated with parameters given in part II are listed in table 3 and compared with experimental values. These are generally satisfactory, although calculated values are rather too small, particularly in the case of acetylene. For ethylene and acetylene, it should be noted that Karplus [14] has indicated that substantial (positive) contributions to the vicinal coupling constants arise by polarization of the π electrons. In a molecular orbital theory, inclusion of these effects require a fuller treatment involving configuration interaction.

REFERENCES

- [1] POPL, J. A., and SANTRY, D. P., 1964, *Mol. Phys.*, **7**, 269.
- [2] POPL, J. A., and SANTRY, D. P., 1965, *Mol. Phys.*, **9**, 301.
- [3] LYNDEN-BELL, R. M., and SHEPPARD, N., 1964, *Proc. roy. Soc. A*, **269**, 385.
- [4] KARPLUS, M., and ANDERSON, D. H., 1959, *J. chem. Phys.*, **30**, 6.
- [5] KARPLUS, M., 1959, *J. chem. Phys.*, **30**, 11.
- [6] ALEXANDER, S., 1961, *J. chem. Phys.*, **34**, 106.
- [7] KARPLUS, M., 1962, *J. Amer. chem. Soc.*, **84**, 2458.
- [8] RAMSEY, N. F., 1953, *Phys. Rev.*, **91**, 303.
- [9] MCCONNELL, H. M., 1956, *J. chem. Phys.*, **24**, 460.
- [10] POPL, J. A., and SANTRY, D. P., 1964, *Mol. Phys.*, **8**, 1.
- [11] MULLER, N., and PRITCHARD, D. E., 1959, *J. chem. Phys.*, **31**, 768.
- [12] FREI, K., and BERNSTEIN, H. J., 1963, *J. chem. Phys.*, **38**, 1216.
- [13] CONROY, H., 1960, *Advances in Organic Chemistry, Methods and Results* (New York: Interscience), p. 265.
- [14] KARPLUS, M., 1960, *J. chem. Phys.*, **33**, 1842.
- [15] COULSON, C. A., and LONGUET-HIGGINS, H. C., 1947, *Proc. roy. Soc. A*, **191**, 39.

Double long-range spin-spin couplings between aldehydic and aromatic protons in the N.M.R. spectra of salicylaldehydes

by DORA G. DE KOWALEWSKI and VALDEMAR J. KOWALEWSKI

Department of Physics, Faculty of Exact Sciences,
The University, Buenos Aires, Argentina

(Received 28 September 1964)

A detailed method of analysis of the N.M.R. spectra of some salicylaldehydes, which makes use of the splittings of the combination lines, shows that in some of them there is more than one long-range interaction between the formyl and the ring protons. It is shown that the splittings of the combination lines are equal if the aldehyde proton is coupled to the proton in position three only, and are different if there is another coupling present. In this way, the magnitudes and relative signs of the $J_{\text{OCH}-3}$ and $J_{\text{OCH}-4}$ or $J_{\text{OCH}-6}$ are determined in the 5-bromo, 5-chloro, 5-hydroxy and 4-hydroxy-salicylaldehydes. These couplings are of the order of 0.10 c.p.s., $J_{\text{OCH}-4}$ being positive and $J_{\text{OCH}-6}$ being negative with respect to $J_{\text{OCH}-3}$.

1. INTRODUCTION

In the previous work of this series [1] several long-range couplings across five bonds were reported in some di-substituted benzaldehydes. Due to the fact that the 2,4 dihydroxibenzaldehyde was the only one that did not show coupling with the aromatic proton in position five but with the proton in position three, the study of the N.M.R. spectra of all commercially available salicylaldehydes was undertaken under different conditions: at room temperature, near the boiling point of the solutions and at two different frequencies, 60 and 19.25 Mc/sec.

An improvement of the method of analysis of the high resolution spectra, which was now made with an ABCD computer programme, and in the experimental technique, gave indication that in some salicylaldehydes the formyl proton, which is coupled with the proton in position three of the ring with a coupling constant of about 0.5 c.p.s., is also feebly coupled (~ 0.10 c.p.s.) sometimes to proton four, across six bonds and sometimes to proton six across four bonds, but with a negative sign with respect to the main 0.5 c.p.s. coupling.

No long-range coupling was observed at all in 3-methoxy- and 3,5 dichloro-salicylaldehydes, this being attributed to the stereospecificity of the long-range coupling [2, 3] and to the absence of a proton in position three to couple with.

Though no structural data on salicylaldehydes are available, the works of Porte *et al.* [4], Reeds [5] and Forsén and Åkermark [6] in the infra-red and by N.M.R. show that the chemical shift of the OH signal towards lower fields gives a measure of the strength of the internal hydrogen bond between the CHO and

the OH and that this is proportional to the corresponding CO infra-red shifts. It was observed by the authors that in most of the salicylaldehydes studied (5Cl; 5Br; 5OH; 4OH) the OH signal is always present to the left of the OCH peak (0.5–1.5 p.p.m.), this one being already far to the left (*circa*—10.0 p.p.m. with respect to tetramethylsilane) giving an indication of the existence of an internal hydrogen bond.

This should give, as a consequence, a very high value of the energy barrier against internal rotation for the carbonyl group. On the other hand it was observed that, within the range of temperature used (23–130°C), the two long-range couplings were temperature independent, suggesting a rigid character of the bond $C_{ald}-C_{arom}$.

2. EXPERIMENTAL

The N.M.R. spectra were taken with a Varian DP-60 instrument operating at either of two frequencies 60 and 19.25 Mc/sec, using the usual high resolution technique and the Varian high temperature device. The spectra were field swept with the field increasing from left to right and the calibration was made by the usual side band technique. The spectrum of each substance was taken several times rejecting the records with too big sweep irregularities and averaging the remaining ones. As a consequence, no perfect fit should be expected between the theoretical and any single experimental spectrum.

All substances were studied in several solvents (dimethylformamide, dimethylsulphoxide, benzene, acetone, ethyl maleate) at room and at the highest temperature each solution could withstand without boiling. No significant change of the values of the long-range coupling constants was observed which could be ascribed to the temperature, the main effect being a marked narrowing of the lines. This narrowing allowed the direct observation of splittings of up to 0.2 c.p.s. Similar narrowing was also observed in acetone solution and for this reason this was the solvent mainly used.

3. METHOD OF CALCULATION

Only di-substituted compounds were studied in order to avoid assignment uncertainties on the basis of the accepted relation: $J_{ortho} > J_{meta} > J_{para}$. While in the previous paper [1] the spectra, which were almost of the ABCX type, were studied solving with the computer the ABC part and adding, as a simple splitting, the effect of the long-range coupling, in the present work all spectra were solved as ABCD cases using an iterative procedure described elsewhere [7]. All theoretical spectra were checked, whenever possible, at both frequencies, the chemical shifts for the lower frequency being obtained from the 60 Mc spectra and keeping the values of the J -coupling constants. The method of calculation used throughout has the following properties:

(1) Each proton gives rise to eight transitions. Each coupling constant J_{ij} gives rise to four splittings S_{ij} all four being usually different or, at most, two and two equal. A given splitting S_{ij} appearing in the group of lines due to the i th nucleus also appears, with exactly the same value in the group of lines due to nucleus j . Using this property, the main long-range coupling across five bonds was calculated with better precision, not from the splitting of the aldehyde

'doublet' but from the splittings of the corresponding ring proton. (The aldehyde 'doublet' is formed from a total of eight imperfectly overlapping transitions.)

(2) The iterative programmes used make use of the following fitting criterion: assuming that the correct assignment has already been made, the position of each group of lines in a spectrum is characterized by the average frequency of these lines, $\bar{\nu}_i$. Each spin-spin coupling constant is characterized by the average splitting \bar{S}_{ij} it produces. A given theoretical spectrum is considered a good fit if the $\bar{\nu}_{ij}$'s and \bar{S}_{ij} 's are reproduced, this last part being determined by a least squares criterion. No use is made of the measured intensities of the lines, this being only used for checking the assignment. (The existence of a negative coupling constant can simply be proved assuming a negative value for the corresponding \bar{S}_{ij} and checking the resulting intensities.) No use is made at all in this method of the combination lines. Calculations, as well as experiments, show that if in an ABX spectrum $J_{AB} \sim \delta_{AB}$ two combination lines appear near the X (or C) group of lines [8]. The position of these lines is quite sensitive to δ_{AB} . If now we perturb the ABC spectrum introducing the Y (or D) proton, we observe the following things: if only one of the possible J_{Di} couplings is non-zero, both combination lines appear as doublets with splittings S_1 and S_2 , S_1 being usually very nearly, and if not equal to S_2 . If now we introduce another coupling $J_{Dj} \neq 0$ it comes out that $S_1 \neq S_2$. Since in this case one of the S 's is smaller than the average of S_1 and S_2 while the other one is bigger, it was tried and verified that the sum $\Sigma = |S_1| + |S_2|$ is usually proportional to one of the J 's while the difference $\Delta = |S_1| - |S_2|$ is proportional to the other one.

There is sometimes an uncertainty, but this can usually be overcome by a careful study of the linewidth and the relative intensities of the ABC part of the spectrum. This was possible in the present case due to the very good resolution available, which was, for all practical purposes, limited only by the natural linewidth.

4. RESULTS

4.1. 5-bromosalicylaldehyde

This substance is probably the best example of the outlined method. Figure 1 shows the spectrum of this substance dissolved in acetone, at room temperature and at 60 Mc/sec, from which it is evident that the aldehyde splitting is due to the ring proton in position three. This spectrum was calculated with the iterative programme assuming $S_{BD} = S_{CD} = 0$ and the following set of parameters was obtained (in c.p.s. and taking as zero the mid-point of the ABC group):

$$\begin{aligned} \nu_A &= 24.45, & \nu_B &= -18.07, & \nu_C &= -31.17, & \nu_D &= -150.90, \\ J_{AB} &= 8.85, & J_{AC} &= 0.36, & J_{AD} &= 0.56, & J_{BC} &= 2.58, & J_{BD} &= J_{CD} = 0. \end{aligned}$$

The 19.25 Mc/sec spectrum (figure 2) shows the combination lines as two small doublets near the two triplets of the A proton, and $S_1 < S_2$. (The left-hand side doublet is here always labelled S_1 .) To determine the influence of the several long-range couplings upon S_1 and S_2 , a set of spectra was calculated with the computer (with a simple non-iterative programme) using for the chemical shifts the values deduced from the 60 Mc/sec spectrum and varying slowly and

successively each parameter. In the first trial it was assumed that $J_{BD}=J_{CD}=0$ and J_{AD} , the main coupling was varied. Table 1 shows the results obtained:

J_{AD}	S_1	S_2	Σ	Δ
0.40	0.35	0.39	0.74	-0.04
0.45	0.39	0.44	0.83	-0.05
0.50	0.43	0.49	0.92	-0.06
0.55	0.48	0.53	1.01	-0.05
0.60	0.51	0.58	1.09	-0.07
0.65	0.55	0.62	1.18	-0.07

Table 1.

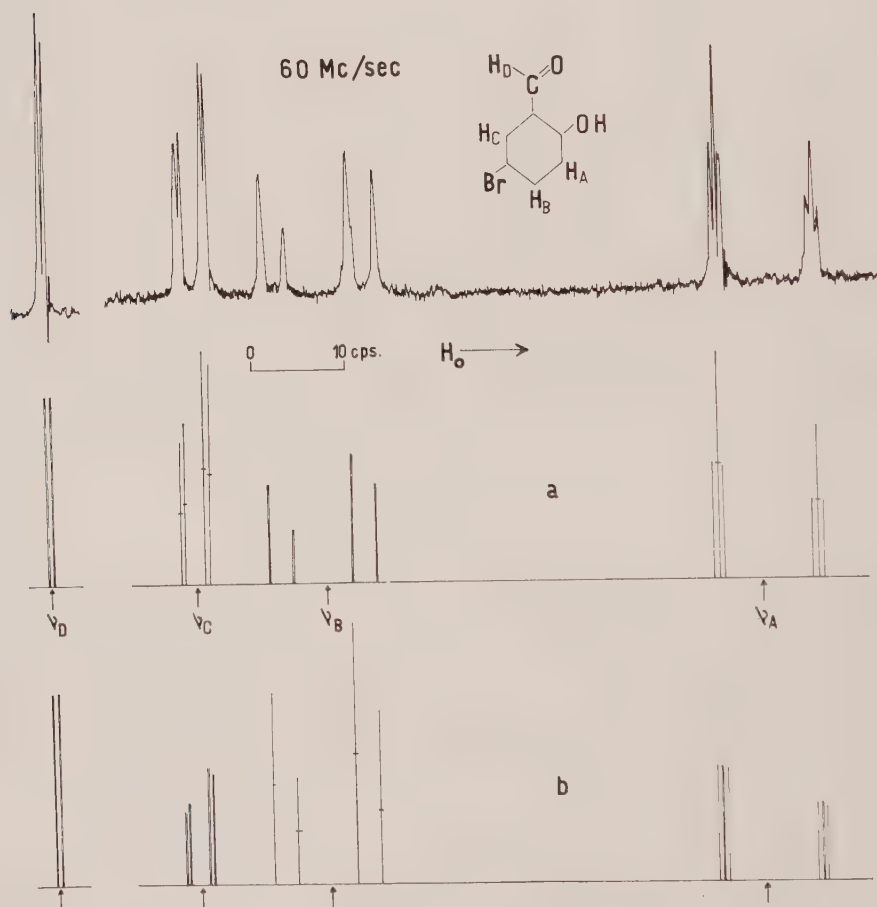


Figure 1. 60 Mc/sec N.M.R. spectrum of 5-bromosalicylaldehyde dissolved in acetone and at room temperature, with two possible theoretical solutions as given by the computer analysis of the combination lines: (a) with $J_{BD}=0.15$ c.p.s. and (b) with $J_{CD}=-0.15$ c.p.s. The relative height and larger half-width of the B lines shows (a) to be the correct solution.

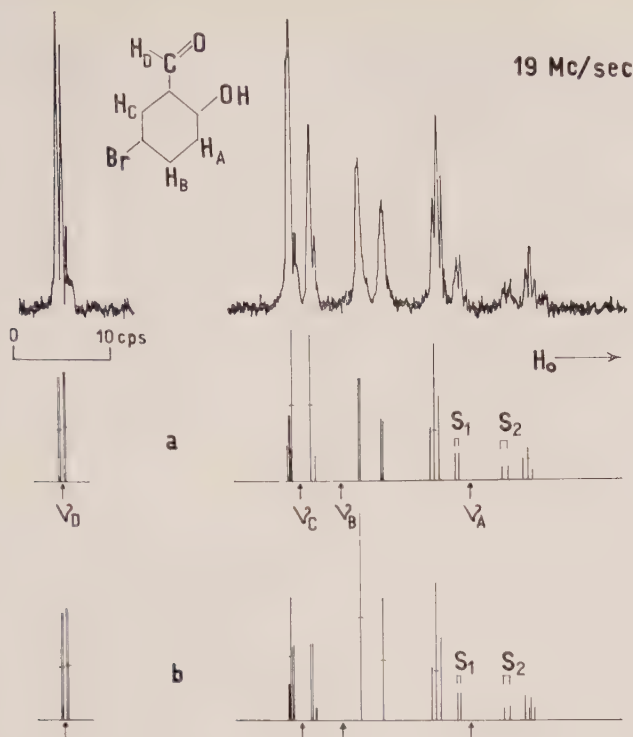


Figure 2. 19.25 Mc/sec spectrum of 5-bromosalicylaldehyde showing clearly the combination doublets S_1 and S_2 . Here too the intensities pattern favour the solution (a) with $J_{BD}=0.15$ c.p.s. The splitting due to this coupling cannot be resolved and the aldehyde signal appears thus as a doublet.

As it can be seen from this table, the difference of both combination splittings is practically independent of J_{AD} while the sum is directly proportional to it. The experimental values are: $S_1=0.39$ c.p.s. and $S_2=0.64$ c.p.s., which give $\Sigma=1.03$ and $\Delta=-0.25$. Interpolating the value of Σ we obtain for $J_{AD}=0.56$ in (accidentally, of course) perfect agreement with the result of the iterative programme. Taking now this value of J_{AD} for granted, assuming $J_{CD}=0$ and varying slowly J_{BD} the following set of results is obtained:

J_{BD}	S_1	S_2	Σ	Δ
0.15	0.41	0.65	1.06	-0.24
0.10	0.43	0.60	1.03	-0.17
0.05	0.46	0.58	1.04	-0.12
0.00	0.49	0.54	1.03	-0.05
-0.05	0.51	0.51	1.02	0.00
-0.10	0.55	0.47	1.02	0.08
-0.15	0.57	0.44	1.01	0.13

Table 2.

If we consider the experimental results with $\Delta = -0.25$ we are led immediately to the conclusion that $J_{BD} = 0.15$, but if we now try varying J_{CD} while keeping $J_{BD} = 0$ (and $J_{AD} = 0.56$) we obtain:

J_{CD}	S_1	S_2	Σ	Δ
0.15	0.59	0.44	1.03	0.15
0.10	0.55	0.47	1.02	0.07
0.05	0.53	0.51	1.04	0.02
0.00	0.49	0.54	1.03	-0.05
-0.05	0.45	0.58	1.03	-0.13
-0.10	0.41	0.61	1.02	-0.20
-0.15	0.39	0.64	1.03	-0.25

Table 3.

This gives us a solution with $J_{CD} = -0.15$ c.p.s. To decide against both possibilities we will observe the experimental spectra. In both of them, at 60 as well as at 19.25 Mc/s the B lines show a slightly larger linewidth than the other ones. If we now draw the theoretical spectra given by both solutions (case (a) $J_{BD} = 0.15$ and case (b) with $J_{CD} = -0.15$), it can be seen that in both cases the second long-range coupling introduces a splitting, the result of which is a slight widening of the corresponding lines and a decrease of the intensity due to an imperfect overlapping of its components (see Appendix). On this basis, it is quite evident that the solution (a), with $J_{BD} = 0.15$ c.p.s. across six bonds, is the correct one.

4.2. 5-chlorosalicylaldehyde

This case is quite similar to the previous one and only the 19.25 Mc/s spectrum (figure 3) is given to show the combination doublets S_1 and S_2 . The fact that the theoretical spectrum was calculated from the parameters obtained at 60 Mc/s plus the unavoidable sweep errors accounts for the observed differences in the positions of the groups of lines. Nevertheless the fine details are quite clear, like the quartets of the A lines and the combination doublets. (The 'fine structure' in the second aldehyde peak is merely due to 'wiggles'.) An analysis similar to the previous one with the experimental values $S_1 = 0.36$ and $S_2 = 0.64$ gives the following set of parameters for this substance (at 60 Mc/s):

$$\nu_A = 19.00, \quad \nu_B = -12.95, \quad \nu_C = -25.72, \quad \nu_D = -163.73, \\ J_{AB} = 8.94, \quad J_{AC} = 0.26, \quad J_{AD} = 0.50, \quad J_{BC} = 2.53, \quad J_{BD} = 0.10, \quad J_{CD} = 0.00.$$

4.3. 2,4 dihydroxybenzaldehyde

The 60 Mc/sec spectrum of this substance was studied in a previous paper [1] showing a long-range coupling of 0.51 c.p.s. between the aldehyde and the ring proton in position three (H_A). The ABCD analysis made lately confirm this value. The spectrum at 19.25 Mc/sec of this substance taken in acetone solution at room temperature shows (figure 4) two combination doublets with

an average splitting of $S_1=0.50$ and $S_2=0.30$ c.p.s. If we vary J_{BD} keeping $J_{CD}=0$ we obtain:

J_{BD}	S_1	S_2	Σ	Δ
0.15	0.30	0.31	0.61	-0.01
0.10	0.35	0.35	0.70	0.00
0.05	0.39	0.39	0.78	0.00
0.00	0.43	0.43	0.86	0.00
-0.05	0.47	0.47	0.94	0.00
-0.10	0.51	0.51	1.02	0.00
-0.15	0.55	0.55	1.10	0.00

Table 4.

Taking the experimental result $\Sigma=0.80$, we are led to assume that $J_{BD}=0.04$ c.p.s., but this is within experimental error.

If we now try varying J_{CD} , keeping $J_{BD}=0$, we get:

J_{CD}	S_1	S_2	Σ	Δ
0.15	0.28	0.57	0.85	-0.29
0.10	0.34	0.52	0.86	-0.18
0.05	0.38	0.47	0.85	-0.09
0.00	0.43	0.43	0.86	0.00
-0.05	0.50	0.39	0.89	0.11
-0.10	0.53	0.34	0.87	0.19
-0.16	0.58	0.29	0.87	0.28

Table 5.

Our experimental value of $\Delta=0.20$ fits well with $J_{CD}=-0.10$ and since Σ is proportional to J_{BD} and Δ to J_{CD} only, there is no ambiguity in the assignment.

The 19.25 Mc/sec parameters of this spectrum are:

$$\begin{aligned} \nu_A &= 23.15, \quad \nu_B = 19.83, \quad \nu_C = 0.10, \quad \nu_D = -42.03, \\ J_{AB} &= 2.28, \quad J_{AC} = 0.17, \quad J_{AD} = 0.51, \quad J_{BC} = 8.67, \quad J_{BD} = 0, \quad J_{CD} = -0.10. \end{aligned}$$

4.4. 2,5 dihydroxybenzaldehyde

On figure 5 is shown the 60 Mc/sec spectrum of this substance taken in dimethylformamide at *circa* 116°C. Since this is a strongly coupled case, the combination lines are visible even at this frequency. The average experimental values of $S_1=0.36$ and $S_2=0.61$ are definitely different from the theoretical values of 0.44 and 0.49 obtained with the computer assuming only one long-range coupling. The experimental value of $\Sigma=0.97$ gives for J_{AD} the value of 0.55 c.p.s. which compares well with the value of 0.50 given by the iterative programme. (It should be noted here that the uncertainties in the parameters, as given by the iterative programme are highest when dealing with strong coupled

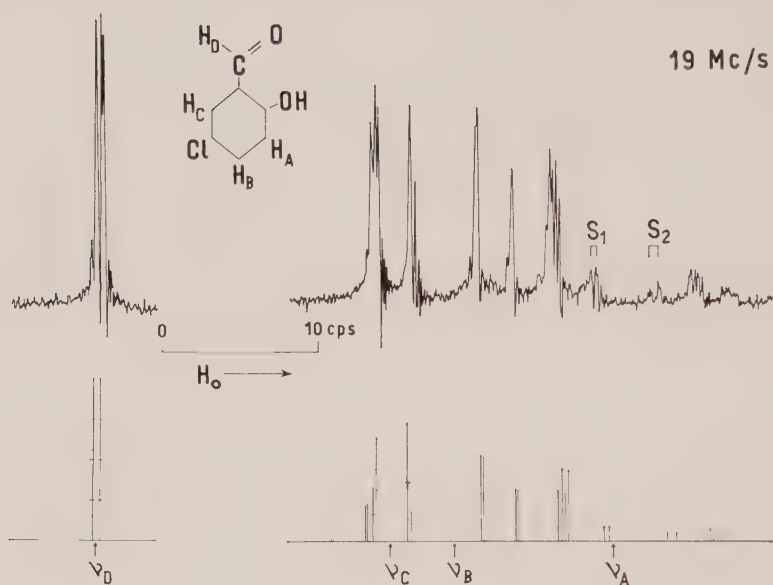


Figure 3. 19.25 Mc/sec spectrum of 5-chlorosalicylaldehyde. The experimental values of S_1 and S_2 lead us to assume the existence of the second long-range coupling $J_{\text{BD}} = 0.10$ c.p.s.

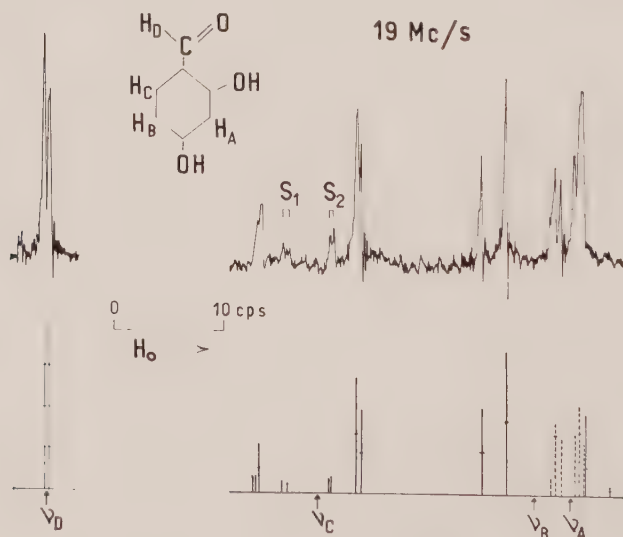


Figure 4. 19.25 Mc/sec spectrum of 2,4 dihydroxybenzaldehyde. The experimental values of S_1 and S_2 point unambiguously to a second long-range coupling $J_{\text{CD}} = -0.10$ c.p.s.

spectra.) Following the analysis as in previous cases one arrives at the conclusion that the coupling is either $J_{BD}=0.10$ (spectrum (a)) or $J_{CD}=-0.10$ (spectrum (b)).

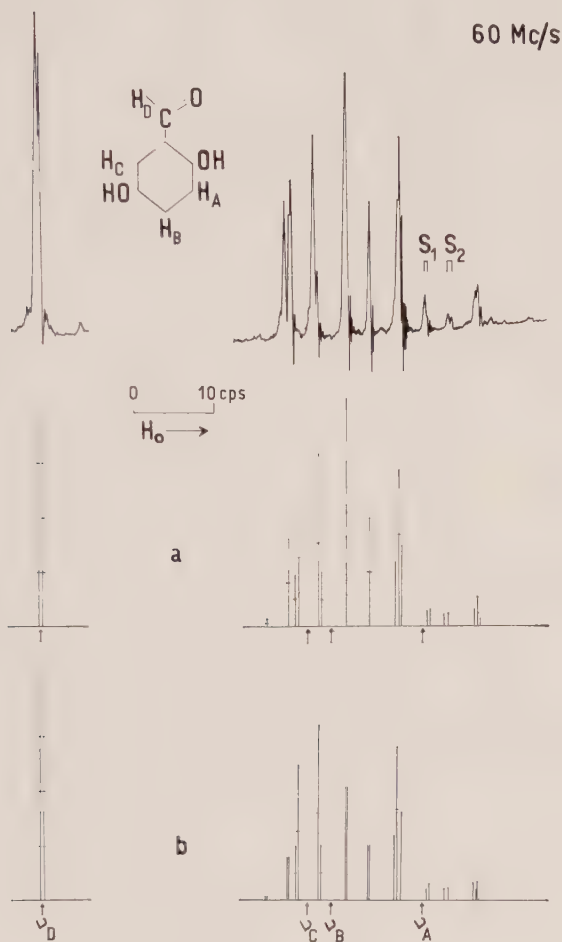


Figure 5. 60 Mc/sec spectrum of 2,5 dihydroxybenzaldehyde on which the combination doublets are clearly visible since we are dealing with a strong coupled spectrum. Two solutions, as given by the computer are possible: (a) with $J_{CD} = -0.10$ c.p.s. and (b) with $J_{BD} = 0.10$ c.p.s. This being a strong coupled case, the splittings S_{CD} are all smaller than J_{CD} in the first case, while in the second one all the splittings S_{BD} are bigger than J_{BD} . This evidently favours solution (a).

The ambiguity cannot be solved so easily as previously but the following things should be noted: in the first case ($J_{BD} = 0.10$), all splittings S_{CD} are bigger than 0.10 c.p.s. (between 0.11 and 0.14). This would lead to the intensities pattern of the spectrum (b) which definitely does not fit with the experimental spectrum. In the second case ($J_{CD} = -0.10$) the corresponding splittings

are all smaller than 0.10 c.p.s. giving thus, by overlapping, lines of practically normal intensity (see Appendix). We are thus led to the conclusion that in the 2,5 dihydroxybenzaldehyde there is very probably a negative coupling of -0.10 c.p.s. between the aldehyde and the proton in position six.

The calculated parameters for the 60 Mc/sec spectrum of this substance are:

$$\begin{aligned} \nu_A &= 4.31, \quad \nu_B = -1.41, \quad \nu_C = -10.27, \quad \nu_D = -200.00, \\ J_{AB} &= 9.01, \quad J_{AC} = 0, \quad J_{AD} = 0.55, \quad J_{BC} = 3.03, \quad J_{BD} = 0, \quad J_{CD} = -0.10. \end{aligned}$$

4.5. 5-nitrosalicylaldehyde

The 19.25 Mc/sec spectrum of this substance in acetone solution at room temperature (figure 6) shows, like all other salicylaldehydes, that the main coupling is with proton three and that $S_1 = S_2 = 0.38$ c.p.s. what, in accordance

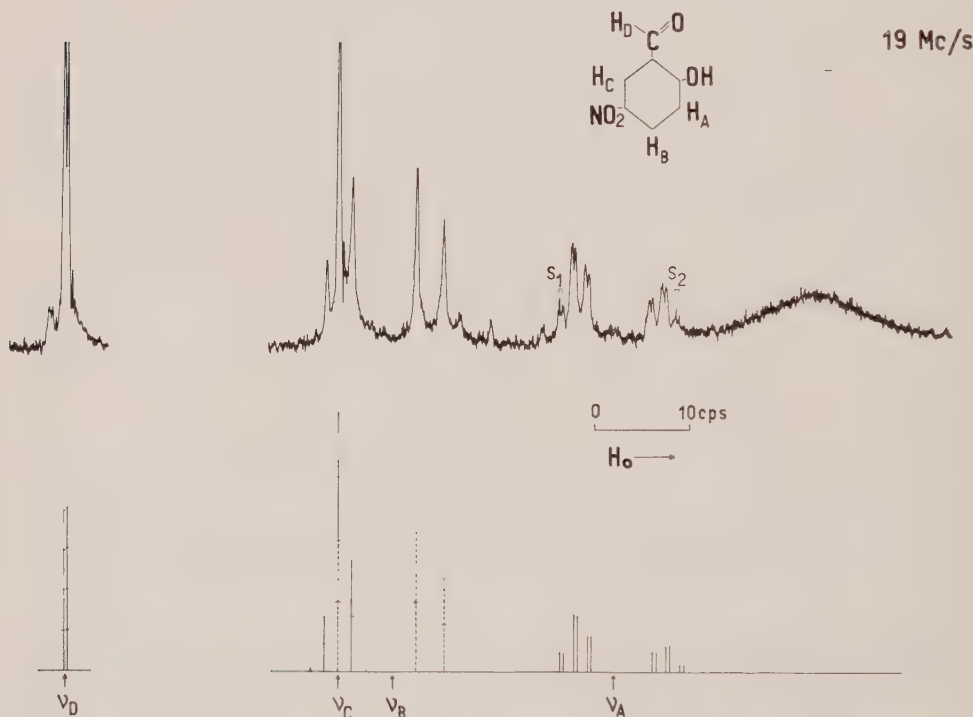


Figure 6. 19.25/sec spectrum of 5-nitrosalicylaldehyde. The two combination doublets around the A group are $S_1 = S_2$ showing that no other long-range coupling, except the one with proton three, is present. The OH peak can be seen as a very wide line on the high field side.

with the computer data should be considered as an indication of the absence of a second long-range coupling. The OH signal appears at the right side of the field which according to many works [4-6] is an indication of the absence of internal H-bond.

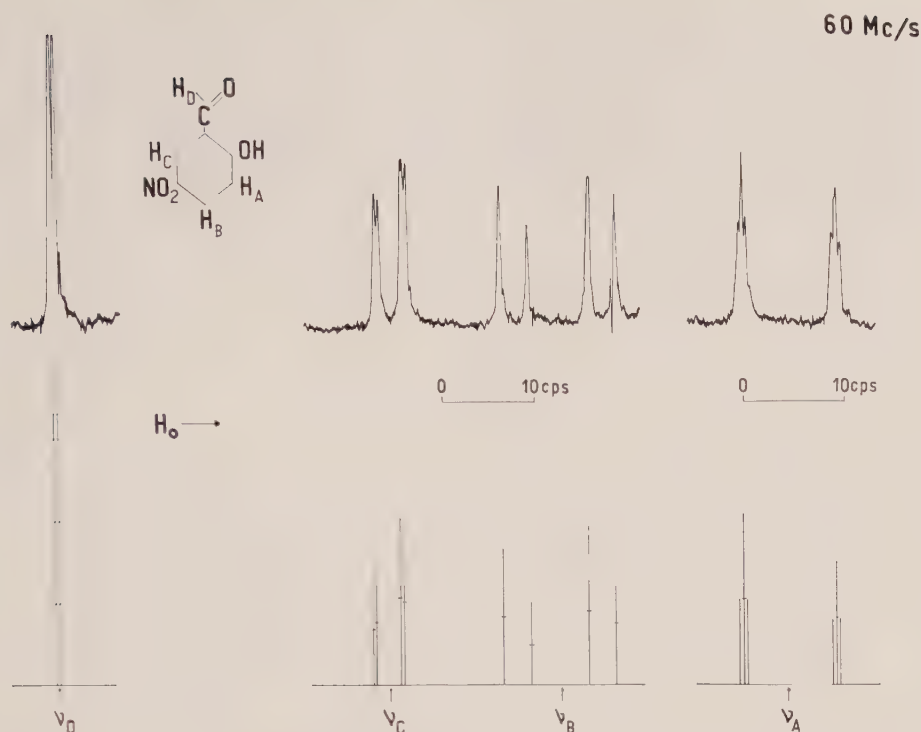


Figure 7. 60 Mc/sec of 5-nitrosalicylaldehyde showing the long-range coupling between the aldehyde and the proton three.

There is no evidence that in acetone solution the B lines (half-width ~ 0.5 c.p.s.) are coupled to the OH proton, as happens in deuteriochloroform [9]. This absence of coupling is confirmed by the 60 Mc/sec spectrum (figure 7), the parameters of which are:

$$\begin{aligned} \nu_A &= 40.51, \quad \nu_B = -31.81, \quad \nu_C = -49.52, \quad \nu_D = -141.42, \\ J_{AB} &= 9.29, \quad J_{AC} = 0.31, \quad J_{AD} = 0.38, \quad J_{BC} = 2.97, \quad J_{BD} = J_{CD} = 0.00. \end{aligned}$$

We would like to thank Dr. R. Ch. de Guber from the Argentine Institute of Calculus for the skilful programming.

The assistance of Mr. J. Linskens in preparing the drawings is gratefully acknowledged.

We like to thank the National Research Council of Argentina (CNICT) and the Ford Foundation for financial support.

APPENDIX

Assuming we have two Lorentzian lines with half-width Δ and height y_0 , separated by a distance $\delta \leq \Delta$, their partial over-lapping gives rise to a 'single' line of height $y \leq 2y_0$. This can be easily calculated and is given by the expression:

$$y = \frac{1 + (\delta/\Delta)^2}{2y_0} y_0 \leq y \leq 2y_0.$$

Figure 8 gives a graph of this function. From it, and assuming a definite value for Δ from the other ring proton signals, the non-resolved separation δ can be obtained by comparing the observed and the calculated intensities.

In spite of the rather low precision with which line intensities are obtained in N.M.R. spectroscopy, the long-range splittings constants obtained in this way agree reasonably well with the values obtained from the theoretical analysis of the spectra.

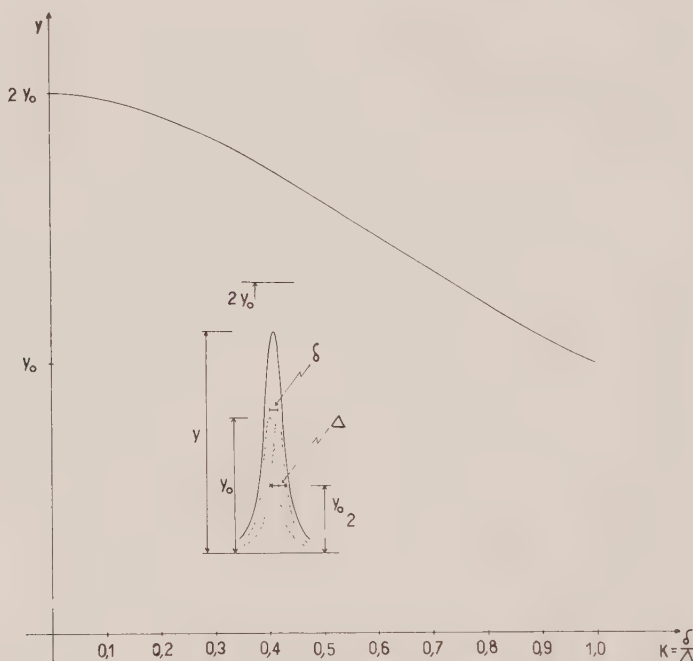


Figure 8. Calculated height of two Lorentzian lines of half-width Δ separated by a distance $\delta \leq \Delta$ as a function of the parameter δ/Δ .

REFERENCES

- [1] KOWALEWSKI, D. G. DE, and KOWALEWSKI, V. J., 1962, *J. chem. Phys.*, **37**, 1009.
- [2] BANWELL, C. N., and SHEPPARD, N., 1962, Communication No. 14 at the General Discussion on High Resolution N.M.R. arranged by the Faraday Society, Oxford, September.
- [3] FREEMAN, R. (private communication).
- [4] PORTE, A. L., GUTOWSKY, H. S., and MOYER HUNSBERGER, I., 1960, *J. Amer. chem. Soc.*, **82**, 5057.
- [5] REEDS, L. W., 1960, *Canad. J. Chem.*, **38**, 249.
- [6] FORSÉN, S., ÅKERMARK, B., 1963, *Acta chem. scand.*, **17**, 1907.
- [7] KOWALEWSKI, V. J., and KOWALEWSKI, D. G. DE, 1962, *J. chem. Phys.*, **36**, 266.
- [8] POPE, J. A., SCHNEIDER, W. G., and BERNSTEIN, H. J., 1959, *High Resolution Nuclear Magnetic Resonance* (New York: McGraw-Hill Book Company).
- [9] FORSÉN, S., and ÅKERMARK, B., 1963, *Acta chem. scand.*, **17**, 1712.

Multiple long range spin-spin couplings in di-substituted benzaldehydes and hindered rotation

by DORA G. DE KOWALEWSKI and VALDEMAR J. KOWALEWSKI

Department of Physics, Faculty of Exact Sciences, The University,
Buenos Aires, Argentina

(Received 28 September 1964)

The analysis of the N.M.R. spectra of the 3-nitro 4-hydroxy; 2-chloro 4-dimethylamino; 2,4 dinitro and 2,4 dimethoxybenzaldehydes shows the existence of a long-range coupling between the aldehyde proton and the ring proton in position five. The splitting of the combination lines allows the determination, in magnitude and relative sign, of another long-range coupling in the first three substances and of three simultaneous long-range couplings in the 2,3 dimethoxybenzaldehyde.

It was verified that these interactions are temperature independent in the range of 23–200°C which is considered as an indication of the rigid character of the bond between the aldehyde and the ring carbons.

1. INTRODUCTION

With the intention to complete the study of the long-range couplings in di-substituted benzaldehydes [1] the spectra of 13 compounds were studied at two different frequencies, 60 and 19.25 Mc/sec with the method described previously [2]. Four of these compounds show combination lines at some frequency and this allowed us to detect, besides the main coupling with proton five, another and eventually a third long-range coupling between the aldehyde and the ring protons.

The experimental procedure and the method of analysis follow exactly the outlines of the previous paper [2].

2. 2-CHLORO 4-DIMETHYLAMINOBENZALDEHYDE

This substance was studied at about 116°C in dimethylformamide solution, since at room temperature the lines are widened and the long-range splittings are barely shown. Figure 1 shows the spectrum of this substance taken at 60 Mc/sec. Since the chemical shifts of the nuclei A and B of the spectrum are very close, combination lines are visible, even at this frequency.

The first unusual thing which was found in this spectrum was that, starting with an initial value for the para splitting $S_{AC}=0.49$ the computer gave a solution $J_{AC}=1.18$ c.p.s., an unusually high value for a para coupling, and the intensities pattern did not fit correctly, specially for the C group of lines. It was then assumed that $S_{AC}=-0.49$. This time the computer gave a solution with $J_{AC}=0.12$ c.p.s. and a correct intensity pattern.

The combination doublets, which are quite clear in this case, have the experimental splittings $S_1=0.38$ and $S_2=0.67$ giving for their sum: $\Sigma=1.05$ and their difference $\Delta=-0.29$. Assuming the existence of only one long-range coupling, the computer solution gave $S_1=0.53$ and $S_2=0.52$. An analysis similar to the one of the salicylaldehydes [2] leads to the conclusion that $J_{AD}=0$ and $J_{CD}=-0.10$, without any ambiguity, since it shows that $J_{AD}\propto\Sigma$ and $J_{CD}\propto\Delta$ only.

The final set of parameters for the 60 Mc/sec spectrum of this substance is (in c.p.s.):

$$\begin{aligned} \nu_A &= 24.56, & \nu_B &= 23.34, & \nu_C &= -35.68, & \nu_D &= -193.00, \\ J_{AB} &= 2.36, & J_{AC} &= 0.12, & J_{AD} &= 0, & J_{BC} &= 8.69, & J_{BD} &= 0.63, & J_{CD} &= -0.10. \end{aligned}$$

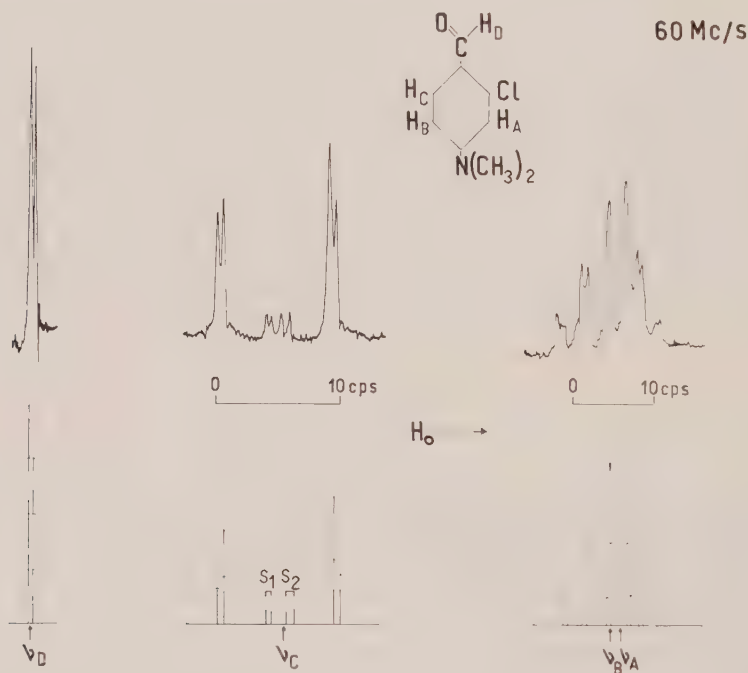


Figure 1. 60 Mc spectrum of 2-chloro 4-dimethylaminobenzaldehyde in dimethyl formamide solution at 116°C . Since $J_{AB} > \delta_{AB}$ combination lines can be seen near the group C. The coupling of the aldehyde proton with the ring proton in position (B) five splits also the combination lines. S_1 is evidently smaller than S_2 and computer analysis shows this to be due to the presence of another long-range coupling of -0.10 c.p.s. with proton C.

3. 3-NITRO, 4-HYDROXYBENZALDEHYDE

Figure 2 shows the 60 Mc/sec spectrum of this substance taken in acetone solution at room temperature, from which is evident the main long-range coupling with proton number five. Figure 3 shows the spectrum of the same substance at 19.25 Mc/sec. The splittings of the C group of lines are now smaller and the triplets are not resolved but the combination doublets S_1 and S_2 can now be seen. While the calculated values for only one long-range coupling are $S_1=0.43$ and $S_2=0.47$, the experimental values are $S_1=0.54$ and $S_2=0.34$ c.p.s., suggesting

the existence of a second long-range coupling. Unfortunately this is not a favourable case and two solutions are possible: either $J_{AD} = -0.15$ or $J_{BD} = 0.15$ c.p.s.

An examination of the 60 Mc/sec spectrum shows the A lines slightly broader than the other ones and slightly smaller than predicted by the computer calculation. Although this effect is perhaps not enough to account for the value of $J_{AD} = -0.15$ c.p.s., in view of the success in the previous cases [2] and the experimental values of S_1 and S_2 , the existence of a second long-range coupling is assumed as probable with the following set of parameters at 60 Mc/sec (in c.p.s.):

$$\nu_A = 15.90, \quad \nu_B = 8.68, \quad \nu_C = -24.58, \quad \nu_D = -134.50, \\ J_{AB} = 1.74, \quad J_{AC} = 8.54, \quad J_{AD} = -0.15, \quad J_{BC} = 0.35, \quad J_{BD} = 0, \quad J_{CD} = 0.49.$$

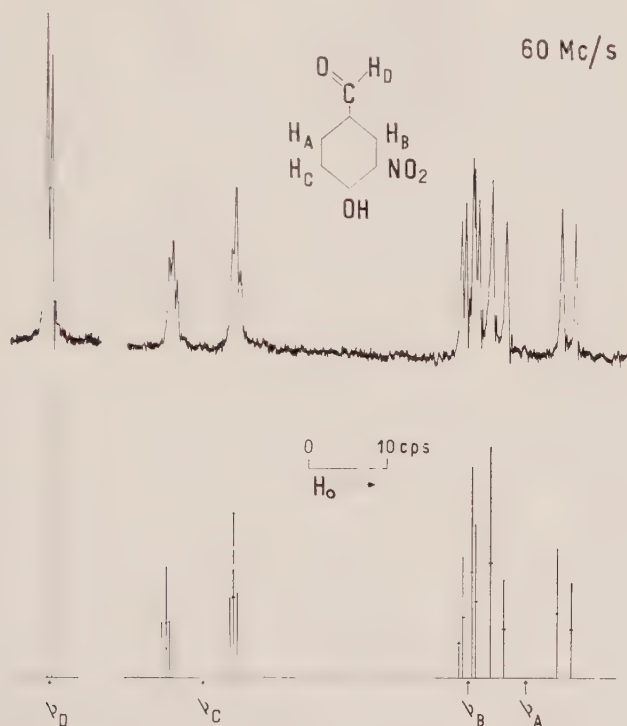


Figure 2. 60 Mc spectrum of 3-nitro, 4-hydroxybenzaldehyde showing the coupling between the aldehyde and the ring proton in position five, across five bonds. The computer gives two solutions: (a) with a second long-range coupling $J_{AD} = -0.15$ or (b) with $J_{BD} = 0.15$ c.p.s. The aspect of the A lines favours solution (a).

4. 2,4 DIMETHOXYBENZALDEHYDE

The 60 Mc spectrum of this substance, which is shown in figure 4, was taken at room temperature in acetone solution. Again, since δ_{AB} is very small, combination lines are visible even at this frequency. The experimental values of the splittings are: $S_1 = 0.87$ and $S_2 = 0.36$ c.p.s. This gives us $\Sigma = 1.23$ and $\Delta = 0.51$ c.p.s. For only one long-range coupling the computer gives $S_1 = 0.71$ and $S_2 = 0.73$. Variation of the remaining parameters J_{BD} and J_{CD} shows that Σ is only a function of J_{BD} while Δ is only a function of J_{CD} . Linear interpolation

gives $J_{BD}=0.15$ and $J_{CD}=-0.25$ c.p.s. without ambiguity. The existence of these couplings is evident from the spectrum of the ring protons too, as a barely resolved fine structure in the C lines, a noticeable widening of the B lines and a certain fine structure of the aldehyde signal which, we should recall, is an unresolved multiplet of eight partially overlapping lines.

The theoretical spectrum of figure 4 was calculated with the following set of parameters:

$$\begin{aligned} \nu_A &= 17.16, & \nu_B &= 15.57, & \nu_C &= -50.03, & \nu_D &= -200.75, \\ J_{AB} &= 2.18, & J_{AC} &= 8.58, & J_{AD} &= 0.91, & J_{BC} &= 0.33, & J_{BD} &= 0.15, & J_{CD} &= -0.25. \end{aligned}$$

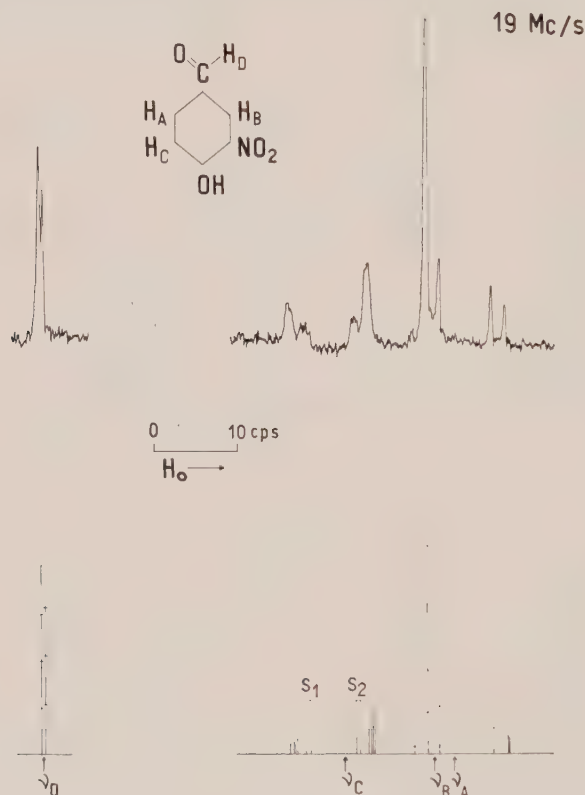


Figure 3. 19.25 Mc spectrum of the same substance of figure 2 showing the splittings S_1 and S_2 . The existence of a second long-range coupling is suspected because $S_1 > S_2$.

5. 2,4 DINITROBENZALDEHYDE

This is a case in which the existence of double long-range coupling is directly evident from the aldehyde signal. This is shown in figure 5 under different conditions: (a) in dimethylsulphoxide at 120°C ; (b) in dimethylformamide at 120°C ; (c) in acetone at room temperature; (d) in ethyl maleate at 190°C and (e) in benzene at 77°C . The 60 Mc spectrum of the ring protons, in acetone solution at room temperature (figure 6) shows the main long-range coupling with proton five and the second one, though not resolved, with proton three this time.

The 19.25 Mc spectrum of this substance shows (figure 7) the combination doublets $S_1=0.24$ and $S_2=0.33$. The long-range spin-spin coupling constants were obtained with the computer by the iterative method as $J_{BD}=0.57$ and $J_{CD}=0.21$ c.p.s. giving, besides, for the combination doublets the values: $S_1=0.22$ and $S_2=0.36$, in good agreement with the experimental values. The next inquiry was directed towards the sign of these couplings. The computer shows that, if both long-range couplings are assumed of different signs and whichever is the negative one, $S_1=0.56$ and $S_2=0.69$. For both couplings negative, the solution is the same as for both positive.

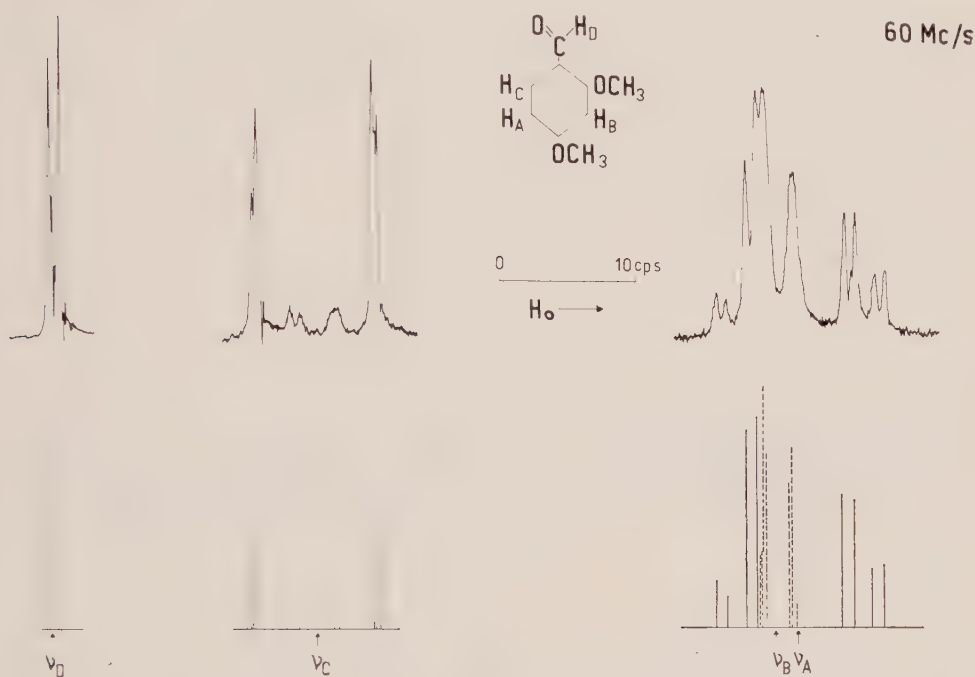


Figure 4. 60 Mc spectrum of 2,4 dimethoxybenzaldehyde showing the combination doublets S_1 and S_2 . Computer analysis gives in this case and without ambiguity: $J_{BD}=0.15$ and $J_{CD}=-0.25$ c.p.s. The existence of these couplings can be, in this case, inferred directly from the B and C lines.

Coming now back to the aldehyde signal, it can be seen from figure 5 that while in dimethylformamide it is a perfect quartet, in benzene it appears as a doublet. Careful measurements were made of all the spectra which show that, with the exception of benzene and within the experimental error, both couplings are solvent and temperature independent. In benzene the second long-range coupling is still present, as can be seen from the widening of the C lines (figure 8), but is definitely smaller. The difference in chemical shift of the ring protons should also be noted.

The 60 Mc parameters for this substance, in acetone solution, are:

$$\begin{aligned} \nu_A &= 29.27, & \nu_B &= -2.15, & \nu_C &= -12.22, & \nu_D &= -103.79, \\ J_{AB} &= 8.35, & J_{AC} &= 0.35, & J_{AD} &= 0, & J_{BC} &= 2.29, & J_{BD} &= 0.57, & J_{CD} &= 0.21. \end{aligned}$$

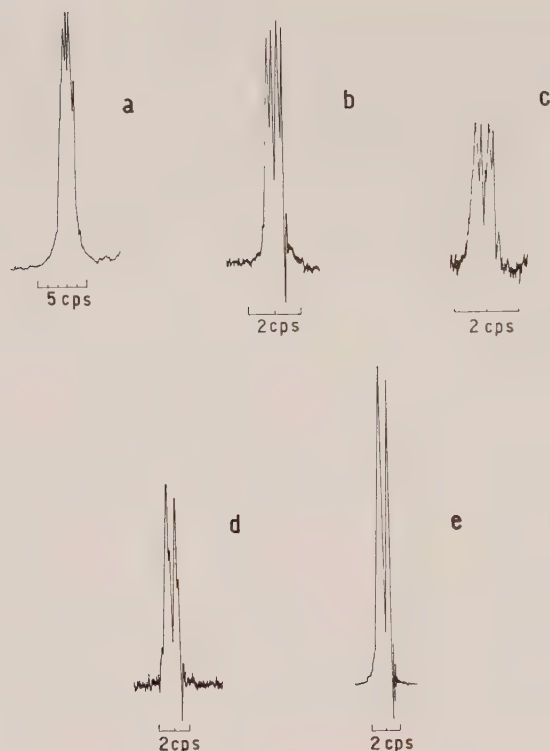


Figure 5. Aldehyde signal of the 2,4 dinitrobenzaldehyde under different conditions, showing directly the presence of two simultaneous long-range couplings. (a) in dimethylsulphoxide solution at 120°C; (b) in dimethylformamide at 120°C; (c) in acetone at room temperature; (d) in ethyl maleate at 190°C; (e) in benzene at 77°C.

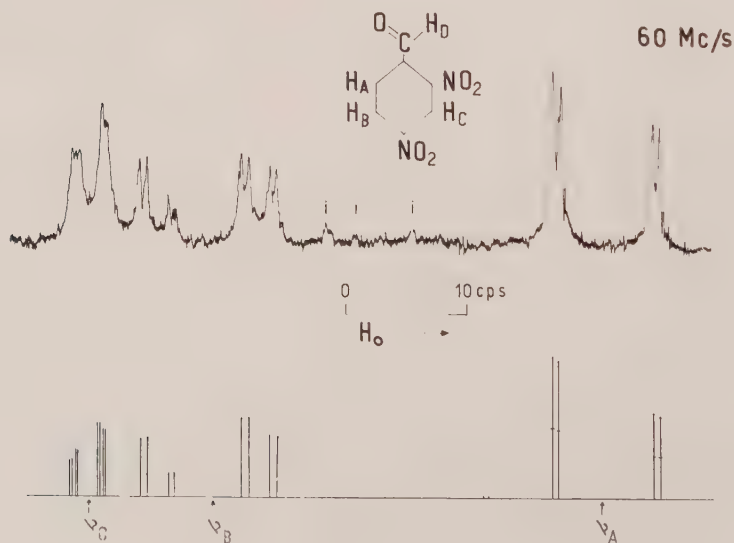


Figure 6. 60 Mc spectrum of 2,4 dinitrobenzaldehyde, in acetone solution and at room temperature, showing the main coupling of the aldehyde and proton five, $J_{BD}=0.57$ c.p.s. and a second with proton three, $J_{CD}=0.21$ c.p.s. (The peaks marked *i* are impurities.)

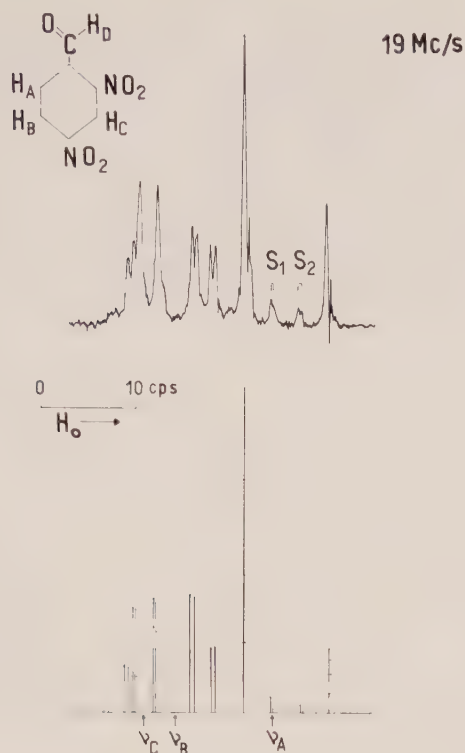


Figure 7. 19.25 Mc spectrum of the previous substance showing the 'combination doublets' S_1 and S_2 . Computer calculation shows both long-range couplings to be of the same sign.

6. DISCUSSION

The main results of this and the preceding paper are that, in benzaldehydes which show a multiple long-range coupling, the couplings with the ring protons in positions three, four and five are (relatively) positive while the coupling with proton six is negative. These results should be compared with those obtained by Hoffman *et al.* [3] in furanaldehydes by triple resonance experiments who determined the signs of similar double long-range couplings with respect to the ring protons. Their result is similar in the sense that only the coupling with the proton in position ortho with respect to the aldehyde group is negative.

McConnell [4] as well as McLachlan [5] have predicted an alternation in the signs of proton-proton spin-spin couplings according to which protons separated an odd number of bonds should have a positive coupling while protons separated an even number of bonds should have a negative coupling. If we try to apply this to benzaldehydes we see this prediction to work well with protons three, five and six but not with proton four, which is separated six bonds and is positive.

Another aspect of the present work is related to the possibility of a hindered internal rotation of the aldehyde group. The independence of the observed couplings with temperature has been already pointed out. All present results seem to confirm the stereospecificity of the long-range couplings in benzaldehydes [6]. According to this the two long-range couplings with protons three and five

in 2, 4 dimethoxy and 2, 4 dinitrobenzaldehydes could be considered as a time average result of the two positions, *cis* and *trans* with respect to the *ortho* substituent. X-ray and neutron diffraction studies by Coppens [7] in some solid *ortho* nitrobenzaldehydes show a rigid planar structure with the formyl proton near the nitro group but without forming hydrogen bond with it, which could account for a rigid structure. Infra-red and Raman studies by Silver and Wood [8] of chloro and methyl benzaldehydes show the existence of a rather high barrier against internal rotation for these compounds (between 4.87 and 7.96 kcal/mol). The results of the present work seem to support the existence of such high barriers. In 2, 4 dinitrobenzaldehyde, for instance, the splittings seem to change slightly

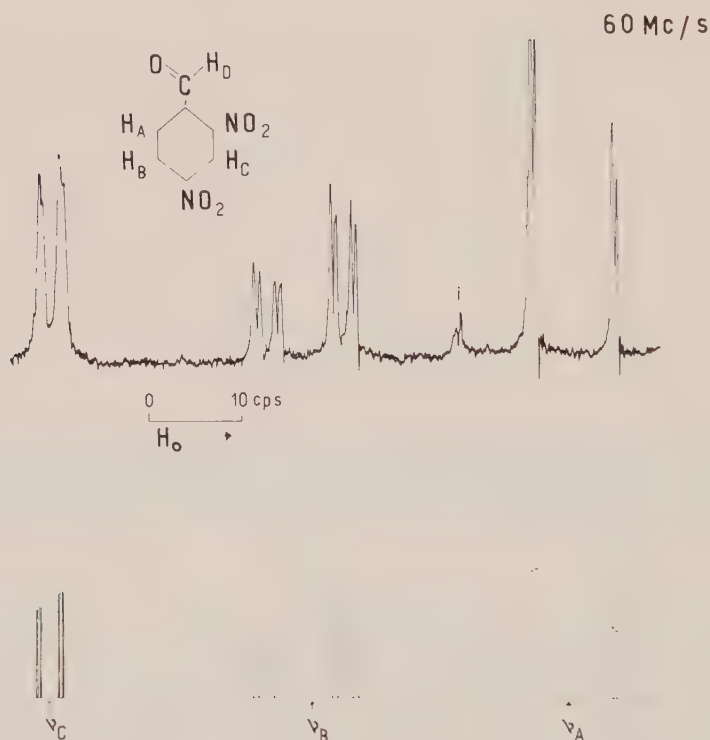


Figure 8. 60 Mc spectrum of the same substance of figure 6 but in benzene solution. The second long-range coupling, though not visible in the aldehyde signal, is seen to be still present as an unresolved fine structure of the C lines.

only when observed at almost 200°C, but it is doubtful whether this is due to the increased amplitude of torsional vibration or a solvent effect similar to the one of benzene, though of smaller magnitude. This is in disagreement with the work of Karabatsos [9] according to which a certain maximum value for this coupling should be expected in the planar structure, independent of substituent, and the different values of the observed splittings of the aldehyde peak could be accounted for as a result of a mixture of isomers of both forms, *cis* and *trans*.

The authors would like to thank Dr. Rebeca Ch. de Guber from the Argentine Institute of Calculus for her skilful programming.

The assistance of Mr. J. Linskens in preparing the drawings is very much appreciated.

Financial support by the National Research Council of Argentina (C.N.I.C.T.) and the Ford Foundation is dutifully acknowledged.

APPENDIX

The following substances, of similar structure, do not show the characteristic long-range coupling across five bonds. As a consequence combination lines are not split and the present method cannot be used to detect eventual long-range

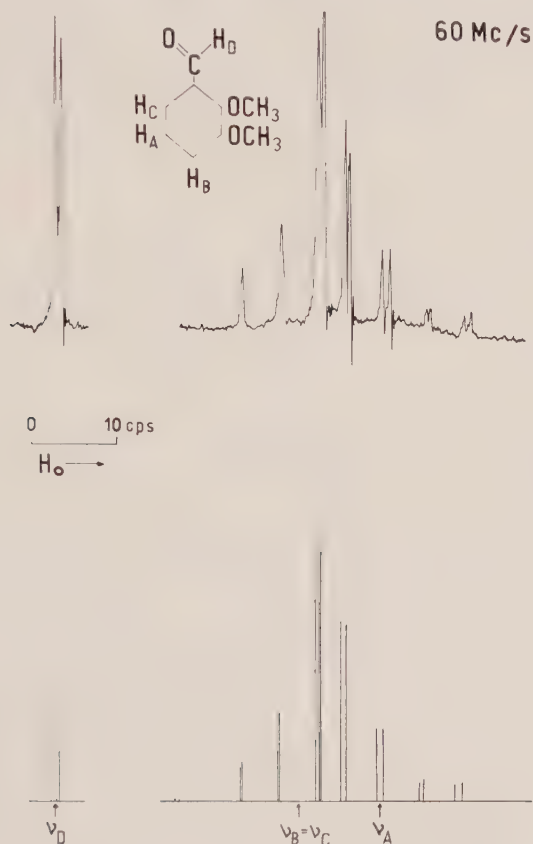


Figure 9. 60 Mc spectrum of 2,3 dimethoxybenzaldehyde showing only one long-range coupling with the aldehyde.

couplings with other ring protons, the existence of which cannot naturally be excluded: 3, 4 dimethoxy; 3 nitro 4 chloro; 2 nitro 5 hydroxy and 2 nitro 5 chloro benzaldehyde.

Another group shows an interaction between the aldehyde and the ring proton in position five, but the ABC ring spectrum is such as to preclude the observation of combination lines, due to lack of intensity or due to its position, at the base of some intense peak. Among these are the 2, 3 dimethoxybenzaldehyde and 3, 4 dichlorobenzaldehyde. The 60 Mc spectrum of the first of these substances is

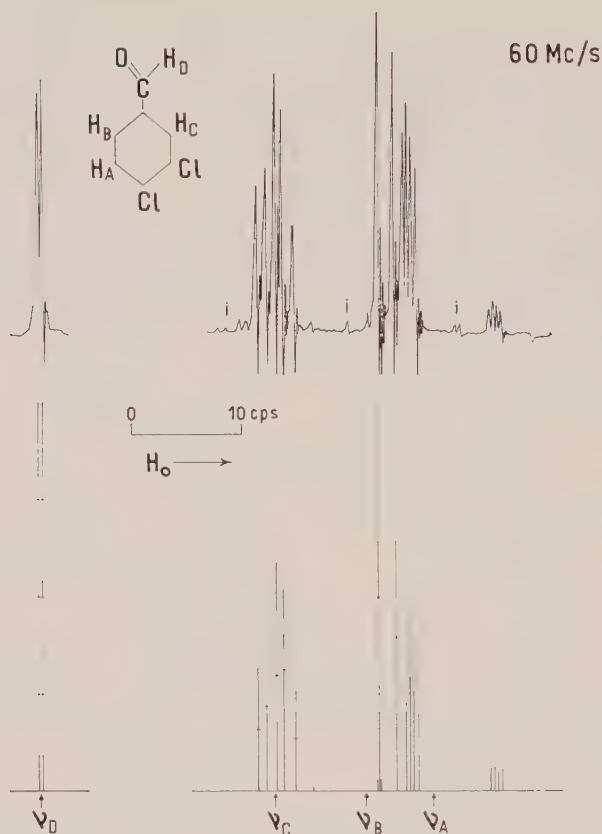


Figure 10. 60 Mc spectrum of 3,4 dichlorobenzaldehyde with a long-range coupling between the aldehyde and proton in position five. (Peaks marked with *i* are impurities.)

shown in figure 9. The theoretical spectrum was calculated with the following set of parameters (in c.p.s.):

$$\nu_A = 1.90, \quad \nu_B = -7.74, \quad \nu_C = -7.74, \quad \nu_D = -194.87, \\ J_{AB} = 7.52, \quad J_{AC} = 7.52, \quad J_{AD} = 0.81, \quad J_{BC} = J_{BD} = J_{CD} = 0.$$

The 60 Mc spectrum of 3,4 dichlorobenzaldehyde is shown in figure 10 and its parameters are (in c.p.s.):

$$\nu_A = 4.79, \quad \nu_B = -1.47, \quad \nu_C = -9.99, \quad \nu_D = -130.00, \\ J_{AB} = 7.83, \quad J_{AC} = 0.32, \quad J_{AD} = 0.48, \quad J_{BC} = 1.92, \quad J_{BD} = J_{CD} = 0.$$

REFERENCES

- [1] KOWALEWSKI, D. G. DE, and KOWALEWSKI, V. J., 1962, *J. chem. Phys.*, **37**, 1009.
- [2] KOWALEWSKI, D. G. DE, and KOWALEWSKI, V. J., 1965, *Mol. Phys.*, **9**, 319.
- [3] HOFFMAN, R. A., GESTBLOM, B., and GRONOWITZ, S., 1963, *J. mol. Spectrosc.*, **11**, 454.
- [4] MCCONNELL, H. M., 1955, *J. chem. Phys.*, **23**, 2454.
- [5] McLACHLAN, A. D., 1959, *Mol. Phys.*, **2**, 223.
- [6] BANWELL, C. N., and SHEPPARD, N., 1962, Communication No. 14 at the Discussion of the Faraday Society, Oxford, 17-19 September.
- [7] COPPENS, P., 1964, *Acta Cryst.*, **17**, 573; 1964, *Ibid.*, **17**, 222.
- [8] SILVER, H. G., and WOOD, J. L., 1964, *Trans. Faraday Soc.*, **60**, 5.
- [9] KARABATSOS, G. J., 1963, *J. Amer. chem. Soc.*, **85**, 3886.

Ligand field parameters of Mo(III) complexes

by C. FURLANI and O. PIOVESANA

Chemical Institute, University of Trieste
and Centro Chimica Comp. Coord. of C.N.R.

(Received 9 November 1964; revision received 29 December 1964)

Spectral absorption data of some octahedral chromophores of Mo^{3+} are reported, together with values of Δ and β_{55} parameters, whenever experimentally attainable. For complexes with sufficiently electronegative ligands, almost complete ligand field spectra can be observed, whereas in other complexes intense charge transfer bands occur; with ligands of low electronegativity, charge transfer bands from the central ion to the ligands are frequently encountered.

1. INTRODUCTION

Literature references on Mo(III) complexes [1–2–3] clearly show striking similarity to the ligand field spectra of the $3d^3$ configuration of Cr^{3+} . We report here new spectra of Mo(III) complexes, and discuss values of the ligand field parameters Δ and β_{55} obtained thereby.

2. EXPERIMENTAL

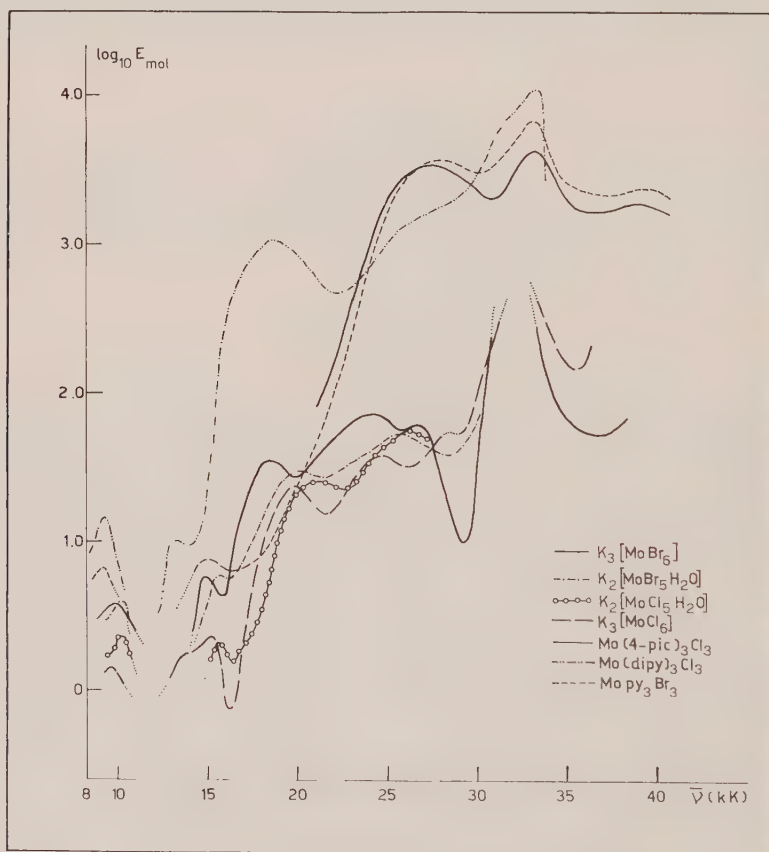
2.1. $[\text{MoX}_6]^{3-}$, $[\text{MoX}_5(\text{H}_2\text{O})]^{2-}$ ($X = \text{Cl}, \text{Br}, \text{I}$)

The absorption spectrum of K_3MoCl_6 had been measured by Hartmann and Schmidt [3], and its assignment confirmed by Jørgensen [2]; on re-measuring this spectrum we have found maximum frequencies slightly different from previous literature reports [3]. Observed bands occur at the same frequencies as in the reflection spectrum of the solid salt, and can therefore be attributed to the pure MoCl_6 chromophore, only in solutions containing $[\text{HCl}] \geq 9 \text{ M}$. With lower $[\text{HCl}]$, spin-allowed bands are shifted towards higher frequencies as a consequence of beginning aquation. Between $[\text{HCl}]$ 1 and 2 M a constant spectrum, attributable to $[\text{MoCl}_5(\text{H}_2\text{O})]^{2-}$ is observed. At about 31 kK (and occasionally also about 28 kK) a spurious band sometimes occurs, which is however absent from fresh solutions. According to the approximate formula by Jørgensen [4] $\bar{\nu}_{\pi \rightarrow \gamma_5} = 51 - 7q + 15$ for Cl, charge transfer $\text{Cl}^- \rightarrow \text{Mo}^{3+}$ should occur at about 45 kK, and $\text{Cl}^- \rightarrow \text{Mo}^{4+}$ at 37 kK. We then suppose that such spurious absorptions are due to charge transfers involving Mo^{4+} or, even more probably, Mo^{5+} . Actually, it is already well known that Mo(V) chloride [5, 6] and bromide [6] species have very intense charge transfer bands in the violet and near ultra-violet region; $[\text{MoOCl}_5]^-$ has been reported [6] to absorb at 28.0 and 32.2 kK, and could well be responsible for the observed spurious bands in $[\text{MoCl}_6]^{3-}$ solutions.

A similar behaviour has been observed of $[\text{MoBr}_6]^{3-}$ and $[\text{MoBr}_5(\text{H}_2\text{O})]^-$; differences from the chlorocompounds include a slight red shift of both spin-allowed and spin-forbidden $d \rightarrow d$ bands, in agreement with the relative position of Cl and Br in the spectrochemical and in the nephelauxetic series.

Identification of the second spin-allowed ligand field transition ${}^4A_{2g} \rightarrow {}^4T_{1g}$ is rather uncertain because of overlapping strong absorptions due to $[\text{MoOBr}_5]^-$ impurities, which are almost unavoidably present (reported at 24.1 and 26.5 kK in reference [6]). The figure 23.2 kK quoted in table 1 and the β_{35} value of table 2 are taken from the reflectance spectrum of the solid; in solution the apparent band maximum is around 24.1 kK.

Attempts to prepare solid Mo(III) hexaiodide complexes, analogously to K_3MoCl_6 and K_3MoBr_6 , proved unsuccessful; however, on dissolving solid K_3MoBr_6 in conc. HI, a deep red solution is obtained, whose spectrum is consistent with expectations for a hexaiodide Mo(III) species, since it exhibits a more pronounced nephelauxetic decrease of β_{55} and β_{35} , and a smaller Δ than $[\text{MoBr}_6]^{3-}$. Such spectrum is also reported in table 1 and tentatively assigned to $[\text{MoI}_6]^{3-}$.



Absorption spectra of some Mo(III) complexes.

2.2. Oxalato-complexes

Solutions prepared by dissolving K_3MoCl_6 in aqueous ammonium oxalate take at first a yellow colour, turning later to red; in such solutions, where we assume presence of oxalato-complexes of Mo(III), although unstable, only the first spin-allowed band is clearly identifiable at ~ 25 kK, and this is in agreement with the position of oxygen ligands after halogens in the spectrochemical series.

2.3. Mo(III)-ethylenediamine and Mo(III)-EDTA

Here too we assumed formation of Mo(III)-ethylenediamine[†] or Mo(III)-EDTA complexes in aqueous solutions prepared from K_3MoCl_6 in 50 per cent en (pH ~ 9), respectively 0.1 M disodium EDTA (pH ~ 6). In both cases yellow solutions are obtained (deeper yellow with en), where molybdenum retains its tervalent state, as we demonstrated polarographically by the absence of any reduction waves before the Mo(III) step; such solutions exhibit only one well-developed band, at about 25 kK for EDTA or 30 kK for en complexes. In agreement with the position of the ligands in the spectrochemical series, we assign this band to $^4A_{2g} \rightarrow ^4T_{2g}$. The spin-forbidden transition around 15 kK is remarkably intense.

2.4. Mo(III)-dipy and Mo(III)-ophen

From the reaction of K_3MoCl_6 with these ligands according to reference [7], we failed to prepare previously claimed [7] $Mo(dipy)_3Cl_3$ and $Mo(ophen)_3Cl_3$, and obtained instead $dipyH[Mo(dipy)Cl_4]$ and $ophenH[Mo(ophen)Cl_4]$ (brown solids; 1:1 electrolytes in nitromethane; Cl found, 25.6 per cent (calcd. for $C_{20}H_{17}N_2Cl_4Mo$, 25.7 per cent) and 23.9 per cent (calcd. for $C_{24}H_{17}N_2Cl_4Mo$, 23.7 per cent).

The only ligand field bands observed of the above complexes are the spin-forbidden ones (8.8 and 13.7 kK for the dipy complex), with a nephelauxetic ratio β_{55} even smaller than in the halocomplexes, probably due to strong delocalization of t_{2g} electrons and conjugation with π orbitals of the ligands. The rather intense, characteristic band around 19 kK occurs at too low frequencies for a $d \rightarrow d$ spin-allowed transition, so we assign it to a charge transfer $Mo \rightarrow dipy$, analogous to the well-known iridium band [8]. The ctf band at 19 kK in Mo(III) lies at about 30–32 kK in Ir(III); this difference of about 13 kK, after correction for interelectronic repulsions, points to an electronegativity difference of 0.4 units, in tolerable agreement with the difference reported by Jørgensen [8] between Mo(III) (1.7) and Ir(III) (2.25).

A broad band between 23 and 27 kK corresponds probably to another ctf to dipy, since again this frequency would be too low for the first spin-allowed $d \rightarrow d$ band. Besides that, very intense absorptions occur at ~33 kK (with structure) and 41 kK (internal dipy transitions). The first $d \rightarrow d$ spin-allowed band is probably masked by the above-discussed absorption at ~33 kK.

2.5. MoX_3L_3 ($X = Cl, Br$; $L = py(9), 4\text{-picoline}$)

Again, the only $d \rightarrow d$ bands observed are the spin-forbidden ones, at frequencies not far from those of the halocomplexes. Two rather intense bands (sometimes with structure) are observed at 26–27 and ~34 kK. These frequencies are too low for a ctf $Cl \rightarrow Mo$ (see discussion for $[MoX_6]^{3-}$), so that they should be due to ctf $Mo \rightarrow L$, and possibly mask spin-allowed $d \rightarrow d$ transitions. We are inclined to assign the band at 26–27 kK mainly to $^4A_{2g} \rightarrow ^4T_{2g}$, intensified by intermixing with a state of ctf to py. Above 38 kK, internal transitions of the pyridines occur, slightly shifted with respect to the free molecules, as already observed by other authors [10].

[†] Also formation of polynuclear Mo(III)-en species might here partially occur.

Complex	Chromophore	Prep.	ν_{\max} (kK)	$\log E_{\text{mol}}$	Assignment
K_3MoCl_6 (in 9 M HCl)	Mo(III)Cl_6	[13]	9.5 14.8 19.4 24.2 28.0 32.2	0.14 0.31 1.37 1.58 var. var. }	${}^4A_{2g} \rightarrow {}^2E_g, {}^2T_{1g}$ $\rightarrow {}^2T_{2g}$ $\rightarrow {}^4T_{2g}$ $\rightarrow a^4T_{1g}$ ctf Mo(IV) or Mo(V)
$\text{K}_2\text{MoCl}_5 \cdot \text{H}_2\text{O}$ (in 1 M HCl)	$\text{Mo(III)Cl}_5\text{O}$	[13]	9.8 15.2 21.0 25.8	0.36 0.32 1.40 1.74	${}^4A_{2g} \rightarrow {}^2E_g, {}^2T_{1g}$ $\rightarrow {}^2T_{2g}$ $\rightarrow {}^4T_{2g}$ $\rightarrow a^4T_{1g}$
K_3MoBr_6 (in 8.8 M HBr)	Mo(III)Br_6	[14]	9.5 14.5 18.3 23.2(†) 26.4 30.8	0.59 0.74 1.52 — var. var. }	${}^4A_{2g} \rightarrow {}^2E_g, {}^2T_{1g}$ $\rightarrow {}^2T_{2g}$ $\rightarrow {}^4T_{2g}$ $\rightarrow a^4T_{1g}$ ctf Mo(IV) or Mo(V)
$\text{K}_2\text{MoBr}_5 \cdot \text{H}_2\text{O}$ (in 1 M HBr)	$\text{Mo(III)Br}_5\text{O}$	[14]	9.8 ₅ 15.3 19.7 25.5	0.60 0.79 1.46 1.71	${}^4A_{2g} \rightarrow {}^2E_g, {}^2T_{1g}$ $\rightarrow {}^2T_{2g}$ $\rightarrow {}^4T_{2g}$ $\rightarrow a^4T_{1g}$
Mo(III)—I^- (from K_3MoBr_6 in 57 per cent aq. HI)	probably Mo(III)I_6	—	9.2 13.8 16.6 ₅ 20.0 ₅	— — — —	${}^4A_{2g} \rightarrow {}^2E_g, {}^2T_{1g}$ $\rightarrow {}^2T_{2g}$ $\rightarrow {}^4T_{2g}$ $\rightarrow a^4T_{1g}$
Mo(III) oxalate (from K_3MoCl_6 in 5 per cent $(\text{NH}_4)_2\text{C}_2\text{O}_4$)	Mo(III)O_6	—	16.6 18.4 ~ 27 sh.	— — ~ 2.2 }	${}^4A_{2g} \rightarrow {}^2T_{2g}$ $\rightarrow {}^4T_{2g}$
Mo(III)—en (from K_3MoCl_6 in 50 per cent aq. en)	Mo(III)N_6	—	(13.0) 20.8 sh. 30.2	— — ~ 2.4	${}^4A_{2g} \rightarrow {}^2T_{2g}(?)$ — ${}^4A_{2g} \rightarrow {}^4T_{2g}$
Mo(III)—EDTA (from K_3MoCl_6 in 0.1 M EDTA)	$\text{Mo(III)N}_2\text{O}_4$	—	15.4 20.6 sh. 24.8	— — ~ 2.3	${}^4A_{2g} \rightarrow {}^2T_{2g}$ — ${}^4A_{2g} \rightarrow {}^4T_{2g}$
$[\text{ModipyCl}_4]^-$ (in nitro- methane)	$\text{Mo(III)N}_2\text{Cl}_4$	[7]	8.8 13.7 18.2 ~ 25 sh. 33.0	— 0.98 3.03 — 3.77	${}^4A_{2g} \rightarrow {}^2E_g, {}^2T_{1g}$ $\rightarrow {}^2T_{2g}$ ctf dipy ctf dipy dipy
$[\text{Mo(ophen)Cl}_4]^-$ (in nitro- methane)	$\text{Mo(III)N}_2\text{Cl}_4$	[7]	9.3 13.5 18.9 22.2 sh. 26.3	0.82 0.96 3.15 — 3.10	${}^4A_{2g} \rightarrow {}^2E_g, {}^2T_{1g}$ $\rightarrow {}^2T_{2g}$ ctf opphen — ctf opphen

Complex	Chromophore	Prep.	$\bar{\nu}_{\max}$ (kk)	$\log E_{\text{mol}}$	Assignment
Mopy ₃ Cl ₃ (in CHCl ₃)	Mo(III)N ₃ Cl ₃	[9]	8.8 14.5 27.2 33.6 39.6	0.85 0.85 3.47 3.41 4.19	$^4A_{2g} \rightarrow ^2E_g, ^2T_{1g}$ $\rightarrow ^2T_{2g}$ ctf py + $^4A_{2g} \rightarrow ^4T_{2g}$ ctf py py
Mopy ₃ Br ₃ (in pyridine)	Mo(III)N ₃ Br ₃	[9]	8.8 14.7 27.2 32.7 39.3	0.81 0.88 3.58 3.85 3.19	$^4A_{2g} \rightarrow ^2E_g, ^2T_{1g}$ $\rightarrow ^2T_{2g}$ ctf py + $^4A_{2g} \rightarrow ^4T_{2g}$ ctf py py
Mo(4-pic) ₃ Cl ₃ (in CHCl ₃)	Mo(III)N ₃ Cl ₃	Present work	8.8 (~13) 27.0 33.0 38.4	— — 3.57 3.68 3.27	$^4A_{2g} \rightarrow ^2E_g, ^2T_{1g}$ $\rightarrow ^2T_{2g}$ ctf 4-pic + $^4A_{2g} \rightarrow ^4T_{2g}$ ctf 4-pic 4-pic
Mo(4-pic) ₃ Br ₃ (in CHCl ₃)	Mo(III)N ₃ Br ₃	Present work	8.8 14.5 27.6 35.8 39.3	0.75 1.10 3.42 4.16 4.21	$^4A_{2g} \rightarrow ^2E_g, ^2T_{1g}$ $\rightarrow T_{2g}$ ctf 4-pic + $^4A_{2g} \rightarrow ^4T_{2g}$ ctf 4-pic 4-pic

† Reflectance spectrum of solid K₃MoBr₆.

Table 1. Absorption spectra of Mo(III) complexes.

Complex	Chromophore	Δ	β_{55}	β_{35}
K ₃ MoCl ₆	Mo(III)Cl ₆	19.4	0.78	0.70
K ₂ MoCl ₅ · H ₂ O	Mo(III)Cl ₅ O	21.0	0.80	0.71
K ₂ MoBr ₆	Mo(III)Br ₆	18.3	0.77	0.70
K ₂ MoBr ₅ · H ₂ O	Mo(III)Br ₅ O	19.7	0.80	—
Mo(III)—I ⁻	Mo(III)I ₆	16.6 ₅	0.74	0.58
[Mo(NCS) ₆] ³⁻	Mo(III)N ₆ †	> 24	0.52	—
Mo(III)—C ₂ O ₄ ⁼	Mo(III)O ₆	≥ 27	0.84	—
Mo(III)—en	Mo(III)N ₆	≥ 30	(0.68)	—
Mo(III)—EDTA	Mo(III)N ₂ O ₄	~ 25	0.79	—
[ModipyCl ₄] ⁻	Mo(III)N ₂ Cl ₄	(≥ 33)	0.72	—
[Mo(ophen)Cl ₄] ⁻	Mo(III)N ₂ Cl ₄	(≥ 33)	0.72	—
Mopy ₃ Cl ₃	Mo(III)N ₃ Cl ₃	(≥ 27)	0.73	—
Mopy ₃ Br ₃	Mo(III)N ₃ Br ₃	(≥ 27)	0.74	—
Mo(4-pic) ₃ Cl ₃	Mo(III)N ₃ Cl ₃	(≥ 27)	0.68	—
Mo(4-pic) ₃ Br ₃	Mo(III)N ₃ Br ₃	(≥ 28)	0.70	—

† See reference [16].

Table 2. Ligand field parameters of Mo(III) complexes (in kk). B for gaseous Mo(III) has been assumed to be 0.61 kk (reference [6], p. 137).

Comparison with the spectrum of Crpy_3Cl_3 [10] shows again a band about 34 kK. The Cr compound exhibits distinctly the two spin-allowed transitions ${}^4A_{2g} \rightarrow {}^4T_{2g}$ at 15.9 and ${}^4A_{2g} \rightarrow {}^4T_{1g}$ at 22.2 kK, while the Mo compounds have an additional band at 26–27 kK. Previous assignments [10, 11] of MoPy_3Cl_3 included ${}^4A_{2g} \rightarrow {}^4T_{2g}$ at 15 or 16 kK, ctf from Cl at 26 kK and ctf to py at 34 kK; while we agree on the assignment of the 34 kK band, we do not think that the band at 16 kK is spin-allowed, on the ground of both its low intensity and a comparison with the spin-forbidden absorptions in other Mo(III) complexes; besides that, a different assignment would imply a too low value of Δ . The band at 26–27 kK cannot be due to ctf from the halogen for the same reasons already discussed for $[\text{MoX}_6]^{3-}$; besides, its position does not vary appreciably between chloro- and bromo-complexes, whereas replacement of Cl through Br would shift a ctf band some 6 kK to the red.

3. DISCUSSION

The spectra reported here for several Mo(III) complexes can to a good extent be satisfactorily interpreted by ligand field theory, thus confirming substantial similarity in behaviour of the $(nd)^3$ configurations in Cr(III) and in Mo(III) . Differences are rather quantitative than qualitative in nature; besides the already known ones ($\Delta_{\text{Mo}^{3+}} > \Delta_{\text{Cr}^{3+}}$; $\beta_{\text{Mo}^{3+}} < \beta_{\text{Cr}^{3+}}$; therefore, and also because $F_{\text{Mo}^{3+}}^k < F_{\text{Cr}^{3+}}^k$, both spin-forbidden transitions within t_{2g}^3 of Mo^{3+} occur at lower frequencies than the first spin-allowed band, whereas ${}^4A_{2g} \rightarrow {}^4T_{2g}$ of Cr^{3+} lies usually between the two spin-forbidden bands), with Mo(III) complexes charge transfer bands are of much more frequent occurrence, particularly with ligands like py, dipy, acac; here, the low optical electronegativity of Mo(III) (1.7 against 1.8 of Cr(III)) enhances charge transfers to the ligands, and this tendency parallels the chemical fact that Mo^{3+} is more reducing than Cr^{3+} . On this ground we can distinguish between two types of Mo(III) complexes: the first one is with highly electronegative ligands (halogens, amines, oxalates) where not only the spin-forbidden, but also the two spin-allowed $d \rightarrow d$ bands (or at least the first one) can be observed, and therefore the ligand field parameters Δ , β_{55} and often also β_{35} can be determined. In the second type, namely with highly conjugated ligands of low electronegativity (pyridines, dipy, ophen, acac), the $d \rightarrow d$ spin-allowed bands are generally masked by intense ctf bands at relatively low frequencies; of the ligand field spectrum, only the spin-forbidden transitions which occur within t_{2g}^3 are observed, and the only ligand field parameter which can be determined directly is β_{55} . To the latter group belongs also Mo(acac)_3 [12].

Values of β_{55} in:

	X = Cl	Br	I
$[\text{MoX}_6]^{3-} (4d)^3$	0.78	0.77	0.74
$[\text{TcX}_6] (4d)^3$	0.65	0.62	0.59
$[\text{ReX}_6] (5d)^3$	0.68	0.64	0.62

Among the halocomplexes, both Δ and β_{55} decrease in the order $\text{Cl} > \text{Br} > \text{I}$; this matches exactly what has been recently reported [15] for $(\text{nd})^3$ of $[\text{TcX}_6]^-$ and $[\text{ReX}_6]^-$ ($\text{X} = \text{F}, \text{Cl}, \text{Br}, \text{I}$). A comparison of β_{55} data from reference [15] and from the present work shows that the trend is the same for Mo(III) as well as for Tc(IV) and Re(IV); absolute β_{55} values are somewhat higher for Mo(III) than for Tc(IV) and for Re(IV), probably as a result of lower optical electronegativity (and therefore covalency) in Mo(III) complexes, and of the lower oxidation state of the central metal ion in molybdenum complexes.

REFERENCES

- [1] HARTMANN, H., and SCHMIDT, H. J., 1957, *Z. phys. Chem.*, **11**, 234.
- [2] JØRGENSEN, C. K., 1962 a, *Absorption Spectra and Chemical Bonding in Complexes* (London: Pergamon Press), p. 291; 1962 b, *Inorganic Complexes* (London: Academic Press).
- [3] MITCHELL, P. C., and WILLIAMS, R. J. P., 1962, *J. chem. Soc.*, p. 4570.
- [4] JØRGENSEN, C. K., 1962, *Absorption Spectra and Chemical Bonding in Complexes* (London: Pergamon Press), p. 154.
- [5] JØRGENSEN, C. K., 1957, *Acta chem. scand.*, **11**, 73.
- [6] EDWARDS, D. A., and FOWLES, G. W. A., 1962, Proc. 7th Int. Conf. Coord. Chem. Stockholm, Abstract 1F8.
- [7] STEELE, M. C., 1957, *Aust. J. Chem.*, **10**, 489.
- [8] JØRGENSEN, C. K., 1957, *Acta chem. scand.*, **11**, 151 and 166.
- [9] ROSENHEIM, A., ABEL, G., and LEWY, R., 1931, *Z. anorg. Chem.*, **197**, 200.
- [10] KÖNIG, E., and SCHLÄFER, H. L., 1960, *Z. phys. Chem.*, **26**, 371.
- [11] KÖNIG, E., 1963, *Naturwissenschaften*, **50**, 641.
- [12] CHRIST, K., and SCHLÄFER, H. L., 1963, *Angew. Chem.*, **75**, 137.
- [13] IRVING, R. J., and STEELE, M. C., 1957, *Aust. J. Chem.*, **10**, 490.
- [14] WARDLAW, W., and HARDING, A. J. I., 1926, *J. chem. Soc.*, p. 1592.
- [15] JØRGENSEN, C. K., and SCHWOCHAU, K., 1965, *Z. Naturf. A* (in the press).
- [16] LEWIS, J., NYHOLM, R. S., and SMITH, P. W., 1961, *J. chem. Soc.*, p. 4590.

The long-range interaction of atoms and molecules

by Y. M. CHAN† and A. DALGARNO

Department of Applied Mathematics, The Queen's University of Belfast

(Received 26 January 1965)

The long-range interaction between atomic systems is expressed in terms of multipole frequency-dependent polarizabilities of the separate systems and a variational procedure is set up for calculating them. Application is made to a pair of hydrogen atoms with the result that the interaction at a large separation R is given in rydbergs by:

$$-\frac{12.9981}{R^6} - \frac{248.8}{R^8} - \frac{6571}{R^{10}} + O(1/R^{11}),$$

correct to the figures shown. The R^{-6} coefficient agrees with that of Hirschfelder and Löwdin and the R^{-8} coefficient agrees with the calculation of Pauling and Beach. The R^{-10} coefficient is much larger than that obtained by Pauling and Beach who included only the quadrupole-quadrupole contribution.

1. INTRODUCTION

The calculation of the long-range interactions between atoms is an application of perturbation theory for the case when the perturbation may be written as a sum of products, each factor of which refers to a single atom. By making use of the identity

$$\frac{1}{a+b} = \frac{2}{\pi} \int_0^\infty \frac{ab}{(a^2+w^2)(b^2+w^2)} dw \quad (1)$$

(Landau and Lifschitz [1]), it is possible to reduce the original many-centre problem to a number of single centre problems. A formal expression has been derived by Mavroyannis and Stephen [2] and by McLachlan [3] which relates the leading term of the long-range interaction of a pair of atoms to the electric dipole atomic polarizabilities, evaluated at imaginary frequencies, and it is clear that similar expressions describe the higher terms of the series expansion of the interaction. Since methods are available for the calculation of frequency-dependent polarizabilities (cf. Karplus and Kolker [4], Chan and Dalgarno [5],) a new scheme is established for the prediction of long-range forces.

2. LONG-RANGE INTERACTION BETWEEN ATOMS AND MOLECULES

The electrostatic interaction energy of a charge distribution consisting of charges e_i at positions \mathbf{r}_i , measured from its centre of charge, and a second non-overlapping charge distribution of charges e_j at positions \mathbf{r}_j , measured from its

† Commonwealth Scholar. Now at Physics Department, University of Malaya, Malaya.

centre of charge, is given by

$$V(\mathbf{r}, \boldsymbol{\rho}) = \sum_i \sum_j \sum_{m, n, \alpha} \frac{(-)^n 4\pi e_i e_j (m+n)! \delta_{\alpha, -\beta}}{R^{m+n+1} [(2m+1)(2n+1)(m-\alpha)!(m+\alpha)!(n-\alpha)!(n+\alpha)!]^{1/2}} \times \mathcal{Y}_m^\alpha(\mathbf{r}_i) \mathcal{Y}_n^\beta(\mathbf{r}_j) \quad (2)$$

(Rose [6], Fontana [7]) where $\mathcal{Y}_m^\alpha(\mathbf{r})$ is the regular solid spherical harmonic:

$$\mathcal{Y}_m^\alpha(\mathbf{r}) = r^m Y_m^\alpha(\mathbf{r}) \quad (3)$$

and R is the distance between the centres of charge.

Let H_a and H_b be the Hamiltonians of a pair of atoms an infinite distance apart described respectively by eigenfunctions $\psi_0^a(\mathbf{r})$ and $\phi_0^b(\boldsymbol{\rho})$. Then the interaction energy is given correct to second order in $V(\mathbf{r}, \boldsymbol{\rho})$ by:

$$E(R) = \langle \psi_0^a \phi_0^b | V | \psi_0^a \phi_0^b \rangle - \mathbf{S}_s \mathbf{S}_t \frac{|\langle \psi_0^a \phi_0^b | V | \psi_s^a \phi_t^b \rangle|^2}{(E_s^a + E_t^b - E_0^a - E_0^b)}, \quad (4)$$

where ψ_s^a and E_s^a are the eigenfunctions and eigenvalues of H_a and ϕ_t^b and E_t^b are the eigenfunctions and eigenvalues of H_b . The evaluation of the first-order term is trivial. The second-order term may be written, using (1), as:

$$E_2(R) = \frac{-2}{\pi} \mathbf{S}_s \mathbf{S}_t \int_0^\infty \frac{(E_s^a - E_0^a)(E_t^b - E_0^b) |\langle \psi_0^a \phi_0^b | V | \psi_s^a \phi_t^b \rangle|^2}{\{(E_s^a - E_0^a)^2 + \omega^2\} \{(E_t^b - E_0^b)^2 + \omega^2\}} d\omega. \quad (5)$$

Substituting (2), (5) may be simplified to:

$$E_2(R) = \frac{-2}{\pi} \cdot 16\pi^2 e^4 \sum_{m, n, \alpha} \frac{\{(m+n)!\}^2 \delta_{\alpha, -\beta}}{R^{2(m+n+1)} (2m+1)(2n+1)(m-\alpha)!(m+\alpha)!(n-\alpha)!(n+\alpha)!} \times \int_0^\infty A_m^\alpha(\omega) B_n^\beta(\omega) d\omega, \quad (6)$$

where

$$A_m^\alpha(\omega) = \mathbf{S}_s \frac{(E_s^a - E_0^a) |\langle \psi_0^a | \sum_i \mathcal{Y}_m^\alpha(\mathbf{r}_i) | \psi_s^a \rangle|^2}{(E_s^a - E_0^a)^2 + \omega^2} \quad (7)$$

with a similar expression for $B_n^\beta(\omega)$. Replacing ω in (7) by iu yields

$$A_m^\alpha(iu) = \mathbf{S}_s \frac{(E_s^a - E_0^a) |\langle \psi_0^a | \sum_i \mathcal{Y}_m^\alpha(\mathbf{r}_i) | \psi_s^a \rangle|^2}{(E_s^a - E_0^a)^2 - u^2}, \quad (8)$$

which is, apart from an external factor, the 2^m -pole dynamic polarizability at the frequency u .

Expression (8) can be evaluated by writing it in the form:

$$A_m^\alpha(iu) = \frac{1}{2} \mathbf{S}_s \frac{|\langle \psi_0^a | \sum_i \mathcal{Y}_m^\alpha(\mathbf{r}_i) | \psi_s^a \rangle|^2}{(E_s^a - E_0^a) + u} + \frac{1}{2} \mathbf{S}_s \frac{|\langle \psi_0^a | \sum_i \mathcal{Y}_m^\alpha(\mathbf{r}_i) | \psi_s^a \rangle|^2}{(E_s^a - E_0^a) - u} \quad (9)$$

and using a familiar sum rule (cf. Dalgarno [8]) to give:

$$A_m^\alpha(iu) = -\frac{1}{2} \left\langle \psi_0^a \left| \sum_i \mathcal{Y}_m^\alpha \right| (\chi(+)) + \chi(-) \right\rangle, \quad (10)$$

where

$$(H_a - E_0^a \pm u) \chi(\pm) + \left\{ \sum_i \mathcal{Y}_m^\alpha - \left\langle \psi_0^a \left| \sum_i \mathcal{Y}_m^\alpha \right| \psi_0^a \right\rangle \right\} \psi_0^a = 0. \quad (11)$$

Mavroyannis and Stephen [2] have, in effect, suggested that (11) be solved by a variational method and that (7) be evaluated by replacing u in (10) by $i\omega$.

The procedure presents difficulties in practice since it requires that (10) be obtained as an analytical function of ω but Karplus and Kolker [9] have applied the method with success to the calculation of some R^{-6} coefficients in the uncoupled Hartree-Fock approximation.

We have used a more direct attack on (7) which avoids the requirement that the χ functions be obtained as analytical functions of u or ω . We introduce the function $\Psi_m^\alpha(\omega)$ which is the well-behaved solution of the equation:

$$\{(H^a - E_0^a)^2 + \omega^2\} \Psi_m^\alpha(\omega) + \{\mathcal{Y}_m^\alpha - \langle \psi_0^a | \mathcal{Y}_m^\alpha | \psi_0^a \rangle\} \psi_0^a = \omega^2 \langle \Psi_m^\alpha | \psi_0^a \rangle \psi_0^a \quad (12)$$

(cf. Hirschfelder *et al.* [10]).

Then noting that

$$(E_s^a - E_0^a) \langle \psi_s^a | \mathcal{Y}_m^\alpha | \psi_0^a \rangle = \langle \psi_s^a | \nabla \mathcal{Y}_m^\alpha \cdot \nabla | \psi_0^a \rangle, \quad (13)$$

it follows that

$$A_m^\alpha(\omega) = \langle \Psi_m^\alpha | \nabla \mathcal{Y}_m^\alpha \cdot \nabla | \psi_0^a \rangle. \quad (14)$$

Alternatively,

$$A_m^\alpha(\omega) = \langle \Psi_m^{\alpha'} | \mathcal{Y}_m^\alpha | \psi_0^a \rangle, \quad (15)$$

where

$$\begin{aligned} \{(H_a - E_0^a)^2 + \omega^2\} \Psi_m^{\alpha'} + \{\nabla \mathcal{Y}_m^\alpha \cdot \nabla - \langle \psi_0^a | \nabla \mathcal{Y}_m^\alpha \cdot \nabla | \psi_0^a \rangle\} \psi_0^a \\ = \omega^2 \langle \Psi_m^{\alpha'} | \psi_0^a \rangle \psi_0^a, \end{aligned} \quad (16)$$

this scheme having the advantage that the third-order contributions to $E(R)$ can also be expressed in terms of $\Psi_m^{\alpha'}$.

Equations (12) and (16) can be solved by variational procedures. Thus for equation (12) we minimize:

$$\begin{aligned} J(\omega) = \langle \Psi_m^\alpha | (H_a - E_0)^2 + \omega^2 | \Psi_m^\alpha \rangle - \omega^2 |\langle \Psi_m^\alpha, \psi_0^a \rangle|^2 \\ + 2 \langle \Psi_m^\alpha | \mathcal{Y}_m^\alpha - \langle \psi_0^a | \mathcal{Y}_m^\alpha | \psi_0^a \rangle | \psi_0^a \rangle \end{aligned} \quad (17)$$

with respect to a trial form of Ψ_m^α .

The theory we have presented applies generally to atoms and molecules. Some simplification results for atoms in S states since the polarizabilities are independent of the direction of the perturbing field and A_m^α can be written as $A_m(\omega) = A_m^0(\omega)$. Then

$$\begin{aligned} E_2(R) = -\frac{2}{\pi} \cdot 16\pi^2 e^4 \sum_{m,n} \frac{\{(m+n)!\}^2}{R^{2(m+n+1)}} \frac{1}{(2m+1)(2n+1)} \\ \times \int_0^\infty A_m(\omega) B_n(\omega) d\omega \sum_{\alpha=-m,n}^{\alpha=+m,n} \frac{1}{(m-\alpha)!(m+\alpha)!(n-\alpha)!(n+\alpha)!}, \end{aligned} \quad (18)$$

where m, n is the lesser of m and n . The leading terms are given by:

$$\begin{aligned} E_2(R) = -\frac{2}{\pi} \cdot 16\pi^2 e^4 \left\{ \frac{2}{3R^6} \int_0^\infty A_1(\omega) B_1(\omega) d\omega \right. \\ + \frac{1}{R^8} \int_0^\infty \{A_1(\omega) B_2(\omega) + A_2(\omega) B_1(\omega)\} d\omega \\ + \frac{4}{5R^{10}} \int_0^\infty \{A_1(\omega) B_3(\omega) + A_3(\omega) B_1(\omega)\} d\omega \\ \left. + \frac{14}{5R^{10}} \int_0^\infty A_2(\omega) B_2(\omega) d\omega + O(R^{-12}) \right\}. \end{aligned} \quad (19)$$

3. LONG-RANGE INTERACTION OF TWO HYDROGEN ATOMS

We have calculated $A_1(\omega)$, $A_2(\omega)$ and $A_3(\omega)$ for a hydrogen atom in its ground state by minimizing (17) with respect to the trial function:

$$\Psi_m(\mathbf{r}) = \sum_{p=0}^3 a_p r^p \mathcal{Y}_m^0(\mathbf{r}) \psi_0^a(r). \quad (20)$$

Machine limitations restricted us to four terms in (20), but this was sufficient to ensure accuracy to six significant figures for $A_1(\omega)$ and to four significant figures for $A_2(\omega)$ and $A_3(\omega)$. The trial function (20) is sufficiently flexible to yield Ψ_m exactly both for zero and for infinite values of ω , where (12) can be solved in terms of elementary functions. Thus

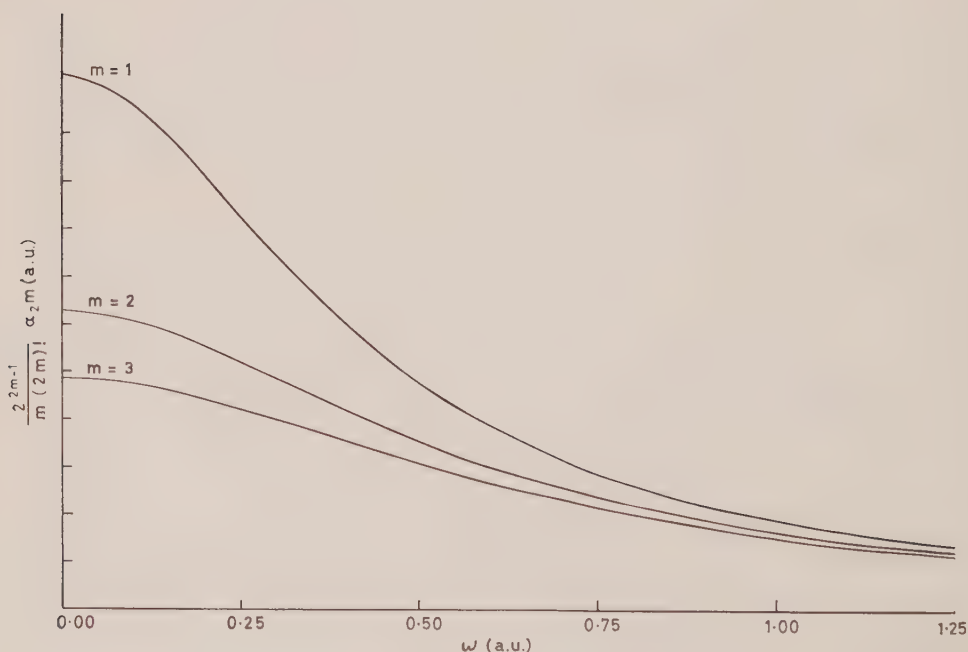
$$\Psi_1^a(\omega=0) = \frac{1}{12} (2r^2 + 11r + 22) \mathcal{Y}_1^0(\mathbf{r}) \psi_0^a, \quad (21)$$

$$\Psi_2^a(\omega=0) = \frac{1}{36} (6r^2 + 26r + 39) \mathcal{Y}_2^0(\mathbf{r}) \psi_0^a, \quad (22)$$

$$\Psi_3^a(\omega=0) = \frac{1}{1440} (36r^2 + 141r + 188) \mathcal{Y}_3^0(\mathbf{r}) \psi_0^a, \quad (23)$$

and

$$\Psi_m^a(\omega=0) \sim -\frac{1}{\omega^2} \mathcal{Y}_m^0(\mathbf{r}) \psi_0^a. \quad (24)$$



The dipole, quadrupole and octupole polarizabilities of atomic hydrogen at imaginary frequencies $i\omega$.

The dipole, quadrupole and octupole polarizabilities at imaginary frequencies ω are illustrated in the figure, the scales being chosen so that they all behave asymptotically as $1/\omega^2$. The actual limiting values of the polarizabilities are in atomic units:

$$\alpha_{2m}(\omega=0) = \frac{8\pi}{(2m+1)} A_m(\omega=0) = \frac{(2m+2)!(m+2)}{2^{2m+1}m(m+1)} \quad (25)$$

(cf. Dalgarno [11]) and

$$\alpha_{2m}(\omega=\infty) = \frac{8\pi}{2m+1} A_m(\omega=\infty) = \frac{m(2m)!}{2^{2m-1}\omega^2}. \quad (26)$$

Carrying out the numerical integrations in (19), we find that $E_2(R)$ is given in rydbergs by:

$$E_2(R) = -\frac{12.9981}{R^6} - \frac{248.8}{R^8} - \frac{(2270+4301)}{R^{10}} + O(R^{-12}), \quad (27)$$

correct to the figures shown. From a direct variational approach to the two-centre problem, Pauling and Beach [12] obtained:

$$E_2(R) = -\frac{12.99806}{R^6} - \frac{248.798}{R^8} - \frac{2270.42}{R^{10}} \quad (28)$$

and Hirschfelder and Löwdin [12] obtained:

$$E_2(R) = -\frac{12.998052}{R^6} - \frac{289.6994}{R^8} \dagger. \quad (29)$$

Our R^{-6} coefficient agrees with that of Hirschfelder and Löwdin but our R^{-8} coefficient does not. However, our R^{-8} coefficient does agree with the earlier calculations of Pauling and Beach. Our value for the quadrupole-quadrupole contribution to the R^{-10} coefficient agrees with the calculation of Pauling and Beach, who overlooked the larger dipole-octupole contribution (cf. Dalgarno and Lewis [14]).

A referee has suggested that the wave functions and polarizabilities may be useful in other connections. They are tabulated in the Appendix.

The research reported has been sponsored by Cambridge Research Laboratories OAR through the European Office, Aerospace Research, United States Air Force, under Grant No. AF 61 (052)-780. It has in addition been partly supported by the Atomic Energy Research Establishment, Harwell.

REFERENCES

- [1] LANDAU, L. D., and LIFSHITZ, E. M. 1958, *Statistical Physics* (London: Pergamon Press); 1960, *Electrodynamics of Continuous Media* (London: Pergamon Press).
- [2] MAVROYANNIS, C., and STEPHEN, M. J., 1962, *Mol. Phys.*, **5**, 629.
- [3] McLACHLAN, A. D., 1962, *Proc. roy. Soc. A*, **271**, 387.
- [4] KARPLUS, M., and KOLKER, H. J., 1963, *J. chem. Phys.*, **39**, 2997.
- [5] CHAN, Y. M., and DALGARNO, A., 1965, *Proc. phys. Soc., Lond.*, **85**, 1455.
- [6] ROSE, M. E., 1958, *J. Math. Phys.*, **37**, 215.
- [7] FONTANA, P. R., 1961, *Phys. Rev.*, **123**, 1865.

† Professor Hirschfelder (private communication) has discovered an error in this work. The corrected value for the R^{-8} coefficient is 248.790, in harmony with our result.

- [8] DALGARNO, A., 1962, *Quantum Theory*, Vol. 1, Ed. D. R. Bates (London: Academic Press).
- [9] KARPLUS, M. and KOLKER, H. J., 1964, *J. chem. Phys.*, **41**, 3955.
- [10] HIRSCHFELDER, J. O., BROWN, W. B., and EPSTEIN, S. T. 1964, *Advances in Quantum Chemistry*, Vol. 1 (New York: Academic Press).
- [11] DALGARNO, A., 1962, *Advanc. Phys.*, **11**, 281.
- [12] PAULING, L., and BEACH, J. Y., 1935, *Phys. Rev.*, **47**, 686.
- [13] HIRSCHFELDER, J. O., and LÖWDIN, P. O., 1959, *Mol. Phys.*, **2**, 229.
- [14] DALGARNO, A., and LEWIS, J. T., 1956, *Proc. phys. Soc., Lond. A*, **69**, 57.

APPENDIX

ω (A.U)	$a_0(\omega)$	$a_1(\omega)$	$a_2(\omega)$	$a_3(\omega)$	$\alpha_2(\omega)$
0	1.833(0)	9.167(-1)	1.667(-1)	0.000(0)	4.500(0)
0.1	1.746(0)	8.694(-1)	1.592(-1)	-2.055(-3)	4.250(0)
0.2	1.534(0)	7.604(-1)	1.374(-1)	-5.849(-3)	3.654(0)
0.3	1.285(0)	6.440(-1)	1.053(-1)	-8.025(-3)	2.978(0)
0.4	1.056(0)	5.460(-1)	7.049(-2)	-7.899(-3)	2.382(0)
0.5	8.665(-1)	4.686(-1)	3.955(-2)	-6.410(-3)	1.905(0)
0.6	7.163(-1)	4.068(-1)	1.531(-2)	-4.530(-3)	1.538(0)
0.7	5.984(-1)	3.561(-1)	-2.157(-3)	-2.788(-3)	1.258(0)
0.8	5.061(-1)	3.131(-1)	-1.381(-2)	-1.392(-3)	1.042(0)
0.9	4.332(-1)	2.760(-1)	-2.102(-2)	-3.613(-4)	8.747(-1)
1.0	3.751(-1)	2.438(-1)	-2.508(-2)	-3.603(-4)	7.427(-1)
1.2	2.897(-1)	1.911(-1)	-2.740(-2)	-1.139(-3)	5.520(-1)
1.4	2.313(-1)	1.510(-1)	-2.591(-2)	-1.397(-3)	4.247(-1)
1.6	1.901(-1)	1.198(-1)	-2.292(-2)	-1.392(-3)	3.360(-1)
1.8	1.596(-1)	9.582(-2)	-1.971(-2)	-1.283(-3)	2.720(-1)
2.0	1.365(-1)	7.720(-2)	-1.671(-2)	-1.136(-3)	2.244(-1)
2.5	9.767(-2)	4.652(-2)	-1.088(-2)	-7.865(-4)	1.481(-1)
3.0	7.404(-2)	2.921(-2)	-7.117(-3)	-5.307(-4)	1.048(-1)
3.5	5.828(-2)	1.903(-2)	-4.750(-3)	-3.604(-4)	7.800(-2)
4.0	4.711(-2)	1.283(-2)	-3.253(-3)	-2.496(-4)	6.025(-2)
4.5	3.889(-2)	8.889(-3)	-2.278(-3)	+1.760(-4)	4.791(-2)
5.0	3.262(-2)	6.317(-3)	-1.631(-3)	1.267(-4)	3.900(-2)
6.0	2.385(-2)	3.416(-3)	-8.919(-4)	6.981(-5)	2.727(-2)
7.0	1.815(-2)	1.983(-3)	-5.206(-4)	4.090(-5)	2.013(-2)
8.0	1.274(-2)	9.766(-4)	-2.577(-4)	2.031(-5)	1.546(-2)
9.0	1.035(-2)	6.457(-4)	-1.708(-4)	1.348(-5)	1.224(-2)
10.0	8.573(-3)	4.428(-4)	-1.173(-4)	9.273(-6)	9.929(-3)
11.0	7.210(-3)	3.147(-4)	-8.375(-5)	6.643(-6)	8.216(-3)
12.0	6.148(-3)	2.285(-4)	-6.087(-5)	4.831(-6)	6.910(-3)
25.0	1.311(-3)	1.047(-5)	-2.829(-6)	2.271(-7)	1.598(-4)
50.0	3.989(-4)	1.020(-6)	-2.868(-7)	2.38 (-8)	3.999(-4)

Table 1. Frequency dependent dipole polarizability and wave function†

† $1.833(t) \equiv 1.833 \times 10^t$.

ω (A.U.)	$a_0(\omega)$	$a_1(\omega)$	$a_2(\omega)$	$a_3(\omega)$	$\alpha_4(\omega)$
0	1.083(0)	7.222(-1)	1.667(-1)	0.000(0)	1.504(1)
0.1	1.063(0)	6.993(-1)	1.656(-1)	-1.476(-3)	1.452(1)
0.2	1.006(0)	6.479(-1)	1.586(-1)	-4.611(-3)	1.326(1)
0.3	9.134(-1)	6.004(-1)	1.388(-1)	-6.992(-3)	1.164(1)
0.4	8.027(-1)	5.683(-1)	1.083(-1)	-7.614(-3)	9.976(0)
0.5	6.916(-1)	5.466(-1)	7.405(-2)	-6.805(-3)	8.477(0)
0.6	5.908(-1)	5.276(-1)	4.201(-2)	-5.272(-3)	7.180(0)
0.7	5.053(-1)	4.990(-1)	1.575(-2)	-3.587(-3)	6.107(0)
0.8	4.366(-1)	4.795(-1)	-4.400(-3)	-2.097(-3)	5.222(0)
0.9	3.812(-1)	4.495(-1)	-1.847(-2)	-8.865(-4)	4.496(0)
1.0	3.381(-1)	4.168(-1)	-2.761(-2)	1.679(-5)	3.903(0)
1.2	2.792(-1)	3.478(-1)	-3.520(-2)	1.038(-3)	2.699(0)
1.4	2.381(-1)	2.872(-1)	-3.597(-2)	1.477(-3)	2.352(0)
1.6	2.106(-1)	2.337(-1)	-3.296(-2)	1.542(-3)	1.891(0)
1.8	1.901(-1)	1.893(-1)	-2.881(-2)	1.447(-3)	1.549(0)
2.0	1.740(-1)	1.533(-1)	-2.458(-2)	1.292(-3)	1.284(0)
2.5	1.421(-1)	9.197(-2)	-1.591(-2)	8.886(-4)	8.646(-1)
3.0	1.186(-1)	5.663(-2)	-1.018(-2)	5.849(-4)	6.173(-1)
3.5	9.881(-2)	3.630(-2)	-6.687(-3)	3.906(-4)	4.618(-1)
4.0	8.348(-2)	2.392(-2)	-4.480(-3)	2.650(-4)	3.607(-1)
4.5	7.064(-2)	1.646(-2)	-3.112(-3)	1.852(-4)	2.853(-1)
5.0	6.051(-2)	1.154(-2)	-2.200(-3)	1.317(-4)	2.327(-1)
6.0	4.552(-2)	6.000(-3)	-1.150(-3)	6.908(-5)	1.630(-1)
7.0	3.497(-2)	3.552(-3)	-6.886(-4)	4.169(-5)	1.204(-1)
8.0	2.780(-2)	2.089(-3)	-4.036(-4)	2.435(-5)	9.256(-2)
9.0	2.249(-2)	1.339(-3)	-2.592(-4)	1.566(-5)	7.332(-2)
10.0	1.848(-2)	9.369(-3)	-1.833(-4)	1.117(-5)	5.950(-2)
11.0	1.548(-2)	6.495(-3)	-1.272(-4)	7.750(-1)	4.924(-2)
12.0	1.313(-2)	4.664(-4)	-9.153(-5)	5.590(-6)	4.142(-2)
25.0	3.132(-3)	4.667(-5)	-9.835(-5)	6.343(-7)	9.585(-3)
50.0	7.965(-4)	2.294(-6)	-4.699(-7)	2.957(-8)	2.399(-3)

Table 2. Frequency dependent quadrupole polarizability and wave function.

ω (A.U.)	$a_0(\omega)$	$a_1(\omega)$	$a_2(\omega)$	$a_3(\omega)$	$\alpha_8(\omega)$
0	1.306(-1)	9.792(-2)	2.500(-2)	0.000(0)	1.313(2)
0.1	1.307(-1)	9.456(-2)	2.531(-2)	-1.821(-4)	1.280(2)
0.2	1.271(-1)	8.911(-2)	2.505(-2)	-5.622(-4)	1.193(2)
0.3	1.198(-1)	8.438(-2)	2.336(-2)	-9.080(-4)	1.075(2)
0.4	9.708(-2)	8.658(-2)	1.681(-2)	-1.012(-3)	9.468(1)
0.5	8.828(-2)	8.856(-2)	1.409(-2)	-9.528(-4)	8.251(1)
0.6	7.182(-2)	9.212(-2)	8.734(-3)	-7.628(-4)	7.139(1)
0.7	5.912(-2)	9.317(-2)	4.193(-3)	-5.483(-4)	6.184(1)
0.8	4.849(-2)	9.285(-2)	4.485(-4)	-3.362(-4)	5.369(1)
0.9	4.098(-2)	9.034(-2)	-2.289(-3)	-1.601(-4)	4.681(1)
1.0	3.367(-2)	8.776(-2)	-4.470(-3)	-5.530(-5)	4.101(1)
1.2	3.216(-2)	7.450(-2)	-5.851(-3)	1.332(-4)	3.197(1)
1.4	2.843(-2)	6.402(-2)	-6.428(-3)	2.178(-4)	2.543(1)
1.6	2.927(-2)	5.229(-2)	-5.887(-3)	2.253(-4)	2.062(1)
1.8	2.945(-2)	4.268(-2)	-5.193(-3)	2.137(-4)	1.700(1)
2.0	3.010(-2)	3.431(-2)	-4.383(-3)	+1.881(-4)	1.422(1)
2.5	2.795(-2)	2.078(-2)	-2.874(-3)	1.314(-4)	9.605(0)
3.0	2.563(-2)	1.251(-2)	-1.788(-3)	8.362(-5)	6.887(0)
3.5	2.204(-2)	8.179(-3)	-1.205(-3)	5.772(-5)	5.164(0)
4.0	1.968(-2)	5.057(-3)	-7.437(-4)	3.543(-5)	4.011(0)
4.5	1.667(-2)	3.613(-3)	-5.443(-4)	2.646(-4)	3.200(0)
5.0	1.445(-2)	2.529(-3)	-3.839(-4)	1.876(-5)	2.611(0)
6.0	1.104(-2)	1.312(-3)	-2.004(-4)	9.829(-6)	1.831(0)
7.0	8.684(-3)	6.916(-4)	-1.044(-4)	5.059(-6)	1.354(0)
8.0	6.892(-3)	4.218(-4)	-6.403(-5)	3.115(-6)	1.041(0)
9.0	5.597(-3)	2.627(-4)	-3.966(-5)	1.921(-6)	8.244(-1)
10.0	4.672(-3)	1.409(-4)	-2.006(-5)	9.169(-7)	6.692(-1)
11.0	3.861(-3)	1.259(-4)	-1.927(-5)	9.441(-7)	5.538(-1)
12.0	3.313(-3)	6.839(-5)	-9.719(-6)	4.428(-7)	4.659(-1)
25.0	8.421(-4)	-2.636(-5)	+4.884(-6)	-2.740(-7)	1.080(-1)
50.0	2.012(-4)	-8.333(-7)	1.652(-7)	-9.751(-9)	2.699(-2)

Table 3. Frequency dependent octupole polarizability and wave function.

The Renner effect in a nearly linear molecule, with application to NH_2

by R. N. DIXON

Department of Chemistry, University of Sheffield

(Received 5 May 1965)

The theory developed by Renner, and Pople and Longuet-Higgins, for vibronic interactions in a triatomic molecule has been extended to allow both component states of an electronic Π state to have double minima potentials. The energy levels for this model have been found by diagonalization of a truncated infinite Hamiltonian matrix using a computer. This theory has been applied to the experimental data for NH_2 , and it is concluded that the excited state is bent. The equilibrium angle is $144^\circ \pm 5^\circ$, and the barrier height is $777 \pm 100 \text{ cm}^{-1}$. However, only the lowest vibronic level of the excited state lies below the potential maximum. The complete array of energy levels suggests that the usual Hamiltonian for vibronic interaction overestimates the importance of vibronic effects at large displacements from the linear configuration. Vibronic effects are also shown to be negligible for the lower levels of the ground state of NH_2 .

1. INTRODUCTION

Dressler and Ramsay [1] have analysed the electronic absorption spectrum of gaseous NH_2 , and have shown that it arises from a transition from the ground state, with a valence angle of $103^\circ 20'$, to an excited state which is linear or nearly linear. The unusual and complex pattern of vibrational levels in the excited state was interpreted as an example of the 'Renner effect' [2]; that is, a vibronic interaction which arises from the resolution upon bending of an orbital degeneracy. A single ${}^2\Pi_u$ state of linear NH_2 correlates in the bent molecule with both the ground state and the upper state of the bands. The theory developed by Renner has been extended by Pople and Longuet-Higgins [3] to cope with such a large vibronic splitting, using first-order perturbation theory. This theory gives satisfactory agreement with experiment for the higher levels of the excited state, which were the levels observed by Dressler and Ramsay.

Herzberg and Johns [4] have recently observed an electronic absorption spectrum of BH_2 which is similar to that of NH_2 , with a bent ground state and a linear excited state which both correlate with one ${}^2\Pi_u$ state of linear BH_2 . Combination of this observation with Walsh's molecular orbital scheme for AH_2 molecules [5] suggests a need to re-examine the NH_2 data to determine the valence angle for the equilibrium configuration of the excited state.

Eaton, Johns and Ramsay [6] have recently extended the observations on NH_2 to lower frequencies, and have detected the lowest vibrational levels of the excited state for the vibronic species $\Sigma, \Pi, \Delta, \Phi, \Gamma$ and H . The theory of Pople and Longuet-Higgins is not expected to be quantitatively accurate for these levels; and the author has found on attempting to extend this theory that a perturbation expansion does not converge rapidly for low quantum numbers.

On the other hand, the influence of a double minimum in the bending vibrational potential for the upper state will be greatest on these lowest levels. The present work was undertaken in order to determine this potential function for the upper state of NH_2 .

2. THEORY

Both Renner, and Pople and Longuet-Higgins, considered a simplified Hamiltonian for the vibronic interaction in a triatomic molecule. The bending of the molecule is represented by a coordinate r and a phase angle ϕ with respect to a space-fixed reference plane (figure 1). θ is the angle conjugate to the electronic angular momentum in a space-fixed coordinate system, and without loss of generality this can be considered as the angular coordinate of a single electron.

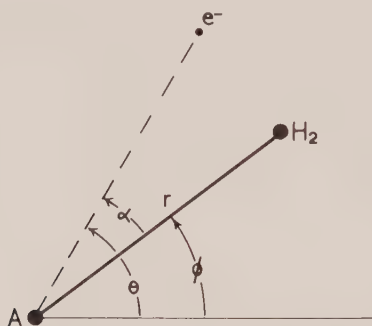


Figure 1. The coordinate system.

In the absence of vibronic coupling between θ and ϕ the electronic wavefunction will include an angular factor $\exp(\pm i\Lambda\theta)$. The above authors have shown that the vibronic coupling *within the two components* of an orbitally degenerate state may be approximated as follows. In the Born-Oppenheimer (fixed nucleus) approximation we may associate vibrational potential functions $V^+(r)$ and $V^-(r)$ with the two component states of the bent molecule, and it is assumed that the electronic wavefunctions of these two components contain angular factors $\cos(\Lambda\alpha)$ and $\sin(\Lambda\alpha)$ respectively for all values of r , ($\alpha = \theta - \phi$). The molecular Hamiltonian is then:

$$\begin{aligned}\mathcal{H} &= \mathcal{H}_0 + \mathcal{H}_1 + \mathcal{H}_2[\exp(2i\Lambda\alpha) + \exp(-2i\Lambda\alpha)], \\ \mathcal{H}_0 &= V_0(r) + \frac{p^2}{2m} + \frac{p_\phi^2}{2mr^2}, \\ \mathcal{H}_1 &= \frac{1}{2}[V^+(r) + V^-(r)] - V_0(r), \\ \mathcal{H}_2 &= \frac{1}{2}[V^+(r) - V^-(r)],\end{aligned}\tag{1}$$

where p and p_ϕ are conjugate to r and ϕ respectively, m is the reduced mass for the bending vibration, and $V_0(r)$ is a convenient zero-approximation potential function, usually chosen to be harmonic.

Renner treated the case of a Π state in which both $V^+(r)$ and $V^-(r)$ are harmonic. Pople and Longuet-Higgins used a first-order perturbation method for a Π state in which the potentials had both quadratic and quartic terms, so that the lower potential had a double minimum, but the upper curve has a minimum at

the linear configuration. In this paper we shall allow both curves to have double minima, and find the energy levels by diagonalization of a truncated infinite matrix.

Let the zero-approximation potential be quadratic:

$$V_0(r) = \frac{1}{2}kr^2. \quad (2)$$

We may now transform the energy into units of the zero-approximation harmonic oscillator vibration frequency

$$hc\omega_0 = \frac{h}{2\pi} \sqrt{\left(\frac{k}{m}\right)},$$

and the bending coordinate into dimensionless units:

$$q = \left[\frac{2\pi}{h} \sqrt{(mk)} \right]^{1/2} r. \quad (3)$$

Double minimum potential functions can be constructed in a very flexible form by using a combination of quadratic functions and Gaussian functions. We shall choose $V_0(r)$ to be the potential to which the upper curve becomes asymptotic at high values of r . Let us assume that V^+ is the upper potential surface V' , and V^- is V'' , as in NH_2 . Then

$$\left. \begin{aligned} V'(q) &= \frac{1}{2}q^2 + \alpha' [\exp(-\beta' q^2) - 1], \\ V''(q) &= \frac{1}{2}q^2 + \alpha'' [\exp(-\beta'' q^2) - 1]. \end{aligned} \right\} \quad (4)$$

Basis functions for the evaluation of the matrix of \mathcal{H} may be chosen to be products of the electronic factor $\exp(\pm i\Lambda\theta)$ and the eigenfunctions of the zero-approximation two-dimensional harmonic oscillator:

$$|\Lambda, v, l\rangle = \frac{1}{2\pi} R_{v,l}(q^2) \exp(i\Lambda\theta) \exp(il\phi) \quad (5)$$

and the matrix is diagonal in the only good angular momentum quantum number:

$$K = \Lambda + l \quad (6)$$

[2, 3]. Eigenfunctions of the Hamiltonian may therefore be expanded as linear combinations of the functions $|\Lambda, v, K + \Lambda\rangle$ and $|\Lambda, v, K - \Lambda\rangle$.

We will now restrict the discussion to electronic Π states ($\Lambda = \pm 1$).

Pople and Longuet-Higgins have shown that the matrix elements of the perturbation to \mathcal{H}_0 can be expressed in terms of vibrational matrix elements:

$$\begin{aligned} \langle \mp 1, v, K \pm 1 | (\mathcal{H} - \mathcal{H}_0) | \mp 1, v', K \pm 1 \rangle &= \langle v, K \pm 1 | \mathcal{H}_1 | v', K \pm 1 \rangle, \\ \langle \pm 1, v, K \mp 1 | (\mathcal{H} - \mathcal{H}_0) | \mp 1, v', K \pm 1 \rangle &= \langle v, K \mp 1 | \mathcal{H}_2 \exp(\mp 2i\phi) | \\ &\quad v', K \pm 1 \rangle, \end{aligned} \quad (7)$$

and have given expressions for the matrix elements of quadratic and quartic terms. The matrix elements of the Gaussian terms in \mathcal{H}_1 have been given by the author in an earlier paper [7], and it therefore remains to find the matrix elements of the Gaussian terms in \mathcal{H}_2 . Pople and Longuet-Higgins have used a sign convention for the vibrational wavefunctions in which the matrix elements of powers of q are positive. Since this is different from that used in reference [7] the quadratic terms have been taken from an earlier paper by Shaffer [8] to avoid errors in sign.

By examination of the expansion formula for the associated Laguerre polynomials of argument $\rho = q^2$ it is deduced that:

$$\rho L_{l+k}^l(\rho) = -(k+1)(l+k) L_{l+k-1}^{l-2}(\rho) + \sum_{r=0}^k \frac{(l-1)(l+k)!}{(l-2+r)!} L_{l-2+r}^{l-2}(\rho), \quad (8)$$

whence

$$\begin{aligned} \exp(-2i\phi)|v, K+1\rangle = & - \left[\frac{v-K+1}{v+K+1} \right]^{1/2} |v, K-1\rangle \\ & + \sum_{v'=K-1}^{v-2} \left\{ \frac{[\frac{1}{2}(v-K-1)]! [\frac{1}{2}(v'+K-1)]!}{[\frac{1}{2}(v+K+1)]! [\frac{1}{2}(v'-K+1)]!} \right\}^{1/2} |v', K-1\rangle. \end{aligned} \quad (9)$$

The matrix elements of $\mathcal{H}_2 \exp(-2i\phi)$ may therefore be calculated from those of \mathcal{H}_2 using equation (9) and the rules of matrix multiplication; and those of $\mathcal{H}_2 \exp(+2i\phi)$ by using the Hermitian property of the Hamiltonian matrix. (Note, however, that although the expansion of equation (9) is complete, it is not possible to give a closed expression for $\exp(2i\phi)|v, K-1\rangle$, since there will be a remainder term proportional to q^{K-1} .) This method is very convenient for evaluation using a computer, since the matrix elements of $\mathcal{H}_2 [\exp(2i\alpha) + \exp(-2i\alpha)]$ may then be calculated from the matrix elements of the terms in \mathcal{H}_1 which are needed elsewhere in the Hamiltonian matrix.

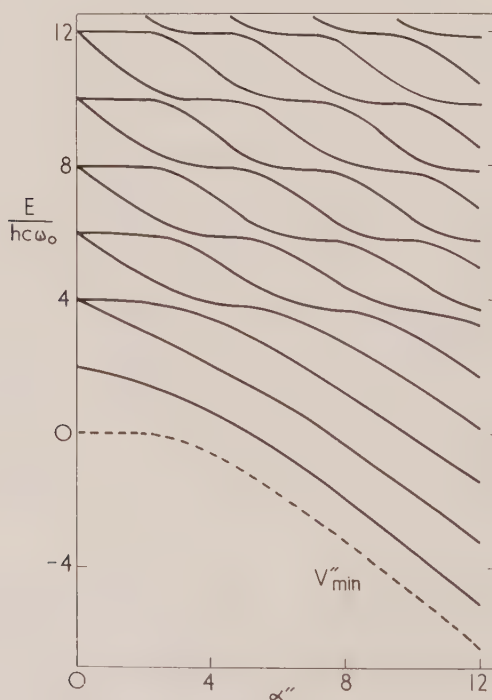


Figure 2. The calculated pattern of Δ vibronic levels for a II state in which the upper state is harmonic, but the lower state is perturbed by a Gaussian of constant width but varying height. $0 \leq \alpha'' \leq 12$, $\beta'' = 0.25$, $h'' = 1$. The lower component state has a double minimum for $\alpha'' > 2$.

A programme has been written for the Sheffield University Mercury Computer to calculate the Hamiltonian matrix using the first $(n+1)$ functions $|1, v, K-1\rangle$ and the first n functions $|-1, v, K+1\rangle$ (i.e. $v \leq K-1+2n$), and to find the eigenvalues of this matrix, where $n \leq 19$.

Both Renner, and Pople and Longuet-Higgins, have shown that within the approximation of the Hamiltonian of equation (1) the Σ^+ vibronic levels are associated with $V^+(r)$, and the Σ^- levels with $V^-(r)$, and that their term values are equal to those of a molecule in an orbitally non-degenerate state with these potential functions, but with $l \equiv \Lambda$. The Σ levels associated with the potentials of equation (4) may therefore be calculated using the method of reference [7].

Renner has also shown that if the term values with $K > 0$ are calculated as a function of the parameters of $V^+(q)$ and $V^-(q)$, and these two potentials are very different, then there are strong 'avoided crossings' between the curves for the lower levels of the upper state and higher levels of the lower state. Figure 2 gives the pattern of Δ vibronic levels calculated using the method outlined above for an electronic Π state in which $V'(q)$ is strictly harmonic, but $V''(q)$ is perturbed by a Gaussian term of constant width but increasing height. It is seen that as α'' increases the closest approach between the lower levels associated with $V'(q)$ and higher levels associated with $V''(q)$ becomes an appreciable fraction of the vibrational spacing. It is therefore expected that the accurate reproduction of the experimental data for levels with $K > 0$ will be extremely dependent on the form of both potentials over a wide range of values of q , and on the accuracy of the assumptions implicit in the Hamiltonian of equation (1).

3. APPLICATION TO NH_2

Pople and Longuet-Higgins determined the coefficients of a quadratic + quartic form for $V'(q)$ by using an expression which gives a reasonable fit to Dressler and Ramsay's term values for the higher Σ^+ levels of NH_2 ;

$$T(\text{cm}^{-1}) = 9650 + 597(v+1) + 11.5(v+1)^2. \quad (10)$$

However, the observed separation between the two lowest Σ^+ levels, 1158 cm^{-1} [6], is 173 cm^{-1} less than that predicted by this equation, indicating a strong anharmonicity at low q values.

Trial values of the parameters α' and β' in the potential $V'(q)$ (equation (4)) were chosen to calculate the ratios of the first three $\Sigma^+ - \Sigma^+$ intervals, using the method of reference [7] with $l=1$ (i.e. the intervals between the levels $(0, 1, 0)$; $(0, 3, 0)$; $(0, 5, 0)$; and $(0, 7, 0)$). It was found that a potential with a minimum at the linear configuration could not produce all three of the observed ratios to better than ~ 4 per cent ($\equiv 50 \text{ cm}^{-1}$). The closest fit was obtained using:

$$\alpha' = 10.0, \beta' = 0.0775, \omega_0 = 1078 \text{ cm}^{-1}, T_0 = 11286 \text{ cm}^{-1}, \quad (11)$$

giving a mean error for the first five Σ^+ levels of $\pm 2 \text{ cm}^{-1}$. (T_0 is the electronic energy of the linear configuration with respect to the lowest level of the ground state). The higher Σ^+ levels are not so closely fitted by these parameters (figure 3). However these levels are known to be perturbed by Fermi resonance between levels $(0, v'_2, 0)$ and $(1, v'_2 - 4, 0)$, and the discrepancies are of the order of magnitude of the Fermi resonance interaction constant [1]. The parameters of equation (11) give a potential with a double minimum and a barrier height of 777 cm^{-1} , and with the observed bond length of 0.976 \AA the equilibrium angle is calculated

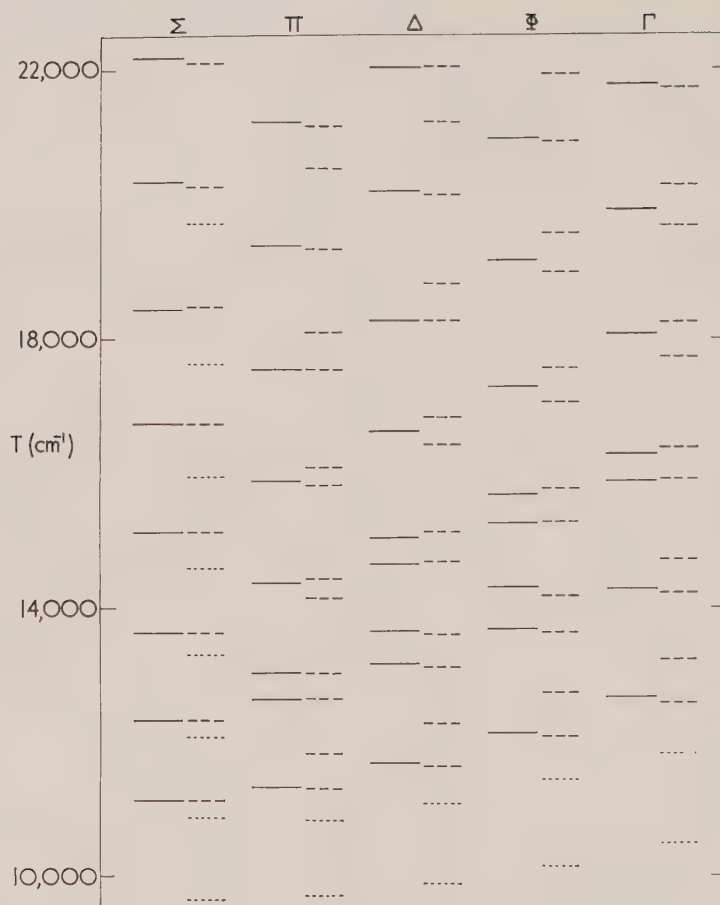


Figure 3. Comparison between the observed vibronic term values for NH_2 (—) with those calculated using the parameters of equations (11) and (13) (---). Levels which may be closely associated with the lower component state are dotted (- - - -).

to be 144° . With these values the $(0, 1, 0)\Sigma^+$ level lies 164 cm^{-1} below the potential maximum, and all other Σ^+ levels lie above it. The parameters of this potential are therefore not well-determined, and the estimated errors in the barrier height and equilibrium angle are $\pm 100\text{ cm}^{-1}$ and $\pm 5^\circ$ respectively.

The parameters of $V''(q)$ may be determined from the known data on the ground state of NH_2 , as in reference [3]. Three suitable data are: $\omega_2'' = 1497.3\text{ cm}^{-1}$ (ΔG_2^1 value) [6]; T_0 (equation (11)) and the ground-state valency angle of 103.4° [1]; and these are related to α'' , β'' , h'' (and $\eta'' = 2\alpha''\beta''/h''$) by:

$$\left. \begin{aligned} \frac{T_e}{hc\omega_0} &= \frac{\alpha''}{\eta''}(\eta'' - 1 - \ln \eta''), \\ q_{\min}^2 &= \frac{2\alpha'' \ln \eta''}{h''\eta''}, \\ h'' \ln \eta'' &= \frac{1}{2} \left[\frac{\omega_e''}{\omega_0} \right]^2 \end{aligned} \right\} \quad (12)$$

In using these equations the ground-state anharmonic constant x''_{22} was assumed to be -20 cm^{-1} , by analogy with H_2O [9], giving :

$$\alpha'' = 26.891, \quad \beta'' = 0.05388, \quad h'' = 0.6991. \quad (13)$$

These potential curves are shown in figure 4, and indicate that the vertical transition from the lowest vibrational level of the ground-state to the Σ^+ levels of the excited state should involve the $(0, 9, 0) \Sigma^+$ level. This transition is indeed the strongest observed [1], giving added weight to the suggestion of a bent excited state.

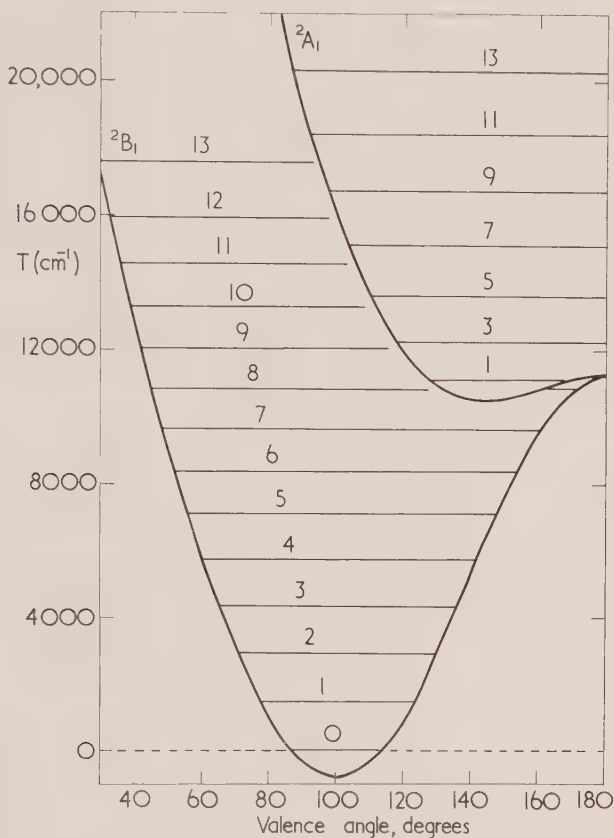


Figure 4. Calculated potential energy curves for the 2B_1 and 2A_1 states of NH_2 , and the calculated Σ levels. The Σ^- (ground state) levels are given vibrational quantum numbers v_2 appropriate to a bent state, whereas the Σ^+ levels (excited state) are numbered as for a linear molecule.

The energy levels with $0 \leq K \leq 4$ were calculated using these two potential functions, and the results are compared with experiment [1, 6] in figure 3. Small variations were made in the parameters of $V''(q)$, but it was found impossible to produce shifts of more than about 50 cm^{-1} in levels corresponding to observed transitions without departing radically from the input data discussed above, and in general all levels in a given energy range were shifted by similar amounts.

4. DISCUSSION

The measure of agreement between the observed and calculated term values for the higher levels of the NH_2 excited state is very similar to that given by the method of Pople and Longuet-Higgins, and is very much better for the more recently observed lower levels. The calculations give a satisfactory explanation for the separations between the pairs of levels observed for each K value at low vibrational quantum numbers. Thus figure 3 justifies the assumption that realistic Born-Oppenheimer potential functions can be obtained from the Σ levels with l set equal to Λ . However, the comparison worsens as K increases, as might be expected from the conclusion drawn in § 2. It is interesting to consider figure 3 in the light of probable contributions to inaccuracies in the calculations, since we can then give a critical evaluation of the Hamiltonian of equation (1).

The set of basis functions used ($v \leq \sim 40$) should be adequate to represent all eigenvalues of the Hamiltonian with turning points at $q \leq 9$ (\equiv a valence angle of 40°), corresponding to ground state levels with term values less than $15\,000\text{ cm}^{-1}$. Higher levels of the ground state, and any excited state levels with which these levels strongly interact, are likely to be considerably in error due to (a) truncation of the infinite matrix, (b) inadequacies of the potential functions for large values of q , and (c) neglect of interactions with the other degrees of freedom. The method of the appendix shows that first-order vibronic interactions are determined mainly by low q values (i.e. near the linear configuration), and the comparison between Pople and Longuet-Higgins' first-order treatment and that of this paper shows that these errors are not very important for the higher levels of the excited state, except where there are Fermi resonance interactions. The most serious errors in the method are therefore likely to be for those levels which exhibit strong upper state-lower state interactions, since a wide range of q values may contribute to the interaction matrix elements.

Figure 3 indicates that 'local interactions' between higher ground-state levels and lower excited state levels persist to higher term values in the calculations than in the observations. This could be partly due to the errors discussed above, but it seems more likely that the electronic wavefunctions of the two states do not remain in the relationship of 'pure precession' [10] for large values of q , with a consequent over-emphasis on vibronic interactions. The application of the principles of directed valence to a simple LCAO-MO description of AH_2 molecules [5], gives the $(b_1 - \pi_u)$ orbital as a pure p_x atomic orbital on atom A for all valence angles, whereas the $(a_1 - \pi_u)$ orbital involves s - p hybridization, so that at a valence angle 2β it is:

$$(a_1 - \pi_u) = \cot \beta \cdot s_A + \sqrt{(1 - \cot^2 \beta)} \cdot p_{z_A}. \quad (14)$$

Consequently the importance of local vibronic interactions will be considerably less than predicted by the above model for levels with turning points at valence angles near 90° ; that is, for all but the few lowest excited state levels for each K value greater than zero. This is qualitatively in agreement with figure 3.

We may conclude that it is possible to obtain a moderately accurate representation of the whole of the complex vibronic structure of a Π state exhibiting a 'strong Renner effect' with this model. There can be no doubt that the equilibrium configuration of the first excited state of NH_2 is not linear but shows a double minimum in the potential function for the bending vibration, in accord with a

suggestion made by Walsh [11], but at variance with a semi-empirical calculation of the electronic energy made by Jordan and Longuet-Higgins [12]. However, a close fit to experiment will require a considerably more elaborate Hamiltonian than that used in this work, and it is extremely doubtful that a perturbation expansion will be sufficiently accurate for all vibrational levels.

I am indebted to Dr. D. A. Ramsay for making his experimental data on the lower excited levels of NH_2 available to me in advance of publication.

APPENDIX

Weak vibronic effects in a moderately bent state

The electronic angular momentum $\Lambda\hbar$ of a state which is orbitally degenerate when linear will be largely quenched for the lower vibrational levels of a considerably bent component state. The effects of vibronic interaction may then be evaluated by expressing the Hamiltonian in a rotating coordinate system (cf. equation (1));

$$\mathcal{H} = \mathcal{H}_e + \mathcal{H}_v + \mathcal{H}_r + \mathcal{H}_{\text{evr}}. \quad (15)$$

\mathcal{H}_e is the Born-Oppenheimer (fixed nucleus) electronic Hamiltonian, and has eigenvalues which are the vibrational potential energy functions V^+ and V^- ; $V^\pm + \mathcal{H}_v$ is the vibrational Hamiltonian; and \mathcal{H}_r is the rigid rotor Hamiltonian. The vibronic interaction about the nearly linear axis of the molecule can be evaluated using the normal method for the coupling of internal angular momenta to overall rotation;

$$\mathcal{H}_{\text{evr}} = \frac{p_\alpha^2}{2mr^2} - \frac{p_\alpha p_\phi}{mr^2}, \quad (16)$$

p_α is the electronic angular momentum which is conjugate to $\alpha = (\theta - \phi)$. In order to evaluate the matrix elements of \mathcal{H}_{evr} we will ignore the dependence of the electronic wavefunctions upon vibrational coordinates, and assume as above, that:

$$\psi^+ = \cos \Lambda\alpha; \quad \psi^- = \sin \Lambda\alpha. \quad (17)$$

The unperturbed wavefunctions Ψ are products of electronic wavefunctions ψ^\pm , vibrational wavefunctions $\chi_{v_1}^\pm$, and rotational wavefunctions $\exp(iK\phi)$. The first term of \mathcal{H}_{evr} contributes to matrix elements which are electronically diagonal:

$$\langle \Psi^\pm | \mathcal{H}_{\text{evr}} | \Psi^\pm \rangle = \Lambda^2 \langle \chi_{v_1}^\pm | \frac{\hbar^2}{2mr^2} | \chi_{v_1}^\pm \rangle. \quad (18)$$

For the lowest vibrational levels of a moderately bent state the vibrational amplitude is small compared with the equilibrium value of the bending coordinate, so that these matrix elements are equal to $\hbar c A^\pm \Lambda^2$ if $v_1 = v_2$, and zero otherwise. Hence these terms result only in a small shift of origin which is different for the two states. The second term in \mathcal{H}_{evr} is electronically non-diagonal, with matrix elements:

$$\langle \Psi^+ | \mathcal{H}_{\text{evr}} | \Psi^- \rangle = i\Lambda K \langle \chi_{v_1}^+ | \frac{\hbar^2}{mr^2} | \chi_{v_2}^- \rangle. \quad (19)$$

For the lower vibrational levels of a bent component state we may evaluate the effect of these terms using second-order perturbation theory, and for a given level of one state we may assume a constant energy denominator in summing over the levels of the other state. To this approximation the perturbation to the term values is:

$$\frac{4\Lambda^2 K^2 A^{\pm 2}}{\Delta E_{\text{vert}}} \quad (20)$$

The vibronic interaction therefore results in a modification of the rotational constants of each level, so that they are no longer related to the form of only one potential energy function:

$$\left. \begin{array}{l} \text{Upper component state:} \quad A'_{\text{eff}} = A' \left[1 + \frac{4\Lambda^2 A'}{\Delta E'} \right], \\ \text{Lower component state:} \quad A''_{\text{eff}} = A'' \left[1 - \frac{4\Lambda^2 A''}{\Delta E''} \right], \end{array} \right\} \quad (21)$$

where the ΔE values are vertical excitation energies evaluated at the equilibrium configuration of the state concerned.

Substitution of the values of A'' and $\Delta E''$ for the ground state of NH_2 into equation (21) shows that vibronic interactions are negligible in this case, even neglecting the probable departure from the relationship of pure precession. However, vibronic interactions will become significant for bent component states of HAB or AH_2 molecules with valence angles greater than about 120° and ΔE values of a few thousand cm^{-1} , for which A_{eff} could differ from A by 10 per cent or more. Thus if vibronic interactions are completely ignored the observed A values will lead to a valence angle for the lower component state which is too bent, and an angle for the upper component state which is too near linear.

REFERENCES

- [1] DRESSLER, K., and RAMSAY, D. A., 1959, *Phil. Trans. A*, **251**, 553.
- [2] RENNER, R., 1934, *Z. Phys.*, **92**, 172.
- [3] POPLE, J. A., and LONGUET-HIGGINS, H. C., 1958, *Mol. Phys.*, **1**, 372.
- [4] HERZBERG, G., and JOHNS, J. W. C. (to be published).
- [5] WALSH, A. D., 1953, *J. chem. Soc.*, p. 2260.
- [6] EATON, D. R., JOHNS, J. W. C., and RAMSAY, D. A. (to be published).
- [7] DIXON, R. N., 1964, *Trans. Faraday Soc.*, **60**, 1363.
- [8] SHAFFER, W. H., 1944, *Rev. mod. Phys.*, **16**, 245.
- [9] HERZBERG, G., 1945, *Infrared and Raman Spectra of Polyatomic Molecules* (New York: D. van Nostrand, Inc.).
- [10] VAN VLECK, J. H., 1929, *Phys. Rev.*, **33**, 467.
- [11] WALSH, A. D., quoted in LAIDLER, K. J., and RAMSAY, D. A., 1958, *Canad. J. Chem.*, **36**, 1.
- [12] JORDAN, P. C. H., and LONGUET-HIGGINS, H. C., 1962, *Mol. Phys.*, **5**, 121.

Fluorescence decay times of naphthalene and naphthalene excimers

by NOBORU MATAGA

Department of Chemistry, Faculty of Engineering Science, Osaka University,
Toyonaka, Osaka, Japan

and MASAO TOMURA and HITOSHI NISHIMURA

Department of Physics, Institute of Technology, Osaka City University,
Sugimotocho, Sumiyoshiku, Osaka, Japan

(Received 26 January 1965)

Fluorescence spectra and fluorescence decay times of naphthalene and methylnaphthalenes in solution have been measured under various conditions, i.e. in several different solvents and at different temperatures from 300°K to 100°K.

Furthermore, the concentration dependence of the fluorescence decay time was examined in detail in order to determine the fluorescence lifetime of the excimer. The mechanism of the excimer formation and decomposition reaction is discussed on the basis of observed results.

1. INTRODUCTION

The concentration dependence of the relative fluorescence yield of naphthalene in *n*-hexane was studied in detail by Dammers-deKlerk [1] and it was found that the yield decreased a little with increasing concentration up to 10^{-3} mol/l. and closely approached a constant value (about 75 per cent of the yield at infinite dilution) at concentrations higher than 10^{-2} mol/l. These results, which indicate a very small concentration quenching of fluorescence, have been explained by assuming that at higher concentrations transient dimers are formed by interaction between excited and unexcited naphthalene molecules and that these dimers can fluoresce at practically the same wavelength region as the excited monomer.

In relation to Dammers-deKlerk's study, Berlman and Weinreb [2] have examined the decay time of naphthalene in several different solvents, exciting the solutions by a pulsed beam of 75 kev electrons. However, their results seem to be not very conclusive. They were not able to identify the decay time of the excited dimer because of some inconsistent results. Furthermore, the excitation by the electron pulse complicated the interpretation of the observed results because the exciting energy is absorbed by the solvent, which then transfers part of the excitation energy to the solute, in contrast to the case of ultra-violet excitation.

On the other hand, Döller and Förster [3] have confirmed that the excimer of naphthalene, quite similar to the case of pyrene, is formed only in a very concentrated solution ($\gtrsim 0.5$ mol/l.) and that an excimer fluorescence spectrum quite different from the monomer fluorescence can be observed clearly.

In view of the circumstances described above, it appears to be necessary to study the fluorescence decay processes of naphthalene under various conditions using ultra-violet light instead of high energy radiation for the excitation.

2. EXPERIMENTAL PROCEDURE

2.1. Purification of materials

Naphthalene was recrystallized from ethanol and sublimated in a vacuum. α - and β -methylnaphthalenes were distilled several times in a vacuum. *n*-hexane and cyclohexane were dried over metallic sodium, distilled fractionally and the distillates were passed through a column of silica gel. Liquid paraffin was passed many times through a column of silica gel and then it was confirmed that the absorption at $270\text{ m}\mu$ was absent and that no luminescence from impurity was detectable under irradiation at the wavelengths for exciting the naphthalenes. Analytical grade toluene was distilled fractionally. Acetonitrile was refluxed repeatedly over phosphorous pentoxide, distilled into potassium carbonate and fractionally distilled from it. All solutions for the measurements were carefully de-aerated by the ordinary procedure of repeated freezing, evacuation and melting.

2.2. Apparatus and measurement

The photometer for the measurement of fluorescence spectra has been described elsewhere [4]. The cuvette for the solution was fused quartz tube which has a flat window and which contained a few millilitres of solution.

The lifetime measurement was conducted as follows. A specially designed condenser of a few hundreds pF [5] was charged to $2000\sim 3000\text{ v}$. Pulsed light was produced by discharging this condenser through a gap of about 1 mm between small electrodes in air. The inductance of the discharging circuit was about $1\text{ m}\mu$ henry. The half value width of the light pulse was $8\sim 10\text{ ns}$. Although the half value width of the light pulse was very small, there follows a tail, which has a few per cent of the intensity of the main pulse, and which has a decay time of about 15 ns . This tail arises because of the relaxational oscillation of the discharging circuit and the discharge due to the recombinations of produced ions.

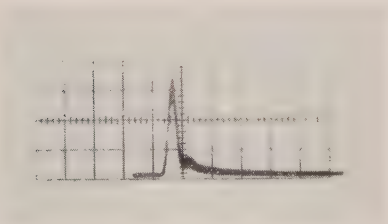


Figure 1. Oscilloscope of exciting light pulse. The larger division in the ordinate is equal to 50 ns .

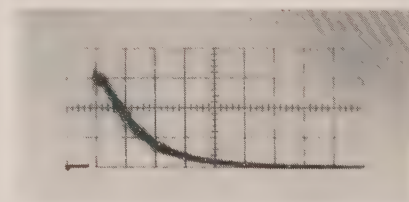


Figure 2. Oscilloscope of fluorescence decay curve of 0.1 mol/l . naphthalene in cyclohexane at 30°C (monomer fluorescence band). The larger division in the ordinate is equal to 50 ns .

The solution in the cuvette was irradiated by the pulsed light which was made monochromatic through a monochromator. The luminescence from the solution was received by a photomultiplier of 1P28 type. Appropriate filters were used to separate the monomer and dimer emissions. Responses from the photomultiplier were guided to a synchroscope (Tektronix 585) and the decay curves were photographed. The time constant of the guiding circuit was about 4 ns .

Examples of oscillograms of the pulsed light and the fluorescence decay curve of solution are shown in figures 1 and 2 respectively.

3. EXPERIMENTAL RESULTS

The concentration dependence of the fluorescence spectrum of α -methyl-naphthalene is shown in figure 3. Our result for naphthalene agrees with that of Döller and Förster [3] and also with the result of Berlman and Weinreb [2] in that the fluorescence of excimers is observable only in the case of very high concentration. In the case of pure liquid of α -methyl-naphthalene, only the excimer fluorescence can be observed. However, we have not observed any remarkable change of the fluorescence spectra at room temperature in the case of solutions more dilute than ~ 0.01 mol/l.

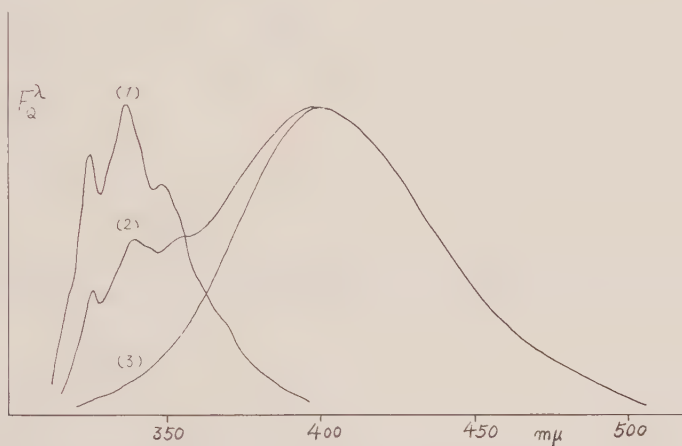


Figure 3. Fluorescence spectra of α -methylnaphthalene at 30°C . (1) 1.42×10^{-3} mol/l. in toluene, (2) 2.0 mol/l. in toluene, (3) pure liquid.

Fluorescence decay times were evaluated by the semi-logarithmic plot as it is shown in figure 4, for which the oscillogram of the decay curve is already indicated in figure 2.

In relation to the previous study [2], we have examined in detail the temperature dependence of the fluorescence decay time of naphthalene monomer in liquid paraffin, *n*-hexane and toluene. The results for liquid paraffin and *n*-hexane are shown in figures 5 and 6 respectively. In addition to this, we have evaluated the relative fluorescence yield ϕ at various temperatures by the equation,

$$\phi = \int_0^\infty I_0 \exp(-t/\tau) dt = I_0 \tau,$$

where τ is the decay time and I_0 is the fluorescence intensity at $t=0$. The temperature dependence of the fluorescence yield was practically the same as that of the fluorescence decay time in the case of liquid paraffin and *n*-hexane solutions, as it is shown in figure 6 for the latter. However, in the case of toluene solution, the decrease of the fluorescence yield at higher temperature was a little larger than that of the decay time. This fact seems to indicate the existence of very rapid quenching processes by some impurity in the solution or by solvent molecules themselves, which may be diminished at low temperature.

The concentration dependences of the decay times of the monomer and the excimer components of the fluorescence spectrum, respectively, were examined carefully. It was possible that any decay curve we measured was fitted practically,

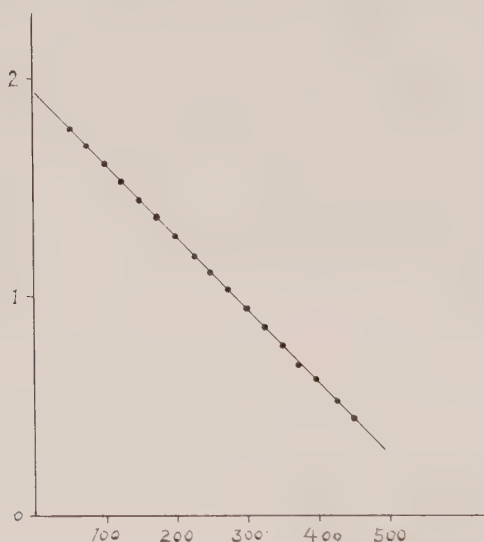


Figure 4. Semi-logarithmic plot of the fluorescence decay curve. Abscissa: $\log I(t)$ in arbitrary scale; ordinate: t in the unit of nanoseconds.

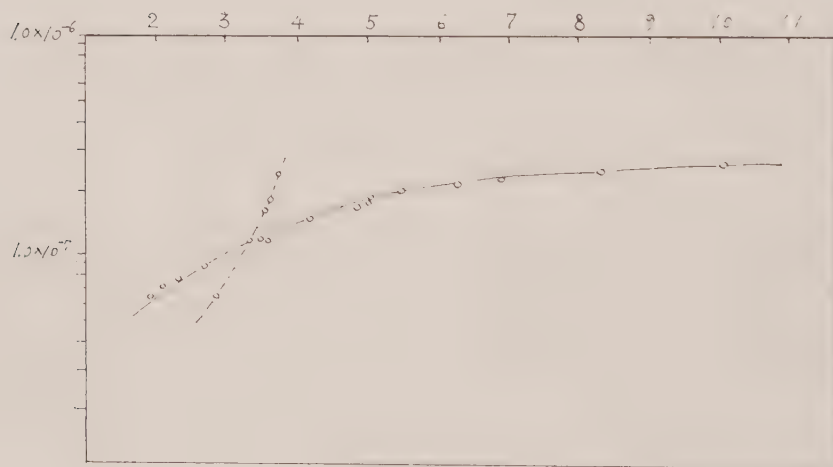


Figure 5. $\log \tau' \sim 1/T$ relation for naphthalene (3×10^{-3} mol/l.) in liquid paraffin. Abscissa: τ' (sec) in logarithmic scale; ordinate: $10^3/T$ ($^{\circ}\text{K}^{-1}$). The broken line indicates the results given in reference [2].

at least in the range from 100 to 3 of the intensity scale, to a single exponential curve of the form, $I(t) = I_0 \exp(-t/\tau)$. Moreover, the rise time of the excimer fluorescence as well as that of the monomer fluorescence was practically the same as the effective decay time of the exciting light pulse. These behaviours of naphthalene and methylnaphthalenes are quite different from those of pyrene, where

double exponential decay curves are observed and the rise time of the excimer fluorescence is longer, in some appropriate concentration range, than the effective decay time of the light pulse [6].

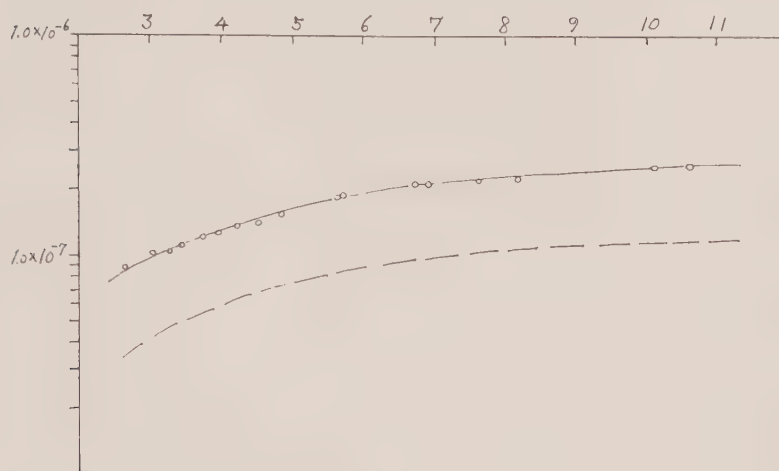


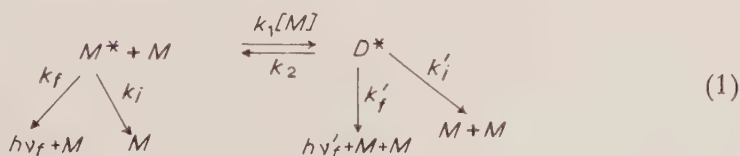
Figure 6. $\log \tau' \sim 1/T$ and $\log \phi \sim 1/T$ relations for naphthalene (1×10^{-4} mol/l.) in *n*-hexane. The broken line represents $\log \phi$ in arbitrary scale.

Contrary to our results, Berlman [2] has observed double exponential decay in the case of dilute as well as fairly concentrated solutions of naphthalene, which seems to indicate some complicating mechanisms due to the excitation by the high energy radiation.

The decay time of the monomer fluorescence (τ') in the case of dilute solutions, where the excimer formation is not observed, and the decay time of the excimer fluorescence (τ'') determined with highly concentrated solutions, are collected in the table. A remarkable feature which can be seen from the table is the fact that τ' is approximately equal to τ'' in all cases examined here.

4. DISCUSSION

The kinetic behaviour of the excimer formation and decomposition may be expressed as follows:



From this scheme, the time dependence of the fluorescence intensity of monomer, $I_M(t)$, and that of excimer, $I_D(t)$, are calculated as follows [6]:

$$\left. \begin{aligned} I_M(t) &= k_f \{ [M^*]_0 / (\beta - \alpha) \} \{ (\beta - \alpha) \exp(-\alpha t) + (\mu - \alpha) \exp(-\beta t) \}, \\ I_D(t) &= k_f' \{ [M^*]_0 k_1 [M] / (\beta - \alpha) \} \{ \exp(-\alpha t) - \exp(-\beta t) \}, \end{aligned} \right\} \quad (2)$$

where $[M^*]_0$ is concentration of excited monomer at $t=0$ and

$$\frac{\alpha}{\beta} = [(\mu + \nu) \mp \{(\nu - \mu)^2 + 4k_1 k_2 [M]\}^{1/2}] / 2, \quad (3)$$

$$\left. \begin{aligned} \mu &= k_f + k_i + k_1 [M] = (1/\tau_M) + k_1 [M], \\ \nu &= k_f' + k_i' + k_2 = (1/\tau_D) + k_2. \end{aligned} \right\} \quad (4)$$

In (3), $-$ sign corresponds to α and $+$ sign to β .

Solvent	[M] (mol/l.)	τ' (ns)	τ'' (ns)	Temperature ($^{\circ}$ K)
Naphthalene				
Cyclohexane	1.0×10^{-4}	120	—	295
	1.0×10^{-3}	120	—	295
	1.0×10^{-2}	120	—	295
	1.0×10^{-1}	120	—	295
	1.0	120	117	295
<i>n</i> -hexane	1.0×10^{-4}	110	—	291
	Saturated solution (≈ 1.0)	66	70	291
Toluene	1.3×10^{-4}	110	—	291
	3.0×10^{-4}	100	—	291
	5.0×10^{-2}	105	110	291
	5.0×10^{-1}	110	110	291
	2.8	90	80	301
Liquid paraffin	3.0×10^{-3}	117	—	291
	1.0	110	110	291
	2.0	110	110	291
Acetonitrile	3.0×10^{-3}	118	—	298
α -methylnaphthalene				
<i>n</i> -hexane	1.3×10^{-3}	77	—	291
Toluene	1.4×10^{-3}	83	—	291
	2.06	69	67	291
Liquid paraffin	0.1	96	95	291
	1.0	82	83	291
Pure liquid		—	60	291
β -methylnaphthalene				
Toluene	2.03	26	28	291
Pure liquid		—	20	313

Fluorescence decay times of naphthalene and α - β -methylnaphthalenes.

Since β is evidently larger than α as can be seen from (3) and because the observed decay curves are accurately single exponential, we can safely conclude that β is much larger than α and we are actually observing the decay curve of $\exp(-\alpha t)$ in both the monomer and the excimer fluorescence. Moreover, since τ' is almost equal to τ'' as is shown in the table, which indicates that the concentration dependence of α is rather small, τ_D is certainly very close to τ_M . If $\tau_D = \tau_M = 1/\kappa$, we can see from (3) that $\alpha = \kappa$ and $\beta = \kappa + k_2 + k_1 [M]$. Thus α is independent of concentration. On the other hand, the spectral evidence indicates that excimer dissociation is fast at room temperature. Therefore, under the conditions where the excimer band is observed it can be assumed that,

$$k_1[M] \gg 1/\tau_M \quad \text{and} \quad k_2 \gg 1/\tau_D.$$

Accordingly, from (3), $\beta \gg \alpha$ in accord with the observed exponential decay. If τ_D is a little different from τ_M , i.e. $1/\tau_D - 1/\tau_M \approx \delta\kappa$, then the decay constants can be calculated approximately as follows:

$$\begin{aligned} \alpha &\approx 1/\tau_M + \delta\kappa/2 - (\delta\kappa/2)(k_2 - k_1[M])/(k_2 + k_1[M]), \\ \beta &\approx 1/\tau_M + \delta\kappa/2 + k_2 + k_1[M] + (\delta\kappa/2)(k_2 - k_1[M])/(k_2 + k_1[M]). \end{aligned}$$

When $[M]$ become very large, α converges to $1/\tau_D$. Therefore, $\alpha (=1/\tau' = 1/\tau'')$ will change from $1/\tau_M$ for dilute solutions where no excimer band can be observed to $1/\tau_D$ for very concentrated solutions or pure liquid. The decay times in a highly concentrated solution and in a pure liquid are a little smaller than in less concentrated solution. This circumstance may arise if τ_D is a little smaller than τ_M , i.e. $\delta\kappa > 0$. It may be possible also that, at very high concentration, the excimer may be deactivated non-radiatively by some interactions with the ground state monomers or with some unknown impurities.

It may be concluded that $\tau_M \approx 100$ ns and τ_D is almost the same as or a little smaller than τ_M .

The largest possible value of k_1 can be estimated by:

$$k_1 = 8RT/3000\eta, \quad (5)$$

where R is the gas constant, T is the absolute temperature and η is the viscosity coefficient of solvent. The value of k_1 is equal to about 10^{10} l./mol sec at room temperature in the case of ordinary solvents, which are not very viscous, as used here.

In the case of pyrene [6], the experimental value of k_1 is practically the same as that calculated by (5). In the present case, k_2 may be much larger than that of pyrene, because the excimer formation is not observed in dilute solutions. Because of these facts, it seems to be reasonable to assume that $\beta \gtrsim 10^9 \text{ sec}^{-1}$ in highly concentrated solutions of naphthalenes where the excimer fluorescence can be observed clearly. This assumption agrees with the observed fact that the rise time of the dimer fluorescence is practically the same as the effective decay time of the light pulse and that either the observed decay curve of the excimer fluorescence or that of the monomer fluorescence is single exponential.

On the other hand, the wave number difference of the monomer and the excimer fluorescence of naphthalene is not very different from that of pyrene. This fact seems to indicate that the destabilization energy (δE) due to dimerization in the ground state of naphthalene is larger than that of pyrene, as it is shown in figure 7. In the case of pyrene, it has been established [6] that $\delta E = 3370 \text{ cm}^{-1}$ and the energy difference D between the monomer and the excimer fluorescent state is equal to 2760 cm^{-1} . The D value of naphthalene must be smaller than that of pyrene, because the dissociation reaction occurs much faster in the case of

naphthalene than in the case of pyrene. Accordingly, the lower limit of the δE value of naphthalene can be estimated from the observed frequencies of the fluorescence spectra, i.e. $\delta E > 4340 \text{ cm}^{-1}$. The circumstances for the excimers of α - and β -methylnaphthalene seem to be quite similar to the case of naphthalene. The general feature of the potential energy curves obtained by theoretical calculation [7] which includes charge resonance interaction as well as the exciton type interaction, is in qualitative agreement with those given in figure 7.

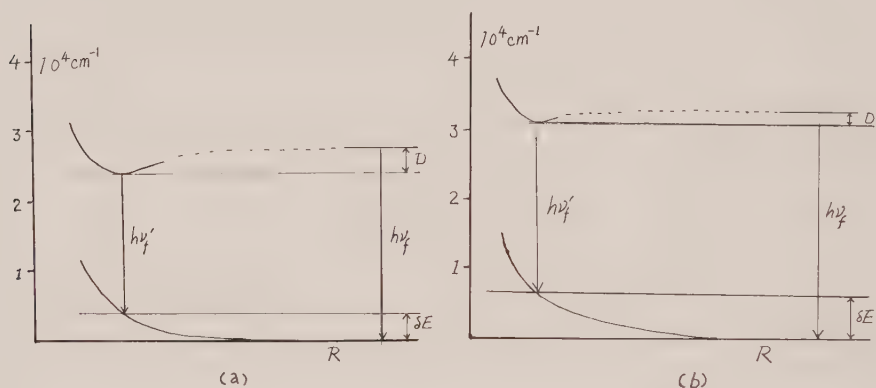


Figure 7. Potential energy diagram for excimer formation and decomposition processes. (a) pyrene, (b) naphthalene.

In the case of pyrene [6], it has been established that $k_f = 1.5 \times 10^6 \text{ sec}^{-1}$, $k_i = 0.81 \times 10^6 \text{ sec}^{-1}$, $k_f' = 1.2 \times 10^7 \text{ sec}^{-1}$ and $k_i' = 0.39 \times 10^7 \text{ sec}^{-1}$ in cyclohexane solution, from the observed values of the lifetimes and fluorescence quantum yields of the monomer and the excimer, respectively. Moreover, it has been shown that k_f' value is approximately independent of the nature of solvent and temperature, which seems to indicate that the excimer has a stable steric configuration [8].

The fluorescence quantum yield of naphthalene in *n*-hexane at room temperature is 0.375 [9]. Then, $k_f = 3.4 \times 10^6 \text{ sec}^{-1}$ and $k_i = 5.7 \times 10^6 \text{ sec}^{-1}$, by taking $\tau_M = 110 \text{ ns}$. However, we cannot assess the k_f' and k_i' values for naphthalene, because we do not have accurate value of the quantum yield of the excimer fluorescence.

As far as our experimental results are concerned, there is no positive result which supports Dammers-deKlerk's conclusion [1], since the observed lifetime does not show any change more than experimental error in the concentration range from 10^{-4} to 10^{-1} mol/l .

Now, the natural radiative lifetime of naphthalene, estimated from the observed fluorescence quantum yield and decay time, is about 290 ns, which is almost the same as that calculated from the oscillator strength of α -band in the absorption spectrum. We can see from figures 5 and 6 that the fluorescence lifetime of naphthalene at 100°K is 260 ~ 270 ns which is rather close to the natural radiative lifetime. Therefore, the value of k_i at 100°K is about $1/15 \sim 1/20$ of that at room temperature, which seems to mean that the collisional deactivations by solvent molecules are diminished at low temperatures. We have plotted

$$\log k_i = \log (1/\tau' - 1/\tau_0')$$

against $1/T$, where τ_0' is the low temperature limiting value and assumed to be ~ 280 ns, and have obtained approximate linear relations. Therefore, the temperature dependent part of k_i can be expressed as, $k_i = k_i^0 \exp(-\delta\epsilon/kT)$. The values of $\delta\epsilon$ were estimated to be 280 cm^{-1} and 270 cm^{-1} for *n*-hexane and paraffin solutions, respectively.

According to Berlman and Weinreb [2], the fluorescence decay time of naphthalene monomer in liquid paraffin is markedly longer than the decay times in cyclohexane and benzene. Furthermore, they have observed a very large temperature dependence of the decay time in liquid paraffin, as it is shown in figure 5. These results are not in agreement with ours as shown in the table and figure 5, and seem to indicate some complications induced by the high energy radiation. Since the solvent molecules are primarily excited in the case of high energy radiation, if a non-trivial time is necessary for energy transfer from the solvent molecules to the solute molecules and the transfer process involves some temperature dependent molecular interaction processes, the observed discrepancy between the results of high energy and the ultra-violet excitation may be expected.

The authors express their thanks to Mr. K. Ezumi and Mr. T. Mitani for their assistance in the experimental measurements.

REFERENCES

- [1] DAMMERS-DEKLERK, A., 1958, *Mol. Phys.*, **1**, 141.
- [2] BERLMAN, I. B., and WEINREB, A., 1962, *Mol. Phys.*, **5**, 313.
- [3] DÖLLER, E., and FÖRSTER, TH., 1962, *Z. phys. Chem.*, **31**, 274; *Ibid.*, **34**, 132.
- [4] MATAGA, N., TORIHASHI, Y., and KAIFU, Y., 1962, *Z. phys. Chem.*, **34**, 379. MATAGA, N., and KAIFU, Y., 1964, *Mol. Phys.*, **7**, 137.
- [5] TOMURA, M., 1963, *Buturi*, **81**, 654 (in Japanese).
- [6] BIRKS, J. B., DYSON, D. J., and MUNRO, I. H., 1963, *Proc. roy. Soc.*, A, **275**, 575.
- [7] MURRELL, J. N., and TANAKA, J., 1964, *Mol. Phys.*, **7**, 363.
- [8] BIRKS, J. B., LUMB, M. D., and MUNRO, I. H., 1964, *Proc. roy. Soc.*, A, **280**, 289.
- [9] IVANOVA, T. V., KUDRYASHOV, P. I., and SVESHNIKOV, B. YA., 1961, *Doklad. Akad. Nauk. SSSR.*, **138**, 572.

Electron resonance studies of fluorine hyperfine interactions

by A. CARRINGTON, A. HUDSON and H. C. LONGUET-HIGGINS

Department of Theoretical Chemistry, University of Cambridge

(Received 23 February 1965)

Radicals derived from five fluoronitrobenzenes have been prepared and their E.S.R. spectra measured. The hyperfine splittings are discussed and evidence is presented for steric hindrance of a nitro group when it has two orthofluorine neighbours.

1. INTRODUCTION

The first fluorine-containing radical studied in solution by electron spin resonance was the fluoranil semiquinone [1, 2]. Since then a number of radicals showing fluorine hyperfine interactions have been investigated including the anions of para and meta-fluoronitrobenzene [3, 4], para-fluoroacetophenone and 2,7-difluorofluorenone [5, 6]. Fluorine contact interactions have been observed in the ^{19}F nuclear resonance spectra of substituted nickel aminotroponimineates [7, 20]. These latter studies showed that the sign of the fluorine coupling in the C-F fragment is positive, in contrast to the negative coupling in the C-H fragment. This may be taken as evidence for electron delocalization between carbon and fluorine; similar conclusions were reached in a single crystal study of x-irradiated mono-fluoroacetamide [8].

In earlier studies [1, 3] the sign of the fluorine splitting was assumed to be negative, and the results were interpreted in terms of equation (1), similar to that proposed by McConnell for proton hyperfine interactions [9]:

$$a_{\text{F}} = Q^{\text{C}} \rho_{\text{C}}. \quad (1)$$

By analogy with the theory of ^{13}C hyperfine interactions [10, 11] Eaton and co-workers suggested the use of the equation:

$$a_{\text{F}} = Q^{\text{C}} \rho_{\text{C}} + Q^{\text{F}} \rho_{\text{F}} \quad (2)$$

rather than equation (1). In equation (2) the first term arises from spin polarization of the C-F σ bonding electrons due to unpaired spin on the carbon atom and the second term represents the spin polarization of fluorine 1s and 2s electrons due to spin density in a $2p\pi$ orbital on fluorine; one expects Q^{C} to be negative and Q^{F} to be positive. Accurate values of the constants are not yet available although a number of estimates have been made [7, 8, 20].

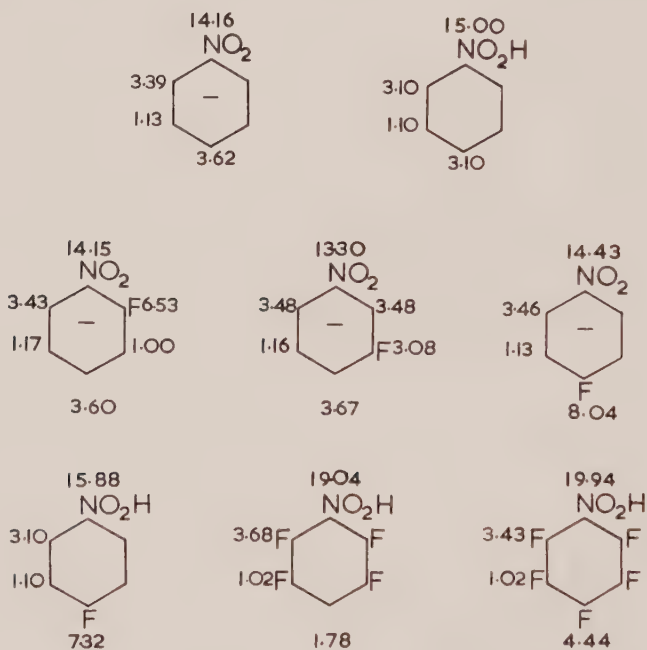
In this paper the spectra of radicals derived from five fluorinated nitrobenzenes are presented. The fluorine splittings are interpreted in terms of equation (2), the spin densities being calculated by means of the approximate S.C.F. method of McLachlan [12].

2. MEASUREMENT AND ANALYSIS OF THE SPECTRA

The monofluoronitrobenzenes were purchased from L. Light & Co. and pentafluoronitrobenzene from the University of Birmingham. A sample of tetrafluoronitrobenzene was kindly donated by Professor W. K. R. Musgrave.

The anion radicals of meta and para-fluoronitrobenzene were generated photochemically by ultra-violet irradiation of dilute solutions in methanol containing sodium methoxide [13]. The ortho-fluoronitrobenzene radical anion was prepared in a flow system by reduction with alkaline sodium dithionite [14] the solvent being aqueous ethanol. Reproductions of the spectra of the three monofluoro derivatives are to be found elsewhere [18].

Tetra and pentafluoronitrobenzene were found to undergo rapid solvolysis under the conditions used to prepare the other radicals. It was however possible to prepare radicals by irradiation of degassed solutions in tetrahydrofuran [15]. The radicals formed are neutral species and their electron spin resonance spectra show the presence of a small doublet splitting due to abstraction of an α -hydrogen from the solvent. The transferred proton is probably attached to one of the oxygen atoms of the nitro group [16, 17]. The corresponding neutral radical from parafluoronitrobenzene was also prepared in this way, for purposes of comparison. All spectra were recorded on a Varian 100 kc/s spectrometer, irradiations being carried out in the multipurpose cavity with a high-pressure mercury lamp.



In the solvents used all of the radicals show a large nitrogen splitting which divides the spectrum into three groups of lines and makes the remainder of the analysis straightforward. Splitting constants were assigned by comparison with the unfluorinated species since fluorine substitution appears to have little effect on the odd electron distribution. The observed hyperfine splittings in gauss are given in the figure.

The spectra in aqueous alcohol show interesting line-width effects which were noted by Ayscough, Sargent and Wilson [4]; these have been considered in detail elsewhere [18].

3. THEORY

The results obtained for the three monofluoro derivatives indicate that fluorine substitution has little effect on the distribution of the unpaired electron. The ring proton splittings are almost constant, irrespective of the position of the fluorine atom. Furthermore, the fluorine splitting in each molecule is roughly twice as large as the corresponding proton splitting. These observations suggest that, for the three radicals under consideration, there is an approximately linear relationship between the fluorine splitting and the spin density on the adjacent carbon atom, the proportionality constant Q^C in equation (1) being 50 ± 10 gauss.

A new feature emerges from the results obtained for the tetra and pentafluoro derivatives. The fluorine splittings are now roughly equal to the corresponding proton splittings in nitrobenzene itself; at the same time, the nitrogen splitting is some 5 to 6 gauss larger. These results suggest that steric hindrance due to the presence of two ortho fluorine atoms forces the nitro group out of the plane of the molecule. The unpaired electron is therefore more localized on the nitro group, and the nitrogen splitting is increased. The consequent decrease of spin density in the ring system accounts for the relatively small fluorine splittings.

	$C_6H_5NO_2^-$ exp.†	$C_6H_5NO_2^-$ calc.‡	$2-FC_6H_4NO_2^-$ calc.‡	$3-FC_6H_4NO_2^-$ calc.‡	$4-FC_6H_4NO_2^-$ calc.‡
N	—	0.3219	0.3235	0.3227	0.3273
O	—	0.1827	0.1811	0.1831	0.1832
F	—	—	0.0093	0.0057	0.0108
1	—	-0.0371	-0.0423	-0.0369	-0.0423
2	0.151	0.1508	0.1356	0.1558	0.1511
3	-0.050	-0.0538	-0.0473	-0.0508	-0.0546
4	0.161	0.1559	0.1554	0.1536	0.1449
5	-0.050	-0.0538	-0.0555	-0.0532	-0.0546
6	0.151	0.1508	0.1591	0.1482	0.1508

† The values in the first column (apart from sign) have been obtained by dividing the observed values of a_H by 22.5 gauss.

‡ The calculated values have been obtained by McLachlan's method using the parameters $\alpha_N = \alpha_C + 2.20\beta_{cc}$, $\alpha_O = \alpha_C + 1.88\beta_{cc}$, $\alpha_F = \alpha_C + 1.60\beta_{cc}$, $\beta_{CN} = 1.20\beta_{cc}$, $\beta_{NO} = 1.67\beta_{cc}$, $\beta_{CF} = 0.70\beta_{cc}$ and an auxiliary inductive parameter of $0.1\beta_{cc}$ for the carbon adjacent to the fluorine.

Spin densities in the anions of nitrobenzene and its monofluoro-derivatives.

It therefore appears that all of our results may be interpreted in terms of equation (1). However, we are *not* suggesting that the fluorine splitting depends only on the carbon atom spin density. A single crystal study of the $CHFCNH_2$ radical by Cook *et al.* shows quite clearly that the unpaired electron is partially delocalized into a fluorine p_π orbital and that the resulting fluorine interaction depends on both ρ_C and ρ_F . The apparent linear relationship involving only ρ_C which we have observed must arise because the ratio ρ_C/ρ_F is approximately constant and this conclusion is confirmed by spin density calculations.

For the monofluoro compounds, we have carried out approximate S.C.F. calculations using the method due to McLachlan with appropriate molecular orbital parameters for fluorine [8] and the nitro group [19]. The resulting spin densities are shown in the table. We have not thought it worthwhile to make corresponding calculations for the polyfluoro derivatives because of uncertainty in the choice of a resonance integral for the C-N bond. It may however be noted that the *relative* spin densities at the various ring positions in the benzyl radical are unaltered by reducing the resonance integral of the exocyclic carbon-carbon bond, at least in the Hückel approximation, and that if the coulomb integral of the antibonding orbital of the nitro group is approximately α_c , the same will be true for the nitrobenzene anion. It is therefore not surprising that in the polyfluoro derivatives the spin densities in the ring are apparently in the same ratio as in the nitrobenzene anion itself. The observed increase in the nitrogen coupling is consistent with the assumption that the spin density in the ring is approximately halved.

We should like to thank the D.S.I.R. for the purchase of the Varian Spectrometer and the award of a maintenance grant to A. H.

REFERENCES

- [1] ANDERSON, P. H., FRANK, P. J., and GUTOWSKY, H. S., 1960, *J. chem. Phys.*, **32**, 196.
- [2] EASTMAN, J. W., ANDROES, G. M., and CALVIN, M., 1962, *Nature, Lond.*, **193**, 1067.
- [3] MAKI, A. H., and GESKE, D. H., 1961, *J. Amer. chem. Soc.*, **83**, 1852.
- [4] AYSCOUGH, P. B., SARGENT, F. P., and WILSON, R., 1963, *J. chem. Soc.*, p. 5418.
- [5] RIEGER, P. H., and FRAENKEL, G. K., 1962, *J. chem. Phys.*, **37**, 2811.
- [6] DEHL, R., and FRAENKEL, G. K., 1963, *J. chem. Phys.*, **39**, 1793.
- [7] EATON, D. R., JOSEY, A. D., PHILLIPS, W. D., and BENSON, R. E., 1962, *Mol. Phys.*, **5**, 407.
- [8] COOK, R. J., ROWLANDS, J. R., and WHIFFEN, D. H., 1963, *Mol. Phys.*, **7**, 31.
- [9] McCONNELL, H. M., 1956, *J. chem. Phys.*, **24**, 632.
- [10] McLACHLAN, A. D., DEARMAN, H. H., and LEFEBVRE, R., 1960, *J. chem. Phys.*, **33**, 65.
- [11] KARPLUS, M., and FRAENKEL, G. K., 1961, *J. chem. Phys.*, **35**, 1312.
- [12] McLACHLAN, A. D., 1960, *Mol. Phys.*, **3**, 233.
- [13] RUSSELL, G. A., and GEELS, E. J., 1963, *Tet. Letters*, **20**, 1333.
- [14] KOLKER, P. L., and WATERS, W. A., 1964, *J. chem. Soc.*, p. 1136.
- [15] LAGERCRANTZ, C., and YHLAND, M., 1962, *Acta chem. scand.*, **16**, 1043.
- [16] WARD, R. L., 1963, *J. chem. Phys.*, **39**, 2588.
- [17] CARRINGTON, A., and HUDSON, A. (unpublished results).
- [18] CARRINGTON, A., HUDSON, A., and LUCKHURST, G. R., 1965, *Proc. roy. Soc.*, **A**, **284**, 582.
- [19] RIEGER, P. H., and FRAENKEL, G. K., 1963, *J. chem. Phys.*, **39**, 609.
- [20] EATON, D. R., JOSEY, A. D., BENSON, R. E., PHILLIPS, W. D., and CAIRNS, T. L., 1962, *J. Amer. chem. Soc.*, **84**, 4100.

Electric fields in fluorocyclohexanes and the magnitude of ^{19}F chemical shifts

by J. W. EMSLEY

Department of Chemistry, University of Durham

(Received 2 November 1964)

The ^{19}F high resolution N.M.R. spectra of the four compounds $\text{C}_6\text{F}_{11}\text{Cl}$, $\text{C}_6\text{F}_{11}\text{Br}$, $\text{C}_6\text{F}_{10}\text{Cl}_2$ and $\text{C}_6\text{F}_{10}\text{Br}_2$ have been recorded under identical conditions, and the chemical shifts obtained compared with those of the axial and equatorial nuclei in perfluorocyclohexane. It is shown that the magnitude of the chemical shift of ^{19}F nuclei more than two bonds removed from the chlorine or bromine atoms can be accounted for satisfactorily in terms of intramolecular electric fields, provided that the structure of the molecules is that of an asymmetrically distorted chair form.

1. INTRODUCTION

It has been shown recently [1, 2] that the magnitude of the chemical shift of a ^{19}F nucleus in a fluoroaromatic compound can be predicted from the magnitude of π -electron charge densities and the resultant electric fields at the fluorine nucleus. The chemical shift may be written as a sum of two terms:

$$\delta = \delta(\text{electronic}) + \delta(\text{electric}), \quad (1)$$

where δ is the chemical shift relative to some convenient reference compound. The success achieved in calculating the chemical shift in aromatic compounds, in particular when the other substituents are halogen atoms, suggests that the chemical shifts of ^{19}F nuclei in saturated fluorocarbons should also be amenable to the same kind of treatment. $\delta(\text{electronic})$ will be zero for saturated molecules, and the chemical shift will be determined by the magnitude of $\delta(\text{electric})$; that is

$$\delta = \delta(\text{electric}) = -A\Delta E_z - B(\Delta E^2 + \Delta\langle E^2 \rangle). \quad (2)$$

In equation (2) E is the electric field at the fluorine nucleus arising from point dipoles placed at the centre of any polar bonds in the molecule, and E_z is the component of this field acting along the bond direction $\text{C} \rightarrow \text{F}$. $\langle E^2 \rangle$ is the time-averaged square of the electric fields produced by fluctuating dipoles in the bonds, and is given approximately by [3]:

$$\langle E^2 \rangle = \sum_i 3P_i I_i / r_i^6, \quad (3)$$

where P_i is the polarizability of the electron group, I_i is the first ionization potential, and r_i is the distance separating the fluorine atom from the electron group. The values of r_i and P_i are taken to be those of electrons in bonds rather than atomic properties [1, 2]. The symbols Δ in equation (2) indicate that the quantities are relative to a fluorine nucleus in a reference compound. The constants A and B have been shown to have the values $B = (15 - 45) \times 10^{-18}$ e.s.u. and

$$A \sim -10 \times 10^{-12} \text{ e.s.u. [4, 5].}$$

Compounds with single atom substituents, that is Cl, Br, I and H, are the simplest type with which to test the validity of equation (2), and the ^{19}F chemical shifts in a number of series of such fluorinated aliphatic compounds have been measured; for example CF_3X , $\text{C}_2\text{F}_5\text{X}$, *n* $\text{C}_3\text{F}_7\text{X}$ and *iso* $\text{C}_3\text{F}_7\text{X}$ [6]. However, these compounds are unsuitable for testing equation (2). In the case of CF_3X compounds the ^{19}F chemical shifts will be determined by the inductive effect of X as well as the electric fields; moreover, the point-dipole approximation used in all the electric field calculations is invalid for the short distances involved in such molecules. The other series do contain fluorine nuclei sufficiently distant from X for the inductive effect to be small, but in each case the N.M.R. spectra of samples at temperatures accessible in this laboratory ($\sim -100^\circ\text{C}$ to 200°C) are of mixtures of rapidly interconverting isomers whose relative abundancies are unknown. For the application of equation (2) it is necessary to know the precise geometry of the molecule, and for this reason the most suitable compounds to study are cyclic aliphatic fluorocarbons. The compounds chosen for this investigation are the cyclohexanes $\text{C}_6\text{F}_{11}\text{Cl}$, $\text{C}_6\text{F}_{11}\text{Br}$, $\text{C}_6\text{F}_{10}\text{Cl}_2$ and $\text{C}_6\text{F}_{10}\text{Br}_2$, which were available or could be easily prepared.

2. EXPERIMENTAL

The four compounds available were $\text{C}_6\text{F}_{11}\text{Cl}$, $\text{C}_6\text{F}_{11}\text{Br}$, $\text{C}_6\text{F}_{10}\text{Cl}_2$ and $\text{C}_6\text{F}_{10}\text{Br}_2$. The two undecafluorocyclohexanes were obtained from Dr. R. D. Chambers of this laboratory, and used without further purification. The two decafluorocyclohexanes were prepared by ultra-violet irradiation of decafluorocyclohexene in the presence of halogen, and were shown by gas phase chromatography to contain less than 5 per cent impurity after re-distillation. The N.M.R. spectra were recorded on an A.E.I. R.S.2 spectrometer operating at 60 Mc/s.

For an accurate test of the validity of equation (2) it is necessary to know the chemical shifts of the fluorine nuclei in isolated molecules, and this could be attained by measuring the spectra of gaseous samples at low pressure. However, the compounds under investigation have an N.M.R. spectrum whose component peaks are very broad and show a poor signal to noise ratio, consequently it was necessary to study the spectra of solutions of these compounds. The effect of a solvent on the chemical shift of a fluorine nucleus is determined almost entirely by intermolecular dispersion forces, and for similar compounds should show the same dependence on concentration; therefore, it should be adequate to compare ^{19}F shifts measured at the same dilution in the same solvent and relative to a common internal reference sample [7, 8]. The aim of the present investigation is to compare the chemical shifts of axial and equatorial ^{19}F nuclei in substituted fluorocyclohexanes with the corresponding shifts in perfluorocyclohexane, C_6F_{12} , so that it would be convenient to use C_6F_{12} as an internal reference compound. However, C_6F_{12} is difficult to handle and a poor solvent for studies at low temperatures, consequently, a secondary standard CFCl_3 , which also served as solvent, was used. The spectrum of a 0.7 M solution of perfluorocyclohexane in CFCl_3 and trifluoromethyl benzene at -66°C shows an AB quartet with chemical shifts relative to CFCl_3 of 12.4.24 p.p.m. (axial) and 14.2.44 (equatorial) [9]; the spectrum at room temperature consists of a single, broad peak with a chemical shift of 133.23 ± 0.01 p.p.m. from CFCl_3 , and it was confirmed that this value is unchanged for a 20 per cent v/v solution of C_6F_{12} in trichlorofluoromethane. The N.M.R. spectra of 20 per cent (v/v) solutions in CFCl_3 were recorded, and the

Solvent	Concentration of $C_6F_{11}Cl$ v/v per cent	Line positions in cycles sec^{-1} relative to $CFCl_3$									
		1	2	3	4	5	6	7	8	9	10
$CFCl_3$	90	6744	7036	7254	7539	7993	8163	8280	8382	8454	8673
$CFCl_3$	20	6766	7057	7267	7532	8000	8175	8279	8386	8457	8671
Acetone	10	6734	7019	7228	7513	7964	8138	8244	8353	8423	8637
CH_3OH	10	6722	7015	7225	7506	7967	8149	8253	8353	8426	8648
Cyclohexane	10	6769	7060	7273	7554	8004	8185	8289	8394	8469	8681

Table 1. Line positions in the ^{19}F spectrum of $C_6F_{11}Cl$ in different solvents relative to an internal sample of $CFCl_3$.

results referred to perfluorocyclohexane. In order to check that a large solvent effect from some unsuspected interaction was not present in these compounds, the spectrum of $C_6F_{11}Cl$ was recorded at low dilution, ~ 10 per cent (v/v), in a number of solvents with 10 per cent $CFCl_3$ as reference compound, and the results are shown in table 1 together with the line positions in a 90 per cent (v/v) solution in $CFCl_3$. The results show that the variation in line positions between different solvents is at most 40 cycles sec^{-1} , and that the effect of diluting with $CFCl_3$ is to change the line positions by no more than 20 cycles sec^{-1} . Sufficient quantities of each compound were not available for any extensive dilution experiments, and it was assumed that recording spectra as 20 per cent (v/v) solutions in $CFCl_3$ would give rise to an error of not more than 10 cycles sec^{-1} .

The spectra of the four compounds at room temperature are shown in the figure, and it will be noticed that the individual peaks are broad, having a width at half height of approximately 70 cycles sec^{-1} . Because of this the line positions were recorded by placing an audio-frequency sideband of the $CFCl_3$ signal on each side of each peak and separated by 200 cycles sec^{-1} . At least five spectra were recorded for each compound and the standard deviations of the mean line positions was approximately 5 cycles sec^{-1} . Table 2 shows the mean line positions, together with relative intensities obtained by measuring the area under each peak.

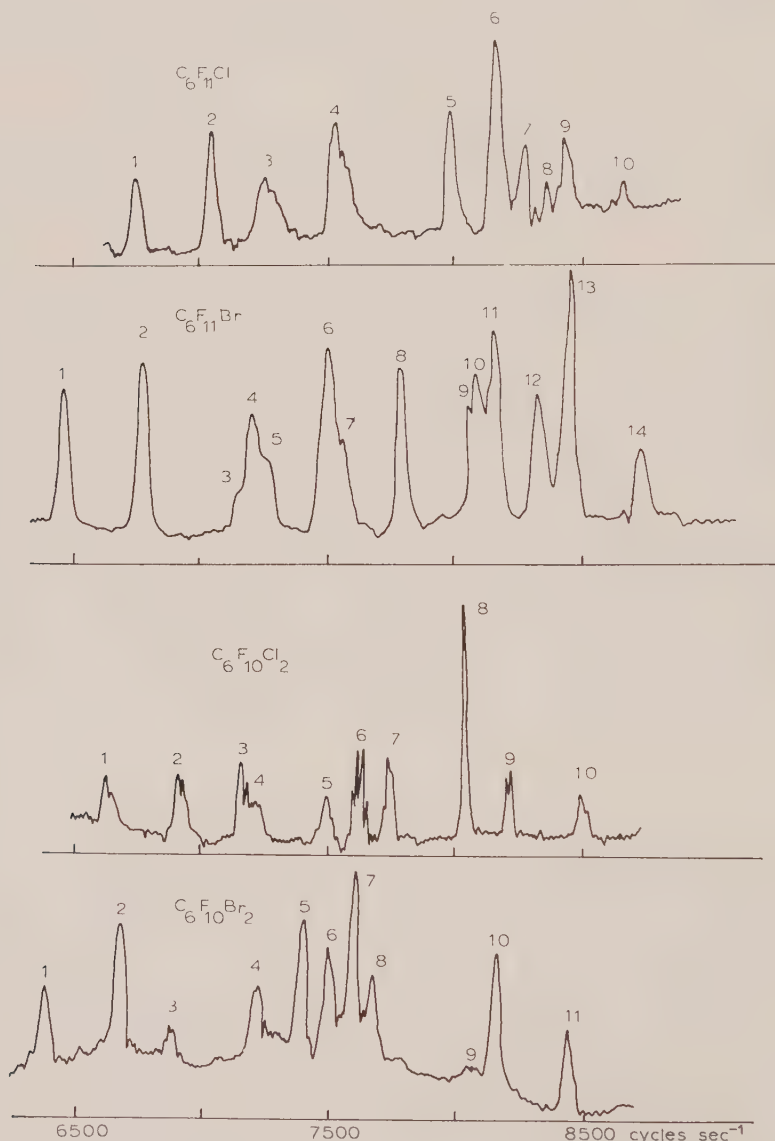
3. N.M.R. RESULTS

3.1. Undecafluoromonochlorocyclohexane. $C_6F_{11}Cl$

The ^{19}F N.M.R. spectrum of this compound has been recorded previously at 40 Mc/s by Feeney and Sutcliffe [10], who used the pure liquid and measured line positions relative to an external sample of trifluoroacetic acid. It was decided to re-examine this compound as a 20 per cent (v/v) solution in $CFCl_3$ so that a comparison could be made with perfluorocyclohexane. Feeney and Sutcliffe showed that the spectrum did not change over the temperature range $-29^\circ C$ to $+80^\circ C$, and so rejected the possibility that the molecule is interconverting at a fast enough rate to give an averaged N.M.R. spectrum. They concluded that the molecule exists as a fixed conformation with the chlorine atom in an equatorial position [10, 11]. We have confirmed that no substantial changes in the spectrum occur in the wider temperature range of $-100^\circ C$ to $+100^\circ C$. The spectrum recorded at room temperature, shown in the figure, contains ten peaks compared with the

nine peaks observed at 40 Mc/s by Feeney and Sutcliffe; the additional peak arises from increased chemical shifts at higher frequency.

The ^{19}F spectrum of a $\text{C}_6\text{F}_{11}\text{X}$ compound should show three sets of AB quartets arising from the three different types of $-\text{CF}_2-$ group, and a single peak from the fluorine on the same carbon atom as X, that is, thirteen peaks in all. The spectrum of $\text{C}_6\text{F}_{11}\text{Cl}$ contains only ten peaks, so that there must be some overlap, making an assignment to individual AB quartets more difficult. However, a trial assignment can be checked in two ways; firstly by noting that the value of the coupling constant between two fluorine nuclei on the same carbon atom, $J_{\text{FF}}(\text{geminal})$, is



The ^{19}F N.M.R. spectra of 20 per cent v/v solutions in CFCl_3 of $\text{C}_6\text{F}_{11}\text{Cl}$, $\text{C}_6\text{F}_{11}\text{Br}$, $\text{C}_6\text{F}_{10}\text{Cl}_2$ and $\text{C}_6\text{F}_{10}\text{Br}_2$.


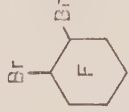
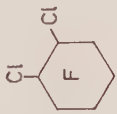
Compound	Peak	Shift from CFCl_3 (cycles sec ⁻¹)	Relative intensity	Compound	Peak	Shift from CFCl_3 (cycles sec ⁻¹)	Relative intensity	
	1	6766	2.0		1	6501	2.0	
	2	7057			2	6787		
	3	7267	3.0		3	7153	3.5	
	4	7532			4	7209		
	5	8000	1.2		5	7266	1.3	
	6	8175	2.2		6	7495		
	7	8279	0.8		7	7548	2.5	
	8	8386	0.6		8	7780		
	9	8457	0.8		9	8037	1.0	
	10	8671	0.4		10	8071		
	1	6648	2.0		11	8131	1.5	
	2	6932			12	8307		
	3	7143	2.0		13	8410	1.5	
	4	7220			14	8698		
	5	7495	1.5		1	6381	2.0	
	6	7627	1.2		2	6675		
	7	7742	2.8		3	6867	0.25	
	8	8036	2.0		4	7204		
	9	8215			5	7378	2.0	
	10	8488			6	7482		

Table 2. Line positions in the ^{19}F spectra of 20 per cent v/v solutions in CFCl_3 of $\text{C}_6\text{F}_{11}\text{Cl}$, $\text{C}_6\text{F}_{11}\text{Br}$, $\text{C}_6\text{F}_{10}\text{Cl}_2$ and $\text{C}_6\text{F}_{10}\text{Br}_2$ at room temperature. Positive shifts are to high field of the reference.

Solvent	Concentration $C_6F_{11}Cl$ v/v per cent	Peak separations $\Delta(i-j) = J_{FF}$ in cycles sec^{-1}				
		$\Delta(1-2)$	$\Delta(3-4)$	$\Delta(5-7)$	$\Delta(6-9)$	$\Delta(8-10)$
$CFCI_3$	90	292	285	287	291	291
$CFCI_3$	20	291	265	278	282	285
Acetone	10	285	284	279	284	284
CH_3OH	10	293	281	287	276	295
Cyclohexane	10	291	281	284	284	287

Table 3. Geminal F-F coupling constants J_{FF} for $C_6F_{11}Cl$ in different solvents.

Solvent	Concentration C ₆ F ₁₁ Cl v/v per cent	δ _{ijkl} cycles sec ⁻¹			φ _{ij} cycles sec ⁻¹					
		δ _{1, 2, 5, 7}	δ _{3, 4, 6, 9}	δ _{3, 4, 8, 10}	φ _{1, 2}	φ _{5, 7}	φ _{3, 4 (6, 9)}	φ _{6, 9}	φ _{3, 4 (8, 10)}	φ _{8, 10}
CFCI ₃	90	1215	866	1094	6907	8122	7418	8284	7414	8507
CFCI ₃	20	1194	874	1095	6932	8125	7417	8291	7412	8507
Acetone	10	1195	864	1088	6895	8088	7393	8258	7389	8477
CH ₃ OH	10	1207	879	1098	6888	8095	7388	8267	7380	8479
Cyclohexane	10	1198	868	1088	6933	8131	7435	8304	7430	8518

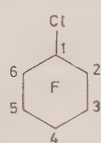
Table 4. Chemical shifts of ^{19}F nuclei in $C_6F_{11}Cl$ in different solvents. δ_{ijkl} is the chemical shift between geminal fluorine nuclei, and derived from the AB quartet $ijkl$. ϕ_{ij} is the chemical shift of each ^{19}F nucleus referred to $CFCl_3$.

of the order of 270–300 cycles sec^{-1} , and secondly by a closer examination of the data in table 1 on the spectrum of $\text{C}_6\text{F}_{11}\text{Cl}$ in different solvents. The value of $J_{\text{FF}}(\text{geminal})$ will remain unchanged by solvents, so that the separation of both the A and B doublets in each AB quartet will be independent of solvent, even though the chemical shifts of A and B may change considerably. On this basis, and using their relative intensities, the following peaks were assigned to AB quartets:

- (1) 1, 2, 5, 7 overall intensity \equiv 4 fluorines,
- (2) 3, 4, 6, 9 overall intensity \equiv 4 fluorines,
- (3) 3, 4, 8, 10 overall intensity \equiv 2 fluorines,

with peak 6 also containing the peak arising from the fluorine on the same carbon atom as chlorine. The values of the coupling constants and internal chemical shifts in different solvents are given in tables 3 and 4 respectively, and these results show the above assignment to be correct, for, although the shifts relative to CFCl_3 vary by amounts of up to 45 cycles sec^{-1} , the values of $J_{\text{FF}}(\text{geminal})$ and δ_{ijk} remain constant with the standard deviation of 5 cycles sec^{-1} .

Assuming that substitution of fluorine by chlorine affects the chemical shifts of neighbouring nuclei more than distant ones, and that axial fluorines resonate at lower fields than equatorial fluorine nuclei [9], then the most probable allocation of chemical shifts ϕ_{ij} to positions of fluorine nuclei is:



Position of ^{19}F nucleus	Chemical shift relative to CFCl_3 (cycles sec^{-1})
2 and 6 axial	$\phi_{1,2} = 6932$
2 and 6 equatorial	$\phi_{5,7} = 8125$
3 and 5 axial	$\phi_{3,4(6,9)} = 7417$
3 and 5 equatorial	$\phi_{6,7} = 8291$
4 axial	$\phi_{3,4(8,10)} = 7412$
4 equatorial	$\phi_{8,10} = 8507$
1 axial	8175

3.2. Undecafluoromonobromocyclohexane. $\text{C}_6\text{F}_{11}\text{Br}$

The ^{19}F N.M.R. spectrum of a 20 per cent (v/v) solution in CFCl_3 was recorded at -100°C , $+100^\circ\text{C}$ and at room temperature. There was no significant difference between the three spectra, so that the spectrum obtained at room temperature can be taken to be that of a single fixed conformational isomer, most probably with bromine in an equatorial position. The recorded spectrum contains fourteen resolved lines, but the eleven fluorines in $\text{C}_6\text{F}_{11}\text{Br}$ should give rise to a maximum of thirteen peaks, so that at least one peak must originate from an impurity. The lines were assigned to AB quartets on the basis of the magnitude of $J_{\text{FF}}(\text{geminal})$, the relative intensities of the peaks, and the magnitude of the chemical shifts. In this way the most probable assignment of peaks to AB quartets is:

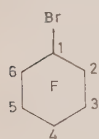
- (1) 1, 2, 8, 10,
- (2) 4, 6, 11, 13,
- (3) 5, 7, 13, 14,

and of the three remaining peaks, 12 was assigned to the fluorine on the same carbon

atom as the bromine, and 3 and 9 were attributed to an impurity. The latter peaks do not have companion peaks at a distance of ~ 290 cycles sec^{-1} , and so are unlikely to be components of AB quartets. The coupling constant J_{ij} and chemical shifts δ_{ijkl} are calculated to be:

- (1) $J_{1,2}=286$, $J_{8,10}=291$, $\delta_{1,2,8,10}=1246$ cycles sec^{-1} .
- (2) $J_{4,6}=285$, $J_{11,13}=279$, $\delta_{4,6,11,13}=877$ cycles sec^{-1} .
- (3) $J_{5,7}=273$, $J_{13,14}=288$, $\delta_{5,7,13,14}=1109$ cycles sec^{-1} .

Making the same assumptions as in the case of $\text{C}_6\text{F}_{11}\text{Cl}$, the assignment of chemical shifts ϕ_{ij} , relative to CFCl_3 , of fluorine nuclei in $\text{C}_6\text{F}_{11}\text{Br}$ is:



Position of ^{19}F nucleus	Chemical shift relative to CFCl_3 (cycles sec^{-1})
2 and 6 axial	$\phi_{1,2} = 6661$
2 and 6 equatorial	$\phi_{8,10} = 7907$
3 and 5 axial	$\phi_{4,6} = 7374$
3 and 5 equatorial	$\phi_{11,13} = 8251$
4 axial	$\phi_{5,7} = 7424$
4 equatorial	$\phi_{13,14} = 8534$
1 axial	8307

3.3. 1,2 *dichloro decafluorocyclohexane*. $\text{C}_6\text{F}_{10}\text{Cl}_2$

The ^{19}F spectrum of this compound may arise from a number of possible isomeric forms, and the maximum number of lines which each isomeric form can produce is as follows:

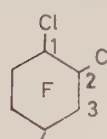
- | | |
|---|-----------|
| (a) both Cl atoms in equatorial positions | 9 peaks, |
| (b) both Cl atoms in axial positions | 9 peaks, |
| (c) interconversion between (a) and (b) | 9 peaks, |
| (d) position 1 axial, position 2 equatorial | 18 peaks, |
| (e) position 1 equatorial, position 2 axial | 18 peaks, |
| (f) interconversion between (d) and (e) | 9 peaks. |

Possibilities (c) and (f) may be eliminated, because the spectrum showed no substantial change over the temperature range -100°C to $+100^\circ\text{C}$. The spectrum recorded at room temperature shows ten peaks, two of which (6 and 3) can be attributed to impurities since they do not lie ~ 290 cycles sec^{-1} from other peaks in the spectrum and do not form part of an AB quartet. This leaves eight peaks, which reduces the possible structures to (a) or (b), with (a) the more probable on steric grounds. The most probable assignment of peaks to AB quartets with the coupling constants J_{ij} and chemical shifts δ_{ijkl} are:

- (1) 1, 2, 7, 8 $J_{1,2}=283$, $J_{7,8}=295$, $\delta_{1,2,7,8}=1058$ cycles sec^{-1} .
- (2) 4, 5, 9, 10 $J_{4,5}=275$, $J_{9,10}=273$, $\delta_{4,5,9,10}=955$ cycles sec^{-1} .

The fluorines on the same carbon atoms as chlorine give rise to part of peak 8.

The assignment of chemical shifts to fluorine nuclei in the molecule $C_6F_{10}Cl_2$ is on the same basis as in $C_6F_{11}Cl$ and $C_6F_{11}Br$, and is:

	Position of fluorine	Chemical shift relative to
		$CFCl_3$ (cycles sec^{-1})
	3 and 6 axial	$\phi_{1,2} = 6808$
	3 and 6 equatorial	$\phi_{7,8} = 7858$
	4 and 5 axial	$\phi_{4,5} = 7377$
	4 and 5 equatorial	$\phi_{9,10} = 8332$
	1 and 2 axial	8036

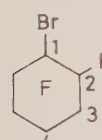
3.4. 1,2 dibromo decafluorocyclohexane. $C_6F_{10}Br_2$

The ^{19}F N.M.R. spectrum of $C_6F_{10}Br_2$ does not change substantially over the temperature range $-100^\circ C$ to $+100^\circ C$, so that the spectrum recorded at room temperature can be taken to be that of the fixed isomer with both bromines in equatorial positions. The spectrum contains eleven peaks of which two (3 and 9) arise from an impurity. The remaining nine peaks can be assigned to two AB quartets and a single peak from the two fluorine nuclei which are in $-CF-Br$ groups, as follows:

$$(1) \ 1, 2, 5, 8 \quad J_{1,2} = 294, \ J_{5,8} = 278, \ \delta_{1,2,5,8} = 989 \text{ cycles } sec^{-1}.$$

$$(2) \ 4, 6, 10, 11 \quad J_{4,6} = 277, \ J_{10,11} = 274, \ \delta_{4,6,10,11} = 896 \text{ cycles } sec^{-1}.$$

The assignment of chemical shifts to fluorine nuclei is on the same basis as in the preceding examples, and is given below:

	Position of ^{19}F nucleus	Chemical shift relative to
		$CFCl_3$ (cycles sec^{-1})
	3 and 6 axial	$\phi_{1,2} = 6557$
	3 and 6 equatorial	$\phi_{5,8} = 7496$
	4 and 5 axial	$\phi_{4,6} = 7364$
	4 and 5 equatorial	$\phi_{10,11} = 8261$
	1 and 2 axial	7591.

4. DISCUSSION

The structures of these compounds have not been determined experimentally, but it may be assumed that they have structures which approximate to the symmetrical chair form adopted by cyclohexane. The magnitudes of the electric field components E_z , E^2 and $\langle E^2 \rangle$ were calculated assuming symmetrical chair structures with C-C bond lengths and angles as in cyclohexane, and values of C-Cl, C-F and C-Br bond lengths taken as the average values in aliphatic compounds. The various vector quantities and internuclear distances were calculated by placing the molecules in the coordinate system suggested by Corey and Sheen [12]. The changes in electric fields arising from replacement of a fluorine by chlorine or bromine in an equatorial position were calculated by assuming that each C-F, C-Cl or C-Br bond contained a point dipole at the bond centre and acting in the bond direction, with carbon as the positive pole. The molecular parameters used in these calculations are given in table 5.

X	r_{C-X} [13] (Å)	μ_{C-X} [14] (Debye)	P_{C-X} [15] ($\times 10^{24}$ cm ³)	I_{C-X} [16] ($\times 10^{12}$ ergs)
F	1.32	1.40	0.683	28.5
Cl	1.80	1.55	2.508	20.8
Br	1.94	1.56	3.567	18.8
C	1.55	0	0.579	18.03

Table 5. The molecular parameters used in calculating electric fields in fluorocyclohexanes

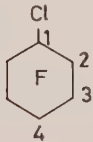
¹⁹ F nucleus	$\Delta E_z \times 10^{-6}$ e.s.u.	$\Delta E^2 \times 10^{-12}$ e.s.u.
	2 axial 2 equatorial 3 axial 3 equatorial 4 axial 4 equatorial	-0.01464 -0.01464 0.00240 0.00096 0.00156 0.00050
		-0.00161 -0.00161 0.00072 0.00004 0.00038 0.00004

Table 6. Calculated values of ΔE_z and ΔE^2 for fluorine nuclei in $C_6F_{11}Cl$ relative to perfluorocyclohexane.

Because of the similarity in the values of the bond dipole moments of C-F, C-Cl and C-Br bonds, and the magnitude of the constants A and B in equation (2), it is unlikely that changes in E_z and E^2 will have an appreciable effect on the chemical shift produced by substituting these halogens in place of fluorine. This was checked by carrying out the necessary calculations in detail for $C_6F_{11}Cl$, and table 6 gives the values of ΔE_z and ΔE^2 for the fluorine nuclei in this molecule relative to the axial and equatorial positions in perfluorocyclohexane. The results show that changes in E_z and E^2 should give rise to chemical shifts of no more than 0.2 p.p.m. consequently these terms have been neglected in the rest of the calculations. The changes in chemical shifts which are observed when fluorine is replaced by chlorine or bromine must arise from changes in the magnitude of $\langle E^2 \rangle$, the time-averaged square electric field, so that δ , the chemical shift relative to perfluorocyclohexane is given by:

$$\delta = -B \cdot \Delta \langle E^2 \rangle. \quad (4)$$

Table 7 gives the calculated values of $\Delta \langle E^2 \rangle$ for the fluorine nuclei in the four compounds studied, together with the observed shifts referred to the same position, axial or equatorial, in perfluorocyclohexane.

The first point to be noted from the data in table 7 and the form of equation (4) is that the chemical shifts produced by replacing an equatorial fluorine in position 1 should be equal at both axial and equatorial fluorine nuclei in positions 2 and 6, whereas, for both the chloro and bromo derivatives the axial and equatorial fluorine nuclei at these positions have different chemical shifts relative to C_6F_{12} . This discrepancy could be explained by assuming that the value of the constant B was different for the two fluorines, but this is not very probable because B depends upon the nature of the C-F bond which is identical for axial and equatorial positions

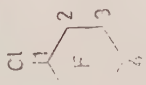
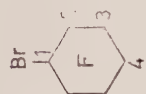
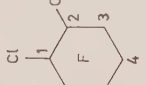
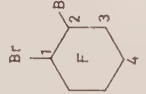
¹⁹ F nucleus	$\Delta\langle E^2 \rangle$ $\times 10^{-12}$ e.s.u.	Chemical shift p.p.m.		¹⁹ F nucleus	$\Delta\langle E^2 \rangle$ $\times 10^{-12}$ e.s.u.	Chemical shift p.p.m.	
		Calculated	Observed			Calculated	Observed
 Cl 2 3 F 4 5 6	2 ax.	7.86	8.72	 Br 1 2 F 3 4 5 6	-0.31557	11.95	13.23
	2 eq.	7.86	7.02		-0.43469	11.95	10.67
	3 ax.	0.67	0.63		-0.43469	1.09	1.33
	3 eq.	0.28	4.25		-0.03965	0.45	4.92
	4 ax.	0.44	0.72		-0.01642	0.66	0.50
	4 eq.	0.12	0.65		-0.02415	0.19	0.21
	1 ax.		-12.02		-0.00678		
 Cl 1 2 F 3 4 5 6	1,2 ax.	8.53	-9.70	 Br 1 2 F 3 4 5 6	-0.34251	13.03	-2.28
	3 ax.	8.14	10.78		-0.47434	12.40	14.95
	3 eq.	1.11	11.48		-0.45111	1.75	17.50
	4 ax.	0.40	1.28		-0.06380	0.64	1.50
	4 eq.		3.57		-0.02320		4.75

Table 7. The calculated values of the mean square electric field $\Delta\langle E^2 \rangle$, and the observed and calculated chemical shifts of ¹⁹F nuclei in the compounds C₆F₁₁Cl, C₆F₁₁Br, C₆F₁₀Cl₂, C₆F₁₀Br₂ relative to perfluorocyclohexane.

[1, 5]. A more likely explanation is that these molecules do not have a symmetrical chair structure so that axial and equatorial fluorines are no longer equidistant from their neighbours.

In the molecules $C_6F_{11}Cl$ and $C_6F_{11}Br$ the fluorines in the positions 2 and 6 show the largest chemical shifts relative to C_6F_{12} , and two separate values of the constant B have been calculated, one for each molecule, which when substituted into equation (4) reproduce the average shifts of the fluorines in these positions. The values of B obtained have been used to calculate the shifts of the fluorine nuclei in all other positions in both these molecules and the dichloro and dibromo derivatives of C_6F_{12} , and the results are shown in table 8. The two values of B used in these calculations are:

$$C_6F_{11}Cl \text{ and } C_6F_{10}Cl_2. \quad B = 24.92 \times 10^{-18} \text{ e.s.u.}$$

$$C_6F_{11}Br \text{ and } C_6F_{10}Br_2. \quad B = 27.48 \times 10^{-18} \text{ e.s.u.}$$

The data in table 7 show that for the two molecules $C_6F_{11}Cl$ and $C_6F_{11}Br$ there is good agreement between the observed and calculated chemical shifts, except for the discrepancy already noted, and the large difference between observed and calculated values for the positions 3 equatorial. In both molecules there is an observed shift approximately 4 p.p.m. larger than the calculated value, which could arise from a departure from the symmetrical chair structure for these molecules. Replacing an equatorial fluorine atom by either chlorine or bromine will lead to increased steric strain in the molecule, which can be relieved most easily by the equatorial fluorine atoms moving away from the larger atom in the equatorial plane. Such a distortion would increase the distances between the equatorial fluorines at positions 2 and 6 and the equatorial substituent, whilst leaving the axial fluorines at these positions relatively undisturbed. It would also decrease the distance between the equatorial fluorine at position 3 and its fluorine neighbours. The net result of all these changes would be to have unequal chemical shifts for axial and equatorial fluorines in positions 2 and 6, and to increase the downfield shift of the equatorial fluorine in position 3. A precise calculation of the shifts in such a distorted molecule is not practicable because of the large number of parameters involved, but because of the r^{-6} dependence of $\Delta\langle E^2 \rangle$, then the magnitude of the distortion necessary would be small, probably of the order of 0.2 Å.

The agreement between calculated and observed chemical shifts of the fluorine nuclei in the 1,2 dichloro and dibromo decafluorocyclohexanes is again good, except for the equatorial fluorines in the positions 3 and 4, which are 3–5 p.p.m. to low field of the calculated values. In both these equatorial positions the fluorine is in a similar position to one of the substituents as the equatorial fluorine at position 3 in the $C_6F_{11}X$ compounds, and the large shift could arise from the same sort of distortion of the molecules.

It can be concluded that equation (4) probably does describe correctly the magnitude of ^{19}F chemical shifts produced by substituting chlorine or bromine for fluorine, but that accurate structures of these compounds would have been known before any definite conclusions could be drawn. The order of magnitude of the constant B necessary to reproduce the observed chemical shifts, $(25\text{--}27) \times 10^{-18}$ e.s.u., is within the range of values determined previously [1, 2, 5, 6]. It is less than the value found for fluoroaromatic compounds of approximately $42\text{--}49 \times 10^{-18}$ e.s.u., which is to be expected of C–F bonds with less double bond

character [5]. If the molecules are distorted from the chair form, then the value of B would probably have to be increased in magnitude to explain the observed shifts.

4.1. Perfluorocyclohexane. C_6F_{12}

If the chemical shifts produced by replacing a fluorine by chlorine and bromine can be explained by the change in the magnitude of $\langle E^2 \rangle$, then the same phenomenon should explain the magnitude of the chemical shift between axial and equatorial fluorine nuclei in perfluorocyclohexane. Differences in E_z and E^2 may also be important and have been calculated, together with $\Delta\langle E^2 \rangle$. The results are:

$$\Delta E_z = 0.04848 \times 10^6 \text{ e.s.u.},$$

$$\Delta E^2 = -0.09327 \times 10^{12} \text{ e.s.u.},$$

$$\Delta\langle E^2 \rangle = -0.30327 \times 10^{12} \text{ e.s.u.};$$

in each case Δ refers to the differences (equatorial-axial). If A is assumed to be -10×10^{-12} e.s.u., the value found for C-F in CHF_3 , and B is given a value of 26.20×10^{-18} e.s.u., being the mean of the two values used in the calculations on $C_6F_{11}Cl$ and $C_6F_{11}Br$, then the shift calculated with equation (2) is:

$$\delta \text{ (equatorial-axial)} = 10.87 \text{ p.p.m.},$$

compared with the value of 18.2 p.p.m. found by Tiers [9]. The calculated value is of the correct sign, that is it predicts that the axial fluorine will resonate at lowest field, but the magnitude is too small by 7.3 p.p.m. The correct magnitude of the axial-equatorial shift can be obtained by retaining the same value of A , but increasing B to 44.89×10^{-18} e.s.u.; however, distortion from the chair form would also change the calculated value.

I am indebted to Dr. J. Hutchinson and Mr. J. Cook for preparing the samples of $C_6F_{10}Cl_2$ and $C_6F_{10}Br_2$, and to Dr. R. D. Chambers for the gift of the samples of $C_6F_{11}Cl$ and $C_6F_{11}Br$. I would also like to acknowledge the many discussions I have had on this subject with Dr. L. Phillips.

REFERENCES

- [1] BODEN, N., EMSLEY, J. W., FEENEY, J., and SUTCLIFFE, L. H., 1964, *Mol. Phys.*, **8**, 133.
- [2] BODEN, N., EMSLEY, J. W., FEENEY, J., and SUTCLIFFE, L. H., 1964, *Mol. Phys.*, **8**, 467.
- [3] BUCKINGHAM, A. D., BERNSTEIN, H. J., and RAYNES, W. T., 1963, *J. chem. Phys.*, **38**, 3481.
- [4] PETRAKIS, L., and BERNSTEIN, H. J., 1962, *J. chem. Phys.*, **37**, 2731.
- [5] PETRAKIS, L., and BERNSTEIN, H. J., 1963, *J. chem. Phys.*, **38**, 1562.
- [6] EMSLEY, J. W., FEENEY, J., and SUTCLIFFE, L. H., 1965, *High Resolution Nuclear Magnetic Resonance Spectroscopy* (Oxford: Pergamon Press).
- [7] FILIPOVITCH, G., and TIERS, G. V. D., 1959, *J. phys. Chem.*, **63**, 761.
- [8] GLICK, R. E., and EHRENSON, S. J., 1958, *J. phys. Chem.*, **62**, 1599.
- [9] TIERS, G. V. D., 1960, *Proc. chem. Soc.*, p. 389.
- [10] FEENEY, J., and SUTCLIFFE, L. H., 1960, *Trans. Faraday Soc.*, **56**, 1559.
- [11] FEENEY, J., and SUTCLIFFE, L. H., 1961, *J. phys. Chem.*, **65**, 1894.
- [12] COREY, E. J., and SNEEN, R. A., 1955, *J. Amer. chem. Soc.*, **77**, 2505.

- [13] TABLES OF INTERATOMIC DISTANCES AND CONFIGURATION IN MOLECULES AND IONS, 1958, Ed., L. E. Sutton (London: The Chemical Society).
- [14] SUTTON, L. E., 1955, *Determination of Organic Structures by Physical Methods*, Eds., E. A. Braude, and F. C. Nachod (New York: Academic Press).
- [15] LE FÈVRE, R. J. W., 1961, *Journal and Proceedings of the Royal Society of New South Wales*, **95**, 1.
- [16] LANDOLT, H. H., and BERNSTEIN, R., 1950, *Zahlenwerte und Functionen* (Berlin: Julius Springer-Verlag), I Band, I Teil.

RESEARCH NOTES

E.P.R. studies of ionic association of pyrazine negative ion and alkali metal cations

by J. dos SANTOS-VEIGA† and A. F. NEIVA-CORREIA
Laboratório de Física e Engenharia Nucleares, Sacavém, Portugal

(Received 22 March 1965)

In solutions of pyrazine negative ion obtained by alkali metal reduction Carrington and Santos-Veiga [1], McDowell *et al.* [2] and recently Atherton and Goggins [3] observed E.P.R. spectra characteristic of the interaction of the unpaired electron with the alkali metal nucleus. We resumed this type of study with the purpose of achieving a more detailed knowledge of this type of ionic association.

Special care was taken in the measurement of the metal hyperfine splitting constants namely, very slow variation of the field and a calibration in each run (recording the spectrum of tetracene positive ion [4]), so as to avoid doubt as to their changes with temperature.

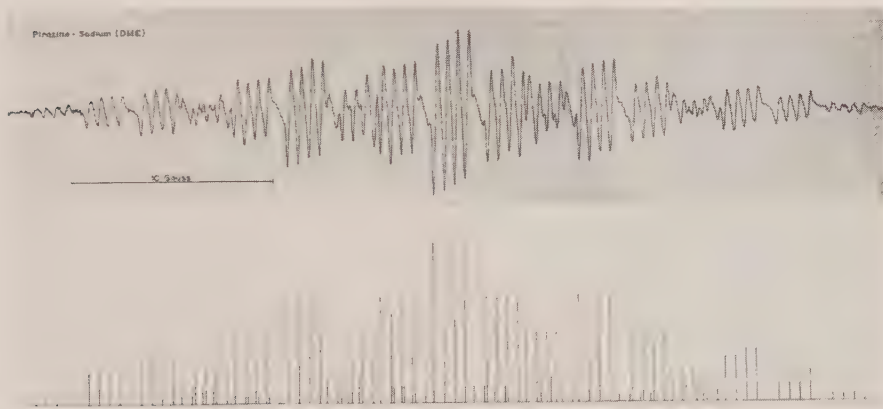


Figure 1. E.P.R. spectrum of pyrazine-sodium in DME.

We re-investigated the system pyrazine-sodium-tetrahydrofuran and found that contrary to the observations of Atherton and Goggins [3] the sodium splitting is temperature dependent with a negative coefficient. As the nitrogen and proton splittings ($a_N = 7.19$ gauss; $a_H = 2.63$ gauss) did not change with temperature within the error of ± 2 per cent we could use a_N as an internal calibration too. In the system pyrazine-sodium-1, 2-dimethoxyethane we observed the same pattern with the only difference that a_{Na} is lower by about 10 per cent. The spectrum recorded at 24°C is shown in figure 1.

We studied also the system pyrazine-potassium-1, 2-dimethoxyethane and obtained complete resolution of the spectrum showing ^{39}K splitting, thus the ions

† From the University of Coimbra, Portugal.

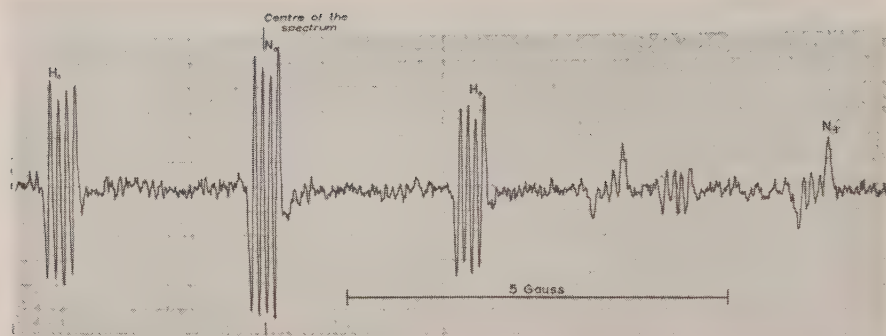


Figure 2. Central part of the E.P.R. spectrum of pyrazine-potassium in DME.

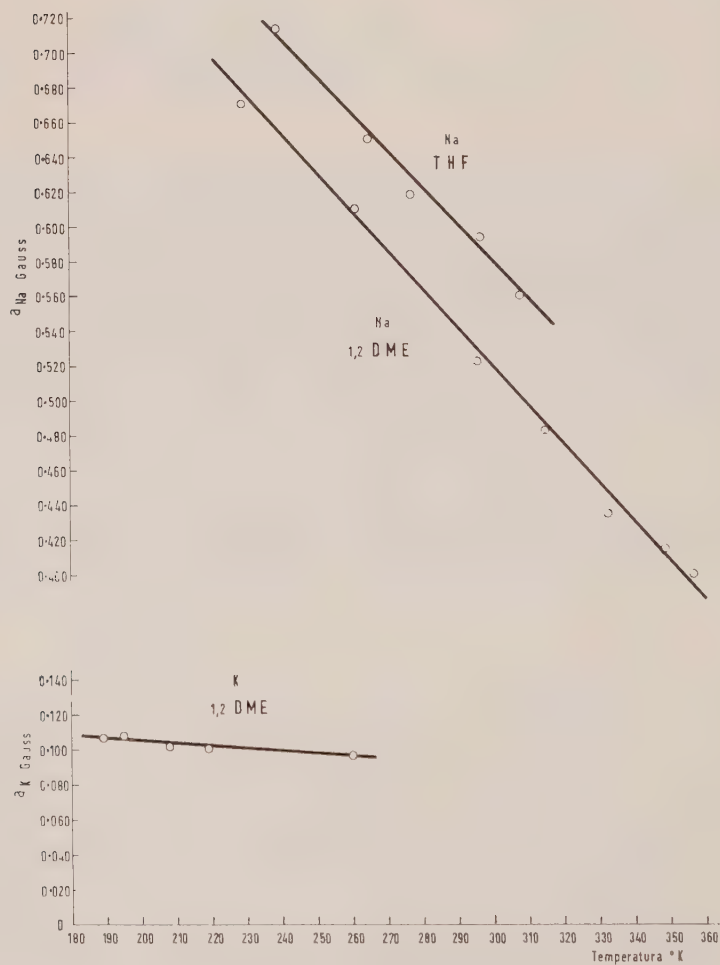


Figure 3.

are associated in pairs like pyrazine-sodium. The central part of this spectrum (recorded at -58°C) is shown in figure 2.

Noting that the groups of lines marked H_0 and N_{-1} should have the same intensity, the alternation of line width reported by Atherton and Goggins [3] is clearly observed. The widening only affects the groups for which the combined spin of the two ^{14}N nuclei is odd. This agrees with an intramolecular exchange as described by de Boer and Mackor [5] in which the potassium ion migrates back and forth between the two nitrogen atoms modifying alternately the unpaired electron density of these positions and so causing a time dependent modulation of a_N . The negative temperature dependence of a_K is less marked than that of a_{Na} .

The metal splittings for the three systems are plotted as a function of temperature in figure 3. Positive temperature dependence was described by Atherton and Weissman [6] for naphthalene-sodium and by de Boer and Mackor [5] for pyracene-sodium and explained by assuming that the cation resides near the nodal plane of the lowest antibonding π orbital and that as the temperature increases it stays longer in regions of higher spin density. Nishiguchi *et al.* [7] reported negative temperature dependence for the system biphenyl-potassium. Noting that as the lowest antibonding π orbital of biphenyl has no nodal plane between the 1 and 1' or 2 and 3 carbon positions they suggest that when temperature decreases the cation approaches a position near the 1-1' or the 2-3 bond thus increasing a_K . We interpret the negative dependence observed in the pyrazine systems in a similar way. As can be inferred from the linewidth alternation effect the alkali cation moves near a bisecting plane containing the two nitrogen atoms because of their net negative charge. The lowest antibonding π orbital is symmetrical about this plane and the spin density is highest near the nitrogen atoms. At lower temperatures the cation stays longer near these and gives a higher splitting constant; as the temperature increases the cation spends more time at the intermediate positions where the unpaired electron density is lower.

The offer of the E.P.R. spectrometer to the LFEN by the International Atomic Energy Agency is thankfully acknowledged: and we thank Mr. J. Furtado Coelho for many useful discussions.

REFERENCES

- [1] CARRINGTON, A., and DOS SANTOS-VEIGA, J., 1962, *Mol. Phys.*, **5**, 21.
- [2] McDOWELL, C. A., PAULUS, K. F., and ROWLANDS, J. R., 1962, *Proc. chem. Soc.*, p. 60.
- [3] ATHERTON, N. M., and GOGGINS, A. E., 1964, *Mol. Phys.*, **8**, 98.
- [4] HYDE, J. S., and BROWN, H. W., 1962, *J. chem. Phys.*, **37**, 368.
- [5] DE BOER, E., and MACKOR, E., 1964, *J. Amer. chem. Soc.*, **86**, 1513.
- [6] ATHERTON, N. M., and WEISSMAN, S. I., 1961, *J. Amer. chem. Soc.*, **83**, 1330.
- [7] NISHIGUCHI, H., NAKAI, Y., NAKAMURA, K., ISHIZU, K., DEGUCHI, Y., and TAKAKI, H., 1964, *J. chem. Phys.*, **40**, 241.

Note on the paper
“Proton spin-lattice relaxation in aqueous ionic solutions”

by Jones and Powles†

by BURTON P. FABRICAND

Hudson Laboratories of Columbia University
Dobbs Ferry, New York

(Received 19 March 1965)

In a paper by Jones and Powles [1] it is claimed that the effect of the solute on the proton spin-lattice relaxation times in ionic solutions is not linear with concentration for concentrations above $\frac{1}{4}N$ contrary to conclusions reached by Hertz [2] and Fabricand *et al.* [3]. The data on which this claim is based are shown in figure 1 of reference [1]. I should like to point out that even with the data points shown, the curve labelled $MgCl_2$ is easily fitted by a straight line up to a concentration of $1N$, and the curves labelled $NaCl$ and $RbCl$ are easily fitted by a straight line up to a concentration of $2N$. Only the curve labelled KCl is badly fitted by a straight line. However, let us consider the errors in measurement stated in reference [1]. There is a ± 2 per cent error in the relaxation time measurement which leads to an error of $\pm 0.006 \text{ sec}^{-1}$ in the reciprocal relaxation time, and there is a temperature error of $\pm \frac{1}{2}^\circ C$ which leads to an error of $\pm 0.002 \text{ sec}^{-1}$, using the data on temperature variation presented in figure 2 of reference [1]. Taking the square root of the sum of the squares of these errors, I find an error in each individual data point of figure 1 of $\pm 0.006 \text{ sec}^{-1}$, which amounts to three times the diameter of each data point in that figure. With this error, the curve labelled KCl is now easily fitted by a straight line up to $2N$. The claim of non-linearity in the data is certainly not warranted by these results.

The $RbCl$ curve in figure 1 of reference [1] is in sharp disagreement with the results reported in references [2] and [3], where this curve lies under the KCl curve. It is possible that unknown transition metal impurities in the samples of reference [1] contributed to these measurements. A concentration of only one part per million of this type of impurity will cause about a 4 per cent error in a relaxation time measurement. All samples used in reference [3] were analysed to better than one part in ten million by the powerful analytical technique of atomic absorption spectroscopy [4].

Two further points should be mentioned. In our laboratory, we found it necessary to control sample temperatures to much better than $\frac{1}{2}^\circ C$ to get reproducible results when measuring the very small deviations of proton relaxation times

† This work was supported by the Office of Naval Research under Contract Nonr-266(84). Reproduction in whole or in part is permitted for any purpose of the United States Government. Hudson Laboratories of Columbia University Contribution No. 215.

in solution from those in pure water, especially at low concentrations. Our apparatus controls the temperature to 0.01°C . Secondly, we feel that concentrations should be measured by molality rather than normality, since the main interest in this work is in the fraction of water molecules near ions and the fraction not near ions. If the data of reference [1] were plotted using molality, the curves would appear even more linear.

REFERENCES

- [1] JONES, G. T., and POWLES, J. G., 1964, *Mol. Phys.*, **8**, 607.
- [2] HERTZ, H. G., 1963, *Berichte der Bunsengesellschaft*, **67**, 311.
- [3] FABRICAND, B. P., GOLDBERG, S. S., LEIFER, R., and UNGAR, S. G., 1964, *Mol. Phys.*, **7**, 425.
- [4] FABRICAND, B. P., SAWYER, R. R., UNGAR, S. G., and ADLER, S., 1962, *Geochim. et cosmoch. Acta*, **26**, 1023.

The angular overlap model, an attempt to revive the ligand field approaches

by CLAUS E. SCHÄFFER

Chemistry Department I (Inorganic Chemistry), University of Copenhagen,
H. C. Ørsted Institute, Universitetsparken 5, Copenhagen Ø, Denmark

and CHR. KLIXBÜLL JØRGENSEN

Cyanamid European Research Institute, Cologny (Geneva) Switzerland

(Received 12 October 1964)

A general method for the calculation of orbital energy differences within a partially filled l -shell of a central ion in an inorganic chromophore is described. The angular overlap model covers σ , π and δ anti-bonding (as well as bonding) effects, and it is shown that the consequence of the model is identical with that of a singular contact term potential acting close to each ligand nucleus. Because of this the model can also treat chromophores containing different ligands, each new ligand contributing one σ and one π (and one δ) radial parameter. In this way fewer parameters are involved than in usual ligand field approaches.

Selected symmetries of chromophores, cubic, pentagonal, tetragonal, and trigonal, are used to illustrate the applications of the model.

1. INTRODUCTION

The orbital energy differences in an inorganic chromophore MX_N between the orbitals of a partially filled l -shell were recently estimated by Jørgensen *et al.* [1]. These authors proposed and used a model somewhat analogous to that of Wolfsberg and Helmholz [2], a model in which the anti-bonding energy effect upon a given symmetry-adapted combination of l -orbitals is supposed to be proportional to the square of the group overlap integral, S_{MX} , between that central ion orbital and a corresponding symmetry-adapted linear combination of σ -orbitals. If the ligands are identical and at equal distances from the central ion, the anti-bonding energy is approximately expressed ([3], p. 93) as:

$$\Xi^2 \cdot \sigma^* = H_X^2 \cdot S_{MX}^2 / (H_M - H_X), \quad (1)$$

provided the diagonal element of one electron energy, H_X , of the σ -orbitals is much more negative than the energy, H_M , of the l -orbitals considered ($0 > H_M \gg H_X$). S_{MX} is written as a coefficient, Ξ , times the similar group overlap integral, S_{MX}^* , in which an s -function has been used instead of the angular part of the l -orbital. Because σ^* is the same for different γ_n orbitals (corresponding to the same l -shell) the anti-bonding energies of these orbitals will be proportional to the Ξ^2 -values of each particular γ_n .

In this paper, we shall define in more general terms the quantity, Ξ , and introduce the symbols, Ξ_σ , Ξ_π and Ξ_δ , to take into account the effect of σ , π and δ -bonding; Ξ_σ corresponds to Ξ of [1]. Furthermore, we shall define the

contact term potentials V_λ ($\lambda = \pi$ and $\lambda = \delta$), each consisting of two terms, which together with V_σ (V_{sing} of [1]) make up five contact terms in all. Finally, we shall show that the appropriate matrix elements of these potentials are identical with the energies obtained from the Ξ^2 -method.

The matrix elements consist of additive contributions from each ligand, a result which makes the model applicable also to complexes in which the ligands, and thus the σ^* -values, are different.

The general model taking account of σ , π and δ -anti-bonding as well as bonding effects is used to show that, if corresponding radial parameters are identical in a tetrahedral and an octahedral complex, the d -orbital set will split in the tetrahedral complex $-\frac{4}{9}$ times as much as in the corresponding octahedral complex. This is the same result as that of the electrostatic model [4]. It is shown for other cubic cases that there exist similar relations to the octahedral splitting, a subject which has been treated also by Schmidtke [5].

Finally a few cases of lower symmetry are discussed briefly.

2. THE ANGULAR OVERLAP MODEL

As the first approximation of the angular overlap model, the central ion l -orbital is written† as a product of an angular and a radial function. As a consequence of this, the overlap integral, S_{MX} , between the l -orbital and a ligand orbital is likewise factorized so that:

$$S_{MX} = \Xi \cdot S_{MX}^*, \quad (2)$$

where Ξ is a coefficient accounting for the influence of the angular function of the central ion. We shall attach to it two sub-indices λ and ω , λ indicating whether we are concerned with a σ , π or δ overlap, and ω specifying the particular orbital (for $\lambda > 0$) of the not necessarily degenerate set. Furthermore, we shall specify the central ion orbital, M , and either the ligand orbital (latin capital letter), or the linear combination of ligand orbitals (greek letter), e.g.:

$$\Xi_\sigma[d_{z^2}, X_i] \quad \text{or} \quad \Xi_{\pi\omega}[d_{xy}, \chi_n].$$

These terms are related to group overlap coefficients: if X is an orbital of a ligand placed on the z -axis of the Cartesian coordinate system then the ratio $(\Xi_\delta[d_{z^2}, \chi_n]) / (\Xi_\delta[d_{xy}, X])$, for example, is an expression for the coefficient g which expresses the number of times the group overlap integral G is greater than the appropriate diatomic overlap integral S , usually expressed [2] as $G[d_{z^2}, \chi_n] = gS[d_\delta, X]$.

In [1] Ξ^2 was defined for a metal orbital M and a ligand σ -linear combination χ , which were proper basis functions for irreducible representations of the molecular symmetry group. This definition was (and is) valid for cases in which the symmetry is so high as to make each given symmetry type γ_n represented only once among the set of l -orbitals. Further, if more than one linear combination of ligand σ -orbitals had non-vanishing overlap integrals with an l -orbital of given γ_n , only such combinations were considered in [1] which involved topologically separated ligand atoms.

Perkins and Crosby [6] have given an analysis of this model considering only σ -bonding and proposed the use of non-symmetry adapted functions. They thereby had to introduce non-diagonal elements.

† This is strictly only possible in a spherically symmetrical core field.

In the general case, more overlap integrals will be different from zero and the quantity Ξ^2 of [1] should be substituted by

$$\sum_{n=1}^N \Xi^2[M, \chi_n],$$

the sum of the Ξ^2 quantities taken for all the ligand linear combinations, or, equally well,

$$\sum_{j=1}^N \Xi^2[M, X_j]$$

where no linear combinations of localized ligand orbitals are formed. Using this extended version of the model, which we shall call *the angular overlap model*, the diagonal matrix element of the central ion orbital M must be written:

$$\sigma^* \sum_{n=1}^N (\Xi[M, \chi_n])^2 = \sigma^* \sum_{j=1}^N (\Xi[M, X_j])^2. \quad (3)$$

Similarly, non-diagonal elements connecting two different metal orbitals M and M' may appear and are given by:

$$\sigma^* \sum_{n=1}^N \Xi[M, \chi_n] \Xi[M', \chi_n] = \sigma^* \sum_{j=1}^N \Xi[M, X_j] \Xi[M', X_j]. \quad (4)$$

It is not necessary, but often faster, to symmetry-adapt the M orbital or the ligand orbital linear combinations, provided the above general definitions are used.

In the following we shall attach sub-indices $\pi(\lambda=1)$ and $\delta(\lambda=2)$ to σ^* , no sub-index indicating $(\lambda=0)$. For Ξ values, similarly σ , π , and δ sub-indices will be used in the expressions (3) and (4).

For chromophores possessing so high a symmetry that each γ_n is represented only once for the l -value considered, either non-symmetry-adapted central ion orbitals can be used [6], and the inherent non-diagonal elements tolerated, or the symmetry-adapted central ion orbitals must be employed. With our present definitions, the symmetry adaptation of the ligand orbitals does not influence the number of non-diagonal elements, although the number of terms in both diagonal and non-diagonal elements can be reduced considerably by such a symmetry adaptation.

In cases [6] where the symmetry gives rise to a γ_n which occurs more than once for a given l -value, non-diagonal elements are unavoidable.

3. EVALUATION OF Ξ -VALUES

With the central ion M placed at the origin of a cartesian coordinate system and the ligand X at unit distance, $\Xi_\sigma[M, X]$ can be found [1] as the value of the function M (normalized to 4π) at the position of the ligand. In order to estimate Ξ_π and Ξ_δ values in a similar way, the position $(0, 0, 1)$ was chosen for X and a number of auxiliary points introduced:

$$\left. \begin{array}{ll} a: (\epsilon, 0, 1), & a': (-\epsilon, 0, 1), \\ b: (0, \epsilon, 1), & b': (0, -\epsilon, 1), \\ c: (\frac{1}{2}\sqrt{2}\epsilon, \frac{1}{2}\sqrt{2}\epsilon, 1), & c': (-\frac{1}{2}\sqrt{2}\epsilon, -\frac{1}{2}\sqrt{2}\epsilon, 1), \\ d: (\frac{1}{2}\sqrt{2}\epsilon, -\frac{1}{2}\sqrt{2}\epsilon, 1), & d': (-\frac{1}{2}\sqrt{2}\epsilon, \frac{1}{2}\sqrt{2}\epsilon, 1), \\ A: (1, 0, 0), & \\ B: (0, 1, 0), & \\ C: (\frac{1}{2}\sqrt{2}, \frac{1}{2}\sqrt{2}, 0), & \\ D: (\frac{1}{2}\sqrt{2}, -\frac{1}{2}\sqrt{2}, 0), & \end{array} \right\} \quad (5)$$

$\Xi_{\pi a}[M, X]$ of a π -orbital $X_{\pi a}$ on X is found as the limiting value of the difference between the functional values of M at a and at a' , divided by ϵ , the infinitesimal distance between a and X ,

$$\Xi_{\pi a}[M, X] = \left[\frac{M(a) - M(a')}{\epsilon} \right] \lim_{\epsilon \rightarrow 0} = 2 \frac{\partial M}{\partial x}. \quad (6)$$

This particular π -orbital corresponds to the same row of an irreducible representation as p_x and d_{zx} and will accordingly be called π_{\cos} in the following. The similar expression for the orthogonal π -orbital $X_{\pi b}$ is:

$$\Xi_{\pi b}[M, X] = \left[\frac{M(b) - M(b')}{\epsilon} \right] \lim_{\epsilon \rightarrow 0} = 2 \frac{\partial M}{\partial y} \quad (7)$$

corresponding to p_y and d_{yz} and πb will in the following be called π_{\sin} . Another set of orthogonal π -orbitals, e.g. $X_{\pi c}$ and $X_{\pi d}$ could have been chosen equally well, $X_{\pi c}$ would then have corresponded to $(p_x + p_y)$ and $(d_{zx} + d_{yz})$ and $X_{\pi d}$ to $(p_x - p_y)$ and $(d_{zx} - d_{yz})$.

$\Xi_{\delta ab}[M, X]$ of a δ -orbital $X_{\delta ab}$ is found as the limiting value of the sum of the functional values of M at a and a' , minus the sum of its functional values at b and b' , divided by ϵ^2 :

$$\Xi_{\delta ab} = \left[\frac{M(a) + M(a') - M(b) - M(b')}{\epsilon^2} \right] \lim_{\epsilon \rightarrow 0} = \frac{\partial^2 M}{\partial x^2} - \frac{\partial^2 M}{\partial y^2}, \quad (8)$$

corresponding to $d_{x^2-y^2}$. The expression for the orthogonal δ -orbital is:

$$\Xi_{\delta cd} = \left[\frac{M(c) + M(c') - M(d) - M(d')}{\epsilon^2} \right] \lim_{\epsilon \rightarrow 0} = 2 \frac{\partial^2 M}{\partial x \partial y}, \quad (9)$$

corresponding to d_{xy} . In the following, the orbitals δab and δcd will be called δ_{\cos} and δ_{\sin} , and we shall use the general symbol $\Xi_{\lambda\omega}$, where if $\lambda = \pi$ or δ , ω stands for cos or sin, or a specific linear combination of these orbitals.

It is interesting to note that the differential operators have a similar form to the corresponding central atom orbitals. For ϕ -orbitals the expression for the differential operators are:

$$\left. \begin{aligned} \Xi_{\phi \cos} &= \frac{1}{4} \left[\frac{\partial^3 M}{\partial x^3} - 3 \frac{\partial^3 M}{\partial x \partial y^2} \right] \\ \Xi_{\phi \sin} &= \frac{1}{4} \left[\frac{\partial^3 M}{\partial y^3} - 3 \frac{\partial^3 M}{\partial x^2 \partial y} \right], \end{aligned} \right\} \quad (10)$$

corresponding to the ϕ -orbitals $f_{x^3-3xy^2}$ and $f_{y^3-3x^2y}$. Now, in order to obtain more general expressions for Ξ_{π} and Ξ_{δ} the coordinates given above for X and for the auxiliary points (5) will be considered as defining vectors radiating from the origin. Thus the following equations are obtained:

$$\left. \begin{aligned} a &= X + \epsilon A, \\ a' &= X - \epsilon A, \\ b &= X + \epsilon B, \text{ etc.} \end{aligned} \right\} \quad (11)$$

If the coordinates of $X(0, 0, 1)$ are transformed into general coordinates (x, y, z) of our fixed coordinate system, the same transformation will change the coordinates of the normals A, B , etc. to, say, (p_A, q_A, r_A) , (p_B, q_B, r_B) , etc. giving the general expressions for Ξ_{λ} in table 1.

Such a transformation can be performed by a matrix identical with that of table 2, working on the column vectors $\begin{bmatrix} z \\ x \\ y \end{bmatrix}$. If (x, y, z) are written as $(\sin \theta \cos \phi, \sin \theta \sin \phi, \cos \theta)$, (p, q, r) will likewise be written as functions of θ and ϕ and such a transformation leads to the following expression for:

$$\Xi_{\lambda\omega}[M, X_j] = \mathcal{N}_\lambda F_{M\lambda\omega}(\theta_j, \phi_j), \quad (12)$$

where \mathcal{N}_λ takes the values:

$$\left. \begin{aligned} \lambda=0 &: \sqrt{(2l+1)}, \\ \lambda=1 &: [2(2l+1)l(l+1)]^{1/2}, \\ \lambda=2 &: [\tfrac{1}{2}(2l+1)(l-1)l(l+1)(l+2)]^{1/2}, \\ \lambda=3 &: [\tfrac{1}{32}(2l+1)(l-2)(l-1)l(l+1)(l+2)(l+3)]^{1/2} \end{aligned} \right\} \quad (13)$$

and ω specifies the particular one of a possibly (if $\lambda > 0$) degenerate set of ligand orbitals, again up to a similarity transformation. $F_{M\lambda\omega}$ is a function of the

M	Ξ_σ	$\Xi_{\pi a}$	$\Xi_{\delta ab}$
p_z	$\sqrt{3}z$	$2\sqrt{3}r_A$	
p_x	$\sqrt{3}x$	$2\sqrt{3}p_A$	
p_y	$\sqrt{3}y$	$2\sqrt{3}q_A$	
d_{z^2}	$\tfrac{1}{2}\sqrt{5}(2z^2 - x^2 - y^2)$	$2\sqrt{45}zr_A$	$\sqrt{45}[r_A^2 - r_B^2]$
d_{zx}	$\sqrt{15}zx$	$2\sqrt{15}[xr_A + zp_A]$	$2\sqrt{15}[p_Ar_A - p_Br_B]$
d_{yz}	$\sqrt{15}yz$	$2\sqrt{15}[yr_A + zq_A]$	$2\sqrt{15}[q_Ar_A - q_Br_B]$
$d_{x^2-y^2}$	$\tfrac{1}{2}\sqrt{15}(x^2 - y^2)$	$2\sqrt{15}[xp_A - yq_A]$	$\sqrt{15}[(p_A^2 - q_A^2) - (p_B^2 - q_B^2)]$
d_{xy}	$\sqrt{15}xy$	$2\sqrt{15}[xq_A + yp_A]$	$2\sqrt{15}[p_Aq_A - p_Bq_B]$

Table 1. $\Xi_{\lambda\omega}[M, X]$ for X having coordinates (x, y, z) with normals at M with coordinates (p_A, q_A, r_A) etc. (see text). M represents all p and d cartesian orbitals. For $\Xi_{\pi b}$ and $\Xi_{\delta cd}$ the expressions are analogous to those of $\Xi_{\pi a}$ and $\Xi_{\delta ab}$. Division of these expressions by \mathcal{N}_λ will transform the Ξ -terms into F -terms (equation (12)).

	σ	π_{\cos}	π_{\sin}
p_z	$\cos \theta$	$-\sin \theta$	0
p_x	$\sin \theta \cos \phi$	$\cos \theta \cos \phi$	$-\sin \phi$
p_y	$\sin \theta \sin \phi$	$\cos \theta \sin \phi$	$\cos \phi$
	$p_{z'}$	$p_{x'}$	$p_{y'}$

Table 2. $F_{\lambda\omega}(p)$ matrix.

spherical polar coordinates θ and ϕ and is characterized by the central ion orbital and ligand orbital which overlap. We shall call $F_{M\lambda\omega}$ the *angular overlap integral*. With reference to equations (3) and (4) we shall be able to speak about a single angular overlap integral and a group angular overlap integral. For a single ligand the F -function can be written as an element of a real orthogonal

matrix F . Tables 2 and 3 give this matrix for cartesian p and d orbitals. In general linear combinations† of the columns $F_{M\pi a}$ and $F_{M\pi b}$ and of the columns $F_{M\delta ab}$ and $F_{M\delta cd}$ are required when more ligands are considered.

4. EQUIVALENCE OF THE ANGULAR OVERLAP MODEL AND A PERTURBATION MODEL WITH A SINGULAR POTENTIAL *

We shall assume that overlap between the orbital, X_j , localized on the ligand, j , and orbitals of other ligands can be neglected. For N ligands we can write N linear combinations of such localized ligand orbitals, the combinations being linearly independent. We shall choose these as the orthogonal functions, ($n = 1, 2, 3, \dots, N$):

$$\chi_n = \sum_{j=1}^N a_{nj} X_j, \quad (14)$$

where

$$\sum_{n=1}^N a_{ni} a_{nj} = \delta[i, j].$$

$\Xi_{\lambda\omega}$ for the combination can now be written

$$\Xi_{\lambda\omega}[M, \chi_n] = \mathcal{N}_\lambda \sum_{j=1}^N a_{nj} F_{M\lambda\omega}(\theta_j, \phi_j), \quad (15)$$

\mathcal{N}_λ times the group angular overlap integral. The $\lambda\omega$ -part of the matrix element connecting the central ion orbitals M and M' through the ligand combination χ_n is:

$$\Xi_{\lambda\omega}[M, \chi_n] \Xi_{\lambda\omega}[M', \chi_n] = \mathcal{N}_\lambda^2 \sum_{i=1}^N \sum_{j=1}^N a_{ni} a_{nj} F_{M\lambda\omega}(\theta_i, \phi_i) F_{M'\lambda\omega}(\theta_j, \phi_j) \quad (16)$$

and this expression should now be summed over all the combinations, χ_n with $\lambda\omega$ symmetry,

$$\begin{aligned} \sum_{n=1}^N \Xi_{\lambda\omega}[M, \chi_n] \Xi_{\lambda\omega}[M', \chi_n] &= \mathcal{N}_\lambda^2 \sum_{i=1}^N \sum_{j=1}^N \sum_{k=1}^N a_{ni} a_{nj} F_{M\lambda\omega}(\theta_i, \phi_i) F_{M'\lambda\omega}(\theta_j, \phi_j) \\ &= \mathcal{N}_\lambda^2 \sum_{i=1}^N \sum_{j=1}^N \delta[i, j] F_{M\lambda\omega}(\theta_i, \phi_i) F_{M'\lambda\omega}(\theta_j, \phi_j) = \mathcal{N}_\lambda^2 \sum_k F_{M\lambda\omega}(\theta_k, \phi_k) F_{M'\lambda\omega}(\theta_k, \phi_k). \end{aligned} \quad (17)$$

† Our field transformation matrix (fixed coordinate system, table 2) working on the orthogonal linear combinations of coordinates

$$\cos(\alpha) \cdot a + \sin(\alpha) \cdot b \text{ and } -\sin(\alpha) \cdot a + \cos(\alpha) \cdot b$$

(and similar combinations of c and d) is equivalent to $F^{(p)}_{\{\alpha, \theta, \phi\}}$ working on the coordinates a and b . $F^{(p)}_{\{\alpha, \theta, \phi\}}$ is the Eulerian field rotation matrix acting within the fixed (z, x, y) -coordinate frame. It is defined as a rotation α around the z -axis followed by a rotation θ around the y -axis and finished by a rotation ϕ , again around the z -axis, all counter-clockwise rotations in the right-handed (z, x, y) -coordinate system. $F^{(p)}_{\{\alpha, \theta, \phi\}}$ is equivalent to $\mathfrak{z}^{(1)}_{(\phi, \theta, \alpha)}$ of [5], and the similar $F^{(d)}_{\{\alpha, \theta, \phi\}}$ matrix (equivalent to $\mathfrak{z}^{(2)}_{(\phi, \theta, \alpha)}$ of [5]) can be obtained from our F -matrix (table 3) by keeping the first column unchanged and by forming the linear combinations

$$\begin{aligned} &\cos \alpha \cdot (\pi_{\cos}) + \sin \alpha \cdot (\pi_{\sin}), \\ &-\sin \alpha \cdot (\pi_{\cos}) + \cos \alpha \cdot (\pi_{\sin}), \\ &\cos 2\alpha \cdot (\delta_{\cos}) + \sin 2\alpha \cdot (\delta_{\sin}), \\ &\text{and } -\sin 2\alpha \cdot (\delta_{\cos}) + \cos 2\alpha \cdot (\delta_{\sin}) \end{aligned}$$

of the other columns. It should be noted that $F_{\{\phi, \theta, \pi-\phi\}}$ is a symmetrical matrix.

	σ	π_{\cos}	π_{\sin}	δ_{\cos}	δ_{\sin}
d_{z^2}	$\frac{1}{4}(1+3\cos 2\theta)$	$-\frac{1}{2}\sqrt{3}\sin 2\theta$	0	$\frac{1}{4}\sqrt{3}(1-\cos 2\theta)$	0
d_{zx}	$\frac{1}{2}\sqrt{3}\sin 2\theta\cos\phi$	$\cos 2\theta\cos\phi$	$-\cos\theta\sin\phi$	$-\frac{1}{2}\sin 2\theta\cos\phi$	$\sin\theta\sin\phi$
d_{yz}	$\frac{1}{2}\sqrt{3}\sin 2\theta\sin\phi$	$\cos 2\theta\sin\phi$	$\cos\theta\cos\phi$	$-\frac{1}{2}\sin 2\theta\sin\phi$	$-\sin\theta\cos\phi$
$d_{x^2-y^2}$	$\frac{1}{4}\sqrt{3}(1-\cos 2\theta)\cos 2\phi$	$\frac{1}{2}\sin 2\theta\cos 2\phi$	$-\sin\theta\sin 2\phi$	$\frac{1}{4}(3+\cos 2\theta)\cos 2\phi$	$-\cos\theta\sin 2\phi$
d_{xy}	$\frac{1}{4}\sqrt{3}(1-\cos 2\theta)\sin 2\phi$	$\frac{1}{2}\sin 2\theta\sin 2\phi$	$\sin\theta\cos 2\phi$	$\frac{1}{4}(3+\cos 2\theta)\sin 2\phi$	$\cos\theta\cos 2\phi$
	$d_{(z')^2}$	$d_{x'^2-x}$	$d_{y'^2-z'}$	$d_{(x')^2-(y')^2}$	$d_{x'y'}$

Table 3. $F_{\lambda\omega}^{(d)}$ matrix.

It is seen that such a matrix element consists of a sum of contributions from each of the ligands. If M is the same central ion orbital as M' , we have the diagonal element:

$$\mathcal{N}_\lambda^{-2} \sum_{k=1}^N F_{M\lambda\omega}^2(\theta_k, \phi_k). \quad (18)$$

Because of the product form of the matrix elements an orbital whose diagonal element is equal to zero will only have vanishing non-diagonal elements. This is physically understandable if only anti-bonding effects are considered, because otherwise a linear combination of central ion orbitals would have a negative anti-bonding energy.

It is an important consequence of the additivity of contributions from the ligands that the model can be extended to molecules where the ligands, and thus the σ_λ^* -values of equations (3) and (4), are different.

The general matrix element can then be written:

$$\sum_{\lambda\omega} \sum_{j=1}^N \sigma_{\lambda\omega j}^* \Xi_{\lambda\omega}[M, X_j] \Xi_{\lambda\omega}[M', X_j] = \sum_{\lambda\omega} \sum_{j=1}^N \mathcal{N}_\lambda^{-2} \sigma_{\lambda\omega j}^* F_{\lambda\omega}[M, X_j] F_{\lambda\omega}[M', X_j], \quad (19)$$

where σ^* has been provided with a sub-index referring to the ligand j and placed after the summation sign. For l -electrons the first summation comprises $(2l+1)$ terms.

It is convenient to include the constant \mathcal{N}_λ^{-2} into the radial term [5] and re-write the matrix element as:

$$\sum_{\lambda\omega} \sum_{j=1}^N e_{\lambda\omega j} F_{\lambda\omega}[M, X_j] F_{\lambda\omega}[M', X_j]. \quad (20)$$

In [1] and [6] it was pointed out that matrix elements of the singular potential:

$$V_\sigma = \sum_{k=1}^N \sigma_k^* \delta(x-x_k) \delta(y-y_k) \delta(z-z_k) = \sum_{k=1}^N \sigma_k^* \delta(\theta-\theta_k) \delta(\phi-\phi_k) \quad (21)$$

taken with respect to the normalized l -orbitals were identical with those of the Ξ^2 method. The same result would have been obtained using the functions $\mathcal{N}_\sigma F_\sigma$, because these are identical with the l -orbitals.

In accordance with equation (20) a general singular potential:

$$V_{\lambda\omega} = \sum_{j=1}^N e_{\lambda\omega j} \delta(x-x_j) \delta(y-y_j) \delta(z-z_j) = \sum_{j=1}^N e_{\lambda\omega j} \delta(\theta-\theta_j) \delta(\phi-\phi_j) \quad (22)$$

can be defined. The matrix elements of this operator with respect to $F_{\lambda\omega}$ functions are identical with those of the angular overlap model.

5. SOME SUM RULES

From the normality of the columns of the F matrices (tables 2 and 3) together with the result that the contributions from the ligands are additive, it follows that the sum of the diagonal angular matrix elements (with respect to $\lambda\omega$ ligand orbitals) of all the central ion orbitals of a given l -shell is equal to the number N of ligands:

$$\sum_{M,n} (F_{\lambda\omega}[M, \chi_n])^2 = \sum_{M,j} (F_{\lambda\omega}[M, X_j])^2 = N \quad (23)$$

forming $(2l+1)$ equations. From the normality of the rows of the F -matrices another $(2l+1)$ equations of the same form as equation (23) may be obtained. Here the summation is carried out over all $\lambda\omega$ -contributions to the angular overlap of a particular central atom orbital, and the equation states that the total angular bonding capacity of any orbital is equal to the number of ligands.

Equation (23) is a generalization of equation (8) of [1]. It is perhaps worth mentioning that the radial factor may cause some $\lambda\omega$ -contributions to effectively vanish in actual physical situations.

The F -matrices need further comment. The l -functions in the column to the left of the matrices are the cartesian l -functions relative to our fixed (x, y, z) -coordinate system which also defines the polar coordinates θ and ϕ . The $\lambda\omega$ columns of the matrix give the coefficients to these functions in the linear combination which has an angular overlap integral of unity with a $\lambda\omega$ -function on the ligating atom, whose coordinates are θ and ϕ . These linear combinations are pure cartesian l -functions relative to a (x', y', z') coordinate system with z' -axis in the central ion-ligand direction and the same origin (the central ion position) as the (x, y, z) system. For $\theta \neq \frac{0}{\pi}$ the axes of the right-handed (x', y', z') coordinate system are fixed in such a way that x' lies in the plane determined by the axes z and z' . For $\theta = \frac{0}{\pi}$, ϕ should be defined as having the value 0.

The rows of the F -matrices give the decomposition of the cartesian (x, y, z) l -functions into those of the (x', y', z') system. The square of such a coefficient corresponding to a $\lambda\omega$ column is an expression of the fraction to which the l -orbital in question may participate in a bond of $\lambda\omega$ -symmetry, its total angular capacity [5] for bond formation being the sum of the squares of these coefficients, i.e. unity. The transposed F -matrices are, with a real basis, irreducible representations of the three dimensional rotation group.

6. APPLICATIONS OF THE MODEL TO CUBIC STRUCTURES

Jørgensen and Schmidtke [7] have found that the d -orbital splitting in a tetrahedral complex should be $-\frac{4}{9}$ of that in an octahedral complex, when σ overlap is considered. This is also true when π and δ overlaps are considered [5].

The contribution to the orbital energy difference Δ is for the octahedron:

$$\Delta_{\text{oct}} = E_{e_g} - E_{t_{2g}} = (3e_{\sigma} + 3e_{\delta}) - (4e_{\pi} + 2e_{\delta}) = 3e_{\sigma} - 4e_{\pi} + e_{\delta} \quad (24)$$

and for the tetrahedron:

$$\Delta_{T_d} = E_e - E_{t_2} = \left(\frac{8}{3}e_{\pi} + \frac{4}{3}e_{\delta}\right) - \left(\frac{4}{3}e_{\sigma} + \frac{9}{8}e_{\pi} + \frac{16}{9}e_{\delta}\right) = -\frac{4}{3}e_{\sigma} + \frac{16}{9}e_{\pi} - \frac{4}{9}e_{\delta} = -\frac{4}{9}\Delta_{\text{oct}}. \quad (25)$$

Here the δ -contribution to $E_{t_{2g}}$ can, e.g. be found by looking at the d_{zx} -orbital. The general expression for the coefficient to e_{δ} is:

$$\sum_{j=1}^N \left(\frac{1}{2} \sin 2\theta_j \cos \phi_j \right)^2 + (\sin \theta_j \sin \phi_j)^2. \quad (26)$$

The contribution from the ligands on the z -axis ($\theta=0$ and $\theta=\pi$) and on the x -axis ($\theta=\pi/2, \phi=0$ and $\theta=\pi/2, \phi=\pi$) vanishes, and we are left with a contribution to the second term from the ligands on the y -axis ($\theta=\pi/2, \phi=\pi/2$ and $\theta=\pi/2, \phi=3\pi/2$). These make up the coefficient 2 to e_{δ} of $E_{t_{2g}}$ (equation (24) second parenthesis).

The other coefficients have been obtained in a similar way.

For the hexahedron (the cube) Δ is twice Δ_{T_d} (equation (25)), i.e. $-\frac{8}{9}\Delta_{\text{oct}}$. For the tetrakis-hexahedron or triakis-octahedron, which is a superposition of a cube and an octahedron, Δ is:

$$2\Delta_{T_d} + \Delta_{\text{oct}} = \left(-\frac{8}{9} + 1\right)\Delta_{\text{oct}} = \frac{1}{9}\Delta_{\text{oct}} \quad (27)$$

<i>d</i> -orbital	<i>D_{∞h}</i> -linear (2) rep. <i>e_σ</i> <i>e_π</i> <i>e_δ</i>	<i>D_{3h}</i> -triangular (3) rep. <i>e_σ</i> <i>e_π</i> <i>e_δ</i>	<i>D_{4h}</i> -square (4) rep. <i>e_σ</i> <i>e_π</i> <i>e_δ</i>	<i>D_{5h}</i> -pentagonal (5) rep. <i>e_σ</i> <i>e_π</i> <i>e_δ</i>
$\frac{1}{2}\sqrt{5}(2z^2 - x^2 - y^2)$	σ_g^+ 2 0 0	a_1' $\frac{3}{2}$ 0 $\frac{9}{4}$	a_{1g} 1 0 3	a_1' $\frac{5}{4}$ 0 $\frac{15}{4}$
$\sqrt{15}zx$ $\sqrt{15}yz$	π_g { 0 2 0 0 2 0	e'' { 0 $\frac{3}{2}$ $\frac{3}{2}$ 0 $\frac{3}{2}$ $\frac{3}{2}$	e_g { 0 2 2 0 2 2	e_1'' { 0 $\frac{5}{2}$ $\frac{5}{2}$ 0 $\frac{5}{2}$ $\frac{5}{2}$
$\frac{1}{2}\sqrt{15}(x^2 - y^2)$ $\sqrt{15}xy$	δ_g { 0 0 2 0 0 2	e' { $\frac{3}{2}$ $\frac{3}{2}$ $\frac{3}{2}$ 0 $\frac{3}{2}$ $\frac{3}{2}$	b_{1g} 3 0 1 b_{2g} 0 4 0	e_2' { $\frac{15}{8}$ $\frac{5}{4}$ $\frac{5}{4}$ $\frac{15}{8}$ $\frac{5}{4}$ $\frac{5}{4}$

Table 4. Energies of *d*-orbitals in terms of the radial parameters *e_σ*, *e_π*, and *e_δ*. The orbitals are renormalized to 4π. The number of ligands are given in parenthesis to the symmetry. The classification of the orbitals in terms of irreducible representations (rep.) of the appropriate point groups are included, the main symmetry axis being always chosen as the *z*-axis. For the square the *x* and *y* axes pass through the corners of the square.

provided the distances to all 14 ligands, and thus the radial parameters, are the same. For the tetradecahedron (cubo-octahedron) the results are

$$E_{e_g} - E_{t_{2g}} = (\frac{3}{2}e_{\sigma} + 6e_{\pi} + \frac{9}{2}e_{\delta}) - (3e_{\sigma} + 4e_{\pi} + 5e_{\delta}) = -\frac{1}{2}\Delta_{\text{oct}}.$$

Schmidtke [5] also has obtained these results but he did not include π and δ terms in all cases.

7. STRUCTURES OF LOWER SYMMETRY

In table 4 are listed some results obtained for lower symmetry systems with monatomic ligands. The linear case (2 ligands) can be directly superposed on each of the other three systems (forming the bipyramids) without changing their point group, and the energy can be obtained by adding the individual contributions with or without the same value for the radial parameters e_{λ} . E.g. addition of $D_{\infty h}$ to D_{4h} using the same values for the e_{λ} parameters will make up the octahedral case of equation (24).

Also half the energy contributions from $D_{\infty h}$, corresponding to $C_{\infty v}$ (one ligand), can be added without difficulty, thus forming the monopyramids. Hereby, however, the xy -plane of symmetry disappears, the point groups reduce to C_{3v} , C_{4v} , and C_{5v} , and the gerade-ungerade and prime-double prime symbols vanish. For the triangular case complications might have arisen from non-diagonal elements connecting the two e -components of the C_{3v} symmetry of the monopyramid. These, however, vanish in this particular case. Problems of this kind will be reserved for a forthcoming paper.

It should be noted that the sum of the numbers in the e_{σ} columns is equal to the number of ligands N , and the sum of the numbers in the e_{π} and e_{δ} columns (which correspond to two orbitals) is $2N$. Further the sum of the numbers in each row corresponding to a particular symmetry is also N . These rules have been discussed in § 5.

8. CONCLUSION

It is not easy to make a general statement as to the range of approximate validity of the angular overlap model. In principle negative e_{λ} values, corresponding to bonding effects on the l -orbital, may occur and will have to be treated by the model identically with positive (anti-bonding effects) e_{λ} -values. As the angular treatment is independent of the choice of sign for the semi-empirical parameter e_{λ} , all results obtained from the angular functions will be valid for bonding as well as anti-bonding contributions to e_{λ} , even though the approximations may turn out to be less justified in one case than in the other.

In a subsequent paper we shall show how the model, in contrast to the electrostatic model, accounts for the small splitting of energy levels which experimentally is found in tris(bidentate)octahedral complexes.

Further we shall develop the qualitative ideas of Griffith and Orgel [8] about the splitting of the energy levels in hexacoordinated, approximately octahedral complexes with different ligands, using a method similar to that of Yamatera [9] but which is more general [10].

We would like to thank Drs. G. A. Crosby, W. G. Perkins, and H.-H. Schmidtke for communicating to us their results prior to publication.

REFERENCES

- [1] JØRGENSEN, C. K., PAPPALARDO, R., and SCHMIDTKE, H.-H., 1963, *J. chem. Phys.*, **39**, 1422.
- [2] WOLFSBERG, M., and HELMHOLZ, L., 1952, *J. chem. Phys.*, **20**, 837.
- [3] JØRGENSEN, C. K., 1962, *Orbitals in Atoms and Molecules* (London: Academic Press).
- [4] BALLHAUSEN, C. J., 1954, *Math.-fys. Medd., Selsk.*, **29**, no. 4.
- [5] SCHMIDTKE, H.-H., 1964, *Z. Naturforsch.*, **19a**, 1502.
- [6] PERKINS, W. G., and CROSBY, G. A., 1965, *J. chem. Phys.*, **42**, 407.
- [7] JØRGENSEN, C. K., and SCHMIDTKE, H.-H., 1963, *Z. phys. Chem.*, **38**, 118.
- [8] GRIFFITH, J. S., and ORGEL, L. E., 1956, *J. chem. Soc.*, 4981.
- [9] YAMATERA, H., 1958, *Bull. chem. Soc., Japan*, **31**, 95.
- [10] SCHÄFFER, C. E., and JØRGENSEN, C. K., 1965, *Math.-fys. Medd., Selsk.*, **34**, no. 13.

Solvent effects on the visible spectra of nitrobenzene anion radicals

by JAMES Q. CHAMBERS† and RALPH N. ADAMS

Department of Chemistry, The University of Kansas,
Lawrence, Kansas

(Received 18 February 1965)

The correlation of solvent shifts of the optical and E.P.R. spectra of the anion of nitrobenzene in N,N-dimethylformamide with added water is consistent with the picture of hydrogen-bonding or solvation of the $\text{NB}^{\cdot-}$.

1. INTRODUCTION

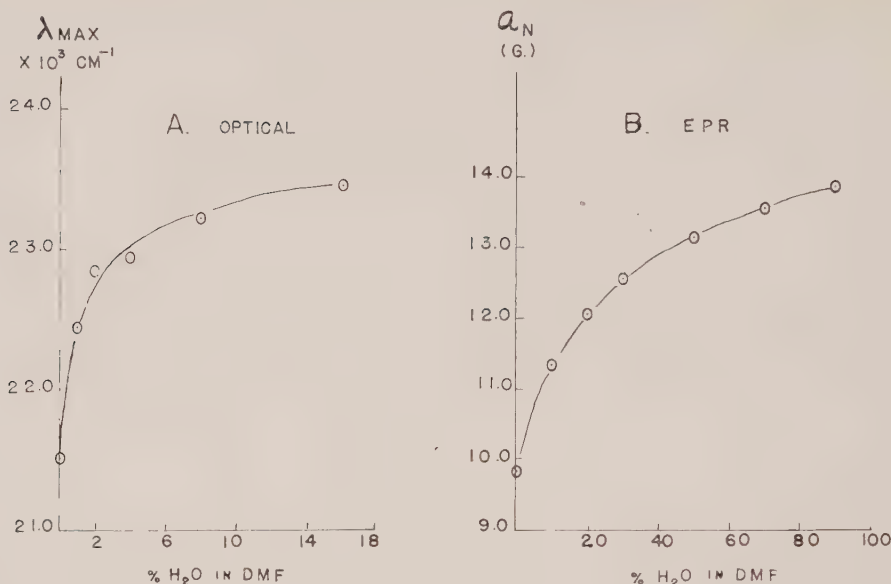
The anion radicals of nitrobenzene ($\text{NB}^{\cdot-}$) and substituted nitrobenzenes have been studied extensively in the past few years. The electron paramagnetic resonance (E.P.R.) spectra of these anions are well characterized in a variety of solvents. Of particular interest is the large solvent effect on the ^{14}N hyperfine coupling constants (a_{N}) in the E.P.R. spectra of these anions [1]. The changes in a_{N} are understood fairly well in terms of solvation or hydrogen bonding of the anion radicals with hydroxylic solvents. A quantitative treatment has been given by Gendell *et al.* [2] and a large body of experimental evidence has been collected on various solvents systems [2–5]. The present work concerns the correlation of the solvent shift of the visible absorption spectrum of $\text{NB}^{\cdot-}$ with the change in a_{N} .

The visible spectrum of $\text{NB}^{\cdot-}$ in N,N-dimethylformamide (DMF) was first reported by Kemula and Sioda [6]. The spectrum has also been described in dimethoxyethane (DME) by Nagakura and co-workers [7] and in alkaline aqueous media by Kastening [8]. Kemula and Sioda electrochemically generated $\text{NB}^{\cdot-}$ directly in a spectrophotometric cell. Our method differs slightly in that we make $\text{NB}^{\cdot-}$ by controlled potential coulometry and, in a closed system, transfer the radical ion via a peristaltic pump to a Cary recording spectrophotometer. The electrochemical generation techniques are well known [1–4] and the spectrophotometric measurements were conventional.

2. RESULTS AND DISCUSSION

In DMF containing 0.1 M tetraethylammonium perchlorate (TEAP) as supporting electrolyte, the absorption maximum of $\text{NB}^{\cdot-}$ is at $465\text{ m}\mu$ ($21.5 \times 10^3\text{ cm}^{-1}$) and has a molar extinction of $1.1 \times 10^3\text{ cm}^2\text{ mole}^{-1}$. The absorption maximum shows a rather strong blue shift with increasing amounts of water in DMF (a shift of *ca.* 1900 cm^{-1} for 20 per cent H_2O –DMF). The blue shift parallels the increase in a_{N} in the E.P.R. spectrum, i.e. there is a sharp change for small quantities of water which gradually levels out. The optical and E.P.R. data are compared in the figure. (Due to instability of $\text{NB}^{\cdot-}$ at

† Present address: Department of Chemistry, University of Colorado, Boulder, Colorado.



Comparison of solvent effects on optical and E.P.R. spectra. A. Variation of λ_{max} with water addition. B. Variation of a_N with water addition. Solvent system: DMF-0.1 M TEAP with added water as indicated.

increasing water concentrations, reliable optical data can be obtained only up to about 20–30 per cent H₂O-DMF.)

According to Nagakura *et al.* the long wavelength transition in $\text{NB}^{\cdot-}$ (which occurs at 560 $\text{m}\mu$ in DME) is between two low lying energy levels ($W_1 \rightarrow W_2$) whose wave functions contain large contributions from a charge transfer configuration in addition to contributions from locally excited states both in the benzene ring and the nitro group. The calculations of Nagakura are, in general, analogous to those of Murrell *et al.* [9–11] and Heilbronner and co-workers [12] in which charge transfer states are admixed with ground and locally excited states for the calculation of optical spectra.

Using the notation of Nagakura the optical ground state of $\text{NB}^{\cdot-}$ (W_1) contains a 54 per cent contribution from the charge transfer configuration (ψ_{14}'). This is decreased to 36 per cent in the excited state (W_2), i.e. the 560 $\text{m}\mu$ transition corresponds to displacement of an electron from the nitro function to the ring. Since it is clear from the E.P.R. data that the ground state of $\text{NB}^{\cdot-}$ is strongly solvated by water in DMF, the excited state will be less solvated. In the sense of the Franck-Condon principle in solvent shifts of optical spectra as discussed by Pimentel [13] and others [14], a blue shift with water or hydroxylic solvents would be expected for $\text{NB}^{\cdot-}$. The magnitude of the shift (*ca.* 1900 cm^{-1}) appears to be consistent with predictions by Pimentel [13].

The absorption maximum of $\text{NB}^{\cdot-}$ is obviously solvent sensitive and it is not surprising that the value for DMF found in this study (465 $\text{m}\mu$) differs from that reported in dimethoxyethane (560 $\text{m}\mu$). Further, Kemula and Sioda found two peaks at 435 and 465 $\text{m}\mu$ with NaNO_3 as the supporting electrolyte. The

peak at 435 m μ , which is not observed in this study using the large tetraethylammonium cation, very likely arises from an ion-pair type interaction. Such behaviour is consistent with the properties of NB \cdot^- as shown in this work. Sodium and other metal ions exert a marked influence on a_N of NB \cdot^- in DMF [15]. A thorough study of the effects of metal ions on the optical spectra of NB \cdot^- is in progress.

We are indebted to T. Layloff for valuable discussions during the course of this work. These studies were sponsored by the Air Force through the Air Force Office of Scientific Research and NASA through CRES 40-D at the University of Kansas.

REFERENCES

- [1] PIETTE, L. H., LUDWIG, P., and ADAMS, R. N., 1961, *J. Amer. chem. Soc.*, **83**, 3909; 1962, *Ibid.*, **84**, 4212.
- [2] GENDELL, J., FREED, J. H., and FRAENKEL, G. K., 1962, *J. chem. Phys.*, **37**, 2832.
- [3] CHAMBERS, J. Q., LAYLOFF, T., and ADAMS, R. N., 1964, *J. phys. Chem.*, **68**, 661.
- [4] LUDWIG, P., LAYLOFF, T., and ADAMS, R. N., 1964, *J. Amer. chem. Soc.*, **86**, 4568.
- [5] PANNELL, J., 1964, *Mol. Phys.*, **7**, 317, 599.
- [6] KEMULA, W., and SIODA, R., 1962, *Bull. Acad. polon. Sci.*, **10**, 507; 1963, *Nature, Lond.*, **197**, 588.
- [7] ISHITANI, A., KUWATA, K., TSUBOMURA, H., and NAGAKURA, S., 1963, *Bull. chem. Soc., Japan*, **36**, 1357.
- [8] KASTENING, B., 1964, *Electrochim Acta*, **9**, 241.
- [9] LONGUET-HIGGINS, H. C., and MURRELL, J. N., 1955, *Proc. phys. Soc., Lond. A*, **68**, 601.
- [10] MURRELL, J. N., 1955, *Proc. phys. Soc., Lond. A*, **68**, 969; 1963, *Tetrahedron*, Suppl. 2, **19**, 223.
- [11] GODFREY, M., and MURRELL, J. N., 1964, *Proc. roy. Soc. A*, **278**, 71.
- [12] GRINTER, R., and HEILBRONNER, E., 1962, *Helv. chim. acta*, **45**, 2496.
- [13] PIMENTEL, G. C., 1957, *J. Amer. chem. Soc.*, **79**, 3323.
- [14] MURRELL, J. N., 1963, *The Theory of the Electronic Spectra of Organic Molecules* (New York: John Wiley & Sons).
- [15] KITAGAWA, T., LAYLOFF, T., and ADAMS, R. N., 1964, *Analyt. Chem.*, **36**, 925.

Calculation on some excited states of helium and lithium

by D. B. COOK and J. N. MURRELL

The Department of Chemistry, Sheffield University

(Received 11 December 1964)

Rydberg defects for some excited states of Li and He have been calculated using anti-symmetrized products of core and Rydberg orbital wave functions. Electron exchange makes an important contribution to the defect for the s and p series. For the s series electron correlation is relatively unimportant, for the p series correlation accounts for about 40 per cent of the defect and for the d series (and higher) correlation accounts for nearly all the defect. The relevance of these results to Rydberg defects of heavier atoms and molecules is briefly discussed.

1. INTRODUCTION

In this paper we present some calculations on the excited states of helium and lithium. The work was undertaken as a preliminary to an investigation of Rydberg states of molecules. The question we asked ourselves was: to what accuracy can we calculate Rydberg defects using the type of approximate wave functions that are available for molecules?

Helium and lithium are the simplest systems whose term values (energies relative to ionization) follow the Rydberg formula. Helium has the advantage that the wave functions of the positive ion are known exactly, and lithium is the simplest example of one electron outside a closed shell.

A similar, but less extensive investigation on the 2P states of lithium has recently been given by Coulson and Stamper [1]. However, there is an error in one of their calculations and as a result some of their conclusions need modifying. There are also some early calculations on helium and lithium by Eckhart [2] which we have re-examined.

We will first examine a wave function built up from a hydrogen orbital, ϕ , and a wave function ψ^+ which is an eigenfunction of the positive ion, the two being combined in an anti-symmetrized product.

For lithium the states will be doublets:

$$^2\psi = \mathcal{A}\psi^+(2,3)\phi(1) \quad (1)$$

(\mathcal{A} is the anti-symmetrizing operator). Their energy is given by:

$$\frac{\langle ^2\Psi | \mathcal{H} | ^2\Psi \rangle}{\langle ^2\Psi | ^2\Psi \rangle} = E^+ + E_H + \frac{\langle \mathcal{A}\psi^+(2,3)\phi(1) | - (Z-1)/r_1 + 1/r_{12} + 1/r_{13} | \psi^+(2,3)\phi(1) \rangle}{\langle \mathcal{A}\psi^+(2,3)\phi(1) | \psi^+(2,3)\phi(1) \rangle}, \quad (2)$$

where Z is the nuclear charge, E^+ is the energy of the positive ion and E_H the appropriate hydrogen energy. (To get this expression one makes use of the fact that ψ^+ and ϕ are eigenfunctions of the positive ion and of the hydrogen atom respectively.)

The deviation from the energy $E^+ + E_H$, which may be called the defect energy, is given by:

$$-\Delta = C + X,$$

where Δ is taken to be positive if the state has an energy lower than $E^+ + E_H$. C is the coulomb energy of the electron density ϕ^2 in the potential field of the positive ion less one unit of nuclear charge:

$$C = \frac{\langle \psi^+(2, 3)\phi(1) | - (Z-1)/r_1 + 1/r_{12} + 1/r_{13} | \psi^+(2, 3)\phi(1) \rangle}{\langle \mathcal{A}\psi^+(2, 3)\phi(1) | \psi^+(2, 3)\phi(1) \rangle}. \quad (3)$$

This is usually called the penetration term. X is the exchange energy between the outer electron and the positive core:

$$X = \frac{\langle (\mathcal{A}-1)\psi^+(2, 3)\phi(1) | - (Z-1)/r_1 + 1/r_{12} + 1/r_{13} | \psi^+(2, 3)\phi(1) \rangle}{\langle \mathcal{A}\psi^+(2, 3)\phi(1) | \psi^+(2, 3)\phi(1) \rangle}. \quad (4)$$

Expressions (3) and (4) both contain a normalizing integral in the denominator. If ψ^+ is expressed in terms of orbitals and ϕ is orthogonal to all the orbitals in ψ^+ , then this normalizing integral will be unity.

The corresponding states of the helium atom are either singlets or triplets. Their energies can likewise be expressed in terms of the coulomb and exchange energies defined above. The defects of the singlet ($^1\Delta$) and triplet ($^3\Delta$) states are given by:

$$\left. \begin{aligned} -^1\Delta &= C - X, \\ -^3\Delta &= C + X. \end{aligned} \right\}$$

Tables 1 and 2 give the results for the p, d and f series based on the wave function described above. For He^+ the eigenfunction ψ^+ is known exactly; for Li^+ we have used two different approximate wave functions. The first one is based on the best Slater-type-orbital (S.T.O.) and the second is the accurate Hartree-Fock function given by Roothaan [5]. In table 1 we have included the ratios $X/\frac{1}{2}(^1\Delta - ^3\Delta)$ and $C/\frac{1}{2}(^1\Delta + ^3\Delta)$ which give a measure of the accuracy to which the exchange and coulomb energies are calculated if it is assumed that the orbitals for the singlet and triplet series are the same.

The calculated coulomb and exchange terms are both found to vary approximately as $1/n^3$, as does the observed defect. This means that the relative accuracy of the calculated defect is independent of n .

For the ^3P series of helium one calculates about 60 per cent of the observed defect. For the ^2P series of lithium the percentage is about the same (55 per cent)

Outer orbital	$-X$	$-C$	$^1\Delta$ calc.	$^1\Delta$ obs.	$^3\Delta$ calc.	$^3\Delta$ obs.	$X/\frac{1}{2}(^1\Delta - ^3\Delta)$ (per cent)	$C/\frac{1}{2}(^1\Delta + ^3\Delta)$ (per cent)
2p	839	228	-611	-244	1067	1804	82	34
3p	271	78	-193	-85	349	561	84	33
4p	117	34	-83	-39.5	151	236	85	35
3d	2.8	0.76	-2.04	14.5	3.6	17.8	170	2.4
4d	1.6	0.43	1.03	6.7	2.0	8.6	168	2.8
4f	0.01	0.00	-0.01	≈ 0.20	0.01	≈ 0.81	—	—

Table 1. Calculated defects for helium based on the wavefunction described in the text†.

† Calculations have been made for each series up to $n=9$, and the results not quoted can be obtained on application to the authors.

when the Hartree–Fock wave function is used for the positive ion, but rather poorer (~ 50 per cent) when the best S.T.O. is used†.

We have also examined the effect of introducing electron correlation into the wave function of Li^+ , Mulliken has recently asked whether this is important [3]. We took a wave function

$$\Psi = {}^1\psi(1s^2) + \lambda {}^1\psi(2p^2)$$

where the $1s$ orbital is the best S.T.O. already described and $\psi(2p^2)$ is a 1S function formed from the configuration $2p^2$, in which the exponential factor of the $2p$ S.T.O. (ζ) and λ were both varied to minimize the total energy. The best values were $\zeta = 4.2$, $\lambda = 0.0305$, and this simple function gave 39 per cent of the correlation energy of Li^+ . However, the $2p^2$ part of the wave function only contributes about 11 cm^{-1} to the defect of the $1s^2 2p$ (2P) state. One can therefore assume that correlation in the core is not an important factor in determining the Rydberg defect. That is, an accurate Hartree–Fock wave function of the core is about as good as an exact eigenfunction for calculating a Rydberg defect.

Outer orbital	S.T.O. $1s$				S.C.F. $1s$				
	$-X$	$-C$	${}^2\Delta$ calc.	Δ calc./ Δ obs. (per cent)	$-X$	$-C$	${}^2\Delta$ calc.	Δ calc./ Δ obs. (per cent)	${}^2\Delta$ obs.
2p	372	179	551	48	421	206	627	54	1151
3p	124	61	185	50	140	71	211	57	370
4p	54	27	81	51	61	31	92	58	160
3d	0.67	0.36	1.03	9	0.88	0.52	1.40	12	12.1
4d	0.39	0.18	0.57	10	0.52	0.30	0.82	14	5.8
4f	0.00	0.00	0.00	—	0.00	0.04	0.04	—	—

Table 2. Calculated for lithium similar to those given in table 1, but taking the best S.T.O. $1s$ for the ground state of Li^+ $1s = (2.6875)^{3/2} \pi^{-1/2} \exp(-2.6875r)$ and Roothaan's S.C.F. function for ground state of Li^{++} .

† Calculations have been made for each series up to $n = 9$, and the results not quoted can be obtained on application to the authors.

The calculations show that the exchange term is always larger than the coulomb (penetration) terms and for the P series makes a large contribution to the total defect. It is not therefore a good approximation to neglect the anti-symmetrizing operator in the wave function for the Rydberg state, as has been suggested [3], for orbitals which have no precursors in the core‡.

The accuracy of the calculated defects for the singlet states of helium is much less than for the triplets. However, if we compare $-X$ and $-C$ with $\frac{1}{2}({}^1\Delta - {}^3\Delta)$ and $\frac{1}{2}({}^1\Delta + {}^3\Delta)$ respectively, we can see that the large error for the singlet states

† A similar calculation by Coulson and Stamper [1] gave a considerable improvement using the Hartree–Fock wave function (91 per cent of the observed defect) but their calculation was in error by a factor of 2 in the exchange energy (private communication, Coulson and Stamper).

‡ The term precursor has been introduced by Mulliken, and we include a discussion of it at the end of this paper.

is due to the fact that the calculated value of C is in poor agreement with the mean defect of the singlet and triplet states. On the basis of our choice of wave function, this mean defect is to be identified with the coulomb term (C), but as we shall shortly see, a considerable part of this mean defect is due to correlation between the Rydberg electron and the core (which is called the polarization effect in early work).

The calculated defects for the D states are considerably worse (on a percentage basis) than those for the P states. Examination of the helium results shows that it is not the exchange energy which is seriously at fault, although this does overestimate the singlet-triplet splitting. The electron correlation energy gets relatively more important as the quantum number l of the Rydberg orbital increase.

The S states present a new feature because a hydrogenic outer orbital is not orthogonal to the orbitals of the inner core. In this case, exchanging one electron between the core and the Rydberg gives, in addition to the two-electron integrals, one-electron terms which dominate the exchange integral and make it negative. The calculated defect energy for both the $1s2s(^3S)$ state of helium and the $1s^22s(^2S)$ state of lithium are negative, whereas a large positive defect is observed. The calculated energy for the 1S state of helium is lower than that observed, a situation which can arise because we have not made this state orthogonal to the ground state. The results are summarized in table 3.

	$-X$	$-C$	Δ calc.	Δ obs.
Helium $1s\ 2s(^3S)$	-5424	4722	-702	11035
Helium $1s\ 2s(^1S)$	-5424	4722	10146	4613
Lithium $1s^2\ 2s(^2S)$	-12116	6652	-5464	16066

Table 3. Calculated energies of the (2s) S states using a hydrogen 2s orbital and the best S.T.O. for the case.

The next step in the analysis was to investigate a wave function which still represents one electron outside a core, but does not restrict the outer orbital to be a hydrogen wave function, or the wave function of the core to be an eigenfunction of the positive ion. This type of calculation was carried out for some states of helium and lithium by Eckhart [2] and some of his results were corrected by Wilson [4].

We have calculated the defect in the 2p states using anti-symmetrized products of outer orbital and inner core, but where the effective nuclear charge of both inner and outer orbitals (ζ_1 and ζ_2 respectively) were allowed to vary. In this type of calculation it is misleading to look at the absolute values of X and C as given by (3) and (4). When ζ_1 and ζ_2 are varied to minimize the total energy, both X and C become larger, as apparently required by experiment, but this is to a large extent offset by the increase in zeroth order energy of the state, $E^+ + E_H$. For this reason we quote only the total calculated defect for these calculations. Our results are shown in table 4. It is clear that the outer electron has almost no effect on the size of the inner core and that although the outer orbital may be expanded or contracted through the influence of the core, this has rather little effect on the absolute value of the energy. For example, expressed as a percentage of the observed defect,

the helium $1s2p$ (3P) state energy, relative to the hydrogenic value, is improved from 59 per cent with $\zeta_1=2.00$, $\zeta_2=0.500$, to 69 per cent with $\zeta_1=1.99$, $\zeta_2=0.545$. The comparable improvement for the lithium 2P ($2p$) state is 4 per cent.

Helium $1s\ 2p$ (3P) observed $\Delta=1804\text{ cm}^{-1}$

$\zeta_{1s} \backslash \zeta_{2p}$	0.500 (hydrogen)	0.545 (best)
2.00 (ion)	1067	1248
1.99 (best)	1143	1285

Helium $1s\ 2p$ (1P) observed $\Delta=-244$

$\zeta_{1s} \backslash \zeta_{2p}$	0.500 (hydrogen)	0.485 (best)
2.00 (ion & best)	-611	-537

Lithium $1s^2\ 2p$ (2P) observed $\Delta=1151$

$\zeta_{1s} \backslash \zeta_{2p}$	0.500 (hydrogen)	0.522 (best)
2.6875 (ion)	551	585
2.6865	551	595

Table 4. The effect of varying the exponent of the $1s$ and $2p$ orbitals on the calculated defect (cf. tables 1 and 2).

A necessary criterion for the best $3p$ orbital is that the $3p$ state shall be orthogonal to the $2p$. In the absence of an exact eigenfunction for the $2p$ state we must use the condition that the $3p$ be orthogonal to the approximate $2p$ wave function that has been calculated. There are two obvious functions to try: a hydrogenic $3p$ function having the same effective nuclear charge as the best hydrogenic $2p$ and the best S.T.O. for $3p$ made orthogonal to the best hydrogenic $2p$. The results are shown in table 5; they confirm a result which has been known for ground state orbitals for a long time, that the orthogonalized S.T.O. is the better choice. The nature of the inner loops in an outer orbital is not directly determined by the effective nuclear charge of the core but by the condition of orthogonality to inner orbitals.

Outer orbital	Δ	ζ_{3p}
Screened hydrogenic ($3p$) _{STO} - $\langle 2p 3p\rangle(2p)$ _{STO}	186 199	0.348($=\frac{2}{3}\zeta_{2p}$) 0.30

Table 5. Calculations for $1s^2\ 3p$ (2p) state of Li (cf. table 2).

The calculations in table 3 show that when the Rydberg orbital has a precursor in the core then a hydrogen function gives a very poor calculated defect. In these cases it is very important to take a wave function built up from a non-hydrogenic Rydberg orbital and possibly a core wave function which is not an eigenfunction of the ion. We have compared the best screened hydrogenic 2s orbital with the best S.T.O. The results are shown in table 6. As in the case of the 3p orbitals one finds that the latter is the better function, and for both the ^3S states of helium and the ^2S states of lithium one can obtain a wave function which gives about 95 per cent of the observed defect. The best single determinant wave function for the ground state of lithium gives 97.5 per cent of the observed defect. The remaining 2.5 per cent would imply a correlation energy of 403 cm^{-1} .

Outer orbital	Helium (^3S)	Lithium (^2S)
Best screened hydrogenic	9217 ($\zeta=0.765$)	9788 ($\zeta=0.886$)
Best S.T.O.	10420 ($\zeta=0.57$)	15584 ($\zeta=0.637$)
Observed	11035	16066

Table 6. Calculated defects for the 2s orbitals.

Relative to the total defect a wave function which introduces no correlation between the outer electron and the core is better for the S series than for the P, and for the D series and beyond this type of wave function gives practically none of the observed defect. The absolute value of the correlation energy of the S series is about the same for the P series, but it then becomes rather small for the D series.

We turn now to a brief analysis of these correlation energies. An explanation of the Rydberg defect of orbitals which have no precursor in the core was given as early as 1924 by Born and Heisenberg [6]. Their explanation was based on a semi-classical model in which the outer electron polarized the inner core and was attracted by the induced dipole. This model was put into modern quantum mechanics by Mayer and Mayer [7] and their work has been frequently quoted [8] as a source for obtaining the polarizabilities of ions. However there is a rather serious deficiency in the Mayers' work which is that it is not based on an anti-symmetrized wave function, and we have already shown that a considerable part of the defect of the P series of helium and lithium comes from the exchange terms.

In the Mayers' theory the interaction between the outer electron and the core is introduced through a perturbation term in the Hamiltonian and which they write as $H' = H_a + H_b$:

$$H_a = -\frac{\mathbf{R} \cdot \mathbf{r}}{r^3},$$

$$H_b = -\frac{1}{2} \frac{1}{r^3} \left[\left(\frac{\mathbf{R} \cdot \mathbf{r}}{r} \right)^2 - R^2 \right],$$

where \mathbf{r} is the position vector of the Rydberg electron and $\mathbf{R} = \sum \mathbf{r}_i$ is the sum of the position vectors of the electrons in the core. H_a represents the interaction of the outer electron with a dipolar distortion of the core; H_b represents the interaction of the outer electron with a quadrupolar distortion of the core. H' represents the

first terms in the expansion of the Hamiltonian under the condition that the outer electron is always further from the nucleus than the electrons of the core: this is not necessarily a good approximation. In the Mayers' theory H_a and H_b can be considered as independent perturbations, but this is only true if one uses non-anti-symmetrized functions since in this case by symmetry any two states that can interact under the influence of H_a will not interact under the influence of H_b and vice versa. It is not however true for anti-symmetrized functions as we can see from the following examples.

Consider the $1s2p_0$ (the zero indicates a z -component of angular momentum of zero). This can interact with the 3P state arising from the configuration $(np)(md)$. The Hamiltonian matrix element between these states will involve integrals of the type:

$$\langle 1s2p_0 || \frac{1}{r_{12}} || np_0md_0 \rangle;$$

there are two contributions to this matrix element as follows:

$$\begin{aligned} \langle 1s2p_0 || \frac{1}{r_{12}} || np_0md_0 \rangle = & \int \int 1s(1)2p_0(2) \frac{1}{r_{12}} np_0(1)md_0(2) d\tau_1 d\tau_2 \\ & - \int \int 1s(1)2p_0(2) \frac{1}{r_{12}} np_0(2)md_0(1) d\tau_1 d\tau_2. \end{aligned} \quad (5)$$

The first represents the interaction of the dipolar density $1snp_0(1)$ with the dipolar part of $np_0md_0(2)$: on the assumption that electron (1) is always closer to the nucleus than electron (2) the perturbation to electron (2) can be expressed by the dipolar term H_a . The second integral represents the interaction of the quadrupolar density $1smd_0(1)$. With the quadrupolar part of $2p_0np_0(2)$. Again this may be represented by the quadrupolar perturbation term H_b provided electron (2) is always outside electron (1). It is clear however that the dipolar and quadrupolar perturbations are not separable in this case, but in fact oppose each other.

We have examined the effect of the excited state $2p'3d(^3P)$ on the energy of the $1s2p(^3P)$ state of helium. This was done by maximizing the second-order interaction energy:

$$\frac{5}{2} \langle 1s2p_0 || \frac{1}{r_{12}} || 2p'_0(\zeta)3d_0(\eta) \rangle^2 / \Delta E(\zeta, \eta)$$

with respect to the Slater exponents ζ and η of the $2p'$ and $3d$ orbitals. $\Delta E(\zeta, \eta)$, the energy separation between the two 3P states was calculated using the average energy of all states obtained from the $2p'3d$ configuration. The maximum stabilization was obtained with $\zeta=1.88$, $\eta=1.28$. With these parameters the dipolar and quadrupolar parts of the matrix element (5) had the values 0.0274 and 0.0040 A. U. respectively, so that although one can say that the predominant part of the interaction is dipolar, the quadrupolar part reduces the matrix element by about $\frac{1}{7}$. The stabilization energy calculated in this way is 130 cm^{-1} which is 25 per cent of the correlation energy (taking this as that part of the defect not given by the best single determinant function that we used—see table 4).

The effect of this excited configuration is perhaps better interpreted as separating the electrons from the region where the $1s$ and $2p$ orbitals overlap than as polarizing the inner core in the field of the outer electron. The calculations we have made indicate that a configuration interaction treatment of this correlation energy is likely to be more slowly convergent than a similar calculation for the correlation energy of two electrons in the same orbital (e.g. the helium atom problem).

2. CONCLUSIONS

The results of our calculations on helium and lithium are summarized below.

The p series

About 60 per cent of the total defect can be attributed to penetration and exchange energies and the rest to correlation energy. The exchange energy is larger than the penetration and so it is certainly necessary to work with an anti-symmetrized wave function. Providing the core wave function is built up from reasonably good S.T.O.'s for the positive ion, the coulomb and exchange contributions are calculated quite accurately. There is very little improvement in using accurate Hartree-Fock functions for the core or in using a core wave function which includes correlation. There is also very little improvement in the total energy if the core and Rydberg orbitals are varied to minimize the total energy (that is, one does not restrict them to bring good wave functions for the positive ion and a hydrogen function, respectively).

The s series

A very poor value is calculated for the Rydberg defect from a wave function based on an eigenfunction of the core and a hydrogen orbital. It is essential to vary both the core and the Rydberg orbital to minimize the total energy. However, a wave function obtained in this way (e.g. the best single determinant function for the ground state of lithium) gives a very good calculated defect. The correlation energy in this case is a small part of the total defect energy, although in absolute magnitude it is comparable to the correlation energy for the P series.

The d series

The Rydberg defect is almost entirely due to correlation between the outer electron and the electrons of the core.

Finally, there are two general comments which hold for all series. When the coulomb and exchange contributions to the defect are of opposite sign, as they are for the singlet states of He (and as they will be for all singlet excited states of closed-shell molecules) then the relative accuracy to which one can calculate the Rydberg defect is much worse. Also, for Rydberg orbitals which are not the first members of a series (e.g. $2s$, $3p$) it is better to take S.T.O.'s orthogonalized to the lower members of the series rather than hydrogen orbitals based on the effective nuclear charge of the first member.

One can reasonably expect to generalize these results to more complex atoms. The results for the s series will hold for any Rydberg series which has an orbital of the same l -value in the core. The results for the p series will hold if the Rydberg orbital has a l -value one greater than the highest l value of the core orbitals; and the d series results will apply to those having l two or more greater than the highest l value of the core orbitals.

The generalization to molecules is much more suspect and has still to be tested. Mulliken classifies Rydberg orbitals of molecules into two classes in the following manner. Each Rydberg orbital is assigned to a Rydberg series (a series being a set of states whose term values fit the general formula $-R/(n-\delta)^2$). If the first member of this series (e.g. 1s, 2p, 3d, 4f) is to be correlated with a core orbital (the series has a precursor in the core) then the Rydberg orbital is said to be penetrating and has a large defect. If the first member of the series is itself a Rydberg orbital then the orbital is non-penetrating and has a small defect. We would expect that the wave functions and energies of the penetrating orbitals should be subject to the same criterion as the s states of helium and lithium. On the other hand, we expect that Mulliken's non-penetrating orbitals should really fall into two classes, those whose first member has an l value greater by one than the highest l value of the core orbitals (analogous to the p series of helium and lithium) and those of still higher l value (cf. the d series).

The weakness of the Mulliken classification lies in deciding whether the first member of the Rydberg series is to be correlated with a core orbital or not. For small molecules (e.g. NH_3), one can take this correlation relative to the united atom orbitals (in this case Ne); an investigation on this type of molecule will be reported in a later publication. But for large molecules this is clearly unsatisfactory as the united atom orbitals would be occupied to very high quantum numbers. There is clearly a great deal more work necessary before one can give a confident classification of Rydberg states of large molecules.

REFERENCES

- [1] COULSEN, C. A., and STAMPER, J., 1963, *Mol. Phys.*, **6**, 609.
- [2] ECKHART, C., 1930, *Phys. Rev.*, **36**, 878.
- [3] MULLIKEN, R. S., 1964, *J. Amer. chem. Soc.*, **86**, 3183.
- [4] WILSON, E. B., 1933, *J. chem. Phys.*, **1**, 210.
- [5] Roothaan, C. C. J., 1960, *Rev. mod. Phys.*, **32**, 186.
- [6] BORN, M., and HEISENBERG, W., 1924, *Z. Phys.*, **23**, 407.
- [7] MAYER, J. E., and MAYER, M. E., 1933, *Phys. Rev.*, **43**, 605.
- [8] BUCKINGHAM, A. D., 1959, *Quart. Rev. chem. Soc.*, **13**, 183.

Détermination des signes relatifs des constantes de couplage ^{31}P - ^1H dans le tripropyl phosphate par R.M.N. dans le champ magnétique terrestre†

par E. DUVAL, J. RANFT‡ et G. J. BÉNÉ

Institut de Physique Expérimentale
de l'Université de Genève, Suisse

(Received 21 December 1964)

Le spectre protonique du tripropyl phosphate dans le champ magnétique terrestre est étudié. Les valeurs absolues des constantes d'interaction ayant été déterminées par le spectre à 100 Mc/s, il est alors possible de comparer le spectre en champ faible aux spectres calculés par un ordinateur. Cette comparaison permet de déterminer les signes relatifs des constantes d'interaction phosphore-proton. Une interprétation théorique du couplage spin (noyau)-spin (noyau) fixe les signes absolus des constantes d'interaction phosphore-proton.

1. INTRODUCTION

Dans le champ magnétique terrestre, c'est-à-dire à 0,45 Gs les déplacements chimiques sont pratiquement nuls, et ainsi la fréquence de résonance d'un noyau quelconque est tout simplement proportionnelle au rapport gyromagnétique de ce noyau. Pour une telle valeur du champ magnétique, la fréquence de résonance du proton se situe à 1925 c/s et celle du phosphore à 780 c/s. Si alors les constantes d'interaction entre proton et phosphore sont inférieures à 10 c/s, ce qui est le cas pour le produit étudié ici, les projections des spins suivant la direction du champ magnétique peuvent être considérées comme de bons nombres quantiques par rapport à cette interaction qui a pour effet, finalement, d'introduire un déplacement chimique fictif entre les protons de groupes différents. Ce 'déplacement chimique effectif' est égal à la demi-différence des constantes d'interaction phosphore-proton.

Remarquons enfin que le spectre protonique est symétrique, une partie se rapportant au phosphore dans l'état $+\frac{1}{2}$ l'autre au phosphore dans l'état $-\frac{1}{2}$.

Ces différentes constatations nous permettent de voir que les signes relatifs des constantes d'interaction phosphore-proton apparaissent dans les spectres en champ faible, les déplacements chimiques effectifs n'ayant pas la même valeur si les constantes sont de mêmes signes ou de signes différents.

Il est en général nécessaire de comparer les résultats des spectres en champ faible aux spectres calculés électroniquement car les déplacements chimiques effectifs étant de l'ordre de 4 c/s et les constantes d'interaction entre protons de l'ordre de 8 c/s, la structure de ces spectres est en général très complexe. Pour le calcul nous nous servons des valeurs absolues des constantes de couplage obtenues en champ fort où il est plus facile de les déterminer directement. Ces

† Recherche financée par le fonds national suisse pour la recherche scientifique.

‡ Physicien invité, de l'Université Karl Marx de Leipzig.

valeurs pourront d'ailleurs être améliorées par l'étude du spectre en champ faible où la précision peut atteindre aisément $\pm 0,02$ c/s; en particulier lorsque le groupe de protons interagissant avec le phosphore interagit lui-même avec un autre groupe de protons en nombre pair. On sait en effet que dans ce cas, une fréquence de transition à la valeur $\nu_H + \frac{1}{2}J_{P-H}$ correspondant au phosphore dans l'état $-\frac{1}{2}$, ν_H étant la fréquence de résonance du proton, J_{P-H} la constante d'interaction phosphore-proton qui est alors déterminée par la distance des deux raies correspondant à ces transitions.

La technique de R.M.N. en champ faible nous a déjà permis de déterminer les signes relatifs des constantes d'interaction phosphore-proton dans les triéthyl phosphate [1] et phosphite [2] et de préciser les valeurs des constantes d'interaction des protons du groupe méthyle qui sont inférieures à 1 c/s.

Nous allons maintenant exposer les résultats de l'étude du spectre du tripropyl phosphate que nous comparerons à ceux déjà obtenus sur d'autres produits organo-phosphorés.

2. SPECTRES EN CHAMP FORT

Afin de pouvoir calculer le spectre en champ faible nous avons déterminé les valeurs absolues des constantes d'interaction du tripropyl phosphate

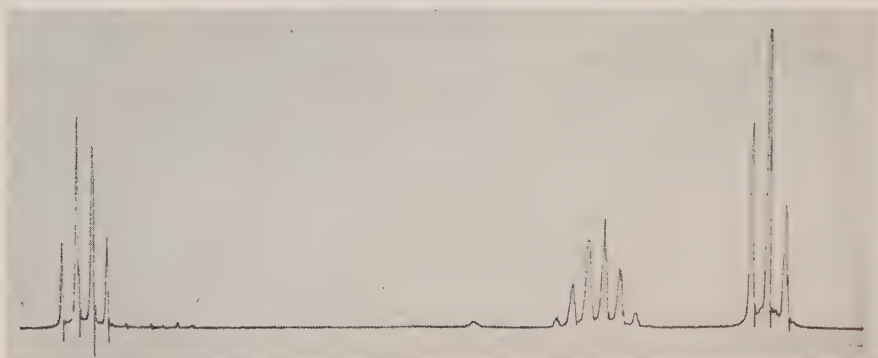
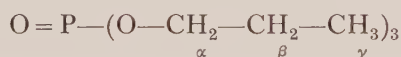


Figure 1. Spectre à 100 Mc/s.

à l'aide des spectres à 60 et 100 Mc/s.

Chaque multiplet de ces spectres a été examiné soigneusement après l'avoir obtenu par un balayage lent. Le multiplet correspondant aux protons α se compose de deux triplets légèrement décalés qui nous permettent de déterminer $|J_{P-H\alpha}|$ et $|J_{H\alpha-H\beta}|$. Le multiplet correspondant aux protons β est plus complexe. Nous devons utiliser le calcul exact fait par Corio [3] dans le cas A_2B_3 pour déterminer $|J_{H\beta-H\gamma}|$, le rapport

$$\left| \frac{J_{H\beta-H\gamma}}{\delta_{H\beta} - \delta_{H\gamma}} \right| (\delta_{H\beta-H\gamma}, \text{ étant le déplacement chimique effectif})$$

étant de l'ordre de 0,1 à 100 Mc/s. Ces trois premières constantes d'interaction étant déterminées, on peut alors évaluer la valeur approximative de $|J_{P-H\beta}|$.

Finalement nous avons les valeurs suivantes :

$$|J_{\text{P-H}\alpha}| = 7,6 \text{ c/s}, \quad |J_{\text{P-H}\beta}| \simeq 0,8 \text{ c/s}, \quad |J_{\text{P-H}\gamma}| \simeq 0, \quad |J_{\text{H}\alpha-\text{H}\beta}| = 6,8 \text{ c/s}$$

$$|J_{\text{H}\beta-\text{H}\gamma}| = 7,5 \text{ c/s}.$$

3. SPECTRES EN CHAMP FABLE.

DÉTERMINATION DES SIGNES RELATIFS

Comme nous l'avons déjà fait remarquer les termes de couplage du phosphore avec les protons peuvent se traiter comme des déplacements chimiques.

Les déplacements chimiques effectifs entre les différents groupes de protons sont alors égaux à :

$$\delta_{\text{H}\alpha-\text{H}\beta} = \frac{J_{\text{P-H}\alpha} - J_{\text{P-H}\beta}}{2},$$

$$\delta_{\text{H}\alpha-\text{H}\gamma} = \frac{J_{\text{P-H}\alpha}}{2},$$

$$\delta_{\text{H}\beta-\text{H}\gamma} = \frac{J_{\text{P-H}\beta}}{2}.$$

$J_{\text{P-H}\beta}$ est considéré comme nul. Il peut être facile de rectifier cette valeur par la suite lors de la comparaison spectre expérimental—spectre théorique.

L'emploi du programme de Swalen a permis de calculer les spectres théoriques correspondant à différentes valeurs de $J_{\text{P-H}\beta}$, soit : 0,6 c/s, 0,8 c/s, 1,0 c/s, les signes

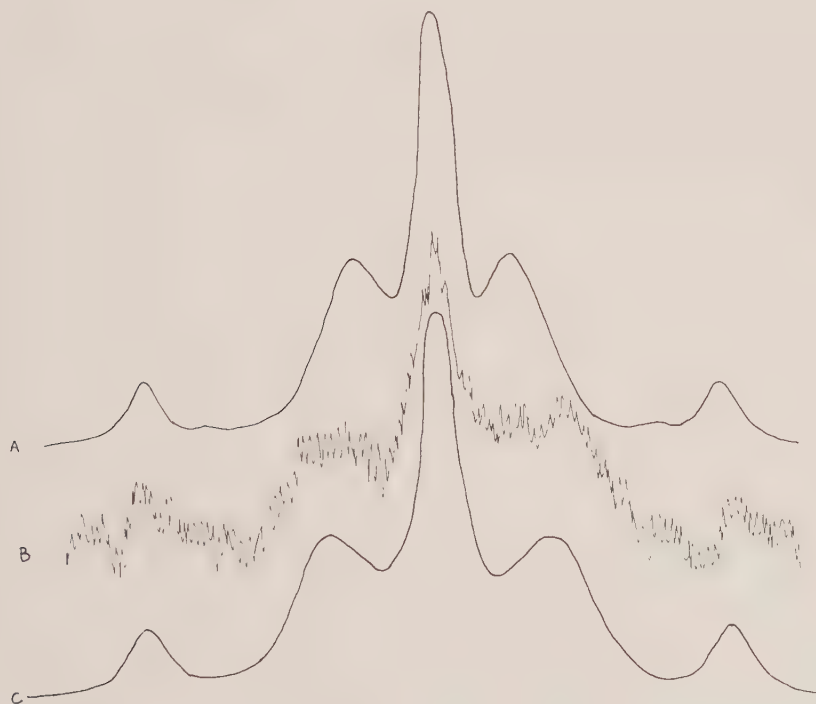


Figure 2. Comparaison spectre expérimental spectres calculés pour $J_{\text{P-H}\beta} = 0,8 \text{ c/s}$.

A: Spectre calculé: $J_{\text{P-H}\alpha}$ et $J_{\text{P-H}\beta}$ sont de signes différents.

B: Spectre expérimental.

C: Spectre calculé: $J_{\text{P-H}\alpha}$ et $J_{\text{P-H}\beta}$ sont de mêmes signes.

relatifs de $J_{P-H\alpha}$ et $J_{P-H\beta}$ étant identiques ou différents. La largeur de raie a été fixée à 0,4 c/s, valeur déterminée pour le triméthyl-phosphate.

L'accord entre spectre théorique et spectre expérimental est pour $J_{P-H\alpha}$ et $J_{P-H\beta}$ de mêmes signes.

Nous ne pouvons préciser mieux la valeur absolue de $J_{P-H\beta}$, les spectres théoriques différant peu entre $J_{P-H\beta}=0,6$ c/s et $J_{P-H\beta}=1$ c/s; nous espérons pouvoir le faire lorsque le rapport signal sur bruit de notre appareil sera amélioré. Le spectre nous permet de justifier la valeur de $J_{P-H\alpha}$ trouvée en champ fort, cette constante correspondant à la distance des deux pics extrêmes, conformément à ce qui a été dit auparavant.

4. DISCUSSION

Dans une publication antérieure [4] il a été montré que l'interaction spin (noyau)–spin (noyau) était fonction des intégrales d'échange entre électrons. Le fait que les intégrales d'échange inter-atomiques soient en général négatives et les, intégrales d'échange intra-atomique positives donne la possibilité aux constantes de couplage d'être soit positives soit négatives suivant le nombre d'atomes intervenant entre les deux noyaux interagissant. Nous avons admis dans une première approximation que la constante de couplage était due à l'interaction électronique à travers la chaîne moléculaire et d'autre part à l'interaction directe des électrons des atomes auxquels appartiennent les noyaux interagissant. Donc pour autant que l'on puisse admettre que le signe de l'intégrale d'échange entre deux électrons ne varie pas avec la distance des deux atomes, on voit que le premier processus donne une contribution de même signe que le processus direct si le nombre d'atomes intermédiaires est pair, de signe différent si le nombre d'atomes intermédiaires est impair.

Puisque $J_{PH\alpha}$ et $J_{PH\beta}$ sont de même signe ce serait le processus direct qui serait prépondérant dans le couplage P–H β .

Substances	$J_{P-H\alpha}$ (c/s)	$J_{P-H\beta}$ (c/s)	Signes relatifs	Réf.
$(CH_3-CH_2-CH_2O)_3 P=O$	7,6	0,8	Identiques	Cet article
$(CH_3-CH_2O)_3 P=O$	8,4	0,84	Identiques	[1]
$(CH_3-CH_2O)_3 P$	7,9	0,55	Contraires	[2]
$(CH_3-CH_2)_3 P$	0,5	13,7	Contraires	[5]

D'après ce tableau, il en est de même pour le triéthyl phosphate, tandis que les signes sont différents pour les triéthyl phosphite et phosphine. Il semble alors que l'intégrale d'échange des électrons du phosphore avec ceux du proton soit sensible au caractère 's' des électrons de liaison du phosphore ce qui n'est pas étonnant car celui-ci influence la forme et l'étendue des orbitales de liaison.

Nous remercions le Docteur Melera de Varian (Zurich) qui a bien voulu se charger de prendre les spectres à 60 et 100 Mc/s. Nous sommes reconnaissant d'autre part au Docteur Swalen qui nous a fourni le programme pour le calcul des spectres, ainsi qu'au CERN qui a mis l'ordinateur IBM 7090 à notre disposition

RÉFÉRENCES

- [1] BÉNÉ, G. J., DUVAL, E., FINAZ, A., et HOCHSTRASSER, G., 1963, *C.R. Acad. Sci. Paris*, **256**, 2365.
- [2] BÉNÉ, G. J., DUVAL, E., FINAZ, A., HOCHSTRASSER, G., et KOÏDÉ, S., 1963, *Phys. Letters*, **7**, 34.
- [3] CORIO, P. L., 1960, *Chem. Rev.*, **60**, 363.
- [4] KOÏDÉ, S., et DUVAL, E., 1964, *J. chem. Phys.*, **41**, 315.
- [5] NARASIMHAN, P. T., et ROGERS, M. T., 1961, *J. chem. Phys.*, **34**, 1049.

The distortions of the ethylene molecule in its low-lying excited states—a four-electron treatment

by LOUIS BURNELLE

Research Institute for Advanced Studies (Martin Company),
1450 South Rolling Road, Baltimore, Maryland 21227

and CLOTILDE LITT

Institut d'Astrophysique, Université de Liège,
Cointe-Sclessin, Belgium

(Received 10 February 1965)

Calculations have been carried out on the low-lying excited states of ethylene, with a view of determining whether there appears a pyramidal arrangement of the bonds around each carbon atom, in addition to the twisting of the two CH_2 groups. The two π -electrons and the two electrons of the CC σ -bond are treated as valence electrons; the core is formed by four hybrids pointing toward the hydrogen atoms, whose effect is neglected. The interaction between the valence electrons and the core is taken explicitly into account, but variation of the core energy with the distortions is neglected. It is found that in the (twisted) T state a flapping of the two CH_2 groups produces a significant stabilization (0.7 eV for a tetrahedral arrangement of the bonds), whereas in the V state it causes an increase in energy. It appears from the study of the flapping in the non-twisted molecule that the relative stabilities of the cis- and trans-conformations in the ground state are not predicted correctly. This lack of success, which has been encountered also with other approximations in similar problems, stresses the need for more accurate calculations.

1. INTRODUCTION

The purpose of this work is to study the changes of shape undergone by ethylene in its first excited states. The idea that the molecule loses its planarity when it is electronically excited had already been introduced many years ago. Indeed, in 1931, Olson [1] suggested that a twisting might take place in the excited state corresponding to the absorption observed in the 2000 Å region. Mulliken [2] then deduced from semi-quantitative considerations that the molecule was twisted by 90° in its T and V states[†]. The vibrational structure of the $N \rightarrow V$ absorption system was later found to be in agreement with such a distortion in the V state [4].

On the other hand, the development of molecular orbital theory made feasible more quantitative theoretical approaches. Thus Mulliken and Roothaan carried out a semi-empirical treatment of the two-electron problem [5]; likewise Parr and Crawford assimilated the molecule to a two-electron system in a core

[†] The notations N , T , V and Z are now widely adopted (see for example references [3] and [4]) and we will adhere to them.

field but introduced fewer empirical parameters [6]. Very recently the question of the twisting taking place in the T , V and Z states was tackled by Moskowitz and Harrison [7] who took into account all 16 electrons of the molecule.

The results of all the above studies agree on the point that in its first three excited states the two CH_2 groups make an angle of 90° with each other, so that the twisting in those states leaves no doubt. However, the question that other distortions might appear in addition to the twisting was raised by Walsh some time ago [8]. Walsh suggested that there would be a pyramidal arrangement of the bonds around each carbon atom; this would correspond to the excited orbital's acquiring some s character, which, according to Walsh, would stabilize the orbital. He also suggested that each carbon atom would be slightly out of the mirror plane bisecting the HCH angle of the other CH_2 group.

Since the spectrum of ethylene is fairly diffuse and complicated, the experimental detection of the distortions suggested by Walsh is practically impossible in the present stage of experimental techniques. We believe that this is one of the cases where it appears that only a quantitative theoretical treatment can solve the question.

In a study on the mechanism of the electrophilic additions on the double CC bond [9], we have been led recently to find arguments in favour of the structure proposed by Walsh [8]. Calculations have indicated that these reactions very probably proceed through the twisted configuration [9]. These additions are known to be stereospecific [10] and to interpret this peculiarity we have suggested that in ethylene and its derivatives the excited state has a structure involving a trans-flapping and a twisting.

The determination of the geometrical structure of the low-lying states of ethylene thus appears to be important from two points of view: first for our understanding of the properties of molecular orbitals, and second for our comprehension of the chemical reactivity of ethylenic compounds†.

In investigating the energy changes associated with the flapping of the two CH_2 groups our main purpose was thus to determine whether flapping would lower the energy of the twisted molecule in its excited states. But for the sake of completeness we have also included the flapping in the planar molecule (this gives rise to a *cis*- or a *trans*-arrangement of the two CH_2 groups), in the various states which have been considered.

When the molecule is flapped a change of hybridization takes place, the $2p\pi$ atomic orbitals of the carbons being now mixed with the s -type orbitals. Conversely, the sp^2 hybrids forming the CH bonds will lose some of their s character, the more so as the bending increases, and when a tetrahedral arrangement of the bonds will be reached, they will have become sp^3 hybrids. The situation is therefore basically different from that which results from a mere twisting of the two CH_2 groups, in which case no change of hybridization takes place and the π -electron approximation may be invoked to carry out a two-electron treatment.

2. METHOD OF CALCULATION

In view of the very nature of the problem, it has been decided to treat the molecule as a four-electron system. The two electrons of the CC σ -bond have thus been included in the valence electrons and the interactions (coulombic

† It is to be mentioned that extended Hückel calculations on ethylene have not detected any departure from a trigonal arrangement of the bonds in the first excited state (see reference [11]).

and exchange) between the four valence electrons and the core was explicitly taken into account. Moreover, the core was modified with the bending. To simplify the problem, the hydrogen atoms have been neglected and the CH bonds assimilated to hybrids pointing toward the hydrogens. The core was built from MO's which were linear combinations of these hybrids. The 1s electrons of the carbons were supposed to be collapsed on the nuclei, because if the W_p approximation [12] is used and if it is supposed that the mixing of the 1s orbitals with the other MO's is negligible, the effect of the inner-shell electrons is actually included in the semi-empirical parameter which is used for W_p . This is the procedure which has been adopted.

One electron was allotted to each of the core MO's. In calculating the interaction energy between the core and the valence electrons we have merely divided by two the term which one would obtain by supposing that the core orbitals are doubly occupied.

For example, suppose we calculate the energy of a closed-shell configuration (the extension to the open-shell configurations we have considered is straightforward). It is known [13] that the electronic energy of the system is given by:

$$E = 2 \sum_{i=1}^k H_i + \sum_{i,j} (2J_{ij} - K_{ij}), \quad (1)$$

where the summation extends over all the k doubly occupied MO's and the symbols J , K and H refer to the coulomb, exchange and one-electron operators, respectively. Now we divide the k occupied orbitals into s core orbitals and $k-s$ valence orbitals. The energy can then be divided into several terms:

$$E = 2 \sum_{i=1}^s H_i + \sum_{i=1}^s \sum_{j=1}^s (2J_{ij} - K_{ij}) + 2 \sum_{l=s+1}^k H_l + \sum_{l=s+1}^k \sum_{m=s+1}^k (2J_{lm} - K_{lm}) \\ + 2 \sum_{i=1}^s \sum_{l=s+1}^k (2J_{il} - K_{il}). \quad (2)$$

The first two terms constitute the core energy, which has been considered as a constant. The third and fourth refer similarly to the valence orbitals, while the last one represents the interaction between the doubly occupied valence orbitals and the doubly occupied core orbitals. In the case of the singly occupied orbitals treated below, the factor 2 in the last term above has to be replaced by unity.

It is convenient to introduce at this point the one-electron energies, defined as follows if one adopts our assumption concerning the singly occupied core orbitals:

$$\epsilon_i = H_i + \sum_{i=1}^s (J_{ii} - 1/2 K_{ii}). \quad (3)$$

These are the eigenvalues of what we may call the core hamiltonian:

$$H^c = H + \sum_i (J_i - 1/2 K_i). \quad (4)$$

Then the component of the electronic energy which is to be calculated can be written:

$$E = 2 \sum_{l=s+1}^k \epsilon_l + \sum_{l=s+1}^k \sum_{m=s+1}^k (2J_{lm} - K_{lm}). \quad (5)$$

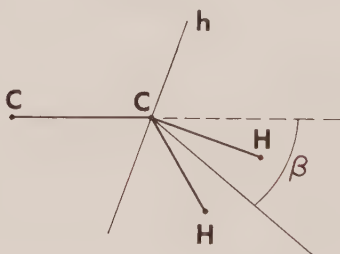
The energy has been calculated for the electronic configurations represented by the following determinantal wave functions:

$$\begin{aligned}
 \Phi_1 &= |(\dots \text{core} \dots) \sigma \bar{\sigma} \pi \bar{\pi}| \\
 \Phi_V &= \sqrt{\frac{1}{2}} \{ |(\dots \text{core} \dots) \sigma \bar{\sigma} \pi \bar{\pi}^*| - |(\dots \text{core} \dots) \sigma \bar{\sigma} \bar{\pi} \pi^*| \} \\
 \Phi_T &= \begin{cases} \sqrt{\frac{1}{2}} \{ |(\dots \text{core} \dots) \sigma \bar{\sigma} \pi \bar{\pi}^*| + |(\dots \text{core} \dots) \sigma \bar{\sigma} \bar{\pi} \pi^*| \} \\ \text{or } |(\dots \text{core} \dots) \sigma \bar{\sigma} \pi \pi^*| \\ \text{or } |(\dots \text{core} \dots) \sigma \bar{\sigma} \bar{\pi} \bar{\pi}^*| \end{cases} \\
 \Phi_2 &= |(\dots \text{core} \dots) \sigma \bar{\sigma} \pi^* \bar{\pi}^*|
 \end{aligned} \tag{6}$$

Here, σ represents the orbital associated with the CC σ -bond and π is the bonding orbital formed by the $2p\pi$ AO's or by the hybrids derived from them when the molecule flaps; similarly, π^* is the corresponding anti-bonding orbital. In the expressions above, as usual, the absence of a bar denotes a spin orbital with α spin, the presence of a bar, a spin orbital with β spin.

Φ_1 and Φ_2 belong to the same symmetry and configuration interaction between the two states has been taken into account.

It may be convenient to describe briefly the derivation of the expressions for the MO's. First, the four hybrids centred on each carbon atom have been determined in the following way. The amount of flapping is measured by the angle β between the prolongation of the CC bond and the bisector of the HCH angle, as indicated in the figure. It has been supposed that as the CH_2 groups flap the HCH angle is modified in such a way that the three angles formed by the bonds emanating from each carbon atom remain equal to each other. It has further been assumed that the hybrid derived from the $2p\pi$ AO of a given carbon follows the motion of the CH_2 group by remaining oriented along the h axis, which bisects the supplement of β (see figure). The expressions for the hybrids



can be derived from the orthonormality conditions, once their direction is imposed by the indicated procedure. The expressions thus obtained will not be reproduced here. The $2s$ orbitals used in the treatment were made orthogonal to the corresponding $1s$ AO's.

Then from the hybrids localized molecular orbitals were built: the three valence MO's σ , π , π^* plus four MO's associated with the CH bonds, which will be designated by the collective label ψ_{CH} . Some of these MO's belong to the same irreducible representation and it was therefore necessary to orthogonalize them. This was done by Schmidt's orthogonalization method. The number of vectors to be orthogonalized varied in each case, according to the geometric configuration of the molecule. Table 1 lists the various configurations which

have been considered, together with their corresponding point groups. Table 2, on the other hand, gives the irreducible representations which the MO's belong to and thus indicates which orbitals were to be orthogonalized.

Geometrical configuration	Point groups
Planar	$D_{2h} = V_h$
Twisted by 90° , non-flapped	D_{2d}
Cis-flapped	C_{2v}
Trans-flapped	C_{2h}
Twisted by 90° and flapped	C_2

Table 1. Point groups of the various geometrical configurations.

For example, in the planar molecule one of the ψ_{CH} MO's was to be made orthogonal to σ ; in the twisted and flapped molecule, σ and two of the ψ_{CH} MO's were to be made orthogonal to π , etc., etc.

The electronic energies of the four electronic configurations have the following expressions:

$$E_1 = E_{\text{core}} + 2\epsilon_\sigma + 2\epsilon_\pi + J_{\sigma\sigma} + J_{\pi\pi} + 2(2J_{\sigma\pi} - K_{\sigma\pi}),$$

$$E_2 = E_{\text{core}} + 2\epsilon_\sigma + 2\epsilon_{\pi^*} + J_{\sigma\sigma} + J_{\pi^*\pi^*} + 2(2J_{\sigma\pi^*} - K_{\sigma\pi^*}),$$

$$E_V = E_{\text{core}} + 2\epsilon_\sigma + \epsilon_\pi + \epsilon_{\pi^*} + J_{\sigma\sigma} + J_{\pi\pi^*} + K_{\pi\pi^*} + 2J_{\sigma\pi} - K_{\sigma\pi} + 2J_{\sigma\pi^*} - K_{\sigma\pi^*},$$

$$E_T = E_{\text{core}} + 2\epsilon_\sigma + \epsilon_\pi + \epsilon_{\pi^*} + J_{\sigma\sigma} + J_{\pi\pi^*} - K_{\pi\pi^*} + 2J_{\sigma\pi} - K_{\sigma\pi} + 2J_{\sigma\pi^*} - K_{\sigma\pi^*}.$$

Geometrical configuration	Irreducible representations of the MO's
Planar	$\pi: B_{3u}, \pi^*: B_{2g}$ $\sigma: A_{1g}$ $\psi_{CH}: 1A_{1g} + 1B_{1u} + 1B_{2u} + 1B_{3g}$
Twisted by 90° , non-flapped	$\pi, \pi^*: E$ (degenerate pair) $\sigma: A_1$ $\psi_{CH}: E$ (degenerate pair) + $1A_1 + 1B_2$
Cis-flapped	$\pi: A_1, \pi^*: B_1$ $\sigma: A_1$ $\psi_{CH}: 1A_1 + 1A_2 + 1B_1 + 1B_2$
Trans-flapped	$\pi: B_u, \pi^*: A_g$ $\sigma: A_g$ $\psi_{CH}: 1A_g + 1B_g + 1B_u + 1A_u$
Twisted by 90° and flapped	$\pi: A, \pi^*: B$ $\sigma: A$ $\psi_{CH}: 2A + 2B$

Table 2. Symmetry properties of the different MO's.

In the calculation of the one-electron energies we have used the W_p approximation, according to the following procedure.

Consider first ϵ_π . If we write π in the form:

$$\pi = C(\psi_A + \psi_B), \quad (7)$$

where ψ_A and ψ_B are appropriate hybrids centred on atom A and atom B, respectively, and C is a normalization coefficient, then

$$\epsilon_\pi = 2C^2(\int \psi_A^* H^c \psi_A dt + \int \psi_B^* H^c \psi_A dt). \quad (8)$$

The W_p approximation [12] may be expressed by the following equation:

$$T\psi_A - Z_c\psi_A/r_A + \sum_p (J_p - 1/2 K_p)\psi_A = W_{\text{hybr}}\psi_A, \quad (9)$$

where the p 's are the hybrids constituting the core in the appropriate atomic valence state. In the non-flapped case, for instance, the p 's will be three sp^2 hybrids and W_{hybr} will be equal to the standard value of W_{2p} . When the flapping angle is such that a tetrahedral structure is reached, then the p 's will be sp^3 hybrids and W_{hybr} will be the valence state ionization potential corresponding to the process $C(\text{te te te te}) \rightarrow C^+(\text{te te te})$.

Now, on the other hand,

$$H^c\psi_A = T\psi_A - Z_c\psi_A/r_A - Z_c\psi_A/r_B + \sum_i (J_i - 1/2 K_i)\psi_A. \quad (10)$$

The i 's are here the MO's forming the core *in the molecule*.

By replacing in equation (10) $H^c\psi_A$ by expression (12) and taking (11) into account one finally arrives at:

$$\begin{aligned} \epsilon_\pi = W_{\text{hybr}} + 2C^2\{ & -Z_c[(C_B : \psi_A\psi_A) + (C_B : \psi_A\psi_B)] \\ & + \sum_i [J_{iA} - 1/2 K_{iA} + (ii : \psi_A\psi_B) - 1/2 (i\psi_A : i\psi_B)] \\ & - \sum_p [J_{pA} - 1/2 K_{pA} + (pp : \psi_A\psi_B) - 1/2 (p\omega_A : p\psi_B)]\}. \end{aligned} \quad (11)$$

For $\epsilon_{\pi*}$ a very similar expression is arrived at. In the same way, if σ is written:

$$\sigma = C'(\chi_A + \chi_B), \quad (12)$$

where χ_A and χ_B are pointing toward each other, one obtains:

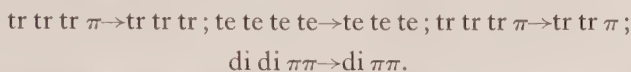
$$\begin{aligned} \epsilon_\sigma = W_x + 2C'^2\{ & -Z_c[(C_B : \chi_A\chi_A) + (C_B : \chi_A\chi_B)] \\ & + \sum_i [(ii : \chi_A\chi_A) - 1/2 (i\chi_A : i\chi_A) + (ii : \chi_A\chi_B) - 1/2 (i\chi_A : i\chi_B)] \\ & - \sum_q [(qq : \chi_A\chi_A) - 1/2 (q\chi_A : q\chi_A) + (qq : \chi_A\chi_B) - 1/2 (q\chi_A : q\chi_B)]\}. \end{aligned} \quad (13)$$

Here, the q 's represent the three hybrids centred on atom A different from χ_A and the i 's have the same meaning as before. W_x is the valence state ionization potential associated with the removal of an electron from the hybrid engaged in the formation of the CC σ -bond.

W_{hybr} and W_x are the only semi-empirical parameters which have been introduced in the calculations. As for all the integrals appearing in the above equations, it has not been attempted to adjust them through a semi-empirical procedure and their theoretical values have been used. The reason for adopting this procedure is that we feel that at present too little is known concerning the adjustment of integrals involving σ -type orbitals or σ and π orbitals simultaneously. In the calculations the value of 1.59 has been used for the orbital exponent of the 2s and 2p orbitals. Use of the value of 1.625 which is preferred at present would certainly not affect the results significantly. The CC bond length has been taken equal to 1.34Å.

Systematic derivations of valence state ionization potentials have been carried out recently by Pilcher and Skinner [14] and by Hinze and Jaffe [15].

We have utilized for W_{hybr} and W_x the values derived by the latter authors. In the cases giving rise to intermediate hybridization, we have made a four-point Lagrange interpolation, using for the determination of W_{hybr} the four ionization potentials corresponding to the following processes:



For W_x it has appeared logical rather to use for the first point the value corresponding to the process $\text{sppp} \rightarrow \text{spp}$.

3. RESULTS AND DISCUSSION

Let us consider first the results concerned with the non-flapped molecule and examine only the effect of the twisting. Table 3 lists the energies of the four electronic states which have been treated, represented by the symbols used by Parr and Crawford [6]: i.e. Φ_N and Φ_Z result from the C.I. between Φ_1 and Φ_2 ; Φ_V and Φ_T have been defined on page 4. The overall picture emerging from

$\theta = 0$		$\theta = \pi/2$
E_N	0	2.33
E_T	3.80	2.21
E_V	12.14	10.17
E_Z	16.36	10.29

Table 3. Energies of the planar and twisted molecules (ev).

the table is quite satisfactory: the molecule is found to be twisted in its three excited states, the barrier increasing as the states tend to be higher in energy. It is also noticed that for $\theta = 90^\circ$ the energy of the T state becomes lower than that of the ground state. All these features are in agreement with earlier works [5, 6]. The calculated barrier in the ground state is in good agreement with the experimental value, 2.66 ev [16]. The value found for the $N \rightarrow T$ excitation, 3.80 ev also compares reasonably well with the observed value, 4.6 ev [17, 18]. The calculated excitation energy for the $N \rightarrow V$ transition is too large (experimentally, $[E_V - E_N]_{\theta=0}$ is 7.6 ev [4]). This discrepancy is characteristic of the treatments where the two-electron integrals are not adjusted semi-empirically. Even the most refined calculations [7] are not exempt from this shortcoming.

As a matter of fact, the figures gathered in table 3 are quite close to the results of the two-electron treatment of Parr and Crawford [6]. Thus, as far as the twisting is concerned, the explicit inclusion of the electrons of the CC σ -bond does not bring significant improvements. This was to be expected, on the grounds of the argument given above, page 4.

As regards the flapping in the *twisted* molecule, table 4 gives the energies of the various states, for different values of the flapping angle β . The value of $\beta = 54.7^\circ$ corresponds to a tetrahedral arrangement of the bonds. It appears that as the twisted molecule flaps, the energy of the V and Z states increases constantly. On the other hand, the flapping causes a persistent lowering of the energy of the T state, in agreement with Walsh's idea [8].

It is noticed that no minimum appears in the variation of E_T as a function of β . This shortcoming is a consequence of the approximations inherent to the treatment. In view of the assumptions underlying the calculations one cannot, of course, expect an extremely accurate description of the energy variation as a function of the flapping. It may be appropriate to recall here that the primary purpose of this study was to detect whether or not a flapping takes

	$\beta = 0^\circ$	$\beta = 10^\circ$	$\beta = 20^\circ$	$\beta = 40^\circ$	$\beta = 54.7^\circ$
E_N	2.33	2.31	2.26	2.00	1.56
E_T	2.21	2.20	2.15	1.91	1.48
E_V	10.17	10.26	10.53	11.49	12.28
E_Z	10.29	10.37	10.63	11.58	12.37

Table 4. Effect of the flapping in the twisted configuration†.

† Energies are in electron volts, measured with reference to the energy of the planar ground state.

place in the excited states and that it was not expected to get a detailed description of the potential curve. The two simplifications which affect the results most are undoubtedly the following ones : (1) the neglect of the hydrogen atoms, (2) the assumption that the core energy remains constant through the distortions. The non-bonded interaction between the hydrogen atoms must certainly give rise to an increase in energy when the molecule flaps. Use of the various potentials which have been suggested for the non-bonded interaction [19] indicates that the effect should be of the order of 0.1ev when β reaches 54.7° , which is not sufficient to produce a minimum in the energy curve. The change in the core must also act in the same direction as the non-bonded interaction between the hydrogens; the change in hybridization indeed gives rise to a weakening of the bonds in the molecule, so this must correspond to an increase in energy. We have not attempted to calculate the contribution due to this factor, especially since by keeping the CC bond length constant some stabilizing effect has been ignored.

We now turn to the flapping of the non-twisted molecule. We will consider only the results obtained for the ground state. Table 5 gives the energies of the cis- and trans-configurations corresponding to several values of the flapping angle. The effects due to the approximations involved in the treatment, which

	$\beta = 20^\circ$		$\beta = 40^\circ$		$\beta = 54.7^\circ$	
	Cis	Trans	Cis	Trans	Cis	Trans
E_N	0.060	0.183	0.160	0.657	0.065	1.003

Table 5. Effect of the flapping in the non-twisted ground state†.

† The energy units and the reference energy are the same as in table 3 and table 4.

we have already noticed in discussing the results collected in table 4, are here again quite apparent. First, the energy of the *trans*-molecule is higher than that of the *cis*-molecule, for all values of the flapping angle. Experimentally it is known [20] that the vibration frequencies corresponding to the two flapping modes are quite close to each other, the *cis*-flapping frequency being slightly larger than the other one (949 cm^{-1} , compared to 943 cm^{-1} for the *trans* mode). For infinitely small distortions it therefore requires less energy to flap the molecule in the *trans* form than in the *cis* form. Although nothing is known as regards the behaviour of the potential energy curves for larger distortions angles, it is very likely that this relative stability of the *trans* form persists when the angle β is increased. The lack of success of our method in this respect of the problem is not too surprising, if one bears in mind that π -orbital calculations give rise to a similar difficulty. Without introducing nuclear repulsion, such calculations predict, for example, that the *cis* form of butadiene is the most stable [21, 22], contrary to experimental evidence. The method used in the present work is not free from the defects of other semi-empirical approximate treatments. It is also noticed that while the energy curve for the *trans* conformations rises constantly, that curve relative to the *cis* shows a less satisfactory behaviour.

4. CONCLUSIONS

The results of the calculations indicate that in the first excited triplet state the conformation of the ethylene molecule involves a twisting and a flapping of the CH_2 groups. In the corresponding singlet state, it is found that a flapping in the twisted molecule causes an increase in energy. Both effects are quite sharp. However, the lack of success encountered by the method when dealing with the flapping in the planar system clearly indicates that the approximations made are not quite satisfactory. On the basis of this observation more calculations are intended which will take into account all the electrons in the system.

We are very grateful to Dr. Carl Moser, Directeur de Recherche au C.N.R.S., for providing us with the values of the integrals required in the calculations. We are also thankful to Professor C. Manneback, of the University of Louvain, for useful discussions. Finally, we express our indebtedness to Mr. Jon R. Hamann, of R.I.A.S., who has read our manuscript.

REFERENCES

- [1] OLSEN, A. R., 1931, *Trans. Faraday Soc.*, **27**, 69.
- [2] MULLIKEN, R. S., 1932, *Phys. Rev.*, **41**, 751; 193, *Ibid.*, **43**, 297; 1942, *Rev. mod. Phys.*, **14**, 265.
- [3] MURRELL, J. N., 1963, *The Theory of the Electronic Spectra of Organic Molecules* (London: Methuen).
- [4] WILKINSON, P. G., and MULLIKEN, R. S., 1955, *J. chem. Phys.*, **23**, 1895.
- [5] MULLIKEN, R. S., and ROTHMAN, C. C. J., 1947, *Chem. Rev.*, **4**, 29.
- [6] PARR, R. G., and CRAWFORD, JR., B. L., 1948, *J. chem. Phys.*, **16**, 526.
- [7] MOSKOWITZ, J. W., and HARRISON, M. C., 1965, *J. chem. Phys.*, **42**, 1726.
- [8] WALSH, A. D., 1953, *J. chem. Soc.*, p. 2325.
- [9] BURNELLE, L., 1963, *Tetrahedron*, **21**, 49.
- [10] GOULD, E. W., 1959, *Mechanism and Structure in Organic Chemistry* (New York: Holt, Rinehart & Winston), p. 523.
- [11] HOFFMAN, R. (private communication).

- [12] GOEPPERT-MAYER, M., and SKLAR, A. K., 1938, *J. chem. Phys.*, **6**, 645.
- [13] DAUDEL, R., LEFEBVRE, R., and MOSER, C., 1959, *Quantum Chemistry* (New York: Interscience), p. 470.
- [14] PILCHER, G., and SKINNER, H. A., 1962, *J. inorg. nucl. Chem.*, **24**, 937.
- [15] HINZE, J., and JAFFE, H. H., 1961, *J. Amer. chem. Soc.*, **84**, 540, and subsequent papers.
- [16] RABINOVITCH, B. S., DOUGLAS, J. E., and LOONEY, F. S., 1952, *J. chem. Phys.*, **20**, 1807.
- [17] EVANS, D. F., 1960, *J. chem. Soc.*, p. 1735.
- [18] MULLIKEN, R. S., 1960, *J. chem. Phys.*, **33**, 1596.
- [19] FISCHER-HJALMARS, I., 1963, *Tetrahedron*, **19**, 1805.
- [20] CRAWFORD, B. L., LANCASTER, J. E., and INSKEEP, R. G., 1953, *J. chem. Phys.*, **21**, 678.
- [21] PARR, R. G., and MULLIKEN, R. S., 1950, *J. chem. Phys.*, **18**, 1338.
- [22] LONGUET-HIGGINS, H. C., and MURRELL, J. N., 1955, *Proc. phys. Soc., Lond., A*, **68**, 601.

H-H and ^{13}C -H coupling constants in pyridazine

by V. M. S. GIL†

Department of Chemistry, University of Sheffield

(Received 29 December 1964; revision received 2 February 1965)

Analysis of the proton and ^{13}C -H satellite N.M.R. spectra of pyridazine has given the following H-H coupling constants: $J_{34} = 5.05$ c.p.s., $J_{35} = 1.85$ c.p.s., $J_{45} = 8.00$ c.p.s., $J_{36} = \pm 1.40$ c.p.s.; the ^{13}C -H couplings are 183 c.p.s. and 168 c.p.s. respectively for the 3 (or 6) and 4 (or 5) positions.

1. INTRODUCTION

In this paper an analysis is given of the proton and ^{13}C -H satellite N.M.R. spectra of pyridazine. The same spectra have recently been the subject of a paper by Tori and Ogata [1]. However, the ^{13}C -H satellites which they report are not so well resolved as ours and their analysis of these satellites is not correct because it is based on the invalid assumption that they are first-order spectra. A similar study was made by Reddy and Goldstein on furan [2], but the analysis they give is also incorrect for the same reasons.

2. RESULTS AND DISCUSSION

2.1. The experimental spectra

The spectra were recorded on a Varian HR 100 Mc/s spectrometer using the pure liquid and TMS as an internal standard.

The main proton resonance spectrum of pyridazine (AA'XX' system) consists of two symmetrical quartets. The high-field quartet (A-spectrum) due to protons 4,5 is shown in figure 1.

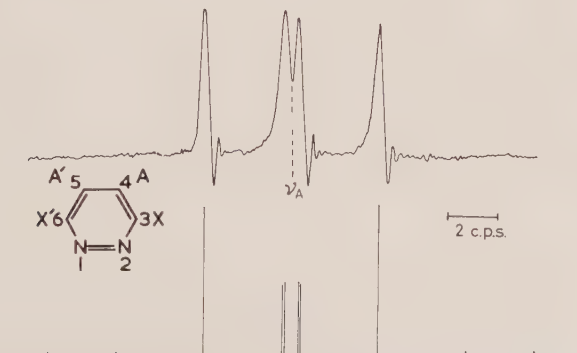


Figure 1. The observed and calculated spectrum of 4,5-protons of pyridazine.

† Present address: Department of Chemistry, University of Coimbra, Portugal.

The analysis of an AA'XX' spectrum [3] shows that the separation of the outer lines in the quartet (6.95 c.p.s.) is:

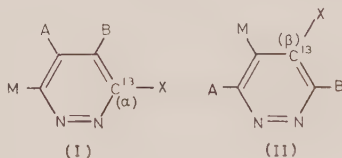
$$N = J_{34} + J_{35} = 6.95 \text{ c.p.s.} \quad (1)$$

The two inner lines are unresolved doublets and from their separation one can obtain the following combination of coupling constants

$$\frac{1}{2}(K^2 + L^2)^{1/2} + \frac{1}{2}(M^2 + L^2)^{1/2} - \frac{1}{2}(K + M) \simeq 0.65 \text{ c.p.s.}, \quad (2)$$

where $K = J_{45} + J_{36}$, $M = J_{45} - J_{36}$, $L = J_{34} - J_{35}$. It has been assumed that couplings between protons ortho to each other are positive and that $J_{45} > |J_{36}|$ and $J_{34} > |J_{35}|$. Equations (1) and (2) are the limit of the information that can be obtained from the analysis of this spectrum.

If there is one ^{13}C nucleus in the pyridazine ring then the proton spectrum can be interpreted as if each proton H had a chemical shift of $\nu_{\text{H}} \pm \frac{1}{2}J_{^{13}\text{CH}}$ [4], the positive sign being for those molecules when ^{13}C has α spin and the negative sign for those when ^{13}C has β spin; ν_{H} is the chemical shift in the ^{12}C molecule. With a natural abundance of ^{13}C , one sees a pair of satellites to each of the normal proton signals which are due to the transitions of the proton directly bonded to the ^{13}C atom. The coupling between the ^{13}C nucleus and the bonded proton is much larger than any other ^{13}C -H or H-H coupling constant; therefore, each of the two outer satellites may be interpreted as the X spectrum of an ABMX system. There is indirect evidence that, for a hydrogen directly bound to a ^{13}C , $J_{^{13}\text{CH}}$ is positive [5]. It follows that the low-field ^{13}C -H satellite of protons 3,6 is due to the transitions of the X spin in molecule (I), and the high-field satellite corresponding to protons 4,5 arises from the X transitions in molecule (II)†.



A first-order analysis of these spectra would be valid only if $|\nu_{\text{A}} - \nu_{\text{B}}| \gg |J_{\text{AB}}|$ which is a condition not attained for the present molecule.

The X-spectrum of an ABMX system consists of two doublets centred on ν_{X} with line intensities 1, two doublets centred on $\nu_{\text{X}} + \frac{1}{2}J_{\text{MX}}$ with total intensity 2, and another pair of doublets, centred on $\nu_{\text{X}} - \frac{1}{2}J_{\text{MX}}$, with total intensity 2 [6, 7].

The observed high-field satellite of the 4,5-proton signal is shown in figure 2. The separation between the lines of intensity 1 symmetrically displaced in respect to ν_{X} , combined with the value for J_{MX} obtained from the transitions centred on $\nu_{\text{X}} + \frac{1}{2}J_{\text{MX}}$ and $\nu_{\text{X}} - \frac{1}{2}J_{\text{MX}}$, gives:

$$\left. \begin{aligned} J_{45} &= 8.05 \text{ c.p.s.}, \\ J_{34} + J_{35} &= 6.85 \text{ c.p.s.} \end{aligned} \right\} \quad (3)$$

The low-field satellite (protons 3,6) is shown in figure 3. The rather broad nature of this spectrum is due to the nitrogen electric quadrupole moment.

† We shall be concerned only with the outer satellites; the inner satellites partially overlap each other and it would be a poor approximation to treat them as the X part of an ABMX system because the chemical shift between protons A, B and the ^{13}C bonded proton becomes much smaller than for molecules (I) and (II).

In a similar way as for the high-field satellite one gets:

$$\left. \begin{aligned} J_{36} &= \pm 1.35 \text{ c.p.s.}, \\ J_{34} + J_{35} &= 6.95 \text{ c.p.s.} \end{aligned} \right\} \quad (4)$$

The value for $J_{34} + J_{35}$ compares favourably with the values obtained above.

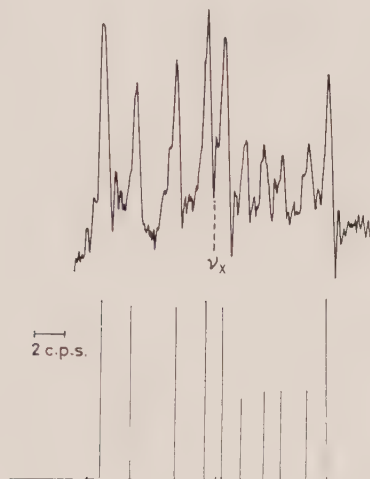


Figure 2. The high-field ^{13}C -H satellite (X-spectrum of molecule II) of pyridazine and the calculated spectrum for $\delta = 2.4$ c.p.s.

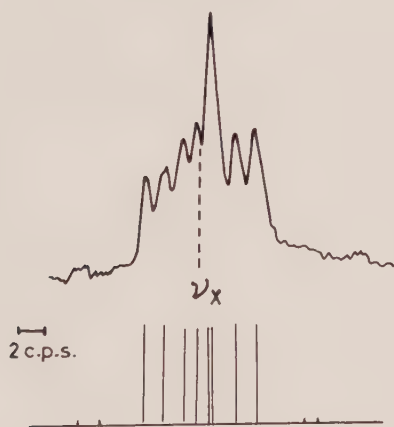


Figure 3. The observed and calculated low-field ^{13}C -H satellite (X-spectrum of molecule I) of pyridazine.

2.2. The calculated spectra and long-range ^{13}C -H couplings

In the previous sections three independent values for $J_{34} + J_{35}$ have been determined (1), (3) and (4). If a value of 6.90 ± 0.05 c.p.s. is taken, then

$$\left. \begin{aligned} J_{45} &= 8.00 \pm 0.05 \text{ c.p.s.}, \\ J_{36} &= \pm 1.40 \pm 0.05 \text{ c.p.s.}, \end{aligned} \right\} \quad (5)$$

and, by substituting these quantities into (2), one gets $L = J_{34} - J_{35} = 3.2$ c.p.s. and

$$\left. \begin{aligned} J_{34} &= 5.05 \pm 0.05 \text{ c.p.s.}, \\ J_{35} &= 1.85 \pm 0.05 \text{ c.p.s.} \end{aligned} \right\} \quad (6)$$

The A-part of the main spectrum calculated with these values is shown in figure 1.

In contrast to the main spectrum, the structure of the ^{13}C -H satellites depends not only on the various H-H coupling constants but also on long-range ^{13}C -H coupling, the reason being that the frequency and intensity of the lines centred about $\nu_X \pm \frac{1}{2}J_{MX}$ depend on $\nu_A - \nu_B \equiv \delta$ which is

$$\frac{1}{2}(J_{^{13}\text{CB}} - J_{^{13}\text{CA}}) \text{ and } \frac{1}{2}(J_{^{13}\text{CA}} - J_{^{13}\text{CB}})$$

respectively for the high-field and low-field satellites.

There are two δ values for which the calculated high-field satellite is in good agreement with the observed spectrum: $\delta = +0.85 \pm 0.1$ c.p.s. and $\delta = +2.40 \pm 0.1$ c.p.s. The theoretical spectrum for $\delta = 2.40$ c.p.s. is shown in figure 2 and is independent of the sign of $J_{AB} \equiv J_{36}$. The low-field satellite (figure 3) is best reproduced for $\delta = +1.0 \pm 0.1$ c.p.s. if J_{36} is positive or $\delta = -1.0 \pm 0.1$ c.p.s. if J_{36} is negative.

Since $J_{^{13}\text{CA}}$, a ^{13}C -H coupling across three bonds, is probably very nearly zero, 2δ must then approach the value for a ^{13}C -H coupling across two bonds. Therefore, either $+1.7$ c.p.s. or $+4.8$ c.p.s. are approximately the coupling constant between a 3-proton and a 4- ^{13}C nucleus. Similarly, the coupling between a 3- ^{13}C nucleus and a 4-proton is: $+2.0$ c.p.s. if $J_{36} < 0$ or -2.0 c.p.s. if $J_{36} > 0$ †.

The coupling constants between each proton and the directly bonded ^{13}C are 183 ± 1 c.p.s. and 168 ± 1 c.p.s., respectively for the 3 and 4 positions.

3. CONCLUSION

We conclude by noting some differences between the coupling constants we have found for pyridazine and those previously reported (in brackets) [1]:

$$\begin{aligned} J_{34} &= 5.05 \text{ c.p.s. (4.9)}; J_{35} = 1.85 \text{ c.p.s. (2.0)}; J_{45} = 8.00 \text{ c.p.s. (8.4)} \\ J_{36} &= \pm 1.40 \text{ c.p.s. (3.5)}. \end{aligned}$$

The major difference is found for the coupling between protons ortho to the nitrogen atoms. This coupling constant is of some theoretical interest since it is known that coupling between protons ortho to the same nitrogen atom in azabenzenes is always abnormally small (0 to 0.4 c.p.s.) [3, 8]. Its sign could not however be determined from the spectra.

It has also been found that the coupling constants between a 4- ^{13}C and a 3-proton in pyridazine (1.7 or 4.8 c.p.s.) has the same sign as the bonded ^{13}C -H coupling, and that J_{36} and the coupling constant between a 3- ^{13}C nucleus and a 4-proton (± 2.0 c.p.s.) have opposite signs. Values for ^{13}C -C-H coupling

† If a similar analysis of the furan ^{13}C -H satellites reported by Reddy and Goldstein [2] is carried out, one gets proton coupling constants that are equal to those obtained by those authors by a first-order treatment, within the experimental error. A δ value of -3.5 ± 1 c.p.s. is found for the low-field satellite whereas, for the high-field one, good agreement is obtained for $\delta \geq 3$ c.p.s. These values suggest that in furan the coupling constant between an α - ^{13}C nucleus and a β -proton is about $+7.0 \pm 2$ c.p.s. and that between a β - ^{13}C and an α -proton of at least $+6$ c.p.s.

constants vary from +49.2 c.p.s. for acetylene to -4.5 c.p.s. for ethane, and -2.4 c.p.s. in ethylene [9]. Changes in the ^{13}C -C-H angle seem to be a primary factor; for example, the ^{13}C -C-H coupling in cis-dichloroethylene is zero and in the trans-isomer is ± 15.7 c.p.s. [10]. In vinyl bromide CH couplings through two bonds have been found to have values ranging from -8.5 to +5.8 c.p.s. [11]. A long-range CH coupling of ± 4.9 c.p.s. has been found in a benzene derivative, 1,2,4,5-tetrachlorobenzene [12].

The variation of the ^{13}C -H coupling constants in the diazabenzenes will be the subject of a forthcoming paper.

The author is greatly indebted to Dr. D. H. Whiffen and Professor J. N. Murrell for most illuminating and encouraging discussions. Thanks are also due to the National Physical Laboratory (Teddington) for guest worker facilities and to the Comissão Coordenadora da Investigação para a NATO (Portugal) for the award of a Postgraduate Scholarship.

REFERENCES

- [1] TORI, K., and OGATA, M., 1964, *Chem. Pharm. Bull. Japan*, **12**, 272.
- [2] REDDY, G. S., and GOLDSTEIN, J. H., 1962, *J. Amer. chem. Soc.*, **84**, 583.
- [3] POPLÉ, J. A., SCHNEIDER, W. G., and BERNSTEIN, H. J., 1959, *High-Resolution Nuclear Magnetic Resonance* (McGraw-Hill).
- [4] BANWELL, C. N., and SHEPPARD, N., 1961, *Proc. roy. Soc. A*, **263**, 136.
- [5] POPLÉ, J. A., and SANTRY, D. P., 1964, *Mol. Phys.*, **8**, 1, and references therein.
- [6] LEE, J., and SUTCLIFFE, L. H., 1958, *Trans. Faraday Soc.*, **54**, 308.
- [7] RAO, B. D. N., and VENKATESWARLU, P., 1960, *Proc. Indian. Acad. Sci.*, p. 109.
- [8] REDDY, G. S., HOBGOOD, R. T., and GOLDSTEIN, J. H., 1962, *J. Amer. chem. Soc.*, **84**, 336.
- [9] LYNDEN-BELL, R. M., and SHEPPARD, N., 1962, *Proc. roy. Soc. A*, **269**, 385.
- [10] MULLER, N., 1962, *J. chem. Phys.*, **37**, 2729.
- [11] LYNDEN-BELL, R. M., 1963, *Mol. Phys.*, **6**, 537.
- [12] HUTTON, H. M., REYNOLDS, W. F., and SCHAEFER, T., 1962, *Canad. J. Chem.*, **40**, 1758.

Normal coordinate analysis of XeF_4 in the Urey-Bradley Field†

by WALTER A. YERANOS

Department of Chemistry, Northern Illinois University, Illinois 60115

(Received 2 November 1964)

Using published infra-red and Raman data, the normal coordinates, the Urey-Bradley force constants, and the contribution of these force constants to the different normal modes of XeF_4 have been determined. The analysis has been carried out using a Fortran II programme written specifically for the IBM 1620 computer, and within the formalism of Wilson's G - F matrix method. Furthermore, using a recently reported semi-empirical M.O. scheme for XeF_4 , the vibronic interactions responsible for the symmetry-forbidden $2a_{2u} \rightarrow 3e_u$ electronic transition at 44.15 kK are discussed qualitatively.

1. INTRODUCTION

Presently, it is accepted that the XeF_4 molecule is square planar with an average Xe-F bond distance of 1.95 Å [1, 2]. Since the molecule is centrosymmetric, the exclusion principle holds and one expects, from group theoretical considerations [3], three Raman active, three infra-red active and an inactive mode of vibration. The band assignments [4, 5] as well as the calculated frequencies in the Urey-Bradley field are given in table 1.

As usual, the analysis of the vibrational problem reduces to the solution of the secular determinant:

$$|GF - I\lambda| = 0,$$

where F is the force constant matrix, G is the inverse kinetic energy matrix and the λi 's ($\equiv 4\pi^2 c^2 \tilde{\nu} i^2$) are the frequency parameters [6, 7].

In matrix notation the above secular determinant takes the convenient and familiar form:

$$L^{-1}GFL = \Lambda,$$

where $LL^{-1} = I$, and $LL' = G$. It should be noted that Λ is a diagonal matrix having the frequency parameters λi on its diagonal.

2. THE SYMMETRY COORDINATES

The 3N-6 normal vibrations of XeF_4 in D_{4h} symmetry, can be expressed most conveniently in terms of four in-plane Xe-F bond stretches, of four in-plane angle bends, and of two out-of-plane angle bends of the trans bonds (see figure). The symmetry coordinates belonging to the different irreducible representations in D_{4h} symmetry were generated by the projection operator

$$P_{\lambda k}^{(j)} = \frac{l_j}{h} \sum_R \Gamma^{(j)}(R)_{\lambda k} \cdot R [8].$$

† Supported by the Dean's fund for Research at Northern Illinois University.








	Act.	Observed	Calculated	Vibr. mode
$\bar{\nu}_1(a_{1g})$	R	543	543	
$\bar{\nu}_2(a_{2u})$	IR	291	291	
$\bar{\nu}_3(b_{1g})$	R	235	235	
$\bar{\nu}_4(b_{1u})$	i.a.	(221)	(231)	
$\bar{\nu}_5(b_{2g})$	R	502	502	
$\bar{\nu}_6(e_u)$	IR	586	587	
$\bar{\nu}_7(e_u)$	IR	123	182	

Table 1. Observed and calculated frequencies (in cm^{-1}) of XeF_4 .

After the elimination of the redundant coordinate, these are:

$$S_1(a_{1g}) = \frac{1}{2} (\delta R_1 + \delta R_2 + \delta R_3 + \delta R_4),$$

$$S_2(a_{2u}) = \frac{R'}{\sqrt{2}} (\delta \gamma_{13} + \delta \gamma_{24}),$$

$$S_3(b_{1g}) = \frac{R}{2} (\delta \alpha_{12} - \delta \alpha_{23} + \delta \alpha_{34} - \delta \alpha_{41}),$$

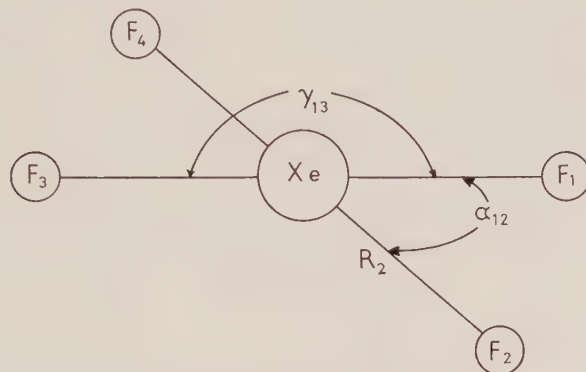
$$S_4(b_{1u}) = \frac{R'}{\sqrt{2}} (\delta \gamma_{24} - \delta \gamma_{13}),$$

$$S_5(b_{2g}) = \frac{1}{2} (\delta R_1 - \delta R_2 + \delta R_3 - \delta R_4),$$

$$S_6(e_u) = \frac{1}{\sqrt{2}} (\delta R_1 - \delta R_3),$$

$$S_7(e_u) = \frac{R}{2} (\delta \alpha_{12} - \delta \alpha_{34} + \delta \alpha_{41} - \delta \alpha_{23}),$$

where the internal coordinates involving angle bends have been multiplied by the proper internuclear distances so that *all* force constants be calculated in units of $\text{mdyn}/\text{\AA}$. It should be noticed that only one symmetry coordinate of a pair of degenerate coordinates (e_u species) is given.



Internal coordinates of XeF_4 .

3. THE G AND F MATRIX ELEMENTS

The kinetic energy matrix elements [9, 10] as well as the force constant matrix elements in the Urey-Bradley field [11] are given in table 2, where μ_Y is the reciprocal of the atomic weight of nucleus Y, and the force constants $K(\text{Xe}-\text{F})$, $H_\alpha(\text{F}_1-\text{Xe}-\text{F}_2)$, $H_\gamma(\text{F}_1-\text{Xe}-\text{F}_3)$, and $F(\text{F} \dots \text{F})$ are the standard stretching, angle bending and repulsion constants of the Urey-Bradley field.

Species	G matrix		F matrix	
a_{1g}	$G_{1,1}$	μ_F	$F_{1,1}$	$K(\text{Xe}-\text{F}) + 2F(\text{F} \dots \text{F})$
a_{2u}	$G_{2,2}$	$2(\mu_F + 4\mu_{\text{Xe}})$	$F_{2,2}$	$H_\gamma(\text{F}_1-\text{Xe}-\text{F}_3)$
b_{1g}	$G_{3,3}$	$4\mu_F$	$F_{3,3}$	$H_\alpha(\text{F}_1-\text{Xe}-\text{F}_2) + 0.55F(\text{F} \dots \text{F})$
b_{1u}	$G_{4,4}$	$2\mu_F$	$F_{4,4}$	$H_\gamma(\text{F}_1-\text{Xe}-\text{F}_3)$
b_{2g}	$G_{5,5}$	μ_F	$F_{5,5}$	$K(\text{Xe}-\text{F}) - 0.2F(\text{F} \dots \text{F})$
e_u	$G_{6,6}$	$\mu_F + 2\mu_{\text{Xe}}$	$F_{6,6}$	$K(\text{Xe}-\text{F}) + 0.9F(\text{F} \dots \text{F})$
e_u	$G_{6,7} = G_{7,6}$	$-2\sqrt{2}\mu_{\text{Xe}}$	$F_{6,7} = F_{7,6}$	$\sqrt{2}(0.45)F(\text{F} \dots \text{F})$
e_u	$G_{7,7}$	$2(\mu_F + 2\mu_{\text{Xe}})$	$F_{7,7}$	$H_\alpha(\text{F}_1-\text{Xe}-\text{F}_2) + 0.55F(\text{F} \dots \text{F})$

Table 2. G and F matrix elements of XeF_4 in D_{4h} .

4. EVALUATION OF FORCE CONSTANTS

The four force constants of the previous section can readily be determined from the linear relationships emanating from the $\tilde{\nu}_1$, $\tilde{\nu}_2$, $\tilde{\nu}_3$ and $\tilde{\nu}_5$ frequencies of table 1. These are given in table 3.

It is indeed interesting to note that the calculated frequency for the $\tilde{\nu}_6(e_u)$ vibration, based on these force constants, differs only by 0.17 per cent from the observed. It is also interesting to find that the $\tilde{\nu}_7(e_u)$ frequency is significantly

higher than the original assignment of Claassen *et al.* [1, 2]. It is indeed higher than its sister mode in the XeOF_4 molecule. It is perhaps worth while to mention that, at present, the 123 cm^{-1} band is tentatively assigned to an HF rotation [12].

$K(\text{Xe-F})$	$H_\alpha(\text{F}_1\text{-Xe-F}_2)$	$H_\gamma(\text{F}_1\text{-Xe-F}_3)$	$F(\text{F} \dots \text{F})$
2.86_0	0.03_4	0.30_0	0.21_8

Table 3. The Urey-Bradley potential constants of XeF_4 (in $\text{mdyn}/\text{\AA}$).

5. THE DETERMINATION OF THE NORMAL COORDINATES

The normal coordinates Q of XeF_4 are given by the relation:

$$Q = L^{-1}S,$$

where L has been defined previously.

To determine L^{-1} , we have followed the procedure described by Miyazawa [13]. It should be remembered that although the matrices G and F are individually symmetric, their product GF is not†. To diagonalize GF we followed the following procedure:

(i) Diagonalize G , such that

$$U'GU = V$$

(ii) Form the $V^{1/2}$ matrix, taking the square roots of the diagonal matrix elements of V .

(iii) Construct the matrix \mathbf{F} .

$$\mathbf{F} = (UV^{1/2})'F(UV^{1/2}).$$

(iv) Diagonalize \mathbf{F} , such that

$$C'\mathbf{F}C = (UV^{1/2}C)'F(UV^{1/2}C) = \Lambda.$$

(v) Set

$$L = UV^{1/2}C$$

and find its inverse.

	S_1	S_2	S_3	S_4	S_5	S_6	S_7
Q_1	4.35_8						
Q_2		2.45_3					
Q_3			2.17_9				
Q_4				3.08_2			
Q_5					4.35_8		
Q_6						3.87_5	0.12_8
Q_7						0.70_3	2.78_2

Table 4. Normal coordinates of XeF_4 in the Urey-Bradley field.

† A manuscript is in preparation entitled "A Computer Program for Vibrational Analyses" with C. Givens of the Computer Center of Northern Illinois as co-author and will shortly be submitted for publication.

The normal coordinates of XeF_4 in the Urey-Bradley field and with respect to the set of force constants determined by us are given in table 4.

The potential energy distribution, which displays the contribution of the various Urey-Bradley force constants to the different normal modes [14], is given in table 5.

	K	H_α	H_γ	F
$\tilde{\nu}_1$	0.867 ₇	0.000 ₀	0.000 ₀	0.132 ₃
$\tilde{\nu}_2$	0.000 ₀	0.000 ₀	1.000 ₀	0.000 ₀
$\tilde{\nu}_3$	0.000 ₀	0.223 ₁	0.000 ₀	0.776 ₉
$\tilde{\nu}_4$	0.000 ₀	0.000 ₀	1.000 ₀	0.000 ₀
$\tilde{\nu}_5$	1.015 ₅	0.000 ₀	0.000 ₀	-0.15 ₅
$\tilde{\nu}_6$	0.954 ₆	0.000 ₇	0.000 ₀	0.044 ₇
$\tilde{\nu}_7$	0.021 ₀	0.231 ₉	0.000 ₀	0.747 ₁

Table 5. The potential energy distribution in XeF_4 .

6. VIBRONIC INTERACTIONS

The far ultra-violet spectrum of XeF_4 has been studied experimentally and theoretically by several investigators [15]. It is generally accepted that the weak absorption band at 44.15 kK, with an oscillator strength of 8×10^{-3} at 0° , is due to a vibronically allowed transition between the one-electron molecular orbitals $\psi_i(a_{2u})$ and $\psi_f(e_u)$. It can be shown [16] that, within the framework of the Herzberg-Teller approximation [17], the theoretical oscillator strength for an electronic transition between states \mathbf{k} and \mathbf{k}' is given by:

$$f_{k \rightarrow k'} = 1.085 \times 10^{11} \nu_{kk'} G_{k'} \times \left\{ M_{kk'}^2(0) + \sum_a \frac{h}{8\pi^2 \tilde{\nu}_a} \cdot \text{ctnh} \left(\frac{h\tilde{\nu}_a}{2kT} \right) \cdot \left[\sum_{s \neq k} \left(\frac{\partial \bar{\lambda}_{ks}}{\partial Q_a} \right)_0 \cdot M_{sk'}(0) + \sum_{s \neq k'} \left(\frac{\partial \bar{\lambda}_{k's}}{\partial Q_a} \right)_0 \cdot M_{ks}(0) \right]^2 \right\},$$

where $\nu_{kk'}$ is the energy separation of the levels \mathbf{k} and \mathbf{k}' in Kaysers, $G_{k'}$ is the degeneracy of the upper level \mathbf{k}' , $\tilde{\nu}_a$ is the frequency of the vibration in cm^{-1} which induces the vibronic transition, $M_{st}(0)$ is the transition moment between levels s and t in the equilibrium configuration, and $(\partial \bar{\lambda}_{st}/\partial Q_a)_0$ is the vibronic perturbation energy per unit displacement in the normal coordinate Q_a , resulting from the coupling of the electronic states s and t .

Since the XeF_4 molecule is centro-symmetric, the first term in the braces of the above expression vanishes identically for *all* transitions between levels of the same parity. It should be noted, on the other hand, that the temperature-dependent, vibronically allowed transitions can *only* occur when

$$\Gamma_i \otimes \Gamma_f \otimes \Gamma_q \otimes \Gamma_{\text{vib.}} \Rightarrow \Gamma_1 (\equiv A_{1g}).$$

Applying this to XeF_4 , one finds that the transition $\psi(a_{2u}) \rightarrow \psi(e_u)$ at 44.15 kK is due to the combined effects of the $\tilde{\nu}_2(291\text{ cm}^{-1})$ vibration which induces X and Y polarized transitions, and of the $\tilde{\nu}_6(586\text{ cm}^{-1})$ and $\tilde{\nu}_7(182\text{ cm}^{-1}?)$ vibrations which induce Z polarized transitions in D_{4h} . We are presently studying the theoretical vibronic interactions in XeF_4 and will soon publish our results.

The author wishes to express his gratitude to Professor M. J. Joncich and Dean John Skok of Northern Illinois University for their encouragement, and to Professor H. H. Claasen for making available to him the data necessary for this investigation.

REFERENCES

- [1] BURNS, J. H., ARGON, P. A., and LEVY, H. A., 1963, *Noble-Gas Compounds*, Ed. H. H. Hyman (Chicago: University of Chicago Press), p. 211.
- [2] BOHN, R. K., KATADA, K., MARTINEZ, J. V., and BAUER, S. H., 1963, *J. chem. Phys.*, **67**, 1569.
- [3] TINKHAM, M., 1964, *Group Theory and Quantum Mechanics* (New York: McGraw-Hill Book Co. Inc.).
- [4] CLAASEN, H. H., CHERNICK, C. C., and MALM, J. G., 1963, *J. Amer. chem. Soc.*, **85**, 1927.
- [5] CLAASEN, H. H., CHERNICK, C. C., and MALM, J. G., 1963, *Noble-Gas Compounds*, Ed. H. H. Hyman (Chicago: University of Chicago Press), p. 287.
- [6] WILSON, E. B., Jr., 1939, *J. chem. Phys.*, **7**, 1041.
- [7] WILSON, E. B., Jr., DECIUS, J. C., and CROSS, P. C., 1955, *Molecular Vibrations* (New York: McGraw-Hill Book Co. Inc.).
- [8] NIELSEN, J. R., and BERRYMAN, L. N., 1949, *J. chem. Phys.*, **17**, 659.
- [9] FERIGLE, S. M., and MEISTER, A. G., 1951, *J. chem. Phys.*, **19**, 982.
- [10] DECIUS, J. C., 1948, *J. chem. Phys.*, **16**, 1025.
- [11] UREY, H. C., and BRADLEY, C. A., 1931, *Phys. Rev.*, **38**, 1969.
- [12] HYMAN, H. H., 1964, *Science*, **145**, 773.
- [13] MIYAZAWA, T., 1958, *J. chem. Phys.*, **29**, 246.
- [14] OVEREND, J., and SCHERER, J. R., 1960, *J. chem. Phys.*, **32**, 1286, 1296, 1720; 1960, *Ibid.*, **34**, 446.
- [15] LOHR, L. L., Jr., and LIPSCOMB, W. N., 1963, *J. Amer. chem. Soc.*, **85**, 240. RUNDLE, R. E., 1963, *J. Amer. chem. Soc.*, **85**, 112. WILSON, E. G., JORTNER, J., and RICE, S. A., 1963, *J. Amer. chem. Soc.*, **85**, 815. JORTNER, J., RICE, S. A., and WILSON, E. G., 1963, *J. chem. Phys.*, **38**, 2302. BOUDREAUX, E. A., 1964, *J. chem. Phys.*, **40**, 246.
- [16] YERANOS, W. A., 1964, Doctor's Dissertation, University of Illinois, Urbana.
- [17] HERZBERG, G., and TELLER, E., 1933, *Z. phys. Chem. B*, **21**, 410.

Urey-Bradley potential constants of sulphur compounds : SF₅Cl

by WALTER A. YERANOS

Department of Chemistry, Northern Illinois University,
DeKalb, Illinois, 60115

(Received 29 December 1964)

Using previously published infra-red and Raman data, the Urey-Bradley force constants of SF₅Cl have been determined. The analysis has been carried within Wilson's G - F matrix method and the constants evaluated by the use of a computer programme (MV-E1D) which refines the differences of the experimental and calculated frequencies in the least-squares sense. To enhance our statistical analysis, we have also included the molecular vibrations of SF₆ in our least-squares fit. Finally, assuming the transferability of the Urey-Bradley force constants, the normal coordinates as well as the potential energy distribution of both SF₅Cl and SF₆ have been determined.

1. INTRODUCTION

The infra-red and Raman spectra as well as the band assignments of SF₅Cl have been reported by Cross *et al.* [1]. In a subsequent paper, Venkatesvarlu and Sathianandan [2] have also reported a vibrational analysis of SF₅Cl in a 'modified generalized valence field force'. A closer examination of their investigation, however, shows that 13 force constants have been determined from only 11 observed frequencies, and that this has been done in the absence of any supplementary isotopic, vibrational-rotational interaction, coriolis zeta interaction, etc. data.

In the present investigation we have re-examined the vibrational analysis of SF₅Cl. Using slightly different symmetry coordinates than Venkatesvarlu *et al.*, and containing the potential field to the standard Urey-Bradley field, we have endeavoured to fix six force constants from a total of 16 experimental frequencies. This has been done by assuming the transferability of the Urey-Bradley force constants which enabled us to use the observed frequencies of SF₆ [3], in our least-squares fit.

A diagram depicting the 'general' geometry of the molecules under consideration is given in the figure. Since the geometric parameters for SF₅Cl are not yet available, we have assumed that the S-F distance in SF₅Cl was identical to the one obtained for SF₅OF [4], and that the distance S-Cl was the sum of the covalent radii of S and Cl [5].

It should be noted that although SF₅Cl and SF₆ belong to different point groups, they have an identical number of internal degrees of freedom. The symmetry distribution of the vibrations of SF₅Cl in the C_{4v} point group is given by :

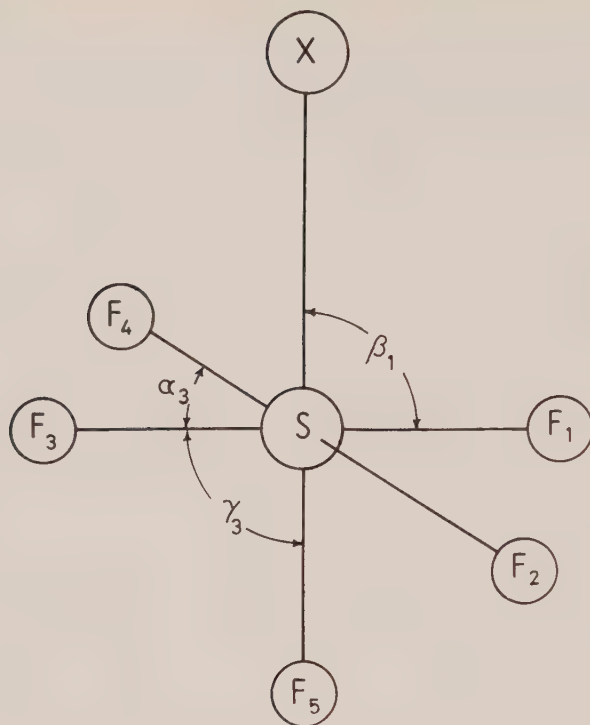
$$\Gamma_{\text{vibr.}} = 4A_1 \oplus 2B_1 \oplus B_2 \oplus 4E$$

and SF₆ in the O_h point group, by :

$$\Gamma_{\text{vibr.}} = A_{1g} \oplus E_g \oplus 2T_{1u} \oplus T_g \oplus T_{2u}.$$

Finally, it should be mentioned that we have chosen the following convenient set of internal coordinates: $\delta r_1, \delta r_2, \delta r_3, \delta r_4, \delta r_5, \delta r_6$ ($\equiv \delta r_x$ in C_{4v}), $\delta \alpha_1, \delta \alpha_2, \delta \alpha_3, \delta \alpha_4, \delta \beta_1, \delta \beta_2, \delta \beta_3, \delta \beta_4, \delta \gamma_1, \delta \gamma_2, \delta \gamma_3$, and $\delta \gamma_4$ (see figure) and have sought force constants which will satisfy

$$L^{-1}GFL = \Lambda \sim \Lambda_{\text{obs.}},$$



The 'general' geometry of the molecules under investigation. In the case of SF_6 , $\text{X}=\text{F}$, and of SF_5Cl , $\text{X}=\text{Cl}$. In the SF_5Cl molecule, $d(\text{S}-\text{F})$ is taken as 1.53 \AA , and $d(\text{S}-\text{Cl})$ as 2.00 \AA .

where G is the inverse kinetic energy matrix, F the force constant matrix, Λ the diagonal matrix of the frequency parameters $\lambda_i (\equiv 4\pi^2 c^2 \tilde{\nu}_i^2)$, and L the transformation matrix from the normal to the symmetry coordinates which are obtained by the methods of group theory [6, 7].

2. G AND F MATRIX ELEMENTS

The potential energy V and the kinetic energy T of a vibrating molecule can be given, in terms of the previously mentioned symmetry coordinates and in matrix notation, as:

$$2V = S'FS$$

and

$$2T = \dot{S}'G^{-1}\dot{S},$$

where G^{-1} is the kinetic energy matrix and satisfies the relationship $LL' = G$.

The vibrational problems under consideration have been solved within the framework of Wilson's G - F matrix method [8, 9], and the potential energy has been restricted to the Urey-Bradley field [10], such that

$$V = \frac{1}{2} \sum K_i (\delta r_i)^2 + \frac{1}{2} \sum H_{jk} r_j r_k (\delta \alpha_{jk})^2 + \frac{1}{2} \sum F_{jk} (\delta q_{jk})^2 + \text{linear terms}$$

where K , H and F are the usual bond stretching, angle bending and repulsive force constants of the Urey-Bradley field.

As mentioned earlier we have assumed transferability of force constants in the Urey-Bradley field.

3. DETERMINATION OF FORCE CONSTANTS AND DISCUSSION

The force constants have been determined as mentioned in our previous papers [11, 12]. In brief, a refinement process was used such that the variance χ in

$$\chi=\delta\lambda'.W.\delta\lambda$$

attained a minimum, and that the changes in the F matrix were so small that the changes in the frequencies were negligible. That is:

$$L_s^{-1}(G_0F_0+\Delta F_s)L=s\Lambda_s=\Lambda_{s-1},$$

where s denotes the iteration index.

Some of our trial set of force constants were obtained from a previous analysis of the SF_6 molecule [13], while others were estimated by comparison to other molecules [14]. Our starting, as well as the converged force constants are given in table 1, while the frequencies obtained from them are listed in table 2. It should be noted that the analysis has been carried in the *standard* Urey-Bradley field and consequently we have not included the interaction constants h and k proposed by Hiraishi *et al.* [13].

	$K(S-F)$	$K(S-Cl)$	$H(F-S-F)$	$H(F-S-Cl)$	$F(F \dots F)$	$F(F \dots Cl)$
Initial	3.75 ₀	2.79 ₃	0.40 ₀	0.30 ₆	0.75 ₀	0.27 ₅
Converged	3.67 ₂	2.62 ₆	0.36 ₀	0.30 ₆	0.83 ₃	0.28 ₆

Table 1. Urey-Bradley force constants of SF_5Cl (in mdyn/Å).

	Mode	Act.	Exp.	Calc. 1	Calc. 2	$\Delta\tilde{\nu}$ per cent† (2)
SF_5Cl	$\tilde{\nu}_1(a_1)$	R, IR	834	888	880	— 6
	$\tilde{\nu}_2(a_1)$	R, IR	703	715	722	— 3
	$\tilde{\nu}_3(a_1)$	R, IR	599	557	558	7
	$\tilde{\nu}_4(a_1)$	R, IR	404	406	404	0
	$\tilde{\nu}_5(b_1)$	R	624	601	598	4
	$\tilde{\nu}_6(b_2)$	R	396	350	353	11
	$\tilde{\nu}_7(b_2)$	R	504	538	541	— 7
	$\tilde{\nu}_8(e)$	R, IR	916	937	928	— 1
	$\tilde{\nu}_9(e)$	R, IR	579	549	548	5
	$\tilde{\nu}_{10}(e)$	R, IR	442	459	456	— 3
	$\tilde{\nu}_{11}(e)$	R, IR	270	282	280	— 4
SF_6	$\tilde{\nu}_1(a_{1g})$	R	776	777	791	— 2
	$\tilde{\nu}_2(e_g)$	R	642	618	617	4
	$\tilde{\nu}_3(t_{1u})$	IR	932	950	940	— 1
	$\tilde{\nu}_4(t_{1u})$	IR	613	546	550	10
	$\tilde{\nu}_5(t_{2g})$	R	522	539	541	— 4
	$\tilde{\nu}_6(t_{2u})$	i.a.	344†	381	383	— 11

† Inferred from combination bands.

‡ $\Delta\tilde{\nu}=(\tilde{\nu}_{\text{obs.}}-\tilde{\nu}_{\text{calc.}})$ to the nearest wave number.

Table 2. Observed and calculated frequencies in cm^{-1} .

	S_1	S_2	S_3	S_4	S_5	S_6	S_7	S_8	S_9	S_{10}	S_{11}
Q_1	0.88 ₈	-2.75 ₃	-0.83 ₅	-0.27 ₉	4.33 ₇	-0.47 ₇	3.33 ₄	2.78 ₄	-0.03 ₉	-0.18 ₅	-0.15 ₈
Q_2	0.90 ₉	0.57 ₆	3.99 ₀	-0.76 ₅	0.44 ₁	4.69 ₂		-2.00 ₀	2.01 ₀	-1.78 ₆	-1.88 ₀
Q_3	-1.44 ₅	-2.95 ₅	1.53 ₈	2.06 ₃				1.28 ₃	2.42 ₉	-0.37 ₇	2.95 ₇
Q_4	4.90 ₁	0.36 ₆	-0.13 ₅	2.63 ₁				-0.99 ₂	-2.19 ₅	-4.79 ₄	2.12 ₇
Q_5											
Q_6											
Q_7											
Q_8											
Q_9											
Q_{10}											
Q_{11}											

Table 3. Normal coordinates of SF_5Cl .

The normal coordinates of SF_5Cl and SF_6 , based on the force constants determined in this investigation, can be found in tables 3 and 4. While the potential energy distribution matrices which are given by:

$$P.E.D. = \Lambda^{-1} \cdot (JZ) \cdot \Phi,$$

where (JZ) is the Jacobian matrix and Φ is a diagonal matrix having the calculated force constants on its diagonal, are found in tables 5 and 6.

	S_1	S_2	S_3	S_4	S_5	S_6
Q_1	4.35 ₉	4.35 ₉	2.79 ₄ 2.50 ₀	-0.13 ₇ 2.13 ₀	2.17 ₉	3.08 ₂
Q_2						
Q_3						
Q_4						
Q_5						
Q_6						

Table 4. Normal coordinates of SF_6 .

	$K(S-F)$	$K(S-Cl)$	$H(F-S-F)$	$H(F-S-Cl)$	$F(F \dots F)$	$F(F \dots F)$
$\tilde{\nu}_1$	0.62 ₂	0.13 ₈	0.05 ₉	0.06 ₅	0.11 ₅	0.00 ₂
$\tilde{\nu}_2$	0.53 ₄	0.05 ₅	0.02 ₅	0.02 ₈	0.35 ₈	0.00 ₂
$\tilde{\nu}_3$	0.27 ₂	0.18 ₂	0.11 ₇	0.13 ₀	0.29 ₇	0.00 ₁
$\tilde{\nu}_4$	0.03 ₅	0.44 ₇	0.08 ₃	0.09 ₂	0.05 ₆	0.28 ₈
$\tilde{\nu}_5$	0.91 ₀	0.00 ₀	0.00 ₁	0.00 ₁	0.07 ₂	0.01 ₆
$\tilde{\nu}_6$	0.02 ₇	0.00 ₀	0.25 ₆	0.28 ₅	0.27 ₃	0.15 ₉
$\tilde{\nu}_7$	0.00 ₀	0.00 ₀	0.44 ₀	0.00 ₀	0.56 ₀	0.00 ₀
$\tilde{\nu}_8$	0.82 ₉	0.00 ₀	0.08 ₄	0.01 ₈	0.07 ₃	0.00 ₆
$\tilde{\nu}_9$	0.00 ₆	0.00 ₀	0.41 ₂	0.00 ₃	0.57 ₉	0.00 ₁
$\tilde{\nu}_{10}$	0.00 ₅	0.00 ₀	0.35 ₀	0.12 ₀	0.46 ₁	0.06 ₄
$\tilde{\nu}_{11}$	0.00 ₅	0.00 ₀	0.08 ₆	0.53 ₁	0.10 ₅	0.27 ₃

Table 5. The potential energy distribution in SF_5Cl .

	$K(S-F)$	$H(F-S-F)$	$F(F \dots F)$
$\tilde{\nu}_1$	0.52 ₄	0.00 ₀	0.47 ₆
$\tilde{\nu}_2$	0.86 ₃	0.00 ₀	0.13 ₇
$\tilde{\nu}_3$	0.80 ₉	0.10 ₉	0.08 ₂
$\tilde{\nu}_4$	0.01 ₀	0.39 ₈	0.59 ₂
$\tilde{\nu}_5$	0.00 ₀	0.44 ₀	0.56 ₀
$\tilde{\nu}_6$	0.00 ₀	0.44 ₀	0.56 ₀

Table 6. The potential energy distribution in SF_6 .

Finally, it should be noted that the percentage error in the frequencies is in general less than 10 per cent. It is indeed the belief of the present investigator that force constant calculations, are more valid for investigations where anharmonicity corrections are taken into consideration. But, alas, in the present molecules such corrections are impossible and one should perhaps be content with our set of force constants.

The author wishes to extend his gratitude to Professor Michael J. Joncich for his encouragement and Mr. Clyde C. Givens of the Computer Center of Northern Illinois University for his expert assistance.

REFERENCES

- [1] CROSS, L. H., ROBERTS, H. L., GROGGIN, P., and WOODWARD, L. A., 1960, *Trans. Faraday Soc.*, **56**, 945.
- [2] VENKATESVARLU, K., and SATHIANANDAN, K., 1961, *Optika i Spektroskopiya*, **11**, 24.
- [3] GAUNT, J., 1953, *Trans. Faraday Soc.*, **49**, 1122. YOST, DON M., STEFFENS, C. C., and CROSS, S. T., 1934, *J. chem. Phys.*, **2**, 311.
- [4] CRAWFORD, R. A., DUDLEY, F. B., and HEDBERG, K., 1959, *J. Amer. chem. Soc.*, **81**, 5287.
- [5] INTERATOMIC DISTANCES, 1958, Chemical Society, Special publication No. 11.
- [6] NIELSEN, J. R., and BERRYMAN, L. N., 1949, *J. chem. Phys.*, **17**, 659.
- [7] TINKHAM, M., 1964, *Group Theory and Quantum Mechanics* (New York: McGraw-Hill Book Co. Inc.).
- [8] WILSON, E. B., 1949, *J. chem. Phys.*, **7**, 1041.
- [9] FERIGLE, SALVADOR M., and MEISTER, ARNOLD G., 1951, *J. chem. Phys.*, **19**, 982.
- [10] UREY, H. C., and BRADLEY, C. A., 1931, *Phys. Rev.*, **38**, 1969.
- [11] YERANOS, WALTER A., and FOSS, FRED D., 1965, *Mol. Phys.*, **9**, 87.
- [12] YERANOS, WALTER A., and GIVENS, CLYDE C. (unpublished bulletin).
- [13] HIRAISHI, J., NAKAGAWA, I., and SHIMANOUCI, T., 1964, *Spectrochim. Acta*, **20**, 819.
- [14] SHIMANOUCI, T., and NAKAGAWA, I., 1962, *Spectrochim. Acta*, **18**, 89.

The dipole moment of dihexamethylbenzenecobalt

by B. J. NICHOLSON and H. C. LONGUET-HIGGINS

Department of Theoretical Chemistry, University Chemical Laboratory,
Lensfield Road, Cambridge

(Received 25 March 1965)

The unexpected dipole moment of dihexamethylbenzenecobalt is examined in the light of the 'pseudo-Jahn-Teller effect', which is found to offer a qualitative explanation.

1. INTRODUCTION

Fischer and Lindner recently reported that dihexamethylbenzenecobalt (CoAr_2) has a dipole moment of $1.78 \pm 0.07D$ in benzene and cyclohexane at 25°C [1], in contrast with CrAr_2 , which has no dipole moment [2]; the evidence suggests that FeAr_2 relates to CrAr_2 in structure, since they have similar x-ray powder photographs, CoAr_2 differing in this respect. The infra-red spectra of the three compounds were recorded; down to 700 cm^{-1} they are alike and closely related to the spectrum of free Ar, but below that CoAr_2 is sharply distinguished. Some spectroscopic data is tabulated in table 1, where parallels between CrAr_2 and $\text{Cr}(\text{C}_6\text{H}_6)_2$ are clear.

FeCp_2 [13]†	$\text{Cr}(\text{C}_6\text{H}_6)_2$ [14]‡	CrAr_2 [1]†	FeAr_2 [1, 2]†	CoAr_2 [1]†
669 vw	673 vw			671 m
624 vw, br	626 vw			625 m
567 vw, br				564 m
	512 vw			537 m, br
490 s	490 s	490 s		504 m, br
478 s	459 s	454 s	465 w	468 m
	425 s			
	418 vw	389 w	371 w	419 w, br
		313 v br	362 w	

Table 1. Infra-red spectra of some sandwich molecules in the range $690\text{--}250\text{ cm}^{-1}$. Cp = cyclopentadienyl, Ar = hexamethylbenzene, s = strong, m = medium, w = weak intensity, br = broad, v = very. † In Nujol mull, ‡ in KBr pellet.

It thus appears probable that CrAr_2 and FeAr_2 have normal sandwich structures, but that CoAr_2 does not; this seemingly anomalous situation is here investigated by the methods of den Boer, den Boer and Longuet-Higgins [3], who attempted to explain the apparent distortion of $\text{Cr}(\text{C}_6\text{H}_6)_2$ from D_{6h} to D_{3d} symmetry by a 'pseudo-Jahn-Teller effect': if low-lying excited states can mix heavily with the ground state when a distortion occurs, the distortion may become energetically

profitable. We test the possibility of D_{6h} models of CrAr_2 , FeAr_2 and CoAr_2 developing dipole moments in this way.

2. THEORETICAL APPROACH

The usual approximation for calculations on sandwich compounds is that the outer electrons move in an effective field provided by the nuclei and the inner electrons (including those forming sigma bonds in the aromatic moiety); the Hamiltonian due to the framework is then a sum of one-electron operators. For an excited state to cause a distortion by the pseudo-Jahn-Teller effect the perturbation produced by the distortion must have a non-zero matrix element between this state and the ground state. It follows that only one-electron excitations, with no change in spin multiplicity, need consideration. Also the perturbation has the symmetry of the distortion, and this must be A_{2u} or E_{1u} to generate a dipole moment in a D_{6h} molecule. The number of available excited states is thus strictly curtailed.

First-order perturbation theory describes the normal Jahn-Teller effect, while the pseudo-Jahn-Teller effect is a second-order perturbation. The lowering of the electronic energy which occurs on mixing in the excited states is given by $\sum_n (|M_n|^2 / \Delta E_n)$, where M_n is the matrix element between the ground state and the n th excited state, and ΔE_n is the energy difference between the two states in the undistorted molecule; it will be found later that the matrix elements are proportional to the extent of distortion. We therefore estimate the energy which would be necessary to produce a particular small distortion if no significant pseudo-Jahn-Teller effect were operative, the relevant force constants being obtained from other sandwich molecules; if this energy is less than the lowering of the electronic energy produced by the distortion, distortion will occur. In practice it is more convenient to calculate the matrix elements and the energy required for distortion, and to use these to obtain critical values for the excitation energies; if it appears probable that the actual excitation energies are less than these critical values, distortion will be expected.

To apply this theory a knowledge of the electronic structures of CrAr_2 , FeAr_2 and CoAr_2 is needed. There has been much work on the electronic structure of ferrocene (FeCp_2), to which [4-6] provide access; there is some agreement that the main source of bonding is the e_{1g} interaction (to use the notation of Dunitz and Orgel [7]), but considerable disagreement about the quantitative aspects of the problem. We need the order of the lowest anti-bonding orbitals, but this is still a matter for debate. Perhaps the commonest description, following [7], places the ($e_{1g}d$) anti-bonding orbitals below the ($e_{1u}p$), ($a_{2u}p$) and ($a_{1g}s$). All these orbitals are localized more on the metal atom than on the ligands, with ($e_{1g}d$) the most delocalized. The letters d , s and p denote the $3d$, $4s-3d$ or $4p$ character of the metal orbital involved, and the group representation symbols have their usual symmetry connotations for sandwich molecules (six-fold symmetry may be assumed for the Ar rings since slight distortions to three-fold symmetry, as may occur for $\text{Cr}(\text{C}_6\text{H}_6)_2$ [8], would negligibly alter the conclusions). The energies of the important e_1 and e_2 ring orbitals should be similar for Cp and Ar when the effect of the methyl groups is allowed for, so we take the above orbital order as applying to all the Ar sandwiches. Some other possibilities will be discussed at the end.

We can now write down the electronic configurations that would be expected for the ground states of CrAr_2 , FeAr_2 and CoAr_2 if they have normal sandwich structures. CrAr_2 would have a totally symmetrical singlet ground state $^1A_{1g}$, in accordance with the general theory. The two additional electrons in FeAr_2 , and probably the three in CoAr_2 , would enter $(e_{1g}d)$ to give $^3A_{2g}$ and $^2E_{1g}$ ground states respectively (we do not consider the possibility that exchange forces might cause the third extra electron in CoAr_2 to enter the orbital next above $(e_{1g}d)$, thus producing a quartet ground state). The magnetic measurements [1] agree with these suggestions, but for CoAr_2 , where the actual structure is obviously not a normal sandwich, the observation of a doublet ground state does not resolve the ambiguity; the doublet and quartet states could cross during the distortion.

For CrAr_2 , with a $^1A_{1g}$ ground state, we look for $^1E_{1u}$ and $^1A_{2u}$ excited states to allow respectively E_{1u} and A_{2u} distortions. All the experimental and theoretical evidence indicates that the relevant excitation energies are too large to allow heavy mixing of excited and ground states, so there is no reason to expect CrAr_2 to distort from a normal sandwich structure. FeAr_2 and CoAr_2 , however, have as their highest occupied orbitals the anti-bonding $(e_{1g}d)$, which are not far below suitable vacant $(e_{1u}p)$ and $(a_{2u}p)$ orbitals.

For FeAr_2 an A_{2u} distortion will mix the $^3A_{2g}$ ground state with $^3A_{1u}$ excited states, and an E_{1u} distortion will lead to mixing with $^3E_{1u}$ excited states. The only such states which need serious consideration are the $^3A_{1u}$ state obtained by exciting an electron from $(e_{1g}d)$ into $(e_{1u}p)$, and the $^3E_{1u}$ state produced by excitation from $(e_{1g}d)$ into $(a_{2u}p)$. We now calculate the matrix elements of the two types of perturbation between the ground state and these excited states.

The figure shows our choice of axes for the undistorted molecule. We define the complex orbitals (e_{+1g}) and (e_{-1g}) in such a way that they are interchanged by reflection in the xz plane, and likewise (e_{+1u}) and (e_{-1u}) ; we have suppressed the symbols d and p without risk of ambiguity, and we also abbreviate $(a_{2u}p)$ to (a_{2u}) . Ignoring the closed shell we may write the wave functions for the two outermost electrons as:

$$\begin{aligned} ^3A_{2g} & \quad |e_{+1g}{}^\alpha e_{-1g}{}^\alpha\rangle & (-) \\ ^3A_{1u} & \quad \sqrt{(1/2)}[|e_{+1g}{}^\alpha e_{-1u}{}^\alpha\rangle - |e_{-1g}{}^\alpha e_{+1u}{}^\alpha\rangle] & (-) \\ ^3E_{1u+} & \quad \sqrt{(1/2)}[|e_{+1g}{}^\alpha a_{2u}{}^\alpha\rangle + |e_{-1g}{}^\alpha a_{2u}{}^\alpha\rangle] & (+) \\ ^3E_{1u-} & \quad \sqrt{(1/2)}[|e_{+1g}{}^\alpha a_{2u}{}^\alpha\rangle - |e_{-1g}{}^\alpha a_{2u}{}^\alpha\rangle] & (-) \end{aligned}$$

where the symbols in brackets on the right indicate the symmetry with respect to the xz plane; the chosen components of $^3E_{1u}$ are correct zeroth-order functions for perturbations which are symmetric or anti-symmetric about that plane. The A_{2u} distortion, which we shall denote by H_1 , is necessarily symmetric, but we shall find it convenient to consider E_{1u} distortions, denoted by H_2 , which are anti-symmetric about the xz plane (and hence symmetric about the yz plane). The relevant non-vanishing matrix elements are then easily found to be:

$$\langle ^3A_{2g} | H_1 | ^3A_{1u} \rangle = \sqrt{(1/2)}[\langle e_{-1g} | H_1 | e_{-1u} \rangle + \langle e_{+1g} | H_1 | e_{+1u} \rangle] = M_1$$

and

$$\langle ^3A_{2g} | H_2 | ^3E_{1u+} \rangle = \sqrt{(1/2)}[\langle e_{-1g} | H_2 | a_{2u} \rangle - \langle e_{+1g} | H_2 | a_{2u} \rangle] = M_2.$$

M_1 is real and M_2 pure imaginary.

CoAr_2 , with a ${}^2E_{1g}$ ground state, would be subject to normal Jahn-Teller distortions of E_{2g} symmetry. But all E_{2g} vibrations in sandwich molecules are vibrations within the aromatic rings and, as spectra show [9], are not particularly sensitive to the bonding with the metal; ($e_{1g}d$) electrons, in orbitals localized more on the metal atom than on the ligand, would not be expected to cause large Jahn-Teller distortions within the rings. In support we note the x-ray evidence [10] that no large static distortions occur in CoCp_2 , also a molecule usually described as having a degenerate ground state. The normal Jahn-Teller effect cannot, of course, offer an explanation for the dipole moment of CoAr_2 (CoCp_2 has no dipole moment [11]). In treating the pseudo-Jahn-Teller effect we assume that CoAr_2 has a degenerate ground state (the same results would be obtained if we took the non-degenerate ground state obtained after an E_{2g} distortion, except that more exact definitions of the excitation energies than we require would involve the small normal Jahn-Teller stabilization energy).

This ${}^2E_{1g}$ ground state will be mixed with ${}^2E_{1u}$ excited states by A_{2u} distortions, and with ${}^2A_{1u}$, ${}^2A_{2u}$ and ${}^2E_{2u}$ states by E_{1u} distortions. As for FeAr_2 we restrict consideration to states obtained by one-electron excitations from ($e_{1g}d$) to ($e_{1u}p$) or ($a_{2u}p$), but for CoAr_2 these excitations yield more states of interest, namely three distinct ${}^2E_{1u}$ states belonging to the configuration ($e_{1g}d$)²($e_{1u}p$)¹ and three more states, of species ${}^2A_{1u}$, ${}^2A_{2u}$ and ${}^2E_{2u}$, arising from ($e_{1g}d$)²($a_{2u}p$)¹. With respect to the xz plane the symmetric and anti-symmetric components of the ground state have the wave functions:

$${}^2E_{1g\pm} \quad \sqrt{(1/2)}[|e_{+1g}{}^\alpha e_{+1g}{}^\beta e_{-1g}{}^\alpha\rangle \pm |e_{-1g}{}^\alpha e_{-1g}{}^\beta e_{+1g}{}^\alpha\rangle].$$

A convenient orthonormal set of ${}^2E_{1u}$ wave functions is:

$$\begin{aligned} {}^2E_{1u\pm}{}^a & \quad \sqrt{(1/2)}[|e_{+1g}{}^\alpha e_{+1g}{}^\beta e_{-1u}{}^\alpha\rangle \pm |e_{-1g}{}^\alpha e_{-1g}{}^\beta e_{+1u}{}^\alpha\rangle], \\ {}^2E_{1u\pm}{}^b & \quad (1/2)[|e_{+1g}{}^\alpha e_{-1g}{}^\beta e_{+1u}{}^\alpha\rangle - |e_{+1g}{}^\beta e_{-1g}{}^\alpha e_{+1u}{}^\alpha\rangle] \\ & \quad \pm (1/2)[|e_{-1g}{}^\alpha e_{+1g}{}^\beta e_{-1u}{}^\alpha\rangle - |e_{-1g}{}^\beta e_{+1g}{}^\alpha e_{-1u}{}^\alpha\rangle], \\ {}^2E_{1u\pm}{}^c & \quad \sqrt{(1/12)}[2|e_{+1g}{}^\alpha e_{-1g}{}^\alpha e_{+1u}{}^\beta\rangle - |e_{+1g}{}^\alpha e_{-1g}{}^\beta e_{+1u}{}^\alpha\rangle - |e_{+1g}{}^\beta e_{-1g}{}^\alpha e_{+1u}{}^\alpha\rangle] \\ & \quad \pm \sqrt{(1/12)}[2|e_{-1g}{}^\alpha e_{+1g}{}^\alpha e_{-1u}{}^\beta\rangle - |e_{-1g}{}^\alpha e_{+1g}{}^\beta e_{-1u}{}^\alpha\rangle - |e_{-1g}{}^\beta e_{+1g}{}^\alpha e_{-1u}{}^\alpha\rangle]. \end{aligned}$$

Although these wave functions will not diagonalize the complete Hamiltonian, they do diagonalize the one-electron part of the Hamiltonian, and it will be an adequate approximation to regard them as describing three states of equal excitation energy, ΔE_1 , above the ground state. The matrix elements of an A_{2u} distortion H_1 between the ground state and these excited states are:

$$\begin{aligned} \langle {}^2E_{1g+} | H_1 | {}^2E_{1u+}{}^a \rangle &= \langle {}^2E_{1g-} | H_1 | {}^2E_{1u-}{}^a \rangle \\ &= (1/2)[\langle e_{-1g} | H_1 | e_{-1u} \rangle + \langle e_{+1g} | H_1 | e_{+1u} \rangle] = M_1/\sqrt{2}, \\ \langle {}^2E_{1g+} | H_1 | {}^2E_{1u+}{}^b \rangle &= \langle {}^2E_{1g-} | H_1 | {}^2E_{1u-}{}^b \rangle = -M_1/2, \\ \langle {}^2E_{1g+} | H_1 | {}^2E_{1u+}{}^c \rangle &= \langle {}^2E_{1g-} | H_1 | {}^2E_{1u-}{}^c \rangle = -\sqrt{3}M_1/2, \end{aligned}$$

so that the depression of the energy of ${}^2E_{1g+}$, or of ${}^2E_{1g-}$, by interaction with the three ${}^2E_{1u}$ states in question is:

$$-(1/2 + 1/4 + 3/4)|M_1|^2/\Delta E_1 = -3|M_1|^2/2\Delta E_1.$$

Under an E_{1u} distortion the ${}^2E_{1g}$ ground state is mixed with the following three states:

$$\begin{aligned} {}^2A_{1u} & \quad \sqrt{(1/6)}[2|e_{+1g}{}^\alpha e_{-1g}{}^\alpha a_{2u}{}^\beta\rangle - |e_{+1g}{}^\alpha e_{-1g}{}^\beta a_{2u}{}^\alpha\rangle - |e_{+1g}{}^\beta e_{-1g}{}^\alpha a_{2u}{}^\alpha\rangle] \quad (-) \\ {}^2A_{2u} & \quad \sqrt{(1/2)}[|e_{+1g}{}^\alpha e_{-1g}{}^\beta a_{2u}{}^\alpha\rangle - |e_{+1g}{}^\beta e_{-1g}{}^\alpha a_{2u}{}^\alpha\rangle] \quad (+) \\ {}^2E_{2u\pm} & \quad \sqrt{(1/2)}[|e_{+1g}{}^\alpha e_{+1g}{}^\beta a_{2u}{}^\alpha\rangle \pm |e_{-1g}{}^\alpha e_{-1g}{}^\beta a_{2u}{}^\alpha\rangle] \quad (\pm) \end{aligned}$$

The symbols on the extreme right again indicate whether the state is symmetric or anti-symmetric about the xz plane. For an E_{1u} distortion H_2 which is anti-symmetric about the xz plane the non-vanishing matrix elements between the ground state and these excited states are found to be:

$$\begin{aligned}\langle {}^2E_{1g+}|H_2|^2A_{1u}\rangle &= (\sqrt{3}/2)[\langle e_{-1g}|H_2|a_{2u}\rangle - \langle e_{+1g}|H_2|a_{2u}\rangle] = \sqrt{(3/2)}M_2, \\ \langle {}^2E_{1g-}|H_2|^2A_{2u}\rangle &= M_2/\sqrt{2}, \\ \langle {}^2E_{1g+}|H_2|^2E_{2u-}\rangle &= \langle {}^2E_{1g-}|H_2|^2E_{2u+}\rangle = M_2/\sqrt{2}.\end{aligned}$$

Setting the excitation energies all equal to ΔE_2 we conclude that H_2 depresses the energies of ${}^2E_{1g+}$ and ${}^2E_{1g-}$ by amounts equal to $2|M_2|^2/\Delta E_2$ and $|M_2|^2/\Delta E_2$ respectively, the former being the larger and consequently of more significance for the pseudo-Jahn-Teller effect.

Summarizing, we find that if ΔE_1 and ΔE_2 are the energies needed to excite an electron from $(e_{1g}d)$ to $(e_{1u}p)$ and $(a_{2u}p)$ respectively, then the second-order stabilizations produced by A_{2u} and E_{1u} distortions are as shown below, where for completeness we have given the corresponding results for the as yet unreported MnAr_2 :

	A_{2u}	E_{1u}
MnAr_2	$ M_1 ^2/2\Delta E_1$	$ M_2 ^2/\Delta E_2$
FeAr_2	$ M_1 ^2/\Delta E_1$	$ M_2 ^2/\Delta E_2$
CoAr_2	$3 M_1 ^2/2\Delta E_1$	$2 M_2 ^2/\Delta E_2$

Of the three compounds, it can be seen that CoAr_2 is the most likely to undergo pseudo-Jahn-Teller distortions.

3. EVALUATION OF THE MATRIX ELEMENTS

We discuss the A_{2u} ring-metal stretching mode (ω_1), the E_{1u} ring-rocking mode (ω_2) and the E_{1u} ring-metal-ring bending mode (ω_3), which are shown in the figure; the other modes of these symmetries are distortions within the ligands. Denoting the carbon $2p_z$ orbitals by $\phi_1, \phi_2 \dots \phi_6$ for one ring and $\chi_1, \chi_2 \dots \chi_6$ for the other, ϕ_r and χ_r being diametrically opposed, we expand the molecular orbitals occurring in M_1 and M_2 as:

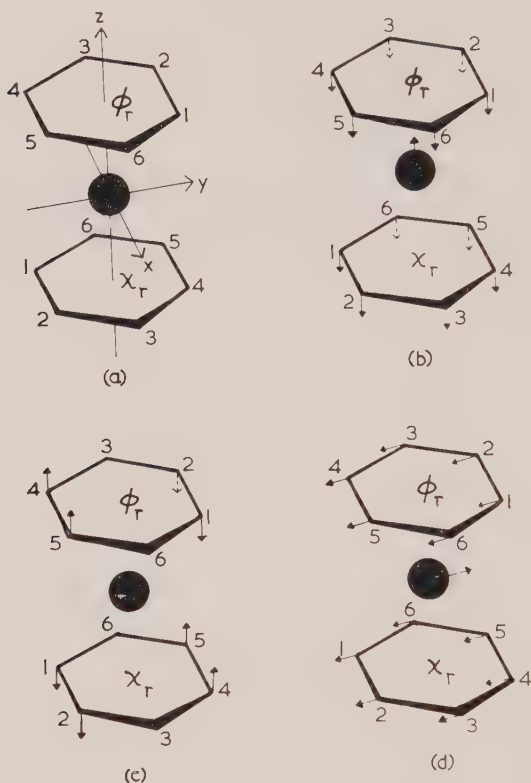
$$\begin{aligned}(e_{+1g}) &= \sqrt{(1-\lambda)}d_{+1} - \sqrt{(\lambda/12)}\sum_r W^r(\phi_r + \chi_r), \\ (e_{+1u}) &= \sqrt{(1-\mu)}p_{+1} - \sqrt{(\mu/12)}\sum_r W^r(\phi_r - \chi_r), \\ (a_{2u}) &= \sqrt{(1-\nu)}p_0 - \sqrt{(\nu/12)}\sum_r (\phi_r - \chi_r),\end{aligned}$$

where $W = \exp(i\pi/3)$ and λ, μ, ν are delocalization parameters. The anti-bonding nature of these orbitals determines the central signs, their g or u character the final signs.

Substitution of these expansions into M_1 and M_2 can be simplified by investigating the effect of distortion on the various integrals. Those of type $\langle \phi_r | H | \phi_s \rangle$, where r may equal s , are insensitive to the distortions we are considering, as structural changes within the rings are not involved; they cancel in the symmetrical molecule. Those caused by interaction between orbitals of different rings may safely be neglected. Those of type $\langle d | H | p \rangle$ must vanish in the undistorted molecule and will change little during the distortions if, as we shall assume, the carbon atoms are almost neutral; that this is an approximation is, of course, shown by the dipole moment of CoAr_2 .

To evaluate M_1 for ω_1 we examine $\langle e_{+1g} | H | e_{+1u} \rangle$ (the subscripts on H_1 and H_2 can now be safely dropped). Expanding this expression gives:

$$\begin{aligned} \langle e_{+1g} | H | e_{+1u} \rangle = & -\sqrt{[(1-\lambda)\mu/12]} \sum_r W^r [\langle d_{+1} | H | \phi_r \rangle - \langle d_{+1} | H | \chi_r \rangle] \\ & -\sqrt{[\lambda(1-\mu)/12]} \sum_r W^{-r} [\langle \phi_r | H | p_{+1} \rangle + \langle \chi_r | H | p_{+1} \rangle]. \end{aligned}$$



Some modes of vibration of a sandwich molecule: (a) choice of axes; (b) A_{2u} ring-metal stretching, ω_1 ; (c) E_{1u} ring-rocking, ω_2 ; (d) E_{1u} ring-metal-ring bending, ω_3 .

From the angular properties of d_{+1} and p_{+1} it follows that in the undistorted molecule

$$\langle d_{+1} | H | \phi_r \rangle = W^{-r} \beta_1 = \langle d_{+1} | H | \chi_r \rangle$$

and

$$\langle \phi_r | H | p_{+1} \rangle = W^r \beta_2 = -\langle \chi_r | H | p_{+1} \rangle,$$

where β_1 and β_2 are resonance integrals thus defined. If in the distortion the metal atom moves nearer the ring with orbitals ϕ_r by an amount q , then

$$\begin{aligned} \langle d_{+1} | H | \phi_r \rangle &= W^{-r} (\beta_1 - \gamma_1), \\ \langle d_{+1} | H | \chi_r \rangle &= W^{-r} (\beta_1 + \gamma_1), \\ \langle \phi_r | H | p_{+1} \rangle &= W^r (\beta_2 - \gamma_2), \\ \langle \chi_r | H | p_{+1} \rangle &= -W^r (\beta_2 + \gamma_2), \end{aligned}$$

where $\gamma = |\beta'q|$ and $\beta' = d\beta/dq$. Hence:

$$\sum_r W^r [\langle d_{+1} | H | \phi_r \rangle - \langle d_{+1} | H | \chi_r \rangle] = - \sum_r (2\gamma_1) = -12\gamma_1,$$

and

$$\sum_r W^{-r} [\langle \phi_r | H | p_{+1} \rangle + \langle \chi_r | H | p_{+1} \rangle] = - \sum_r (2\gamma_2) = -12\gamma_2,$$

so

$$\langle e_{+1g} | H | e_{+1u} \rangle = + \sqrt{[12(1-\lambda)\mu]\gamma_1} + \sqrt{[12\lambda(1-\mu)]\gamma_2}.$$

The complex conjugacy of the two terms in M_1 then gives us that

$$|M_1|^2 = 24 [\sqrt{[(1-\lambda)\mu]\gamma_1} + \sqrt{[\lambda(1-\mu)]\gamma_2}]^2.$$

For the E_{1u} modes we consider:

$$\begin{aligned} \langle e_{+1g} | H | a_{2u} \rangle &= - \sqrt{[(1-\lambda)\nu/12]} \sum_r [\langle d_{+1} | H | \phi_r \rangle - \langle d_{+1} | H | \chi_r \rangle] \\ &\quad - \sqrt{[\lambda(1-\nu)/12]} \sum_r W^{-r} [\langle \phi_r | H | p_0 \rangle + \langle \chi_r | H | p_0 \rangle]. \end{aligned}$$

In the undistorted molecule we define β_3 by:

$$\langle \phi_r | H | p_0 \rangle = \beta_3 = - \langle \chi_r | H | p_0 \rangle.$$

The component of ω_2 which is anti-symmetric about the xz plane is that shown in the figure; four carbon atoms are stationary and the other eight move parallel to the hexad axis for small distortions. Imagining twelve metal-carbon bonds, we see that, for those that change, the individual alterations are similar to those for ω_1 , but are differently interrelated. We therefore retain q for the extent of distortion to simplify the notation. Then we find:

$$\begin{aligned} \langle \phi_r | H | p_0 \rangle &= \beta_3 - n_r \gamma_3, \\ \langle \chi_r | H | p_0 \rangle &= -(\beta_3 + n_r \gamma_3), \\ \langle d_{+1} | H | \phi_r \rangle &= W^{-r} (\beta_1 - n_r \gamma_1), \\ \langle d_{+1} | H | \chi_r \rangle &= W^{-r} (\beta_1 + n_r \gamma_1), \end{aligned}$$

where $n_r = 0, \pm 1$ according to the formula $n_r = 2 \sin(r\pi/3)/\sqrt{3}$. Hence:

$$\sum_r [\langle d_{+1} | H | \phi_r \rangle - \langle d_{+1} | H | \chi_r \rangle] = - \sum_r 2W^{-r} n_r \gamma_1 = i4\sqrt{3}\gamma_1$$

and

$$\sum_r W^{-r} [\langle \phi_r | H | p_0 \rangle + \langle \chi_r | H | p_0 \rangle] = - \sum_r 2W^{-r} n_r \gamma_3 = i4\sqrt{3}\gamma_3,$$

so

$$\langle e_{+1g} | H | a_{2u} \rangle = -i2\sqrt{[(1-\lambda)\nu]\gamma_1} - i2\sqrt{[\lambda(1-\nu)]\gamma_3}.$$

This gives

$$|M_2|^2 = 8 [\sqrt{[(1-\lambda)\nu]\gamma_1} + \sqrt{[\lambda(1-\nu)]\gamma_3}]^2.$$

For ω_3 , which we do not discuss in detail, a similar expression is obtained, but the interpretations of γ_1 and γ_3 are different as they must be defined with respect to a different distortion coordinate.

The most important quantities required in evaluating these expressions are γ_1 , γ_2 and γ_3 , which, as noted, can be thought of as representing changes in the resonance integrals of the individual metal-carbon bonds and so are similar for ω_1 and ω_2 . If we assume β_1 changes exponentially during these distortions by a factor $\exp(-q/a_1)$, then $\beta_1' = -\beta_1/a_1$. β_1 will probably be slightly less than the much discussed C-C resonance integral of Hückel Molecular Orbital Theory, but as estimates of this vary (e.g. -1.1 ev in [3], -2.6 ev in [7]) we cannot hope to be definite about β_1 and must rest content with showing that plausible values make a pseudo-Jahn-Teller distortion a tenable suggestion. Again, assessments

of the matrix element for the e_{1g} interaction in FeCp_2 (which equals $\sqrt{10}\beta_1$) range from an empirically based guess of -2 eV [7] to calculations such as [6] which give around -7 eV †. Thus $-0.7\text{ eV} > \beta_1 > -2.2\text{ eV}$ seems likely. The matrix elements for the e_{1u} and a_{2u} interactions ($\sqrt{10}\beta_2$ and $\sqrt{10}\beta_3$ respectively) are found to be larger than for the e_{1g} interaction in [6], but are thought to be smaller, though still considerable, in [7]; we follow [7] and put $\beta_2 = 0.6\beta_1$, $\beta_3 = 0.3\beta_1$. a_1 is investigated with the usual assumption that resonance integrals are proportional to overlap integrals; calculation of these for different values of q by the methods of [7] suggest that this parameter is about 1 \AA . Inspection of the informative diagrams in [6] support this and indicate that a_2 has a similar value, while a_3 may be larger. Reasonable conclusions for FeCp_2 are $\beta_1' = 1.25\text{ eV/\AA}$, $\beta_2' = 0.6\beta_1'$, $\beta_3' = 0.2\beta_1'$, and we adopt these for CrAr_2 . As anti-bonding electrons are added to Cp sandwiches each one increases the ring-metal distance by about 0.1 \AA [12], thus decreasing β , and hence β' , by about one-tenth if a is 1 \AA ; allowing for this we take β_1' for FeAr_2 and CoAr_2 as 1.0 eV/\AA and 0.9 eV/\AA respectively, with β_2' and β_3' in proportion. Within the present approximations this last distinction is not significant in an absolute sense, but it does affect the relative values for FeAr_2 and CoAr_2 .

For ω_3 the situation is more complicated. The motion of each carbon atom can be split into two components, the one a vibration perpendicular to the hexad axis, which, as far as the individual resonance integrals are concerned, has a resemblance to the motion parallel to this axis in ω_2 , and the other an oscillation about the hexad axis, which can be treated as in [3] and does not alter β_3 , since β_3 has no angular variation about this axis. A detailed analysis shows that the two components produce out-of-phase effects on β_1 so that β_1' is small and may be of either sign with respect to β_3' . As a square must be taken, and β_3' is small, the results are too sensitive to the numerical choices to be worth giving; we merely remark that $|M_2|^2$ will be some 10 to 20 times smaller for ω_3 than for ω_2 .

The evaluation also requires the delocalization parameters λ, μ, ν , which are not as crucial as the resonance integrals. $\lambda = 0.3$, $\mu = 0.2$, $\nu = 0.1$, are reasonable and consistent with our other assumptions. The matrix elements can now be calculated, at least approximately, and we turn to a consideration of the force constants for ω_1 , ω_2 , and ω_3 .

4. ESTIMATION OF THE FORCE CONSTANTS

ω_1 and ω_2 appear in the infra-red as strong absorptions around 450 cm^{-1} ; data for several sandwich molecules are shown in table 2. The frequencies fall naturally into two columns and the usual assignments are given (except for NiCp_2) though it is possible that the column headings ω_1 and ω_2 should be interchanged there and in this discussion. The 355 cm^{-1} absorption for NiCp_2 has been assigned to both ω_1 and ω_2 [9] or to ω_1 definitely and perhaps also to ω_2 [13]. The general trends, however, clearly indicate that it is ω_2 and that ω_1 would be expected, by extrapolation from FeCp_2 and CoCp_2 , to lie below 250 cm^{-1} , the limit of the observations. Treating these molecules as linear XY_2 systems with the rings

† In case of confusion we should point out that β_1 as here defined is not the same as $\beta(e_{1g})$ in [6], which is a core integral and is about 30 eV . β_1 corresponds to the overall off-diagonal element for the e_{1g} interaction, which can be immediately obtained by working back from the given eigenvalues and eigenvectors.

Compound and reference		ω_2 (cm^{-1})	ω_1 (cm^{-1})	k_1 ($\text{mdynes}/\text{\AA}$)	Departure from 'eighteen-electron rule'
VCp ₂	[13]	422 s	379 s	2.0	-3
CrCp ₂	[13]	429 s	408 m	2.3	-2
V(C ₆ H ₆) ₂	[14]	470 s	424 s	2.5	-1
Cr(C ₆ H ₆) ₂	[14]	490 s	459 s	2.9	0
CrAr ₂	[1]	490 s	454 s	3.2	0
FeCp ₂	[13]	490 s	478 s	3.1	0
CoCp ₂	[13]	464 m	355 s	2.0	+1
NiCp ₂	[13]	355 s			+2

Table 2. The A_{2u} ring-metal stretching (ω_1) and E_{1u} ring-rocking (ω_2) fundamentals for some sandwich molecules. k_1 is discussed in the text. Abbreviations are as in table 1.

as point masses allows the calculation of approximate force constants for the metal-ring bond (k_1) and for the interaction between the two bonds (k_{12}), given the A_{2u} and A_{1g} ring-metal stretching frequencies [15]; the latter are available only for FeCp₂ and Cr(C₆H₆)₂, for both of which k_{12} is small and about 0.5×10^5 dynes/cm. For the other compounds $k_1 - k_{12}$ is obtainable from the A_{2u} fundamental ω_1 ; the quoted values of k_1 assume that k_{12} retains the above value. For NiCp₂, k_1 will be about 1×10^5 dynes/cm if ω_1 is about 250 cm^{-1} . k_1 is seen to depend more on the electronic structure than on the ligand; for molecules with fewer electrons than FeCp₂ k_1 and both fundamentals decrease slowly and steadily as weakly bonding electrons are removed. On adding anti-bonding electrons the changes are larger and more erratic; the two fundamentals surprisingly differ sharply for CoCp₂ and, most probably, for NiCp₂, instead of depending similarly on the metal-ring bonding as for the earlier members of the series. Also the extent of the drop in k_1 is not anticipated from the molecular orbital descriptions. The calculations of [6] assign the extra electrons to ring orbitals unaffected by compound formation and [7] estimates that the e_{1g} interaction gives not more than two-thirds of the bonding energy so that each anti-bonding electron removes at most one-sixth of it (this is compatible with the heats of formation of FeCp₂ and NiCp₂, after allowing for valence state promotion energies). The pseudo-Jahn-Teller effect may be partly responsible for these observations; inspection of the orbitals involved shows that it is only likely to affect ω_1 and ω_2 in sandwich molecules with anti-bonding electrons, where it could contribute to the decreases in these frequencies. There is no reason to expect it to alter the different fundamentals by the same amount. The A_{1g} ring-metal stretching frequencies for CoCp₂ and NiCp₂ would illuminate the situation.

To test the importance of the pseudo-Jahn-Teller effect we require an estimate of the force constant which would apply if the anti-bonding electrons were weakening the bonds only in the normal way and not by the pseudo-Jahn-Teller effect. This is probably best gleaned from the frequency that changes least (albeit erratically), which is ω_2 in the assignment of table 2. We take for this test force constant k_t values of 2.0×10^5 and 1.5×10^5 dynes/cm for molecules with two and three anti-bonding electrons respectively (i.e. FeAr₂ and CoAr₂). For the

sake of argument we use these values for both ω_1 and ω_2 . The force constant for ω_3 can be estimated from its frequency by the XY_2 approximation; this frequency is available only for $FeCp_2$, whence a value of 0.16×10^5 dynes/cm is found†. This is about one-twentieth of k_1 . The spectra of $FeAr_2$ and $CoAr_2$ below 690 cm^{-1} are of doubtful interpretation, so force constants have not been estimated for these compounds. The weakness of the absorptions of $FeAr_2$ is quite out of character for ω_1 or ω_2 (the remainder of this spectrum is of comparable intensity to those of $CoAr_2$ and $CrAr_2$) and analogy with $NiCp_2$ suggests that the 465 cm^{-1} absorption is not a fundamental, though there could be one around 360 cm^{-1} . We suspect that neither fundamental has been observed, which might indicate that the pseudo-Jahn-Teller effect is of importance for both. Most of the absorptions of $CoAr_2$ in the quoted range are near-coincidences with weaker lines in the spectra of $Cr(C_6H_6)_2$ and $FeCp_2$, though two are presumably related, in the distorted structure, to the fundamentals of a normal sandwich molecule.

5. RESULTS AND DISCUSSION

The energy required to produce ω_1 or ω_2 distortions is, with the above assumptions, $k_t q^2$ (two ring-metal bonds are involved). For example, if $|M_1|^2/\Delta E_1$ is greater than $k_t q^2$, ω_1 distortion will occur. Thus distortion will be expected if ΔE_1 is less than a certain critical value ΔE_{1c} given by $\Delta E_{1c} = |M_1|^2/k_t q^2$. The results are as follows:

	ΔE_{1c} (for ω_1)	ΔE_{2c} (for ω_2)
$FeAr_2$	0.9 eV	0.1 eV
$CoAr_2$	1.5 eV	0.2 eV

ΔE_{2c} for ω_3 will be of the same order of magnitude as for ω_2 , since both the matrix element and the force constant are smaller. These results might well be increased or decreased by at least a factor of two. E_{1g} distortions have not been discussed, but the situation is similar, save for the numerical details, to that for E_{1u} distortions, if $(a_{2u}p)$ is replaced by $(a_{1g}s)$ in the analysis. It is quite possible that the excitation energies are near these critical values and that the pseudo-Jahn-Teller effect becomes of significance as anti-bonding electrons are added to sandwich molecules; the point when distortions rather than decreases in ω_1 , ω_2 or ω_3 result could well be reached between $FeAr_2$ and $CoAr_2$, as extrapolation of ω_1 for $FeCp_2$ and $CoCp_2$ suggests. Thus while the sensitivity of $FeAr_2$ and $CoAr_2$ to air and heat is an expected consequence of the presence of anti-bonding electrons, the distortion rather than the complete dissociation of $CoAr_2$ is only expected when the pseudo-Jahn-Teller effect is considered.

No quantitative forecast of the structure of $CoAr_2$ can be attempted from these results. The normal Jahn-Teller effect gives terms linear in q against quadratic force constant terms, so distortion must occur and an expression for its expected extent can easily be written. The pseudo-Jahn-Teller effect, however, gives terms quadratic in q and so may not lead to a distortion, but if it does the distortion may well be large, though difficult to estimate because it is controlled by steric repulsions and other higher-order terms. What we have

† This value is misprinted in [13].

shown is that in CoAr_2 the normal sandwich structure is quite likely to be unstable; unfortunately there are many ways in which such a structure might distort. Though an ω_1 distortion is at first sight favoured, the results are approximate; in particular, ΔE_{2c} is less than ΔE_{1c} partly because the a_{2u} interaction was assumed less than the e_{1u} , but if this is so ΔE_2 will be less than ΔE_1 , quite possibly by 1 eV. (If ΔE_2 for CoAr_2 , between doublet ground and excited states, is very small, then, as noted earlier, the ground state in the undistorted molecule may in fact be the quartet state corresponding to the excited doublet state.) Combinations of A_{2u} , E_{1u} and E_{1g} distortions may occur. Steric effects of the methyl groups may be important.

The size of the dipole moment shows that the distortion must be considerable, but offers no further guidance. There are some other sandwich molecules with distortions of the sort we have discussed for CoAr_2 , and their dipole moments are of the same order of magnitude. BeCp_2 , with a dipole moment of about $2.4D$ (depending on the solvent), undergoes an ω_1 distortion, which can be explained by an ionic model [16]. PbCp_2 and SnCp_2 , with dipole moments of about $1.5D$ and $1.0D$ (depending on the solvent) [17], are suggested on infra-red evidence to have structures resulting from E_{1u} distortions, with each ring symmetrically bound, but with a ring-metal-ring angle substantially different from 180° ; this has been rationalized by the concept of sp^2 hybridization [18]. An alternative, equivalent, description can be offered in terms of the pseudo-Jahn-Teller effect. PbCp_2 , if it had a normal sandwich structure, would probably have as its highest occupied orbital one of mainly metal $6s$ character, below vacant ones of mainly $6p_{0,\pm 1}$ character. Excitations to these vacant orbitals would give suitable excited states for E_{1u} and A_{2u} distortions. The similarity of the two descriptions is apparent, and our treatment of CoAr_2 can be thought of as an investigation into the likelihood of hybridization of metal $3d_{\pm 1}$ with $4p_{0,\pm 1}$ orbitals, the gain in bond strength being compared with the necessary promotion energies. A novel distortion is shown by $\text{CpRhC}_6(\text{CF}_3)_6$: the metal atom is bonded to a 'butadiene unit' of the benzene nucleus, which is dihedral, while the bonding to the Cp ring is normal; the 'eighteen-electron rule' then holds [19]. This has been ascribed to the effects of the electron-attracting trifluoromethyl groups [19], and discussion in terms of the pseudo-Jahn-Teller effect is of doubtful value. A distortion of this type for CoAr_2 (which would involve an 'allyl' rather than a butadiene unit of one benzene nucleus if the eighteen-electron rule were to be obeyed) is not expected if the above suggestion is correct. These precedents provide no clear pointer to the structure of CoAr_2 ; the spectra of BeCp_2 , PbCp_2 and SnCp_2 do not have the same features as CoAr_2 from 690 – 250 cm^{-1} , and the similarity of the spectra of CoAr_2 , FeAr_2 , CrAr_2 and Ar above 700 cm^{-1} suggest that distortions within the rings do not occur.

6. CONCLUSIONS

It is obviously not feasible to examine all other conceivable descriptions of the electronic structure of a D_{6h} model of CoAr_2 , but the more important possibilities will be noted. Though the final conclusions from the experimental evidence for $\text{Cr}(\text{C}_6\text{H}_6)_2$ agree with our assumptions, it was earlier thought that ($e_{1u}p$) came below ($e_{1g}d$) [20]; if so, excitation of an ($e_{1u}p$) electron to ($e_{1g}d$) or ($a_{1g}s$) would give results for A_{2u} or E_{1u} distortions similar to those already obtained.

The calculations of [6] have ($e_{2u}R$) as the lowest vacant orbitals for FeCp_2 , followed by ($e_{2g}R$) and ($e_{1g}d$), where R indicates orbitals localized more on the rings than the metal. Excitations from ($e_{2u}R$) to ($e_{2g}R$) and ($e_{1g}d$) would provide excited states suitable for A_{2u} and E_{1u} distortions. Steric interaction between the methyl groups may be partly relieved by staggering of the rings to give D_{6d} symmetry. A D_{6h} model was used because the treatment is then a little simpler, and the g, u distinction is an aid to clarity, but a D_{6d} model gives analogous results.

The approach of this paper is not above criticism. The lowering of the electronic energy caused by distortion has been described by resonance integrals, but has then been compared to an energy expressed in terms of force constants. It would be preferable to relate the force constants directly to the resonance integrals, but this is no simple matter. The convenient cancellation of the distortion coordinate q occurs only because of the choice of an exponential dependence of β on q , as opposed to the parabolic form of kq^2 . But the basic principle, that low-lying excited states can give rise to distortion, is well established.

To sum up, it seems reasonable to suggest that the pseudo-Jahn-Teller effect is of importance in sandwich molecules with anti-bonding electrons, that it is partly responsible for the large changes observed in the A_{2u} ring-metal stretching and E_{1u} ring-rocking fundamentals, and that the dipole moment of CoAr_2 is less surprising than at first sight.

One of us (B. J. N.) acknowledges with thanks financial support from D.S.I.R.

REFERENCES

- [1] FISCHER, E. O., and LINDNER, H. H., 1964, *J. organometal. Chem.*, **2**, 222.
- [2] FISCHER, E. O. (private communication).
- [3] DEN BOER, D. H. W., DEN BOER, P. C., and LONGUET-HIGGINS, H. C., 1962, *Mol. Phys.*, **5**, 387.
- [4] SCOTT, D. R., and BECKER, R. S., 1961, *J. chem. Phys.*, **35**, 516. Erratum, *Ibid.*, 2246.
- [5] WILKINSON, G., and COTTON, F. A., 1959, *Prog. inorg. Chem.*, **1** (New York).
- [6] DAHL, J. P., and BALLHAUSEN, C. J., 1961, *Math. fys. Medd.*, **33**, No. 5.
- [7] DUNITZ, J. D., and ORGEL, L. E., 1955, *J. chem. Phys.*, **23**, 954.
- [8] JELLINEK, F., 1963, *J. organometal. Chem.*, **1**, 43.
- [9] LIPPINCOTT, E. R., and NELSON, R. D., 1958, *Spectrochim. Acta*, **10**, 307.
- [10] PFAB, W., and FISCHER, E. O., 1953, *Z. anorg. all. Chem.*, **274**, 317.
- [11] FISCHER, E. O., and SCHREINER, S., 1959, *Chem. Ber.*, **92**, 938.
- [12] SCHNEIDER, R., and FISCHER, E. O., 1963, *Naturwissenschaften*, **50**, 349.
- [13] FRITZ, H. P., and SCHNEIDER, R., 1960, *Chem. Ber.*, **93**, 1171.
- [14] FRITZ, H. P., LÜTTKE, W., STAMMREICH, H., and FORNERIS, R., 1961, *Spectrochim. Acta*, **17**, 1068.
- [15] HERZBERG, G., 1945, *Infrared and Raman Spectra of Polyatomic Molecules* (New York).
- [16] ALMENNINGEN, A., BASTIANSEN, O., and HAALAND, A., 1964, *J. chem. Phys.*, **40**, 3434.
- [17] DAVE, L. D., EVANS, D. F., and WILKINSON, G., 1959, *J. chem. Soc.*, p. 3684.
- [18] FRITZ, H. P., and FISCHER, E. O., 1961, *J. chem. Soc.*, p. 547.
- [19] CHURCHILL, M. R., and MASON, R., 1963, *Proc. chem. Soc.*, p. 365.
- [20] BERRY, R. S., 1961, *J. chem. Phys.*, **35**, 2025.

The absorption spectra of solid CO and N₂†

by M. BRITH and O. SCHNEPP

Department of Chemistry, Israel Institute of Technology, Haifa, Israel

(Received 13 April 1965)

The absorption spectra of CO and N₂ solids were investigated in the wavelength region 1600–1150 Å at temperatures ranging from 10°K to 30°K. For CO two electronic transitions were observed: $A^1\Pi \leftarrow X^1\Sigma^+$, 13 vibrational bands measured between 1570 Å and 1250 Å; $d^3\Delta \leftarrow X^1\Sigma^+$, 7 vibrational bands measured between 1300 Å and 1225 Å. The spectra are simply related to the molecular transitions and can be interpreted on the basis of existing theory of the excited states of molecular crystals of cubic symmetry. Davydov splitting has been clearly resolved for a number of bands of the $A \leftarrow X$ transition, and the experimental splitting energy can be quantitatively accounted for if the f -number of this transition is 0.16. The observed relative intensities of the components are in agreement with theoretical prediction. For N₂ also two electronic transitions have been observed: $a^1\Pi_g \leftarrow X^1\Sigma_g^+$, 8 vibrational bands measured between 1460 Å and 1250 Å; $w^1\Delta_u \leftarrow X^1\Sigma_g^+$, 11 bands measured between 1400 Å and 1170 Å. Here again Davydov splitting was observed but the theoretical interpretation of the splitting energy and the relative intensities of the components is complicated by the fact that the corresponding molecular transitions are dipole forbidden. The assignment of the latter transition is confirmed.

1. INTRODUCTION

CO and N₂ are very well-known molecules. The absorption spectrum of CO in the gas phase has been investigated by Hopfield and Birge [1] and again more recently by several authors [2–4]. Above 1200 Å the ‘Fourth Positive’ bands of CO of the allowed transition $A^1\Pi \leftarrow X^1\Sigma^+$ are the most prominent in the spectrum. Apart from this transition other known systems are: $a^3\Pi_r \leftarrow X^1\Sigma^+$ (Cameron bands) [4], $a'^3\Sigma^+ \leftarrow X^1\Sigma^+$ [3, 4], $e^3\Sigma^- \leftarrow X^1\Sigma^+$ [3, 4] and $d^3\Delta \leftarrow X^1\Sigma^+$ [4]. These are forbidden systems and are very weak in intensity.

The absorption spectrum of N₂ in the gas phase was first investigated by Hopfield and Birge [5] and has recently been the subject of a number of studies [2, 5–10]. The most intense systems in absorption at wavelengths longer than 1200 Å are: $a^1\Pi_g \leftarrow X^1\Sigma_g^+$ [6, 8], $B^3\Sigma_u^- \leftarrow X^1\Sigma_g^+$ [10, 7], $a'^1\Sigma_u^- \leftarrow X^1\Sigma_g^+$ [10, 7], $w^1\Delta_u \leftarrow X^1\Sigma_g^+$ [7]. All of these transitions are forbidden but the Lyman–Birge–Hopfield system ($a \leftarrow X$) is the most intense.

The absorption spectrum of CO and N₂ has here been investigated in the solid, in the region 1600 Å–1200 Å with the object of studying the perturbation of the electronic and vibrational states of the molecule by the crystal field. Preliminary work on the absorption spectra of these molecules in the solid has been reported by Dressler [11].

† Supported by the Air Force Office of Scientific Research under Contract AF61(052)–428 through the European Office of Aerospace Research (OAR), United States Air Force. Based on dissertation to be presented to the Senate, Israel Institute of Technology, by M. Brith in partial fulfilment of the requirements for the degree of Doctor of Science.

Electronic spectra of many molecular crystals have previously been studied and interpreted on the basis of the theoretical work of Davydov and others [12]. However, these investigations have mostly been concerned with the crystals of polyatomic molecules.

2. EXPERIMENTAL

In these experiments the N_2 and CO gases were deposited on a window of LiF cooled to $20^\circ K$. The experimental arrangement was similar to that described by Schnepf and Dressler [13]. Experiments were also carried out in which the sample of deposited gas was annealed at $30^\circ K$. In this case the temperature was regulated by a flow of cold He gas into the cryostat. This procedure permitted subsequent cooling to $10^\circ K$ and was applied to CO. In other experiments with solid N_2 the annealing at $30^\circ K$ was made possible by an arrangement similar to that described by Savitsky and Hornig [14] and by the use of liquid hydrogen as coolant.

The spectra were photographed on a 2m Eagle mounting grating spectrograph with a dispersion of 7.5 \AA/mm in first order and a resolution of 50 000. Tanaka [15] light sources of Kr and Ar were used.

Serious difficulties were caused by the strong absorption by a film of ice which deposited on the cold window during the experiment. The water vapour originated presumably from desorption from the warm outer walls of the cryostat. Further difficulty was encountered due to scattering of the light by the thick layers of solid deposit which were needed in the case of N_2 . The first difficulty was overcome partly by spreading silicone high vacuum grease over the walls of the cryostat after first heating the appropriate part of the cryostat in a drying oven.

The thicknesses of the solid deposits were some tens of angstroms for CO and several microns for N_2 . These values were estimated from the volume of the deposited gas, taking into account that the total amount of gas supplied was deposited as a solid over an area of 50 cm^2 . This figure is based on measurements of thicknesses of solid deposits by observing the appearance of interference colours in similar experimental arrangements.

Tracings of the plates were prepared with the aid of a micro densitometer. Frequencies of the band centres were measured from the plates and also from the tracings. The wavelengths were measured by the distance of the bands from the $H_I = 1215.7 \text{ \AA}$ line and the dispersion was determined with the help of impurity lines of N,C,O. The measurements were reproducible to 0.2 \AA . The bands are $400\text{--}1000 \text{ cm}^{-1}$ wide for solid CO and $200\text{--}400 \text{ cm}^{-1}$ wide for solid N_2 . The accuracy of measurement was about $\pm 30 \text{ cm}^{-1}$ in the case of CO and $\pm 20 \text{ cm}^{-1}$ in the case of N_2 . The widths of the bands at half intensity were measured from the tracings. The splitting of the bands were measured directly from the plates. Relative intensities were measured by the usual densitometric methods with an accuracy of 30 per cent.

The intensity ratios of the split components of the vibronic bands of CO ($A \leftarrow X$) were determined from the peak heights. The relative intensities of the vibronic bands including both split components were determined by graphical integrations of the absorption curves. This method was not applicable to the individual split components because of the excessive overlap. In the case of N_2 the relative intensities of the vibronic bands were determined from the peak heights.

3. EXPERIMENTAL RESULTS

3.1. CO

The absorption spectrum of CO was investigated in the solid state in the region 1600 Å–1200 Å. Plates A and B in figure 1 represent one set of experiments in which the temperature of the cold window was kept at 20°K and the absorption spectra of different thicknesses of deposit were recorded. The thicknesses varied from several molecular layers to 100 Å. Another experiment was carried out in which the gas was deposited at 30°K and after a short time was cooled down to 10°K (figure 1C).

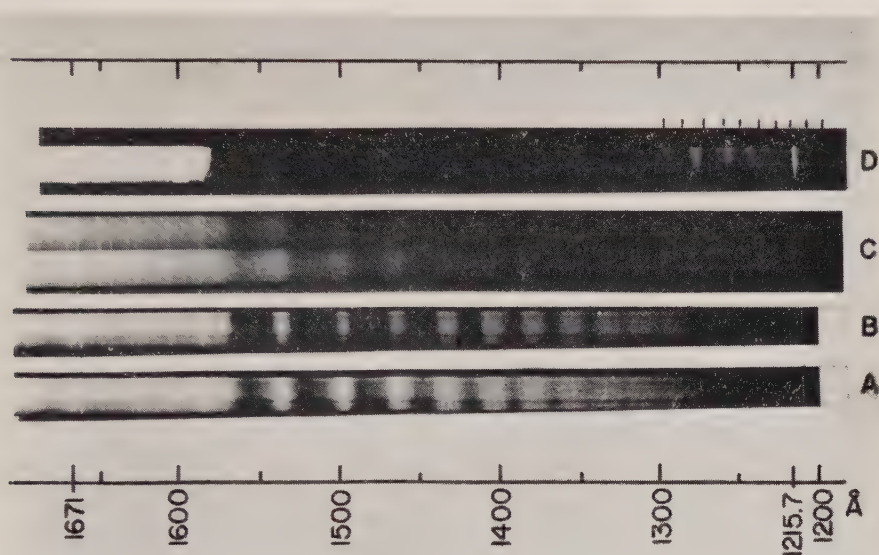


Figure 1. Absorption spectrum of solid CO in the 1200–1600 Å region; A, B: temperature 20°K; C: temperature 10°K (the solid sample annealed to 30°K). The sample thickness in A, B is five times that in C; sample thickness in D is 1000 times that in A, B. The marked bands in D are those of the $d^3\Delta \leftarrow X^1\Sigma^+$ transition. Sources: A–C: krypton; D: argon.

3.1.1. Transition $A^1\Pi \leftarrow X^1\Sigma^+$

Table 1 summarizes the experimental results. The table also includes the frequencies of the band centres in the gas (calculated from Hopfield and Birge's vibrational constants) and the calculated Franck–Condon factors [16]. The table also contains the vibrational frequency intervals in the gas and solid spectra and the shift of the band centres of the solid compared to the spectrum of the gas. The solid spectrum contains 13 bands, (0, 0) to (12, 0).

The widths of the bands vary appreciably along the progression. The first bands are wide, their widths vary from 920 cm⁻¹ (0, 0) to 1030 cm⁻¹ (1, 0), fall off to 770 cm⁻¹ at (3, 0) and narrow gradually to 460 cm⁻¹ (5, 0). The widths of the bands (7, 0) to (12, 0) are fairly equal at 400 cm⁻¹.

v'	λ (Å) solid	ν (cm ⁻¹) solid	ν (cm ⁻¹) gas	$\Delta\nu$ (cm ⁻¹) solid-gas shift of centre of band	Width (cm ⁻¹)	Splitting (cm ⁻¹)	Intensity arbitrary units ± 30 per cent	Franck-Condon factors	Vibrational intervals (cm ⁻¹) in solid	Vibrational intervals (cm ⁻¹) in gas
0	1566.6 1555.3	63833 64296	64747	-683	920	460	3.3	0.11		
1	1530.3 1517.1	65347 65915	66228	-598	1030	570	3.6	0.21	1569	1481
2	1494.3 1483.6	66921 67404	67674	-515	980	480	2.2	0.23	1529	1446
3	1459.3 1451.2	68526 68908	69086	-414	780	380	1.3	0.18	1513	1412
4	1426.1	70121	70464	-343	660		0.9	0.11	1449	1378
5	1398.8	71490	71807	-317	460		0.45	0.069	1369	1343
6	1373.4	72812	73116	-304	400		0.16	0.03	1322	1309
7	1350.2	74063	74390	-327			0.07	0.01	1251	1274
8	1328.1	75301	75629	-328			0.04		1238	1239
9	1307.0	76515	76834	-319					1214	1205
10	1287.0	77700	78005	-305					1185	1171
11	1268.1	78850	79141	-291					1150	1136
12	~1250	~79990	80243						~1140	1102

Table 1. Summary of absorption spectrum of solid CO, transition $A^1\Pi \leftarrow X^1\Sigma^+$, and comparison with the spectrum of the gas.

The first four bands are the most prominent in the progression and the second band is the most intense, the intensity falling off gradually along the progression. The calculated Franck–Condon factors [16] for this transition were recently found to be in good agreement with gas phase experiments [17]. Comparison of the band intensities in the solid with the calculated Franck–Condon factors shows that quantitatively the intensity distribution in the transition in the solid is different from that of the gas for the lower vibrational levels.

The first four strong bands are clearly split into two components overlapping one another (see figures 1 A, 2). The intensities of the two components are quite different (intensity ratio 1.5 ± 0.2) and also the widths of the components differ slightly. The more intense component is the lower in energy.

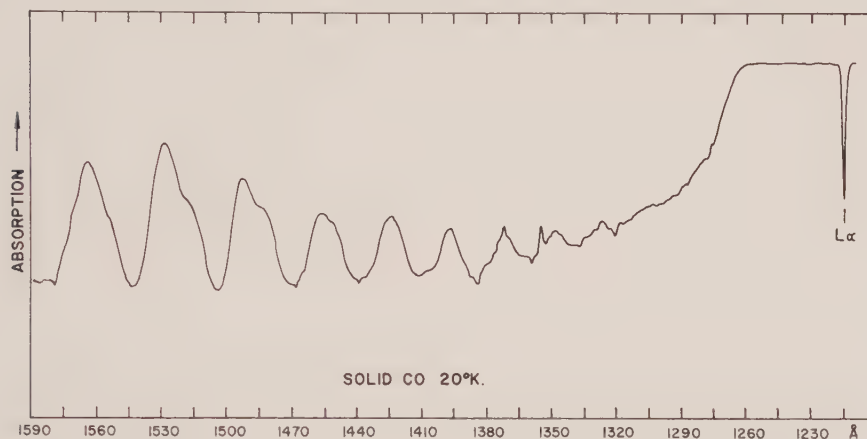


Figure 2. Tracing of the absorption spectrum of solid CO at 20°K.
Transition : $A^1\Pi \leftarrow X^1\Sigma^+$.

The magnitude of the splitting of these bands like their width, varies with the intensity of the band. The splitting of the second band is the largest, 570 cm^{-1} . The splitting of the first and third amounts to 460 cm^{-1} and 480 cm^{-1} and that of the fourth 380 cm^{-1} (see table 1). The splittings were measured from the plates and are accurate to $\pm 50\text{ cm}^{-1}$. In the other bands which are less intense the splitting is not apparent since it is smaller than the widths of the component bands. In the 'weak coupling' approximation [20] the magnitude of the splitting of a band is predicted to be proportional to its intensity in the gas. Assuming this approximation to be applicable, the splitting of the (5,0) band can be calculated from that of the (3,0) band and from the ratio of their Franck–Condon factors. In this way we predict a splitting of 150 cm^{-1} for the (5,0) band, whereas the width of the band is 460 cm^{-1} . In the same way we calculate 20 cm^{-1} for the splitting of the (7,0) band, whereas the band width is 400 cm^{-1} . It is therefore clear that the splitting can only be observed in the first few and most intense bands.

The bands are shifted to lower energies compared to the gas spectrum. The shift is largest for the (0,0) band (700 cm^{-1}), decreases gradually from band to band to 350 cm^{-1} for the (4,0) band and is constant for the other bands at $300\text{--}330\text{ cm}^{-1}$ (see table 1).

3.1.2. Transition $d^3\Delta \leftarrow X^1\Sigma^+$

The last bands of the $A \leftarrow X$ transition (9, 0)–(12, 0) are very weak in intensity. In order to record them relatively thick layers of CO had to be deposited and the spectrum was recorded with an Ar source. Beside these bands there appeared another progression of bands which extended to 1230 Å. This was the limit of measurement because of the loss of intensity due to light scattering. The intervals between these bands are 750–670 cm^{-1} , much smaller than the intervals for the last bands of the $A \leftarrow X$ progression (1200–1140 cm^{-1}). These intervals also do not converge appreciably, and the bands are somewhat narrower than the $A \leftarrow X$ bands. These bands are assigned as the (16, 0) to (22, 0) bands of the transition $d^3\Delta \leftarrow X^1\Sigma^+$ on the basis of frequency and the progression forming vibrational intervals [4, 18]. This transition involves a very large change in equilibrium internuclear distance ($\Delta r_e = 0.271 \text{ Å}$). Its intensity maximum lies in the region of the bands (9, 0) to (12, 0) and the ratio of the intensity of the (19, 0) band to the (10, 0) band in the gas [4] is 1/10. The intensity of this transition in the gas compared to the strong bands of the $A \leftarrow X$ transition is 1/1000, from which we obtain an intensity ratio of about 1/10000 for the intensity of the observed bands to the intensity of the strong bands of the $A \leftarrow X$ transition in the gas. In this work the ratio between the thicknesses of deposited layers required for the observation of these two absorption systems was roughly 1/3000 which is of the correct order of magnitude.

v'	λ (Å) solid	ν (cm^{-1}) solid	ν (cm^{-1}) gas	$\Delta\nu$ (cm^{-1}) solid–gas; shift of centre of band	Vibrational intervals (cm^{-1}) in gas	Vibrational intervals (cm^{-1}) in solid
15			76611			
16	1298.2	77030	77405	–380	794	
17	Masked by $A \leftarrow X$		78186		781	
18	1273.0	78554	Masked by $A \leftarrow X$			$\Delta\nu(16,0)–(18,0)$ 1524
19	1260.6	79327	79719	–390		748
20	~1249	~80060	80425	–370	706	730
21	1238.5	80743	81142	–400	717	687
22	1228.2	81420				673

Table 2. Summary of absorption spectrum of solid CO, transition $d^3\Delta \leftarrow X^1\Sigma^+$, and comparison with the spectrum of the gas.

In table 2 the measured wave lengths and frequencies are listed. The frequencies are compared to the frequencies of the band heads of the $d \leftarrow X$ transition in the gas [4]. The assignment of vibrational quantum numbers was somewhat arbitrary and may be in error. However, this assignment gives a shift of 380–400 cm^{-1} to lower energy for all the measured bands comparable to the shift of the $A \leftarrow X$ system.

Because of the great widths and intensities of the $A \leftarrow X$ bands, they mask the first members of the $d \leftarrow X$ progression. Nevertheless, some weak bands were

observed in the spectrum of a deposition layer of about 100 times that required to observe the strong $A \leftarrow X$ bands. These might be some of the more intense bands of the $d \leftarrow X$ progression.

3.2. N₂

The absorption spectrum of solid N₂ in the region 1600 Å–1200 Å was investigated at 20°K and 30°K. Also experiments were performed in which the sample was deposited at 30°K and subsequently cooled to 10°K. The spectra were identical for all these procedures. The thicknesses of deposited sample were about 3×10^3 – 3×10^4 times those needed for CO, i.e. about 1–10 μ . The spectra are represented in figures 3, 4. There are two absorption systems in the spectrum of the solid. The first progression consists of 8 bands which are broader and more intense. The second progression extends to shorter wavelengths and 11 bands of this system could be measured.

3.2.1. Transition $a^1\Pi_g \leftarrow X^1\Sigma_g^+$

The first progression represents the molecular $a^1\Pi_g \leftarrow X^1\Sigma_g^+$ transition which is analogous to the $A^1\Pi \leftarrow X^1\Sigma^+$ transition in CO. The intensity of this transition in N₂ in the gas phase is about 10^{-4} times that of the CO transition. This factor is an estimate obtained by comparing Tanaka's optical paths and

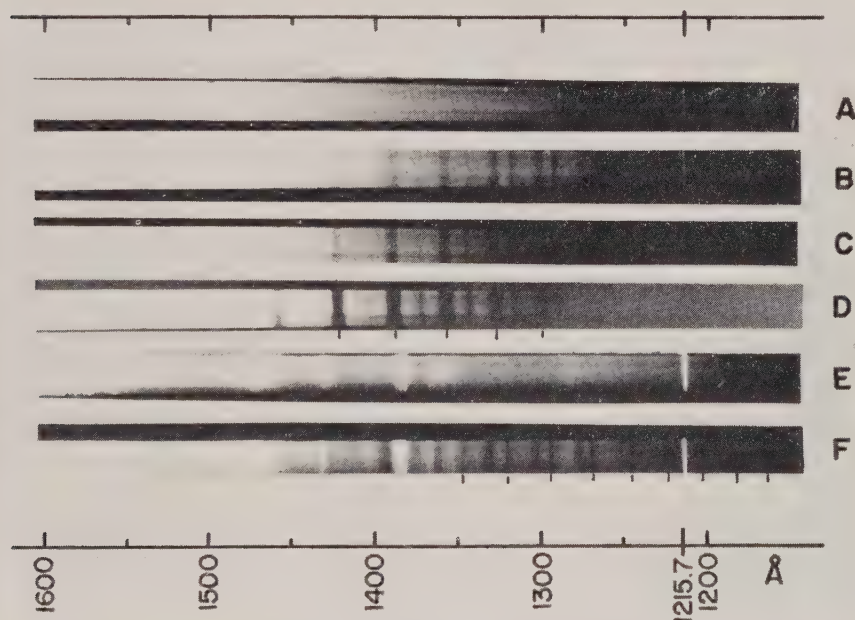


Figure 3. Absorption spectrum of solid N₂ in the 1150–1500 Å region, temperature 20°K. A: background krypton continuum; the thickness of sample in D is five times that in B, C. The markings in D indicate the separation between the split components of the bands of the $a^1\Pi_g \leftarrow X^1\Sigma_g^+$ transition; E: background argon continuum; F: the marked bands belong to the $w^1\Delta_u \leftarrow X^1\Sigma_g^+$ transition.

pressures for which the strongest bands of these transitions appeared [4, 6]. The ratio of the absorption intensities of N_2 and CO in the solid was found to be about 3×10^{-4} from a comparison between the volumes of the gases deposited. Table 3 summarizes the experimental data and includes the frequencies of the gas (calculated from Wilkinson's vibrational constants [8]) and calculated Franck-Condon factors [19]. As in the case of CO the perturbation by the crystal field manifests itself in the splitting of the bands and in their frequency shift.

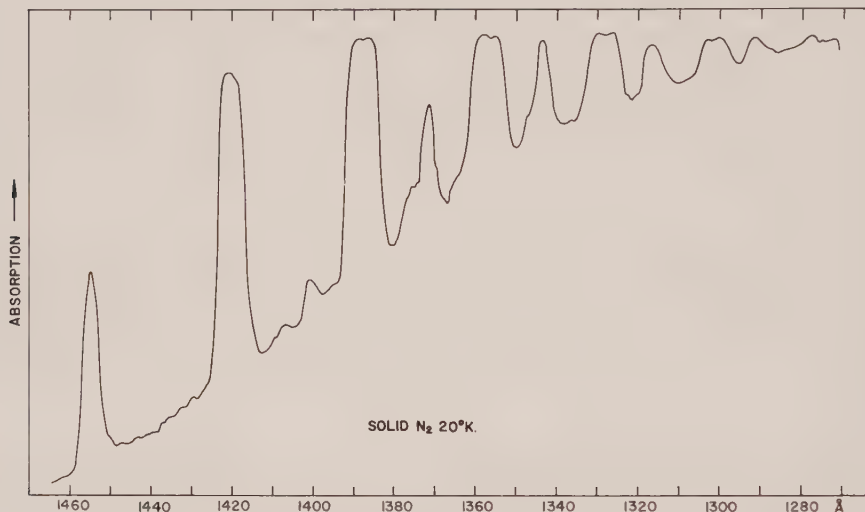


Figure 4. Tracing of the absorption spectrum of solid N_2 . The broader bands are those of the transition $a^1\Pi_g \leftarrow X^1\Sigma_g^+$ and are seen to be split.

The bands are much narrower than those of the parallel but much more intense transition in CO. The range of band widths is $200\text{--}400\text{ cm}^{-1}$ as compared to $300\text{--}1100\text{ cm}^{-1}$ for CO. The first band is appreciably weaker in intensity than the others and is also the narrowest (210 cm^{-1} wide). The widths of the most intense bands (2, 0) to (5, 0) vary from 340 cm^{-1} (2, 0) to 380 cm^{-1} (4, 0) to 330 cm^{-1} (5, 0).

There is no close agreement between the different authors concerning the intensity of the different bands in the gas phase. The intensity variation along the progression in the solid seems to follow the intensity variation in the gas as given by Tanaka [6]. However, the first band (0, 0) is relatively much less intense in the solid.

Also in N_2 a crystal field splitting has been observed but its magnitude is smaller than in CO. The splitting is apparent only in the strong bands (2, 0), (3, 0), (4, 0) and can be seen clearly only in the spectrum of a very thick sample (see figure 3 D and figure 4). The magnitude of the splitting of these bands, all of which are of about the same intensity, is $160\text{--}180\text{ cm}^{-1}$. The splittings were measured from the plates, the accuracy being about $\pm 30\text{ cm}^{-1}$.

As in CO the bands are shifted to lower energies. The magnitude of the shift ($270\text{--}200\text{ cm}^{-1}$) is smaller than in CO ($700\text{--}300\text{ cm}^{-1}$). The magnitude of the shift varying from 270 cm^{-1} for the (0, 0) band to 210 cm^{-1} for the (3, 0) band and is constant for the other bands at $215\text{--}200\text{ cm}^{-1}$ (see table 3).

v'	λ (Å) solid	ν (cm ⁻¹) solid	ν (cm ⁻¹) gas	$\Delta\nu$ (cm ⁻¹) solid-gas shift of centre of band	Width (cm ⁻¹)	Splitting (cm ⁻¹)	Intensity arbitrary units accuracy ± 30 per cent	Franck-Condon factors	Vibrational intervals (cm ⁻¹) in solid	Vibrational intervals (cm ⁻¹) in gas
0	1456.0	68681	68951	-270	210		1	0.05		
1	1421.2	70363	70618	-255	280	~ 140	3	0.13	1682	1667
2	1390.1 1387.0	71935 72095	72256	-241	340	160	5	0.18	1652	1638
3	1359.3 1356.1	73569 73739	73867	-213	370	170	6	0.19	1639	1611
4	1330.6 1327.4	75154 75335	75450	-215	380	180	8	0.15	1591	1583
5	1303.6 1300.8	76713 76873	77006	-213	330	160	8	0.11	1548	1556
6	1276.6	78333	78534	-201	290				1540	1528
7	~ 1252.0	~ 79870	80033							1499

Table 3. Summary of absorption spectrum of N₂, transition $a^1\Pi_g \leftarrow X^1\Sigma_g^+$ and comparison with the spectrum of the gas.

v'	λ (Å) solid	ν (cm ⁻¹) solid	ν (cm ⁻¹) gas	$\Delta\nu$ (cm ⁻¹) solid-gas	Width (cm ⁻¹)	Splitting (cm ⁻¹)	Intensity arbitrary units ± 30 per cent	Intensity in the gas, Tanaka [7]	Vibrational intervals in solid (cm ⁻¹)	Vibrational intervals in gas (cm ⁻¹)
0	1401.6	71347	71740	-390			0.2			
1	1373.0 1372.0	72833 72886	73276	-380	130	50	1	1	1539	1535
2	1345.0 1344.0	74345 74404	74787	-380	160	60	3	2	1518	1512
3	1319.0 1317.6	75815 75896	76278	-380	200	80	9	3	1492	1491
4	1294.1 1292.8	77274 77351	77745	-390	190	80	12	3	1455	1468
5	1269.1	78796	79184	-390	190			4	1445	1439
6	1246.6	80218	80609	-390				5	1422	1425
7	1225.2	71619	82009	-390				7	1401	1401
8	1204.9	82994	83379	-390				6	1375	1370
9	1185.7	84338	84722	-390				6	1344	1343
10	~ 1167.3	~ 85666	86050	-380				5	~ 1328	1328

Table 4. Summary of absorption spectrum of N₂, transition $w^1\Delta_g \leftarrow X^1\Sigma_g^+$, and comparison with the spectrum of the gas.

3.2.2. Transition $w^1\Delta_u \leftarrow X^1\Sigma^+_g$

The second observed progression of bands belongs to the $w^1\Delta_u \leftarrow X^1\Sigma^+_g$ molecular transition, and this assignment is confirmed by our observation which proves that the transition originates from $v''=0$ of the ground state [7]. This absorption system in the solid is almost equal in intensity to the $a \leftarrow X$ system. In the gas phase the intensity of this transition is about 5×10^{-3} that of the $a \leftarrow X$ transition [7].

This progression contains 11 bands (see figures 3, 4). The magnitude of Δr_e is greater in this transition than for the $a \leftarrow X$ transition [8, 10] ($\Delta r_e = 0.166 \text{ \AA}$ compared to $\Delta r_e = 0.123 \text{ \AA}$) and therefore the intensity is spread over more bands. The spectrum was recorded with a Kr lamp (figures 3 B, C, D) and with an Ar lamp (figure 3 F). The last bands of this progression are only barely discernible in this spectrum because of the very small intensity of the light source in this region but their absorption is intense. The experimental data concerning this transition are given in table 4. The table includes also the band head frequencies and intensities of the gas which were taken from Tanaka [7]. The bands of this transition are narrower (widths about $130\text{--}200 \text{ cm}^{-1}$) than those of the $a \leftarrow X$ transition (widths $200\text{--}400 \text{ cm}^{-1}$).

The bands (3, 0) to (9, 0) are the most intense bands and the (0, 0) band is relatively weak. This is in agreement with the intensity distribution reported for the gas spectrum. The intense bands are split into two components which differ very much in their widths. The width of the narrow component is $20\text{--}30 \text{ cm}^{-1}$ of a total of $130\text{--}200 \text{ cm}^{-1}$, the longer wavelength component being the narrower. The magnitude of the splitting is about $50\text{--}80 \text{ cm}^{-1}$. The splitting is seen clearly only in the spectrum recorded with the Kr lamp since with the Ar lamp less contrasty plates were used. This splitting cannot be seen in the tracings of the plates. The shifts which are given in the table are the differences between band centres of the wide components and the band heads in the gas. The magnitude of this shift is constant at -380 to -390 cm^{-1} .

4. DISCUSSION

Comparing the spectra of the molecules CO and N₂ in the gas to their spectra in the solid we can conclude that there is no great perturbation of the potential curve of the diatomic molecule by the crystal field apart from an electronic energy shift and crystal splitting of the exciton states.

The crystal field splitting is small compared to the vibrational energies both in CO and N₂ and therefore we can restrict our discussion to the weak coupling approximation [20]. In this approximation the splitting energy of the different bands in a progression is proportional to the square of the Franck-Condon overlap integrals between the vibrational functions of the ground and excited molecular states, i.e. the splitting energy is divided among the different bands parallel to the intensity. As we have shown, both in the case of solid CO and in the case of solid N₂, the observations qualitatively confirm the theoretical prediction in this respect.

The variation of the width of the bands also parallels the variation in intensity. The overall width of the bands is the sum of a contribution of the splitting energy and another of a broadening which may be ascribed to excitation of lattice modes.

The molecules CO and N₂ are isoelectronic and have, therefore, parallel electronic configurations. These two molecules crystallize in similar structures. Solid α -CO (stable below 61.5°K [22]) and solid α -N₂ (stable below 35.6°K [22])

have very nearly face-centred cubic structures if we consider molecular centres only with four molecules in the unit cell. The figure axes of the molecules are oriented along body diagonals of the cube. The accurate crystal space group for both solids is $P2_13(T^4)$ but $\alpha\text{-N}_2$ is very nearly $[21] \text{Pa}3 (T_h^6)$. The molecular centres in the case of $\alpha\text{-N}_2$ are displaced by 0.17 \AA from the centro-symmetric positions of $\text{Pa}3$ along the (111) directions so that the symmetry is reduced to $P2_13$. Although the centre of symmetry is thereby destroyed, the transition $a \leftarrow X$ is not intensified in the solid. Therefore we feel justified in dealing with the problem as though the space group were $\text{Pa}3$.

The degeneracy of the excited π -states of CO and N_2 is not removed by the symmetry of the site (C_3, C_{3i} respectively). Nevertheless, there occurs a crystal field splitting which is of the Davydov type [12]. This splitting arises from interactions between molecules on translationally non-equivalent sites. Because there are four different sites in the unit cell and the molecular excited states are doubly degenerate, eight different one site exciton functions can be constructed. These are given by [12, 23] :

$$\Psi_j^\alpha(\mathbf{k}) = \sum_a \exp(i\mathbf{k} \cdot \mathbf{r}_a) \psi_{j,a}^\alpha. \quad (1)$$

This function represents the propagation of an α -excitation along the molecules of the j th sub-lattice. This propagation is modulated by the wave vector. In this expression \mathbf{r}_a is the position vector of the centre of the a th cell and α designates one of the two components of the degenerate molecular state. The function $\psi_{j,a}^\alpha$ is a localized wavefunction of the crystal which is a product function in which every molecule is in its ground state except the molecule in the j th site of the a th unit cell which is excited to the α -state. These eight functions form a basis for a representation which reduces to $E + 2F$ in the case of CO (${}^1\Pi$) (factor group T) and to $E_g + 2F_g$ in the case of N_2 (${}^1\Pi_g$) (factor group T_h), all for the case $\mathbf{k} = 0$, where F and E designate triply and doubly degenerate representations respectively.

In the case of CO (factor group T) transitions to the two F states are dipole allowed as the translations X, Y, Z belong to the F representation. The transition to the doubly degenerate state, which belongs to the representation E, is forbidden. In the case of N_2 (factor group T_h) the dipole transition to the F_g excited state is forbidden. However, the electric quadrupole and magnetic dipole transitions are allowed since the terms XY, XZ, YZ and the rotations R_x, R_y, R_z belong to F_g . The transition to the doubly degenerate state which belongs to the representation E_g still remains forbidden.

Fox and Hexter [23] calculated the energies and intensities of the transitions between exciton states in cubic crystals. Their calculations are applicable to molecular crystals having cubic symmetry, four molecules in the unit cell and site symmetry C_3 at least, provided that the molecular transition is dipole allowed. The problem is treated in the approximation of dipole-dipole interaction and for the case $\mathbf{k} = 0$. These calculations are valid for the case $a \ll D \ll \lambda$, where a is the unit cell parameter, D the sample dimension and λ the wavelength of the exciting radiation. We shall here refer to their solution for the case of spherical samples.

In the approximation of dipole-dipole interaction the result of the energy calculation is as follows:

$$\left. \begin{aligned} \Delta E &= \Delta\omega^r + D - A \pm 2|J|, \\ A \pm 2|J| &= 2/3 p^2 h_1 a^{-3} (1 \pm \sqrt{7}), \end{aligned} \right\} \quad (2)$$

where

$$J = \sum_q \langle \phi_p^\alpha \phi_q^0 | V_{pq} | \phi_p^0 \phi_q^\beta \rangle,$$

$$A = \sum_q \langle \phi_p^\alpha \phi_q^0 | V_{pq} | \phi_p^0 \phi_q^\alpha \rangle = \sum_q \langle \phi_p^\beta \phi_q^0 | V_{pq} | \phi_p^0 \phi_q^\beta \rangle,$$

$$D = \sum_l \langle \phi_k^r \phi_l^0 | V_{kl} | \phi_k^r \phi_l^0 \rangle - \langle \phi_k^0 \phi_l^0 | V_{kl} | \phi_k^0 \phi_l^0 \rangle.$$

ϕ_p, ϕ_q are the molecular functions of different molecular sites; α, β designate the two degenerate molecular states.

The magnitude of the Davydov electronic splitting is then given by:

$$\Delta E_{\text{split}} = 4\sqrt{7/3} p^2 h_1 a^{-3} \quad (3)$$

and accordingly the splitting of a vibronic band is given by

$$\Delta E_{\text{split}}^{v'v''} = \Delta E_{\text{split}} q_{v'v''} \quad (4)$$

where $q_{v'v''}$ is the appropriate Franck-Condon overlap factor. Here h_1 is the lattice sum structure parameter [24], p is the transition dipole of the free molecule which can be estimated if the oscillator strength of the molecular transition is known.

The f -number for the transition $A^1\Pi \leftarrow X^1\Sigma^+$ in CO has recently been measured [25]. It was found to have the value 0.08. Using this value and the Franck-Condon factor values measured by the same authors for the first three bands and the theoretical value [16] for the fourth and fifth bands, the values for the splitting energies were calculated. These are given in table 5 where they are compared to the experimental results.

v'	$q_{v'v''}$	$\Delta\nu$ (cm ⁻¹) calc. (first order)	$\Delta\nu$ (cm ⁻¹) calc. (second order included)	$\Delta\nu$ (cm ⁻¹) expt.
0	0.11	130	160	460 ± 50
1	0.25	280	320	570 ± 50
2	0.25	270	265	480 ± 50
3	0.18	180	160	380 ± 50
4	0.11	115	90	

Table 5. Calculated and experimental band splittings of the $A^1\Pi \leftarrow X^1\Sigma^+$ transition in CO.

These calculations were carried out to second order [26], i.e. including mixing between the vibronic states of the excited electronic state $^1\Pi$ in the crystal field in the dipole-dipole approximation. It is clear from table 5 that the dipole approximation is inadequate and accounts for about one-half of the observed splitting. Therefore a complete monopole calculation using good molecular wave-functions of the type carried out recently for anthracene [27] is indicated.

The intensity ratio of the two F states (see eqn. 3) is predicted by the dipole theory to be 1.47 for spherical particles. This value is independent of h_1 and is the same for all the bands of the progression in the first order approximation. The experimental ratio measured in this work was 1.5 ± 0.2 , in satisfactory agreement with the theory.

Fox and Hexter [23] predict that the band structure will be affected by the shape of the crystallites. No change of the spectrum was observed here when the conditions of sample preparation were varied.

Only the last bands of the $d \leftarrow X$ transition in CO could be identified. As expected, this transition is not intensified in the solid.

It is well known that a considerable extent of disorder persists in the CO crystal at low temperature and this is ascribed to the arbitrary sense of the C-O axis [28]. This disorder may be expected to contribute to the line widths of the absorption spectrum. It would not affect the splitting terms in the dipole approximation but would affect the shift through the D^r term.

The theoretical scheme of Fox and Hexter was here applied to the forbidden transition $a^1\Pi_g \leftarrow X^1\Sigma_g^+$ in N_2 . As already described this transition is allowed both by an electric quadrupole and by a magnetic dipole mechanism. The two molecular functions α and β of the Π_g state were chosen so as to transform like xz and yz respectively (x, y, z are the molecular axes, z being the figure axis). These terms belong to the Π_g representation in the point group $D_{\infty h}$ and quadrupole transitions to these states will accordingly be permitted by the corresponding quadrupole moment elements.

The intermolecular potential was taken to be that of a quadrupole-quadrupole interaction, this being the lowest non-vanishing term in the expansion of the potential in a multipole-multipole series when the molecular transition dipole is forbidden. In this approximation the Hamiltonian matrix elements are sums of interactions between the transition quadrupole moment components (xz), (yz) of one molecule and those of all molecules of a single sublattice. The eight one-site exciton functions built from the molecular α and β -states form the basis from which the Hamiltonian matrix is constructed.

The molecular interaction potential is given by:

$$V_{12}(1) = \frac{1}{r_{12}} = f(x_1' y_1' z_1', x_2'' y_2'' z_2''), \quad (5)$$

where 1 and 2 designate the two interacting molecules, primes and double primes denote coordinate systems with orientations characteristic of those molecules. Only the terms $(x_1' z_1')(x_2'' z_2'')$; $(y_1' z_1')(y_2'' z_2'')$; $(x_1' z_1')(y_2'' z_2'')$; $(y_1' z_1')(x_2'' z_2'')$ of the expanded potential are required, since other terms do not contribute.

The Hamiltonian matrix elements have the form:

$$H_{ij}^{\alpha, \beta} = \sum_{r_{iq}}' F_{ip, jq}^{\alpha, \beta}(\mathbf{r}_{jq}) q_{ip}^{\alpha} q_{jq}^{\beta}. \quad (6)$$

Here in any matrix element the i th molecule of some arbitrary unit cell p is taken as the origin and the sum is over all molecules in the j th sub-lattice. Here \mathbf{r}_{jq} is the position vector of the molecule at the j th site of the q th unit. The prime on the summation indicates that the origin molecule is to be excluded from the summation. The symbol q_{ip}^{α} represents the transition quadrupole moment to the α th molecular state of the i th site and the p th unit cell. The $F(\mathbf{r})$ depend on the lattice structure and are derived from differential coefficients in the expansion (5) of $1/r$.

The Hamiltonian matrix elements were calculated as the sums of nearest-neighbour interactions. As the next-to-nearest neighbour molecules contributed only about 1 per cent to the energy, more distant molecules were not included.

In order to diagonalize the Hamiltonian matrix, combinations between one site exciton functions, derived from the xz and yz molecular states respectively, were chosen so as to give resultant functions which transform like XZ, YZ, XY respectively, where these six functions belong to the representation F_g . Two additional functions of the type $(X^2 - Y^2)$ and $(X^2 + Y^2 - 2Z^2)$ belong to the representation E_g . The molecular quadrupole transition moment components xz, yz were analogously transformed to crystal quadrupole moment terms. These transformations are of the form:

$$m_{ff'} = \sum_{FF'} m_{FF'} \Phi_{fF} \Phi_{f'F'}, \quad (7)$$

where ff' are molecular axes, FF' are crystal axes and $\Phi_{fF} \Phi_{f'F'}$ are the direction cosines between the two axis systems.

The secular determinant is then factored into three 2×2 determinants which are identical and belong to the F_g representation and a fourth already diagonalized two-dimensional problem which belongs to the E_g representation. The E_g problem is not of interest here.

The roots of the F_g problem are calculated to be:

$$\Delta E = \Delta\omega^r + D - \frac{830 \pm 1720}{2} \frac{q^2}{4a^5}. \quad (8)$$

Accordingly the splitting energy is given by:

$$\Delta E_{\text{split}} = \frac{1720q^2}{4a^5}, \quad (9)$$

where $q = q_{xz} = q_{yz}$ is the molecular transition quadrupole. The value of the molecular transition quadrupole can be calculated if functions of the ground and excited states of the molecule are known. The value of q can also be evaluated from the oscillator strength of the transition. Alternatively if the splitting energy is attributed to quadrupole terms only, the quadrupole transition moment can be evaluated from the experimental splitting energy and an oscillator strength can be evaluated from it. Mulliken and Wilkinson [9] have shown that the contribution of the electric quadrupole transition probability is 0.13 of the total for the $a \leftarrow X$ electronic band system. The relation between the molecular transition quadrupoles q_{xz}, q_{yz} and the oscillator strength f is given by [29]:

$$q^2 = \langle m | xz | n \rangle^2 = \langle m | yz | n \rangle^2 = \frac{5}{16} \frac{e^2 h^0 \cdot 13 f}{\pi^4 m_e \bar{\nu}_{mn}^3 c} \quad (10)$$

where $\bar{\nu}_{mn}$ is the frequency in cm^{-1} , m_e the mass of the electron. Substitution in (9) gives the splitting energy:

$$\Delta E_{\text{split}} (\text{cm}^{-1}) = \frac{5}{64} \frac{1720}{a^5} \frac{e^2 h^0 \cdot 13 f}{\pi^4 m_e \bar{\nu}_{mn}^3 c} \left(\frac{1}{hc} \right). \quad (11)$$

The experimental splitting energy of the band (3, 0) is 170 cm^{-1} and the Franck-Condon overlap factor [19] has a value of 0.19. From these values we get the oscillator strength: $f_{N_2}(a \leftarrow X) = 10^{-5}$. As the oscillator strength in the analogous but dipole-allowed transition of CO is estimated to be about 0.16, the intensity of the transition in N₂ is expected to be 6×10^{-5} times that in CO. The observed intensity ratio is about 10^{-4} , in satisfactory agreement with the prediction.

The intensity ratio for the transition to the two F_g states which we get according to this calculation is 5/1 whereas the experimental value is close to unity. The transition is not intensified in the solid since the high crystal symmetry does not allow interaction of the excited g state with states to which the electronic transition is dipole allowed. However, mixing with higher electronic g states is possible and is assumed to be responsible for the above lack of agreement between theory and experiment.

The transition $w^1\Delta_u \leftarrow X^1\Sigma_g^+$ in N_2 is intensified in the solid by a factor of 10^2 since it becomes dipole allowed in the crystal symmetry; the reducible representation of the four molecules in the unit cell in the excited Δ_u state reduces to $2F_u + E_u$ in the factor group T_h (in the same way as the representation of the Π_u state). The intensification of this transition in the solid is due to mixing of the exciton wave functions which belong to F_u with other exciton wave functions which belong to the same irreducible representation and are derived from molecular $^1\Sigma_u^+$ or $^1\Pi_u$ states to which dipole transitions are allowed. In the region 1000–800 Å there are many molecular absorption systems [30] which are intense and the upper states of which are of symmetries $^1\Sigma_u^+$ or $^1\Pi_u$. Quantitative treatment of this mixing may be formulated in terms of an interaction between the transition dipole of the perturbing $^1\Sigma_u^+$ or $^1\Pi_u$ state with the transition octupole of the Δ_u state; the direct product of $\Pi_g \times \Pi_u$ reduces to $\Sigma_u^+ + \Sigma_u^- + \Delta_u$ in $D_{\infty h}$. As expected, the bands of this transition are split due to interaction between two different F_u states in the same way as already described for the $^1\Pi_g \leftarrow ^1\Sigma_g^+$ transition in N_2 and for $^1\Pi \leftarrow ^1\Sigma^+$ in CO. As described in a previous section the bands are in fact observed to be split into two components of very different widths.

It was assumed here that the annealed N_2 deposit crystallized in the α -form which is the stable form of solid N_2 below 36.5°K, whereas the β -form is stable between 35.6°K and 63.1°K. The structure [31] of the β -form is such that the molecular centres form an hexagonal close-packed lattice. The space group is $P6_3/mmc$ (D_{6h}^4) and there are two parallel molecules in the primitive unit cell. In this case the four-fold representation of the 2 molecules in the unit cell in the Π_g molecular state reduces to $2E_{1g}$ (the factor group being D_{6h}). The quadrupole transition to one of the two degenerate states is forbidden and therefore no splitting should be observed. The results obtained confirm, therefore, the assumption that the sample was in the α -form.

REFERENCES

- [1] HOPFIELD, J. J., and BIRGE, R. T., 1927, *Phys. Rev.*, **29**, 922.
- [2] WATANABE, K., ZELIKOFF, MURRAY, and INN, EDWARD C. Y., 1953, "Absorption Coefficients of Several Atmospheric Gases", Geographical Research Papers No. 21.
- [3] HERZBERG, G., and HUGO, T. J., 1955, *Canad. J. Phys.*, **33**, 757.
- [4] TANAKA, Y., JURSA, A. S., and LEBLANC, F., 1957, *J. chem. Phys.*, **26**, 862.
- [5] BIRGE, R. T., and HOPFIELD, J. J., 1928, *Astrophys. J.*, **68**, 257.
- [6] TANAKA, Y., 1955, *J. opt. Soc. Amer.*, **45**, 663.
- [7] TANAKA, Y., OGAWA, M., and JURSA, R. S., 1964, *J. chem. Phys.*, **40**, 3690.
- [8] WILKINSON, P. G., 1957, *Astrophys. J.*, **126**, 1.
- [9] WILKINSON, P. G., and MULLIKEN, R. S., 1957, *Astrophys. J.*, **126**, 10.
- [10] WILKINSON, P. G., and MULLIKEN, R. S., 1959, *J. chem. Phys.*, **31**, 678.
- [11] DRESSLER, K., 1962, *J. Quant. Spectrosc. Radiat. Transfer*, **2**, 683.
- [12] SCHNEPP, O., 1963, *Annu. Rev. phys. Chem.*, **14**, 35.
- [13] SCHNEPP, O., and DRESSLER, K., 1960, *J. chem. Phys.*, **33**, 49.
- [14] SAVITSKY, G., and HORNIG, D. F., 1962, *J. chem. Phys.*, **36**, 2634.

- [15] TANAKA, Y., 1955, *J. opt. Soc. Amer.*, **45**, 710.
- [16] JARMAIN, W. R., EBISVAKI, R., and NICHOLLS, R. W., 1960, *Canad. J. Phys.*, **38**, 510.
- [17] SILVERMAN, S. M., and LASSETTRE, E. N., 1961, *J. chem. Phys.*, **41**, 3727.
- [18] CARROLL, P. K., 1962, *J. chem. Phys.*, **36**, 2861.
- [19] JARMAIN, W. R., FRASER, P. A., and NICHOLLS, R. W., 1955, *Astrophys. J.*, **122**, 55.
- [20] SIMPSON, W. T., and PETERSON, D. L., 1957, *J. chem. Phys.*, **26**, 588. WITKOWSKI, A., and MOFFITT, W., 1960, *J. chem. Phys.*, **33**, 872.
- [21] JORDAN, H., SMITH, H., WARREN, STREIB, W. E., and LIPSCOMB, W. N., 1964, *J. chem. Phys.*, **41**, 756.
- [22] LANDOLT-BÖRSTEIN, *Atom und Molekular Physik*, 4 Teil Kristalle (Berlin, Göttingen, Heidelberg : Springer-Verlag).
- [23] FOX, D., and HEXTER, R. M., 1964, *J. chem. Phys.*, **41**, 1125.
- [24] LUTTINGER, J. M., and TISZA, L., 1946, *Phys. Rev.*, **70**, 954.
- [25] HESSER, J. E., and DRESSLER, K., unpublished
- [26] CRAIG, D. P., 1955, *J. chem. Soc.*, p. 2302.
- [27] SILBEY, R., JORTNER, J., and RICE, S. A., 1965, *J. chem. Phys.* **42**, 1515.
- [28] CLAYTON, J. O., and GIAUQUE, W. F., 1932, *J. Amer. chem. Soc.*, **54**, 2610.
- [29] BOHM, D., 1951, *Quantum Theory* (New York: Prentice Hall Inc.), p. 426;
KAUTZMANN, W., 1957, *Quantum Theory* (New York: Academic Press Inc.), p. 654.
- [30] WORLEY, R. F., 1943, *Phys. Rev.*, **64**, 207.
- [31] STREIB, W. E., JORDAN, T. H., and LIPSCOMB, W. N., 1962, *J. chem. Phys.*, **37**, 2962.

RESEARCH NOTES

Long-range interaction of two 1s-hydrogen atoms expressed in terms of natural spin-orbitals†

by J. O. HIRSCHFELDER

University of Wisconsin Theoretical Chemistry Institute, Madison,
Wisconsin

and P. O. LÖWDIN

Quantum Chemistry Group, University of Uppsala, Uppsala, Sweden

(Received 5 May 1965)

A numerical error in the calculation of B_8/R^8 was discovered. The corrected result agrees with the old Pauling and Beach value and recent calculations by Chan and Dalgarno and by Bell.

In our paper [1], there is a trivial mistake in equations (60) and (61) which has the unfortunate effect of changing most of the numerical values in §5, the *Calculation of the Inverse Eighth Power Dispersion Energy*, $-B_8R^8$. Equations (60) and (61) should read:

If $n=n''$ and $n'=n'''$,

$$\int \Omega_{n1; n'2}^* \mathcal{H} \Omega_{n1; n'2} d\tau = \frac{2}{5}(n-2) + \frac{2}{7}(n' - \frac{29}{12}). \quad (60)$$

If $n=n''$ but $n' \neq n'''$,

$$\begin{aligned} \int \Omega_{n1; n'2}^* \mathcal{H} \Omega_{n1; n''2} d\tau &= \left(\frac{\epsilon_{n'2}}{\epsilon_{n''2}} \right) \left(\frac{2n'}{7} - \frac{4}{21} \right), \quad n''' > n' \\ &= \left(\frac{\epsilon_{n''2}}{\epsilon_{n'2}} \right) \left(\frac{2n''}{7} - \frac{4}{21} \right), \quad n''' < n'. \end{aligned} \quad (61)$$

The corrected tables 6, 7, 8, 9 and 10 are given.

From the corrected table 8 it appears that the calculations including twelve configurations now give the result:

$$B_8 = 124.395,$$

which now agrees with the value of $B_8 = 124.399$ obtained by Pauling and Beach [2] and the recent results of 124.4 and 124.40 obtained by Chan and Dalgarno [3] and by Bell [4] respectively. Using our best values of B_6 and B_8 , we calculate the energy of the system of two hydrogen atoms to be:

$$E = -1 - 6.499026/R^6 - 124.395/R^8. \quad (120)$$

† Most of this work was carried out at Uppsala University and was supported by the Aeronautical Research Laboratory, Wright Air Development Center of the Air Research and Development Command through its European Office under a contract with Uppsala University. A small part of this work was supported by the United States Air Force under Contract AF33(616)-3414 with the University of Wisconsin, monitored by Aeronautical Research Laboratory, Wright Development Center.

	$\overline{2p} \ \overline{3d}$	$\overline{3p} \ \overline{3d}$	$\overline{2p} \ \overline{4d}$	$\overline{3p} \ \overline{4d}$	$\overline{4p} \ \overline{4d}$	$\overline{2p} \ \overline{5d}$	$\overline{3p} \ \overline{5d}$	$\overline{4p} \ \overline{5d}$	$\overline{5p} \ \overline{5d}$	$\overline{4p} \ \overline{3d}$	$\overline{5p} \ \overline{3d}$	$\overline{5p} \ \overline{4d}$
$\overline{2p} \ \overline{3d}$	0.166667	0.223607	0.251976	0	0	0.125988	0	0	0	0.129099	0.084515	0
$\overline{3p} \ \overline{3d}$	0.223607	0.566667	0	0.251976	0	0	0.125988	0	0	0.519615	0.340168	0
$\overline{2p} \ \overline{4d}$	0.251976	0	0.452381	0.223607	0.129099	0.476190	0	0	0	0	0	0.084515
$\overline{3p} \ \overline{4d}$	0	0.251976	0.223607	0.852381	0.519615	0	0.476190	0	0	0	0	0.340168
$\overline{4p} \ \overline{4d}$	0	0	0.129099	0.519615	1.252381	0	0	0.476190	0	0.251976	0	0.851050
$\overline{2p} \ \overline{5d}$	0.125988	0	0.476190	0	0	0.738095	0.223607	0.129099	0.084515	0	0	0
$\overline{3p} \ \overline{5d}$	0	0.125988	0	0.476190	0	0.223607	1.138095	0.519615	0.340168	0	0	0
$\overline{4p} \ \overline{5d}$	0	0	0	0	0.476190	0.129099	0.519615	1.538095	0.851050	0.125988	0	0
$\overline{5p} \ \overline{5d}$	0	0	0	0	0	0.084515	0.340168	0.851050	1.938095	0	0.125988	0.476190
$\overline{4p} \ \overline{3d}$	0.129099	0.519615	0	0	0.251976	0	0	0.125988	0	0.966667	0.851050	0
$\overline{5p} \ \overline{3d}$	0.084515	0.340168	0	0	0	0	0	0	0.125988	0.851050	1.366667	0.251976
$\overline{5p} \ \overline{4d}$	0	0	0.084515	0.340168	0.851050	0	0	0	0.476190	0	0.251976	1.652381

Table 6. The relevant part of the energy matrix \mathbf{H} of order twelve used in calculating B_8 .

	$\overline{2p} \overline{3d}$	$\overline{3p} \overline{3d}$	$\overline{2p} \overline{4d}$	$\overline{3p} \overline{4d}$	$\overline{4p} \overline{4d}$	$\overline{2p} \overline{5d}$	$\overline{3p} \overline{5d}$	$\overline{4p} \overline{5d}$	$\overline{5p} \overline{5d}$	$\overline{4p} \overline{3d}$	$\overline{5p} \overline{3d}$	$\overline{5p} \overline{4d}$
$\overline{2p} \overline{3d}$	0.921445	-0.127844	-0.157705	0.034980	0.003520	-0.023940	0.001877	0.001284	0.000360	-0.024813	-0.005613	-0.000122
$\overline{3p} \overline{3d}$	-0.127844	0.743355	0.034980	-0.112354	0.041512	0.001877	-0.020375	0.004317	0.002201	-0.176628	-0.039233	0.003307
$\overline{2p} \overline{4d}$	-0.157705	0.034980	0.804889	-0.105884	-0.021362	-0.215014	0.042501	0.005933	0.000406	0.003520	-0.000122	-0.005274
$\overline{3p} \overline{4d}$	0.034980	-0.112354	-0.105884	0.656553	-0.148198	0.042501	-0.158201	0.053597	0.007077	0.041512	0.003307	-0.034863
$\overline{4p} \overline{4d}$	0.003520	0.041512	-0.021362	-0.148198	0.589171	0.005933	0.053597	-0.137584	0.061467	-0.097501	0.045362	-0.184700
$\overline{2p} \overline{5d}$	-0.023940	0.001877	-0.215014	0.042501	0.005933	0.646823	-0.072122	-0.017551	-0.005254	0.001284	0.000360	0.000406
$\overline{3p} \overline{5d}$	0.001877	-0.020375	0.042501	-0.158201	0.053597	-0.072122	0.542687	-0.107341	-0.030906	0.004317	0.002201	0.007077
$\overline{4p} \overline{5d}$	0.001284	0.004317	0.005933	0.053597	-0.137584	-0.017551	-0.107341	0.490284	-0.139330	-0.017877	0.006635	0.061467
$\overline{5p} \overline{5d}$	0.000360	0.002201	0.000406	0.007077	0.061467	-0.005254	-0.030906	-0.139330	0.399817	0.006635	-0.014304	-0.091064
$\overline{4p} \overline{3d}$	-0.024813	-0.176628	0.003520	0.041512	-0.097501	0.001284	0.004317	-0.017877	0.006635	0.664719	-0.217942	0.045362
$\overline{5p} \overline{3d}$	-0.005613	-0.039233	-0.000122	0.003307	0.045362	0.000360	0.002201	0.006635	-0.014304	-0.217942	0.514028	-0.061240
$\overline{5p} \overline{4d}$	-0.000122	0.003307	-0.005274	-0.034863	-0.184700	0.000406	0.007077	0.061467	-0.091064	0.045362	-0.061240	0.463089

Table 7. The matrix $\mathbf{T} = (\mathbf{H}_{22}^{(0)} + \mathbf{1})^{-1}$ of order twelve used in calculating B_8 . This matrix was found by successive inversions.

Here the energy is in units of e^2/a_0 and length is in units of a_0 . From table 10 it is easy to express the wavefunction in terms of the natural spin orbitals. Thus, the corrections to $\Psi_2(a1, b2)$ of equations (114) to (119) are obvious with the exception that the corrected value of N should be

$$N = 1 - 3.699363/R^6 - 60.25968/R^8. \quad (115)$$

The energy calculated with the wave function of equation (114), using only two sets of natural orbitals, agrees almost perfectly with equation (120). In a similar manner, the corrections to $\Psi_1(a1, b2)$ of equation (122) are obvious with the exception that the coefficient of $\psi_{100}(a1) \psi_{100}(b2)$ should be

$$1 - 3.698772/R^6 - 60.23270/R^8.$$

In this case the energy is

$$E(\text{one natural orbital}) = -1 - 6.497066/R^6 - 124.3022/R^8.$$

Other misprints and errata in this paper are

- p. 231 Equation (10). There is broken type; r_{b2} should be raised to the l th power.
- p. 233 Equation (30). Type has fallen out; should read $\Theta_{k,l}$.
- p. 253 Equation (137). The $(2/n)$ should be raised to the $l+2$ power instead of the $l-2$.
- p. 254 Equation (144). The number should be 7242 instead of 724.2. As a result, each of the entries in table 12 should be multiplied by $1.7783 = 10^{1/4}$.
- p. 256 Equation (A11). The superscripts on I should be $(2l+1)$, $(2l+2)$, $(2l+3)$.

Number of configurations considered	Last configuration in the sequence equation (58) considered	Value of B_8 obtained
1	$\overline{2p} \ \overline{3d}$	115.7143
2	$\overline{3p} \ \overline{3d}$	118.9687
3	$\overline{2p} \ \overline{4d}$	123.7356
4	$\overline{3p} \ \overline{4d}$	124.0932
5	$\overline{4p} \ \overline{4d}$	124.0933
6	$\overline{2p} \ \overline{5d}$	124.2107
7	$\overline{3p} \ \overline{5d}$	124.2121
8	$\overline{4p} \ \overline{5d}$	124.2123
9	$\overline{5p} \ \overline{5d}$	124.2123
10	$\overline{4p} \ \overline{3d}$	124.3866
11	$\overline{5p} \ \overline{3d}$	124.3950
12	$\overline{5p} \ \overline{4d}$	124.3950

Table 8.

$i \backslash j$		1	2	3	4	5	6	7
	1	$\overline{2p}$	$\overline{3p}$	$\overline{4p}$	$\overline{5p}$	$\overline{3d}$	$\overline{4d}$	$\overline{5d}$
	1	0	0	0	0	-3.385604	0.579447	0.087959
	2	0	0	0	0	0.469729	-0.128525	-0.006896
	3	0	0	0	0	0.091170	-0.012933	-0.004718
	4	0	0	0	0	0.020625	0.000447	-0.001322
	5	-3.385604	0.469729	0.091170	0.020625	0	0	0
	6	0.579447	-0.128525	-0.012933	0.000447	0	0	0
	7	0.087959	-0.006896	-0.004718	-0.001322	0	0	0

Table 9. Matrix of coefficients $C_{il;j1}^{(4)}$. Here $C_{i1;j1}^{(4)} = C_{i-1;j-1}^{(4)} = 3 \cdot 1/2 C_{i0;j0}^{(4)}$. The notation is explained in the text.

Root, n	1	2	3	4
γ_{n1}	-1.110371	-0.014029	-0.000541	-0.000059
$\alpha_{1n}^0(1)$	0.987527	0.151308	0.041400	0.014000
$\alpha_{2n}^0(1)$	-0.155451	0.979596	0.103400	0.074000
$\alpha_{3n}^0(1)$	-0.024599	-0.100704	0.989300	-0.103000
$\alpha_{4n}^0(1)$	-0.004444	-0.085769	0.094400	0.991000
$R\alpha_{5n}(1)$	3.078907	4.496008	-1.011930	26.943136
$R\alpha_{6n}(1)$	-0.533619	2.634795	3.794453	-6.381085
$R\alpha_{7n}(1)$	-0.079303	-0.509096	3.445209	1.746203
$G_{nn}(1)/\gamma_{n1}^2$	9.770709	27.415409	27.291343	769.700024

Table 10. Constants for natural orbitals having $m=1$. All the constants are the same for $m=-1$.

REFERENCES

- [1] HIRSCHFELDER, J. O., and LÖWDIN, P. O., 1959, *Mol. Phys.*, **2**, 229.
- [2] PAULING, L., and BEACH, J. Y., 1935, *Phys. Rev.*, **47**, 686.
- [3] CHAN, Y. M., and DALGARNO, A., 1965, *Mol. Phys.*, **9**, 349.
- [4] BELL, R. J., 1965, *Proc. phys. Soc., Lond.*, **86**, 239,

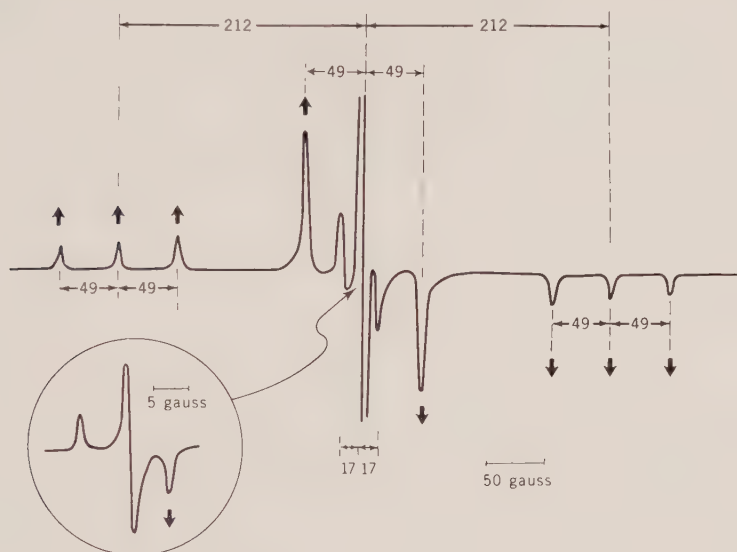
Electron spin resonance spectrum of the NF_2 radical isolated in a neon matrix at 4°K

by PAUL H. KASAI and EARL B. WHIPPLE

Union Carbide Research Institute, Tarrytown, New York

(Received 9 June 1965)

Although several electron spin resonance studies of the NF_2 radical have been reported [1-5], no unambiguous assignment of the spectrum has been made which includes the anisotropic parts of the hyperfine interactions with both nitrogen and fluorine nuclei. Since the recent discovery [6] of preferential



E.S.R. spectrum of NF_2 radical isolated in Ne matrix at 4°K . The magnetic field increases from left to right and the sharp peak at the centre of the spectrum is shown inside the circle on an expanded field scale with reduced gain. The microwave frequency was 9.43 kMc.

orientation of radicals trapped in neon matrices makes it possible to assign macroscopically observed principal tensor components to molecular axes, a re-study of the NF_2 spectrum using matrix isolation techniques was undertaken. A spectrum of randomly oriented NF_2 in neon at 4°K is shown in the figure. The overall pattern has the characteristic asymmetry expected for a system with severe hyperfine anisotropy, and can be interpreted in terms of the following parameters:

$$\left. \begin{aligned} A_x(\text{N}) &= 49 \pm 0.5 \text{ gauss}, \\ A_y(\text{N}) &= A_z(\text{N}) = 0 \pm 1.0 \text{ gauss}, \\ A_x(\text{F}) &= 212 \pm 2.0 \text{ gauss}, \\ A_y(\text{F}) &= A_z(\text{F}) = -16.9 \pm 1.0 \text{ gauss}. \end{aligned} \right\} \quad (1)$$

$A_x(\text{N})$, for example, indicates the x -component of the hyperfine interaction with the nitrogen nucleus. The actual orientation of these axes relative to the

molecular structure will be elaborated later. The sharp line at the centre of the spectrum is due mostly to transitions in which the two fluorine nuclei are in the anti-parallel spin state and the nitrogen nucleus is in the $m_I = 0$ state. At higher resolution this line shows two asymmetric side peaks (see figure) indicative of an orthorhombic g -tensor. The one at the higher field is at the centre of the spacings due to $A_x(\text{N})$ and $A_x(\text{F})$ mentioned above. The corresponding g -values are:

$$\left. \begin{aligned} g_x &= 2.0011 \pm 0.0005, \\ g_y &= 2.0079 \pm 0.0005 \\ g_z &= 2.0042 \pm 0.0005. \end{aligned} \right\} \quad (2)$$

and

The design of the cryostat used is essentially that of Jen *et al.* [7], but with one important modification. The sapphire rod upon which the matrix is formed has a flat spatula shape and can be rotated about its vertical axis. It has been found that with this geometry a molecule with a well-defined plane exhibits a strong tendency to orient its plane parallel to the plane of the rod within the matrix [6]. Oriented samples could be prepared by pre-heating the NF_2 to about 300° before deposition, and in their spectra all components identified with the x -axis (marked with arrows in the figure) became stronger at the expense of the remaining lines when the magnetic field was applied perpendicular to the plane of the rod, and vice-versa. On this basis, the x -axis could be fixed perpendicular to the molecular plane.

The NF_2 ground state is expected to be $^2\text{B}_1$ with the unpaired electron in an anti-bonding π orbital:

$$\Phi_0 = \alpha \phi_{px}(\text{N}) - \frac{\beta}{2} [\phi_{px}(\text{F}_1) + \phi_{px}(\text{F}_2)], \quad (3)$$

where ϕ_{px} represents the p_x valence orbital of the respective atom. The lowest excited state would probably be $^2\text{A}_1$ with the unpaired electron in the non-bonding nitrogen orbital directed away from the fluorine atoms along the C_{2v} axis. Since g_y shows the largest deviation from the free-spin value, the y -axis must be identified with the direction perpendicular to the x and the C_{2v} axes of the molecule. The hyperfine interactions are made up of isotropic and 'dipolar' parts of the forms:

$$\left. \begin{aligned} A_x(\text{N}) &\cong A_{\text{iso}}(\text{N}) + 2A_{\text{dip}}(\text{N}) \\ A_y(\text{N}) &\cong A_z(\text{N}) \cong A_{\text{iso}}(\text{N}) - A_{\text{dip}}(\text{N}), \\ A_{\text{iso}}(\text{N}) &= g_{n,\text{N}} \beta_n \frac{8\pi}{3} |\Phi_0(0)_{\text{N}}|^2 \\ A_{\text{dip}}(\text{N}) &= g_{n,\text{N}} \beta_n \frac{2}{5} \alpha^2 \left\langle \frac{1}{r^3} \right\rangle_{\text{N}, 2p}. \end{aligned} \right\} \quad (4)$$

and

Here, $\Phi_0(0)_{\text{N}}$ stands for the value of Φ_0 at the nitrogen nucleus, and $\langle 1/r^3 \rangle_{\text{N}, 2p}$ stands for $\langle 1/r^3 \rangle$ of the nitrogen $2p$ atomic function. Similar expressions should also hold for the hyperfine interaction with the fluorine nuclei. Substituting the values given in (1) into these equations, one obtains:

$$\left. \begin{aligned} A_{\text{iso}}(\text{N}) &= 16 \pm 1 \text{ gauss}, \\ A_{\text{iso}}(\text{F}) &= 59 \pm 1 \text{ gauss}, \\ A_{\text{dip}}(\text{N}) &= 16 \pm 1 \text{ gauss} \\ A_{\text{dip}}(\text{F}) &= 76 \pm 1 \text{ gauss}. \end{aligned} \right\} \quad (5)$$

and

The value obtained above for the isotropic part are in excellent agreement with the values reported by Farmer *et al.* [4], 17 ± 2 gauss and 60 ± 2 gauss for the nitrogen and the fluorine nuclei, respectively. Also, from $\langle 1/r^3 \rangle$ averages computed from spectroscopic data [8] one can estimate:

$$g_{n,N} \beta_n^{\frac{2}{5}} \left\langle \frac{1}{r^3} \right\rangle_{N, 2p} \cong 15 \text{ gauss}$$

and

$$g_{n,F} \beta_n^{\frac{2}{5}} \left\langle \frac{1}{r^3} \right\rangle_{F, 2p} \cong 500 \text{ gauss.}$$

One therefore obtains $\alpha^2 \cong 1$ and $\beta^2 \cong 0.3$ for Φ_0 as given in equation (3). Because of the nature of approximations involved in equation (4) and in the estimate of $\langle 1/r^3 \rangle$, these values should not be taken too literally. They are consistent, however, with the picture that the unpaired electron is in the anti-bonding π orbital of equation (3). For this function the values of $|\Phi_0(0)_N|^2$ and $|\Phi_0(0)_F|^2$ are both zero, and there should not be any isotropic parts to the hyperfine interactions. The values of $|\Phi_0(0)_N|^2$ and $|\Phi_0(0)_F|^2$ inferred from the observed isotropic parts are indeed very small, being about equal, respectively, to the $|\phi(0)_N|^2$ and to one-quarter of the $|\phi(0)_F|^2$ expected for $2p$ orbitals with exchange polarization of the core electrons [9]. More details will be published soon.

REFERENCES

- [1] PIETTE, L. H., JOHNSON, F. A., BOOMAN, K. A., and COLBURN, C. B., 1961, *J. chem. Phys.*, **35**, 1481.
- [2] ADRIAN, F. J., COCHRAN, E. L., and BOWERS, V. A., 1962, *Advance in Chemistry Series*, **36**, 50.
- [3] DOORENBOS, H. E., and LOY, B. R., 1963, *J. chem. Phys.*, **39**, 2393.
- [4] FARMER, J. B., GERRY, M. C. L., and McDOWELL, C. A., 1964, *Mol. Phys.*, **8**, 253.
- [5] COLBURN, C. B., ETTINGER, R., and JOHNSON, F. A., 1964, *J. inorg. Chem.*, **3**, 455.
- [6] KASAI, P. H., WELTNER, W. Jr., and WHIPPLE, E. B., 1965, *J. chem. Phys.*, **42**, 1120.
- [7] JEN, C. K., FONER, S. N., COCHRAN, E. L., and BOWERS, V. A., 1958, *Phys. Rev.*, **112**, 1169.
- [8] BARNES, R. G., and SMITH, W. V., 1954, *Phys. Rev.*, **93**, 95.
- [9] GOODINGS, D. A., 1961, *Phys. Rev.*, **123**, 1706.

Dielectric constants of homogeneous mixtures

by H. LOOYENGA

Central Laboratory TNO, Delft

(Received 5 April 1965)

A new simple formula for the dielectric constants of homogeneous mixtures is derived. This formula contains expression $(\epsilon^{1/3} - 1)$ instead of the usual quantity $(\epsilon - 1)/(\epsilon + 2)$ (Clausius-Mosotti, Debye). Similarly, function $(n^{2/3} - 1)$ replaces $(n^2 - 1)/(n^2 + 2)$ in the Lorentz-Lorenz formula.

The application of the resulting modified definitions of molar refraction and of molar polarization is discussed on the basis of experimental data.

The determination of dipole moments of organic molecules can be improved by the use of this new formula. No additional parameters are needed, and calculations are as simple as in the usual Debye method.

1. INTRODUCTION

In a preceding paper [1], a simple formula was derived for the dielectric constant of a heterogeneous mixture:

$$\epsilon = [(\epsilon_2^{1/3} - \epsilon_1^{1/3})v_2 + \epsilon_1^{1/3}]^3, \quad (1)$$

where ϵ_1 and ϵ_2 are the dielectric constants of the components, and v_2 is the volume fraction of the second component. An alternative derivation, also fitted for complex dielectric constants, can be given in the following way.

The dielectric constant, ϵ , is a function of v_2 . We consider two mixtures, a and b , with volume fractions of the second component:

$$v_{2a} = v_2, \quad v_{2b} = v_2 + \Delta v_2. \quad (2)$$

We now add $\delta \text{ cm}^3$ of b to $(1 - \delta) \text{ cm}^3$ of a , δ being a small quantity. The resulting dielectric constant can be calculated with the equation of Bruggeman [1], or with the one of Böttcher [1]. When higher powers of δ are neglected, both equations lead to the same formula:

$$\epsilon = \epsilon_a + \frac{3\epsilon_a(\epsilon_b - \epsilon_a)}{2\epsilon_a + \epsilon_b} \delta. \quad (3)$$

The coefficient of δ in equation (3) is exact. The absence of higher powers of δ corresponds to neglecting the mutual interaction of spherical particles of dielectric constant ϵ_b in a medium of dielectric constant ϵ_a .

The volume fraction of the second pure component in the resulting mixture is given by:

$$(1 - \delta)v_2 + \delta(v_2 + \Delta v_2) = v_2 + \delta \cdot \Delta v_2. \quad (4)$$

Function $\epsilon(v_2 + \Delta v_2)$ can be expanded in Taylor's series:

$$\epsilon(v_2 + \Delta v_2) = \epsilon(v_2) + \Delta v_2 \epsilon'(v_2) + \frac{1}{2}(\Delta v_2)^2 \epsilon''(v_2). \quad (5)$$

Insertion of this expansion into equation (3) yields:

$$2[\epsilon'(v_2)]^2 = 3\epsilon(v_2) \cdot \epsilon''(v_2). \quad (6)$$

The solution of this differential equation with the proper boundary conditions is easily shown to be equation (1). Equation (1) has also been given by Landau and Lifshitz [2], but the present derivation (and also the derivation given in [1]) clearly shows the limitations of this formula. This does not involve the shapes of the particles, but corresponds to a certain lack of randomness in the mixture composed as described above [1]. In real homogeneous mixtures, however, there is always some lack of randomness, because a molecule of the first component has either a positive or a negative preference to molecules of its own kind.

On the other hand, equation (1) has the advantage that it does not contain the shapes or the dielectric inhomogeneities of the particles. For this reason, equation (1) can also be applied to homogeneous mixtures, which is the subject of this paper.

2. GENERAL CONSIDERATIONS

If we neglect, for the moment, volume changes in mixing pure liquids, equation (1) can be generalized to:

$$\epsilon^{1/3} = \sum_k \epsilon_k^{1/3} v_k.$$

Because $\sum_k v_k = 1$, this equation can also be written as:

$$\epsilon^{1/3} - 1 = \sum_k (\epsilon_k^{1/3} - 1) v_k. \quad (7)$$

Böttcher [3] has shown that the Debye equation:

$$\frac{\epsilon - 1}{\epsilon + 2} = \frac{4\pi}{3} \sum_k N_k \left(\alpha_k + \frac{\mu_k^2}{3kT} \right), \quad (8)$$

where N_k = the number of molecules k per cm^3 , α_k = the polarizability of a molecule and μ_k = its dipole moment, can be written in a form analogous to equation (7):

$$\frac{\epsilon - 1}{\epsilon + 2} = \sum_k \frac{\epsilon_k - 1}{\epsilon_k + 2} v_k. \quad (9)$$

It will now be shown that similarly equation (7) can be written as:

$$\epsilon^{1/3} - 1 = \frac{4\pi}{3} \sum_k N_k \left(\alpha_k + \frac{\mu_k^2}{3kT} \right). \quad (10)$$

We first note that for $\epsilon \approx 1$, as in the diluted gas phase, expressions $(\epsilon^{1/3} - 1)$ and $(\epsilon - 1)/(\epsilon + 2)$ are equivalent in first and second order:

$$\epsilon^{1/3} - 1 = \frac{1}{3}(\epsilon - 1) - \frac{1}{9}(\epsilon - 1)^2 + \frac{5}{81}(\epsilon - 1)^3 - \dots, \quad (11a)$$

$$(\epsilon - 1)/(\epsilon + 2) = \frac{1}{3}(\epsilon - 1) - \frac{1}{9}(\epsilon - 1)^2 + \frac{3}{81}(\epsilon - 1)^3 - \dots \quad (11b)$$

In order to arrive at a molecular interpretation, the easiest system to discuss is the diluted gas phase. In the limiting situation of infinite dilution, the polarizations of the individual molecules due to an external electric field are independent, and equations (8) and (10) hold exactly, because $\epsilon \gg 1$; see equations (11).

Equations (7) and (9) are both of the form:

$$f(\epsilon) = \sum_k f(\epsilon_k) v_k \quad \text{with} \quad f(1) = 0. \quad (12)$$

If such an equation is valid, we can fruitfully introduce a hypothetical process of dilution with vacuum. The ϵ_k corresponding to vacuum is 1 and its $f(\epsilon_k) = 0$. If a liquid is thus diluted with a large amount of vacuum to a hypothetical gas phase, the dielectric constant of this gas phase is given by :

$$f(\epsilon_{\text{gas}}) = (1 - v_{\text{vac}})f(\epsilon_{\text{liq}}),$$

where v_{vac} = the volume fraction of vacuum. On the other hand :

$$N_{k, \text{gas}} = (1 - v_{\text{vac}})N_{k, \text{liq}}$$

and :

$$f(\epsilon_{\text{gas}}) = \frac{4\pi}{3} \sum_k N_{k, \text{gas}} \left(\alpha_k + \frac{\mu_k^2}{3kT} \right)$$

Therefore :

$$f(\epsilon_{\text{liq}}) = \frac{4\pi}{3} \sum_k N_{k, \text{liq}} \left(\alpha_k + \frac{\mu_k^2}{3kT} \right). \quad (13)$$

Taking $f(\epsilon) = (\epsilon - 1)/(\epsilon + 2)$, formula (13) is in fact the Debye equation, cf. (8). But $f(\epsilon) = (\epsilon^{1/3} - 1)$ yields equation (10), which has to be preferred on the strength of previous arguments in this paper.

For the interpretation of gas phase measurements, equation (8) can be used as well as equation (10).

Sometimes, for example in the case of water, the extrapolation of gas phase measurements to the liquid phase with the aid of equation (8) leads to infinite or negative values of ϵ , the right hand side being ≥ 1 [4]. This does not occur if we use equation (10) instead of equation (8).

In this context a pure liquid is considered as a mixture of an arbitrary vacuum fraction and a corresponding compressed liquid. This assumption does not alter equation (8) and (10).

Therefore, equation (10) can also be applied to mixtures with volume contraction. In this process of mixing, some vacuum is lost.

In analogy with its usual definition, the molar polarization [5] is now defined on the basis of equation (10) as :

$$[P]_k = (\epsilon_k^{1/3} - 1) \frac{M_k}{d_k}, \quad (14)$$

where ϵ_k = the dielectric constant of pure component k , M_k is the molecular weight of this component, and d_k is its density. For a mixture, equation (10) can be transformed into† :

$$[P] \equiv (\epsilon^{1/3} - 1) \frac{\bar{M}}{d} = \sum_k x_k [P]_k \equiv [\bar{P}] \quad (15)$$

along the same lines, with the aid of Maxwell's relation $\epsilon = n^2$, the new definition of the molar refraction is :

$$[R]_k = (n_k^{2/3} - 1) \frac{M_k}{d_k}. \quad (16)$$

For a mixture we have :

$$[R] \equiv (n^{2/3} - 1) \frac{\bar{M}}{d} = \sum_k x_k [R]_k \equiv [\bar{R}]. \quad (17)$$

† In this paper, the mean value $\bar{\Omega}$ of a quantity Ω is defined as $\sum_k x_k \Omega_k$ with x_k = the molar fraction of component k .

For pure organic substances, the values of the molar refraction according to the new definition (equation (16)) are only about 4 per cent higher than those according to the usual definition by Lorentz-Lorenz [6] (for example compare table 2).

Even our new equations (15) and (17) cannot be expected to hold exactly for practical mixtures.

In the first place, equation (1) is not an exact formula, but it contains some approximations involving a certain lack of randomness in the mixtures. However, one need not expect that this approximation will introduce serious errors, because we can formally vary this lack of randomness. This can be done varying the assumed radii of the spherical particles with volume fraction $v_2 + \Delta v_2$ (compare equation (2)). Another variation can be illustrated with the following example: we can make a mixture with $v_2 = \frac{1}{2}$ by direct mixing of the pure components, but also by mixing equal parts of two mixtures with $v_2 = \frac{1}{4}$ and $v_2 = \frac{3}{4}$. Applying equation (1) to both ways, the same ultimate value of the dielectric constant is obtained.

In the second place, however, we must assume that, in mixing pure components, the states of the individual molecules remain unchanged. This will be approximately true for mixtures of organic components with weak van der Waals interactions. In the same way, $[R]_k$ is not entirely independent of temperature, because most organic liquids are in fact composed of a mixture of conformations. These equilibria are temperature-dependent.

In the next chapter, equations (10), (14), (15), (16) and (17) will be applied to a number of practical examples.

3. PRACTICAL APPLICATIONS

3.1. *The molar refraction*

A simple, but crucial, question in this field is the independence of the molar refraction for a pure substance of temperature. The usual Lorentz-Lorenz definition reads:

$$[R] = \frac{n^2 - 1}{n^2 + 2} \frac{M}{d} = \frac{4\pi}{3} N_A \alpha, \quad (18)$$

N_A is Avogadro's number and α is the molecular polarizability. Because α is supposed to be independent of temperature, $[R]$ should also be constant. In practice this is, however, not the case. It has been tried to improve formula (18) by replacing empirically function $(n^2 - 1)/(n^2 + 2)$ by another function of n [7]. Although some improvement was obtained, these equations are not very useful in view of lack of theoretical background.

In table 1, a number of molar refractions of hydrocarbons are collected. Clearly, the new definition according to equation (16) means a considerable improvement on formula (18).

It must, however, be noted that even the best formula of the type $[R] = f(n)M/d$ cannot give an exact independence of the physical conditions for all substances. In the first place, the polarizability, α , depends on the pressure. This even holds for noble gases, as Ten Seldam [9] has shown.

Table 1. Molar refractions. Calculated from data of the American Petroleum Research Project 44 [8]. $[R] = (n^2 - 1)M/d$.

Compound	$[R]_{20}$	$\Delta \times 10^3$	$\Delta_{L.L.} \times 10^3$
<i>n</i> -pentane	26.036	10	20
<i>n</i> -hexane	30.900	9	21
<i>n</i> -heptane	35.769	0	15
<i>n</i> -octane	40.637	2	17
<i>n</i> -nonane	45.517	— 3	13
<i>n</i> -decane	50.386	5	22
<i>n</i> -hexadecane	79.619	6	21
Cyclopentane	24.021	1	11
Methylcyclopentane	28.917	1	14
1,1-dimethylcyclopentane	33.773	0	12
1,cis-2-dimethylcyclopentane	33.630	6	19
1,trans-2-dimethylcyclopentane	33.789	5	19
1,cis-3-dimethylcyclopentane	33.810	— 3	12
1,trans-3-dimethylcyclopentane	33.851	2	14
Ethylcyclopentane	33.720	— 1	13
Cyclohexane	28.866	1	13
1-hexene	30.532	0	12
1,2-pentadiene	25.954	1	14

Compound	$[R]_{20}$	$\Delta \times 10^3$	$\Delta_{L.L.} \times 10^3$
1,cis-3-pentadiene	26.912	— 1	14
1,trans-3-pentadiene	27.136	— 1	14
1,4-pentadiene	25.231	— 13	0
Cyclohexane	28.264	4	17
Cyclopentene	23.365	5	16
Benzene	27.637	1	16
Toluene	32.795	2	18
1-methylnaphthalene	52.669	1	26
Styrene	38.795	15	33
<i>o</i> -xylene	37.816	7	23
<i>m</i> -xylene	37.929	2	19
<i>p</i> -xylene	37.966	7	24
1,2,3-trimethylbenzene	42.796	— 1	17
1,2,4-trimethylbenzene	42.978	0	19
1,3,5-trimethylbenzene	43.064	— 2	17
Thiophene	25.849	0	14
Thiacyclopentane	27.650	— 2	11
2-Thiapropane	19.962	3	13

$$\Delta = [R]_{25^\circ\text{C.}} - [R]_{20^\circ\text{C.}} \quad \Delta_{L.L.} = [(n^2 - 1)/(n^2 + 2)][M/d]_{25^\circ\text{C.}} - [(n^2 - 1)/(n^2 + 2)][M/d]_{20^\circ\text{C.}}$$

In the second place, in many organic molecules a number of conformational isomers with slightly different free energies may occur. Because these isomers will have different polarizabilities, their mean polarizability will be a function of the temperature due to shifts in their mutual equilibria. To avoid this complication, special emphasis should be laid on rigid molecules like benzene and thiophene (table 1).

In table 2, the molar refractions of nine isomeric heptanes are shown. According to the principle of additivity of atomic refractions, all these values should be equal. This is only approximately the case. Relative to the usual Lorentz-Lorenz refraction, the temperature dependence is greatly reduced. There is also a slight reduction of the difference between the highest and the lowest value, viz. from 0.34 to 0.28.

Compound	$[R]_{20}$	$\Delta \times 10^3$	$\left(\frac{n^2-1}{n^2+2} \frac{M}{d}\right)_{20}$	$\Delta_{L.L.} \times 10^3$
3-ethylpentane	35.524	-5	34.283	+ 9
2,3-dimethylpentane	35.558	-3	34.324	+11
3,3-dimethylpentane	35.561	-1	34.332	+13
2,3,3-trimethylpentane	35.596	-1	34.374	+13
3-methylhexane	35.680	-5	34.460	+ 9
<i>n</i> -heptane	35.769	0	34.550	+15
2-methylhexane	35.795	-7	34.591	+ 8
2,4-dimethylpentane	35.805	-1	34.619	+13
2,2-dimethylpentane	35.806	-2	34.617	+12

Table 2. Molar refractions of nine heptanes. Calculated from data of the American Petroleum Research Project 44 [8]. For the assignment of the abbreviations see table 1. $\lambda = 589.3$ nm.

x_2	$[R]_{\text{exp}}$	$[R]_{\text{calc}}$	$\{[R]_{\text{calc}} - [R]_{\text{exp}}\} \times 10^3$	$\Delta n \times 10^5 \dagger$ Scholte
0	40.357	40.357	0	+ 1
0.17412	38.156	38.155	-1	- 9
0.36798	35.703	35.703	0	-18
0.54403	33.476	33.477	+1	-22
0.72226	31.223	31.223	0	-21
0.86104	29.465	29.468	+3	-10
1.00000	27.713	27.710	-3	+ 1

$\dagger \Delta n = n$ calculated by Scholte— n measured by Scholte.

Table 3. The experimental and calculated refractions of mixtures of 2,3,4-trimethylpentane (1) and carbontetrachloride (2). Measurements by Scholte [9]. $t = 25^\circ\text{C}$. $\lambda = 589.3$ nm.

In table 3, the additivity of the molar refractions according to formula (17) is shown. A mixture of two apolar liquids is chosen, because in that case the chance of specific interactions is as small as possible. The second column is given by:

$$[\bar{R}]_{\text{calc}} = 40.3570x_1 + 27.7104x_2. \quad (19)$$

This formula gives the best fit to the experimental values. The constants were calculated by the method of least squares.

It is interesting to note that the mean molar volume is not additive. It is given to a reasonable approximation by:

$$\bar{V} = 159.574x_1 + 97.116x_2 + 1.188x_1x_2. \quad (20)$$

Obviously, the empirical principle of additivity of molar refractions makes that this deviation from the linearity of \bar{V} is not reflected in $[\bar{R}]$.

Scholte has calculated n with Böttcher's formula, containing the radii of the molecules as parameters, but these radii were determined from the temperature dependence of refractive index and of density of the pure components. In the last column, the deviations of the calculated refractive indices from the experimental values are given. It is easily seen that, since $n \approx 1.4$, an error in $[R]$ of 10^{-3} corresponds to an error in n of 10^{-5} . In this case, equation (12) seems to fit the experiments better than Böttcher's formula.

Mol. fraction Na I	$[R]_{\text{exp}}$	$[R]_{\text{calc}}$	$\Delta \times 10^3$	With the Lorentz-Lorenz formula		
				$[R]_{\text{exp}}$	$[R]_{\text{calc}}$	$\Delta \times 10^3$
0	3.791	3.792	+2	3.693	3.699	+6
0.01279	4.002	4.003	+1	3.890	3.892	+2
0.02243	4.161	4.161	0	4.039	4.038	-1
0.03398	4.351	4.351	0	4.215	4.213	-2
0.05044	4.622	4.621	-1	4.466	4.462	-4
0.06970	4.939	4.937	-2	4.758	4.754	-4
0.09065	5.282	5.281	-1	5.072	5.071	-1
0.11732	5.718	5.719	+1	5.469	5.474	+5

Table 4. The molar refractions of solutions of sodium iodide in water. Measurements by Scholte [10]. $t = 25^\circ\text{C}$. $\lambda = 656.3 \text{ nm}$.

In table 4, the result is seen of the application of equation (12) to solutions of sodium iodide in water. The mol. fraction of sodium iodide is not as reliable as the other experimental results of Scholte. This is due to the great hygroscopy of sodium iodide. Constants $[R]_k$ in equation (17) were also calculated by means of least squares. The values in the second column of table 4 are calculated from this linear equation.

3.2. The dielectric constant of mixtures of apolar liquids

In this field, no new interesting aspects are expected to appear; ϵ will behave in the same way as n^2 in the preceding chapter. Scholte measured also the dielectric constant of the same mixtures as mentioned in table 3. He calculated, using Böttcher's formula, in the same manner the dielectric constants of the mixtures from data of the pure components. Also in this case it turns out that equation (15) is closer to the experimental values than Böttcher's formula. The results are collected in table 5.

Weight fraction CCl ₄	0.22114	0.43949	0.61639	0.77788	0.89299
Density d	0.81336	0.94113	1.07858	1.24524	1.40022
Dielectric constant $\epsilon(\text{exp.})$	2.0044	2.0402	2.0806	2.1310	2.1784
ϵ , calc. with equation (8) ($\mu=0$)	2.0031	2.0388	2.0787	2.1288	2.1773
ϵ , calc. by Scholte	2.0033	2.0390	2.0790	2.1292	2.1776
ϵ , calc. with equation (10)	2.0038	2.0401	2.0803	2.1305	2.1785
$[\epsilon(\text{equation 8}) - \epsilon(\text{exp.})] \times 10^5$	-13	-14	-19	-22	-11
$[\epsilon(\text{Scholte}) - \epsilon(\text{exp.})] \times 10^5$	-11	-12	-16	-18	-8
$[\epsilon(\text{equation 10}) - \epsilon(\text{exp.})] \times 10^5$	-6	-1	-3	-5	+1

Table 5. The dielectric constants for mixtures of 2,3,4-trimethylpentane and carbon-tetrachloride. Measurements by Scholte [11]. $d(\text{C}_8\text{H}_{18})=0.71585$, $\epsilon(\text{C}_8\text{H}_{18})=1.9767$, $d(\text{CCl}_4)=1.58412$, $\epsilon(\text{CCl}_4)=2.2367$.

3.3. The dielectric constants of mixtures with a polar component

This subject is of great interest in physical chemistry. The main goal is the determination of the dipole moment of a molecule with the aid of equation (10). In general, the temperature dependence of ϵ is not measured, but the first term in the right hand side of equation (8) is estimated from the molar refraction at optical frequencies. Especially for large dipoles, the second term is predominant and the errors introduced by this estimation are not large.

Of course, measurements in diluted gas phase are theoretically more reliable, but accurate measurements are difficult, and impossible with most organic substances, because of their low vapour pressure at reasonably low temperatures.

The calculation of the dielectric constants with equation (8) at high concentrations of the polar component with gas phase-determined μ_k and α_k yields in some cases even $\epsilon < 0$. Therefore, only diluted solutions are measured. But also in this case the results are doubtful, as Böttcher [12] pointed out. On the basis of formula (8), one expects a linear relation of type:

$$(\epsilon - 1)\bar{M}/(\epsilon + 2)d = [\bar{P}] = [P]_0 + x\{[P]_1 - [P]_0\}, \quad (21)$$

where x = the molar fraction of the dipolar solute and $[P]_0$ and $[P]_1$ are the molar polarizations of solvent and solute. But, in general, the experimental data do not fit in formula (21).

Therefore, the experimental results are extrapolated to $x \rightarrow 0$. Several authors have proposed different procedures of extrapolation. Böttcher [13] reviewed these methods, the best known equation is that of Halverstadt and Kumler [14].

If, however, function $(\epsilon - 1)/(\epsilon + 2)$ is replaced by $(\epsilon^{1/3} - 1)$ it turns out that equation (10) can be used directly. We thus start with the theoretically better founded equation (7), and avoid the time-consuming extrapolations of $\partial d/\partial x$ and $\partial \epsilon/\partial x$ separately to $x \rightarrow 0$.

As a first example, we show the results of the application of equation (15) to measurements by De Vos [15] on diluted solutions of chlorobenzene in benzene. De Vos carefully extrapolated his measurements of the dielectric constant to zero frequency. In table 6, the results at 298°K. are shown. The experimental values of $[P]$ were fitted, with least squares, into an equation of type (10), yielding:

$$[P] = 28.188 + 64.540x. \quad (22)$$

In the third column of table 6, the deviations are listed. The largest deviation

8×10^{-3} corresponds to an error in ϵ of 4×10^{-4} . Equation (22) yields $[P]$ ($\text{C}_6\text{H}_5\text{Cl}$) = 92.728. The non-dipole contribution to this $[P]$ can be estimated from the molar refraction of chlorobenzene in the sodium-*D*-line yielding, on the basis of the data of De Vos, $[R]_D = 33.011$. The dipole moment can be calculated with the well-known formula [15]:

$$\mu = 0.01281\{[P] - [R]_D\}^{1/2} \quad (23)$$

yielding

$$\mu = 1.709D.$$

x	$[P]_{\text{exp}}$	$\Delta[P] \times 10^3$
0.000000	28.189	-1
0.004852	28.504	-3
0.008338	28.727	-1
0.011070	28.904	-2
0.011974	28.961	0
0.015052	29.151	+8
0.017614	29.318	+7
0.020933	29.544	-5
0.021803	29.592	+3
0.024736	29.789	-5
0.028111	30.004	-2

x = mol. fraction of chlorobenzene. $\Delta[P] = [P]$ (equation 22) — $[P]_{\text{exp}}$.

Table 6. The dielectric constants of dilute solutions of chlorobenzene in benzene at 298°K. Measurements by De Vos [15].

The same can be done with De Vos's measurements at 308°K. Three concentrations had to be skipped, because the deviations were much larger than usual. A dipole moment of 1.711*D* was obtained. At 318°K, two measurements had to be skipped. The resulting dipole moment is then 1.707*D*. The gas phase measurements, quoted by De Vos [15], give 1.69–1.72*D*.

De Vos [15] compared the results of different formulae applied to his above-mentioned experimental data. He first calculated μ by Halverstadt-Kumler's [14], secondly by Böttcher's [16] formula, and in the third place by a formula of Scholte [16]. The treatment of the spherical molecular model of Böttcher was extended by Scholte to an ellipsoidal model. The dimensions of this model were fitted to the molecular shape. All these results are collected in table 7. Obviously, the discrepancy between vapour phase measurements and dilute solutions can be removed by use of formula (10). In vapour phase, $\epsilon \approx 1$ and equations (8) and (10) become equivalent.

In table 8, some dipole moments of 1-chloro-1-methylcyclohexane are compared. As in the case of chlorobenzene, the values obtained on the basis of equation (10) are higher than those obtained by the usual method of Halverstadt and Kumler. It is interesting to note that the difference in results between carbon tetrachloride and benzene is smaller than that calculated by Maaskant. The data of Maaskant's table D seem to be a little extraordinary.

One can, however, never hope to have exact accordance between dipole moments of one substance in different solvents. There are always some specific

Method of calculation	Temperature (°K)		
	298	308	318
Halverstadt-Kumler } calculations	1.587	1.589	1.589
Böttcher } by	1.577	1.575	1.571
Scholte } De Vos [15]	1.741	1.736	1.730
Calculation based on equation (10)	1.709	1.711	1.707

Table 7. Dipole moments of chlorobenzene in Debye units from measurements [15] on dilute solutions.

Table in the thesis of Maaskant	C	D	E	F
Solvent	CCl ₄	CCl ₄	C ₆ H ₆	C ₆ H ₆
μ , calculated with H.-K. [14] by Maaskant	2.16	2.18	2.10	2.11
μ , calculated on basis of equation (10)	2.30	2.35	2.27	2.26

Table 8. The dipole moment of 1-chloro-1-methylcyclohexane in Debye units based on measurements by Maaskant [17].

interactions which influence the total apparent dipole moment. This holds especially for highly melting organic substances. Their solubility is always due to rather strong specific interactions with the solvent.

A large part of organic molecules can occur in different conformational isomers. An example is 1,2-dichloro-ethane; the *trans* conformation is the most stable one and has no dipole moment. The *skew* conformation has a dipole moment of at least one *D*.

On the basis of the Böttcher's treatment [18] of the interaction energy of a dipole and its surrounding dielectric, one can make a very rough estimate of the extra stabilization of the skew conformation which is 0.1 kcal/mol in non-polar solvents and can amount to 1–2 kcal/mol in polar solvents. Even this 1 kcal/mol can cause a clear deviation in the apparent dipole moment.

3.4. The dielectric constant of pure polar liquids

In principle it is possible to calculate the dipole moment of a molecule from the temperature dependence of the dielectric constant of the pure liquid.

In practice, however, most dipolar liquids are associated to some extent. Because it has to be expected that the degree of association greatly depends on temperature, equation (10) cannot be used, although calculation of the dipole moment at one single temperature, with the aid of a reasonable estimate of α , may be possible.

An example of a compound which may give reasonable results, is bromoform. The molecule is rigid; therefore the temperature dependence of α may be expected

$t^{\circ}\text{C}$	$\left[(\epsilon^{1/3} - 1) \frac{M}{d} \right]_{\text{exp.}}$	$\left[(\epsilon^{1/3} - 1) \frac{M}{d} \right]_{\text{equation (24)}}$
18.26	55.53	55.54
18.45	55.52	55.52
26.01	54.97	54.96
29.29	54.74	54.73
35.35	54.31	54.31
40.53	53.97	53.96
42.42	53.85	53.84
50.57	53.31	53.33
50.68	53.32	53.32

Table 9. The molar polarizability of bromoform according to Scholte [19].

to be very small. The large bromine atoms avoid association. The results are shown in table 9, and fit into the equation:

$$(\epsilon^{1/3} - 1) \frac{\bar{M}}{d} = 33.366 + \frac{6461.5}{T} \quad (24)$$

yielding $\mu = 1.03D$. Scholte [19] finds $0.78D$, Buckingham and Le Fèvre [20] determined the dipole moment in gas phase to be $1.00 \pm 0.02D$.

REFERENCES

- [1] LOOYENGA, H., 1965, *Physica*, **31**, 401.
- [2] LANDAU, L. D., and LIFSHITZ, E. M., 1960, *Electrodynamics of Continuous Media* (London: Pergamon Press), p. 46.
- [3] BÖTTCHER, C. J. F., 1952, *Theory of Electric Polarisation* (Amsterdam: Elsevier), p. 203.
- [4] *Loc. cit.*, pp. 200–201.
- [5] *Loc. cit.*, p. 206.
- [6] *Loc. cit.*, pp. 267–268.
- [7] *Loc. cit.*, pp. 266–267.
- [8] ROSSINI, F. D., PITZER, K. S., ARNETT, R. L., BRAUN, R. M., and PIMENTEL, G. C., 1953, *Selected Values of Physical and Thermodynamical Properties of Hydrocarbons and Related Compounds* (Pittsburg: Carnegie Press).
- [9] TEN SELDAM, C. A., 1953, Thesis, Utrecht.
- [10] SCHOLTE, T. G., 1950, Thesis, Leiden, p. 50.
- [11] SCHOLTE, T. G., 1950, Thesis, Leiden, p. 68.
- [12] BÖTTCHER, C. J. F., the same book as in references [3]—[7].
- [13] BÖTTCHER, C. J. F., the same book as in references [3]—[7].
- [14] HALVERSTADT, I. F., and KUMLER, W. D., 1942, *J. Amer. chem. Soc.*, **64**, 2988.
- [15] DE VOS, F. C., 1958, Thesis, Leiden, pp. 100–102.
- [16] SCHOLTE, T. G., 1950, Thesis, Leiden, p. 75.
- [17] MAASKANT, W. J. A., 1963, Thesis, Leiden, pp. 85–87, 92.
- [18] BÖTTCHER, C. J. F., 1952, *Theory of Electric Polarisation* (Amsterdam: Elsevier).
- [19] SCHOLTE, T. G., 1950, Thesis, Leiden, p. 73.
- [20] BUCKINGHAM, A. D., and LE FÈVRE, R. J. W., 1953, *J. chem. Soc.*, p. 3432.

A two-electron atomic integral

by P. J. ROBERTS

Department of Natural Philosophy, University of Glasgow

(Received 31 March 1965; revision received 28 May 1965)

A two-electron atomic integral occurring in the atomic many-body problem is evaluated in closed form. The correlation factor used is a positive integral power of the distance between the two electrons.

1. INTRODUCTION

Szász [1] formulated the atomic many-body problem in terms of wavefunctions taking account of the correlations between the electrons in an atom. In the lowest approximation he constructed the many-electron wavefunction from two-electron functions which accounted for electron-pair correlations only. Such pair functions may be designated 'binary' wavefunctions, and each binary function consists of the product of two one-electron atomic orbitals with a binary correlation factor (BWF). The BWF is a function of the distance between the two electrons, and was chosen by Szász [1] to be a positive integral power of the inter-electronic distance. It is customary to use as one-electron orbitals the well-known Slater atomic functions.

With BWF's of the type mentioned above, the simplest two-electron integral occurring in the atomic many-body theory [1] has an integrand which is a product of two one-electron atomic orbitals with an integral power of the inter-electronic separation. In the case where only Coulomb forces occur between the electrons, this integral power will be greater than or equal to minus one. Several different methods [1-7] have been published for calculating the atomic multi-electron integrals, but no closed formula has yet been given in the literature for the integral mentioned above. We show below that this integral can be computed in closed form.

2. MATHEMATICAL DERIVATION

We write the two-electron atomic integral in the general form considered by Calais and Löwdin [5]:

$$I = \int dV f(r_1) g(r_2) h(r) Y_{lm}(\theta_1, \phi_1) Y_{\lambda\mu}(\theta_2, \phi_2), \quad (1)$$

where the subscripts 1 and 2 refer to the two electrons, r is the distance between them, and Y is the complex spherical harmonic normalized to unity over the whole unit sphere [8]. The integration is over the whole of configuration space for the two electrons.

Equation (1) can be reduced to a three-fold integral by expanding $h(r)$ in spherical harmonics, followed by completion of the angular integrations. The result is [5]:

$$I = (-1)^m 2\pi \delta(\lambda, l) \delta(m, -\mu) \int_0^\infty f(r_1) r_1^2 dr_1 \int_0^\infty g(r_2) r_2^2 dr_2 \int_0^\pi h(r) P_l(\cos \theta) \sin \theta d\theta, \quad (2)$$

where δ is the usual delta function, P is the Legendre polynomial, and θ is the angle between the electronic radial vectors \mathbf{r}_1 and \mathbf{r}_2 .

We now restrict our consideration to the correlation factor :

$$h(r) = r^n, \quad (3)$$

where n is an arbitrary integer. In this case the final integral over θ in equation (2) has been evaluated by Chapman [9] and Sack [10], and we merely quote the result :

$$J = \int_0^\pi r^n P_l(\cos \theta) \sin \theta d\theta = 2(-\tfrac{1}{2}n)_l y^n (x/y)^l F[l - \tfrac{1}{2}n, -\tfrac{1}{2} - \tfrac{1}{2}n : l + \tfrac{3}{2} : x^2/y^2] / (\tfrac{3}{2})_l, \quad (4)$$

where x and y are the least and greatest in magnitude, respectively, of r_1 and r_2 , and F is the hypergeometric function of Gauss.

Equation (4) is valid for arbitrary values of n , positive or negative, integral or non-integral, and has been independently derived by the author from the Taylor series for $h(r)$. In what follows, however, we shall only be concerned with integral values of n greater than or equal to minus one, as in this case the hypergeometric function is a terminating series. For positive even n , the factor $(-\tfrac{1}{2}n)_l$ causes J to vanish identically when $l > \tfrac{1}{2}n$.

Expanding the hypergeometric function as a power series, we obtain :

$$J = \sum_s C(n, l, s) x^{l+2s} y^{l+2s-n}, \quad (5)$$

where

$$C(n, l, s) = 2(-\tfrac{1}{2}n)_{l+s} (-\tfrac{1}{2} - \tfrac{1}{2}n)_{s/s} ! (\tfrac{3}{2})_{l+s}, \quad (6)$$

and the sum terminates at the term $s = \tfrac{1}{2}n - l$ when n is even, and at the term $s = \tfrac{1}{2}(n+1)$ when n is odd, provided $n \geq -1$.

We are now in a position to evaluate equation (2) when f and g are radial Slater functions, i.e.

$$f(r) = r^p \exp(-ar), \quad g(r) = r^q \exp(-br), \quad h(r) = r^n, \quad n \geq -1, \quad p \geq l, \quad q \geq \lambda, \quad (7)$$

where p, q , are positive integers or zero, and a, b are positive variation parameters. Here the Slater orbitals have been chosen in unnormalized form.

Substituting equations (5) and (7) into equation (2) we obtain :

$$\begin{aligned} I = & 2\pi(-1)^m \delta(l, \lambda) \delta(m, -\mu) \sum_s C(n, l, s) \int_0^\infty \int_0^{r_1} dr_1 dr_2 \\ & \times \{ r_1^{n-l-2s+p+2} \exp(-ar_1) r_2^{l+2s+q+2} \exp(-br_2) \\ & + r_1^{n-l-2s+q+2} \exp(-br_1) r_2^{l+2s+p+2} \exp(-ar_2) \}, \end{aligned} \quad (8)$$

where the second radial integral has been transformed by using Dirichlet's theorem on double integrals.

Examining the powers of r_1 which occur in the integrand of equation (8), we observe that, owing to the restrictions on the s summation,

$$\begin{aligned} l & \leq n - l - 2s, \quad n \text{ even}, \\ n - l - 2s + p + 2 & \geq p - l + 1, \quad n \text{ odd}, \\ n - l - 2s + q + 2 & \geq q - l + 1, \quad n \text{ odd}. \end{aligned} \quad (9)$$

Since the integral I is only non-zero when $l = \lambda$, and p and q obey the regularity conditions stated in equation (7), it is obvious that the integers on the right hand

side of equation (9) are always positive when n is greater than or equal to minus one. Thus, only positive integral powers of r_1 and r_2 occur in the integrand of equation (8), so that the integral I is a linear combination of integrals of the type:

$$K = \int_0^\infty dr_1 r_1^u \exp(-ar_1) \int_0^{r_1} dr_2 r_2^v \exp(-br_2), \quad (10)$$

where u and v are positive integers.

Equation (10) is easily evaluated by means of a formula due to Boys [11]:

$$K = (-\partial/\partial a)^u (-\partial/\partial b)^v [1/a(a+b)] \\ = \sum_{r=0}^u u! (u+v-r)! / (u-r)! a^{r+1} (a+b)^{u+v+1-r}. \quad (11)$$

Comparing equations (10) and (11) with equation (8), we see that the integral I reduces to a finite series (over s) of simple analytic expressions such as equation (11), and is thus given in closed form.

The author is indebted to Dr. Robert A. Sack for his constructive criticism of an earlier draft of this paper and for drawing his attention to reference [9]. Dr. Sack has derived useful recurrence relations for integrals of the type K .

REFERENCES

- [1] SZÁSZ, L., 1961, *J. chem. Phys.*, **35**, 1072.
- [2] JAMES, H. M., and COOLIDGE, A. S., 1936, *Phys. Rev.*, **49**, 688.
- [3] FOCK, V., VESSELOV, M., and PETRASHEN, M., 1940, *J. exp. theor. Phys.*, **10**, 723.
- [4] WALSH, P., and BOROWITZ, S., 1959, *Phys. Rev.*, **115**, 1206.
- [5] CALAIS, J. L., and LÖWDIN, P. O., 1962, *J. mol. Spectrosc.*, **8**, 203.
- [6] ÖHRN, Y., and NORDLING, J., 1963, *J. chem. Phys.*, **39**, 1864.
- [7] HINZE, J., and PITZER, K. S., 1964, *J. chem. Phys.*, **41**, 3484.
- [8] EDMONDS, A. R., 1957, *Angular Momentum in Quantum Mechanics* (Princeton: Princeton University Press).
- [9] CHAPMAN, S., 1916, *Quart. J. pure appl. Math.*, **47**, 16.
- [10] SACK, R. A., 1964, *J. Math. Phys.*, **5**, 245.
- [11] BOYS, S. F., 1950, *Proc. roy. Soc. A*, **201**, 125.

Electron paramagnetic resonance study of the photo-excited triplet state of pyrene-*d*-10

by S. W. CHARLES†, P. H. H. FISCHER‡ and C. A. McDOWELL

Department of Chemistry, The University of British Columbia,
Vancouver 8, B.C., Canada

(Received 2 June 1965)

Electron paramagnetic resonance absorption has been observed at room temperature in pyrene-*d*-10 orientated in fluorene when irradiated with light from an AH6 mercury lamp. Measurements were made at a frequency of 9.4 Gc.p.s. The long principal magnetic axis in the plane of the pyrene-*d*-10 was taken as the *x*-axis, the short axis in the plane to be the *y*-axis, and the normal to the plane to be the *z*-axis. The results have been described by the spin Hamiltonian.

$$H = |\beta| \mathbf{H} \cdot \mathbf{g} \cdot \mathbf{S} + D(S_z^2 - 1/3 \mathbf{S}^2) + E(S_x^2 - S_y^2)$$

with $S = 1$,

$$\begin{aligned} g_{xx} &= 2.0028 \pm 0.0005, \\ g_{yy} &= 2.0023 \pm 0.0005, \\ g_{zz} &= 2.0019 \pm 0.0005, \\ D/hc &= \pm 0.06577 \pm 0.00005 \text{ cm}^{-1}, \\ E/hc &= \mp 0.03162 \mp 0.00005 \text{ cm}^{-1}. \end{aligned}$$

The pyrene-*d*-10 does not fit perfectly into a fluorene substitutional site. The pyrene plane is inclined to the fluorene crystal *b* axis at $30^\circ 0' \pm 15'$, as compared to $34^\circ 50'$ for the fluorene host molecules.

1. INTRODUCTION

Hutchison and Mangum [1,2] were the first to observe the electron paramagnetic resonance spectrum of the photo-excited triplet state of an organic molecule in a single crystal, namely naphthalene oriented in durene. Further studies of this system have been made [3,4] while other systems, quinoxaline in durene [5], phenanthrene in diphenyl and in fluorene [6], quinoline and isoquinoline in durene [7] have been reported recently. In this paper we wish to report the results of the triplet state magnetic resonance study of photo-excited pyrene-*d*-10 oriented in a single crystal of fluorene§. In contrast to previous studies, the present investigation was conducted at room temperature.

2. CRYSTAL STRUCTURES

(a) Fluorene

X-ray crystallographic investigations by Iball [8] and by Burns and Iball [9] have shown that fluorene crystallizes orthorhombically, space group

† On leave of absence from the Department of Physics, University College of North Wales, Bangor, Great Britain.

‡ Present address: Max-Planck Institut f. mediz. Forschung, Institut f. Chemie Heidelberg/Germany, Jahnstrasse 29.

§ On completion of this work a note by O. H. Griffith on the E.S.R. of photo-excited undeuterated pyrene oriented in fluorene, appeared in *J. phys. Chem.*, **69**, 1429 (1965).

D_{2h}^{16} - $Pnam$, with four planar molecules per unit cell, and unit cell edge lengths $a = 8.49 \pm 0.01$, $b = 5.721 \pm 0.008$, and $c = 18.97 \pm 0.10$ Å. They also showed that the plane of the molecules is inclined to the crystal b -axis at $34^\circ 50'$, and that the molecular x -axis (long axis) is parallel to the crystallographic c -axis. See figures 1 and 2.

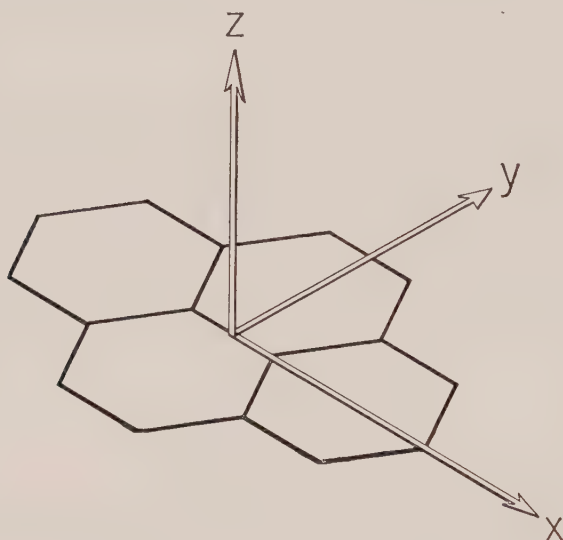


Figure 1. Pyrene axis system.

(b) *Pyrene in fluorene*

From an analysis of the polarized absorption spectrum of pyrene in fluorene at 77°K , Bree and Vilkos [10] concluded that the pyrene molecules do not exactly occupy a substitutional site in the fluorene host lattice, but that the long axis (x -axis), has moved away from the c -axis in the ac plane. Furthermore they suggest that rotation of pyrene molecules about the b -crystal axis could lead to minimization of the interaction between protons of neighbouring molecules.

3. EXPERIMENTAL WORK

A Varian V-4500 X-band spectrometer was employed. The static magnetic field was supplied by a 6 in. magnet, modulated at a frequency of 100 Kc.p.s., and directly calibrated using a proton resonance magnetometer. The microwave field was polarized perpendicular to the static magnetic field for all measurements. The microwave frequency was measured using a Hewlett Packard counter and transfer oscillator. Frequencies ranged from 9.4 to 9.5 Gc.p.s. for all measurements.

The crystal under investigation was grown from a melt, and contained 1.12×10^{-4} mole fraction pyrene- d -10 in fluorene. Assuming that the long axes (x) of the pyrene molecules are nearly parallel to the crystal c -axis, the crystal was mounted on the cleavage ab face, so that it could be rotated about the crystal c -axis in the static magnetic field H . At certain orientations, maximum projections in the ab -plane of the pyrene molecular z and y axes became parallel to

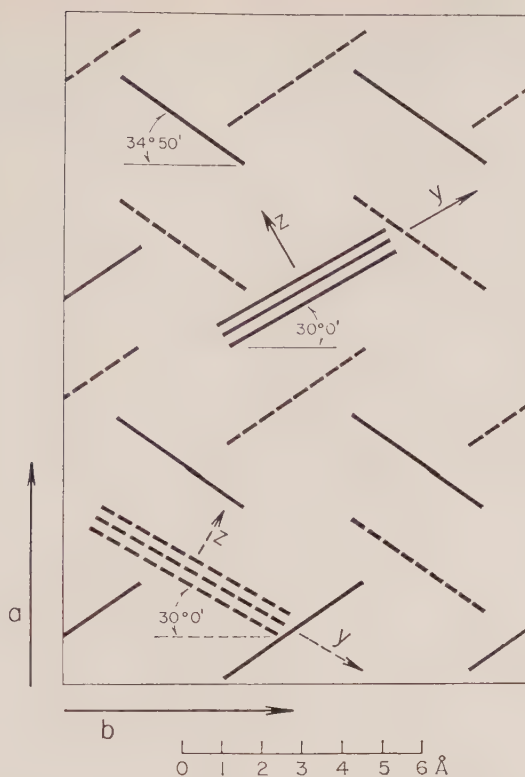


Figure 2. Positions of the two crystallographically inequivalent pyrene molecules in fluorene lattice.

the field. The molecular z -axis was located in the ab plane by examining the resonance field strength as a function of small rotations (within the range $\pm 5^\circ$) about an axis both in the ab plane and perpendicular to the maximum projection of z in ab . Then by small rotations about z with c directed along H it was shown that x was parallel to c . Thus the orientations of the principal magnetic planes of the molecule with respect to the crystal faces were deduced.

Photo-excitation of pyrene molecules was effected by continuously irradiating with an AH6 high pressure mercury arc. The orange-red phosphorescence of the pyrene molecules remained visible for at least 5 sec after removal of the mercury arc.

4. RESULTS AND DISCUSSION

In figures 3, 4 and 5 are shown the results for the magnitude of field strength $|H|$ at which resonance is observed for various angles of H in the principal magnetic planes of one set of the two crystallographically inequivalent pyrene-*d*-10 molecules present. For each of these two sets of molecules two absorptions are found because of the zero field splitting of the triplet state.

Stationary points of $|H|$ versus angle of rotation are reached when H passes through the x , y , or z axes of the pyrene molecules. Rotation about the x -axis of pyrene (equivalent to rotation about the fluorene x -axis and the crystallographic

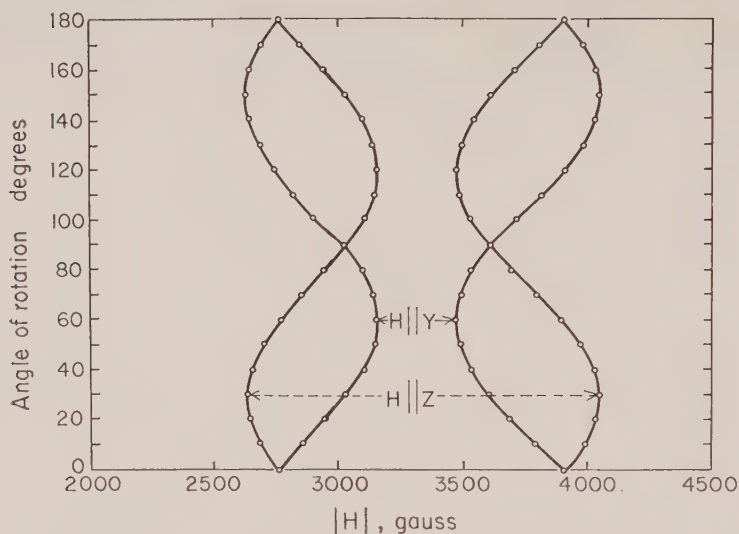


Figure 3. $|H|$ for resonance versus angle of rotation of H in fluorene (and pyrene) yz plane.

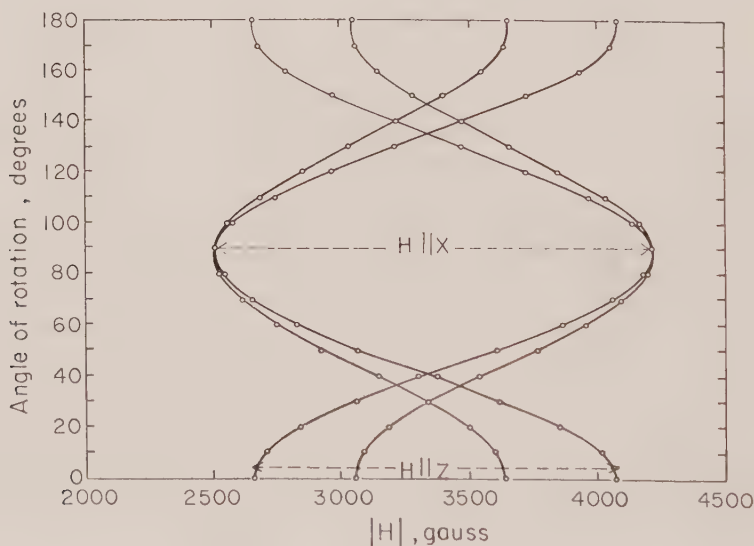


Figure 4. $|H|$ for resonance versus angle of rotation of H in pyrene xz plane.

c -axis), see figure 2 indicated that at 30° , H passed through the z -axis of the first set of the two sets of magnetically inequivalent pyrene molecules, at 60° through the y -axis of the second set, at 120° through the y -axis of the first set, and at 150° again through the z -axis of the second set. This information enabled us to construct Teflon wedges to support the crystal, so that the above procedure could be applied to rotation about the y and z axes of the pyrene molecules,

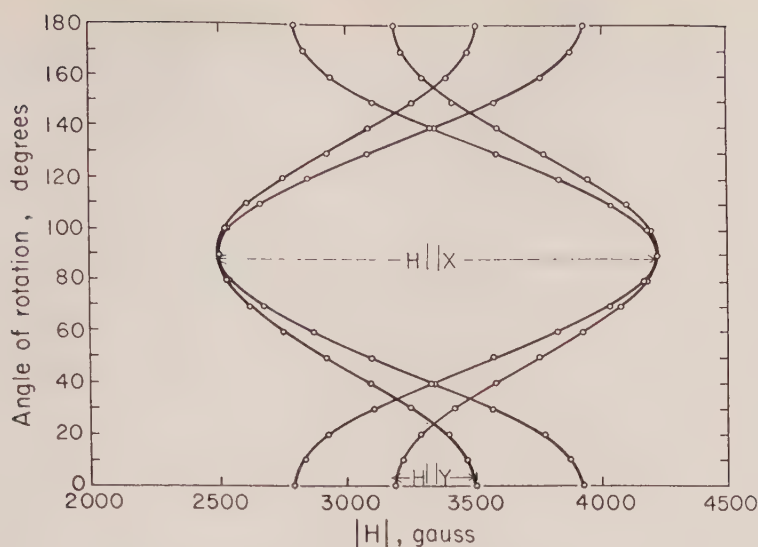


Figure 5. $|H|$ for resonance versus angle of rotation of H in pyrene xy plane.

since these axes do not coincide with the fluorene y and z axes. Whereas the xy planes of the fluorene host molecules make an angle of $34^\circ 50'$ with the bc crystal plane, the pyrene xy planes make an angle of $30^\circ 0' \pm 15'$ with the bc crystal plane, see figure 2. It was difficult to make a more accurate estimate of the latter angle, as the change of resonant field near the stationary points is quite small.

As a check for consistency in our reading and the correctness of the angles of the wedges supporting the crystal, approximate values of g , given by $2h\nu/\beta(H_L + H_H)$ were calculated. ν is the microwave frequency, β the Bohr magneton and H_L and H_H refer to the low and high field measurements when H is parallel to a magnetic axis. See table 1.

	x -axis		y -axis		z -axis	
g_x	—	—	2.0053	2.0053	2.0055	2.0055
g_y	2.0268	2.0271	2.0267	2.0267	—	—
g_z	2.0132	2.0133	—	—	2.0130	2.0132

Table 1. Axis of pyrene molecule about which H rotates.

The magnitude of the three high field-low field absorption peak separations along the principal axes of the fine structure tensor are approximately 0.161, 0.029, and 0.132 cm^{-1} . These values are found when H is parallel to the pyrene x -axis, y -axis and z -axis respectively.

In the presence of a magnetic field H the spin triplet is described approximately by the Hamiltonian:

$$H = |\beta| \mathbf{H} \cdot \mathbf{g} \cdot \mathbf{S} + D(S_z^2 - 1/3 \mathbf{S}^2) + E(S_x^2 - S_y^2).$$

The assumption is made that the molecular axes and the principal axes of the spin-spin coupling tensor coincide. This leads to the following energy levels for H parallel to x , y and z (15), (2).

$$\begin{aligned}
H\|x \quad W_{\mp 1} &= \frac{1}{2}(D+E) \mp [\frac{1}{4}(D+E)^2 + g^2\beta^2 H^2]^{1/2}, \\
W_0 &= D-E, \\
H\|y \quad W_{\mp 1} &= \frac{1}{2}(D-E) \mp [\frac{1}{4}(D-E)^2 + g^2\beta^2 H^2]^{1/2}, \\
W_0 &= D+E, \\
H\|z \quad W_{\mp 1} &= D \mp [\frac{1}{4}(D-E)^2 + g^2\beta^2 H^2]^{1/2}, \\
W_0 &= 0.
\end{aligned}$$

From these relationships it will be seen that the high field-low field separations are given approximately by $(D-3E)/hc$, $(D+3E)/hc$ and $-2D/hc$ for the x -axis, y -axis and z axis respectively. The sum of these three terms is zero and thus the signs for our experimental values can only be ± 0.161 , ∓ 0.029 and $\mp 0.132 \text{ cm}^{-1}$. These values lead to the approximate values for the zero-field parameters $D/hc = \pm 0.0660 \text{ cm}^{-1}$ and $E/hc = \mp 0.0317 \text{ cm}^{-1}$.

Self consistent values of the zero field parameters and the g -tensor were obtained by using the approximate values of D/hc , E/hc , and g_x , g_y and g_z given in table 1 and employing the Newton-Raphson method for obtaining the real roots of the above set of simultaneous algebraic equations. The method was applied to the difference expressions $W_1 - W_0 = h\nu$, etc. for five out of the six possible expressions and solving them for the five unknowns so that the difference between $h\nu$ (experimental) and $h\nu$, calculated using the self-consistent values of the five unknowns, was less than 1 part in 10^7 for all five expressions. The sixth expression was used as a check for these values and gave a difference $h\nu(\text{exp.}) - h\nu(\text{calc.})$ of less than 1 part in 4000. The errors listed in table 2 are maximum values obtained by assuming the error of part 1 in 4000 was the result of an error concentrated in one term only. Thus the actual errors in these five terms are expected to be less than those quoted. These self consistent values are given in table 2.

Parameter	Value
D/hc	$\pm 0.06577 \pm 0.00005 \text{ cm}^{-1}$
E/hc	$\mp 0.03162 \pm 0.00005 \text{ cm}^{-1}$
g_{xx}	2.0028 ± 0.0005
g_{yy}	2.0023 ± 0.0005
g_{zz}	2.0019 ± 0.0005

Table 2.

The experimental results do not enable us to determine the absolute sign of the zero field parameters D and E . They do show however that these parameters must have opposite signs. In the light of other experimental work [2, 5, 6] and from theoretical considerations [11] it seems reasonable to assign a positive value to D and a negative value to E .

Calculations are in progress to determine theoretical values of D and E by the method of van der Waals and ter Maten [11] and will be the subject of a further publication. Pariser-type calculations of the wave function for the excited states of pyrene indicate that a ${}^3B_{3u}^+$ state is the lowest triplet state for pyrene and that it is *ca.* 2.1 eV above the ground state. This compares well with the

experimental value of $16\,800\text{ cm}^{-1}$ (2.1 eV), obtained by McClure [12] for pyrene in a rigid glass at 77°K †. For this state we have found the configuration mixture to be:

$$\begin{aligned} &0.9921(h; h') + 0.0813(g; g') + 0.0254(f; f') \\ &- 0.0695(e; e') - 0.0295(d; d') - 0.0312(c; c') \\ &- 0.0429\{(c; h') + (h; c')\}. \end{aligned}$$

using van der Waals and ter Maten's nomenclature.

5. HYPERFINE SPLITTING

Although the signals obtained with the x , y or z axes of the pyrene molecules parallel to the static field were intense, a careful study at these (and other) orientations did not reveal any hyperfine structure. Perhaps this is to be expected in view of the fact that the ratio $\mu_{\text{H}}/\mu_{\text{D}} \simeq 6.7$. It has been shown for other aromatic triplet systems, that the spin-density distributions of the lowest triplet state and of the corresponding negative ion are similar [13]. Assuming this to be the case for the system under investigation, and employing experimentally determined spin densities of the pyrene negative ion [14], the following deuterium-coupling constants, including the isotropic and dipolar contributions, have been calculated. These are:

$H\ x$	$a_1 = 0.07\text{ G},$	$H\ y$	$a_1 = 0.21\text{ G},$	$H\ z$	$a_1 = 0.14\text{ G},$
	$a_2 = 0.87\text{ G},$		$a_2 = 0.57\text{ G},$		$a_2 = 0.64\text{ G},$
	$a_3 = 0.38\text{ G},$		$a_3 = 0.24\text{ G},$		$a_3 = 0.28\text{ G},$

where subscript 1 refers to the carbon atoms lying on the molecular x -axis, 2 to the adjacent carbon atoms, and 3 to the remaining set of carbon atoms of the 3 types of non-equivalent sets. Employing these coupling constants an overall deuterium splitting of 10.28, 7.32, and 7.92 G is calculated for H parallel to the molecules' x , y , or z axes respectively, a ratio of 1.41:1:1.08. Neglecting the very small splitting of deuterium attached to carbon atoms 1, the line shapes for all three orientations will be similar and consequently the widths at maximum slopes should be in the same ratio. Experimentally we find a ratio of 1.54:1:1.19. Owing to the presence of a small, but not accurately known amount of undeuterated or partially deuterated pyrene the experimentally determined overall linewidths are greater than those calculated. The fact that the above ratios are quite similar would seem to lend support to the ${}^3B_{3u}^+$ assignment, however, the lack of hyperfine splitting prevents us from assigning the symmetry of the triplet state with absolute certainty.

A short-lived phosphorescence ($< 0.5\text{ sec}$) of undeuterated pyrene oriented in fluorene was observed, but the E.P.R. signal was of insufficient signal to noise ratio for hyperfine splitting to be observed. No noticeable increase in the lifetime of the phosphorescent state or the intensity of the E.P.R. signal was observed, even upon lowering the temperature to 4°K .

† O. H. Griffith determined the maximum of the only line discovered in the 77°K phosphorescence spectrum of pyrene-doped fluorene to be $16\,750 \pm 60\text{ cm}^{-1}$.

6. COMMENTS

On completion of this work a note by O. H. Griffith on the E.P.R. of pyrene-*h*-10 oriented in a fluorene host lattice was published. Our results indicate that his assumption that the pyrene molecule is in a perfectly substitutional site is not true. Rather a slight re-orientation, a rotation of *ca.* 5° about the *c* crystal axis, takes place. Due to the different choice of molecular axes, Griffith's values of the zero field parameters differ numerically from ours. With his choice of molecular axes our values of *D* and *E* are consistent.

We are indebted to Miss V. V. B. Vilkos for kindly preparing the crystals investigated, and to Professor A. Bree for much helpful discussion. We also thank Dr. F. G. Herring for computational help and Professor R. Lefebvre for kindly supplying us with pyrene SCF calculations. We wish to acknowledge with thanks the receipt of generous financial support from the National Research Council of Canada.

REFERENCES

- [1] HUTCHISON, C. A., Jr., and MANGUM, B. W., 1958, *J. chem. Phys.*, **29**, 952.
- [2] HUTCHISON, C. A., Jr., and MANGUM, B. W., 1961, *J. chem. Phys.*, **34**, 908.
- [3] HORNIG, A. W., and HYDE, J. S., 1963, *Mol. Phys.*, **6**, 33.
- [4] SCHMILLEN, A., and FOERSTER, G. V., 1961, *Z. Naturf., A*, **16**, 320.
- [5] VINCENT, J. S., and MAKI, A. H., 1963, *J. chem. Phys.*, **39**, 3088.
- [6] BRANDON, R. W., GERKIN, R. E., and HUTCHISON, C. A., Jr., 1964, *J. chem. Phys.*, **41**, 3717.
- [7] VINCENT, J. S., and MAKI, A. H., 1965, *J. chem. Phys.*, **42**, 865.
- [8] IBALL, J., 1936, *Z. Kristallogr.*, **91**, 397.
- [9] BURNS, D. M., and IBALL, J., 1955, *Proc. roy. Soc. A*, **227**, 200.
- [10] BREE, A., and VILKOS, V. V. B., 1964, *J. chem. Phys.*, **40**, 3125.
- [11] VAN DER WAALS, J. H., and TER MATEN, G., 1964, *Mol. Phys.*, **8**, 301, and others.
- [12] McCLURE, D. S., 1949, *J. chem. Phys.*, **17**, 910.
- [13] McLACHLAN, A. D., 1962, *Mol. Phys.*, **5**, 51.
- [14] HOIJTINK, G. T., TOWNSEND, J., and WEISSMAN, S. I., 1961, *J. chem. Phys.*, **34**, 507.
- [15] STEVENS, K. W. H., 1952, *Proc. roy. Soc. A*, **214**, 237.

Long range interactions between three hydrogen atoms

by Y. M. CHAN and A. DALGARNO

Department of Applied Mathematics, The Queen's University of Belfast

(Received 31 May 1965)

The three-body interaction energy for three hydrogen atoms a , b and c at large distances R_{ab} , R_{bc} and R_{ca} from each other is calculated to be $21.6425 (3 \cos \theta_a \cos \theta_b \cos \theta_c + 1)/R_{ab}^3 R_{bc}^3 R_{ca}^3$ atomic units, where θ_a , θ_b and θ_c are the internal angles of the triangle abc . The calculation is carried out by transforming the three-body problem into three one-body problems.

1. INTRODUCTION

The non-additive contribution to the long range interactions between three distant atoms has been discussed in a number of papers [1-10] but in no case has a precise calculation of its magnitude been carried out. A simple extension of a procedure used by Chan and Dalgarno [11] for hydrogen atoms makes possible a very accurate prediction for three hydrogen atoms.

2. THEORY

The interaction potential V_{ab} of a charge distribution consisting of charges e_i at positions \mathbf{r}_i , measured from its centre of charge a and a second non-overlapping charge distribution of charges e_j at positions \mathbf{r}_j , measured from its centre of charge b , is given by:

$$V_{ab} = \sum_i \sum_j \sum_{m,n,\alpha} \frac{(-)^n 4\pi e_i e_j (m+n)! \delta_{\alpha,-\beta}}{R_{ab}^{m+n+1} [(2m+1)(2n+1)(m-\alpha)!(m+\alpha)!(n-\alpha)!(n+\alpha)!]^{1/2}} \times \mathcal{Y}_m^\alpha(\mathbf{r}_i) \mathcal{Y}_n^\beta(\mathbf{r}_j) \quad (1)$$

[12, 13], where $\mathcal{Y}_m^\alpha(\mathbf{r})$ is the regular solid spherical harmonic:

$$\mathcal{Y}_m^\alpha(\mathbf{r}) = r^m Y_{n,\alpha}(\mathbf{r}) \quad (2)$$

and R_{ab} is the distance between the centres of charge.

The interaction potential for three non-overlapping charge distributions, centred at a , b and c is the sum of the two-body potentials:

$$V_{abc} = V_{ab} + V_{bc} + V_{ca}. \quad (3)$$

The non-additive contribution to the change in energy arising from the potential V occurs first in the third order of perturbation theory [1, 4] and for three identical atoms it may be expressed as:

$$E_{abc} = 6 \sum_s \frac{\langle O_a O_b | V_{ab} | s_a s_b \rangle \langle s_b O_c | V_{bc} | O_b s_c \rangle \langle s_c s_a | V_{ca} | O_c O_a \rangle}{(E_s^a + E_s^b - E_0^a - E_0^b)(E_s^c + E_s^a - E_0^c - E_0^a)}, \quad (4)$$

where s_a represents the s_a th excited state of atom a with eigenvalue E_s^a and the summation is over all states s_a , s_b and s_c for which the denominator does not vanish [4]. Writing (1) symbolically in the form $V_{ab} = V_a V_b$, (4) may be reduced to :

$$E_{abc} = 6 \int_s \frac{|\langle O_a | V_a | s_a \rangle \langle O_b | V_b | s_b \rangle \langle O_c | V_c | s_c \rangle|^2}{(E_s^a - E_0^a + E_s^b - E_0^b)(E_s^c - E_0^c + E_s^a - E_0^a)} \quad (5)$$

which, on using the identity :

$$\frac{1}{a+b} = \frac{2}{\pi} \int_0^\infty \frac{ab}{(a^2 + \omega^2)(b^2 + \omega^2)} d\omega, \quad (6)$$

may be written in product form :

$$\begin{aligned} E_{abc} = & \frac{24}{\pi^2} \int_0^\infty d\omega \int_0^\infty d\omega' \mathbf{S}_{s_a} \frac{(E_s^a - E_0^a) |\langle O_a | V_a | s_a \rangle|^2}{(E_s^a - E_0^a)^2 + \omega^2} \\ & \times \mathbf{S}_{s_b} \frac{(E_s^b - E_0^b) |\langle O_b | V_b | s_b \rangle|^2 (E_s^b - E_0^b)}{\{(E_s^b - E_0^b)^2 + \omega^2\} \{(E_s^b - E_0^b)^2 + \omega'^2\}} \\ & \times \mathbf{S}_{s_c} \frac{(E_s^c - E_0^c) |\langle O_c | V_c | s_c \rangle|^2}{(E_s^c - E_0^c)^2 + \omega'^2}. \end{aligned} \quad (7)$$

Following [11], we introduce a function $\Phi_a(\omega)$ such that :

$$\{(H_a - E_0^a)^2 + \omega^2\} \Phi_a(\omega) + \{\nabla V_a \cdot \nabla - \langle O_a | \nabla V_a \cdot \nabla | O_a \rangle\} \psi_0^a = \omega^2 (\Phi_a, \psi_0^a) \psi_0^a, \quad (8)$$

where H_a is the Hamiltonian of the unperturbed atom a and ψ_0^a is its eigenfunction. Then (7) becomes :

$$E_{abc} = \frac{24}{\pi^2} \int_0^\infty d\omega \int_0^\infty d\omega' V_a(\omega) \langle \Phi_b(\omega), \Phi_b(\omega') \rangle U_c(\omega'), \quad (9)$$

where

$$U_c(\omega) = \langle \Phi_a, V_a \psi_0^a \rangle \quad (10)$$

is the polarizability evaluated at an imaginary frequency $i\omega$, which enters the calculations for a pair of atoms [11].

In the case of three hydrogen atoms at large distances apart, (9) can be reduced to :

$$E_{abc} = \frac{\gamma_{abc} (3 \cos \theta_a \cos \theta_b \cos \theta_c + 1)}{R_{ab}^3 R_{bc}^3 R_{ca}^3}, \quad (11)$$

where θ_a , θ_b and θ_c are the inner angles of the triangle formed by the three atoms and

$$\gamma_{abc} = \frac{72}{\pi^2} \int_0^\infty d\omega \int_0^\infty d\omega' u(\omega) \langle \phi(\omega), \phi(\omega') \rangle u(\omega'), \quad (12)$$

where

$$u(\omega) = \langle \phi(\omega), z\psi_0 \rangle \quad (13)$$

and

$$\{(H - E_0)^2 + \omega^2\}\phi(\omega) + \frac{\partial \psi_0}{\partial z} = 0, \quad (14)$$

z being the cartesian coordinate of the electron.

3. CALCULATIONS

Equation (14) may be solved by minimizing the functional:

$$J = \langle \phi_t | (H - E_0)^2 + \omega^2 | \phi_t \rangle + 2 \left\langle \phi_t \left| \frac{\partial}{\partial z} \right| \psi_0 \right\rangle, \quad (15)$$

with respect to a trial function ϕ_t . For ϕ_t , we adopted:

$$\phi_t(\mathbf{r}) = \sum_{p=0}^n a_p r^{p-1} z \psi_0(\mathbf{r}) \quad (16)$$

and the convergence of ν_{abc} for n increasing up to 6 is shown in the table. Convergence is rapid and the long range non-additive three-body interaction is:

$$\frac{21.6425(3 \cos \theta_a \cos \theta_b \cos \theta_c + 1)}{R_{ab}^3 R_{bc}^3 R_{ca}^3} \quad (17)$$

correct to the figures shown.

Number of parameters	ν_{abc}
2	22.0044
3	21.6580
4	21.6437
5	21.6427
6	21.6425

Long range interaction of three hydrogen atoms.

Midzuno and Kihara [4] have given a simple formula for γ_{abc} :

$$\gamma_{abc} = \frac{3}{4} \alpha_b \nu_{ac}, \quad (18)$$

where α_b is the polarizability and ν_{ac} is the magnitude of the coefficient of the R^{-6} term in the long range two-body interaction. Using $\alpha_b = 4.5$ and $\nu_{ac} = 6.50$, (18) yields 21.9 in close agreement with the result of our more elaborate calculations†.

It is of interest to note that ν_{ac} may be expressed in terms of $\phi_t(\mathbf{r})$ [11] and for $n=6$ we obtain a value 6.49904 compared to the most accurate value available 6.499026 [14].

The research reported has been sponsored by Cambridge Research Laboratories OAR through the European Office, Aerospace Research, United States Air Force, under Grant No. AF 61 (052)-780. It has in addition been partly supported by the Atomic Energy Research Establishment, Harwell.

† Dr. R. J. Bell informs us in a private communication that he has recently derived a value of 21.643 ± 0.002 by an extension of a summation technique used to evaluate two-body interactions [15].

REFERENCES

- [1] AXILROD, B. M., and TELLER, E., 1943, *J. chem. Phys.*, **11**, 299.
- [2] MUTO, Y., 1943, *Proc. phys.-math. Soc. Japan*, **17**, 629.
- [3] AXILROD, B. M., 1949, *J. chem. Phys.*, **17**, 1349.
- [4] MIDZUNO, Y., and KIHARA, T., 1956, *J. phys. Soc. Japan*, **11**, 1045.
- [5] KIHARA, T., 1958, *Advanc. chem. Phys.*, **1**, 267.
- [6] McLACHLAN, A. D., 1963, *Mol. Phys.*, **6**, 423.
- [7] MUSER, J. I., 1963, *J. chem. Phys.*, **39**, 2409.
- [8] KESTNER, N. R., and SINANOGLU, O., 1963, *J. chem. Phys.*, **38**, 1730.
- [9] LINDER, B., and HOERNSCHEMEYER, D., 1964, *J. chem. Phys.*, **40**, 622.
- [10] LINDER, B., 1964, *J. chem. Phys.*, **40**, 2003.
- [11] CHAN, Y. M., and DALGARNO, A., 1965, *Mol. Phys.* **9**, 349.
- [12] ROSE, M. E., 1958, *J. Math. Phys.*, **37**, 215.
- [13] FONTANA, P. R., 1961, *Phys. Rev.*, **123**, 1865.
- [14] HIRSCHFELDER, J. O., and LOWDIN, P. O., 1959, *Mol. Phys.*, **2**, 229.
- [15] BELL, R. J., 1965, *Proc. phys. Soc., Lond.* **86**, 17.

An electron spin resonance and polarographic study of the sulphone group

by R. GERDIL and E. A. C. LUCKEN

Cyanamid European Research Institute, Cologne/Geneva, Switzerland

(Received 24 May 1965)

The electron spin resonance spectra of the radical anions of diphenyl sulphone, dibenzothiophene S, S-dioxide and thianthrene S, S, S', S'-tetroxide have been measured and the proton hyperfine splitting constants assigned to the various protons by measurement of the spectra of deuterio and methyl derivatives.

The experimentally determined spin populations were correlated by molecular orbital calculations, using the formalism of Koch and Moffit to describe the sulphone group, and it is shown that irrespective of the mutual orientation of this group and the conjugated system it may be described as far as the electron spin resonance spectra are concerned as contributing a vacant symmetric orbital to the conjugated system whose coulomb integral (α_{SO_2}) and sulphur carbon resonance integral ($\beta_{\text{C-SO}_2}$) are given by $\alpha_{\text{SO}_2} = \alpha_{\text{C}} - 2.0\beta$, $\beta_{\text{C-SO}_2} = 0.8\beta$ where α and β are the carbon coulomb integral and carbon-carbon resonance integrals respectively. The polarographic half wave reduction potentials of these compounds and some of their methyl derivatives dissolved in anhydrous dimethylformamide were also determined and the effect of methyl substitution on this quantity is also well described by the above parameters for the sulphone group. Finally a difference between the results obtained here and those previously obtained by Vincow from the electron spin resonance spectrum of thioxanthone S, S-dioxide radical anion is noted and discussed.

1. INTRODUCTION

The electronic structure [1] of the sulphone group and the manner and extent of its interaction with an adjacent unsaturated carbon atom [2] have been the subject of extensive theoretical and experimental [3] investigations. Although some conjugative interaction seems well-established it does not appear to have the extreme orientation dependence of, say, that of the analogous nitro group whose effect is quite different if coplanarity of the nodal planes of the nitro π -system and carbon π -system is prevented. This of course is to some extent an expected consequence of the supposed use of the sulphur atom 3d orbitals in forming double bonds with the adjacent oxygen or carbon atoms.

The use of proton hyperfine structure in the electron spin resonance spectra of unsaturated organic free-radicals is now well-established as a method of investigating molecular wave-functions [4] and since diaryl sulphones have been shown to form metastable radical-anions by their reaction with potassium at low temperatures in ethereal solvents [5] we have investigated the spectra of a number of suitable compounds. In a recent paper [6] we showed that the effect of methyl substituents on the polarographic half-wave reduction potential of reducible conjugated systems was also a useful test of molecular wave functions, which gives results similar to those provided by electron spin resonance spectra and we also report here the results of an investigation of these same sulphones by this method.

In these ways we have attempted to obtain an adequate molecular orbital description of the sulphone group, particularly with respect to its conjugative ability and to determine what differences arise in this description, if any, as the mutual orientation of the sulphone group and the unsaturated system is changed.

2. RESULTS

Radical anions have been formed from dibenzothiophene S, S-dioxide (an example of Case I conjugation as explained below), diphenyl sulphone (Case II conjugation) and thianthrene S, S, S', S'-tetroxide in which the orientation of the sulphone group is such that the conjugation is intermediate between these two extremes. The proton hyperfine splitting constants in the electron spin resonance spectra of these three compounds are shown in table 1, together with the assignments of these constants to the various different protons in the molecules. For the

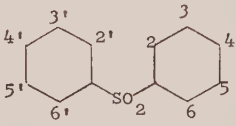
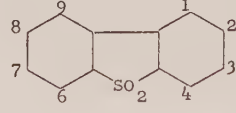
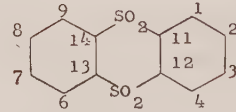
Compound	Splitting constants ± 0.03 gauss			
	a_1	a_2	a_3	a_4
(I) 	—	2.41	0.65	4.64
(II) 	< 0.2	2.50	2.16	< 0.4
(III) 	< 0.2	2.14	2.14	< 0.2

Table 1. Splitting constants of unsubstituted sulphone radical anions: diphenyl sulphone (I); dibenzothiophene S, S-dioxide (II); thianthrene S, S, S', S'-tetroxide (III).

thianthrene derivative these assignments follow from the spectra of the 2,7 dichloro and dimethyl compounds which are given in table 2. For dibenzothiophene S, S-dioxide the spectra of the 2,8, the 3,7 and the 4,6-dimethyl derivatives show that the two large proton splittings derive from the protons at the 2,8 and 3,7 positions (table 2). This is confirmed by the spectra of the 2,8 and 4,6-dideuterio derivatives (figure 1) which moreover show that the larger of these two splittings arises from the 2,8 protons. The assignment and the absolute values of the splitting constants reported here do not agree with those reported by Eargle and Kaiser [7]; we have, however, repeated these measurements on a number of occasions. The splitting constant of the para protons in diphenylsulphone follows directly from the spectrum (figure 2) while the assignment of the smallest splitting constant to the meta protons follows from the spectrum of the 3,3'-dimethyl derivative (table 2).

Compound	Spectrum
2,8-dimethyl dibenzo-thiophene dioxide	9 bands with approximately bi-nominal intensity ratios. Mean band separation 2.39 gauss.
3,7-dimethyl dibenzo-thiophene dioxide	Complex spectrum containing over 70 lines for which over-lapping made an unambiguous analysis difficult. Total width of 17.6 gauss shows that the methyl splitting is large.
4,6-dimethyl dibenzo-thiophene dioxide	1 : 4 : 6 : 4 : 1 quintet of separation 2.3 gauss. The lines within each band are not resolved.
3,3'-dimethyl diphenyl-sulphone	$a_2 = 2.10$, $a_6 = 2.24$, $a_{\text{methyl}} = a_5 = 0.59$, $a_4 = 4.89 \text{ gauss} \pm 0.03 \text{ gauss}$.
2,7-dimethyl thianthrene tetroxide	9 bands in approximately bi-nominal intensity ratios. Mean band separation 2.16 gauss.
2,7-dichloro thianthrene tetroxide	1 : 2 : 1 triplet of bands, separation 2.35 gauss.

Table 2. Electron spin resonance spectra of substituted radical anions.

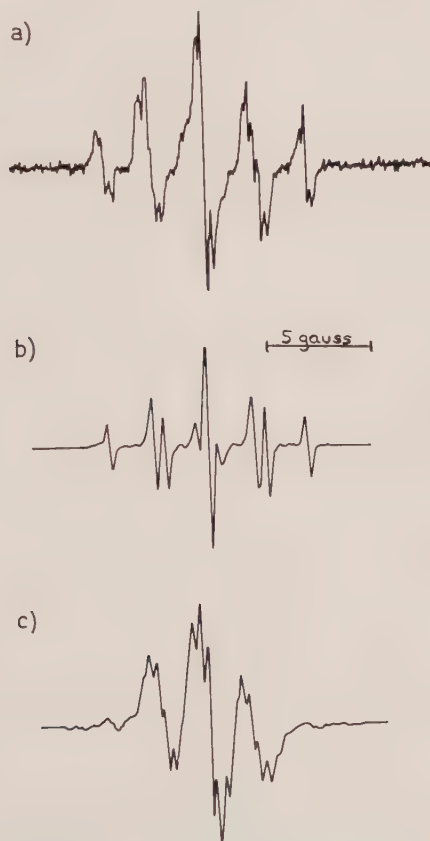


Figure 1. Electron spin resonance spectra of the radical anions of : (a) dibenzothiophene S, S-dioxide, (b) 4,6 dideuteriodibenzothiophene S, S-dioxide, (c) 2,8 dideuteriodibenzothiophene S, S-dioxide, formed by reaction with potassium in dimethoxyethane at 200°K. In (c) the small outer peaks are due to traces of undeuterated material.

The half-wave potentials (HWP) of the sulphones and their dimethylated derivatives reported here (table 3) are part of a more extensive polarographic study of the sulphone group which will be published later. Two well-defined waves of approximately equal height were observed for most of the compounds in anhydrous dimethylformamide (DMF) by using a dropping control device. The HWP of the first wave ($E_{1/2}^1$) corresponds to the uptake of one electron followed by the formation of the corresponding radical anion. This was demonstrated by controlled potential electrolysis in the cavity of the E.S.R. spectrometer.



Figure 2. Electron spin resonance spectrum of the radical anion of diphenyl sulphone formed by reaction with potassium in dimethoxyethane at 200°K.

Compound	$-E_{1/2}^1(\text{V})^\dagger$	I_d^\ddagger
Diphenylsulphone (I)	2.063	1.99
3,3'-dimethyl-	2.097	2.04
4,4'-dimethyl-	2.181	2.46
Dibenzothiophene dioxide (II)	1.732	1.90
2,8-dimethyl-	1.810	1.80
3,7-dimethyl-	1.814	1.85
4,6-dimethyl-	1.779	2.07
Thianthrene tetroxide (III)	1.311	1.77
2,7-dimethyl-	1.400	1.67

† Versus sat. Ag/AgCl electrode.

‡ [mA . lit . mole⁻¹ . mg^{-2/3} sec^{1/6}].

Table 3. Polarographic reduction potentials in anhydrous DMF.

For the present purpose only the first reduction wave is of significance and therefore only $E_{1/2}^1$ and I_d^1 values are listed in the table. A shift $\Delta E_{1/2}$ to more negative HWP was observed for all methylated derivatives and was calculated according to :

$$\Delta E_{1/2} = E_{1/2} (\text{methyl derivative}) - E_{1/2} (\text{parent compound}).$$

3. MOLECULAR ORBITAL CALCULATIONS

The coordinate system which, following Moffit [1], we use to describe the molecular orbitals of the sulphone group is shown in figure 3. The sulphur atom uses four essentially $3s3p^3$ hybrid orbitals to form single bonds to each of the

(a)	Available atomic orbitals and combinations thereof	(b) Symmetry		Moffit's nomenclature
		xz	yz	
π	$\phi_0(2p_x)$	S	A	$\phi_0(2p\pi)$
	$\frac{1}{\sqrt{2}} [\phi_0(2p_x) + \phi_0(2p_x)]$	S	A	$\phi_0(2pb_1)$
	$\frac{1}{\sqrt{2}} [\phi_0(2p_x) - \phi_0(2p_x)]$	A	A	$\phi_0(2pa_2)$
π	$\phi_R(2p\pi)$	A	S	$\phi_R(2p_y)$
	$\frac{1}{\sqrt{2}} [\phi_R(2p_y) + \phi_R'(2p_y)]$	A	S	$\phi_R(2pb_2)$
	$\frac{1}{\sqrt{2}} [\phi_R(2p_y) - \phi_R'(2p_y)]$	A	A	$\phi_R(2pa_2)$
	$\frac{1}{\sqrt{2}} [\phi_R(2p\pi) + \phi_R'(2p\pi)]$	S	S	$\phi_R(2pa_1)$
	$\frac{1}{\sqrt{2}} [\phi_R(2p\pi) - \phi_R'(2p\pi)]$	S	A	$\phi_R(2pb_1)$
σ, π	$\phi_S(3p_x)$	S	A	$\phi_S(3pb_1)$
σ, π	$\phi_S(3p_y)$	A	S	$\phi_S(3pb_2)$
σ	$\phi_S(3p_z)$	S	S	$\phi_S(3pa_1)$
π	$\phi_S(3d_{z^2})$	S	S	$\phi_S(3da_1)$
π, σ	$\phi_S(3d_{xz})$	S	A	$\phi_S(3db_1)$
π	$\phi_S(3d_{yz})$	A	S	$\phi_S(3db_2)$
π	$\phi_S(3d_{xy})$	A	A	$\phi_S(3da_2)$
π	$\phi_S(3d_{x^2-y^2})$	S	S	$\phi_S(3da_1')$

Table 4. Atomic orbitals available for the construction of a MO model of conjugated sulphones. (a) Type of bonding in which the orbitals are preferentially involved. Most of the a.o. involved in σ -bonding have been left out of the table. (b) Symmetry is given with respect to the xz - and yz -plane of figure 3.

oxygen and carbon atoms and we will not discuss these further. In table 4 are shown the orbitals which are available for π -type delocalization, together with their symmetry classification and Moffit's nomenclature. Moffit showed that the remaining four electrons, two on the sulphur atom and one on each of the oxygen atoms, are accommodated on molecular orbitals of the form:

$$S, A: \Psi(xb_1) = \gamma_0 \phi_0(2pb_1) + \gamma_s \phi_s(3p_x) + \gamma'_s \phi_s(3d_{xz}),$$

$$A, A: \Psi(va_2) = \delta_0 \phi_0(2pa_2) + \delta_s \phi_s(3d_{xy})$$

and estimated that the residual charge on the sulphur atom was approximately +0.5.

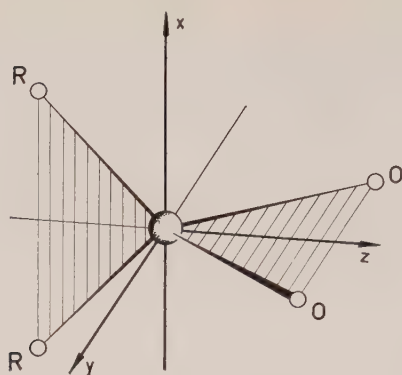


Figure 3. Reference frame for the tetrahedral sulphone R_2SO_2 . The sulphur atom is located at the centre; the O-S-O group lies in the yz -plane, and the R-S-R group lies in the xz -plane.

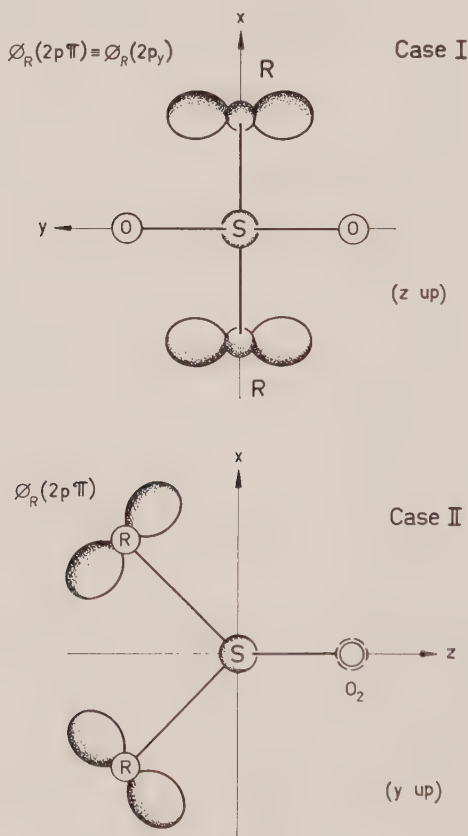


Figure 4. Two extreme orientations of the group $R \pi$ -orbital with respect to the SO_2 -group. Case I conjugation: the nodal plane of $\phi_R(2p\pi)$ lies in the xz -plane and its main axis is parallel to the O-S-O plane. Case II conjugation: the nodal plane of $\phi_R(2p\pi)$ is perpendicular to the xz -plane and its main axis lies in the xz -plane. The planes xz and yz are planes of symmetry.

Two extreme situations arise with the RSR' group according to whether the nodal plane of $\phi_R(2p\pi)$ lies in, or perpendicular to the $R-S-R'$ plane. These two situations are illustrated in figure 4 and are called by Koch and Moffit [2] Case I and Case II conjugation.

In Case I, $\phi_R(2p\pi)$ is identical with a carbon ($2p_y$) orbital and interactions can formally take place in the following ways:

$$\begin{aligned} A, S: \phi_R + \phi_{R'} &\leftrightarrow \phi_S(3p_y); \quad \phi(3d_{yz}). \\ A, A: \phi_R - \phi_{R'} &\leftrightarrow \Psi(va_2). \end{aligned}$$

The interaction of symmetry A, S does not affect the SO_2 -group, but simply contributes to the overall delocalization particularly as the sulphur atom has a formal charge of about $+0.5$. In the totally antisymmetrical combination, interaction can occur with the doubly occupied $\Psi(va_2)$ orbital and then affects the SO_2 group properties.

For Case II conjugation the following interactions are theoretically possible:

$$\begin{aligned} S, S: \phi_R + \phi_{R'} &\leftrightarrow \phi_S(3d_{z^2}); \quad \phi_S(3d_{x^2-y^2}). \\ S, A: \phi_R - \phi_{R'} &\leftrightarrow \Psi(xb_1). \end{aligned}$$

The interaction with $\Psi(xb_1)$ is expected to be small because of the strong bonding character of this sulphone orbital. Therefore, the main interaction will occur with the totally symmetric vacant d -orbitals which will also contribute to the overall delocalization.

The carbon atomic orbitals $\phi_R, \phi_{R'}$ are of course not isolated but form part of a conjugated system. It is therefore appropriate to replace them by molecular orbitals χ_R^i and $\chi_{R'}^j$ of which in general there will be a large number. Moreover although if the groups R and R' are independent as in diphenyl sulphone, the combinations $\chi_R^i \pm \chi_{R'}^i$ are degenerate; when R and R' are connected, as in dibenzothiophene S, S-dioxide, they in general have different energies. In figure 5 (extreme left-hand and right-hand columns) are shown the energy levels for two hypothetical molecules in which the groups R and R' are independent and which can take up either the Case I or Case II orientations. The only molecular orbitals shown are those corresponding to highest occupied and lowest unoccupied levels. In the central column of figure 5 are shown the molecular π -orbitals of the sulphone group, the order and approximate values of their energies is that given by Moffit. Finally in the two remaining columns are shown the resultant molecular orbitals for the two neutral sulphones corresponding to Case I and Case II conjugation.

Although the details of the diagram will be different from one molecule to another, calculations, on both diphenyl sulphone and dibenzothiophene dioxide for a wide range of the parameters used to describe the various orbitals of the sulphone group, reveal that for the neutral molecules in Case I conjugation the lowest unoccupied orbital—and thus the orbital holding the unpaired electron in the radical-anion—is always $A, S (=b_2)$ while for Case II conjugation it is $S, S (=a_1)$. These have in common the fact that they both arise from the symmetrical combinations $\chi_R^i + \chi_{R'}^i$. Therefore, since the distribution of spin population is largely determined by the odd electron distribution, a satisfactory description of the sulphone group in so far as the electron spin resonance spectra of the radical anions is concerned will be obtained in both cases by treating the sulphone group as

supplying a vacant symmetric orbital to the conjugated system while the molecular orbital parameters ascribed to the remaining sulphone orbitals will not affect the theoretical odd electron distribution. This fact has already been noted by Vincow for Case I conjugation in his discussion of the electron spin resonance spectrum of the thioxanthone S, S-dioxide radical-anion [8].

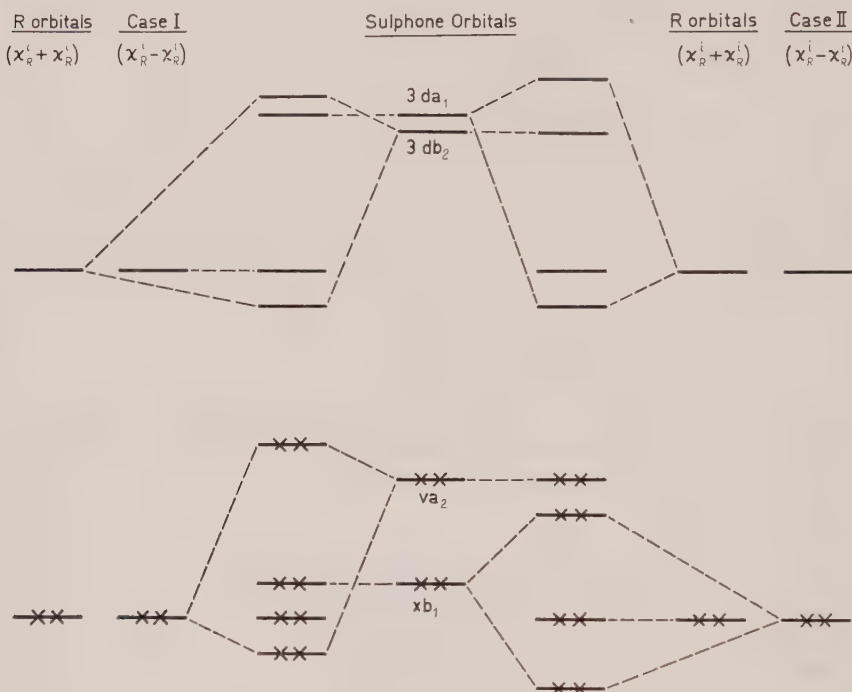


Figure 5. Correlation diagram for the conjugation of sulphones. The unlabelled levels to the left and right of the central column are the resultant molecular orbitals for Case I and Case II conjugation respectively.

The investigation reported here has of course been enormously simplified by this coincidence. Nevertheless it should be clearly realized that it imposes a limitation on the sensitivity of the electron spin method in this particular case since the proton hyperfine spectra only reveal part of the behaviour of the sulphone group.

With this model of the sulphone group the Hückel molecular π -orbitals of the molecule were calculated in the usual way. The coulomb integral of the vacant orbital and its resonance integral with the adjacent carbon $2p_\pi$ orbital were expressed as:

$$\begin{aligned}\alpha_{\text{SO}_2} &= \alpha + \gamma\beta, \\ \beta_{\text{C-SO}_2} &= \delta\beta,\end{aligned}$$

where α and β are the coulomb integral of a carbon $2p_\pi$ orbital and the carbon-carbon $2p_\pi$ resonance integral respectively. From these orbitals is obtained the odd electron population at an atom r , given by the square of the coefficients C_{or} of

$\delta \backslash \gamma$	-3.0	-2.0	-1.0	
Diphenylsulphone				
0.4	0.0484	0.0522	0.0500	a_2
	0.0360	0.0306	0.0104	a_3
	0.1601	0.1496	0.0868	a_4
0.6	0.0562	0.0628	0.0663	a_2
	0.0304	0.0228	0.0075	a_3
	0.1540	0.1392	0.0938	a_4
0.8	0.0660	0.0749	0.0823	a_2
	0.0247	0.0166	0.0053	a_3
	0.1482	0.1332	0.1026	a_4
Dibenzothiophene dioxide				
0.4	0.0730	0.0608	0.0241	a_1
	0.0298	0.0370	0.0507	a_2
	0.1498	0.1389	0.0758	a_3
	0.0080	0.0026	0.0061	a_4
0.6	0.0553	0.0384	0.0167	a_1
	0.0429	0.0550	0.0627	a_2
	0.1350	0.1108	0.0520	a_3
	0.0007	0.0016	0.0257	a_4
0.8	0.0388	0.0255	0.0165	a_1
	0.0583	0.0696	0.0737	a_2
	0.1132	0.0833	0.0405	a_3
	0.0022	0.0157	0.0473	a_4
Thianthrene tetroxide				
0.4	0.0007	0.0021	0.0080	a_1
	0.1114	0.0962	0.0453	a_2
0.6	0.0030	0.0072	0.0175	a_1
	0.0983	0.0786	0.0441	a_2
0.8	0.0080	0.0155	0.0313	a_1
	0.0857	0.0675	0.0459	a_2

Table 5. Odd-electron populations in the radical anions of diphenyl sulphone, dibenzothiophene dioxide and thianthrene dioxide, calculated for various values of the coulomb integral $\alpha_{OS_s} = \alpha + \gamma\beta$ and the carbon-sulphur resonance integral, $\beta_{C-SO_2} = \delta\beta$ of the sulphone group.

the atomic orbital ϕ_r in the singly-occupied molecular orbital ψ_0 , (where $0=j+1$, first antibonding MO). From this the spin-population, ρ_r , was calculated according to McLachlans' equation [9]:

$$\rho_r = C_{or}^2 + \lambda \sum_s C_{or}^2 \pi_{rs},$$

where π_{rs} is the atom-atom polarizability and λ is a parameter whose order of magnitude is unity and to which we have assigned the value 1.2.

The hyperfine coupling constant of the proton attached to atom r was then calculated from the equation:

$$a_r = Q\rho_r,$$

where Q has been given the value 25 gauss.

Since spin-populations are obtained by applying a first-order correction to the odd-electron populations we initially calculated the odd-electron distribution ($C_{j+1,r}^2$) for the three molecules under study for a wide range of parameter values. These results are shown in table 5.

4. DISCUSSION

(a) *E.S.R. spectra*

For diphenyl sulphone it was apparent that a value of $\gamma = -2.0$, $\delta = 0.8$ should yield satisfactory results and therefore a complete spin-population calculation was performed for these values to yield the spin-population distribution and hyperfine splitting constants shown in table 6. The agreement with experiment is extremely good.

For dibenzothiophene dioxide, the example of Case I conjugation, it is evident that the situation is much less straightforward. In order to achieve high spin-population in the 2 and 3 positions it is certainly necessary to use parameter values in the same region as those employed for Case II conjugation. However, the odd-electron population at position 3 is calculated to be greater than that in position 2 while experimentally the converse is true.

A complete spin-population calculation was, however carried out for $\gamma = -2.0$, $\delta = 0.8$ with the results shown in table 6. The best that can be said for them is that the pattern and order of magnitude of splitting constants is correctly predicted. From the results shown in table 5, it is apparent that the simple description of the sulphone group used here is not completely adequate, nevertheless similar parameter values can be used to describe the sulphone group in both Case I and Case II conjugation.

A possible cause of the poor agreement between theory and experiment might be an effect of the sulphone group on the β carbon atoms. Thus Rieger and Fraenkel [10] observed that in aromatic carbonyl compounds where the carbonyl group is locked in the plane of the ring the coupling constants of the two ortho and meta protons were considerably different and ascribed this to a decrease in the coulomb integral of the carbon atom adjacent to the oxygen atom of the carbonyl group brought about by the large negative charge on the oxygen atom. However it did not seem profitable to introduce yet another parameter into the description of the sulphone group and this hypothesis was not pursued further.

In thianthrene tetroxide which is non-planar [11] and where the conjugation is presumably intermediate between Case I and II almost all the parameter values tried produce the correct pattern of splitting constant, i.e. large on the 2,3,7,8 and small on the 1,4,6,9 positions. The results of a spin population calculation for the same parameter values as used previously, $\gamma = -2.0$, $\delta = 0.8$, are shown in table 6 and again fair agreement with experiment is obtained. Although it is difficult to say quantitatively what is the effect of the bending of the molecule on the resonance integral β_{C-SO_2} it is likely that it will be reduced. It is perhaps significant that the agreement with experiment for thianthrene S, S-tetroxide for the parameter values $\gamma = -2.0$, $\delta = 0.6$ is much better for both E.S.R. (table 6) and polarographic (figure 6) results.

A feature of the spectrum of this radical is the weak satellites flanking each line whose intensities suggest that they are due to ^{13}C in natural abundance in one of the three possible positions. The fourfold symmetry of the molecule makes it

Position	ρ_r	a_r
Diphenyl sulphone radical anion $\gamma = -2.0, \delta = 0.8$		
2	0.0874	2.18
3	-0.0224	0.56
4	0.1786	4.46
Dibenzothiophene dioxide radical anion $\gamma = -2.0, \delta = 0.8$		
1	0.0006	0.015
2	0.0659	1.65
3	0.0844	2.11
4	-0.0060	0.15
Thianthrene tetroxide radical anion $\gamma = -2.0, \delta = 0.8$		
1	-0.0119	0.30
2	0.0717	1.79
11	0.1259	—
$\gamma = -2.0, \delta = 0.6$		
1	-0.0257	0.64
2	0.0807	2.17
11	0.1387	—

Table 6. Spin populations and proton hyperfine coupling constants in the radical anions of diphenyl sulphone, dibenzothiophene dioxide and thianthrene dioxide calculated for the odd electron populations from McLachlan's equation with $\lambda = 1.2$, $Q = 25$ gauss.

impossible, however, to decide which position gives rise to the splitting. The coupling constant is 2.04 gauss, and from the sharpness of the spectrum all other ^{13}C coupling constants must be considerably less than this. From the spin density distribution calculated for $\gamma = -2.0$, $\delta = 0.8$ and using the theory and parameter values of Karplus and Fraenkel [12] the ^{13}C coupling constants for the 1 and 2 positions may be calculated as -3.18 and $+1.72$ gauss respectively, while for $\gamma = -2.0$, $\delta = 0.6$ they are -4.05 and $+2.24$. For the carbon atoms bonded to the sulphone groups the parameters Q_{CS}^{C} and Q_{SC}^{C} are not available. However, it would seem probable that because of the high spin population on these atoms they would have a ^{13}C splitting of greater than 2.5 gauss. These estimates are therefore inconclusive and further discussion is pointless until the carbon atom giving rise to the splitting should be known.

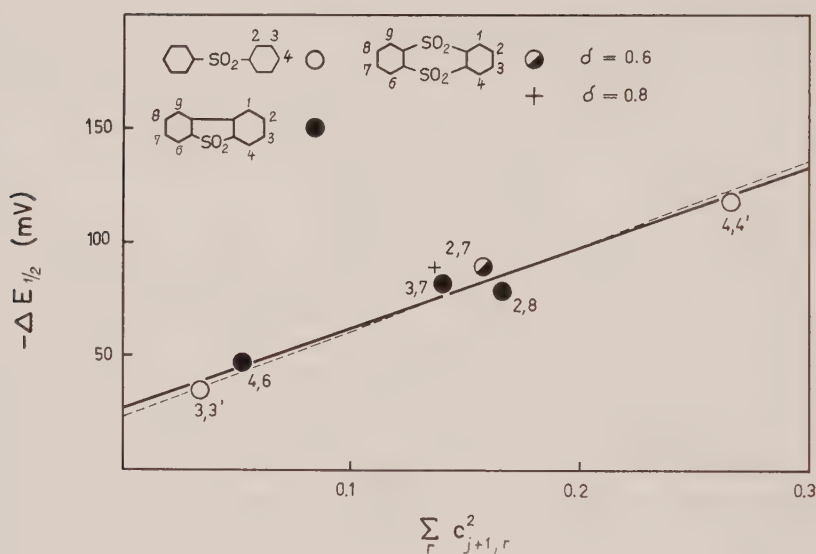


Figure 6. Dependence of the HWP shifts on the inductive effect of the methyl groups for $\gamma = -2.0$ and $\delta = 0.8$. The numbers refer to the site of the substitution. The dotted line depicts the polarographic correlation for the methyl substituted dibenzothiofenenes and dibenzofurans.

It may be concluded that the values $\gamma = -2.0$ and $\delta = 0.8$ give a fairly good description of the sulphone group both in Case I and II conjugation. It remains to compare this result with that previously obtained by Vincow for Case I conjugation in a study of thioxanthone dioxide radical anion [8]. Excellent agreement with experiment was obtained with the values $\gamma = -3.0$, $\delta = 0.4$, however reference to table 5 shows that this would produce completely incorrect values for dibenzothiofene dioxide. Vincow, however, performed no experiments which enabled him to assign the splitting constants to the four different atoms on this molecule and his assignments were based on agreement with theory and the argument that this placed the largest splitting constants ortho and para to the carbonyl group in agreement with the spectrum of benzophenone ketyl. At the time Vincow wrote his paper, the spectrum of diphenylsulphone radical anion

was unknown; the measurements reported here show that the splitting constants ortho and para to the sulphone group are even larger than in the case of the carbonyl compound. This argument is, therefore, invalid, and it is our opinion that the large splitting constants in thioxanthone dioxide are probably due to the protons in the 2 and 3 positions by analogy with the spectra of the 'unmixed' radical anions of anthrasemiquinone [13, 14] and thianthrene tetroxide, although we have no experimental evidence to offer on this point. Unfortunately, however, the spin populations in thioxanthone dioxide radical anion with $\gamma = -2.0$ and $\delta = 0.7$, taken from Vincow's paper are 0.0668, 0.0049, 0.109 and -0.0324 for the 1,2,3 and 4 positions respectively, compared with the experimental spin densities, of 0.135, 0.102, 0.036 and 0.023. (Note that the order in which these numbers are given does not imply an assignment to particular protons.)

It would seem, therefore, that we have arrived at an impasse. A solution to the problem could lie in the values used by Vincow to describe the carbonyl group, although these give satisfactory results for the *p*-benzosemiquinones [12]. However, until the assignment of the splitting constants has been determined experimentally, further discussion on this point would be vain.

(b) Polarographic reduction

The interpretation of the variations $\Delta E_{1/2}$ occurring in the HWP of the compounds under methyl-substitution is based on the assumption that $\Delta E_{1/2}$ is proportional to the first order inductive perturbation produced by the methyl groups on the lowest antibonding MO($j+1$). This was recently shown to be true for dibenzothiophene and dibenzofuran [6] and is now successfully applied to support the choice of the MO's used to account for the observed HFS constants of the sulphones. Inspection of tables 3 and 5 shows that only two sets of parameters give good correlation between the potential shifts and the inductive effect. When the values $\gamma = -2.0$, $\delta = 0.8$ are used (which also gives the best results for the E.S.R.-calculations) the data are closely distributed along the formerly determined regression line of other dimethylated isologs (figure 6). The other set of values $\gamma = -1.0$ and $\delta = 0.6$ also yields a good correlation among the experimental data but the regression line has a slightly different orientation from the preceding one. On polarographic ground alone it is of course not possible to make an unambiguous choice between the two correlations.

Dimethylthianthrene tetroxide, which displays a steric configuration of the sulphone group intermediate between those of dibenzothiophene dioxide and diphenyl sulphone, gives the less satisfactory fitting of the regression line when a planar configuration of the molecule is assumed ($\gamma = -2.0$, $\delta = 0.8$). It is however interesting to point out that when a smaller value for $\beta_{\text{C-SO}_2}$ is used for thianthrene tetroxide, which is consistent with a bending of the molecule, a significant improvement of the polarographic correlation (see figure 6) as well as of the E.S.R. calculations, is obtained.

5. EXPERIMENTAL

Electron spin resonance spectra were measured at -70°C on a 'Microspin' spectrometer at a radiofrequency of 9600 Mc/s. The field sweep was calibrated at frequent intervals against a solution of the naphthalene radical anion in dimethoxyethane.

Preparation of sulphones. Diphenyl sulphone was a purified commercial product. Thianthrene S, S, S', S'-tetroxide [15] and its 2,7 dichloro and dimethyl [16] derivatives, dibenzothiophene S, S-dioxide [17] and the dimethyl diphenylsulphone [18] were prepared by standard methods. The preparation of the deuterated and methylated dibenzothiophene S, S-dioxides is given in reference [19].

Preparation of radical anions. The radical anions were performed as in reference [19].

Molecular orbital calculations. These were performed in part on an IBM 1620 computer and in part on an Elliot 803 computer. The Hückel molecular orbitals were determined in the usual way and the atom-atom polarizabilities determined from them. For the calculations performed on the IBM instrument the spin densities were then calculated by hand from these data, for the remainder of the calculations a programme was devised for the Elliot 803 which gave the odd electron densities and $1/\lambda$ times the corrections which produce the spin densities from these (i.e. the second term in McLachlan's equation). This procedure enabled the effect of changes Q and λ to be investigated with great ease.

Polarography. The reductions were carried out in anhydrous DMF with 0.15 M tetra-*n*-butylammonium iodide as supporting electrolyte. The method (rapid polarography) and the apparatus are the same as described elsewhere [6].

We thank Professor E. Heilbronner for kindly carrying out the calculations on the IBM 1620 and Dr. G. Klopman for his help in programming the calculations for the Elliot 803.

REFERENCES

- [1] MOFFIT, W. E., 1950, *Proc. roy. Soc. A*, **200**, 409.
- [2] KOCH, H. P., and MOFFIT, W. E., 1951, *Trans. Faraday Soc.*, **47**, 7.
- [3] PRICE, C. C., and OAE, S., 1962, *Sulfur Bonding* (Ronald Press).
- [4] CARRINGTON, A., 1963, *Quart. Rev. chem. Soc., Lond.*, **17**, 67.
- [5] Gerdil, R., and Lucken, E. A. C., 1963, *Proc. chem. Soc., Lond.*, p. 144.
- [6] Gerdil, R., and Lucken, E. A. C., to be published.
- [7] EARGLE, D. H., and KAISER, E. T., 1964, *Proc. chem. Soc., Lond.*, p. 22.
- [8] VINCOW, G., 1962, *J. chem. Phys.*, **37**, 2484.
- [9] McLACHLAN, A. D., 1960, *Mol. Phys.*, **3**, 233.
- [10] RIEGER, P. H., and FRAENKEL, G. K., 1962, *J. chem. Phys.*, **37**, 2811.
- [11] HOSOYA, S., 1963, *Acta Cryst.*, **16**, 310.
- [12] KARPLUS, M., and FRAENKEL, G. K., 1961, *J. chem. Phys.*, **35**, 1312.
- [13] BRANDON, R. W., and Lucken, E. A. C., 1961, *J. chem. Soc.*, p. 4273.
- [14] VINCOW, G., and FRAENKEL, G. K. 1961, *J. chem. Phys.*, **34**, 1333.
- [15] GRAEBE, C., 1876, *Annalen*, **179**, 181.
- [16] BAW, H., BENNETT, G. M., and DEARNS, P., 1934, *J. chem. Soc.*, p. 683.
- [17] GILMAN, H., and ESMAY, D. L., 1952, *J. Amer. chem. Soc.*, **74**, 2021.
- [18] TRUCE, W. E., TATE, D. P., and BURDGE, B. N., 1960, *J. Amer. chem. Soc.*, **82**, 2874.
- [19] Gerdil, R., and Lucken, E. A. C., 1965, *J. Amer. chem. Soc.*, **87**, 213.

The intensity of the symmetry-forbidden electronic band of biphenylene

by J. W. HILPERN

Department of Chemistry, The University, Sheffield 10

(Received 31 May 1965)

The intensity of the symmetry-forbidden B_{1g} electronic band of biphenylene has been calculated. A value a sixth of that observed for the $358\text{ m}\mu$ band is obtained suggesting that it is possibly part of the B_{1g} band.

1. INTRODUCTION

Murrell and Pople [1] have applied the general theory of Herzberg and Teller [2] of the absolute intensity of weak, symmetry forbidden bands to the intensities of the symmetry forbidden bands of benzene. We were interested in the intensity of the lowest-forbidden B_{1g} electronic band of biphenylene. It has been suggested by Hilpern [3] that the medium intense ($\epsilon_{\text{max}} = 10^4$) band at $\lambda_{\text{max}} = 358\text{ m}\mu$ is B_{1g} and made allowed by a b_{2u} vibration. Hochstrasser [4] suggested that a b_u vibration occurred in the weak band at $392\text{ m}\mu$. It has been postulated [3] that this band is the origin of the medium intense band at $358\text{ m}\mu$ and we are concerned with a larger effect of a b_u vibration giving rise to this medium intense band. The assignment of the allowed band ($\epsilon_{\text{max}} = 10^5$) at $248\text{ m}\mu$ is reasonably well established [3, 5] and has B_{3u} symmetry. Before we could apply Murrell and Pople's method we had first to calculate the b_{2u} normal vibrations.

2. CALCULATION OF b_{2u} NORMAL VIBRATIONS

There are five b_{2u} normal vibrations (in plane) of biphenylene if we ignore the hydrogen atoms.

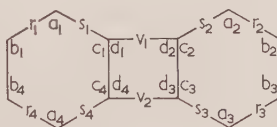


Figure 1. Internal valence coordinates of biphenylene.

We take the seven symmetry coordinates:

$$\begin{aligned} S_1 &= \frac{1}{2}(r_1 + r_2 - r_3 - r_4), \\ S_2 &= \frac{1}{2}(s_1 + s_2 - s_3 - s_4), \\ S_3 &= 1/\sqrt{2}(v_1 - v_2), \\ S_4 &= R/2(a_1 + a_2 - a_3 - a_4), \\ S_5 &= R/2(b_1 + b_2 - b_3 - b_4), \\ S_6 &= R/2(c_1 + c_2 - c_3 - c_4), \\ S_7 &= R/2(d_1 + d_2 - d_3 - d_4). \end{aligned}$$

Removal of the redundancy gives rise to five independent symmetry coordinates :

$$\begin{aligned} S_1' &= -\sqrt{3}(S_1 + S_2) + \frac{2S_4}{R} + \frac{(S_5 + S_6)}{R}, \\ S_2' &= S_1 - S_2, \\ S_3' &= -\sqrt{3}(S_1 + S_2) + \frac{2S_4}{R} - \frac{(S_5 + S_6)}{R}, \\ S_4' &= S_5 - S_6, \\ S_5' &= \frac{1}{2}S_3 - \frac{1}{2}\frac{S_7}{R}. \end{aligned}$$

The G matrix was calculated in terms of vector for each atom, cf. Wilson, Decius and Cross [6]:

$$G_{ll'} = \sum_{\alpha=1}^{12} \mu_{\alpha} \mathbf{S}_{l\alpha} \cdot \mathbf{S}_{l'\alpha},$$

using normalized symmetry coordinates. The G matrix becomes:

G	S_1'	S_3'	S_5'	S_2'	S_4'
S_1'	μ_c	$\frac{\mu_c}{\sqrt{5}}$	$\frac{\mu_c}{2}$	0	0
S_3'		μ_c	$\frac{\mu_c}{2\sqrt{5}}$	0	0
S_5'			μ_c	$0.34\mu_c$	$-0.65\mu_c$
S_2'				μ_c	$-0.56\mu_c$
S_4'					μ_c

where $\mu_c = 0.08328$.

The F matrix for internal coordinates was formed and transformed by β , the transformation matrix, to the F matrix for symmetry coordinates:

$$F_{\text{symm coord}} = \beta F_{\text{int coord}} \beta'.$$

The FG matrix was obtained.

We initially took the same valence force constants as Scully and Whiffen [7], taking only diagonal force constants. The units are m dyn/Å

$$f_{aa} = f_{bb} = f_{cc} = f_{dd} = 1.0; \quad f_{ss} = f_{rr} = f_{vv} = 5.5.$$

Diagonalization of the FG matrix using these force constants gave five roots, the highest value corresponding to a frequency of 624 cm^{-1} . Hochstrasser [4] gave a value of 792 cm^{-1} as the b_u vibration he observes. Increasing f_{dd} , the valence force constant for the central restricted 90° angle to 3 m dyn/Å gives roots, the highest value corresponding to a frequency of 785 cm^{-1} :

$$\nu_1 = 505 \text{ cm}^{-1},$$

$$\nu_2 = 785 \text{ cm}^{-1},$$

$$\nu_3 = 79 \text{ cm}^{-1},$$

$$\nu_4 = 222 \text{ cm}^{-1},$$

$$\nu_5 = 135 \text{ cm}^{-1}.$$

The L matrix, the matrix of the characteristic vectors of the roots, is also obtained and from these the five normal vibrations, Q_K ,

$$Q_K = \sum_{l=1}^5 L_{Kl} S_l.$$

The vibrations are normalized so that the sum of the squares of the displacements is unity and are shown in figure 2.

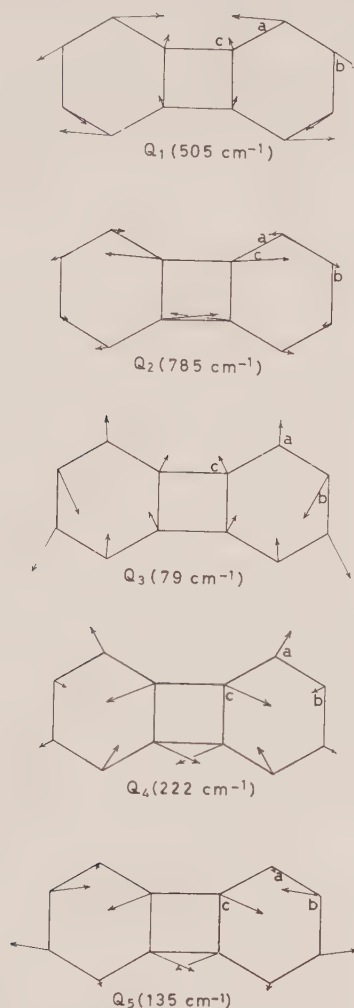


Figure 2. Normal coordinates of biphenylene, $b_2 u$. Angles as shown and the magnitude of the displacement vector given in brackets:

$$\begin{aligned}
 Q_1 : & \quad a = 34^\circ(0.42), \quad b = 58^\circ(0.25), \quad c = 72^\circ(0.11), \\
 Q_2 : & \quad a = 23^\circ(0.12), \quad b = 69^\circ(0.07), \quad c = 25^\circ(0.48), \\
 Q_3 : & \quad a = 117^\circ(0.21), \quad b = 28^\circ(0.42), \quad c = 63^\circ(0.16), \\
 Q_4 : & \quad a = 91^\circ(0.24), \quad b = 63^\circ(0.12), \quad c = 67^\circ(0.42), \\
 Q_5 : & \quad a = 31^\circ(0.05), \quad b = 98^\circ(0.31), \quad c = 67^\circ(0.39).
 \end{aligned}$$

It should be emphasized that this method is very approximate. One cannot strictly transfer force constants from molecule to molecule although Scully and Whiffen [7] and Freeman and Ross [8] have had some success in interpreting in plane vibrations of naphthalene using Whiffen's [9] force constants from benzene; these are also the force constants used here. Increasing the force constant of the central angle is reasonable since it is much more restricted but a detailed analysis for a molecule with a similarly restricted angle is not available.

In view of the fact that this force constant gave a reasonable result it was used. It was not considered useful to put in the off-diagonal elements since the calculation is already approximate.

3. CALCULATION OF THE INTENSITY OF THE LOWEST SYMMETRY FORBIDDEN BAND OF BIPHENYLENE

The method followed was that outlined by Murrell and Pople [1]. The transition density, $\rho_{p\beta}$, was calculated.

The wave functions are:

$$p = \psi_1^{-1} \quad (B_{1g}),$$

$$\beta = \frac{1}{\sqrt{2}} (\psi_1^{-2} + \psi_2^{-1}) \quad (B_{3u}),$$

so

$$\begin{aligned} \rho_{p\beta} &= \left\langle \psi_1^{-1} \left| \frac{1}{\sqrt{2}} (\psi_1^{-2} + \psi_2^{-1}) \right. \right\rangle \\ &= \frac{1}{\sqrt{2}} \{ \langle \psi_1^{-1} | \psi_1^{-2} \rangle + \langle \psi_1^{-1} | \psi_2^{-1} \rangle \} \\ &= \frac{1}{\sqrt{2}} (\theta_{-1}\theta_{-2} + \theta_2\theta_1), \end{aligned}$$

where θ_1, θ_{-1} and θ_2, θ_{-2} are the highest and second highest bonding and anti-bonding molecular orbitals respectively [10].

This is expanded in terms of atomic orbitals and product terms $\phi_\sigma \phi_\tau$ ($\sigma \neq \tau$) omitted, $\rho_{p\beta}$ can then be represented as in figure 3, each coefficient measuring a density $-e\phi_\sigma^2$ at position σ . The interaction energy of this density function with the five perturbing sets of dipoles is estimated by replacing the distribution $-K\phi_\sigma^2$ by a point charge $-Ke$ at position σ and evaluating its energy in the field of all the dipoles (there is no interaction between the dipole at centre σ and the charge distribution σ_σ^2). The interaction energies are $-0.110(Q_1)e^2$, $-0.156e^2(Q_2)$, $-0.070e^2(Q_3)$, $0.119e^2(Q_4)$, $-0.021e^2(Q_4)$. The ratio for the oscillator strengths is given by:

$$\frac{f_p}{f_\beta} = \frac{E_p}{F_\beta(F_\beta - F_p)} \times \frac{h}{8\pi^2\mu} \times \frac{(\text{interaction energy})^2}{\text{normal vibration frequency (cm}^{-1}\text{)}}.$$

Energy of the β band is $40\,250\text{ cm}^{-1}$. Mean energy of p band $29\,410\text{ cm}^{-1}$. The results of substituting for each b_{2u} normal vibration are given in the table.

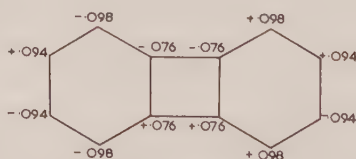


Figure 3. Transition density, ρ_β .

The calculated intensity on mixing B_{1g} and B_{3u} (allowed) electronic states by a b_{2u} vibration is thus seen to be about $\frac{1}{6}$ of the observed value (assuming that the $358\text{ m}\mu$ band is indeed part of the lowest electronic band).

Normal coordinate		f_p/f_β	ν_Q (cm ⁻¹)
Q_1		0.0020	505
Q_2		0.0037	784
Q_3		0.0073	79
Q_4		0.0075	222
Q_5		0.0008	135
Total	f_p/f_β	0.0213	observed 0.138

4. DISCUSSION OF RESULTS

The assumptions made are similar to those of Murrell and Pople namely:

- (1) biphenylene has been taken as a twelve electron system;
- (2) the transition density functions have been represented by point charges at the nuclei;
- (3) we have ignored any contributions to the intensity arising from the C-H vibrations;
- (4) that the ground state remains unchanged during the vibrations: b_{3u} vibrations in the ground state would contribute to the intensity. C-H vibrations would also tend to increase the intensity so that a calculated oscillator strength lower than that observed is to be expected.

The first semi-empirical formalism proposed for the description of vibronic interactions was made by Craig [11] in a valence bond computation. He proposed that the net interaction of the benzene π electrons with the vibrating carbon nuclei is essentially of a dipolar character; each carbon atom acting towards the π electrons on its non-neighbours as a small dipole, but being completely screened by the combined σ and π electrons from the electrons π on its neighbours. This assumption gave good agreement with experiment.

Murrell and Pople [1] used Craig's model in a molecular orbital framework but did not carry over Craig's nearest neighbour screening hypothesis and obtained less good agreement with experiment. However, Pople and Sidman [12] have used the Murrell and Pople unscreened charge-dipole model on formaldehyde with considerable success. A clue to the high value of oscillator strength calculated by Murrell and Pople lies, perhaps, in the third semi-empirical method developed by Liehr and Moffitt [13-16]. They point out that the Jahn-Teller 'splitting' of degenerate states must be analysed with some care when the forces tending to lower symmetry are of the same order as retreating forces encountered during typical vibrations, as in benzene. They thus treat the vibrational and electronic motions on the same level and obtain good agreement with experiment for the oscillator strengths of the symmetry forbidden bands of benzene. It thus appears that the model of Murrell and Pople probably gives good agreement when degenerate transitions are not involved, as for formaldehyde. The oscillator strength of the 393 m μ band alone is 0.002 and the calculated value for the B_{1g} band is thus ten times larger. We are investigating the p band (B_{1g}) of biphenylene and for the symmetry forbidden p band of benzene Murrell and Pople calculated a (maximum) value four times that of the observed, for the α band ten times that observed.

In view of the high oscillator strength obtained by Murrell and Pople in similar calculations the assignment remains ambiguous. However it does make possible the assignment that the $358\text{ m}\mu$ band is part of the first electronic level (0-0 band $393\text{ m}\mu$).

The author would like to thank Dr. M. Randic for help and advice on the normal coordinate analysis, Dr. J. N. Murrell for advice on the intensity calculations and Mr. K. Miller for reading the manuscript. She would also like to thank the Air Force Cambridge Research Laboratories for sponsoring the work under Contract AF 61 (052)-848 through the European Office of Aerospace Research (OAR), United States Air Force.

REFERENCES

- [1] MURRELL, J. N., and POPLER, J. A., 1956, *Proc. phys. Soc., Lond. A*, **69**, 245.
- [2] HERZBERG, G., and TELLER, E., 1933, *Z. phys. Chem. B*, **21**, 410.
- [3] HILPERN, J. W., 1965, *Trans. Faraday Soc.*, **61**, 605.
- [4] HOCHSTRASSER, R. M., 1961, *Canad. J. Chem.*, **39**, 765.
- [5] CLAR, E., 1952, *Aromatische Kohlenwasserstoffe* (Berlin: Springer-Verlag), p. 279.
- [6] WILSON, E. B., DECIUS, J. C., and CROSS, P. C., 1955, *Molecular Vibrations* (London: McGraw-Hill), p. 61.
- [7] SCULLY, D. B., and WHIFFEN, D. H., 1960, *Spectrochim. Acta*, **16**, 1410.
- [8] FREEMAN, D. E., and ROSS, I. G., 1960, *Spectrochim. Acta*, **16**, 1393.
- [9] WHIFFEN, D. H., 1955, *Phil. Trans. A*, **248**, 131.
- [10] COULSON, C. A., and DAUDEL, R., *Dictionary of Molecular Constants*, Vol. II.
- [11] CRAIG, D. P., 1950, *J. chem. Soc.*, p. 59.
- [12] POPLER, J. A., and SIDMAN, J. W., 1957, *J. chem. Phys.*, **27**, 1270.
- [13] LIEHR, A. D., and MOFFITT, W., 1956, *J. chem. Phys.*, **25**, 1074.
- [14] LIEHR, A. D., and MOFFITT, W., 1957, *Phys. Rev.*, **106**, 1195.
- [15] LIEHR, A. D., 1957, *Ann. Phys., Lpz.*, **1**, 221.
- [16] LIEHR, A. D., 1960, *Rev. mod. Phys.*, **32**, 435.

Multipolar theory of dielectric polarization in dense mixtures

by S. KIELICH

Department of Physics, A. Mickiewicz University, Poznan, Poland

(Received 19 February 1965; revision received 12 June 1965)

By statistical mechanics and a multipole tensor formalism, an expression for the dielectric polarization of dense mixtures is derived, of such generality as to account for certain new factors of a molecular nature not taken into account in hitherto-existing theories. The general results are discussed in some special cases of dipolar, quadrupolar, octopolar, etc. systems and applied to moderately dense gases, in which the second dielectric virial coefficient provides the basis for determining molecular multipole moments or multipole polarizabilities of order higher than dipolar. This indirect method yields a quadrupole moment of 5×10^{-26} e.s.u. cm² for the CO₂ molecule and an octopole moment of 4×10^{-34} e.s.u. cm³ for the CH₄ molecule.

1. INTRODUCTION

The statistical theory of isotropic dielectrics initiated by Kirkwood [1] and Yvon [2] has been modified and further developed in various ways by several authors [3–18]. Most theoretical work on dielectric polarization dealt with one-component systems of identical non-polar spherical molecules [1–7], dipolar molecules [8–14] and quadrupolar molecules [15–19]. Brown [3], Harris and Brush [20] and Buckingham [21] discussed the application of the statistical mechanical theory of dielectric polarization [8–12] to dilute solutions of dipolar molecules in a non-polar solvent. A virial theory of dielectric polarization of compressed gas mixtures has been given by Buckingham and Raab [22] (see also ref. [23]).

The importance of investigating the dielectric polarization in various substances resides primarily in the possibility of obtaining information not only on the molecular dipole moments themselves, as already shown by Debye, but moreover on the higher order molecular moments such as quadrupolar [15–19], octopolar [23–25] or hexadecapolar [26]. Obviously, such information on the molecular multipole moments of order higher than dipolar can be obtained only when, in the medium under investigation, molecular interactions are sufficiently apparent. These interactions will lead to an effect consisting in the induction, in any given molecule of the dense medium, of a dipole moment by the electric field of the permanent quadrupoles [15–19], octopoles [23–25], etc. of its neighbours. Clearly, such data on molecular multipole moments will be of a rather orientational character. Nevertheless, this indirect method deserves further study.

The present investigation is aimed at deriving a statistical-molecular theory of dielectric polarization for multi-component systems on the basis of the existing theories. A consistent and general tensor formalism will be developed which

enables us to obtain a general expression for the dielectric polarization in terms of multipole permanent moments and multipole polarizability tensors of molecules of arbitrary symmetry as well as of statistical averages of inverse powers of the mutual distances between molecules interacting in pairs, triplets, etc. The theory thus generally formulated can be applied to a wide range of vastly varying special cases beyond the one-component systems mostly discussed hitherto, comprising two-, three-component systems, etc., consisting of quadrupolar, octopolar or hexadecapolar unlike molecules.

In the Appendices we give in explicit form the first, second- and third-order multipole moments induced in a molecule by a strong inhomogeneous electric field as well as the higher-order energies of interactions between multipolar molecules. Various aspects of intermolecular energies have been discussed and developed in suitable approaches by several authors (see refs. [27–31] and the papers cited there); a tensor formalism for the multipole expansion of intermolecular energy was given by Frenkel [27], Carlson and Rushbrooke [28] and later by Jansen [31], whose general and concise tensor notation we use in the present paper.

2. GENERAL THEORY

We shall consider a medium of volume V placed in an external, in general inhomogeneous electric field with the potential ϕ . The tensor of the electric permittivity of such a medium is given in general by the equation [17, 32]:

$$(\epsilon - \mathbf{U}) \cdot \mathbf{E} = 4\pi \sum_{n=1}^{\infty} (-1)^{n-1} \frac{2^n n!}{(2n)!} \nabla^{n-1} [n-1] \mathbf{P}^{(n)}, \quad (1)$$

in which $\mathbf{P}^{(n)}$ is the 2^n -pole electric polarization operator of the medium and \mathbf{E} the homogeneous electric field in the medium; \mathbf{U} is the second-rank unit tensor, ∇ the differential operator and the symbol $[n]$ denotes n -fold contraction of the product of two tensors of rank n .

In the presence of the electric field at thermodynamical equilibrium of the system we have by classical statistical mechanics

$$\mathbf{P}^{(n)} = \frac{\int \frac{\mathbf{M}_T^{(n)}}{V} \exp \left\{ -\frac{U(\tau, \phi)}{kT} \right\} d\tau}{\int \exp \left\{ -\frac{U(\tau, \phi)}{kT} \right\} d\tau}, \quad (2)$$

wherein $\mathbf{M}_T^{(n)}(\tau, \phi)$ and $U(\tau, \phi)$ are respectively the 2^n -pole total electric moment and potential energy of the system at configuration τ in the electric field with potential ϕ .

In the case here considered we have:

$$U(\tau, \phi) = U(\tau, 0) - \sum_{n=1}^{\infty} \frac{2^n n!}{(2n)!} \int_0^{E_0^{(n)}} \mathbf{M}_T^{(n)}[n] d\mathbf{E}^{(n)}, \quad (3)$$

where $U(\tau, 0)$ is the potential energy of the system in the absence of an external electric field ($\phi=0$) and $\mathbf{E}^{(n)} = -\{\nabla^n \phi\}_0$ is the strength of the external electric field of ∇ -degree n within the medium and $\mathbf{E}_0^{(n)}$ —at a large distance from the medium or in the absence of the medium (*in vacuo*).

If the medium contains N_1 molecules of the first species, N_2 of the second, . . . , and N_i of the i th species, its multipole electric moment is given by:

$$\mathbf{M}_T^{(n)} = \sum_i \sum_{p=1}^{N_i} {}_T\mathbf{M}_{pi}^{(n)}, \quad (4)$$

where ${}_T\mathbf{M}_{pi}^{(n)}$ is the total 2^n -pole electric moment of the p th molecule of species i . Generally, when the electric field is present, ${}_T\mathbf{M}_{pi}^{(n)}$ can be expanded in the form:

$${}_T\mathbf{M}_{pi}^{(n)} = \mathbf{M}_{pi}^{(n)(0)} + \mathbf{M}_{pi}^{(n)(1)} + \mathbf{M}_{pi}^{(n)(2)} + \mathbf{M}_{pi}^{(n)(3)} + \dots = \sum_{s=0}^{\infty} \mathbf{M}_{pi}^{(n)(s)} \quad (5)$$

with $\mathbf{M}_{pi}^{(n)(0)} \equiv \mathbf{M}_{pi}^{(n)}$ denoting the 2^n -pole electric moment of the isolated molecule in the zeroth approximation, i.e. the permanent multipole moment in the absence of electric fields (see Appendix A).

In the case when the molecule of a medium is acted on by the total electric field $\mathbf{E}_0^{(n)} + \mathbf{F}_{pi}^{(n)}$ of degree n the multipole moment of order $s \geq 1$ induced in the p th molecule of species i is of the form:

$$\begin{aligned} \mathbf{M}_{pi}^{(n)(s)} = & \frac{1}{s!} \sum_{n_1=1}^{\infty} \dots \sum_{n_s=1}^{\infty} \frac{2^{n_1+\dots+n_s} n_1! \dots n_s!}{(2n_1)! \dots (2n_s)!} \\ & \times {}^{(n)}\mathbf{A}_{pi}^{(n_1+\dots+n_s)} [n_1 + \dots + n_s] (\mathbf{E}_0^{(n_1)} + \mathbf{F}_{pi}^{(n_1)}) \dots (\mathbf{E}_0^{(n_s)} + \mathbf{F}_{pi}^{(n_s)}) \end{aligned} \quad (6)$$

with $\mathbf{A}_{pi}^{(n_1+\dots+n_s)}$ denoting the s th-order multipole polarizability tensor of a molecule p of species i . This tensor describes the s th-order polarization of the 2^n -pole moment caused by the s th power of the electric field of degree n_s (see Appendix A).

The molecular electric field $\mathbf{F}_{pi}^{(n)}$ of degree n at the centre of the p th molecule of species i due to the other $N-1$ molecules of the system in the presence of an external electric field is defined in general as [32]:

$$\mathbf{F}_{pi}^{(n)} = \sum_j \sum_{\substack{q=1 \\ q \neq p}}^{N_j} \sum_{m=1}^{\infty} (-1)^m \frac{2^m m!}{(2m)!} {}^{(n)}\mathbf{T}_{pq}^{(m)} [m] {}_T\mathbf{M}_{qj}^{(m)}, \quad (7)$$

wherein

$${}^{(n)}\mathbf{T}_{pq}^{(m)} = -\nabla^{n+m} \left(\frac{1}{r_{pq}} \right)$$

is the tensor of rank $n+m$ describing the $(2^n$ -pole)– $(2^m$ -pole) interactions between the molecules p and q separated by a distance r_{pq} (see Appendix B); here, the differential operator ∇^{n+m} is directed from molecule q to p .

Equation (1) with the expressions (2)–(7) provide the basis for the general theory of the electric permittivity of a multi-component system whose components consist of molecules possessing multipole permanent electric moments as well as induced multipole moments of the first, second, third, etc. orders given by (6) for $s=1, 2, 3, \dots$. The multipole polarization operator (2) can, in general, be expanded in powers of the applied field \mathbf{E}_0 and its derivatives. Thus, the theory as formulated above is applicable not only to the case of a weak electric field but to the cases of non-linear variations of the electric permittivity tensor as produced by the square of a homogeneous electric field ($\mathbf{E} \equiv \mathbf{E}^{(1)} = -\nabla\phi$), by the gradient of an electric field ($\mathbf{E}^{(2)} = \nabla\mathbf{E}$), or by electric fields of higher degrees,

such as the gradient of a field gradient ($\mathbf{E}^{(3)} = \nabla \nabla \mathbf{E}$), and so forth. Obviously, a theory thus generally formulated is, in its explicit form, apt to present obstacles of a mathematical nature; this, however, is compensated by its wide range of applicability to various special cases, of which only some—and we might well say the simplest—are discussed in detail in this paper.

In the case when the applied electric field is weak and homogeneous, and when for convenience the isotropic medium is represented as a macroscopic spherical sample in vacuum for which $(\epsilon + 2)\mathbf{E} = 3\mathbf{E}_0$, equation (1) yields by (2) and (3) for the Clausius–Mossotti function:

$$\frac{\epsilon - 1}{\epsilon + 2} V = P_D + P_O, \quad (8)$$

where

$$P_D = \frac{4\pi}{3} \left\langle \frac{\partial}{\partial E_0} (\mathbf{M}_T^{(1)} \cdot \mathbf{e}) \right\rangle \quad (9a)$$

is the distortional or deformational polarizability of the medium and

$$P_O = -\frac{4\pi}{3kT} \left\langle (\mathbf{M}_T^{(1)} \cdot \mathbf{e}) \frac{\partial U}{\partial E_0} \right\rangle = \frac{4\pi}{3kT} \langle (\mathbf{M}_T^{(1)} \cdot \mathbf{e})^2 \rangle \quad (9b)$$

is its orientational polarizability; \mathbf{e} is a unit vector in the direction of the applied electric field \mathbf{E}_0 .

The brackets in (9) denote the statistical average at zero external electric field:

$$\langle X \rangle = \frac{\int X(\tau, 0) \exp \left\{ -\frac{U(\tau, 0)}{kT} \right\} d\tau}{\int \exp \left\{ -\frac{U(\tau, 0)}{kT} \right\} d\tau}. \quad (10)$$

3. DISTORTIONAL POLARIZATION

We now discuss the distortional polarizability of (9a) which in the approximation of the first-order dipole moment given by (6) for $s=1$ and $n=1$ is of the form:

$$P_D = \frac{4\pi}{3} \sum_i \sum_{p=1}^{N_i} \left\{ \langle \mathbf{e} \cdot {}^{(1)}\mathbf{A}_{pi}^{(1)} \cdot \mathbf{e} \rangle + \sum_{n=1}^{\infty} \frac{2^n n!}{(2n)!} \left\langle \mathbf{e} \cdot {}^{(1)}\mathbf{A}_{pi}^{(n)} [n] \frac{\partial \mathbf{F}_{pi}^{(n)}}{\partial E_0} \right\rangle \right\}. \quad (11)$$

This is a general equation for P_D containing the effects due to induced multipole interactions of unlike molecules of the system; beyond the Kirkwood–Yvon effect from fluctuations in the induced dipole moments ($n=1$), equation (11) contains similar effects from quadrupole ($n=2$), octopole ($n=3$), etc. moments induced in the molecules by the molecular field gradient $\mathbf{F}_{pi}^{(2)}$, gradient of field gradient $\mathbf{F}_{pi}^{(3)}$, etc. of the other molecules.

By methods of statistical mechanics, equation (11) with (7) can be expressed formally as follows:

$$P_D = \sum_i x_i P_D^{(i)} + \sum_{ij} x_i x_j P_D^{(ij)} + \sum_{ijk} x_i x_j x_k P_D^{(ijk)} + \dots, \quad (12)$$

where $x_i = N_i/N$ is the mole fraction of the i th component of the system.

The first term in (12) expresses the well-known additivity of distortional polarizability:

$$P_D^{(ij)} = \frac{4\pi}{3} N a_i \quad (13)$$

of the individual components consisting of non-interacting molecules possessing the mean dipole polarizabilities $a_i = {}^{(1)}\mathbf{A}_i^{(1)} : \mathbf{U}/3$.

The second, third and further terms of (12) responsible for the derivations from additivity of P_D arise from the interactions between unlike molecules in a dense medium. The quantities $P_D^{(ij)}$ and $P_D^{(ijk)}$ are in general of a very complicated form and, in the special case when the correlation functions do not depend on the mutual orientations of the molecules, are given as follows:

$$\begin{aligned} P_D^{(ij)} = & \frac{2\pi}{9} \sum_{n=1}^{\infty} \sum_{m=1}^{\infty} \frac{2^n (n!)^2 m! (2n+2m)!}{(2n)! (2n+1)! (2m)!} \\ & \times \{ a_i^{(2m)} ({}^{(1)}\mathbf{A}_j^{(n)} [n+1] {}^{(n)}\mathbf{A}_j^{(1)}) + ({}^{(1)}\mathbf{A}_i^{(n)} [n+1] {}^{(n)}\mathbf{A}_i^{(1)}) a_j^{(2m)} \} \\ & \times \int \int r_{pq}^{-2(n+m+1)} n_{ij}^{(2)}(\mathbf{r}_p, \mathbf{r}_q) d\mathbf{r}_p d\mathbf{r}_q, \quad (14) \end{aligned}$$

$$\begin{aligned} P_D^{(ijk)} = & \frac{4\pi}{27} \sum_{n=1}^{\infty} (n+1)(2n+1) \{ a_i a_j a_k^{(2n)} + a_i a_j^{(2n)} a_k + a_i^{(2n)} a_j a_k \} \\ & \times \int \int \int (r_{pq} r_{qr})^{-(n+2)} P_{n+1} \left(\frac{\mathbf{r}_{pq} \cdot \mathbf{r}_{qr}}{r_{pq} r_{qr}} \right) n_{ijk}^{(3)}(\mathbf{r}_p, \mathbf{r}_q, \mathbf{r}_r) d\mathbf{r}_p d\mathbf{r}_q d\mathbf{r}_r. \quad (15) \end{aligned}$$

Here,

$$a_i^{(2n)} = \frac{2^n n!}{(2n+1)!} {}^{(n)}\mathbf{A}_i^{(n)} [2n] \mathbf{U}^n \quad (16)$$

is the mean value of the 2^n -pole electric polarizability of a molecule of species i due to an electric field of degree n and P_{n+1} is the Legendre polynomial of degree $n+1$. In (14), $n_{ij}^{(2)}(\mathbf{r}_p, \mathbf{r}_q)$ is the binary distribution function for a pair of molecules p and q of species i and j at positions \mathbf{r}_p and \mathbf{r}_q , whereas in (15) $n_{ijk}^{(3)}(\mathbf{r}_p, \mathbf{r}_q, \mathbf{r}_r)$ is the ternary distribution function for triples of molecules p , q and r of species i , j and k at positions \mathbf{r}_p , \mathbf{r}_q and \mathbf{r}_r .

If the higher-order terms are neglected, we obtain from (14):

$$\begin{aligned} P_D^{(ij)} = & \frac{4\pi}{9} \int \int \{ [a_i(\mathbf{a}_j : \mathbf{a}_j) + (\mathbf{a}_i : \mathbf{a}_i) a_j] r_{pq}^{-6} + [a_i ({}^{(1)}\mathbf{A}_j^{(2)} :: {}^{(2)}\mathbf{A}_j^{(1)}) \\ & + ({}^{(1)}\mathbf{A}_i^{(2)} :: {}^{(2)}\mathbf{A}_i^{(1)}) a_j] r_{pq}^{-8} + \frac{4}{5} [a_i ({}^{(1)}\mathbf{A}_j^{(3)} :: {}^{(3)}\mathbf{A}_j^{(1)}) + ({}^{(1)}\mathbf{A}_i^{(3)} :: {}^{(3)}\mathbf{A}_i^{(1)}) a_j] r_{pq}^{-10} \\ & + 5 [q_i(\mathbf{a}_j : \mathbf{a}_j) + (\mathbf{a}_i : \mathbf{a}_i) q_j] r_{pq}^{-8} + \frac{28}{3} [q_i ({}^{(1)}\mathbf{A}_j^{(2)} :: {}^{(2)}\mathbf{A}_j^{(1)}) + ({}^{(1)}\mathbf{A}_i^{(2)} :: {}^{(2)}\mathbf{A}_i^{(1)}) q_j] r_{pq}^{-10} \\ & + 12 [q_i ({}^{(1)}\mathbf{A}_j^{(3)} :: {}^{(3)}\mathbf{A}_j^{(1)}) + ({}^{(1)}\mathbf{A}_i^{(3)} :: {}^{(3)}\mathbf{A}_i^{(1)}) q_j] r_{pq}^{-12} + \dots \} n_{ij}^{(2)}(\mathbf{r}_p, \mathbf{r}_q) d\mathbf{r}_p d\mathbf{r}_q, \quad (17) \end{aligned}$$

where, by (16), $q_i \equiv a_i^{(4)} = \mathbf{U} : {}^{(2)}\mathbf{A}_i^{(2)} : \mathbf{U}/15$ is the mean quadrupole polarizability describing the quadrupole moment ${}^{(2)}\mathbf{A}_i^{(2)} : \mathbf{F}_i^{(2)}$ induced in the molecule of species i by the molecular electric field gradient $\mathbf{F}_i^{(2)}$. In (17), ${}^{(1)}\mathbf{A}_i^{(2)}$, ${}^{(1)}\mathbf{A}_i^{(3)}$, \dots are the

tensors of dipole polarizabilities describing the dipole moments ${}^{(1)}\mathbf{A}_i^{(2)} : \mathbf{F}_i^{(2)}$ and ${}^{(1)}\mathbf{A}_i^{(3)} : \mathbf{F}_i^{(3)}$ induced in the molecule by the field gradient $\mathbf{F}_i^{(2)}$ and gradient of field gradient $\mathbf{F}_i^{(3)}$. Alternatively, the quadrupole polarizability tensor ${}^{(2)}\mathbf{A}_i^{(1)}$ and octopole polarizability tensor ${}^{(3)}\mathbf{A}_i^{(1)}$ define the quadrupole moment ${}^{(2)}\mathbf{A}_i^{(1)} \cdot \mathbf{F}_i^{(1)}$ and octopole moment ${}^{(3)}\mathbf{A}_i^{(1)} : \mathbf{F}_i^{(1)}$ induced in the molecule by the field $\mathbf{F}_i^{(1)}$.

The successive terms in equation (17) with (A5) correspond to the term discussed strictly in explicit form by Jansen and Solem [17] on the basis of quantum-mechanical perturbation theory.

As a particular case of interest, we shall consider that of molecules with centres of inversion for which (17) yields in a good approximation:

$$P_D^{(ij)} = \frac{4\pi}{9} \iint \{ [a_i(\mathbf{a}_j : \mathbf{a}_j) + (\mathbf{a}_i : \mathbf{a}_i)a_j] r_{pq}^{-6} + 5[q_i(\mathbf{a}_j : \mathbf{a}_j) + (\mathbf{a}_i : \mathbf{a}_i)q_j] r_{pq}^{-8} \} n_{ij}^{(2)}(\mathbf{r}_p, \mathbf{r}_q) d\mathbf{r}_p d\mathbf{r}_q, \quad (18)$$

or, if the molecules possess moreover the axial symmetry:

$$P_D^{(ij)} = \frac{4\pi}{3} \iint \{ a_i a_j [a_i(1 + 2\kappa_i^2) + a_j(1 + 2\kappa_j^2)] r_{pq}^{-6} + 5[q_i a_j^2(1 + 2\kappa_j^2) + a_i^2(1 + 2\kappa_i^2)q_j] r_{pq}^{-8} \} n_{ij}^{(2)}(\mathbf{r}_p, \mathbf{r}_q) d\mathbf{r}_p d\mathbf{r}_q, \quad (19)$$

where $\kappa_i = (a_{zz}^{(i)} - a_{xx}^{(i)})/3a_i$ is a parameter determining the anisotropy of dipole polarizability.

For a one-component system with molecules possessing the isotropic dipole polarizability ($a_i \neq 0, \kappa_i = 0$) but no quadrupole polarizability ($q_i = 0$), equation (19) yields the result of De Boer *et al.* [4].

We now consider the further contributions to P_D from induced dipole moments of the second and third orders given by (6) for $n = 1$ and respectively for $s = 2$ and $s = 3$. In the zeroth approximation by unweighted averaging over all possible orientations of molecules $\partial \mathbf{M}_{pi}^{(1)}/\partial E_0$ vanishes, whereas $\partial \mathbf{M}_{pi}^{(3)}/\partial E_0$ is non-zero and yields the following contribution to distortional polarization:

$$P_D^{(ij)} = \frac{\pi}{9} \sum_{n=1}^{\infty} \sum_{m=1}^{\infty} \frac{2^{n+m}(n!m!)^2(2n+2m)!}{(2n)!(2n+1)!(2m)!(2m+1)!} \times \{ (\mathbf{U} : {}^{(1)}\mathbf{C}_i^{(1+2n)}[2n]\mathbf{U}^n)(\mathbf{M}_j^{(m)}[m]\mathbf{M}_j^{(m)}) + (\mathbf{M}_i^{(n)}[n]\mathbf{M}_i^{(n)})(\mathbf{U} : {}^{(1)}\mathbf{C}_j^{(1+2m)}[2m]\mathbf{U}^m) \} \times \iint r_{pq}^{-2(n+m+1)} n_{ij}^{(2)}(\mathbf{r}_p, \mathbf{r}_q) d\mathbf{r}_p d\mathbf{r}_q, \quad (20)$$

where ${}^{(1)}\mathbf{C}_i^{(1+2n)}$ is the third-order dipole polarizability tensor of the molecule of species i due to the second power of the electric field of degree n .

In the case of molecules possessing only the third-order mean dipole polarizability $c_i = \mathbf{U} : {}^{(1)}\mathbf{C}_i^{(2)} : \mathbf{U}/5$, the expression (20) becomes:

$$P_D^{(ij)} = \frac{5\pi}{27} \sum_{n=1}^{\infty} \frac{2^n(n+1)!n!}{(2n)!} \{ c_i(\mathbf{M}_j^{(n)}[n]\mathbf{M}_j^{(n)}) + (\mathbf{M}_i^{(n)}[n]\mathbf{M}_i^{(n)})c_j \} \iint r_{pq}^{-2(n+2)} n_{ij}^{(2)}(\mathbf{r}_p, \mathbf{r}_q) d\mathbf{r}_p d\mathbf{r}_q. \quad (21)$$

Hitherto, in the foregoing calculations we have considered the simpler cases when in the definition (10) the potential energy $U(\tau, 0) = U(\mathbf{r})$ depended only on the positional variables \mathbf{r} of the molecules. If in general $U(\tau, 0)$ consists besides $U(\mathbf{r})$ also of that part of $V(\mathbf{r}, \boldsymbol{\omega})$ which depends both on the positional and orientational variables \mathbf{r} and $\boldsymbol{\omega}$ of the molecules, we can obtain some further contributions to P_D . However, we shall restrict these supplementary calculations to the contribution resulting from the second-order dipole moment $\mathbf{M}_{pi}^{(2)}$. By (6) for $s=2$ and $n=1$ we have:

$$\left\{ \frac{\partial \mathbf{M}_{pi}^{(2)}}{\partial \mathbf{E}_0} \right\}_{\mathbf{E}_0=0} = \sum_{n=1}^{\infty} \frac{2^n n!}{(2n)!} {}^{(1)}\mathbf{B}_{pi}^{(1+n)} [1+n] \mathbf{e} \mathbf{F}_{0pi}^{(n)} + \dots, \quad (22)$$

where ${}^{(1)}\mathbf{B}^{(1+n)}$ is the second-order dipole polarizability tensor due to the molecular electric field $\mathbf{F}_0^{(n)}$ of ∇ -degree n at $\mathbf{E}_0=0$.

In the case when $V(\mathbf{r}, \boldsymbol{\omega})$ arises from electrostatic interaction between the 2^n -pole permanent electric moment of one molecule and the 2^m -pole permanent electric moment of another, i.e. when (see Appendix B)

$$V(\mathbf{r}, \boldsymbol{\omega}) = -\frac{1}{2} \sum_{ij} \sum_{p=1}^{N_i} \sum_{q=1}^{N_j} \sum_{n=1}^{\infty} \sum_{m=1}^{\infty} (-1)^m \frac{2^{n+m} n! m!}{(2n)!(2m)!} \mathbf{M}_{pi}^{(n)} [n] {}^{(n)}\mathbf{T}_{pq}^{(m)} [m] \mathbf{M}_{qj}^{(m)} \quad (23)$$

is non-zero, we obtain by (9a) and (22) the following contribution:

$$P_D^{(ij)} = \frac{2\pi}{9kT} \sum_{n=1}^{\infty} \sum_{m=1}^{\infty} \frac{2^{n+m} (2n+2m)! (n! m!)^2}{(2n)!(2n+1)!(2m)!(2m+1)!} \{ (\mathbf{U} : {}^{(1)}\mathbf{B}_i^{(1+n)} [n] \mathbf{M}_i^{(n)}) \times (\mathbf{M}_j^{(m)} [m] \mathbf{M}_j^{(m)}) + (\mathbf{M}_i^{(n)} [n] \mathbf{M}_i^{(n)}) (\mathbf{U} : {}^{(1)}\mathbf{B}_j^{(1+m)} [m] \mathbf{M}_j^{(m)}) \} \times \int \int r_{pq}^{-2(n+m+1)} n_{ij}^{(2)}(\mathbf{r}_p, \mathbf{r}_q) d\mathbf{r}_p d\mathbf{r}_q \quad (24)$$

which, as we see, in contradistinction to the preceding contributions (14) and (20), depends directly on the temperature.

If, in particular, the molecules possess only the permanent dipole moment $\mathbf{M}_i^{(1)} = \mu_i \mathbf{k}$, expressions (21) and (24) yield:

$$P_D^{(ij)} = \frac{10\pi}{27} \left\{ c_i \mu_i^2 + \mu_i^2 c_j + \frac{6\mu_i \mu_j}{5kT} (b_i \mu_j + \mu_i b_j) \right\} \int \int r_{pq}^{-6} n_{ij}^{(2)}(\mathbf{r}_p, \mathbf{r}_q) d\mathbf{r}_p d\mathbf{r}_q \quad (25)$$

where $b_i = \mathbf{U} : {}^{(1)}\mathbf{B}_i^{(2)} \cdot \mathbf{k}/3$ is the mean second-order dipole polarizability.

Analogously in the case of molecules with permanent quadrupole moments $\mathbf{M}_i^{(2)} = \boldsymbol{\Theta}_i$, expressions (21) and (24) reduce to:

$$P_D^{(ij)} = \frac{10\pi}{27} \int \int \left\{ [c_i (\boldsymbol{\Theta}_j : \boldsymbol{\Theta}_j) + (\boldsymbol{\Theta}_i : \boldsymbol{\Theta}_i) c_j] r_{pq}^{-8} + \frac{56}{25kT} [(\mathbf{U} : {}^{(1)}\mathbf{B}_i^{(3)} : \boldsymbol{\Theta}_i) \times (\boldsymbol{\Theta}_j : \boldsymbol{\Theta}_j) + (\boldsymbol{\Theta}_i : \boldsymbol{\Theta}_i) (\mathbf{U} : {}^{(1)}\mathbf{B}_j^{(3)} : \boldsymbol{\Theta}_j)] r_{pq}^{-10} \right\} n_{ij}^{(2)}(\mathbf{r}_p, \mathbf{r}_q) d\mathbf{r}_p d\mathbf{r}_q. \quad (26)$$

In a similar way we can calculate some other contributions to P_D dependent on T^{-1} and T^{-2} (see refs. [22, 23, 32]).

4. ORIENTATIONAL POLARIZATION

In the absence of an external electric field ($\mathbf{E}_0=0$) all directions of $\mathbf{M}^{(1)}$ with respect to \mathbf{e} have the same probability, so that $(\mathbf{M}^{(1)} \cdot \mathbf{e})^2$ appearing in (9b) can

be averaged over all directions and we obtain for the orientational polarizability of multi-component systems:

$$P_0 = \frac{4\pi}{9kT} \langle \mathbf{M}_T^{(1)} \cdot \mathbf{M}_T^{(1)} \rangle = \frac{4\pi}{9kT} \sum_{ij} \left\langle \sum_{p=1}^{Ni} \sum_{q=1}^{Nj} \mathbf{r}_p \mathbf{M}_{pi}^{(1)} \cdot \mathbf{r}_q \mathbf{M}_{qj}^{(1)} \right\rangle. \quad (27)$$

We shall discuss this equation only for the case when the system consists of molecules presenting no permanent electric dipoles ($\mathbf{M}_{pi}^{(1)} = 0$) but possessing permanent electric moments of higher orders $n \geq 2$. Up to the first-order induced dipole moment resulting from (6) for $s=1$ and $n=1$ at $\mathbf{E}_0=0$,

$$\mathbf{M}_{pi}^{(1)} = \sum_{n=1}^{\infty} \frac{2^n n!}{(2n)!} {}^{(1)}\mathbf{A}_{pi}^{(n)} [n] \mathbf{F}_{0pi}^{(n)}, \quad (28)$$

equation (27) yields:

$$P_0 = \frac{4\pi}{9kT} \sum_{ij} \sum_{n=1}^{\infty} \sum_{m=1}^{\infty} \frac{n 2^{n+m} n! m!}{(2n)!(2m)!} \left\langle \sum_{p=1}^{Ni} \sum_{q=1}^{Nj} ({}^{(1)}\mathbf{A}_{pi}^{(n)} [n] \mathbf{F}_{pi}^{(n)}) \cdot ({}^{(1)}\mathbf{A}_{qj}^{(m)} [m] \mathbf{F}_{qj}^{(m)}) \right\rangle. \quad (29)$$

With the molecular electric field of (7) this equation can be represented in the form:

$$P_0 = \sum_{ij} x_i x_j P_0^{(ij)} + \sum_{ijk} x_i x_j x_k P_0^{(ijk)} + \dots, \quad (30)$$

where in the special case when $V(\mathbf{r}, \omega) = 0$ we have:

$$\begin{aligned} P_0^{(ij)} = & \frac{4\pi}{9kT} \sum_{n=1}^{\infty} \sum_{m=1}^{\infty} \frac{2^{n+m} (2n+2m+2)! [n! (m+1)!]^2}{(2n)!(2n+1)!(2m+2)!(2m+3)!} \\ & \times \left\{ ({}^{(1)}\mathbf{A}_i^{(n)} [1+n] {}^{(1)}\mathbf{A}_i^{(n)}) (\mathbf{M}_j^{(1+m)} [1+m] \mathbf{M}_j^{(1+m)}) \right. \\ & - \frac{4m+2}{2n+3} ({}^{(1)}\mathbf{A}_i^{(n)} [1+n] \mathbf{M}_i^{(1+n)}) ({}^{(1)}\mathbf{A}_j^{(m)} [1+m] \mathbf{M}_j^{(1+m)}) \\ & \left. + (\mathbf{M}_i^{(1+m)} [1+m] \mathbf{M}_i^{(1+m)}) ({}^{(1)}\mathbf{A}_j^{(n)} [1+n] {}^{(1)}\mathbf{A}_j^{(n)}) \right\} \\ & \times \int \int r_{pq}^{-2(n+m+2)} n_{ij}^{(2)}(\mathbf{r}_p, \mathbf{r}_q) d\mathbf{r}_p d\mathbf{r}_q, \quad (31) \end{aligned}$$

$$\begin{aligned} P_0^{(ijk)} = & \frac{4\pi}{27kT} \sum_{n=1}^{\infty} \frac{2^n (n+1)! n!}{(2n)!} \{ a_i a_j ({}^{(n)}\mathbf{M}_k^{(n)} [n] \mathbf{M}_k^{(n)}) \\ & + a_i ({}^{(n)}\mathbf{M}_j^{(n)} [n] \mathbf{M}_j^{(n)}) a_k + ({}^{(n)}\mathbf{M}_i^{(n)} [n] \mathbf{M}_i^{(n)}) a_j a_k \} \\ & \times \int \int \int (r_{pq} r_{qr})^{-(n+2)} P_{n+1} \left(\frac{\mathbf{r}_{pq} \cdot \mathbf{r}_{qr}}{r_{pq} r_{qr}} \right) n_{ijk}^{(3)}(\mathbf{r}_p, \mathbf{r}_q, \mathbf{r}_r) d\mathbf{r}_p d\mathbf{r}_q d\mathbf{r}_r. \quad (32) \end{aligned}$$

For molecules possessing only the permanent quadrupole moment expression (31) yields the formula [23]:

$$\begin{aligned} P_0^{(ij)} = & \frac{4\pi}{135kT} \{ 5(\mathbf{a}_i : \mathbf{a}_i)(\boldsymbol{\Theta}_j : \boldsymbol{\Theta}_j) - 6(\mathbf{a}_i : \boldsymbol{\Theta}_i)(\mathbf{a}_j : \boldsymbol{\Theta}_j) \\ & + 5(\boldsymbol{\Theta}_i : \boldsymbol{\Theta}_i)(\mathbf{a}_j : \mathbf{a}_j) \} \int \int r_{pq}^{-8} n_{ij}^{(2)}(\mathbf{r}_p, \mathbf{r}_q) d\mathbf{r}_p d\mathbf{r}_q, \quad (33) \end{aligned}$$

which in the case of axial symmetry assumes the simpler form :

$$P_0^{(ij)} = \frac{2\pi}{15kT} \{5a_i^2(1+2\kappa_i^2)\Theta_j^2 - 12a_i\kappa_i\Theta_i a_j\kappa_j\Theta_j + 5\Theta_i^2 a_j^2(1+2\kappa_j^2)\} \int \int r_{pq}^{-8} n_{ij}^{(2)}(\mathbf{r}_p, \mathbf{r}_q) d\mathbf{r}_p d\mathbf{r}_q. \quad (34)$$

Formula (33) or (34) determines the contribution to P_0 from the effect consisting in the induction, in a given molecule of the medium, of a dipole moment by the electric field of the quadrupoles of its neighbours [15, 16]. This formula, when applied to a single-component system, yields immediately the result derived by Jansen [17].

In the case of molecules having only isotropic dipole polarizability of the first-order the general expression (31) can be simplified to :

$$P_0^{(ij)} = \frac{2\pi}{9kT} \sum_{n=2}^{\infty} \frac{2^n(n+1)!n!}{(2n)!} \{a_i^2(\mathbf{M}_j^{(n)}[n]\mathbf{M}_j^{(n)}) + (\mathbf{M}_i^{(n)}[n]\mathbf{M}_i^{(n)})a_j^2\} \int \int r_{pq}^{-2(n+2)} n_{ij}^{(2)}(\mathbf{r}_p, \mathbf{r}_q) d\mathbf{r}_p d\mathbf{r}_q, \quad (35)$$

or to the still simpler form :

$$P_0^{(ij)} = \frac{2\pi}{9kT} \sum_{n=2}^{\infty} (n+1) \{a_i^2(M_j^{(n)})^2 + (M_i^{(n)})^2 a_j^2\} \int \int r_{pq}^{-2(n+2)} n_{ij}^{(2)}(\mathbf{r}_p, \mathbf{r}_q) d\mathbf{r}_p d\mathbf{r}_q \quad (36)$$

if the molecules possess moreover the axial symmetry, i.e. when

$$\mathbf{M}_i^{(n)}[n]\mathbf{M}_i^{(n)} = \frac{(2n)!}{2^n(n!)^2} \{M_i^{(n)}\}^2, \quad (37)$$

where $M_i^{(n)}$ is the 2^n -pole scalar electric moment of an axially symmetric molecule of species i .

Formula (35) can be used, *i. a.*, in the case of tetrahedrally symmetric molecules (e.g. CH_4) having the octopole, $M_{xyz}^{(3)} \equiv \Omega$, and hexadecapole, $M_{xxzz}^{(4)} \equiv \Phi$ electric moments ; namely, we obtain in this case the formula :

$$P_0^{(ij)} = \frac{32\pi}{15kT} \int \int \left\{ (a_i^2 \Omega_j^2 + \Omega_i^2 a_j^2) r_{pq}^{-10} + \frac{25}{7} (a_i^2 \Phi_j^2 + \Phi_i^2 a_j^2) r_{pq}^{-12} \right\} n_{ij}^{(2)}(\mathbf{r}_p, \mathbf{r}_q) d\mathbf{r}_p d\mathbf{r}_q, \quad (38)$$

which describes the effect arising in a dense medium owing to each molecule gaining a dipole moment under the influence of the electric fields of octopoles and hexadecapoles of its neighbours. For $\Phi=0$ and a one-component system, this effect was first computed by Johnston *et al.* [24] and measured in methane.

For $\Omega=0$, formula (38), in turn, can be applied to octahedral molecules (e.g. SF_6), in which case the first non-zero permanent moment is hexadecapolar Φ .

We shall now calculate the contributions to P_0 arising from the potential energy $V(\mathbf{r}, \boldsymbol{\omega})$ given by (23). However, we assume for simplicity that the multipolar molecules of the system are isotropically polarizable and mutually

interacting in pairs only. Thus, by (10), (23) and (27) we obtain an additional contribution to $P_0^{(ij)}$ dependent directly on T^{-2} :

$$P_0^{(ij)} = \frac{4\pi}{9k^2T^2} \sum_{n=2}^{\infty} \sum_{m=2}^{\infty} \frac{2^{n+m}n!m!(n+m+1)!}{(2n+1)!(2m+1)!} a_i a_j (\mathbf{M}_i^{(n)}[n]\mathbf{M}_i^{(n)}) \\ \times (\mathbf{M}_j^{(m)}[m]\mathbf{M}_j^{(m)}) \int \int r_{pq}^{-(2n+2m+5)} n_{ij}^{(2)}(\mathbf{r}_p, \mathbf{r}_q) d\mathbf{r}_p d\mathbf{r}_q. \quad (39)$$

This expression yields for axially symmetric quadrupolar molecules:

$$P_0^{(ij)} = \frac{8\pi}{15k^2T^2} a_i a_j \Theta_i^2 \Theta_j^2 \int \int r_{pq}^{-13} n_{ij}^{(2)}(\mathbf{r}_p, \mathbf{r}_q) d\mathbf{r}_p d\mathbf{r}_q \quad (40)$$

or, for molecules possessing the tetrahedral symmetry:

$$P_0^{(ij)} = \frac{256\pi}{35k^2T^2} a_i a_j \Omega_i^2 \Omega_j^2 \int \int r_{pq}^{-17} n_{ij}^{(2)}(\mathbf{r}_p, \mathbf{r}_q) d\mathbf{r}_p d\mathbf{r}_q, \quad (41)$$

if the term with hexadecapole moment can be neglected.

Quite similarly, expressions (31), (35) and (39) can be applied for other kinds of molecular symmetry, but we shall refrain here from writing the results obtained in the various special cases [32].

5. APPLICATION TO GASEOUS SYSTEMS AND DISCUSSION

In the case of very dense systems, $P^{(ij)}$ and $P^{(ijk)}$ cannot in general be reduced to a form suitable for numerical calculations and for subsequent comparison of equations (8), (12) and (30) with the experimental data. Only in the exceptional case of imperfect but not too dense gases can we confine ourselves to pairwise interaction between the molecules for which $P^{(ij)}$ can be reduced in general to a form adapted to numerical evaluations. In this case of moderately dense gases, the binary distribution function can be expressed as follows [4]:

$$n_{ij}^{(2)}(\mathbf{r}_p, \mathbf{r}_q) = \rho^2 \exp \left\{ - \frac{u_{ij}(r_{pq})}{kT} \right\} \{1 + O(\rho)\}, \quad (42)$$

with $\rho = N/V$ denoting the average number of molecules of the system and $u_{ij}(r_{pq})$ the potential energy of radial interactions between molecules p and q of species i and j separated by a distance r_{pq} .

If u_{ij} in (42) is the Lennard-Jones potential of the form:

$$u_{ij}(r_{pq}) = 4\epsilon_{ij} \left\{ \left(\frac{\sigma_{ij}}{r_{pq}} \right)^s - \left(\frac{\sigma_{ij}}{r_{pq}} \right)^t \right\}, \quad (43)$$

we have:

$$\int \int r_{pq}^{-n} n_{ij}^{(2)}(\mathbf{r}_p, \mathbf{r}_q) d\mathbf{r}_p d\mathbf{r}_q = \frac{6b_{ij}\rho}{sy_{ij}^4 \sigma_{ij}^n} H_n^{s-t}(y_{ij}), \quad (44)$$

wherein [33]

$$H_n^{s-t}(y_{ij}) = y_{ij}^{2(2s+3-n)/s} \sum_{m=0}^{\infty} \frac{1}{m!} y_{ij}^{2m(s-t)/s} \Gamma \left(\frac{mt+n-3}{s} \right), \quad (45)$$

with ϵ_{ij} and σ_{ij} denoting the well-known central force parameters and $y_{ij} = 2(\epsilon_{ij}/kT)^{1/2}$ and $b_{ij} = \frac{2}{3}\pi N\sigma_{ij}^3$.

With the help of (44) the quantity $P^{(ij)}$ discussed in §§ 3 and 4 can be written as :

$$P^{(ij)} = V^{-1} \{ B_p^{(ij)} + O(\rho) \}, \quad (46)$$

where $B_p^{(ij)}$ is the second virial coefficient of dielectric polarization.

In cases when the values of the molecular parameters ϵ_{ij} and σ_{ij} are known, we can use expressions (44) and (46) for evaluating $B_p^{(ij)}$ numerically; obviously, according to the system dealt with, one will have to assume such values of the molecular quadrupole, octopole, etc. moments as to achieve satisfactory agreement with the experimental data available for the second dielectric virial coefficient. In this way we can obtain information concerning the values of the multipole electric moments of various molecules.

For the sake of simplicity we shall carry out the evaluation of B_p only for a one-component gas. In the case of a quadrupolar gas we obtain from equations (19), (34), (40), (44) and (46), if the anisotropy in polarizabilities are neglected,

$$B_D = \frac{24b^2}{5y^4} \left(\frac{a}{\sigma^3} \right)^2 \left\{ \left(\frac{a}{\sigma^3} \right) H_6^{s-t}(y) + 5 \left(\frac{q}{\sigma^5} \right) H_8^{s-t}(y) + \dots \right\}, \quad (47)$$

$$B_O = \frac{3b^2}{5y^2} \left(\frac{\Theta^2}{\sigma^5 \epsilon} \right) \left\{ \left(\frac{a}{\sigma^3} \right)^2 H_8^{s-t}(y) + 36 \left(\frac{q}{\sigma^5} \right)^2 H_{12}^{s-t}(y) + \frac{y^2}{10} \left(\frac{a}{\sigma^3} \right)^2 \left(\frac{\Theta^2}{\sigma^5 \epsilon} \right) H_{13}^{s-t}(y) \right\}. \quad (48)$$

Similarly we obtain for B_O in the case of tetrahedral molecules possessing only the octopole moment Ω ,

$$B_O = \frac{48b^2}{55y^2} \left(\frac{a}{\sigma^3} \right)^2 \left(\frac{\Omega^2}{\sigma^7 \epsilon} \right) \left\{ H_{10}^{s-t}(y) + \frac{3y^2}{7} \left(\frac{\Omega^2}{\sigma^7 \epsilon} \right) H_{17}^{s-t}(y) \right\}. \quad (49)$$

The table compares the values of $B_p^{\text{calc}} = B_D + B_O$ calculated from equations (47) and (48) for N_2 and CO_2 and equations (47) and (49) for CH_4 with the experimental data [18, 24]. We have performed the theoretical calculation for simplicity for $s=12$ and $t=6$ (in this case the functions H_n^{12-6} are to be found tabulated in ref. [34]) with the help of the following molecular data [30, 35] for N_2 : $\epsilon/k = 91.5^\circ K$, $\sigma = 3.681 \text{ \AA}$, $a = 1.76 \times 10^{-24} \text{ cm}^3$, for CO_2 : $\epsilon/k = 190^\circ K$, $\sigma = 3.996 \text{ \AA}$, $a = 2.92 \times 10^{-24} \text{ cm}^3$, and for CH_4 : $\epsilon/k = 137^\circ K$, $\sigma = 3.882 \text{ \AA}$, $a = 2.60 \times 10^{-24} \text{ cm}^3$.

It is seen from the table that good agreement between the calculated and experimental values of the second dielectric virial coefficients is obtained if the quadrupole moment of the N_2 molecule is $\Theta = 1.5 \times 10^{-26} \text{ e.s.u. cm}^2$ and that of the CO_2 molecule is [18] $\Theta = 5 \times 10^{-26} \text{ e.s.u. cm}^2$ with the octopole moment of the CH_4 molecule amounting to $\Omega = 4 \times 10^{-34} \text{ e.s.u. cm}^3$. We note also that the second virial coefficient B of the equation of state yields $\Theta = 1.8 - 1.9 \times 10^{-26} \text{ e.s.u. cm}^2$ for the N_2 molecule, $\Theta = 4.59 - 5.0 \times 10^{-26} \text{ e.s.u. cm}^2$ for the CO_2 molecule [35, 36] and $\Omega = 5 \times 10^{-34} \text{ e.s.u. cm}^3$ for the CH_4 molecule [33].

It is evident that further research in this direction can be fruitful and will surely bring much interesting information on the electric multipole moments and multipole polarizabilities of molecules.

In concluding, it should be stressed that the total dielectric polarization P of a multi-component system can be expanded in a power series in the mole fraction,

$$P = \sum_i x_i P_i + \sum_{ij} x_i x_j P_{ij} + \sum_{ijk} x_i x_j x_k P_{ijk} + \dots, \quad (50)$$

where the first term represents the additivity rule, while the subsequent terms account for deviations therefrom. The quantities P_{ij} and P_{ijk} are non-zero only for systems in which interactions occur both between molecules of the same species and between those of various components in dense systems. The expressions obtained here for P_{ij} and P_{ijk} allow to state that investigation of deviations of P from additivity can be a source, *i.a.*, of information concerning the permanent and induced electric multipoles of molecules of various species as well as on the nature and magnitude of the forces with which they interact in the dense mixture.

Gas	$T^{\circ}\text{K}$	B_D	B_O	$B_P^{\text{calc}} = B_D + B_O$	B_P^{exper}
N_2 $\Theta = 1.5 \times 10^{-24} \text{ e.s.u. cm}^2$	242	1.9	1.9	3.8	$4.2 (\pm 1.0) [24]$
	296	1.8	1.4	3.2	$2.0 (\pm 1.0) [24]$
CO_2 $\Theta = 5 \times 10^{-26} \text{ e.s.u. cm}^2$	323	9.8	40.9	50.7	49.7 [18]
	348	9.6	37.3	46.9	46.4 [18]
CH_4 $\Omega = 4 \times 10^{-34} \text{ e.s.u. cm}^3$	242	5.5	3.5	9.0	$9.0 (\pm 0.4) [24]$
	315	5.3	2.9	8.2	$7.3 (\pm 1.8) [24]$

Calculated and experimental values of the second polarization virial coefficient in cm^6/mol^2 .

APPENDIX A

Quantum mechanical form of first-, second- and third-order multipole moments

We now consider, for simplicity, a system of identical, non-interacting molecules subjected to an external inhomogeneous electric field. The Hamiltonian of a molecule is $H = H_0 + H'$, where H_0 is the Hamiltonian of the non-perturbed (isolated) molecule and

$$H' = - \sum_{n=1}^{\infty} \frac{2^n n!}{(2n)!} \mathbf{M}^{(n)}[n] \mathbf{E}_0^{(n)} \quad (\text{A1})$$

is the perturbation Hamiltonian resulting from interaction between the 2^n -pole moment operator of the molecule [33]

$$\mathbf{M}^{(n)} = \sum_v e_v r_v^n \mathbf{Y}^{(n)}(\mathbf{r}_v) \quad (\text{A2})$$

and an external electric field $\mathbf{E}_0^{(n)} = -\{\nabla^n \phi\}_0$ of ∇ -degree n^\dagger . In (A2), e_v is the v th electric charge of the molecule with radius vector \mathbf{r}_v and the operator $\mathbf{Y}^{(n)}$ of order n is given by:

$$\begin{aligned} \mathbf{Y}^{(n)}(\mathbf{r}_v) &= \frac{(-1)^n}{n!} r_v^{n+1} \nabla^n \left(\frac{1}{r_v} \right) \\ &= \frac{1}{n! r_v^n} \{ (2n-1)!! \mathbf{r}_{v1} \mathbf{r}_{v2} \dots \mathbf{r}_{vn} - (2n-3)!! r_v^2 \sum \mathbf{U}_{12} \mathbf{r}_{v3} \dots \mathbf{r}_{vn} + \dots \\ &\quad + (-1)^k (2n-2k-1)!! r_v^{2k} \sum \mathbf{U}_{12} \dots \mathbf{U}_{2k-1, 2k} \mathbf{r}_{v2k+1} \dots \mathbf{r}_{vn} + \dots \}, \quad (\text{A3}) \end{aligned}$$

where \mathbf{U}_{12} is the unit second-rank tensor and $\sum \mathbf{U}_{12} \mathbf{r}_{v3} \dots \mathbf{r}_{vn}$, etc. are sums of terms resulting from the one written out by interchanging the indices 1, 2, \dots n .

† By ∇ -degree n we mean n -fold application of the operator ∇ .

Using (A 1) and the quantal perturbation method we obtain in turn for the first-, second- and third-order multipole moments induced in the molecule by the external electric field :

$$\left. \begin{aligned} \mathbf{M}^{(n)} &= \sum_{n_1=1}^{\infty} \frac{2^{n_1} n_1!}{(2n_1)!} {}^{(n)}\mathbf{A}^{(n_1)}[n_1] \mathbf{E}_0^{(n_1)}, \\ \mathbf{M}^{(n)} &= \frac{1}{2} \sum_{n_1=1}^{\infty} \sum_{n_2=1}^{\infty} \frac{2^{n_1+n_2} n_1! n_2!}{(2n_1)!(2n_2)!} {}^{(n)}\mathbf{B}^{(n_1+n_2)}[n_1+n_2] \mathbf{E}_0^{(n_1)} \mathbf{E}_0^{(n_2)}, \\ \mathbf{M}^{(n)} &= \frac{1}{6} \sum_{n_1=1}^{\infty} \sum_{n_2=1}^{\infty} \sum_{n_3=1}^{\infty} \frac{2^{n_1+n_2+n_3} n_1! n_2! n_3!}{(2n_1)!(2n_2)!(2n_3)!} \\ &\quad \times {}^{(n)}\mathbf{C}^{(n_1+n_2+n_3)}[n_1+n_2+n_3] \mathbf{E}_0^{(n_1)} \mathbf{E}_0^{(n_2)} \mathbf{E}_0^{(n_3)}. \end{aligned} \right\} \quad (\text{A } 4)$$

Here, the first-order multipole polarizability tensor or, simply, the multipole polarizability tensor

$${}^{(n)}\mathbf{A}^{(n_1)} = \hbar^{-1} \sum_{k \neq g} \omega_{kg}^{-1} (\mathbf{M}_{gk}^{(n)} \mathbf{M}_{kg}^{(n_1)} + \mathbf{M}_{gk}^{(n_1)} \mathbf{M}_{kg}^{(n)}) \quad (\text{A } 5)$$

characterizes the linear or first-order polarization of the 2^n -pole electric moment of a molecule due to an electric field of degree n_1 ; $\mathbf{M}_{gk}^{(n)}$ is the matrix element for the transition from the ground state g to the excited state k with the frequency ω_{gk} in the absence of perturbation.

Similarly the quantum-mechanical expressions for the second- and third-order multipole polarizability tensors are of the form :

$$\begin{aligned} {}^{(n)}\mathbf{B}^{(n_1+n_2)} &= -\hbar^{-2} P(n, n_1, n_2) \left\{ \sum_{k \neq g} \omega_{kg}^{-2} \mathbf{M}_{gk}^{(n)} \mathbf{M}_{kg}^{(n_1)} \mathbf{M}_{gg}^{(n_2)} \right. \\ &\quad \left. - \sum_{k \neq g} \sum_{l \neq g} \omega_{kg}^{-1} \omega_{lg}^{-1} \mathbf{M}_{gk}^{(n)} \mathbf{M}_{kl}^{(n_1)} \mathbf{M}_{lg}^{(n_2)} \right\}, \end{aligned} \quad (\text{A } 6)$$

$$\begin{aligned} {}^{(n)}\mathbf{C}^{(n_1+n_2+n_3)} &= \hbar^{-3} P(n, n_1, n_2, n_3) \left\{ \sum_{k \neq g} \omega_{kg}^{-3} \mathbf{M}_{gk}^{(n)} \mathbf{M}_{kg}^{(n_1)} \mathbf{M}_{gg}^{(n_2)} \mathbf{M}_{gg}^{(n_3)} \right. \\ &\quad - \sum_{k \neq g} \sum_{l \neq g} \omega_{kg}^{-1} \omega_{lg}^{-1} [\omega_{kg}^{-1} \mathbf{M}_{gk}^{(n)} \mathbf{M}_{kg}^{(n_2)} \mathbf{M}_{gl}^{(n_1)} \mathbf{M}_{lg}^{(n_3)} + \omega_{lg}^{-1} \mathbf{M}_{gk}^{(n)} \mathbf{M}_{kl}^{(n_1)} \mathbf{M}_{lg}^{(n_2)} \mathbf{M}_{gg}^{(n_3)} \\ &\quad \left. + \omega_{kg}^{-1} \mathbf{M}_{gk}^{(n)} \mathbf{M}_{gg}^{(n_1)} \mathbf{M}_{gk}^{(n_2)} \mathbf{M}_{gl}^{(n_3)}] + \sum_{k \neq g} \sum_{l \neq g} \sum_{m \neq g} \omega_{kg}^{-1} \omega_{lg}^{-1} \omega_{mg}^{-1} \mathbf{M}_{gk}^{(n)} \mathbf{M}_{kl}^{(n_1)} \mathbf{M}_{lm}^{(n_2)} \mathbf{M}_{mg}^{(n_3)} \right\}, \end{aligned} \quad (\text{A } 7)$$

where $P(n, n_1, n_2, \dots)$ denotes a symmetrizing operation over all permutations of n, n_1, n_2, \dots .

The numerical values of diagonal matrix elements of the second- and third-order multipole polarizability tensors of (A 6) and (A 7) can be calculated directly by methods discussed in the paper of Dalgarno [37] for the case of first-order multipole polarizability.

The effect of molecular interactions on the multipole polarizability tensors (A 5)–(A 7) can be calculated, e.g., by a method analogical to that elaborated by Jansen *et al.* [5, 17].

APPENDIX B

Higher-order intermolecular energies

We consider two non-overlapping molecular systems p and q which have in general 2^n -pole and 2^m -pole electric moments, respectively. The vector connecting the centres of these interacting molecular systems is \mathbf{r}_{pq} , and \mathbf{r}_{pv} and \mathbf{r}_{qv}

are radius vectors of their electric charges e_{pv} and $e_{q\mu}$. The energy of electrostatic interaction between the two molecular systems

$$u_{pq} = \sum_v \sum_\mu \frac{e_{pv} e_{q\mu}}{|\mathbf{r}_{pq} - \mathbf{r}_{pv} + \mathbf{r}_{q\mu}|} \quad (\text{B } 1)$$

may be expanded in the following form [31, 33]:

$$u_{pq} = - \sum_{n=0}^{\infty} \sum_{m=0}^{\infty} (-1)^m \frac{2^{n+m} n! m!}{(2n)!(2m)!} \mathbf{M}_p^{(n)} [n]^{(n)} \mathbf{T}_{pq}^{(m)} [m] \mathbf{M}_q^{(m)}, \quad (\text{B } 2)$$

where the multipole interaction tensor is of the form:

$${}^{(n)}\mathbf{T}_{pq}^{(m)} = -\nabla^{n+m} \left(\frac{1}{r_{pq}} \right) = (-r_{pq})^{-(n+m+1)} \mathbf{Y}^{(n+m)}(\mathbf{r}_{pq}) \quad (\text{B } 3)$$

with ${}^{(n)}\mathbf{T}_{pq}^{(m)} = (-1)^{n+m(m)} \mathbf{T}_{qp}^{(n)}$ and $\mathbf{Y}^{(n+m)}(\mathbf{r}_{pq})$ defined by (A 3) if n is replaced by $n+m$ and \mathbf{r} by \mathbf{r}_{pq} .

We now generalize the equation (B 2) to the case of a multi-component system containing $N_1, N_2, \dots, N_i, \dots$ molecular systems of the first, second, \dots i th species, and obtain for the total first-order (or electrostatic) energy of molecular interactions:

$$V^{(1)} = -\frac{1}{2} \sum_{ij} \sum_{p=1}^{N_i} \sum_{q=1}^{N_j} \sum_{n=0}^{\infty} \sum_{m=0}^{\infty} (-1)^m \frac{2^{n+m} n! m!}{(2n)!(2m)!} \mathbf{M}_{pi}^{(n)} [n]^{(n)} \mathbf{T}_{pq}^{(m)} [m] \mathbf{M}_{qj}^{(m)}, \quad (\text{B } 4)$$

or, in concise form:

$$V^{(1)} = -\frac{1}{2} \sum_i \sum_{p=1}^{N_i} \sum_{n=0}^{\infty} \frac{2^n n!}{(2n)!} \mathbf{M}_{pi}^{(n)} [n] \mathbf{F}_{0pi}^{(n)}, \quad (\text{B } 5)$$

where the molecular electric field of degree n at the centre of the molecular system p of species i due to the electric multipoles of all the other molecular systems is given by:

$$\mathbf{F}_{0pi}^{(n)} = \sum_j \sum_{q=1}^{N_j} \sum_{m=0}^{\infty} (-1)^m \frac{2^m m!}{(2m)!} {}^{(n)}\mathbf{T}_{pq}^{(m)} [m] \mathbf{M}_{qj}^{(m)}. \quad (\text{B } 6)$$

Similarly, the second-order intermolecular energy may be expanded in the following form:

$$V^{(2)} = -\frac{1}{2} \sum_i \sum_{p=1}^{N_i} \sum_{n=1}^{\infty} \sum_{m=1}^{\infty} \frac{2^{n+m} n! m!}{(2n)!(2m)!} \mathbf{F}_{0pi}^{(n)} [n] {}^{(n)}\mathbf{A}_{pi}^{(m)} [m] \mathbf{F}_{0pi}^{(m)}, \quad (\text{B } 7)$$

or by (B 6) in explicit form:

$$V^{(2)} = -\frac{1}{2} \sum_{ijk} \sum_{p=1}^{N_i} \sum_{q=1}^{N_j} \sum_{r=1}^{N_k} \sum_{n=1}^{\infty} \sum_{m=1}^{\infty} \sum_{n_1=0}^{\infty} \sum_{m_1=0}^{\infty} (-1)^{n+m_1} \frac{2^{n+m+n_1+m_1} n! m! n_1! m_1!}{(2n)!(2m)!(2n_1)!(2m_1)!} \\ \times \mathbf{M}_{qj}^{(n_1)} [n_1] {}^{(n_1)}\mathbf{T}_{qp}^{(n)} [n] {}^{(n)}\mathbf{A}_{pi}^{(m)} [m] {}^{(m)}\mathbf{T}_{pr}^{(m_1)} [m_1] \mathbf{M}_{rk}^{(m_1)}. \quad (\text{B } 8)$$

In general we have for the $(s+1)$ -order energy of intermolecular interactions ($s=1, 2, \dots$):

$$V = - \frac{1}{s+1} \sum_i \sum_{p=1}^{N_i} \sum_{n=1}^{\infty} \frac{2^n n!}{(2n)!} \mathbf{M}_{pi}^{(n)} [n] \mathbf{F}_{0pi}^{(n)}, \quad (\text{B } 9)$$

where

$$\mathbf{M}_{pi}^{(s)} = \frac{1}{s!} \sum_{n_1=1}^{\infty} \dots \sum_{n_s=1}^{\infty} \frac{2^{n_1+\dots+n_s} n_1! \dots n_s!}{(2n_1)! \dots (2n_s)!} \times {}^{(n)}\mathbf{A}_{pi}^{(n_1+\dots+n_s)} [n_1 + \dots + n_s] \mathbf{F}_{0pi}^{(n_1)} \dots \mathbf{F}_{0pi}^{(n_s)} \quad (\text{B } 10)$$

is the s th-order multipole moment induced in a molecular system p of species i by molecular electric fields of (B 6).

It is clear that by appropriate simplifying assumptions we can obtain directly from the general expressions (B 4) and (B 8) the special results derived previously by Debye, Keesom and others (see e.g. [30]).

By (A 3) and (B 3), we obtain the following identity:

$${}^{(n)}\mathbf{T}_{pq}^{(m)} [n+m] {}^{(n)}\mathbf{T}_{rs}^{(m)} = \frac{(2n+2m)!}{2^{n+m}} (r_{pq} r_{rs})^{-(n+m+1)} P_{n+m} \left(\frac{\mathbf{r}_{pq} \cdot \mathbf{r}_{rs}}{r_{pq} r_{rs}} \right), \quad (\text{B } 11)$$

which has been recurred to in the course of the present investigation. If in particular $P=r$ and $q=s$ we have $P_{n+m}(1)=1$, and (B 11) yields the identity derived by Jansen [31].

The computations of the various contributions to P_D and P_0 were performed with the help of the following unweighted orientational average:

$$\langle \mathbf{M}_p^{(n)} \mathbf{M}_p^{(m)} \rangle_{\omega} = \begin{cases} \frac{1}{2n+1} (\mathbf{M}_p^{(n)} [n] \mathbf{M}_p^{(n)}) \mathbf{U}^n & \text{for } n=m, \\ 0 & \text{for } n+m \text{ odd.} \end{cases} \quad (\text{B } 12)$$

REFERENCES

- [1] KIRKWOOD, J. G., 1936, *J. chem. Phys.*, **4**, 952.
- [2] YVON, J., 1937, *Recherches sur la théorie cinétique des liquides* (Paris: Herman et Cie).
- [3] BROWN, W. F., Jr., 1950, *J. chem. Phys.*, **18**, 1193, 1200; 1956, *Dielectrics, Encyclopedia of Physics*, Vol. **17** (Berlin: Springer-Verlag).
- [4] DE BOER, J., VAN DER MAESEN, F., and TEN SELDAM, C. A., 1953, *Physica*, **19**, 265.
- [5] JANSEN, L., and MAZUR, P., 1955, *Physica*, **21**, 193, 208.
- [6] ISIHARA, A., and HANKS, R. V., 1962, *J. chem. Phys.*, **36**, 433. ISIHARA, A., 1963, *J. chem. Phys.*, **38**, 2437.
- [7] KAUFMAN, A. N., and WATSON, K. M., 1961, *Phys. Fluids*, **4**, 931.
- [8] KIRKWOOD, J. G., 1939, *J. chem. Phys.*, **7**, 911.
- [9] FRÖHLICH, H., 1949, *Theory of Dielectrics* (Oxford University Press).
- [10] ROSENBERG, R., and LAX, M., 1953, *J. chem. Phys.*, **21**, 424.
- [11] HARRIS, F. E., and ALDER, B. J., 1953, *J. chem. Phys.*, **21**, 1031, 1351. HARRIS, F. E., 1955, *J. chem. Phys.*, **23**, 1662.
- [12] BUCKINGHAM, A. D., 1956, *Proc. roy. Soc. A*, **238**, 235. BUCKINGHAM, A. D., and POPL, J. A., 1955, *Trans. Faraday Soc.*, **51**, 1179.
- [13] COLE, R. H., 1957, *J. chem. Phys.*, **27**, 33.
- [14] MANDEL, M., and MAZUR, P., 1958, *Physica*, **24**, 116.
- [15] BUCKINGHAM, A. D., and POPL, J. A., 1955, *Trans. Faraday Soc.*, **51**, 1029.
- [16] ZWANZIG, R. W., 1956, *J. chem. Phys.*, **25**, 211.
- [17] JANSEN, L., and SOLEM, A. D., 1956, *Phys. Rev.*, **104**, 1291. JANSEN, L., 1958, *Rev. Phys.*, **112**, 434.

- [18] JOHNSTON, D. R., and COLE, R. H., 1962, *J. chem. Phys.*, **36**, 318.
- [19] BIRNBAUM, G., and MARYOTT, A. A., 1962, *J. chem. Phys.*, **36**, 2026, 2032.
- [20] HARRIS, F. E., and BRUSH, S. G., 1956, *J. Amer. chem. Soc.*, **78**, 1280.
- [21] BUCKINGHAM, A. D., 1956, *Trans. Faraday Soc.*, **52**, 1551.
- [22] BUCKINGHAM, A. D., and RAAB, R. E., 1958, *Trans. Faraday Soc.*, **54**, 623.
- [23] KIELICH, S., 1962, *Bull. Acad. Polon. Sci., Sér. math. astr. et. phys.*, **10**, 485, 493, 657.
- [24] JOHNSTON, D. R., OUDEMANS, G. J., and COLE, R. H., 1960, *J. chem. Phys.*, **33**, 1310.
- [25] KIELICH, S., 1963, *Acta phys. polon.*, **24**, 389; 1965, *Ibid.*, **27**, 457.
- [26] KIELICH, S., 1964, *Acta phys. polon.*, **25**, 39.
- [27] FRENKEL, J., 1926, *Lehrbuch der Elektrodynamik*, Vol. I (J. Springer).
- [28] CARLSON, B. C., and RUSHBROOKE, G. S., 1950, *Proc. Camb. phil. Soc.*, **46**, 626.
- [29] POPLÉ, J. A., 1954, *Proc. roy. Soc. A*, **221**, 498, 508.
- [30] HIRSCHFELDER, J. O., CURTISS, Ch. F., and BIRD, R. B., 1954, *Molecular Theory of Gases and Liquids* (New York: J. Wiley).
- [31] JANSEN, L., 1958, *Phys. Rev.*, **110**, 661.
- [32] KIELICH, S., 1965, *Acta phys. polon.*, **27**, 305.
- [33] KIELICH, S., 1965, *Physica*, **31**, 444.
- [34] BUCKINGHAM, A. D., and POPLÉ, J. A., 1955, *Trans. Faraday Soc.*, **51**, 1173.
- [35] KIELICH, S., 1962, *Physica*, **28**, 511, 1123.
- [36] ORCUTT, R. H., 1963, *J. chem. Phys.*, **39**, 605.
- [37] DALGARNO, A., 1962, *Advanc. Phys.*, **11**, 281.

Quadrupole relaxation in solutions of electrolytes

by C. DEVERELL, D. J. FROST† and R. E. RICHARDS

Physical Chemistry Laboratory, South Parks Road, Oxford

(Received 27 May 1965)

Nuclear resonance line widths are recorded for ^{79}Br , ^{81}Br and ^{127}I in aqueous solutions of salts of the alkali metals and alkaline earth metals.

The line width is determined by quadrupole relaxation and is shown to depend on bulk viscosity and on salt concentration according to an equation $\Delta\nu = A\eta + Bc\eta$, where A and B are constants. B is close to zero for strongly hydrated ions, but significant for K^+ , Rb^+ and Cs^+ . At very high concentration the equation no longer holds.

1. INTRODUCTION

Many nuclei with spin quantum number $I > \frac{1}{2}$ possess an electric quadrupole moment which can interact strongly with local electric field gradients. In liquids this interaction provides an important mechanism for nuclear relaxation. The quadrupole interaction energy may be many times greater than the accompanying magnetic dipole interaction and often dominates the relaxation process and determines the observed line width. The general theory of quadrupole relaxation in liquids has been given by Abragam and Pound [1], who derived the following equation for the relaxation rate:

$$T_1^{-1} = \frac{3}{40} \frac{4I(I+1) - 3}{I^2(2I-1)^2} \cdot \left(\frac{eQ}{\hbar} \right)^2 \cdot \left\langle \left(\frac{d^2V}{dZ^2} \right)^2 \right\rangle \cdot \tau_c, \quad (1)$$

where eQ is the quadrupole moment of the nucleus, $\langle (d^2V/dZ^2)^2 \rangle$ is the mean square electric field gradient at the nucleus, and τ_c is a correlation time describing the random molecular motions that give rise to the electric field.

A study of the relaxation times of nuclei with $I > \frac{1}{2}$ present in ions in electrolyte solutions can yield information concerning the electric fields in the neighbourhood of these ions. The varying inhomogeneous fields can arise from the thermal motions of the dipolar solvent molecules and of neighbouring ions; these may either be the vibrational motions of the ligands or solvent molecules, if a complex ion is formed, or the random translational and rotational diffusion of the other particles in solution in cases where the ion containing the resonating nucleus has little interaction with the solvent molecules.

There are two major difficulties in the application of the general formula obtained by Abragam and Pound to the study of quadrupole relaxation in electrolyte solutions. There is considerable uncertainty in the evaluation of the correlation times and it is extremely difficult to evaluate the mean square electric field gradient. The two theories that have been proposed to interpret quadrupole relaxation in these solutions take up opposing standpoints as to the source of the fluctuating field gradients that initiate relaxation. The earlier theory proposed by Valiev [2] attributes them to the translational and rotational motion of nearby water molecules, whilst the second interpretation offered by Hertz [3] assumes that the fields also contain an important contribution from the other ions present in the solution.

† Present Address: Unilever Research Laboratories, Colworth House, Bedford.

Valiev uses a simple model for his calculation. He assumes that the ion that contains the nucleus has little interaction with the solvent molecules and that all the particles present in solution may be assumed to undergo free translational and rotational diffusion. Large ions such as bromide, iodide, potassium, rubidium, and caesium might be expected to fit such a description. Considering the fields arising from the rotational and translational diffusion of the water molecules, he derives the following expression for the case where $I = 5/2$:

$$T_2^{-1} = \frac{216}{875} \pi^2 \cdot \left(\frac{eQ(1+\gamma)}{\hbar} \right)^2 \frac{\mu^2}{(2a)^2} \cdot \frac{N}{V} \cdot \frac{\eta}{kT}; \quad (2)$$

$(1+\gamma)$ is the anti-shielding factor, which corrects for the distortion of the electron shells from spherical symmetry by nearby electric charges, μ is the dipole moment of the water molecule, $2a$ is the separation of the ion and water molecule, η is the viscosity of the solution. The correlation time is assumed to be proportional to the bulk viscosity of the solution.

Hertz first calculates an expression for the line width at infinite dilution, assuming that the electric fields arise from the rotational motion of the water molecules. The equation he derives is similar in form to that of Valiev. If one puts $\tau_c = 4\pi a^3 \eta / 3kT$,

$$T_2^{-1} = 0.24 \frac{32\pi^2}{15} \cdot \left(\frac{eQ \cdot P(1+\gamma)}{\hbar} \right)^2 \mu^2 C_{\text{H}_2\text{O}} \frac{a^3}{r_0^5} \frac{\eta}{kT}; \quad (3)$$

$P = 2\epsilon + 3/5\epsilon$, and is a polarization factor which takes into account the effect of the ion on the solvent surrounding it. $C_{\text{H}_2\text{O}}$ is the concentration of water molecules.

These authors differ, however, in their interpretation of the change of line width with increasing concentration. Valiev neglects ionic effects and assigns the change in line width to an increase in the correlation times for rotational and translational diffusion. Since these are dependent on the viscosity he predicts a linear dependence of line width upon viscosity. Hertz attributes the increases in line width to two effects; the correlation time effect and the additional electric fields of the other ions in solution. It was not possible at that time to decide which of these two terms are most important. Taking into account the translational diffusion of these ions, and using a simple model in which the nucleus is surrounded by a uniform distribution of ions outside a sphere of radius d he calculates the following expressions:

$$T_2^{-1} = \frac{8\pi}{5} \left(\frac{eQ(1+\gamma)P}{\hbar} \right)^2 \left\{ \frac{\mu^2 N k \tau_c}{r_0^5} + \sum \frac{\nu_i z_i^2 e^2 C}{3d^3} \tau_i \right\}, \quad (4)$$

where C is the concentration of the ions, τ_i is the correlation time for the diffusion of the ions. In his interpretation of experimental results, Hertz did not use the viscosity as a measure of the correlation time, and assumed that the increase of line width with increasing concentration arises mainly from the decrease in the separation of the ions. Using his theoretical expression for the line width he attempts to calculate minimum values of the effective distance of approach of the ions with the aid of measured line widths.

In an earlier paper, Richards and Yorke [4] have described measurements of line widths of bromine resonances in the bromide ion. These measurements showed that the viscosity of the solution is of great importance in determining the line width and this paper describes further work.

2. EXPERIMENTAL

The same apparatus and procedure were used as by Richards and Yorke [4]. Modulation corrections to the line widths were made by using different modulation amplitudes and extrapolating to zero amplitude.

3. RESULTS

3.1. Bromine resonances

The resonances of ^{79}Br and ^{81}Br nuclei were measured for all solutions. For the solutions in which $\Delta\nu/\eta$ was constant, the ratio of this quantity for the two isotopes was within experimental error equal to the ratio of the squares of the quadrupole moments of ^{79}Br and ^{81}Br . In the figures which follow, the results refer to ^{79}Br resonances because these are the broader, so that modulation corrections are less important.

3.2. Alkaline earth ions

In all the solutions the line widths increase with concentration and are closely proportional to the viscosity of the solution. The results are given in tables 1 to 4. The relation between line width and viscosity is illustrated in figure 1. In figure 2 the line width for magnesium bromide solutions and $\Delta\nu/\eta$ are plotted against concentration.

Concentration (moles/kg H_2O)	Viscosity (c.p.s.)	^{81}Br line width (c/s)	^{79}Br line width (c/s)
0.49	1.08	432	500
1.00	1.28	490	594
1.77	1.54	569	696
2.33	2.04	774	1000
2.78	2.39	941	1254
3.31	3.39	1376	2037
4.08	4.16	1885	2830
4.92	6.04	2960	4820

Table 1. Magnesium bromide.

Concentration (moles/kg H_2O)	Viscosity (c.p.s.)	^{81}Br line width (c/s)	^{79}Br line width (c/s)
0.46	1.01	406	480
0.87	1.10	431	525
1.46	1.25	474	590
2.26	1.47	554	707
2.68	1.59	611	805
3.43	1.95	763	1079

Table 2. Calcium bromide.

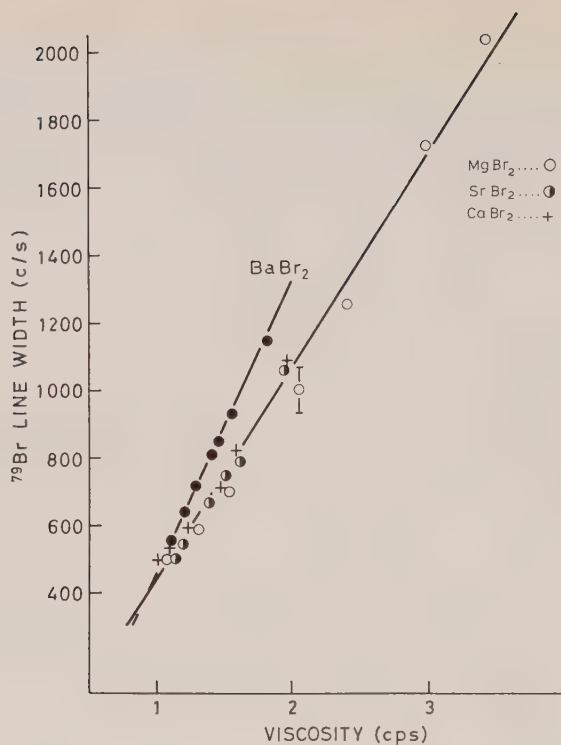


Figure 1. ^{79}Br line widths in solutions of alkaline earth bromides.

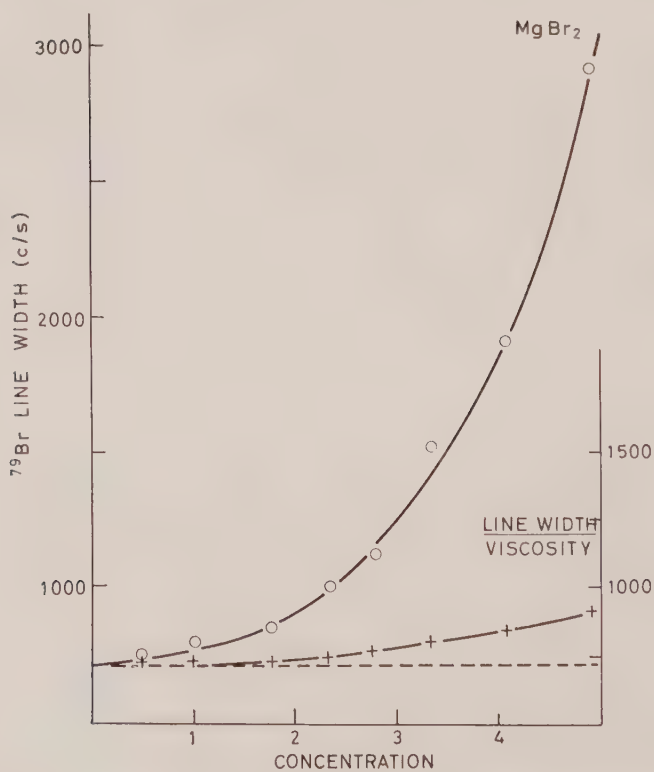


Figure 2. ^{79}Br line width and ^{79}Br line width/viscosity in magnesium bromide solutions.

Concentration (moles/kg H ₂ O)	Viscosity (c.p.s.)	⁸¹ Br line width (c/s)	⁷⁹ Br line width (c/s)
0.51	1.04	330	468
0.79	1.12	370	503
1.05	1.18	385	545
1.62	1.37	478	668
1.93	1.49	538	755
2.23	1.60	583	803
2.82	1.93	738	1060
4.33	2.71	1183	1725

Table 3. Strontium bromide.

Concentration (moles/kg H ₂ O)	Viscosity (c.p.s.)	⁸¹ Br line width (c/s)	⁷⁹ Br line width (c/s)
0.68	1.03	428	507
0.99	1.10	443	549
1.28	1.18	477	636
1.60	1.26	516	725
1.91	1.39	552	819
2.21	1.42	566	848
2.57	1.57	656	935
2.74	1.78	772	1147

Table 4. Barium bromide.

Concentration (moles/kg H ₂ O)	Viscosity (c.p.s.)	⁸¹ Br line width (c/s)	⁷⁹ Br line width (c/s)
0.53	1.00	310	415
1.06	1.05	345	390
1.67	1.09	348	460
2.69	1.23	363	478
3.58	1.34	400	498
4.45	1.44	448	563
5.45	1.60	485	650
6.32	1.77	538	738
7.28	1.95	635	985
8.03	2.08	708	1090

Table 5. Lithium bromide.

3.3. *Alkali metals*

The measurements of line width and viscosity are summarized in tables 5 to 7. In figure 3 the variation of $\Delta\nu/\eta$ with concentration is shown for Li⁺, K⁺, Rb⁺, Cs⁺.

Concentration (moles/kg H ₂ O)	Viscosity (c.p.s.)	⁸¹ Br line width (c/s)	⁷⁹ Br line width (c/s)
0.82	0.90	280	361
1.20	0.89	284	362
1.46	0.88	285	370
2.14	0.88	285	365
2.40	0.88	291	369
2.96	0.89	299	375
4.38	0.91	307	391
4.64	0.93	316	399
5.44	0.95	320	414

Table 6. Potassium bromide.

Concentration (moles/kg H ₂ O)	Viscosity (c.p.s.)	⁸¹ Br line width (c/s)	⁷⁹ Br line width (c/s)
0.29	0.90	313	385
0.52	0.87	320	390
1.81	0.85	333	420
2.21	0.85	333	440
3.34	0.85	343	470
4.12	0.86	355	480
5.42	0.88	388	518

Table 7. Rubidium bromide.

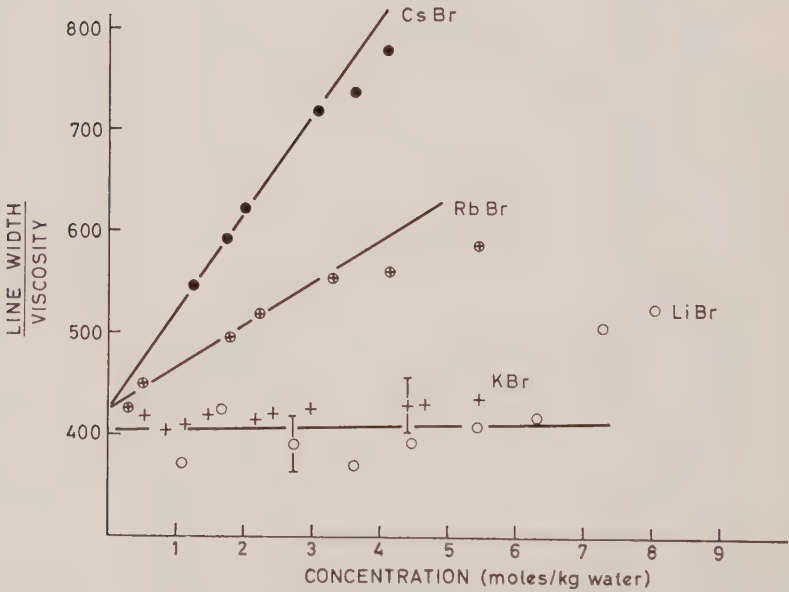


Figure 3. ⁷⁹Br line width/viscosity in solutions of alkali metal bromides.

4. IODINE RESONANCES

The results of measurements of ^{127}I resonances are given in tables 8 to 11. The variation of $\Delta\nu/\eta$ with concentration is shown in figure 4.

Concentration (moles/kg H_2O)	Viscosity (c.p.s.)	^{127}I line width (c/s)
0.53	0.93	1000
1.61	0.97	1180
3.08	1.07	1350
3.56	1.12	1465
4.42	1.21	1625
5.54	1.35	2010
6.87	1.60	2563

Table 8. Sodium iodide.

Concentration (moles/kg H_2O)	Viscosity (c.p.s.)	^{127}I line width (c/s)
1.01	0.85	995
1.39	0.85	986
1.70	0.84	1003
2.46	0.83	1026
2.74	0.83	1037
3.30	0.84	1076
4.80	0.86	1135
5.22	0.87	1154
6.63	0.93	1224
8.80	1.04	1317

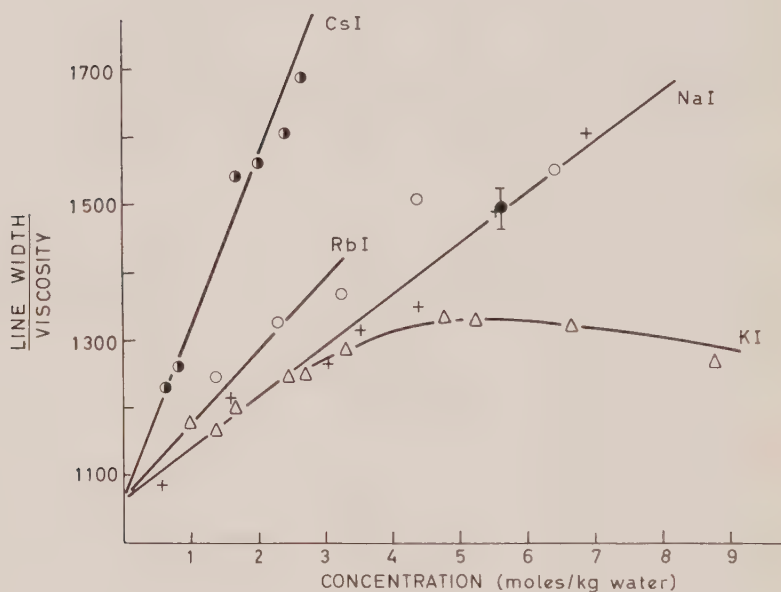
Table 9. Potassium iodide.

Concentration (moles/kg H_2O)	Viscosity (c.p.s.)	^{127}I line width (c/s)
1.36	0.83	1035
2.29	0.84	1110
3.24	0.83	1135
4.37	0.82	1235
5.60	0.85	1263
6.92	0.89	1375

Table 10. Rubidium iodide.

Concentration (moles/kg H ₂ O)	Viscosity (c.p.s.)	¹²⁷ I line width (c/s)
0.65	0.86	1062
0.81	0.86	1086
1.21	—	1198
1.68	0.80	1238
2.01	0.81	1255
2.42	0.80	1280
2.64	0.80	1351

Table 11. Caesium iodide.

Figure 4. ¹²⁷I line width/viscosity in solutions of alkali metal iodides.

5. DISCUSSION

If the broadening of these nuclear resonances is caused by electric quadrupole relaxation, then whatever the mechanism, the line widths of two isotopic species having the same spin quantum number I in a given solution must depend on the ratio of the squares of the quadrupole moments of the nuclei. This is found to be the case for ⁷⁹Br and ⁸¹Br in all the solutions studied. For example, in solutions of the alkaline earths, the ratios of the slopes of the plots of $\Delta\nu$ against η were found to be 1.35, 1.30, 1.41 and 1.42. The expected ratio is 1.39.

The two mechanisms which have been considered as a source of quadrupole relaxation are ion-solvent and ion-ion interactions. The relative importance of these effects depends on the salt concerned. In either case it is important to have some measure of the variation of the correlation times τ_c and τ_i in these solutions. Ideally these quantities should be measured from relaxation time and

diffusion coefficient measurements on the appropriate nuclei for each solution. Few of these data are available, however, and so we turn to a readily measurable parameter. There is good evidence [5] that in solutions of small molecules the molecular correlation times are approximately linearly proportional to the bulk viscosity of the liquid. The viscosity is easily measured for these solutions and so we shall use its variations as a measure of the variation of τ_c and τ_i . Equation (4) may then be re-written:

$$\Delta\nu = A\eta + Bc\eta, \quad (5)$$

where A and B are constants, A depending mainly on solvent and B mainly on the cation, and c is the concentration of the salt. For solutions of strongly hydrated ions, B is likely to be small and the line width will depend only on the solvent. This is illustrated for LiBr in figure 5. The line width varies steeply with concentration, but $\Delta\nu/\eta$ remains constant as expected if B is small for Li^+ . On the other hand, for CsBr (figure 5), $\Delta\nu/\eta$ rises linearly with concentration, showing that B is significant and ion-ion interactions are playing an important part.

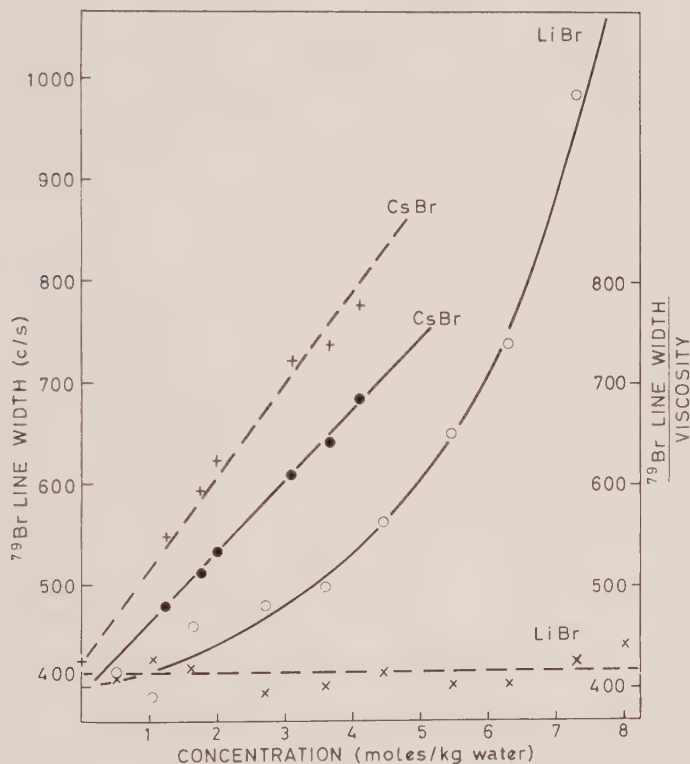


Figure 5. Comparison of ^{79}Br line width and ^{79}Br line width/viscosity in caesium bromide and lithium bromide solutions.

Similar consideration of the other salt solutions shows that the results can be fitted very satisfactorily to equation [5] at concentrations not exceeding 4 molal, above which deviations often seem to occur. The values of A and B obtained are given in table 12.

The agreement between experiment and equation (5) is shown for sodium iodide in figure 6.

For LiBr and NaBr, $B=0$ and the line width arises almost entirely from ion-solvent interaction. This is no doubt because the Li and Na ions are strongly solvated, so that the anions and cations do not approach closely enough to produce an electric field gradient at the Br nucleus. The larger cations are less strongly solvated and ion-ion interaction becomes progressively more important. The

Bromides		Iodides	
A $\text{sec}^{-1} \text{poise}^{-1}$ $\times 10^{-2}$	B $\text{sec}^{-1} \text{poise}^{-1}$ $\text{molal}^{-1} \times 10^{-2}$	A $\text{sec}^{-1} \text{poise}^{-1}$ $\times 10^{-2}$	B $\text{sec}^{-1} \text{poise}^{-1}$ $\text{molal}^{-1} \times 10^{-2}$
Li 400	~ 0	—	—
Na 394	~ 0	1067	70
K 400	7	1067	70
Rb 427	40	1067	105
Cs 426	97	1067	240

Table 12.

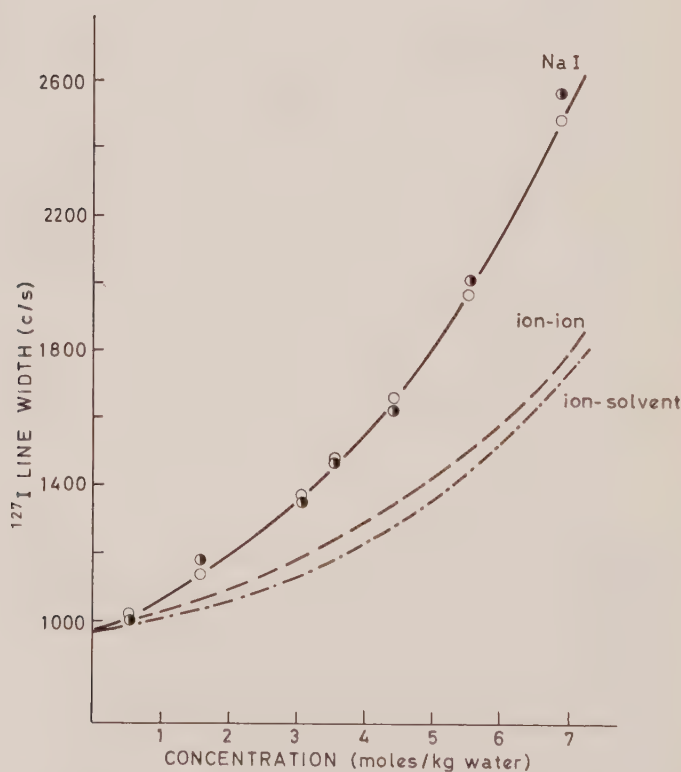


Figure 6. ^{127}I line width in sodium iodide solutions, showing relative contributions from ion-solvent and ion-ion interactions.

● experimental.

○ equation 5.

occurrence of a non-zero value of the constant B may be correlated with measurements of the resonance signal from the nuclei of cations present in these solutions. Wertz [6] has found that the line width of the ^{23}Na signal remains constant in sodium bromide solutions, but it increases with concentration in sodium iodide solutions. Measurements we have made on the ^{87}Rb resonance line width shows that it is dependent upon the concentration of iodide and bromide ions, the broadening effect of the iodide ion being greater than that of the bromide ion. It seems likely that this broadening may be assigned to an ion-ion interaction, which also accounts for a significant value of the constant B . Although the qualitative increase in the value of B is easy to understand, it is doubtful whether much significance can be attached to the absolute values, in view of the many unknown parameters involved.

At concentrations greater than 4 molal, equation (5) usually gives too large a line width, suggesting some form of saturation of the ion-ion interactions. It is important to appreciate that even at high concentrations and for salts with large values of B , the viscosity of the solution plays an important role in determining the line width.

The results on the solutions of the bromides of the alkaline earths can be fitted to equation (5) with $A = 420\text{--}450 \times 10^2 \text{ sec}^{-1} \text{ poise}^{-1}$ and with B very close to zero. This would be expected from the strong solvation of the doubly charged cations. However, there is a small variation of $\Delta\nu/\eta$ with concentration which is illustrated on a large scale in figure 7. It appears that the ion-ion interactions increase with concentration faster than a linear term in B (equation (5)) can account for.

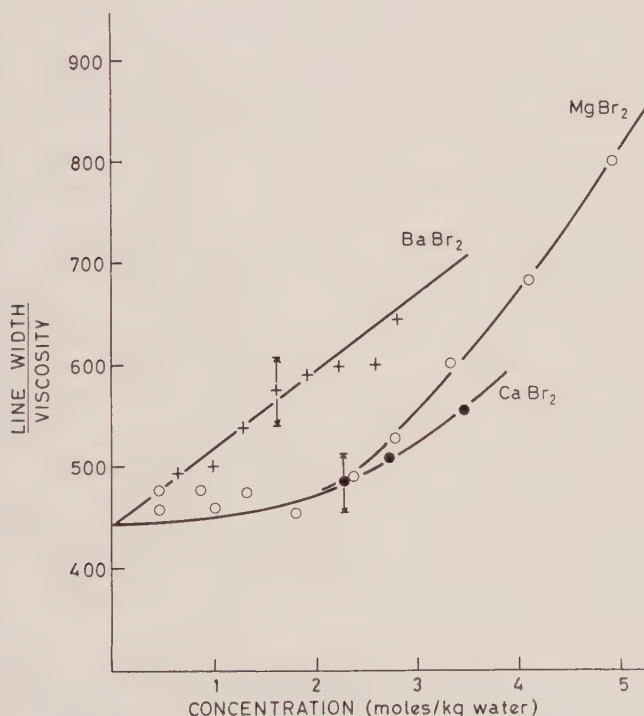


Figure 7. ^{79}Br line width/viscosity in solutions of alkaline earth bromides.

However, this only occurs at such high concentrations that the molar ratio of water to salt is approaching 10 : 1, where our simple model can hardly be expected to hold.

Non-aqueous solvents

A similar analysis can be applied to the results of Richards and Yorke [4]. For a two component solvent, the constants in equation (4) will differ, but will be constant for a given solvent composition.

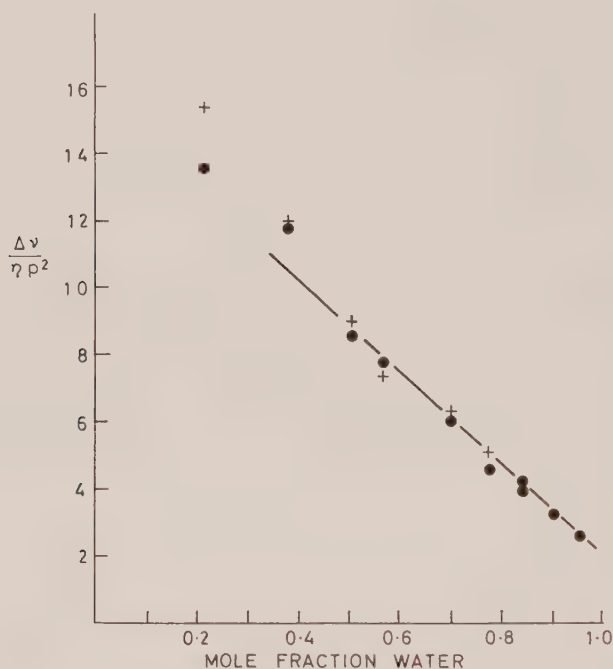


Figure 8. ^{79}Br resonances of solutions of sodium bromide in methanol/water mixtures.

For solvents of constant composition, the line width should therefore vary linearly with viscosity, provided ion-ion interactions are small. The results obtained by Richards and Yorke for sodium bromide are consistent with this conclusion in mixtures of methanol and water and of glycine and water of various compositions. For a methanol/water mixture with weight fraction of water 0.75 ($\epsilon = 67$), $\Delta\nu/\eta$ in solutions of sodium bromide was $715 \times 10^2 \text{ sec}^{-1} \text{ poise}^{-1}$ and independent of salt concentration. For a similar mixture with weight fraction of water 0.5 ($\epsilon = 55$), $\Delta\nu/\eta$ showed a slow increase with concentration from 1074×10^2 to $1320 \times 10^2 \text{ sec}^{-1} \text{ poise}^{-1}$. The greater the proportion of non aqueous component of the solvent the greater is $\Delta\nu/\eta$ (figure 8). This may arise from the longer correlation time of the larger molecule for a given bulk viscosity. At the lower dielectric constants, there is an increasing contribution from cation-anion interactions.

6. CONCLUSIONS

The line widths of bromine and iodine resonances in solutions of salts depend on electric quadrupole relaxation. The electric field gradients concerned with the

relaxation can be caused by ion-solvent and by ion-ion interactions, the relative importance of these depending on the cation. In any case the viscosity of the solution has an important influence on the line width, because of its relation to the molecular and ionic correlation times. The ion-solvent interactions are dominant when the cation is strongly hydrated (alkaline earths, Li^+ and Na^+), but ion-ion interactions become most important for weakly solvated cations (Rb^+ , Cs^+).

We thank the Hydrocarbon Research Group of the Institute of Petroleum for grants in aid of apparatus. We are also grateful to the Science Research Council for financial assistance and for a Maintenance Grant (C.D.).

Note added in proof.—A recent paper by Valier [*Zhur. strukt. khim.*, 1964, **5**, 477] discusses the role of ion-ion interactions in the nuclear quadrupole relaxation of diamagnetic ions. The equation derived is similar to that of Hertz [3], and the predicted dependence on the concentration and viscosity of the salt solutions is in agreement with the experiments described above.

REFERENCES

- [1] ABRAGAM, A., and POUND, R. V., 1953, *Phys. Rev.*, **92**, 943.
- [2] VALIEV, K. A., and KHABIBULLIN, B. M., 1961, *Russ. J. phys. Chem.*, **35**, 1118.
- [3] HERTZ, H. G., 1961, *Z. Elektrochem.*, **65**, 20.
- [4] RICHARDS, R. E., and YORKE, B. A., 1963, *Mol. Phys.*, **6**, 289.
- [5] BLOEMBERGEN, N., PURCELL, E. M., and POUND, R. V., 1948, *Phys. Rev.*, **73**, 679.
- [6] JARDETSKY, O., and WERTZ, J. E., 1960, *J. Amer. chem. Soc.*, **82**, 318.

Nuclear magnetic energy levels and symmetry wave functions for six chemically equivalent spin $\frac{1}{2}$ nuclei with $C_{3v} \times C_i$ symmetry

by A. NESZMÉLYI

Central Research Institute for Chemistry,
Hungarian Academy of Sciences, Budapest, Hungary

(Received 1 June 1965)

The nuclear Zeeman energy levels of six chemically equivalent and interacting spin $\frac{1}{2}$ nuclei with $C_{3v} \times C_i$ symmetry are calculated and the symmetry adapted spin-functions are given.

The factoring of the spin-Hamiltonian according to the irreducible representations of the symmetry point group and F_z , the expectation value of the total spin component in the z direction, greatly reduces the numerical work required for theoretical calculation of spectra [1] or for the derivation of N.M.R. parameters from experimental spectra by machine iteration [2]. The idea of sub-spectral analysis in terms of local symmetry groups has been extended recently [3] to the analysis of all types of N.M.R. spectra.


	
$C_{3v} \times C_i$	$S(6)$
E	(1)(2)(3)(4)(5)(6)
C_3^+ C_3^-	(123)(456) (132)(465)
$\sigma_{d_{14}}$ $\sigma_{d_{36}}$ $\sigma_{d_{25}}$	(1)(23)(4)(56) (12)(3)(45)(6) (13)(2)(46)(5)
i	(14)(25)(36)
S_6^- S_6^+	(153426) (162435)
C_{2_1} C_{2_2} C_{2_3}	(14)(26)(35) (16)(25)(34) (15)(24)(36)

Table 1. Elements of the symmetry group $C_{3v} \times C_i$ as permutations of the symmetric group $S(6)$. The cyclohexane structure represents the symmetry.

The basic symmetry functions which belong to the various irreducible representations of the symmetry group of n chemically equivalent nuclei A_n , are given in the literature for up to four spin $\frac{1}{2}$ nuclei [1, 4]. The partition of the 2^n symmetry functions among the irreducible representations and F_z values are summarized for $n \leq 4$ and extended for the case $n=6$ in [3]. The symmetry functions themselves are usually not required for most of the calculations. However, in some cases it has been found useful to know the A_6 symmetry functions and energy levels and a derivation for the $C_{3v} \times C_i$ group was worked out. (D_6 , D_{3d} and D_{3h} are isomorphic to $C_{3v} \times C_i$.) The group elements and their expressions as permutations of the symmetric group $S(6)$ are given in table 1. The cyclohexane structure was taken as the representative of the $C_{3v} \times C_i$ symmetry.

The Hamiltonian for the six-spin system was chosen so as to describe all the possible spin-spin couplings. Let J_{12} , J_{13} and J_{14} denote the coupling constant between the first, second and third neighbours, then the spin-Hamiltonian in units of h is as follows:

$$H = \nu_A F_z + \sum_{k=1}^6 \mathbf{I}_k \cdot (J_{12} \mathbf{I}_{k+1} + J_{13} \mathbf{I}_{k+2} + \frac{1}{2} J_{14} \mathbf{I}_{k+3}).$$

Here \mathbf{I}_k denotes the spin vector operator of the k th particle. (When in the course of summation any of the indices exceed six, subtract six from its value.)

$C_{3v} \times C_i$	A_{1g}			A_{1u}			A_{2g}			A_{2u}			E_g			E_u			Number of energy levels	Number of allowed transitions
D_6 D_{3d} D_{3h}	A_1 A_{1g} A_1			B_2 A_{2u} A_2''			A_2 A_{2g} A_2			B_1 A_{1u} A_1''			E_1 E_u E''			E_2 E_g E'				
F F_z	3	1	1	2	0	0	0	1	2	1	1	2	1	0						
3	1														1			1		
2	1			1					1			1			4			4		
1	1	1	1	1				1	1	1	1	1	1		10			10		
0	1	1	1	1	1	1	1	1	1	1	1	1	1	1	14			10		
-1	1	1	1	1				1	1	1	1	1	1		10			4		
-2	1			1					1			1			4			1		
-3	1														1					
Total:																		44	30	

Table 2. Classification of the basic symmetry functions of the A_6 system with $C_{3v} \times C_i$ symmetry.

Irred. repr.	$2F+1$ $nD_j F_z$	N^{-2}	Simultaneous eigenfunctions of F^2 , F_z and of the symmetry operators
A_{1g}	${}^7A_{1g}^3$	1	aa
	${}^7A_{1g}^2$	6	$(1+i)(ea+ba+ac)$
	${}^7A_{1g}^1$	15	$[ee+bb+cc+(1+i)(cb+ce+af+da+ag+eb)]$
	${}^7A_{1g}^0$	20	$(1+i)(cf+gb+de+ah+bd+gc+fe+dc+eg+fb)$
	${}^3_1A_{1g}^1$	12	$(1+i)(cb+ce+af+da-ag-eb)$
	${}^3_1A_{1g}^0$	24	$(1+i)(3cf-gb-de-ah)$
A_{1u}	${}^5_2A_{1u}^1$	60	$(1+i)[-4(ee+bb+cc)+cb+ce+af-da-ag-eb]$
	${}^5_2A_{1u}^0$	120	$(1+i)[3cf+3(gb+de+ah)-2(bd+gc+fe+dc+eg+fb)]$
	${}^5_1A_{1u}^2$	6	$(1-i)(ea+ba+ac)$
	${}^5_1A_{1u}^1$	6	$(1-i)(cb+ce+af)$
	${}^5_1A_{1u}^0$	36	$(1-i)(3cf+gb+de+ah-bd-gc-fe-dc-eg-fb)$
	${}^1_1A_{1u}^0$	8	$(1-i)(3cf-gb-de-ah)$
A_{2g}	${}^1_2A_{1u}^0$	72	$(1-i)[3cf+gb+de+ah+2(bd+gc+fe+dc+eg+fb)]$
	${}^1A_{2g}^0$	12	$(1+i)(bd+gc+fe-dc-eg-fb)$
	${}^3A_{2u}^1$	6	$(1-i)(da+ag+eb)$
	${}^3A_{2u}^0$	12	$(1-i)(bd+gc+fe-dc-eg-fb)$
	${}^5E_g^2$	12	$(1+i)(2ea-ba-ac)$
	${}^5E_g^1$	4	$(1+i)(ba-ac)$
E_g	${}^5E_g^1$	48	$[-2(2ee-bb-cc)+(1+i)(2cb-ce-af+2da-ag-eb)]$
	${}^5E_g^0$	16	$[-2(bb-cc)+(1+i)(ce-af+ag-eb)]$
	${}^5E_g^0$	8	$(1+i)(-bd+fe-dc+ef)$
	${}^5E_g^0$	24	$(1+i)(bd-2gc+fe-dc-eg+2fb)$
	${}^3_1E_g^1$	24	$(1+i)(2cb-ce-af-2da-ag-eb)$
	${}^3_1E_g^1$	8	$(1+i)(ce-af-ag+eb)$
	${}^3_1E_g^0$	12	$(1+i)(2gb-de-ah)$
	${}^3_1E_g^0$	4	$(1+i)(de-ah)$
	${}^3_2E_g^1$	48	$[2(2ee-bb-cc)+(1+i)(2cb-ce-af+2da-ag-eb)]$
	${}^3_2E_g^1$	16	$[2(bb-cc)+(1+i)(ce-af+ag-eb)]$
	${}^3_2E_g^0$	24	$(1+i)(bd-2gc+fe-dc+eg-2fb)$
	${}^3_2E_g^0$	8	$(1+i)(bd-fe-dc+eg)$
E_u	${}^5E_u^3$	12	$(1-i)(2ea-ba-ac)$
	${}^5E_u^3$	4	$(1-i)(ba-ac)$
	${}^5E_u^1$	48	$(1-i)(2cb-ce-af-3ag+3eb)$
	${}^5E_u^1$	16	$(1-i)(ce-cf+2da-ag-eb)$
	${}^5E_u^0$	72	$(1-i)[2(2gb-de-ah)-bd+gc-fe-dc-eg+2fb]$
	${}^5E_u^0$	24	$(1-i)[2(de-ah)-bd+fe+dc-eg]$
	${}^3E_u^1$	16	$(1-i)(2cb-ce-af+ag-eb)$
	${}^3E_u^1$	48	$(1-i)(3ce-3af-2da+ag+eb)$
	${}^3E_u^0$	8	$(1-i)(bd-fe+dc-eg)$
	${}^3E_u^0$	24	$(1-i)(-bd+2gc-fe+dc+eg-2fb)$
	${}^1E_u^0$	36	$(1-i)(2gb-de-ah+bd-2gc+fe+dc+eg-2fb)$
	${}^1E_u^0$	12	$(1-i)(de-ah+bd-fe-dc+eg)$

Table 3. Normalized symmetry-functions for the A_6 spin-system with $C_{3v} \times C_i$ symmetry. The basic product functions are designated by two-letter symbols, where $a = \alpha\alpha\alpha$, $b = \alpha\alpha\beta$, $c = \alpha\beta\alpha$, $d = \alpha\beta\beta$, $e = \beta\alpha\alpha$, $f = \beta\alpha\beta$, $g = \beta\beta\alpha$ and $h = \beta\beta\beta$. The operator i changes the order of the letters, so e.g. $(1 \pm i)(ah-2bc) = ah-2bc \pm ha \mp 2cb = \alpha\alpha\alpha\beta\beta\beta - 2\alpha\alpha\beta\alpha\beta\alpha \pm (\beta\beta\beta\alpha\alpha\alpha - 2\alpha\beta\alpha\alpha\alpha\beta)$.

Starting from the 64 orthonormal basic products:

$$\psi = \prod_{j=1}^6 \phi_{m_j}(j), \quad (m_j = \frac{1}{2} \quad \text{or} \quad -\frac{1}{2}), \quad \phi_{1/2} = \alpha, \quad \phi_{-1/2} = \beta,$$

we generated symmetry adapted functions using the symmetrizing operator [5, 6]:

$$W_{ts}^k = \frac{d_k}{g} \sum_{R \in G} D^k(R)_{ts}^* \cdot R.$$

The functions:

$$u_t^{(k)} = W_{ts}^k \psi, \quad (t = 1, 2, \dots, d_k)$$

transform as partners according to the t th column of the k th irreducible representation D^k , of dimension d_k of the group G of order g .

Designation of the symmetry-function $2F+1D_j$	Diagonal matrix elements. Take the sum of the indicated multiples of			Off Diagonal matrix elements	Exact eigenvalues
	J_{12}	J_{13}	$\frac{1}{2}J_{14}$		
${}^7A_{1g}$	$\frac{3}{2}$	$\frac{3}{2}$	$\frac{3}{2}$	—	
${}^3_1A_{1g}$	-1	+1	$-\frac{5}{2}$	$\frac{\sqrt{5}}{2}(-J_{12}+J_{13}) + \nu_A F_z$	$\nu_A F_z - J_{12} - \frac{1}{4}J_{14} \pm \sqrt{[(J_{13}-J_{14})^2 + \frac{5}{4}(J_{13}-J_{12})^2]}$
${}^3_2A_{1g}$	-1	-1	$\frac{3}{2}$		
${}^5A_{1u}$	$-\frac{1}{2}$	$\frac{3}{2}$	$-\frac{1}{2}$	—	
${}^1_1A_{1u}$	0	0	$-\frac{9}{2}$	$\frac{3}{2}(-J_{12}+J_{13})$	$-J_{12} - \frac{5}{4}J_{14} \pm \sqrt{[(J_{12}-J_{14})^2 + \frac{9}{4}(J_{13}-J_{12})^2]}$
${}^1_2A_{1u}$	-2	0	$-\frac{1}{2}$		
${}^3A_{2u}$	$\frac{1}{2}$	$-\frac{3}{2}$	$-\frac{1}{2}$	—	
${}^1A_{2g}$	$-\frac{3}{2}$	$-\frac{3}{2}$	$+\frac{3}{2}$	—	
5E_g	0	0	$\frac{3}{2}$	—	
3_1E_g	$\frac{1}{2}$	$-\frac{1}{2}$	$-\frac{5}{2}$	$\frac{-J_{12}+J_{13}}{\sqrt{2}} + \nu_A F_z$	$\nu_A F_z - \frac{1}{4}(J_{12}+3J_{13}+J_{14}) \pm \sqrt{[(\frac{3}{4}J_{12} + \frac{1}{4}J_{13}-J_{14})^2 + \frac{1}{2}(J_{13}-J_{12})^2]}$
3_2E_g	-1	-1	$\frac{3}{2}$		
5E_u	1	0	$-\frac{1}{2}$	—	
3E_u	-1	0	$-\frac{1}{2}$	—	
1E_u	$-\frac{1}{2}$	$-\frac{3}{2}$	$-\frac{1}{2}$	—	

Table 4. Matrix elements of the Hamiltonian between the symmetry functions of table 3. The exact eigenvalues of the A_g system with the symmetry $C_{3v} \times C_i$ coincide with the diagonal matrix elements if the representation of a given multiplicity occurs only once.

In the basic functions $u_i^{(k)}$ the 64 dimensional representation Γ_{64} of $C_{3v} \times C_i$ generated by the basic products appears in reduced form:

$$\Gamma_{64} = 13A_{1g} \oplus A_{2g} \oplus 11E_g \oplus 7A_{1u} \oplus 3A_{2u} \oplus 9E_u.$$

Here A_{1g}, A_{2g}, \dots are the irreducible representations of the group $C_{3v} \times C_i$. The direct components of Γ_{64} belong to one of the values of F_z , since every $u_i^{(k)}$ has a definite value of F_z and functions of different F_z do not mix. Further factoring may be obtained taking into account that not only F_z but also F^2 , the square of the total angular momentum commutes with the Hamiltonian of an A_n system [7].

Table 2 shows the classification of the symmetry functions according to F_z, F and the irreducible representations of the symmetry group. The corresponding symbols of the isomorphic groups are also given.

The normalized symmetry functions are collected in table 3. The second column contains the multiplicity $M=2F+1$ and the F_z values as upper indices. The third column gives the inverse square of the normalization factor N . Functions belonging to negative F_z values are not shown, these may be obtained from the $+F_z$ functions by simple interchanging of all α and β spin-functions.

The number of energy levels of the A_6 system with the given symmetry and the allowed transitions are to be seen in table 2. Of course, in pure A_6 systems these transitions are not observable.

The matrix elements of the Hamiltonian are given in table 4. Off-diagonal elements occur only in those cases, when more than one eigenfunctions exist with the same eigenvalues of F^2 and F_z and each of them transform according to the same column of an irreducible representation of the symmetry point group. (A left subscript distinguishes these functions in table 3.) To get the exact eigenvalues shown in the third column of table 4, it was necessary to solve only three second-order problems, because the corresponding pairs of the two A_{1g} and E_g triplet sets have identical matrix elements.

REFERENCES

- [1] CORIO, P., 1961, *Chem. Rev.*, **60**, 363.
- [2] SWALEN, J. D., and REILLY, C. A., 1962, *J. chem. Phys.*, **37**, 21.
- [3] DIEHL, P., JONES, R. G., and BERNSTEIN, H. J., 1965, *Canad. J. Chem.*, **43**, 81.
- [4] MCCONNEL, H. M., MCLEAN, A. D., and REILLY, C. A., 1955, *J. chem. Phys.*, **23**, 1152.
- [5] MELVIN, M. A., 1956, *Rev. mod. Phys.*, **28**, 18.
- [6] ALTMANN, S. L., 1962, *Quantum Theory*, Ed. D. R. Bates (New York), p. 143.
- [7] POPL, J. A., SCHNEIDER, W. G., and BERNSTEIN, H. J., 1959, *High-resolution Nuclear Magnetic Resonance* (New York).

The relationship between electron spin rotation coupling constants and g -tensor components

by R. F. CURL, JR.†

Mathematical Institute, Oxford University

(Received 7 September 1964; revision received 19 November 1964)

The Hamiltonian (Pauli approximation) which gives rise to the spin-rotation coupling tensor and the electron spin g tensor is set up for a $^2\Sigma$ polyatomic molecule. A relationship between the spin-rotation interaction and the Zeeman effect is suggested. The magnitudes of those terms which prevent this relationship from being exact are estimated. The relationship should be valid to two significant figures in the correction of the g factor from that of the free electron in most cases. Some comparisons with experiment are made.

1. INTRODUCTION

The relationship between nuclear-spin rotation coupling constants and diamagnetic shielding of the nucleus has been discussed by Ramsey [1] and by Hameka [2]. It is clear that such a relationship should probably also be found for the case of the electron. The Hamiltonian involved was discussed by Van Vleck [3, 4]. However, he did not consider the particular relationship sought here.

This relationship is that the components of the g tensor be related to those of the spin-rotation tensor by the equation:

$$g_{ij} = g_e \delta_{ij} - \hbar^{-2} \sum_k \epsilon_{ik} I_{kj}, \quad (1)$$

where $g_e = 2.0023$, I_{kj} is the inertial tensor component, ϵ_{ik} is the spin-rotation tensor component.

Suppose that quantum mechanical treatment of the electronic motion has been made for the nuclei fixed and the electrostatic Hamiltonian. Then the spin-rotation interaction can be treated by introducing additional terms in the Hamiltonian which are treated as perturbations. Certain terms will contribute in first-order perturbation and some in second-order perturbation. The first-order perturbation contribution arises from the interaction of the magnetic field generated by the rotation of the nuclei with the electron spin magnetic moment. The second-order perturbation contribution arises from two different Hamiltonian terms.

If the Hamiltonian is of the form:

$$H = H^{(0)} + H_a^{(1)} + H_b^{(1)}, \quad (2)$$

† On leave from the Department of Chemistry, Rice University.

then the second-order energy is given by

$$E_j^{(2)} = \sum_i' \frac{|\langle i | H_a^{(1)} + H_{bR}^{(1)} | j \rangle|^2}{E_j^{(0)} - E_i^{(0)}}. \quad (3)$$

One of the terms, $H_a^{(1)}$, is the interaction between the electron spin and the electronic orbital angular momentum. The other term, $H_{bR}^{(1)}$, is the interaction between the molecular rotation and the electronic orbital angular momentum.

The Zeeman effect can also be treated as a perturbation. The first-order contribution consists of the interaction of the electron spin magnetic moment with the field (which dominates). This appears as two terms. One is the interaction of the bare electron with the field. The other is the interaction of the electron spin, external field and other electrons which gives rise to the diamagnetic shielding of the electron spin magnetic moment from the external field. This term is gauge dependent and the overall expression for the energy only becomes gauge independent when the second-order perturbation terms are considered. Obviously the second-order perturbation terms are also gauge dependent.

The second-order energy involves two Hamiltonian terms as in equations (2) and (3). For the Zeeman effect one of these terms, $H_a^{(1)}$, is electron spin-electronic orbital interaction, the same term as is found in the spin rotation interaction. The other term, $H_{bZ}^{(1)}$, is the interaction between the external field and the magnetic moment of electronic orbital angular momentum. This term is gauge dependent. If the origin of the vector potential is taken to be the centre of mass, $H_{bZ}^{(1)}$ can be related to $H_{bR}^{(1)}$. From this equation (1) can be derived if the first-order perturbation contribution to the spin rotation interaction and to the electron magnetic moment shielding in the Zeeman effect can be neglected.

The terms contributing in first order are different from those contributing in second-order. There is therefore no reason that the second-order perturbation contribution of one sort of term should not dominate the first-order perturbation contribution of another sort of term. The point to be decided is whether this is indeed the case. This can be approached by experimental tests of the relationship (1) (*vide infra*), by estimating the second-order effects [6] or by comparison of estimates of the first-order effect to experiment. Most consideration will be devoted to the last approach.

In order to see how the second-order contributions lead to the relationship, equation (1), consider the terms† $H_a^{(1)}$, $H_{bR}^{(1)}$, $H_{bZ}^{(1)}$

$$H_a^{(1)} = \sum_j \boldsymbol{\eta}_{sj} \cdot \mathbf{S}_j, \quad (4a)$$

$$H_{bR}^{(1)} = -\mathbf{L} \cdot \boldsymbol{\mu} \cdot \mathbf{M}, \quad (4b)$$

$$H_{bZ}^{(1)} = \hbar^{-1} \mu_B (\mathbf{L} \cdot \mathbf{H}), \quad (4c)$$

where $\boldsymbol{\eta}_{sj}$ is the spin orbit coupling operator for electron j , \mathbf{S}_j is the electron spin operator for electron j , \mathbf{L} is the electronic orbital angular momentum about the centre of mass, $\boldsymbol{\mu}$ is the inverse inertial constant tensor, \mathbf{M} is the rotational angular momentum, \mathbf{H} is the external field, μ_B is the Bohr magneton. The origin of these terms is considered in detail below and in [6].

† Symbols in bold face sans serif are second rank tensors.

In second-order perturbation these lead to the effective Hamiltonians:

$$\begin{aligned} \langle i|H_{\text{SR}}|i'\rangle &= \langle i|\mathbf{S} \cdot \boldsymbol{\epsilon} \cdot \mathbf{N}|i'\rangle \\ &= \sum_{l \neq l_0, i''} \frac{2\langle l_0 i|H_a^{(1)}|li''\rangle \langle li''|H_{bR}^{(1)}|l_0 i'\rangle}{E_0 - E_l}, \end{aligned} \quad (5a)$$

$$\begin{aligned} \langle i|H_Z|i'\rangle &= \langle i|\mu_B(\mathbf{S} \cdot \mathbf{g} \cdot \mathbf{H})|i'\rangle \\ &= \sum_{l \neq l_0, i''} \frac{2\langle l_0 i|H_a^{(1)}|li''\rangle \langle li''|H_{bZ}^{(1)}|l_0 i'\rangle}{E_0 - E_l} + g_e \mu_B \langle i|(\mathbf{H} \cdot \mathbf{S})|i'\rangle, \end{aligned} \quad (5b)$$

where $\mathbf{N} = \hbar^{-1}\mathbf{M}$ and the term $g_e \mu_B(\mathbf{H} \cdot \mathbf{S})$ comes from the first-order interaction of the bare electron spin magnetic moment and the external field.

The effective Hamiltonians arise from a Van Vleck perturbation treatment. In this treatment the Wigner-Eckart theorem is used to allow the replacement [3, 6] of \mathbf{S}_j with $k_j \mathbf{S}$. The \mathbf{S} can then be extracted [3] from the matrix elements to give an effective Hamiltonian. The excitation to state l is an electronic excitation. In this virtual excitation the nuclei do not move (Franck-Condon principle). Therefore the tensor, $\boldsymbol{\mu}$, can also be extracted from the matrix elements. In addition \mathbf{H} and \mathbf{N} can be extracted to give effective Hamiltonians. Thus one has:

$$H_{\text{SR}} = \mathbf{S} \cdot \boldsymbol{\epsilon} \cdot \mathbf{N} = \mathbf{S} \cdot \left[\sum_{l \neq l_0, j} \frac{-2\langle l_0 | k_j \boldsymbol{\eta}_{sj} | l \rangle \langle l | \mathbf{L} | l_0 \rangle}{E_0 - E_l} \right] \cdot \boldsymbol{\mu} \cdot \hbar \mathbf{N}, \quad (6a)$$

$$\begin{aligned} H_Z &= \mu_B(\mathbf{S} \cdot \mathbf{g} \cdot \mathbf{H}) \\ &= g_e \mu_B(\mathbf{S} \cdot \mathbf{H}) + \hbar^{-1} \mu_B \mathbf{S} \cdot \left[\sum_{l \neq l_0, j} \frac{2\langle l_0 | k_j \boldsymbol{\eta}_{sj} | l \rangle \langle l | \mathbf{L} | l_0 \rangle}{E_0 - E_l} \right] \cdot \mathbf{H}. \end{aligned} \quad (6b)$$

NO ₂		
$(g_{aa} - g_e)^a$	$(g_{bb} - g_e)$	$(g_{cc} - g_e)$
-0.0113	-0.0008	+0.0034
$-\epsilon_{aa}/2A^b$	$-\epsilon_{bb}/2B$	$-\epsilon_{cc}/2C$
-0.01128	-0.000304	+0.00388
ClO ₂		
$(g_{aa} - g_e)^c$	$(g_{bb} - g_e)$	$(g_{cc} - g_e)$
+0.0065	+0.0160	+0.0013
$-\epsilon_{aa}/2A^d$	$-\epsilon_{bb}/2B$	$-\epsilon_{cc}/2C$
+0.01333	+0.01089	-0.00027

^a ZELDES, H., and LIVINGSTON, R., 1961, *J. chem. Phys.*, **35**, 563.

^b Reference [5].

^c COLE, T., 1960, *Proc. nat. Acad. Sci., Wash.*, **46**, 506.

^d CURL, R. F., HEIDELBERG, R. F., and KINSEY, J. L., 1962, *Phys. Rev.*, **125**, 1993.

Experimental test of the postulated relationship between spin rotation tensors and *g* tensors.

The identity of the expression in brackets and $\mathbf{l} = \boldsymbol{\mu}^{-1}$ lead to the desired relationship equation (1).

There is little experimental data on spin-rotation coupling constants. For non-linear molecules the spin-rotation coupling constants of only NO_2 and ClO_2 are available. There is data for the molecules NO , OH , O_2 , and SO . However, none of these molecules is in a $^2\Sigma$ state. The presence of two unpaired electrons or electronic orbital angular momentum is a complication we wish to avoid.

When the validity of the relationship (1) is tested for the two molecules NO_2 [5] and ClO_2 [6], it is found to hold quite accurately for NO_2 but very poorly for ClO_2 . This is shown in the table. The analysis below only serves to make this discrepancy for ClO_2 more perplexing.

2. PROCEDURE

The procedure to be followed consists of first writing the Hamiltonian in the Pauli approximation for a fixed coordinate system. The invariance of the Hamiltonian to choice of origin of the vector potential (gauge invariance) is verified. Then a Lagrangian which will give this Hamiltonian is introduced.

The Hamiltonian for the rotating vibrating molecule is set up by the method of Wilson and Howard [7] using the Lagrangian previously found.

The various terms in the Hamiltonian are examined. Estimates are made of the magnitude of the terms which contribute to each of the two tensors.

The approach used here may also be used to derive the relationship of Ramsey for the nuclear case. It is interesting to compare this derivation to Ramsey's. The derivation by the present method is given in the Appendix. The approach used here is more formal than Ramsey's and initially appears to lead to a quite different conclusion.

3. THE PAULI APPROXIMATION

The Hamiltonian for a two electron system has been given by Bethe and Salpeter [8]. Because all interactions are of the two body type, it is immediately possible to generalize to the n -electron system. Several terms in this Hamiltonian cannot contribute to either of the interactions we are interested in either first or second order and can be omitted. Transcribing then the terms we require from Bethe and Salpeter [8] we have (for the two electron case):

$$H = (1/2m)(p_1^2 + p_2^2) + (e/mc)(\mathbf{A}_1 \cdot \mathbf{p}_1 + \mathbf{A}_2 \cdot \mathbf{p}_2) \\ + (\mu_B/mc)[(\mathcal{E}_1 \times \mathbf{p}_1) \cdot \mathbf{S}_1 + (\mathcal{E}_2 \times \mathbf{p}_2) \cdot \mathbf{S}_2 + 2er_{12}^{-3}(\mathbf{r}_{21} \times \mathbf{p}_2) \cdot \mathbf{S}_1 \\ + 2er_{12}^{-3}(\mathbf{r}_{12} \times \mathbf{p}_1) \cdot \mathbf{S}_2] - e\phi_1 - e\phi_2, \quad \mathbf{A}_1 = \frac{1}{2}[\mathbf{H} \times \boldsymbol{\rho}_1]. \quad (7)$$

This Hamiltonian is not gauge invariant. Gauge invariance is necessary. This may be easily verified by considering that for an asymmetric molecule no point in the molecule suggests itself as the origin of the vector potential. Clearly a Hamiltonian is necessary which is independent of the origin.

Such a Hamiltonian is:

$$H = (1/2m)[\mathbf{p}_1 + (e/c)\mathbf{A}_1]^2 + (1/2m)[\mathbf{p}_2 + (e/c)\mathbf{A}_2]^2 \\ + (\mu_B/mc)[\mathcal{E}_1 \times (\mathbf{p}_1 + e/c\mathbf{A}_1) \cdot \mathbf{S}_1 + (\mu_B/mc)[\mathcal{E}_2 \times (\mathbf{p}_2 + e/c\mathbf{A}_2) \cdot \mathbf{S}_2 - e\phi_2 - e\phi_1], \quad (8)$$

or in general:

$$H = (1/2m) \sum_i (\mathbf{p}_i + e/c\mathbf{A}_i)^2 + \mu_B/mc \sum_i [\mathcal{E}_i \times (\mathbf{p}_i + e/c\mathbf{A}_i)] \cdot \mathbf{S}_i \\ + \sum_{\alpha} (1/2m_{\alpha}) [\mathbf{p}_{\alpha} - (Z_{\alpha}e/c)\mathbf{A}_{\alpha}]^2 + \sum_{\alpha>\beta} \frac{Z_{\alpha}Z_{\beta}e^2}{r_{\alpha\beta}} - \sum_{\alpha i} \frac{Z_{\alpha}e^2}{r_{\alpha i}} + \sum_{i>j} \frac{e^2}{r_{ij}}, \quad (9)$$

$$\mathbf{A}_i = (\tfrac{1}{2})(\mathbf{H} \times \boldsymbol{\rho}_i) - 2\mu_B \sum_{j \neq i} r_{ij}^{-3} (\mathbf{S}_j \times \mathbf{r}_{ji}), \quad (10a)$$

$$\mathbf{A}_{\alpha} = (\tfrac{1}{2})(\mathbf{H} \times \boldsymbol{\rho}_{\alpha}) - 2\mu_B \sum_i r_{i\alpha}^{-3} (\mathbf{S}_i \times \mathbf{r}_{i\alpha}), \quad (10b)$$

$$\mathcal{E}_i = -e \sum_{j \neq i} \mathbf{r}_{ji} r_{ij}^{-3} + \sum_{\alpha} Z_{\alpha} e r_{\alpha i}^{-3} \mathbf{r}_{\alpha i}. \quad (10c)$$

and $\mathbf{r}_{ij} = \mathbf{r}_j - \mathbf{r}_i$.

The electrons are indicated by Latin indices, the nuclei by Greek indices. The Hamiltonian should be invariant to shift of the origin of the vector potential. This shift is the replacement of all the $\boldsymbol{\rho}_i$ and $\boldsymbol{\rho}_{\alpha}$ with $\boldsymbol{\rho}_i'$, $\boldsymbol{\rho}_{\alpha}'$ where $\boldsymbol{\rho}_i' = \boldsymbol{\rho}_i + \mathbf{R}$. The invariance can be demonstrated by the method described by Chan and Das [9].

This Hamiltonian is similar to but different from that given by Stone [10]. The difference seems to be that the vector potential of an electron is given entirely by the external field in Stone's Hamiltonian, no contributions from the electron magnetic moments to the vector potential are included.

4. THE LAGRANGIAN

In order that the Hamiltonian may be set up in a coordinate system rotating with the molecule, a Lagrangian which will give the Hamiltonian (9) is needed. The Hamiltonian is obtained from the Lagrangian by the usual procedure:

$$\mathbf{p}_i = \frac{\partial L(q, \dot{q})}{\partial \dot{q}_i} = f_i(q, \dot{q}). \quad (11)$$

Inverting, we have:

$$\dot{q}_i = g_i(q, p). \quad (12)$$

Then the Hamiltonian is

$$H = \sum_i \dot{q}_i p_i - L(\dot{q}, q) \quad (13)$$

or in terms of q 's, p 's:

$$H = \sum_i g_i(q, p) p_i - L(g(q, p), q). \quad (14)$$

A Lagrangian which gives the Hamiltonian is:

$$L = \tfrac{1}{2} \sum_i m v_i^2 + \tfrac{1}{2} \sum_{\alpha} m_{\alpha} v_{\alpha}^2 - e/c \sum_i \mathbf{A}_i \cdot \mathbf{v}_i - \mu_B/c \sum_i (\mathcal{E}_i \times \mathbf{v}_i) \cdot \mathbf{S}_i \\ + \sum_{\alpha} (Z_{\alpha}e/c) \mathbf{A}_{\alpha} \cdot \mathbf{v}_{\alpha} - \sum_{\alpha>\beta} Z_{\alpha}Z_{\beta}e^2/r_{\alpha\beta} + \sum_{\alpha i} Z_{\alpha}e^2/r_{\alpha i} \\ - \sum_{i>j} e^2/r_{ij} + (\mu_B^2/2mc^2) \sum_i (\mathbf{S}_i \times \mathcal{E}_i)^2. \quad (15)$$

The last term may be omitted without affecting any terms of interest to us.

5. ROTATING COORDINATE SYSTEM

The procedure of Wilson and Howard [7] is now to be followed to separate molecular translation from the other motions and to approximately separate molecular rotation from vibration and electronic motions.

A rotating translating coordinate system is introduced. In terms of this coordinate system the velocities are:

$$\mathbf{v}_i = \dot{\mathbf{R}} + \boldsymbol{\omega} \times \mathbf{r}_i + \dot{\mathbf{r}}_i, \quad (16)$$

where \mathbf{R} is the vector to the origin of the moving coordinate system from the origin of a stationary axis system, $\boldsymbol{\omega}$ is the angular velocity of rotation of the moving coordinate system and \mathbf{r}_i is the position of the i th particle in the moving system.

Six conditions are necessary to specify the moving coordinate system. By choosing three of these of be:

$$\sum_i m \mathbf{r}_i + \sum_{\alpha} m_{\alpha} \mathbf{r}_{\alpha} = 0, \quad (17)$$

the translation of the molecule as a whole is separated from other motions. By choosing the other three conditions to be the Eckhart conditions:

$$\sum_{\alpha} m_{\alpha} (\mathbf{a}_{\alpha} \times \mathbf{r}_{\alpha}) = 0, \quad (18)$$

where \mathbf{a}_{α} is the equilibrium position of the α th nucleus in the moving frame, the maximum separation of rotation and vibration is achieved. Substituting the velocities (16) and their subsidiary conditions (17) and (18) into the Lagrangian (15), the result is:

$$\begin{aligned} 2L = & M\dot{\mathbf{R}}^2 + 2\dot{\mathbf{R}} \cdot \left[\sum_{\alpha} (Z_{\alpha}e/c) \mathbf{A}_{\alpha} - (e/c) \sum_i \mathbf{A}_i - (\mu_B/c) \sum_i (\mathbf{S}_i \times \boldsymbol{\mathcal{E}}_i) \right] \\ & + \boldsymbol{\omega} \cdot \mathbf{l}_n + \boldsymbol{\omega} \cdot \mathbf{l}_e + \boldsymbol{\omega} \cdot 2\boldsymbol{\omega} \cdot \sum_{\pi} m_{\alpha} (\boldsymbol{\delta}_{\alpha} \times \dot{\mathbf{r}}_{\alpha}) + 2\boldsymbol{\omega} \cdot \sum_i m (\mathbf{r}_i \times \dot{\mathbf{r}}_i) \\ & + 2\boldsymbol{\omega} \cdot \sum_{\alpha} (Z_{\alpha}e/c) (\mathbf{r}_{\alpha} \times \mathbf{A}_{\alpha}) + 2\boldsymbol{\omega} \cdot \sum_i (-e/c) (\mathbf{r}_i \times \mathbf{A}_i) \\ & + 2\boldsymbol{\omega} \cdot \sum_{\alpha} (-\mu_B/c) \mathbf{r}_{\alpha} \times (\mathbf{S}_{\alpha} \times \boldsymbol{\mathcal{E}}_{\alpha}) + \sum_i m_{\alpha} \dot{\mathbf{r}}_{\alpha}^2 + \sum_i m \dot{\mathbf{r}}_i^2 \\ & + 2 \sum_{\alpha} (Z_{\alpha}e/c) \mathbf{A}_{\alpha} \cdot \dot{\mathbf{r}}_{\alpha} + 2 \sum_i (-e/c) \mathbf{A}_i \cdot \dot{\mathbf{r}}_i - 2 \sum_i (\mu_B/c) (\mathbf{S}_i \times \boldsymbol{\mathcal{E}}_i) \cdot \dot{\mathbf{r}}_i \\ & - 2V + 2(\mu_B^2/2mc^2) \sum_i (\mathbf{S}_i \times \boldsymbol{\mathcal{E}}_i)^2, \quad (19) \end{aligned}$$

where

$$M = n_e m + \sum_{\alpha} m_{\alpha},$$

n_e = number of electrons,

$$\mathbf{l}_n = \sum_{\alpha} m_{\alpha} (r_{\alpha}^2 \mathbf{1} - \mathbf{r}_{\alpha} \mathbf{r}_{\alpha}),$$

$$\mathbf{l}_e = m \sum_i (r_i^2 \mathbf{1} - \mathbf{r}_i \mathbf{r}_i),$$

$$\boldsymbol{\delta}_{\alpha} = \mathbf{r}_{\alpha} - \mathbf{a}_{\alpha}.$$

The coordinates of the nuclei in the moving coordinate system are not all independent because of the six conditions defining the system. If there are

N nuclei there are only $3N-6$ independent coordinates rather than $3N$. This can be accounted for by introducing the normal coordinates such that:

$$\sum_{\alpha=1}^N m_{\alpha} \dot{\mathbf{r}}_{\alpha}^2 = \sum_{K=1}^{3N-6} \dot{Q}_K^2, \quad (20a)$$

$$\delta_{\alpha} = \sum_K \mathbf{l}_K^{\alpha} Q_K, \quad (20b)$$

where the coefficients \mathbf{l}_K^{α} are constants for infinitesimal displacements. Equation (19) can be re-written:

$$\begin{aligned} 2L = & M\dot{\mathbf{R}}^2 + 2\dot{\mathbf{R}} \cdot \mathbf{S}_T + \boldsymbol{\omega} \cdot \mathbf{l}_n \cdot \boldsymbol{\omega} + \boldsymbol{\omega} \cdot \mathbf{l}_e \cdot \boldsymbol{\omega} + 2\boldsymbol{\omega} \cdot \sum_K \mathbf{C}_K \dot{Q}_K \\ & + 2\boldsymbol{\omega} \cdot \sum_i m(\mathbf{r}_i \times \dot{\mathbf{r}}_i) + 2\boldsymbol{\omega} \cdot \mathbf{S}_R + 2\boldsymbol{\omega} \cdot \sum_i (-e/c)(\mathbf{r}_i \times \mathbf{A}_i) \\ & - 2\boldsymbol{\omega} \cdot \sum_i (\mu_B/c)\mathbf{r}_i \times (\mathbf{S}_i \times \mathcal{E}_i) + \sum_i m\dot{\mathbf{r}}_i^2 + \sum_K \dot{Q}_K^2 + 2 \sum_K S_K \dot{Q}_K \\ & + 2 \sum_i (-e/c)\mathbf{A}_i \cdot \dot{\mathbf{r}}_i - 2 \sum_i (\mu_B/c)(\mathbf{S}_i \times \mathcal{E}_i) \cdot \dot{\mathbf{r}}_i \\ & - 2V + 2(\mu_B^2/2mc^2) \sum_i (\mathbf{S}_i \times \mathcal{E}_i)^2, \quad (21) \end{aligned}$$

where

$$\begin{aligned} \mathbf{S}_T &= \sum_{\alpha} (Z_{\alpha}e/c)\mathbf{A}_{\alpha} + \sum_i (-e/c)\mathbf{A}_i - \sum_i (\mu_B/c)(\mathbf{S}_i \times \mathcal{E}_i), \\ \mathbf{C}_K &= \sum_{\alpha, L} (\mathbf{l}_L^{\alpha} \times \mathbf{l}_K^{\alpha}) Q_L, \\ \mathbf{S}_R &= \sum_{\alpha} (Z_{\alpha}e/c)(\mathbf{r}_{\alpha} \times \mathbf{A}_{\alpha}), \\ S_K &= \sum_{\alpha} (Z_{\alpha}e/c)\mathbf{A}_{\alpha} \cdot \mathbf{l}_K^{\alpha}. \end{aligned}$$

The procedure outlined in equations (11), (12), (13) and (14) may now be followed and yields:

$$\begin{aligned} H = & \frac{1}{2} \left(\mathbf{M} - \mathbf{m} - \mathbf{L} + \sum_K S_K \mathbf{C}_K - \mathbf{S}_R \right) \cdot \boldsymbol{\mu} \cdot \left(\mathbf{M} - \mathbf{m} - \mathbf{L} + \sum_K S_K \mathbf{C}_K - \mathbf{S}_R \right) \\ & + (1/2M)(\mathbf{P} - \mathbf{S}_T)^2 + (1/2m) \sum_i [\mathbf{p}_i + e/c\mathbf{A}_i + (\mu_B/c)(\mathbf{S}_i \times \mathcal{E}_i)]^2 \\ & + \left(\frac{1}{2}\right) \sum_K (P_K - S_K)^2 + V - (\mu_B^2/2mc^2) \sum_i (\mathbf{S}_i \times \mathcal{E}_i)^2, \quad (22) \end{aligned}$$

where

$$\begin{aligned} \mathbf{m} &= \sum_K \mathbf{C}_K P_K, \\ \mathbf{L} &= \sum_i \mathbf{r}_i \times \mathbf{p}_i, \\ \boldsymbol{\mu} &= \left[\mathbf{l}_n - \sum_K \mathbf{C}_K \mathbf{C}_K \right]^{-1}, \end{aligned}$$

\mathbf{M} is the rotational angular momentum conjugate to $\boldsymbol{\omega}$, \mathbf{P} is conjugate to $\dot{\mathbf{R}}$, \mathbf{p}_i to $\dot{\mathbf{r}}_i$, and P_K to \dot{Q}_K .

This is the classical Hamiltonian. The quantum mechanical Hamiltonian can be obtained by inserting factors at the left, in the middle and at the right of the quadratic forms in (22). To a first approximation the molecule can be assumed

rigid. Then the quantum mechanical Hamiltonian can be written as follows (dropping the translation as well):

$$H = \frac{1}{2}(\mathbf{M} - \mathbf{L} - \mathbf{S}_R) \cdot \boldsymbol{\mu} \cdot (\mathbf{M} - \mathbf{L} - \mathbf{S}_R) + \frac{1}{2m} \sum_i [\mathbf{p}_i + (e/c)\mathbf{A}_i + (\mu_B/c)(\mathbf{S}_i \times \mathcal{E}_i)]^2 + \frac{1}{2} \sum_K (p_K - S_K)^2 - \frac{1}{2m} \sum_i \mu_B^2/c^2 (\mathbf{S}_i \times \mathcal{E}_i)^2 + V. \quad (23)$$

6. SPIN-ROTATION INTERACTION

The spin-rotation interaction is a bilinear form in the electron spins and the rotational angular momentum \mathbf{M} ($\mathbf{M} = \hbar \mathbf{N}$). There are contributions in first-order perturbation from a similar bilinear form in the Hamiltonian to be found in $-\mathbf{M} \cdot \boldsymbol{\mu} \cdot \mathbf{S}_R$ and from second-order perturbation involving the cross product between $-\mathbf{M} \cdot \boldsymbol{\mu} \cdot \mathbf{L}$ and

$$\sum_i [(e/mc)\mathbf{A}_i + (\mu_B/mc)(\mathbf{S}_i \times \mathcal{E}_i)] \cdot \mathbf{p}_i = \sum_j \eta_{sj} \cdot \mathbf{S}_j.$$

The first-order part is:

$$-\mathbf{M} \cdot \boldsymbol{\mu} \cdot \sum_{\alpha} (Z_{\alpha} e/c)(\mathbf{r}_{\alpha} \times \mathbf{A}_{\alpha}) \quad (24)$$

or

$$-\mathbf{M} \cdot \boldsymbol{\mu} \cdot \sum_{\alpha, i} (-2\mu_B Z_{\alpha} e/c) r_{\alpha i}^{-3} [\mathbf{r}_{\alpha} \times (\mathbf{S}_i \times \mathbf{r}_{i\alpha})]. \quad (25)$$

This can be re-written:

$$\sum_{\alpha i} (2\mu_B Z_{\alpha} e/c) r_{\alpha i}^{-3} [(\boldsymbol{\omega}' \times \mathbf{r}_{\alpha}) \cdot (\mathbf{S}_i \times \mathbf{r}_{i\alpha})], \quad (26)$$

$$\boldsymbol{\omega}' = \mathbf{M} \cdot \boldsymbol{\mu}.$$

7. THE ZEEMAN EFFECT

An external magnetic field is introduced by adding $\frac{1}{2}(\mathbf{H} \times \boldsymbol{\rho}_i)$ to the vector potential of all particles \mathbf{A}_i . The location of the origin of the vector potential associated with the external field at the centre of mass is helpful. Then the Zeeman effect can be most easily compared with the spin-rotation coupling. This choice of gauge means that $\boldsymbol{\rho}_i = \mathbf{r}_i$.

The Zeeman effect consists of two completely different types of terms. The one of interest here is a bilinear form in the electron spin and magnetic field. The other which is ignored here is a bilinear form in the rotational angular momentum and magnetic field.

The bilinear form in S and H can arise in first-order perturbation from such forms already present in the Hamiltonian or such a form can arise in second-order perturbation as the cross product of linear terms in the Hamiltonian. Consider first the first-order terms. These are to be found in:

$$\frac{1}{2} \mathbf{S}_R \cdot \boldsymbol{\mu} \cdot \mathbf{S}_R, \quad (27a)$$

$$-(\mu_B e/mc^2) \sum_i \mathbf{A}_i \cdot (\mathcal{E}_i \times \mathbf{S}_i), \quad (27b)$$

$$\frac{1}{2} (e^2/mc^2) \sum_i \mathbf{A}_i^2, \quad (27c)$$

$$\frac{1}{2} \sum_K S_K^2. \quad (27d)$$

The contribution of the first and last terms are completely negligible. They correspond to diamagnetic shielding of the electron by circulation of nuclear charge.

Examining the terms of interest in (27 *b*) it is seen that

$$\begin{aligned}
 - (e\mu_B/2mc^2) \sum_i (\mathbf{H} \times \mathbf{r}_i) \cdot (\mathcal{E}_i \times \mathbf{S}_i) &= (e^2\mu_B/2mc^2) \sum_{i \neq j} r_{ij}^{-3} (\mathbf{H} \times \mathbf{r}_i) \cdot (\mathbf{r}_{ji} \times \mathbf{S}_i) \\
 &\quad - (e^2\mu_B/2mc^2) \sum_{i, \alpha} Z_\alpha r_{i\alpha}^{-3} (\mathbf{H} \times \mathbf{r}_i) \cdot (\mathbf{r}_{\alpha i} \times \mathbf{S}_i), \quad (28)
 \end{aligned}$$

while (27 *c*) is:

$$- (e^2\mu_B/mc^2) \sum_{i \neq j} r_{ij}^{-3} (\mathbf{H} \times \mathbf{r}_i) \cdot (\mathbf{S}_j \times \mathbf{r}_{ji}). \quad (29)$$

The term from equation (23) which contributes in second-order perturbation is

$$(e/mc) \sum_i \mathbf{A}_i \cdot \mathbf{p}_i$$

in particular

$$(e/2mc) \mathbf{H} \cdot \sum_i \mathbf{l}_i$$

which is $(e/2mc) \mathbf{H} \cdot \mathbf{L}$. The cross product between this and

$$\sum_i [(e/2mc) \mathbf{A}_i + (\mu_B/mc)(\mathbf{S}_i \times \mathcal{E}_i)] \cdot \mathbf{p}_i$$

in second-order perturbation constitutes the second-order perturbation contribution. The second-order perturbation contribution to the spin-rotation coupling involves the same sort of cross product with $(e/2mc) \mathbf{H} \cdot \mathbf{L}$ replaced by $\mathbf{M} \cdot \boldsymbol{\mu} \cdot \mathbf{L}$. The perturbation is a Van Vleck perturbation to excited electronic states in which \mathbf{M} participates as a number not an operator. The resulting effective Hamiltonian has interaction constants related by (1) (remembering that $\boldsymbol{\mu}^{-1} = \mathbf{I}$, $e/2mc = \mu_B/\hbar$ and $\mathbf{M} = \hbar \mathbf{N}$).

8. ESTIMATION OF TERMS

The terms in the spin-rotation and g tensor which arise from second-order perturbations are related exactly by (1). In order to find out whether this relationship (1) is valid it is necessary to estimate the first-order terms (24), (28) and (29).

Several approximations will be required in order to estimate these terms. The first is that the ground state wave function is reasonably well approximated by a single Slater determinant:

$$\begin{aligned}
 \psi_0 &= (N!)^{-1/2} |\phi_1(1) \alpha \phi_1(2) \beta \dots \phi_{(N-1)/2}(N-2) \alpha \\
 &\quad \times \phi_{(N-1)/2}(N-1) \beta \phi_{(N+1)/2}(N) \alpha|, \quad (30)
 \end{aligned}$$

where the ϕ_i are an orthonormal set.

Use of this wave function in the calculation of the expectation value of the various terms of (26), (28) and (29) proceeds straightforwardly. The terms in the nuclear coordinates and the coordinates of one electron are one electron operators. From the familiar Hartree-Fock case it is apparent that the sums of one electron operators go over to sums of expectation values over the individual

spin-orbitals. However, the sums reduce to only one term, that over the spin-orbital of the odd electron, because of the cancellation of the other terms. The term with $\phi_i\alpha$ will be cancelled by the term $\phi_i\beta$ because of the \mathbf{S}_i in the operator:

$$\left\langle \sum_i \mathbf{B}(i) \cdot \mathbf{S}_i \right\rangle = \int \phi_N'(x) \mathbf{B}(x) \cdot \mathbf{S} \phi_N'(x) dx, \quad (31)$$

where $\phi_N'(x)$ is the spin-orbital associated with the odd electron.

An analogous but more complicated situation holds for the two electron operators. Again use of the wave function (30) leads to familiar results. The sum of two electron operators go over to sums of expectation values over pairs of spin orbitals minus the exchanged pairs. Again because of the presence of the spin operator one sum drops out and one of the two spin orbitals is always that for the odd electron. One sum over electrons still remains. The importance of these results is that the sums appearing in (26), (28) and (29) are not additive, but there is large cancellation. Only terms arising from the odd electron have to be considered.

Consider first the term (25). It is known experimentally that

$$A_s/2A (\sim B_s/2B, C_s/2C)$$

is of the order 10^{-2} . This is to be compared to a typical element of (25), the trace for instance:

$$\sum_{\alpha} (4\mu_B Z_{\alpha} e/c) \langle (\mathbf{r}_{\alpha} \cdot \mathbf{r}_{\alpha e})/r_{\alpha e}^3 \rangle = \sum_{\alpha} (2\hbar Z_{\alpha} e^2/mc^2) \langle (\mathbf{r}_{\alpha} \cdot \mathbf{r}_{\alpha e})/r_{\alpha e}^3 \rangle, \quad (32)$$

where the subscript e refers to the odd electron. The factor \hbar is combined with another \hbar from $\mathbf{M} = \hbar \mathbf{N}$ and μ to give the rotational constants $\hbar^2 \mu/2$. Use has been made in going from (25) to (32) of expression (31). Thus the dimensionless quantity:

$$(2/mc^2) \sum_{\alpha} Z_{\alpha} e^2 \left\langle \frac{\mathbf{r}_{\alpha} \cdot \mathbf{r}_{\alpha e}}{r_{\alpha e}^3} \right\rangle. \quad (33)$$

is compared to 10^{-2} . The quantity in brackets above varies as $r_{\alpha e}^{-2}$. This is intermediate between $r_{\alpha e}^{-3}$ which is a property of the wave function in the immediate neighbourhood of the nucleus and $r_{\alpha e}^{-1}$ which is a property of the wave function over the whole molecule. The quantity $r_{\alpha e}^{-2}$ can be thought of as a property of the wave function on the atom. Molecule wave functions on the atom should be expanded in atomic states.

The expression in the brackets will average to zero if the atomic wave function has a definite parity. Thus it is expected to be much smaller for ClO_2 in which the odd electron is in a $p\pi$ orbital of parity $(-)$ on the atoms than is NO_2 in which the odd electron is in a $2s2p$ hybrid on the N of mixed parity. When the hybridization involves (as it does for NO_2) orbitals of the same principal quantum number there is much cancellation because the radial portions of the wave functions have different numbers of nodes. The $2s$ orbital has one radial node the $2p$ none. The expression (33) has been evaluated by numerical integration of the Hartree-Fock wave function [11] on the N atom. The cancellation from the radial node of $2s$ is large. Large cancellation might be fortuitous. The expression (33) for the integration up to the node of $2s$ is 0.0005 assuming sp^2 hybridization with the wave function located on the N .

Now the contributions of (28) and (29) to the *g* tensor need to be estimated. The second term in (28) can be expected to dominate, since the electric field of the nuclei should be larger than that of the electrons in order that the odd electron be bound to the molecule. The first term in (28) should cancel part of the second term. The second term in (28) can be re-written (using (31)):

$$\begin{aligned} & - (1/2mc^2) \sum_{\alpha} Z_{\alpha} e^2 \langle r_{\alpha e}^{-3} (\mathbf{H} \times \mathbf{r}_e) \cdot (\mathbf{r}_{\alpha e} \times \mathbf{S}_e) \rangle \\ & = - (1/2mc^2) \sum_{\alpha} Z_{\alpha} e^2 \langle r_{\alpha e}^{-3} (\mathbf{H} \times \mathbf{r}_{\alpha}) \cdot (\mathbf{r}_{\alpha e} \times \mathbf{S}_e) \rangle \\ & \quad - (1/2mc^2) \sum_{\alpha} Z_{\alpha} e^2 \langle r_{\alpha e}^{-3} (\mathbf{H} \times \mathbf{r}_{\alpha e}) \cdot (\mathbf{r}_{\alpha e} \times \mathbf{S}_e) \rangle. \end{aligned} \quad (34)$$

The coefficient μ_B in (28) has been dropped in order to give the dimensionless *g* tensor. The first term in (34) is closely related to (24) and (32). Essentially it differs only by a factor of $-\frac{1}{2}$. The trace of the second term which is useful for comparison is:

$$(1/mc^2) \sum_{\alpha} Z_{\alpha} e^2 \langle \mathbf{r}_{\alpha e}^{-1} \rangle = -V_{Ne}/mc^2, \quad (35)$$

the average nuclear potential energy divided by the electron rest energy. If *V* is in A.U. (1 A.U. = 2 Rydbergs) then $mc^2 = \alpha^{-2}$ ($\alpha = 1/137$). For hydrogenic orbitals $V_{Ne} = -\sum_{\alpha} (C_{\alpha} Z_{\alpha}/n_{\alpha})^2$ where C_{α}^2 is the fractional importance of atom α in

the odd electron ϕ . For NO_2 Z is about 7.5, n_e is about 2. $C_N^2 \sim 0.5$, $C_O^2 \sim 0.25$. Therefore $\bar{V}_{Ne} \sim -14$ or $\bar{V}_{Ne}/mc^2 \sim -0.0007$. For ClO_2 $Z_{\text{Cl}} = 17$, $n_{\text{Cl}} = 3$, $C_{\text{Cl}}^2 = 0.5$, $Z_0 = 8$, $n_0 = 2$, $C_0^2 = 0.25$. Therefore $\bar{V}_{Ne} \sim -25$ or $\bar{V}_{Ne}/mc^2 \sim -0.0012$. These numbers are to be compared with 0.01.

The expression (29) is more difficult to evaluate. It can be expanded (dropping μ_B again):

$$\begin{aligned} & -\alpha^2 e^2 \sum_j \langle r_{ej}^{-3} (\mathbf{H} \times \mathbf{r}_j) \cdot (\mathbf{S}_e \times \mathbf{r}_{ej}) \rangle_{\text{ex}} = -\alpha^2 e^2 \sum_j \langle r_{ej}^{-3} (\mathbf{H} \times \mathbf{r}_e) \cdot (\mathbf{S}_e \times \mathbf{r}_{ej}) \rangle_{\text{ex}} \\ & \quad -\alpha^2 e^2 \sum_j \langle r_{ej}^{-3} (\mathbf{H} \times \mathbf{r}_{ej}) \cdot (\mathbf{S}_e \times \mathbf{r}_{ej}) \rangle_{\text{ex}}, \end{aligned} \quad (36)$$

where the subscript ex on the brackets indicates that the exchange of electrons *j* and *e* should be subtracted if different from zero.

The first term of expression (36) is just twice the first term of (28). The trace of the second term is $-\alpha^2$ times twice the coulomb repulsion of the other electrons on the odd electron minus the exchange. These terms should be of the same magnitude as the nuclear term previously evaluated.

In general the electron terms cancel part of the terms arising from nuclei because the nuclear and electronic charges are of opposite sign.

9. DISCUSSION

The admittedly approximate consideration of the first order term in the spin rotation and *g* tensor indicates that the relationship (1) should hold approximately. Perhaps nine-tenths of these tensors come from the second-order coupling involving the electronic angular momentum.

The agreement of the experimental results for NO_2 with the relationship (1) is therefore gratifying. Indeed the agreement is, if anything, better than could be expected. On the other hand, the discrepancies in the case of ClO_2 are larger (~ 0.005) than expected (~ 0.001).

APPENDIX

Derivation of Ramsey's formula

Consider a $^1\Sigma$ diatomic molecule AB with nucleus A with spin 1 nucleus B with spin 0. The equation (23) for this case becomes:

$$H = (1/2\mu R^2)(\mathbf{M} - \mathbf{L} - \mathbf{S}_R)^2 + (1/2m) \sum_i (\mathbf{p}_i + (e/c)\mathbf{A}_i)^2 + \frac{1}{2}(P_V - S_V)^2 + V, \quad (\text{A } 1)$$

with

$$\mu = \frac{m_A m_B}{m_A + m_B},$$

$$\mathbf{A}_i = r_{Ai}^{-3}(\gamma \hbar \mathbf{I} \times \mathbf{r}_{Ai}) + \frac{1}{2}(\mathbf{H} \times \mathbf{p}_i),$$

$$\mathbf{S}_R = (Z_B e/c) R^{-3} [\mathbf{r}_B \times (\hbar \gamma \mathbf{I} \times \mathbf{R})] + \hbar c^{-1} [\gamma - (Z_A e/2M_A c)] [\mathbf{r}_A \times (\mathbf{I} \times \mathcal{E}_A)] \\ + (Z_B e/c) [\mathbf{r}_B \times \frac{1}{2}(\mathbf{H} \times \mathbf{p}_B)] + (Z_A e/c) [\mathbf{r}_A \times \frac{1}{2}(\mathbf{H} \times \mathbf{p}_A)],$$

$$\mathbf{R} = \mathbf{r}_B - \mathbf{r}_A,$$

$$\mathbf{r}_B = (\mu/M_B)\mathbf{R}.$$

At its equilibrium position the electric field on nucleus A is zero. In the ground vibrational state the electric field is approximately zero. To a first approximation the second term in \mathbf{S}_R can be neglected. Likewise the terms in S_V can be neglected. The third and fourth terms of \mathbf{S}_R can be neglected.

If the origin of the vector potential associated with the external field H is taken to be the centre of mass $\mathbf{p}_i = \mathbf{r}_i$ then the second-order portions of the spin rotation and shielding tensors are related by the Larmor conditions for the electron.

When the shielding is averaged over all directions this gives the relationship:

$$\sigma - (e^2/3mc^2) \sum_i \langle r_{Ai}^{-3} (\mathbf{r}_{Ai} \cdot \mathbf{r}_i) \rangle \\ = (2\mu_B \mu R^2/3\hbar \gamma) [C_W - (Z_B e/c\mu R^3)(\mu/M_B)\hbar \gamma]. \quad (\text{A } 2)$$

This formula would be the same as Ramsey's [12]:

$$\sigma - (e^2/3mc^2) \sum_i \langle r_{Ai}^{-1} \rangle = (2\mu_B \mu R^2/3\hbar \gamma) [C_W - (\hbar \gamma Z_B e/c\mu R^3)], \quad (\text{A } 3)$$

except for the choice of origin for the vector potential at the centre of mass rather than the nucleus in question, and for a factor μ/M_B in the second term on the right-hand side of (A 2). These differences can be made to disappear from (A 2) by shifting the origin of the vector potential to the nucleus in question and simultaneously shifting the origin of \mathbf{L} from the centre of mass to the nucleus in question A . When this is done the shift in \mathbf{L} generates an additional term:

$$(\gamma/c\mu R^2)\mathbf{M} \cdot [\mathbf{r}_A \times (\mathcal{E}_{\text{Ael}} \times \mathbf{I})],$$

where \mathcal{E}_{Ael} is the contribution of the electrons to the electric field at nucleus A . Since the total field \mathcal{E}_A was previously assumed to be zero:

$$\mathcal{E}_A = \mathcal{E}_{AB} + \mathcal{E}_{\text{Ael}} = 0,$$

$\mathcal{E}_{\text{Ae}} = -\mathcal{E}_{AB}$, \mathcal{E}_{AB} is the electric field at A from B and S_R' becomes:

$$S_R' = (Z_B e \hbar \gamma/c) R^{-3} [\mathbf{r}_B \times (\mathbf{I} \times \mathbf{R})] - (\hbar \gamma/c) [\mathbf{r}_A \times (\mathbf{I} \times \mathcal{E}_{AB})]. \quad (\text{A } 4)$$

Then when S_R' is used in place of S_R the formula found by Ramsey (A 3) is obtained.

The author wishes to express his appreciation for a NATO post-doctoral Fellowship, which made this work possible.

REFERENCES

- [1] RAMSEY, N. F., 1950, *Phys. Rev.*, **78**, 699.
- [2] HAMEKA, H. F., 1962, *Rev. mod. Phys.*, **34**, 87.
- [3] VAN VLECK, J. H., 1951, *Rev. mod. Phys.*, **23**, 213.
- [4] VAN VLECK, J. H., 1932, *The theory of Electric and Magnetic Susceptibilities* (Oxford).
- [5] BIRD, G. R., *et al.*, 1964, *J. chem. Phys.*, **40**, 3378.
- [6] CURL, R. F., 1962, *J. chem. Phys.*, **37**, 779.
- [7] WILSON, E. B., and HOWARD, J. B., 1936, *J. chem. Phys.*, **4**, 260. See also ALLEN H. C., and CROSS, P. C., 1963, *Molecular Vib-Rotors* (New York: Wiley), Chap. I.
- [8] BETHE, H. A., and SALPETER, E. E., 1957, *Handbuch der Physik*, Vol. XXXV (Berlin: Springer), p. 267, equation (39.14).
- [9] CHAN, S. I., and DAS, T. P., 1962, *J. chem. Phys.*, **37**, 1527.
- [10] STONE, A. J., 1963, *Proc. roy. Soc. A*, **271**, 424.
- [11] HARTREE, D. R., and HARTREE, W., 1948, *Proc. roy. Soc.*, **193**, 299.
- [12] RAMSEY, N. F., 1956, *Molecular Beams* (Oxford), p. 164, equation (VI 53). There appears to be a factor 2 necessary in the sum over i .

RESEARCH NOTE

Electron spin resonance of the N_2O_2^+ radical

by R. P. A. MUNIZ† and J. DANON

Centro Brasileiro de Pesquisas Físicas, Rio de Janeiro, Brazil

(Received 15 June 1965)

The existence of the N_2O_2^+ radical has been suggested on the basis of chemical reactions [1, 2]. The structure of this radical, which is an interesting case of single electron bond, is probably a nitric oxide-nitrosonium ion $[\text{ON} \cdot \text{NO}]^+$, with the two groups united by one electron. We have found evidence of this radical in the E.P.R. spectrum of irradiated sodium nitroprusside.

Single crystals of $\text{Na}_2\text{Fe}(\text{CN})_5\text{NO} \cdot 2\text{H}_2\text{O}$, irradiated at 77°K with 2 mev electrons from a linear accelerator, upon examination on a Varian 4500 3 cm spectrometer, shows the presence of a number of paramagnetic centres. One of them has been reported in a previous note [3] and will be described in more detail in a next publication [4].



Spectrum of irradiated $\text{Na}_2\text{Fe}(\text{CN})_5\text{NO} \cdot 2\text{H}_2\text{O}$ taken with the magnetic field parallel to the a -axis of the crystal. The strong triplet in the centre of the spectrum has been described. The two quintets at the two extremes are due to N_2O_2^+ . The wings on the sides of the triplet are both quintets also. By rotation of the crystal each of them splits into two quintets and move across the spectrum.

The paramagnetic species identified as N_2O_2^+ in irradiated sodium nitroprusside appears as eight quintets which move and cross each other as the crystal is rotated in the magnetic field. It is quite stable at room temperature and the

† On leave of absence from the Universidade de Brasilia, Brazil.

relative intensities of the lines in any one quintet are 1 : 2 : 3 : 2 : 1, as can be seen in the figure, which shows the spectrum taken with the magnetic field parallel to the a -axis of the sodium nitroprusside single crystal. These quintets are 20 to 30 times less intense than the other components of the spectrum.

The observed relative intensities of the components of the quintets suggest that this paramagnetic centre is a radical in which two nitrogens share equally an electron. A similar radical has been reported [5] and identified as N_2O_4^- , formed by irradiation of NaNO_2 single crystals. The g -values and hyperfine splittings, however, are quite different from the ones reported here, as can be seen in the table below.

Spectrum	g_x	g_y	g_z	A_x	A_y	A_z	References
Quintet	1.899	2.108	2.028	8 G	8 G	8 G	Present work
Quintet	2.0055	2.0047	2.0142	8 G	2 G	2 G	Ref. [5]

Replacement of the ^{14}N (Spin 1) by ^{15}N (Spin $\frac{1}{2}$) exclusively at the NO position, by synthesizing $\text{Na}_2\text{Fe}(\text{CN})_5 \text{ } ^{15}\text{NO} \cdot 2\text{H}_2\text{O}$, turns the quintet into a triplet. This shows that the observed paramagnetic species is genetically connected with the NO displaced by irradiation from its position in the nitroprusside ion. This NO is, in fact, observed in the E.P.R. spectrum as an unstable triplet and, as NO^+ , in the infra-red spectrum [4].

The association of these two species forming the N_2O_2^+ radical accounts for the observed E.P.R. spectrum. The multiplicity of these quintets can be accounted for if one supposes that the N_2O_2^+ is formed at different lattice sites, with different but definite orientations, related to the crystal structure. This supposition is supported by the observed angular variation of the spectrum [4].

This work was supported by the Conselho Nacional de Pesquisas.

REFERENCES

- [1] ADDISON, C. C., and LEWIS, J., 1955, *Quart. Rev.*, **9**, 115.
- [2] SEEL, F., 1958, *Recent Aspects of the Inorganic Chemistry of Nitrogen* (Chemical Society Special Publication).
- [3] DANON, J., MUNIZ, R. P. A., and PANEPUCCI, H., 1964, *J. chem. Phys.*, **41**, 3651.
- [4] DANON, J., MUNIZ, R. P. A., TOSI, L., and ALMEIDA, I. G. (to be submitted to *J. chem. Phys.*).
- [5] TATENO, JUN, and GESI, KAZUO, 1964, *J. chem. Phys.*, **40**, 1317.

INDEX OF AUTHORS (WITH THE TITLES OF PAPERS)

- ABRAHAM, R. J., and CAVALLI, L.: The influence of substitution on CH . CF and CF . CF coupling constants, 67
- ADAMS, RALPH, N., *see* CHAMBERS, JAMES Q.
- ANDERSON, A., and WALMSLEY, S. H.: Far infra-red spectra of molecular crystals. IV. Ammonia, hydrogen sulphide and their fully deuterated analogues, 1
- BARANOWSKI, B., *see* POPIELAWSKI, J.
- BARNETT, M. P., *see* DAHL, J. P.
- BARUA, A. K., CHAKRABORTI, P. K., and SARAN, ANIL: Formation of dimers in polar gases, 9
- BÉNÉ, G. J., *see* DUVAL, E.
- BHALLA, K. C., and KHUBCHANDANI, P. G.: Molecular orbitals for H_2^+ using A.O.'s with angularly dependent Z_{eff} , 229
- BHALLA, K. C., and KHUBCHANDANI, P. G.: Variation calculations for H_2^+ using A.O.'s with angularly dependent Z_{eff} , 291
- BRITH, M., and SCHNEPP, O.: The absorption spectra of solid CO and N_2 , 473
- BUNKER, P. R.: The vibrational selection rules and torsional barrier of ferrocene, 247
- BUNKER, P. R.: The vibrational selection rules and torsional barrier of methylsilylacetylene, 257
- BURNELLE, LOUIS, and LITT, CLOTILDE: The distortions of the ethylene molecule in its low-lying excited states—a four-electron treatment, 433
- CARRINGTON, A., HUDSON, A., and LONGUET-HIGGINS, H. C.: Electron resonance studies of fluorine hyperfine interactions, 377
- CARRINGTON, A., LONGUET-HIGGINS, H. C., MOSS, R. E., and TODD, P. F.: Isotope effects in electron spin resonance: the negative ion of cyclo-octatetraene-1-d, 187
- CARRINGTON, A., LONGUET-HIGGINS, H. C., and TODD, P. F.: The tricyano-sym-triazine anion: a permanent Jahn-Teller distortion?, 211
- CARRINGTON, A., and SMITH, I. C. P.: The electron spin resonance spectrum and spin density distribution of the benzyl radical, 137
- CAVALLI, L., *see* ABRAHAM, R. J.
- CHAKRABORTI, P. K., *see* BARUA, A. K.
- CHAMBERS, JAMES, Q., and ADAMS, RALPH, N.: Solvent effects on the visible spectra of nitrobenzene anion radicals, 413
- CHAN, Y. M., and DALGARNO, A.: The long-range interaction of atoms and molecules, 349
- CHAN, Y. M., and DALGARNO, A.: Long-range interactions between three hydrogen atoms, 525
- CHARLES, S. W., FISCHER, P. H. H., and McDOWELL, C. A.: Electron paramagnetic resonance study of the photo-excited triplet state of pyrene-*d*-10, 517
- CHILD, M. S., and ROACH, A. C.: The Jahn-Teller effect in ReF_6 , 281
- COHEN, A. D., and McLAUCHLAN, K. A.: The high-resolution nuclear magnetic resonance spectrum of 2-carbomethoxy 5,6-dimethyl benzofuran, 49
- COOK, D. B., and MURRELL, J. N.: Calculation on some excited states of helium and lithium, 417
- CURL, JR., R. F.: The relationship between electron spin rotation coupling constants and *g*-tensor components, 585
- DAHL, J. P., and BARNETT, M. P.: Expansion theorems for solid spherical harmonics, 175
- DALGARNO, A., *see* CHAN, Y. M.
- DANON, J., *see* MUNIZ, R. P. A.
- DA SILVEIRA, ANTONIO, MARQUES, MANUEL A., ET MARQUES, NOEMIO, M.: Nouvelles recherches sur l'existence de cations complexes de structure définie dans les solutions d'électrolytes, 271
- DE BOER, E., and MACLEAN, C.: Spin densities in the alkyl groups of alkyl-substituted naphthalene negative ions, determined by N.M.R., 191

- DEGUCHI, Y., *see* NISHIGUCHI, H.
- DE KOWALEWSKI, DORA, G., and KOWALEWSKI, VALDEMAR J.: Double long-range spin-spin couplings between aldehydic and aromatic protons in the N.M.R. spectra of salicylaldehydes, 319
- DE KOWALEWSKI, DORA G., and KOWALEWSKI, VALDEMAR J.: Multiple long-range spin-spin couplings in di-substituted benzaldehydes and hindered rotation, 331
- DEVERELL, C., FROST, D. J., and RICHARDS, R. E.: Quadrupole relaxation in solutions of electrolytes, 565
- DIXON, W. T.: The molecular orbital theory of some simple radicals, 201
- DIXON, R. N.: The Renner effect in a nearly linear molecule, with application to NH_2 , 357
- DOS SANTOS-VEIGA, J., and NEIVA-CORREIA, A. F.: E.P.R. studies of ionic association of pyrazine negative ion and alkali cations, 395
- DUVAL, E., RANFT, J., et BÉNÉ, G. J.: Détermination des signes relatifs des constantes de couplage ^{31}P - ^1H dans le tripropyl phosphate par R.M.N. dans le champ magnétique terrestre, 427
- EMSLEY, J. W.: Electric fields in fluorocyclohexanes and the magnitude of ^{19}F chemical shifts, 381
- FABRICAND, BURTON P.: Note on the paper "Proton spin-lattice relaxation in aqueous ionic solutions", 399
- FISCHER, HANNS: Rapid proton exchange of the free radical $\cdot\text{CH}_2\text{OH}$ as studied by E.S.R., 149
- FISCHER, P. H. H., *see* CHARLES, S. W.
- FOSS, FRED D., *see* YERANOS, WALTER A.
- FROST, D. J., *see* DEVERELL, C.
- FURLANI, C., and PIOVESANA, O.: Ligand field parameters of Mo(III) complexes, 341
- GERDIL, R., and LUCKEN, E. A. C.: An electron spin resonance and polarographic study of the sulphone group, 529
- GIBBONS, W. A., and GIL, V. M. S.: Studies of sterically hindered and overcrowded molecules. Part I. Proton magnetic resonance studies of the relative steric and electronic effects of the methyl and *t*-butyl groups, 163
- GIBBONS, W. A., and GIL, V. M. S.: Studies of sterically hindered and overcrowded molecules. Part II. Comparative proton magnetic resonance studies of substituent effects in monoderivatives of benzene, mesitylene and 1,3,5-tri-*t*-butylbenzene, 167
- GIL, V. M. S.: The relative signs of the proton coupling constants in the pyridine ring—the N.M.R. spectrum of 2,2'-dipyridine, 97
- GIL, V. M. S.: H-H and ^{13}C -H coupling constants in pyridazine, 443
- GIL, V. M. S., *see* GIBBONS, W. A.
- GROSS, J. M., and SYMONS, M. C. R.: The electron spin resonance spectra of paradinitrobenzene anions, 287
- GUGGENHEIM, E. A.: The new equation of state of Longuet-Higgins and Widom, 43
- GUGGENHEIM, E. A.: Variations on van der Waals' equation of state for high densities, 199
- HALL, G. G., *see* LORQUET, J. C.
- HILPERN, J. W.: Calculation of a triplet ground state for 1,2-diphenylphenanthro[1]-cyclobutane, 295
- HILPERN, J. W.: The intensity of the symmetry-forbidden electronic band of biphenylene, 543
- HIRSCHFELDER, J. O., and LÖWDIN, P. O.: Long-range interaction of two 1s-hydrogen atoms expressed in terms of natural spin-orbitals, 491
- HUDSON, A., *see* CARRINGTON, A.
- HUGHES, FLOYD, and PATTEN, FRANK W.: Microwave diamagnetic resonance associated with polysiloxanes, 233
- HURST, R. P., *see* STUART, J. D.

ISHIZU, K., *see* NISHIGUCHI, H.

JØRGENSEN, CHR. KLIXBÜLL, *see* SCHÄFFER, CLAUS E.

KASAI, PAUL H., and WHIPPLE, EARL B.: Electron spin resonance spectrum of the HF_2 radical isolated in a neon matrix at 4°K , 497

KHUBCHANDANI, P. G., *see* BHALLA, K. C.

KIELICH, S.: Multipolar theory of dielectric polarization in dense mixtures, 549

KIMURA, K., and NAGAKURA, A.: Vacuum ultra-violet absorption spectra of various mono-substituted benzenes, 117

KOWALEWSKI, VALDEMAR J., *see* DE KOWALEWSKI, DORA G.

LITT, CLOTILDE, *see* BURNELLE, LOUIS

LOEWENSTEIN, A., and SHPORER, M.: Cobalt-59 spin-spin coupling and isotope shifts in $\text{K}_3\text{Co}(\text{CN})_6$, 293

LONGUET-HIGGINS, H. C., *see* CARRINGTON, A.

LONGUET-HIGGINS, H. C., *see* NICHOLSON, B. J.

LOOYENGA, H.: Dielectric constants of homogeneous mixtures, 501

LORQUET, J. C.: The electronic structure of ionized molecules. II. Alkanes, 101

LORQUET, J. C., and HALL, G. G.: The electronic structure of ionized molecules. III. Field ionization, 29

LÖWDIN, P. O., *see* HIRSCHFELDER, J. O.

LUCKEN, E. A. C., *see* GERDIL, R.

LUCKHURST, G. R.: Solvent and temperature effects in the electron spin resonance spectrum of the hexamethylacetone-sodium ion-quartet, 179

MCDOWELL, C. A., *see* CHARLES, S. W.

McLAUCHLAN, K. A., *see* COHEN, A. D.

MACLEAN, C., *see* DE BOER, E.

MARQUES, MANUEL A., *see* DA SILVEIRA, ANTONIO

MARQUES, NOEMIO M., *see* DA SILVEIRA, ANTONIO

MASON, R., PHILLIPS, D. C., and ROBERTSON, G. B.: The electron distribution of the bonded hydrogen atom in carbon-hydrogen bonds, 277

MATAGA, NOBORU, TOMURA, MASAO, and NISHIMURA, HITOSHI: Fluorescence decay time of naphthalene and naphthalene excimers, 367

MOSS, R. E., *see* CARRINGTON, A.

MUNIZ, R. P. A., and DANON, J.: Electron spin resonance of the N_2O_2^+ radical, 599

MURRELL, J. N., *see* COOK, D. B.

NAGAKURA, S., *see* KIMURA, K.

NAKAMURA, K., *see* NISHIGUCHI, H.

NAKAI, Y., *see* NISHIGUCHI, H.

NEIVA-CORREIA, A. F., *see* DOS SANTOS-VEIGA, J.

NESZMÉLYI, A.: Nuclear magnetic energy levels and symmetry wave functions for six chemically equivalent spin $\frac{1}{2}$ nuclei with $C_{3v} \times C_i$ symmetry, 579

NICHOLSON, B. J., and LONGUET-HIGGINS, H. C.: The dipole moment of dihexamethylbenzenecobalt, 461

NISHIGUCHI, H., NAKAI, Y., NAKAMURA, K., ISHIZU, K., DEGUCHI, Y., and TAKAKI, H.: Weak association between alkali metal ions and mononegative ions of aromatic hydrocarbons, 153

NISHIMURA, HITOSHI, *see* MATAGA, NOBORU

PATTEN, FRANK W., *see* HUGHES, FLOYD

PHILLIPS, D. C., *see* MASON, R.

PIOVESANA, O., *see* FURLANI, C.

- POPIELAWSKI, J., and BARANOWSKI, B.: Statistical mechanics of transport processes in adsorbed gases, 59
- POPLE, J. A., and SANTRY, D. P.: A molecular orbital theory of hydrocarbons. II. Ethane, ethylene and acetylene, 301
- POPLE, J. A., and SANTRY, D. P.: A molecular orbital theory of hydrocarbons. III. Nuclear spin coupling constants, 311
- PRYCE, M. H. L., SINHA, K. P., and TANABE, Y.: On the tetragonal distortion of octahedral systems in an E_g electronic state, 33
- RANFT, J., *see* DUVAL, E.
- RICHARDS, R. E., *see* DEVERELL, C.
- ROACH, A. C., *see* CHILD, M. S.
- ROBERTS, P. J.: A two-electron atomic integral, 513
- ROBERTSON, G. B., *see* MASON, R.
- ROWLINSON, J. S.: A test of Kihara's intermolecular potential, 197
- ROWLINSON, J. S.: Self-consistent approximations for molecular distribution functions, 217
- SAMS, JOHN R.: Quantum second virial coefficient of a two-dimensional Lennard-Jones gas, 17
- SAMS, JOHN R.: Quantum second virial coefficient of a one-dimensional Lennard-Jones gas, 77
- SAMS, JOHN R.: Two-dimensional second virial coefficients of krypton on graphite carbon 195
- SANTRY, D. P., *see* POPLE, J. A.
- SARAN, ANIL, *see* BARUA, A. K.
- SCHNEPP, O., *see* BRITH, M.
- SCHÄFFER, CLAUS E., and JØRGENSEN, CHR. CLIXBÜLL: The angular overlap model, an attempt to revive the ligand field approaches, 401
- SHPORER, M., *see* LOEWENSTEIN, A.
- SINHA, K. P., *see* PRYCE, M. H. L.
- SMITH, I. C. P., *see* CARRINGTON, A.
- STUART, J. D., and HURST, R. P.: A study of the valence electron approximation: application to LiH, 265
- SYMONS, M. C. R., *see* GROSS, J. M.
- TAKAKI, H., *see* NISHIGUCHI, H.
- TANABE, Y., *see* PRYCE, M. H. L.
- TODD, P. F., *see* CARRINGTON, A.
- TOMURA, MASAO, *see* MATAGA, NOBORU
- WALMSLEY, S. H., *see* ANDERSON, A.
- WHIPPLE, EARL B., *see* KASAI, PAUL H.
- YERANOS, WALTER A.: Normal coordinate analysis of XeF_4 in the Urey-Bradley field, 449
- YERANOS, WALTER A.: Urey-Bradley potential constants of sulphur compounds: SF_5Cl , 455
- YERANOS, WALTER A., and FOSS, FRED D.: Normal coordinate analysis of Re(VII)O_4^- , $\text{Re(VII)O}_3\text{Cl}$ and $\text{Re(VII)O}_3\text{Br}$, 87